Michael Y. Henein
Editor

Clinical Echocardiography

Third Edition

MOREMEDIA

Springer

Clinical Echocardiography

Michael Y. Henein
Editor

Clinical Echocardiography

Third Edition

Springer

Editor
Michael Y. Henein
Imperial College London
London, UK

ISBN 978-3-031-95893-9 ISBN 978-3-031-95894-6 (eBook)
https://doi.org/10.1007/978-3-031-95894-6

© The Editor(s) (if applicable) and The Author(s), under exclusive license to Springer Nature Switzerland AG 2004, 2012, 2025

This work is subject to copyright. All rights are solely and exclusively licensed by the Publisher, whether the whole or part of the material is concerned, specifically the rights of translation, reprinting, reuse of illustrations, recitation, broadcasting, reproduction on microfilms or in any other physical way, and transmission or information storage and retrieval, electronic adaptation, computer software, or by similar or dissimilar methodology now known or hereafter developed.
The use of general descriptive names, registered names, trademarks, service marks, etc. in this publication does not imply, even in the absence of a specific statement, that such names are exempt from the relevant protective laws and regulations and therefore free for general use.
The publisher, the authors and the editors are safe to assume that the advice and information in this book are believed to be true and accurate at the date of publication. Neither the publisher nor the authors or the editors give a warranty, expressed or implied, with respect to the material contained herein or for any errors or omissions that may have been made. The publisher remains neutral with regard to jurisdictional claims in published maps and institutional affiliations.

This Springer imprint is published by the registered company Springer Nature Switzerland AG
The registered company address is: Gewerbestrasse 11, 6330 Cham, Switzerland

If disposing of this product, please recycle the paper.

Foreword

By definition, nerve transfer is a surgical technique in which a nearby healthy nerve is sacrificed to serve as a donor for an injured, more important recipient nerve. Historically, credit should be given to Harris and Low (1903), who first proposed this technique. Many others have contributed with new methods or modifications of the original approach. Names such as Tuttle (1913), Vulpian and Stoffel (1920), Foerster (1929), and Lurje (1948) should also be remembered as pioneers in the field of nerve transfers.

In more recent years, increasing knowledge in nerve anatomy, microsurgical techniques, and nerve regeneration—as well as the remarkable publications of Narakas, Gu, Oberlin, Leechavengvongs, Mackinnon, and Samardzic—has significantly advanced the acceptance and use of nerve transfer procedures in many types of nerve injuries.

Peripheral nerve transfers have been performed primarily in cases of brachial plexus injuries and, in recent years, have become the preferred method of treatment for many specialists—even without surgical exploration of the plexus. In many cases, the functional outcomes achieved with nerve transfers surpass those obtained through traditional nerve repair or tendon transfers.

The editors—Fernando Guedes, Christian Heinen, Lukas Rasulic, Alexander Shin, and Mariano Socolovsky—have brought together a distinguished group of authors from various specialties, all experts in peripheral nerve surgery from around the world, to create this important book: *Nerve Transfers for Brachial Plexus Reconstruction After Trauma*."

The editors, as well as all contributing authors, should be congratulated for publishing such an outstanding book. It will undoubtedly become an indispensable resource for all specialists interested in the surgical treatment of brachial plexus injuries.

It is an honor to have been invited to write this foreword.

Head – Peripheral Nerve Surgery Unit, Department of Neurosurgery
University of São Paulo Medical School
São Paulo, SP, Brazil

Mario G. Siqueira

Preface

Over the past seven decades, clinical cardiology has demonstrated that Doppler echocardiography is a cornerstone of optimal practice. While many technologies come and go, those that endure prove to be truly essential—and echocardiography is one such technology. In the 1950s, Edler, with great humility, could not have anticipated that his invention of the first echocardiograph would one day become an "imaging stethoscope" in cardiology clinics worldwide, especially in the West. Over the years, dedicated scientists and engineers have continually improved this technology: adding 2D imaging to M-mode, then spectral and myocardial Doppler, followed by myocardial deformation and perfusion evaluation. The cross-sectional limitations of earlier technologies have now been overcome through 3D and 4D echocardiography, enabling accurate volumetric and valve assessments.

In addition to its unique accessibility across all patient settings—clinics, hospital wards, intensive care units, emergency rooms, and operating theaters—Doppler echocardiography has recently experienced a significant increase in demand. Pediatric and fetal echocardiography are now well-established practices. Moreover, patients from respiratory, oncology, renal, stroke, and certain neurology specialties are increasingly referred for echocardiographic assessment. This wider application underscores the clinical necessity of understanding the interplay between various organ systems and provides more accurate explanations for symptoms and physical findings, while also guiding optimal management strategies.

This third edition of Clinical Echocardiography has been compiled with updated 17 previously published chapters in addition to 5 new chapters, in response to the increasing demand by clinicians and physiologists. The book offers a clinical approach to the anatomical and physiological assessment of various cardiovascular syndromes, using different Doppler echocardiographic modalities, as well as serving as a reference guide for optimal current management.

London, UK — Michael Y. Henein

Contents

1 Mitral Valve 1
Michael Y. Henein, Matteo Lisi, Matteo Cameli, Federico Landra, Mary Sheppard, Harry Smith, John R. Pepper, Mario Petro, and Michael Rigby

2 Aortic Valve 35
Michael Y. Henein, Matteo Cameli, Matteo Lisi, Federico Landra, Mary Sheppard, John R. Pepper, Harry Smith, Mario Petro, and Michael Rigby

3 Tricuspid Valve 67
Michael Y. Henein, Mary Sheppard, John R. Pepper, and Michael Rigby

4 Pulmonary Valve 83
Michael Y. Henein, Mary Sheppard, John R. Pepper, and Michael Rigby

5 Valve Substitutes 95
Michael Y. Henein, Matteo Cameli, Matteo Lisi, Federico Landra, Mary Sheppard, and John R. Pepper

6 Infective Endocarditis 105
Matteo Lisi, Matteo Cameli, Sergio Mondillo, and Michael Y. Henein

7 Coronary Artery Disease 115
Michael Y. Henein, Ibadete Bytyçi, and Michael Rigby

8 Stress Echocardiography 151
Eugenio Picano and Lauro Cortigiani

9 Dilated Cardiomyopathy 161
Michael Y. Henein, Ibadete Bytyçi, Mary Sheppard, and John R. Pepper

10 Hypertrophic Cardiomyopathy 183
Michael Y. Henein, Per Lindqvist, Mary Sheppard, and John R. Pepper

11 Restrictive Cardiomyopathy 201
Michael Y. Henein, Per Lindqvist, and Mary Sheppard

12 Pulmonary Hypertension 215
Michael Y. Henein, Per Lindqvist, and Mary Sheppard

13 Echocardiography in Advanced Heart Failure 227
Francesca M. Righini, Luca Martini, Matteo Lisi, Matteo Cameli, and Michael Y. Henein

14 Cardio-oncology 249
Ibadete Bytyçi and Michael Y. Henein

15 The Left Atrium 261
Alessandro Campora, Matteo Lisi, Matteo Cameli, and Michael Y. Henein

16 Cardiac Tumors 277
Michael Y. Henein, Mary Sheppard, and Michael Rigby

17 Pericardial Disease 289
Michael Y. Henein and Mary Sheppard

18 Simple Adult Congenital Heart Lesions 307
Wei Li and Michael Y. Henein

19 Percutaneous Device Closure of Atrial Septal Defect (ASD) and Patent Foramen Ovale (PFO) 321
Evelyn M. Lee, Kwang How Mok, Ting Ting Low, and Leonard M. Shapiro

20 Carotid Scanning 351
Eugenio Picano and Ana Cristina Camarozano

21 Diseases of the Aorta 357
Michael Y. Henein, Mary Sheppard, Harry Smith, John R. Pepper, and Mario Petro

22 Cardiac Function and Renal Disease 371
Bernd Stegmayr and Michael Y. Henein

Index 381

Mitral Valve

1

Michael Y. Henein, Matteo Lisi, Matteo Cameli, Federico Landra, Mary Sheppard, Harry Smith, John R. Pepper, Mario Petro, and Michael Rigby

Anatomy

The mitral valve is composed of two leaflets, an annulus, chordae tendineae, and two papillary muscles. The anterior (aortic) leaflet is attached to the root of the aorta in direct continuity with the aortic valve and the membranous septum, and has a trapezoidal shape involving one-third of the circumference of the annulus (Fig. 1.1). The posterior leaflet has a quadrangular shape, is continuous with the posterior wall of the left atrium and is longer than the anterior leaflet, occupying two-thirds of the circumference of the mitral annulus (Fig. 1.2). The posterior leaflet is generally divided into three scallops, but this may vary. The two leaflets coapt at the zone of apposition leaving an overlapping segment 5-mm long. The chordal anatomy of the mitral valve is complicated, with around 12 primary chordae arising from each papillary muscle, the anterolateral and the posteromedial, which then divide into secondaries and numerous tertiary branches which attach themselves to the margins of the two leaflets (Videos 1.1 and 1.2). The papillary muscles themselves are continuous with the trabeculae and subendocardial layer of the ventricular wall. The normal diameter of the mitral annulus is approximately 3 cm with a circumference

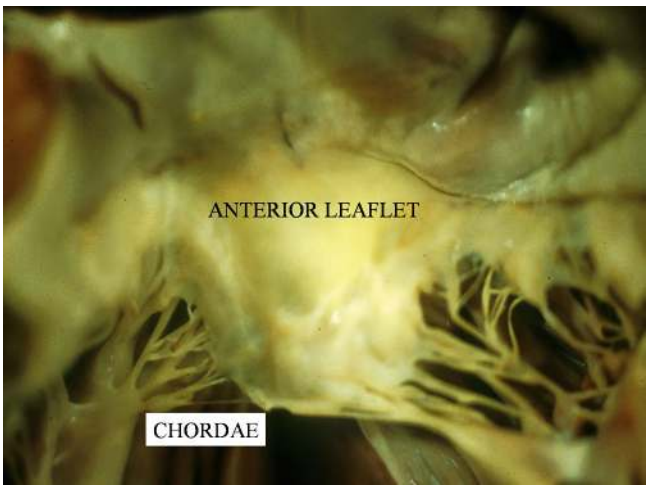


Fig. 1.1 Normal mitral valve with large "apron" like anterior leaflet in direct continuity with the aortic valve and posterior leaflet. Note the attached chordae and papillary muscles

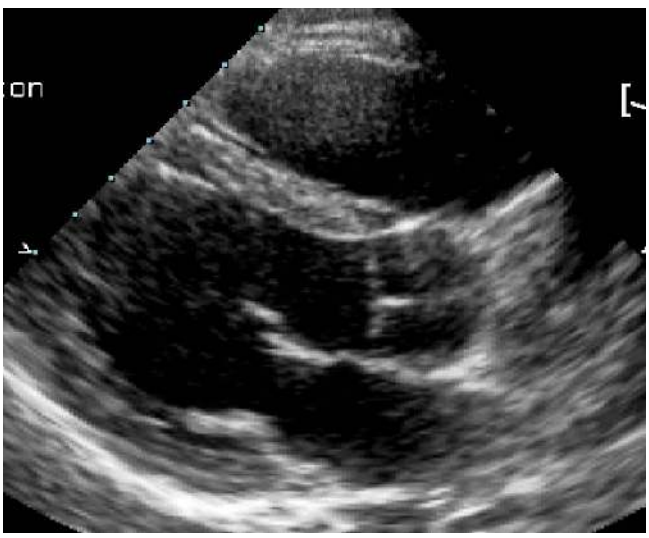


Fig. 1.2 Parasternal 2D long axis view showing anterior (extending from the posterior aortic wall) and posterior (extending from the left atrial posterior wall) mitral valve leaflets

Supplementary Information The online version contains supplementary material available at https://doi.org/10.1007/978-3-031-95894-6_1.

M. Y. Henein (✉)
Imperial College London, London, UK

Univesity of Siena, Siena, Italy
e-mail: m.henein@imperial.ac.uk

M. Lisi
Ospedale S. Maria delle Croci, Ravenna, Italy

M. Cameli · F. Landra
Univesity of Siena, Siena, Italy

M. Sheppard · H. Smith · J. R. Pepper · M. Petro · M. Rigby
Royal Brompton Hospital, London, UK

© The Author(s), under exclusive license to Springer Nature Switzerland AG 2025

M. Y. Henein (ed.), *Clinical Echocardiography*, https://doi.org/10.1007/978-3-031-95894-6_1

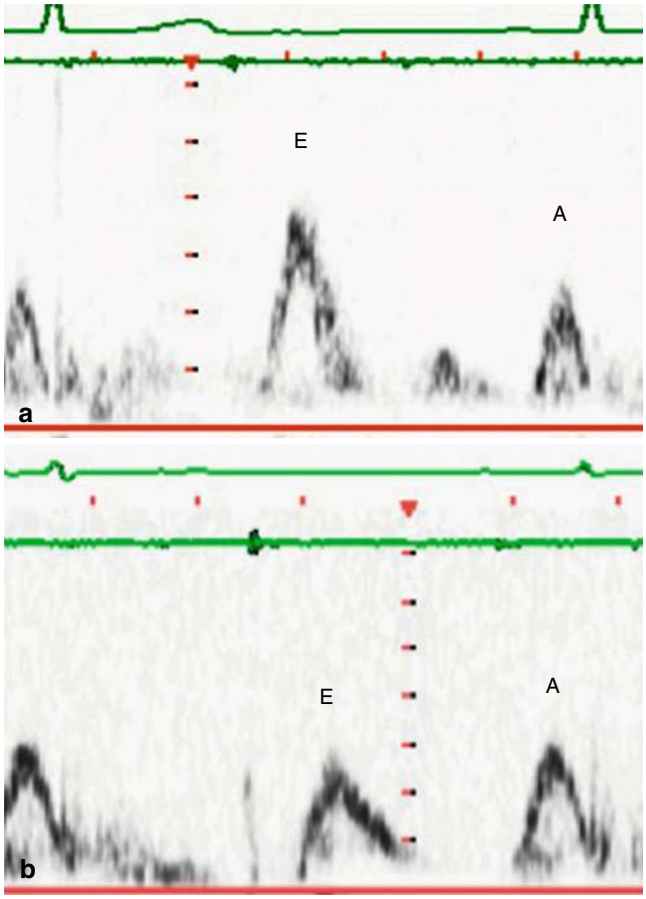


Fig. 1.3 Transmitral Doppler flow velocities from (**a**) young subject showing dominant early diastolic component and (**b**) an elderly showing dominant late diastolic component

of 8–9 cm. The annulus is not a passive structure, so in addition to its normal movement toward the apex in systole, the contraction of the posterior myocardial muscle shortens the annular diameter by 25%, making its dynamics a very important component in the mechanism of mitral valve competence (Fig. 1.3) [1].

Physiology

Optimum function of the mitral valve depends on the integral function of all its components: leaflets, chordae, annulus, and papillary muscles, as well as the left atrium and the left ventricle (Fig. 1.4). Left atrial cavity enlargement and shape change result in mitral annular dilatation and hence overall valve dysfunction and incompetence. A normal mitral valve does not close passively. In addition to the pressure difference between the ventricle and the atrium in systole, the annular contraction and papillary muscle contraction play an important role in maintaining the competence of the mitral valve. The mitral valve orifice cross-sectional area is

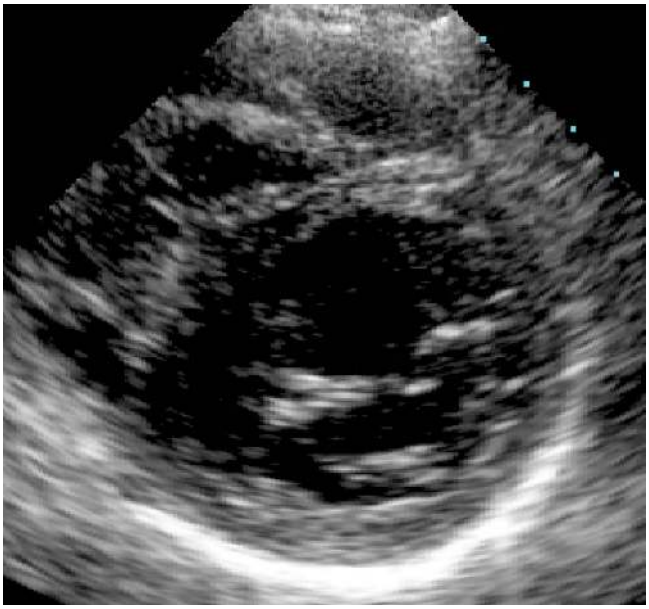


Fig. 1.4 Minor axis view of the left ventricle at the level of the papillary muscles. Note their relationship with different segments of the left ventricle

approximately 5.0 cm^2, allowing left ventricular filling to occur predominantly in early diastole (approximately two-thirds of stroke volume) at a peak rate of 50–100 cm/s. The remaining one-third of the stroke volume passes through the mitral valve during atrial systole. During diastasis, ventricular volume remains unchanged [2]. With exercise and increase in heart rate, diastasis shortens and the early and late filling components approximate until they summate and become indistinguishable [3]. With age, the filling pattern reverses so that dominant left ventricular filling occurs in late diastole [4].

Mitral Stenosis

Rheumatic fever is the leading cause of mitral stenosis (MS), followed by degenerative MS. Less common causes include congenital MS, malignant carcinoid disease, inflammatory and infiltrative disorders, tumors, and drug-induced valve disease.

Congenital Mitral Stenosis

Congenital mitral stenosis is a relatively rare group of anomalies with considerable variations in the morphological features. Normally included in this diagnosis is cortriatriatum and supravalvar mitral membrane which can be identified from the four chamber and long axis sections (Fig. 1.5). Characteristically, color flow Doppler reveals acceleration

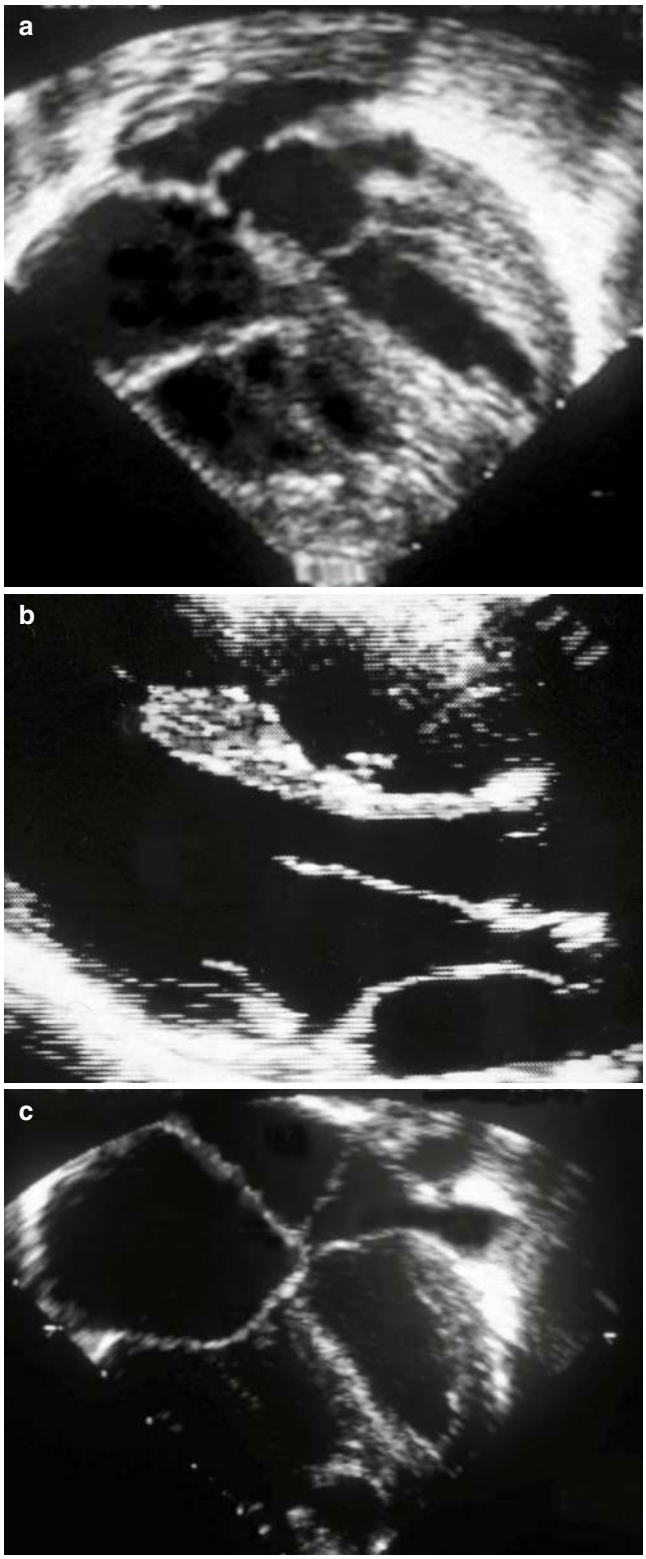


Fig. 1.5 (**a**, **b**) Subcostal views from two patients with cor triatriatum, one parallel to mitral valve leaflets and the other at oblique angle. (**c**) Subcostal view from a patient with supravalvar membrane

proximal to the mitral valve leaflets. It is not unusual, however, for the supravalvar mitral stenosis to be associated with thickened mitral valve leaflets and chordal abnormalities as well. It is unusual to find isolated mitral valve stenosis. In addition to thickened and dysplastic leaflets, anomalies of the chordae and of the papillary muscles may be detected. In the classical parachute mitral valve, all the chordae insert into a single papillary muscle.

Rheumatic Mitral Stenosis

Rheumatic mitral stenosis affects 10/100,000, predominantly in the Middle East, India, and Far East. Mitral stenosis develops progressively after the occurrence of rheumatic fever in childhood [5]. It results in fusion of the commissures, thickened leaflets, and eventually fibrosis. In the early stages, the anterior mitral leaflet is pliable showing a doming motion in diastole and possibly a degree of leaflet prolapse in systole. The posterior leaflet is always stiff due to the commissural fusion. Thickening of the valve affects predominantly the tips and the leaflet body but tends to spare the base (Fig. 1.6) [6]. The subvalvular apparatus may also be involved; the chordae are thickened and fused and the papillary muscles are scarred due to spread of fibrosis into the inferobasal myocardium. Eventually, the mitral ring and leaflets may calcify [7]. Long-standing mitral stenosis may be complicated by dilatation of the left atrium, atrial fibrillation, and develop-

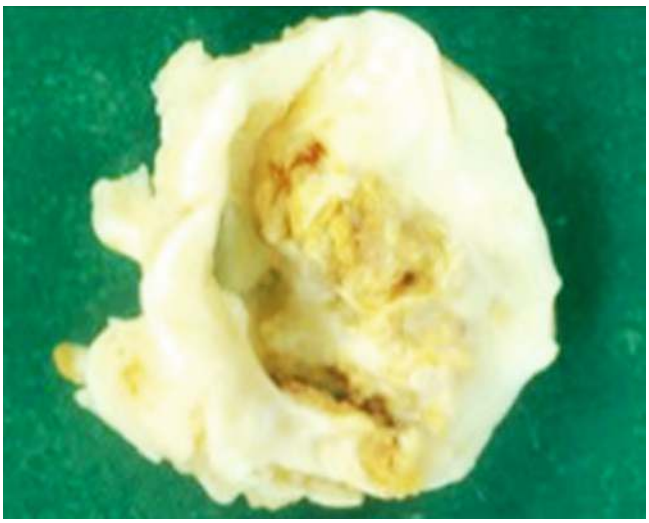


Fig. 1.6 Pathology section from rheumatic MVD showing the stenotic orifice with fish-mouth appearance. Note the commissural fusion and leaflet calcification. View from the left atrium

ment of mural thrombus. Mitral stenosis may also result in pulmonary venous congestion, pulmonary hypertension, right ventricular hypertrophy and dilatation, and functional tricuspid regurgitation.

Pathophysiology As the disease progresses, the leaflets thicken, the commissures fuse, and the mitral valve area falls. With an area of 2.5 cm^2, symptoms start to appear as transmitral pressure drop becomes influenced by valve area, rhythm, duration of diastasis, and ventricular diastolic function (Figs. 1.7 and 1.8). With a valve area of 2.5 cm^2, peak left ventricular filling rate falls and diastasis is lost. This is of no physiological consequence at rest, but with exercise, left ventricular filling is only maintained by a significant rise in left atrial pressure and consequently pressure drop between the left atrium and left ventricle. As the valve area becomes progressively smaller, a pressure drop develops at rest. This is usually associated with a fall in cardiac output, increase in pulmonary vascular resistance, and worsening symptoms. In severe mitral stenosis, the pressure difference between the left atrium and left ventricle may be as high as 25–30 mmHg, and valve area less than 1 cm^2 in comparison to the normal valve area of 5 cm^2. The increase in heart rate does not significantly change the effective mitral orifice area compared to the aortic stenotic area. This could be explained by the lesser number of commissures assisting in the opening of the valve compared to those of the aortic valve. Subvalvular apparatus involvement with fibrosis may itself contribute to the degree of stenosis [8]. In some patients, the chordal severity of fibrosis and narrowing may become the flow limiting level rather than the leaflets tips. The important consequence of mitral stenosis is its effect on left atrial pressure, size, and the pulmonary vasculature. As the disease progresses and valve area falls, left atrial emptying reduces, left atrial size and pressure increase, and the pulmonary venous pressure also increases. Long-standing conditions may result in irreversible post-capillary pulmonary hypertension secondary to the raised left atrial pressure (Videos 1.3 and 1.4).

In order to gain a flow-independent measure of the degree of narrowing, mitral valve area is frequently calculated. A number of methods have been proposed for this, but none is entirely satisfactory. There is no agreed gold standard against which noninvasive measures can be calibrated, and when compared with one another, correlation coefficients are usually too low to be applicable in individual patients. Furthermore, it is questionable whether the complex hemodynamic disturbance to atrioventricular flow can be summed up in a simple statement of area.

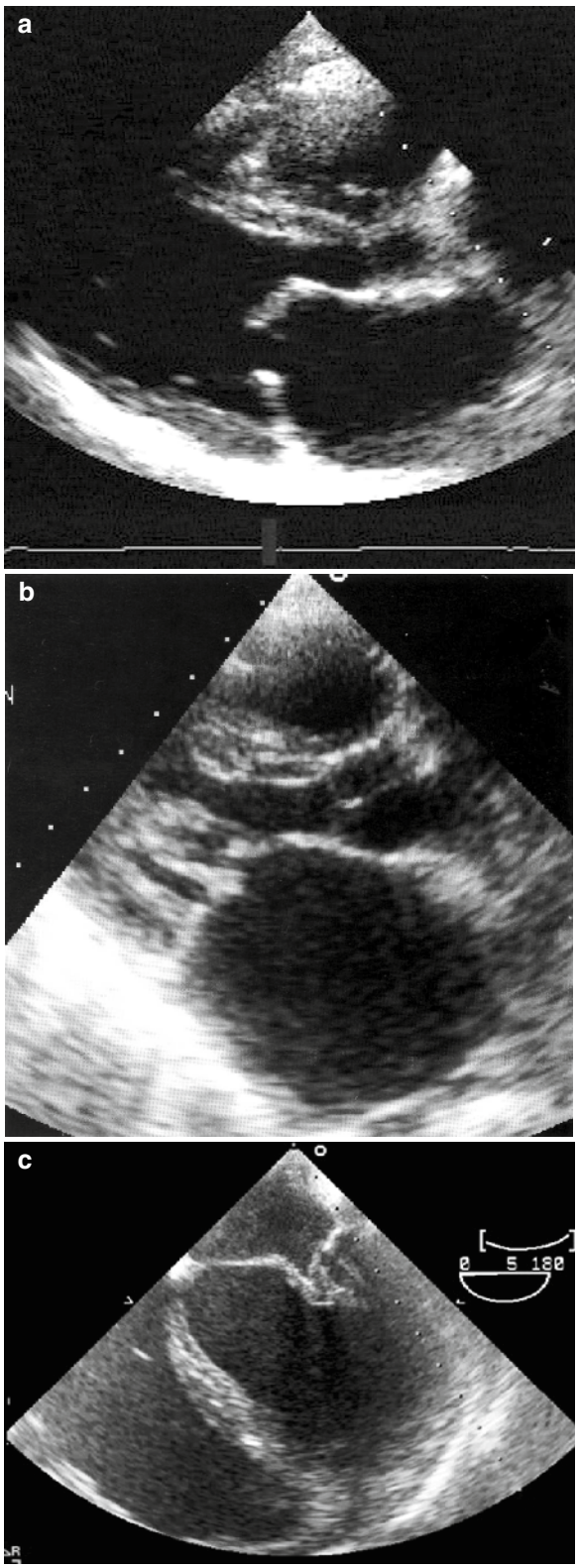


Fig. 1.7 (**a**) 2D parasternal long axis view showing rheumatic mitral valve leaflets. Note the thickening and bowing of the anterior leaflet in diastole. (**b**) Similar view from a patient with fibrosed subvalvar apparatus causing subvalvar stenosis. (**c**) Trans-esophageal views from a patient with fibrosed subvalvar apparatus

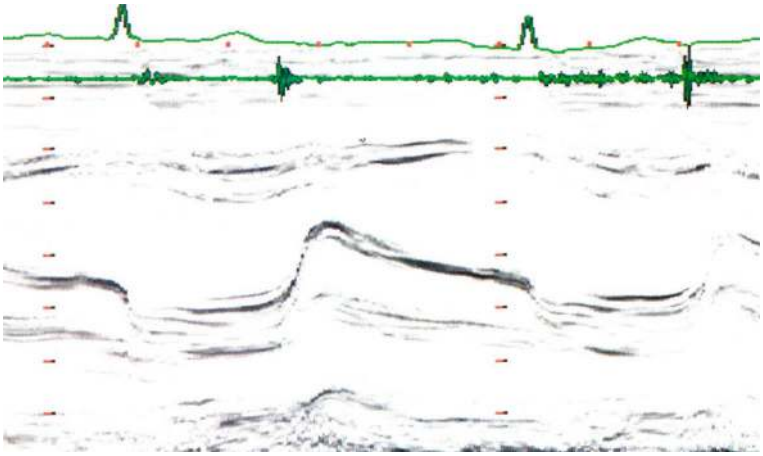


Fig. 1.8 Mitral valve M-mode echogram from the same patient. Note the characteristic pattern of stiff rheumatic anterior leaflet in diastole and the anterior movement of the posterior leaflet, due to commissural fusion

Assessment of Severity of Mitral Stenosis

Mitral Valve Area

A number of methods have been used with varying accuracy.

(a) *Planimetry Technique*: It involves tracing the inner border of the mitral valve opening in diastole (Fig. 1.9). This has been shown to correlate with valve area measured by catheterization [9]. It has its limitations particularly in the presence of significant leaflet tip calcification, poor border detection, and varying degrees of opening time due to atrial fibrillation.

(b) *Vena Contracta*: The width of color flow jet in two orthogonal planes correlates with planimetry estimated values of mitral valve area [10].

(c) *Flow Convergence Method* (*Proximal Isovelocity Area—PISA*). Blood flow through a narrowed orifice converges in a series of proximal isovelocity hemispheres (isovelocity surface area). In mitral stenosis, it can be demonstrated by mosaic color Doppler on the atrial side in diastole (Fig. 1.10). The flow rate is calculated by $2\pi r^2 v$, where r is the distance to a contour of velocity v, defined by the change in color at the aliasing boundary. The narrowed orifice area can be calculated by dividing peak flow rate by maximal velocity through the orifice (obtained from the continuous wave Doppler). Mitral valve area calculated by this method has been shown to correlate with that obtained by conventional catheterization. However, flow convergence method is subject to geometric complexities of the mitral valve orifice [11].

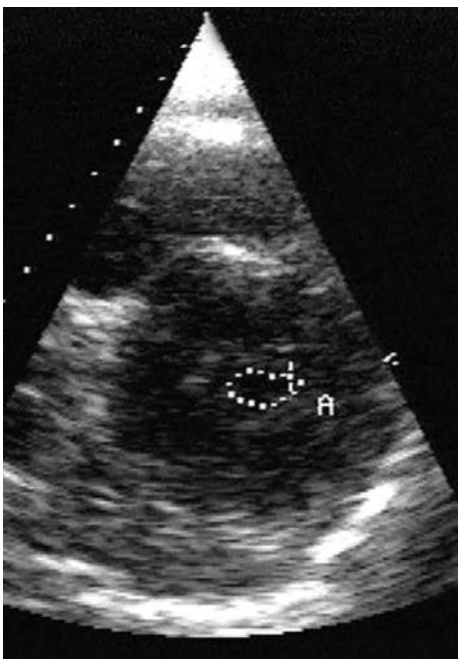


Fig. 1.9 Parasternal short axis view of a rheumatic mitral valve showing a traced valve area of 1.0 cm^2

(d) *Transmitral -Pressure Drop*: Using modified Bernoulli equation ($4\,V^2$), peak and minimum mitral pressure drop can be measured and mean value calculated (Fig. 1.11) [12].

(e) *Pressure ½ Time*: This is the time taken by the early diastolic transmitral pressure to drop to ½ its peak value (or the time taken for initial velocity divided by square root of 2 which is 1.4). Mitral area is then calculated as a constant (220) divided by pressure ½ time (Fig. 1.12). Although mitral pressure ½ time has been found to correlate with invasively measured mitral valve area, it too has major limitations, particularly in patients with atrial fibrillation, and fast heart rate. Also pressure ½ time depends on the left ventricular inflow resistance due to the funnel shape of the mitral apparatus including both orifice and subvalvar components. More resistance at the subvalvar apparatus may slow the pressure decline across the inflow tract, so that pressure ½ time is usually smaller than that obtained from 2D planimetry. The opposite is seen in patients with concomitant aortic regurgitation or left ventricular hypertrophy, when pressure ½ time overestimates the degree of mitral stenosis. It may therefore provide unreliable values after mitral valvuloplasty. The main reason for underestimating the accuracy of this method is the fact that it relies on the pressure fall which is frequently not exponential [13, 14].

(f) *Continuity Equation*: This is based on the principle of mass and energy conservation. The flow at all points along a tube is constant and equals the product of mean velocity and the cross-sectional area. Mitral valve area is calculated as the product of aortic or pulmonary annular cross-sectional area and the ratio of the respective valve velocity time integral to that of the mitral stenotic continuous wave velocity. Although a more complex approach, this method is preferable in patients with additional significant aortic regurgitation in whom pressure ½ time overestimates mitral valve area [15].

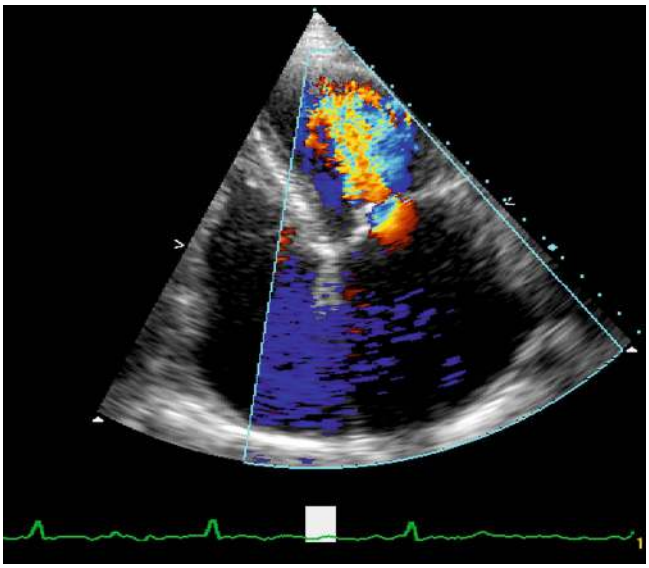


Fig. 1.10 Transmitral flow convergence velocities from a patient with mitral stenosis. Note the change in velocity before the stenotic orifice

The common practice now is to study most patients with significant mitral valve disease by transesophageal echocardiography since it provides a more detailed assessment of the mitral valve, subvalvar apparatus, and the presence of left atrial spontaneous contrast and appendage clots. Mitral valve area measurements can also be obtained from transesophageal images as described above.

In general, mitral valve area >1.5 cm^2 is usually considered mild stenosis, between 1.0 and 1.5 cm^2 moderate, and <1 cm^2 as severe stenosis.

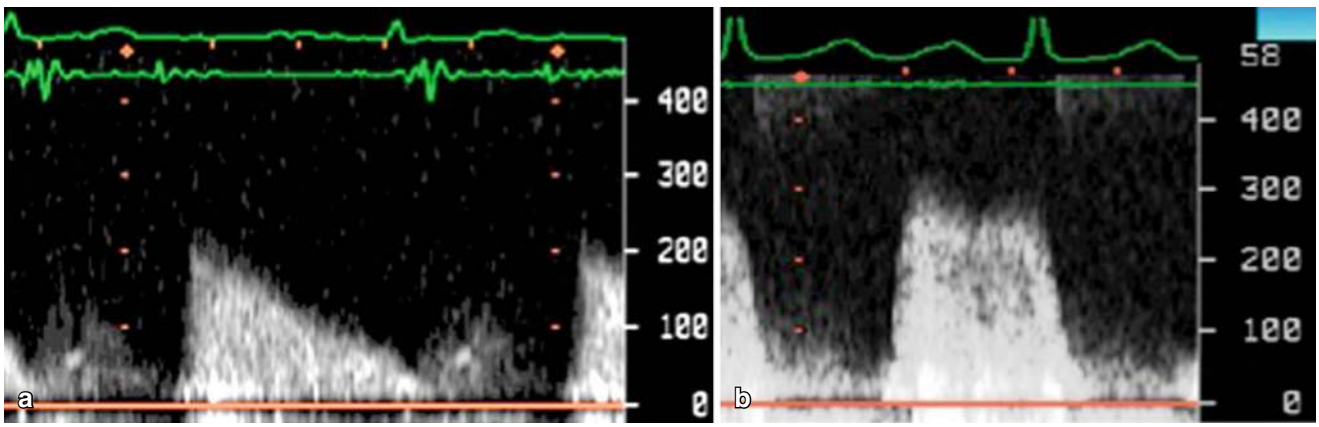


Fig. 1.11 LV filling velocities by CW Doppler, showing raised early diastolic pressure drop component giving a mean of 8 mmHg (**a**) and another patient with severe stenosis and mean pressure drop of 20 mmHg (**b**)

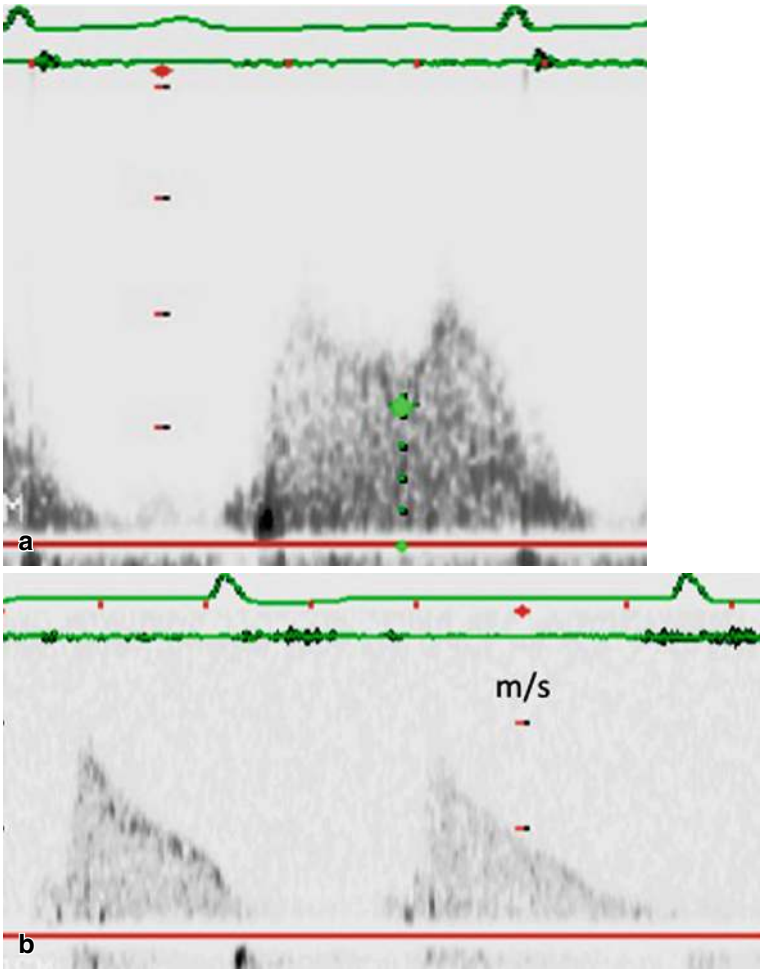


Fig. 1.12 Transmitral Doppler flow velocities from 2 patients with mitral stenosis showing pressure 1/2 time limitations

Clinical Picture and Disturbed Physiology

Symptoms can develop at any time after the onset of acute rheumatic fever, but usually significant mitral stenosis matures years after the first episode of rheumatic fever. The commonest manifestation is breathlessness, reduction of exercise tolerance, or palpitation, usually the result of increased left atrial pressure and atrial fibrillation. Hemoptysis and paroxysmal nocturnal dyspnea may be related to pulmonary venous congestion. Systemic embolic disease, fluid retention, and symptoms of right-sided congestion are common in untreated cases. Venous pressure is raised if there is tricuspid regurgitation, organic involvement of tricuspid valve, or pulmonary hypertension. The characteristic opening snap is heard when the leaflets are still pliable, but it disappears as the leaflets calcify with reduced mobility. A loud first heart sound is heard preceded by presystolic murmur if the patient is in sinus rhythm or middiastolic murmur.

Complications

(a) *Leaflet Fibrosis and Deformation*: With progressive rheumatic disease, chronic leaflet deformity occurs in the form of fibrosis and stiffness, particularly of the posterior leaflet. Fibrosis and calcification of the anterior leaflet may also occur (Fig. 1.13).

(b) *Left Atrial Dilatation*: Progressive reduction in mitral valve orifice area causes perpetual increase in left atrial pressure and size, particularly in the young and middle-aged patients, followed by pulmonary venous hypertension. Left atrial dilatation is associated with reduction in its mechanical function and hence slow intra-atrial blood circulation. With progressive disease and development of atrial fibrillation, the circulation in the atrium becomes very sluggish and echocardiography may demonstrate spontaneous echo contrast, which is usually clearly seen on transesophageal images (Fig. 1.14; Video 1.5). Such



Fig. 1.13 Apical four chamber view from a patient with rheumatic mitral valve. Note the extent of leaflet thickening and fibrosis

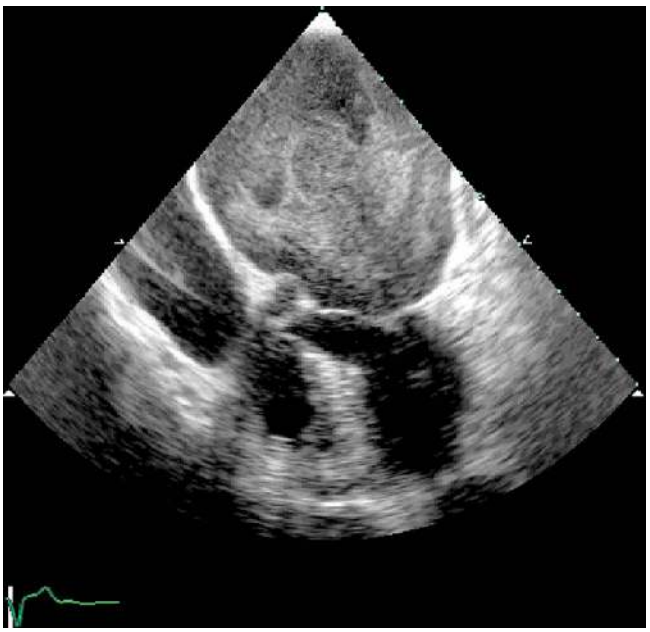


Fig. 1.14 TOE from a patient with rheumatic mitral valve stenosis showing a large left atrium with spontaneous echo contrast

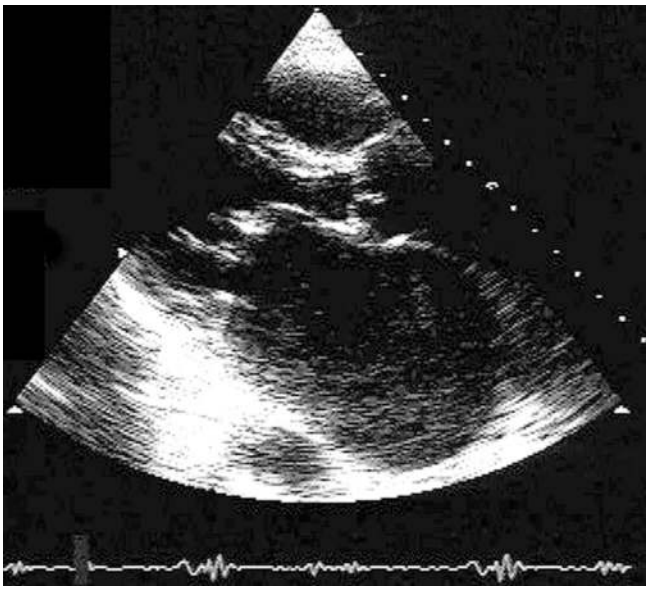


Fig. 1.15 Parasternal view of the LV showing dilated cavity

patients are given anticoagulants in order to avoid clot formation and to reduce the risk of cerebrovascular accidents. Left atrial thrombus formation is very common in patients with severe mitral stenosis: Almost one-fifth of those undergoing surgery have left atrial thrombus, and in one-third of them, the thrombus is restricted to the atrial appendage [6]. Even in patients with sinus rhythm, left atrial thrombus may form in those with dilated left atrium and spontaneous contrast and hence the need for anticoagulation [16, 17].

(c) *Left Ventricular Dysfunction*: In most cases with mitral stenosis, the left ventricle is normal in size and systolic function is well maintained. However, in some patients, diastolic function may be abnormal with raised end-diastolic pressure. This picture could be related to additional pathologies, e.g., hypertension, diabetes, or coronary artery disease rather than primary rheumatic myocardial disease. The latter was suggested years ago, but no convincing evidence has ever substantiated. Left ventricular cavity dilatation is only seen in the presence of additional coronary artery disease (Fig. 1.15). In some patients with rheumatic mitral stenosis, the left ventricle may be impaired. In addition to the characteristic picture of a slow filling ventricle, posterobasal segmental hypokinesia may be seen. This may either be due to primary rheumatic myocardial involvement or secondary to the significant restriction of the posterior leaflet motion and hence its corresponding myocardial segment. Ventricular dysfunction may add to the low stroke volume, raised peripheral resistance, and the development of pulmonary hypertension [18, 19].

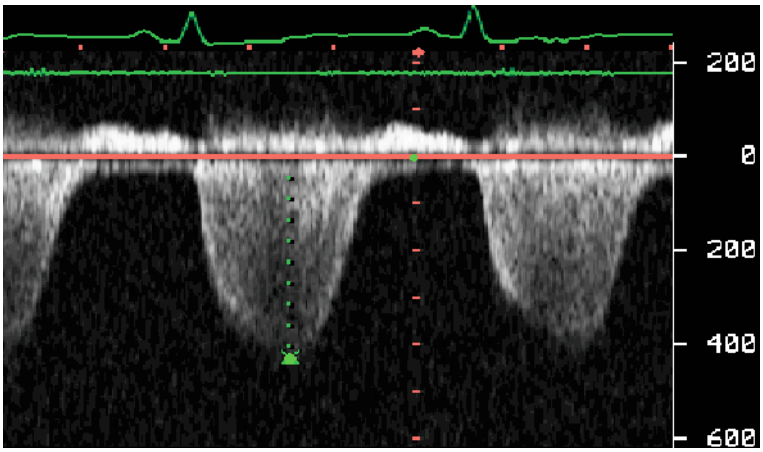


Fig. 1.16 Continuous wave Doppler demonstrating raised RV-RA pressure drop −70 mmHg, from a patient with PHT complicating mitral stenosis

(d) *Pulmonary Hypertension*: With the increase in severity of mitral stenosis and left atrial pressure, the pulmonary venous pressure increases followed by raised pulmonary arterial pressure. Pulmonary artery pressure usually reflects the degree of increase in left atrial pressure in mitral stenosis. It is very rare for pulmonary hypertension to develop with left atrial pressure less than 20 mmHg in the setting of isolated mitral stenosis. Despite that, discrepancy between the two may suggest a raised pulmonary vascular resistance or a pre-capillary primary etiology for pulmonary hypertension. Long-standing mitral stenosis and pulmonary hypertension may result in irreversibly raised pulmonary vascular resistance; even a successful valve surgery and correction of mitral stenosis may not guarantee a normal pressure drop across the pulmonary bed of approximately 10–15 mmHg. Such patients may remain limited by breathlessness despite having successful mitral valve surgery [11]. Pulmonary hypertension is demonstrated as dilated right heart and significant increase in right ventricular to right atrial pressure drop (Fig. 1.16). This may be underestimated as the right atrial pressure rises. Systolic right ventricular pressure may significantly fall after successful mitral valvotomy or valvuloplasty [20, 21].

(e) *Tricuspid Regurgitation*: Even in the absence of organic tricuspid leaflet disease, functional tricuspid regurgitation may be present. This varies in its severity from mild to moderate as the tricuspid ring dilates, particularly as pulmonary hypertension develops. Severe tricuspid regurgitation has been reported to develop years after mitral valve replacement, which significantly limits exercise tolerance in individual patients (Fig. 1.17). Recently some of this tricuspid regurgitation has been shown to be organic in origin, with the leaflets demonstrating signs of disease with fibrosis, calcification, prolapse, and tethering. In contrast to functional regurgitation, severe organic disease results in severe tricuspid annular dilatation, right heart failure, morbid liver complications, and early mortality [22].

(f) *Aortic Valve Disease*: Although the mitral valve is most commonly affected by rheumatic disease, aortic regurgitation may also appear early in life during the subacute phase. Aortic stenosis tends to develop later. Its severity may be significantly underestimated so long as mitral valve stenosis is present. If missed before correction of mitral stenosis, it usually devalues the success of the procedure (Fig. 1.18).

(g) *Tricuspid Valve Stenosis*: Organic tricuspid stenosis is not seen in the absence of mitral stenosis. When it occurs, physical signs are usually mild and overshadowed by those of mitral stenosis. Physiologically, significant pressure drops are much less than across the mitral valve (2–3 mmHg). Tricuspid stenosis must be recognized by echocardiography before correction of mitral stenosis because if left, it results in fluid retention. Tricuspid stenosis is often missed at cardiac catheterization and when confirmed, it always requires an open procedure; thus, it is an absolute contraindication to balloon mitral valvuloplasty. Finally, tricuspid stenosis may develop late after mitral valve surgery for mitral stenosis (Fig. 1.19) [23].

(h) *Right Heart Disease*: With the development of pulmonary hypertension, the right ventricle becomes hypertrophied and its cavity dilates with time. As right ventricular myocardium becomes stiff, diastolic pressures raise and are reflected on right atrial pressure and eventually right atrial dilatation occurs. With progressive tricuspid annulus dilatation, significant tricuspid regurgitation develops. Patients with severe tricuspid regurgitation may develop fluid retention which needs careful management in order to maintain optimum left-sided cardiac output and tissue perfusion. Long-standing significant tricuspid regurgitation itself and raised right atrial pressure may cause further deterioration of right ventricular function and congestive heart failure. By that stage, the myocar-

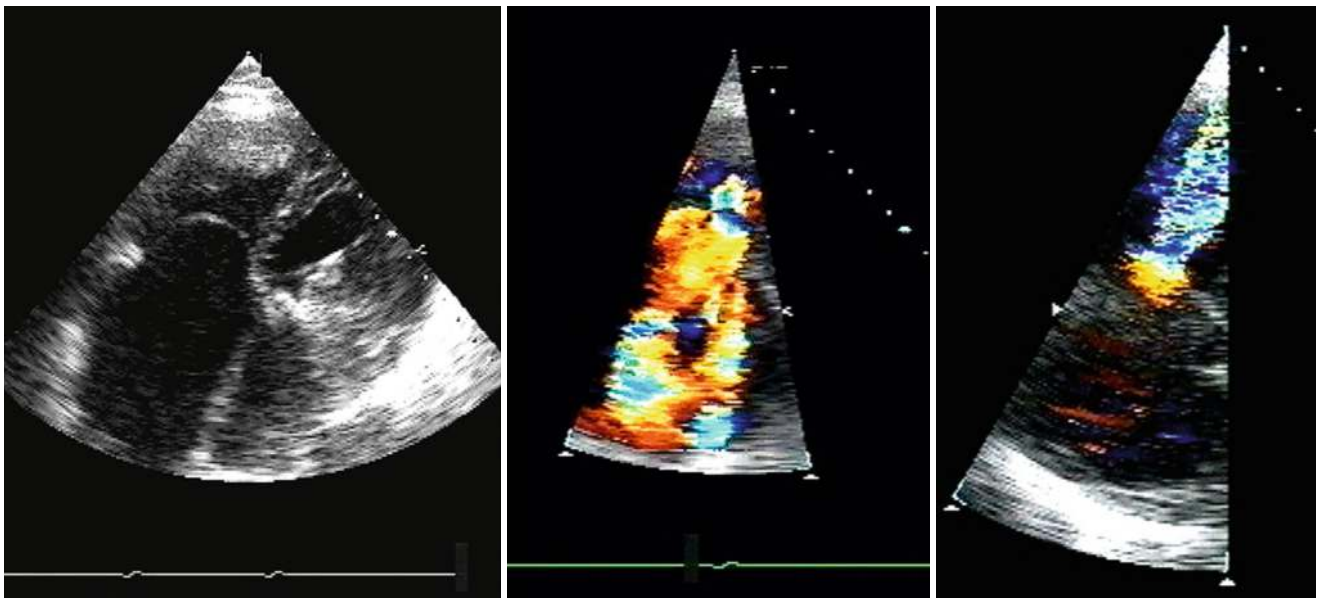


Fig. 1.17 Apical 4 chamber view from a patient with rheumatic heart disease involving mitral, aortic, and tricuspid valves. Note the bowing of the tricuspid valve leaflets in diastole (*left*), tricuspid regurgitation (*middle*) and colour flow Doppler showing PISA (*right*)

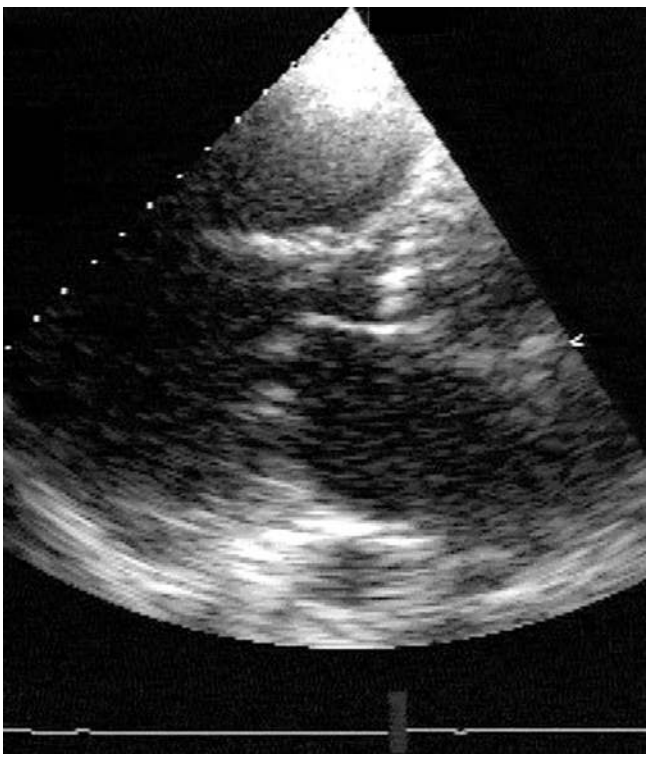


Fig. 1.18 Parasternal long axis view from a patient with rheumatic heart disease involving mitral and aortic valves. Note the classical picture of mitral leaflet involvement and thickening of the aortic cusps

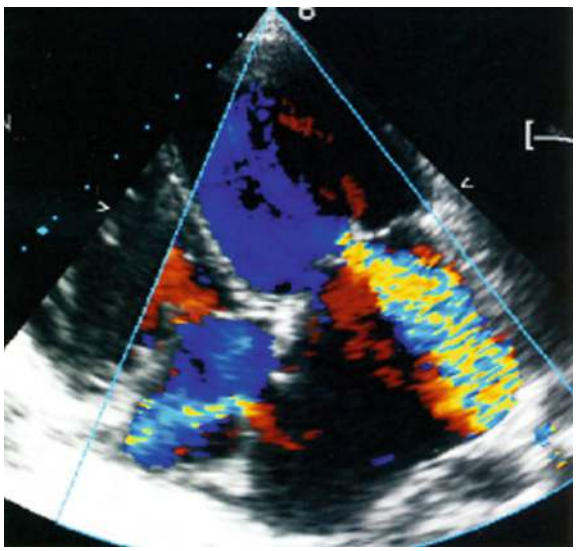


Fig. 1.19 Apical views from a patient with rheumatic mitral valve leaflets after balloon valvuloplasty demonstrating significant regurgitation and atrial shunt across the mid septum

dial damage is usually irreversible despite any successful mitral valve surgery. Fluid retention secondary to tricuspid valve disease should be carefully managed, particularly in patients subjected to mitral valve surgery, who may require the two valves replaced in the same setting. Once irreversible, right ventricular myocardial dysfunction occurs; tricuspid valve surgery adds no symptomatic or prognostic clinical value. In contrast, it significantly increases the surgical risk and perioperative morbidity.

Treatment

Non-interventional

Medical Therapy The only medical treatment in mitral stenosis is the prophylactic measures against rheumatic fever, endocarditis when recommended, and diuretics for raised left atrial pressure. There is no specific treatment which has a direct effect on slowing disease progress. Early intervention in the disease process before the development of atrial fibrillation and enlarged left atrium is highly recommended, provided a conservative procedure is possible. In patients who develop atrial fibrillation, attempts to restore sinus rhythm are usually unsuccessful unless associated with surgery. To maintain sinus rhythm, the organic mitral lesion should be dealt with either interventionally or surgically. In addition to heart rate control, digoxin may keep patients with modestly dilated left atrium in sinus rhythm. Once atrial fibrillation is organized, attention should be diverted to rate control with digoxin, β-blockers, or calcium channel blockers. When atrial fibrillation develops, warfarin is the anticoagulant drug of choice and INR level should be monitored and maintained at 2.5–3.5, independent of the CHA_2DS_2-VASc score to prevent cardiovascular thromboembolic events, including stroke and death [24, 25]. Patients recommended for percutaneous mitral valvuloplasty should receive stable anticoagulation therapy for at least 3 months before procedure and transesophageal echo should exclude left atrial clot. Those who need surgical intervention may receive a Maze procedure as a means for restoring sinus rhythm. This involves surgically creating a single electrical pathway from the sinus node to the AV node while isolating the abnormal electrical activity of the left and right atrial tissues. The success of Maze procedure varies significantly, ranging between 25% and 80% even after an initially successful procedure. Catheter ablation with isolation of pulmonary veins offers an alternative procedure. Procedure effectiveness is progressively lower according to disease severity, but it could be feasibly performed during percutaneous mitral valvuloplasty with benefit in maintaining sinus rhythm [26, 27].

Follow-Up Doppler echocardiography is the main investigation for clinical follow-up of patients with mitral stenosis. The frequency of follow-up is tailored according to individual patient's clinical condition and the severity of mitral valve disease. While it could be every 2 years in a patient with mild stenosis and regurgitation, it needs a shorter follow-up period in another with severe stenosis and evidence of pulmonary hypertension. A closer follow-up should be devised for pregnant women who have mitral stenosis.

Interventional

Valvuloplasty:

This technique uses a percutaneous catheter double balloon or Inoue balloon valvuloplasty. It is only recommended when mitral valve leaflets are pliable and there is no valve calcification including the subvalvar apparatus [28]. Left atrial clot should be excluded by transesophageal echo. The increase in mitral valve area occurs along the plan of commissures and results in increased opening angle provided there is no calcification. An echocardiographic (Abascal) score is used to assess morphologically mitral valve structure and function [29–31]. Assigning a score ranging from 0 to 4 to each of mitral leaflet mobility, thickening, calcification, and subvalvular thickening provides a numerical assessment of the overall valve function. The higher the score, the more anatomically deformed and functionally abnormal is the valve, thus the likelihood of poor outcome after balloon valvuloplasty. Mid- and long-term results of the procedure in well-selected cases are promising. A successful procedure is judged by a >50% increase in mitral valve area. This can be underestimated early after procedure because of the iatrogenically created left to right shunt across the atrial septum (Video 1.6). The latter results from the trans-septal puncture and insertion of the catheters. This shunt has been reported to disappear within 6 months after the procedure. Significant mitral regurgitation may occur in >30% of patients after balloon valvuloplasty. It is usually more severe when the procedure is complicated by a tear in one of the two leaflets. Transesophageal echocardiography is of particular importance before and during mitral valvuloplasty in order to:

(a) Assess valve structure and calcification before procedure.
(b) Exclude left atrial appendage or free wall thrombus.
(c) Guide the way during trans-septal puncture.
(d) Ascertain balloon position across the valve orifice.
(e) Assess pressure drop and mitral valve area after each inflation.
(f) Detect early complication, i.e., leaflet tear, ruptured chordae, or mitral regurgitation that need urgent intervention.
(g) Confirm any perforation of left atrial free wall.
(h) Assess left to right shunt.

Surgery

For symptomatic patients not suitable for mitral valvuloplasty, surgery is the only alternative.

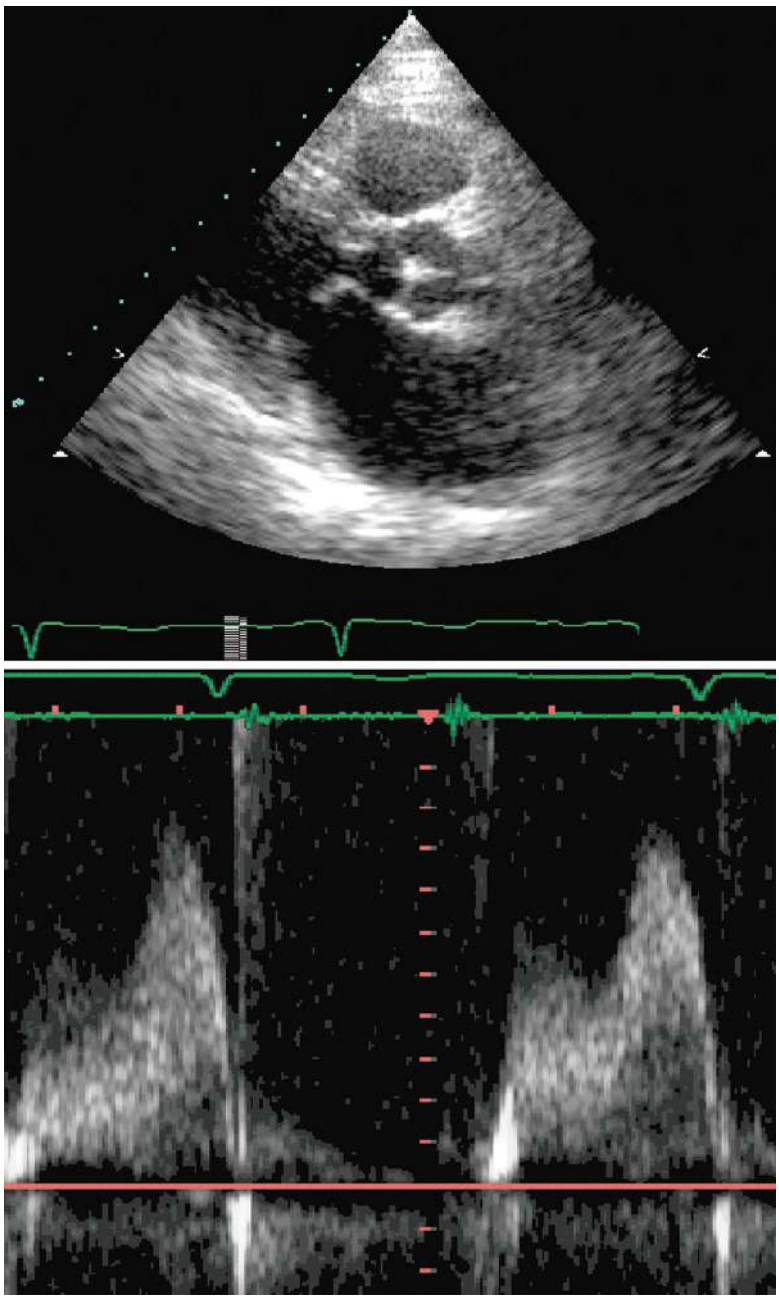


Fig. 1.20 Parasternal long axis view from a patient with rheumatic mitral valve disease and flow velocities after valvotomy

(a) *Closed Mitral Valvotomy*: This is appropriate for young patients who are in sinus rhythm, with no other valve disease, in whom mitral valve leaflets are mobile and not calcified. This is an underrated operation, and up to 40-year follow-up results are exceptionally good.

The procedure aims at opening the mitral valve by applying a dilator through the ventricular apex and feeling the valve leaflets and orifice by the surgeon's finger until the desired valve area is achieved. The first successful operations were carried out in 1948. This operation has been intensively used in the UK and other countries with an average mortality of 3–4% [31].

(b) *Open Valvotomy*: This procedure allows an anatomical repair of the mitral valve under direct vision. Correction of associated rheumatic mitral regurgitation in some cases has been recently undertaken. Open valvotomy requires the use of cardiopulmonary bypass, but can be performed either via a sternotomy or smaller incisions such as a right anterior thoracotomy or with computerized robotic technology via three to four ports in the chest wall (Fig. 1.20).

(c) *Mitral Valve Replacement*: This procedure is required in pure mitral stenosis when the valve is heavily calcified. It involves either a mechanical (St Jude Medical) or a tissue valve (bioprosthesis) substitute with very good long-term follow-up. Despite that, surgical mortality for mitral valve replacement varies according to other comorbidities. While it is in the order of 3% in patients with isolated mitral valve stenosis, it could be as high as 12% in patients with additional pulmonary hypertension. Cryopreserved mitral homografts have been proposed recently [32] as a

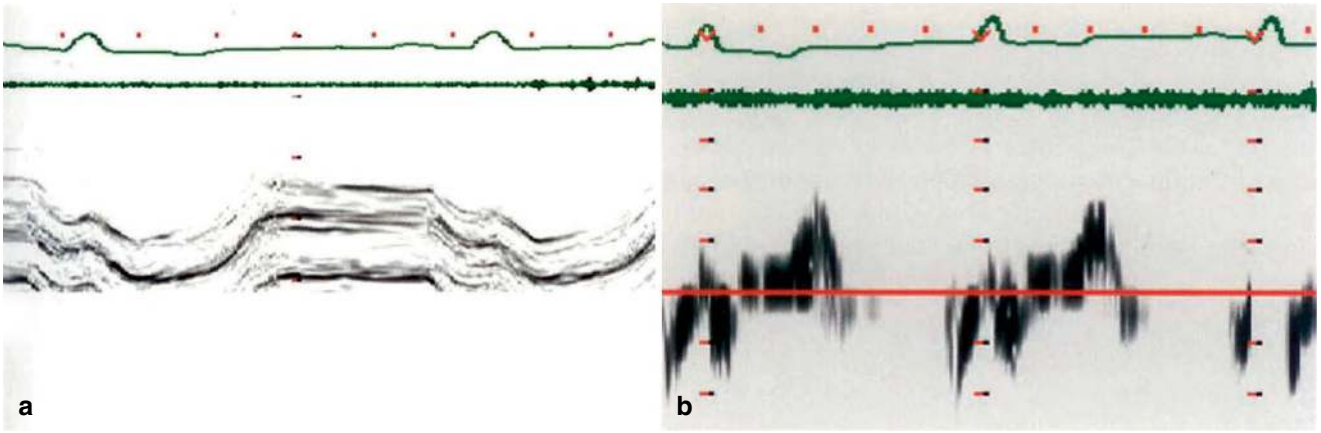


Fig. 1.21 Long axis recording from left ventricular free wall of a patient after mitral valve replacement and cutting of papillary muscles. Note the marked incoordinate behavior and the extent of shortening that takes place in diastole rather than systole M-mode (**a**) and TD1 (**b**)

better option. Although this operation has significant theoretical advantages including better longevity, lack of need for anticoagulants in patients with sinus rhythm, and achieving a low forward gradient, this remains an innovative procedure with a mortality of 25–50% of failing valves within 3 years of implantation [33]. Finally, the use of a pulmonary autograft in a Dacron tube for mitral valve replacement has been proposed, but the general experience is limited [34]. This technique (top-hat) could be ideal for patients who have limited access to anticoagulation clinics, particularly in the developing countries. Traditional procedure of mitral valve replacement involves cutting the heads of the papillary muscles. This resulted in significant asynchrony of the left ventricle, particularly the long axis when its main shortening phase occurs in diastole rather than in systole (Fig. 1.21). The loss of longitudinal function renders the ventricle more spherical in diastole and hence has adverse implications on filling pattern and symptoms. The current surgical approach is to preserve the papillary muscles as much as possible. This change in procedural plan has resulted in maintained long axis function and improvement of ventricular hemodynamics and symptoms after surgery.

(d) *Mitral Valve Repair*: Minimally calcified leaflets with some degree of mitral regurgitation might benefit from a repair procedure under direct visualization of the valve.

The Role of Echocardiography in Patient Selection for Surgery

1. *Assessing Ventricular Function*: In addition to valve assessment, transthoracic echocardiography provides an exceptional means for quantifying ventricular function in these patients. Symptoms may be caused by poor ventricular function, whether as part of the rheumatic cardiac disease or an additional etiology, i.e. coronary artery disease. Raised end-diastolic pressure results in accentuated left ventricular filling velocities and is complicated by pulmonary venous congestion and breathlessness. Additional atrial fibrillation usually worsens the situation by losing the atrial filling component of the left ventricle, hence compromising the stroke volume, particularly when fast. Such severely disturbed physiology should be excluded before accepting mitral valve stenosis as the main cause of symptoms. Furthermore, ignoring such abnormalities before surgery may result in perioperative or early postoperative complications with an increased mortality.
2. *Degree of Valve Calcification*: Transesophageal echocardiography provides additional details on the mitral valve and subvalvar apparatus that may influence decision-making. Pliable leaflets with mild calcification suggest valvotomy whereas extensive calcification requires valve replacement. Subvalvar stenosis by fibrosed chordae and papillary muscles also favors valve replacement. Any evidence for additional endocarditis or possible complications such as "shunt formation" can be dealt with at the time of surgery (Videos 1.7 and 1.8).
3. *Atrial Fibrillation*: Patients with atrial fibrillation and a modestly dilated left atrium may be recommended for elective ablation of the pulmonary veins at the time of mitral valve surgery. When such procedure is performed under transesophageal echo guidance, it may add to its rate of success. Left atrial clot, whether mural or in the atrial appendage, can also be decorticated during the procedure.
4. *Other Valve Disease*: Transthoracic echocardiography provides quantitative assessment of aortic and tricuspid valve involvement, when combined with pulsed and continuous wave Doppler. If found, a balanced physiology should be considered when assessing more than one diseased valve, i.e., tricuspid stenosis tends to underestimate mitral stenosis and mitral stenosis underestimates aortic

stenosis. Transesophageal echocardiography may add more clarity in assessing tricuspid valve anatomy in this condition (Video 1.9).

Mitral Annular Calcification

Mitral annular calcification is usually a disease of the elderly [35], predominantly females [32]. It is also present in other conditions such as hypertension and/or aortic stenosis [33]. Calcification affects the heart either in a patchy manner or uniformly. It usually involves the mitral annulus but can extend into the basal septum, the aortic root, and cusps or rarely the whole of the ventricular basal region. However, if the calcification encroaches on the basal part of the mitral leaflets, it may result in increased filling velocities. It can be associated with mild mitral regurgitation, but more commonly conduction disturbances occur in approximately 50% of patients. When affecting the mitral annulus, the leaflets themselves are usually spared, and the valve does not become stenotic. The combination of mitral annular calcification and aortic calcification has been shown to predict coronary artery calcification too (Fig. 1.22 and 1.23).



Fig. 1.22 Pathological picture showing extensive nodular calcification of the mitral annulus that extends deeply into the myocardium. Note sparing of most of the leaflet apart from base

Management In the absence of significant mitral stenosis, valve replacement is not indicated. When involving the aortic root and cusps leading to stenosis, aortic valve and root replacement is usually successful. Calcification of the mitral annulus is not superficial, but it invades deeply into the myocardium. During surgery, decalcifying the mitral ring for valve replacement may result in myocardial perforation. Mitral valve replacement, therefore, should never be performed for isolated annular calcification. Transcatheter treatment for mitral annular calcification has been proposed in the last decade, initially using the same prothesis used for transcatheter aortic valve replacement. Transesophageal echocardiography is essential for intraprocedure guidance, to exclude left atrial thrombus, guide trans-septal puncture, valve deployment avoiding left ventricular outflow tract obstruction, and for assessing early hemodynamic impact of the valve prothesis and its function [36].

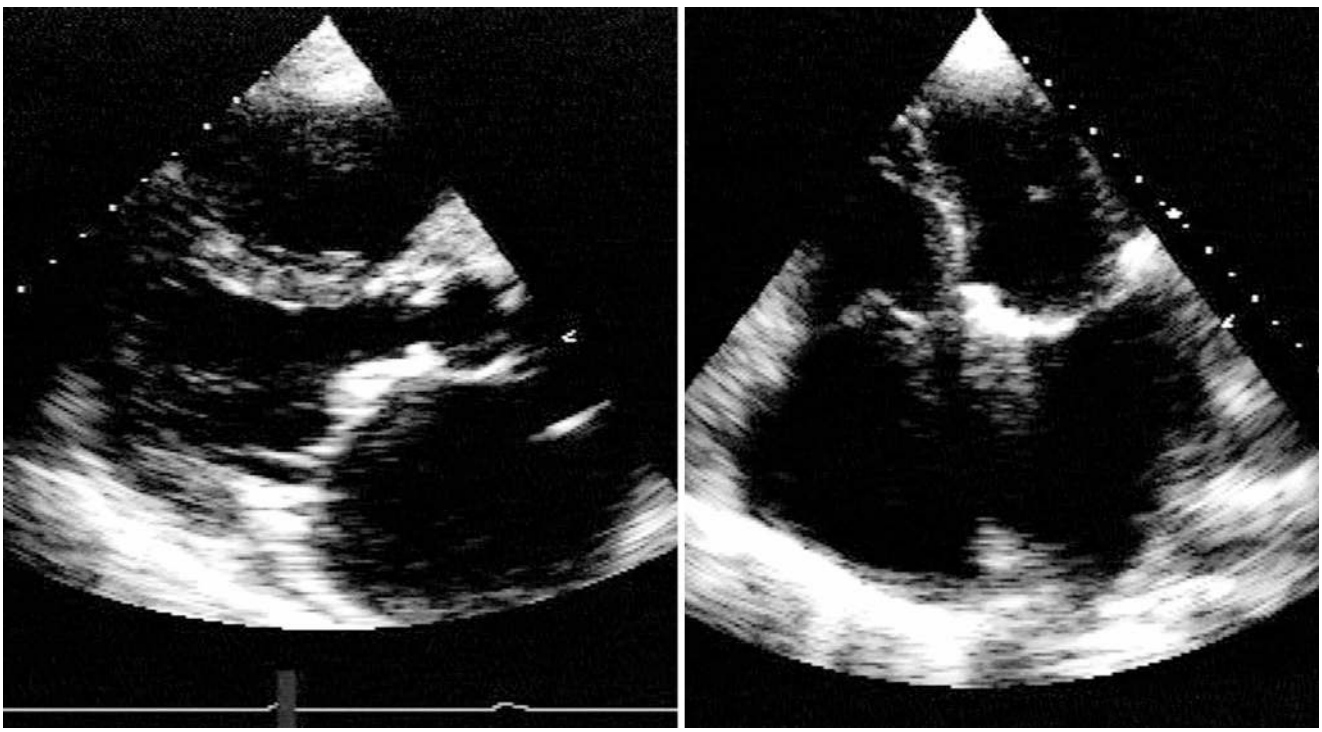


Fig. 1.23 Parasternal and apical view from a patient with mitral annular calcification

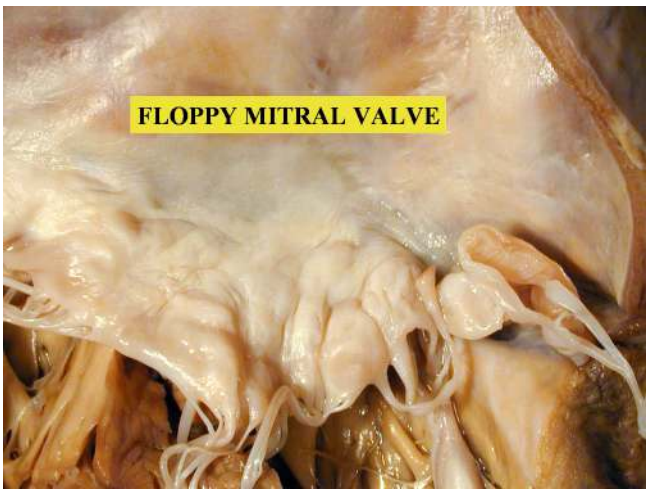


Fig. 1.24 Pathological section from myxomatous mitral valve leaflet showing the thickened leaflet with ballooning between the chordae

Mitral Regurgitation

Mitral regurgitation results from abnormalities affecting different components of the mitral valve: leaflets, annulus, chordae, or papillary muscles. Causes of mitral regurgitation are multiple, in comparison to mitral stenosis. Myocardial disease, when affecting particularly the basal part of the left ventricle, results in mitral regurgitation. Atrial fibrillation and heart failure with preserved ejection fraction may be responsible for left atrial enlargement and consequent secondary - atrial functional mitral regurgitation, linked to annular enlargement, perturbations of annular contraction, and atriogenic leaflet tethering [37]. Less common causes of mitral regurgitation are mitral valve prolapse, myxomatous degeneration, endocarditis, nonischemic dilated cardiomyopathy, and other infiltrative disease and fibrosis (Figs 1.24 and 1.25). Of note, mitral valve prolapse has been recently linked to life threathening arrhythmias, the so-called arrhythmic mitral valve prolapse [38]. Advanced echocardiography may guide risk stratification in asymptomatic patients [39].

Common Causes of Mitral Regurgitation:

A. *Ischemic Mitral Regurgitation*

The most common cause of mitral regurgitation is the ischemic pathology, and the most component of the mitral valve apparatus that is subject to ischemic dysfunction is the posteromedial papillary muscle which is also predisposed to infarction. The vulnerability of the posteromedial papillary muscle to ischemic dysfunction is because it is supplied by a single branch of the posterior descending artery and has only a few collaterals. In contrast, the anterolateral papillary muscle receives blood supply from branches of both the left anterior descending artery and the circumflex artery; so it is less susceptible to ischemia. Ischemic disturbances of left ventricular function contribute to the development of mitral regurgitation through a number of mechanisms: (a) regional wall motion abnormalities with adverse ventricular remod-

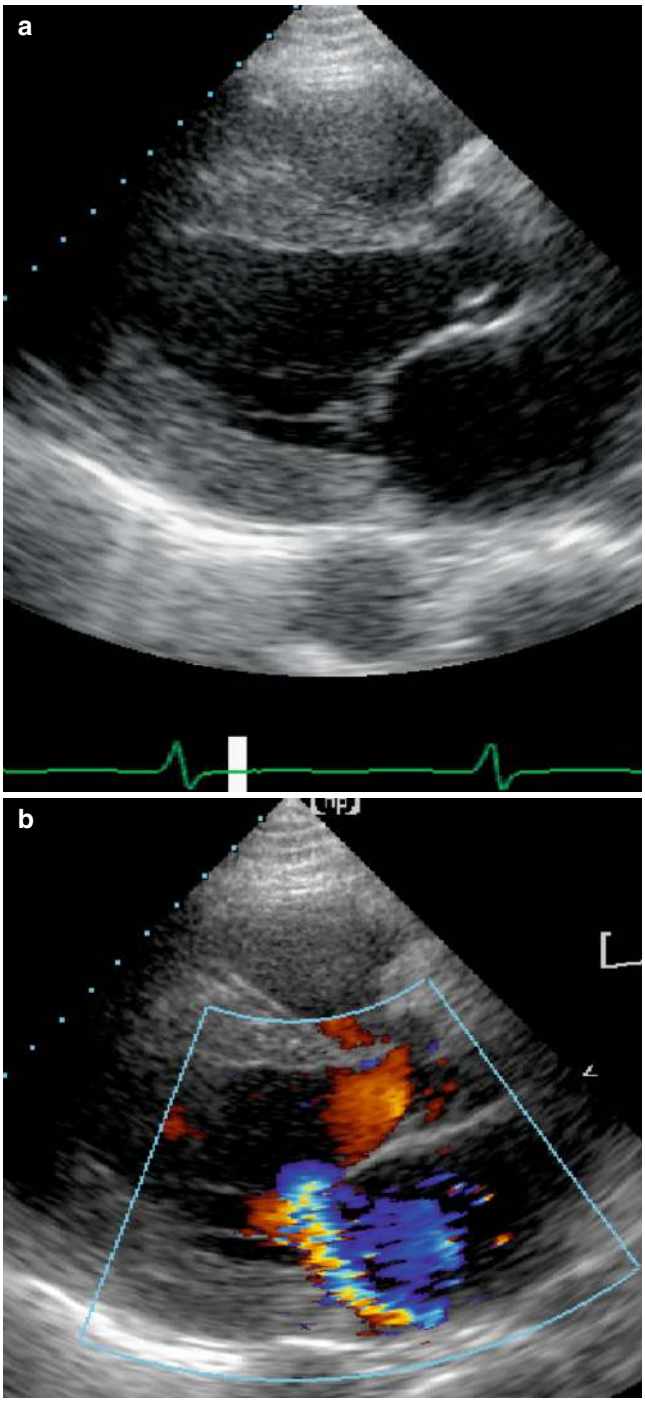


Fig. 1.25 Parasternal view from a patient with hypertensive LV disease and functional mitral regurgitation. Note the LA enlargement

eling and systolic tenting of the valve leaflets, (b) left ventricular dilatation and shape change that alters normal alignment of the papillary muscles and results in leaflet tethering and inadequate closure, and (c) annular dilatation that leads to inadequate annular contraction and leaflet coaption. These mechanisms may contribute to further enlargement of the left ventricle and deterioration of its function which itself would add to the severity of mitral regurgitation. Four clinical presentations are seen in ischemic mitral regurgitation: (i) acute myocardial infarction, (ii) papillary muscle rupture, (iii) reversible ischemic myocardial dysfunction in the presence of preserved left ventricular systolic function, and (iv) end-stage ischemic cardiomyopathy with reduced function.

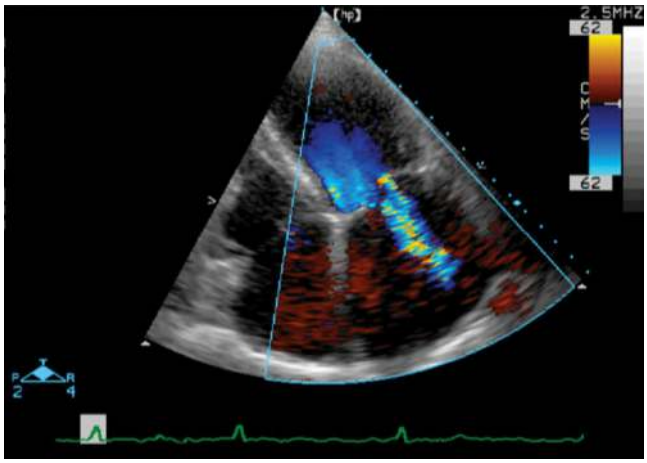


Fig. 1.26 Parasternal views from a patient with functional mitral regurgitation due to ischemic LV disease. Note the normal morphology of the mitral valve, and dilated ring

Acute Myocardial Infarction: Mitral regurgitation is common in acute myocardial infarction, and significant regurgitation complicates up to 15% of cases. Although most such cases present within the context of acute myocardial infarction, some may present with acute development of mitral regurgitation [40]. Most patients presenting with myocardial infarction complicated by mitral regurgitation have right and circumflex coronary artery disease that causes inferior wall dysfunction. Mitral regurgitation therefore does not seem to be related to the infarct size but the extent of ischemic dysfunction and involvement of posteromedial papillary muscle. The resulting poor support to the posterior leaflet, referred to as tethering, causes lack of leaflet coaption and valve incompetence. Severe mitral regurgitation developing after infarction carries poor prognosis with mortality rising up to 25% at 30 days and over 50% at 1 year [41]. The effect of myocardial reperfusion on mitral regurgitation remains controversial.

Papillary Muscle Rupture: Although a rare complication to myocardial infarction, complete papillary muscle rupture causes severe mitral regurgitation and cardiogenic shock which is usually fatal, 70% within 24 hours without emergency surgery. Surgical repair of the papillary muscle is not feasible in most cases because of the extent of the necrotic tissue [42]; so valve replacement is necessary and its risk is influenced by other factors including severe left ventricular dysfunction which usually exists. Papillary muscle rupture occurs 2–5 days after the onset of the infarct. Incomplete rupture, usually of only one head of the papillary muscle, occurs 4–5 days after the infarct with gradual deterioration of mitral regurgitation. This worsens preexisting left ventricular dysfunction.

Ischemic Mitral Regurgitation in a Normal Left Ventricle: Patients with long-standing ischemic myocardial dysfunction may have exertional reversible ischemia. If this affects the posterior wall of the left ventricle, it leads to further deterioration of posterior wall function and consequently the posterior leaflet function and the development of mitral regurgitation (Fig. 1.26) [33, 43]. Exertional breathlessness in these patients does not always have to be due to raised end-diastolic pressure but a sudden increase in left atrial pressure by the development of mitral regurgitation with exercise, particularly in those with dilated left atrium and those with poor atrial compliance. Stress echocardiography is the ideal investigation for demonstrating the ischemic ventricular dysfunction and the development of mitral regurgitation and raised left atrial pressure, hence the beneficial role of antianginal therapy and afterload reduction. Patients who develop significant mitral regurgitation with stress and are accepted for coronary artery bypass graft surgery should receive mitral valve repair, a ring insertion, at the same time of surgical revascularization [44] to avoid potential persistent symptoms despite successful surgery.

Ischemic Mitral Regurgitation in Ventricular Dysfunction: Mitral regurgitation is very common in patients with long-standing ischemic left ventricular dysfunction and those in end-stage ventricular disease. Since, in these patients, valve leaflets appear morphologically normal, the mitral regurgitation is described as "functional." Three-dimensional echocardiographic assessment of the mitral valve proves that the valve itself is not entirely normal, with long-standing progressive changes in the interleaflet relations and subvalvar apparatus. Reducing ventricular pressures may improve left ventricular geometry and lowering blood pressure may reduce mitral regurgitation severity.

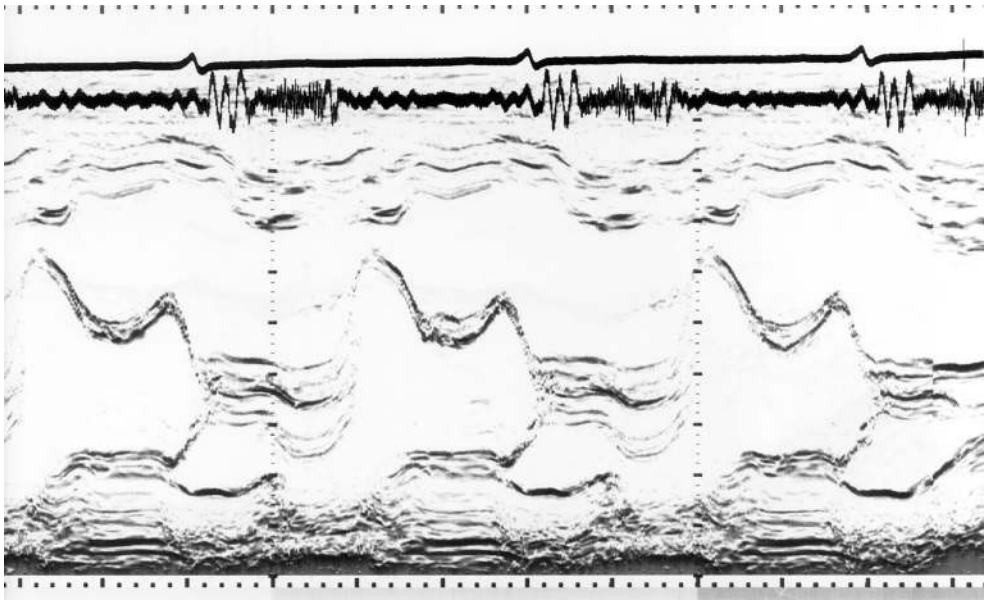


Fig. 1.27 Mitral valve M-mode recording showing systolic prolapse

B. *Myxomatous Degeneration*

This is the most common cause of isolated mitral regurgitation. It is also called degenerative mitral valve disease of the elderly or floppy valve. The disease involves progressive myxomatous degeneration of the mitral leaflets and may range from stretched "normal" appearing leaflet to the full-blown thickened myxomatous ballooned leaflet (Fig. 1.27). The terms prolapse, floppy, redundant, myxomatous, and flail have all been applied to this entity. The classic valve leaflets are thickened, redundant, and increased in area, and prolapse into the left atrium in systole (Fig. 1.28). This process could affect either of the two cusps, most commonly the mid-third of the posterior leaflet. The chordae may become elongated, thinned, and tortuous, predisposing to rupture and acute mitral valve prolapse. In the elderly, myxomatous mitral degeneration is usually asymptomatic. Echocardiographically, mid-late systolic buckling of the leaflets >2–3 mm posterior displacement to the mitral closure point is taken as a clear demonstration of the leaflet prolapse. Particularly when involving the two leaflet tips, myxomatous may be difficult to differentiate from vegetations caused by endocarditis. The diagnosis of mitral leaflet prolapse should be made from the left parasternal view since the combination of the shape change of the mitral valve ring in systole and the valve closure may appear to represent prolapse in other views [34]. In Marfan syndrome, the myxomatous degeneration tends to involve commonly the leaflet tips, particularly the anterior leaflet (Fig. 1.29). This does not always result in significant mitral regurgitation but may remain static and asymptomatic for years. Loss of systolic coaptation and prolapse of one of the two leaflets into the left atrium is a highly sensitive and specific sign of a flail leaflet irrespective of its etiology. Transesophageal echo usually provides clearer images for the leaflets and the degree of loss of coaption. The degree of mitral regurgitation with pure leaflet prolapse may be insignificant and clinical examination reveals a mid-systolic click or late systolic murmur. Mitral prolapse may predispose to infective endocarditis, and prophylactic antibiotics may be recommended for high-risk patients. Simple mitral prolapse may progress to severe mitral regurgitation that requires surgical repair (Figs. 1.30, 1.31, 1.32 and 1.33).

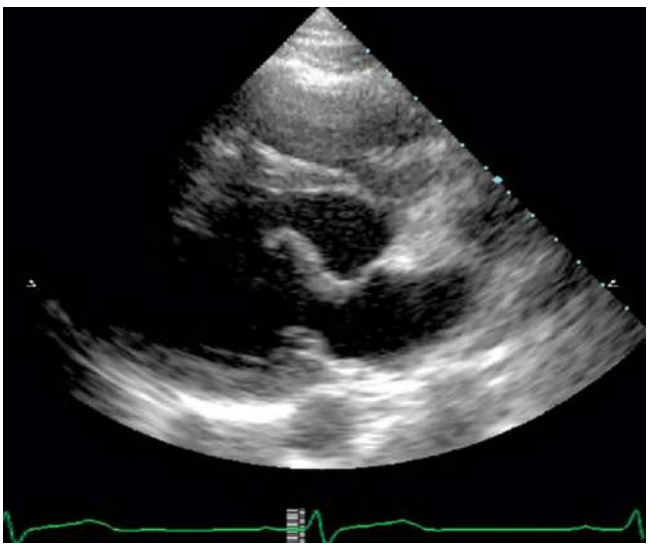


Fig. 1.28 Parasternal views from a patient with myxomatous mitral valve disease

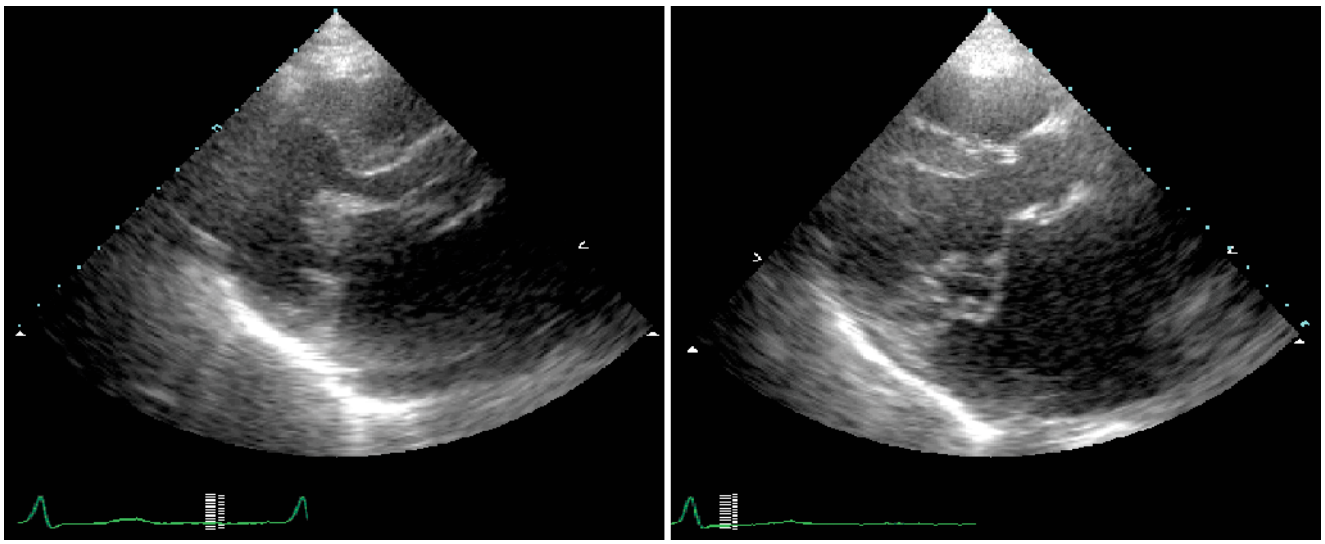


Fig. 1.29 TOE from a patient with MV leaflets showing multiple regurgitation jets



Fig. 1.30 Flail anterior mitral valve leaflet from a patient with Marfan's syndrome

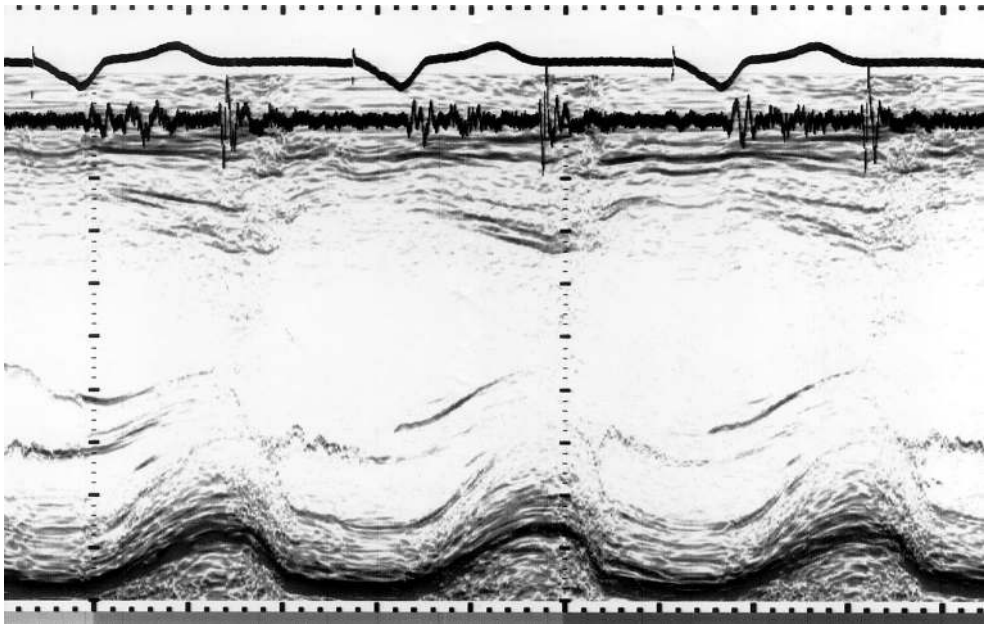
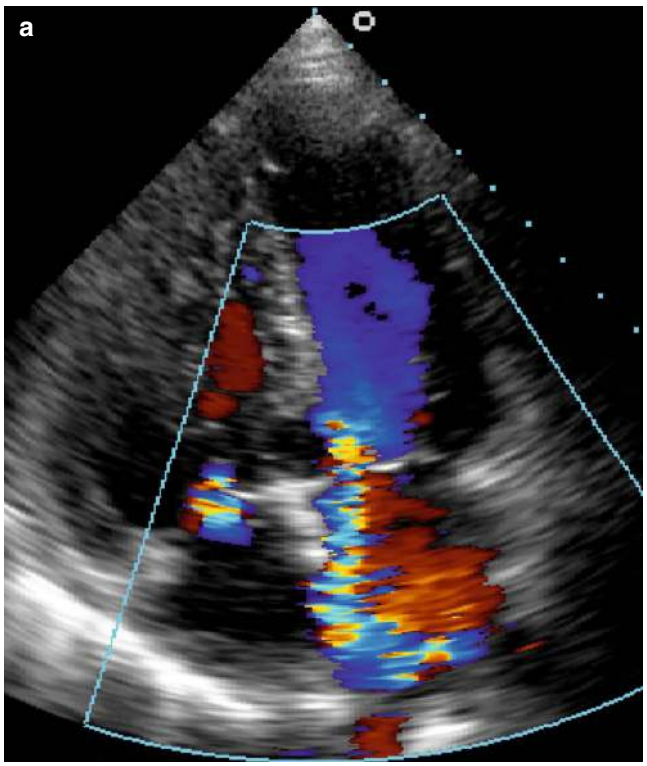


Fig. 1.31 M-mode of active LV minor axis from a patient with severe mitral regurgitation. Note the relative difference between enddiastolic and end-systolic dimension

C. *Congenital Mitral Regurgitation*

The most common form of so-called congenital mitral regurgitation is that found in association with a primum atrial septal defect or other form of atrioventricular septal defect. In general, it is better to describe the systemic atrioventricular valve in this group of anomalies as the left atrioventricular valve rather than the mitral valve. Another important cause of congenital mitral regurgitation is the so-called isolated cleft of the anterior leaflet of the mitral valve. In essence, the valve appears to have three leaflets. The importance of this diagnosis is that in almost every case, it is possible to perform a surgical repair by patching anterior leaflet of the mitral valve, thus avoiding the need for mitral replacement (Video 1.10).



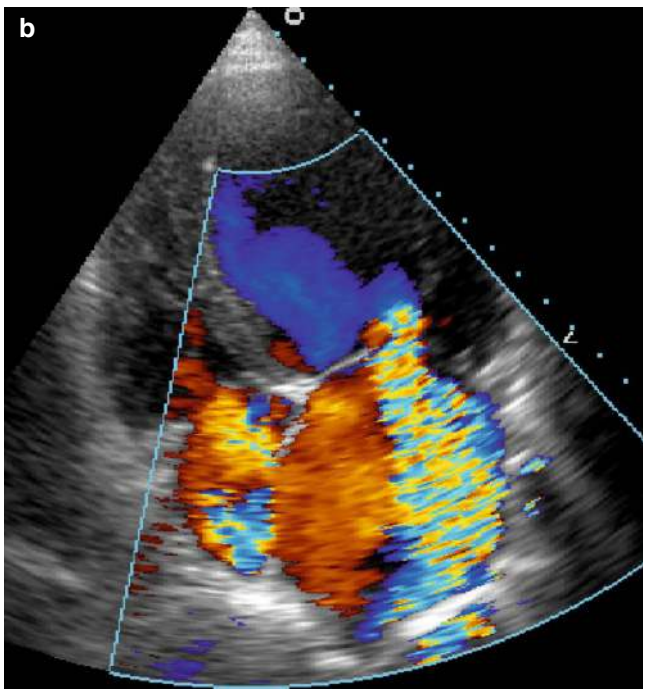


Fig. 1.32 Colour Doppler from 2 patients with mitral regurgitation mild (**a**) and severe (**b**)

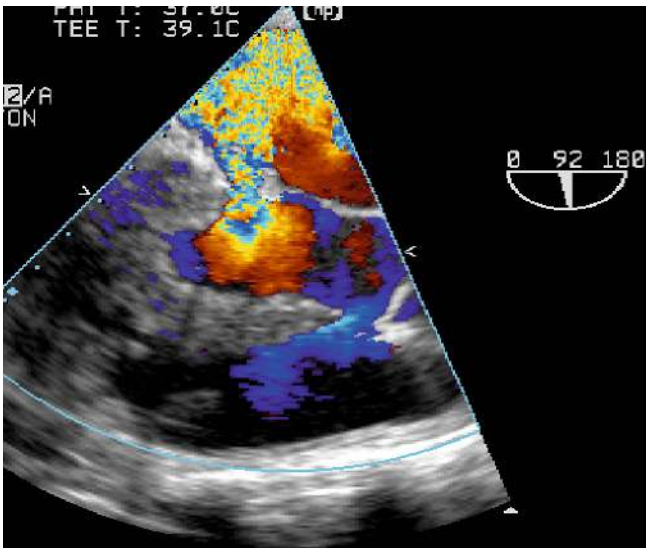


Fig. 1.33 TOE from a patient with prolapsing posterior leaflet

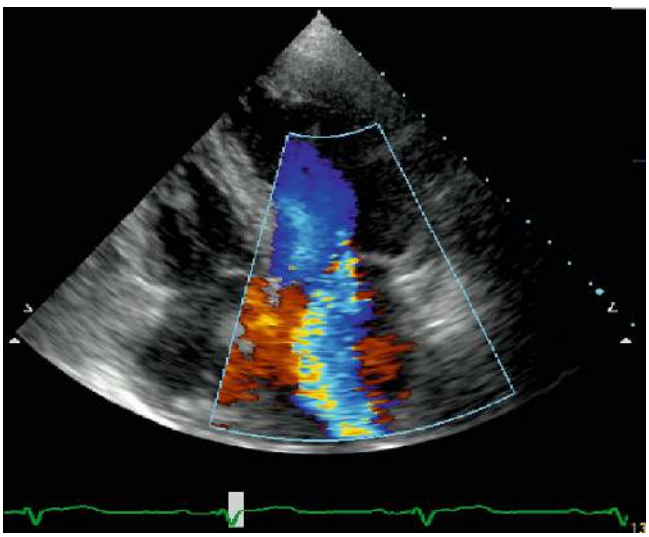


Fig. 1.34 Mitral regurgitation from a patient with anterior leaflet prolapse

Infective Endocarditis

This is a major cause of symptomatic mitral regurgitation (Fig. 1.34) [40]. Vegetations develop on the cusp and vary from small nodules along the line of apposition to large friable masses up to 10 mm in diameter or even more, particularly with fungal infection. Lesions on the anterior (aortic) cusp of the mitral valve may occur in association with aortic valve endocarditis, usually involving the right coronary cusp. Infection of the mitral valve may also cause leaflet rupture and perforation, and hence jet lesions. These jet lesions vary from localized aneurysms to complete cusp perforation resulting in severe mitral regurgitation that requires valve replacement. Endocarditis may affect normal valves particularly in the elderly but more

commonly valves with minor congenital abnormality or floppy valve.

Pathophysiology of Mitral Regurgitation

The regurgitant volume of mitral regurgitation is calculated as the regurgitant flow over the regurgitant area. The flow velocity through the orifice is related to the ventricular–atrial systolic pressure difference. High left ventricular systolic pressures, e.g., systemic hypertension, increases mitral regurgitation volume, and low left ventricular pressure, reduces it. Left atrial pressure in acute mitral regurgitation is raised with a V-wave in late systole due to the increased volume and the velocity of blood entering the left atrium. The absence of a V-wave on the left atrial pressure recording or pulmonary wedge pressure, however, does not exclude the diagnosis of severe mitral regurgitation. With severe mitral regurgitation, the raised retrograde stroke volume into the left atrium causes increased forward flow across the mitral valve into the left ventricle in the succeeding cycle, which increases ventricular activity and the rate of increase of cavity size.

Mitral regurgitation is often a dynamic lesion, and the size of the regurgitant orifice and regurgitant volume may vary with the pressure gradient across the valve and with changes in left ventricular volume and geometry. The effective regurgitant orifice area itself may increase with significantly abnormal ventricular geometry. Thus, successful reduction of left ventricular volume by optimum medical therapy or pacing and improvement of its systolic function may assist in reducing severity of mitral regurgitation and opening the vicious circle.

Isolated mitral regurgitation is associated with a large increase in left ventricular output. The total stroke volume may be increased up to 3–4 times the normal. At the time of aortic valve opening, more than quarter of the stroke volume may have already entered the left atrium. This results into a V-wave which may be as high as 50–60 mmHg. This volume of blood re-enters the left ventricle in early diastole, thus shortening the isovolumic relaxation time and increasing early diastolic filling velocities, resulting in a third heart sound. When mitral regurgitation is very severe, left ventricular and left atrial pressures may equalize at mid-ejection or even earlier. This occurs particularly with ruptured papillary muscle. At first, left ventricular end-diastolic volume does not significantly increase whereas end-systolic is greatly reduced. This results in a significant fall in forward cardiac output that can only be maintained by sinus tachycardia.

Assessing Severity of Mitral Regurgitation

The major determinant of mitral regurgitation severity is the effective regurgitant area, which may be fixed in rheumatic mitral valve disease, bacterial endocarditis, and mitral prolapse. A regurgitant volume of 40 ml signifies a regurgitant fraction (volume of blood regurgitated into the left atrium) of 40% and regurgitant area (mitral valve incompetent area in systole) of 40 mm^2 [41].

(a) *Large LV Stroke Volume*: An increase in left ventricular end-diastolic dimension and fall of end-systolic dimension over time suggests an overloaded ventricle and significant mitral regurgitation (Fig. 1.35) [18, 42]. In these patients, fractional shortening and calculated ejection fraction should not be taken as measures of ventricular function. Absolute end-systolic diameter or volume may be considered as more accurate markers of ventricular disease. An end-systolic diameter >40 mm suggests independent left ventricular disease, the reversibility of which cannot be confirmed [44].

(b) *Color Flow Area:* This is the most widely used technique. Maximum jet areas traced in different views correlate with severity of mitral regurgitation assessed by left ventriculography. A regurgitant area of >8 cm^2 or relative area >40% that of the left atrium suggests severe regurgitation, whereas a jet area of <4 cm^2 or relative area <20% identifies mild mitral regurgitation (Figure 1.36). This method relies on the clear display of a uniform regurgitant jet. If used alone, it may over- or underestimate the regurgitation severity, particularly when the valve leaflets are flail and the jet uniformity is disrupted. Jet areas studied by transesophageal technique also tend to overestimate valve regurgitation [45–47].

(c) *Proximal Isovelocity Surface Area* (*PISA*): As discussed in mitral stenosis, the regurgitant orifice area can be calculated by dividing peak flow rate by maximum velocity through the orifice (obtained from the continuous wave Doppler). A regurgitant orifice area >0.5 cm^2 corresponds to a regurgitant fraction of >50%, thus signifying severe mitral regurgitation that needs surgery (Fig. 1.37). Accurate measurements of flow convergence seem more reliable than color flow area mapping. However, flow convergence method is subject to geometric complexities of the regurgitant orifice that require correction factors as in eccentric jets commonly seen in mitral valve prolapse.

(d) *Vena Contracta*: This is the narrowest cross-sectional area of the jet that immediately exists at the regurgitant orifice. The width of vena contracta has been found to

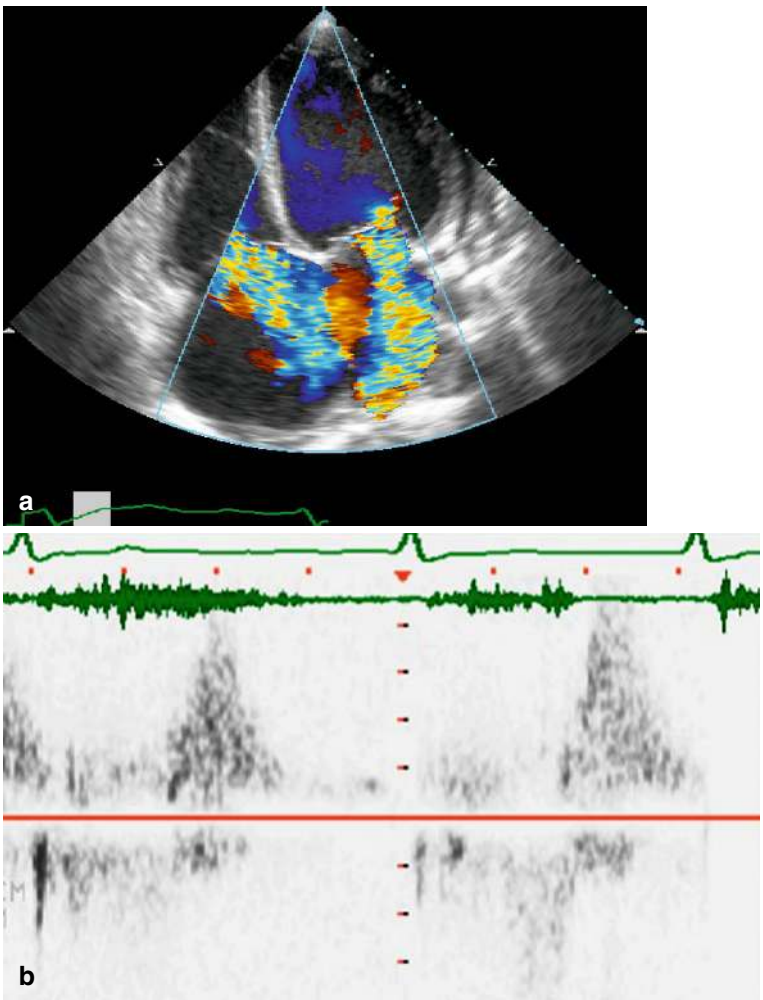


Fig. 1.35 (**a**) Apical 4 chamber view from a patient with severe mitral regurgitation on color Doppler. Note the absolute and relative difference in the regurgitant area with respect to that of the left atrium. (**b**) Pulmanory venous flow showing systolic flow reversal due to severe mitral regurgitation

correlate with the regurgitant volume: A width of >5 mm with a regurgitant volume of 60 ml suggests severe and a width <3 mm is consistent with mild mitral regurgitation. Vena contracta has been suggested to be independent of hemodynamic variables, orifice geometry, and instrument setting and is associated with a low interobserver variability (Fig. 1.38) [48].

(e) *Systolic Flow Reversal in Pulmonary Veins*: This sign is helpful in determining regurgitant severity only when the jet is not eccentric. It is not of great use in patients with severe left ventricular disease in whom the systolic component of pulmonary venous flow is already poor and also in those with eccentric mitral regurgitation jet. Moreover, systolic flow in the pulmonary veins is affected by left atrial compliance, age, rhythm, and eccentric jets [49].

(f) *Continuous Wave Doppler*: Mild mitral regurgitation usually stops well beyond (>80 ms) end-ejection corresponding to the left ventricular pressure decline during isovolumic relaxation period. A short deceleration limb of the retrograde transmitral signal suggests significant regurgitation. As left atrial pressure increases, the retrograde pressure drop across the mitral valve also drops and no longer represents left ventricular pressure. Left atrial pressure can be estimated as the transmitral retrograde pressure drop deducted from systolic blood pressure, particularly when it is low [50].

(g) *Left Atrial Emptying Volume*: Left atrial end-systolic volume – end-diastolic volume >40 ml identifies patients with severe mitral regurgitation [51].

(h) *Continuity Equation*: Relative aortic and mitral stroke volumes using the continuity equation, as previously discussed, determine regurgitation severity [52].

(i) *Three-Dimensional Color Doppler*: With the advent of real-time three-dimensional color Doppler, studies are in the process of evaluating the technique in quantifying the regurgitant volume.

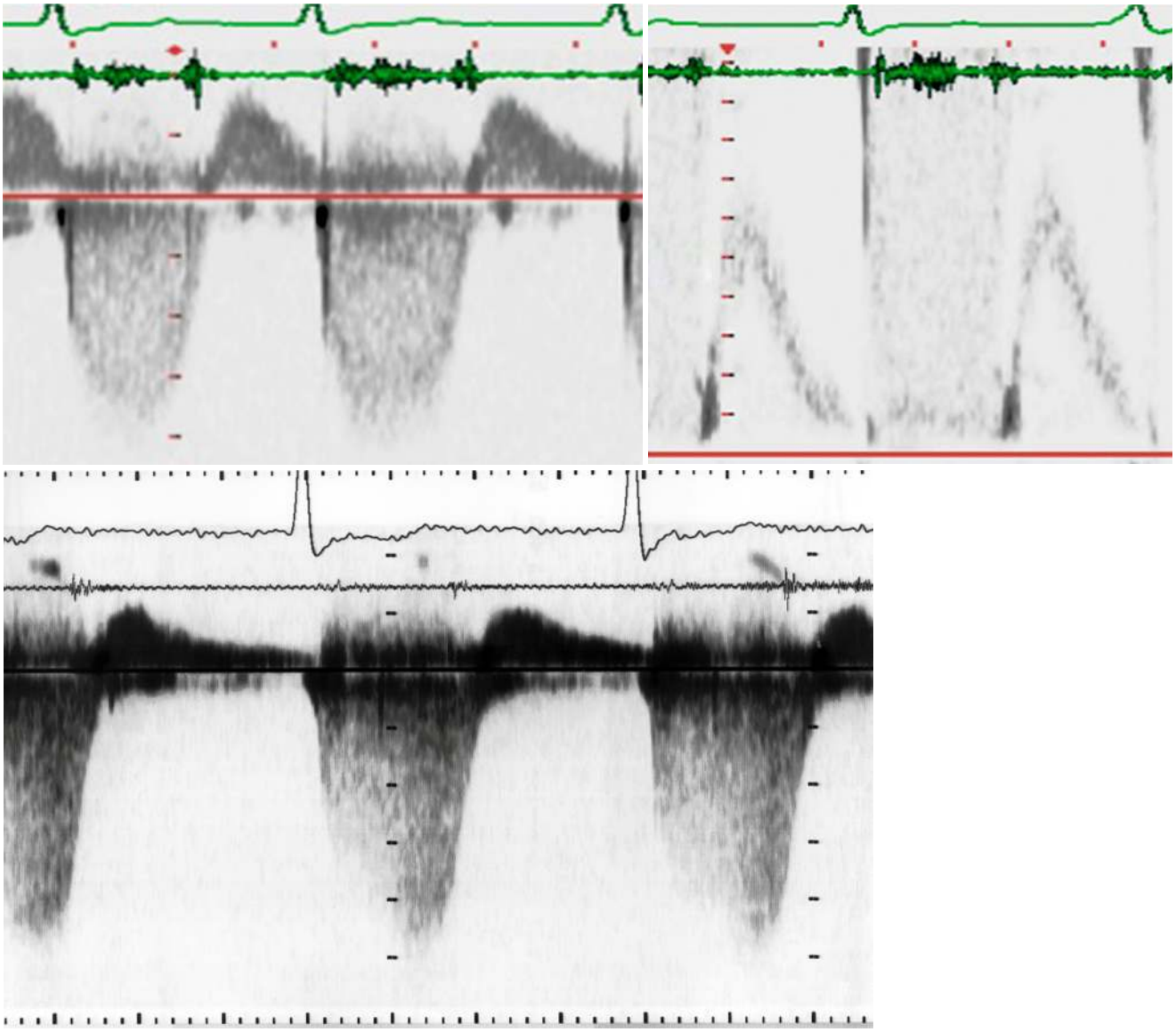


Fig. 1.36 Pulsed and continuous wave Doppler recordings from a patient with severe mitral regurgitation 'top' and another with mild regurgitation 'bottom'. Note the early ending of the CW mitral regurgitation with respect to A2, in severe regurgitation

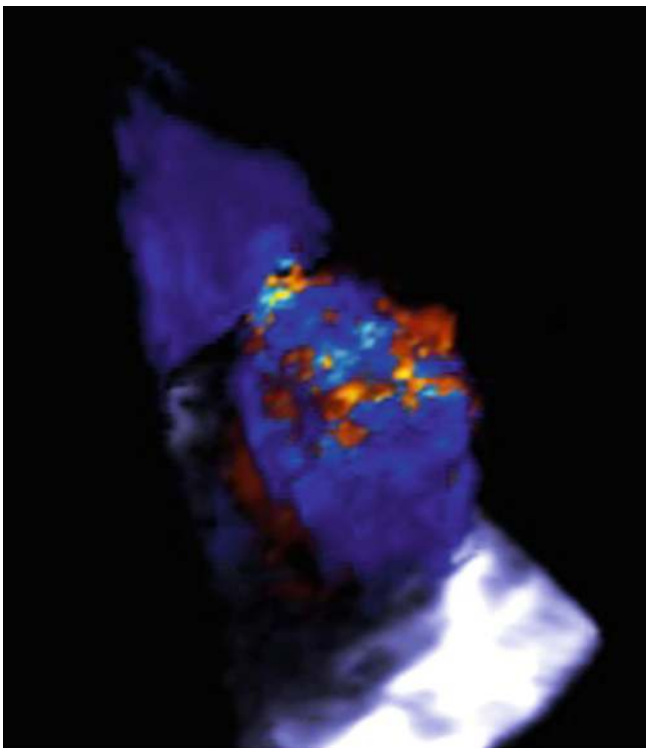


Fig. 1.37 3 dimentional reconstruction of color Doppler mitral regurgitation

Less Common Forms of Mitral Regurgitation

(a) *Ruptured Chordae Tendineae*

This is often a consequence of the myxomatous degeneration process which occurs with age. The development of significant mitral regurgitation is usually gradual. In some cases, it takes an acute onset particularly when it is not a complication of myxomatous degeneration, simply due to chordal rupture (Fig. 1.39). The left ventricle does not dilate acutely. The main symptoms are palpitations and dyspnea. Symptoms tend to improve over the course of the following weeks by which time the ventricle adapts itself to the volume load. Patients may present in intractable pulmonary edema in severe cases. This can be explained on the basis of long-standing mitral regurgitation, leading to a dilated and diseased ventricle. The combination of raised ventricular diastolic pressures and filling pressures worsen the condition and reduce the probabilities of having a possible successful repair and recovery of ventricular function (Fig. 1.40) [53, 54] (Videos 1.11, 1.12, 1.13, 1.14 and 1.15).

(b) *Endomyocardial Fibrosis*

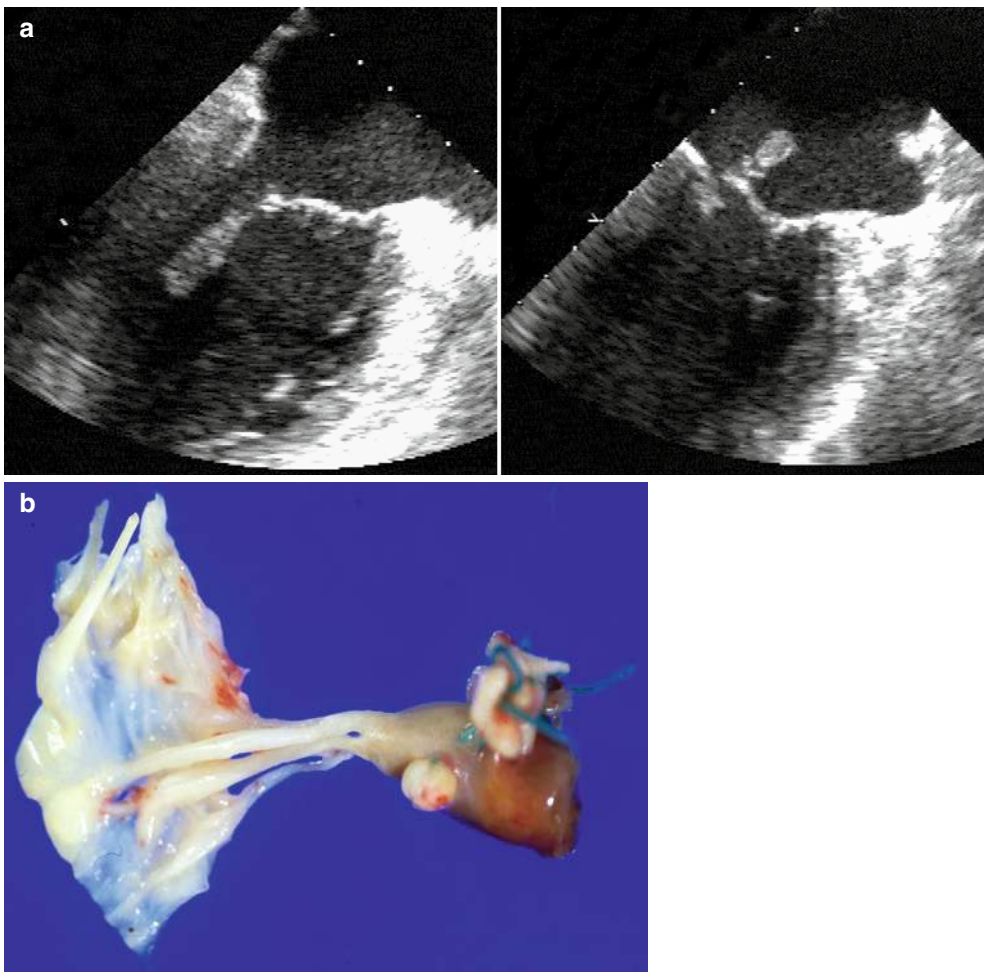


Fig. 1.38 (**a**) TOE from a patient with ruptured posteromedial papillary muscle. Note bouncing of the detached segment into the left atrium in systole. (**b**) Part of mitral valve leaflet with attached chordae and infracted papillary muscle

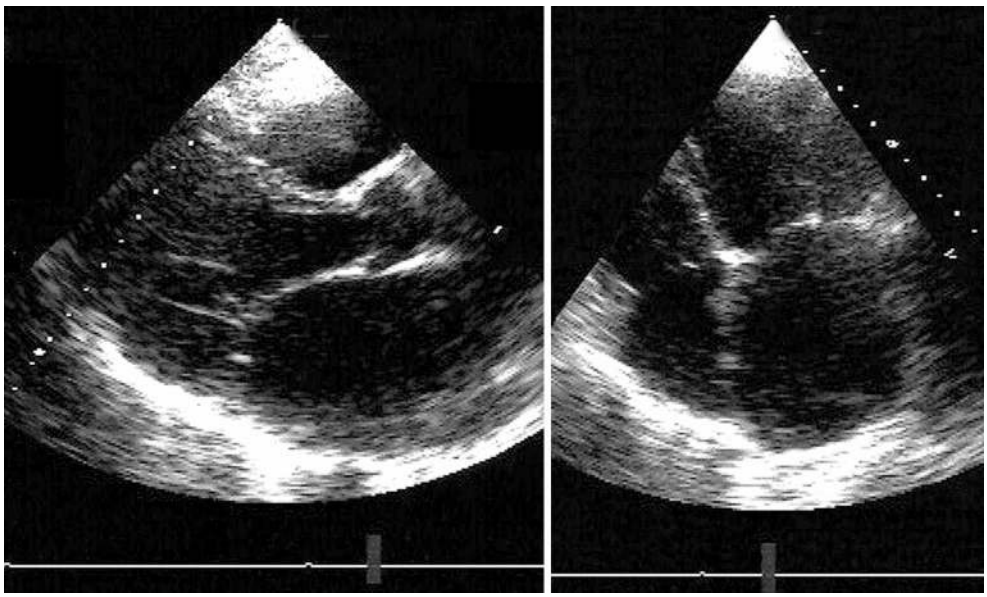


Fig. 1.39 Parasternal long axis views from a patient with severe MR after repair demonstrating significant fall in LV cavity size

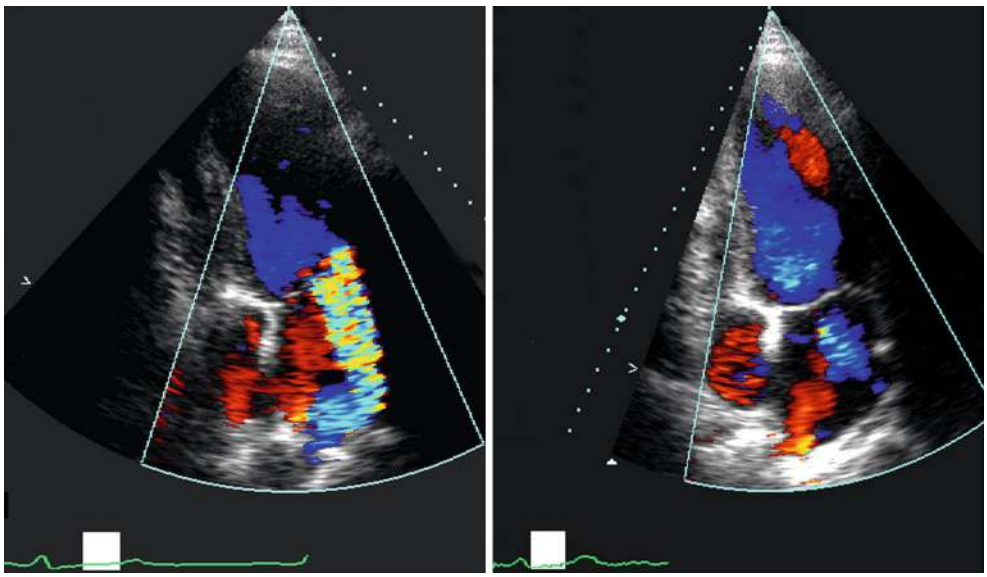


Fig. 1.40 Apical view from a patient with moderate mitral regurgitationat rest (*left*) which became mild with stress (*right*)

This is a fibrosis process that involves the subendocardium and underlying myocardial layer. When affecting the right ventricle, it involves predominantly the apex, then progresses toward the tricuspid valve but spares the outflow tract. In the left ventricle, the inflow tract, apex, and outflow tract are all involved. As the fibrosis affects the papillary muscle, it results in mitral and tricuspid valve regurgitation which can be severe enough to warrant valve replacement. This disease is common in the eastern part of Africa, South India, and Brazil, and rarely affects Europeans. It is usually linked to hypereosinophilia due to helminthic infection (Figs. 1.41 and 1.42).

Stress Echocardiography: Symptomatic patients with no more than moderate mitral regurgitation, particularly caused by ischemic etiology, should be studied by stress echocardiography. It assesses cardiac physiology and the stress-related change in mitral regurgitation severity at the time of symptom development. A drop in systolic blood pressure at fast heart rate is also taken as a marker of worsening regurgitation and compromised forward stroke volume. Patients with primarily left ventricular disease and incompliant cavity may develop raised left atrial pressure as a cause of breathlessness, in the absence of significant mitral regurgitation. Also, those

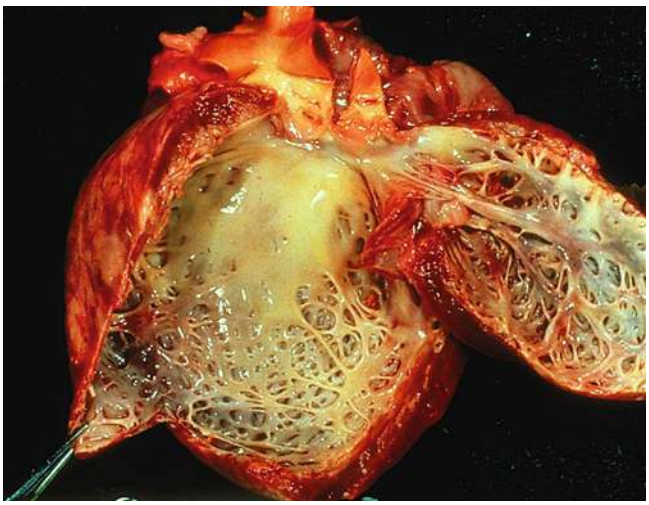


Fig. 1.41 Pathology: Dense pale fibrous tissue lining the endocardium of the left ventricle and extending up to the mitral leaflets

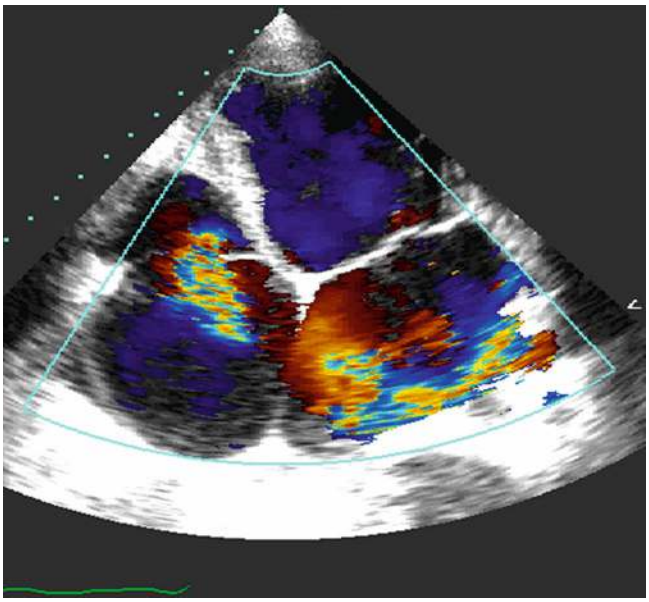


Fig. 1.42 Apical 4 chamber view from a patient with endomyocardial fibrosis. Note the significant fibrosis that is involving the right ventricular apex (*brightness*) and the mitral regurgitation secondary to left-sided involvement

who develop significant arrhythmia at the time of symptoms may need valve repair as a means for symptomatic treatment. Thus, in such patients, stress echocardiography may determine optimum management (Fig. 1.21).

Management of Mitral Regurgitation

Mild and moderate mitral regurgitation are well tolerated and do not require intervention apart from prophylactic antibiotics for potential infection in high-risk patients. Severe mitral regurgitation which causes significant symptoms in spite of medical therapy warrants mitral valve surgery [28]. Medical therapy involves measures of reducing left atrial pressure, e.g., vasodilators, rhythm control in patients with established arrhythmia, and prophylactic measures against thromboembolism, e.g., warfarin. Transcatheter edge-to-edge repair of mitral valve for secondary and less strongly for primary mitral regurgitation has recently received significant attention in patients deemed at high surgical risk [55].

Mitral valve repair is particularly satisfactory for posterior leaflet prolapse and occasionally for anterior leaflet prolapse. Timing of surgery is critical. While it should be at the earliest opportunity for papillary muscle rupture, it could be delayed for 1–2 weeks in case of chordal rupture until hemodynamics settle. This does not justify delaying intervention until patients develop irreversible left ventricular disease, indicated by an increase in end-systolic volume (Figs. 1.43 and 1.44).

The treatment of papillary muscle dysfunction is that of left ventricular disease with particular aim at reducing left ventricular diastolic pressures. Mitral valve replacement in severe left ventricular disease should be avoided as it adds to the disruption of ventricular geometry and hence functional performance. Instead, an undersized mitral ring may be inserted to reduce the inflow diameter and hence the regurgitation, particularly in patients with dilated cardiomyopathy, whose ventricle is resistant to medical therapy. Stress echo may have a role in patient selection for surgical intervention. Mitral regurgitation that increases in severity with stress deserves further attention compared to that which reduces with stress and with enhanced shortening of ventricular basal segment.

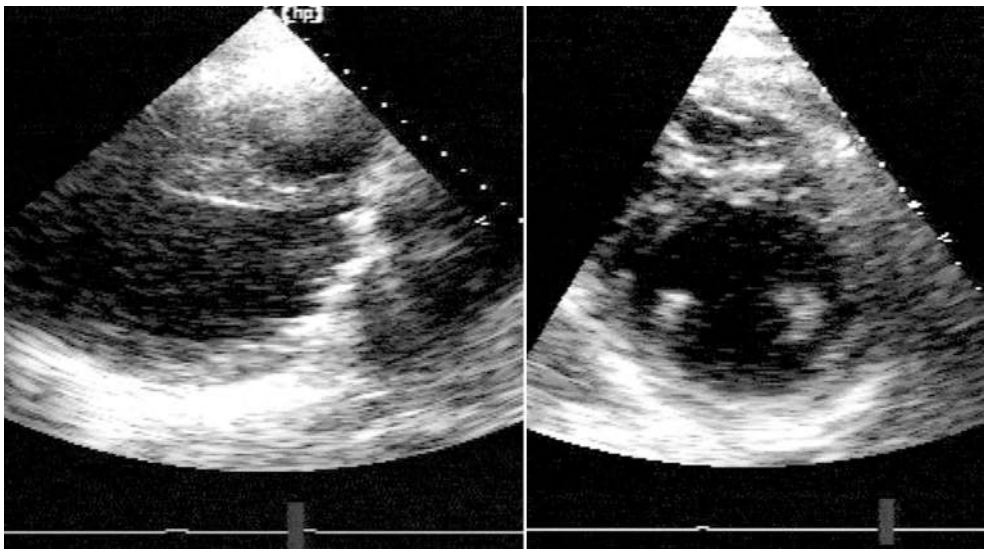


Fig. 1.43 Parasternal long and short axis views of the left heart after mitral valve replacement for significant functional mitral regurgitation. Note the significant increase in LV end-systolic dimension and poor overall systolic function

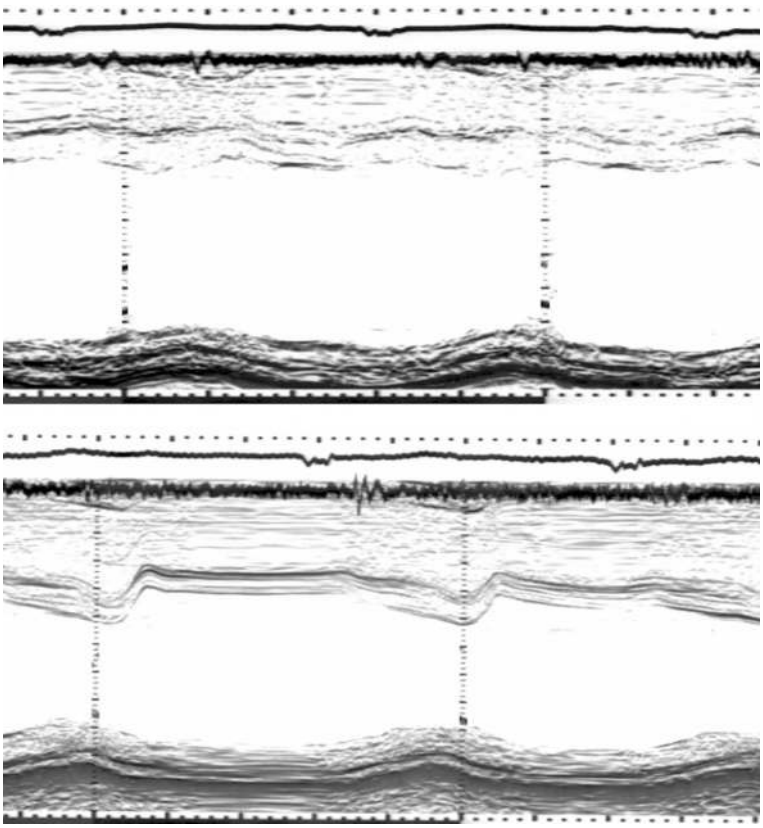


Fig. 1.44 LV minor axis M-mode from a patient with St Jude mitral valve replacement. Note the normalized septal motion 12 months after surgery suggesting significant leak

The Role of Echocardiography in Preoperative and Perioperative Patient Assessment

1. *Before Surgery*

Transesophageal echocardiography is a major diagnostic tool, providing qualitative and quantitative information on the morphology and function of different components of the mitral valve. It provides online details on the exact cause of the mitral regurgitation, functional or organic. In particular, precise identification of the nature of mitral leaflet pathology and the exact scallop disease is crucial for a meticulous surgical strategy. Severe valvular or subvalvular calcification in addition to anterior leaflet involvement reduces the likelihood for successful repair [41, 56]. Preoperative transthoracic echocardiography is equally important in assessing left ventricular size and function [57]. The combination of the two should provide accurate information enough for decision-making on the type of surgery: simple repair, full repair and ring insertion, chordal reimplantation, or mitral valve replacement. Surgical outcome related to left ventricular condition can also be estimated, with end-systolic volume less than 60 ml/m^2 equivalent to end-systolic dimension of 5 cm resulting in better outcome than dimensions more than 5 cm. Left ventricular dysfunction caused by mitral regurgitation may require surgical correction even in the absence of significant symptoms. Such disturbances might worsen in some patients after mitral valve surgery, the reasons for which are not fully understood [58–61] (Videos 1.16 and 1.17).

Intraoperative Assessment

Intraoperative monitoring by transesophageal echo provides early identification of postrepair valve dysfunction so that a second pump run can be established and the dysfunction corrected. A direct assessment of the mode of mitral valve repair can be provided which includes: direct leaflet repair, chordal replacement with Gore-Tex suture, or annuloplasty through insertion of a mitral ring. Intraoperative transesophageal technique also assesses left ventricular function before weaning off the bypass circulation. Thirdly, it identifies any entrapped air in the cardiac chambers. Of course, these findings should be interpreted in the light of specific circumstances: afterload effect, underloaded, or overloaded ventricles, etc. In patients with combined left ventricular dysfunction in the setting of coronary artery disease and mitral regurgitation, intraoperative studies should identify the exact cause of early postoperative slow recovery: whether it is ventricular dysfunction, valve regurgitation, or possibly graft occlusion that needs direct visualization and correction. The same indications for the above apply for postoperative transesophageal echo studies, in addition to identifying early collection of extra cardiac fluid that may have significant hemodynamic effects, irrespective of its volume [62–64].

Surgery

Mitral valve surgery requires open heart surgery and the use of cardiopulmonary bypass circulation. Less invasive approaches are now possible and are available for repair and replacement.

Mitral Valve Repair This operation for mitral prolapse is now a routine practice so that predictable results are widely available. A pathoanatomical directed approach guides contemporary repair techniques which have been shown to be superior to replacement in mitral regurgitation Posterior leaflet repair is by far the commonest operation (80%) and is the most predictable. Good results have been reported with and without the use of a "ring". Anterior leaflet repair is more difficult, results are less predictable, and usually requires the use of a "ring". Traditionally, diseased leaflet resection via surgical excision has been considered the gold standard to mitral valve repair but newer multiple-leaflet preserving techniques have emerged. The nuance distninction between these approaches remains an ongong subject of discussion [65].

In primum inter atrial communications and other forms of atrioventricular septal defect associated with left atrioventricular valve regurgitation, valve repair usually involves the suturing together of part of the superior and inferior bridging leaflets within the left ventricle. Repair of the so-called isolated cleft of the anterior leaflet of the mitral valve can usually be performed by inserting a patch on the anterior leaflet to bridge the cleft. The results of this technique are generally excellent, avoiding the need for mitral valve replacement in virtually every case.

Mitral Valve Replacement There is no ideal valve substitute. The choice lies between a mechanical bileaflet prosthesis and a porcine or bovine, pericardial bioprosthesis. Mechanical valves have the advantage of durability but the disadvantage of life-long anticoagulation, although many of these patients are already committed to warfarin by the presence of atrial fibrillation. Bioprosthetic valves degenerate, and in the mitral position, their life span can be as short as 5 years. Stentless mitral valves are under clinical investigation and include the mitral homograft and a glutaraldehyde-preserved pericardial valve, but medium-term results are not yet available.

Valve Replacement Complications

Mitral valve replacement complications involve para-prosthetic leak, structural valve failure: calcification, tear of leaflet from valve post perforation, obstructed prosthesis due to thrombosis or calcification, thromboembolism, endocarditis, conduction defects.

1. *Para-prosthetic Regurgitation*: This may vary from mild to severe. In the presence of mechanical valves, color Doppler in the transthoracic echo cannot display a uniform regurgitant jet due to the mechanical reflection and therefore may underestimate its importance. A normalized left ventricular septal motion suggests significant leak. Transesophageal echo however is much more sensitive in assessing the exact location and severity of the leak since the valve metal does not distract the ultrasound beam, although it tends to overestimate the regurgitation. Combining left ventricular activity on the M-mode and transesophageal color flow provides a fairly accurate means of assessment. In high-risk patients from a second operation, a para-prosthetic leak can be sealed by a trans-catheter device insertion.
2. *Disintegrating Mitral Xenograft*: The expected durability of these valves is approximately 8 years, and they should thus be followed up annually. Once they show signs of deterioration with rupture or tear of leaflets, they should be replaced as soon as possible, regardless of the severity of regurgitation (Fig. 1.45).
3. *Stuck Mitral Prosthesis*: Although rare, a stuck mitral valve prosthesis may occur, mainly due to thrombosis on the valve preventing its movement. Rapid development of pulmonary edema in a patient with mitral valve prosthesis suggests significant valve dysfunction with associated secondary pulmonary hypertension until otherwise proved. When confirmed, an emergency valve replacement is the only management (Figs. 1.46 and 1.47).
4. *Endocarditis*: This is not uncommon. Prosthetic mitral valve endocarditis is usually difficult to treat medically. Transthoracic echo may or may not show evidence of vegetation. Transesophageal echo is the ideal investigation for this complication. It provides clear images of the valves, and related infection. However, it should not be allowed to overestimate findings. Resistant infection may be eradicated only by valve replacement and debris clearing (Fig. 1.48).
5. *Fibrin Strands/Thrombi*: They can occur on mechanical valves and constitute no real clinical harm. Artificial valve fibrin strands should be differentiated from vegetations (Fig. 1.49).

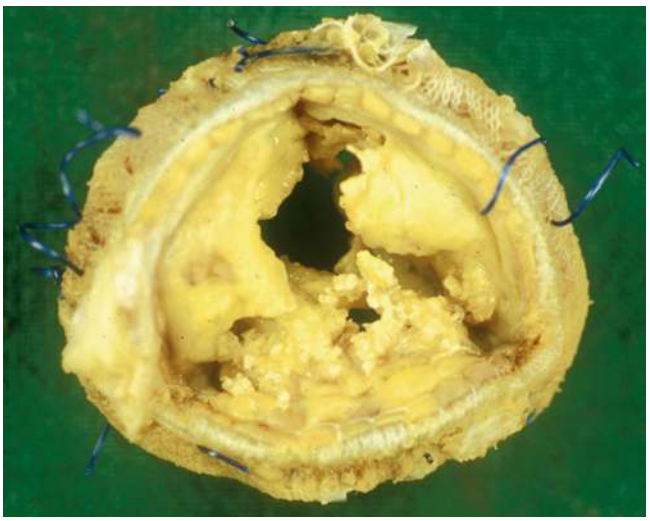


Fig. 1.45 Pathological specimen from a disintegrated MV xenograft

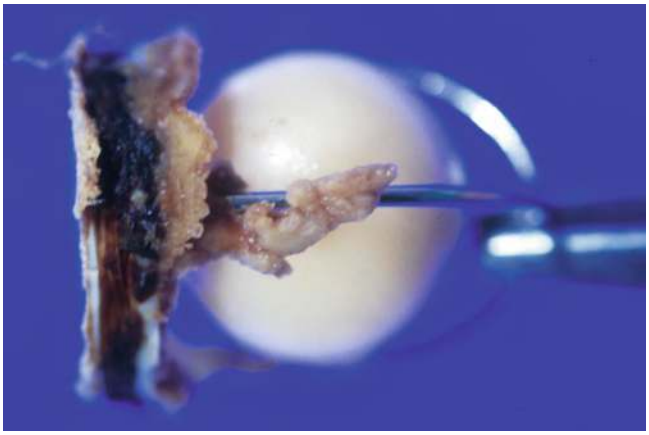


Fig. 1.46 Starr–Edwards ball cage metallic valve excised from the mitral position. Note the stuck ball in the cage by the surrounding clot

Mitral Clip Procedure

Very symptomatic patients in NYHA class III or IV with severe mitral regurgitation represent a significant risk for surgical correction of the leak. Catheter-based mitral valve clip repair (CBMCR) is feasible for selected patients with significant mitral regurgitation, and has proved a satisfactory option for reducing its severity and improving symptoms. Specific criteria for patient selection are well documented including area of leaflet apposition of at least 10 mm [55]. A trans-septal puncture is made and the clip devise is proceeded into the left ventricle under fluoroscopy and transesophageal echo guidance. Two-dimensional transesophageal echocardiography is the standard modality for evaluating

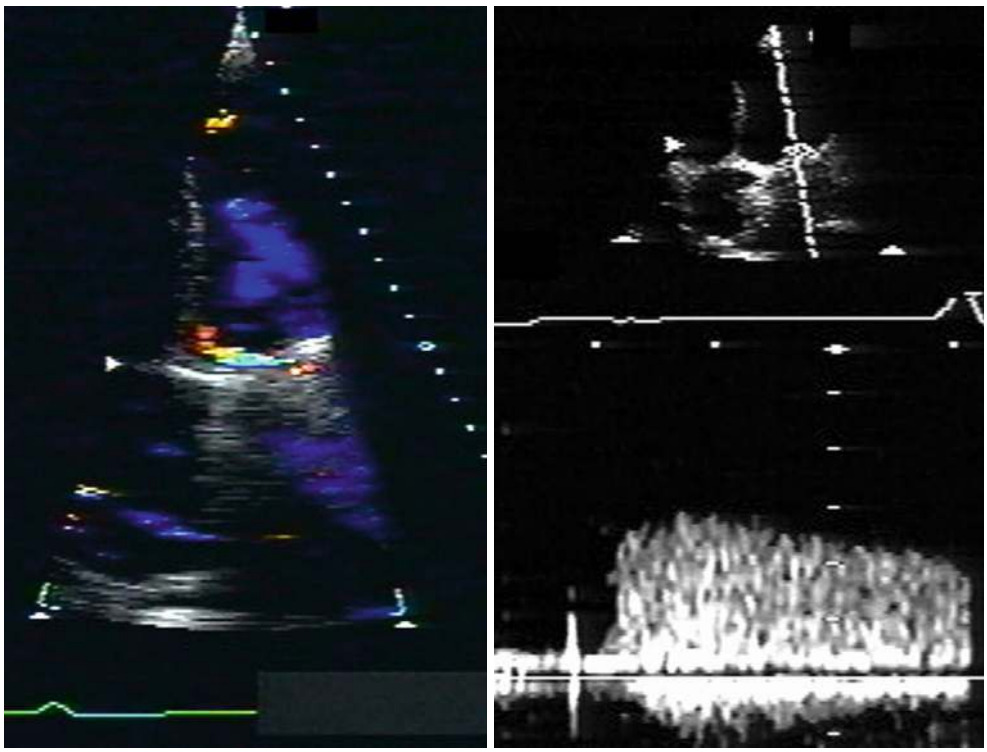


Fig. 1.47 Apical 4 chamber view from a patient with stuck Starr–Edward valve in the mitral position. Note the high forward flow velocities giving rise to a mean pressure drop of 20 mmHg on CW Doppler

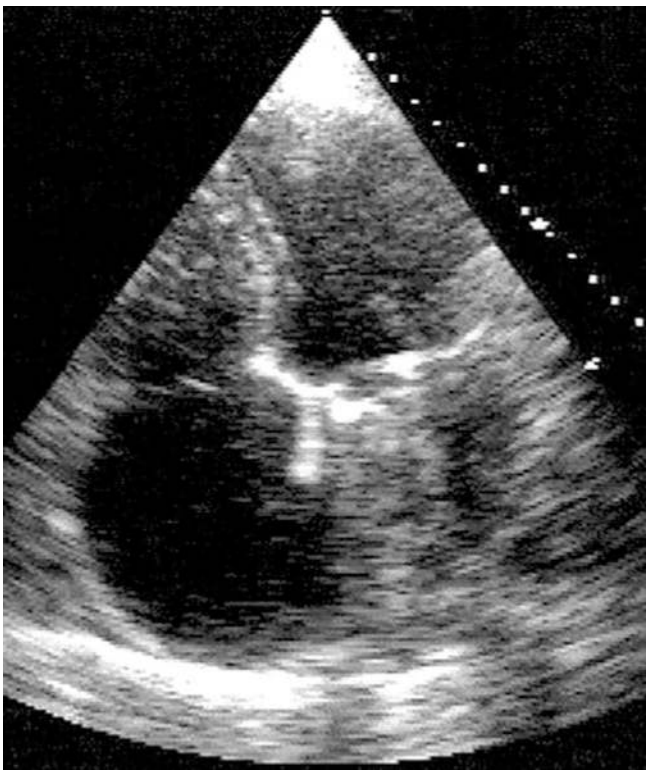


Fig. 1.48 Apical 4 chamber view from a patient with mitral xenograft and large vegetation on the valve



Fig. 1.49 Apical 4 chamber view from a patient with Starr–Edwards mitral prosthesis with small fibrin strands attached to it

mitral regurgitation and procedural guidance [66, 67]. Recently, real-time three-dimensional transesophageal echocardiography became available which offers exquisite pictures of the valve leaflets and attachments. Once the clip is in the ideal position, the device is released and the delivery system is withdrawn. The examination using 2- and 3-D echocardiography allows en face visualization of mitral valve anatomy and mitral regurgitation jet origin, and hence accurate evaluation of the mitral apparatus. Using the two echo techniques may have an effect on the procedure time.

References

1. Yacoub M. Anatomy of the mitral valve chordae and cusps. In: Kalmason D, editor. The Mitral Valve. A Pluridisciplinary Approach. London: Edward Arnold Publishers; 1976. p. 15–20.
2. Daniels SJ, Mintz GS, Kotler MN. Rheumatic tricuspid valve disease: two-dimensional echocardiographic, hemodynamic, and angiographic correlations. Am J Cardiol. 1983;51(3):492–6.
3. Kilner PJ, Henein MY, Gibson DG. Our tortuous heart in dynamic mode—an echocardiographic study of mitral flow and movement in exercising subjects. Heart Vessels. 1997;12(3):103–10.
4. Henein M, Lindqvist P, Francis D, Morner S, Waldenstrom A, Kazzam E. Tissue Doppler analysis of age-dependency in diastolic ventricular behaviour and filling: a cross-sectional study of healthy hearts (the Umea General Population Heart Study). Eur Heart J. 2002;23(2):162–71.
5. Come PC, Riley MF. M mode and cross-sectional echocardiographic recognition of fibrosis and calcification of the mitral valve chordae and left ventricular papillary muscles. Am J Cardiol. 1982;49(2):461–6.
6. Naito M, Morganroth J, Mardelli TJ, Chen CC, Dreifus LS. Rheumatic mitral stenosis:cross-sectional echocardiographic analysis. Am Heart J. 1980;100(1):34–40.
7. Pellikka PA, Tajik AJ, Khandheria BK, Seward JB, Callahan JA, Pitot HC, et al. Carcinoid heart disease. Clinical and echocardiographic spectrum in 74 patients. Circulation. 1993;87(4):1188–96.
8. Gibson DG. Valve disease. In: Weatherall DJ, Ledingham JGG, Warrell DA, editors. Oxford textbook of medicine. New York: Oxford University Press; 1996. p. 2451.
9. Smith MD, Handshoe R, Handshoe S, Kwan OL, DeMaria AN. Comparative accuracy of two-dimensional echocardiography and Doppler pressure half-time methods in assessing severity of mitral stenosis in patients with and without prior commissurotomy. Circulation. 1986;73(1):100–7.
10. Kawahara T, Yamagishi M, Seo H, Mitani M, Nakatani S, Beppu S, et al. Application of Doppler color flow imaging to determine valve area in mitral stenosis. J Am Coll Cardiol. 1991;18(1):85–92.
11. Deng YB, Matsumoto M, Wang XF, Liu L, Takizawa S, Takekoshi N, et al. Estimation of mitral valve area in patients with mitral stenosis by the flow convergence region method: selection of aliasing velocity. J Am Coll Cardiol. 1994;24(3):683–9.
12. Nishimura RA, Rihal CS, Tajik AJ, Holmes DR Jr. Accurate measurement of the transmitral gradient in patients with mitral stenosis: a simultaneous catheterization and Doppler echocardiographic study. J Am Coll Cardiol. 1994;24(1):152–8.
13. Hatle L, Angelsen B, Tromsdal A. Noninvasive assessment of atrioventricular pressure half-time by Doppler ultrasound. Circulation. 1979;60(5):1096–104.
14. Hatle L, Angelsen BA. Doppler ultrasound in cardiology. 2nd ed. Philadelphia: Lea & Febiger; 1985.
15. Nakatani S, Masuyama T, Kodama K, Kitabatake A, Fujii K, Kamada T. Value and limitations of Doppler echocardiography in the quantification of stenotic mitral valve area: comparison of the pressure half-time and the continuity equation methods. Circulation. 1988;77(1):78–85.
16. Shrestha NK, Moreno FL, Narciso FV, Torres L, Calleja HB. Two-dimensional echocardiographic diagnosis of left-atrial thrombus in rheumatic heart disease. A clinicopathologic study. Circulation. 1983;67(2):341–7.
17. Iliceto S, Antonelli G, Sorino M, Biasco G, Rizzon P. Dynamic intracavitary left atrial echoes in mitral stenosis. Am J Cardiol. 1985;55(5):603–6.
18. Gibson DG, Brown D. Measurement of instantaneous left ventricular dimension and filling rate in man, using echocardiography. Br Heart J. 1973;35(11):1141–9.
19. John Sutton MG, Traill TA, Ghafour AS, Brown DJ, Gibson DG. Echocardiographic assessment of left ventricular filling after mitral valve surgery. Br Heart J. 1977;39(12):1283–91.
20. Desideri A, Vanderperren O, Serra A, Barraud P, Petitclerc R, Lesperance J, et al. Long-term (9 to 33 months) echocardiographic follow-up after successful percutaneous mitral commissurotomy. Am J Cardiol. 1992;69(19):1602–6.
21. Weyman AE, Heger JJ, Kronik TG, Wann LS, Dillon JC, Feigenbaum H. Mechanism of paradoxical early diastolic septal motion in patients with mitral stenosis: a cross-sectional echocardiographic study. Am J Cardiol. 1977;40(5):691–9.
22. Veyrat C, Kalmanson D, Farjon M, Manin JP, Abitbol G. Noninvasive diagnosis and assessment of tricuspid regurgitation and stenosis using one and two dimensional echo-pulsed Doppler. Br Heart J. 1982;47(6):596–605.
23. Waller BF. Morphological aspects of valvular heart disease: part II. Curr Probl Cardiol. 1984;9(8):1–74.
24. Connolly SJ, Karthikeyan G, Ntsekhe M, Haileamlak A, El Sayed A, El Ghamrawy A, Damasceno A, Avezum A, Dans AML, Gitura B, Hu D, Kamanzi ER, Maklady F, Fana G, Gonzalez-Hermosillo JA, Musuku J, Kazmi K, Zühlke L, Gondwe L, Ma C, Paniagua M, Ogah OS, Molefe-Baikai OJ, Lwabi P, Chillo P, Sharma SK, Cabral TTJ, Tarhuni WM, Benz A, van Eikels M, Krol A, Pattath D, Balasubramanian K, Rangarajan S, Ramasundarahettige C, Mayosi B, Yusuf S. INVICTUS Investigators. Rivaroxaban in Rheumatic Heart Disease-Associated Atrial Fibrillation. N Engl J Med. 2022;387(11):978–88. https://doi.org/10.1056/NEJMoa2209051. Epub 2022 Aug 28. PMID: 36036525
25. Hindricks G, Potpara T, Dagres N, Arbelo E, Bax JJ, Blomström-Lundqvist C, Boriani G, Castella M, Dan GA, Dilaveris PE, Fauchier L, Filippatos G, Kalman JM, La Meir M, Lane DA, Lebeau JP, Lettino M, Lip GYH, Pinto FJ, Thomas GN, Valgimigli M, Van Gelder IC, Van Putte BP, Watkins CL, ESC Scientific Document Group. ESC Guidelines for the diagnosis and management of atrial fibrillation developed in collaboration with the European Association for Cardio-Thoracic Surgery (EACTS): The Task Force for the diagnosis and management of atrial fibrillation of the European Society of Cardiology (ESC) Developed with the special contribution of the European Heart Rhythm Association (EHRA) of the ESC. Eur Heart J. 2020;42(5):373–498. https://doi.org/10.1093/

eurheartj/ehaa612. Erratum in: Eur Heart J. 2021 Feb 1;42(5):507. Erratum in: Eur Heart J. 2021 Feb 1;42(5):546-547. Erratum in: Eur Heart J. 2021 Oct 21;42(40):4194. PMID: 32860505
26. Chen J, Wang H, Zhao L. Long-term outcomes of radiofrequency catheter ablation for atrial fibrillation in rheumatic heart disease patients with mild mitral stenosis. J Interv Card Electrophysiol. 2019;56(3):313–9. https://doi.org/10.1007/s10840-019-00538-7. Epub 2019 May 4. PMID: 31055689
27. Díez-Delhoyo F, Sánchez De La Nava AM, Sanz-Ruiz R, Ávila P, González-Torrecilla E, Delgado-Montero A, López J, Bermejo J, Arenal Á, Atienza F, Fernández-Avilés F. Combined atrial fibrillation ablation and balloon mitral commissurotomy in patients with rheumatic mitral stenosis. J Cardiovasc Electrophysiol. 2022;33(12):2485–95. https://doi.org/10.1111/jce.15686. Epub 2022 Oct 5. PMID: 36168873
28. Vahanian A, Beyersdorf F, Praz F, Milojevic M, Baldus S, Bauersachs J, Capodanno D, Conradi L, De Bonis M, De Paulis R, Delgado V, Freemantle N, Gilard M, Haugaa KH, Jeppsson A, Jüni P, Pierard L, Prendergast BD, Sádaba JR, Tribouilloy C, Wojakowski W, ESC/EACTS Scientific Document Group. ESC/EACTS Guidelines for the management of valvular heart disease. Eur Heart J. 2021;43(7):561–632. https://doi.org/10.1093/eurheartj/ehab395. Erratum in: Eur Heart J. 2022 Feb 18: PMID: 34453165
29. Abascal VM, Wilkins GT, O'Shea JP, Choong CY, Palacios IF, Thomas JD, et al. Prediction of successful outcome in 130 patients undergoing percutaneous balloon mitral valvotomy. Circulation. 1990;82(2):448–56.
30. Palacios IF, Block PC, Wilkins GT, Weyman AE. Follow-up of patients undergoing percutaneous mitral balloon valvotomy. Analysis of factors determining restenosis. Circulation. 1989;79(3):573–9.
31. Wilkins GT, Weyman AE, Abascal VM, Block PC, Palacios IF. Percutaneous balloon dilatation of the mitral valve: an analysis of echocardiographic variables related to outcome and the mechanism of dilatation. Br Heart J. 1988;60(4):299–308.
32. Roberts WC. Morphologic features of the normal and abnormal mitral valve. Am J Cardiol. 1983;51(6):1005–28.
33. Mintz GS, Kotler MN, Segal BL, Parry WR. Two dimensional echocardiographic evaluation of patients with mitral insufficiency. Am J Cardiol. 1979;44(4):670–8.
34. Segal BL, Likoff W, Kingsley B. Echocardiography. Clinical application in mitral regurgitation. Am J Cardiol. 1967;19(1):50–8.
35. Pomerance A. Pathological and clinical study of calcification of the mitral valve ring. J Clin Pathol. 1970;23(4):354–61.
36. Chehab O, Roberts-Thomson R, Bivona A, Gill H, Patterson T, Pursnani A, Grigoryan K, Vargas B, Bokhary U, Blauth C, Lucchese G, Bapat V, Guerrero M, Redwood S, Prendergast B, Rajani R. Management of patients with severe mitral annular calcification: JACC state-of-the-art review. J Am Coll Cardiol. 2022;80(7):722–38. https://doi.org/10.1016/j.jacc.2022.06.009. PMID: 35953138
37. Farhan S, Silbiger JJ, Halperin JL, Zhang L, Dukkipati SR, Vogel B, Kini A, Sharma S, Lerakis S. Pathophysiology, echocardiographic diagnosis, and treatment of atrial functional mitral regurgitation: JACC state-of-the-art review. J Am Coll Cardiol. 2022;80(24):2314–30. https://doi.org/10.1016/j.jacc.2022.09.046. Erratum in: J Am Coll Cardiol. 2023 Feb 21;81(7):711. PMID: 36480974
38. Sabbag A, Essayagh B, Barrera JDR, Basso C, Berni A, Cosyns B, Deharo JC, Deneke T, Di Biase L, Enriquez-Sarano M, Donal E, Imai K, Lim HS, Marsan NA, Turagam MK, Peichl P, Po SS, Haugaa KH, Shah D, de Riva SM, Bertrand P, Saba M, Dweck M, Townsend SN, Ngarmukos T, Fenelon G, Santangeli P, Sade LE, Corrado D, Lambiase P, Sanders P, Delacrétaz E, Jahangir A, Kaufman ES, Saggu DK, Pierard L, Delgado V, Lancellotti P. EHRA expert consensus statement on arrhythmic mitral valve prolapse and mitral annular disjunction complex in collaboration with the ESC Council on valvular heart disease and the European Association of Cardiovascular Imaging endorsed cby the Heart Rhythm Society, by the Asia Pacific Heart Rhythm Society, and by the Latin American Heart Rhythm Society. Europace. 2022;24(12):1981–2003. https://doi.org/10.1093/europace/euac125. PMID: 35951656
39. Malagoli A, Albini A, Benfari G, Ilardi F, Lisi M, Mandoli GE, Pastore MC, Sperlongano S, Cameli M, D'Andrea A. Arrhythmic mitral valve prolapse: a practical approach for asymptomatic patients. Eur Heart J Cardiovasc Imaging. 2024;25(3):293–301. https://doi.org/10.1093/ehjci/jead332. PMID: 38061000
40. Waller BF, Morrow AG, Maron BJ, Del Negro AA, Kent KM, McGrath FJ, et al. Etiology of clinically isolated, severe, chronic, pure mitral regurgitation: analysis of 97 patients over 30 years of age having mitral valve replacement. Am Heart J. 1982;104(2 Pt 1):276–88.
41. Castello R, Lenzen P, Aguirre F, Labovitz AJ. Quantitation of mitral regurgitation by transesophageal echocardiography with Doppler color flow mapping: correlation with cardiac catheterization. J Am Coll Cardiol. 1992;19(7):1516–21.
42. Upton MT, Gibson DG. The study of left ventricular function from digitized echocardiograms. Prog Cardiovasc Dis. 1978;20(5):359–84.
43. Panidis IP, McAllister M, Ross J, Mintz GS. Prevalence and severity of mitral regurgitation in the mitral valve prolapse syndrome: a Doppler echocardiographic study of 80 patients. J Am Coll Cardiol. 1986;7(5):975–81.
44. Abbasi AS, Allen MW, DeCristofaro D, Ungar I. Detection and estimation of the degree of mitral regurgitation by range-gated pulsed Doppler echocardiography. Circulation. 1980;61(1):143–7.
45. Helmcke F, Nanda NC, Hsiung MC, Soto B, Adey CK, Goyal RG, et al. Color Doppler assessment of mitral regurgitation with orthogonal planes. Circulation. 1987;75(1):175–83.
46. Miyatake K, Izumi S, Okamoto M, Kinoshita N, Asonuma H, Nakagawa H, et al. Semiquantitative grading of severity of mitral regurgitation by real-time two-dimensional Doppler flow imaging technique. J Am Coll Cardiol. 1986;7(1):82–8.
47. Spain MG, Smith MD, Grayburn PA, Harlamert EA, DeMaria AN. Quantitative assessment of mitral regurgitation by Doppler color flow imaging: angiographic and hemodynamic correlations. J Am Coll Cardiol. 1989;13(3):585–90.
48. Eren M, Eksik A, Gorgulu S, Norgaz T, Dagdeviren B, Bolca O, et al. Determination of vena contracta and its value in evaluating severity of aortic regurgitation. J Heart Valve Dis. 2002;11(4):567–75.
49. Klein AL, Obarski TP, Stewart WJ, Casale PN, Pearce GL, Husbands K, et al. Transesophageal Doppler echocardiography of pulmonary venous flow: a new marker of mitral regurgitation severity. J Am Coll Cardiol. 1991;18(2):518–26.
50. Nishimura RA, Tajik AJ. Determination of left-sided pressure gradients by utilizing Doppler aortic and mitral regurgitant signals: validation by simultaneous dual catheter and Doppler studies. J Am Coll Cardiol. 1988;11(2):317–21.
51. Ren JF, Kotler MN, DePace NL, Mintz GS, Kimbiris D, Kalman P, et al. Two-dimensional echocardiographic determination of left atrial emptying volume: a noninvasive index in quantifying the degree of nonrheumatic mitral regurgitation. J Am Coll Cardiol. 1983;2(4):729–36.
52. Bargiggia GS, Tronconi L, Sahn DJ, Recusani F, Raisaro A, De Servi S, et al. A new method for quantitation of mitral regurgitation based on color flow Doppler imaging of flow convergence proximal to regurgitant orifice. Circulation. 1991;84(4):1481–9.
53. Humphries WC Jr, Hammer WJ, McDonough MT, Lemole G, McCurdy RR, Spann JF Jr. Echocardiographic equivalents of a flail mitral leaflet. Am J Cardiol. 1977;40(5):802–7.

54. Mintz GS, Kotler MN, Segal BL, Parry WR. Two-dimensional echocardiographic recognition of ruptured chordae tendineae. Circulation. 1978;57(2):244–50.
55. Hausleiter J, Stocker TJ, Adamo M, Karam N, Swaans MJ, Praz F. Mitral valve transcatheter edge-to-edge repair. EuroIntervention. 2023;18(12):957–76. https://doi.org/10.4244/EIJ-D-22-00725. PMID: 36688459; PMCID: PMC9869401
56. Klein AL, Bailey AS, Cohen GI, Stewart WJ, Duffy CI, Pearce GL, et al. Importance of sampling both pulmonary veins in grading mitral regurgitation by transesophageal echocardiography. J Am Soc Echocardiogr. 1993;6(2):115–23.
57. Lisi M, Cameli M, Mandoli GE, Pastore MC, Righini FM, Flamigni F, D'Ascenzi F, Cavigli L, Focardi M, Rubboli A, Campo G, Mondillo S, Henein MY. Left atrial myocardial intrinsic function remodeling response to repair of primary mitral regurgitation. Echocardiography. 2022;39(10):1264–8. https://doi.org/10.1111/echo.15452. Epub 2022 Sep 8. PMID: 36074005
58. Pastore MC, Mandoli GE, Sannino A, Dokollari A, Bisleri G, D'Ascenzi F, Cavigli L, Pasquini A, Lisi M, Ghionzoli N, Santoro C, Miglioranza MH, Focardi M, Patti G, Valente S, Mondillo S, Cameli M. Two and three-dimensional echocardiography in primary mitral regurgitation: practical hints to optimize the surgical planning. Front Cardiovasc Med. 2021;8(8):706165. https://doi.org/10.3389/fcvm.2021.706165. PMID: 34307510; PMCID: PMC8295501
59. Mandoli GE, Pastore MC, Benfari G, Bisleri G, Maccherini M, Lisi G, Cameli P, Lisi M, Dokollari A, Carrucola C, Vigna M, Montesi G, Valente S, Mondillo S, Cameli M. Left atrial strain as a preoperative prognostic marker for patients with severe mitral regurgitation. Int J Cardiol. 2021;1(324):139–45. https://doi.org/10.1016/j.ijcard.2020.09.009. Epub 2020 Sep 10. PMID: 32920069
60. Cameli M, Lisi M, Righini FM, Massoni A, Natali BM, Focardi M, Tacchini D, Geyer A, Curci V, Di Tommaso C, Lisi G, Maccherini M, Chiavarelli M, Massetti M, Tanganelli P, Mondillo S. Usefulness of atrial deformation analysis to predict left atrial fibrosis and endocardial thickness in patients undergoing mitral valve operations for severe mitral regurgitation secondary to mitral valve prolapse. Am J Cardiol. 2013;111(4):595–601. https://doi.org/10.1016/j.amjcard.2012.10.049. Epub 2012 Dec 1. PMID: 23211360
61. Cameli M, Lisi M, Giacomin E, Caputo M, Navarri R, Malandrino A, Ballo P, Agricola E, Mondillo S. Chronic mitral regurgitation: left atrial deformation analysis by two-dimensional speckle tracking echocardiography. Echocardiography. 2011;28(3):327–34. https://doi.org/10.1111/j.1540-8175.2010.01329.x. Epub 2011 Feb 17. PMID: 21323986
62. Zile MR, Gaasch WH, Carroll JD, Levine HJ. Chronic mitral regurgitation: predictive value of preoperative echocardiographic indexes of left ventricular function and wall stress. J Am Coll Cardiol. 1984;3(2 Pt 1):235–42.
63. Czer LS, Maurer G, Bolger AF, De Robertis M, Resser KJ, Kass RM, et al. Intraoperative evaluation of mitral regurgitation by Doppler color flow mapping. Circulation. 1987;76(3 Pt 2):III108–16.
64. Reichert SL, Visser CA, Moulijn AC, Suttorp MJ, vd Brink RB, Koolen JJ, et al. Intraoperative transesophageal color-coded Doppler echocardiography for evaluation of residual regurgitation after mitral valve repair. J Thorac Cardiovasc Surg. 1990;100(5):756–61.
65. Caldonazo T, Sá MP, Jacquemyn X, Van den Eynde J, Kirov H, Harik L, et al. Respect versus resect approaches for mitral valve repair: a meta-analysis of reconstructed time-to-event data. Am J Cardiol. 2024;213:5–11.
66. Moises VA, Maciel BC, Hornberger LK, Murillo-Olivas A, Valdes-Cruz LM, Sahn DJ, et al. A new method for noninvasive estimation of ventricular septal defect shunt flow by Doppler color flow mapping: imaging of the laminar flow convergence region on the left septal surface. J Am Coll Cardiol. 1991;18(3):824–32.
67. Recusani F, Bargiggia GS, Yoganathan AP, Raisaro A, Valdes-Cruz LM, Sung HW, et al. A new method for quantification of regurgitant flow rate using color Doppler flow imaging of the flow convergence region proximal to a discrete orifice. An in vitro study. Circulation. 1991;83(2):594–604.

Aortic Valve

2

Michael Y. Henein, Matteo Cameli, Matteo Lisi, Federico Landra, Mary Sheppard, John R. Pepper, Harry Smith, Mario Petro, and Michael Rigby

Anatomy

The aortic valve is a passive valve made up of three leaflets which assume the shape of half moons (semi-lunar). Opposite to the mitral valve, there is no true aortic fibrous annulus but a complex root made up of the aortic wall sinuses, left ventricular myocardium, and interleaflet fibrous triangles. The ostia of the coronary arteries are located within the aortic sinuses. The sino-tubular junction is an important anatomic landmark for surgical procedures. It may be that the leaflets of the aortic valve are not passive as they are rich in different types of nerve endings. The function and role of these "nerves" remain obscure (Figs. 2.1 and 2.2).

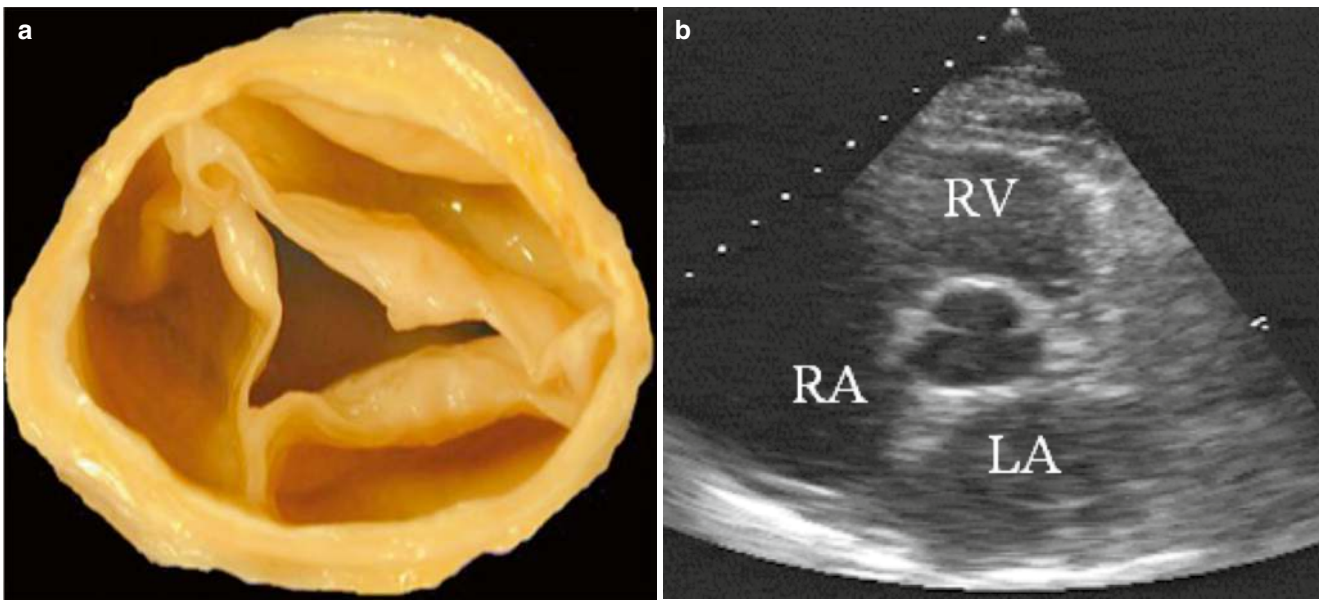


Fig. 2.1 (**a**) Section in the ascending aorta showing a normal tricuspid aortic valve viewed from above and the relation of the leaflets to the coronary arteries arising from the corresponding sinuses. (**b**) Parasternal short axis view of the aortic valve showing the three leaflets and their relation to the surrounding structures

Supplementary Information The online version contains supplementary material available at https://doi.org/10.1007/978-3-031-95894-6_2.

M. Y. Henein (✉)
Imperial College London, London, UK

University of Siena, Siena, Italy
e-mail: m.henein@imperial.ac.uk

M. Cameli · F. Landra
University of Siena, Siena, Italy

M. Lisi
Ospedale S. Maria delle Croci, Ravenna, Italy

M. Sheppard · J. R. Pepper · H. Smith · M. Petro · M. Rigby
Royal Brompton Hospital, London, UK

© The Author(s), under exclusive license to Springer Nature Switzerland AG 2025

M. Y. Henein (ed.), *Clinical Echocardiography*, https://doi.org/10.1007/978-3-031-95894-6_2

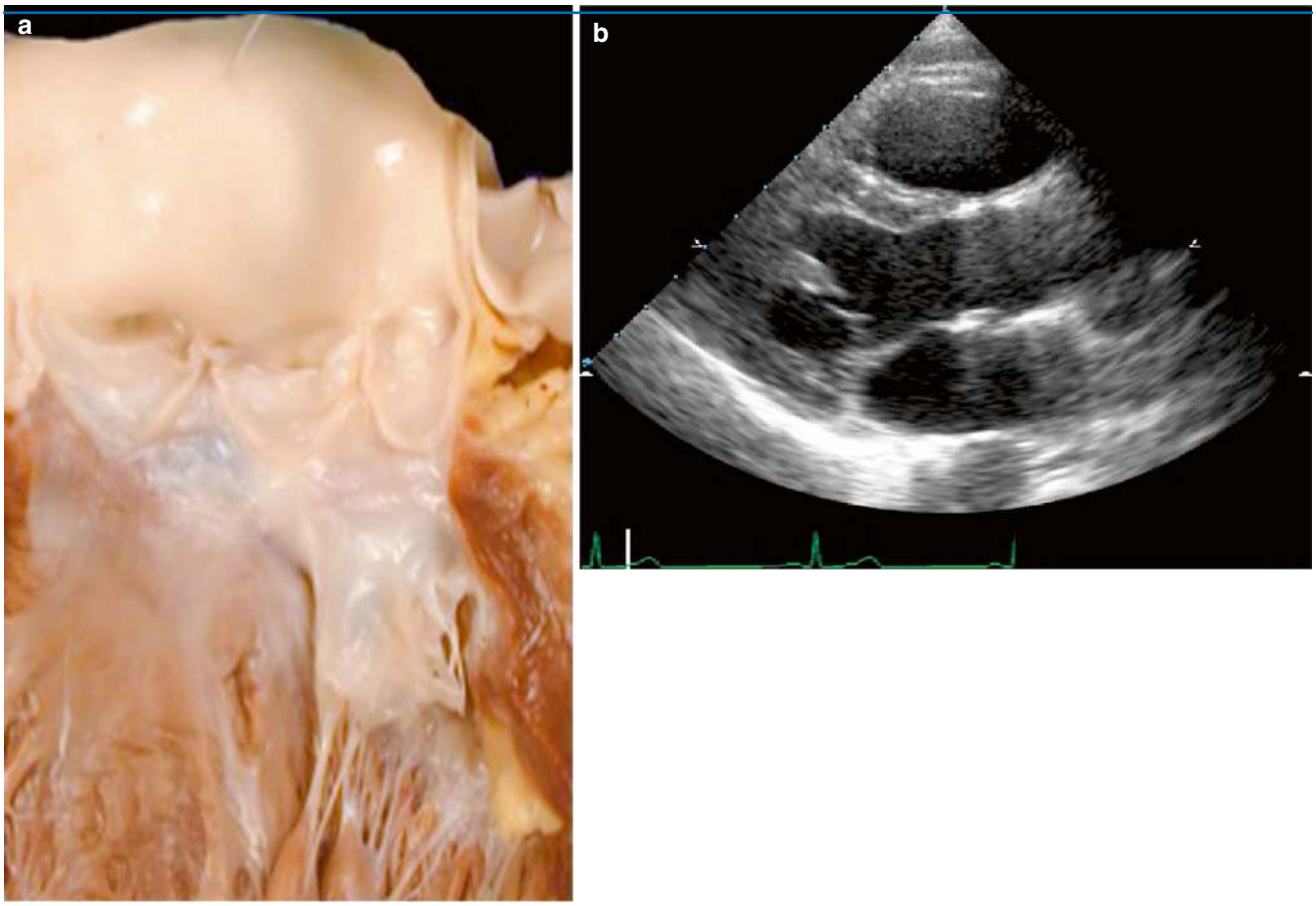


Fig. 2.2 (**a**) Longitudinal section in the left ventricle and ascending aorta showing an opened aortic valve in direct continuity with the anterior leaflet of the mitral valve. (**b**) Parasternal long axis view of the left ventricle and ascending aorta showing opened aortic valve in systole

Aortic Stenosis

Aortic stenosis (AS) is the most common valvular disorder, and its diagnosis is becoming more prevalent in developed nations due to an aging population and advancements in diagnostic methods. It affects approximately 2% of individuals, with prevalence increasing significantly in the elderly [1]. The etiology of aortic valve stenosis is either congenital or acquired. Congenital aortic stenosis can be localized at 3 levels: valvar, supravalvar, or subvalvar.

Etiology

1. *Congenital Cusp Malformation*: A single commissure is seen in infants and young children whereas bicuspid or quadricuspid valves are usually discovered incidentally in young adults (Fig. 2.3). The last two do not usually give rise to any significant hemodynamic abnormality before adulthood, as long as the pressure drop across the valve is not significant. The resulting turbulence at leaflet level adds to the predisposition of these valves to further deformation, fibrosis, calcification, and infective endocarditis [2, 3]. In a bicuspid aortic valve, the commissure is commonly transverse in position and rarely vertical. Mild aortic regurgitation and dilatation of the ascending aorta frequently coexist with a bicuspid valve [4]. When the diagnosis is confirmed, suprasternal imaging is important to exclude aortic coarctation which is also a common association. In congenital aortic stenosis, leaflet movement is limited at the tips rather than at the base, and therefore, M-mode echocardiography may be misleading.

Bicuspid aortic valves are not intrinsically stenotic unless there is also dysplasia of the leaflets or other superimposed pathological change (Video 2.1). The valves may become stenotic due to sclerosis or one of the leaflets may prolapse into the ventricle with subsequent insufficiency. Such valves are highly susceptible to infective endocarditis. The mor-

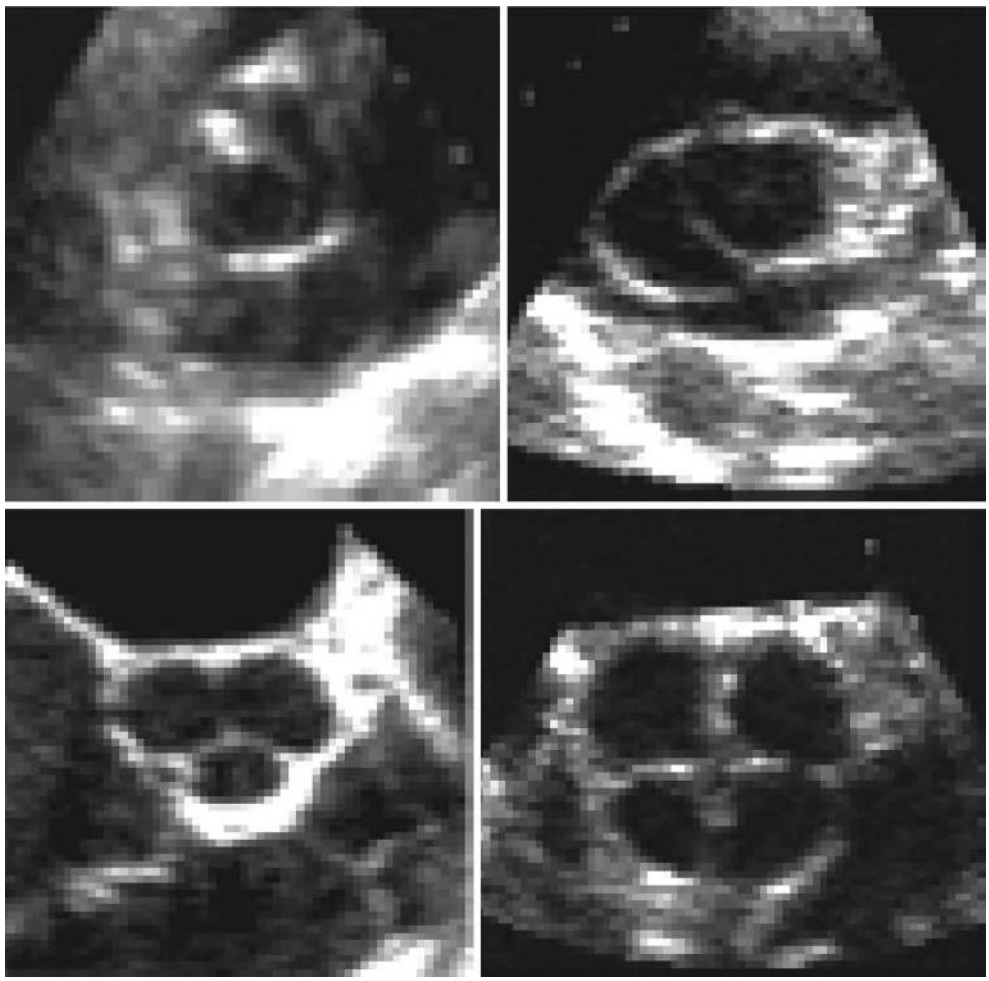


Fig. 2.3 Parasternal short axis view of the aortic valve showing different presentations of cusp formation

phology of the leaflets also varies. The two leaflets can be of equal size or more commonly they are unequal. The larger leaflet almost always has a shallow raphe in its middle part [2]. Most larger leaflets are anterior, and both coronary arteries arise from the sinus above it (Figs. 2.4, 2.5, and 2.6).

2. *Congenital Aortic Tubular Stenosis*: This is a rare congenital disease that presents with uniformly narrowed aortic root and proximal ascending aorta. Management of this condition is complete resection and replacement of the aortic root and proximal (affected segment) ascending aorta (Fig. 2.7). Aortic valve replacement alone in this condition does not absolve symptoms, since patients will be left with residual raised resistance to ejection.
3. *Subaortic Stenosis*: This may be in the form of a fibrous membrane (ridge) below the aortic cusps or hypertrophied upper septum that bulges into the outflow tract. The former is a disease of the young that is usually in the shape of discrete, crescent shaped fibrous shelf or membrane encircling the left ventricular outflow tract. It results in signs of ventricular hypertrophy and significant



Fig. 2.4 Section in a bicuspid aortic valve demonstrating leaflet morphology with one leaflet being larger than the other

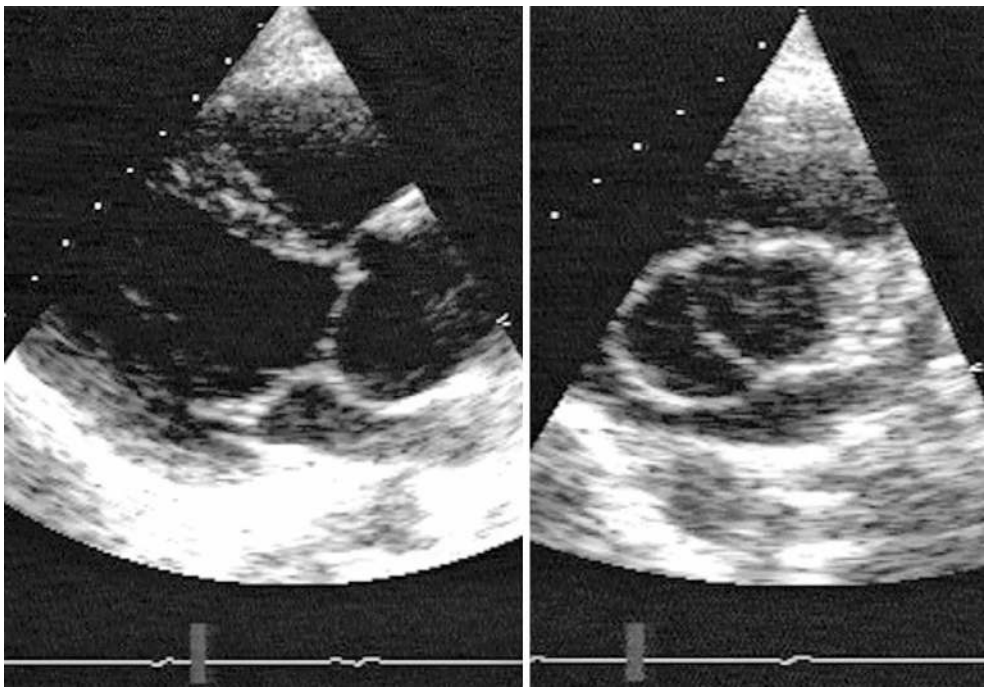


Fig. 2.5 Parasternal long and short axis views from a patient with bicuspid aortic valve showing eccentric closure point

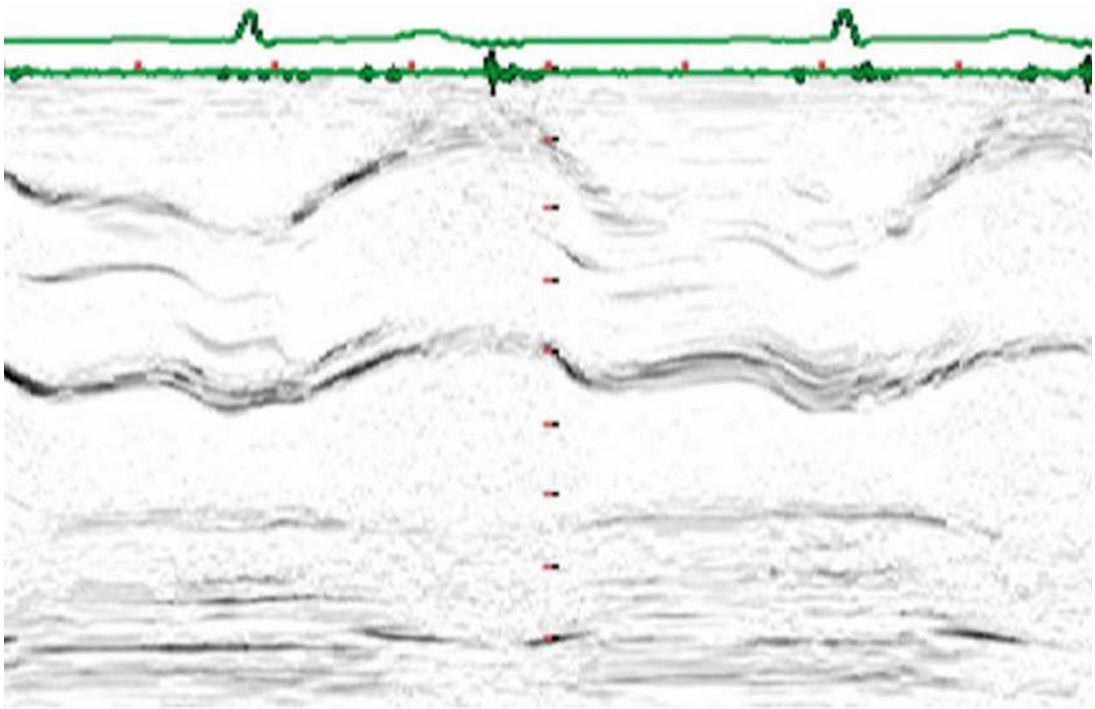


Fig. 2.6 M-mode echogram from a patient with bicuspid aortic valve showing eccentric closure point, frequently seen in this condition

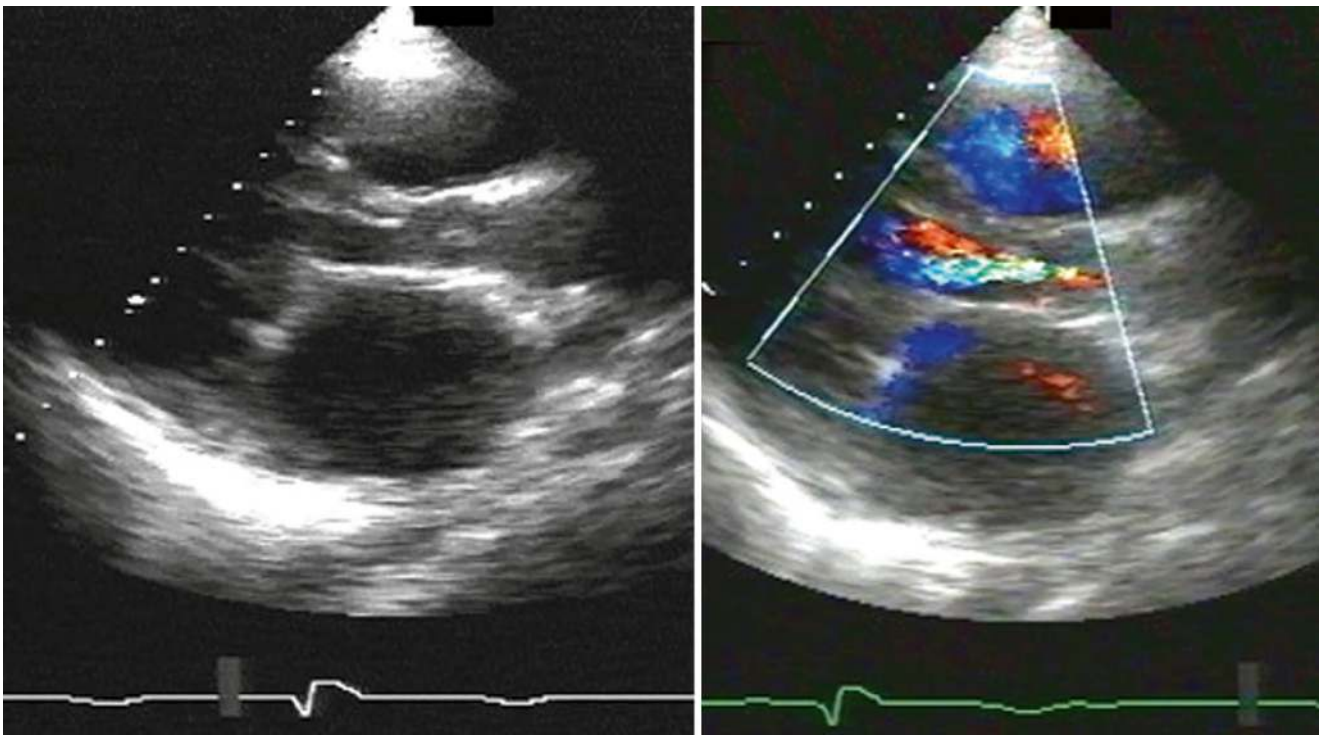


Fig. 2.7 Parasternal long axis view from a patient with tubular narrowing of the aortic root and proximal ascending aorta. Note the normal diameter of the ascending aorta distal to the site of narrowing

outflow tract gradient in the first 3 decades of life. Subaortic fixed narrowing is commonly associated with some degree of aortic regurgitation probably caused by the disturbed vortices in the outflow tract and proximal ascending aorta (Figs. 2.8 and 2.9) [5, 6]. Other congenital cardiac conditions should always be excluded, e.g., atrial septal defect and coarctation of the aorta. When confirmed as the cause of symptoms, surgical excision is the best line of treatment, although it tends to recur unpredictably. Dynamic subaortic stenosis occurring early in life represents a component of hypertrophic cardiomyopathy (Fig. 2.10). Muscular subaortic stenosis is more frequently seen in the elderly with a small left ventricular cavity irrespective of the cause of the hypertrophy [7]. When there is significant outflow tract narrowing, it results in mid-systolic closure of the aortic valve. If the resting pressure drop (gradient) across the outflow tract is not significant in patients limited by exertional symp-

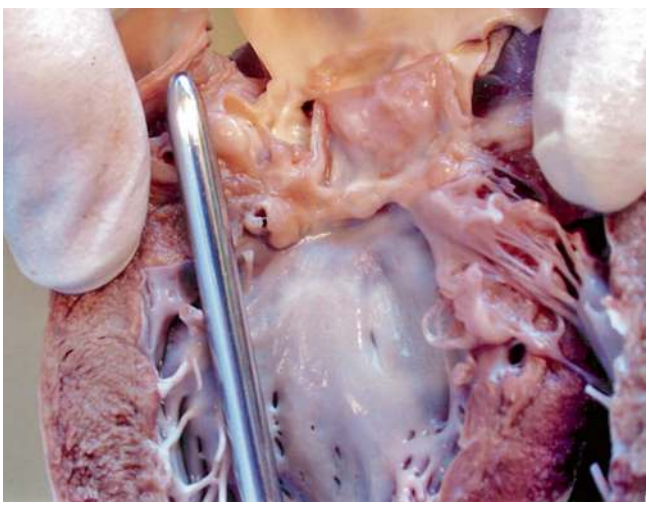


Fig. 2.8 A section in the long axis of the left ventricle and outflow tract from a patient with subaortic stenosis. Note the fibrous ridge beneath the aortic cusps

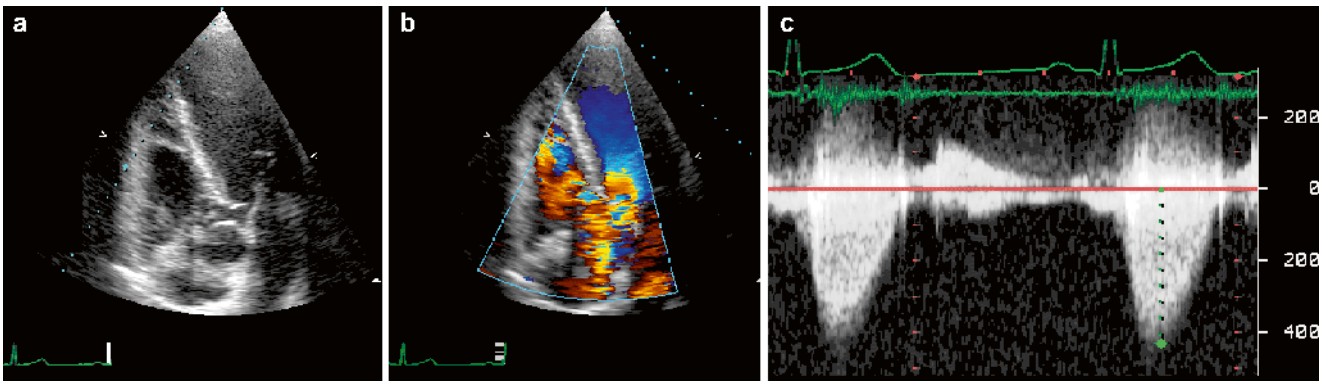


Fig. 2.9 (**a**) Apical 5 chamber view from a young patient with subaortic stenosis. Note the location of the membrane in relation to the valve cusps. (**b**) Color flow Doppler showing aliasing at the site of narrowing. (**c**) Continuous wave Doppler from the same patient showing raised outflow tract pressure drop in the order of 70 mmHg and mild regurgitation

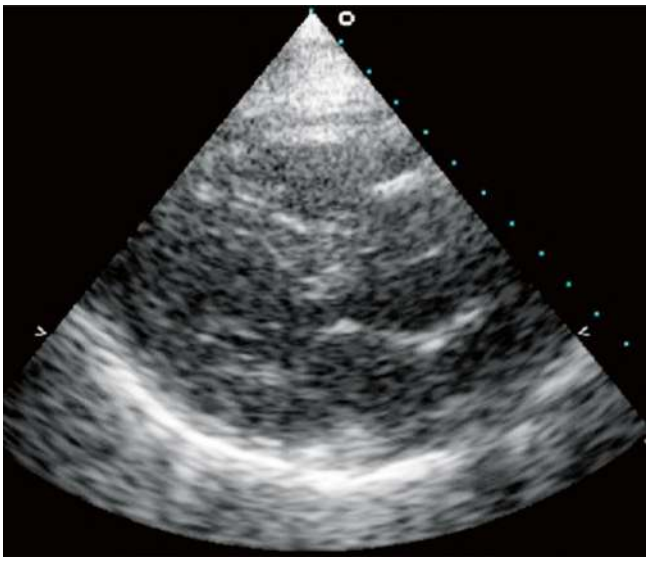


Fig. 2.10 Parasternal long axis view from an elderly lady with hypertrophied upper septum, bulging into the LV outflow tract. Note the normal aortic valve cusps

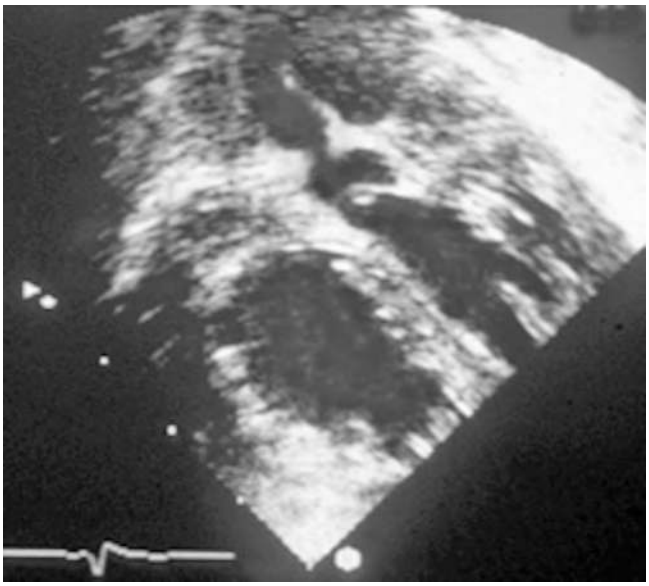


Fig. 2.11 Parasternal long axis view from a patient with supra-aortic stenosis

toms, stress echo is an ideal diagnostic tool for establishing the relationship between potential outflow tract obstruction and symptoms. This condition is discussed in greater detail in Chap. 10.

4. *Supra-aortic Stenosis:* This rare congenital anomaly involves fibrous narrowing of the proximal segment of the ascending aorta distal to the coronary sinuses. It should be diagnosed early in life from routine 2D images with the color Doppler showing localized aliasing at the site of narrowing confirming the diagnosis. Continuous wave high Doppler velocity assesses the degree of stenosis. Supra-aortic stenosis occurs in association with Williams syndrome [8–10] (Fig. 2.11).
5. *Acquired Aortic Stenosis:*
   (a) *Rheumatic Aortic Stenosis:* Like mitral valve disease, rheumatic aortic leaflet involvement is associated with thickening of the edges of cuspis and commissural fusion, best seen in the short axis view. As the disease progresses, the leaflets become fibrotic and calcify, resulting in valve stenosis (Fig. 2.12). Rheumatic aortic valve disease is almost invariably associated with rheumatic mitral valve disease (Fig. 2.13). The degree of aortic stenosis is usually clinically underestimated when associated with significant mitral stenosis which become the volume limiting step before the outflow tract and the aortic valve. Isolated rheumatic aortic stenosis is very rare.



Fig. 2.12 A picture of stenotic rheumatic aortic valve with fusion of the commissures, thickening and calcification of the leaflets

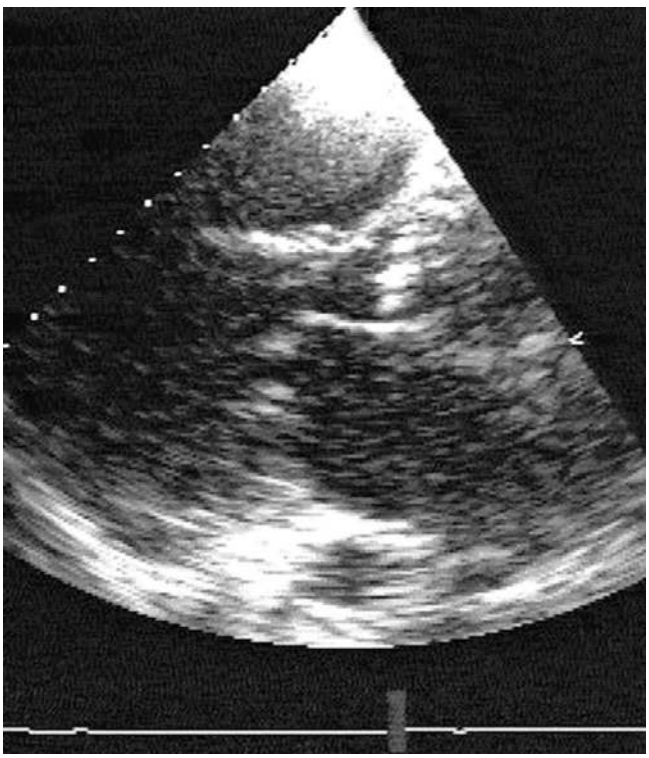


Fig. 2.13 Parasternal long axis view from a patient with combined rheumatic mitral and aortic valve disease

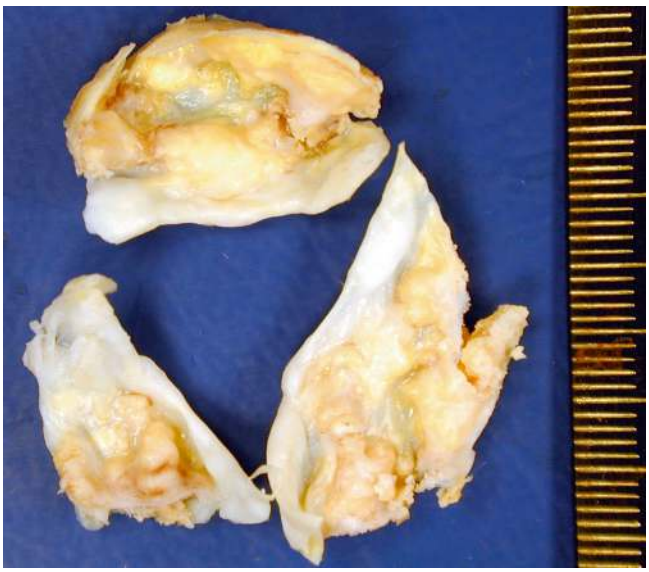


Fig. 2.14 Pathology picture from an 80-year-old patient with senile degenerative calcification of the aortic valve. Note the nodular calcification in each leaflet

(b) *Degenerative or Senile Aortic Stenosis:* This results from calcium deposition on the aortic surface of the valve [11]. As with the mitral valve, calcification in the elderly affects the base and slowly involves the body of the leaflets whereas with rheumatic disease, the opposite occurs and the commissures fuse with calcification [12]. The calcium is deposited as large lumps within the body of each leaflet (Figs. 2.14 and 2.15). The exact etiology of calcific aortic stenosis is not clear. While atherosclerosis with its known risk factors was thought to be an important mechanism, recent findings and meta-analyses are shedding doubt over this theory [13, 14]. In addition, almost 50% of patients with calcific aortic stenosis do not have concomitant atherosclerotic coronary disease to suggest a uniform pathology [15]. A recent evidence has shown a relationship between Lipoprotein a and aortic stenosis [15]. Calcification, identified by echo-dense zones, can be categorized as mild (isolated small echo-dense spots), moderate (multiple larger spots), or severe (widespread thickening and calcification of all cusps). Calcific aortic stenosis is an increasingly important disabling problem in an aging population, affecting 2% of people aged >65 years [11] (Video 2.2).

(c) *Cardiac Amyloidosis*: up to 4–16% of patients >65 years of age undergoing transcatheter aortic valve replacement may be diagnosed with transthyretin cardiac amyloidosis. Cardiac amyloidosis is caused by the extracellular deposition of amyloid fibrils in the heart, a process that

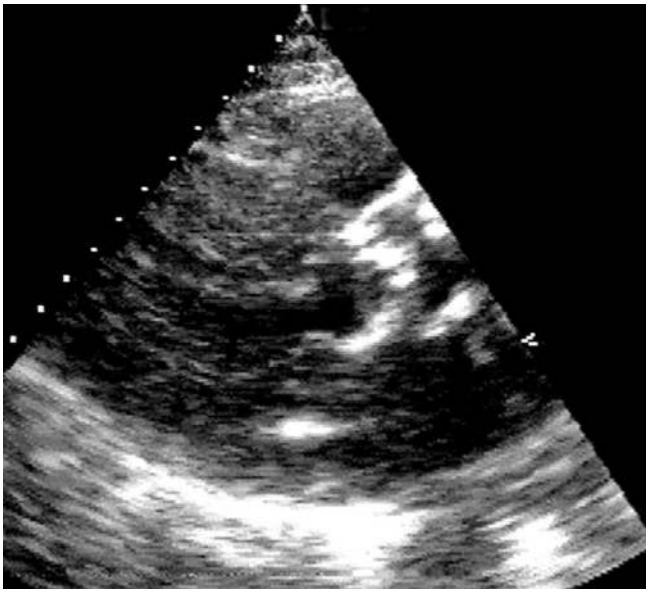


Fig. 2.15 Parasternal long axis view from a patient with calcific AV disease. Note the extent of calcification on the leaflets and the root as well as the mitral annulus

can involve not only the myocardium but also other structures. As such, the infiltrative disease may involve the cardiac valves and shows a high prevalence with aortic stenosis. Many clinical and imaging red flags have been described to assist in recognizing this entity, particularly the presence of granular sparkling myocardium, pericardial effusion, reduced mitral annular s', low-flow low-gradient phenotype, and reduced longitudinal strain with apical sparing [16, 17].

Pathophysiology

Significant aortic stenosis represents a fixed resistance to left ventricular ejection. It results in increased stroke work and hence hypertrophy which may be greater than in the coronary vascular bed, leading to subendocardial ischemia and later fibrosis. The latter is a progressive condition that leads to increased ventricular predisposition to dysfunction and arrhythmias, even in patients with normal diastolic pressures. Aortic calcification may extend to the anterior (aortic) leaflet of the mitral valve. The calcification process may spread to the upper septum to cause conduction disturbances and possibly complete heart block. Later, with the development of severe ventricular disease, the cavity may dilate and its systolic function deteriorate. This results in a rise in filling pressures, functional mitral regurgitation, and signs of heart failure and pulmonary congestion [18].

Assessment of Aortic Stenosis Severity

1. *Extent of Leaflet Separation:* An average value of aortic leaflet separation with respect to the aortic root diameter on an M-mode recording gives an idea about the severity of stenosis. The normal value is in the order of 70%, mild stenosis 50%, and moderate-to-severe stenosis <30% of the aortic root diameter. This method has its obvious limitations, with valve stenosis being overestimated in patients with severe leaflet calcification and those with significant left ventricular disease and low cardiac output [19–21].
2. *Anatomic Valve Area (AVA):* the parasternal short axis window at the level of the aortic valve may allow for direct measurement of the smallest aortic valve area through which blood is forced to pass. Though this assessement is limited by finding a good echocardiographic window, it is more reliable than other grading methods based on hemodynamics, since it may overcome their limitations in cases of low gradient aortic stenosis. As such, AVA values of less than 1 cm^2 are related to a severe aortic stenosis.
3. *Continuous Wave Doppler (CW):* This is the current conventional non-invasive mean for assessing aortic stenosis severity. The peak pressure drop across the aortic valve provides instantaneous assessment, using the modified Bernoulli equation (pressure drop across the aortic valve equals 4 times the recorded squared velocity; $\Delta P = 4V^2$) [22]. This way of assessing aortic pressure has limitations particularly when compared with catheter obtained pressures. Continuous wave pressure drop values are often higher than the peak to peak (left ventricular-aortic) pressure obtained by the pull-back technique possibly because the aortic site of the latter being often the velocity recovery area in the ascending aorta, thus underestimating the difference [23, 24]. When comparing the mean aortic pressure, values of the two techniques are usually close with a mean pressure gradient of 40 mmHg representing severe aortic stenosis in patients with normal LV systolic function and no significant aortic regurgitation. CW Doppler velocities may underestimate aortic pressure drop if the ultrasound beam is not parallel to the high velocity jet (velocity varies inversely with cosine between the two) [25, 26]. In patients with severe left ventricular disease, irrespective of its etiology, the modified Bernoulli equation may underestimate the degree of aortic stenosis because of the limited ability of the left ventricle to generate enough pressure to overcome the valve resistance. Thus, in these patients, the continuity equation is a better method for

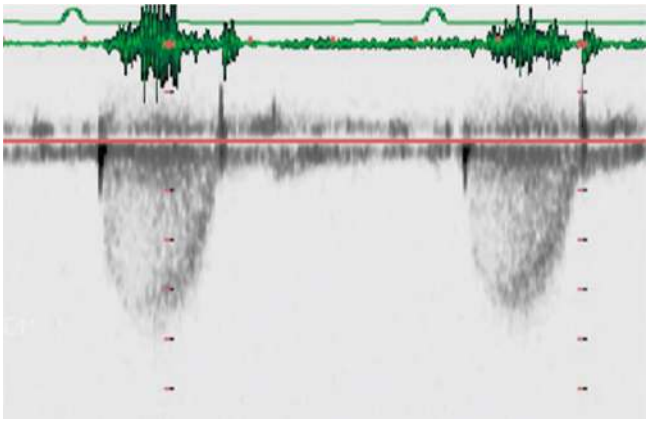


Fig. 2.16 Continuous wave Doppler recording from a patient with severe aortic stenosis and a pressure drop of 90 mmHg

quantifying the severity of stenosis [27] and providing more information (Fig. 2.16).

4. *The Continuity Equation* is the best method for assessing valve area. The blood volume passing through the subvalvular region is the same as that passing through the valve, therefore the ratio of blood flow velocities between aortic and subaortic areas is inversely proportional to the ratio of the cross-sectional area. Subaortic area is calculated $(\text{Diameter}/2)^2 \times 3.14$. Aortic flow is measured from the (VTI) calculated from the CW Doppler and subaortic VTI from that of the PW Doppler.

$$\begin{aligned}\text{Aortic flow} &= \text{Aortic velocity integral} \times \text{Area}_{\text{AV}} \\ &= \text{Subvalvar velocity integral} \times \text{Area}_{\text{LVOT}}.\end{aligned}$$

Since ejection period is almost the same in the two areas, peak velocity may be used rather than integral. A velocity ratio < 0.25 (subaortic) has been shown to be 94% sensitive in detecting severe aortic stenosis [28–31]. This method is ideal for assessing severity of aortic stenosis in patients with poor ventricular systolic function and low-flow low-gradient state (Figs. 2.17 and 2.18).

5. *Color Flow Doppler* demonstrates the exact location of the narrowing, outflow tract versus valve. The narrowest jet width signifies the level at which maximum stenosis is, particularly in patients with combined calcified aortic valve leaflet and subvalvular muscular hypertrophy (Fig. 2.19).

Symptoms and Physiological Disturbances

Breathlessness: In patients with aortic valve disease, symptoms are mainly caused by the resulting ventricular disease. Breathlessness in aortic stenosis is due to raised left ventricular end-diastolic pressure and consequently raised left atrial

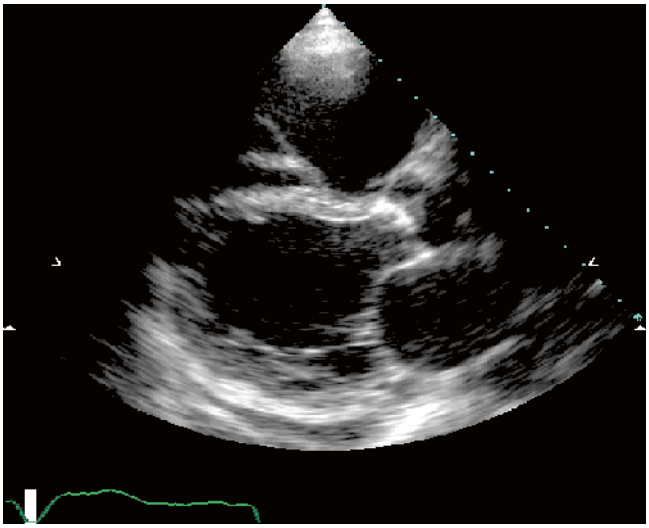


Fig. 2.17 Parasternal long axis view from a patient with calcified aortic valve and dilated ventricle with poor systolic function

pressure that initially appears on exertion then later at rest indicating severe additional left ventricular disease [32]. Mitral regurgitation secondary to outflow tract obstruction also raises left atrial pressure and contributes to patients' breathlessness (Fig. 2.20).

Chest Pain: This is similar to that due to coronary artery disease but the underlying disturbed physiology is mismatch between the bulk of the myocardial mass and the coronary vascular bed as well as the direct effect of abnormal ventricular segmental relaxation on coronary flow in diastole (Fig. 2.21). This has been shown to be associated with significant broadening of QRS duration which normalizes after valve replacement as does segmental ventricular function [33].

Syncope: Syncope in aortic stenosis patients is caused by either exertion-related hypotension as a result of the peripheral vasodilatation and the fixed resistance at the aortic valve level, AV conduction block by calcification, carotid sinus hypersensitivity, or periods of ventricular arrhythmia or even fibrillation. Similar mechanisms underlie the commonly known sudden death in patients with aortic stenosis.

Clinical Signs: A small Bernheim "a" wave might appear in the venous pulse associated with left atrial hypertrophy due to left ventricular hypertrophy. Recent Doppler echocardiographic studies disproved the old belief that Bernheim "a" wave represents right ventricular inlet obstruction and confirmed it to be a sign of atrial cross talk or atrial interaction (Fig. 2.22). Aortic stenosis does not result in raised venous pressure until late when patients develop ventricular disease [34, 35].

Management of Aortic Stenosis

Mild aortic stenosis associated with normal carotid pulse, short systolic murmur with both components of the second

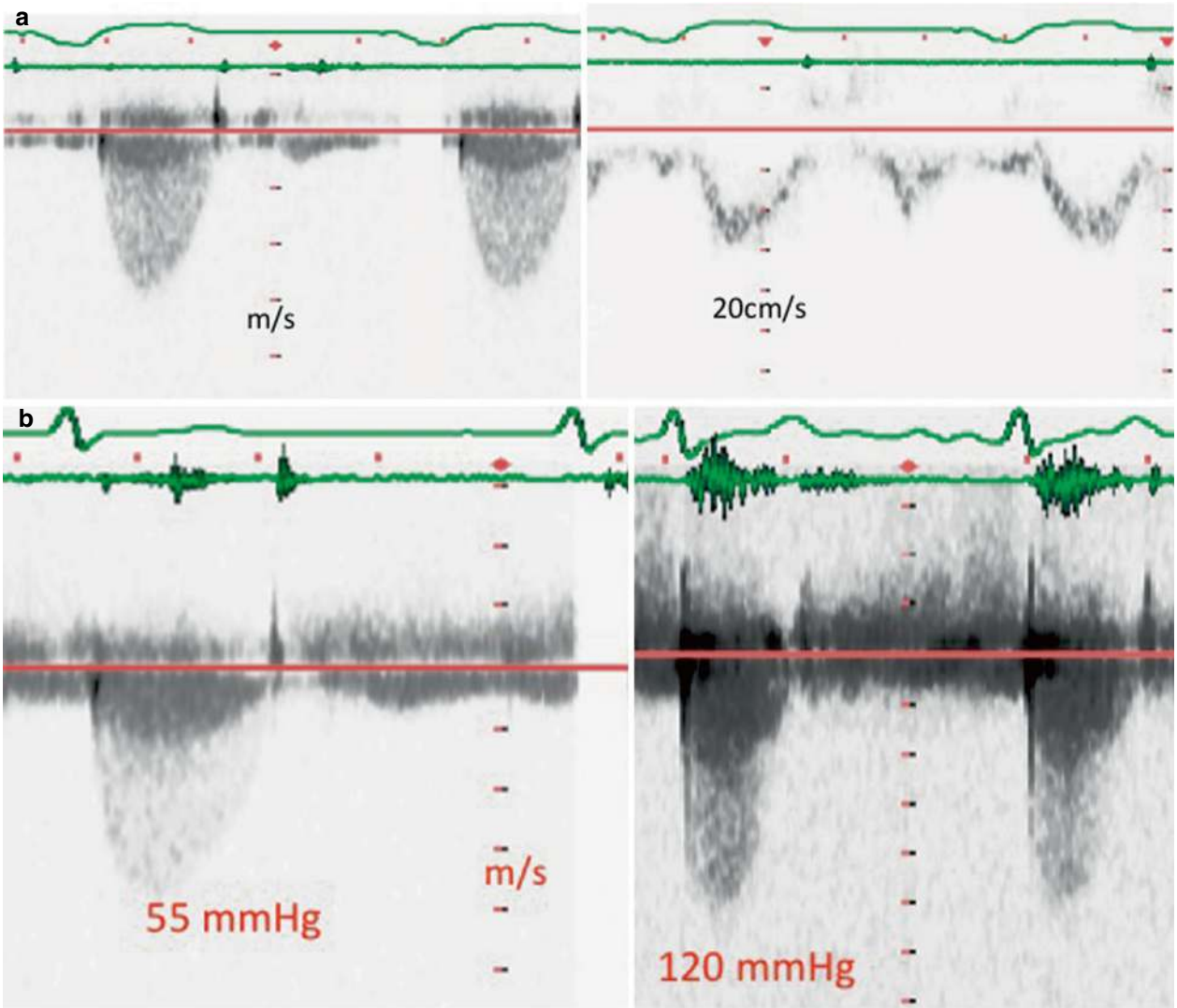


Fig. 2.18 (**a**) Continuous wave Doppler (*left*) from the same patient and pulsed wave Doppler velocities of the LV outflow tract (right). Note the >5 times increase in velocities between the two areas consistent with severe aortic stenosis. (**b**) CW Doppler from a patient with moderate aortic stenosis at rest (*left*) and peak stress (*right*) at the time of symptom development. Note the significant rise in gradient

heart sound audible is managed medically and followed up regularly with an echocardiogram for assessment of aortic pressure drop and left ventricular function. Prophylactic antibiotics are recommended before dental and surgical procedures in high-risk patients [36]. Significant aortic stenosis confirmed by anatomical valve abnormality and a mean pressure drop across the valve of >40 mmHg (valve area of 1 cm^2 or less) in a symptomatic patient is recommended for valve replacement surgery when cardiac output is normal. A diagnostic coronary angiogram, conventional or using CT technique for low atherosclerosis risk patients, is always required in those with aortic stenosis who are >40 years of age. Asymptomatic patients with incidental findings of severe aortic stenosis and a mean gradient >40 mmHg may need to be objectively assessed with a provocation test, i.e. stress echocardiography, for symptoms and bloop pressure drop. Symptom development with exercise has recently been suggested as a marker of a need for surgery [37]. Intervention is also recommended in asymptomatic patients with severe aortic stenosis with left ventricular dysfunction (<50%) and patients with very severe forms of aortic stenosis (mean gradient >60 mmHg), severe calcification or rapid disease progression and those with incipient signs of congestion (elevated BNP levels). In patients with calcified valve leaflets but with low flow and pressure drop due to left ventricular dysfunction, stress echocardiography assist in identifying those patients who need valve replacement. A valve area of <1 cm^2 that remains unchanged with stress is consistent with severe stenosis irrespective of the peak transvalvar pressure drop [38]. Optimum management of heart failure and fluid retention before surgery is usually advised. Finally, conditions such

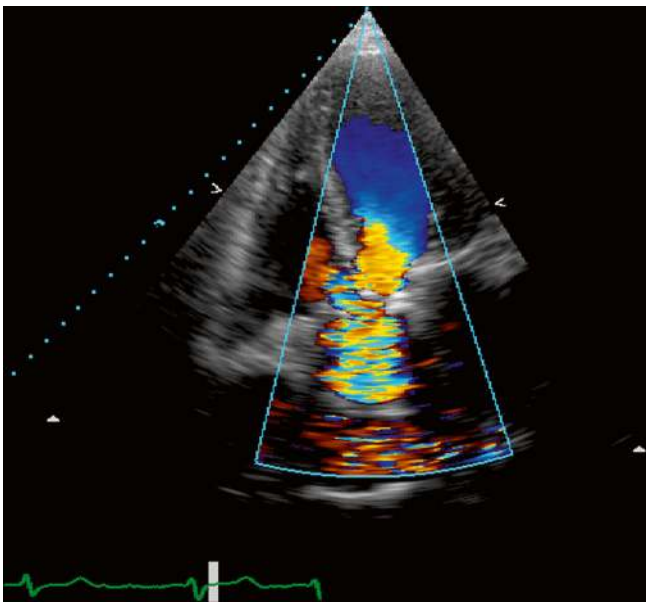


Fig. 2.19 Color flow Doppler from a patient with aortic stenosis. Note the disturbed flow morphology due to the disrupted outflow tract by the calcified leaflets

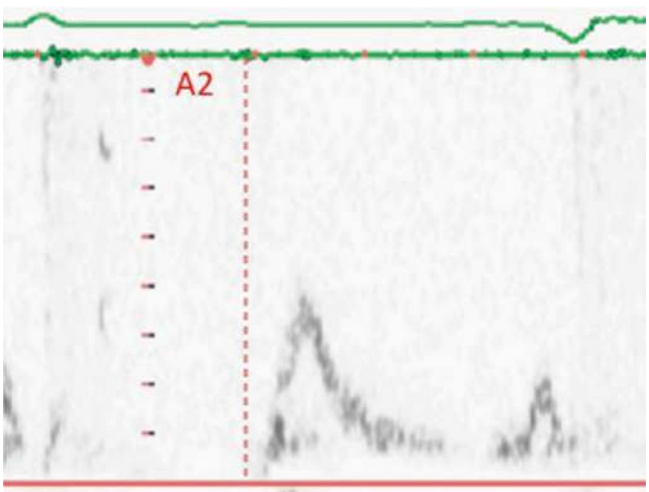


Fig. 2.20 Transmitral Doppler flow velocities from a patient with aortic stenosis limited by exertional breathlessness demonstrating restrictive filling pattern consistent with raised left atrial pressure

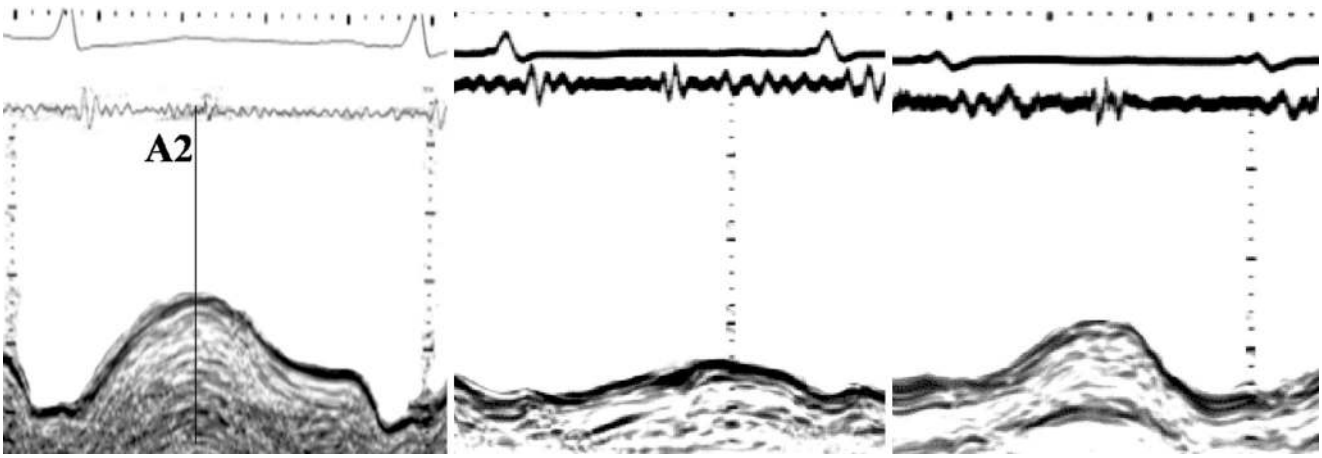


Fig. 2.21 Septal LV long axis recording from a normal (*left*) and a patient with significant aortic stenosis before (*middle*) and after valve replacement (*right*). Note the normalization of long axis lengthening velocities after surgery

as cardiac amyloidosis have been shown to be associated with an atypical form of low-flow low-gradient aortic stenosis, due to the presence of preserved ejection fraction but with low stroke volumes. This entity has been called low-flow low-gradient aortic stenosis with preserved ejection fraction or 'paradoxical' low-flow low-gradient aortic stenosis, and is associated with conditions of significant diastolic impairment.

Aortic Valvuloplasty: This is only advisable in infants and young children in whom the valve leaflets are thin and pliable, but in the majority a valve replacement is required at a later stage [39]. In the elderly, aortic valvuloplasty is not recommended in the management of stenotic valves. Open aortic valvotomy carries similar risks and benefits to valvuloplasty. The problem for the two procedures is the dysplastic valve leaflets for which 2D echo imaging provides more detailed analysis on the extent of disturbed anatomy and leaflet behavior. If ever needed, aortic valvuloplasty may serve as a bridge to complete valve replacement in patients with ignored aortic stenosis who present in late stage heart failure [40].

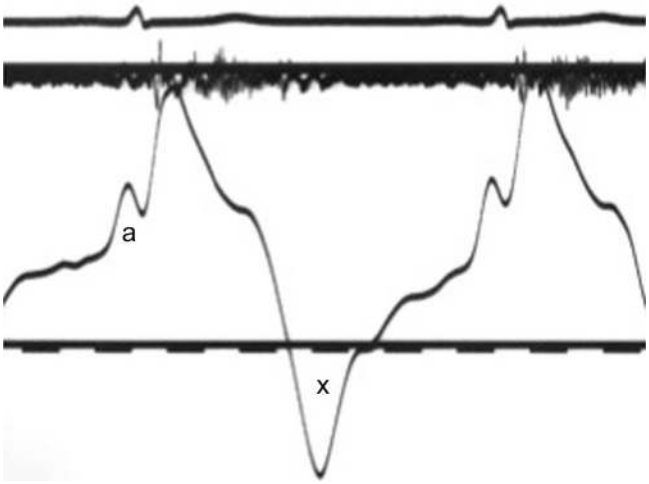


Fig. 2.22 Jugular venous pulse from a patient with aortic stenosis and LV hypertrophy showing Bernheim "a" wave followed by an X descent. Low-flow–low-gradient aortic stenosis with reduced left ventricular function Occurs when the AVA is less than 1 cm2, peak velocity is under 4 m/s, and mean gradient is below 40 mmHg, typically in patients with LV ejection fraction (EF) < 50%. Reduced flow in these cases can be confirmed by a stroke volume index (SVi) of 35 mL/m2 or less, as outlined by the European Society of Cardiology guidelines. Dobutamine echocardiography (DSE) is used to distinguish true severe AS from pseudo-severe AS by assessing contractile reserve. DSE involves administering dobutamine in increasing doses while continuously monitoring ECG, blood pressure, and echocardiographic data. The key diagnostic feature of DSE is the presence of contractile reserve, defined as a 20% or greater increase in stroke volume. In true severe AS, transaortic gradients increase significantly, while AVA remains small. In pseudo-severe AS, gradients stay low, and AVA increases. In cases where gradient and AVA changes are minimal, no clear distinction between the two conditions can be made. To standardize the comparison, a new parameter—the projected AVA at a normal flow rate of 250 mL/s—has been proposed. Low-flow–low-gradient aortic stenosis with preserved left ventricular functionIs characterized by an AVA <1 cm2, peak velocity <4 m/s, and mean gradient <40 mmHg despite a normal LV EF, known as "paradoxical" low-flow–low-gradient severe AS, It occurs in patients with hypertrophied, small ventricles, leading to reduced flow. It is essential to exclude other causes, especially when peak velocity <3.0 m/s and mean gradient <20 mmHg. This condition is commonly seen in elderly patients with hypertension-related LV pathology. Distinguishing between pseudosevere and true severe AS is challenging, and DSE may be less helpful in these cases. Non-contrast CT for assessing valve calcification can provide additional information, with a high calcium score confirming severe AS and a low score making it unlikely. Further research is needed to refine diagnostic approaches

Aortic Valve Surgery

Aortic valve replacement is the only recommended procedure in adults, particularly with calcified cusps. The outcome is complete relief of breathlessness, angina, and syncope. Even in the presence of additional left ventricular disease, aortic valve replacement is the only choice, the results of which are very satisfactory although the risk cannot be ignored. The lower the pre-operative ejection fraction the higher the perioperative mortality in these patients; thus, optimal surgical timing is highly recommended [41–44].

Mechanical or Bioprosthetic Valves: their advantages and disadvantages have been previously outlined. Over the age of 60, there is an increasing trend to use a bioprosthetic valve as the durability has a mean of approximately 15 years and the bleeding complications of long-term anticoagulation start to rise reaching as high as 6 per 100 patients by the age of 70 years [45–47]. There is increasing interest in the use of stentless valves in the aortic position particularly in patients with additional severe left ventricular disease. The recovery of ventricular function in these patients has been found to be much faster and complete when they receive stentless valves compared to stented valves [48–50]. Stentless porcine valves have been developed in order to increase availability. These valves are treated, in the same way as the stented valves, with glutaraldehyde. The durability of these valves at 8 years is 90% which is at least 10% better than current stented porcine valves. Stentless valves have been shown to have superior hemodynamics to stented valves early after operation and postoperatively (Fig. 2.23). This has been shown in terms of improved diastolic function and reduction of left ventricular mass to the normal range [51]. Sutureless aortic valves can be used in patients who would benefit particularly from a shorter bypass time, for example, those with severe kidney dysfunction or the elderly. Perceval valves have been deployed with success in reducing aortic cross-clamp time and cardiopulmonary bypass times. Favorable haemodynamics and accepted durability are amongst the reported benefits but there is a higher trend towards permanent pacemaker implantation and lower post-operative platelet count [52].

Aortic Valve Reconstruction: The Ozaki procedure (aortic valve reconstruction using autologous pericardium) has been performed with success in experience centres. Peak gradients are reportedly lower than Perimount bioprosthesis at 1 year and 6 year follow up but a higher risk of severe regurgitation at the same time points [53].

Homografts: Long-term results of aortic homografts have proved encouraging with freedom from valve degeneration at 15 years in 75%. Both homografts and autografts have advantages in the presence of endocarditis as they contain no artificial material [54, 55]. Both valves once inserted have significantly lower incidence of endocarditis than any other valve. However, they do degenerate eventually with calcification.

Pulmonary Autograft or Ross procedure has unique features. As a living valve, it is able to grow with the patient and therefore is particularly appropriate for patients before the end of puberty. I The patient also remains free from warfarin and other forms of long term anticoagulation. The pulmonary autograft is able to withstand high stress as seen during athletic exercise with heart rates above 170 bpm, where mechanical valves become increasingly inefficient [56, 57]. A recent long term follow up of 108 adults with a median age of 38 years shows impressive long term survival

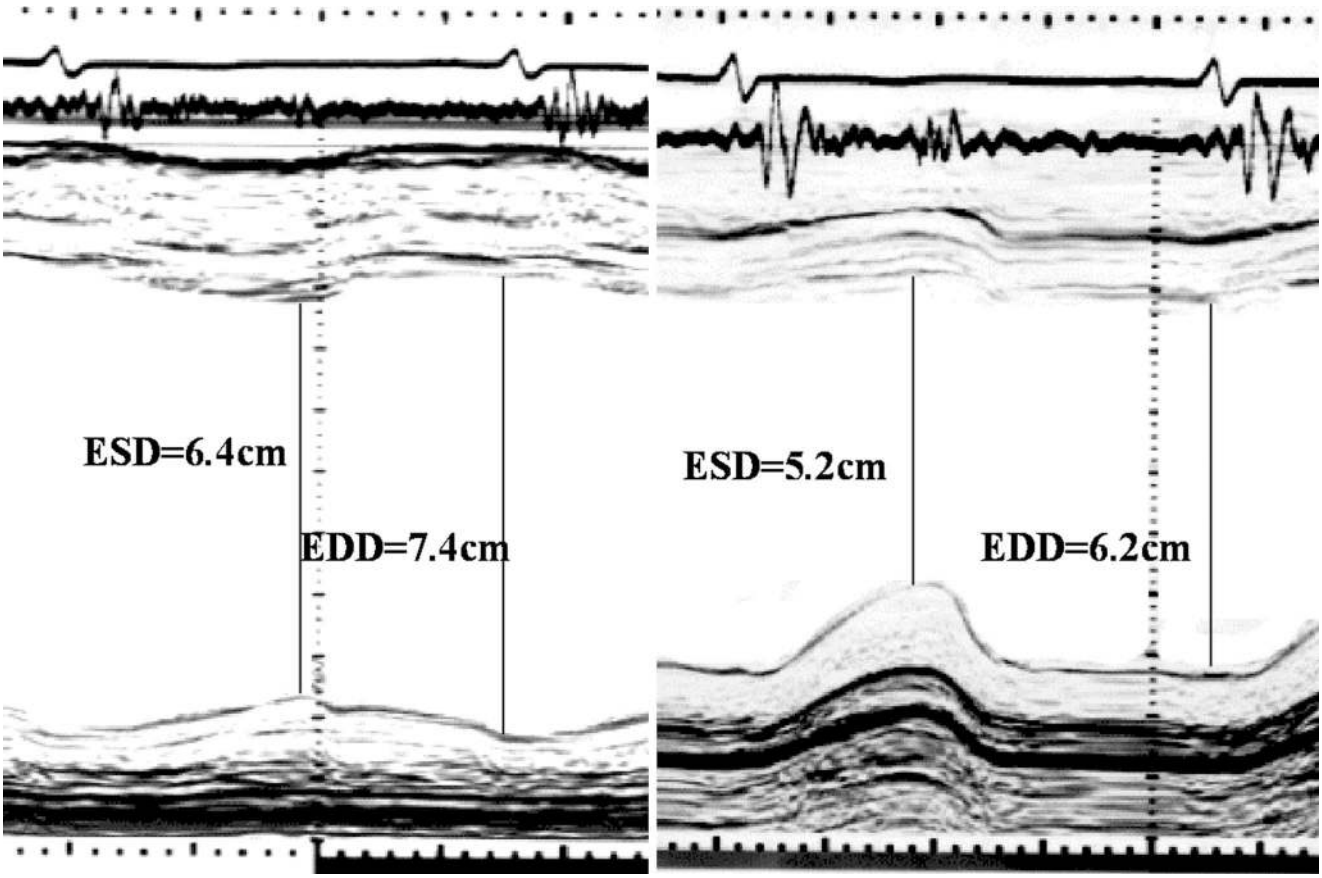


Fig. 2.23 LV minor axis M-mode from a patient with severe aortic stenosis and poor LV systolic function (*left*) and 5 days after valve replacement with a stentless substitute (*right*). Note the significant fall in end-systolic volume and recovery of posterior wall systolic function

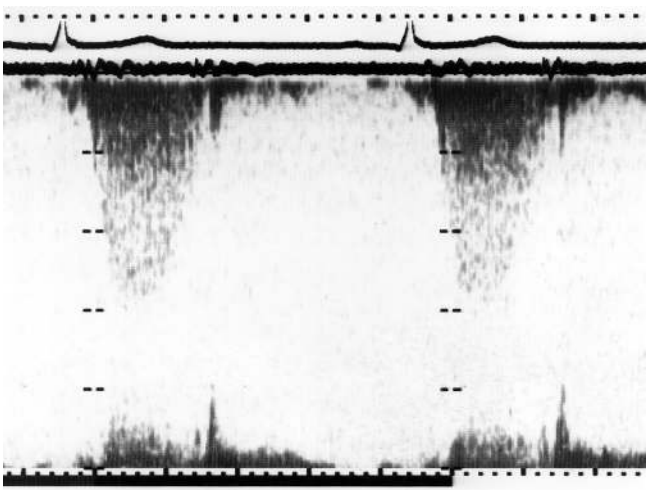


Fig. 2.24 Pulmonary homograft peak velocity by continuous wave Doppler demonstrating a peak velocity of 3.0 m/s

and freedom from reintervention well into the third decade post procedure [58]. Aortic autograft surgery is more complicated and is usually reserved for specialist centers and for patients with a life expectancy in excess of 20 years.

Pulmonary valve homograft velocities tend to increase over the early postoperative months until it settles at a value of 2–3 m/s (Fig. 2.24) [59].

The Role of Echocardiography During Aortic Valve Surgery [60, 61]

Preoperative echocardiographic examination aims at:

(a) Assessing and quantifying the severity of aortic valve stenosis.
(b) Assessment of the extent of left ventricular disease.
(c) Measuring aortic root diameter to guide the size of the valve substitute.
(d) Measuring the pulmonary valve annulus dimensions when pulmonary aortic autograft procedure is planned.
(e) Assessing aortic root and ascending aorta diameter that may be included in the surgical procedure, particularly in patients with bileaflet aortic valve disease who may have additional significant aortopathy and enlargement of ascending aorta.

(f) It may suggest the presence of additional coronary artery disease, based on the presence of myocardial scaring and/or segmental dyskinesia. Coronary angiography should confirm or exclude this.
(g) Identifying additional valve lesions not as or part of the same pathology.

Intraoperative Echocardiography: Transesophageal echo at the beginning of surgery usually confirms transthoracic findings, although pressure drop estimation is difficult due to the technical limitation of aligning the continuous wave Doppler beam with the left ventricular outflow tract axis. Its additional value is mainly for excluding other lesions before operation, i.e., a small VSD or other aortic shunts in patients with congenital valve disease or those with prior history of endocarditis. At the end of the operation, echocardiographic examination helps in confirming perfect placement of the valve substitute and in excluding any para-prosthetic regurgitation that can be dealt with before closing the chest. It also assesses the amount of entrapped air inside the ventricle during the de-airing stage. In patients with difficulty for weaning from the bypass machine, echocardiography assesses the extent of ventricular loading. Finally, careful examination of the proximal segment of the right and left coronary arteries may identify causes for compromised coronary flow which may be contributing to failure of ventricular recovery of function.

Postoperative Echo Examination: Echocardiography is the investigation of choice for assessing ventricular function in the early postoperative period. In patients with slow recovery, transthoracic or transesophageal echo provide detailed evaluation of the valve as well as ventricular function. Patients with high filling pressures may settle with vasodilators whereas those with under-filled ventricles require fluid loading. A high pressure pericardial collection irrespective of its volume may significantly contribute to the clinical deterioration in the early postoperative course. This should be drained in order to secure rapid recovery of cardiac function. Likewise, progressive increase of pericardial collection over the early postoperative period suggests a need for careful monitoring and a need for drainage. Patients who develop high venous pressures and do not respond to diuretic therapy may have signs of postoperative tight pericardium, in the absence of pericardial effusion. A consistent increase in intrapericardial pressure leads to phasic (inspiratory) right heart filling and ejection followed by the left heart (being expiratory). This condition is benign and usually settles within days of the operation without a need for surgical intervention.

Long-Term Follow-Up: Echocardiography is the investigation of choice for the follow-up of patients after aortic valve surgery. Annual transthoracic echocardiographic examination with Doppler provides detailed assessment of valve function as well as left ventricular performance. It should help in discriminating between valve dysfunction and deterioration of ventricular function as two possible causes for symptoms in such patients.

Transcatheter Aortic Valve Implantation (TAVI) Procedure

Patients older than 75 years old or with with high surgical risks for valve replacement with cardiac or noncardiac comorbidities can now be offered TAVI procedure. Ideal patients for this procedure are those with significantly impaired left ventricular function, concomitant renal impairment, or pulmonary hypertension. This procedure aims at replacing the stenotic aortic valve by a bioprosthesis mounted on a stent. This system is introduced to the aortic root usually retrogradely transfemorally (Videos 2.3 and 2.4). Clinical outcome of this procedure has been shown to be satisfactory even in the long term follow-up. Results have shown significant improvement of left ventricular function, reverse remodeling, and significant improvement of symptoms [62, 63].

Indications for TAVI have recently expanding to moderate-risk patients and even to low-risk patients, with median term follow-up proving to be satisfactory. Particularly, hard clinical endpoint such as mortality, disabling stroke and rehospitalization have proved TAVI to be non-inferior to surgical aortic valve replacement. On one hand, TAVI procedure seems to be more commonly associated with a need of pacemaker implantation and paravalvular leaks, also depending on the type of valve used whether ballon expandable or self expandable, while on the other hand acute kidney injury, severe bleeding and new-onset atrial fibrillation appear to be more frequent after the surgical replacement [64–66].

2D and 3D echocardiographies play a pivotal role in choosing such patients and in monitoring their heart during the procedure [67–69]. Attention is paid to:

1. Thorough assessment of the aortic valve leaflets, extent of calcification, and the severity of stenosis.
2. Aortic root dimensions are carefully measured as well as sino-tubular junction and proximal ascending aorta.
3. Intra-procedural transesophageal echo scanning helps in close monitoring of the guide wire insertion, balloon placement before deployment of the valve.
4. Residual valve regurgitation should be carefully assessed using conventional color and continuous wave Doppler.
5. Other related problems or complications should be easily picked up by echocardiography (Fig. 2.25).

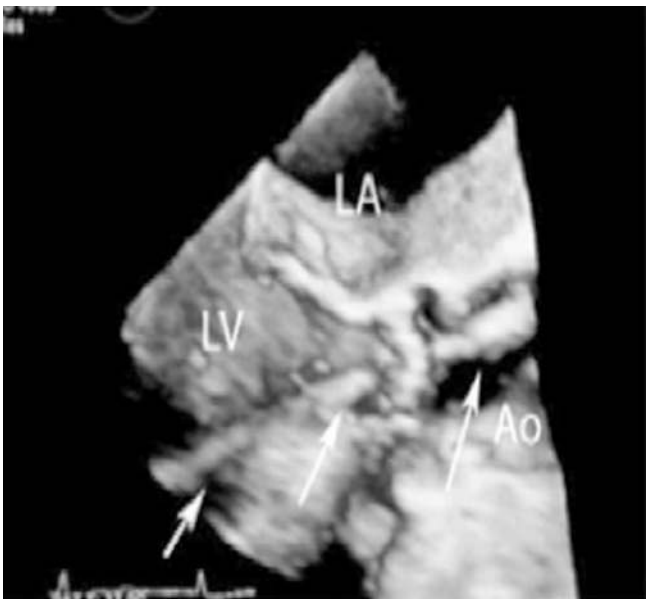


Fig. 2.25 *TAVI* 3D echo during TAVI procedure showing the anatomical structures of the LV outflow tract area and aortic valve as well as the catheter crossing the valve



Fig. 2.26 Pathology picture of rheumatic aortic valve from a patient with severe aortic regurgitation showing leaflet thickening and retraction due to extensive fibrosis

Asymptomatic Severe Aortic Stenosis

Patients with severe aortic stenosis may claim being asymptomatic and hence may not fall into the guidelines category requiring surgical valve replacement. These patients represent a clinical challenge since long-standing significant aortic stenosis results eventually in left ventricular dysfunction which could become irreversible. Therefore, careful monitoring of such patients, for severity of valve stenosis as well as ventricular dysfunction, is of great importance [70–73]. Once left ventricular ejection fraction starts to decrease, asymptomatic patients get an indication for intervention. Similarly, patients with very severe forms of aortic stenosis (mean gradient >60 mmHg), severe calcification or rapid disease progression and those with incipient signs of congestion (elevated BNP levels) are recommended for intervention. Finally, development of symptoms on exercise test or significant blood pressure drop during the same investigation are suggestive of a need for valve replacement.



Fig. 2.27 Transesophageal echo from a young patient with combined rheumatic mitral and aortic valve disease demonstrating aortic regurgitation

Aortic Regurgitation

Etiology

Aortic regurgitation may result from different pathologies affecting either the valve leaflets or the aortic root:

1. *Rheumatic Involvement* of the aortic valve results in thickening of the cusps and fusion of the commissures with retraction of the leaflets and hence regurgitation (Figs. 2.26 and 2.27) [32].
2. *Aortic Leaflet Prolapse*: Aortic prolapse is a rare presentation that results from myxomatous degeneration of the aortic leaflets and their diastolic prolapse into the outflow tract of the left ventricle. This is better viewed from the parasternal long axis images as the leaflet tips meet below the aortic attachment level (Fig. 2.28). Aortic prolapse may be associated with other conditions, e.g., mitral valve prolapse, bicuspid aortic valve disease, or Marfan's disease. Aortic prolapse may also represent a conse-

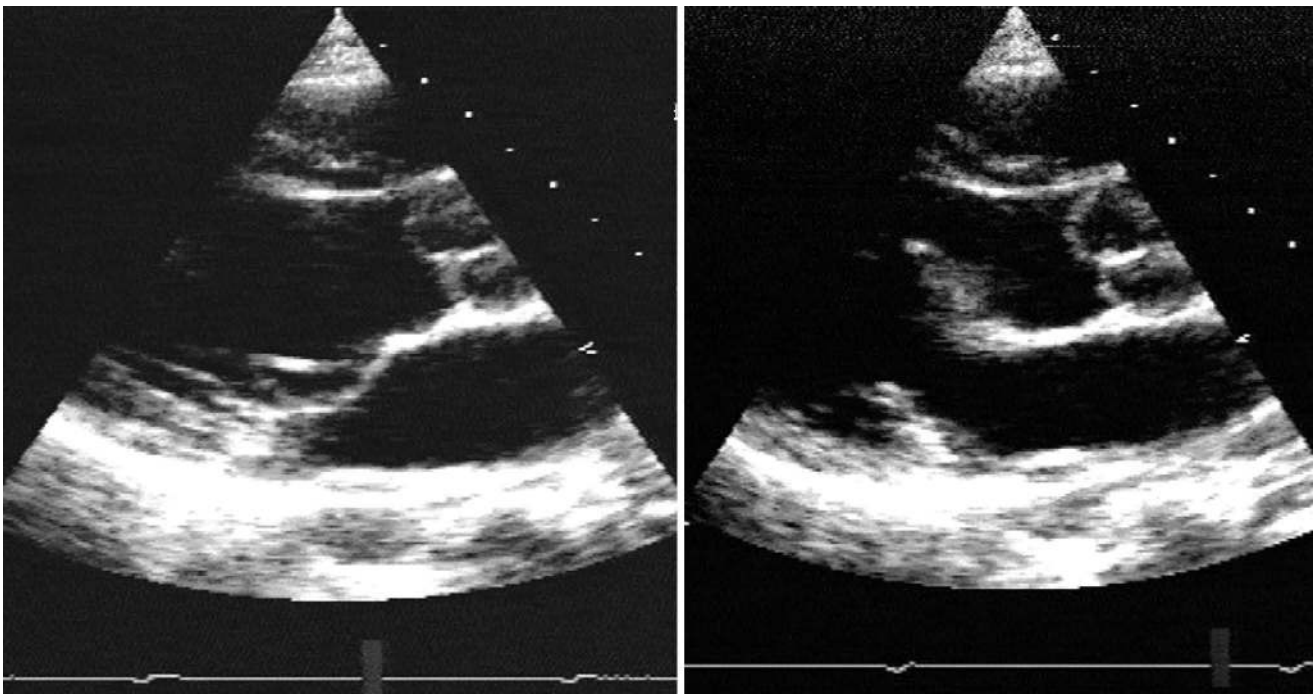


Fig. 2.28 Parasternal long axis view from a patient with aortic regurgitation secondary to leaflet prolapse. Note the level of leaflet prolapse with respect to their attachment points to the aorta

quence of aortic valvuloplasty for valve stenosis in infants and children [74] (Video 2.5).

3. *Aortic Valve Infection (endocarditis)*: With infection, there is formation of vegetations on the surface of the leaflets which can break off and embolize. The leaflets may also perforate. Valve infection complicated by vegetation may result in leaflet prolapse in diastole into the left ventricular outflow tract, causing aortic regurgitation. Aortic root abscess formation is associated with distortion of the valve leaflet and sinus morphology and is much more commonly associated with conduction disturbances (Figs. 2.29, 2.30, 2.31, and 2.32) [75].
4. *Dilatation of Aortic Root* resulting from aneurysm of the ascending aorta, commonly seen with Marfan's syndrome, or isolated medial necrosis (Figs. 2.33 and 2.34). Aneurysmal formation may rarely involve the coronary sinuses resulting in blood stagnation and aortic regurgitation (Fig. 2.35) [76, 77]. Aortic root dilatation may also be associated with more general connective tissue disease, e.g., ankylosing spondylitis, rheumatoid arthritis, Reiter's syndrome, or relapsing polychondritis.
5. *Dissecting Aneurysm:* This may involve the aortic root or proximal ascending aorta. The cause of aortic regurgitation in the two conditions may differ. While in the former the flap tends to hold the cusps opened in diastole, the dissection and false lumen in the latter tend to disturb the normal aortic vortices that close the valve cusps in early diastole (Figs. 2.36, 2.37, and 2.38).
6. *Associated Ventricular Septal Defect:* Small subaortic ventricular septal defect resulting in subaortic blood turbulence may be spontaneously closed by a prolapsing aortic leaflet. This results in significant failure of competent leaflet coaption and hence aortic regurgitation (Fig. 2.39).
7. Syphylitic aortitis causes aortic aneurysm and dilatation of valve area that may involve the coronary ostia.

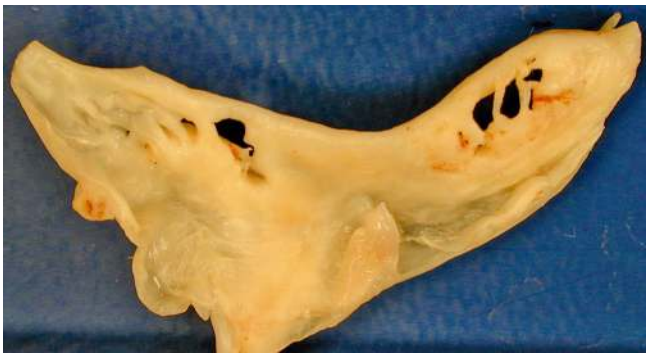


Fig. 2.29 A pathology section from a patient with infective endocarditis causing leaflet perforation and severe aortic regurgitation

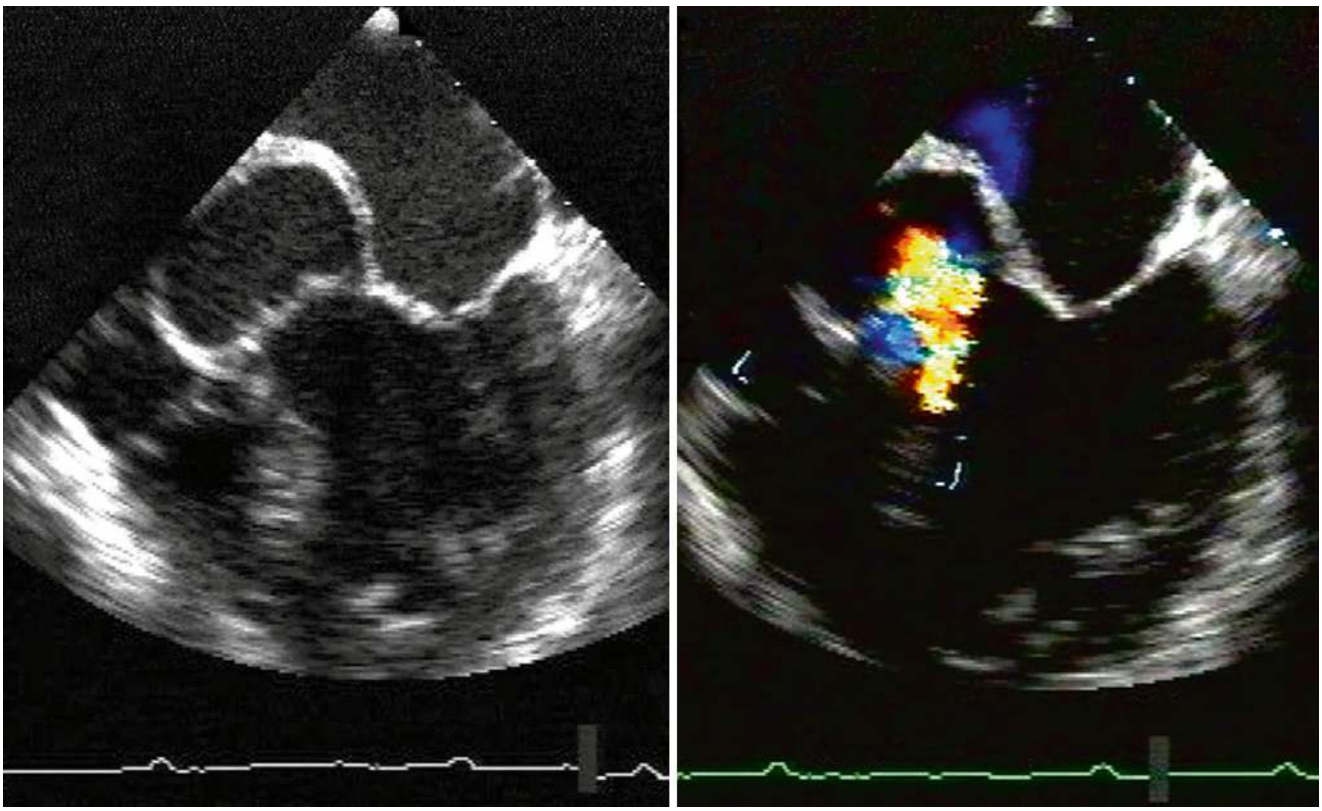


Fig. 2.30 TOE from a patient with severe aortic regurgitation secondary to bacterial endocarditis. Note the abscess cavity in the aortic root which changes its size and shape during the cardiac cycle



Fig. 2.31 Pathological specimen from a patient with aortic regurgitation secondary to infective endocarditis showing vegetation attached to the valve leaflet

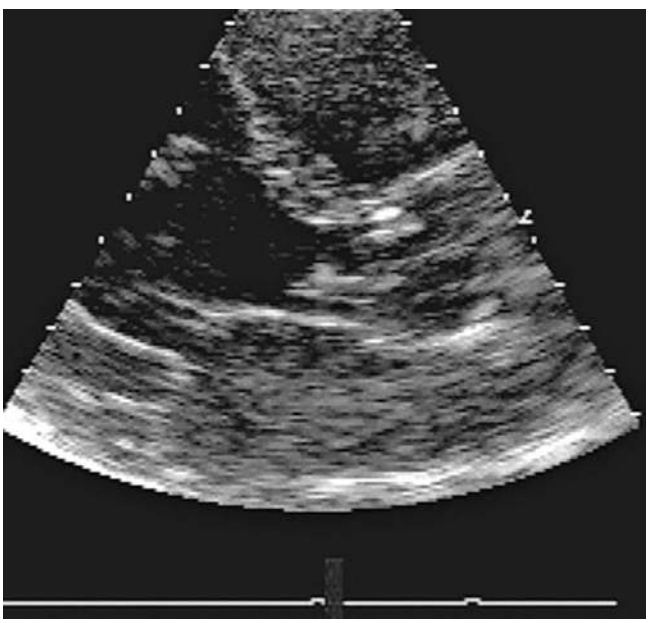


Fig. 2.32 Parasternal long axis view from a patient with infected aortic valve showing a 2-cm long vegetation attached to the aortic cusp and moves freely in the aorta

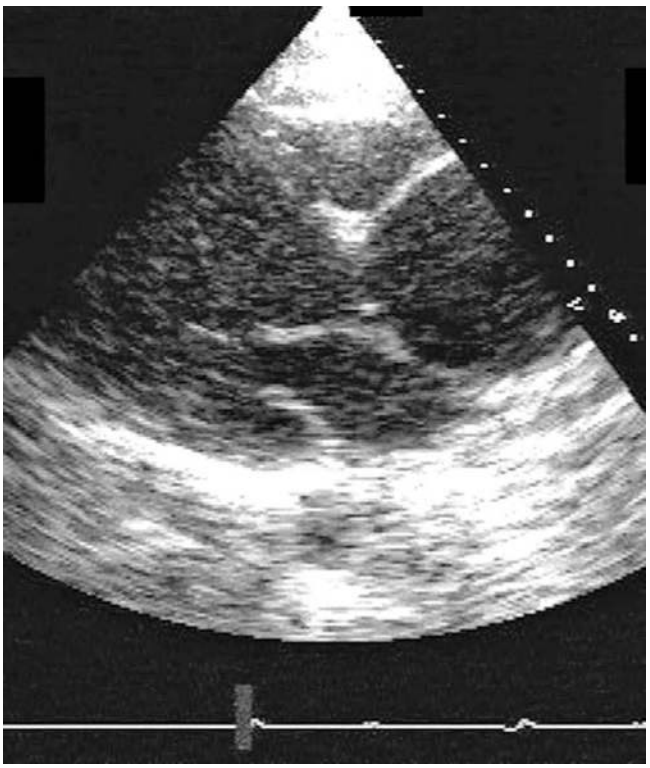


Fig. 2.33 Parasternal long axis view of the LV outflow tract and ascending aorta showing a fusiform aneurysm causing and aortic regurgitation

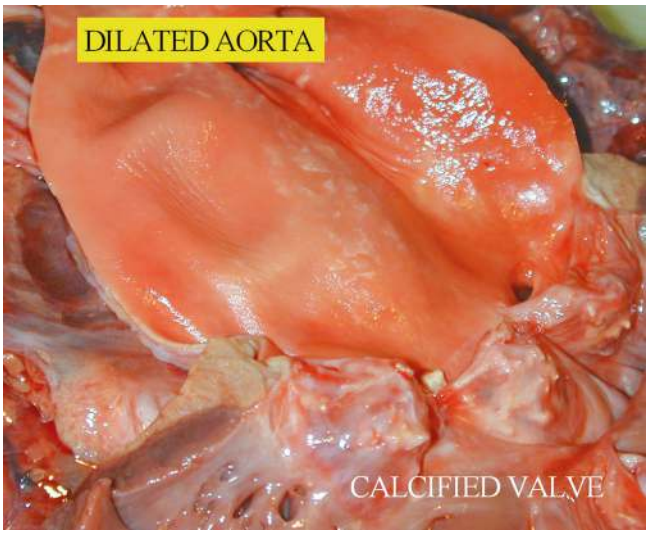


Fig. 2.34 Pathological section of the aortic root from a patient with aneurysm showing generalized dilatation of the wall with calcification of the aortic valve

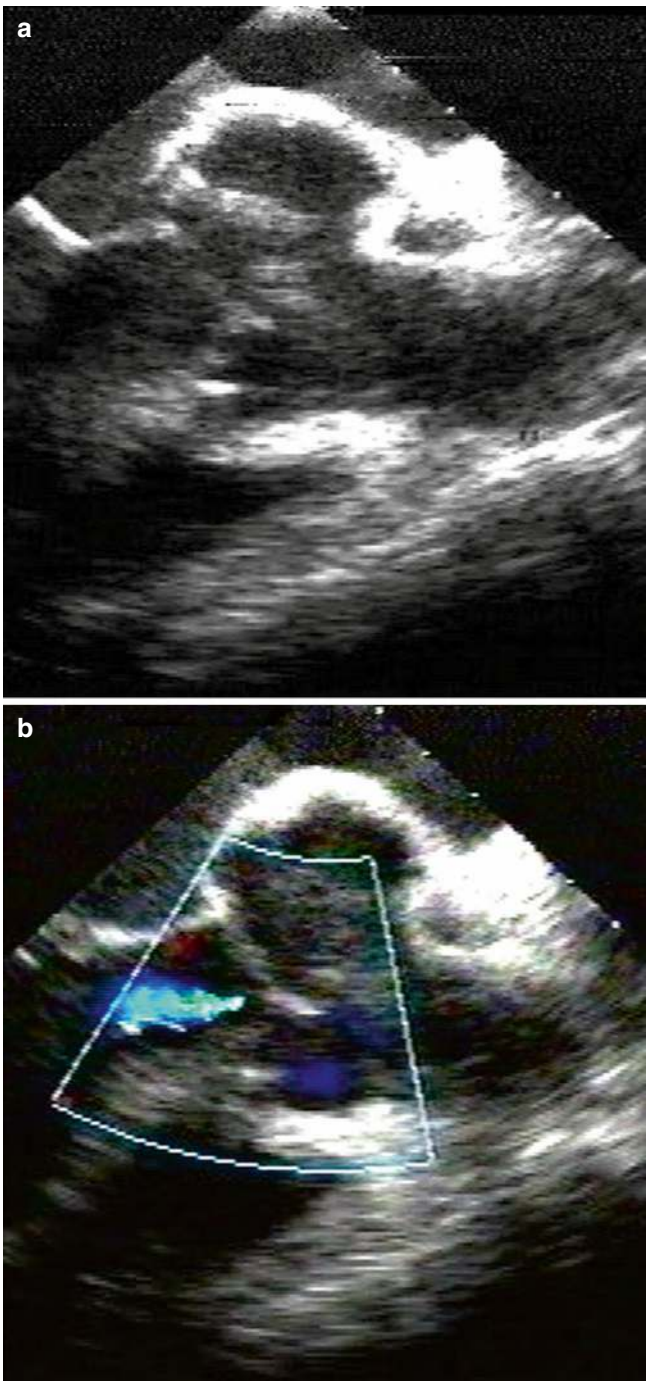


Fig. 2.35 (**a**) Parasternal long axis view from a patient with aneurysmal aortic sinuses with a small clot in the right coronary sinus (cauliflower appearance). (**b**) Mild aortic regurgitation



Fig. 2.36 Pathological section from a patient with dissection in the proximal ascending aorta forming a double barreled aorta

Pathophysiology

Aortic regurgitation is associated with a large left ventricular stroke volume that leads to cavity dilatation. At the same time, the duration of systole is increased, so that the time for coronary filling is correspondingly reduced. In severe regurgitation, the aortic to left ventricular pressure difference in late diastole may be low enough to compromise coronary filling (coronary autoregulation no longer operates at aortic pressures <40 mmHg) which results in ischemic myocardial manifestations.

Acute aortic regurgitation results mainly from cusp perforation caused by infection or from an aging homograft or xenograft (Fig. 2.40). Although the left ventricular cavity becomes overloaded and active, overall ventricular function is maintained since it does not dilate acutely. Acute severe regurgitation results in early mitral valve closure (well before the onset of the QRS) and time-restricted left ventricular filling (Figs. 2.41 and 2.42) [78]. Of course, this should be differentiated from early mitral valve closure associated with first-degree heart block. As mentioned above, mid-diastolic equalization of aortic and left ventricular pressures has its effect on coronary circulation, perpetuating rapid deterioration of ventricular function. Although the left ventricle may not be able to dilate acutely, the large regurgitant volume will result in raised diastolic pressures with its subsequent additional effect on subendocardial blood flow and function (Video 2.6).

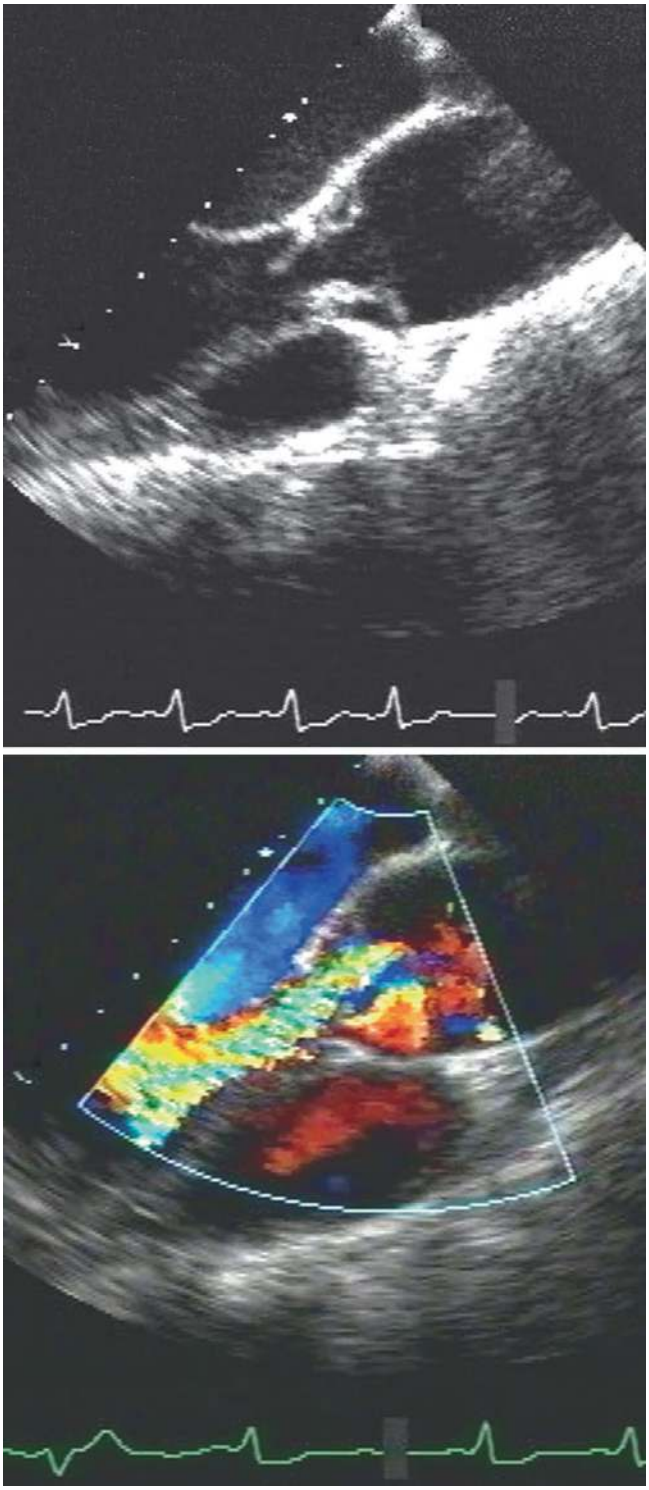


Fig. 2.37 Parasternal long axis view showing a proximal dissection of the aortic root with the flap bouncing back into the left ventricle in diastole (*left*), holding the cusps opened and causing in aortic regurgitation (*right*)



Fig. 2.38 Transesophageal view from a patient with dissection of the ascending aorta 4 cm distal to the cusp level. Note the clotted false lumen

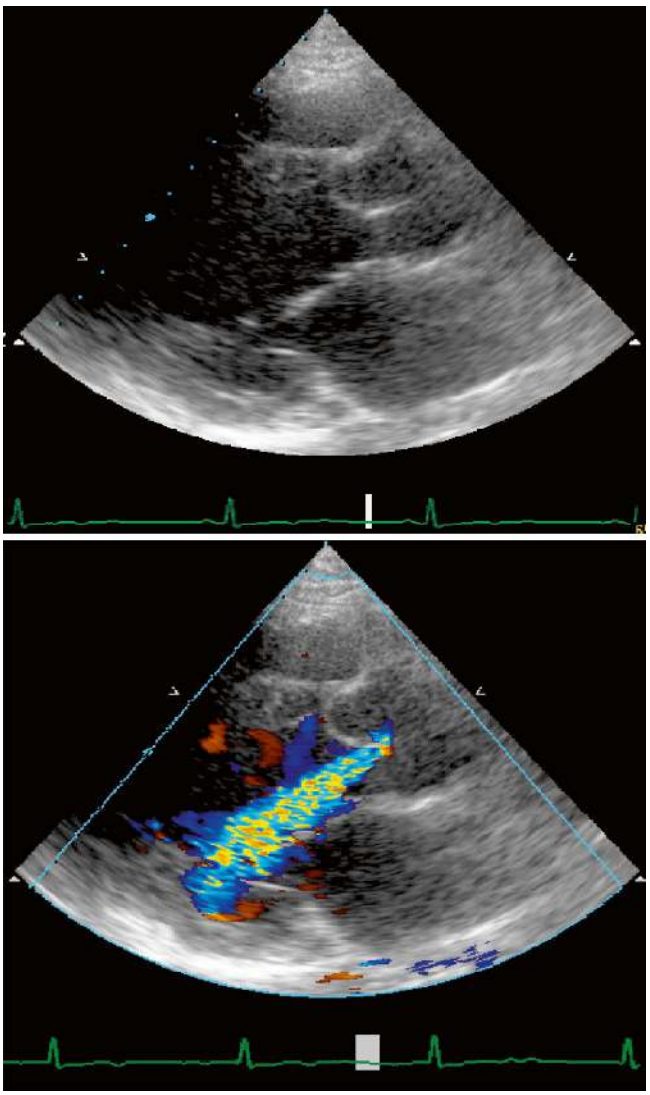


Fig. 2.39 Parasternal long axis view from a patient with aortic regurgitation. Note the prolapsing right coronary cusp closing off a small subaortic VSD (*top*) and resulting aortic regurgitation (*bottom*)

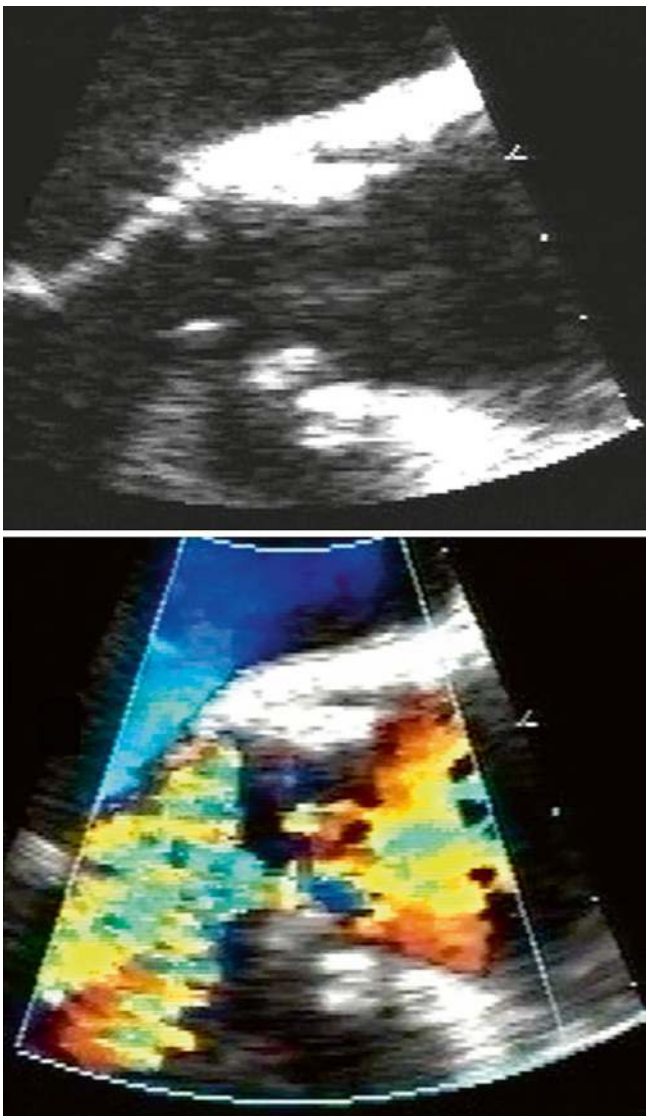


Fig. 2.40 An infected aortic valve xenograft causing a large hole in the right coronary cusp and severe regurgitation

Clinical Picture and Physiological Disturbances

Symptoms: Patients with chronic aortic regurgitation may be asymptomatic for many years. Symptoms develop only as the result of left ventricular disease. Exertional breathlessness is the main limiting symptom with aortic regurgitation which is caused by increased left ventricular diastolic pressure. In late stages, angina may be the result of coronary artery under-perfusion. Aortic root dilatation may be associated with similar symptoms [79].

Signs: All clinical signs are caused by large pulse volume: WaterHammer pulse, Corrigan's sign, DeMusset's sign, visible capillary pulsations in the nail beds (Quinckee's), and Durozier's sign due to retrograde diastolic flow in the femoral artery.

The aortic systolic murmur heard in patients with significant aortic regurgitation is due to the large stroke volume

rather than organic aortic leaflet stiffness and stenosis. P2 is loud when there is secondary pulmonary hypertension. A mid-diastolic murmur caused by a large aortic regurgitant jet hitting the anterior mitral leaflet may be heard at the apex (Austin-Flint) that mimics mitral stenosis. This is usually limiting its movement in diastole and reversing its doming (Fig. 2.43). This results in functional narrowing of mitral valve opening and high velocities (diastolic murmur) [80].

With development of left ventricular disease (increased end-systolic diameter > 5.0 cm) and reduced effective filling period due to the raised end-diastolic pressure, a third heart sound and mitral regurgitation murmur may be heard (Fig. 2.44).

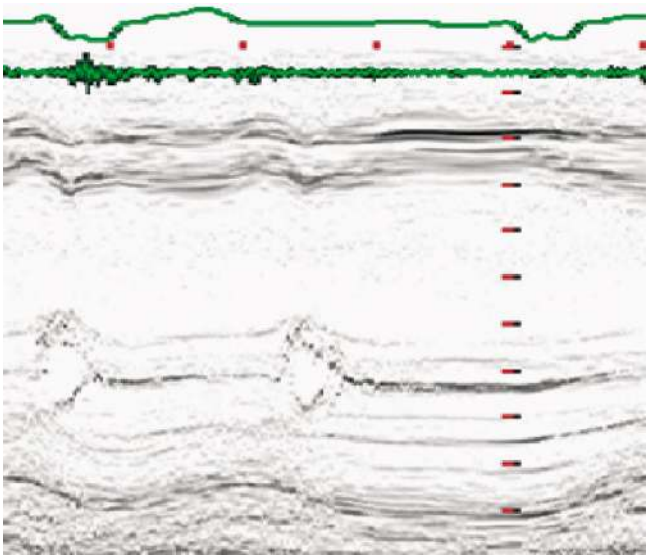


Fig. 2.41 Mitral valve echogram from a patient with acute aortic regurgitation showing early diastolic mitral valve closure

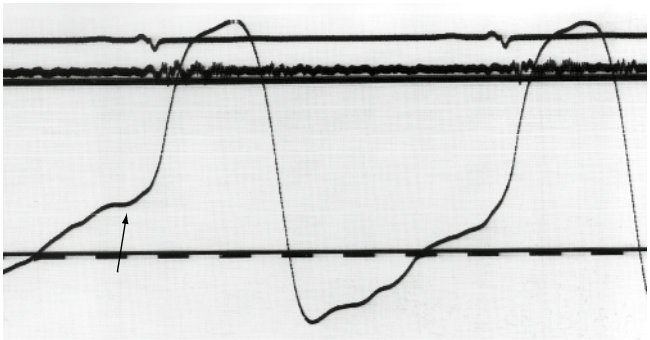


Fig. 2.42 An apexcardiogram from a patient with significant acute aortic regurgitation. Note the raised end-diastolic pressure

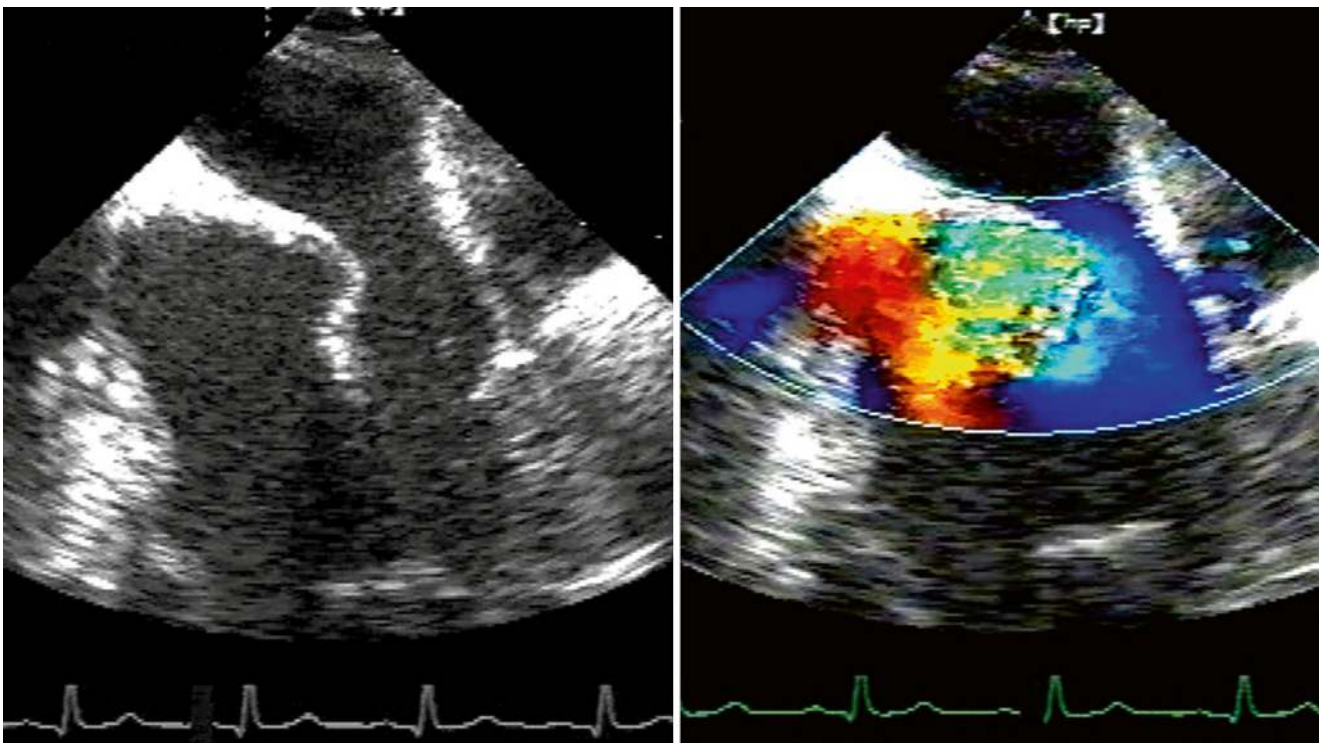


Fig. 2.43 TOE from a patient with severe aortic regurgitation and mid-diastolic mitral stenotic murmur. Note the effect of the aortic regurgitation jet on anterior mitral leaflet morphology and narrowing of the LV inflow tract in diastole (Austin-Flint murmur)

Signs of Aortic Regurgitation May Be Modified with Other Accompanying Conditions

- In infective endocarditis and cusp perforation, the early diastolic murmur sounds musical in quality "seagull murmur." With Homograft or Xenograft degeneration, a loud systolic murmur may be heard and a classical prolapsing and thickened leaflet is seen on 2D echo images.
- In the presence of left ventricular disease, or rheumatic mitral stenosis or pulmonary hypertension, the collapsing pulse and other signs of severe aortic regurgitation may be lost, although the early diastolic murmur remains.
- With very severe aortic regurgitation when the valve is virtually absent, the regurgitant murmur may be inaudible whereas the ventricular cavity is very active and the regurgitant jet diameter almost occupies the whole of the outflow tract.

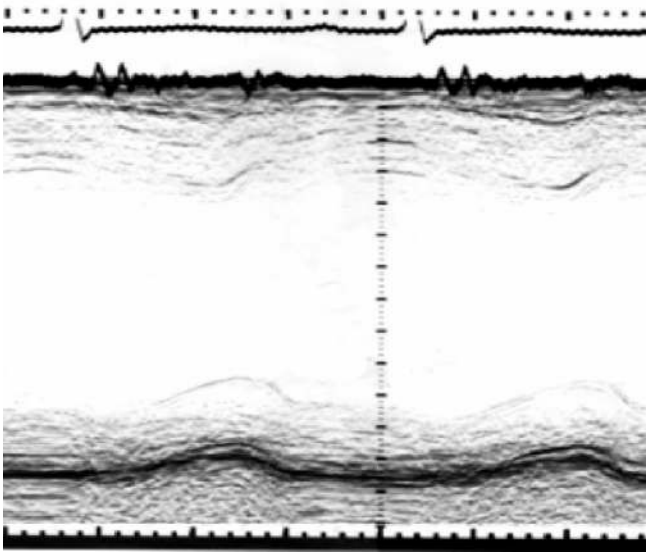


Fig. 2.44 LV M-mode recording from a patient with long-standing severe aortic regurgitation who developed left ventricular disease. Note the significant increase in ventricular end-systolic diameter and volume

Assessing Aortic Regurgitation Severity

Active left ventricular cavity: An increase in left ventricular end-diastolic volume and a fall in end-systolic volume are compatible with a significant overload. The main difference between aortic and mitral regurgitation is that in the former, ventricular loading occurs in early and mid-diastole whereas with mitral regurgitation, it is predominantly early diastolic (Fig. 2.45). An increase in left ventricular minor axis dimension, end-systole >5.0 cm, in the presence of any overload suggests independent ventricular disease even in the absence of significant symptoms. At this stage, recovery of ventricular function even after complete correction of the valve incompetence cannot be guaranteed [81].

Coarse Fluttering of Anterior Mitral Leaflet: This is a common finding in aortic regurgitation. It is caused by the regurgitant jet interfering with the anterior leaflet opening in diastole (Fig. 2.46). This sign however, is not sensitive in estimating regurgitation severity [82].

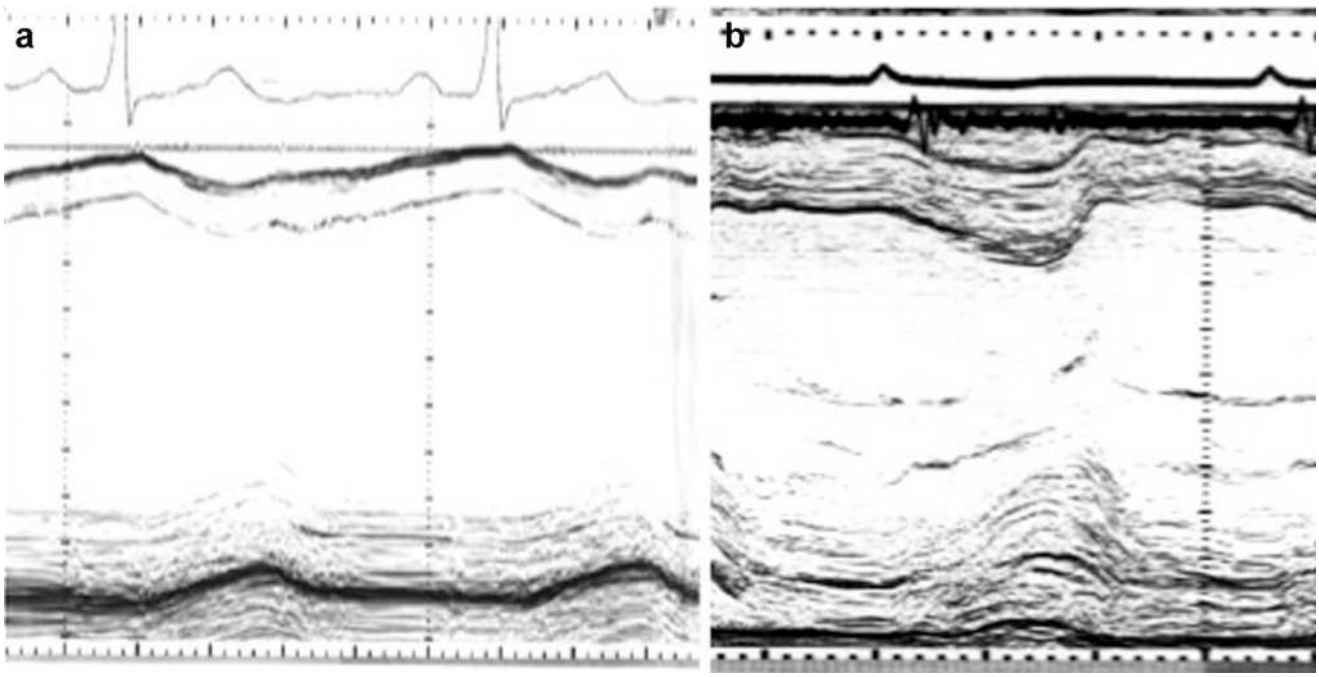


Fig. 2.45 LV M-mode recordings from two patients with overloaded left ventricle caused by aortic regurgitation (**a**) and mitral regurgitation (**b**). Note the difference in loading pattern between the two: early and mid-diastolic with aortic and mainly early diastolic with mitral regurgitation

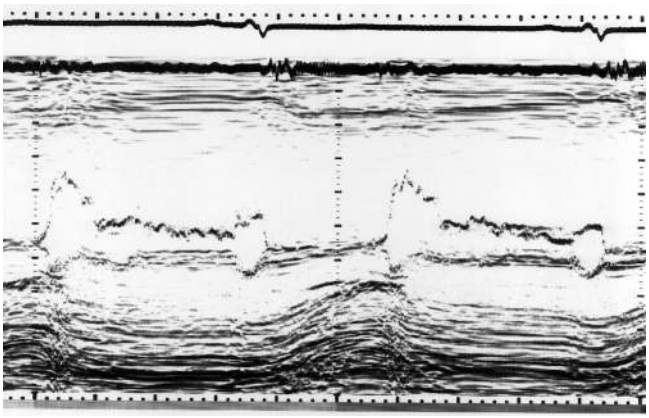


Fig. 2.46 Mitral valve M-mode recording from a patient with aortic regurgitation. Note the course flutter of the anterior leaflet in diastole

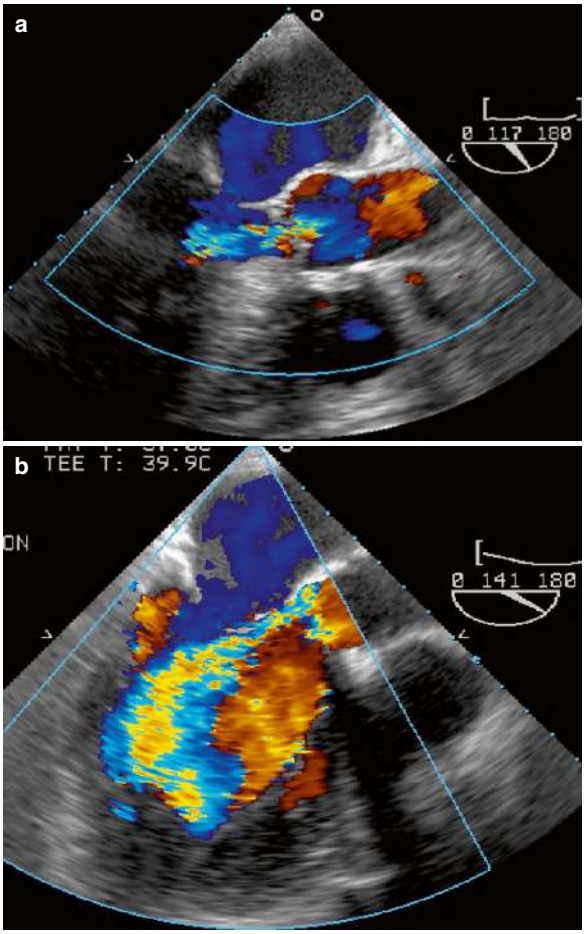


Fig. 2.47 TOE Color flow jet of aortic regurgitation showing mild severity (**a**) and severe regurgitation (**b**). Note the difference in jet distance with respect to the valve level

Color Flow Jet Length: A rough assessment of aortic regurgitation is by measuring the distance of the regurgitant jet with respect to the valve level either: subvalvar (mild), at mid ventricular cavity (moderate), and approaching the apex (severe, Fig. 2.47). Although pulsed wave (PW) Doppler technique is sensitive and specific, it has always been used to offer only a semi-quantitative mean, therefore has become impractical for follow-up studies [83, 84].

Color flow jet diameter and area: This is an accurate way of assessing regurgitation severity, particularly with native valves. A broad jet >12 mm or >65% the aortic root diameter suggests severe regurgitation (Fig. 2.48). Similarly a color flow jet area that occupies over half that of the left ventricular cavity on the apical view (>7.5 cm^2) suggests severe regurgitation whereas an area of 1 cm^2 is compatible with trivial regurgitation (Figs. 2.49 and 2.50). The major limitation of the latter is that the diameter and area, in particular, change over the course of diastole and may be affected by gain setting. Therefore, for follow-up reasons, fixed time measurements should be considered (early diastole) [85].

Continuous Wave Doppler: A rapid fall of aortic to left ventricular diastolic pressure by late diastole, particularly in the absence of raised LV end-diastolic pressure, confirms severe regurgitation. A slow deceleration slope <2 m/s^2 indicates mild regurgitation and a rapid slope >4 m/s^2 indicates severe regurgitation. A pressure ½ time of <300 ms also suggests severe regurgitation (Fig. 2.51). Left ventricular end-diastolic pressure can be calculated as the late diastolic aortic-ventricular pressure drop deducted from the systemic diastolic blood pressure. In patients in whom the aortic regurgitation jet is directed toward the right ventricle, apical continuous wave recordings may be inappropriate, and the left parasternal window may be the optimal site (Fig. 2.52) [86–89].

Diastolic Flow Reversal in the descending aorta or femoral artery (Durozier's sign) confirms significant aortic regurgitation (Fig. 2.53) [90, 91].

Continuity Equation: Aortic regurgitation severity is measured as ratio of the relative regurgitant volume to the left ventricular stroke volume. Therefore, the ideal way for estimating the regurgitant fraction is by measuring mitral valve area and diastolic time flow integral and comparing it with that of the aortic valve. The difference would be taken as regurgitant fraction. The same method can be applied to measure the aortic regurgitant area. Velocity time integral at the valve level and valve area are compared with that 2 cm distal to the valve and valve regurgitant area is calculated. An area of 1.2 cm^2 suggests severe aortic regurgitation. Among the previous measures of aortic regurgitation, severity of regurgitant area is considered the only load-independent marker; however, it is less reliable particularly with dilated aorta [92–95].

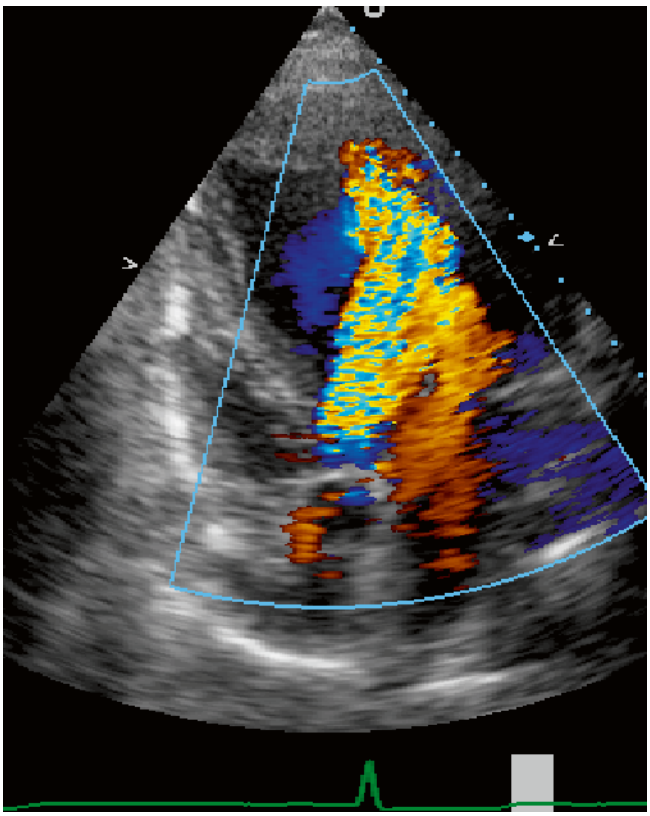


Fig. 2.48 Apical views color flow jet of aortic regurgitation showing a broad jet of 12 mm of severe regurgitation. Note the corresponding difference in regurgitation area with respect to that of the left ventricle

Management

Transthoracic echocardiography usually provides an excellent means of identifying the exact cause of aortic regurgitation and any additional complication, e.g., left ventricular disease. It also assesses other valve anatomy and function and hence, excludes all other possible causes of the clinical findings and auscultation sounds. Even the proximal ascending aorta can be examined for aortic root abscess, aneurysm formation, or the presence of a dissection. In patients with limited transthoracic window, the transesophageal technique should provide detailed assessment of the aortic valve, root, and ascending aorta and identify the exact cause of valve regurgitation. Evidence for infection (vegetation or aortic root abscess) is rarely missed by this technique, but with thickened leaflets, additional evidence for infection in the absence of sizeable vegetation.

Mild and moderate aortic regurgitation require prophylactic antibiotics. Severe aortic regurgitation in symptomatic patients needs aortic valve replacement. In asymptomatic patients, the condition could remain stable for years until signs of disease progression and left ventricular deterioration of function are demonstrated [96, 97]. Calcium channel blockers, e.g., Nifedipine or ACE inhibitors, have been shown to delay the operation by a few years in asymptomatic patients. Cases of sudden death in patients with severe aortic regurgitation and LV end-diastolic diameter of >7.0 cm have been reported. Progressive increase in left ventricular end-

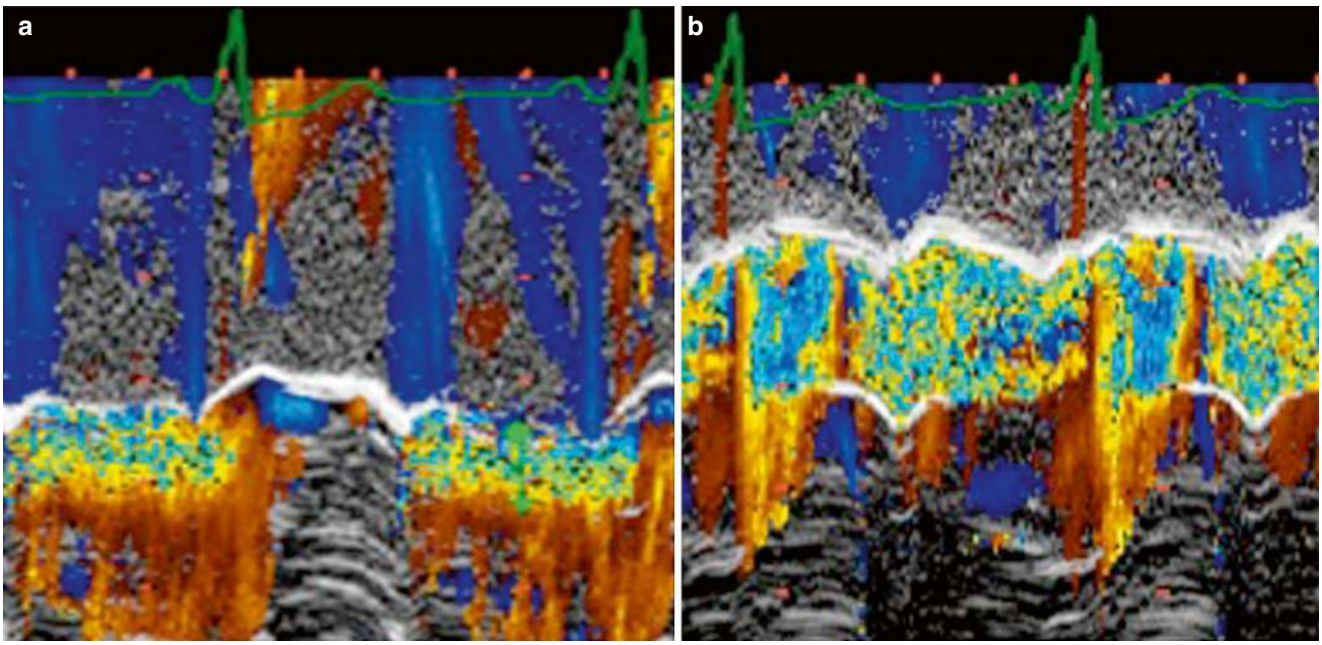


Fig. 2.49 (**a**, **b**) color Doppler M-mode of the aortic root from two patients with mild and severe regurgitation. Note the difference in absolute and relative jet diameter with respect to the aortic root diameter

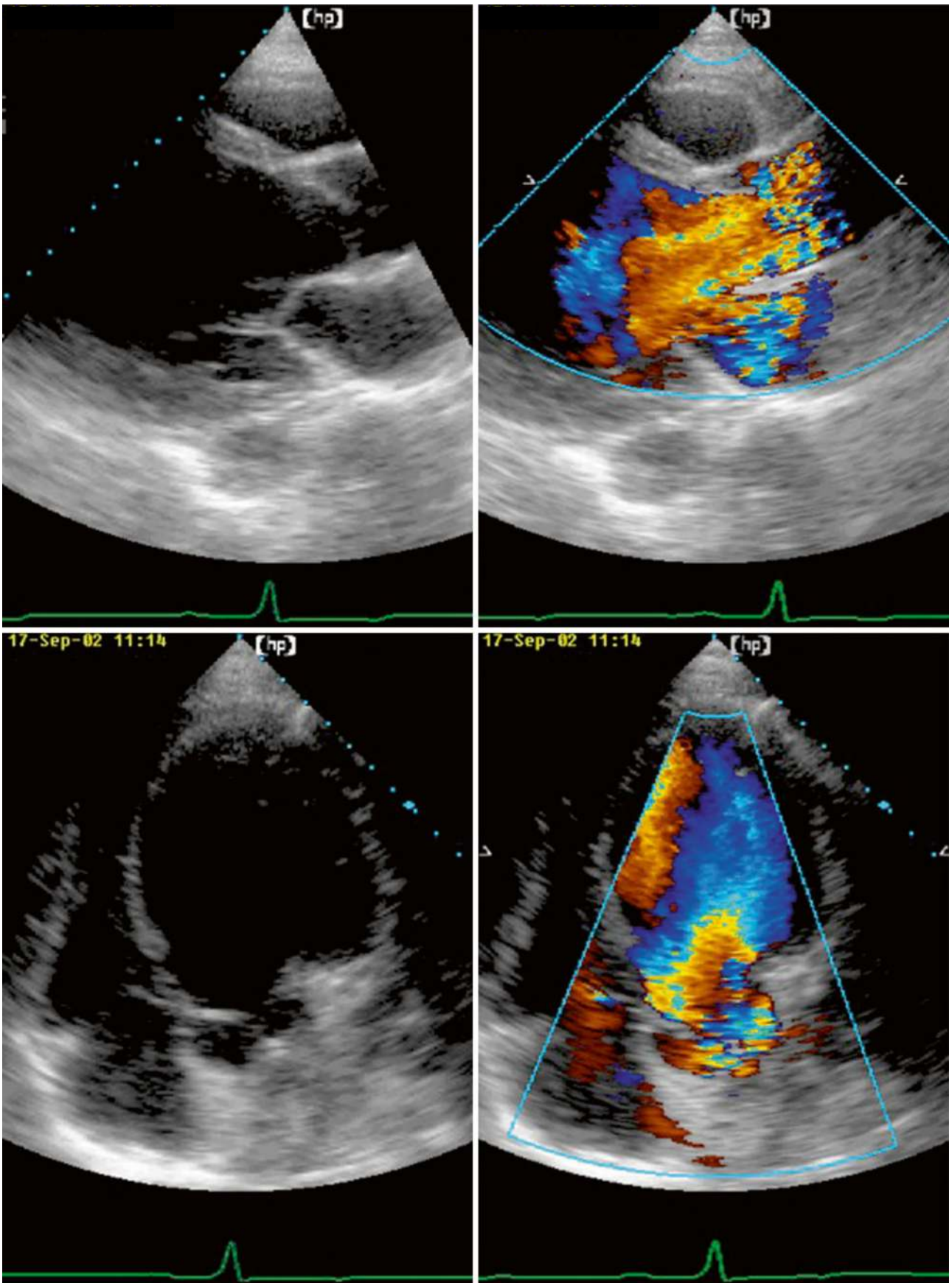


Fig. 2.50 Parasternal long axis view (*top*) from a patient with long standing aortic regurgitation and enlarged LV cavity with poor function. Apical view from the same patient (*bottom*)

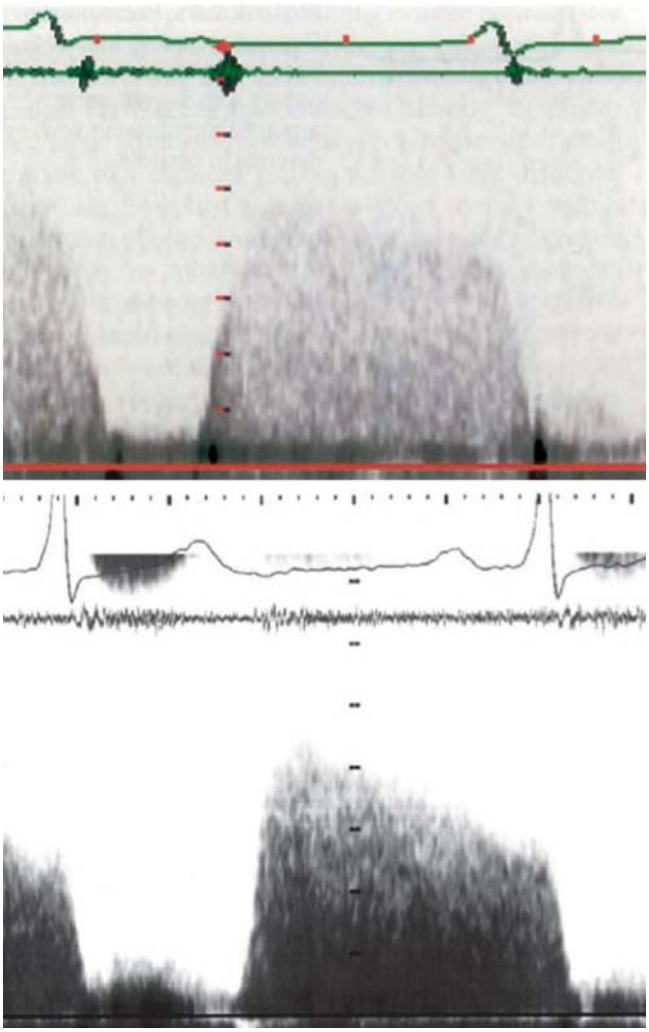


Fig. 2.51 Continuous wave Doppler recording of aortic regurgitation from two patients: mild (*top*) and severe (*bottom*). Note the fast deceleration, and pressure half time with severe regurgitation

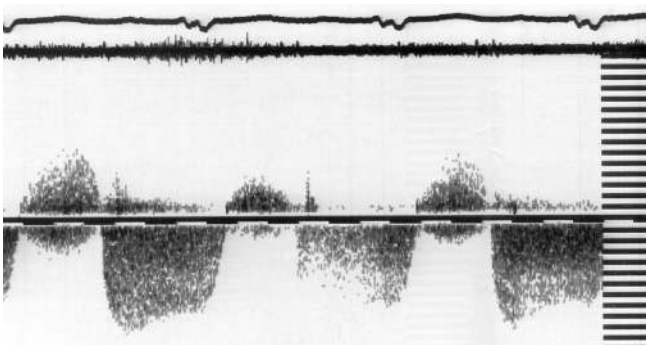


Fig. 2.52 Continuous wave Doppler from a patient with aortic regurgitation recorded from the left parasternal window demonstrating reversed signal

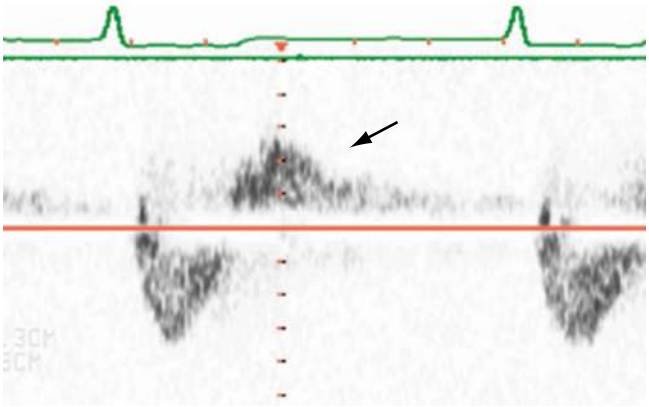


Fig. 2.53 Pulsed wave Doppler recording of the femoral artery from a patient with severe aortic regurgitation showing flow reversal in diastole (*arrow*)

systolic diameter >5.0 cm recommends valve surgery even in the absence of symptoms. If ignored, it may increase the operative mortality and result in poor prognosis [98–101]. Acute aortic regurgitation on the other hand is a surgical emergency. Since it is always due to infective endocarditis, blood cultures should be taken, the organism isolated, and antibiotics started before urgent surgery. Vasodilators may help to stabilize the condition until surgery is available. Aortic regurgitation complicating acute dissection is another surgical emergency.

Other aortic pathologies, e.g., aneurysm or dissection, are always dealt with in the same session either by repair or replacement. Recurrent aortic root and valve infection requires aortic root replacement preferably by a homograft. As in aortic stenosis, in patients with aortic regurgitation and severe left ventricular disease, valve replacement with a low resistance valve substitute (stentless) may result in faster recovery of ventricular function compared with conventional stented ones (Fig. 2.51) [102].

Recently, TAVI has been proposed as an alternative to surgery in patients with pure aortic valve regurgitation. However, the procedure in this context remains challenging, with a significant risk of transcatheter valve embolization and migration, irrespective of the ballon expandable or self expandable architecture [103] (Fig. 2.54).

Surgery for Aortic Regurgitation

Surgical management for aortic regurgitation can be considered according to the anatomical location of the disease process. If it is an issue with the leaflets (calcific degeneration,

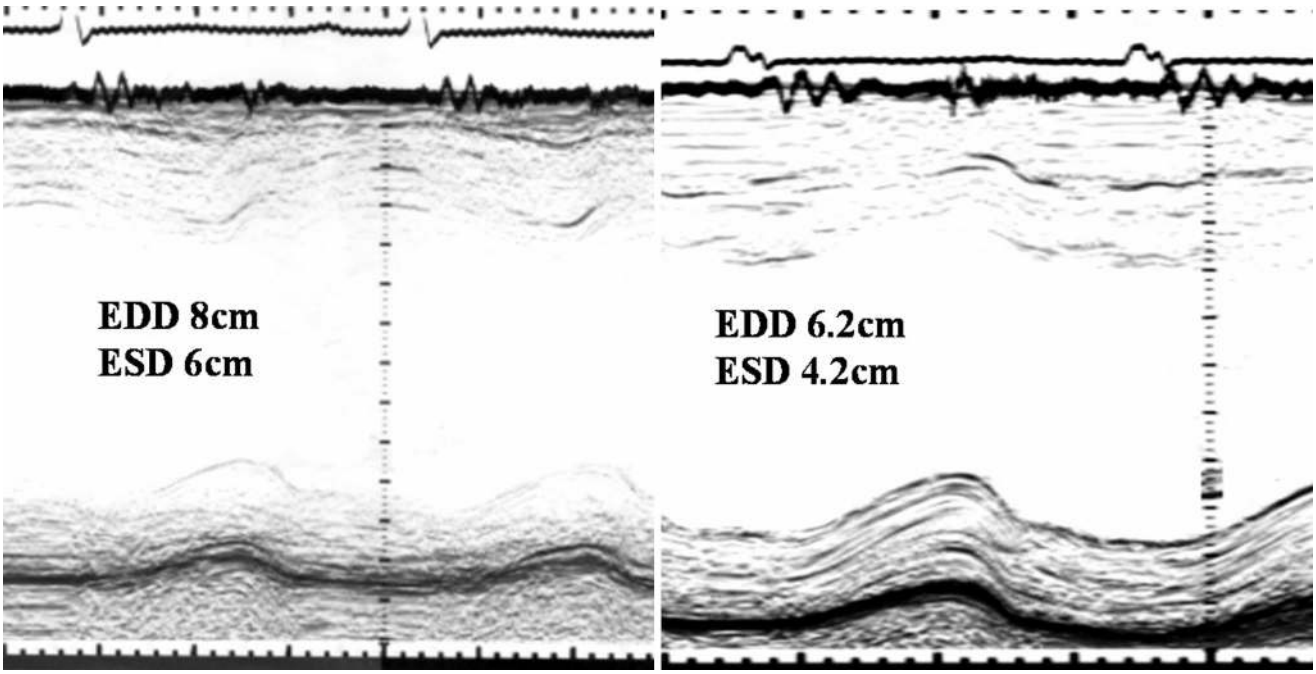


Fig. 2.54 LV M-mode recording from a patient with severe aortic regurgitation and left ventricular disease before (*left*) and after (*right*) valve replacement surgery. Note the significant fall in cavity dimensions and improvement of systolic function as assessed by fractional shortening

rheumatic fever, bicuspid aortic valve), annular (aneurysmal or dissection) or related to infective endocarditis. A patient with aortic regurgitation as a result of root dilation and subsequent cusp prolapse may benefit from a valve sparring root procedure such as a David's or a Yacoub. Alternatively, a patient with destruction of the aortic valve itself would most likely requrie a replacement prosthesis. If regurgitation is the result of aortic dissection with involvement of the valve, replacement or resuspension are options [104].

In recent years, there has been a growing interest in conserving the aortic valve. This has arisen partly because of the experience of aortic valve repair in acute and chronic Stanford type A dissection of the ascending aorta, and partly because in the western world, disease of the aortic root has become the commonest cause of aortic regurgitation [105].

Much recent interest has centered on the surgical management of Marfan's syndrome. Before the era of open-heart surgery, the majority of patients with Marfan's syndrome died of rupture of the aorta often before the age of 30. In 1968, Bentall and DeBono described a composite graft-valve procedure in which a prosthetic valve was sewn into the proximal end of an artificial tubular graft, which in turn was anastomosed to the aortic annulus, with the coronary arteries anastomosed to the side of the graft [106]. This procedure completely removes the defective aortic segment most prone to dissection and rupture. After 30 years experience with this operation, a recent multi-center retrospective report demonstrated the very considerable success that has been achieved [107]. The 30-day mortality was 1.5% for 455 patients who underwent elective repair, 2.6% for the 117 patients who had an urgent repair, and 11.7% for the 103 patients who required emergency repair. Because nearly half the patients with aortic dissection had an aortic root diameter of 6.5 cm or less at the time of operation, it seems sensible to advocate prophylactic repair of aortic aneurysms in Marfan patients when the diameter of the aorta is well below that size.

Despite this, there are some disadvantages to the Bentall operation. These include all the known complications of mechanical prosthetic valves and the possibility of removing a potentially functional aortic valve. Another option is a technique of radical excision of the aortic root and implantation of the coronary ostia (Fagan 1983). Like the Bentall operation, this achieves the objective of removing the defective aortic wall, but in contrast, the patient's own valve leaflets are preserved, resulting in more normal valve function and the avoidance of the complications of an artificial valve. The long-term results of this procedure are excellent for elective operations [108]. Currently in experienced units, prophylactic operation is recommended when the aortic root diameter reaches 5.0 cm. Until that time, patients are generally kept under close scrutiny with a combination of echocardiography and MRA or spiral CT scans performed at 6 monthly intervals. In patients with a family history of a ruptured ascending aorta, elective surgery is recommended even if the diameter is less than 5 cm [109]. In all series so far reported, emergency repair of the ascending aorta invariably emerges as a strong predictor of early mortality [110].

Intraoperative Echo Assistance

Please refer to those for aortic stenosis.

References

1. Iung B, Vahanian A. Epidemiology of valvular heart disease in the adult. Nat Rev Cardiol. 2011;8:162–72.
2. Beppu S, Suzuki S, Matsuda H, Ohmori F, Nagata S, Miyatake K. Rapidity of progression of aortic stenosis in patients with congenital bicuspid aortic valves. Am J Cardiol. 1993;71(4):322–7.
3. Pachulski RT, Chan KL. Progression of aortic valve dysfunction in 51 adult patients with congenital bicuspid aortic valve: assessment and follow up by Doppler echocardiography. Br Heart J. 1993;69(3):237–40.
4. Hahn RT, Roman MJ, Mogtader AH, Devereux RB. Association of aortic dilation with regurgitant, stenotic and functionally normal bicuspid aortic valves. J Am Coll Cardiol. 1992;19(2):283–8.
5. Gewillig M, Daenen W, Dumoulin M, Van der Hauwaert L. Rheologic genesis of discrete subvalvular aortic stenosis: a Doppler echocardiographic study. J Am Coll Cardiol. 1992;19(4):818–24.
6. Borow KM, Glagov S. Discrete subvalvular aortic stenosis: is the presence of upstream complex blood flow disturbances an important pathogenic factor? J Am Coll Cardiol. 1992;19(4):825–7.
7. Henein MY, O'Sullivan C, Sutton GC, Gibson DG, Coats AJ. Stress-induced left ventricular outflow tract obstruction: a potential cause of dyspnea in the elderly. J Am Coll Cardiol. 1997;30(5):1301–7.
8. Nasrallah AT, Nihill M. Supravalvular aortic stenosis. Echocardiographic features. Br Heart J. 1975;37(6):662–7.
9. Usher BW, Goulden D, Murgo JP. Echocardiographic detection of supravalvular aortic stenosis. Circulation. 1974;49(6):1257–9.
10. Weyman AE, Caldwell RL, Hurwitz RA, Girod DA, Dillon JC, Feigenbaum H, et al. Cross-sectional echocardiographic characterization of aortic obstruction. 1. Supravalvular aortic stenosis and aortic hypoplasia. Circulation. 1978;57(3):491–7.
11. Lindroos M, Kupari M, Heikkila J, Tilvis R. Prevalence of aortic valve abnormalities in the elderly: an echocardiographic study of a random population sample. J Am Coll Cardiol. 1993;21(5):1220–5.
12. Brandenburg RO Jr, Tajik AJ, Edwards WD, Reeder GS, Shub C, Seward JB. Accuracy of 2-dimensional echocardiographic diagnosis of congenitally bicuspid aortic valve: echocardiographic-anatomic correlation in 115 patients. Am J Cardiol. 1983;51(9):1469–73.
13. Rossebø AB, Pedersen TR, Boman K, Brudi P, Chambers JB, Egstrup K, et al. Intensive lipid lowering with simvastatin and ezetimibe in aortic stenosis. N Engl J Med. 2008;359(13):1343–56. Epub Sep 2, 2008
14. Chan KL, Teo K, Dumesnil JG, Ni A, Tam J, ASTRONOMER Investigators. Effect of lipid lowering with rosuvastatin on progression of aortic stenosis: results of the aortic stenosis progression observation: measuring effects of rosuvastatin (ASTRONOMER) trial. Circulation. 2010;121(2):306–14. Epub Jan 4, 2010
15. Redlich K, Khaladj N, Peterss S, Pichlmaier M, Shrestha M, Hoy L, et al. Conventional aortic valve replacement in patients with concomitant coronary artery disease and previous coronary artery bypass grafting in the era of interventional approaches. Eur J Cardiothorac Surg. 2011;40(2):455–62. Epub Jan 21, 2011
16. Ljungberg J, Holmgren A, Bergdahl IA, Hultdin J, Norberg M, Näslund U, Johansson B, Söderberg S. Lipoprotein(a) and the Apolipoprotein B/A1 ratio independently associate with surgery for aortic stenosis only in patients with concomitant coronary artery disease. J Am Heart Assoc. 2017;6(12):e007160. https://doi.org/10.1161/JAHA.117.007160.
17. Jaiswal V, Agrawal V, Khulbe Y, Hanif M, Huang H, Hameed M, Shrestha AB, Perone F, Parikh C, Gomez SI, Paudel K, Zacks J, Grubb KJ, De Rosa S, Gimelli A. Cardiac amyloidosis and aortic stenosis: a state-of-the-art review. Eur Heart J Open. 2023;3(6):oead106. https://doi.org/10.1093/ehjopen/oead106. PMID: 37941729; PMCID: PMC10630099.
18. Unger P, Magne J, Vanden Eynden F, Plein D, Van Camp G, Pasquet A, et al. Impact of prosthesis-patient mismatch on mitral regurgitation after aortic valve replacement. Heart. 2010;96(20):1627–32.
19. Chang S, Clements S, Chang J. Aortic stenosis: echocardiographic cusp separation and surgical description of aortic valve in 22 patients. Am J Cardiol. 1977;39(4):499–504.
20. Lesbre JP, Scheuble C, Kalisa A, Lalau JD, Andrejak MT. Echocardiography in the diagnosis of severe aortic valve stenosis in adults. Arch Mal Coeur Vaiss. 1983;76(1):1–12.
21. Williams DE, Sahn DJ, Friedman WF. Cross-sectional echocardiographic localization of sites of left ventricular outflow tract obstruction. Am J Cardiol. 1976;37(2):250–5.
22. Hatle L, Angelsen BA, Tromsdal A. Non-invasive assessment of aortic stenosis by Doppler ultrasound. Br Heart J. 1980;43(3):284–92.
23. Berger M, Berdoff RL, Gallerstein PE, Goldberg E. Evaluation of aortic stenosis by continuous wave Doppler ultrasound. J Am Coll Cardiol. 1984;3(1):150–6.
24. Currie PJ, Seward JB, Chan KL, Fyfe DA, Hagler DJ, Mair DD, et al. Continuous wave Doppler determination of right ventricular pressure: a simultaneous Doppler-catheterization study in 127 patients. J Am Coll Cardiol. 1985;6(4):750–6.
25. Hatle L, Angelsen BA. Doppler ultrasound in cardiology. 2nd ed. Philadelphia: Lea & Febiger; 1985.
26. Lima CO, Sahn DJ, Valdes-Cruz LM, Allen HD, Goldberg SJ, Grenadier E, et al. Prediction of the severity of left ventricular outflow tract obstruction by quantitative two-dimensional echocardiographic Doppler studies. Circulation. 1983;68(2):348–54.
27. Pellikka PA, Nishimura RA, Bailey KR, Tajik AJ. The natural history of adults with asymptomatic, hemodynamically significant aortic stenosis. J Am Coll Cardiol. 1990;15(5):1012–7.
28. Kosturakis D, Allen HD, Goldberg SJ, Sahn DJ, Valdes-Cruz LM. Noninvasive quantification of stenotic semilunar valve areas by Doppler echocardiography. J Am Coll Cardiol. 1984;3(5):1256–62.
29. Richards KL, Cannon SR, Miller JF, Crawford MH. Calculation of aortic valve area by Doppler echocardiography: a direct application of the continuity equation. Circulation. 1986;73(5):964–9.
30. Zoghbi WA, Farmer KL, Soto JG, Nelson JG, Quinones MA. Accurate noninvasive quantification of stenotic aortic valve area by Doppler echocardiography. Circulation. 1986;73(3):452–9.
31. Oh JK, Taliercio CP, Holmes DR Jr, Reeder GS, Bailey KR, Seward JB, et al. Prediction of the severity of aortic stenosis by Doppler aortic valve area determination: prospective Doppler-catheterization correlation in 100 patients. J Am Coll Cardiol. 1988;11(6):1227–34.
32. Panidis IP, Segal BL. Aortic valve disease in the elderly. In: Frankl WS, Brest AN, editors. Valvular heart disease: comprehensive evaluation and management. Philadelphia: F.A. Davis; 1985. p. 289–311.
33. Collinson J, Flather M, Pepper JR, Gibson DG, Henein M. Reversal of ventricular dysfunction and subendocardial ischaemia following aortic valve replacement in patients with severe aortic stenosis. Circulation. 2000;102(18):11–661.
34. Henein MY, Xiao HB, Brecker SJ, Gibson DG. Berheim "a" wave: obstructed right ventricular inflow or atrial cross talk? Br Heart J. 1993;69(5):409–13.

35. Habib G, Hoen B, Tornos P, Thuny F, Prendergast B, Vilacosta I, et al. Guidelines on the prevention, diagnosis, and treatment of infective endocarditis (new version 2009): the Task Force on the Prevention, Diagnosis, and Treatment of Infective Endocarditis of the European Society of Cardiology (ESC). Endorsed by the European Society of Clinical Microbiology and Infectious Diseases (ESCMID) and the International Society of Chemotherapy (ISC) for Infection and Cancer. Eur Heart J. 2009;30(19):2369–413. Epub Aug 27, 2009. No abstract available.
36. Das P, Chambers J. Predictors of outcome in asymptomatic aortic stenosis. N Engl J Med. 2001;344(3):227–9.
37. Schwammenthal E, Vered Z, Moshkowitz Y, Rabinowitz B, Ziskind Z, Smolinski AK, et al. Dobutamine echocardiography in patients with aortic stenosis and left ventricular dysfunction: predicting outcome as a function of management strategy. Chest. 2001;119(6):1766–77.
38. Cowley CG, Dietrich M, Mosca RS, Bove EL, Rocchini AP, Lloyd TR. Balloon valvuloplasty versus transventricular dilation for neonatal critical aortic stenosis. Am J Cardiol. 2001;87(9):1125–7. A10.
39. Buchwald AB, Meyer T, Scholz K, Schorn B, Unterberg C. Efficacy of balloon valvuloplasty in patients with critical aortic stenosis and cardiogenic shock – the role of shock duration. Clin Cardiol. 2001;24(3):214–8.
40. Blitz LR, Gorman M, Herrmann HC. Results of aortic valve replacement for aortic stenosis with relatively low transvalvular pressure gradients. Am J Cardiol. 1998;81(3):358–62.
41. Connolly HM, Oh JK, Orszulak TA, Osborn SL, Roger VL, Hodge DO, et al. Aortic valve replacement for aortic stenosis with severe left ventricular dysfunction. Prognostic indicators. Circulation. 1997;95(10):2395–400.
42. Connolly HM, Oh JK, Schaff HV, Roger VL, Osborn SL, Hodge DO, et al. Severe aortic stenosis with low transvalvular gradient and severe left ventricular dysfunction: result of aortic valve replacement in 52 patients. Circulation. 2000;101(16):1940–6.
43. Pereira JJ, Lauer MS, Bashir M, Afridi I, Blackstone EH, Stewart WJ, et al. Survival after aortic valve replacement for severe aortic stenosis with low transvalvular gradients and severe left ventricular dysfunction. J Am Coll Cardiol. 2002;39(8):1356–63.
44. Hamamoto M, Bando K, Kobayashi J, Satoh T, Sasako Y, Niwaya K, et al. Durability and outcome of aortic valve replacement with mitral valve repair versus double valve replacement. Ann Thorac Surg. 2003;75(1):28–33.
45. John S, Ravikumar E, John CN, Bashi VV. 25-year experience with 456 combined mitral and aortic valve replacement for rheumatic heart disease. Ann Thorac Surg. 2000;69(4):1167–72.
46. Milano A, Guglielmi C, De Carlo M, Di Gregorio O, Borzoni G, Verunelli F, et al. Valve-related complications in elderly patients with biological and mechanical aortic valves. Ann Thorac Surg. 1998;66(6 Suppl):S82–7.
47. Collinson J, Henein M, Flather M, Pepper JR, Gibson DG. Valve replacement for aortic stenosis in patients with poor left ventricular function: comparison of early changes with stented and stentless valves. Circulation. 1999;100(19 Suppl):II1–5.
48. Jin XY, Zhang ZM, Gibson DG, Yacoub MH, Pepper JR. Effects of valve substitute on changes in left ventricular function and hypertrophy after aortic valve replacement. Ann Thorac Surg. 1996;62(3):683–90.
49. Jin XY, Pepper JR, Gibson DG, Yacoub MH. Early changes in the time course of myocardial contraction after correcting aortic regurgitation. Ann Thorac Surg. 1999;67(1):139–45.
50. Rajappan K, Melina G, Bellenger NG, Amrani M, Khaghani A, Pennell DJ, et al. Evaluation of left ventricular function and mass after Medtronic freestyle versus homograft aortic root replacement using cardiovascular magnetic resonance. J Heart Valve Dis. 2002;11(1):60–5.
51. Moises VA, Maciel BC, Hornberger LK, Murillo-Olivas A, Valdes-Cruz LM, Sahn DJ, et al. A new method for noninvasive estimation of ventricular septal defect shunt flow by Doppler color flow mapping: imaging of the laminar flow convergence region on the left septal surface. J Am Coll Cardiol. 1991;18(3):824–32.
52. Powell R, Pelletier MP, Chu MWA, Bouchard D, Melvin KN, Adams C. The Perceval sutureless aortic valve: review of outcomes, complications, and future direction. Innovations (Phila). 2017;12(3):155–73.
53. Unai S, Ozaki S, Johnston DR, Saito T, Rajeswaran J, Svensson LG, et al. Aortic valve reconstruction with autologous pericardium versus a bioprosthesis: the Ozaki procedure in perspective. J Am Heart Assoc. 2023;11:e027391.
54. Carr-White GS, Glennan S, Edwards S, Ferdinand FD, Desouza AC, Pepper JR, et al. Pulmonary autograft versus aortic homograft for rereplacement of the aortic valve: results from a subset of a prospective randomized trial. Circulation. 1999;100(19 Suppl):II103–6.
55. Grocott-Mason RM, Lund O, Elwidaa H, Mazhar R, Chandrasakeran V, Mitchell AG, et al. Long-term results after aortic valve replacement in patients with congestive heart failure. Homografts vs prosthetic valves. Eur Heart J. 2000;21(20):1698–707.
56. Oury JH, Doty DB, Oswalt JD, Knapp JF, Mackey SK, Duran CM. Cardiopulmonary response to maximal exercise in young athletes following the Ross procedure. Ann Thorac Surg. 1998;66(6 Suppl):S153–4.
57. Notenboom ML, Melina G, Veen KM, De Robertis F, Coppola G, De Siena P, et al. Long-term clinical and echocardiographic outcomes following the Ross procedure: a post hoc analysis of a randomized clinical trial. JAMA Cardiol. 2024;9(1):6–14.
58. Porter GF, Skillington PD, Bjorksten AR, Morgan JG, Yapanis AG, Grigg LE. Exercise hemodynamic performance of the pulmonary autograft following the Ross procedure. J Heart Valve Dis. 1999;8(5):516–21.
59. Laske A, Jenni R, Maloigne M, Vassalli G, Bertel O, Turina MI. Pressure gradients across bileaflet aortic valves by direct measurement and echocardiography. Ann Thorac Surg. 1996;61(1):48–57.
60. Morocutti G, Gelsomino S, Spedicato L, Frassani R, Bernardi G, Da Col P, et al. Intraoperative transesophageal echo-Doppler evaluation of stentless aortic xenografts. Incidence and significance of moderate gradients. Cardiovasc Surg. 2002;10(4):328–32.
61. Sousa RC, Garcia-Fernandez MA, Moreno M, Tizon M, Valdeviesos M, Rubio M, et al. The contribution and usefulness of routine intraoperative transesophageal echocardiography in cardiac surgery. An analysis of 130 consecutive cases. Rev Port Cardiol. 1995;14(1):15–27.
62. D'Ascenzi F, Cameli M, Iadanza A, Lisi M, Zacà V, Reccia R, Curci V, Torrisi A, Sinicropi G, Pierli C, Mondillo S. Improvement of left ventricular longitudinal systolic function after transcatheter aortic valve implantation: a speckle-tracking prospective study. Int J Cardiovasc Imaging. 2013;29(5):1007–15. https://doi.org/10.1007/s10554-012-0175-5. Epub 2012 Dec 28. PMID: 23271458.
63. Lisi M, Pastore MC, Fiorio A, Cameli M, Mandoli GE, Righini FM, Cavigli L, D'Ascenzi F, Focardi M, Rubboli A, Campo G, Mondillo S, Henein MY. Left atrial remodeling in response to aortic valve replacement: pathophysiology and myocardial strain analysis. Life (Basel). 2022;12(12):2074. https://doi.org/10.3390/life12122074. PMID: 36556439; PMCID: PMC9788515.
64. D'Ascenzi F, Cameli M, Henein M, Iadanza A, Reccia R, Lisi M, Curci V, Sinicropi G, Torrisi A, Pierli C, Mondillo S. Left atrial remodelling in patients undergoing transcatheter aortic valve implantation: a speckle-tracking prospective, longitudinal study. Int J Cardiovasc Imaging. 2013;29(8):1717–24. https://

doi.org/10.1007/s10554-013-0265-z. Epub 2013 Jul 14. PMID: 23852277.
65. Mack MJ, Leon MB, Thourani VH, Pibarot P, Hahn RT, Genereux P, Kodali SK, Kapadia SR, Cohen DJ, Pocock SJ, Lu M, White R, Szerlip M, Ternacle J, Malaisrie SC, Herrmann HC, Szeto WY, Russo MJ, Babaliaros V, Smith CR, Blanke P, Webb JG, Makkar R, PARTNER 3 Investigators. Transcatheter aortic-valve replacement in low-risk patients at five years. N Engl J Med. 2023;389(21):1949–60. https://doi.org/10.1056/NEJMoa2307447. Epub 2023 Oct 24. PMID: 37874020.
66. Forrest JK, Deeb GM, Yakubov SJ, Gada H, Mumtaz MA, Ramlawi B, Bajwa T, Teirstein PS, DeFrain M, Muppala M, Rutkin BJ, Chawla A, Jenson B, Chetcuti SJ, Stoler RC, Poulin MF, Khabbaz K, Levack M, Goel K, Tchétché D, Lam KY, Tonino PAL, Ito S, Oh JK, Huang J, Popma JJ, Kleiman N, Reardon MJ, Low Risk Trial Investigators. 3-year outcomes after transcatheter or surgical aortic valve replacement in low-risk patients with aortic stenosis. J Am Coll Cardiol. 2023;81(17):1663–74. https://doi.org/10.1016/j.jacc.2023.02.017. Epub 2023 Mar 5. PMID: 36882136.
67. Gallone G, Islas F, Gorla R, Melillo F, Leone PP, Cimaglia P, Pastore MC, Franzone A, Landra F, Bruno F, Scudeler L, Jimenez-Quevedo P, Viva T, Piroli F, Bragato R, Trichilo M, Degiovanni A, Ilardi F, Andreis A, Nombela-Franco L, Maurizio T, Toselli M, Conrotto F, Montorfano M, Manzo R, Cameli M, Patti G, Stefanini G, Testa L, Giannini F, Agricola E, Escaned J, D'Ascenzo F, De Ferrari GM. Stroke volume index and transvalvular flow rate trajectories in severe aortic stenosis treated with TAVR. Eur Heart J Cardiovasc Imaging. 2023;24(8):1052–61. https://doi.org/10.1093/ehjci/jead018. PMID: 36752044.
68. Doguet F, Godin M, Lebreton G, Eltchaninoff H, Cribier A, Bessou JP, et al. Aortic valve replacement after percutaneous valvuloplasty—an approach in otherwise inoperable patients. Eur J Cardiothorac Surg. 2010;38(4):394–9. Epub Mar 2, 2010.
69. Vahanian A, Alfieri OR, Al-Attar N, Antunes MJ, Bax J, Cormier B, et al. Transcatheter valve implantation for patients with aortic stenosis: a position statement from the European Association of Cardio-Thoracic Surgery (EACTS) and the European Society of Cardiology (ESC), in collaboration with the European Association of Percutaneous Cardiovascular Interventions (EAPCI). Eur J Cardiothorac Surg. 2008;34(1):1–8. Epub May 27, 2008.
70. Zhao Y, Lindqvist P, Nilsson J, Holmgren A, Näslund U, Henein MY. Trans-catheter aortic valve implantation – early recovery of left and preservation of right ventricular function. Interact Cardiovasc Thorac Surg. 2011;12(1):35–9. Epub Oct 18, 2010.
71. Amato MC, Moffa PJ, Werner KE, Ramires JA. Treatment decision in asymptomatic aortic stenosis: role of exercise testing. Heart. 2001;86:381–6.
72. Rosenhek R, Binder T, Porenta G, Lang I, Christ G, Schemper M, et al. Predictors of outcome in severe, asymptomatic aortic stenosis. N Engl J Med. 2000;343:611–7.
73. Owen A, Henein MY. Challenges in the management of asymptomatic aortic stenosis. Eur J Cardiothorac Surg. 2011;40:848–50.
74. Allen WM, Matloff JM, Fishbein MC. Myxoid degeneration of the aortic valve and isolated severe aortic regurgitation. Am J Cardiol. 1985;55(4):439–44.
75. Krivokapich J, Child JS, Skorton DJ. Flail aortic valve leaflets: M-mode and two-dimensional echocardiographic manifestations. Am Heart J. 1980;99(4):425–37.
76. DePace NL, Nestico PF, Kotler MN, Mintz GS, Kimbiris D, Goel IP, et al. Comparison of echocardiography and angiography in determining the cause of severe aortic regurgitation. Br Heart J. 1984;51(1):36–45.
77. Imaizumi T, Orita Y, Koiwaya Y, Hirata T, Nakamura M. Utility of two-dimensional echocardiography in the differential diagnosis of the etiology of aortic regurgitation. Am Heart J. 1982;103(5):887–96.
78. Botvinick EH, Schiller NB, Wickramasekaran R, Klausner SC, Gertz E. Echocardiographic demonstration of early mitral valve closure in severe aortic insufficiency. Its clinical implications. Circulation. 1975;51(5):836–47.
79. Morganroth J, Perloff JK, Zeldis SM, Dunkman WB. Acute severe aortic regurgitation. Pathophysiology, clinical recognition, and management. Ann Intern Med. 1977;87(2):223–32.
80. Gibson DG. Valve disease. In: Weatherall DJ, editor. Oxford textbook of medicine. Oxford: Oxford Medical Publications; 1996. p. 2451.
81. Henry WL, Bonow RO, Rosing DR, Epstein SE. Observations on the optimum time for operative intervention for aortic regurgitation. II. Serial echocardiographic evaluation of asymptomatic patients. Circulation. 1980;61(3):484–92.
82. Robertson WS, Stewart J, Armstrong WF, Dillon JC, Feigenbaum H. Reverse doming of the anterior mitral leaflet with severe aortic regurgitation. J Am Coll Cardiol. 1984;3(2 Pt 1):431–6.
83. Esper RJ. Detection of mild aortic regurgitation by range-gated pulsed Doppler echocardiography. Am J Cardiol. 1982;50(5):1037–43.
84. Ciobanu M, Abbasi AS, Allen M, Hermer A, Spellberg R. Pulsed Doppler echocardiography in the diagnosis and estimation of severity of aortic insufficiency. Am J Cardiol. 1982;49(2):339–43.
85. Tribouilloy C, Shen WF, Slama M, Rey JL, Dufosse H, Choquet D, et al. Assessment of severity of aortic regurgitation by M-mode colour Doppler flow imaging. Eur Heart J. 1991;12(3):352–6.
86. Beyer RW, Ramirez M, Josephson MA, Shah PM. Correlation of continuous-wave Doppler assessment of chronic aortic regurgitation with hemodynamics and angiography. Am J Cardiol. 1987;60(10):852–6.
87. Labovitz AJ, Ferrara RP, Kern MJ, Bryg RJ, Mrosek DG, Williams GA. Quantitative evaluation of aortic insufficiency by continuous wave Doppler echocardiography. J Am Coll Cardiol. 1986;8(6):1341–7.
88. Masuyama T, Kodama K, Kitabatake A, Nanto S, Sato H, Uematsu M, et al. Noninvasive evaluation of aortic regurgitation by continuous-wave Doppler echocardiography. Circulation. 1986;73(3):460–6.
89. Masuyama T, Kitabatake A, Kodama K, Uematsu M, Nakatani S, Kamada T. Semiquantitative evaluation of aortic regurgitation by Doppler echocardiography: effects of associated mitral stenosis. Am Heart J. 1989;117(1):133–9.
90. Hoffmann A, Pfisterer M, Stulz P, Schmitt HE, Burkart F, Burckhardt D. Non-invasive grading of aortic regurgitation by Doppler ultrasonography. Br Heart J. 1986;55(3):283–5.
91. Quinones MA, Young JB, Waggoner AD, Ostojic MC, Ribeiro LG, Miller RR. Assessment of pulsed Doppler echocardiography in detection and quantification of aortic and mitral regurgitation. Br Heart J. 1980;44(6):612–20.
92. Enriquez-Sarano M, Seward JB, Bailey KR, Tajik AJ. Effective regurgitant orifice area: a noninvasive Doppler development of an old hemodynamic concept. J Am Coll Cardiol. 1994;23(2):443–51.
93. Kitabatake A, Ito H, Inoue M, Tanouchi J, Ishihara K, Morita T, et al. A new approach to noninvasive evaluation of aortic regurgitant fraction by two-dimensional Doppler echocardiography. Circulation. 1985;72(3):523–9.
94. Reimold SC, Ganz P, Bittl JA, Thomas JD, Thoreau D, Plappert TJ, et al. Effective aortic regurgitant orifice area: description of a method based on the conservation of mass. J Am Coll Cardiol. 1991;18(3):761–8.
95. Zhang Y, Nitter-Hauge S, Ihlen H, Rootwelt K, Myhre E. Measurement of aortic regurgitation by Doppler echocardiography. Br Heart J. 1986;55(1):32–8.

96. Acar J, Michel PL, Luxereau P, Abou JS, Cazaux P, Dorent R, et al. How to manage patients with severe left ventricular dysfunction and valvular regurgitation. J Heart Valve Dis. 1996;5(4):421–9.
97. Borer JS. Aortic valve replacement for the asymptomatic patient with aortic regurgitation: a new piece of the strategic puzzle. Circulation. 2002;106(21):2637–9.
98. Bonow RO, Dodd JT, Maron BJ, O'Gara PT, White GG, McIntosh CL, et al. Long-term serial changes in left ventricular function and reversal of ventricular dilatation after valve replacement for chronic aortic regurgitation. Circulation. 1988;78(5 Pt 1):1108–20.
99. Bonow RO, Lakatos E, Maron BJ, Epstein SE. Serial long-term assessment of the natural history of asymptomatic patients with chronic aortic regurgitation and normal left ventricular systolic function. Circulation. 1991;84(4):1625–35.
100. Borow KM, Green LH, Mann T, Sloss LJ, Braunwald E, Collins JJ, et al. End-systolic volume as a predictor of postoperative left ventricular performance in volume overload from valvular regurgitation. Am J Med. 1980;68(5):655–63.
101. Carabello BA, Spann JF. The uses and limitations of end-systolic indexes of left ventricular function. Circulation. 1984;69(5):1058–64.
102. Jin XY, Pillai R, Westaby S. Medium-term determinants of left ventricular mass index after stentless aortic valve replacement. Ann Thorac Surg. 1999;67(2):411–6.
103. Poletti E, De Backer O, Scotti A, Costa G, Bruno F, Fiorina C, Buzzatti N, Latini A, Rudolph TK, van den Dorpel MMP, Brinkmann C, Patel KP, Panoulas V, Schofer J, Giordano A, Barbanti M, Regazzoli D, Taramasso M, Saia F, Baumbach A, Maisano F, Van Mieghem NM, Søndergaard L, Latib A, Amat Santos IJ, Bedogni F, Testa L. Transcatheter aortic valve replacement for pure native aortic valve regurgitation: the PANTHEON international project. JACC Cardiovasc Interv. 2023;16(16):1974–85. https://doi.org/10.1016/j.jcin.2023.07.026. PMID: 37648345.
104. Fann JI, Glower DD, Miller DC, Yun KL, Rankin JS, White WD, et al. Preservation of aortic valve in type A aortic dissection complicated by aortic regurgitation. J Thorac Cardiovasc Surg. 1991;102(1):62–73; discussion 73–5.
105. Gott VL, Greene PS, Alejo DE, Cameron DE, Naftel DC, Miller DC, et al. Replacement of the aortic root in patients with Marfan's syndrome. N Engl J Med. 1999;340(17):1307–13.
106. Bentall H, De Bono A. A technique for complete replacement of the ascending aorta. Thorax. 1968;23(4):338–9.
107. David TE, Feindel CM. An aortic valve-sparing operation for patients with aortic incompetence and aneurysm of the ascending aorta. J Thorac Cardiovasc Surg. 1992;103(4):617–21.
108. Yacoub MH, Gehle P, Chandrasekaran V, Birks EJ, Child A, Radley-Smith R. Late results of a valve-preserving operation in patients with aneurysms of the ascending aorta and root. J Thorac Cardiovasc Surg. 1998;115(5):1080–90.
109. Coady MA, Rizzo JA, Hammond GL, Mandapati D, Darr U, Kopf GS, et al. What is the appropriate size criterion for resection of thoracic aortic aneurysms? J Thorac Cardiovasc Surg. 1997;113(3):476–91.
110. Lepore V, Jeppsson A, Radberg G, Mantovani V, Bugge M. Aortic surgery in patients with marfan syndrome: long-term survival, morbidity and function. J Heart Valve Dis. 2001;10(1):25–30.

Tricuspid Valve

3

Michael Y. Henein, Mary Sheppard, John R. Pepper, and Michael Rigby

Anatomy

The morphologically right atrioventricular valve has three leaflets (tricuspid): septal, inferior (mural), and anterosuperior which are separated from each other by anteroseptal, superoinferior, and inferoseptal commissures, respectively. The inferior leaflet takes its origin exclusively from the diaphragmatic parietal wall of the ventricle and is often called the mural leaflet. Each commissure is usually supported by the corresponding papillary muscle. The most characteristic and distinguishing feature of the tricuspid valve is the direct attachment of the cords from the septal leaflet to the septum (Fig. 3.1). These chordal attachments to the septal surface are never seen in the morphological left ventricle except when the tricuspid valve straddles and inserts on the left ventricular septal aspect. The reason for this complex arrangement of chordae tendinea is that the atrioventricular valves must close during systole and these prevent them from ballooning into the atria (Videos 3.1 and 3.2).

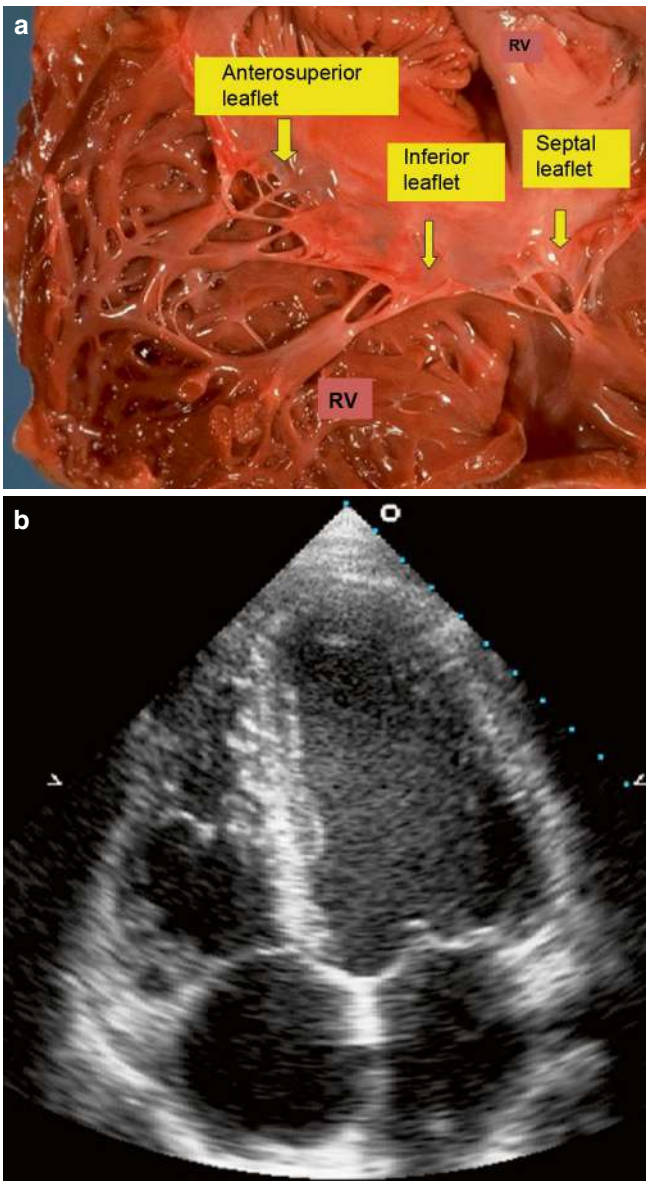


Fig. 3.1 (**a**) Section in the right heart showing the anatomy of the tricuspid valve and its relation to the right atrium and ventricle. (**b**) 2D image of the right heart from the apical view demonstrating the tricuspid septal and anterosuperior leaflets and the trabecular right ventricular apex

Supplementary Information The online version contains supplementary material available at https://doi.org/10.1007/978-3-031-95894-6_3.

M. Y. Henein (✉)
Imperial College London, London, UK

Siena University, Siena, Italy
e-mail: m.henein@imperial.ac.uk

M. Sheppard · J. R. Pepper · M. Rigby
Royal Brompton Hospital, London, UK

© The Author(s), under exclusive license to Springer Nature Switzerland AG 2025

M. Y. Henein (ed.), *Clinical Echocardiography*, https://doi.org/10.1007/978-3-031-95894-6_3

Tricuspid Stenosis

Etiology

Tricuspid stenosis (TS) is rare in adults, and often coexists with tricuspid regurgitation and miral valve disease.

A number of diseases may contribute to the physiological presentation of tricuspid stenosis.

- *Rheumatic valve disease*. This is the most common cause of tricuspid stenosis. The cusps are thickened and the commissures fused so that the valve area becomes small and the valve leaflets dome toward the right ventricle in diastole (Figs. 3.2 and 3.3). In contrast to mitral disease, the subvalvar apparatus is not usually involved [1–3]. As the disease progresses, the right atrium dilates and becomes congested. This is always associated with some degree of tricuspid regurgitation (Fig. 3.4; Video 3.3).
- *Carcinoid Disease*: This is a colonic tumor that secretes 5 hydroxytryptamine which circulates with the blood and affects usually the right heart. The tricuspid valve leaflets become fibrosed and fused so that their movement and opening are restricted (Fig. 3.5) [4, 5].
- *Right Ventricular Pacing*: Tricuspid stenosis may infrequently complicate right ventricular pacing. A pacing wire that perforates one of the three leaflets causes local inflammation, fibrosis, and leaflet stiffness. This can easily be missed by echocardiography if right-sided flow velocities are not carefully studied. Color flow Doppler of the tricuspid valve should give an indication of valve narrowing, and continuous wave Doppler usually confirms significantly raised forward flow velocities (Fig. 3.6). A severe degree of stenosis caused by pacing wires may require valve replacement and insertion of an epicardial lead [6].
- *Functional Tricuspid Stenosis*: When tricuspid valve leaflets are morphologically normal, raised right ventricular inflow velocities can be caused by a number of pathologies:
  (a) *A Large Atrial Septal Defect*: With significant left to right shunt that increases the right atrial stroke volume, right ventricular filling velocities increase. This does not usually result in conventional signs of tricuspid stenosis. After closure of the atrial septal defect, transtricuspid velocities normalize (Fig. 3.7).
  (b) *Localized Pericardial Effusion Behind the Right Atrium*: With progressive increase in a localized effusion pressure, the right atrial free wall may collapse and narrow the inflow tract of the right ventricle, thus resulting in significantly raised velocities (Fig. 3.8). Irrespective of the volume of the pericardial collection, the localized raised pressure is the direct cause

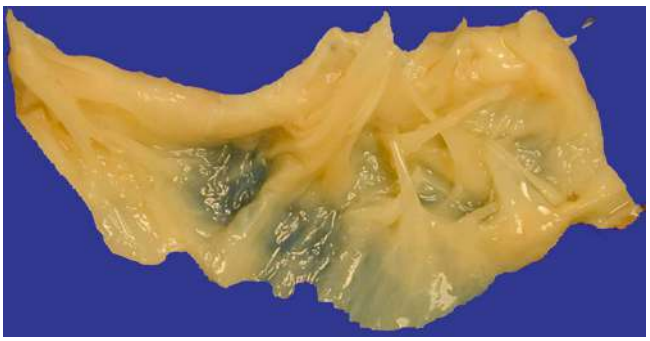


Fig. 3.2 Pathology section from a patient with rheumatic tricuspid valve leaflets

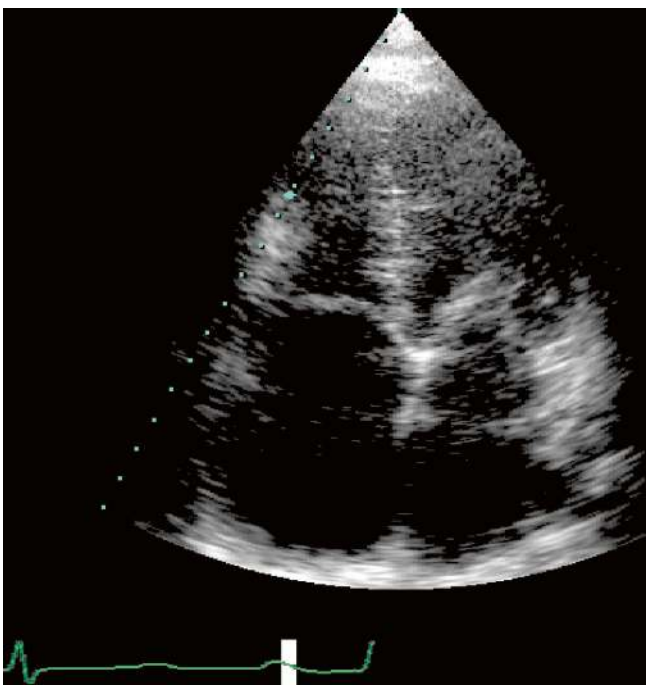


Fig. 3.3 Apical 4 chamber view from a patient with rheumatic mitral and tricuspid valve disease. Note the restricted cusp movement and the valve doming in diastole

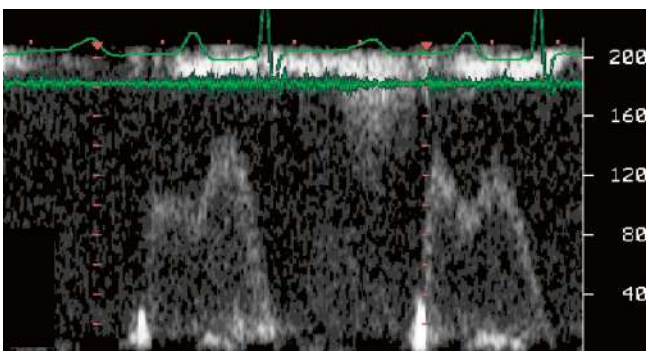


Fig. 3.4 Continuous wave Doppler across the tricuspid valve from the same patient showing high velocities and a mean pressure drop of 4 mmHg

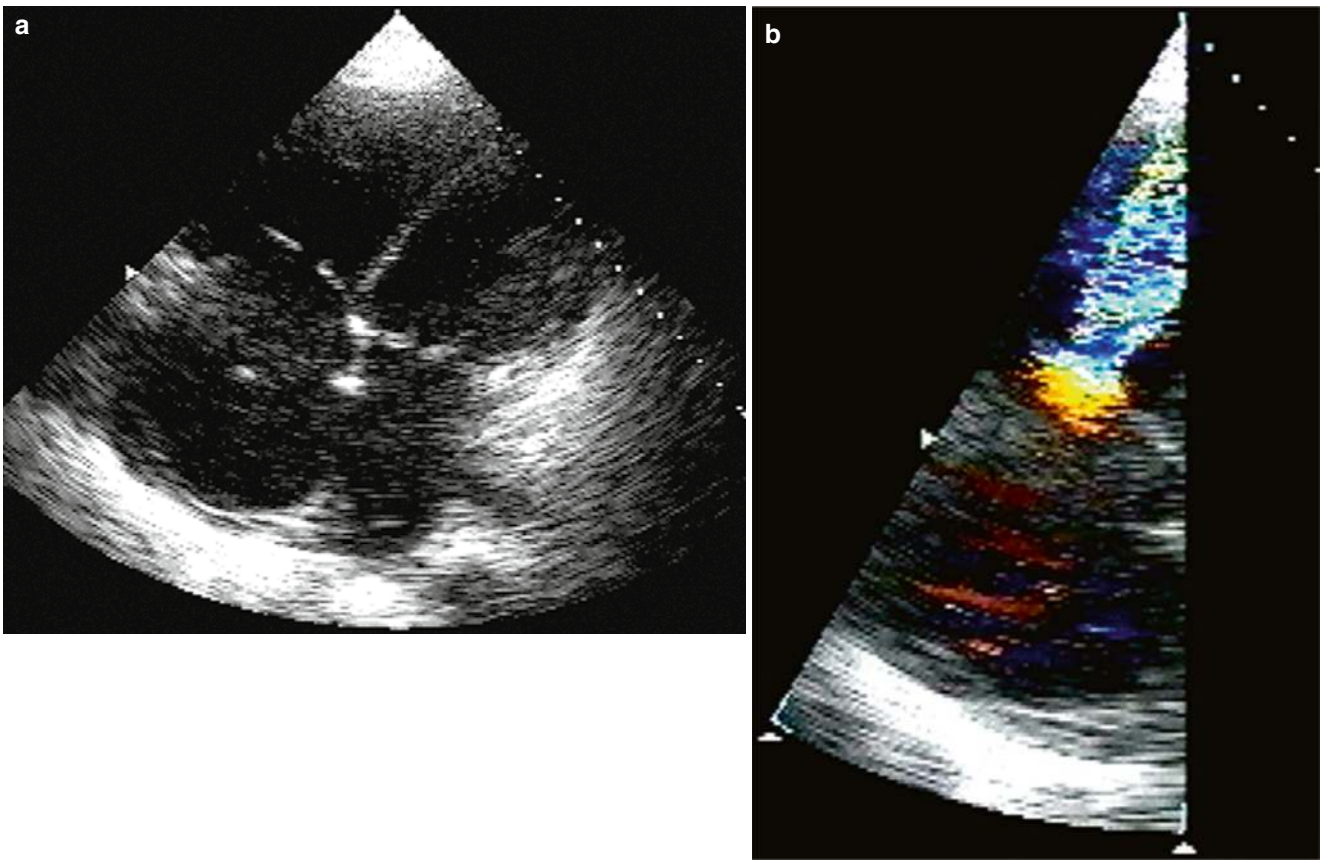


Fig. 3.5 (**a**) Apical 4 chamber view from a patient with carcinoid tricuspid valve disease showing restricted valve opening in diastole and raised flow velocities. (**b**) Color flow Doppler of tricuspid valve forward velocities from the same patient demonstrating aliasing (high velocities) at the leaflet level consistent with restricted valve opening and tricuspid stenosis

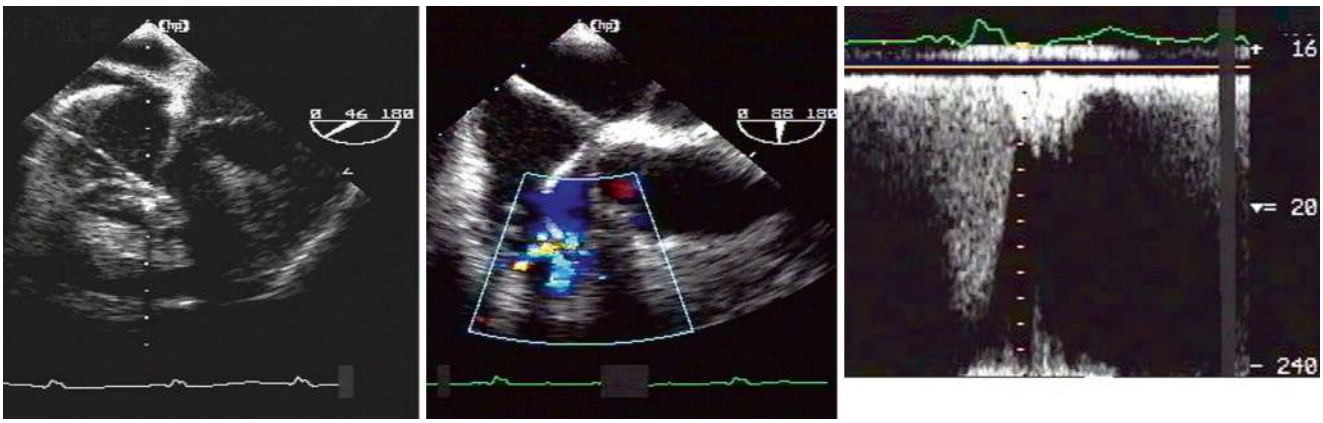


Fig. 3.6 Transesophageal echocardiogram of the right heart showing extensive fibrosis at the site of crossing of the pacemaker leads through the tricuspid valve leaflets. Note the extent of valve fibrosis (*left*) resulting in physiological stenosis shown by aliasing color Doppler (*center*) and raised flow velocities >2 m/s (*right*)

of functional tricuspid stenosis. Draining the pericardial effusion results in complete normalization of valve function and flow velocities.

(c) *Right Atrial Myxoma*: Although rare compared to left atrial myxoma, the tumor narrows the right ventricular inflow tract, causing raised filling velocities. This disturbed physiology normalizes completely after excision of the tumor.

(d) *Right Atrial Secondaries*: Tumors of different histological entities may spread hematologically directly

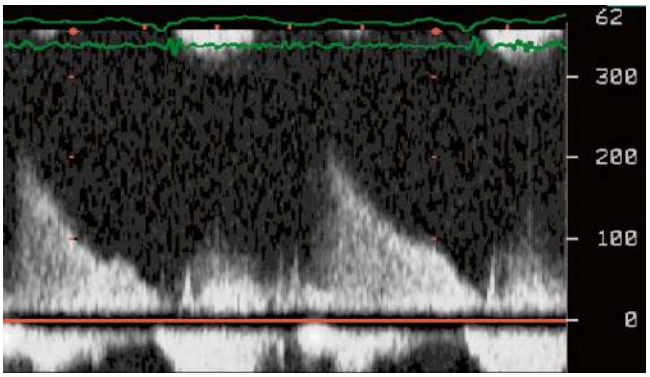


Fig. 3.7 Transtricuspid flow velocities from a patient with atrial septal defect. Note the raised velocities up to 2 m/s before closure

to the right atrium; ovarian sarcoma, renal carcinoma, lymphoma, etc. Large right atrial secondaries may occupy a considerable part of the atrium and interfere with right ventricular inflow tract and filling (Fig. 3.9).

Pathophysiology

Regardless of the etiology, the physiological picture of tricuspid stenosis shares a raised transvalvar forward pressure drop and increased flow velocities. Although this pressure drop is much less than the corresponding pressure across the mitral valve, it results in raised right atrial pressures and systemic venous congestion of varying severity [7–9]. Jugular

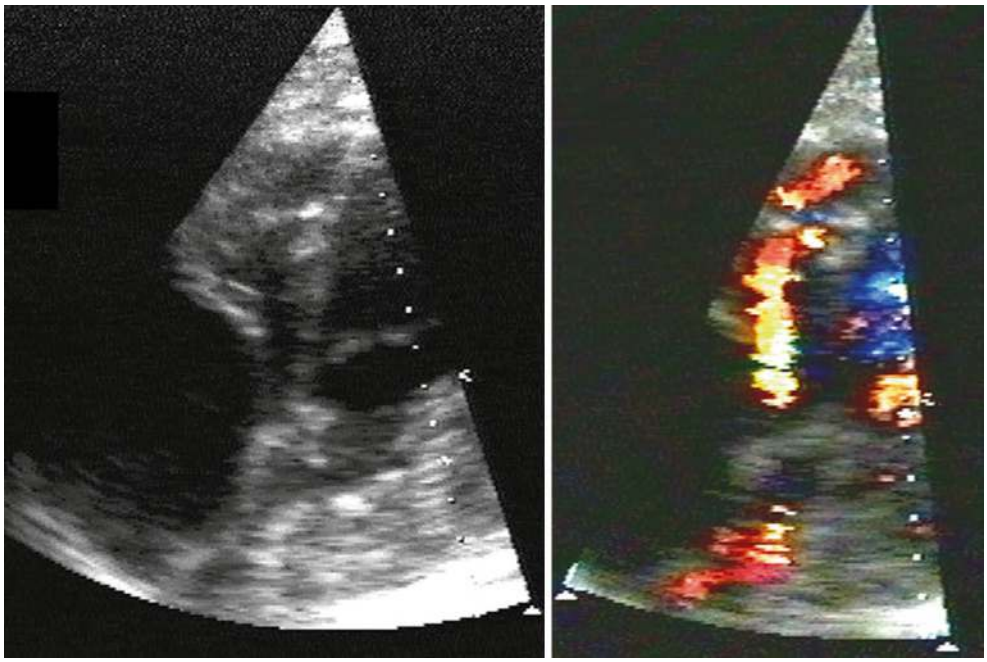


Fig. 3.8 Apical 4 chamber view from a patient with localized pericardial effusion behind the right atrium. Note the collapse of the right atrial free wall (*left*) narrowing the inflow tract of the right ventricle (*left*) and resulting in color aliasing just below the transtricuspid valve level

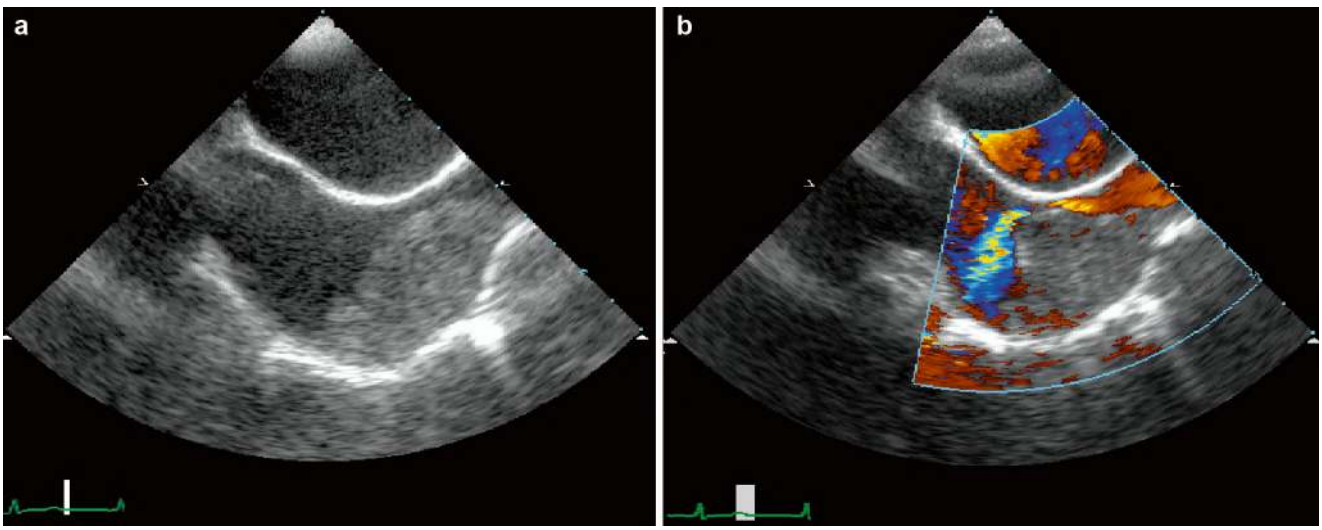


Fig. 3.9 Secondaries invading the right atrium resulting in narrowed inflow (**a**) and high velocities on colour Doppler (**b**)

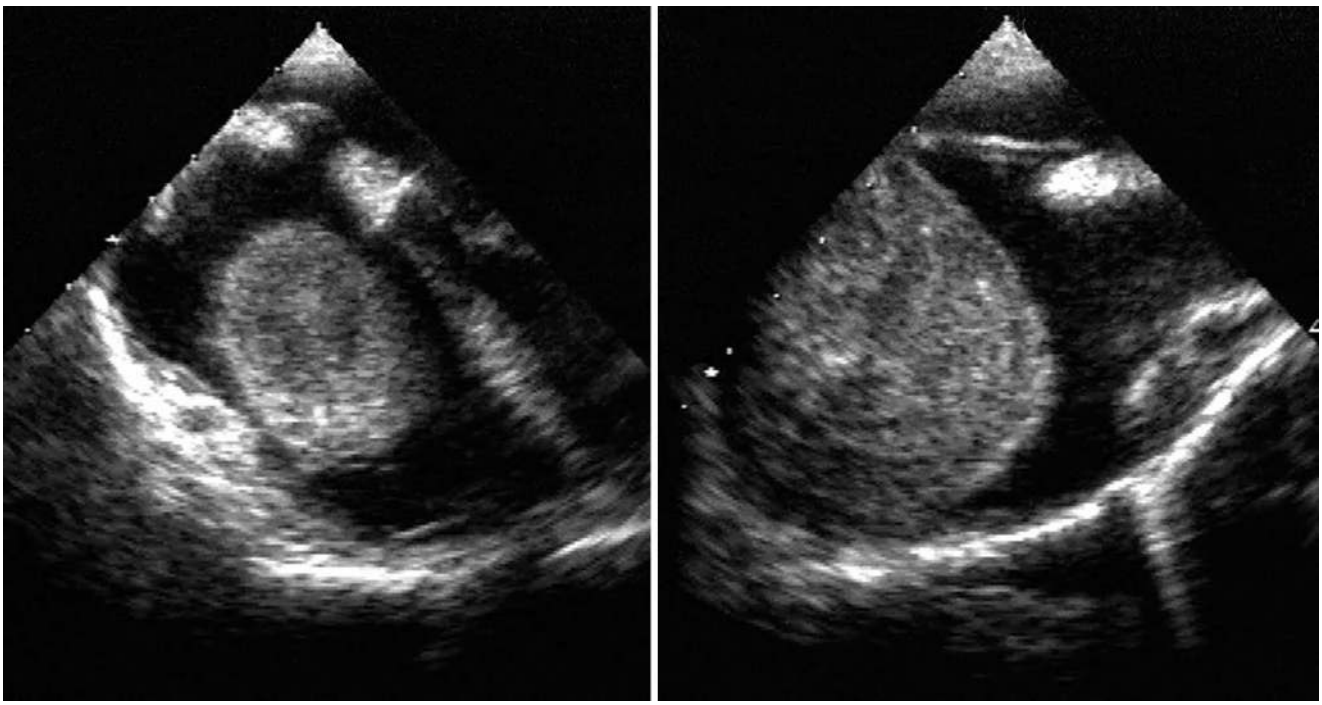


Fig. 3.10 TOE from a patient with renal cell carcinoma invading the inferior vena cava and the right atrium

venous pressure is usually raised demonstrating a slow early diastolic descent consistent with high resistance inflow tract of the right ventricle. Long-standing tricuspid stenosis may result in worsening systemic venous congestion, liver dysfunction, and ascites as well as atrial arrhythmias.

Assessment of Tricuspid Stenosis

Echocardiography is the ideal tool for determining the exact cause of tricuspid stenosis. Conventional 2D imaging helps in assessing right ventricular inflow tract, tricuspid leaflet morphology, and function as well as right atrial size. In addition, extra-cardiac causes which may distort the right atrial cavity shape and function can be detected (pericardial effusion). Disturbed normal color flow Doppler pattern along the vertical axis of the right atrium helps in identifying the level of narrowing. This is usually confirmed by pulsed and continuous wave Doppler, particularly when right ventricular filling velocities are raised.

To accurately assess TS severity, the mean pressure drop across the valve can be derived from the velocity time integral (VTI) of the diastolic continues wave Doppler envelope in the apical four-chamber or parasternal view. A VTI >60 cm and a mean gradient ≥5 mmHg at 70–80 bpm indicate significant TS. The tricuspid valve functional area, calculated by the continuity equation, is challenging due to the known 2DE limitations and stroke volume measurement issues in significant tricuspid or aortic regurgitation. A tricuspid valve area ≤1 cm^2 is considered significant. Transesophageal echocardiography (TOE) is ideal for delineating a clear image of the tricuspid valve leaflets and function. The atrial septum is clearly seen and the extent of tumor invasion of the atrial wall can be assessed. Blood-borne tumor spread can also be assessed by careful study of the inferior vena cava on the TOE images of the right atrium (Fig. 3.10).

Treatment

(a) *Medical*: Systemic venous congestion is usually managed with diuretics. However, a balance should be preserved since with the fixed narrowing of the inflow tract, right ventricular filling relies on the raised right atrial pressure. Radical cure cannot be achieved without correcting the organic lesion.

(b) *Surgical*: Tricuspid valvotomy should be considered at the time of surgery for other valves, particularly with a rheumatic etiology. When missed, it underestimates the surgical success for other procedures, e.g., mitral stenosis. In severe rheumatic tricuspid stenosis, valve replacement is the only option, although this procedure results in some degree of stenosis from the inserted prosthetic valve. Successful drainage of localized pericardial effusion alleviates the associated functional disturbance. Whenever feasible and appropriate, removal of the right atrial space-occupying lesion (tumor) should result in complete recovery of right heart function as long as it

had not invaded the cavity wall. Finally, severe stenosis related to pacing lead might need valve replacement and insertion of and epicardial pacing lead.

Tricuspid Regurgitation

Tricuspid regurgitation (TR) is the retrograde blood from the right ventricle into the right atrium, mainly in systole but rarely in diastole due to restrictive cardiomyopathy or conduction disturbances.

The causes of TR are typically classified into primary (organic), which involves structural changes to the tricuspid valve leaflets, and secondary (functional), where there are no structural abnormalities in the leaflets.

Primary Tricuspid Regurgitation

- *Congenital*: The most common cause of congenital tricuspid regurgitation is Ebstein anomaly. The important echocardiographic features of Ebstein malformation are displacement of the hinge point of the septal and mural (inferior) leaflets of the tricuspid valve from the atrioventricular junction into the body of the inlet compartment of the right ventricle (Figs. 3.11 and 3.12). In most cases, the valve leaflets are dysplastic, but in the more severe cases, the septal or mural leaflets are virtually absent and characteristically the anterosuperior leaflet is large with a so-called sail like motion. Mild-to-moderate valve regurgitation is commonly encountered and an atrial septal defect within the oval fossa usually results in right to left interatrial shunting. Well-recognized associated anomalies with Ebstein anomaly include not only an atrial septal defect but also pulmonary stenosis and ventricular septal defect. Ebstein malformation of the mitral valve is extremely rare, and involvement of the left atrioventricular valve is more likely to be found in congenitally corrected transposition of the great arteries (Video 3.4).
- *Rheumatic Disease*: Severe tricuspid regurgitation has been increasingly recognized after mitral valvotomy or replacement for rheumatic disease, in the absence of significant left-sided disease or pulmonary hypertension; 3-Dimensional echocardiographic studies suggest an organic rheumatic cusp involvement and ring dilatation as the potential underlying pathology for this condition (Figs. 3.14, 3.15, and 3.16) [10].

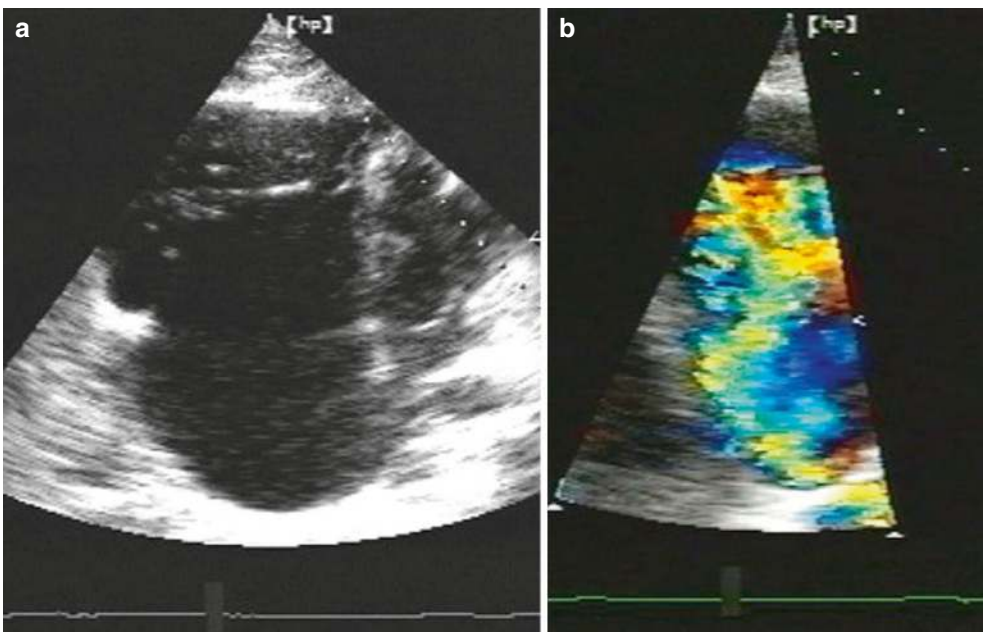


Fig. 3.11 (**a**) Apical 4 chamber view from an adult with Ebstein anomaly and severe tricuspid regurgitation. (**b**) Views from the right ventricle showing thickened ballooned and enlarged tricuspid valve leaflets which are displaced down to the right ventricle. (**c**) A replacement of the mitral valve by a Carpontier Edwards bioprosthesis

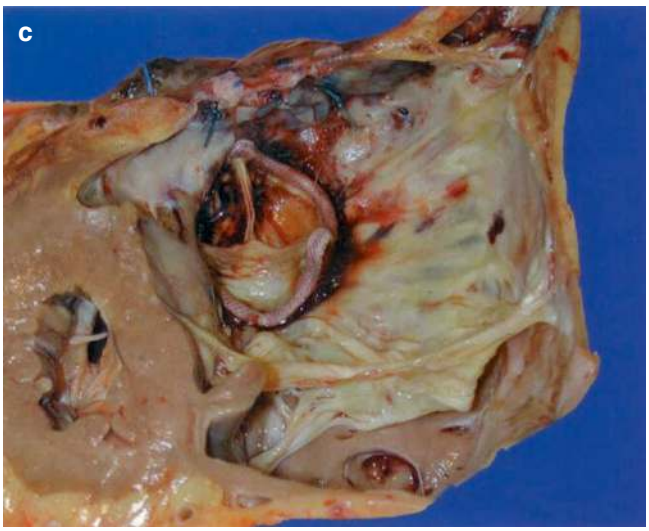


Fig. 3.11 (continued)

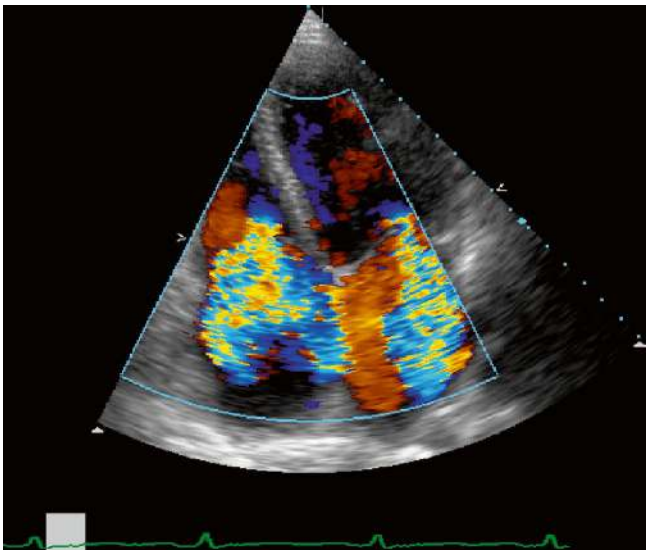


Fig. 3.13 Apical 4 chamber view from a patient with pulmonary hypertension showing dilated right heart and tricuspid regurgitation on color Doppler

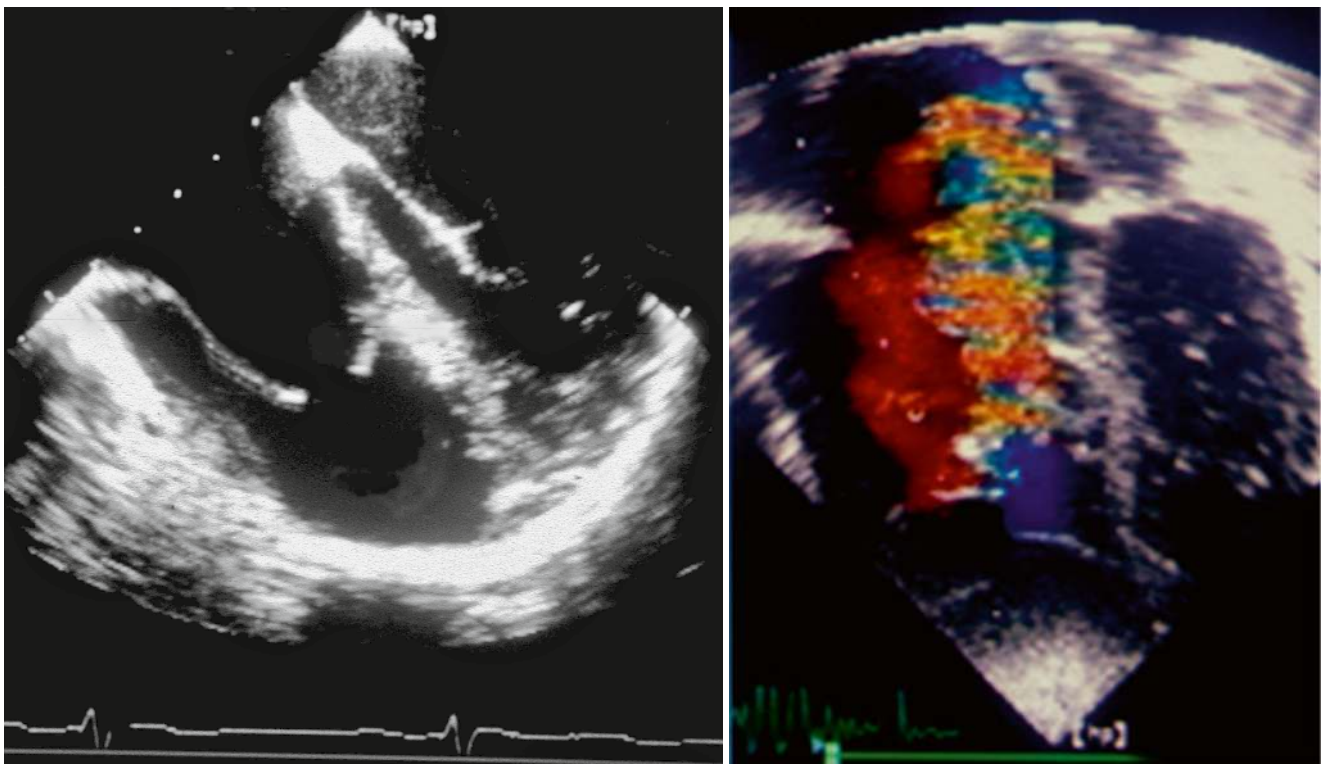


Fig. 3.12 TOE from a patient with Ebstein anomaly showing dilated right heart, apical displacement of the septal tricuspid leaflet (*left*), and severe regurgitation (*right*) on color Doppler

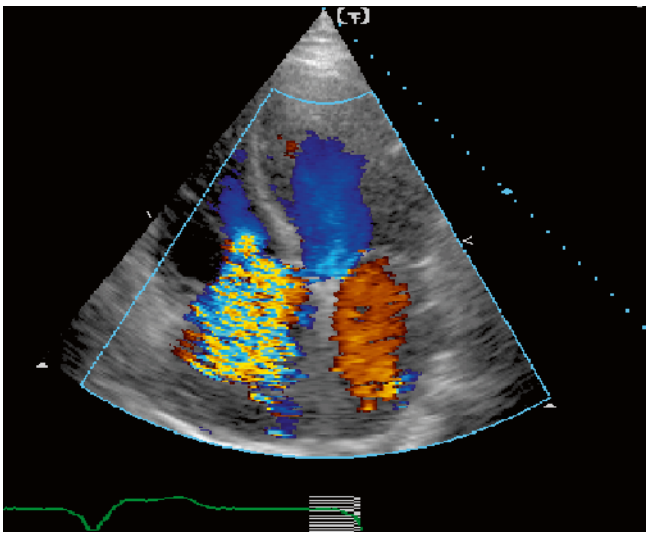


Fig. 3.14 Apical views from a patient with ischaemic heart disease showing significant tricuspid regurgitation

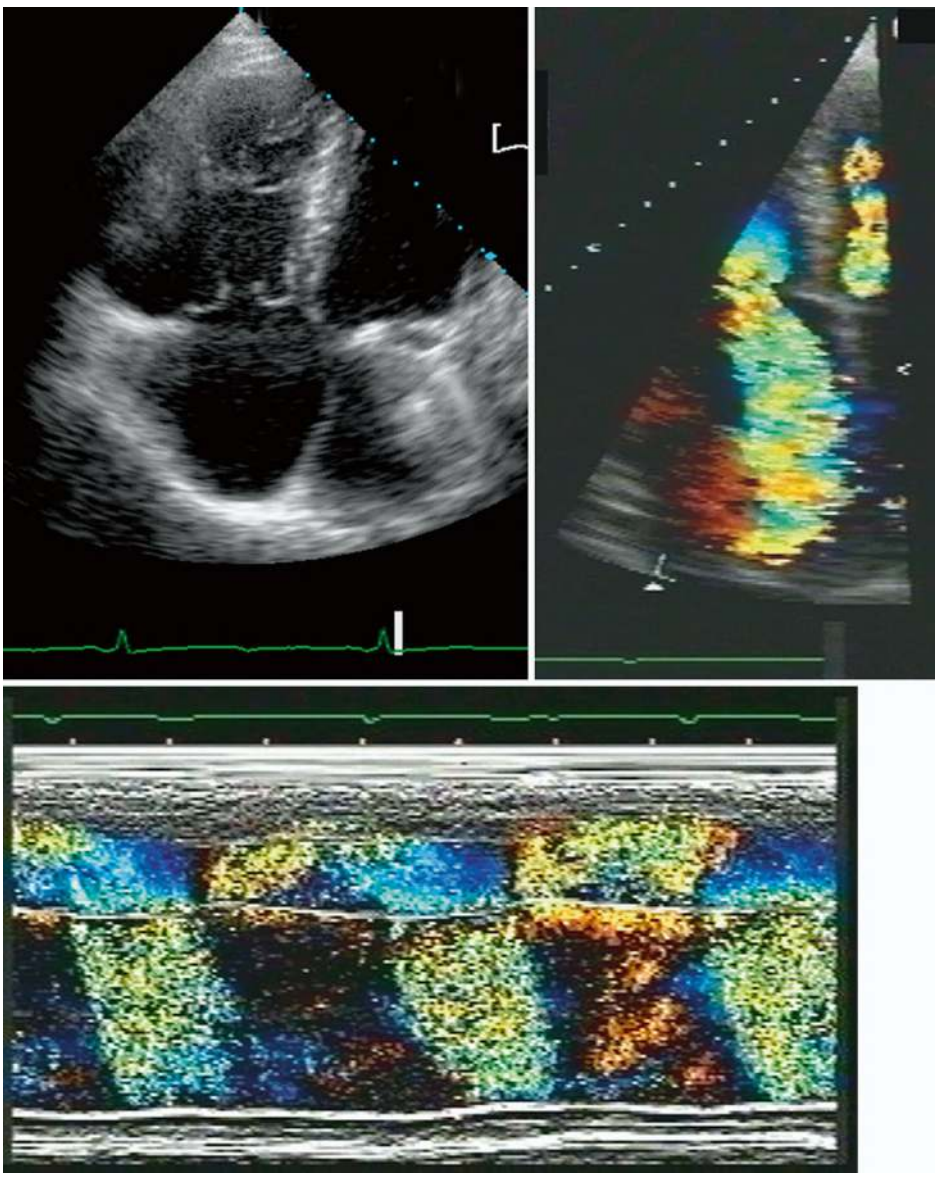


Fig. 3.15 Apical views from a patient with rheumatic mitral valve disease showing involved tricuspid leaflets in the disease process. Note the thickened, short, and failing to coapt leaflets in systole (*left*) resulting in severe regurgitation on color flow Doppler (*right*) which approaches the back of the right atrium on color flow M-mode (*bottom*)

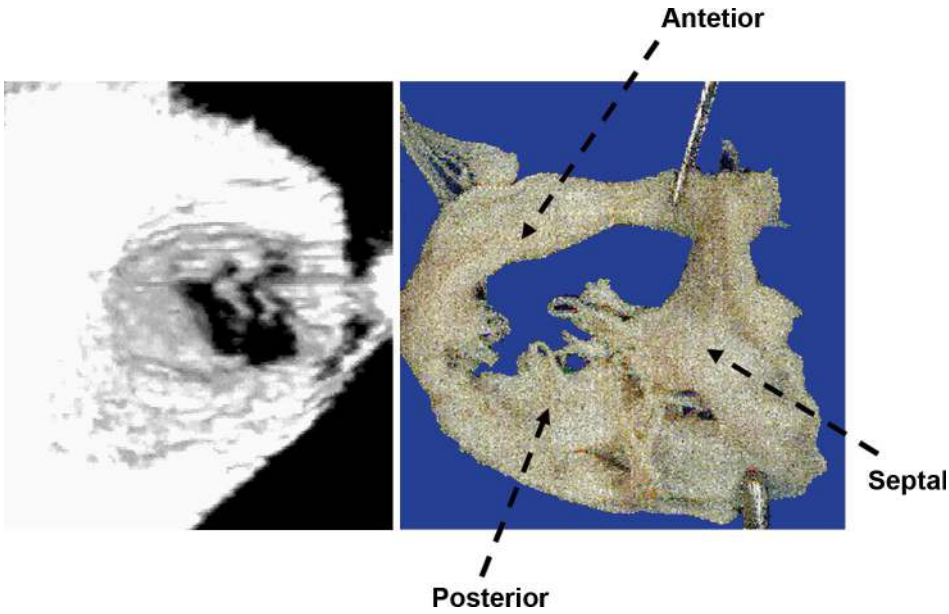


Fig. 3.16 Pathological section from the same patient showing thickened and fibrozed tricuspid leaflets with fused commissures along with the corresponding 3-dimensional echocardiographic images (en face view)

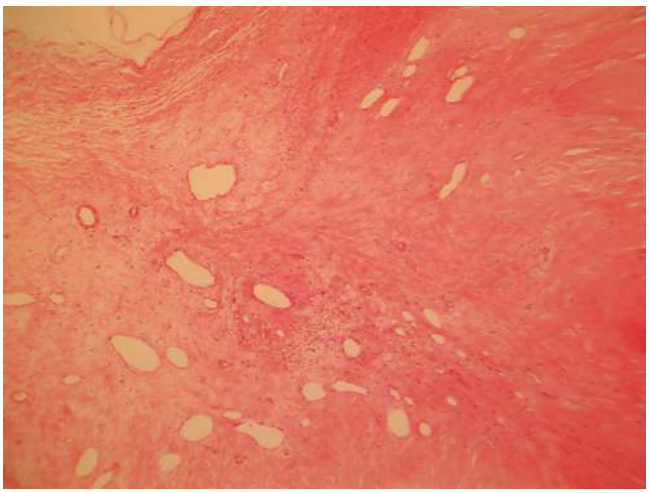


Fig. 3.17 Histological section from the septal leaflet demonstrating vascularization and patchy fibrosis consistent with long-standing inflammatory process

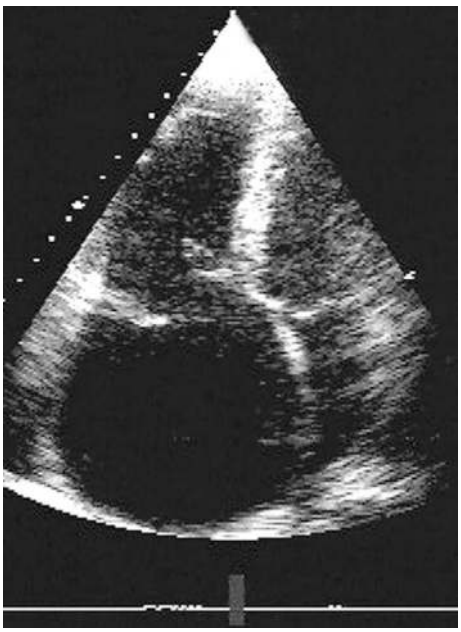


Fig. 3.18 Apical 2D views of the right heart from a drug user showing a vegetation attached to the anterosuperior leaflet of the tricuspid valve and resulting in leaflet prolapse and failure of coaption

- *Endocarditis*: Isolated tricuspid valve endocarditis is less common than other valves, but when present, it may complicate an infected central line or develop in intravenous drug users (Fig. 3.17) [11, 12].
- *Endomyocardial Fibrosis*: Although rare, right-sided endomyocardial fibrosis distorts the inflow tract of the right ventricle and predisposes to severe tricuspid regurgitation (Figs. 3.18 and 3.19). A similar picture is seen with carcinoid syndrome [13].
- *Pacemaker Insertion*: Significant tricuspid regurgitation may develop complicating pacemaker insertion particularly when the lead perforates one of the leaflets (Fig. 3.20). Leaflet fibrosis and retraction develop, resulting in failure of coaption and significant valve incompetence (Video 3.6).
- *Leaflet Prolapse*: Mid-systolic tricuspid valve prolapse may be associated with that of the mitral valve (Figs. 3.21 and 3.22). An example of the association of the two valve dysfunction is seen in Marfan syndrome, although tricuspid regurgitation is usually insignificant compared to mitral regurgitation [14–16].

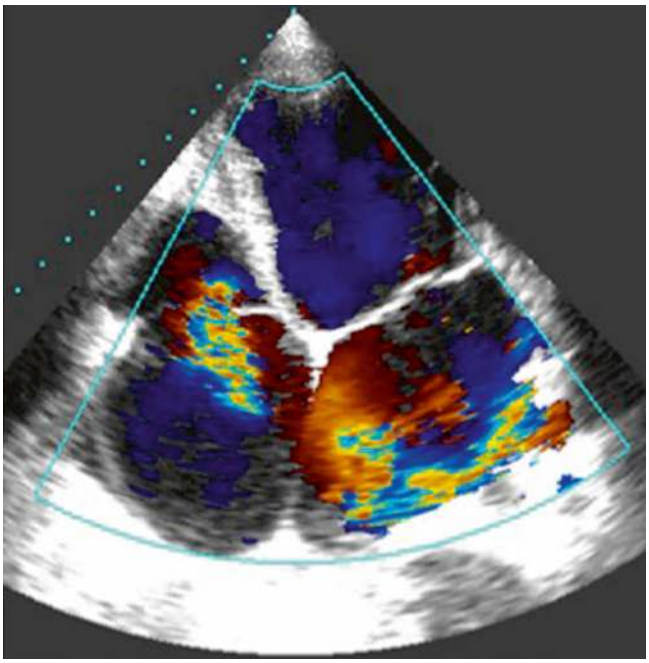


Fig. 3.19 Apical 2D images from a patient with endomyocardial fibrosis showing distorted right ventricular inlet, fibrosed subvalvar apparatus and tricuspid regurgitation

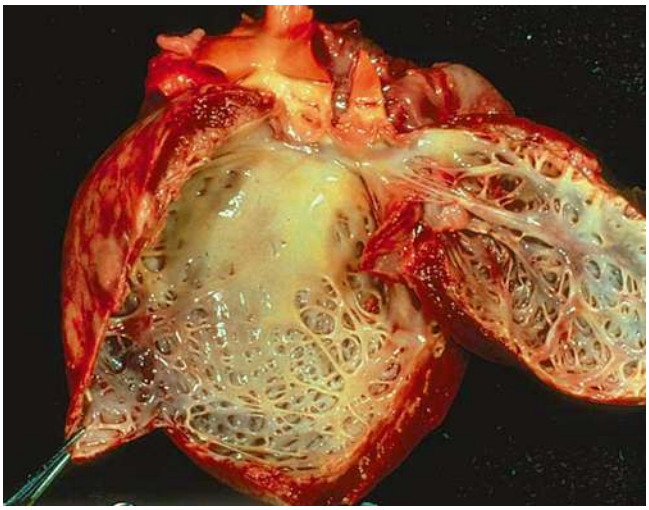


Fig. 3.20 Pathological section from a patient with endomyocardial fibrosis demonstrating extensive subendocardial fibrosis

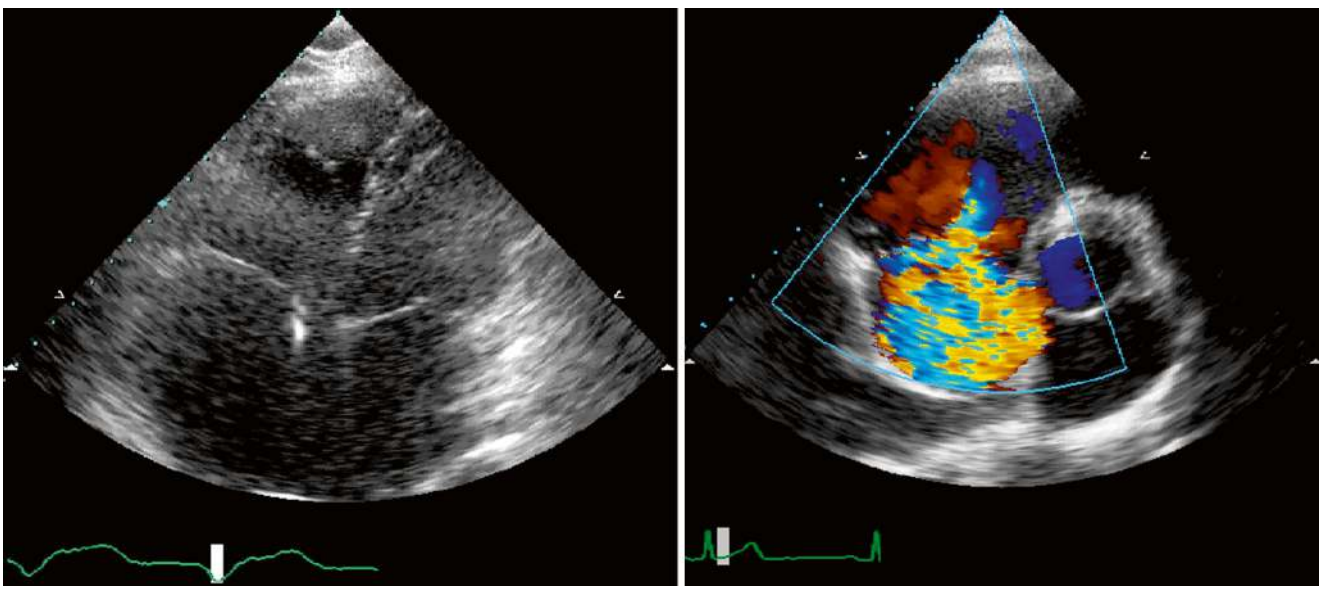


Fig. 3.21 Apical images from a patient with fluid retention after pacemaker insertion. Note the thickened valve leaflets (*left*) and the severe regurgitation (*right*) resulting from localized fibrosis

- *Cardiomyopathy*: Long-standing ischemic myocardial disease of the left ventricle may also involve the right ventricle, particularly in patients with prior right ventricular infarction or ongoing ischemic dysfunction. Progressive ischemic deterioration of the right ventricle may result in dilatation of the basal segment and tricuspid annulus and consequently development of significant regurgitation (Fig. 3.23). A similar picture may be seen in late stage idiopathic dilated cardiomyopathy involving the right heart.
- *Radiotherapy*: Tricuspid regurgitation is an uncommon complication that may appear many years after radiotherapy to the chest. The exact mechanism of valvular regurgitation is poorly understood, but is believed to be caused by slow fibrotic process (Fig. 3.24).

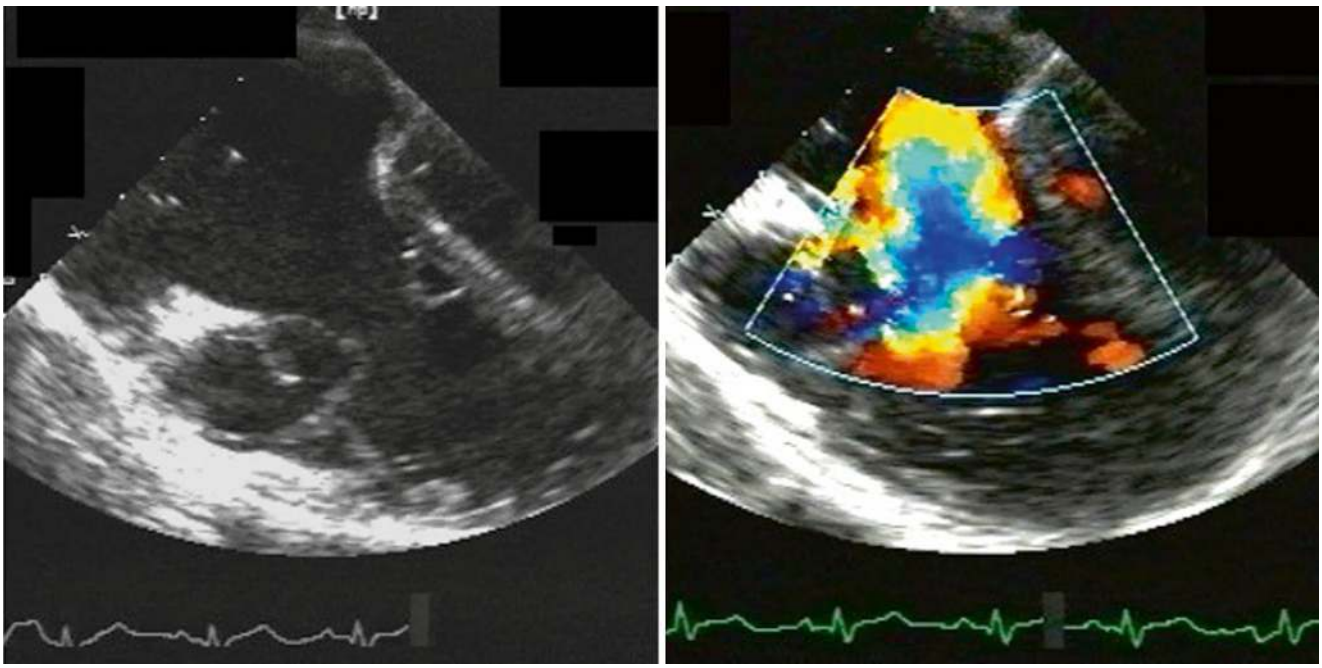


Fig. 3.22 2D images from a patient with congenitally deformed TV leaflets (*left*) resulting in severe regurgitation (*right*)

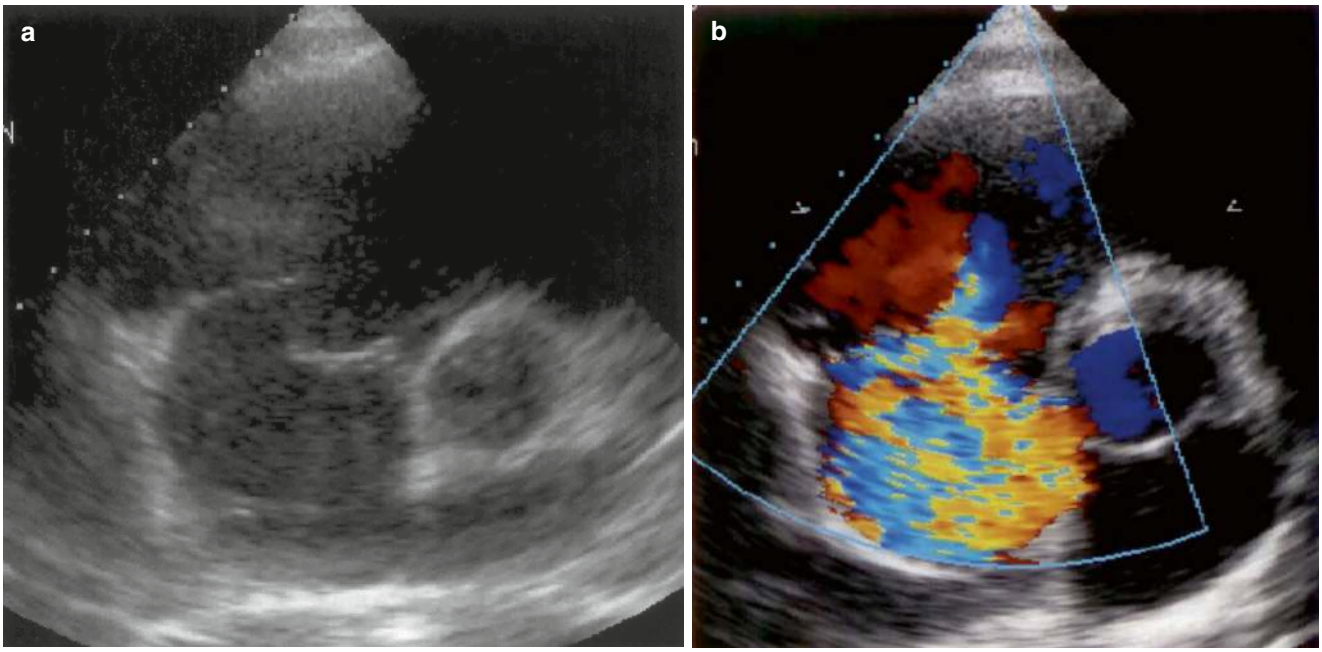


Fig. 3.23 Modified parasternal view from a patient with tricuspid valve prolapse (**a**) causing severe regurgitation (**b**) Note the failure of leaflet coaption

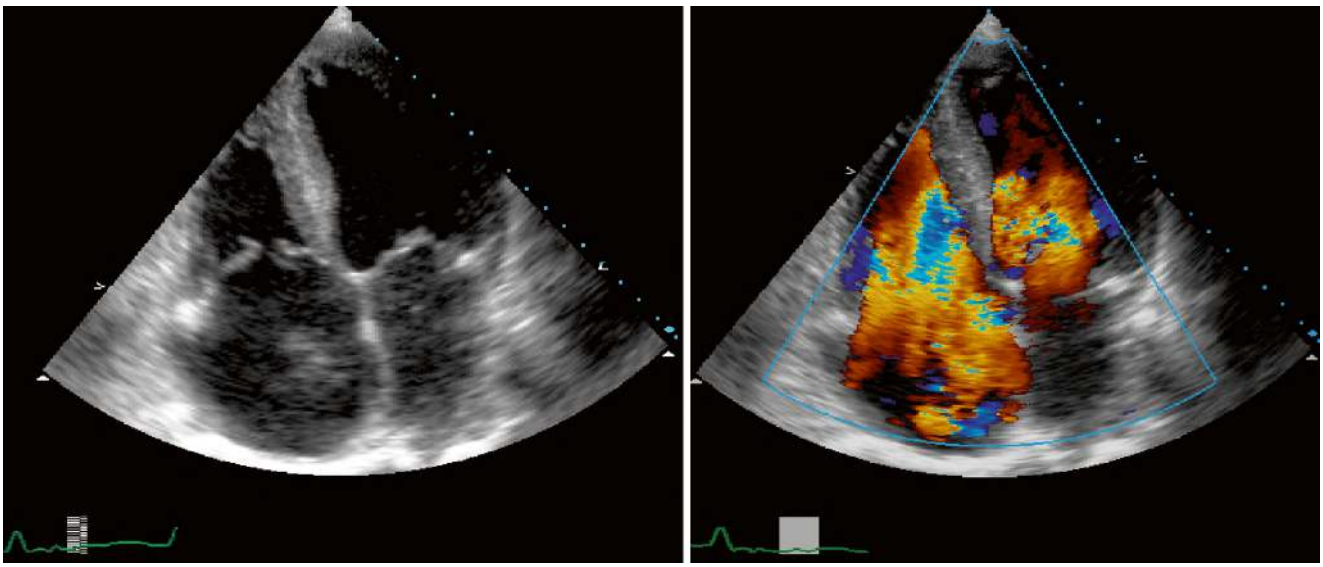


Fig. 3.24 Apical 4 chamber view from a patient with ischemic cardiomyopathy showing dilated 4 chambers (*left*) and severe tricuspid regurgitation on the color Doppler picture (*right*)

Secondary Tricuspid Regurgitation

- *Functional*: Tricuspid regurgitation frequently occurs with dilatation of the right ventricular cavity and tricuspid annulus irrespective of the underlying etiology (Fig. 3.13). It is also seen in patients with pulmonary hypertension and in the end stage of congestive heart failure (Video 3.5).

Pathophysiology

Mild tricuspid regurgitation is common even in 30% of normal people with no cardiac disease. Severe tricuspid regurgitation, irrespective of its etiology, results in signs and symptoms of raised systemic venous pressure. Raised right atrial pressure is transmitted to the venae cava. A systolic "V" wave "from the right ventricle" is seen in the venae cava with the right atrium functioning as a conduit. The systolic "V" wave is followed by a deep wide angled early diastolic venous flow, representing the "Y" descent at the time when the tricuspid valve opens and the right ventricle fills (Fig. 3.25). Long-standing tricuspid regurgitation results in hepatic congestion and fluid retention and eventually renal function impairment. With severe tricuspid regurgitation, the systolic murmur may not be audible due to laminar regurgitation flow.

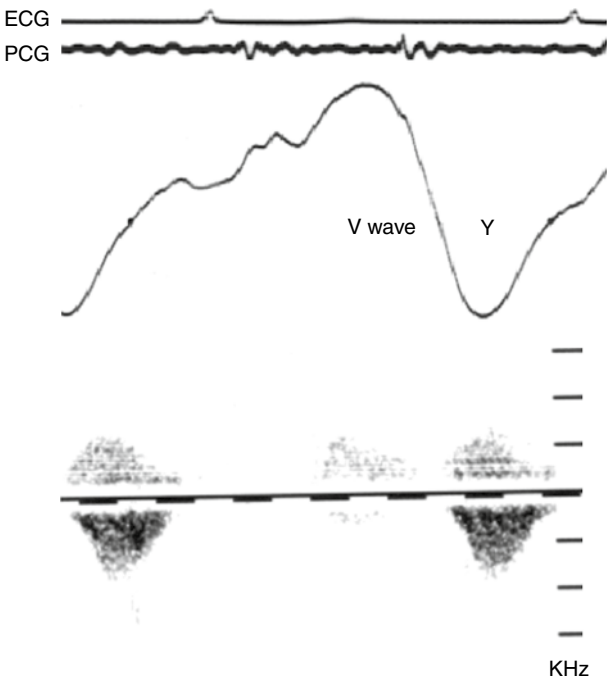


Fig. 3.25 2D image of the tricuspid valve from a patient, 10 years after radiotherapy. Note the normal looking valve morphology, dilated ring, and severe tricuspid regurgitation

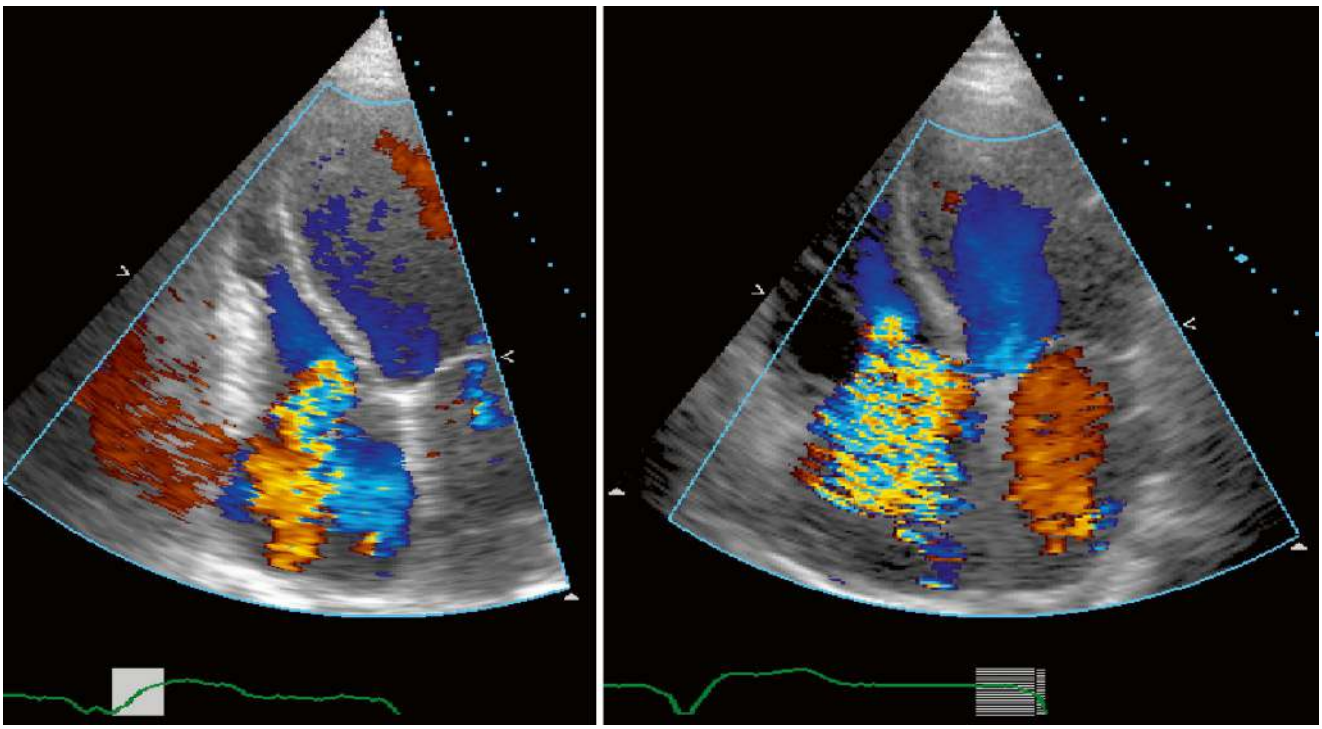


Fig. 3.26 2D images and color Doppler from two patients with tricuspid regurgitation, mild (*left*) and severe (*right*). Note the difference in right atrial size and jet area and diameter

Assessment of Tricuspid Regurgitation

- *Color Flow Doppler*: This is the commonly used echo technique which detects the presence of tricuspid regurgitation, although its absence does not necessarily exclude it. A dilated right atrium and a broad regurgitation jet that approaches the venae cava suggests significant incompetence. A tricuspid regurgitation jet area >40% that of the right atrium is consistent with significant regurgitation (Fig. 3.26) [17].
- *Proximal Isovelocity Convergence Technique*: The same principle as mentioned in the assessment of mitral regurgitation can be applied to determine severity of tricuspid incompetence (Fig. 3.27).
- *Continuous Wave Doppler*: An essential method for assessing severity of tricuspid regurgitation is continuous wave Doppler. It registers the pressure drop between the right ventricle and the right atrium in systole using the modified Bernoulli equation. In the absence of pulmonary valve or right ventricular infundibular stenosis, adding right atrial pressure (approximately 10 mmHg) to the transtricuspid retrograde pressure drop is used to estimate pulmonary artery systolic pressure. Normally with mild functional regurgitation, the higher the pressure drop across the tricuspid valve and the longer it takes to decelerate in early diastole, i.e., after end-ejection (P2), with pulmonary systolic pressure of 80 mmHg is associated with right ventricular—right atrial pressure equalization

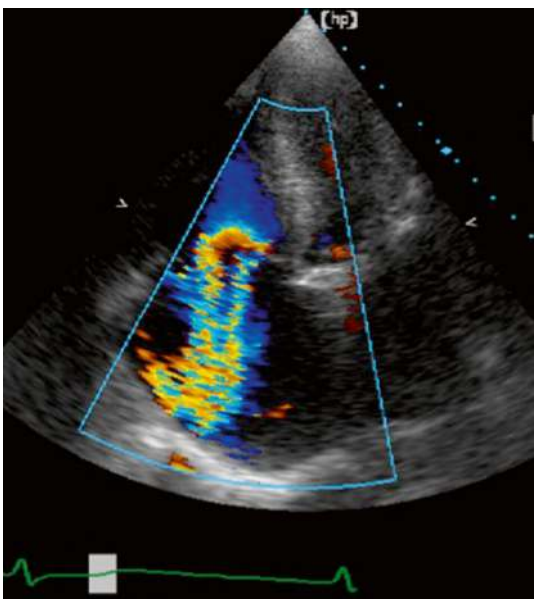


Fig. 3.27 Color flow Doppler of severe tricuspid regurgitation from a patient showing a clear PISA technique at the site of leaflet tips

120 ms after end-ejection. With severe regurgitation and absence of retrograde tricuspid leaflet resistance, the continuous wave Doppler trace becomes more triangular, peaking in early systole and stopping close to end-ejection (Fig. 3.28). This shape represents a reversed V wave in the jugular venous pulse due to pressure equalization between

the right ventricle and the right atrium at end-ejection. In addition, the pressure drop across the valve may fall to as low as 5–10 mmHg due to the increased right atrial pressure. Equalization of forward and backward flow velocity areas suggests free regurgitation. The combination of this picture along with systolic flow reversal in the superior and inferior venae cava or hepatic veins and early diastolic forward flow corresponding to the deep Y descent of the venous pulse confirms the diagnosis of severe regurgitation (Fig. 3.29) [18–20].

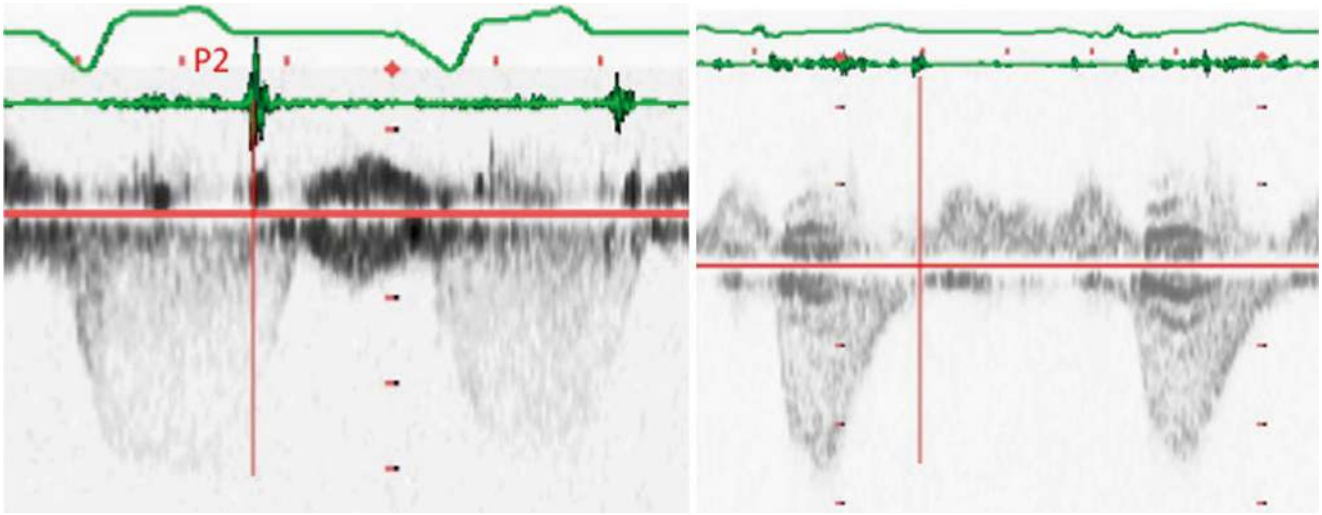


Fig. 3.28 Continuous wave Doppler recordings from two patients with tricuspid regurgitation, mild (*left*) and severe (*right*). Note the low pressure drop and the equalization of right ventricular and atrial pressures in early diastole with severe regurgitation

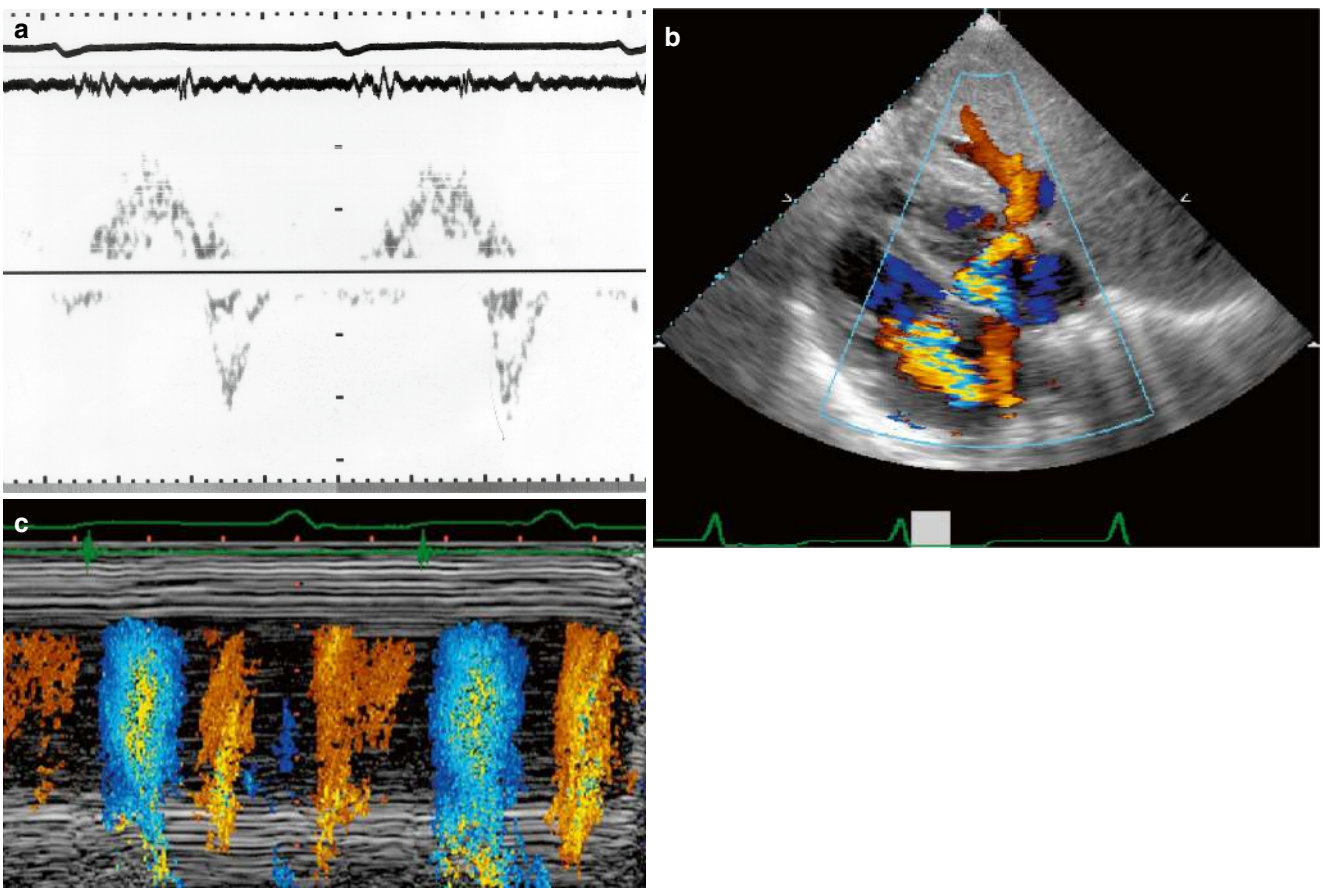


Fig. 3.29 Pulsed wave Doppler velocities from a patient with severe tricuspid regurgitation demonstrating flow reversal in the superior venae cava. (**a**) Respective color flow M-mode showing flow reversal in inferior vena cava (**b**, **c**)

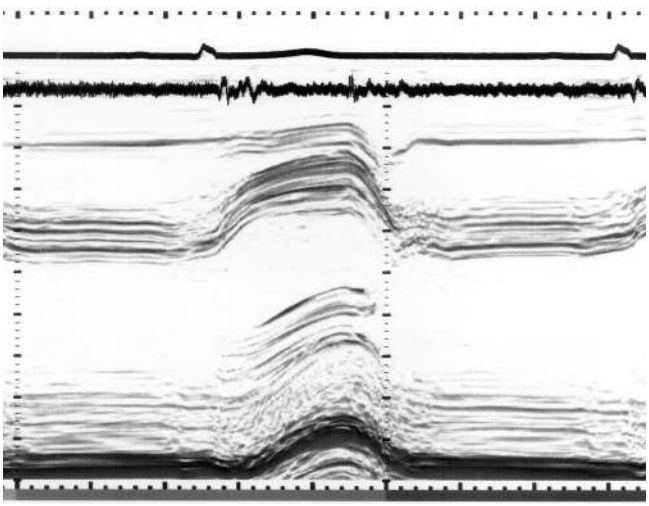


Fig. 3.30 M-mode recording of LV minor axis from a patient with severe tricuspid regurgitation demonstrating reversed septal movement

- *Reversed Septal Movement*: With severe right ventricular volume overload from the tricuspid regurgitation, the interventricular septal movement becomes reversed and the septum functions as part of the right ventricle in systole. This can easily be demonstrated on M-mode images of the left ventricular minor axis (Fig. 3.30).

Treatment

Medical: Medical treatment by diuretics aims at controlling the fluid retention. It may result in significant fall in right ventricular size and hence the extent of tricuspid regurgitation. Moderately severe regurgitation is reasonably tolerated compared to mitral regurgitation. Tricuspid regurgitation secondary to rheumatic mitral valve disease may subside after successful mitral valve surgery, although direct inspection of the tricuspid valve is always recommended for possible plication and repair in an attempt to avoid future incompetence. If the regurgitation is very severe, and the fluid retention requires diuretics in very large doses, enough to cause significant metabolic consequences, valve repair or replacement may be considered.

Surgical Procedures

Tricuspid valve replacement is usually indicated when a prior repair has failed. The repair procedures are less predictable than mitral repair and may involve leaflets only or papillary muscle replacement [21]. Like the mitral valve, tricuspid valve repair can be performed with or without a supporting ring. Furthermore, evidence exists that surgical repair of a dilated tricuspid valve annulus, irrespective of the severity of tricuspid regurgitation, carries better outcome than medical approach [22]. This is based on the suggestion that tricuspid annulus dilatation is an ongoing pathology and a progressive annulus dilatation would sooner or later cause severe regurgitation. The current experience favors the use of large bioprostheses over mechanical valves [23]. Reoperation on the tricuspid valve in cases of persistent tricuspid regurgitation after mitral valve surgery carries a high risk, mostly due to the clinical condition of the patient (including age and the number of previous cardiac interventions) and may well have poor long-term results related to the presence of irreversible right ventricular dysfunction prior to reoperation [23]. In general, tricuspid valve surgery should be considered at the time of left heart valve surgery to avoid potential complications. Many young patients with Ebstein anomaly are symptom-free, but excellent results of surgical repair have been reported in symptomatic patients. A frequent complication of tricuspid valve replacement is heart block due to the close proximity of the AV node to the tricuspid annulus. It is therefore wise to place permanent epicardial electrodes at the time of surgery. These can be easily connected to a pacing box, thus avoiding the problems of running an endocardial lead through a prosthetic valve. Large right atria are usually complicated by arrhythmia (commonly atrial flutter). Trials to control such arrhythmia by right atrial reduction surgery (Maze operation) have been attempted with good results, particularly in Ebstein anomaly. It must be mentioned that tricuspid valve replacement for resistant regurgitation to medical therapy should be performed in a timely fashion before development of intractable right ventricular failure. Late surgery may be followed by residual postoperative raised venous pressure and systemic congestion.

References

1. Daniels SJ, Mintz GS, Kotler MN. Rheumatic tricuspid valve disease: two-dimensional echocardiographic, hemodynamic, and angiographic correlations. Am J Cardiol. 1983;51(3):492–6.
2. Guyer DE, Gillam LD, Foale RA, Clark MC, Dinsmore R, Palacios I, et al. Comparison of the echocardiographic and hemodynamic diagnosis of rheumatic tricuspid stenosis. J Am Coll Cardiol. 1984;3(5):1135–44.
3. Shimada R, Takeshita A, Nakamura M, Tokunaga K, Hirata T. Diagnosis of tricuspid stenosis by M-mode and two-dimensional echocardiography. Am J Cardiol. 1984;53(1):164–8.
4. Pellikka PA, Tajik AJ, Khandheria BK, Seward JB, Callahan JA, Pitot HC, et al. Carcinoid heart disease. Clinical and echocardiographic spectrum in 74 patients. Circulation. 1993;87(4):1188–96.
5. Ross EM, Roberts WC. The carcinoid syndrome: comparison of 21 necropsy subjects with carcinoid heart disease to 15 necropsy subjects without carcinoid heart disease. Am J Med. 1985;79(3):339–54.
6. Heaven DJ, Henein MY, Sutton R. Pacemaker lead related tricuspid stenosis: a report of two cases. Heart. 2000;83(3):351–2.
7. Denning GK, Henneke KH, Rudolph W. Assessment of tricuspid stenosis by Doppler echocardiography. J Am Coll Cardiol. Abstract. 1987.

8. Parris TM, Panidis JP, Ross J, Mintz GS. Doppler echocardiographic findings in rheumatic tricuspid stenosis. Am J Cardiol. 1987;60(16):1414–6.
9. Veyrat C, Kalmanson D, Farjon M, Manin JP, Abitbol G. Noninvasive diagnosis and assessment of tricuspid regurgitation and stenosis using one and two dimensional echo-pulsed Doppler. Br Heart J. 1982;47(6):596–605.
10. Henein MY, Sheppard M, Ho Y, Pepper J, Gibson DG. Evidence for rheumatic valve disease in patients with severe tricuspid regurgitation long after mitral valve surgery – role of 3D reconstruction. J Heart Valve Dis. 2003;12(5):566–72.
11. Ginzton LE, Siegel RJ, Criley JM. Natural history of tricuspid valve endocarditis: a two dimensional echocardiographic study. Am J Cardiol. 1982;49(8):1853–9.
12. Bates ER, Sorkin RP. Echocardiographic diagnosis of flail anterior leaflet in tricuspid endocarditis. Am Heart J. 1983;106(1 Pt 1):161–3.
13. Howard RJ, Drobac M, Rider WD, Keane TJ, Finlayson J, Silver MD, et al. Carcinoid heart disease: diagnosis by two-dimensional echocardiography. Circulation. 1982;66(5):1059–65.
14. Chandraratna PN, Lopez JM, Fernandez JJ, Cohen LS. Echocardiographic detection of tricuspid valve prolapse. Circulation. 1975;51(5):823–6.
15. Rippe JM, Angoff G, Sloss LJ, Wynne J, Alpert JS. Multiple floppy valves: an echocardiographic syndrome. Am J Med. 1979;66(5):817–24.
16. Schlamowitz RA, Gross S, Keating E, Pitt W, Mazur J. Tricuspid valve prolapse: a common occurrence in the click-murmur syndrome. J Clin Ultrasound. 1982;10(9):435–9.
17. Suzuki Y, Kambara H, Kadota K, Tamaki S, Yamazato A, Nohara R, et al. Detection and evaluation of tricuspid regurgitation using a real-time, two-dimensional, color-coded, Doppler flow imaging system: comparison with contrast two-dimensional echocardiography and right ventriculography. Am J Cardiol. 1986;57(10):811–5.
18. Currie PJ, Seward JB, Chan KL, Fyfe DA, Hagler DJ, Mair DD, et al. Continuous wave Doppler determination of right ventricular pressure: a simultaneous Doppler-catheterization study in 127 patients. J Am Coll Cardiol. 1985;6(4):750–6.
19. Sakai K, Nakamura K, Satomi G, Kondo M, Hirosawa K. Hepatic vein blood flow pattern measured by Doppler echocardiography as an evaluation of tricuspid valve insufficiency. J Cardiogr. 1983;13(1):33–43.
20. Chan KL, Currie PJ, Seward JB, Hagler DJ, Mair DD, Tajik AJ. Comparison of three Doppler ultrasound methods in the prediction of pulmonary artery pressure. J Am Coll Cardiol. 1987;9(3):549–54.
21. Dreyfus GD, Souza Neto O, Aubert S. Papillary muscle repositioning for repair of anterior leaflet prolapse caused by chordal elongation. J Thorac Cardiovasc Surg. 2006;132(3):578–84.
22. Dreyfus GD, Corbi PJ, Chan KM, Bahrami T. Secondary tricuspid regurgitation or dilatation: which should be the criteria for surgical repair? Ann Thorac Surg. 2005;79(1):127–32.
23. Vahanian A, Baumgartner H, Bax J, Butchart E, Dion R, Filippatos G, et al. Guidelines on the management of valvular heart disease: the Task Force on the Management of Valvular Heart Disease of the European Society of Cardiology. Eur Heart J. 2007;28(2):230–68. Epub Jan 26, 2007. No abstract available.

Pulmonary Valve

4

Michael Y. Henein, Mary Sheppard, John R. Pepper, and Michael Rigby

Anatomy

The pulmonary valve lies anterior and to the left of the aortic valve. The three pulmonary leaflets assume the shape of half moons (semi-lunar) and are similar but usually not equal in size. The right and left coronary sinuses of the aorta always face the pulmonary valve. The leaflets are thinner and more delicate than the aortic leaflets. Unlike the aortic valve, the pulmonary valve sits on a complete muscular ring of the infundibulum and is not in direct continuity with the tricuspid valve (Fig. 4.1). It is thickest along the closing edge. The delicate pocket-like leaflets are formed primarily of collagen, and they, therefore, open and close passively, with little elastic recoil. In the middle of the free edge of each leaflet is a fibrous mound, the nodule of Arrantius. Coaption of the three nodules ensures complete central closure of the valve orifice during ventricular diastole.

In adults, the pulmonary valve is better viewed from the parasternal short axis window with anterior angulation (Fig. 4.2). It can occasionally be seen from the suprasternal and subcostal views. Normal transpulmonary valve blood velocity is in the order of 75 cm/s in mid-ejection [1]. Acquired pulmonary valve diseases are rare.



Fig. 4.1 Section in the right ventricular outflow tract and pulmonary valves showing the three leaflets

Supplementary Information The online version contains supplementary material available at https://doi.org/10.1007/978-3-031-95894-6_4.

M. Y. Henein (✉)
Imperial College London, London, UK

Siena University, Siena, Italy
e-mail: m.henein@imperial.ac.uk

M. Sheppard · J. R. Pepper · M. Rigby
Royal Brompton Hospital, London, UK

© The Author(s), under exclusive license to Springer Nature Switzerland AG 2025
M. Y. Henein (ed.), *Clinical Echocardiography*, https://doi.org/10.1007/978-3-031-95894-6_4

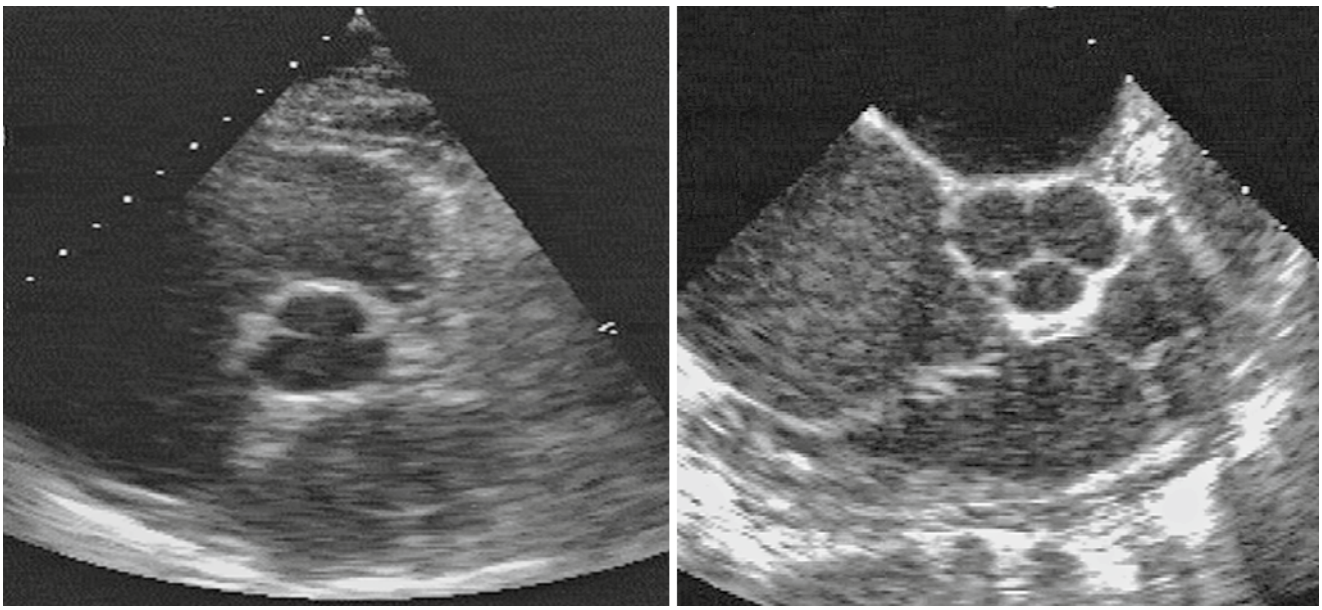


Fig. 4.2 Short axis view of the aortic valve demonstrating normal looking pulmonary valve leaflets and pulmonary artery diameter. Transthoracic (*left*) and transesophageal (*right*)

Pulmonary Stenosis

Pulmonary stenosis can be at three levels: valvular, subvalvar, and supravalvar.

Pumonary Valvular Stenosis

Pulmonary valve stenosis is almost always congenital in origin and can occur alone or in conjuction with other congenital heart disease. It is very rarely rheumatic. Congenital pulmonary stenosis is associated with doming leaflets with total fusion and a single orifice in the middle (Fig. 4.3). In the tetralogy of Fallot, pulmonary valve leaflets are often dysplastic, which are small and thickened and the valve may have only two leaflets [2]. In systole, the leaflets appear doming in the center of the pulmonary artery and are unable to move parallel to the arterial wall as they normally do [3]. In diastole, leaflets may look completely normal since they are not really thickened. Pulmonary stenosis is commonly associated with post-stenotic dilatation of the pulmonary artery which itself may suggest the presence of pulmonary stenosis. Contrary to what occurs with the aortic valve, it is uncommon for the pulmonary valve leaflets to calcify with time [4]. Balloon valvuloplasty is the ideal procedure for managing congenital pulmonary stenosis in children and early adulthood, but the procedure may be complicated by some degree of pulmonary regurgitation particularly in the long term [5]. Similar procedure could be performed in fetuses with pulmonary stenosis or atresia as an attempt to save the ventricle [6]. Rheumatic pulmonary stenosis is extremely rare. Other rare causes of pulmonary valve stenosis are carcinoid disease [7] where kinins released by the carcinoid tumor in the gastro-intestinal tract cause superficial fibrosis of both the tricuspid and pulmonary valves (Video 4.1).

Pulmonary Stenosis Severity

Color flow Doppler shows the level at which maximum aliasing occurs: valvar, subvalvar, or supravalvar. Continuous wave Doppler is the ideal technique for registering peak pulmonary valve velocities that can be translated into a pressure drop by applying the modified Bernoulli equation, $4V^2$. A pressure drop of more than 75 mmHg is considered severe stenosis (Fig. 4.4) [8, 9]. Severe pulmonary stenosis is usually associated with some degree of right ventricular hypertrophy and dysfunction. Significant impairment of right ventricular systolic function and consequently reduction in stroke volume may underestimate the severity of pulmonary stenosis when relying solely on the pulmonary velocities. Recent investigations have shown that patients with significant pulmonary stenosis may have exaggerated left atrial function as a sign of atrial interaction, in a similar way those with aortic stenosis have accentuated right atrial systolic mechanical activity "Bernheim a wave" [10].

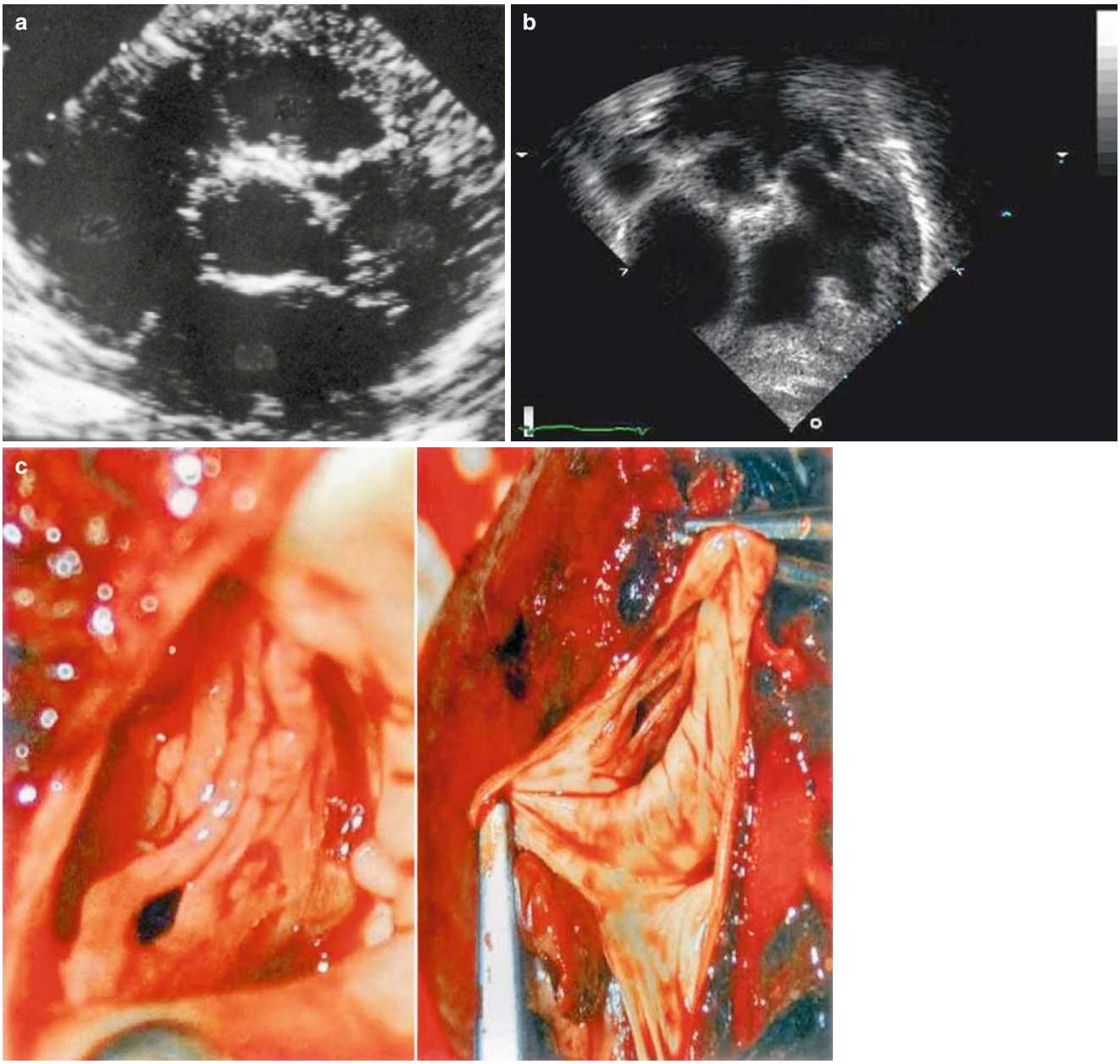


Fig. 4.3 Subcostal views from a patient with deformed pulmonary valve showing stiff and fibrosed leaflets (**a**) and systolic doming (**b**) causing valve stenosis. (**c**) Pathological section from a patient with bicuspid pulmonary valve

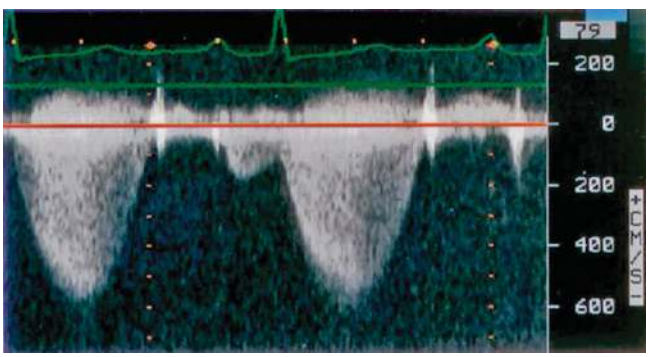


Fig. 4.4 Continuous wave Doppler velocities across a stenotic pulmonary valve registering a value of 4.5 m/s equivalent to a pressure drop of 81 mmHg

Subvalvar Pulmonary Stenosis

Subvalvar pulmonary stenosis is commonly caused by infundibular stenosis or a two-chambered right ventricle either in isolation or together with valvar stenosis or Fallot Tetralogy [11]. Subvalvar pulmonary stenosis can easily be seen on 2D images and confirmed by color Doppler (Figs. 4.5 and 4.6). When it occurs alone, it is often associated with post-stenotic dilatation. It may also be part of other disease conditions such as hypertrophic cardiomyopathy that involves the right heart. Rare causes of subvalvar stenosis include tumors, both primary (angiosarcoma or fibroma) and secondary (melanoma).

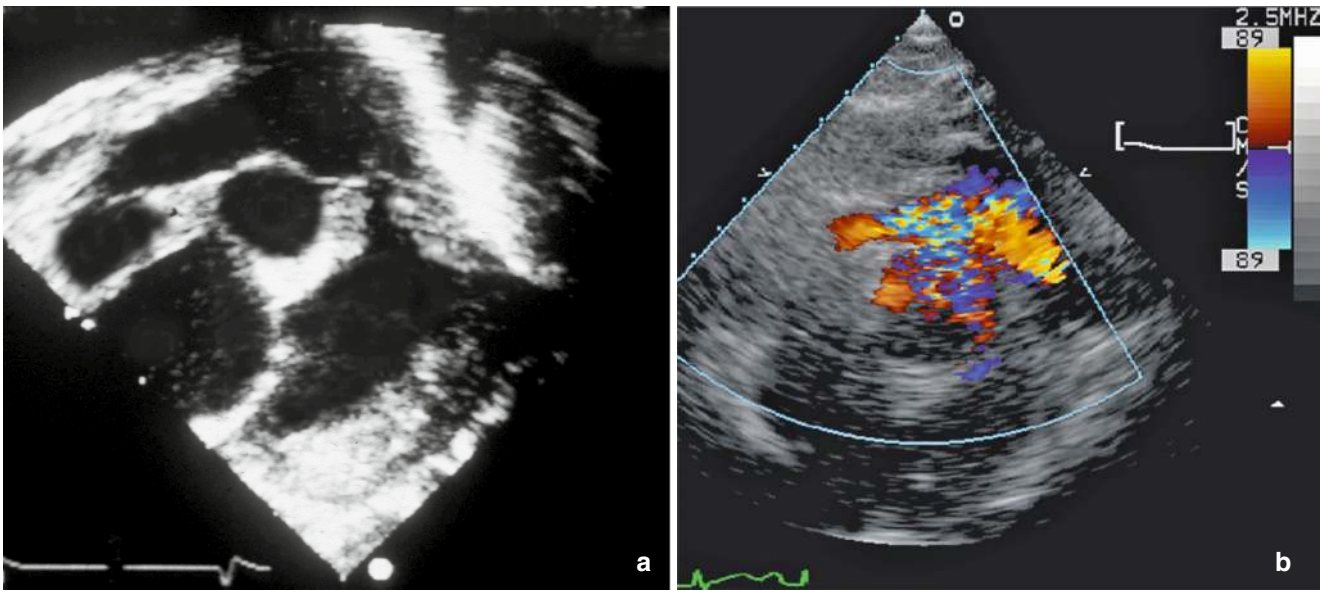


Fig. 4.5 Subcostal views demonstrating subvalvar (infundibular) pulmonary stenosis (**a**) Note the level of narrowing below the valve leaflets (**b**)

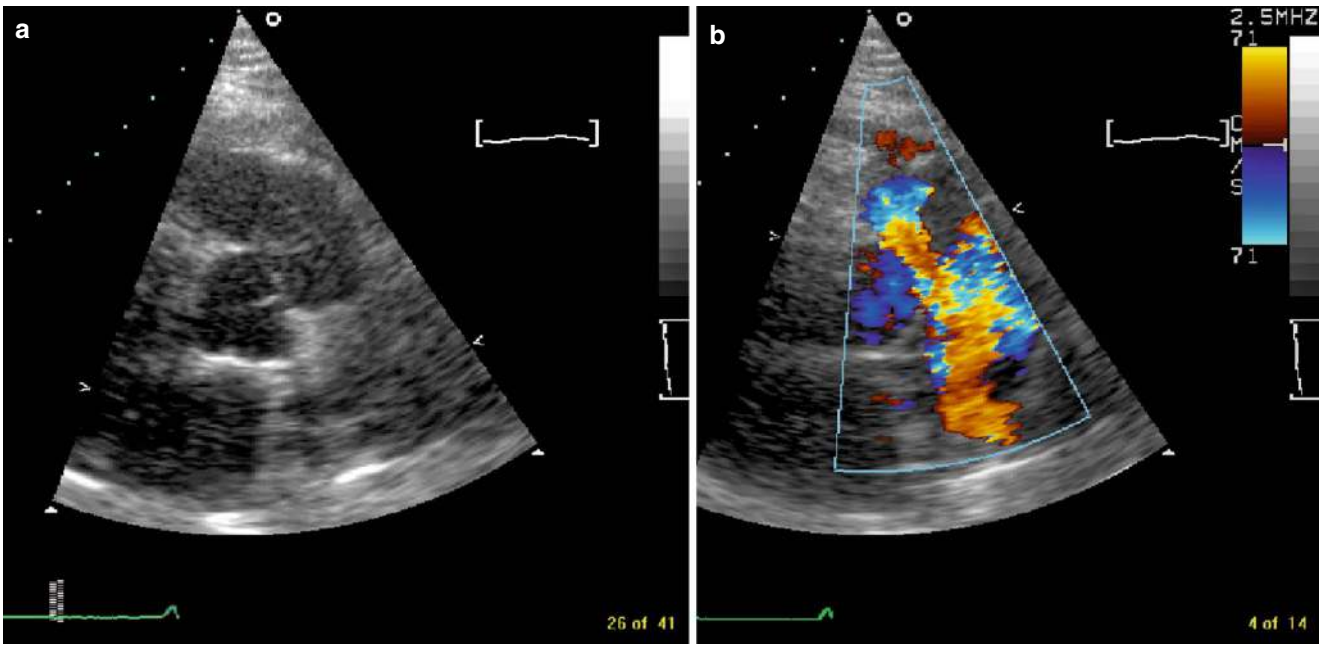


Fig. 4.6 (**a**) 2D images of the pulmonary valve demonstrating subvalvar pulmonary stenosis caused by secondaries (melanoma). (**b**) Color flow Doppler demonstrating the stenosis level beneath the valve. (**c**) Continuous wave Doppler showing peak RV outflow tract velocities 2.0 m/s

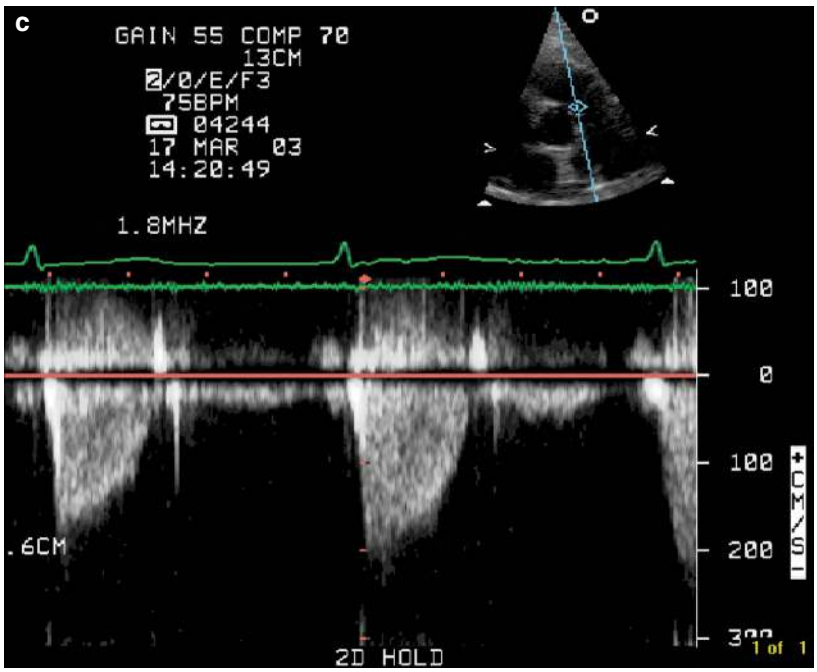


Fig. 4.6 (continued)

Supravalvar Pulmonary Stenosis

Supravalvar pulmonary stenosis occurs in the proximal segment of the pulmonary artery, either in the form of single or multiple narrowings [12, 13] as in Williams syndrome. A typical example occurs following banding of the pulmonary artery as part of the management of significant intracardiac shunting such as multiple ventricular septal defects [14]. However, supravalvar stenosis may also involve only the pulmonary artery branches and spare the main trunk [15]. Once again, color flow Doppler indicates the site of narrowing and continuous wave Doppler can be used to assess the severity of stenosis (Figs. 4.7, 4.8 and 4.9).

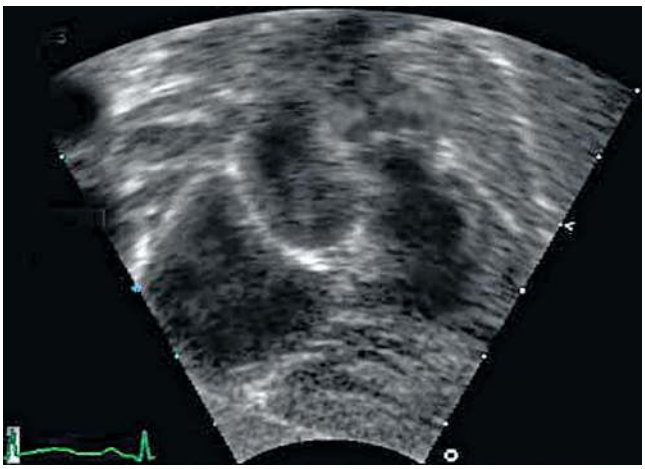


Fig. 4.7 Subcostal views showing supravalvar pulmonary stenosis of the main pulmonary trunk

Treatment

The only management for severe pulmonary stenosis in the adults is valve replacement, by either a homograft or a bioprosthesis [16].



Fig. 4.8 Electron Beam Angiography corresponding to parasternal short axis view from a patient with narrowed left pulmonary artery with respect to a normal right branch

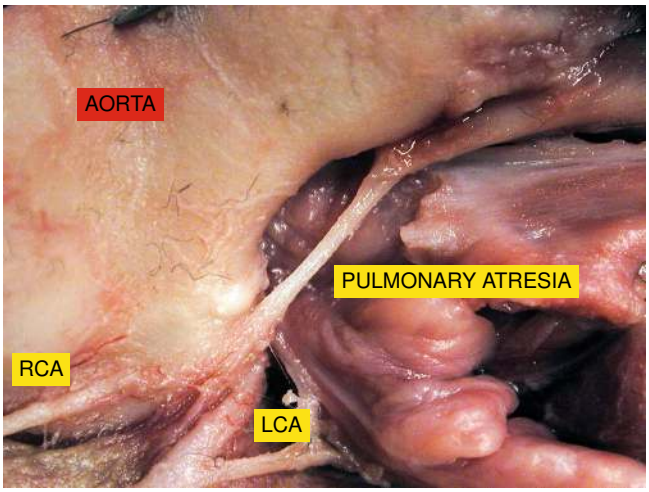


Fig. 4.9 Section in the pulmonary trunk showing thread-like pulmonary artery, no valve was present at the distal end

Pulmonary Regurgitation

Isolated congenital pulmonary regurgitation is rare. In adult congenital heart practice, pulmonary regurgitation is often seen long after pulmonary valvotomy or pulmonary valvuloplasty. It is particularly common after repair of tetralogy of Fallot [17]. The degree of pulmonary regurgitation varies from mild to severe. Significant pulmonary regurgitation may occur secondary to pulmonary artery dilatation and may complicate endocarditis [18]. This is however a rare cause of pulmonary regurgitation (Video 4.2).

Assessment of Pulmonary Regurgitation

1. A color flow jet diameter of more than 7.5 mm suggests significant pulmonary regurgitation when compared with CMR assessment [19] (Fig. 4.10).
2. Continuous wave Doppler velocities are more accurate in discriminating between mild and significant regurgitation [19, 20]. A pulmonary regurgitation signal that shows a sharp decline to meet the baseline, i.e., pressure equalization, in mid-diastole or before the Q wave of the succeeding cycle, is consistent with significant regurgitation. Mild regurgitation demonstrates a measurable retrograde pressure drop between the pulmonary artery and the right ventricle in late diastole. Severe pulmonary regurgitation is usually associated with right ventricular dilatation and increased activity, i.e., to accommodate the increased right ventricular stroke volume (Fig. 4.11).

The severity of pulmonary regurgitation can be assessed using the pulmonary regurgitation index. The pulmonary regurgitation index represents the ratio between the pulmonary regurgitation duration from continuous wave Doppler and total diastolic time expressed as a percent. A pulmonary regurgitation index less than 74% is suggestive of significant regurgitation. In patients with fast heart rate, this index may underestimate the pulmonary regurgitation, and in those with severe right ventricular disease and raised end-diastolic pressure, it may overestimate pulmonary regurgitation severity as the pulmonary artery and right ventricular diastolic pressures will equalize in mid-diastole. In patients with atrial fibrillation, an average of five cycles should be considered for estimating pulmonary regurgitation index.

Complications

Right Ventricular Dilatation

Long-standing pulmonary regurgitation is usually well tolerated by the right ventricle, probably due to the low pressure difference between the pulmonary artery and the right ventricular cavity. Even in patients with severe pulmonary regurgitation, the right ventricular cavity may remain completely normal in terms of size and function. However, follow-up of such patients may reveal varying degrees of right ventricular dilatation (remodeling) and eventually dysfunction (Figs. 4.12 and 4.13). Serial measurements of the right ventricular outflow tract diameter (from the long and short axes) and inflow tract (from the apical four chamber view) can be

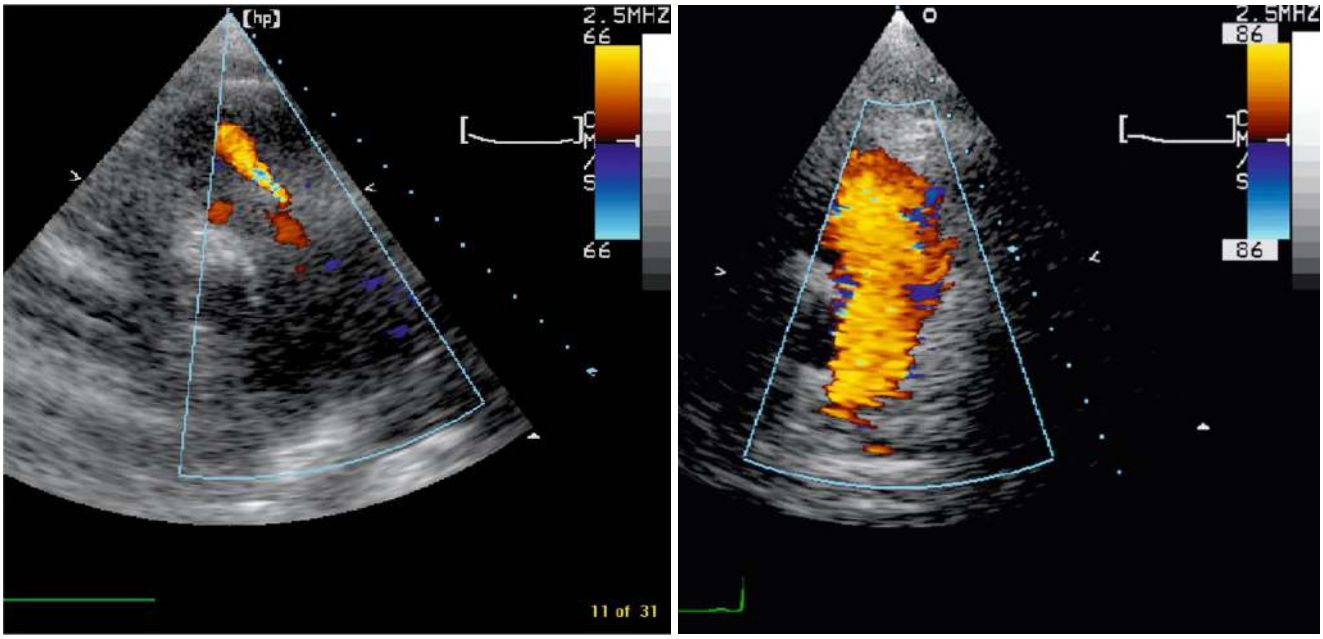


Fig. 4.10 Parasternal short axis view from two patients with pulmonary regurgitation: post pulmonary valvotomy as shown by color flow Doppler mild (*left*) and severe (*right*). Note the narrow pulmonary regurgitation jet in diastole with mild and broad jet (>8 mm) with severe pulmonary regurgitation

used for monitoring changes in ventricular size in patients with pulmonary regurgitation.

Also recent development of arrhythmia should be seen as a sign of deterioration of right ventricular function.

Right Ventricular Dysfunction

In some patients with long-standing pulmonary regurgitation, particularly in the presence of right ventricular dilatation, the intrinsic characteristics of the myocardium may change and become stiff (incompliant). The same physiology is frequently observed in patients with small right ventricular size, particularly those with critical pulmonary stenosis and previous valvotomy. In this situation, the right ventricle may not proportionally dilate [21]. Right ventricular physiology becomes restrictive with (i) an "A" wave in the pulmonary flow velocity (recorded by pulsed wave Doppler) consistent with direct propagation of atrial contraction to the pulmonary artery with the right ventricle itself functioning as a conduit in late diastole; (ii) a giant "A" wave on jugular venous pulse; (iii) a dominant E wave on right ventricular filling pattern with short deceleration time and prominent early diastolic flow in the SVC and IVC (Figs. 4.14, 4.15 and 4.16) [22].

Restrictive right ventricular physiology is commonly associated with varying degrees of tricuspid regurgitation and dilatation of the pulmonary artery. Atriogenic tricuspid regurgitation may develop late in the disease process, particularly in patients with a long PR interval that provokes long tricuspid regurgitation. The effect of this advanced ventricular dysfunction is compromised right ventricular filling time and limited stroke volume and exercise intolerance (Figs. 4.17 and 4.18) [23]. While similar disturbances on the left side can be corrected by DDD pacing and shortening of the atrioventricular delay, no attempts have been proposed to correct long tricuspid regurgitation.

Arrhythmia

Untreated significant pulmonary regurgitation may result in atrial or even ventricular arrhythmias. Early correction of the organic valve disease may protect the patient from potential further deterioration of atrial and ventricular functions and subsequently development of arrhythmias.

Assessment of Right Ventricular Function

Quantification of right ventricular function is not always easy because of its complex anatomy. Long axis movement can easily be studied by recording tricuspid ring movement in systole and diastole using both M-mode and tissue Doppler techniques (Fig. 4.19). Right ventricular free wall (long axis) amplitude has been shown to correlate with overall systolic function assessed by ejection fraction [24]. Also, in early diastole, various degrees of functional impairment can be demonstrated by the lengthening velocity and the presence of dyssynchrony (postejection shortening). Finally, late diastolic amplitude of backward movement of the long axis (towards the atrium) can be used as a marker for assessing right atrial function. Normal right ventricular long axis amplitude is approximately 2.5 ± 0.25 cm [25]. Myocardial

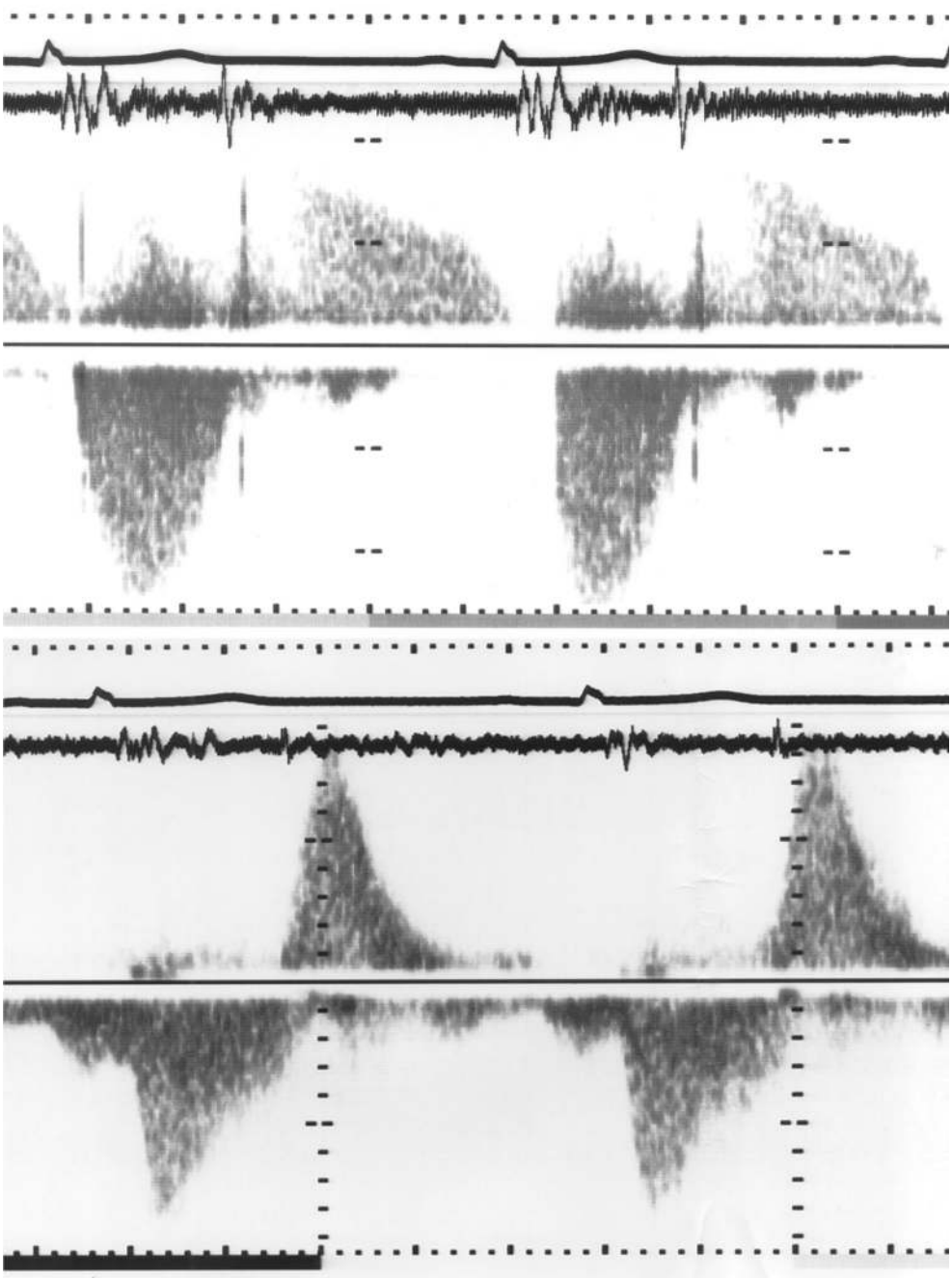


Fig. 4.11 Continuous wave Doppler velocities from two patients with pulmonary regurgitation, mild (*top*) and severe (*bottom*). Note the equalization of pulmonary artery and right ventricular pressures in mid-diastole in the patient with severe regurgitation

tissue Doppler velocities can be used to assess right ventricular free wall function, again in systole and diastole. Normal values range from 9 ± 2 cm/s for systolic velocity to 10 ± 2 cm/s for early diastolic lengthening velocity. Recently, right ventricular function has been assessed using 3D echocardiography and showed comparable volume measurements to those obtained by CMR. In addition, this method has shed light on the compartmental function of the right ventricle: inflow, apex, and outflow tract. Critical measurements have shown significant time delay between the compartmental systolic function, with the inflow tract contracting earlier than the rest, to secure optimum peristaltic function. Also while outflow tract compartment is the closest to relate to peak ejection, this function is transmitted to the inflow tract in patients with pulmonary hypertension [26]. Recently speckle tracking echocardiography has been used to asses right ventricular deformation with promising findings. This can assess global right ventricular strain and strain rate or only the free wall [27]. More results are needed in this field in order to establish the technique for routine clinical application.



Fig. 4.12 Apical four chamber view from a patient with severe pulmonary regurgitation showing a slightly dilated right ventricular cavity but maintained function

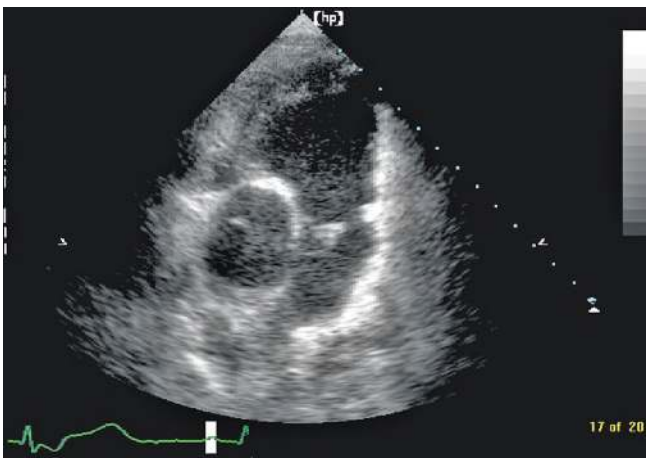


Fig. 4.13 Short axis of the aortic valve and right ventricular outflow tract demonstrating dilated right ventricle

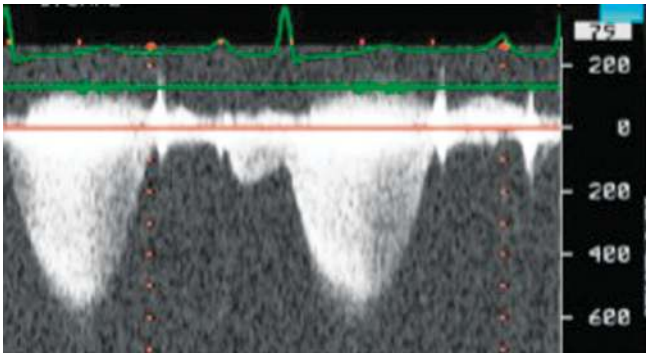


Fig. 4.14 Transpulmonary continuous wave Doppler from a patient with Noonan's syndrome and pulmonary stenosis showing "A" wave consistent with restrictive right ventricular physiology. Note the appearance of an A wave in the pulmonary flow

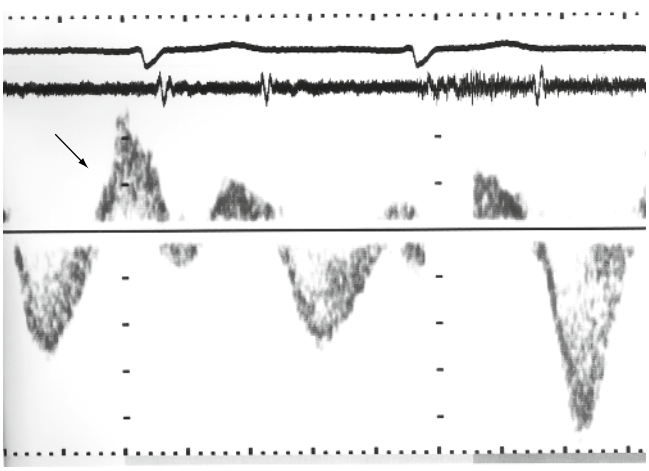


Fig. 4.15 Superior vena caval flow in the same patient showing giant pressure "A" wave

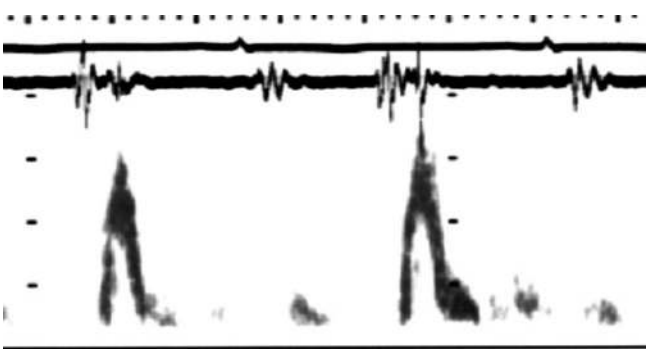


Fig. 4.16 Right ventricular filling pattern from a patient with restrictive physiology showing dominant E wave with very short deceleration time. Note the timing of the peak E ware coincideing with the onset of the third heart sound

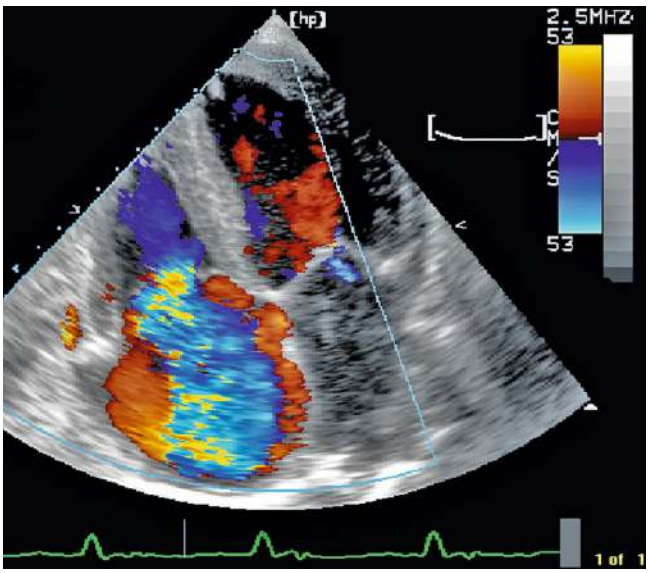


Fig. 4.17 Apical 4 chamber view from a patient with right ventricular disease complicated by tricuspid regurgitation seen by color Doppler

Complications of Restrictive Right Ventricular Disease

1. *Cyanosis:* Restrictive right ventricular physiology with increased diastolic pressure results in raised right atrial pressure and possible shunt reversal at atrial level across an ASD or even a small patent foramen ovale. Patients may experience transient ischemic attacks or cyanosis. Contrast (bubble) echocardiography with a biological contrast (mixed blood and saline) is often useful in confirming the presence of an atrial shunt, particularly with Valsalva maneuver, when the air bubbles cross the septum and appear in the right atrium.
2. *Right heart failure*: Reduced right ventricular function and increased right atrial pressure will be reflected on the systemic circulation and result in salt and water retention and signs and symptoms of right ventricular decompensation.
3. *Arrhythmia:* The increased atrial size and pressure in patients with stiff right ventricle may trigger different forms of arrhythmia: fibrillation or flutter (Fig. 4.20).

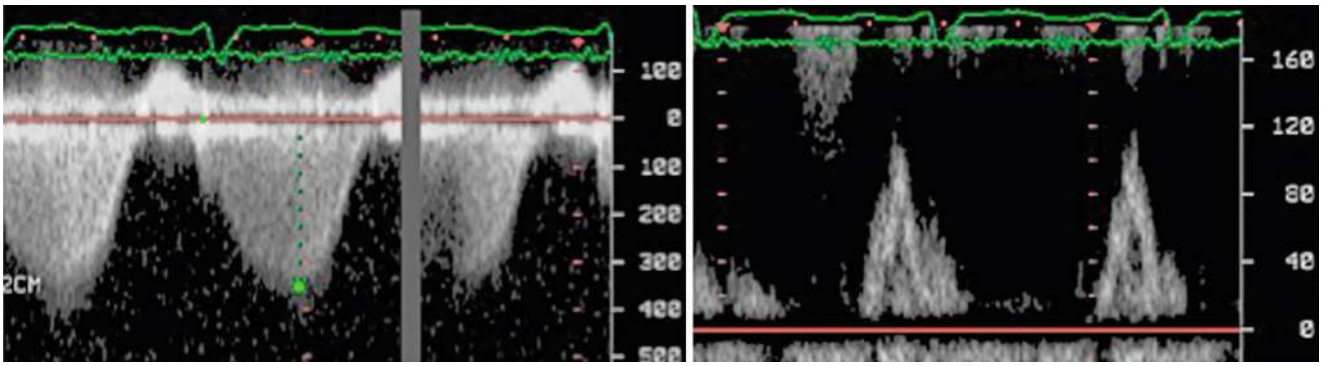


Fig. 4.18 Continuous wave Doppler from a patient with late stage right ventricular disease demonstrating tricuspid regurgitation with atriogenic component (*left*) that limits total right ventricular filling time (*right*)

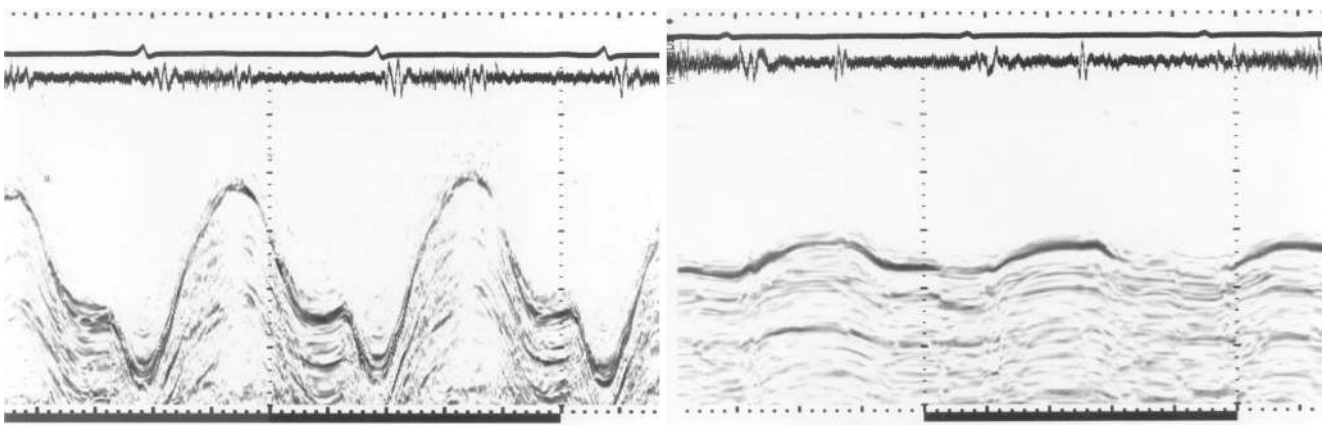


Fig. 4.19 Right ventricular M-mode recording of free wall long axis from a normal subject (*left*) and a patient with severe right ventricular disease (*right*). Note the significant drop in amplitude and velocities

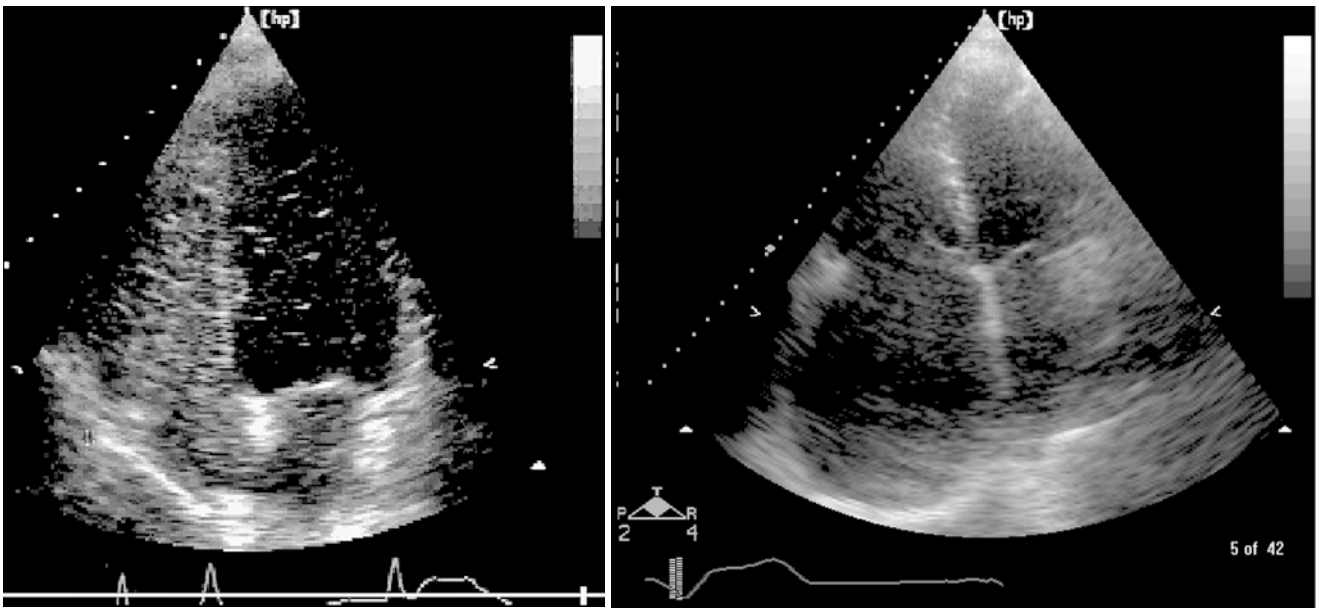


Fig. 4.20 Apical 4 chamber view from a patient with stiff right ventricle and arrhythmia demonstrating disproportionately large right atrium

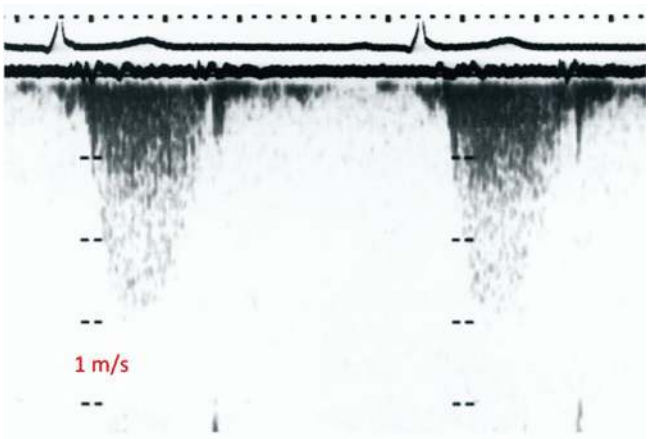


Fig. 4.21 Continuous wave Doppler recording from a patient with pulmonary homograft 12 months after surgery showing a peak velocity of 2 m/s

Management

Although pulmonary valve replacement may be a long-term solution for severe pulmonary regurgitation, there is no consensus regarding the exact time for surgical intervention. Decision making should be based on individual cases and considering other factors, e.g., the presence of early signs of right ventricular disease or arrhythmia. Pulmonary valve replacement by a homograft has proved a very satisfactory operation with excellent clinical outcome. Transvalvar velocities may show some increase over the early postoperative period but remain stable afterward (Fig. 4.21).

Transcatheter pulmonary valve replacement has been investigated and preliminary results are promising [28].

As is the case in restrictive left ventricular physiology, treatment with an ACE-inhibitor may have a substantial role in balancing overall cardiac physiology in patients with restrictive right ventricular disease, but the current literature is lacking the evidence to support this proposal.

References

1. Griffith JM, Henry WL. An ultrasound system for combined cardiac imaging and Doppler blood flow measurement in man. Circulation. 1978;57(5):925–30.
2. Weyman AE, Hurwitz RA, Girod DA, Dillon JC, Feigenbaum H, Green D. Cross-sectional echocardiographic visualization of the stenotic pulmonary valve. Circulation. 1977;56(5):769–74.
3. Leblanc MH, Paquet M. Echocardiographic assessment of valvular pulmonary stenosis in children. Br Heart J. 1981;46(4):363–8.
4. Nishimura RA, Pieroni DR, Bierman FZ, Colan SD, Kaufman S, Sanders SP, et al. Second natural history study of congenital heart defects. Pulmonary stenosis: echocardiography. Circulation. 1993;87(2 Suppl):I73–9.
5. Masura J, Burch M, Deanfield JE, Sullivan ID. Five-year follow-up after balloon pulmonary valvuloplasty. J Am Coll Cardiol. 1993;21(1):132–6.
6. Galindo A, Gutiérrez-Larraya F, Velasco JM, de la Fuente P. Pulmonary balloon valvuloplasty in a fetus with critical pulmonary stenosis/atresia with intact ventricular septum and heart failure. Fetal Diagn Ther. 2006;21(1):100–4.
7. Pellikka PA, Tajik AJ, Khandheria BK, Seward JB, Callahan JA, Pitot HC, et al. Carcinoid heart disease. Clinical and echocardiographic spectrum in 74 patients. Circulation. 1993;87(4):1188–96.
8. Lima CO, Sahn DJ, Valdes-Cruz LM, Goldberg SJ, Barron JV, Allen HD, et al. Noninvasive prediction of transvalvular pressure gradient in patients with pulmonary stenosis by quantitative two-dimensional echocardiographic Doppler studies. Circulation. 1983;67(4):866–71.

9. Johnson GL, Kwan OL, Handshoe S, Noonan JA, DeMaria AN. Accuracy of combined two-dimensional echocardiography and continuous wave Doppler recordings in the estimation of pressure gradient in right ventricular outlet obstruction. J Am Coll Cardiol. 1984;3(4):1013–8.
10. Henein M, Lam YY, Waldenström A, Henein MY. Atrial interaction in the form of 'cross talk' in patients with ventricular outflow tract obstruction. Int J Cardiol. 2011;147(3):388–92.
11. Caldwell RL, Weyman AE, Hurwitz RA, Girod DA, Feigenbaum H. Right ventricular outflow tract assessment by cross-sectional echocardiography in tetralogy of Fallot. Circulation. 1979;59(2):395–402.
12. French JW. Aortic and pulmonary artery stenosis: improvement without intervention? J Am Coll Cardiol. 1990;15(7):1631–2.
13. Wren C, Oslizlok P, Bull C. Natural history of supravalvular aortic stenosis and pulmonary artery stenosis. J Am Coll Cardiol. 1990;15(7):1625–30.
14. Foale RA, King ME, Gordon D, Marshall JE, Weyman AE. Pseudoaneurysm of the pulmonary artery after the banding procedure: two-dimensional echocardiographic description. J Am Coll Cardiol. 1984;3(2 Pt 1):371–4.
15. Rodriguez RJ, Riggs TW. Physiologic peripheral pulmonic stenosis in infancy. Am J Cardiol. 1990;66(20):1478–81.
16. Zubairi R, Malik S, Jaquiss RD, Imamura M, Gossett J, Morrow WR. Risk factors for prosthesis failure in pulmonary valve replacement. Ann Thorac Surg. 2011;91(2):561–5.
17. Brand A, Dollberg S, Keren A. The prevalence of valvular regurgitation in children with structurally normal hearts: a color Doppler echocardiographic study. Am Heart J. 1992;123(1):177–80.
18. Panidis IP, Kotler MN, Mintz GS, Ross J, Weber J. Clinical and echocardiographic correlations in right heart endocarditis. Int J Cardiol. 1984;6(1):17–34.
19. Li W, Davlouros PA, Kilner PJ, Pennell DJ, Gibson D, Henein MY, et al. Doppler-echocardiographic assessment of pulmonary regurgitation in adults with repaired tetralogy of Fallot: comparison with cardiovascular magnetic resonance imaging. Am Heart J. 2004;147(1):165–72.
20. Miyatake K, Okamoto M, Kinoshita N, Matsuhisa M, Nagata S, Beppu S, et al. Pulmonary regurgitation studied with the ultrasonic pulsed Doppler technique. Circulation. 1982;65(5):969–76.
21. Hayes CJ, Gersony WM, Driscoll DJ, Keane JF, Kidd L, O'Fallon WM, et al. Second natural history study of congenital heart defects. Results of treatment of patients with pulmonary valvar stenosis. Circulation. 1993;87(2 Suppl):I28–37.
22. Lam YY, Kaya MG, Goktekin O, Gatzoulis MA, Li W, Henein MY. Restrictive right ventricular physiology: its presence and symptomatic contribution in patients with pulmonary valvular stenosis. J Am Coll Cardiol. 2007;50(15):1491–7. Epub Sep 24, 2007
23. Rowe SA, Zahka KG, Manolio TA, Horneffer PJ, Kidd L. Lung function and pulmonary regurgitation limit exercise capacity in postoperative tetralogy of Fallot. J Am Coll Cardiol. 1991;17(2):461–6.
24. Kaul S, Tei C, Hopkins JM, Shah PM. Assessment of right ventricular function using two-dimensional echocardiography. Am Heart J. 1984;107(3):526–31.
25. Florea VG, Florea ND, Sharma R, Coats AJ, Gibson DG, Hodson ME, et al. Right ventricular dysfunction in adult severe cystic fibrosis. Chest. 2000;118(4):1063–8.
26. Lindqvist P, Calcutteea A, Henein M. Echocardiography in the assessment of right heart function. Eur J Echocardiogr. 2008;9(2):225–34.
27. Lisi M, Camelli M, Mandoli GE, Pastore MC, Righini FM, D'Ascenzi F, Focardi M, Rubboli A, Mondillo S, Henein MY. Detection of myocardial fibrosis by speckle-tracking echocardiography: from prediction to clinical applications. Heart Fail Rev. 2022;27(5):1857–67. https://doi.org/10.1007/s10741-022-10214-0. Epub.
28. Bonhoeffer P, Boudjemline Y, Saliba Z, Hausse AO, Aggoun Y, Bonnet D, et al. Transcatheter implantation of a bovine valve in pulmonary position: a lamb study. Circulation. 2000;102(7):813–6.

Valve Substitutes

5

Michael Y. Henein, Matteo Cameli, Matteo Lisi,
Federico Landra, Mary Sheppard, and John R. Pepper

For the last 40 years, valve replacement with various substitutes in patients with severe valve dysfunction has been practiced, particularly in those with unrepairable valve deformation [1]. Valve Substitutes/artificial valves are essentially of two types: mechanical and bioprostheses.

Mechanical valves are either of the ball-cage type (Starr-Edwards), tilted disc (Bjork-Shiley), or bi-leaflet prosthesis (St. Jude). Although mechanical valves are durable and they correct the organic valve dysfunction, they have a number of potential complications, usually infection, endocarditis particularly of the sewing ring, hemolysis, dehiscence that results in severe regurgitation, and thrombosis. They also require life-long anticoagulation, and this itself has potential complications [2–5].

Bioprosthetic valves or tissue valves, e.g., Hancock porcine valve or Toronto (Stentless porcine valve) are recommended for all patients in whom long-term anticoagulation cannot be afforded and for patients living in countries where regular anticoagulation control is doubtful. They too have their disadvantages: being made of tissue, bioprostheses are subject to infection, calcification, and significant dysfunction (Fig. 5.1). The major disadvantage, however, is the less durability than mechanical valves. Bioprosthetic valve degeneration could be very fast requiring urgent life-saving valve replacement [6–9]. Recently developed pericardial valve bioprostheses have been shown to have the lowest resistance in the outflow tract position and carry a better survival results compared to other old fashioned prostheses [10].

Even if clinical details of the mechanical valve are not available to the sonographer, the chest X-ray may give an idea about the valve shape and struts [11]. Echocardiographic two-dimensional imaging is an excellent tool for assessing valve movement and function [12, 13]. Color Doppler significantly adds to the value of echocardiography in the follow-up of such patients, particularly for demonstrating characteristic flow patterns (Videos 5.1 and 5.2). Color Doppler typically displays two separate jets with a Starr-Edwards ball-cage prosthesis (particularly in the mitral position), an eccentric single jet with the tilted disc (Bjork-Shiley) valve, and a single central jet with the bi-leaflet valve (Fig. 5.2) [14–16].

One disadvantage of color flow Doppler is that it fails to detect valve regurgitation jet from transthoracic images because of the mechanical ultrasound artifact that distracts the image. However, in severe para-prosthetic valve regurgitation, careful angling of the imaging probe should demonstrate the exact site of the dehiscence and the mitral regurgitation jet (Fig. 5.3).

Transesophageal echo is more sensitive than transthoracic echo in detecting the presence and assessing the severity of para-prosthetic valve regurgitation (Fig. 5.4). However, careful interpretation of images should be considered to avoid overestimation of the severity of the incompetence. The same limitations apply to prosthetic valves in the aortic position [17–20].

M-mode echocardiography has become limited in its use in studying prosthetic valve function, simply because it does not provide an accurate quantitative assessment of the mechanical valve apart from the simple display of the M-mode reflection of the moving part of the valve [21]. However, M-mode provides a unique means for assessing the ventricular response to valve regurgitation. Normally, the septal wall of the left ventricle becomes reversed after valve replacement surgery [22]. This has recently been shown to

Supplementary Information The online version contains supplementary material available at https://doi.org/10.1007/978-3-031-95894-6_5.

M. Y. Henein (✉)
Imperial College London, London, UK

Univesity of Siena, Siena, Italy
e-mail: m.henein@imperial.ac.uk

M. Cameli · F. Landra
Univesity of Siena, Siena, Italy

M. Lisi
Ospedale S. Maria delle Croci, Ravenna, Italy

M. Sheppard · J. R. Pepper
Royal Brompton Hospital, London, UK

© The Author(s), under exclusive license to Springer Nature Switzerland AG 2025

M. Y. Henein (ed.), *Clinical Echocardiography*, https://doi.org/10.1007/978-3-031-95894-6_5

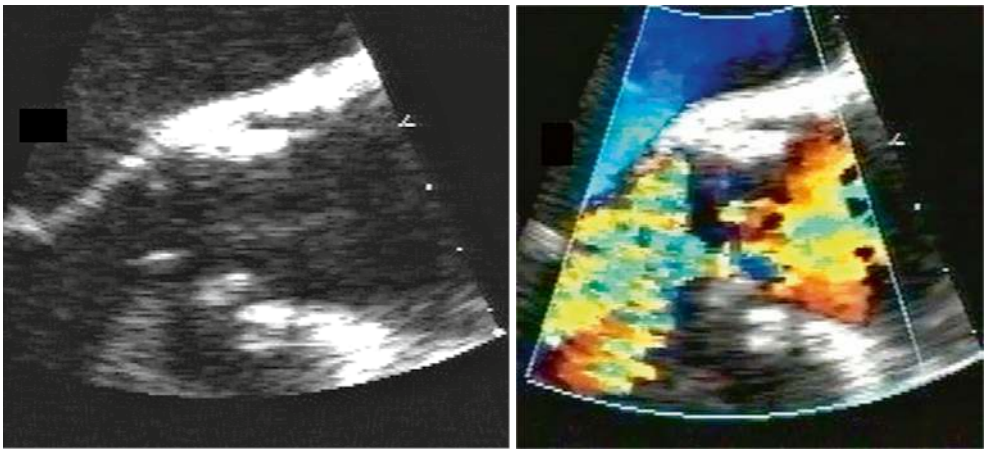


Fig. 5.1 TOE from a patient with a porcine aortic valve. Note the degeneration of the valve leaflets that results in severe mitral regurgitation

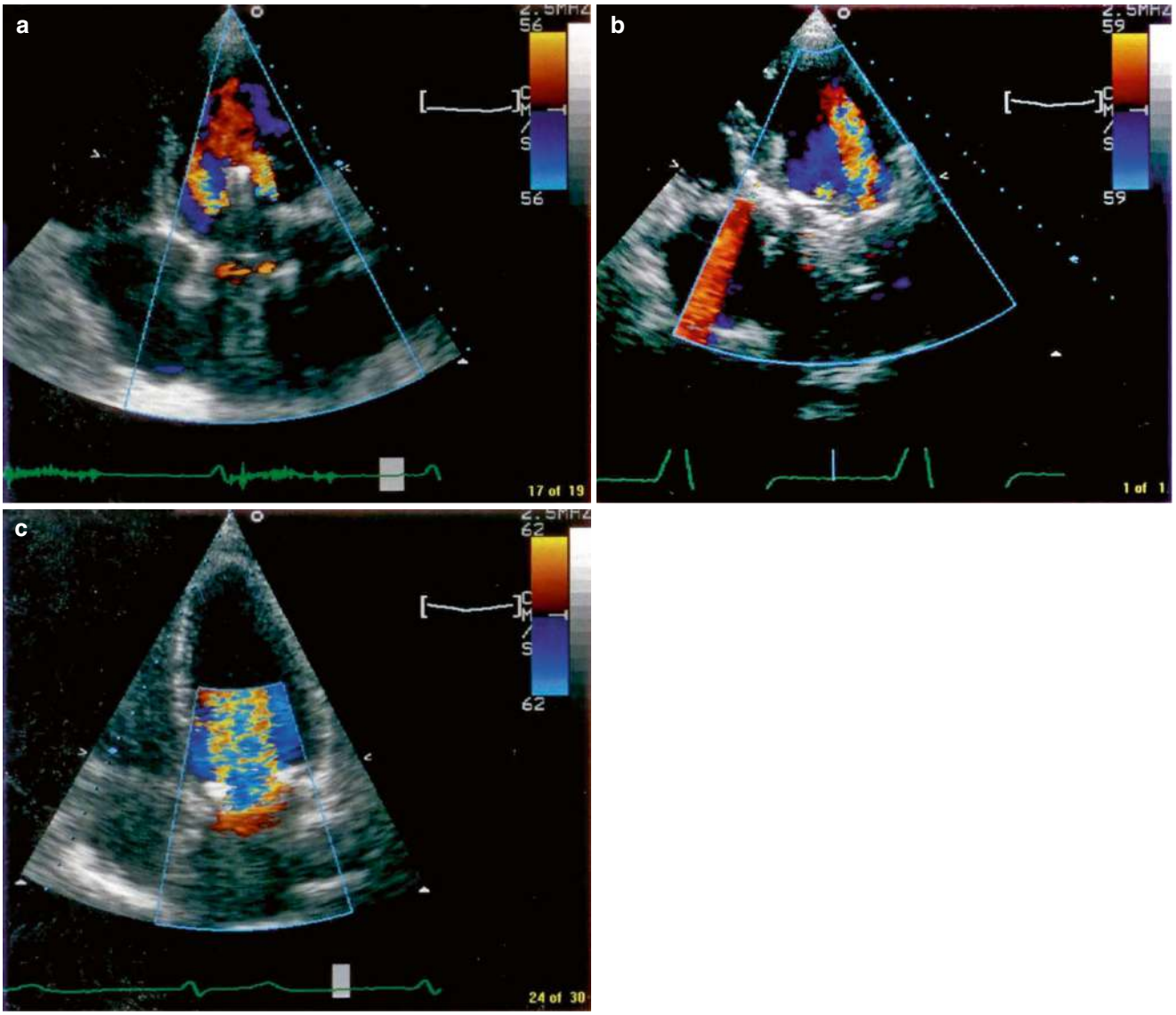


Fig. 5.2 Color flow Doppler recording from 3 mitral prosthetic valves taken from the transthoracic apical 4-chamber views. Note the two jets characterizing a Ball cage (**a**), Bjork-Shiley (**b**) and bileaflet (**c**) valve, eccentric jet with Bjork-Shiley, and central single jet with bi-leaflet valve

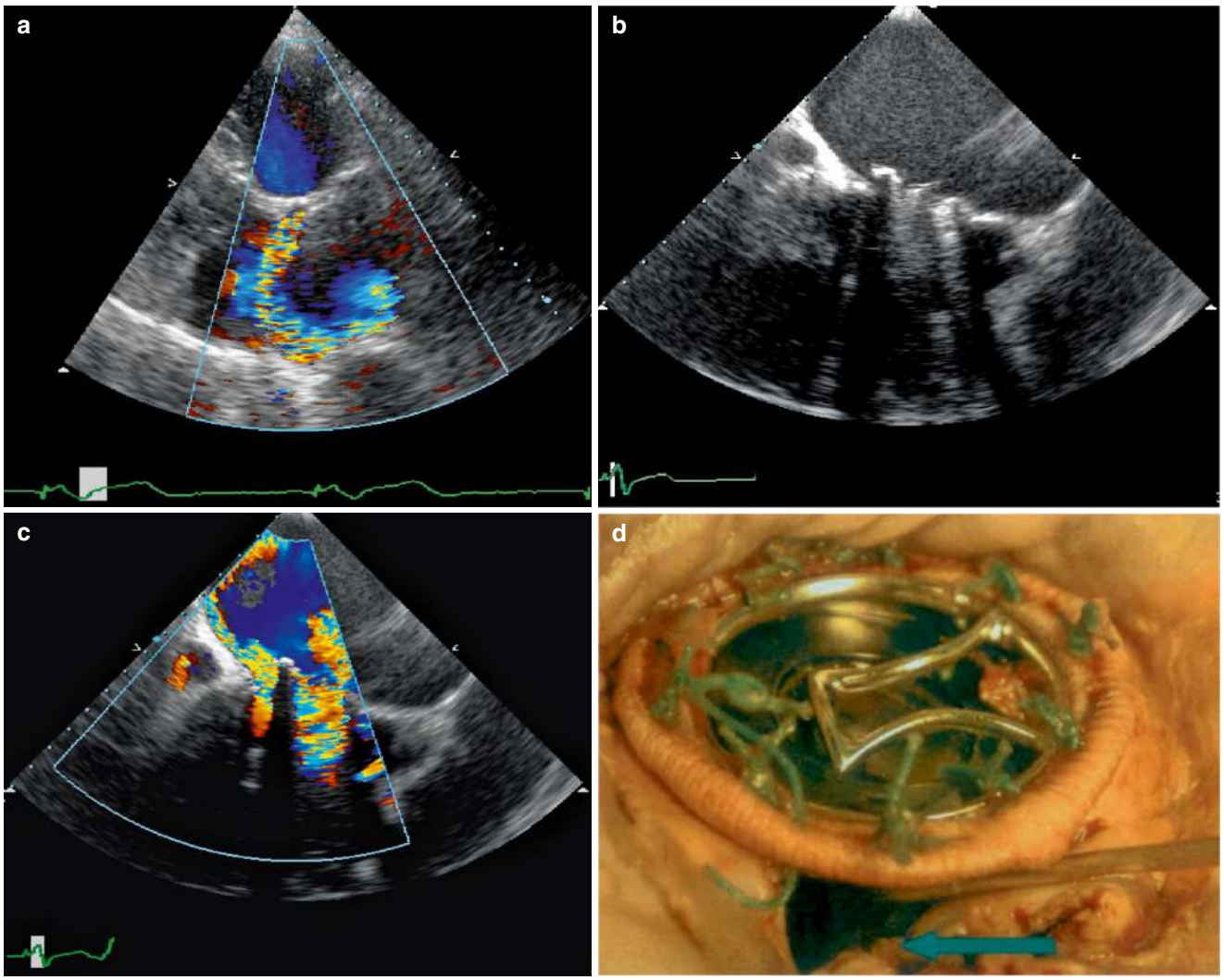


Fig. 5.3 Transthoracic (**a**) and transesophageal (**b**) echo from a patient with dehisced mechanical mitral valve. Note the location of the dehiscent site at the lateral wall (**c**). Pathological specimen (**d**) from a patient with mechanical mitral valve and paravalvular leak caused by loose stitches

correlate with the extent of fall in right ventricular free wall amplitude of motion, known after the bypass circulation. It appears that such reversed septal motion aims at optimizing overall right ventricular function in order to secure optimum stroke volume [23]. With severe para-prosthetic valve regurgitation, M-mode recording of left ventricular minor axis demonstrates a normalized septal movement and an active left ventricular cavity, consistent with significant left ventricular volume overload (Fig. 5.5).

Furthermore, in patients with double valve replacement in whom color flow Doppler may not be conclusive in confirming the origin of the ventricular overload, M-mode of left ventricular minor axis is usually of great help in differentiating between significant mitral and aortic regurgitation. While the increase in left ventricular dimension is exclusively early diastolic with mitral regurgitation, it occurs throughout early and mid-diastole in significant aortic regurgitation (Fig. 5.6).

Continuous wave Doppler is the ideal tool to provide accurate assessment of mechanical valve function. Continuous wave Doppler measures peak forward flow velocities across the mechanical valve which can be converted into pressure drop (gradient) using the modified Bernoulli equation $4V^2$, particularly with high velocities (Fig. 5.7). All valves are somewhat stenotic since they operate on a fixed valve area unlike native valves. However, a comparative increase in velocities and pressure drop during follow-up with respect to postoperative values suggests the development of valve substitute stenosis (Fig. 5.8) [24, 25].

The pressure drop across valves is also affected by its location and the driving pressure of the column of blood passing through it. For instance, the same St. Jude mechanical valve operates at a peak pressure drop of 15 mmHg in the mitral position but operates at a pressure drop of 5–6 mmHg in the tricuspid position (Fig. 5.9) [26].

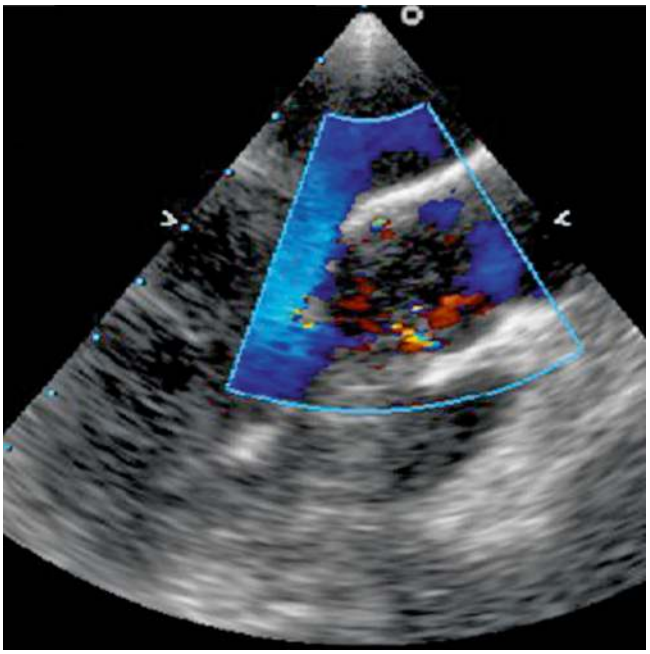


Fig. 5.4 Transesophageal echocardiogram of left ventricular outflow tract and aortic valve demonstrating mild para-prosthetic aortic regurgitation on color flow Doppler

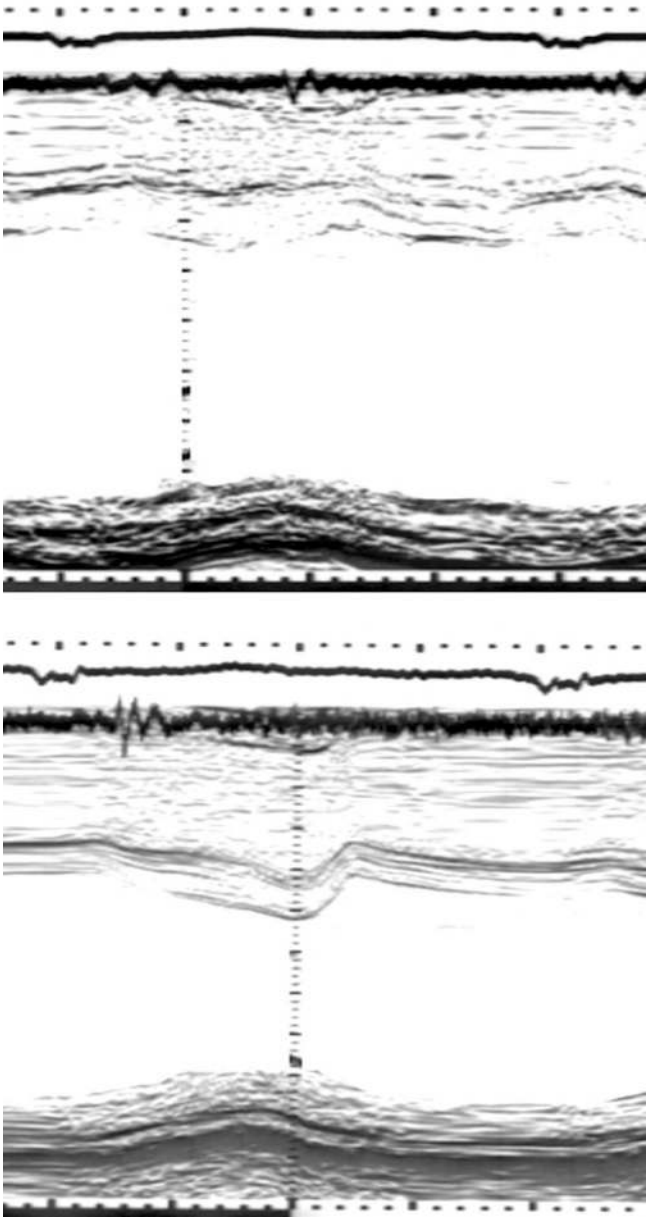


Fig. 5.5 M-mode recording of left ventricular minor axis from a patient 1 year after valve replacement showing reversed septal movement (*top*). The same patient 4 years later after developing severe para-prosthetic mitral regurgitation (*bottom*). Note the dilatation of the ventricle and the extent of cavity activity

Recently, standardized definitions for bioprosthetic aortic and mitral valve dysfunction and failure have been provided [27]. Definition of structural bioprosthetic valve disfunction requires confirmation by imaging of permanent structural changes in the leaflets, struts, or stent and hemodynamic deterioration. On the other hand, non structural bioprosthetic valve disfunction may occur, including any abnormality that is not instrinsic to the prosthetic valve and that causes valve dysfunction, such as prothesis-patient mismatch and paravalvular leak. Transthoracic echocardiography, in addition to confirming the diagnosis, is helpful in defining the progression stage of the dysfunction, depending on the presence of morphological valve deterioration alone or with hemodynamic consequences. Finally, bioprosthetic valve failure is a valve-related death, that needs urgent valve reintervention. This scenario is usually supported by progressive signs of ventricular dysfunction related to the valve related volume or pressure overload with their consequences, e.g pulmonary hypertension.

Most mechanical valves have a small degree of functional regurgitation corresponding to the amount of blood displaced when the valve opens and closes. This may appear only as a weak continuous wave or colour flow Doppler signal. With severe para-prosthetic regurgitation, the continuous wave Doppler signal is strong and the duration of mitral regurgitation is short, thus making the valve opening click very close to the second heart sound (Fig. 5.10) [28, 29]. Colour flow Doppler may also demonstrate evidence for significant regurgitation.

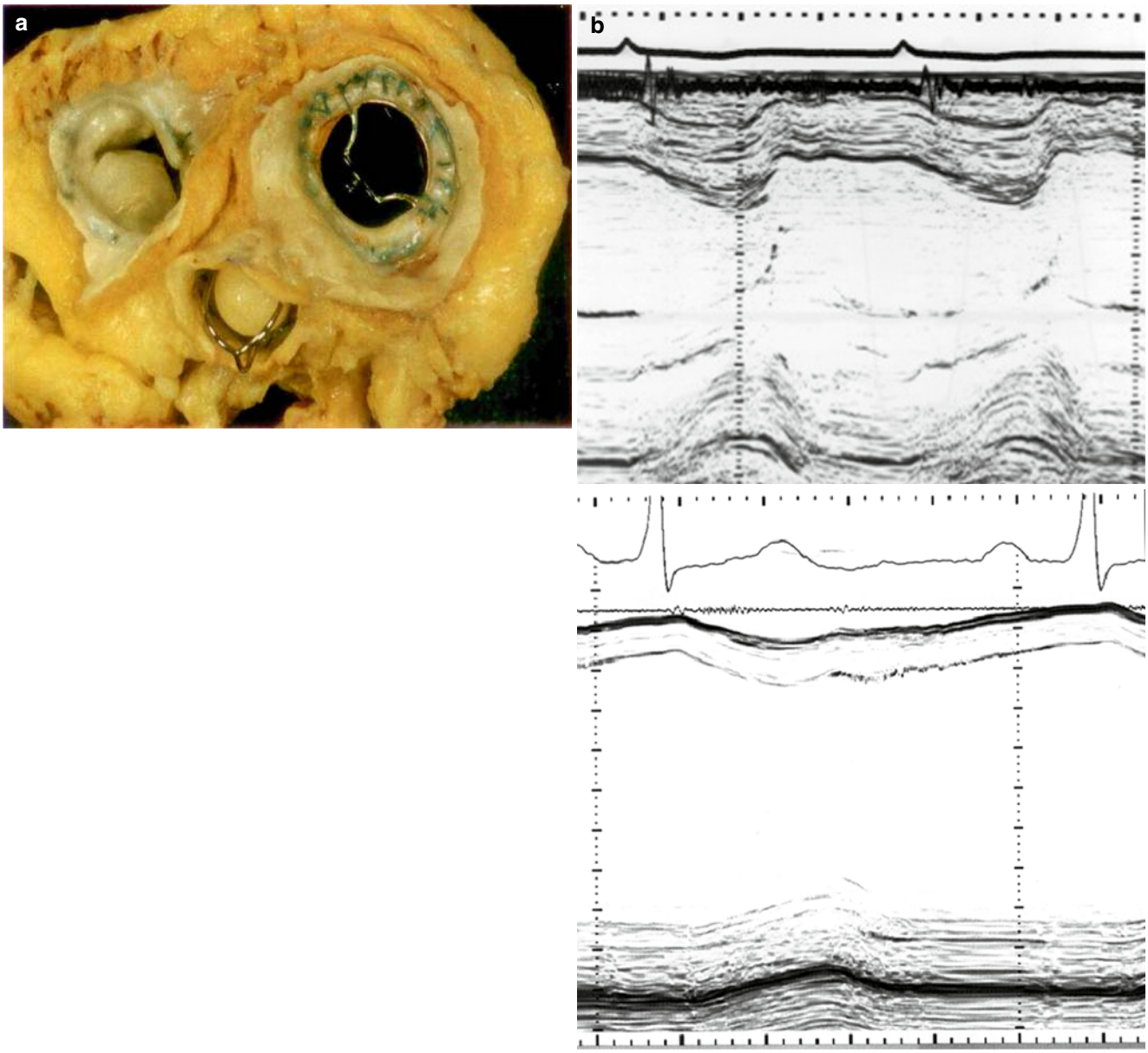


Fig. 5.6 (**a**) Pathological section from a patient with Bjok-Shiley valve in the mitral position, Starr-Edwards in the aortic position, and metal ring around the tricuspid valve leaflets. (**b**) M-mode recording of left ventricular minor axis from two patients, one with severe mitral regurgitation (top) and the other severe aortic regurgitation (bottom). Note the difference in the pattern of left ventricular filling and increase in dimension. While it is exclusively early diastolic in mitral regurgitation, it is throughout early and mid-diastolic in aortic regurgitation

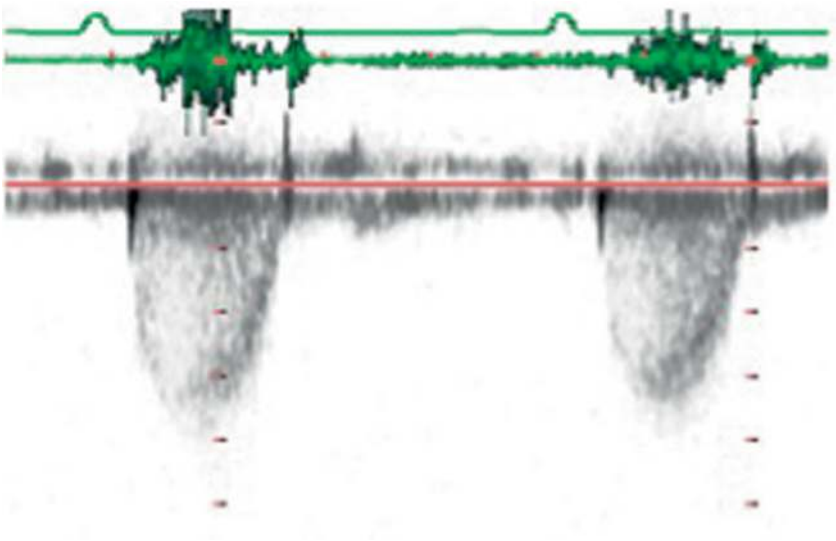


Fig. 5.7 Continuous wave Doppler of transmechanical aortic valve velocities 5 years after surgery when the patient developed signs of heart failure and a pressure drop of 70 mmHg across the valve substitute (*right*)

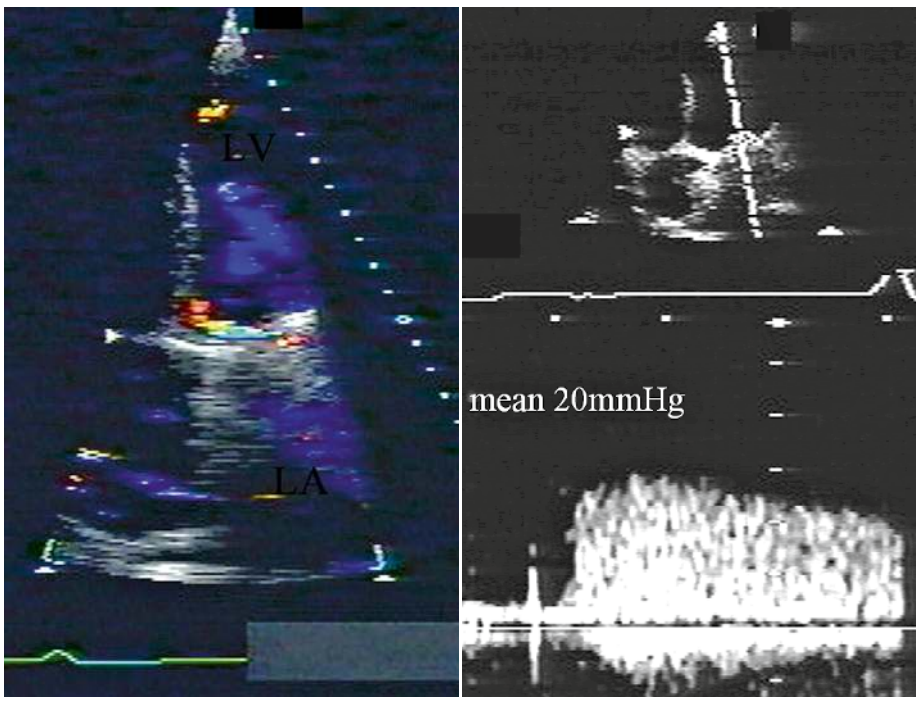


Fig. 5.8 Continuous wave Doppler of transmechanical mitral valve Starr-Edwards prosthesis in the mitral position from a patient showing severe stenosis consistent with stuck mitral valve prosthesis

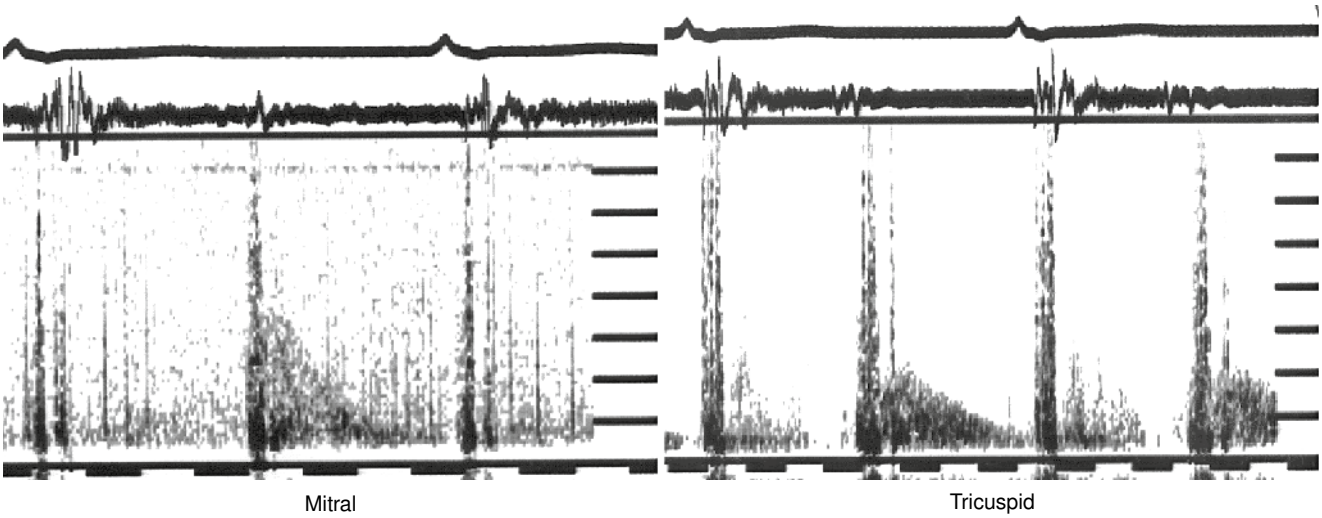


Fig. 5.9 Continuous wave Doppler from two St. Jude's valves, one in the mitral position and the other in the tricuspid position. Note the difference in pressure drop between the two

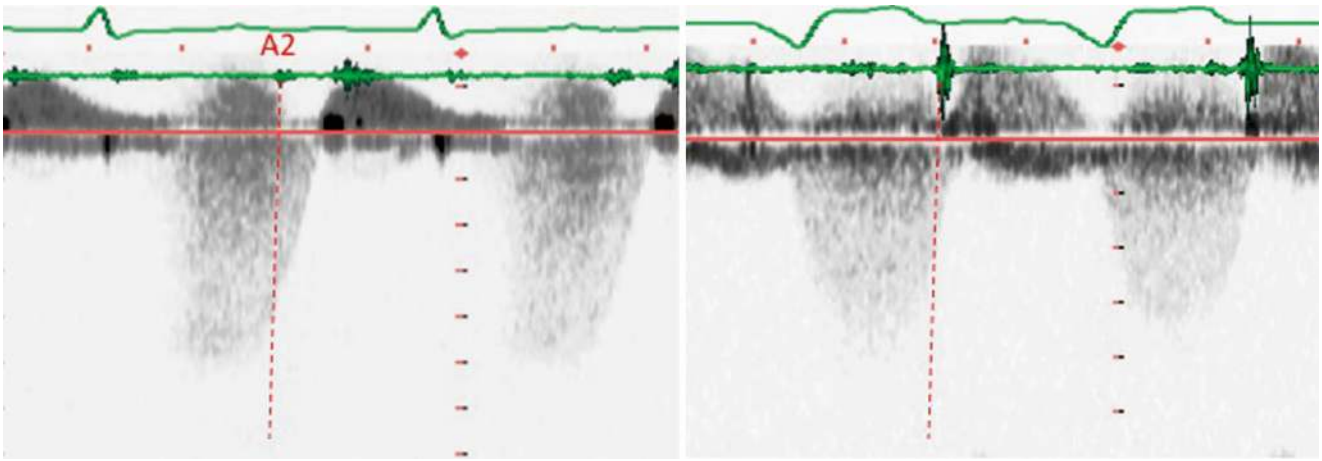


Fig. 5.10 Continuous wave Doppler demonstrating para-prosthetic mitral regurgitation from two patients, mild (*left*) and severe (*right*)

Homografts

Homografts are only feasible for aortic valve replacement either directly in the aortic position or in the pulmonary position as part of Ross procedure (Aortic autograft). Assessment of aortic valve homograft function is exactly the same as for the native valve in Chap. 2. In particular circumstances, the mitral valve can be replaced by a reversed pulmonary valve, the so-called (top hat) operation and the pulmonary valve is replaced by a homograft or a stentless valve substitute (Fig. 5.11). This operation is ideal for patients in whom optimum anticoagulation control cannot be achieved. Although not generally practiced, it has proved a great success in the small number of patients used in.

The same technique can be used in tricuspid valve disease, in patients with severe tricuspid regurgitation particularly those who have contraindication to anticoagulants.

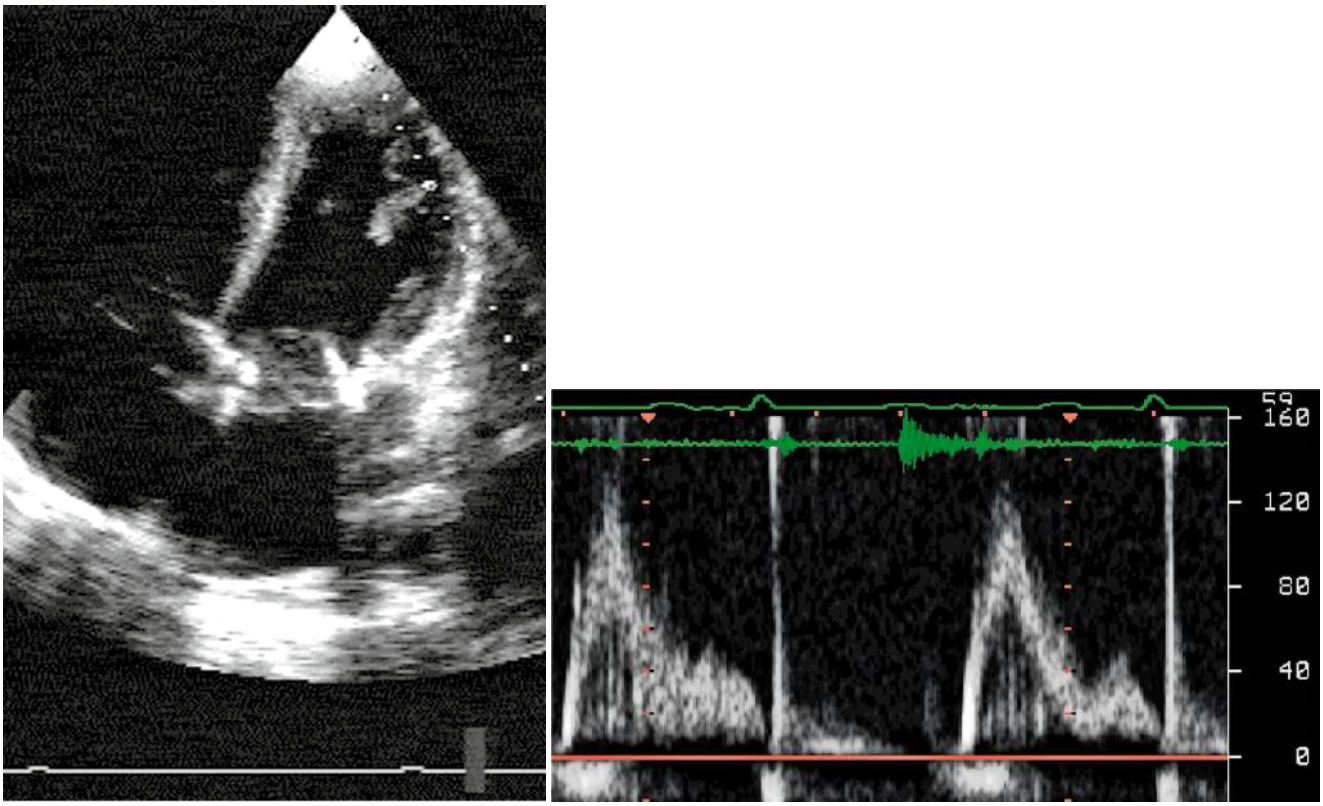


Fig. 5.11 Apical 4-chamber view (*Left*) from a patient with top hat procedure (pulmonary autograft in the mitral position). Note the normal transvalvular flow pattern (*right*)

Endocarditis

All valve substitutes, particularly mechanical and bioprostheses, are subject to infection, since they are made of foreign material, thus seen by the immune system as foreign bodies. Infection may occur in the form of vegetation deposition or may be localized to the sewing ring (Fig. 5.12). Infection in the sewing ring is not usually easy to detect even on transesophageal images (Figs. 5.13 and 5.14). The decision whether to replace a valve suspected of being infected is therefore usually made on clinical grounds. Persistent clinical evidence for endocarditis justifies valve replacement with a homograft, particularly in the aortic position, to clear up the site of infection.

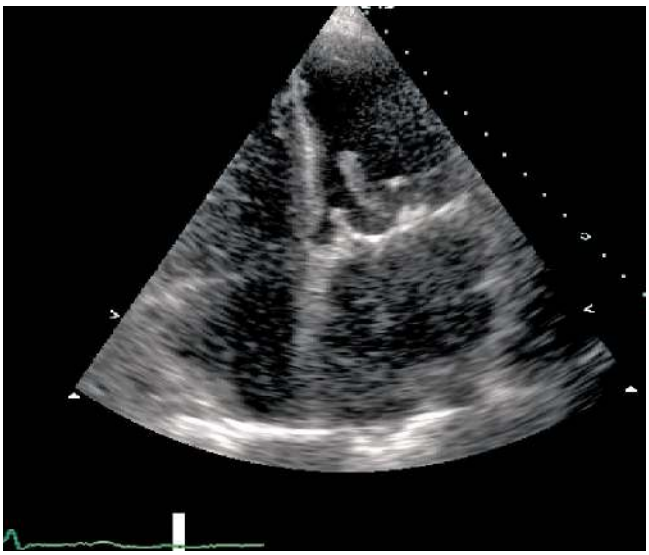


Fig. 5.12 Apical 4-chamber view from a patient with porcine mitral valve, showing large vegetation attached to the valve

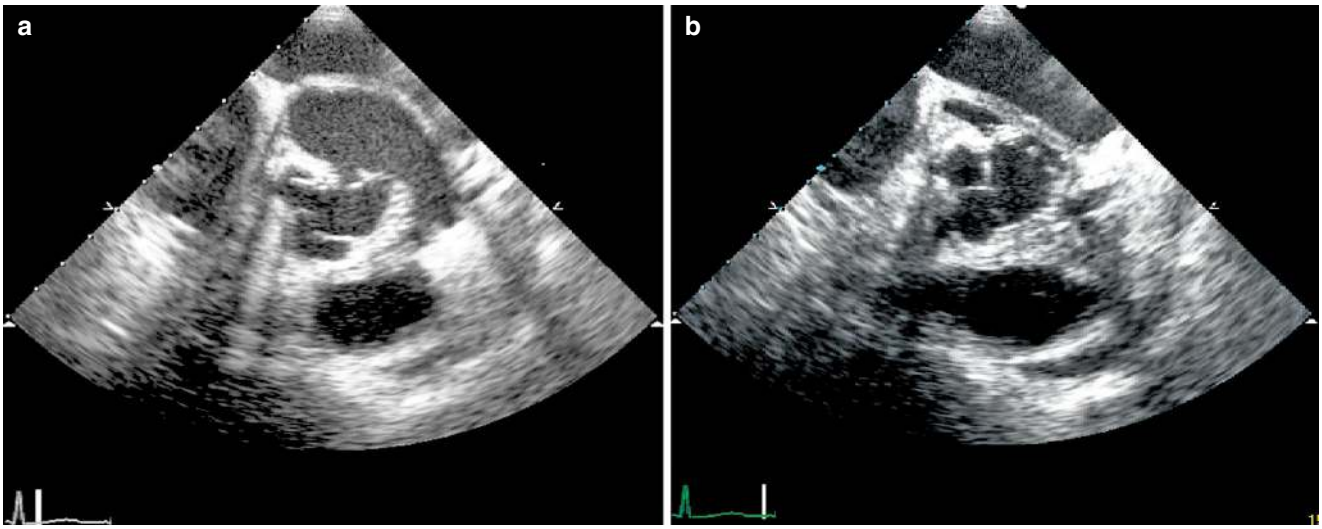


Fig. 5.13 TOE (**a** and **b**) from a patient with clinical evidence for bacterial endocarditis showing an area of dehiscence between the mitral valve prosthesis and aortic root

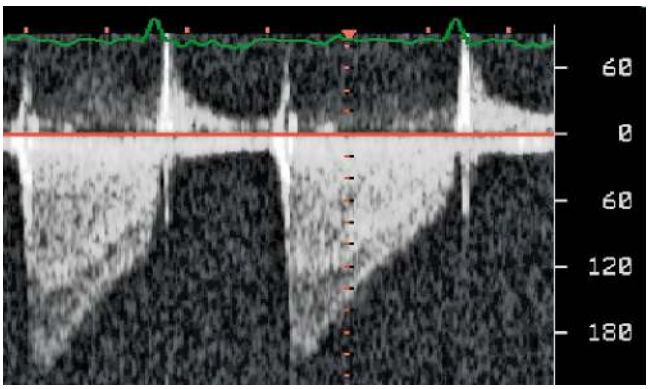


Fig. 5.14 TOE from a patient with Starr-Edward mitral valve prosthesis showing double envelope CW velocity display consistent with partial valve narrowing

Management

Aortic valve replacement by any substitute is the common practice for severe aortic valve disease. While in highly specialized centers, homograft banks are available, in others, mechanical or bioprosthetic valves are the commonly used ones. For severe mitral regurgitation, various repair techniques have proved their success in preserving the native valve. Nevertheless, the frequency of replacing a mitral valve with prosthesis for mitral regurgitation in the United States is much higher than in Europe, 80% vs. 50%. With artificial valves, regular follow-up is needed. Irrespective of technical expertise, a suggested annual follow-up of the valve function and the ventricular function is generally recommended. In patients with valve substitutes who present with acute heart failure, valve dysfunction should be considered the first differential diagnosis until otherwise proved. When clinical diagnosis of endocarditis is made, the artificial valve is the first to be blamed unless clear evidence for infection of another valve is provided. Prophylactic antibiotics in patients with surgically implanted prosthetic valves and with any material used for surgical cardiac valve repair is recommended, as well as for patients with transcatheter implanted aortic and pulmonary valvular prosthesis. Recent guidelines of the European Society of Cardiology recommend prophylactic antibiotic cover for patients at high and intermediate risk for infective endocarditis [30]. Antibiotic prophylaxis should be considered in patients with transcatheter mitrtal and tricuspid valve repair as well.

For more details on endocarditis in general are found in Chap. 6.

References

1. Harken DE, Soroff HS, Taylor WJ. Partial and complete prosthesis is aortic insufficiency. J Thorac Cardiovasc Surg. 1960;40:744–62.
2. Beaudet RL, Poirier NL, Guerraty AJ, Doyle D. Fifty-four months' experience with an improved tilting disk valve (Medtronic-Hall). Thorac Cardiovasc Surg. 1983;2:89–93.
3. Bjork VO, Holmgren A, Olin C, Ovenfors CO. Clinical and haemodynamic results of aortic valve replacement with the Bjork-Shiley tilting disc valve prosthesis. Scand J Thorac Cardiovasc Surg. 1971;5(3):177–91.
4. Nicoloff DM, Emery RW, Arom KV, Northrup WF III, Jorgensen CR, Wang Y, et al. Clinical and hemodynamic results with the St. Jude Medical cardiac valve prosthesis. A three-year experience. J Thorac Cardiovasc Surg. 1981;82(5):674–83.

5. Simon EB, Kotler MN, Segal BL, Parry W. Clinical significance of multiple systolic clicks from Starr-Edwards prosthetic aortic valves. Br Heart J. 1977;39(6):645–50.
6. Cooper DM, Stewart WJ, Schiavone WA, Lombardo HP, Lytle BW, Loop FD, et al. Evaluation of normal prosthetic valve function by Doppler echocardiography. Am Heart J. 1987;114(3):576–82.
7. Fawzy ME, Halim M, Ziady G, Mercer E, Phillips R, Andaya W. Hemodynamic evaluation of porcine bioprostheses in the mitral position by Doppler echocardiography. Am J Cardiol. 1987;59(6):643–6.
8. Hoffmann A, Weiss P, Dubach P, Burckhardt D. Progressive functional deterioration of bioprostheses assessed by Doppler ultrasonography. Chest. 1990;98(5):1165–8.
9. Ryan T, Armstrong WF, Dillon JC, Feigenbaum H. Doppler echocardiographic evaluation of patients with porcine mitral valves. Am Heart J. 1986;111(2):237–44.
10. McClure RS, Narayanasamy N, Wiegerinck E, Lipsitz S, Maloney A, Byrne JG, et al. Pericardial bioprostheses carry better outcome compared to artificial or xenografts. Late outcomes for aortic valve replacement with the Carpentier-Edwards pericardial bioprosthesis: up to 17-year follow-up in 1,000 patients. Ann Thorac Surg. 2010;89(5):1410–6.
11. Mehlman DJ. A guide to the radiographic identification of prosthetic heart valves: an addendum. Circulation. 1984;69(1):102–5.
12. Kotler MN, Mintz GS, Panidis I, Morganroth J, Segal BL, Ross J. Noninvasive evaluation of normal and abnormal prosthetic valve function. J Am Coll Cardiol. 1983;2(1):151–73.
13. Nanda NC, Cooper JW, Mahan EF III, Fan P. Echocardiographic assessment of prosthetic valves. Circulation. 1991;84(3 Suppl):I228–39.
14. Kapur KK, Fan P, Nanda NC, Yoganathan AP, Goyal RG. Doppler color flow mapping in the evaluation of prosthetic mitral and aortic valve function. J Am Coll Cardiol. 1989;13(7):1561–71.
15. Sprecher DL, Adamick R, Adams D, Kisslo J. In vitro color flow, pulsed and continuous wave Doppler ultrasound masking of flow by prosthetic valves. J Am Coll Cardiol. 1987;9(6):1306–10.
16. Zoni A, Botti G, Morozzi L. Color Doppler imaging in mitral prostheses: normal flow pattern of Bjork-Shiley valve. Am J Noninvas Cardiol. 1989;3:261–4.
17. Hixson CS, Smith MD, Mattson MD, Morris EJ, Lenhoff SJ, Salley RK. Comparison of transesophageal color flow Doppler imaging of normal mitral regurgitant jets in St. Jude Medical and Medtronic Hall cardiac prostheses. J Am Soc Echocardiogr. 1992;5(1):57–62.
18. Khandheria BK, Seward JB, Oh JK, Freeman WK, Nichols BA, Sinak LJ, et al. Value and limitations of transesophageal echocardiography in assessment of mitral valve prostheses. Circulation. 1991;83(6):1956–68.
19. Nellessen U, Schnittger I, Appleton CP, Masuyama T, Bolger A, Fischell TA, et al. Transesophageal two-dimensional echocardiography and color Doppler flow velocity mapping in the evaluation of cardiac valve prostheses. Circulation. 1988;78(4):848–55.
20. Taams MA, Gussenhoven EJ, Cahalan MK, Roelandt JR, van Herwerden LA, The HK, et al. Transesophageal Doppler color flow imaging in the detection of native and Bjork-Shiley mitral valve regurgitation. J Am Coll Cardiol. 1989;13(1):95–9.
21. Feldman HJ, Gray RJ, Chaux A, Halpern SW, Kraus R, Allen HN, et al. Noninvasive in vivo and in vitro study of the St. Jude mitral valve prosthesis. Evaluation using two dimensional and M mode echocardiography, phonocardiography and cinefluoroscopy. Am J Cardiol. 1982;49(5):11101–9.
22. Diviggiano EE, Rosi S, Landra F, Marallo C, Scoppa C, Castellani D, Mandoli GE, Pastore MC, Cavigli L, D'Ascenzi F, Cameli M, Focardi M. Reverse septal movement: a step forward in the comprehension of the underlying causes. J Clin Med. 2024;13(4):928. https://doi.org/10.3390/jcm13040928. PMID: 38398242; PMCID: PMC10889416
23. Lindqvist P, Holmgren A, Zhao Y, Henein MY. Effect of pericardial repair after aortic valve replacement on septal and right ventricular function. Int J Cardiol. Nov. 2010;25. [Epub ahead of print]
24. Burstow DJ, Nishimura RA, Bailey KR, Reeder GS, Holmes DR Jr, Seward JB, et al. Continuous wave Doppler echocardiographic measurement of prosthetic valve gradients. A simultaneous Doppler-catheter correlative study. Circulation. 1989;80(3):504–14.
25. Reisner SA, Meltzer RS. Normal values of prosthetic valve Doppler echocardiographic parameters: a review. J Am Soc Echocardiogr. 1988;1(3):201–10.
26. Marti V, Carreras F, Borras X, Pons-Llado G. Doppler echocardiographic findings in normal-functioning St. Jude Medical and Bjork-Shiley mechanical prostheses in the tricuspid valve position. Am J Cardiol. 1991;67(4):307–9.
27. Pibarot P, Herrmann HC, Wu C, Hahn RT, Otto CM, Abbas AE, Chambers J, Dweck MR, Leipsic JA, Simonato M, Rogers T, Sathananthan J, Guerrero M, Ternacle J, Wijeysundera HC, Sondergaard L, Barbanti M, Salaun E, Généreux P, Kaneko T, Landes U, Wood DA, Deeb GM, Sellers SL, Lewis J, Madhavan M, Gillam L, Reardon M, Bleiziffer S, O'Gara PT, Rodés-Cabau J, Grayburn PA, Lancellotti P, Thourani VH, Bax JJ, Mack MJ, Leon MB. Heart valve collaboratory. standardized definitions for bioprosthetic valve dysfunction following aortic or mitral valve replacement: JACC state-of-the-art review. J Am Coll Cardiol. 2022;80(5):545–61. https://doi.org/10.1016/j.jacc.2022.06.002. PMID: 35902178
28. Chen YT, Kan MN, Chen JS, Lin WW, Chang MK, Hu WS, et al. Detection of prosthetic mitral valve leak: a comparative study using transesophageal echocardiography, transthoracic echocardiography, and auscultation. J Clin Ultrasound. 1990;18(7):557–61.
29. Flachskampf FA, O'Shea JP, Griffin BP, Guerrero L, Weyman AE, Thomas JD. Patterns of normal transvalvular regurgitation in mechanical valve prostheses. J Am Coll Cardiol. 1991;18(6):1493–8.
30. Delgado V, Ajmone Marsan N, de Waha S, Bonaros N, Brida M, Burri H, Caselli S, Doenst T, Ederhy S, Erba PA, Foldager D, Fosbøl EL, Kovac J, Mestres CA, Miller OI, Miro JM, Pazdernik M, Pizzi MN, Quintana E, Rasmussen TB, Ristić AD, Rodés-Cabau J, Sionis A, Zühlke LJ, Borger MA, ESC Scientific Document Group. ESC Guidelines for the management of endocarditis. Eur Heart J. 2023;44(39):3948–4042. https://doi.org/10.1093/eurheartj/ehad193. Erratum in: Eur Heart J. 2023 Sep 20;: Erratum in: Eur Heart J. 2024 Jan 1;45(1):56. PMID: 37622656

Infective Endocarditis

6

Matteo Lisi, Matteo Cameli, Sergio Mondillo, and Michael Y. Henein

In recent years, there has been a change in the epidemiological profile of infective endocarditis (IE), with an increase in valvular endocarditis in elderly patients, often as a result of health care–associated procedures, both in patients with native valve disease and patients with prosthetic valves [1–3]. In developed countries, the currently listed predisposing factors for endocarditis are degenerative valve sclerosis, valve prostheses, intravenous drug abuse, and frequent use of invasive procedures [4–6]. In developing countries, however, where the prevalence of rheumatic fever remains high, rheumatic valve disease represents the main risk factor for IE [7]. Furthermore, the emerging and increasing antibiotic resistance among oral streptococci is of concern [8] but whether changes in national guidelines on the use of antibiotic prophylaxis have resulted in an increase in the incidence of IE remains unclear [9–11] There is great variability in IE according to patient's age, with a value of about 3–10 episodes/in every 100,000 person-years in young patients, compared to 14.5 episodes/in every 100,000 person-years in patients between 70 and 80 years of age [12, 13]. In recent years, the incidence of IE has increased [14, 15], becoming a major public health challenge. In 2019, the estimated incidence of IE was 13.8 cases per 100,000 subjects per year, having accounted for 66,300 deaths worldwide [16].

Preventive Measures

Most studies in the literature have focused on dental procedures as a cause of IE, with the use of prophylactic antibiotics to prevent IE in the patients at risk. The scientific hypothesis is based on the assumptions that firstly bacteremia caused by a medical procedure can cause IE, especially in patients with predisposing factors and considered at high risk, and secondly that prophylactic antibiotics can prevent IE [5, 17].

Transient bacteremia is common with manipulation of the teeth and periodontal tissue, and there is a wide variation in reported frequencies of bacteremia related to dental procedures, ranging between 10% and 100%, depending on the procedures used [18, 19]. Transient bacteremia can also occur frequently during routine daily activities unrelated to dental procedures, such as tooth brushing and flossing, use of wooden toothpicks, use of water irrigation devices, and chewing food [20, 21]. Studies showed that in IE caused by *viridans* group streptococci or enterococci, the time elapsing between the bacteremia and the onset of symptoms of IE is usually 7–14 days [22]. Even when there is a close temporal relationship between a dental procedure and IE, it is not always possible to determine with certainty whether the bacteremia which causes IE originated from a dental procedure or from a randomly occurring bacteremia as a result of routine daily activities during the same time period. Good oral hygiene and regular dental check-ups are therefore of fundamental importance to prevent IE, bearing in mind the known high rates of post-procedural bacteremia [23]. One cannot also underestimate the risk of adverse reactions to drugs, both nonfatal reactions, such as rash, diarrhea, and gastrointestinal symptoms, and potentially fatal reactions such as anaphylactic reactions, estimated to occur in 15–25 individuals per one million patients receiving a dose of penicillin [24]. For these reasons, the 2023 ESC guidelines [8] have proposed limiting the indication for antibiotic prophylaxis for IE to high-risk patients (Table 6.1), who are undergoing procedures which carry the highest risk. Moreover

Supplementary Information The online version contains supplementary material available at https://doi.org/10.1007/978-3-031-95894-6_6.

M. Lisi (✉)
Ospedale S. Maria delle Croci, Ravenna, Italy

M. Cameli · S. Mondillo
University of Siena, Siena, Italy

M. Y. Henein
University of Siena, Siena, Italy

Imperial College London, London, UK

© The Author(s), under exclusive license to Springer Nature Switzerland AG 2025

M. Y. Henein (ed.), *Clinical Echocardiography*, https://doi.org/10.1007/978-3-031-95894-6_6

there are such condition considered for patients at intermediate risk of IE for whom antibiotic prophylaxis is not routinely recommended and may be considered on an individual basis [8]. Patients at intermediate risk of IE include those with: (A) rheumatic heart disease; (B) non-rheumatic degenerative valve disease; (C) congenital valve abnormalities including bicuspid aortic valve disease; (D) cardiovascular implanted electronic devices; and (E) hypertrophic cardiomyopathy [5, 8].

To date [8] antibiotic prophylaxis is recommended (in high risk patients; see Table 6.1) in dental extractions, oral surgical procedures, and procedures requiring manipulation of the gingival or periapical region of the teeth (Class: I, LOE: B), while no convincing evidence has been produced on the relationship between bacteraemia from a non-dental procedures and risk of subsequent IE. However, compared with patients with IE not undergoing an invasive procedure, several non-dental invasive procedures were associated with increased risk of IE (such as cardiovascular interventions, skin procedures and wound management, transfusion, dialysis, bone marrow puncture, and endoscopic procedures [25, 26, 27]. Consequentlly, systemic antibiotic prophylaxis may be considered [2023 ESC guidelines, 8] for high-risk patients undergoing an invasive diagnostic or therapeutic procedure of the respiratory, gastrointestinal, genitourinary tract, skin, or musculoskeletal systems (Class IIb, LOE: c).

Table 6.1 Recommendation for antibiotic prophylaxis in patients with cardiovascular disease undergoing oro-dental procedures at increased risk of IE

Recommendations	Class[a]	Level[b]
General prevention measures are recommended in individuals at high and intermediate risk for IE	I	C
Antibiotic prophylaxis is recommended in patients with previous IE	I	B
Antibiotic prophylaxis is recommended in patients with surgically implanted prosthetic valves and with any material used for surgical cardiac valve repair	I	C
Antibiotic prophylaxis is recommended in patients with transcatheter implanted aortic and pulmonary valvular prostheses	I	C
Antibiotic prophylaxis is recommended in patients with untreated cyanotic congenital heart disease, and patients treated with surgery or transcatheter procedures with post-operative palliative shunts, conduits, or other prostheses. After surgical repair, in the absence of residual defects or valve prostheses, antibiotic prophylaxis is recommended only for the first 6 months after the procedure	I	C
Antibiotic prophylaxis is recommended in patients with ventricular assist devices	I	C
Antibiotic prophylaxis should be considered in patients with transcatheter mitral and tricuspid valve repair	IIa	C
Antibiotic prophylaxis may be considered in recipients of heart transplant	IIb	C
Antibiotic prophylaxis is not recommended in other patients at low risk for IE	III	C

Adapted from Delgado V. et al, 2023 ESC Guidelines. [8]
[a]Class of recommendation
[b]Level of evidence

However for high-risk "*patients listed in* Table 6.1" undergoing invasive procedures, prophylactic antibiotics are recommended in the following circumstances with single dose 30–60 min before procedure [8]:

(a) If there is no proven allergy to penicillin or ampicillin:
Amoxicillin (2 g orally for adults, or 50 mg/kg orally for children);
Ampicillin (2 g i.m. or i.v. for adults, or 50 mg/kg i.v. or i.m. for children)

(b) If there is proven allergy to penicillin or ampicillin:
Cephalexin (2 g orally for adults, or 50 mg/kg orally for children);
Azithromycin or clarithromycin (500 mg orally for adults or 15 mg/kg orally for children);
Doxacycline (100 mg orally for adults, or < 45 kg, 2.2 mg/kg orally, >45 kg, 100 mg orally for children);
Cefazolin or ceftriaxoneb (1 g i.m. or i.v. for adults, or 50 mg/kg i.v. or i.m for children)

Diagnostic Criteria for IE and Role of Echocardiography

While the Duke criteria [28] remain the cornerstone for the diagnosis of IE, based upon clinical, echocardiographic, and microbiological findings, 2023 ESC guideline [8] proposed a new diagnostic classification (Table 6.2). Transthoracic and transesophageal echocardiography (TTE and TOE) play a key role in the diagnosis, management, and follow-up of patients with suspected IE [29], and even in those with low probability for IE and no clinical features [30]. The sensitivity of TTE ranges from 40% to 63% and that of TOE from 90% to 100% [31]. In particular, whenever IE is suspected on the basis of clinical and laboratory criteria, patients should be screened by TTE as the first-line imaging modality. TOE is recommended in all patients with high clinical suspicion of IE and a negative or non-diagnostic TTE. Moreover, TOE is also recommended in patients with clinical suspicion of IE, when a prosthetic valve or an intracardiac device is present (for details, see Table 6.3). Recently 2023 ESC guidelines proposed a simple flow chart to be followed in patients with suspected IE [8] (Table 6.3). Right-sided IE accounts for about 5–10% of patients with IE, but its frequency may be increasing as its risk factors are increasing in some countries [32].

Table 6.2 Definitions of the 2023 ESC modified diagnostic criteria of IE

Major criteria
(I) Blood cultures positive for IE
(a) Typical microorganisms consistent with IE from two separate blood cultures: Oral streptococci, *Streptococcus gallolyticus (formely S. bovi)*, HACEK group, *Staphylococcus aureus*, E. faecalis
(b) Microorganism consistent with IE from continuosly positive blood cultures: ≥ 2 blood cultures positive of blood cultures of blood sample drawn >12 h apart. All of 3 or a majority of ≥4 separate cultures of blood (with first and last samples drawn ≥1 h apart)
(c) Single positive blood culture for C. burnetii or phase I IgG antibody titre >1:800.
(II) Imaging positive for IE: Valvular, perivalvular/periprosthetic and foreign material anatomic and metabolic lesions characteristic of IE detected by any of the following imaging techniques: Echocardiography (TTE and TOE) Cardiac CT [18F]-FDG-PET/CT(A) WBC SPECT/CT
Minor criteria
(I) Predisposition conditions (for high or intermediate risk of IE or PWIDs)
(II) Fever defined as temperature >38°C
(III) Embolic vascular dissemination (including those asymptomatic detected by imaging only): Major systemic and pulmonary emboli/infarcts and abscesses Haematogenous osteoarticular septic complications (i.e. spondylodiscitis) Mycotic aneurysms Intracranial ischaemic/haemorrhagic lesions Conjunctival haemorrhages Janeway's lesions
(IV) Immunological phenomena: Glomerulonephritis Osler nodes and Roth spots Rheumatoid factor
(V) Microbiological evidence: Positive blood culture but does not meet a major criterion as noted above Serological evidence for active infection with organism consistent with IE
IE Classification (at admission and during follow-up)
(A) Definite: 2 major criteria 1 major criterion and at least 3 minor criteria 5 minor criteria
(B) Possible: 1 major criterion and 1 or 2 minor criteria 3–4 minor criteria
(C) Negative: Does not meet criteria for definite or possible diagnosis at admission with or without a firm alternative diagnosis

Note: Adapted from Delgado V. et al., 2023 ESC Guidelines [8]
[18F]-FDG-PET/CT 18F-fluorodeoxyglucose positron emission tomography, *CT(A)* computed tomography (angiography), *HACEK* Haemophilus, Aggregatibacter, Cardiobacterium, Eikenella, and Kingella, *IE* infective endocarditis, *Ig* immunoglobulin, *PWID* people who inject drugs, *TOE* transoesophageal echocardiography, *TTE* transthoracic echocardiography, *WBC SPECT/CT* white blood cell single photon emission tomography/computed tomography

Table 6.3 Recommendations for the role of echocardiography in IE.

Recommendations	Class[a]	Level[b]
A. *Diagnosis*		
TTE is recommended as the first-line imaging modality in suspected IE	I	B
TOE is recommended in all patients with clinical suspicion of IE and a negative or non-diagnostic TTE	I	B
TOE is recommended in patients with clinical suspicion of IE, when a prosthetic valve or an intracardiac device is present	I	B
Repeating TTE and/or TEE within 5–7 days is recommended in cases of initially negative examination when clinical suspicion of IE remains high	I	C
TOE is recommended in patients with suspected IE, even in cases with positive TTE, except in isolated right-sided native valve IE with good quality TTE examination and unequivocal echocardiographic findings	I	C
Performing an echocardiography should be considered in S. aureus, E. faecalis, and some Streptococcus spp. Bacteraemia	IIa	B
B. *Follow-up under medical therapy*		
Repeating TTE and/or TOE is recommended as soon as a new complication of IE is suspected (new murmur, embolism, persisting fever and bacteraemia, HF, abscess, AVB)	I	B
TOE is recommended when patient is stable before switching from intravenous to oral antibiotic therapy	I	B
During follow-up of uncomplicated IE, repeat TTE and/or TOE should be considered to detect new silent complications. The timing of repeat TTE and/or TOE depends on the initial findings, type of microorganism, and initial response to therapy	IIa	B
C. *Intraoperative echocardiography*		
Intraoperative echocardiography is recommended in all cases of IE requiring surgery	I	C
D. *Following completion of therapy*		
TTE and/or TOE are recommended at completion of antibiotic therapy for evaluation of cardiac and valve morphology and function in patients with IE who did not undergo valve surgery	I	C

Note: Adapted from Delgado V. et al., 2023 ESC Guidelines [8]
AVB atrioventricular block, *HF* heart failure, *IE* infective endocarditis, *PVE* prosthetic valve endocarditis, *TEE* transoesophageal echocardiography, *TTE* transthoracic echocardiography
[a]Class of recommendation
[b]Level of evidence

Anatomical and Echocardiographic Features of IE

1. Vegetation
   (a) *Echocardiography:* an intracardiac mass attached to a valve or other structure, irrespective of its oscillation (Figs. 6.1, 6.2 and 6.3; Videos 6.1, 6.2 and 6.3)
   (b) *Surgery/necropsy:* Infected mass attached to an endocardial structure or on implanted intracardiac material
2. Abscess
   (a) Echocardiography: Thickened paravalvular area of varying echo intensity (Fig. 6.4)
   (b) *Surgery/necropsy:* Paravalvular cavity with necrosis and purulent material not communicating with the cardiovascular lumen
3. Pseudoaneurysm
   (a) *Echocardiography:* Pulsatile paravalvular echo-free space, with color-Doppler flow (Figs. 6.5 and 6.6; Videos 6.4, 6.5 and 6.6)

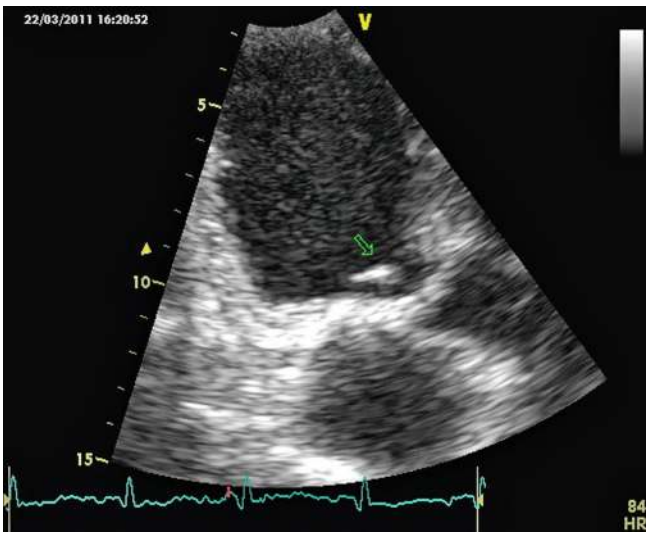


Fig. 6.1 Two-dimensional (2D) transthoracic echocardiography (TTE), apical three chambers view. Aortic valve vegetation (see *arrow*) in a 68-year-old woman (*Enterococcus fecalis*)

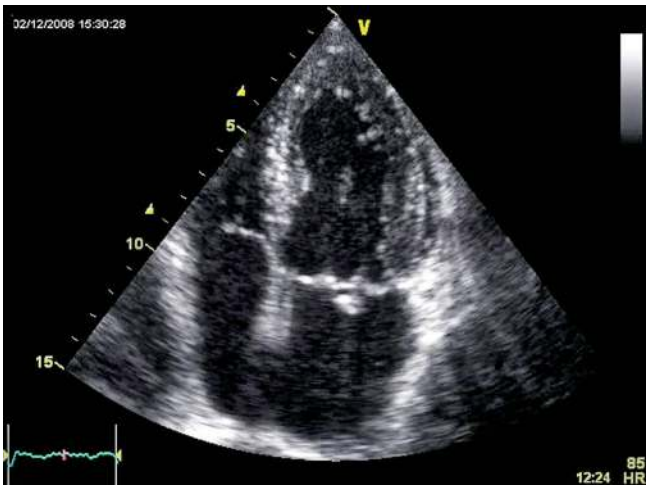


Fig. 6.3 2D TTE, apical four-chamber view. Mitral valve vegetation (attached to the posterior leaflet) in 59-year-old man with mitral valve endocarditis (*Enterococcus gallinarum*)

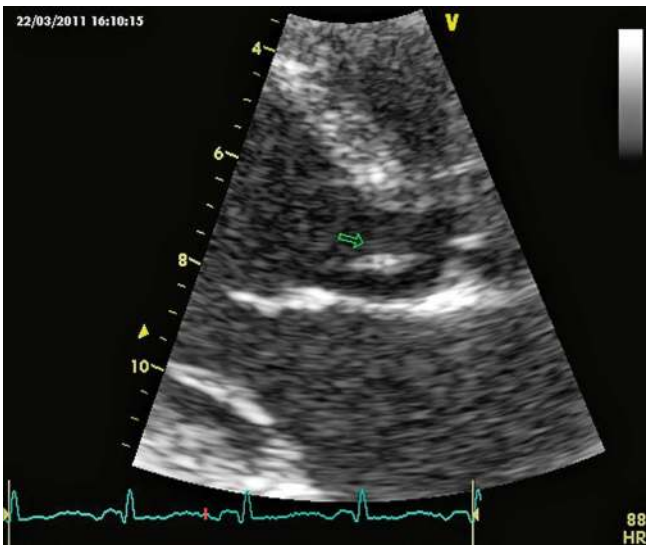


Fig. 6.2 2D TTE, parasternal long axis view. Aortic valve vegetation (see *arrows*) in a 68-year-old woman (*Enterococcus fecalis*)

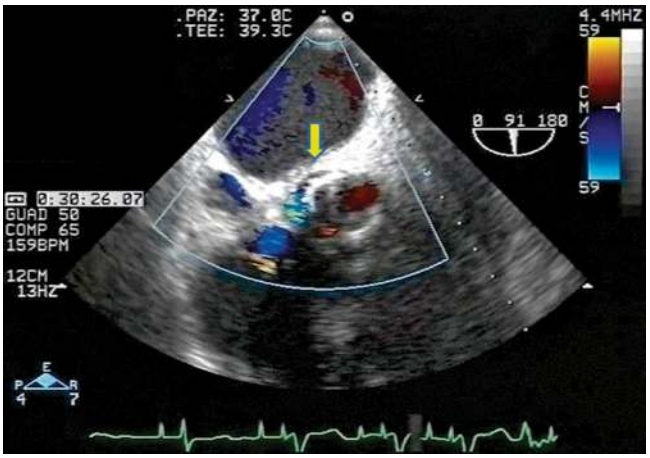


Fig. 6.4 Transesophageal echocardiogram (TOE). Para-prosthetic abscess on a biological aortic prosthesis in a patient undergoing aortic valve replacement 10 days before (see *arrow*)

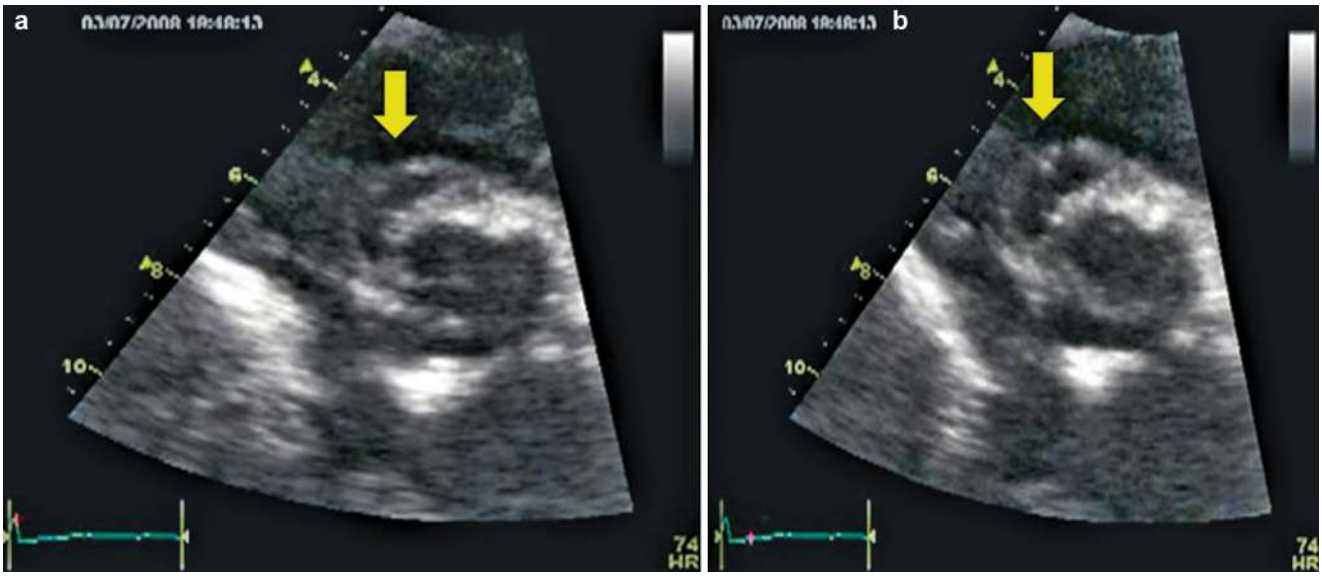


Fig. 6.5 2D TTE, parasternal short axis view. Pseudoaneurysm of aortic biological prosthesis, during diastole (**a**), and during systole (**b**), see *arrows*

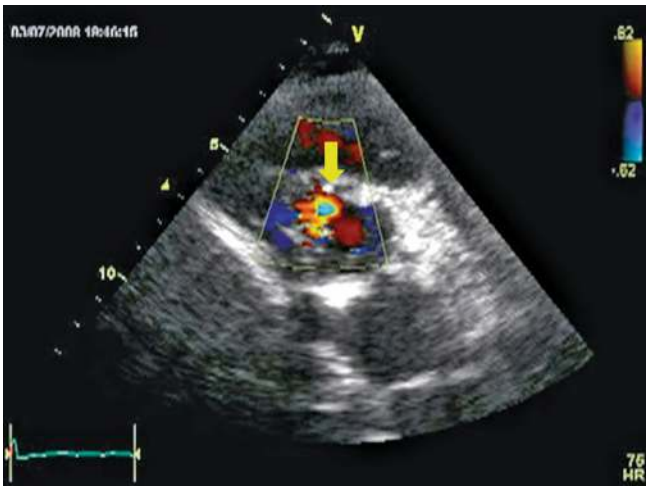


Fig. 6.6 2D TTE, parasternal short axis view. Pseudoaneurysm of aortic biological prosthesis, during systole with color-Doppler that fills the cavity (see *arrow*)

(b) *Surgery/Necropsy:* Paravalvular cavity communicating with the cardiovascular lumen

4. Perforation
   (a) *Echocardiography:* Interruption of endocardial tissue continuity traversed by color-Doppler flow
   (b) *Surgery/necropsy:* Interruption of endocardial tissue continuity
5. Fistula
   (a) *Echocardiography:* Color-Doppler flow communication between two neighboring cavities through a perforation (Fig. 6.7; Videos 6.7 and 6.8)
   (b) *Surgery/Necropsy:* Communication between two neighboring cavities through a perforation
6. Valve Aneurysm
   (a) *Echocardiography:* bulging of valve tissue which is saccular in shape
   (b) *Surgery/necropsy:* Saccular outpouching of valvular tissue
7. Dehiscence of a Prosthetic Valve
   (a) *Echocardiography:* Paravalvular regurgitation identified by TTE/TOE irrespective of prosthesis rocking (Videos 6.9 and 6.10)
   (b) *Surgery/Necropsy:* dehiscence of the prosthesis [5]

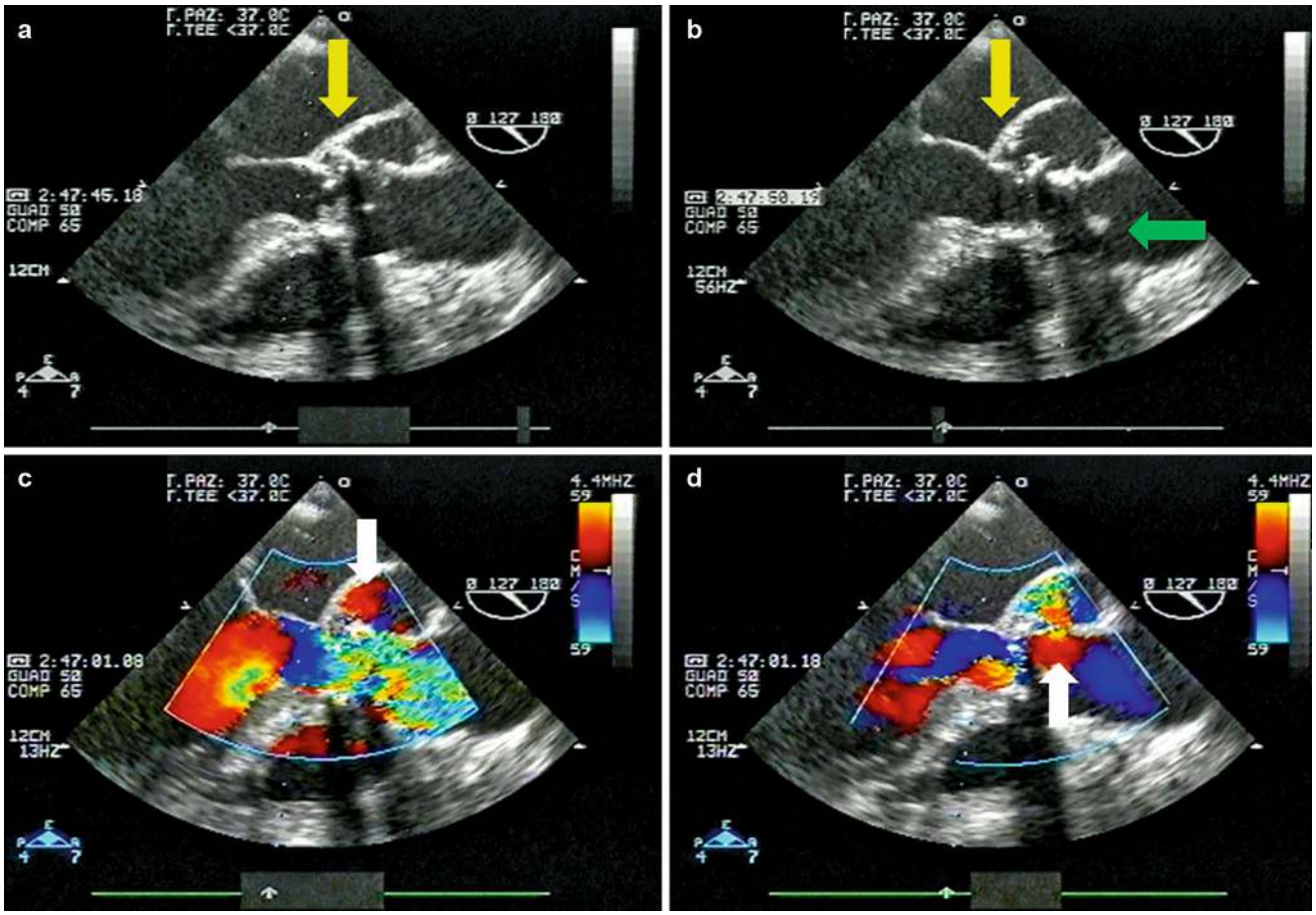


Fig. 6.7 TOE. Post-infectious fistula on biological aortic prosthesis, clearly visible during diastole (**a**) and systole (*yellow arrows*). (**b**) The *green arrow* indicates the vegetation attached to the prosthesis. During systole (**c** and **d**), two communications between the two neighboring cavities (*white arrows*) represented by the aortic bulb and the newly formed para-prosthetic cavity

Indications and Optimal Timing of Surgery in Left-Sided Native Valve IE

The 2023 ESC guidelines introduce the "endocarditis team" as a key role in the management of patients with suspected or confirmed IE in order to provide early and more accurate diagnosis of the primary disease and its complications, uniform antibiotic treatment, optimized timing for surgical intervention, and coordination of post-operative care [8]. Surgical treatment of IE is necessary in about 50% of patients because of severe complications, the commonest of which is heart failure, followed by persistent infection and embolism [33]. Recent changes in the epidemiological profile of the disease explain this trend, with the greater incidence of more virulent organisms and intracardiac material infections [34, 35]. Accurate prognostic classification may help facilitate individual treatment decisions and interpretation of therapeutic interventions in patients with IE. Surgical treatment in patients with left-sided IE is a strong independent predictor of long-term survival. The use of surgery was highly indicated based on age, the presence of heart failure, and intracardiac abscess [36]. Resorting to early surgery in the active phase may help avoid progressive heart failure and irreversible structural damage by severe infection and may prevent systemic embolism [37, 38], but can still be associated with significant risk. The decision to employ surgery must be taken with consideration for the impact on the subsequent risk of potential relapse or post-operative valvular dysfunction, which are always a concern when the material is implanted into infected tissues [39].

Moreover the effect of early surgery on early post-operative mortality is not uniform but might be beneficial in patients with the most severe IE [40]. The three main indications for early surgery in IE, as stated by ESC guidelines, are heart failure, uncontrolled infection, and prevention of embolic events [8] (Table 6.4).

In particular, embolic events are a life-threatening complication and a major cause of morbidity and mortality in patients with IE, with an incidence ranging from 10% to 50%

Table 6.4 Recommendations for the main indications of surgery in IE (native and prosthetic valve endocarditis)

Recommendations	Class[a]	Level[b]
(A) Heart failure		
• Emergency[d] surgery is recommended in aortic or mitral NVE or PVE with severe acute regurgitation, obstruction, or fistula causing refractory pulmonary oedema or cardiogenic shock	I	B
• Urgent[d] surgery is recommended in aortic or mitral NVE or PVE with severe acute regurgitation or obstruction causing symptoms of HF or echocardiographic signs of poor haemodynamic tolerance	I	B
(B) Uncontrolled infection		
• Urgent[c] surgery is recommended in locally uncontrolled infection (abscess, false aneurysm, fistula, enlarging vegetation, prosthetic dehiscence, new AV block)	I	B
• Urgent[c] or non-urgent surgery is recommended in IE caused by fungi or multiresistant organisms according to the haemodynamic condition of the patient	I	C
• Urgent[c] surgery should be considered in IE with persistently positive blood cultures >1 week or persistent sepsis despite appropriate antibiotic therapy and adequate control of metastatic foci	IIa	B
• Urgent[c] surgery should be considered in PVE caused by S. aureus or non-HACEK Gram-negative bacteria	IIa	B
(C) Prevention of embolism		
• Urgent[c] surgery is recommended in aortic or mitral NVE or PVE with persistent vegetations ≥10 mm after one or more embolic episodes despite appropriate antibiotic therapy	I	B
• Urgent[c] surgery is recommended in IE with vegetation ≥10 mm and other indications for surgery	I	C
• Urgent[c] surgery may be considered in aortic or mitral IE with vegetation ≥10 mm and without severe valve dysfunction or without clinical evidence of embolism and low surgical risk	IIb	B

Note: Adapted from Delgado V. et al. 2023 ESC Guidelines [8]
AVB atrioventricular block, *HACEK* Haemophilus, Aggregatibacter, Cardiobacterium, Eikenella, Kingella, *HF* heart failure, *IE* infective endocarditis, *NVE* native valve endocarditis, *PVE* prosthetic valve endocarditis
[a]Class of recommendation
[b]Level of evidence
[c]Urgent, within 3–5 days. Non-urgent, within same hospital admission
[d]Emergency, within 24 h

[41, 42]. Up to 65% of all embolic events involve the central nervous system in cases of left-sided IE [43], while pulmonary embolism is frequent in native right-sided and pacemaker-lead IE.

A recent study showed that the incidence of stroke in patients receiving appropriate antimicrobial therapy was 4.82/1,000 patients in the first week of therapy and fell to 1.71/1,000 patients in the second week, equivalent to a reduction of about 65% (Videos 6.11 and 6.12) [44]. Echocardiography plays a key role in predicting embolic events [45, 46], especially by defining two importan characteristics of vegetation: size and mobility. These represent the most important independent predictors of a new embolic event [47, 48]. Large vegetation >10 mm, severe vegetation mobility, or both are associated with an increased embolic risk, while vegetation length >15 mm represents an independent predictor of 1-year mortality [42] (Figs. 6.8 and 6.9; Videos 6.13, 6.14 and 6.15). Moreover, the risk of embolism is higher in mitral endocarditis compared to aortic endocarditis, especially in staphylococcal IE [49].

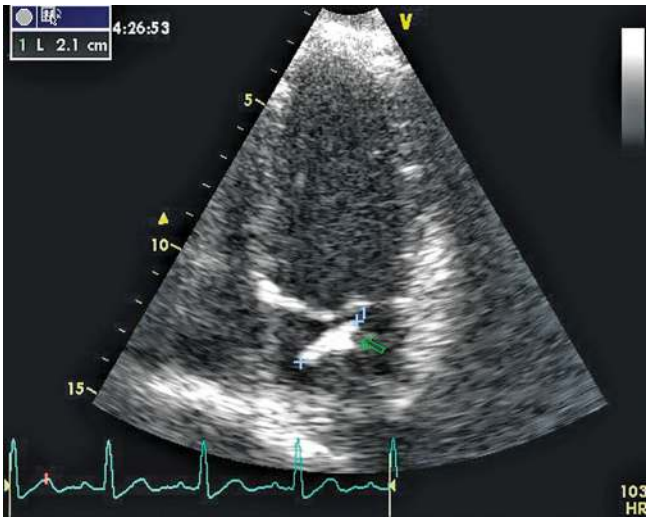


Fig. 6.8 2D TTE. Mitral valve endocarditis (*S. epidermidis*) in a 42-year-old man with a large (21 mm) and mobile vegetation (arrow) attached to the posterior mitral leaflet [see Figs. 6.8 (2D TTE) and 6.9 (3D TTE)]

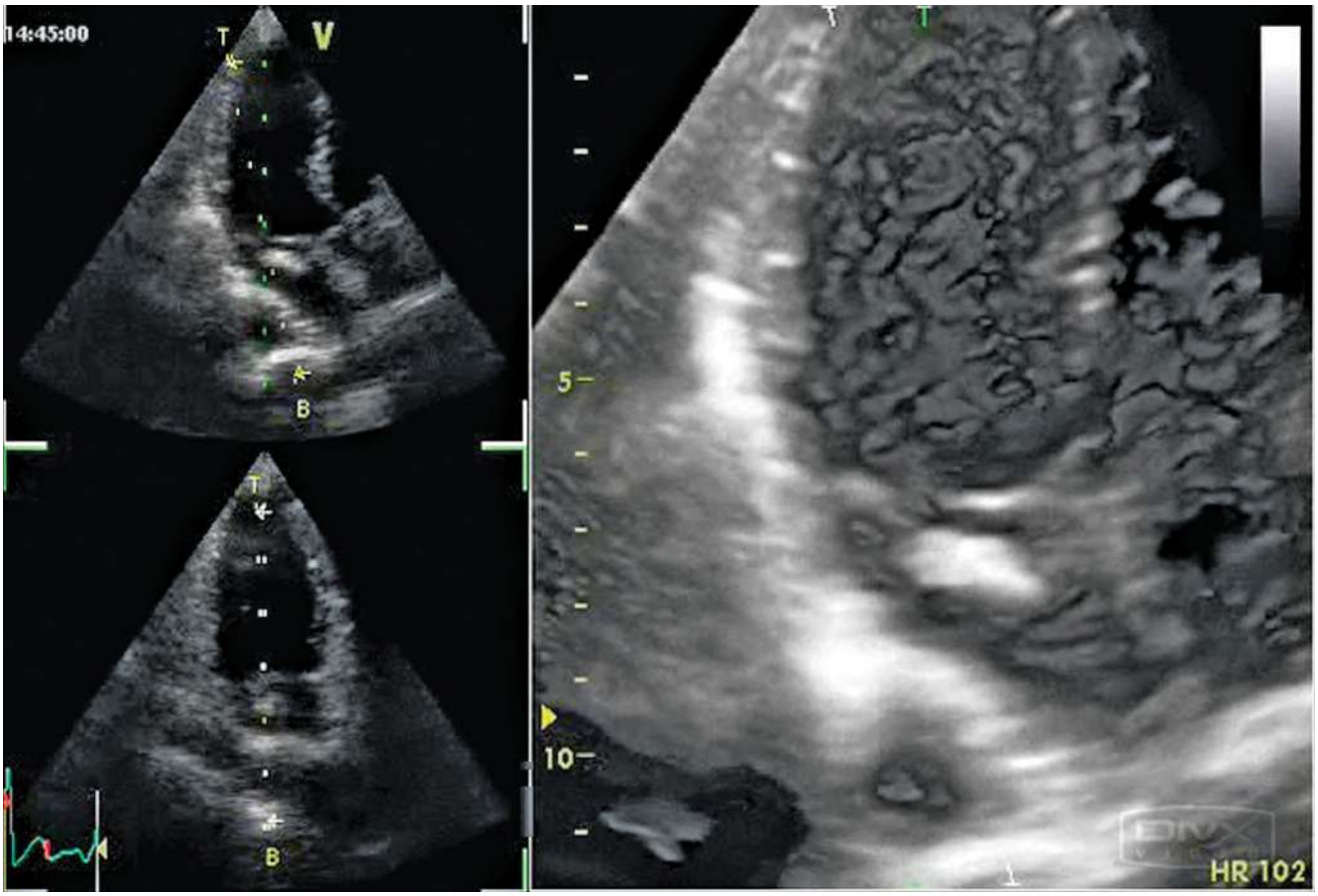


Fig. 6.9 2D TTE and 3D TTE. Mitral valve endocarditis (*S. epidermidis*) in a 42-year-old man with a large (21 mm) and mobile vegetation attached to the posterior mitral leaflet [see Figs. 6.8 (2D TTE) and 6.9 (3D TTE)]

References

1. Moreillon P, Que YA. Infective endocarditis. Lancet. 2004;363:139–49.
2. Hoen B, Alla F, Selton-Suty C, Beguinot I, Bouvet A, Briancon S, et al. Changing profile of infective endocarditis: results of a 1-year survey in France. JAMA. 2002;288:75–81.
3. Hill EE, Herijgers P, Claus P, Vanderschueren S, Herregods MC, Peetermans WE. Infective endocarditis: changing epidemiology and predictors of 6-month mortality: a prospective cohort study. Eur Heart J. 2007;28:196–203.
4. Friedman ND, Kaye KS, Stout JE, McGarry SA, Trivette SL, Briggs JP, et al. Health care-associated bloodstream infections in adults: a reason to change the accepted definition of community-acquired infections. Ann Intern Med. 2002;137:791–7.
5. Habib G, Hoen B, Tornos P, Thuny F, Prendergast B, Vilacosta I, et al. Guidelines on the prevention, diagnosis, and treatment of infective endocarditis (new version 2009): the Task Force on the Prevention, Diagnosis, and Treatment of Infective Endocarditis of the European Society of Cardiology (ESC). Eur Heart J. 2009;30:2369–413.
6. Habib G, Lancellotti P, Antunes MJ, Bongiorni MG, Casalta JP, Del Zotti F, et al. 2015 ESC Guidelines for the management of infective endocarditis: The Task Force for the Management of Infective Endocarditis of the European Society of Cardiology (ESC). Endorsed by: European Association for Cardio-Thoracic Surgery (EACTS), the European Association of Nuclear Medicine (EANM). Eur Heart J. 2015;36(44):3075–128.
7. Nkomo VT. Epidemiology and prevention of valvular heart diseases and infective endocarditis in Africa. Heart. 2007;93:1510–9.
8. Delgado V, Ajmone Marsan N, de Waha S, Bonaros N, Brida M, Burri H, et al. 2023 ESC Guidelines for the management of endocarditis. Eur Heart J. 2023;44(39):3948–4042.
9. Thornhill MH, Gibson TB, Cutler E, Dayer MJ, Chu VH, Lockhart PB, et al. Antibiotic prophylaxis and incidence of endocarditis before and after the 2007 AHA recommendations. J Am Coll Cardiol. 2018;72(20):2443–54.
10. Thornhill MH, Dayer MJ, Nicholl J, Prendergast BD, Lockhart PB, Baddour LM. An alarming rise in incidence of infective endocarditis in England since 2009: why? Lancet. 2020;395(10233):1325–7.
11. Quan TP, Muller-Pebody B, Fawcett N, Young BC, Minaji M, Sandoe J, et al. Investigation of the impact of the NICE guidelines regarding antibiotic prophylaxis during invasive dental procedures on the incidence of infective endocarditis in England: an electronic health records study. BMC Med. 2020;18(1):84.
12. Van der Meer JT, Thompson J, Valkenburg HA, Michel MF. Epidemiology of bacterial endocarditis in The Netherlands. I. Patient characteristics. Arch Intern Med. 1992;152:1863–8.
13. Hogevik H, Olaison L, Andersson R, Lindberg J, Alestig K. Epidemiologic aspects of infective endocarditis in an urban population. A 5-year prospective study. Medicine (Baltimore). 1995;74:324–39.

14. Chen H, Zhan Y, Zhang K, Gao Y, Chen L, Zhan J, Chen Z, Zeng Z. The Global, Regional, and National Burden and Trends of Infective Endocarditis From 1990 to 2019: Results From the Global Burden of Disease Study 2019. Front Med (Lausanne). 2022;9(9):774224.
15. Lisi M, Flamigni F, Russo M, Cameli M, Mandoli GE, Pastore MC, Mele D, Campo G, Henein MY, Rubboli A. Incidence and mortality of infective endocarditis in the last decade: a single center studyJ Cardiovasc Med (Hagerstown). 2023;24(2):105–12.
16. Momtazmanesh S, Saeedi Moghaddam S, Malakan Rad E, Azadnajafabad S, Ebrahimi N, et al. Eur J Prev Cardiol. 2022;29:1287–97.
17. Wilson W, Taubert KA, Gewitz M, Lockhart PB, Baddour LM, Levison M, et al. Prevention of infective endocarditis: guidelines from the American Heart Association: a guideline from the American Heart Association Rheumatic Fever, Endocarditis, and Kawasaki Disease Committee, Council on Cardiovascular Disease in the Young, and the Council on Clinical Cardiology, Council on Cardiovascular Surgery and Anesthesia, and the Quality of Care and Outcomes Research Interdisciplinary Working Group. Circulation. 2007;116:1736–54.
18. Lockhart PB. The risk for endocarditis in dental practice. Periodontol. 2000;2000(23):127–35.
19. Forner L, Larsen T, Kilian M, Holmstrup P. Incidence of bacteremia after chewing, tooth brushing and scaling in individuals with periodontal inflammation. J Clin Periodontol. 2006;33:401–7.
20. Roberts GJ. Dentists are innocent! 'Everyday' bacteremia is the real culprit: a review and assessment of the evidence that dental surgical procedures are a principal cause of bacterial endocarditis in children. Pediatr Cardiol. 1999;20:317–25.
21. Faden HS. Letter: dental procedures and bacteremia. Ann Intern Med. 1974;81:274.
22. Starkebaum M, Durack D, Beeson P. The "incubation period" of subacute bacterial endocarditis. Yale J Biol Med. 1977;50:49–58.
23. Duval X, Leport C. Prophylaxis of infective endocarditis: current tendencies, continuing controversies. Lancet Infect Dis. 2008;8:225–32.
24. Agha Z, Lofgren RP, VanRuiswyk JV. Is antibiotic prophylaxis for bacterial endocarditis cost-effective? Med Decis Making. 2005;25:308–20.
25. Janszky I, Gémes K, Ahnve S, Asgeirsson H, Möller J. Invasive procedures associated with the development of infective endocarditis. J Am Coll Cardiol. 2018;71(24):2744–52.
26. Thornhill MH, Crum A, Campbell R, Stone T, Lee EC, Bradburn M, et al. Temporal association between invasive procedures and infective endocarditis. Heart. 2023;109(3):223–31.
27. Cahill TJ, Harrison JL, Jewell P, Onakpoya I, Chambers JB, Dayer M, et al. Antibiotic prophylaxis for infective endocarditis: a systematic review and meta-analysis. Heart. 2017;103(12):937–44.
28. Durack DT, Lukes AS, Bright DK. New criteria for diagnosis of infective endocarditis: utilization of specific echocardiographic findings. Duke Endocarditis Service. Am J Med. 1994;96:200–9.
29. Sachdev M, Peterson GE, Jollis JG. Imaging techniques for diagnosis of infective endocarditis. Infect Dis Clin North Am. 2002;16:319–37.
30. Knudsen JB, Fuursted K, Petersen E, Wierup P, Mølgaard H, Poulsen SH, et al. Failure of clinical features of low probability endocarditis. The early echo remains essential. Scand Cardiovasc J. 2011; https://doi.org/10.3109/14017431.563863.
31. Evangelista A, Gonzalez-Alujas MT. Echocardiography in infective endocarditis. Heart. 2004;90:614–7.
32. Lassen H, Nielsen SL, Gill SUA, Johansen IS. The epidemiology of infective endocarditis with focus on non-device related right-sided infective endocarditis: A retrospective register-based study in the region of Southern Denmark. Int J Infect Dis. 2020;95:224–30.
33. Tornos P, Iung B, Permanyer-Miralda G, Baron G, Delahaye F, Gohlke-Barwolf C, et al. Infective endocarditis in Europe: lessons from the Euro heart survey. Heart. 2005;91:571–5.
34. Cabell CH, Jollis JG, Peterson GE, Corey GR, Anderson DJ, Sexton DJ, et al. Changing patient characteristics and the effect on mortality in endocarditis. Arch Intern Med. 2002;162:90–4.
35. Fowler VG Jr, Miro JM, Hoen B, Cabell CH, Abrutyn E, Rubinstein E, et al. Staphylococcus aureus endocarditis: a consequence of medical progress. JAMA. 2005;293:3012–21.
36. Aksoy O, Sexton DJ, Wang A, Pappas PA, Kourany W, Chu V, et al. Early surgery in patients with infective endocarditis: a propensity score analysis. Clin Infect Dis. 2007;44:364–72.
37. Vikram HR, Buenconsejo J, Hasbun R, Quagliarello VJ. Impact of valve surgery on 6-month mortality in adults with complicated, left-sided native valve endocarditis: a propensity analysis. JAMA. 2003;290:3207–14.
38. Delahaye F, Celard M, Roth O, de Gevigney G. Indications and optimal timing for surgery in infective endocarditis. Heart. 2004;90:618–20.
39. Tleyjeh IM, Steckelberg JM, Georgescu G, Ghomrawi HM, Hoskin TL, Enders FB, et al. The association between the timing of valve surgery and six-month mortality in left-sided infective endocarditis. Heart. 2008;94:892–6.
40. Thuny F, Beurtheret S, Mancini J, Gariboldi V, Casalta JP, Riberi A, et al. The timing of surgery influences mortality and morbidity in adults with severe complicated infective endocarditis: a propensity analysis. Eur Heart J. 2011;32(16):2027–33.
41. Di Salvo G, Habib G, Pergola V, et al. Echocardiography predicts embolic events in infective endocarditis. J Am Coll Cardiol. 2001;37:1067–76.
42. Thuny F, Di Salvo G, Belliard O, Avierinos JF, Pergola V, Rosenberg V, et al. Risk of embolism and death in infective endocarditis: prognostic value of echocardiography: a prospective multicenter study. Circulation. 2005;112:69–75.
43. Heiro M, Nikoskelainen J, Engblom E, et al. Neurologic manifestations of infective endocarditis: a 17-year experience in a teaching hospital in Finland. Arch Intern Med. 2000;160:2781–7.
44. Dickerman SA, Abrutyn E, Barsic B, Bouza E, Cecchi E, Moreno A, et al. The relationship between the initiation of antimicrobial therapy and the incidence of stroke in infective endocarditis: an analysis from the ICE Prospective Cohort Study (ICE-PCS). Am Heart J. 2007;154:1086–94.
45. Sanfilippo AJ, Picard MH, Newell JB, Rosas E, Davidoff R, Thomas JD, et al. Echocardiographic assessment of patients with infectious endocarditis: prediction of risk for complications. J Am Coll Cardiol. 1991;18:1191–9.
46. Cabell CH, Pond KK, Peterson GE, Durack DT, Corey GR, Anderson DJ, et al. The risk of stroke and death in patients with aortic and mitral valve endocarditis. Am Heart J. 2001;142:75–80.
47. Steckelberg JM, Murphy JG, Ballard D, Bailey K, Tajik AJ, Taliercio CP, et al. Emboli in infective endocarditis: the prognostic value of echocardiography. Ann Intern Med. 1991;114:635–40.
48. Mugge A, Daniel WG, Frank G, Lichtlen PR. Echocardiography in infective endocarditis: reassessment of prognostic implications of vegetation size determined by the transthoracic and the transesophageal approach. J Am Coll Cardiol. 1989;14:631–8.
49. Vilacosta I, Graupner C, San Roman JA, Sarria C, Ronderos R, Fernandez C, et al. Risk of embolization after institution of antibiotic therapy for infective endocarditis. J Am Coll Cardiol. 2002;39:1489–95.

Coronary Artery Disease

7

Michael Y. Henein, Ibadete Bytyçi, and Michael Rigby

Coronary Artery Anomalies

Coronary artery anomalies (CAAs) are rare, occurring in less than 1% of the global population. While they are often discovered incidentally, they can also be a cause of sudden death. Coronary anomalies are a leading cause of cardiac death in young athletes, thus necessitating careful monitoring. Over the last decade, advances in diagnostic technology, including transthoracic and transesophageal echocardiography, as well as other cardiac imaging modalities have been shown to accurately identify patients with anomalous coronary artery disease [1]. CAAs encompass various congenital conditions where one or more of the three main epicardial coronary arteries have an abnormal origin or pathway [2]. Three main types of CAAs are summirezed on Table 7.1 [3–6].

Anomalous origin of the left coronary artery from the pulmonary trunk (ALCAPA) usually presents in early infancy with congestive cardiac failure due to ischemic myocardial dysfunction [2, 3]. The diagnosis can usually be made from the parasternal short axis sections of the great arteries. The most characteristic finding is reversed flow in the left coronary artery demonstrated by color flow Doppler (Fig. 7.1) [6]. Usually the anomalous coronary artery connects to the pulmonary trunk at one of the sinuses, but in some cases the connection may be to the more distal pulmonary arteries. A less common presentation of this condition is in late childhood or early adult life, usually associated with left ventricular dysfunction and mitral regurgitation [1, 3]. In these patients, there is almost always reversed blood flow in the left coronary artery representing a left to right shunt from the right coronary artery into the pulmonary trunk.

Table 7.1 Classification of coronary anomalies

Type of anomaly	Prognosis
Anomalies of origin	
Anomalous pulmonary origin of the coronaries	Generally malignant and needs surgical intervention
ALCAPA	
ARCAPA	
ACCAPA	
Anomalous aortic origin of the coronary arteries	Prognosis varies thus, treatment is individualized
LM from the right aortic sinus of Valsalva	
RCA from the left aortic sinus of Valsalva	
LAD from the right aortic sinus of Valsalva	
LCx from the RCA	
Others	
Anomalies of the course	Surgical intervention
Coronary aneurysm	
Coronary bridging	
Anomalies of termination	Follow up with serial echocardiography
Coronary arteriovenous fistula	Usually, asymptomatic. Mortality during operation till 2%
Coronary stenosis	

Abbreviation: *LM* left main, *LAD* Left anterior descending artery, *RCA* Right coronary artery, *PA* pulmonary artery, *ALCAPA* Origin of left main coronary artery from the pulmonary artery, *ARCAPA* Origin of right coronary artery from the pulmonary artery, *ACCAPA* Origin of circumflex coronary artery from the pulmonary artery

Congenital anomalies of the coronary arteries are also found associating various types of congenital heart disease. The most important of these is complete transposition of the great arteries. Abnormalities such as an intramural course, single coronary artery, or abnormal origin, each add an incremental risk factor for the arterial switch operation performed in early life.

M. Y. Henein (✉)
Imperial Collge London, London, UK

Siena University, Siena, Italy
e-mail: m.henein@imperial.ac.uk

I. Bytyçi
Medical Faculty, University of Prishtina, Prishtina, Kosovo

Clinic of Cardiology, University Clinical Centre of Kosovo, Prishtina, Kosovo

M. Rigby
Royal Brompton Hospital, London, UK

© The Author(s), under exclusive license to Springer Nature Switzerland AG 2025

M. Y. Henein (ed.), *Clinical Echocardiography*, https://doi.org/10.1007/978-3-031-95894-6_7

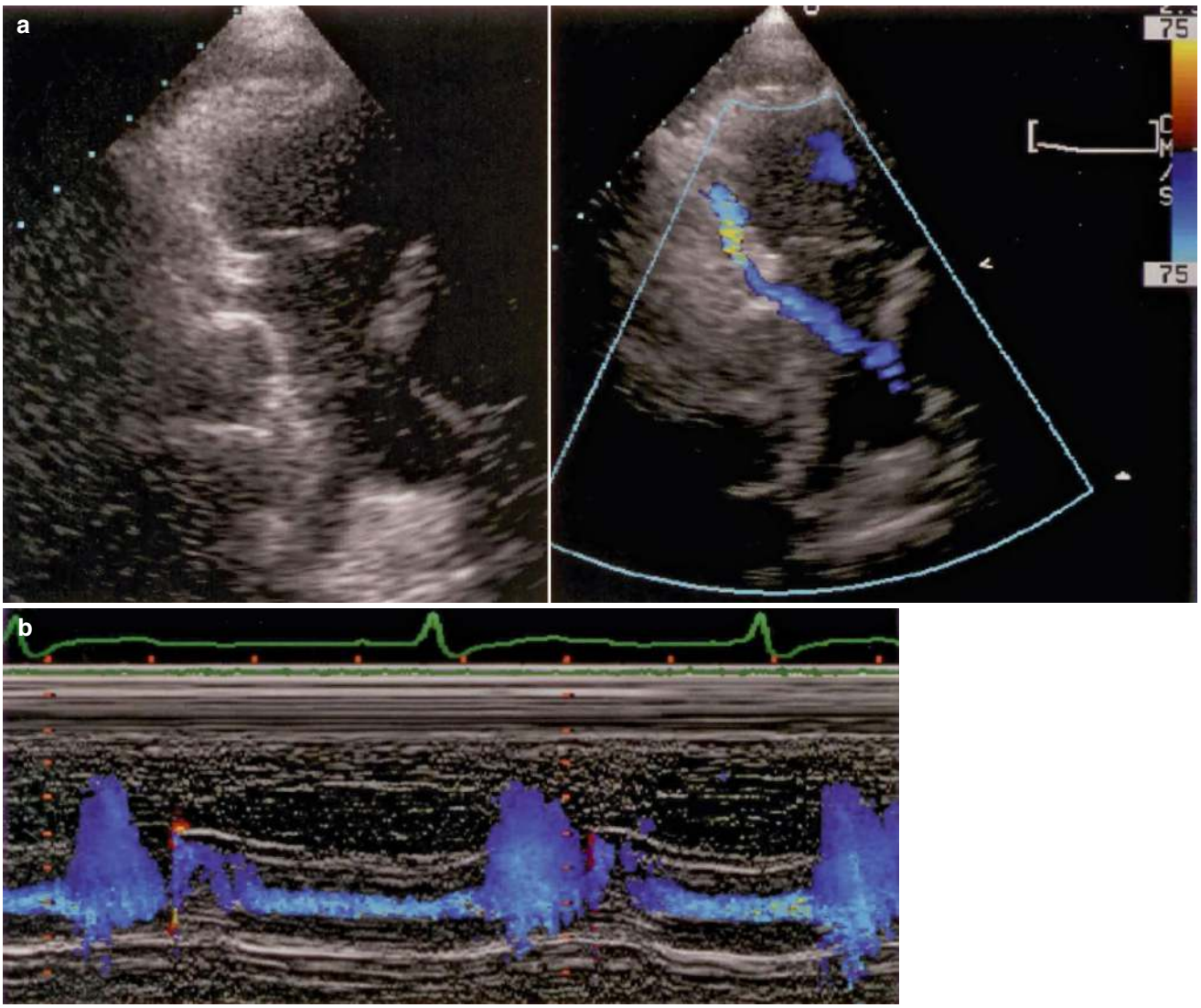


Fig. 7.1 Parasternal short axis view (**a**) from a patient with anomalous left coronary artery origin, arising from the pulmonary artery. Note the continuous retrograde flow in the coronary artery shown on the color M-mode pictures (**b**)

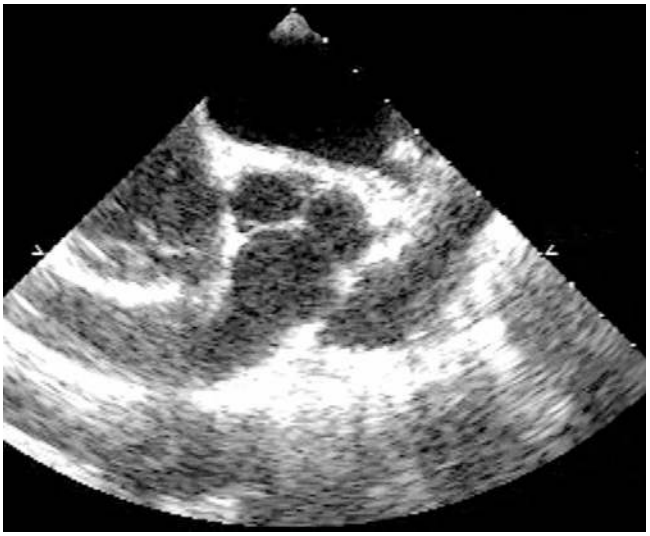


Fig. 7.2 Short axis view of the aortic valve leaflets and root demonstrating a right coronary fistula opening into the right ventricle

Fistula communications from the coronaries may connect to the left or right ventricle, the right atrium, or the pulmonary trunk (Fig. 7.2). They are commonly associated with marked dilatation of the proximal coronary arteries. Color flow Doppler is extremely helpful in the diagnosis of this condition showing at the site of the fistulous communication the characteristic continuous flow profile demonstrated with pulse or continuous wave Doppler [4].

Acquired Coronary Artery Disease

Kawasaki disease is the most common cause of acquired coronary artery anomalies in infants and children. It is characterized by coronary artery aneurysms, the disease often leads to coronary artery stenosis and ischemic heart disease. These aneurysms typically occur in the proximal left and right coronary arteries and can be easily seen from parasternal sections of the aortic valve (Fig. 7.3). However, when aneurysms persist into adulthood, they can be more challenging to define using echocardiography. It is important to recognize that Kawasaki disease in childhood can manifest as ischemic heart disease in young adults [6, 7].

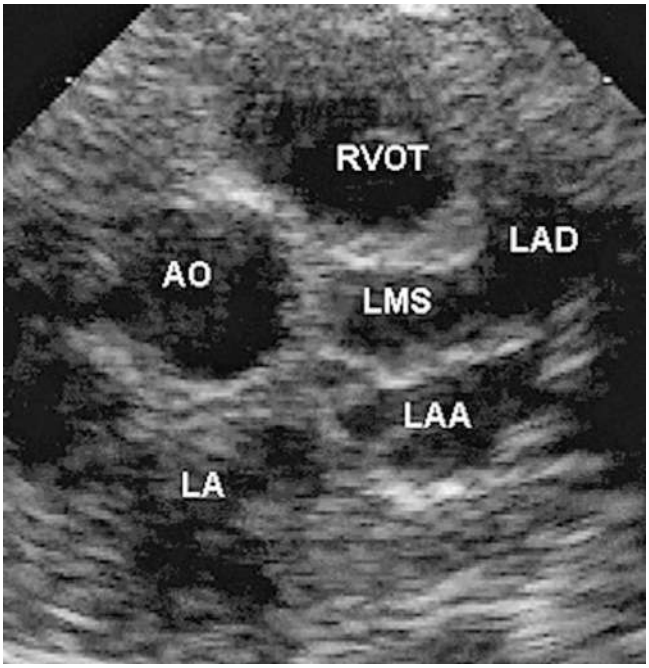


Fig. 7.3 Short axis view of the aortic root and origin of the coronary arteries from a patient with Kawasaki disease. Note the aneurysmal (beaded) appearance of the left coronary artery measured at 12 mm in diameter and its branches

Coronary Artery Anatomy

There are two main coronary arteries which arise from two of the three sinuses of Valsalva, the right coronary and left coronary sinuses respectively (Fig. 7.4). The two coronary arteries have major differences in their branching patterns once they have emerged from their sinuses. After arising from its sinus, the right coronary artery runs around the orifice of the tricuspid valve in the interventricular groove. In this initial course, it usually gives off the sinus nodal artery into the atrial musculature and the infundibular (or conal) artery into the right ventricular muscle mass. The conal/infundibular branch commonly anastomoses with a small branch of the left coronary artery to form the anastomotic ring (of Vieussens). These branches and the ring are sometimes considerably enlarged when there is distal atherosclerotic disease in the right coronary artery. The artery then runs to the acute margin of the heart where it gives rise to the acute marginal artery of the right ventricle and usually a lateral atrial artery. Continuing around the tricuspid orifice the right coronary artery gives off various smaller ventricular branches before, in the majority of hearts, it merges into the posterior interventricular artery. The area of the junction of the posterior interventricular and the atrioventricular grooves is generally called the crux of the heart. Before it forms the posterior descending branch, the right coronary artery itself makes a U-turn into the area of atrioventricular muscular septum and gives off the artery to the atrioventricular node from the apex of the U angle. The foregoing describes the anatomy of the majority of people (i.e., that the artery supplying the posterior descending branch is the right coronary artery). This anatomical arrangement is called right coronary dominance. Although the left coronary artery always supplies a greater mass of muscle than the right coronary artery, it is not usually dominant. Left dominance (posterior descending branch arising from the circumflex artery) is found in only about 15% of people [8, 9].



Fig. 7.4 TOE of the aortic root showing the proximal segments of the right and left coronary arteries

The left coronary artery originates in the left (anterolateral) aortic sinus and passes undivided for up to 2.5 cm as the left main coronary artery between the aorta and the left atrial appendage. It generally bifurcates into anterior descending and circumflex branches, but in about a third of individuals, it trifurcates. The branch between the anterior descending and circumflex branches is called the intermediate branch. The anterior descending branch passes in the anterior interventricular sulcus toward the apex. During its course, it gives a variable number of branches (diagonal branches) to the left ventricle. These, together with their parent branch, are important for arterial and vein graftings. Septal branches, known as septal perforators, arise from proximal LAD and penetrate into septal myocardium. The first perforator is usually the largest and is used in alcohol septal ablation in patients with hypertrophic cardiomyopathy. The course of the circumflex artery is more variable than the other coronary arteries. In some hearts, it terminates almost immediately and often gives off the atrial circumflex artery which runs in the atrial myocardium around the mitral orifice. More commonly, the circumflex artery continues to the obtuse margin of the left ventricle and breaks up into the obtuse marginal arteries which are often embedded within the muscle of the left ventricle. The circumflex artery runs in the left atrioventricular groove and the obtuse marginal branches are often sites for vein grafts. The circumflex artery itself may not be graftable because of its inaccessibility in the left atrioventricular groove [10].

Echocardiographic Imaging of the Coronary Arteries

Transthoracic echocardiography (TTE) allows visualization of the proximal segments of the left and right coronary artery, in particular the left main stem and the proximal left anterior descending artery. Although its sensitivity in detecting significant lesions is debatable, it can detect proximal lumen calcification [6]. Transesophageal echo (TOE) with color flow Doppler provides an ideal noninvasive tool for studying the proximal segments of the right and left coronary arteries. The addition of pulsed wave Doppler assesses coronary flow velocities and may serve as an indirect means to confirm flow-limiting narrowings particularly after coronary bypass surgery [11–13].

Intravascular ultrasound (IVUS) is the commonly used echocardiographic technique for studying coronary luminal disease. It allows direct visualization of the arterial lumen; the luminal surface of the vessel, protruding atherosclerotic plaques, intraluminal thrombi, and intimal flaps can all be assessed by the fiber-optic angioscopy (Fig. 7.5) [14]. During coronary angioplasty, IVUS has been used to guide the operator for optimal stent deployment and management of related complications, e.g., intimal dissection [15]. When combined with Doppler facilities, IVUS scanning may offer detailed assessment of the site and extent of luminal narrowing. It may also assist in optimizing stent positioning. However, IVUS imaging has well-recognized shortcomings. For clear visualization of the arterial wall, coronary flow should be interrupted and replaced with a clear and transparent fluid. Applying this technique is clearly undesirable, particularly in multi-site lesions that require lengthy study time due to unavoidable vessel movement, especially in patients with critical coronary disease. Difficulty in accurate calibration of the measurements and inability to assess arterial structures below the vessel wall add to the limitation of IVUS for routine use. Like conventional angiography, IVUS is unable to assess wall thickness, accurate plaque size, nature of its contents, or plaque stability [16]. However, recent evidence supports that IVUS can provide accurate information on plaque characterization using virtual histology technology [17]. Despite these limitations, intravascular angioscopy has greater sensitivity in identifying non-stenotic atherosclerotic coronary arterial disease compared to conventional angiography. Conceptually, this advantage can be used for the follow-up of non-stenotic coronary disease as is the case in post-transplant coronary artery disease and its response to pharmacological therapy. Finally, IVUS imaging provides a unique means for assessing arterial atherosclerotic "stiffness" as well as endothelial function and its response to different pharmacological agents, e.g., statins [18]. Ideal intravascular ultrasound scanning seems to be the three-dimensional reconstruction online imaging that determines the spatial relationship in the areas of interest. While the two-dimensional images define the circumferential extent of the plaque, the three-dimensional images define the longitudinal extent as well as providing accurate assessment prior to coronary intervention.

Furthermore, recently wall shear stress (WSS) plays a pivotal role in the regulation and maintenance of coronary artery wall function and remodeling. Accurate assessment of WSS can provide valuable insights into the early detection of pathological changes in coronary arteries, potentially pre-

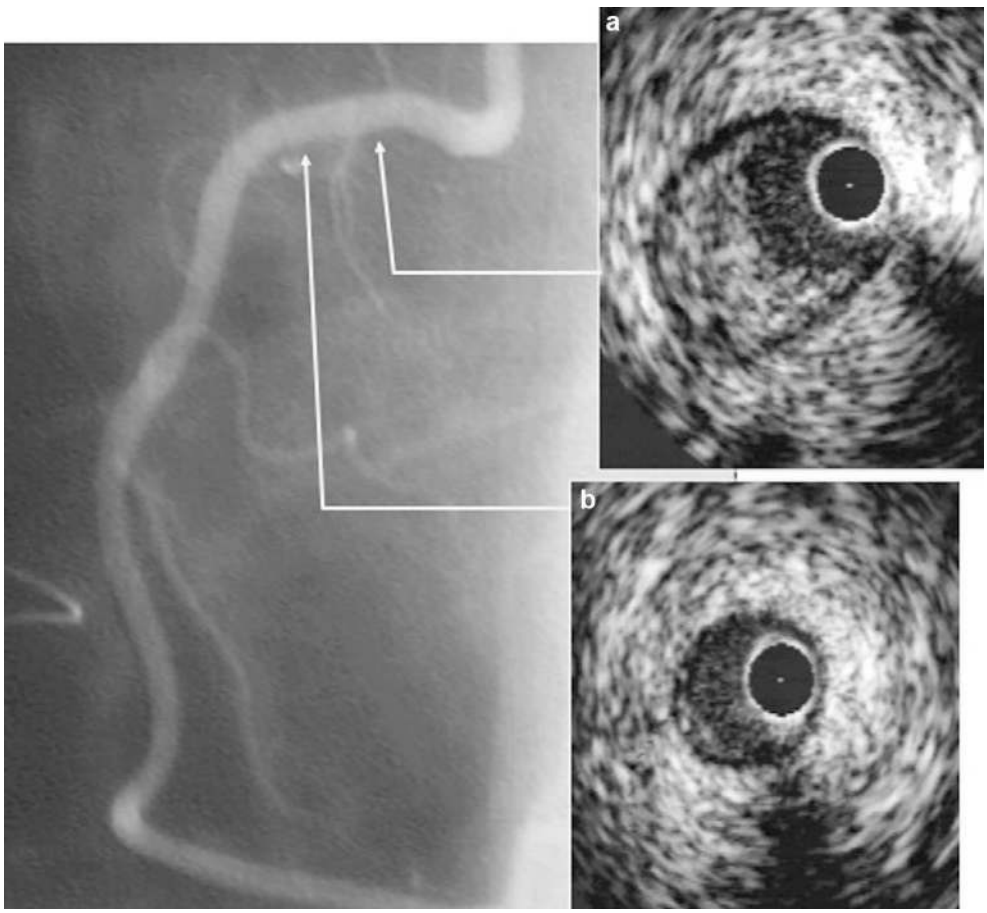


Fig. 7.5 (**a**) Intravascular ultrasound imaging of the proximal segment of the right coronary artery demonstrating plaque formation. (**b**) IVUS image showing plaque characterization using virtual histology technique

venting adverse cardiovascular events. Traditionally, intravascular ultrasound (IVUS) has been employed to measure WSS; however, it is an expensive and invasive technique. Emerging advances in computed tomography coronary angiography (CTCA) and associated software development are poised to offer non-invasive, cost-effective alternatives for routine evaluation of coronary calcification, lesion grading and WSS, thus enhancing the ability of the technique to monitor and diagnose coronary artery conditions effectively [19, 20].

Epicardial cross sectional echocardiographic coronary artery scanning with high-frequency ultrasound transducers has been used intraoperatively to assess coronary artery stenosis, and the results compared with angiography. This way of coronary scanning is able to differentiate poststenotic flow patterns in patients with varying degrees of coronary artery disease, but this technique is currently restricted to research purposes only.

Acute Coronary Syndrome

Acute coronary syndrome (ACS) has become a critical health issue, with its incidence increasing due to the aging population and advances in early disease detection and medical technology. Chest pain is the primary symptom that triggers the diagnostic and therapeutic approach in patients suspected of having ACS, even though physical examinations often show no abnormalities. The resting 12-lead electrocardiogram (ECG) is the first diagnostic tool employed for these patients but often fails to provide a definitive diagosis, so additional diagnostic methods are necessary for early and accurate management of ACS and its complications [21].

Imaging techniques are crucial for identifying ventricular wall motion abnormalities and assessing myocardial viability. TTE is particularly effective for pinpointing the location and extent of ACS and for evaluating potential complications. It plays a vital role in risk stratification by assessing left ventricular ejection fraction (LVEF), right ventricular (RV) function, and detecting any valvular disease or pericardial effusion [22].

Myocardial Infarction

Transthoracic echocardiography is a reliable and non-invasive diagnostic tool capable of detecting myocardial ischemia or scarring (Fig. 7.6). It offers detailed information on various cardiac parameters, including:

(a) Ventricular ejection fraction
(b) Ventricular wall motion abnormalities
(c) Ventricular cavity dimensions and volumes

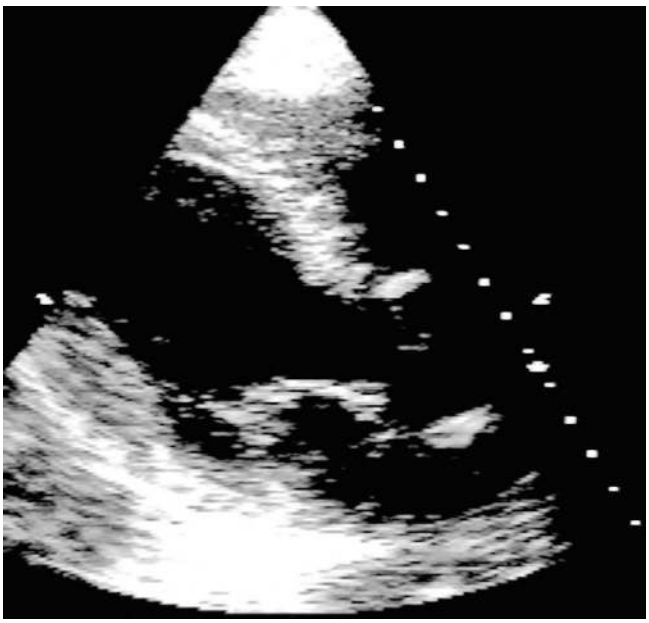


Fig. 7.6 Parasternal long axis view from a patient with anterior myocardial infarction. Note the extent of anterior wall scarring that has spared the proximal anterior segment

(d) Diastolic filling patterns and estimated pressures
(e) Potential complications

Resting 2-dimensional (2D) images combined with M-mode recordings can demonstrate signs of myocardial infarction. In acute infarction, a hypokinetic or akinetic segment in the affected territory corresponding to the electrical changes on the surface ECG supports the diagnosis (Fig. 7.7) [23, 24]. In patients with limited echocardiographic views, the use of left ventricular cavity contrast during the acute presentation has been shown to clearly delineate the endocardium of the dysfunctioning areas [25]. Echocardiography can also be used in the follow-up of these patients, providing important information on the segmental response to thrombolytic therapy, and thereby identifying patients who may need or angioplasty further intervention. In addition, Doppler velocities provide evidence for physiological disturbances which may contribute to delayed recovery, e.g., raised left atrial pressure or significant mitral regurgitation. Scarred segments are the commonest presentation of old myocardial infarction, particularly with Q wave infarction irrespective of its location. The extent of segmental involvement can also predict the site of coronary artery blockage, to some degree, particularly left anterior descending artery disease in anterior infarction. The combination of mid and apical anteroseptal wall infarct and absence of bundle branch block suggests spared proximal left anterior descending artery, with the site of the lesion distal to the first septal branch [26]. The same applies to the posterior wall (Fig. 7.8). Conversely, the extent of fibrosis and scaring is minimal with non-Q wave infarc-

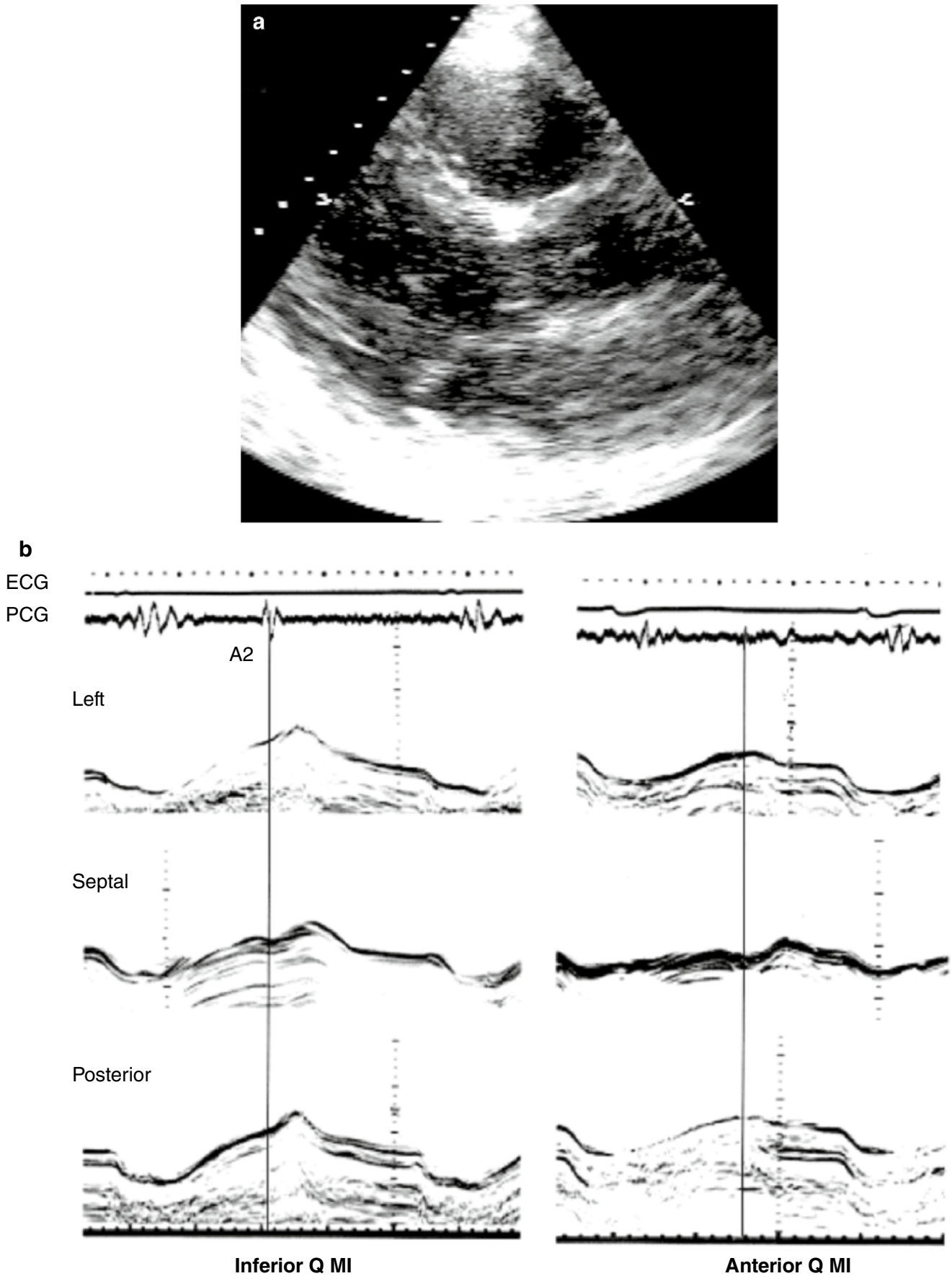


Fig. 7.7 (**a**) Parasternal long axis view from a patient with posterior wall infarction showing scarred and akinetic segment. (**b**) LV long axis recordings from the three segments—left, septal, and posterior demonstrating global incoordination (post-ejection shortening)

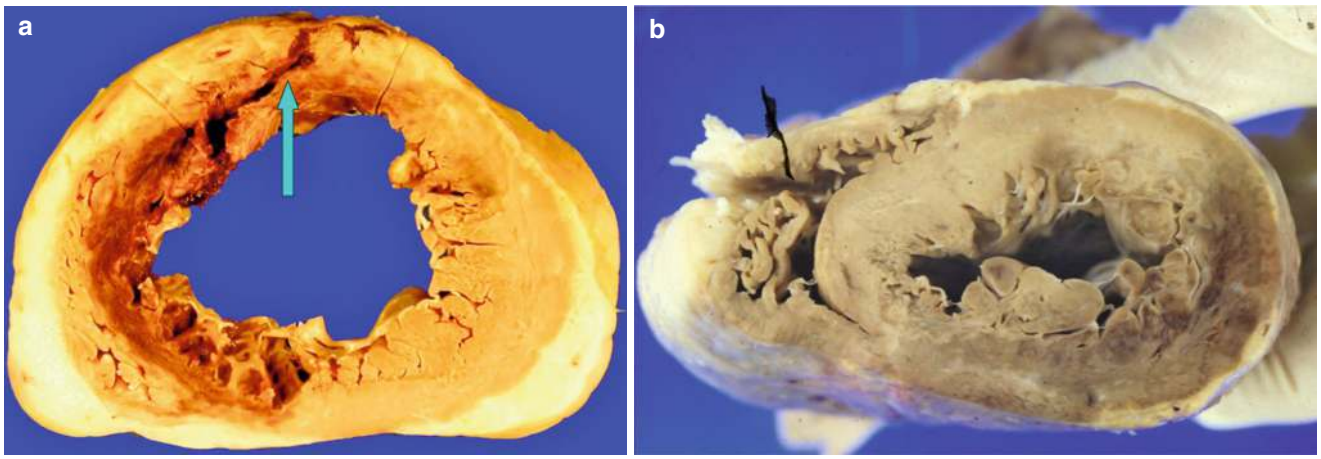


Fig. 7.8 Pathological specimen from two patients (**a**) with anteroseptal infarct with myocardial rupture (arrow) and (**b**) posterolateral infarct extending into posterior aspect of the right ventricle

tion, and the most common presentation is hypokinesia combined with ventricular long axis dysfunction [27], demonstrating frequent incoordination that suggests papillary muscle involvement. With an old infarction, the affected segment appears akinetic with poor thickening fraction.

Right Ventricular Infarction

Right ventricular (RV) infarction should be excluded in patients presenting with low cardiac output and maintained left ventricular systolic function. It occurs in 30% of patients with inferior myocardial infarction who present with hypotension but also may occur in isolation [28]. Numerous echocardiographic markers are available to identify RV myocardial infarction (RV MI), such as TAPSE <10 mm, S′ < 12 cm/s, myocardial performance index (MPI) > 0.7, S′/MPI < 17, or a RV ejection fraction <50%. When present, depressed right ventricular free wall long axis amplitude and the presence of significant incoordination represent sensitive diagnostic criteria for right ventricular infarction, particularly in patients who have not previously undergone cardiac surgery. Assessment of RV free wall amplitude of motion and incoordination with M-mode and tissue Doppler imaging as well as ventricular filling pattern is crucial for confirming the diagnosis (Fig. 7.9). A short early diastolic deceleration time in such cases, particularly in the presence of raised systemic venous pressure that also demonstrates early steep diastolic descent, suggests restrictive right ventricular physiology and associated raised right atrial pressure (Fig. 7.10). A degree of tricuspid regurgitation is usually present in these patients which may vary in severity according to the extent of tricuspid ring dilatation. Management of such patients is critical, since a considerable degree of raised right atrial pressure is required to secure left ventricular filling and hence cardiac output. Recent evidence suggests full recovery of almost 50% of patients presenting with compromised right ventricular function in the setting of inferior myocardial infarction, again limiting the number of patients remaining with stunned or irreversible myocardial damage [29].

Complication of Myocardial Infarction

Following an acute myocardial infarction (MI), several critical mechanical complications may develop, posing immediate life-threatening risks that demand swift diagnosis. TEE becomes indispensable at this stage, providing essential confirmation or exclusion of these complications without delay.

(a) *Ventricular Aneurysms/Pseudoaneurysm:* Both LV aneurysms and pseudoaneurysms are critical mechanical complications that can develop after an acute myocardial infarction. An aneurysm represents segmental full thickness fibrosis of ventricular wall with loss of function. Aneurysmal formation occurs in 10–22% of patients within 3 months of acute infarction [30]. The common site for aneurysm formation is at the apical and antero-apical segments and rarely at the basal posterior wall (Fig. 7.11) [31]. The hinge point or the apical end of the healthy proximal segment determines the edge and the size of the aneurysm [32]. The outward movement of the aneurysm commonly described as "dyskinesia" represents passive movement of the dysfunctioning segment in response to the increased ventricular pressure generated by the rest of the myocardium during systole. The size of the aneurysm depends on the extent of the area affected by the blocked artery. A subjective assessment of relative aneurysm size with respect to that of the ven-

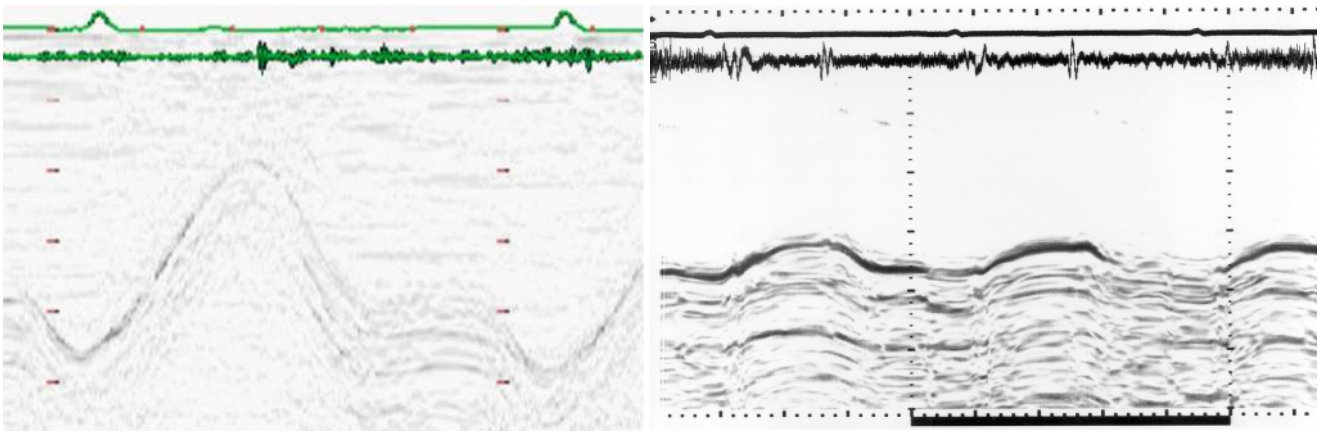


Fig. 7.9 Right ventricular free wall longitudinal motion from a normal subject (*left*) and a patient with right ventricular infarction (*right*). Note the marked reduction in the free wall amplitude of motion in the patient as well as the incoordinate lengthening pattern

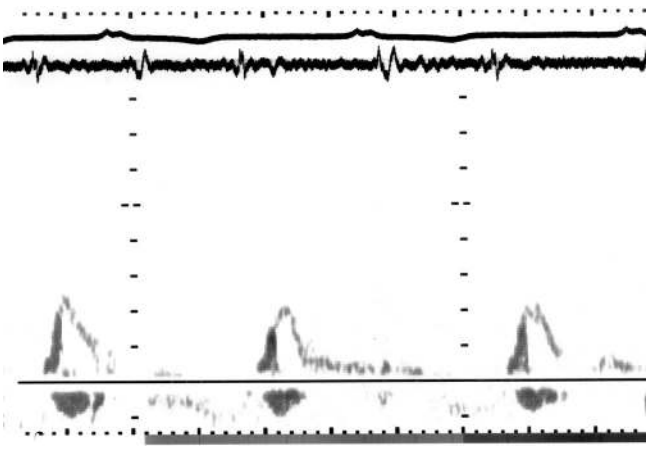


Fig. 7.10 Right ventricular filling velocities from a patient with prior infarction. Note the dominant early diastolic component of filling with short deceleration time consistent with raised RA pressure

tricle has been shown to determine mortality and surgical recovery after aneurysmectomy [33]. In general, the more basal ventricular function that is maintained the better the prognosis. The same applies to the number of coronary arteries involved in the ischemic ventricular process. From a prognostic point of view, a massive anterior infarct with antero-apical aneurysm formation carries a worse prognosis than a localized akinetic segment [34]. Aneurysms also represent a substrate for thrombus formation and hence thromboembolic complications (Fig. 7.12) [35]. The more rapid the development of a ventricular aneurysm after acute infarction, the worse the prognosis [36]. An aneurysm that is noted after 5 days of infarction carries an 80% 1-year mortality. Finally, a true ventricular aneurysm should be differentiated from a false aneurysm that represents a localized myocardial rupture which is sealed by the surrounding parietal pericardium. False aneurysms are usually small in size and carry a better prognosis than a true aneurysm [36]. Two-dimensional echo images are ideal for differentiation between true and false aneurysms.

(b) *Ventricular Septal Rupture:* This is a rare mechanical complication of acute myocardial infarction. When it occurs, it tends to affect the apical third of the anteroseptal segment in anterior myocardial infarction and the proximal part of the posterior septum in inferior infarction. Color flow Doppler is ideal for demonstrating the presence of any left to right shunt, and transvenous echo contrast usually confirms the site of the septal defect and the exact direction of the shunt (Fig. 7.13) [37, 38]. A small apical septal defect is usually protected by the muscle bulk surrounding it. A septal defect associated with hemodynamic disturbances may require either device or surgical closure at the time of revascularization. A sizeable mid-septal defect is usually associated with clinical and hemodynamic instability, and surgical closure is mandatory. Associated left ventricular disease and mitral regurgitation should also be assessed and considered in the management plan.

(c) *Papillary Muscle Rupture:* This is a rare complication of myocardial infarction. Patients present with acute severe mitral regurgitation (MR) and pulmonary edema. A mitral regurgitation murmur may not be heard and if present, may be even difficult to differentiate from that caused by a ventricular septal defect. Echocardiography, particularly TOE, is the initial investigation to determine the exact cause of the valve regurgitation (Fig. 7.14). Urgent surgical repair of papillary muscle rupture is lifesaving procedure [39, 40].

(d) *Mitral Regurgitation:* In patients post-myocardial infarction, echocardiography should routinely include assessment for MR. If detected, the mechanism and severity of MR should be critically determined using either TTE or TOE. Mild mitral regurgitation is a com-

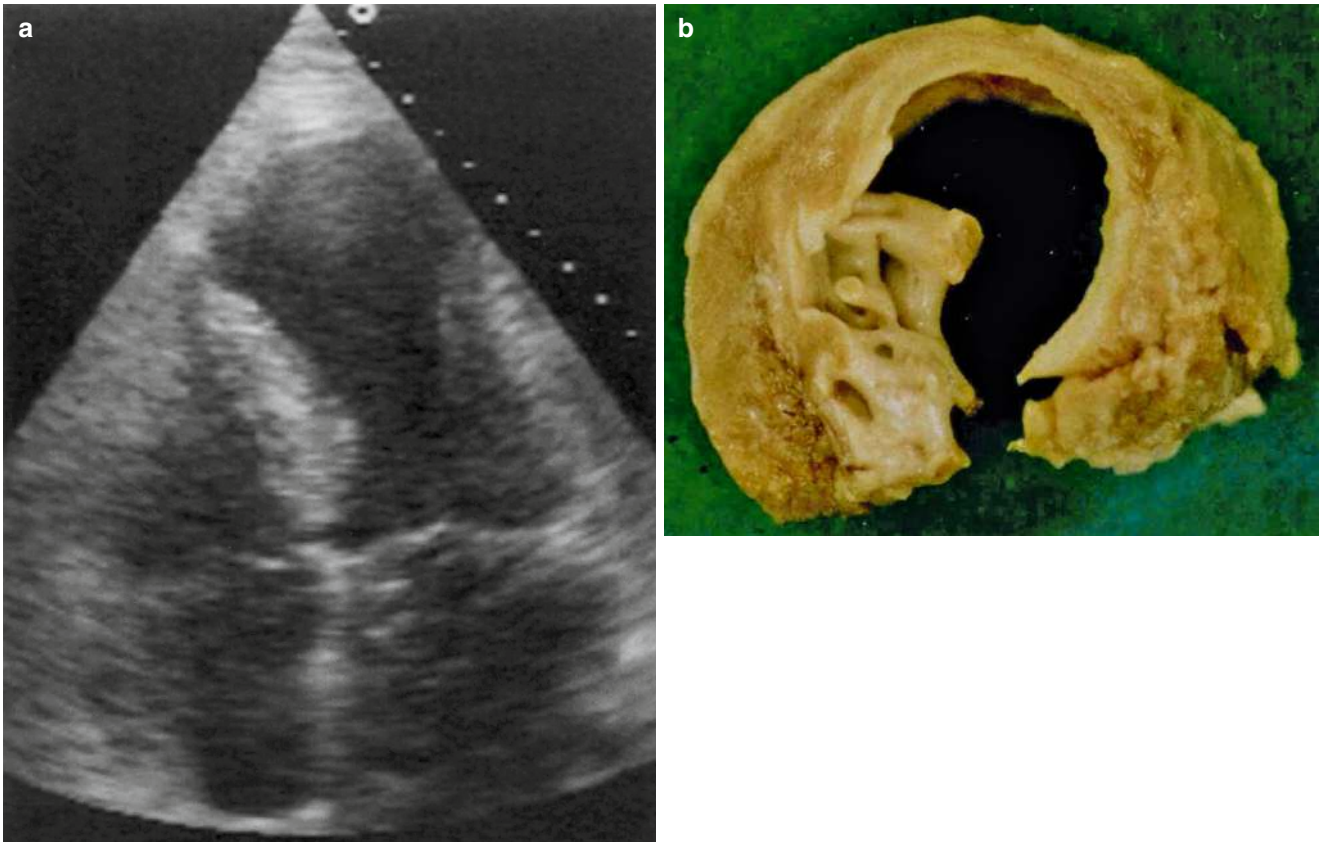


Fig. 7.11 (**a**) Apical 4-chamber view from a patient with anterior infarction complicated by apical aneurysm. Note the site of the aneurysm and the hinge point that marks the edge of the aneurysm. (**b**) Pathological section from a patient with apical aneurysm

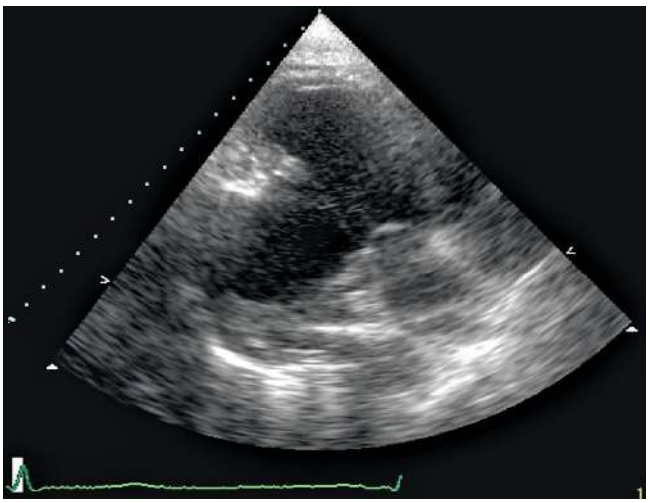


Fig. 7.12 Parasternal long axis view of the left ventricle from a patient with posterior wall aneurysm and clot

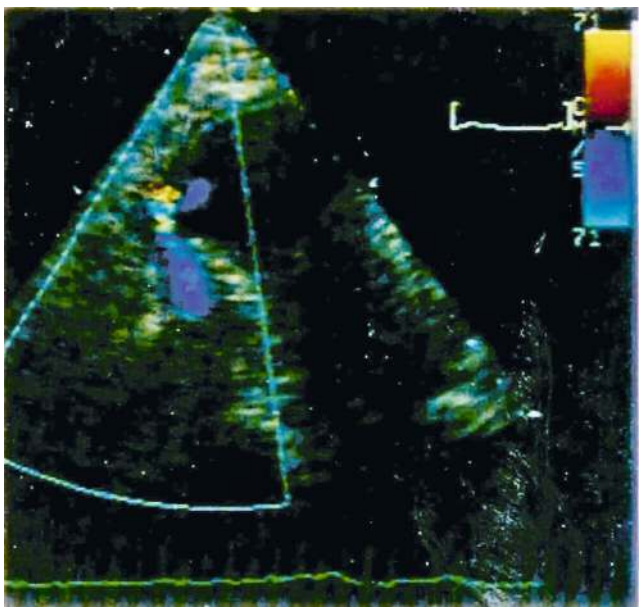


Fig. 7.13 Apical 4-chamber view from a patient with apical ventricular septal defect complicating anterior infarction. Note the left to right shunt on color flow Doppler at the apical level

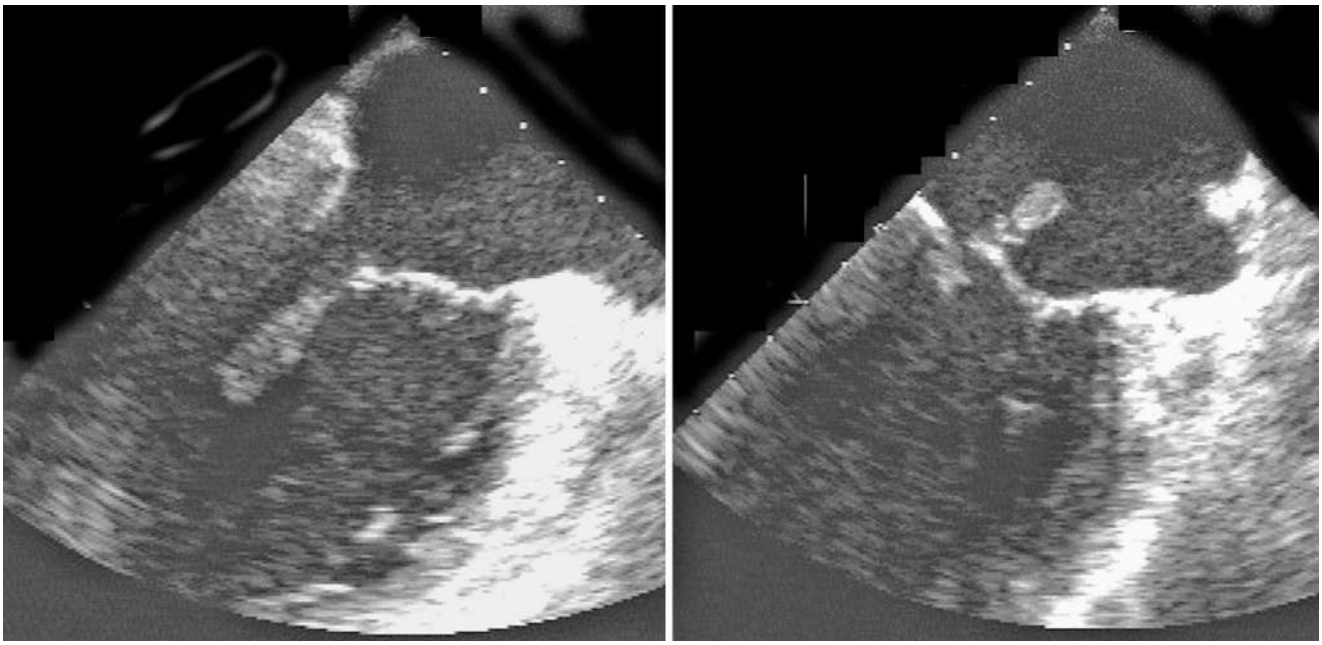


Fig. 7.14 TOE from a patient with posterolateral ruptured papillary muscle. Note the free movement of the detached segment with the mural mitral valve leaflet

mon finding in patients with ventricular disease particularly secondary to coronary artery disease [41]. Functional (secondary) MR may be caused by papillary muscle dysfunction or dyssynchrony of the free wall supporting the papillary muscle [42]. Significant mitral regurgitation may develop either in association with free wall infarction and posterior mitral valve leaflet prolapse caused by papillary muscle dysfunction or as a consequence of progressive deterioration of ventricular function and mitral annular dilatation (Figs. 7.15 and 7.16). While the management of the papillary muscle dysfunction is surgical repair, the appropriate management of ventricular ischemic dysfunction is revascularization and mitral valve repair (annular insertion) in selected cases [43]. Patients with significant left ventricular dyssynchrony who fulfill the criteria for cardiac resynchronization therapy (CRT) may benefit from pacemaker insertion and optimization of A-V delay as means of improving their symptoms as well as survival. Those with intractable mitral regurgitation which is believed to be the direct cause of symptoms and who stand high surgical risk may benefit from mitral valve clip procedure. This recently developed method aims at inserting, transfemorally, a clip device which holds the tips of the middle part of the anterior and posterior mitral valve leaflets, hence creating a biorifice valve. This procedure has become popular in well-selected cases and results in significant reduction of mitral regurgitation and improvement of symptoms. Transesophageal 2D and 3D echocardiography have

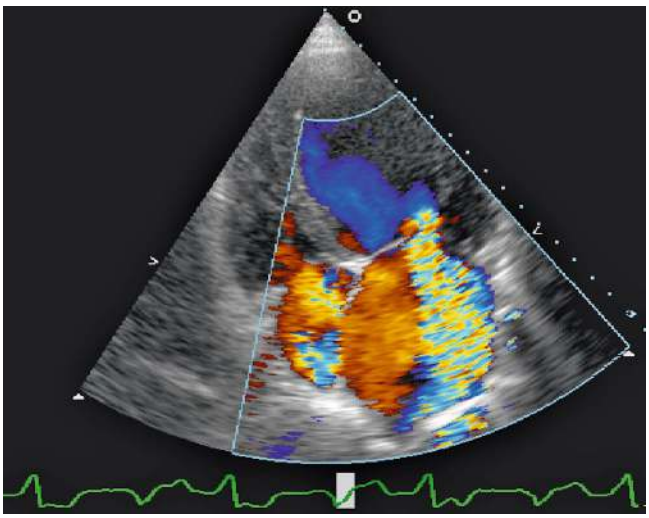


Fig. 7.15 Apical 4-chamber view from a patient with free wall infarction and posterior mitral valve leaflet prolapse. Note the resulting severe regurgitation on the color flow Doppler

proved valuable in guiding toward best device placement and checking any residual mitral regurgitation [44–46].

Stress echocardiography may be needed not only to assess myocardial viability, but also to provide information on severity of the MR, particularly in patients with moderate regurgitation (Fig. 7.17). Patients in whom mitral regurgitation volume drops at peak stress suggest myocardial dysfunction that may respond to revascularization. Those in whom mitral

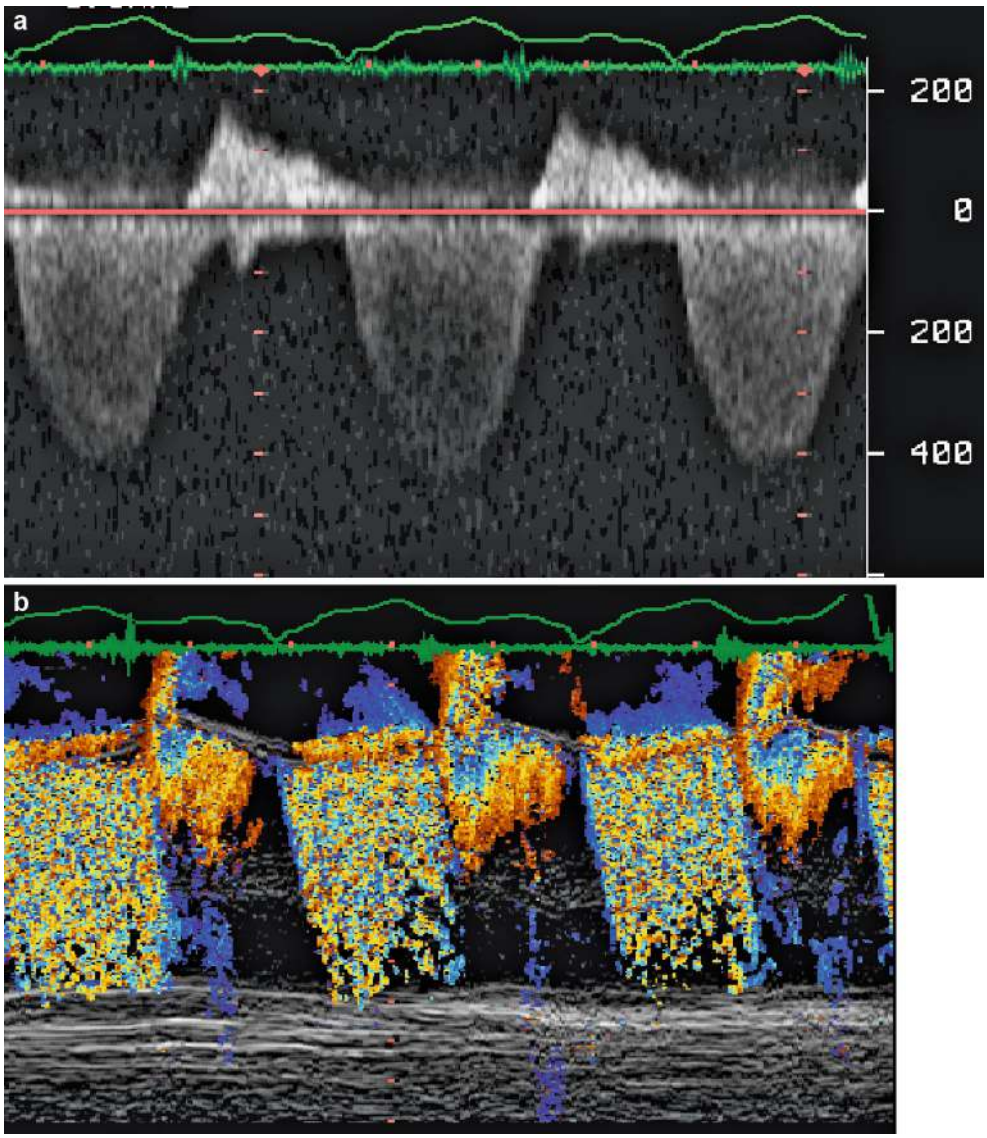


Fig. 7.16 Continuous wave Doppler (**a**) and color Doppler M-mode (**b**) recordings from a patient with ischemic cardiomyopathy and dilated mitral ring showing severe MR

regurgitation worsens at peak stress, usually rare, suggest ischemic left ventricular basal segment which results in annular dilatation. Such patients benefit from additional mitral ring insertion to the CABG procedure. Although current evidence has not shown any additional survival benefit from the combined procedure compared to CABG only, most patients report improved symptoms [47].

(e) *Left Ventricular Thrombus:* LV thrombi are frequently found in extensive anterior infarcts involving the apex. Diagnosis is typically made using echocardiography. While 2D TTE can often detect LV thrombi, it may be challenging when acoustic windows are suboptimal. Somtimes, contrast agents provide a method to distinguish thrombi from trabeculations and strings; however, routine use of contrast after an anterior MI is generally not recommended except for specific cases (e.g., anterior MI with poor acoustic windows) [48].

(f) *Pericardial Effusion:* Pericardial effusion is a common complication after ST elevation myocardial infarction (STEMI), occurring in 4–43% of acute MI cases. It typically appears within the first week and is associated with poor prognosis. Diagnosis is made by echocardiography, which can detect and quantify the effusion and rule out hemorrhagic effusion with tamponade. Causes include pericarditis and hemorrhage from infarcted myocardium, coronary perforation, and myocardial rupture. In pericarditis, effusion is detectable in 60% of cases. Cardiac tamponade results from rapid fluid accumulation in the pericardial space, increasing intrapericardial pressure and reducing cardiac output. Echocardiographic signs of tamponade include right atrial collapse, diastolic RV collapse, and inferior vena cava dilation without inspiratory change. Pulsed wave Doppler can show significant changes in transvalvular velocities during respiration, with compromised left

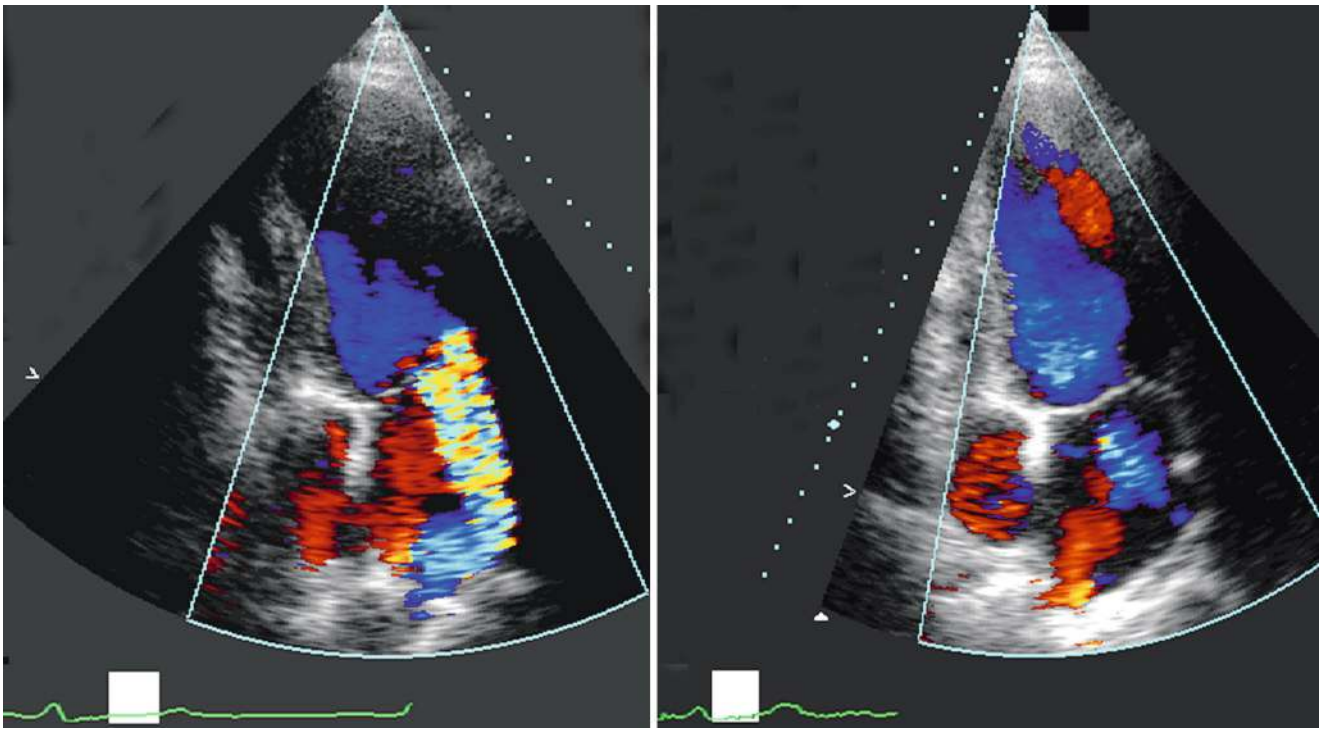


Fig. 7.17 Stress echo images of the apical 4-chamber view from a patient after large anterior infarction showing moderate mitral regurgitation at rest that becomes mild at peak stress

ventricular filling and outflow tract velocities during inspiration. If pericardiocentesis is necessary, echocardiography helps locating the effusion and guiding the needle, with agitated saline contrast confirming the intrapericardial position [49].

(g) *Ischemic Left Ventricular Disease:* Long-standing coronary artery disease, with or without infarction, may result in progressive deterioration of left ventricular function and an increase in left atrial pressure. This is one of the most common causes of breathlessness in these patients (Fig. 7.18). A restrictive ventricular filling pattern is diagnostic of raised left atrial pressure [50]. It is characterized by a short isovolumic relaxation time (<40 ms), dominant early diastolic ventricular filling with short deceleration time (<140 ms). Atrial contraction in late diastole results in retrograde blood flow into the pulmonary veins, thereby exaggerating pulmonary congestion (Fig. 7.19). A longer retrograde "a" wave in the pulmonary veins with respect to the forward transmitral "A" by 30 ms is consistent with raised LV end-diastolic pressure [51]. Furthermore, patients with this degree of ischemic LV disease almost always have some degree of functional mitral regurgitation that adds to the increase in left atrial pressure. A consequence of raised left atrial pressure is the development of secondary pulmonary hypertension. Also, raised left atrial pressure if not treated results in unstable mechanical function and atrial arrhythmia. In addition, raised left atrial pressure is associated with ischemic subendocardium which becomes a substrate for ventricular arrhythmia.

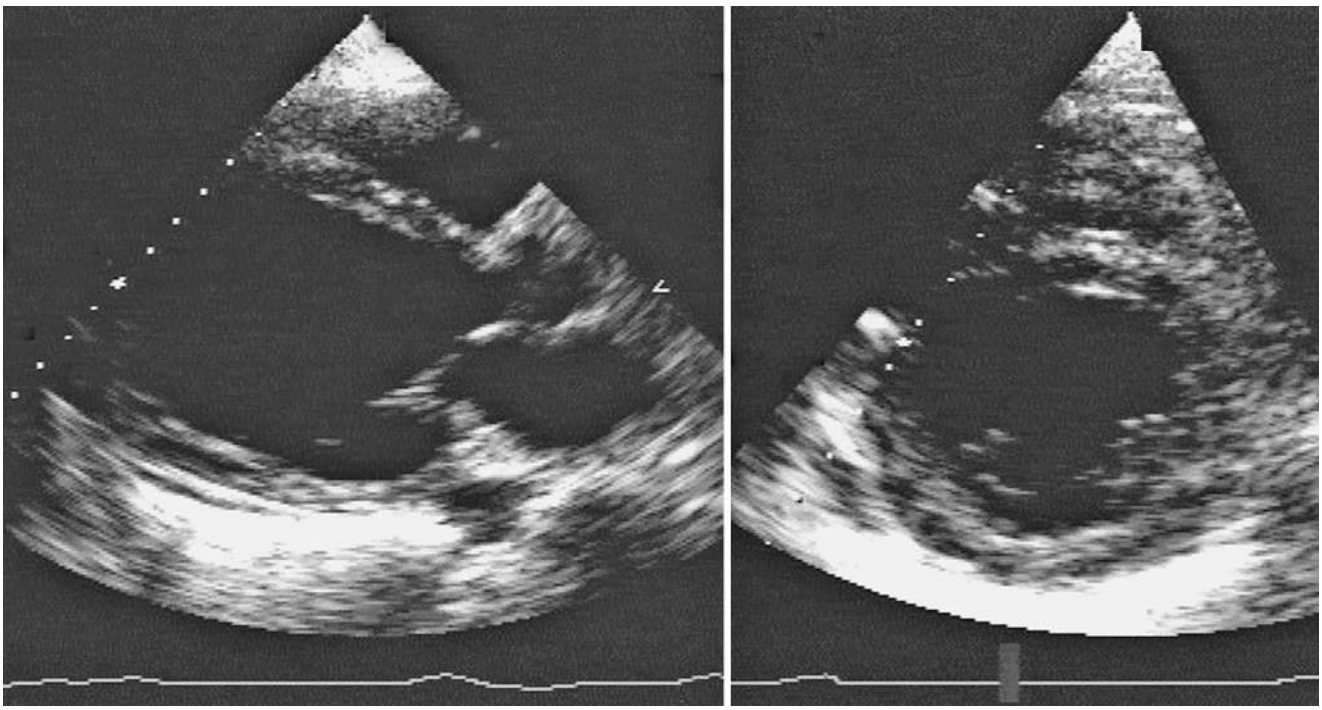


Fig. 7.18 Left ventricular 2D recording from a patient with posterior wall infarction and hypokinetic anterior wall presenting with breathlessness. Note the cavity dilatation and poor overall systolic function (fractional shortening 10%)

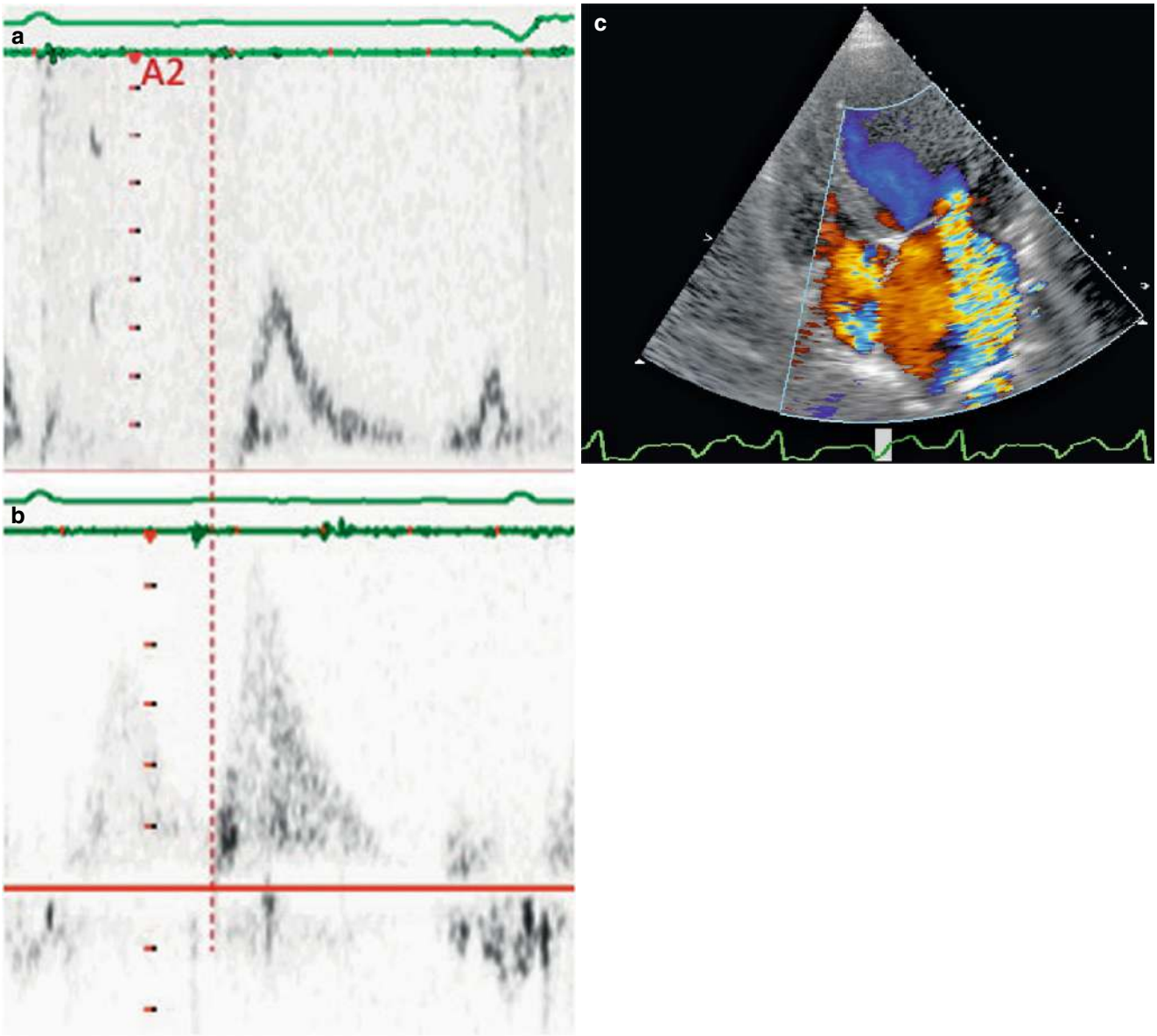


Fig. 7.19 (**a**) Transmitral Doppler flow velocities from the same patient demonstrating typical restrictive LV filling pattern with short IVRT and E wave deceleration time. (**b**) Pulmonary venous Doppler flow velocities showing retrograde flow in late diastole of a significantly longer period compared to that of transmitral Doppler. (**c**) Apical 4-chamber view from the same patient showing enlarged left atrium and severe mitral regurgitation

Myocardial Infarction with Non-obstructive Coronary Arteries

Myocardial infarction with non-obstructive coronary arteries (MINOCA) occurs in 3–15% of all acute MI. Even though these patients are typically younger, more often females, and have fewer cardiovascular risk factors, their prognosis is worse than that of individuals without cardiovascular disease and is comparable to those with myocardial infarction and obstructive CAD [52]. Transthoracic echocardiography is a valuable tool for evaluating cardiac function following a MINOCA event. It helps in diagnosing various conditions such as takotsubo cardiomyopathy and non-ischemic cardiomyopathy and is particularly useful for monitoring the recovery of left ventricular function during follow-up. Additionally, echocardiography can quickly visualize ventricular dysfunction, which is indicative of takotsubo cardiomyopathy, and speckle tracking is used to assess the recovery of myocardial contraction after such events [53, 54].

TEE may be considered if coronary embolism is suspected, offering a more detailed view when necessary. Transthoracic Doppler echocardiography can also assess coronary flow and coronary flow reserve (CFR) at the bedside. CFR is calculated as the ratio of hyperemic diastolic mean (or peak) flow velocity to baseline flow velocity. A CFR cut-off value of 2 is used to detect significant epicardial coronary stenosis and to predict ischemia in the affected myocardial territory. Significant coronary stenosis leads to high proximal resistance to blood flow, whereas in the absence of epicardial stenosis, this resistance is mainly determined by the coronary microcirculation [55].

An algorithm endorsed by ESC and AHA position statements for evaluating myocardial and intracoronary conditions includes cardiac magnetic resonance (CMR) imaging to assess the myocardium, intravascular ultrasound (IVUS), and optical coherence tomography (OCT) to examine intracoronary structures. Additionally, provocative testing for coronary spasm and vasomotor integrity is recommended as part of this comprehensive evaluation [56].

Angina Pectoris

Stable Angina: This is an exertional symptom due to the mismatch of supply and demand of oxygen to the myocardium. The most common cause is coronary artery disease. Resting echocardiography is frequently normal in patients with uncomplicated coronary artery disease. Therefore, stress echo is recommended to demonstrate possible wall motion disturbances during symptom provocation. Exercise or pharmacological stress using adenosine, dipyridamole, or dobutamine are the most common stressors for echocardiographic studies [57]. To accurately localize segmental wall motion abnormalities, echocardiographic societies recommend dividing the ventricle into 17 segments. Each segment should be individually analyzed, incorporating information from different views. A wall motion score index (WMSI) can then be calculated by scoring each segment based on its motion and thickening: 1 = normal or hyperkinetic motion, 2 = hypokinesis, 3 = akinesis (no thickening), 4 = dyskinesis (paradoxical motion), and 5 = aneurysmal (systolic and diastolic deformation). The WMSI is calculated by dividing the sum of these scores by the number of segments visualized (Fig. 7.20) [58].

A normal response to stress is demonstrated by increased segmental thickness and amplitude of endocardial inward movement. Segments are analyzed from the parasternal long axis, short axis, apical 4-chamber, and apical 2-chamber views. The currently available digital storage system in most echocardiographs has made multiple image acquisition easy, and hence, deduction of segmental response at different

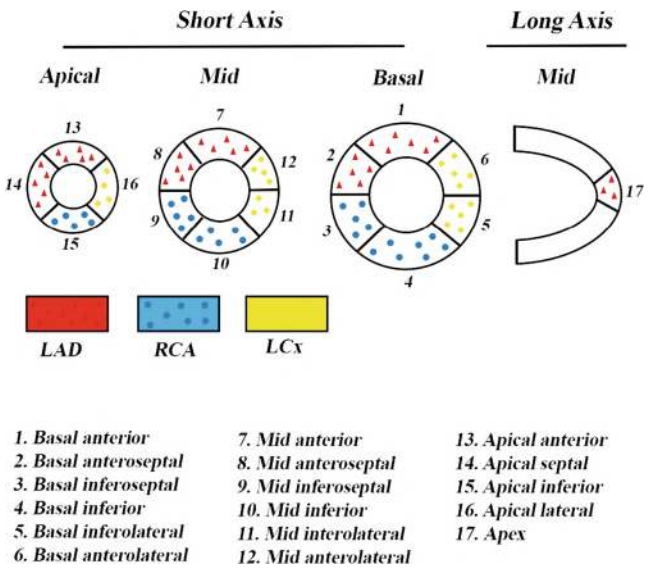


Fig. 7.20 Wall motion score index

stages of stress can be critically assessed. A subjective assessment of the diseased coronary artery can be made according to the distribution of the developed segmental abnormalities [59]. A technical limitation in demonstrating a complete endocardial display at rest and peak stress may limit the use of this test in certain patients but can be overcome by adjusting the harmonic settings. Also, echo contrast agents (e.g., sulfur hexafluoride, or perfluoropropane) have proved to have a significant impact in increasing the definition of the endocardial border throughout the ventricular cavity, by opacifying the whole cavity (Fig. 7.21) [60]. Recently, intravenous myocardial echo contrast has also added to the importance of assessing coronary flow reserve as well as segmental reversible opacification with stress (Fig. 7.22) [61].

To determine the overall ischemic burden, a global score index is obtained from the relative sum of the segmental scores with respect to the number of the segments visualized. This has been shown to be 80% sensitive and 90% specific for diagnosing coronary artery disease [62]. The accuracy of this technique in diagnosing multi-vessel coronary disease is significantly higher than for single vessel disease [63]. The sensitivity of wall motion scoring has proved comparable to that of thallium scanning while specificity is significantly higher [64]. Stress echo has also been shown to predict outcome in patients with ischemic ventricular disease [65]. This subject is dealt with in great detail in Chap. 8.

Although this method of analyzing wall motion behavior with stress is widely used, inherent limitations are present:

1. Analysis of wall motion is subjective in nature, and depends on technical experience; thus lack of objective

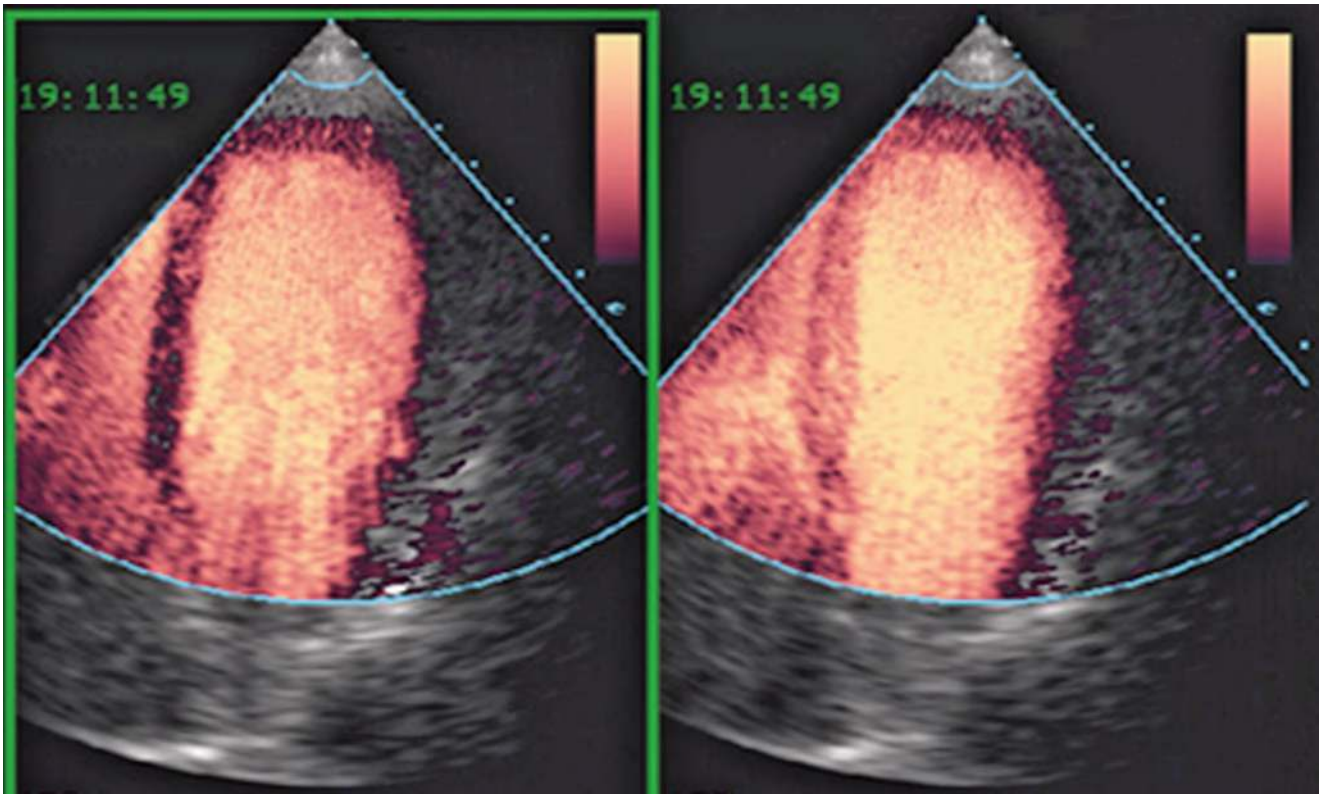


Fig. 7.21 Apical 4-chamber view from a patient with coronary artery disease after injecting echo contrast agent. Note the full opacification of the cavity and the abnormal myocardial perfusion

quantitation makes its reproducibility vary between observers and centers.

2. Wall motion scores are based on the inward movement of the segments in systole that determine the function of the circumferential muscle layer. This method ignores the subendocardial component of the myocardium which is longitudinally orientated. Assessment of longitudinal ventricular function has become now an integral part of resting and stress echo assessment.
3. The technique is unable to register segmental diastolic function that may appear before systolic dysfunction. Current use of tissue Doppler and strain and strain rate techniques incorporate diastolic segmental function.
4. The test terminates when the most significant lesion has caused ischemia. This raises the possibility of underestimating other important coronary disease which may remain undiagnosed.

Stress Long Axis: Stress ventricular long axis demonstrates the mechanical behavior of the subendocardial layer of the myocardium. The myocardial fibers of this layer are longitudinally orientated. They originate from the ventricular apex and insert around the circumference of the mitral and tricuspid valve annuli. In systole, as they contract, they bring the insertion site (mitral and tricuspid annuli) toward their origin (the apex), and in diastole, they move in the opposite direction bringing the annuli back toward the atria in early diastole and again in late diastole, during atrial contraction [66]. These two components of diastolic movement correspond to the "E" and "A" waves of ventricular filling velocities, in early and late diastole. Having the ability to record the long axis function from the valve annulus movement (fibrous landmark) makes the technique highly reproducible. Long axis function can be studied at different segments, anterior, posterior, left, and septal sites, and also at other levels of the ventricle, particularly when using tissue Doppler techniques (Fig. 7.22) [67]. The same principle can be used for studying the free wall function of the right ventricle, which cannot be assessed by other imaging modalities. Finally, measurements of long axis function including amplitude, velocities, timing, and incoordination can be obtained, and thus a comprehensive assessment of systolic and diastolic functions of each of the five longitudinal segments can be performed. Disturbances of the anterior and septal segments usually represent left anterior descending coronary artery disease, left segment represents the circumflex artery disease and posterior and right ventricular free wall the right coronary disease (Fig. 7.23) [68].

Stress long axis technique has shown a significantly higher sensitivity and specificity for diagnosing coronary artery disease when compared with conventional wall motion

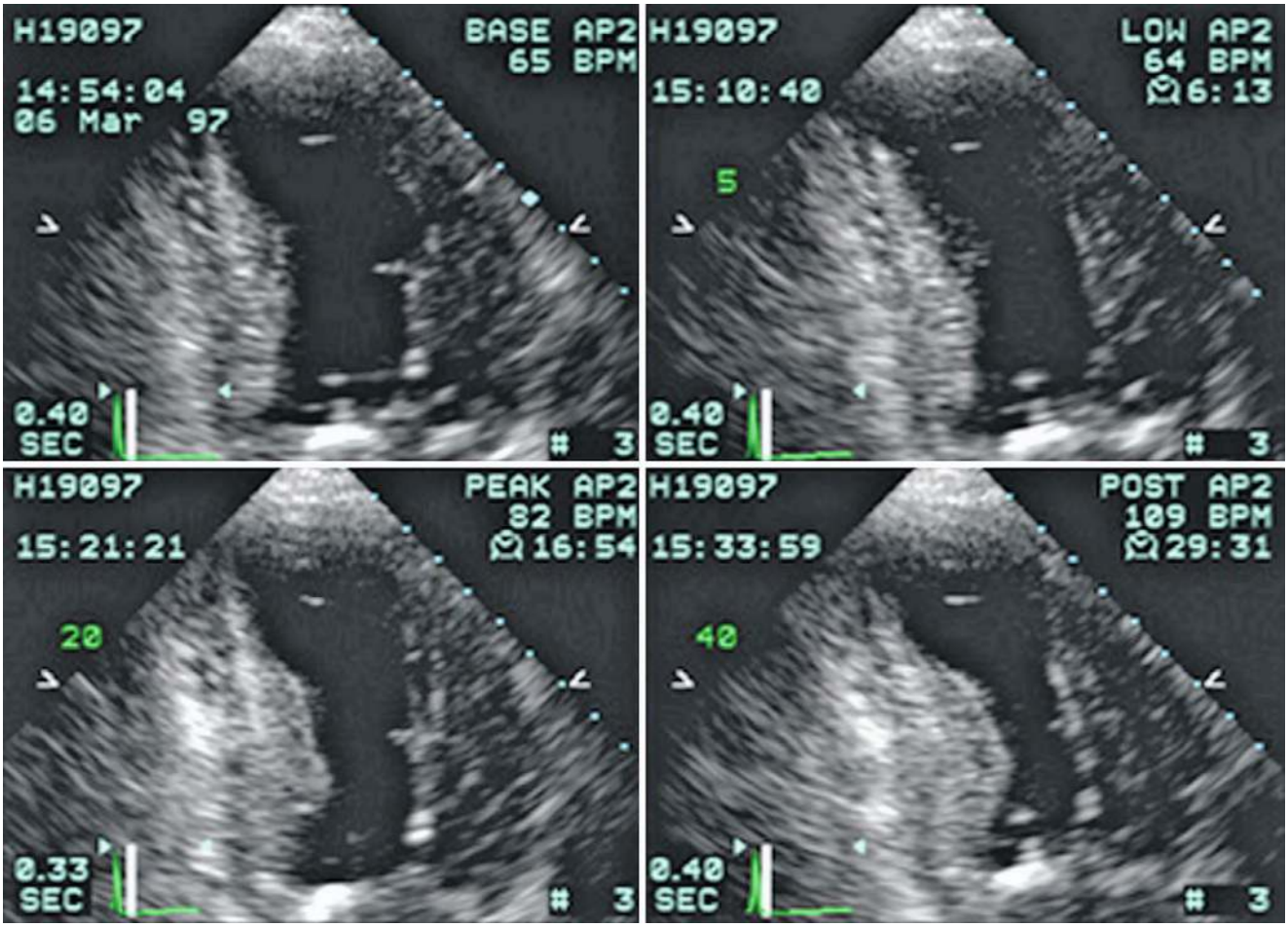


Fig. 7.22 Apical views from a patient with exertional angina at rest (*top*) and peak dobutamine stress (*bottom*). Note the significant development of hypokinesia of the apex with stress consistent with left anterior descending artery disease

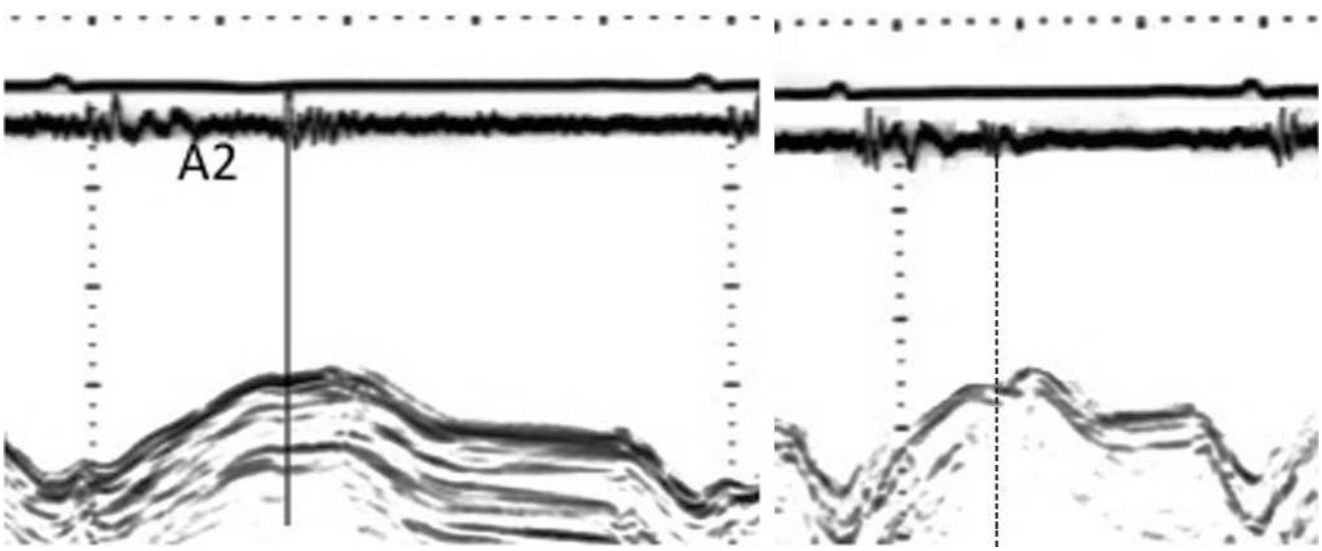


Fig. 7.23 Apical views from a patient with exertional angina at rest (top) and peak dobutamine stress (bottom). Note the significant development of hypokinesia of the apex with stress consistent with left anterior descending artery disease

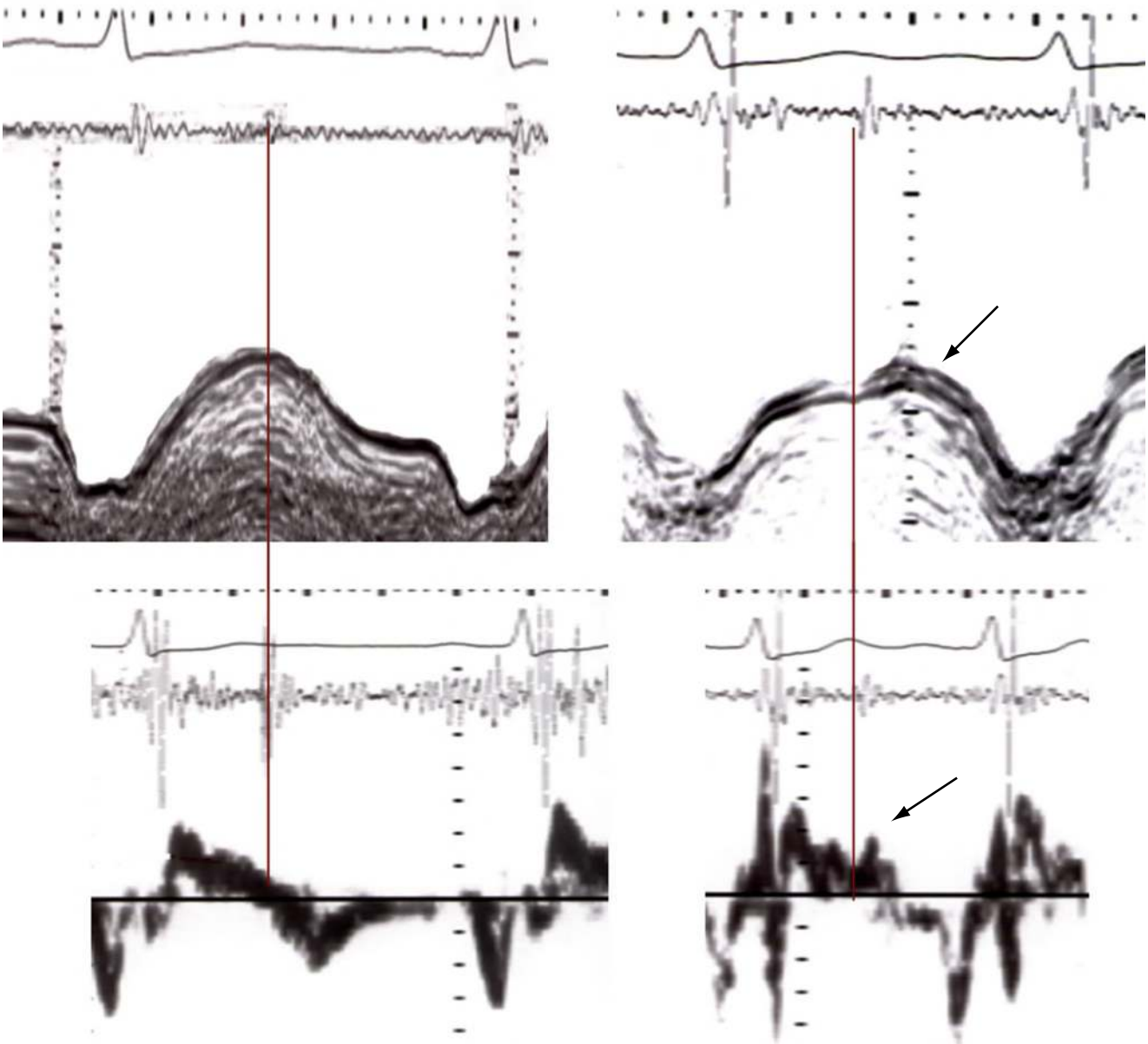


Fig. 7.24 Septal long axis recording from a patient with coronary artery disease at rest (*left*) and peak stress (*right*). Note the fall in amplitude (*top*) and velocities (*bottom*) and the development of incoordination (arrows) in early diastole with stress

score index (Fig. 7.24) [66–69]. Its sensitivity to single vessel disease, particularly that of the right coronary artery, is higher than that of thallium scanning, probably due to its ability to assess right ventricular behavior during stress. A failure of long axis amplitude to increase by 2 mm with stress has been shown as a marker of ischemia, more sensitive than wall motion score index [70]. Likewise a failure of the early diastolic tissue Doppler velocity to increase by 2.5 cm/s is consistent with ischemic behavior, again with a higher sensitivity than wall motion score index [6]. Furthermore, combining ventricular long axis analysis and simultaneous 12 lead ECG at rest and peak stress demonstrates the close relationship between the two, probably based on the anatomical fact that the conduction system runs in the subendocardium (Fig. 7.25) [71–73]. The fall in long

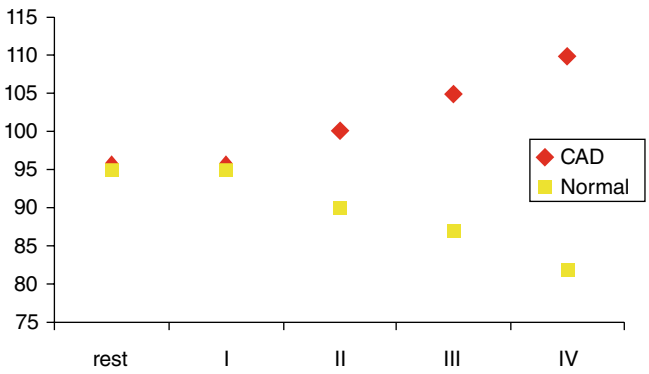


Fig. 7.25 Graph demonstrating the incremental change in QRS duration in normals and in patients with coronary artery disease. Note the progressive broadening of QRS duration in the latter compared with the former

axis amplitude with stress correlates with the delay in ventricular depolarization, or "QRS broadening" seen in patients with coronary artery disease (Fig. 7.26). In addition, detailed analysis of different long axis phases differentiates between the effect of inotropy and conduction disturbances themselves. The delay in the onset of segmental long axis shortening (inward movement) correlates closely with the extent of the delay in depolarization [8]. The latter also correlates with the delay in early diastolic long axis lengthening, resulting in delayed early filling. Furthermore, the exaggerated incoordination seen at peak stress results in very long isovolumic periods that correlate with the drop in cardiac output in patients with ischemic cardiomyopathy [74]. Thus, ventricular long axis analysis not only confirms the presence of coronary artery disease, but distinguishes the global ventricular response to stress. Finally, using the same principle helps in ascertaining the presence of coronary artery disease in patients with left bundle branch block in whom no other non-invasive technique could achieve such result. Shortening of QRS duration at peak stress along with an increase in long axis amplitude excludes coronary artery disease as potential underlying etiology for a dilated ventricle with LBBB [75].

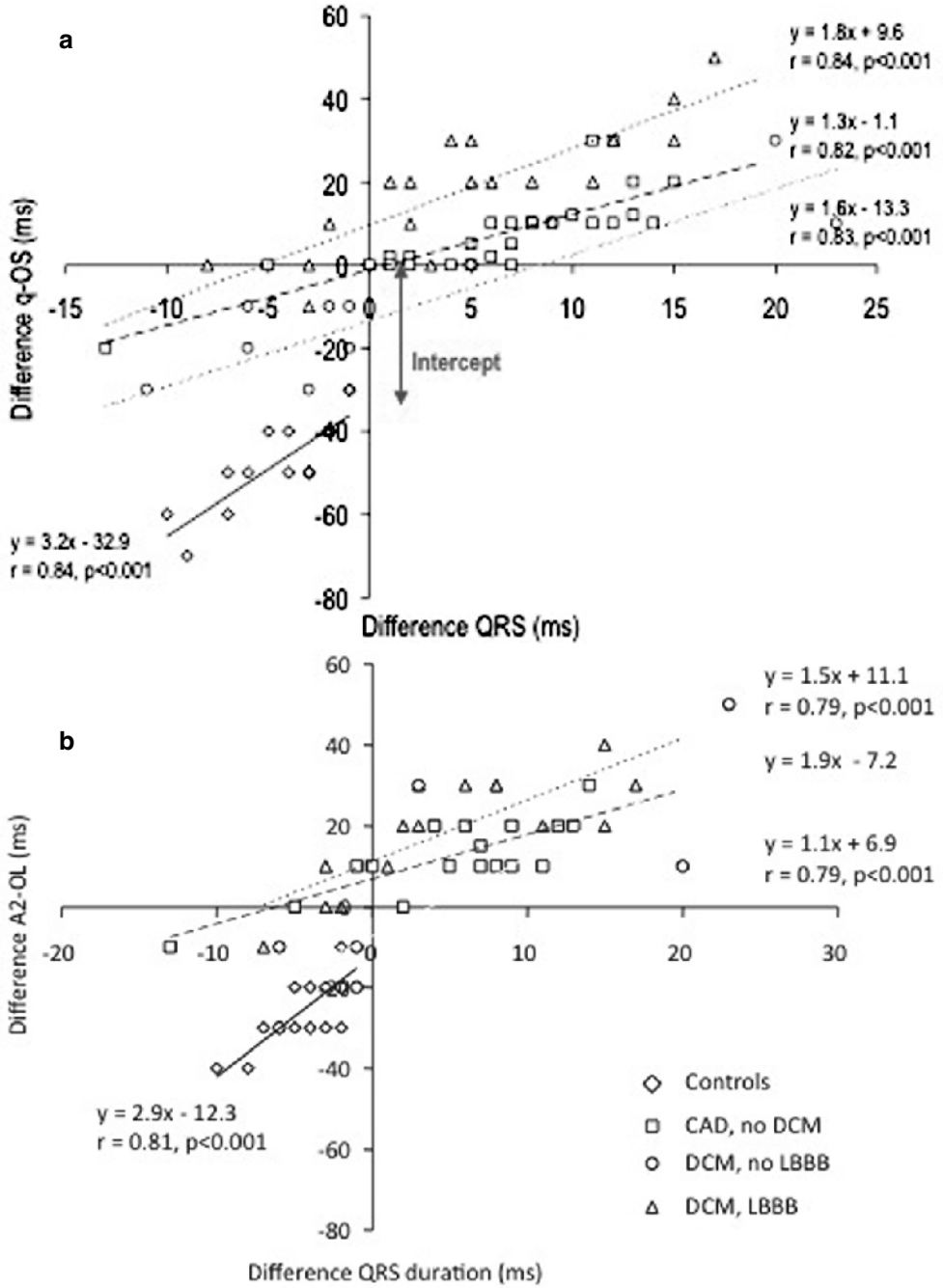


Fig. 7.26 Graph demonstrating a close relationship between QRS broadening and delay in septal onset of shortening (**a**) and lengthening (**b**)

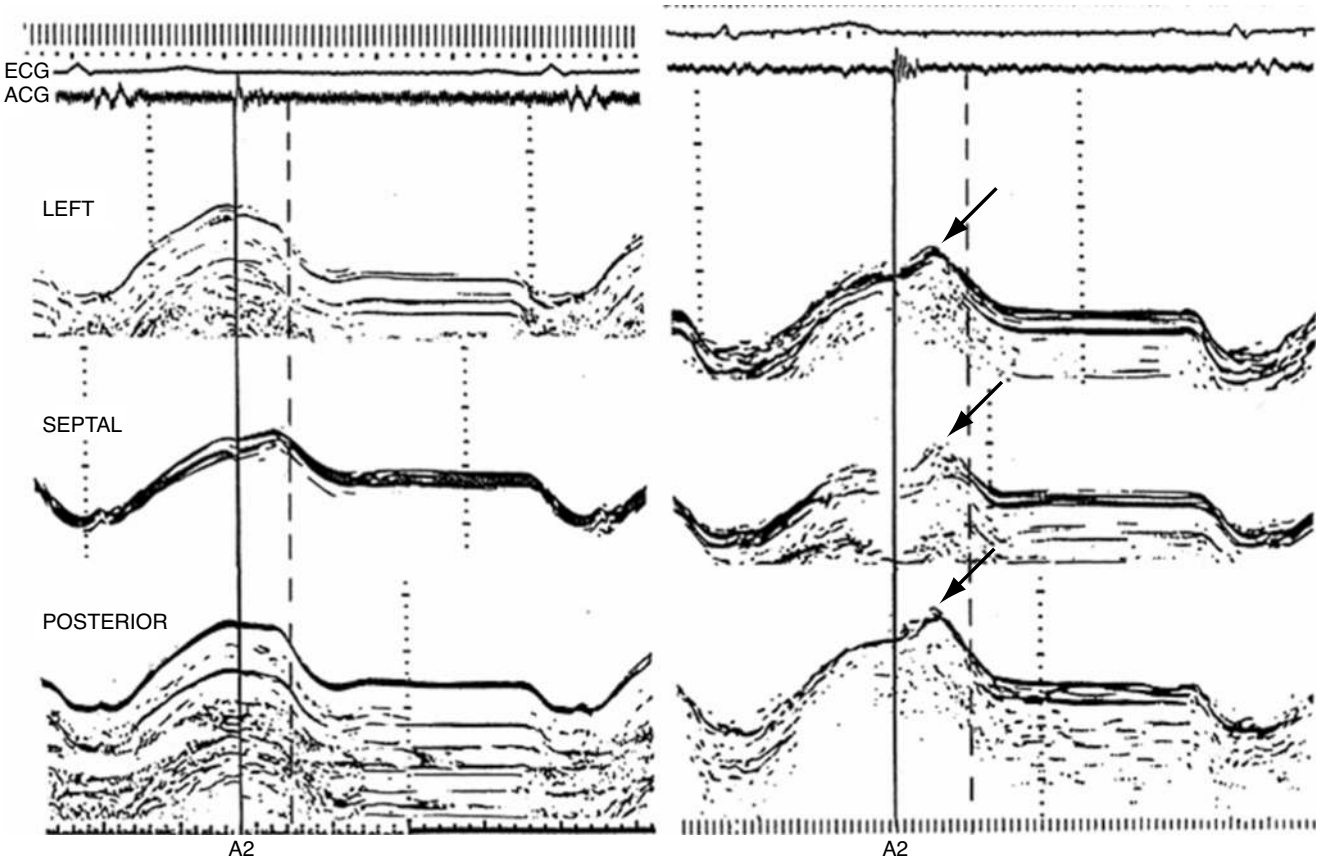


Fig. 7.27 Long axis recordings of the 3 LV long axes, *left*, *septal*, and *posterior* demonstrating universal incoordination pattern, from a patient with unstable angina

Unstable Angina: In patients presenting with unstable angina in whom the coronary arteries prove to be anatomically normal, the resting echocardiography is generally normal. In those with coronary disease, no specific pattern on 2-D images has been identified. However, analysis of ventricular long axis function may demonstrate an exaggerated incoordination/dyssynchrony pattern (post-ejection shortening) in more than one segment (Fig. 7.27) [76]. The extent of this incoordination in early diastole may itself have a mechanical effect in compromising coronary flow, thus perpetuating progression of myocardial ischemia at rest. Complete revascularization of such patients results in regressed incoordination and symptom recovery.

Ischemic Cardiomyopathy

The question of revascularization often arises in patients with ischemic cardiomyopathy and previous myocardial infarction whose symptoms are not medically controlled. The evidence for ischemic myocardium can be demonstrated by various techniques including exercise ECG, stress echo, or myocardial perfusion scanning. Surgical decision making depends on the extent of the viable myocardium whose function is likely to improve with revascularization. This is often referred to as hibernating myocardium. These areas may be hypokinetic at rest so that stress echo, thallium perfusion, or PET scanning are necessary to define such regions [77, 78]. Hibernating myocardium has been defined as a state of persistently impaired myocardial and left ventricular functions at rest due to reduced coronary blood flow that can be partially or completely restored to normal if the myocardial oxygen supply/demand ratio is corrected. Its presence can be demonstrated by a number of techniques. Abnormal thallium or technetium uptake and cardiac magnetic resonance are the current routinely used techniques to assess the degree of myocardial hibernation. Conventional stress echo and wall motion scoring has shown significant accuracy for identifying viable myocardium in different segments with potential implications for selecting suitable patients for surgery and predicting revascularization outcome [79]. Again, the sensitivity of stress echo is significantly improved when using echo contrast agents for delineating clear endocardial border and segmental thickening. Viable segments characteristically show a biphasic response to stress. At low dose stress, local amplitude increases, but at higher doses, it falls again. This

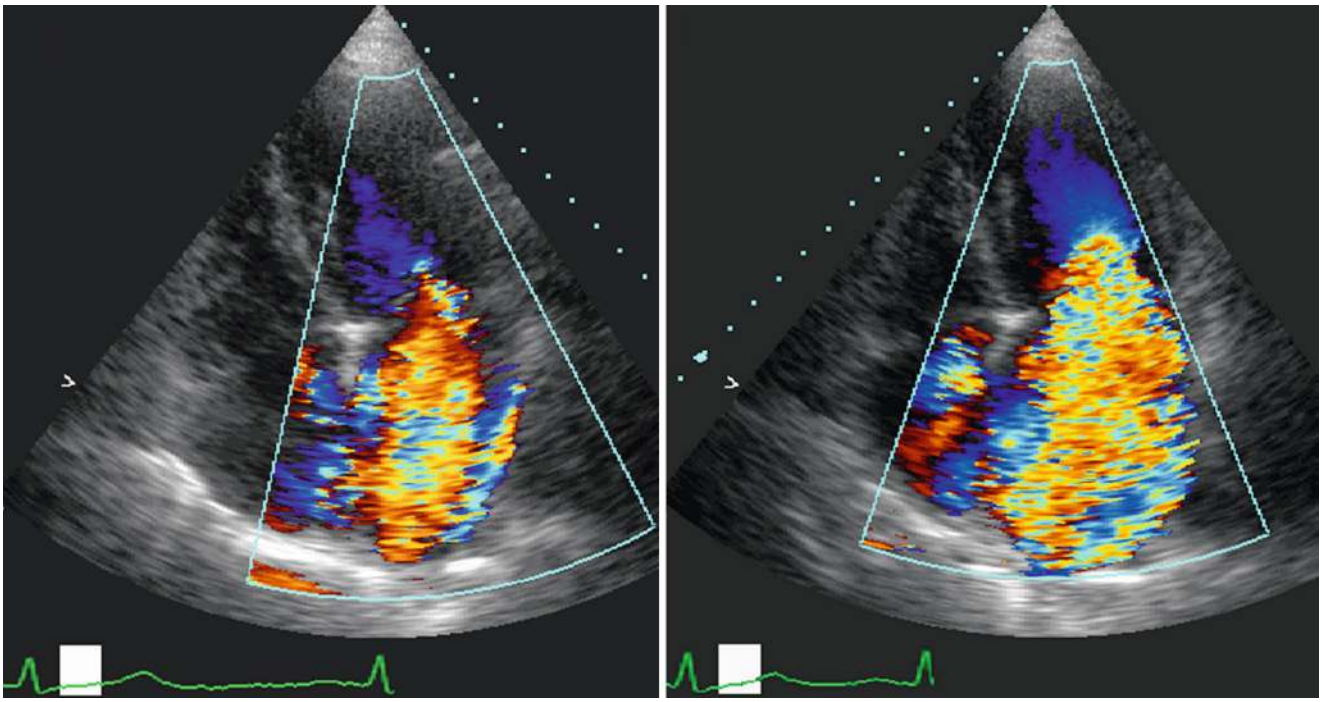


Fig. 7.28 Apical 4-chamber view from a patient with ischemic cardiomyopathy and significant functional mitral regurgitation at rest (*left*) and peak stress (*right*). Note the worsening of mitral regurgitation with stress

biphasic response has been widely used as marker of viable myocardium in patients with ischemic cardiomyopathy [80].

In addition to the other limitations of wall motion scoring, patients with ischemic cardiomyopathy commonly present with secondary complications which may influence the overall pattern of ventricular function. Functional mitral regurgitation, frequently seen in ischemic cardiomyopathy, may overestimate wall motion activity, whereas high left atrial pressure (restrictive physiology) may suppress wall motion. Left bundle branch block is known to affect wall motion behavior even in the absence of coronary disease and is expected, therefore, to affect wall motion score. The severity of mitral regurgitation with stress reduces as the ring diameter falls with the increase in heart rate during stress echo in patients with viable myocardium particularly at the basal ventricular level (Fig. 7.28).

Ventricular Long Axis Function in Ischemic Cardiomyopathy

An increase in long axis amplitude with stress (a normal response) is a reliable sign of viability irrespective of the appearance of additional markers of ischemic dysfunction such as incoordination. A cut-off value of 6 mm amplitude at rest has been shown to be 90% sensitive and 95% specific in predicting surgical recovery (Fig. 7.29). An incremental increase in long axis amplitude with stress by 1.5 mm has proved a more sensitive predictor of the presence of coronary artery disease in patients with dilated cardiomyopathy than the increase in tissue Doppler lengthening velocity or wall motion score index (Fig. 7.30) [60].

Long axis measurements may also provide an opportunity for detailed analysis of ventricular segmental and global function in patients with ischemic cardiomyopathy. With a superimposed ECG, segmental electromechanical behavior can be studied in different phases of the cardiac cycle. In addition to the above markers of ischemic dysfunction, timing with respect to onset of ventricular depolarization and repolarization has been shown to determine the overall performance of the ventricle (stroke volume and cardiac output [81]. In these patients, stress long axis can also demonstrate characteristic incoordination patterns such as early systolic outward movement or post-ejection shortening (in early diastole) which cannot be visualized by wall motion scoring. Finally, long axis disturbances can affect the overall pattern of ventricular filling. The delayed onset of long axis lengthening with respect to end-ejection is associated with a delay of the onset and peak early diastolic filling [82], the consequences of which are increased early diastolic acceleration and compromised filling time (Fig. 7.31). Left ventricular filling pattern during stress may be therefore taken as a surrogate marker of segmental long axis behavior in diastole.

The overall effect of delayed long axis shortening and lengthening and the exaggerated incoordination is significant compromise of LV filling and hence cardiac output with

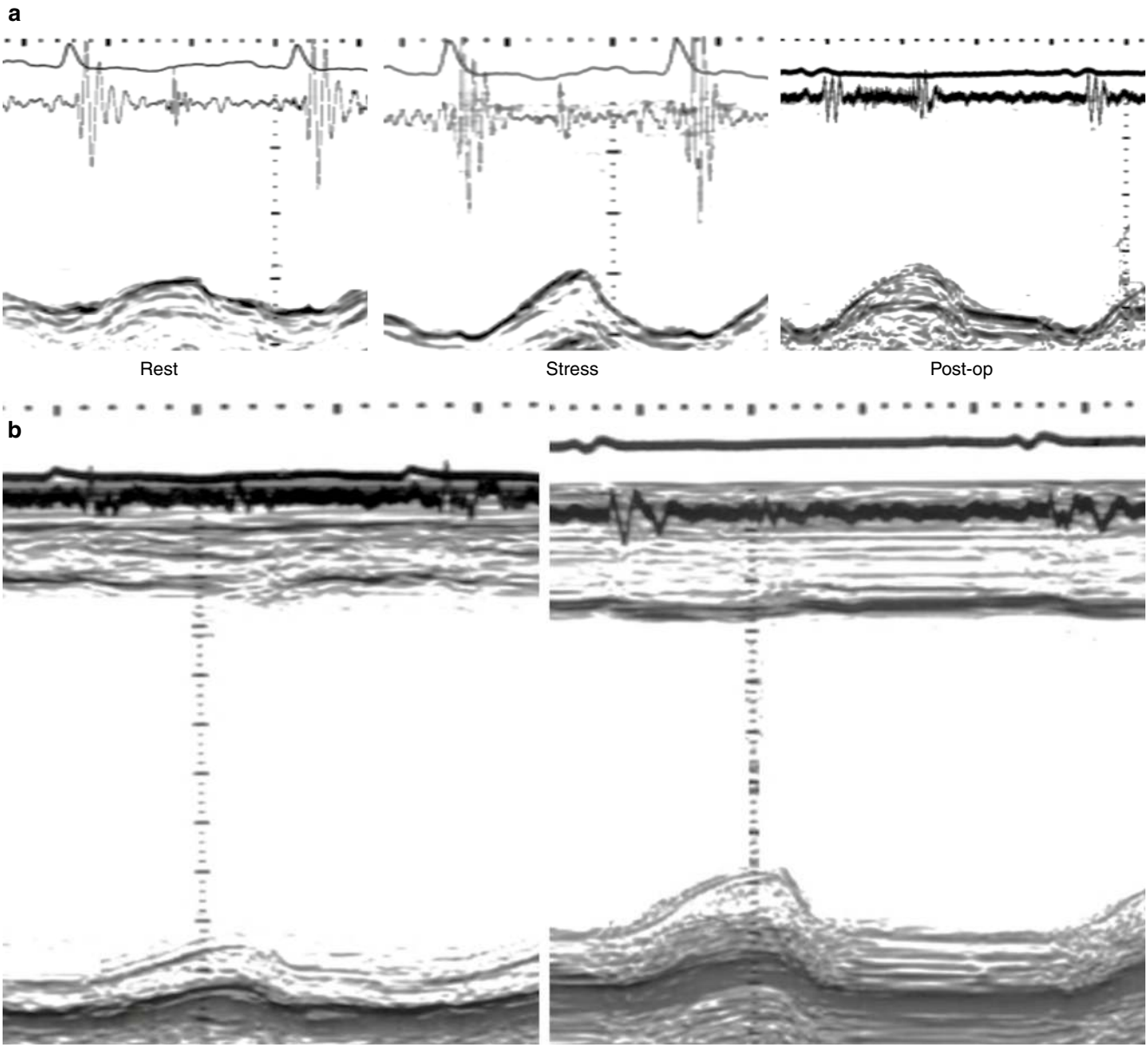


Fig. 7.29 (**a**) LV free wall long axis recording from a patient with ischemic cardiomyopathy at rest (*left*), peak stress (*middle*), and after coronary revascularization (*right*). Note the significant increase in amplitude with stress and complete recovery after surgery. (**b**) LV short axis dimensions and systolic function before and after revascularization showing significant improvement

stress. To enhance diagnostic accuracy, additional parameters can be used. Attenuation of early diastolic LV cavity filling velocity can indicate ischemic dysfunction and suggest the presence of CAD, regardless of its severity. Measurements of reduced longitudinal systolic velocity and prolonged total isovolumic time are also highly accurate (91%) for detecting significant (>50%) coronary branch stenosis (Fig. 7.31). Although these parameters are not typically included in standard stress echo software, they are routinely recorded in transthoracic echocardiograms and can help improve diagnostic accuracy in everyday practice [83]. Similar findings can be demonstrated in the right ventricular free wall behavior, which are difficult to study using other stress techniques (Figs. 7.32 and 7.33).

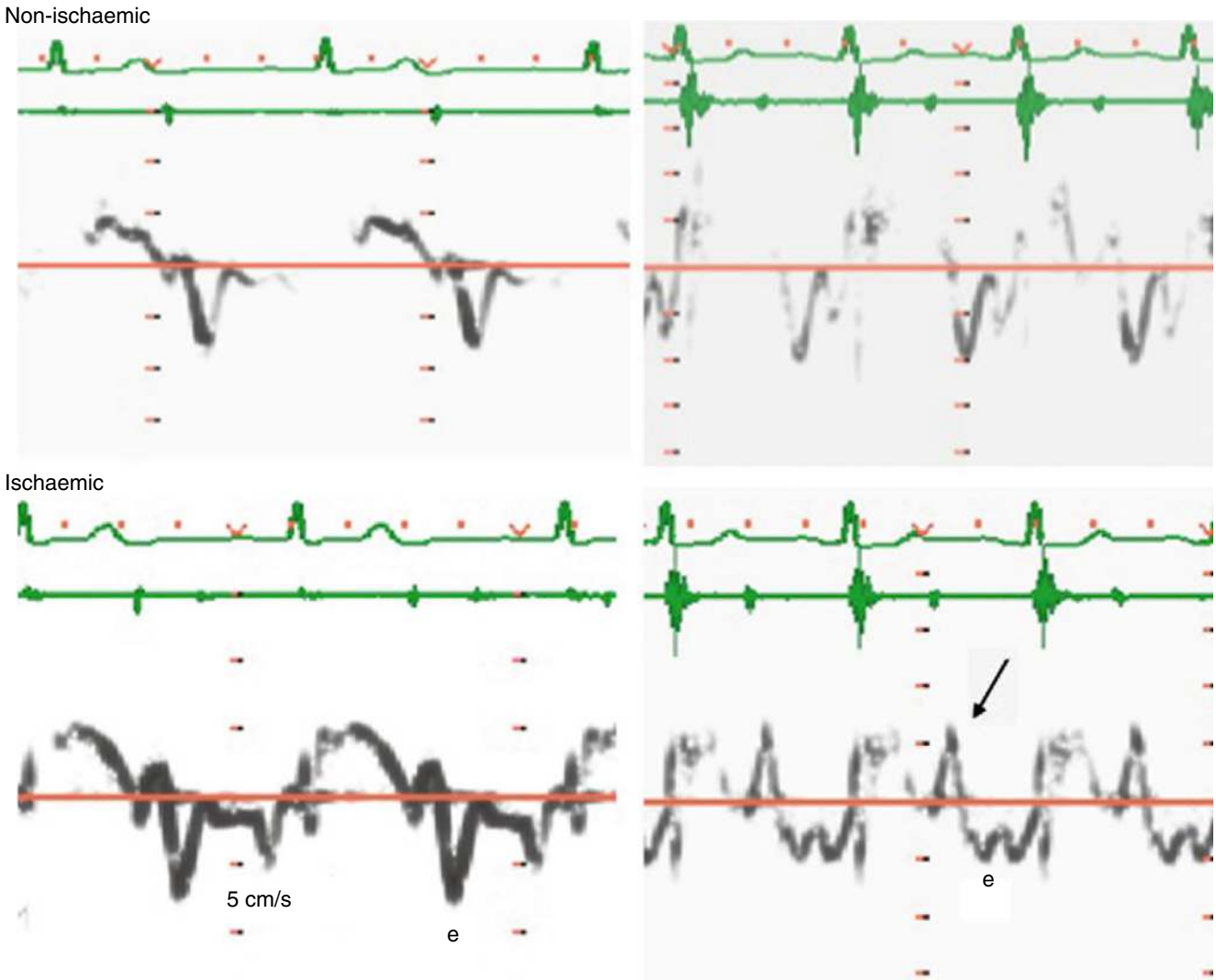


Fig. 7.30 Myocardial tissue Doppler recordings from two patients with dilated cardiomyopathy: nonischemic (*top*) and ischemic (*bottom*) at rest (*left*) and peak stress (*right*). Note the normal increase in early diastolic velocities in the absence of coronary artery disease and the fall of velocities and appearance of incoordination (*arrow*) in coronary disease

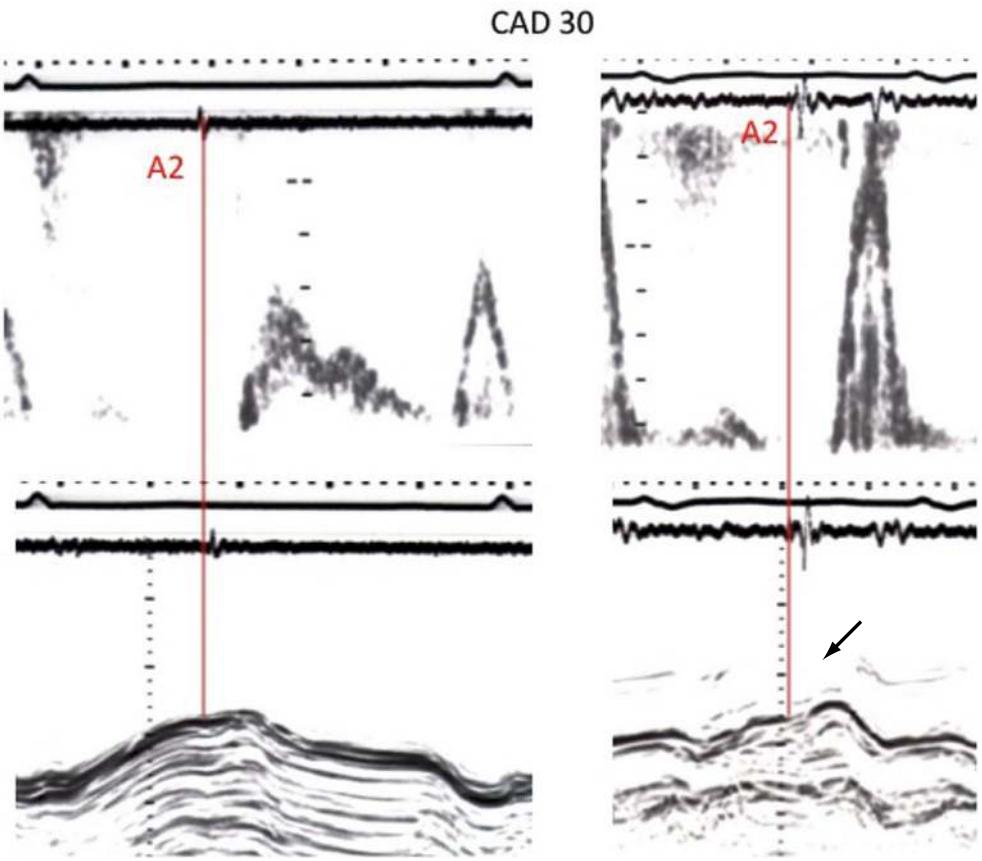


Fig. 7.31 LV septal long axis recording from a patient with ischemic cardiomyopathy along with transmitral filling velocities (*top*) at rest (*left*) and peak stress (*right*). Note the marked development of incoordination (arrow) that compromised early ventricular filling

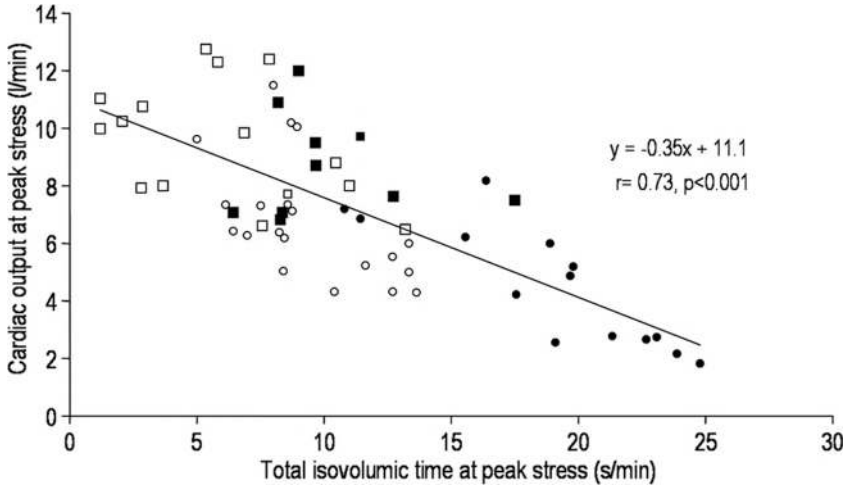


Fig. 7.32 A graph demonstrating the close relationship between stress isovolumic time and peak cardiac output in patients with ischemic cardiomyopathy

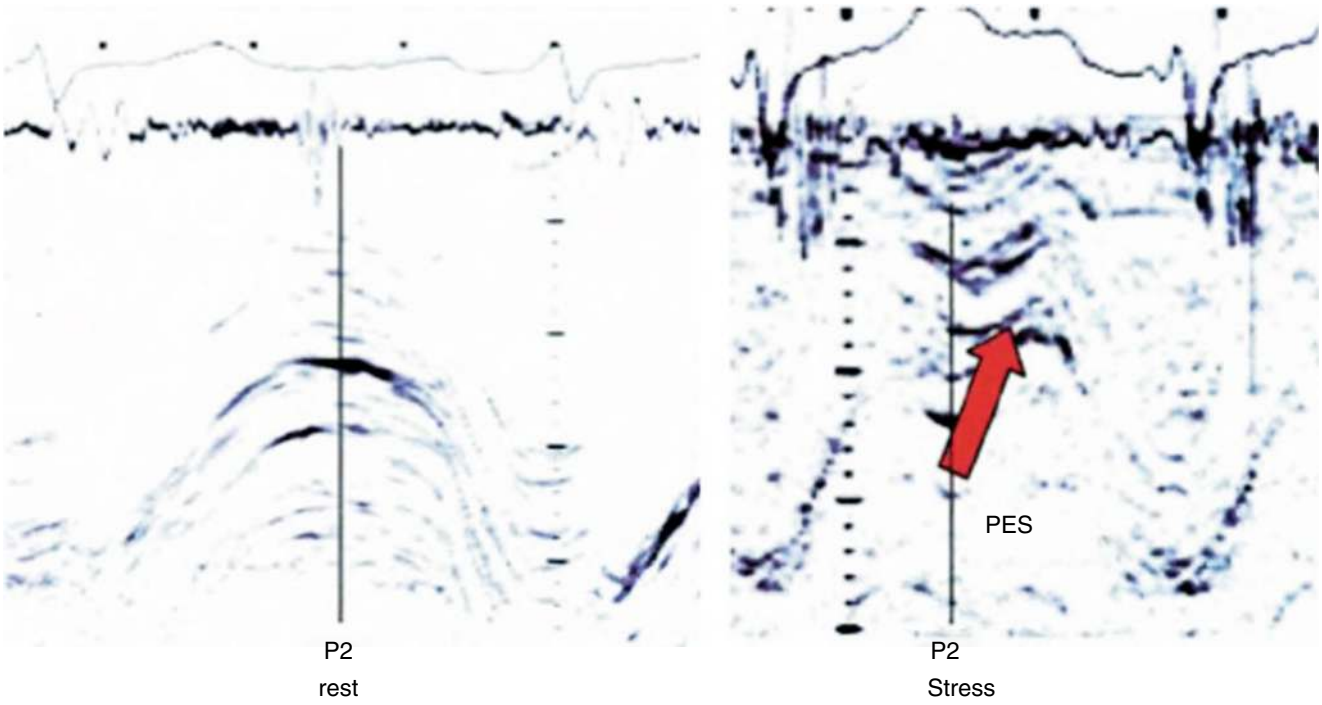


Fig. 7.33 Right ventricular free wall long axis recording from a patient with biventricular ischemic myopathy at rest (*left*) and peak stress (*right*). Note the significantly reduced amplitude at rest which becomes more depressed with stress. Also note the appearance of exaggerated incoordination consistent with ischemic dysfunction (*arrow*)

Management of Coronary Artery Disease

Medical Follow-up: Echocardiography aims at following up segmental as well as overall ventricular function. Transmitral Doppler velocities provide accurate indirect noninvasive markers of filling pressures.

- Optimal use of vasodilators (ACE-Inhibitors and A_2 blockers) as well as others can be monitored.
- Adequate response to ACE-inhibition in patients with restrictive filling results in normalization of left atrial pressure, size, and filling velocities (Fig. 7.34) [84].
- The direct cause of patient's symptoms can be derived from echocardiographic assessment of left ventricular filling time and mitral regurgitation length. Prolonged mitral regurgitation in patients with ischemic cardiomyopathy may cause breathlessness by limiting filling time and stroke volume. This condition, particularly with QRS >150 ms, usually responds favorably to CRT pacing and optimized A-V delay with or without left ventricular lead turned on (Fig. 7.35) [85].

Percutaneous Coronary Intervention (PCI): Echocardiography is not routinely essential during PCI. However, it may be necessary in exceptional cases following PCI related complications, e.g., in patients with hypotension to exclude pericardial tamponade. Ventricular long axis ischemic dysfunction shows early recovery following successful revascularization. The reverse of these findings can be regarded as markers of vessel occlusion (Fig. 7.36 and 7.37) [86].

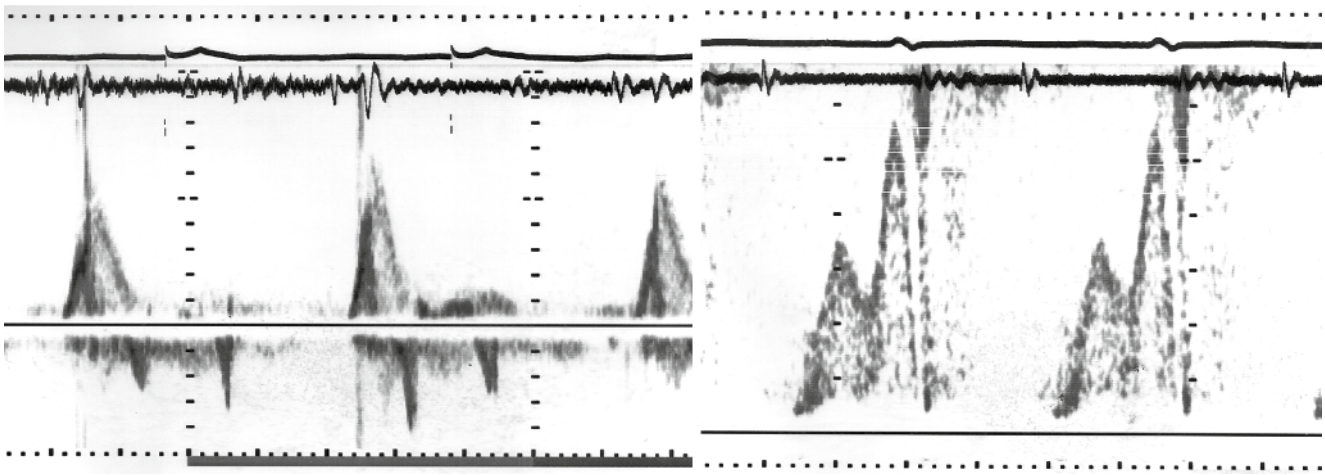


Fig. 7.34 Transmitral Doppler flow velocities from a patient with ischemic cardiomyopathy and limiting dyspnea. Note the restrictive filling pattern (*left*) and third heart sound consistent with raised left atrial pressure which normalizes with ACE-Inhibition (*right*)

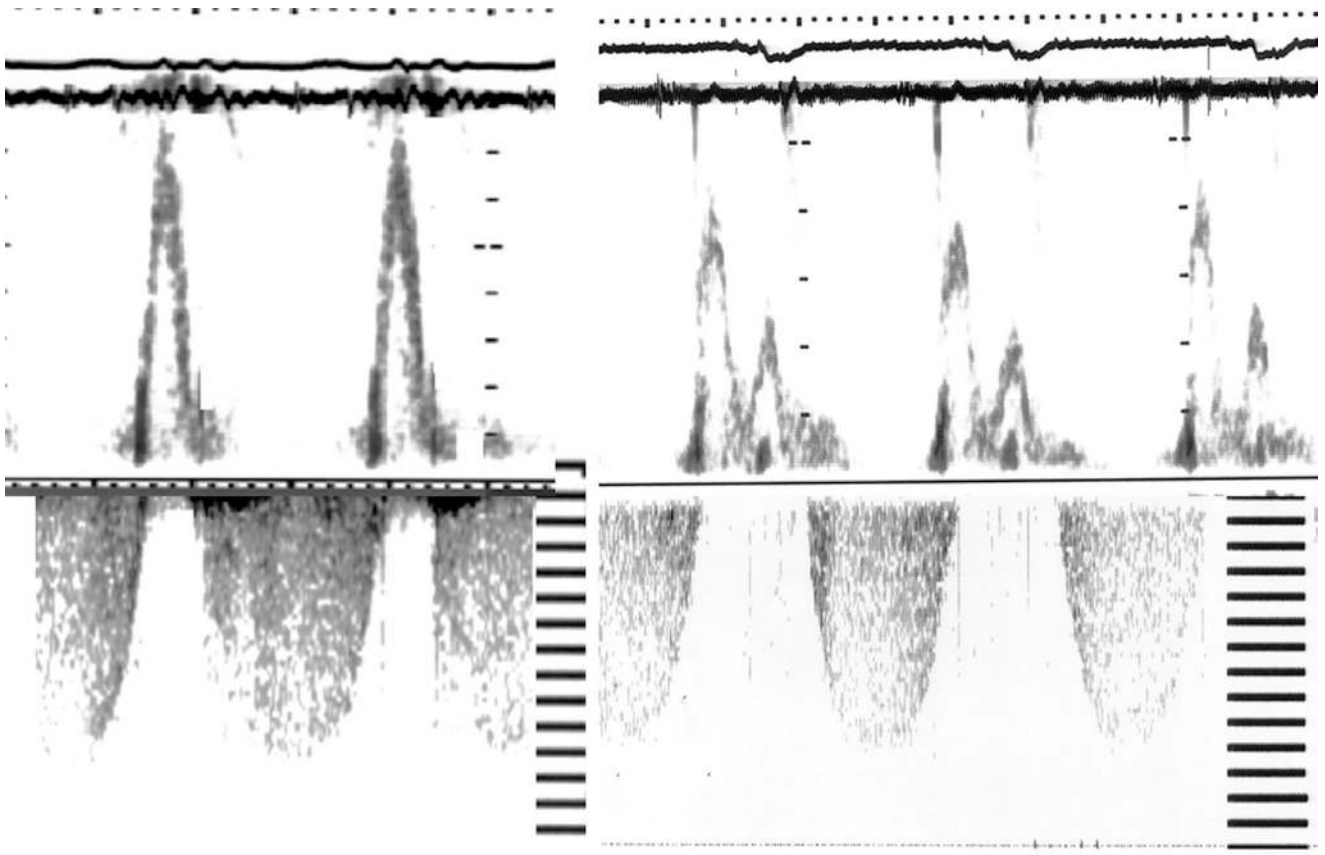


Fig. 7.35 Transmitral Doppler flow velocities from a patient with ischemic cardiomyopathy and resistant dyspnea. Note the short filling time caused by the long mitral regurgitation (*left*) which is shortened by CRT and A-V optimization (*right*)

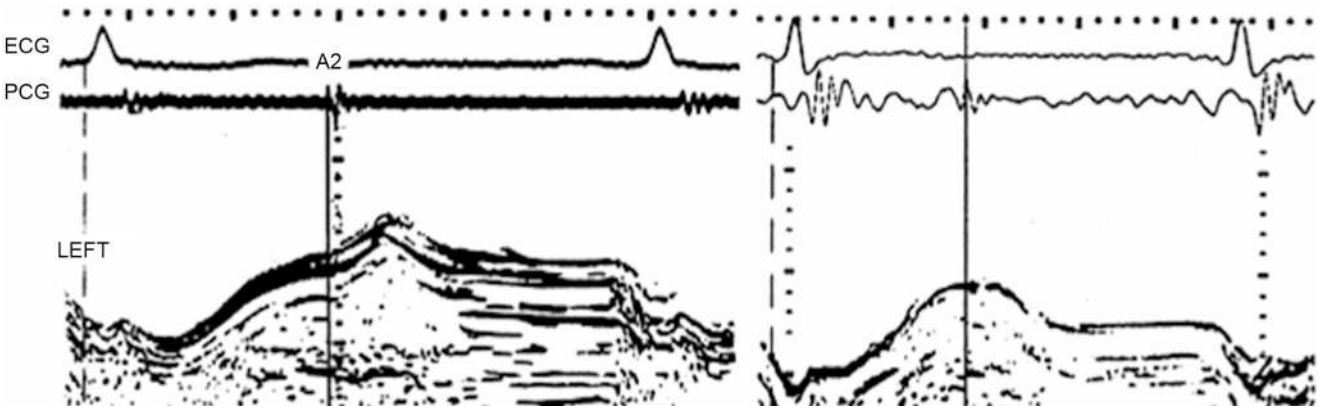
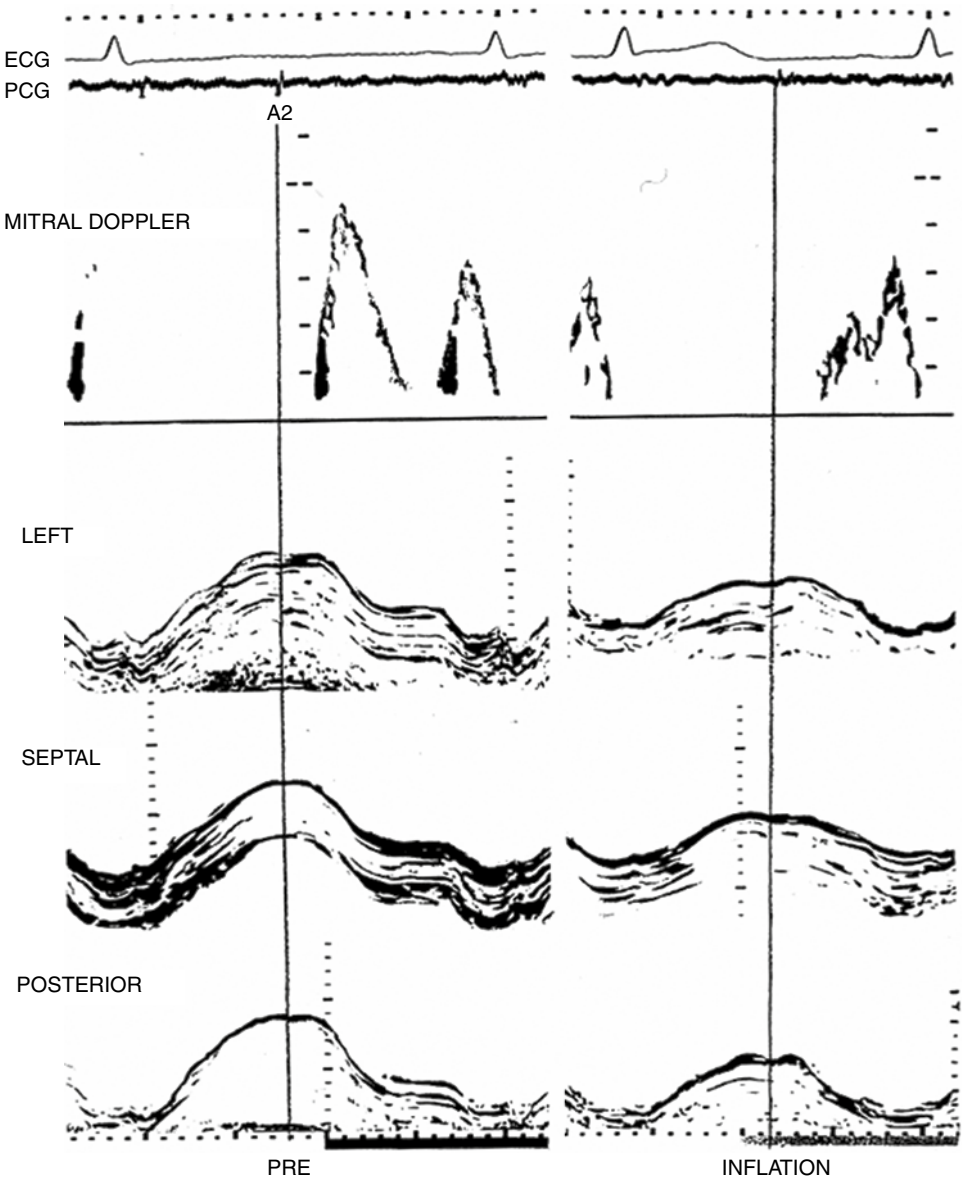


Fig. 7.36 LV free wall long axis recording from a patient with CAD before (*left*) and after (*right*) coronary angioplasty. Note the remarkable normalization of the incoordinate pattern after procedure

Fig. 7.37 LV free wall and septal long axis from a patient during balloon inflation in the proximal LAD. Note the significant fall in long axis amplitude and lengthening velocities



Coronary Artery Bypass Surgery

Intraoperative Echocardiography: Intraoperative echocardiography aims at monitoring global and segmental ventricular function during and after a revascularization procedure. The preoperative study provides a baseline assessment against which postoperative studies can be compared. Transesophageal echocardiography plays an important role for monitoring these patients particularly those with ischemic cardiomyopathy. The 4-chamber view is the most commonly used image, although a transgastric short axis view also provides a satisfactory assessment of left ventricular minor axis function by monitoring segmental thickening as assessed by 2D images and M-mode recordings. Viable segments which remain dysfunctioning after complete revascularization are considered stunned. For academic interest, obtaining a left ventricular pressure recording superimposed on the M-mode trace using an intraventricular catheter tip manometer provides a wealth of information on segmental as well as global power production and cycle efficiency. This technique has shown significant early segmental recovery after revascularization with non-bypass (octopus) procedure when compared with traditional bypass procedure (Fig. 7.38) [87].

Direct visualization of the origin of the coronary artery as well as graft insertion sites may be important in determining the cause of the delay in weaning-off a patient from the bypass circulation. A blocked or kinked graft supplying a vital segment may be the direct cause of such complication. Color flow as well as pulsed wave Doppler showing high velocities at branch origin or graft insertion along with segmental hypokinesia suggests the presence of significant occlusion that needs urgent attention and possible re-intervention (Fig. 7.39).

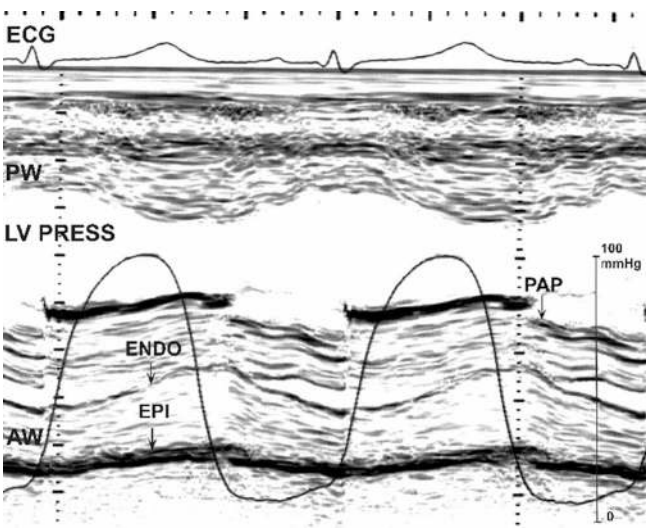


Fig. 7.38 Transgastric left ventricular M-mode recording of the minor axis before establishing the bypass circulation with superimposed LV pressure trace

Finally, intraoperative TOE provides evidence for additional abnormalities that could be dealt with in the same setting, i.e., significant mitral regurgitation that needs leaflet repair or ring insertion, patent foramen ovale, or left atrial appendage clot as a possible cause of transient ischemic attacks (Fig. 7.40 and 7.41).

Intensive Care Unit Echocardiography: Most patients with normal ventricular systolic function before surgery have an uneventful recovery. Those with poor ventricular function may progress more slowly and may require balloon pump insertion. Echocardiographic studies may be requested when recovery is delayed and in those who are ventilator dependent. The transthoracic window is usually limited in such patients so that transesophageal echo is essential for an adequate evaluation. The objective of the TOE in this setting is to assess:

- Regional left ventricular wall motion and estimation of systolic function (ejection fraction).
- Left ventricular filling pattern as a marker of left atrial pressure.
- Evidence for pulmonary hypertension as an indirect marker of raised left atrial pressure.
- Right ventricular systolic function—as a less common cause of an under-filled and poorly functioning left ventricle by 2D and long axis.
- Presence of pericardial effusion, a small localized collection, particularly posterior to the left atrium, may have its deleterious effect on ventricular recovery.

Patients with resistant segmental disturbances may demonstrate clear evidence for ischemic dysfunction with dobutamine stress. Simultaneous documentation of deterioration of segmental wall motion function and ischemic ECG changes at peak stress usually confirms an underlying ischemic cause for the delayed recovery. Emergency coronary angiography and possible re-intervention may be life-saving procedures in such patients.

Postoperative Echocardiography: This aims at providing a baseline data on ventricular function after complete revascularization. It is also helpful for assessing right ventricular function which is known to deteriorate after cardiopulmonary bypass circulation. In addition, any pericardial or left-sided pleural effusion can be assessed. Recurrence of angina-like symptoms can be evaluated using stress echo techniques as discussed above, particularly in patients with conduction disturbances as a possible cause of angina, in whom information provided by other stress techniques may be inconclusive (Fig. 7.42) [88].

It must be mentioned that Doppler echocardiography is an ideal bed-side investigation for indirect assessment of

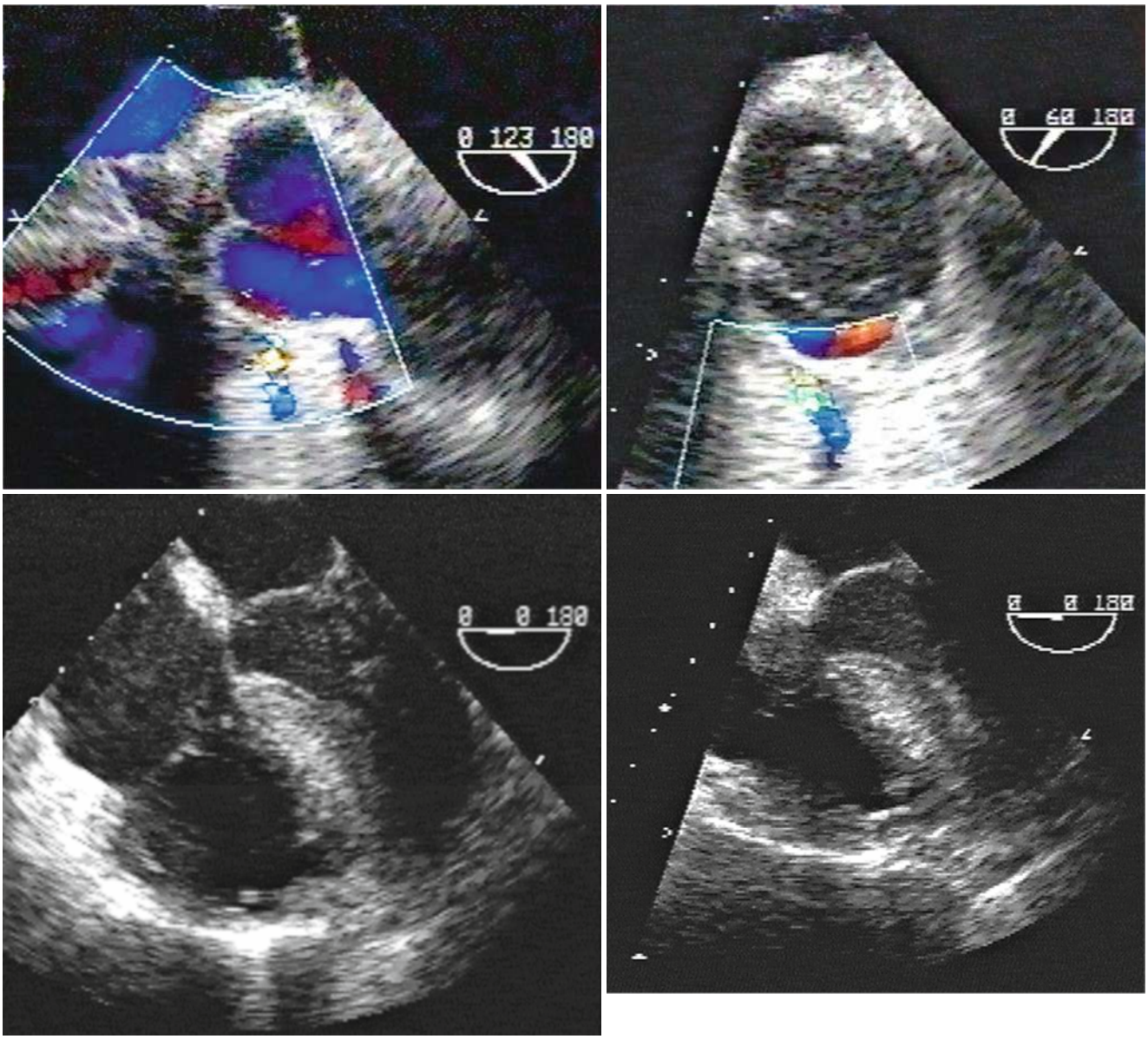


Fig. 7.39 Intraoperative TOE demonstrating high right coronary artery velocities (aliasing) after grafting suggesting graft occlusion or kinking (*top-left*) and apical 4 chamber view showing reduced right ventricular free wall movement (*bottom-left*). Equivalent pictures after releasing the coronary graft obstruction (*right*). Note the significant fall in the right coronary aliasing and normalization of right ventricular function

coronary circulation and myocardial perfusion and mechanical function. With the advent of cardiac CT scanning, it has become now a routine clinical practice to use CT coronary angiography in identifying patients with graft narrowing or obstruction. With one dose of contrast injection, the whole arterial tree and grafts are visualized and could be critically evaluated (Fig. 7.43).

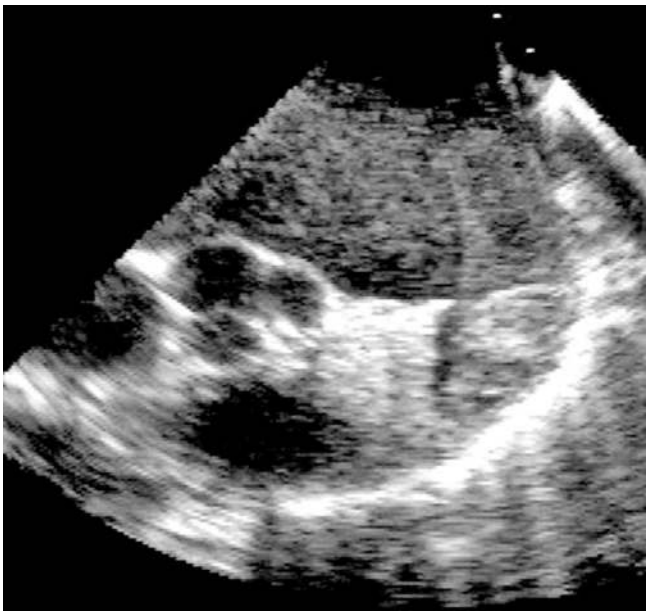


Fig. 7.40 Intraoperative TOE from a patient before CABG surgery showing additional left atrial appendage clot, probably complicating long-standing atrial fibrillation

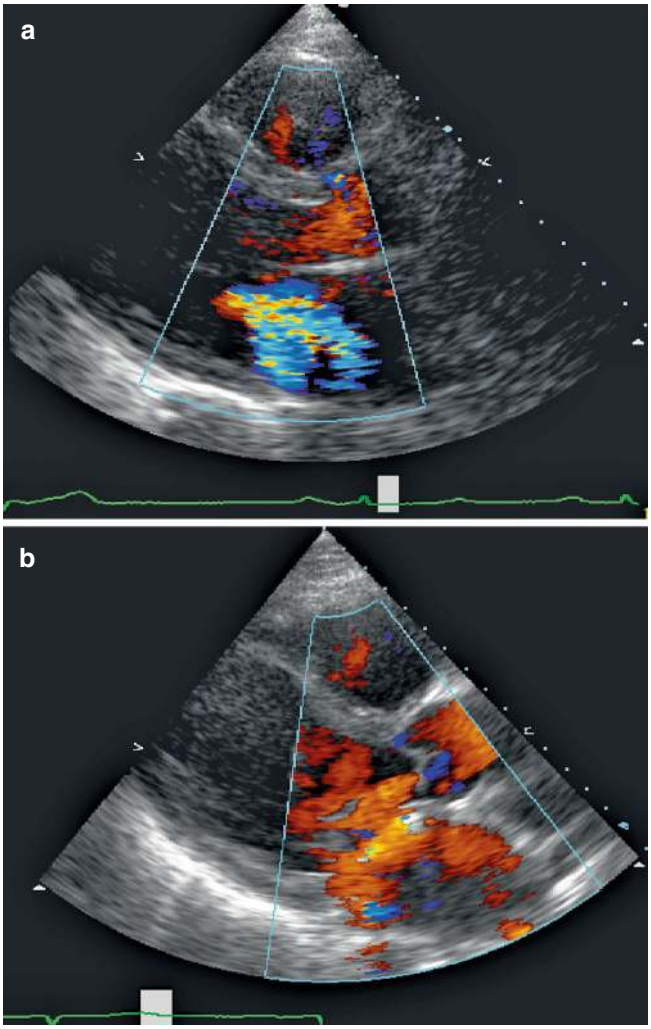


Fig. 7.41 Parasternal views from a patient with ischemic cardiomyopathy and functional mitral regurgitation before (**a**) and after (**b**) CABG and mitral valve repair. Note the disappearance of mitral regurgitation

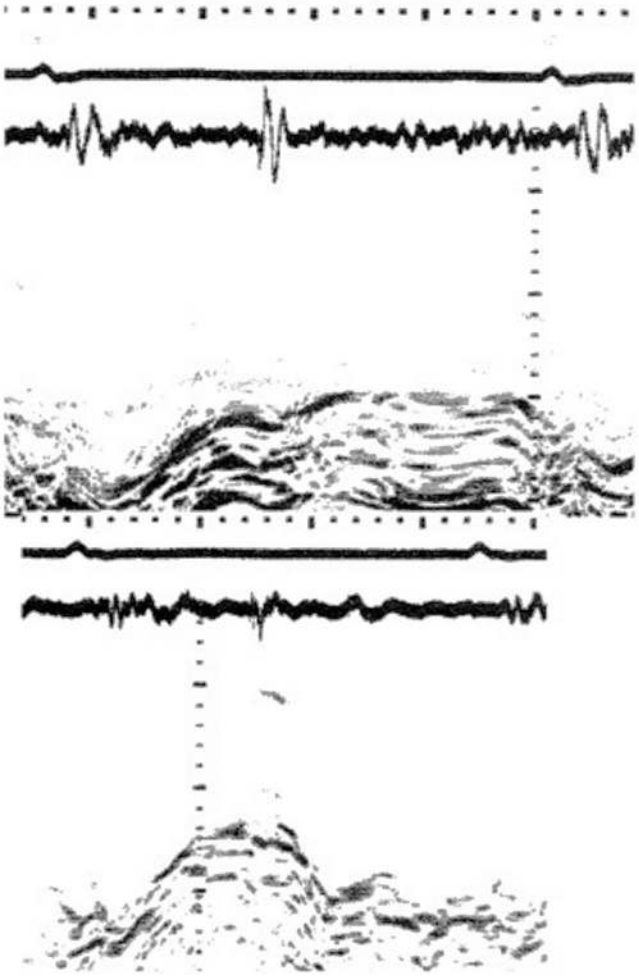


Fig. 7.42 LV long axis recording from the free wall before and after CABG surgery demonstrating significant normalization of function and regression of incoordination



Fig. 7.43 Cardiac CT 3D reconstruction images from a patient with multiple vein grafts and a LIMA to LAD

References

1. Angelini P, Velasco JA, Flamm S. Coronary anomalies: incidence, pathophysiology, and clinical relevance. Circulation. 2002;105:2449–54.
2. Gentile F, Castiglione V, De Caterina R. Coronary artery anomalies. Circulation. 2021;144:983–96.
3. Radke PW, Messmer BJ, Haager PK, Klues HG. Anomalous origin of the right coronary artery: preoperative and postoperative hemodynamics. Ann Thorac Surg. 1998;66:1444–9.
4. Yun G, Nam TH, Chun EJ. Coronary artery fistulas: pathophysiology, imaging findings, and management. Radiographics. 2018;38:688–703.
5. Cheezum MK, Ghoshhajra B, Bittencourt MS, Hulten EA, Bhatt A, Mousavi N, Shah NR, Valente AM, Rybicki FJ, Steigner M, et al. Anomalous origin of the coronary artery arising from the opposite sinus: prevalence and outcomes in patients undergoing coronary CTA. Eur Heart J Cardiovasc Imaging. 2017;18:224–35.
6. Douglas PS, Fiolkoski J, Berko B, Reichek N. Echocardiographic visualization of coronary artery anatomy in the adult. J Am Coll Cardiol. 1988;11(3):565–71.
7. Ae R, Maddox RA, Abrams JY, Schonberger LB, Nakamura Y, Kuwabara M, et al. Kawasaki disease with coronary artery lesions detected at initial echocardiography. J Am Heart Assoc. 2021;10:e019853.
8. Hood JH. Anatomy of the coronary arteries. Semin Roentgenol. 1973;8(1):3–17.
9. Gorlin R. Coronary anatomy. Major Probl Intern Med. 1976;11:40–58.
10. Waller BF. Anatomy, histology, and pathology of the major epicardial coronary arteriesrelevant to echocardiographic imaging techniques. J Am Soc Echocardiogr. 1989;2:232–52.
11. Iliceto S, Marangelli V, Memmola C, Rizzon P. Transesophageal Doppler echocardiography evaluation of coronary blood flow velocity in baseline conditions and during dipyridamole-induced coronary vasodilation. Circulation. 1991;83:61–9.
12. Yamagishi M, Miyatake K, Beppu S, Kumon K, Suzuki S, Tanaka N, et al. Assessment of coronary blood flow by transesophageal two-dimensional pulsed Doppler echocardiography. Am J Cardiol. 1988;62:641–4.
13. Yoshida K, Yoshikawa J, Hozumi T, Yamaura Y, Akasaka T, Fukaya T, et al. Detection of left main coronary artery stenosis by transesophageal color Doppler and two-dimensional echocardiography. Circulation. 1990;81:1271–6.

14. Waller BF, Pinkerton CA, Slack JD. Intravascular ultrasound: a histological study of vessels during life. The new 'gold standard' for vascular imaging. Circulation. 1992;85:2305–10.
15. Yock PG, Fitzgerald PJ, Linker DT, Angelsen BA. Intravascular ultrasound guidance for catheter-based coronary interventions. J Am Coll Cardiol. 1991;17(6 Suppl B):39B–45.
16. Nissen SE, Gurley JC, Grines CL, Booth DC, McClure R, Berk M, et al. Intravascular ultrasound assessment of lumen size and wall morphology in normal subjects and patients with coronary artery disease. Circulation. 1991;84:1087–99.
17. Voros S, Rinehart S, Qian Z, Vazquez G, Anderson H, Murrieta L, et al. Prospective validation of standardized, 3-dimensional, quantitative coronary computed tomographic plaque measurements using radiofrequency backscatter intravascular ultrasound as reference standard in intermediate coronary arterial lesions results from the ATLANTA (Assessment of Tissue Characteristics, Lesion Morphology, and Hemodynamics by Angiography with Fractional Flow Reserve, Intravascular Ultrasound and Virtual Histology, and Noninvasive Computed Tomography in Atherosclerotic Plaques) I Study. JACC Cardiovasc Interv. 2011;4:198–208.
18. Hiro T, Kimura T, Morimoto T, Miyauchi K, Nakagawa Y, Yamagishi M, et al. Effect of intensive statin therapy on regression of coronary atherosclerosis in patients with acute coronary syndrome: a multicenter randomized trial evaluated by volumetric intravascular ultrasound using pitavastatin versus atorvastatin (Japan-ACS [Japan assessment of pitavastatin and atorvastatin in acute coronary syndrome] study). J Am Coll Cardiol. 2009;54:293–302.
19. Bajraktari A, Bytyçi I, Henein MY. High coronary wall shear stress worsens plaque vulnerability: a systematic review and meta-analysis. Angiology. 2021;72:706–14.
20. Bajraktari A, Bytyçi I, Henein MY. The relationship between coronary artery wall shear strain and plaque morphology: a systematic review and meta-analysis. Diagnostics (Basel). 2020;10:91.
21. Pottle A. Prevalence and patterns of cognitive impairment in acute coronary syndromepatients: a systematic review. Eur J Prev Cardiol. 2020;27:281–3.
22. Lancellotti P, Price S, Edvardsen T, Cosyns B, Neskovic AN, et al. The use of echocardiography in acute cardiovascular care: recommendations of the European Association of Cardiovascular Imaging and the Acute Cardiovascular Care Association. Eur Heart J Cardiovasc Imaging. 2015;16:119–46.
23. Buda AJ, Zotz RJ, Gallagher KP. Characterization of the functional border zone around regionally ischemic myocardium using circumferential flow-function maps. J Am Coll Cardiol. 1986;8:150–8.
24. Horowitz RS, Morganroth J, Parrotto C, Chen CC, Soffer J, Pauletto FJ. Immediate diagnosis of acute myocardial infarction by two-dimensional echocardiography. Circulation. 1982;65:323–9.
25. Kaul S, Pandian NG, Gillam LD, Newell JB, Okada RD, Weyman AE. Contrast echocardiography in acute myocardial ischemia. III. An in vivo comparison of the extent of abnormal wall motion with the area at risk for necrosis. J Am Coll Cardiol. 1986;7:383–92.
26. Engelsen DJ, Gorgels AP, Cheriex EC, De Muinck ED, Ophuis AJ, Dassen WR, et al. Value of the electrocardiogram in localising the occlusion site in the left anterior descending coronary artery in acute anterior myocardial infarction. J Am Coll Cardiol. 1999;34:389–95.
27. O'Sullivan CA, Ramzy IS, Duncan A, Li W, Henein MY. The effect of the Q wave infarct on left ventricular electromechanical function. Int J Cardiol. 2003;92:71–6.
28. Ramzy IS, O'Sullivan CA, Lam YY, Dancy M, Tei C, Henein MY. Right ventricular stunning in inferior myocardial infarction. Int J Cardiol. 2009;136(3):294–9.
29. Pasternack RC, Braunwald E, Sobel BE. Acute myocardial infarction. In: Braunwald E, editor. Heart disease. Philadelphia: W.B. Saunders; 1992. p. 1255–60.
30. Gong FF, Vaitenas I, Malaisrie SC, Maganti K. Mechanical complications of acute myocardial infarction: a review. JAMA Cardiol. 2021;6:341–9.
31. Visser CA, Kan G, David GK, Lie KI, Durrer D. Echocardiographic-cineangiographic correlation in detecting left ventricular aneurysm: a prospective study of 422 patients. Am J Cardiol. 1982;50:337–41.
32. Catherwood E, Mintz GS, Kotler MN, Parry WR, Segal BL. Two-dimensional echocardiographic recognition of left ventricular pseudoaneurysm. Circulation. 1980;62:294–303.
33. Barrett MJ, Charuzi Y, Corday E. Ventricular aneurysm: cross-sectional echocardiographic approach. Am J Cardiol. 1980;46:1133–7.
34. Matsumoto M, Watanabe F, Goto A, Hamano Y, Yasui K, Minamino T, et al. Left ventricular aneurysm and the prediction of left ventricular enlargement studied by two-dimensional echocardiography: quantitative assessment of aneurysm size in relation to clinical course. Circulation. 1985;72:280–6.
35. Jordan RA, Miller RD, Edwards JE, Parker RL. Thromboembolism in acute and healed myocardial infarction: intracardiac mural thrombosis. Circulation. 1952;6:1–6.
36. Rueda B, Panidis IP, Gonzales R, McDonough M. Left ventricular pseudoaneurysm: detection and postoperative follow-up by color Doppler echocardiography. Am Heart J. 1990;120:990–2.
37. Drobac M, Gilbert B, Howard R, Baigrie R, Rakowski H. Ventricular septal defect after myocardial infarction: diagnosis by two-dimensional contrast echocardiography. Circulation. 1983;67:335–41.
38. Smyllie JH, Sutherland GR, Geuskens R, Dawkins K, Conway N, Roelandt JR. Doppler color flow mapping in the diagnosis of ventricular septal rupture and acute mitral regurgitation after myocardial infarction. J Am Coll Cardiol. 1990;15:1449–55.
39. Chirillo F, Totis O, Cavarzerani A, Bruni A, Risica G, Cuzzato V. Transesophageal echocardiographic findings in partial and complete papillary muscle rupture complicating acute myocardial infarction. Cardiology. 1992;81:54–8.
40. Koenig K, Kasper W, Hofmann T, Meinertz T, Just H. Transesophageal echocardiography for diagnosis of rupture of the ventricular septum or left ventricular papillary muscle during acute myocardial infarction. Am J Cardiol. 1987;59:362.
41. Barzilai B, Gessler C Jr, Perez JE, Schaab C, Jaffe AS. Significance of Doppler-detected mitral regurgitation in acute myocardial infarction. Am J Cardiol. 1988;61:220–3.
42. Alam M, Thorstrand C, Rosenhamer G. Mitral regurgitation following first-time acute myocardial infarction—early and late findings by Doppler echocardiography. Clin Cardiol. 1993;16:30–4.
43. Izumi S, Miyatake K, Beppu S, Park YD, Nagata S, Kinoshita N, et al. Mechanism of mitral regurgitation in patients with myocardial infarction: a study using real-time two-dimensional Doppler flow imaging and echocardiography. Circulation. 1987;76:777–85.
44. Feldman T, Cilingiroglu M. Percutaneous leaflet repair and annuloplasty for mitral regurgitation. J Am Coll Cardiol. 2011;57:529–37.
45. Franzen O, Baldus S, Rudolph V, Meyer S, Knap M, Koschyk D, et al. Acute outcomes of MitraClip therapy for mitral regurgitation in high-surgical-risk patients: emphasis on adverse valve morphology and severe left ventricular dysfunction. Eur Heart J. 2010;31:1373–81.
46. Swaans MJ, Van den Branden BJ, Van der Heyden JA, Post MC, Rensing BJ, Eefting FD, et al. Three-dimensional transoesophageal echocardiography in a patient undergoing percutaneous mitral valve repair using the edge-to-edge clip technique. Eur J Echocardiogr. 2009;10(8):982–3. Epub Aug 4, 2009
47. Benedetto U, Melina G, Roscitano A, Fiorani B, Capuano F, Sclafani G, et al. Does combined mitral valve surgery improve survival when compared to revascularization alone in patients with ischemic mitral regurgitation? A meta-analysis on 2479 patients. J Cardiovasc Med (Hagerstown). 2009;10:109–14.

48. Steg PG, James SK, Atar D, et al. ESC guidelines for the management of acute myocardial infarction in patients presenting with ST-segment elevation. Eur Heart J. 2012;33:2569–619.
49. Lancellotti P, Price S, Edvardsen T, et al. The use of echocardiography in acute cardiovascular care: recommendations of the European Association of Cardiovascular Imaging and the Acute Cardiovascular. Eur Heart J Acute Cardiovasc Care. 2015;4(1):3–5.
50. Lancellotti P, et al. The use of echocardiography in acute cardiovascular care: recommendations of the European Association of Cardiovascular Imaging and the Acute Cardiovascular Care Association. Eur Heart J Cardiovasc Imaging. 2015;16(2):119–46.
51. Appleton CP, Hatle LK, Popp RL. Relation of transmitral flow velocity patterns to left ventricular diastolic function: new insights from a combined hemodynamic and Doppler echocardiographic study. J Am Coll Cardiol. 1988;12(2):426–40.
52. Montone RA, Niccoli G, Fracassi F, Russo M, Gurgoglione F, Cammà G, et al. Patients with acute myocardial infarction and non obstructive coronaryarteries: safety and prognostic relevance of invasive coronary provocative tests. Eur Heart J. 2018;39:91–8.
53. Montone RA, Jang I-K, Beltrame JF, Sicari R, Meucci MC, Bode M, et al. The evolving role of cardiac imaging in patients with myocardial infarction and non-obstructive coronary arteries. Prog Cardiovasc Dis. 2021;68:78–87.
54. Sucato V, Testa G, Puglisi S, Evola S, Galassi AR, Novo G. Myocardial infarction with non-obstructive coronary arteries (MINOCA): intracoronary imaging-based diagnosis and management. J Cardiol. 2021;77:444–51.
55. Liang K, Nakou E, Del Buono MG, Montone RA, D'Amario D, Bucciarelli-Ducci C. The role of cardiac magnetic resonance in myocardial infarction and non-obstructive coronary arteries. Front Cardiovasc Med. 2022;8:821067.
56. Rossvoll O, Hatle LK. Pulmonary venous flow velocities recorded by transthoracic Doppler ultrasound: relation to left ventricular diastolic pressures. J Am Coll Cardiol. 1993;21(7):1687–96.
57. Bytyci I, Bytyqi S, Abazi G, Bajraktari G, Henein MY. Diagnostic accuracy of non-invasive investigations for coronary artery disease in hypertensive patients: a meta-analysis. Arch Med Sci. 2024;21:167. https://doi.org/10.5114/aoms/188782.
58. Moller JE, Hillis GS, Oh JK, et al. Wall motion score index and ejection fraction for risk stratification after acute myocardial infarction. Am Heart J. 2006;151:419–25.
59. Barbieri A, Bursi F, Mantovani F, Valenti C, Quaglia M, Berti E, et al. Prognostic impact of left ventricular mass severity according to the classification proposed by the American Society of Echocardiography/European Association of Echocardiography. J Am Soc Echocardiogr. 2011;24:1383–91.
60. Berthe C, Pierard LA, Hiernaux M, Trotteur G, Lempereur P, Carlier J, et al. Predicting the extent and location of coronary artery disease in acute myocardial infarction by echocardiography during dobutamine infusion. Am J Cardiol. 1986;58(13):1167–72.
61. Bytyçi I, Bengrid TM, Henein MY. Longitudinal myocardial function is more compromised in cardiac syndrome X compared to insignificant CAD: role of stress echocardiography and calcium scoring. Clin Physiol Funct Imaging. 2022 Jan;42(1):35–42.
62. Sakata Y, Kodama K, Adachi T, Lim YJ, Ishikura F, Fuji H, et al. Comparison of myocardial contrast echocardiography and coronary angiography for assessing the acute protective effects of collateral recruitment during occlusion of the left anterior descending coronary artery at the time of elective angioplasty. Am J Cardiol. 1997;79(10):1329–33.
63. Bytyçi I, Alves L, Alves O, Lopes C, Bajraktari G, Henein MY. Left ventricular myocardial and cavity velocity disturbances are powerful predictors of significant coronary artery stenosis. J Clin Med. 2022;11(20):6185.
64. Marwick TH, Nemec JJ, Pashkow FJ, Stewart WJ, Salcedo EE. Accuracy and limitations of exercise echocardiography in a routine clinical setting. J Am Coll Cardiol. 1992;19(1):74–81.
65. Picano E, Parodi O, Lattanzi F. Comparison of dipyridamole-echocardiography test and exercise thallium-201 for diagnosis of coronary artery disease. Am J Noninv Cardiol. 1989;3:85–92.
66. Sawada SG, Ryan T, Conley MJ, Corya BC, Feigenbaum H, Armstrong WF. Prognostic value of a normal exercise echocardiogram. Am Heart J. 1990;120:49–55.
67. Henein MY, Gibson DG. Normal long axis function. Heart. 1999;81:111–3.
68. Henein M, Lindqvist P, Francis D, Morner S, Waldenstrom A, Kazzam E. Tissue Doppler analysis of age-dependency in diastolic ventricular behaviour and filling: a cross-sectional study of healthy hearts (the Umea General Population Heart Study). Eur Heart J. 2002;23:162–71.
69. Henein MY, Gibson DG. Long axis function in disease. Heart. 1999;81:229–31.
70. Mishra MB, Lythall DA, Chambers JB. A comparison of wall motion analysis and systolic left ventricular long axis function during dobutamine stress echocardiography. Eur Heart J. 2002;23:579–85.
71. von Bibra H, Tuchnitz A, Klein A, Schneider-Eicke J, Schömig A, Schwaiger M. Regional diastolic function by pulsed Doppler myocardial mapping for the detection of left ventricular ischemia during pharmacologic stress testing: a comparison with stress echocardiography and perfusion scintigraphy. J Am Coll Cardiol. 2000;36:444–52.
72. O'Sullivan CA, Henein MY, Sutton R, Coats AJ, Sutton GC, Gibson DG. Abnormal ventricular activation and repolarisation during dobutamine stress echocardiography in coronary artery disease. Heart. 1998;79:468–73.
73. Duncan AM, O'Sullivan CA, Carr-White GS, Gibson DG, Henein MY. Long axis electromechanics during dobutamine stress in patients with coronary artery disease and left ventricular dysfunction. Heart. 2001;86:397–404.
74. Duncan AM, Francis DP, Henein MY, Gibson DG. Limitation of cardiac output by total isovolumic time during pharmacologic stress in patients with dilated cardiomyopathy: activation-mediated effects of left bundle branch block and coronary artery disease. J Am Coll Cardiol. 2003;41:121–8.
75. Duncan AM, Francis DP, Gibson DG, Henein MY. Differentiation of ischemic from nonischemic cardiomyopathy during dobutamine stress by left ventricular long-axis function: additional effect of left bundle-branch block. Circulation. 2003;108:1214–20.
76. Henein MY, Patel DJ, Fox KM, Gibson DG. Asynchronous left ventricular wall motion in unstable angina. Int J Cardiol. 1997;59:37–45.
77. Pierard LA, De Landsheere CM, Berthe C, Rigo P, Kulbertus HE. Identification of viable myocardium by echocardiography during dobutamine infusion in patients with myocardial infarction after thrombolytic therapy: comparison with positron emission tomography. J Am Coll Cardiol. 1990;15:1021–31.
78. Senior R, Lahiri A. Role of dobutamine echocardiography in detection of myocardial viability for predicting outcome after revascularization in ischemic cardiomyopathy. J Am Soc Echocardiogr. 2001;14:240–8.
79. Senior R. Role of contrast echocardiography for the assessment of left ventricular function. Echocardiography. 1999;16(7, Pt 2):747–52.
80. Henein MY, Tossavainen E, A'roch R, Söderberg S, Lindqvist P. Can Doppler echocardiography estimate raised pulmonary capillary wedge pressure provoked by passive leg lifting in suspected heart failure? Clin Physiol Funct Imaging. 2019;39:128–34.

81. Meza MF, Ramee S, Collins T, Stapleton D, Milani RV, Murgo JP, et al. Knowledge of perfusion and contractile reserve improves the predictive value of recovery of regional myocardial function postrevascularization: a study using the combination of myocardial contrast echocardiography and dobutamine echocardiography. Circulation. 1997;96:3459–65.
82. Picano E, Pierard L, Peteiro J, Djordjevic-Dikic A, Sade LE, et al. Eur The clinical use of stress echocardiography in chronic coronary syndromes and beyond coronary artery disease: a clinical consensus statement from the European Association of Cardiovascular Imaging of the ESC. Heart J Cardiovasc Imaging. 2024;25:e65–90.
83. Bytyçi I, Alves L, Alves O, Lopes C, Bajraktari G, Henein MY. Left ventricular myocardial and cavity velocity disturbances are powerful predictors of significant coronary artery stenosis. J Clin Med. 2022;11:6185.
84. Henein MY, Lindqvist P. Diastolic function assessment by echocardiography: a practical manual for clinical use and future applications. Echocardiography. 2020;37:1908–18.
85. Henein MY, Amadi A, O'Sullivan C, Coats A, Gibson DG. ACE inhibitors unmask in coordinate diastolic wall motion in restrictive left ventricular disease. Heart. 1996;76:326–31.
86. Brecker SJ, Xiao HB, Sparrow J, Gibson DG. Effects of dual-chamber pacing with short atrioventricular delay in dilated cardiomyopathy. Lancet. 1992;340(8831):1308–12.
87. Henein MY, Priestley K, Davarashvili T, Buller N, Gibson DG. Early changes in left ventricular subendocardial function after successful coronary angioplasty. Br Heart J. 1993;69:501–6.
88. Koh TW, Carr-White GS, DeSouza AC, Ferdinand FD, Pepper JR, Gibson DG. Effect of coronary occlusion on left ventricular function with and without collateral supply during beating heart coronary artery surgery. Heart. 1999;81:285–91.

Stress Echocardiography

8

Eugenio Picano and Lauro Cortigiani

Introduction

Stress echocardiography (SE) with the ABCDE protocol integrates comprehensive echocardiography with physical, pharmacological, or electrical pacing stress to assess the functional reserves of the heart [1]. Stress-induced regional wall motion abnormality (RWMA) serves as an early and specific marker of ischemia resulting from epicardial artery stenosis. However, ischemia may also manifest without RWMA, particularly in the presence of open coronary arteries. Ideally, a cardiovascular functional test assesses more globally the different vulnerabilities of the patient, extending well beyond the epicardial coronary artery stenosis and including a dynamic evaluation of the heart-lung unit, cardiac diastolic and systolic left ventricular (LV) function potentially altered by myocardial fibrosis or necrosis, coronary microcirculation, and the cardiac autonomic balance.

From Epicardial Artery Stenosis to Patient Vulnerability

Beyond RWMA, additional markers are valuable to capture the diverse phenotypes of myocardial ischemia and patient vulnerability. With the comprehensive ABCDE protocol, the focus shifts from coronary stenosis to the vulnerable patient and evaluates multiple aspects of patient susceptibility to disease, from epicardial coronary artery reserve (step A) to diastolic reserve and pulmonary congestion (step B), global LV systolic contractile reserve impaired by myocardial ischemia, fibrosis or necrosis (step C), coronary microvascular dysfunction in step D (by Doppler), and cardiac sympathetic autonomic reserve in step E by heart rate with ECG (Fig. 8.1).

Conceptually, ABCDE-SE scans five independent and complementary pathophysiological targets each independently contributing to the overall vulnerability profile of the patient (Fig. 8.2).

Semantically, the five steps are also linked to the underlying imaging modality or main sign. Step A remains the first and most important and stands for abnormality of regional function. Step B indicates B-lines assessed by lung ultrasound scan (LUS). Step C is the LV contractile reserve evaluated by volumetric echocardiography, with mandatory quantitative assessment of end-diastolic volume (EDV) and end-systolic volume (ESV) of the LV. Step D is the Doppler-based assessment of coronary flow velocity reserve (CFVR) in the mid-distal left anterior descending (LAD) artery. Step E is the imaging-independent assessment of heart rate reserve (HRR) and ECG changes by electrocardiogram (ECG).

E. Picano (✉)
University Clinical Center of Serbia, Belgrade, Serbia

L. Cortigiani
San Luca Hospital, Lucca, Italy

© The Author(s), under exclusive license to Springer Nature Switzerland AG 2025

M. Y. Henein (ed.), *Clinical Echocardiography*, https://doi.org/10.1007/978-3-031-95894-6_8

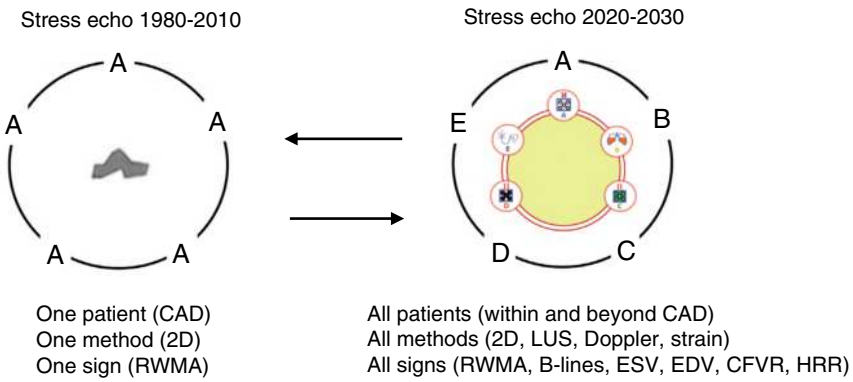


Fig. 8.1 The conceptual approach of advanced SE: from vulnerable stenosis to vulnerable patient. Left panel: In the classical or conventional approach used for 40 years, SE solely focused on the hemodynamic significance of coronary stenosis. Right panel: The advanced ABCDE protocol employed in the last 5 years shifts the focus to the patient as a whole, assessing vulnerability to ischemia (step A with RWMA), pulmonary congestion (step B), LV contractile and preload reserve (step C), coronary microcirculation (step D), and chronotropic reserve (step E). (Reproduced under an open-access Creative Common CC BY license from the article by Picano et al. [5])

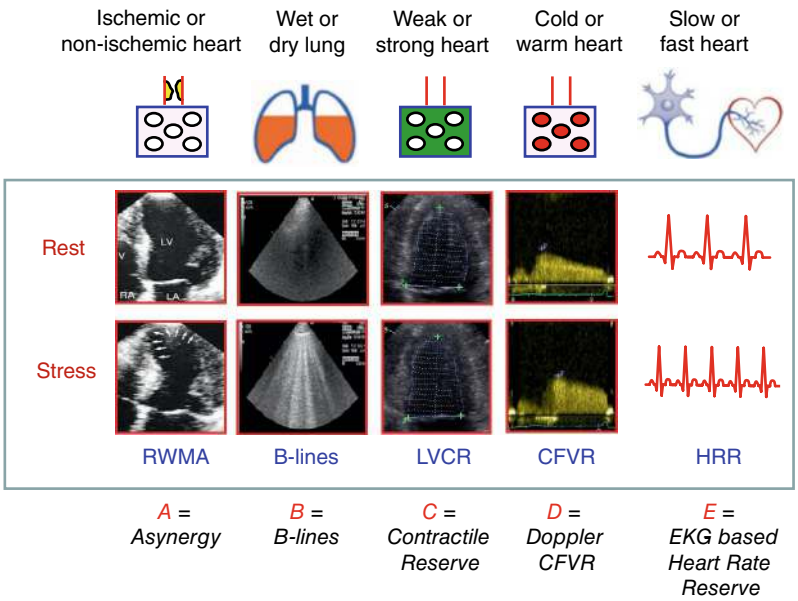


Fig. 8.2 The targets of integrated ABCDE-SE. The 5 pathophysiological targets of ABCDE-SE: epicardial coronary artery stenosis and inducible ischemia (with RWMA), step A; lung water and diastolic function (with B-lines), step B; myocardial functional reserve (with ESV reduction for systolic reserve and EDV increase for diastolic reserve), step C; coronary microcirculatory function (with CFVR), step D; cardiac autonomic balance and sympathetic reserve (with HRR), step E. (Reproduced under open access Creative Common CC BY license from the article by Picano et al. [5])

Methodology

General Test Protocol

During SE, a 12-lead ECG and cuff blood pressure are recorded in resting condition and each minute throughout the examination. Imaging biomarkers must always complement and integrate clinical, electrocardiographic, and blood pressure changes during stress (Fig. 8.3).

ABCDE protocol is based on four imaging (ABCD) and one non-imaging, electrocardiographic step (step E) (Table 8.1).

Diagnostic endpoints of SE include maximum workload (for exercise testing) or maximum dose (for pharmacological), achievement of target heart rate, echocardiographic positivity (akinesis of >2 out of 17 LV segments), severe chest pain, or electrocardiographic positivity (>2 mV ST-segment shift). Submaximal nondiagnostic endpoints are non-tolerable symptoms or asymptomatic side effects such as hypertension (systolic blood pressure >220 mmHg or diastolic blood pressure >120 mmHg), symptomatic hypotension (>40 mmHg drop in blood pressure), supraventricular arrhythmias (supraventricular tachycardia or atrial fibrillation), and complex ventricular arrhythmias (ventricular tachycardia or frequent, polymorphic premature ventricular beats) [2, 4].

A fully normal ABCDE response is shown in Fig. 8.4.

A fully abnormal ABCDE response is shown in Fig. 8.5.

Step A Analysis of the study is usually performed using a 17-segment model of the LV [2]. Regional wall motion is

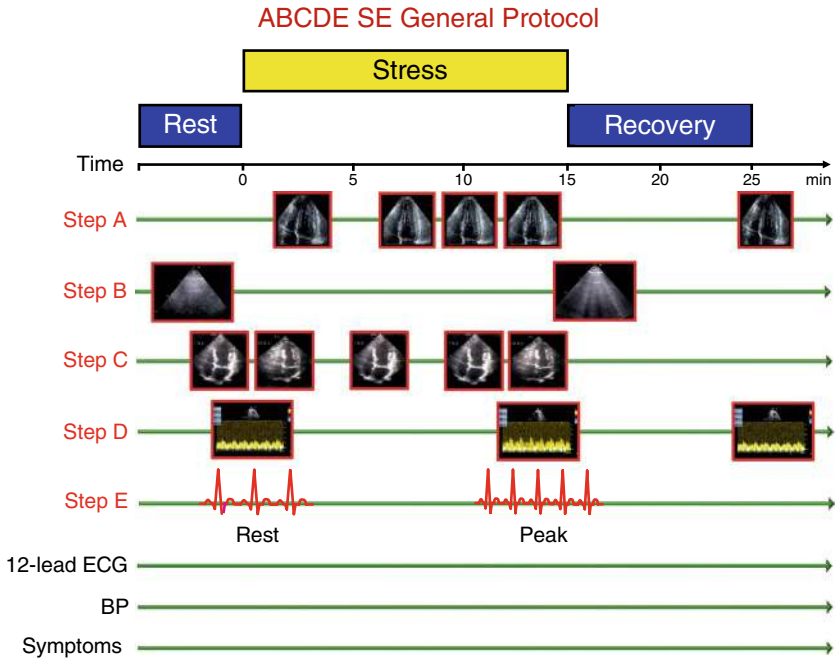


Fig. 8.3 The ABCDE-SE protocol. The completion of the test from the preparation phase to the written response takes about 30′. The recovery phase is optional and advised in presence of test positivity. Step A and step C require the very same images. Step E requires only one ECG lead. Step B can be completed in the early (<30 s) recovery phase. Intermittent imaging of the LAD flow is performed at rest and peak stress with the same transducer used for continuous 2-dimensional imaging (2DE) of wall motion. BP, blood pressure; CFVR, coronary flow velocity reserve; ECG, electrocardiogram; LUS, lung ultrasound scan; RWMA, regional wall motion abnormalities; SE, stress echocardiography. (Reproduced under open access Creative Common CC BY license from the article by Picano et al. [5])

Table 8.1 General test protocol

	Technique	Stress timing	Parameter	Meaning
Step A	2D	Peak	WMSI	Regional LV systolic function
Step B	LUS	Early post	B-lines	PCWP+CVP
Step C	Volumetric 2D	Peak	EDV, ESV	Global LV systolic function
Step D	Color+PWD	Peak	Diastolic-CFV	Coronary microvascular function
Step E	ECG	Peak	Heart rate	ANS

ANS autonomic nervous system, *CMF* coronary microvascular function, *CVP* central venous pressure, *PCWP* pulmonary capillary wedge pressure

semiquantitatively graded from 1 to 4 as follows: 1 = normal or hyperkinetic; 2 = hypokinetic; 3 = akinetic; 4 = dyskinetic. Dividing the sum of individual segment scores by the number of interpretable segments gives the wall motion score index [2, 4]. In the normal response, the wall motion score index is 1.0 at rest and peak stress (Fig. 8.4). In the ischemic response, the wall motion score index is higher at peak stress compared to rest, with RWMA involving at least 2 contiguous segments (Fig. 8.5). A viable segment with akinesis at rest is normal during stress. A necrotic segment shows an

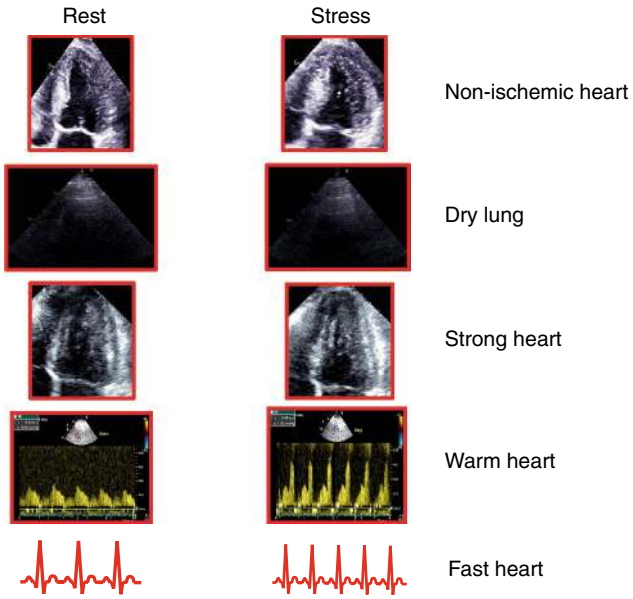


Fig. 8.4 The fully normal ABCDE-SE response. From top to bottom, the five different ABCDE steps of SE with a fully normal response from rest (left column) to stress (right column). The normal response is shown for a non-ischemic (step A) heart, without pulmonary congestion (step B), with a normal reduction in end-systolic volume (step C), the normal increase in coronary flow velocity (step D), and heart rate (step E) during stress. (Modified and adapted from Picano et al. [7] http://creativecommons.org/licenses/by/4.0/)

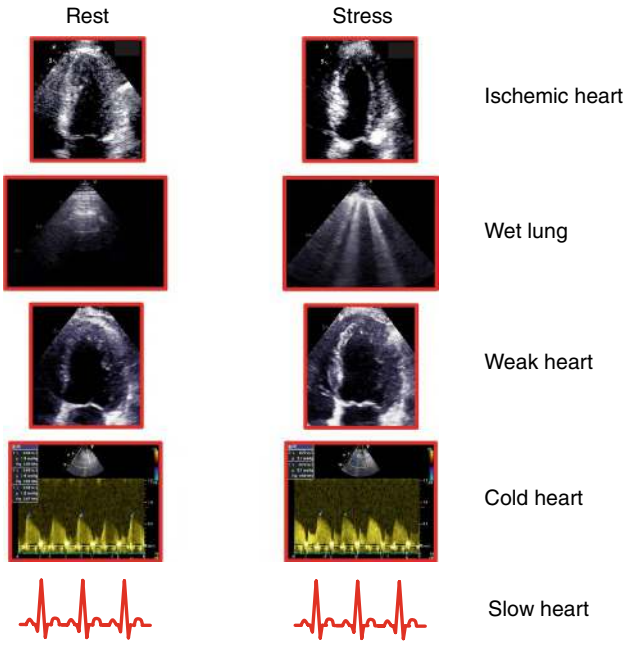


Fig. 8.5 The fully abnormal ABCDE-SE response. From top to bottom, the five different ABCDE steps of SE with a fully abnormal response from rest (left column) to stress (right column). The abnormal response is shown for an ischemic RWMA (step A), with pulmonary congestion and B-lines (step B), lack of reduction of end-systolic volume (step C), blunted increase in coronary flow velocity (step D), and modest increase in heart rate (step E) during stress. (Modified and adapted from Picano et al. [7]. http://creativecommons.org/licenses/by/4.0/)

abnormal, fixed wall motion abnormality at rest and during stress. The presence of inducible RWMA is associated with a reduction of fractional flow reserve. Step A abnormality can be considered an index of altered epicardial coronary artery flow reserve.

Step B Patients are examined with the cardiac transducer. A four-site simplified scan is adopted. Scanned regions are two per side on the right and left hemithorax in the third intercostal space. LUS starts from the mid-axillary line to the anterior axillary line and from the anterior axillary to the mid-clavicular line. LUS is performed at rest and in the 1 min during the early recovery phase. The highest number of B-lines in each single intercostal space is counted and then summed across all four spaces. Each site has a possible score from 0 (black lung, horizontal A-lines) to 10 (white lung, coalescing B-lines). The cumulative number of stress B-lines across all 4 sites are categorized as absent (score points 0–1); mild (2–4); moderate (5–9); and severe (≥10 points). LUS imaging quality remains unchanged during stress [2]. In the normal response, LUS shows normal horizontal A-lines at rest and peak stress (Fig. 8.4). An increase in B-lines from rest to stress ≥2 is a criterion of positivity with all stresses (Fig. 8.5). The stress-induced increase of B-lines is directly related to the amount of pulmonary congestion and extravascular lung water, due to either an increase in pulmonary capillary wedge pressure (in left heart failure) or an increase in central venous pressure (in right heart failure), or both. Step B abnormality can be considered an index of altered LV diastolic reserve.

Step C Quantitative volumetric echocardiography is required for the assessment of LV global contractility with force, also known as elastance, and calculated as the ratio of systolic blood pressure by cuff sphygmomanometer divided by end-systolic volume (ESV) of the LV. LV end diastolic volume (EDV) is also measured. The method of choice is Simpson's biplane, but an apical single plane or even linear method in non-distorted LV is useful. Measurements are made much easier, faster, and more reproducible with automated methods based on artificial intelligence and measuring in real-time EDV and ESV. Force (also known as LV elastance) is measured as systolic blood pressure/ESV. The rest-to-stress change in force (also known as ventricular elastance) is an index of LV contractile reserve, with the normal response characterized by a decrease in ESV with an increase in systolic blood pressure, indicating a normal hypercontractile response. A change of step C, with a reduced systolic reserve, can be observed in the absence of RWMA. The abnormal cut-off is stress-dependent and higher for stronger inotropic stresses like exercise and dobutamine (abnormal <1.8) compared to weaker vasodilator stresses (abnormal <1.2) [2]. An increase in LV contractile reserve (LVCR) with a reduction of ESV from rest to stress is the normal response with all stresses (Fig. 8.4). An increase in ESV from rest to stress is abnormal with all stresses (Fig. 8.5). The rest to-stress change in EDV is an index of preload reserve, with the normal response characterized by an increase of EDV at intermediate stages of stress, before marked tachycardia. The reduction of LV contractile reserve is directly related to the amount of myocardial ischemia, fibrosis, or necrosis.

Step D Coronary flow in the mid-distal portion of the LAD is imaged from the low parasternal long-axis view and/or modified three-chamber view under the guidance of colour-Doppler flow mapping. Coronary flow velocity by pulsed-wave Doppler assessment is biphasic, with a lower peak during systole and a higher peak during diastole when myocardial extravascular resistance is lowest. Vendor-specific settings are pre-adjusted to optimize coronary flow imaging, and color flow velocity is best set at 20–30 cm/s, with wall motion filters off. Peak diastolic flow is the simplest and the easiest parameter to obtain, with about 95% feasibility [2]. In the normal response, rest coronary flow velocity in the LAD increases at least two-fold during stress (Fig. 8.4). An increase in coronary flow velocity from rest to stress ≤2.0 is a criterion of positivity with all stresses (Fig. 8.5). The reduc-

tion of coronary flow velocity reserve (CFVR) is due to epicardial critical coronary artery stenosis or coronary microvascular dysfunction. In the presence of angiographically normal coronary arteries, Step D abnormality can be considered an index of reduced coronary microvascular reserve.

Imaging-independent step E Step E is named from an ECG and measures the peak stress/rest ratio of heart rate. The higher the value of chronotropic reserve the better the cardiac sympathetic reserve. The abnormal cut-off is stress-dependent, and higher for exercise and dobutamine compared to vasodilator stresses. A normal increase in HRR is >1.80 for exercise or dobutamine, and >1.22 for vasodilators (Fig. 8.4). Step E abnormality (Fig. 8.5) can be considered an index of reduced cardiac sympathetic reserve and cardiac autonomic dysfunction.

In contemporary populations studied on therapy and with a low pre-test probability of disease and several comorbidities, the positivity rate of RWMA dropped off and the diagnostic accuracy decreased [2]. With the ABCDE protocol, a significant CAD is often found in the absence of RWMA, and with solitary phenotypes (only one sign present) of the other steps. The presence of organic CAD is more likely with more advanced ABCDE scores ≥3 [6].

Specific Test Protocols

Exercise, dobutamine, vasodilators, and pacing are the most commonly utilized stressors for echocardiographic testing:

1. *Exercise:* Exercise echocardiography can be conducted using either a treadmill or bicycle protocol. In a treadmill test, scanning during exercise may not always be feasible, thus post-exercise imaging is typically relied upon. Bicycle exercise SE can be performed in either an upright or recumbent posture [2–4].
2. *Dobutamine:* The standard dobutamine stress protocol involves continuous intravenous infusion of dobutamine in 3-min increments, starting at 5 μg/kg/min and incrementally increasing to 10, 20, 30, and 40 μg/kg/min. If no endpoint is reached, atropine (up to 1 mg) may be added to the 40 μg/kg/min dobutamine infusion. For applications beyond CAD, such as aortic stenosis or heart failure, lower doses (maximum 20 μg/kg/min), longer steps (5 min instead of 3), and no atropine are recommended [2–4].
3. *Dipyridamole:* The standard dipyridamole protocol involves an intravenous infusion of 0.84 mg/kg over 6 min. Aminophylline should be readily available for immediate administration in case of adverse dipyridamole-related events and is routinely infused at the end of the test regardless of the result [2–4].
4. *Adenosine:* Adenosine is typically infused at a maximum dose of 140 μg/kg/min over 6 min. If intolerable side effects occur, dose down-titration is an option [2–4].
5. *External Pacing:* The presence of a permanent pacemaker enables the conduct of a pacing stress test in a completely noninvasive manner by externally programming the pacemaker to increase frequencies. Pacing is initiated at 100 bpm and increased by 10 bpm every 2 min until reaching the target heart rate or other standard endpoints [2]. A limiting factor, however, is that some pacemakers cannot be programmed to reach the target heart rate.

Coronary vasospasm is a cause of ischemia with normal coronary arteries during exercise or dobutamine, and more rarely after aminophylline administration with dipyridamole and causes 10% of false positive results, with true ischemia and RWMA with open coronary arteries [8, 9]. The selective tests for coronary vasospasm are ergonovine and hyperventilation. Ergonovine echocardiography is very useful in well-selected patients with angina, normal coronary arteries, and negative stress tests [10, 11]. During hyperventilation, a reduction of coronary flow velocity despite the increase in heart rate and systolic blood pressure is suggestive of coronary microvascular or epicardial vasospasm [12] The risks of vasospasm testing outside the catheterization laboratory testing should be weighed against the risks of missing the diagnosis of a potentially life-threatening disease. Vasospasm may cause myocardial infarction, unstable angina, and sudden death, if unrecognized and especially if treated with beta-blockers, which may exacerbate vasospastic vulnerability by blocking beta-2 adrenergic receptor-mediated coronary vasodilation and leaving vasoconstrictor alpha-1 tone unopposed.

Prognostic Value

Each of the five steps has independent and incremental value over the other steps and can be further titrated into a mild, moderate, or severe abnormality according to predetermined cutoff values (Table 8.2). This approach considerably expands the potential of SE, previously based exclusively on the site, extent, and severity of wall motion abnormalities summarized in the peak wall motion score index value. The positivity rate and the negative predictive value of a test based only on RWMA sharply declined in the last four decades [13]. This negative predictive value for all-cause death sharply increases when test negativity for RWMA is combined with the negativity of other steps [14–23].

In patients with chronic coronary syndromes and heart failure, the risk stratification is especially efficient with a

Table 8.2 Criteria of severity for risk stratification with vasodilator ABCDE protocol

	Lowest risk	Mild risk	Moderate risk	Severe risk
Step A-WMSI	1.0	1.08–1.29	1.30–1.69	≥1.70
Step B-Blines	0–1	2–4	5–9	≥10
Step C-LVCR[a]	>1.20	1.10–1.20	1.0–1.09	≤1.0
Step D-CFVR	>2.61	2.17–2.60	1.81–2.16	≤1.80
Step E-HRR[a]	>1.41	1.27–1.40	1.16–1.26	≤1.15
ABCDE score	0	1	2–3	4–5

[a]Values for step C and step E are stress-dependent, with higher cutoff values for exercise and dobutamine (abnormal <1.80). WMSI, wall motion score index

simple cumulative ABCDE score (from 0, all steps normal, to 5, all steps abnormal). The annual mortality rate is <0.5% in patients with a score of 0 and increases progressively to 10-fold higher values in patients with a score of 5 [23].

SE Outside Coronary Artery Disease

ABCDE protocol is a core protocol suitable for all patients and all stresses, and in specific cases, it can be further integrated by the assessment of specific structures and functions with additional patient-tailored steps. Current guidelines support the use of SE with seven key markers in various clinical scenarios (Table 8.3):

1. RWMA: Employed in chronic coronary syndromes, heart transplant recipients for rejection monitoring, Kawasaki disease, detection of coronary anomalies, and post-switch operation ischemia assessment.
2. CFVR: Utilized in patients with INOCA.
3. E/e′ Ratio: Applied in diastolic SE for evaluating heart failure with preserved ejection fraction.
4. Tricuspid Regurgitant Velocity Jet: Employed in diastolic SE, valvular heart disease, and pulmonary hypertension assessment.
5. Transvalvular Gradient Assessment with Simultaneous Stroke Volume Reserve Evaluation: Indicated in low-flow, low-gradient aortic stenosis with reduced ejection fraction to assess severity and contractile reserve.
6. LV Outflow Tract Obstruction and mitral regurgitation in Hypertrophic Cardiomyopathy.
7. Right Ventricular Contractile Reserve in Repaired Tetralogy of Fallot.

Stresses are any (exercise, vasodilator, dobutamine) for induction of RWMA, vasodilator for INOCA, exercise or dobutamine for step R, and dobutamine for low-flow, low-gradient aortic stenosis with reduced ejection fraction to assess severity and contractile reserve. For all other indications, exercise is the only stress, since other stresses such as dobutamine in hypertrophic cardiomyopathy can elicit intraventricular gradients through unphysiological mechanisms and can be both fidangerous and misleading.

Indications, Contraindications, Feasibility, and Safety

Exercise is the only physiological stress modality and the safest. It is the initial choice for SE in all patients capable of exercise [3]. Semi-supine exercise is the most suitable exercise modality for SE, although also the peak treadmill and upright bicycle are excellent choices. Vasodilators are preferred for combined assessment of ischemia and CFVR. Dobutamine is preferred for combined assessment of ischemia and viability, and it is particularly indicated in patients with aortic stenosis and low-flow low-gradient aortic stenosis with reduced LV ejection fraction.

Contraindications to all forms of SE include unstable hemodynamic conditions and symptomatic severe aortic stenosis. Exercise is not indicated in patients unable to exercise maximally and resting systolic blood pressure >180 mmHg. Patients with a history of recent serious atrial or ventricular arrhythmias, or moderate-to-severe hypertension, are unsuitable candidates for dobutamine SE and should be referred for safer vasodilator stress [3]. Patients with a history of bronchospasm or in therapy with anti-asthmatic agents should not undergo vasodilator stress, since adenosine is a bronchoconstrictor, and can be referred to dobutamine, a bronchodilator through its beta-1 receptor agonist activity. Bradyarrhythmias and resting systolic blood pressure <80 mmHg also are a contraindication to vasodilator stress. Atropine coadministration with dobutamine should be avoided in patients with acute angle glaucoma and untreated urinary retention.

Dobutamine carries the highest incidence of limiting side effects (10%) and serious adverse events (1 in 350) [24, 25], with approximately 20% of negative tests associated with troponin elevation [26, 27]. Dipyridamole exhibits the least limiting side effects (5%) and serious adverse events (1 in 700), though patients with bronchospastic tendencies should not receive it. Adenosine, while associated with frequent side effects, has a low incidence of life-threatening complications, such as myocardial infarction, ventricular tachycardia, and shock, with a single fatal myocardial infarction in approximately 10,000 cases. Despite being subjectively less tolerated, adenosine is considered one of the safest pharmacological stress agents [3]. Regadenoson, with its selective stimulation of A2 adenosine receptors, is employed for selective assessment of CFVR with fewer side effects compared to other vasodilators (Table 8.4).

Table 8.3 Specific test protocol outside CAD

	Technique	Disease	Parameter	Meaning
Step F	Color	CCS,HF,HCM,VHD	MR grade	MR severity
Step G	CW-Doppler	HCM,VHD	LVOTG,valvular gradient	Intraventricular or transvalvular gradient
Step L	2D, Strain	VHD, HF	LAVI, LASr	LA myopathy
Step P	CW-Doppler	Pulmonary hypertension	SPAP from TRV	Pulmonary hemodynamics
Step R	M-mode	Right heart failure	TAPSE	RV reserve

ANS autonomic nervous system, *CCS* chronic coronary syndromes, *CMF* coronary microvascular function, *CVP* central venous pressure, *CW* continuous wave, *HCM* hypertrophic cardiomyopathy, *HF* heart failure, *LASr* left atrial strain of the reservoir phase, *LA* left atrium, *LAVI* left atrial volume index, *LVOTG* LV outflow tract gradient, *MR* mitral regurgitation, *PCWP* pulmonary capillary wedge pressure, *RV* right ventricular, *SPAP* systolic pulmonary artery pressure, *TAPSE* tricuspid annular plane systolic excursion, *TRV* tricuspid regurgitant velocity, *VHD* valvular heart disease

Table 8.4 Specific test indications and contraindication

	Indication	Contraindication	Major side effects	Success rate (%)
Exercise	First line	SBP >180 mmHg, submaximal exercise	1 in 1000	85
Dobutamine	Ischemia+Viability	Tachy-Arrhythmias, SBP >180 mmHg	1 in 350	90
Vasodilator	Ischemia+CFVR	Low BP, asthma, bradyarrhythmias	1 in 700	95
Pacing	Permanent AAI-or DDD-PM	None	1 in 2000	95
Ergonovine	Suspect vasospasm	High BP	1 in 350	98

BP blood pressure, *SBP* systolic blood pressure

Competence

The interpretation of SE demands extensive expertise in echocardiography and should exclusively be conducted by physicians with specialized training in the technique [3]. The diagnostic accuracy achieved by an experienced echocardiographer who is inexperienced in SE is comparable to chance outcomes [28]. Nonetheless, proficiency in SE can typically be attained after conducting approximately 100 studies, allowing individuals to reach a plateau of diagnostic accuracy [29]. The training load can be higher for CFVR, with around 200 studies [30]. Given the potential for life-threatening complications associated with stress testing, both the cardiologist and attending nurse should hold certifications in Basic and Advanced Life Support [31].

The advent of artificial intelligence software facilitates the automatic or semi-automatic provision of LV volumes for step C. B-lines are straightforward to acquire and analyze. Step D is more difficult to acquire and easier to analyze than RWMA. Step E, characterized by operator independence, is automatically provided by modern echo machines (Table 8.5).

Prior experience in resting echocardiography and LUS is indispensable before embarking on SE. The fundamental skills needed for imaging the heart and lungs under resting conditions are largely transferrable to stress imaging scenarios. Infrastructure and proficiency in cardiac resuscitation are imperative. The utilization of exercise and pharmacological stress agents mandates a fundamental understanding of their mechanisms of action, safety profiles, anticipated side effects, and antidotes. Notably, superior SE outcomes are achieved when basic standard equipment is operated by individuals with extensive experience, compared to advanced standard equipment in the hands of novices [31].

Table 8.5 Competency in ABCDE SE

	Training (studies)	Maintenance (per year)	Imaging difficulty	Analysis complexity
Step A	100	50	Moderate	Moderate
Step B	25	25	Low	Low
Step C	25	25	Moderate	Moderate
Step D	200	50	High	Low
Step E	10	10	Nil	Nil

The Use of Ultrasound-Enhancing Agents and New Technologies

The inclusion of ultrasound-enhancing agents (UCA) enhances the quality of echocardiographic images for assessing RWMA, EDV, ESV, and occasionally CFVR. Myocardial perfusion imaging holds significant clinical promise, albeit lacking approval from regulatory bodies such as the Food and Drug Administration and the European Medicines Agency. The advantages of UCA must be weighed against additional costs ranging from 25 to 50 dollars per examination and heightened risk. Safety assessment must consider minor side effects occurring in 1 out of 100 cases, including headaches or back pain due to microembolism, and major,

life-threatening complications occurring in 1 out of 10,000 cases, such as anaphylactic reactions. Anaphylactic reactions can arise from complement-activated pseudo-allergy (CARPA) for all UCAs or immediate hypersensitivity responses to the polyethylene glycol (PEG) component found in the excipients of Sonovue and Lumify (absent in Optison). All UCAs entail potential environmental ramifications. The gas within the bubbles comprises either perfluoropropane or sulfur hexafluoride, both categorized as greenhouse gases with perfluoropropane persisting for 9250 years and sulfur hexafluoride for 25,200 years. Consequently, greenhouse gas emissions during production and utilization are noteworthy, although the contrast agents utilized per examination are minimal with a modest per patient and global environmental impact.

Among emerging technologies, global longitudinal strain remains stable at heart rates below 110 beats per minute, providing valuable insights into global LV systolic reserve under vasodilator stress, low-level exercise, and low-dose dobutamine. A stress-induced absolute increase in the global longitudinal strain ≤2 is deemed abnormal. Additionally, peak atrial longitudinal strain can offer informative data, with a reduction during stress or a subnormal increase (less than 10%) indicating abnormality and potentially aiding in the characterization of left atrial function during stress. Real-time three-dimensional echocardiography surpasses two-dimensional methods in accuracy for volumetric echocardiography and is especially valuable for step C assessment, necessitating ESV for contractile reserve evaluation and EDV for preload reserve assessment.

Artificial Intelligence holds promise in revolutionizing diagnostic assessment and data management across all domains, mitigating operator reliance on image acquisition and analysis.

Comparison with Other Imaging Techniques

Current guidelines recommend the utilization of functional testing based on local expertise and physician preference [32, 33]. While this approach is pragmatic and inevitable, it overlooks three crucial considerations that have garnered increasing significance for healthcare policymakers and patients: the economic, radiological, and environmental sustainability of medical procedures [34]. SE emerges as a markedly more cost-effective option compared to alternative techniques, with a direct cost approximately tenfold lower than that of positron emission tomography stress tests. Moreover, SE entails no radiation exposure, unlike the radiation associated with cardiac positron emission tomography equivalent to 150 chest X-rays or single-photon emission tomography scintigraphy equivalent to 500 chest X-rays exposure in a single session [35] (Table 8.6). As a comparison, the cost of a coronary CT adopted as the standard for an anatomy-driven approach is two-fold that of a SE, with a radiation dose of about 200 chest X-rays and a carbon cost of about 10 kg of CO_2 equivalent emissions.

The radiation issue aspect holds particular significance in cardiology, given that patients undergo repetitive testing involving imaging and invasive fluoroscopy procedures, some of which entail considerable radiation exposure (Fig. 8.6).

The carbon footprint of SE stands at approximately 1 kg of carbon dioxide emissions per examination, contrasting starkly with the 50-fold higher emissions associated with stress cardiovascular magnetic resonance and the ten-fold higher emissions of nuclear cardiology testing. While individual economic, radiological, and carbon costs per examination may seem modest, they cumulatively contribute to a significant societal burden, including population health implications and environmental impact [34]. As pressure mounts on policymakers and patients for environmentally conscious, sustainable, and safe medical practices, it becomes increasingly challenging to justify diagnostic strategies that overlook these societal considerations [34, 35].

In the context of the triple-bottom-line approach to sustainable healthcare, SE emerges as the preferable initial choice when multiple tests are suitable for a given indication [36].

Table 8.6 Sustainability of functional testing in CAD

	SE	Stress PET	Stress SPECT	Stress-CMR
Economic cost (€)	100	1000	500	500
Radiation cost (Chest X-rays)	0	150	500	0
Carbon cost (CO_2 equivalent)	1	10	10	50

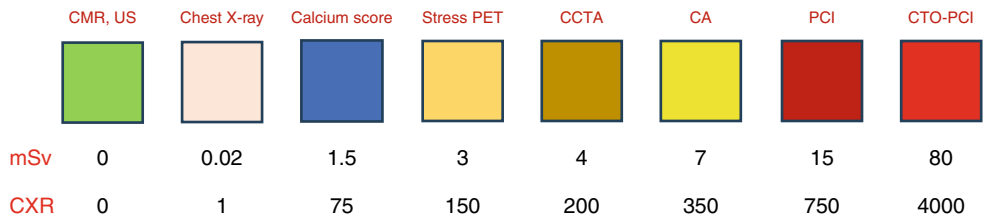


Fig. 8.6 The radiation dose of common cardiac imaging and invasive fluoroscopy procedures. CMR, cardiovascular magnetic resonance; CT, computed tomography; CXR, chest X-rays; CRT, cardiac resynchronization therapy; CTO, chronic total occlusion of coronary artery; NM, nuclear medicine; PCI, percutaneous coronary interventions; PET, positron emission tomography; SPECT, single-photon emission tomography; US, ultrasound. (Redrawn and adapted from original data in Refs. [33, 35]. Reproduced under open access Creative Common CC BY license from the article by Picano et al. [36])

References

1. Picano E. Stress echocardiography. 7th ed. Springer: Heidelberg New York; 2023.
2. Picano E, Pierard L, Peteiro J, Djordjevic-Dikic A, Sade LE, Cortigiani L, et al. The clinical use of stress echocardiography in chronic coronary syndromes and beyond coronary artery disease: a Clinical Consensus Statement from the European Association of Cardiovascular Imaging of the ESC. Eur Heart J Cardiovasc Imaging. 2024;25:e65.
3. Lancellotti P, Pellikka PA, Budts W, Chaudhry FA, Donal E, Dulgheru R, et al. The clinical use of stress echocardiography in non-ischaemic heart disease: recommendations from the European Association of Cardiovascular Imaging and the American Society of Echocardiography. Eur Heart J Cardiovasc Imaging. 2016;17:1191–229.
4. Pellikka PA, Arruda-Olson A, Chaudhry FA, Chen MH, Marshall JE, Porter TR, Sawada SG. Guidelines for performance, interpretation, and application of stress echocardiography in ischemic heart disease: from the American Society of Echocardiography. J Am Soc Echocardiogr. 2020;33:1–41.
5. Picano E, Zagatina A, Wierzbowska-Drabik K, Borguezan Daros C, D'Andrea A, Ciampi Q. Sustainability and versatility of the ABCDE protocol for stress echocardiography. J Clin Med. 2020;9:3184.
6. Gaibazzi N, Ciampi Q, Cortigiani L, Wierzbowska-Drabik K, Zagatina A, Djordjevic-Dikic A, et al. Stress Echo 2030 Study Group. Multiple phenotypes of chronic coronary syndromes identified by ABCDE stress echocardiography. J Am Soc Echocardiogr. 2023;S0894-7317(23):00652–1.
7. Picano E, Ciampi Q, Wierzbowska-Drabik K, et al. The new clinical standard of integrated quadruple stress echocardiography with ABCD protocol. Cardiov Ultrasound. 2018;16:22.
8. Mansencal N, El Hajjaji I, El Mahmoud R, Digne F, Dubourg O. Prevalence of coronary artery spasm during dobutamine stress echocardiography. Am J Cardiol. 2012;109:800–4.
9. Picano E, Lattanzi F, Masini M, Distante A, L'Abbate A. Aminophylline termination of dipyridamole stress as a trigger of coronary vasospasm in variant angina. Am J Cardiol. 1988;62(10 Pt 1):694–7.
10. Song JK, Lee SJ, Kang DH, Cheong SS, Hong MK, Kim JJ, et al. Ergonovine echocardiography as a screening test for diagnosis of vasospastic angina before coronary angiography. J Am Coll Cardiol. 1996;27:1156–61.
11. Om SY, Yoo SY, Cho GY, Kim M, Woo Y, Lee S, et al. Diagnostic and prognostic value of ergonovine echocardiography for noninvasive diagnosis of coronary vasospasm. JACC Cardiovasc Imaging. 2020 Sep;13(9):1875–87.
12. Dikic AD, Dedic S, Jovanovic I, Boskovic N, Giga V, Nedeljkovic I, et al. Stress Echo 2030 study group of the Italian Society of Echocardiography, Cardiovascular Imaging (SIECVI). Noninvasive evaluation of dynamic microvascular dysfunction in ischemia and no obstructive coronary artery disease patients with suspected vasospasm. J Cardiovasc Med (Hagerstown). 2024;25(2):123–31.
13. Cortigiani L, Urluescu ML, Coltelli M, Carpeggiani C, Bovenzi F, Picano E. Apparent declining prognostic value of a negative stress echocardiography based on regional wall motion abnormalities in patients with normal resting left ventricular function due to the changing referral profile of the population under study. Circ Cardiovasc Imaging. 2019;12:e008564.
14. Cortigiani L, Azzolina D, Ciampi Q, Lorenzoni G, Gaibazzi N, Rigo F, Gherardi S, et al. Machine learning algorithms for prediction of survival by stress echocardiography in chronic coronary syndromes. J Pers Med. 2022;12(9):1523.
15. Scali MC, Zagatina A, Ciampi Q, Cortigiani L, D'Andrea A, Daros CB, et al. Stress Echo 2020 Study Group of the Italian Society of Echocardiography and Cardiovascular Imaging. Lung ultrasound and pulmonary congestion during stress echocardiography. JACC Cardiovasc Imaging. 2020 Oct;13(10):2085–95.
16. Cortigiani L, Ciampi Q, Carpeggiani C, Lisi C, Bovenzi F, Picano E. Additional prognostic value of heart rate reserve over left ventricular contractile reserve and coronary flow velocity reserve in diabetic patients with negative vasodilator stress echocardiography by regional wall motion criteria. Eur Heart J Cardiovasc Imaging. 2022;23(2):209–16.
17. Ciampi Q, Zagatina A, Cortigiani L, Gaibazzi N, Borguezan Daros C, Zhuravskaya N, et al. Stress Echo 2020 Study Group of the Italian Society of Echocardiography and Cardiovascular Imaging. Functional, anatomical, and prognostic correlates of coronary flow velocity reserve during stress echocardiography. J Am Coll Cardiol. 2019;74(18):2278–91.
18. Schroder J, Michelsen MM, Mygind ND, Suhrs HE, Bove KB, Bechsgaard DF, et al. Coronary flow velocity reserve predicts adverse prognosis in women with angina and no obstructive coronary artery disease: results from the iPOWER study. Eur Heart J. 2021;42:228–39.
19. Kelshiker MA, Seligman H, Howard JP, Rahman H, Foley M, Nowbar AN, et al. Coronary flow reserve and cardiovascular outcomes: a systematic review and meta-analysis. Eur Heart J. 2022;43(16):1582–93.
20. Elhendy A, Mahoney DW, Khandheria BK, Burger K, Pellikka PA. Prognostic significance of impairment of heart rate response to exercise: impact of left ventricular function and myocardial ischemia. J Am Coll Cardiol. 2003;42(5):823–30.

21. Lauer MS, Mehta R, Pashkow FJ, Okin PM, Lee K, Marwick TH. Association of chronotropic incompetence with echocardiographic ischemia and prognosis. J Am Coll Cardiol. 1998;32(5):1280–6.
22. Cortigiani L, Ciampi Q, Carpeggiani C, Bovenzi F, Picano E. Prognostic value of heart rate reserve is additive to coronary flow velocity reserve during dipyridamole stress echocardiography. Arch Cardiovasc Dis. 2020;113(4):244–51.
23. Ciampi Q, Zagatina A, Cortigiani L, Wierzbowska-Drabik K, Kasprzak JD, et al. Prognostic value of stress echocardiography assessed by the ABCDE protocol. Eur Heart J. 2021;42:3869–78.
24. Varga A, Garcia MA, Picano E. Safety of stress echocardiography (from the international stress Echo complication registry). Am J Cardiol. 2006;98:541–3.
25. Picano E, Mathias W Jr, Pingitore A, Bigi R, Previtali M, on behalf of the EDIC study group. Safety and tolerability of dobutamine-atropine stress echocardiography: a prospective, large scale, multicenter trial. Lancet. 1994;344:1190–2.
26. Samaha E, Avila A, Helwani MA, Ben Abdallah A, Jaffe AS, Scott MG, et al. High-sensitivity cardiac troponin after cardiac stress test: a systematic review and meta-analysis. J Am Heart Assoc. 2019;8:e008626.
27. Medilek K, Zaloudkova L, Borg A, Brozova L, Stasek J. Myocardial injury in stress echo cardiography: comparison of dobutamine, dipyridamole, and dynamic stressors-single center study. Echocardiography. 2022;39:1171–9.
28. Popescu BA, Stefanidis A, Fox KF, Cosyns B, Delgado V, Di Salvo GD, et al. Training, competence, and quality improvement in echocardiography: the EACVI recommenda tions: update 2020. Eur Heart J Cardiovasc Imaging. 2021;21:1305–19.
29. Wiegers SE, Ryan T, Arrighi JA, Brown SM, Canaday B, Damp JB, et al. ACC/AHA/ASE advanced training statement on echocardiography (revision of the 2003 ACC/AHA clinical competence statement on echocardiography): a report of the ACC Competency Management Committee. J Am Soc Echocardiogr. 2019;32:919–43.
30. Michelsen MM, Pena A, Mygind ND, Frestad D, Gustafsson I, Hansen HS, et al. Coronary flow velocity reserve assessed by transthoracic Doppler: the iPOWER study: factors influencing feasibility and quality. J Am Soc Echocardiogr. 2016;29:709–16.
31. Picano E, Ciampi Q, Arbucci R, Cortigiani L, Zagatina A, Celutkiene J, et al. Stress Echo 2030: the new ABCDE protocol defining the future of cardiac imaging. Eur Heart J Suppl. 2023;25(Suppl C):C63–7.
32. Knuuti J, Wijns W, Saraste A, Capodanno D, Barbato E, Funck-Brentano C, et al. ESC Scientific Document Group. 2019 ESC Guidelines for the diagnosis and management of chronic coronary syndromes. Eur Heart J. 2020;41(3):407–77.
33. Gulati M, Levy PD, Mukherjee D, Amsterdam E, Bhatt DL, Birtcher KK, et al. 2021 AHA/ACC/ASE/CHEST/SAEM/SCCT/SCMR Guideline for the Evaluation and Diagnosis of Chest Pain: A Report of the American College of Cardiology/American Heart Association Joint Committee on Clinical Practice Guidelines. J Am Coll Cardiol. 2021;78:e187–285.
34. Picano E. Economic, ethical, and environmental sustainability of cardiac imaging. Eur Heart J. 2023;44(45):4748–51.
35. Picano E, Vañó E, Rehani MM, Cuocolo A, Mont L, Bodi V, Bar O, et al. The appropriate and justified use of medical radiation in cardiovascular imaging: a position document of the ESC Associations of Cardiovascular Imaging, Percutaneous Cardiovascular Interventions and Electrophysiology. Eur Heart J. 2014;35:665–72.
36. Picano E, Vano E. Updated estimates of radiation risk for cancer and cardiovascular disease: implications for cardiology practice. J Clin Med. 2024;13:2066.

Dilated Cardiomyopathy

9

Michael Y. Henein, Ibadete Bytyçi, Mary Sheppard, and John R. Pepper

Dilated cardiomyopathy (DCM) is characterized by left ventricular (LV) or biventricular dilatation, increased end diastolic volume (LVEDV >112 mL/m^2 corrected for age and body surface area), and reduced systolic function (typically ejection fraction <45% and or a fractional shortening <25%), in the absence of coronary artery disease or conditions with pressure/volume overload, e.g. arterial hypertension or valvular heart disease. To enhance specificity, a cut-off of 117 mL/m^2 for LV enlargement was also proposed in familial assessments [1, 2].

Etiology

The causes of DCM can be either genetic or non-genetic;

(a) Genetic—The primary genes associated with a predominant cardiac phenotype. Approximately 20–25% of cases follow an autosomal dominant pattern of inheritance [3].
(b) Familial x-linked cardiomyopathy—This is a familial condition in which the abnormality is in the centromeric half of the dystrophic genome region in the heart. This explains its link to Duchenne muscular dystrophy gene locus [4].
(c) Peri-partum cardiomyopathy—It occurs during pregnancy, usually manifests late in the last trimester, and its prognosis is much better than idiopathic cardiomyopathy [5, 6].
(d) Viral cardiomyopathy—This form of myocardial disease commonly occurs following viral upper respiratory tract infection in adults or gastrointestinal infection in children. Children with viral cardiomyopathy may completely recover and have a better prognosis than adults [7, 8].
(e) Toxic and overload cardiomyopathy—It can be related to alcohol, arsen, cobalt, anabolic/androgenic steroids etc. The risk of these elements is proportional to the entity and the duration of alcohol intake. Despite the severity of impairment of ventricular systolic function, the disease tends to gradually recover after abstinence of alcohol [3].
(f) Endocrinogical diseases—Conditions such as Cushing's diseae, acromegaly, hypo/hyperthyreosis, pheochromocitoma, Adisson disease, etc. may cause myocardial disease and dilated cardiomyopathy [3].
(g) Nutritional deficience—caused by selenium, thiamine, zink, copper and caranitin deficinece may cause dilated cardiomyopathy but they are rare and present in peadiatric patients.
(h) Less common causes include auto-organ antibodies to x and b myosin heavy chain isoform and complicating Acquired Immune Deficiency Syndrome (AIDS) [9, 10].

Hypokinetic non-dilated cardiomyopathy (HNDC) is another condition marked by left ventricular or biventricular global systolic dysfunction without cavity dilation, with LVEF of less than 45%, that cannot be explained by abnormal loading conditions or coronary artery disease. Relatives of individuals with DCM or HNDC are at risk of developing the condition themselves and should undergo clinical, echocardiographic and genetic screening [3, 10].

Supplementary Information The online version contains supplementary material available at https://doi.org/10.1007/978-3-031-95894-6_9.

M. Y. Henein (✉)
Imperial College London, London, UK

Siena University, Siena, Italy
e-mail: m.henein@imperial.ac.uk

I. Bytyçi
Medical Faculty, University of Prishtina, Prishtina, Kosovo

Clinic of Cardiology, University Clincial Centre of Kosovo, Prishtina, Kosovo

M. Sheppard · J. R. Pepper
Royal Brompton Hospital, London, UK

© The Author(s), under exclusive license to Springer Nature Switzerland AG 2025

M. Y. Henein (ed.), *Clinical Echocardiography*, https://doi.org/10.1007/978-3-031-95894-6_9

The myocardial disease and its consequences in DCM may remain silent for a while until it is accidentally discovered on a routine check up or identified following clinical presentation with congestive heart failure (Fig. 9.1) [11].

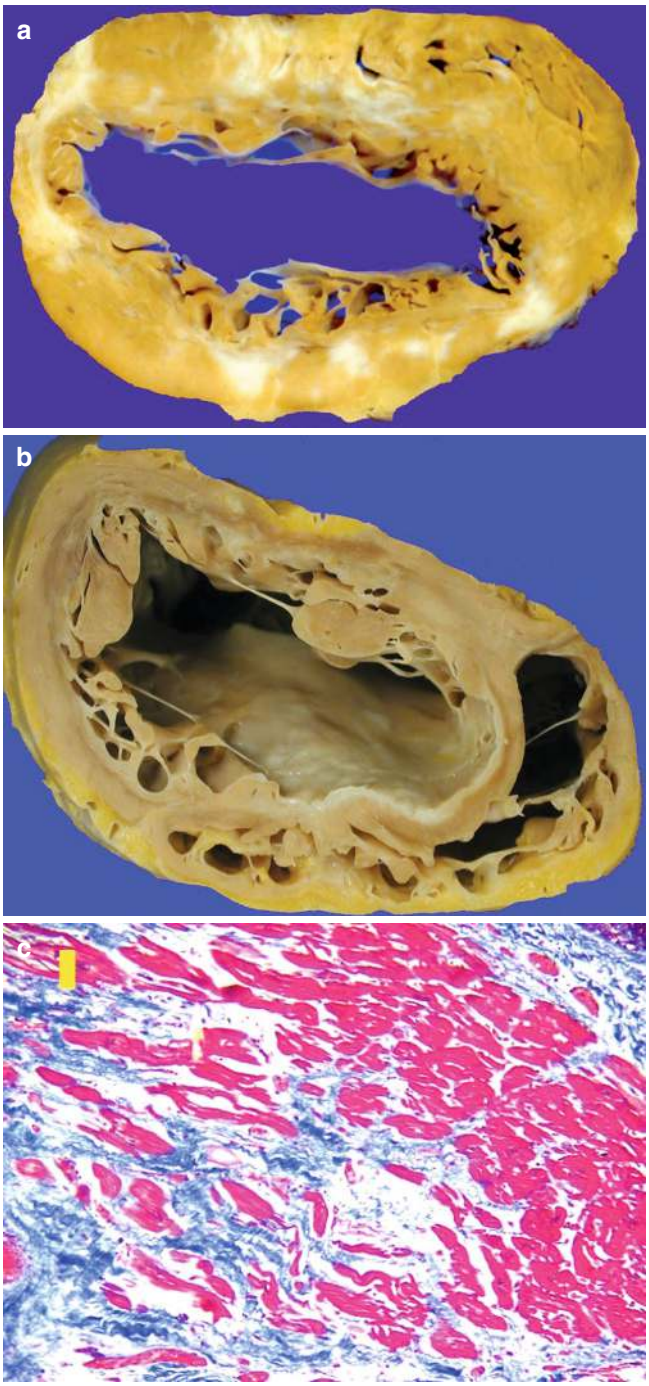


Fig. 9.1 (**a**) Transverse section showing end-stage dilated cardiomyopathy with thin walls and extensive scarring. (**b**) Universal thinning of the left ventricular wall with endocardial thickening. (**c**) Trichrome stain showing myocytes in red and collagen in blue replacing the myocytes

Echocardiographic Finding

Echocardiography remains the key technique for diagnosing and monitoring various heart conditions. It is known for its cost-effectiveness, low risk, and is patient friendly hence its routine use for regular patient follow-up. Furthermore, recent advances in echocardiographic technologies and equipments have significantly improved its performance, reinforcing its advantages over other imaging modalities [12–14]. Table 9.1 provides a summary of the key echocardiographic features associated with DCM [2, 3, 15].

Table 9.1 Echocardiographic findings in dilated cardiomyopathy

Echocardiographic parameters	Cut-off/findings	Note
The main findings		
LV dilatation	LV diameters >2SD from normal according to normo-grams (Z scores >2SD)	Corrected for age and body surface area
LV systolic dysfunction	EF <45% or FSh <25%	Impaired global contractility
Increased LV end-diastolic volume	LVEDV >112 mL/m^2	Corrected for age and body surface area
LV wall thinning	Common finding	
Associated findings		
LV spherical remodelling	Long-axis diameter (L) preserved and transversal (l) increased	Increased sphericity index is common
LV diastolic dysfunction	Restrictive pattern or pseudonormalization of mitral inflow	Indicator of bad prognosis
LV systolic dyssynchrony	Qualitative and quantitative evaluation	A selection criterion for CRT
LV thrombus	May be present	Prognosis and treatment
LA dilatation	LAVI index >34 ml/m^2	Associated with MR, AF
Dilated RV	TAPSE <14 mm, RV FAC <35%	Due to biventricular involvement or PH
Mitral regurgitation	Frequent	Frequent functional MR
Tricuspid regurgitation	Frequent	

Abbreviations: *LA* left atrium, *LV* left ventricle, *EDV* End diastolic volume, *RV* Right ventricle, *MR* Mitral regurgitation, *TR* Tricuspid regurgitation, *AF* Atrial fibrillation, *CRT* Cardiac resynchronization therapy, *LAVI* Left atrium volume indexed, *RV FAC* Right vcentricular fractional area change, *TAPSE* Tricuspid annual plane systolic excursion, *SD* Standard deviation, *PH* pulmonary hypertension

Echocardiographic Main Findings

Ventricular Structure and Function Transthoracic echocardiography (TEE) demonstrates a dilated left ventricle (LV) with increased systolic and diastolic dimensions and reduced systolic function (ejection fraction and or fractional shortening). Besides EF, fractional shortening, dP/dT, and cardiac output, tissue Doppler mitral annulus velocity and speckle tracking deformation in th form of cavity strain are also used parameters for assessing systolic function and are less load dependent [2]. Compared to 2D echocardiography, 3D echocardiography is particularly useful when studying LV shape changes since 3D echocardiography does not rely on a geometric model [2, 3]. There is no definitive echocardiographic picture that depicts different clinical stages of the disease apart from the difference in cavity size [16]. The left ventricular cavity shows globally impaired segmental function with reduced thickening fraction and normal or reduced wall thickness. Patients with DCM may demonstrate localized segmental dysfunction, making a possible definitive differentiation between idiopathic and ischemic etiology difficult [17–20]. Almost 50% of patients with ideopathic dilated cardiomyopathy have clear evidence for segmental wall motion abnormalities. As the disease progresses, the left ventricle further dilates, resulting in increased wall stress (Laplace's Law), increased myocardial oxygen consumption, reduced systolic function, and altered myocardial architecture, and hence a vicious circle. In late stages, the ventricle becomes spherical in shape rather than ellipsoid, characterized by an increased transverse diameter (l) and a preserved long-axis diameter (L), along with normal or reduced wall thickness. The reduction in the overall ventricular systolic performance, can be easily identified using 2D echocardiography in the parasternal long-and short- axis view [21, 22] (Fig. 9.2; Videos 9.1, 9.2, and 9.3).

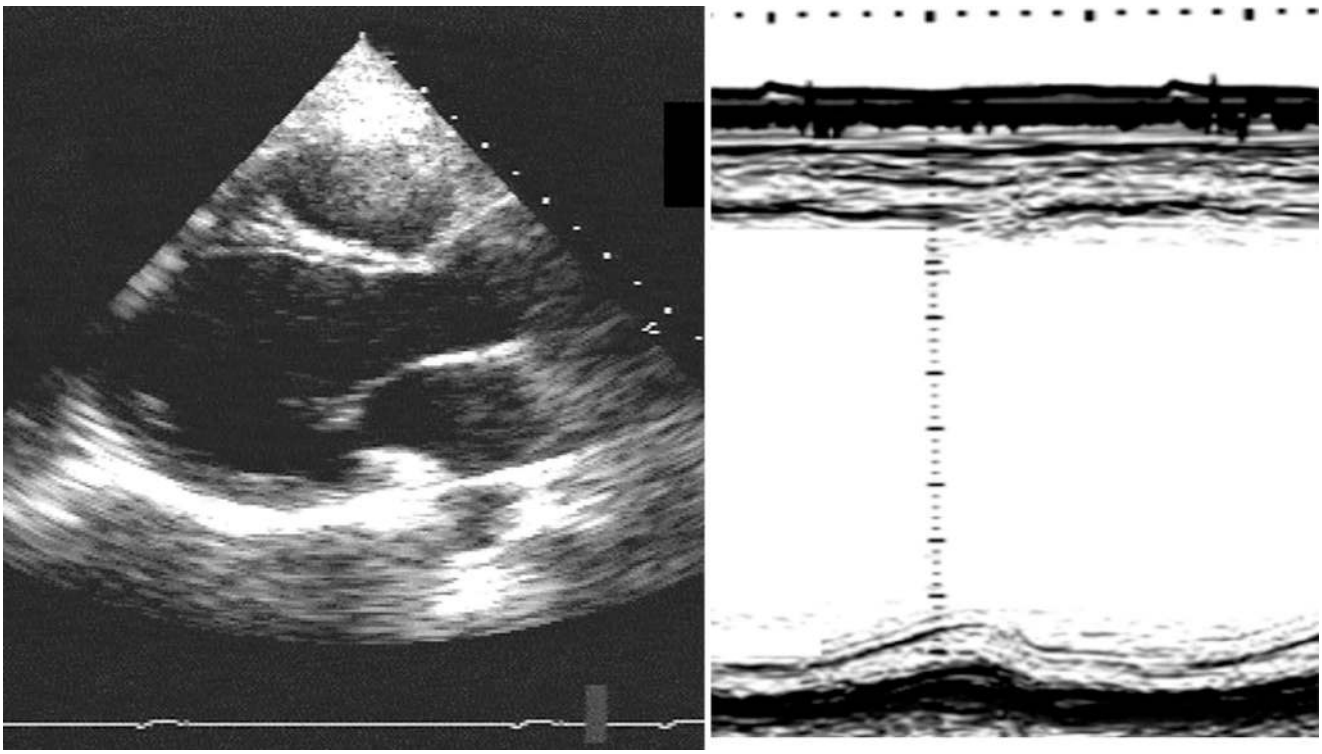


Fig. 9.2 Parasternal long axis view from a patient with DCM (*left*). Corresponding M-mode recording of the basal ventricular region (*right*)

Echocardiograhic Associated Findings

Left Ventricular Diastolic Dysfunction: There is no diagnostic filing pattern for DCM. In early stages LV filling may be normal for age or show a slow ventricular relaxation pattern, characterized by long isovolumic relaxation time, with prolonged early diastolic filling deceleration time and predominant late diastole filling component. In later stages as the ventricle becomes stiff and incompliant, the end diastolic pressure rises, left ventricular filling becomes of the '*restrictive pattern'* characterized by a short deceleration time of the E wave (<150 ms) and an raised E/A ratio (>2) on transmitral pulsed wave Doppler velocity recordings and prolonged flow reversal in the pulmonary veins (Fig. 9.3) [23, 24]. This is often associated with some degree of mitral regurgitation. In early diastole, restrictive LV filling is also characterized by a raised atrioventricular pressure gradient which is transferred across the interventricular septum to the right side of thr heart and result in a delay or complete suppression of early diastolic right ventricular filling (ventricular interaction effect) [25]. Successful pressure offloading of the left atrium (LA) by vasodilators, particularly rennin angiotensin system blocking agents results in normalization of left and right ventricular filling pattern [26].

Left Atrial Dilatation: LA dimensions and volume are estimated by 2D/3D echocardiography in the apical four chamber view. Dilated LA is a notable echocardiographic feature of dilated cardiomyopathy [27]. This increase is primarily due to diastolic dysfunction and varying degrees of mitral regurgitation. Data indicate that the minimal atrial volume assessed at ventricular end-diastole provides a better prediction of outcomes compared to the maximal left atrial volume measured at ventricular end-systole [28, 29].

Mitral Regurgitation: As the left ventricle dilates the pathology involves the basal region and results in dilatation of the mitral annulus and failure of optimum coaption of the mitral valve leaflets. In late stages of the disease when the ventricle becomes spherical, the papillary muscles are displaced laterally causing significantly raised chordal tension. This results in disturbed leaflet movement, suboptimum valve closure and valvular incompetence (Fig. 9.4) [30]. Furthermore, ventricular dyssynchrony is another common cause for mitral regurgitation in dilated cardiomyopathy, which regresses after cardiac resynchronization therapy [31]. Various mechanisms have been proposed suggesting significant deformation of the mitral valve apparatus as an attempt to compensate for the ventricular dysfunction and cavity enlargement [32] (Video 9.4).

Mitral regurgitation in dilated cardiomyopathy varies in severity, from mild in the early disease to severe in late stages (Fig. 9.5). The retrograde pressure drop across the mitral valve aids in estimating left atrial pressure, when the left atrial pressure is raised and the pressure drop across the mitral valve is low (Fig. 9.6). Left atrial pressure is estimated as the difference between systolic blood pressure and systolic retrograde transmitral valve pressure drop.

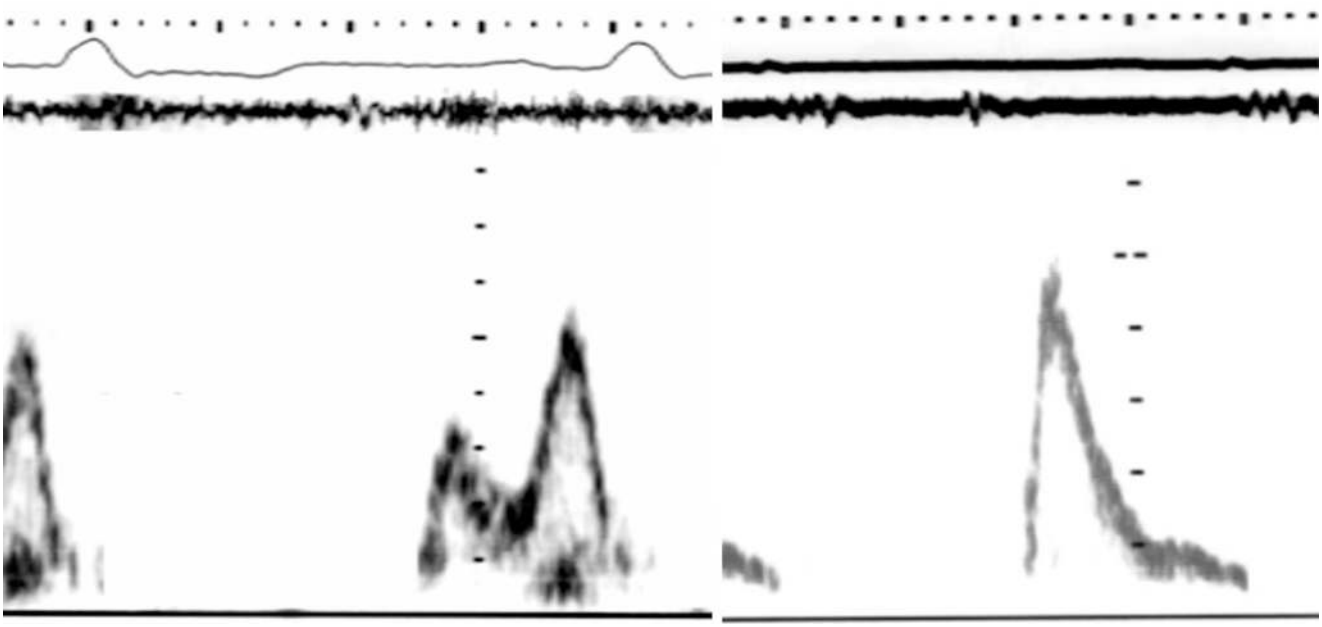


Fig. 9.3 LV filling pattern from two patients with DCM, slow relaxation (*left*) and restrictive high filling pressures (*right*)

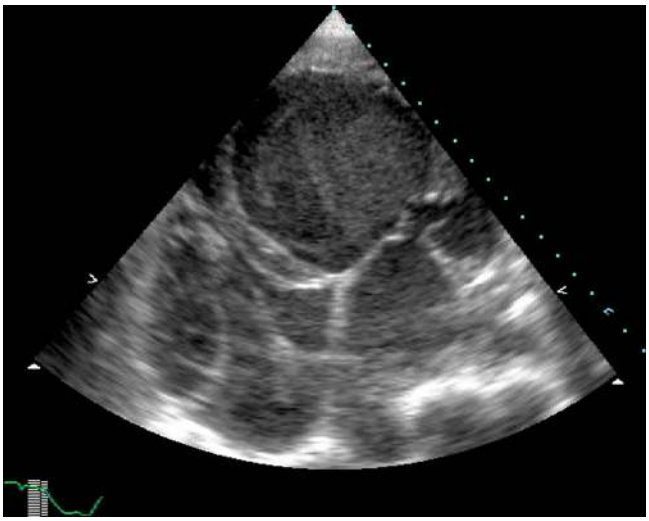


Fig. 9.4 Apical 4 chamber view from a patient with late-stage DCM showing spherical-shaped LV cavity

Raised Left Atrial Pressure: Raised left atrial pressure manifests late in the disease as the left ventricular diastolic pressures rise, resulting in LA dilatation and remodeling, impairment of function and tendency to arrhythmia [33, 34]. Even in patients with maintained sinus rhythm, atrial contraction is resisted by ventricular stiffness and high left ventricular end diastolic pressure. This causes backward flow in the pulmonary veins that adds to the pulmonary venous congestion. Retrograde flow in the pulmonary veins, occurring during atrial systole which is more than 30 ms longer than the transmitral "A" wave duration suggests raised left ventricular end diastolic pressure (Fig. 9.7) [35, 36]. Patients with severe left ventricular disease and raised left atrial pressure often present with a poor systolic component of the pulmonary venous flow consistent with depressed movement of the ventricular long axis in systole and consequently limited atrial enlargement. The higher the left atrial pressure the more ischemic the subendocardium and hence the perpetual

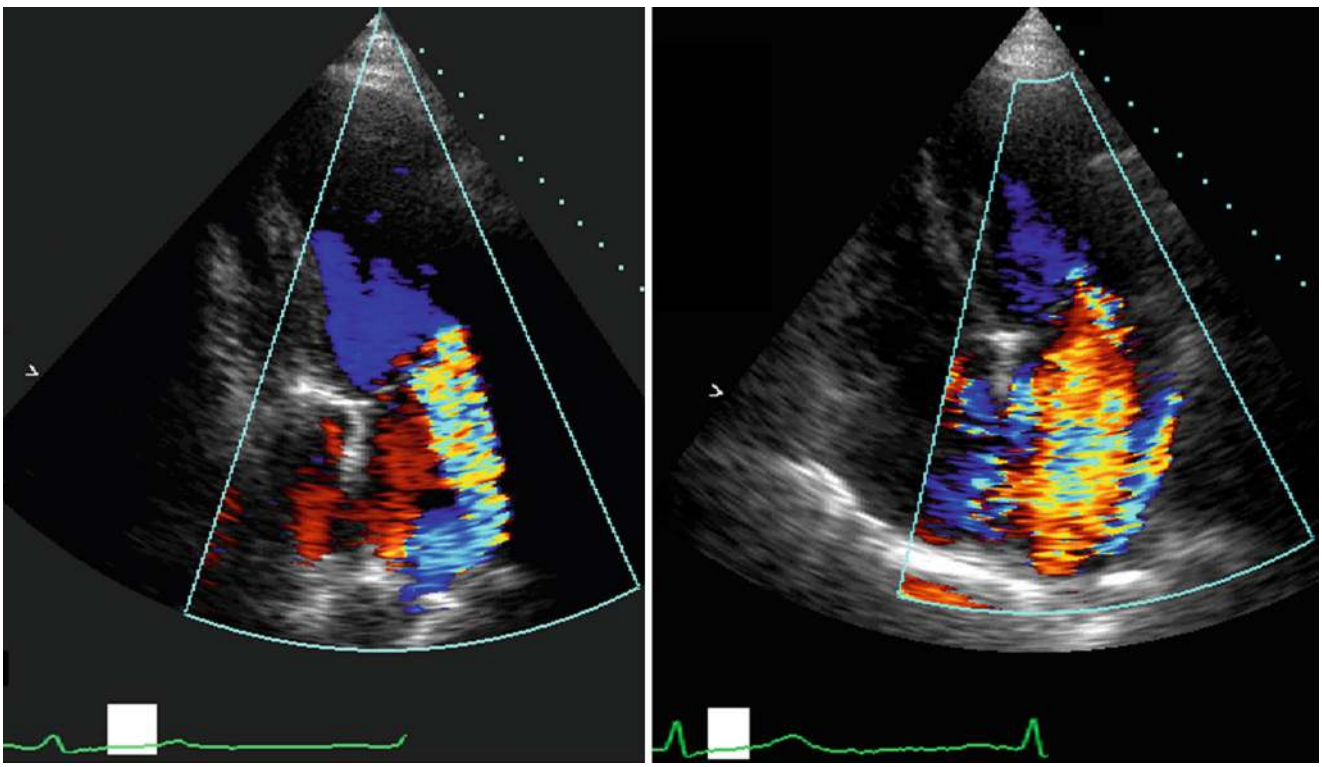


Fig. 9.5 Apical 4 chamber views from two patients with DCM showing mitral regurgitation on color flow Doppler. Mild (*left*) severe (*right*)

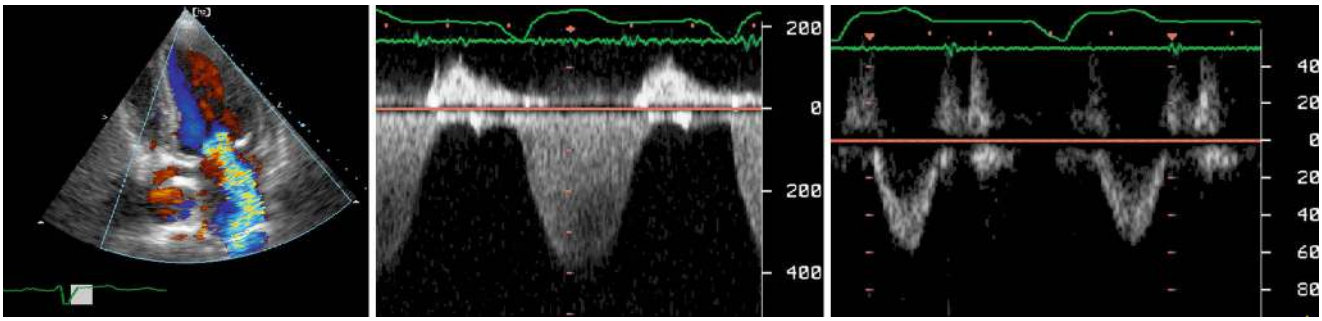


Fig. 9.6 Apical 4 chamber image of a DCM patient with severe mitral regurgitation on color Doppler (*left*) and continuous wave Doppler (*middle*). Note the peak LV-LA pressure drop is 60 mmHg suggesting severely raised left atrial pressure and low cardiac output state, low aortic velocity (right)

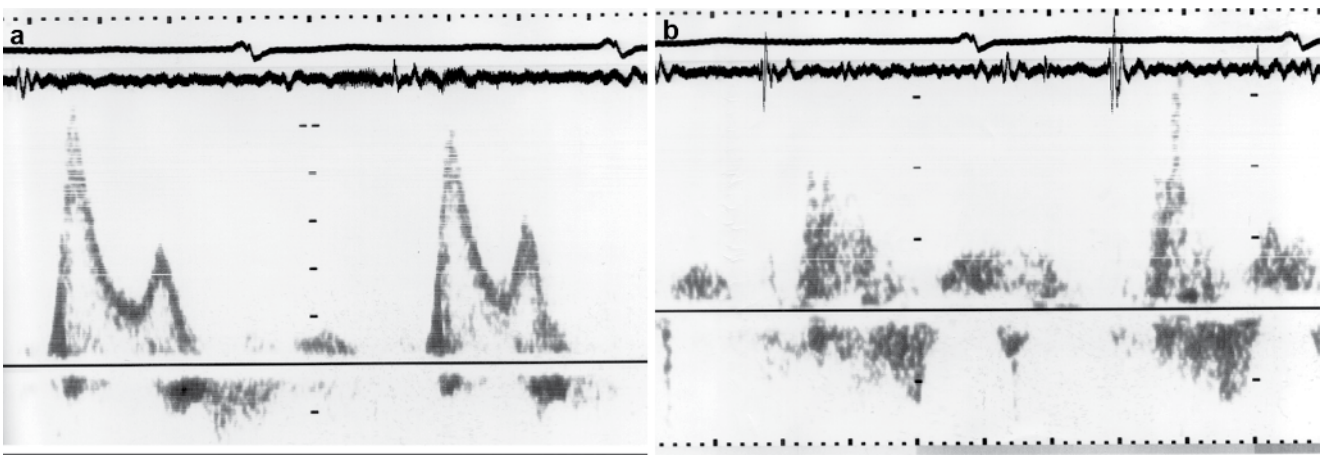


Fig. 9.7 Transmitral flow from a patient with restrictive left ventricular filling and raised left atrial pressures (**a**) and corresponding pulmonary venous flow (**b**). Note the longer duration of the pulmonary venous flow in late diastole compared with the forward mitral flow

deterioration of left ventricular function, further cavity enlargement of both ventricle and atrium, and established atrial fibrillation.

Pulmonary Hypertension: Raised LA pressure, complicating left ventricular disease and mitral regurgitation, may cause pulmonary hypertension (post-capillary). Pulmonary venous hypertension is difficult to diagnose echocardiographically. A short "E" wave deceleration time is a good marker of raised pulmonary wedge pressure. The progressively developing pulmonary arterial hypertension affects the size and function of the right heart. The right ventricle becomes hypertrophied, its function impaired, and the cavity itself dilates because of its thin myocardium. The right atrium also dilates. Pulmonary artery pressure can be estimated from peak tricuspid regurgitation pressure drop added to the estimated right atrial pressure (Fig. 9.8). This can easily be achieved from the collapsibility of the hepatic veins [36]. Although this equation tends to underestimate peak pulmonary artery pressure, it helps in assessing disease progression in symptomatic patients and in monitoring their response to treatment [37].

Tricuspid Regurgitation: As is the case with other causes of right ventricular enlargement and dilatation of the tricuspid annulus, tricuspid regurgitation is common and varies in severity in dilated cardiomyopathy [38]. Severe tricuspid regurgitation may be present in late disease or if the primary pathology involves the right ventricle. In this case the right atrium and right ventricle are both dilated, the right atrial pressure is increased and the peak right ventricular–right atrial pressure drop falls. This fall in pressure drop should not be taken as a sign of reduction of pulmonary artery pressure, particularly in patients who show clinical deterioration, but as a sign of increasing right atrial pressure (Fig. 9.9).

Left Ventricular Thrombus: Late stages of DCM and increased ventricular diastolic pressure are characterized by slow intraventricular circulation, and spontaneous intracavitary echo contrast may be seen. With significantly high early

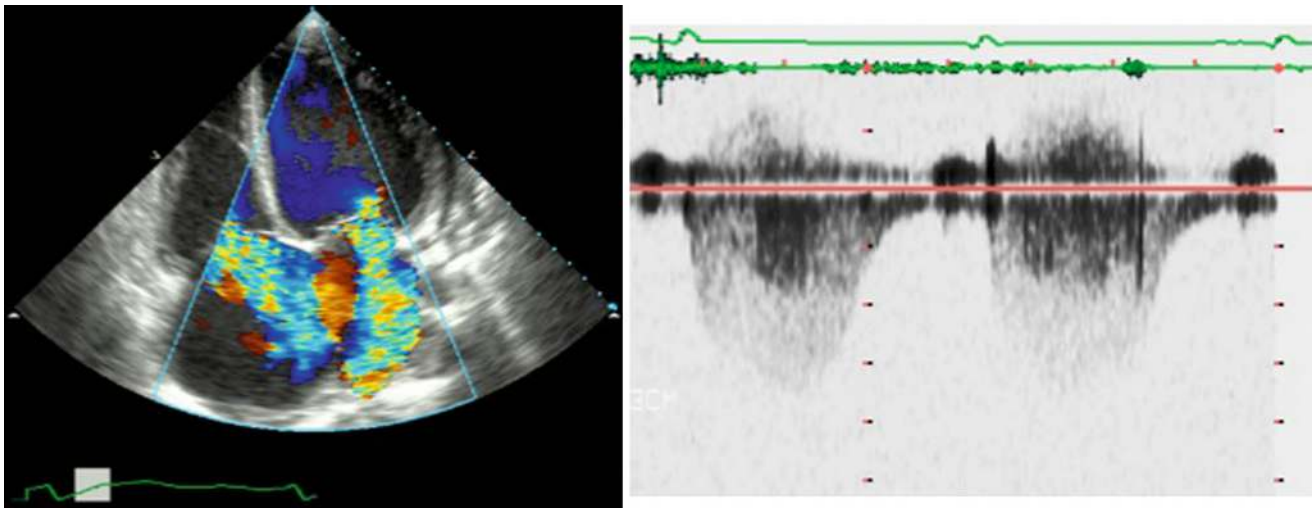


Fig. 9.8 Apical views from a patient with DCM and long-standing raised left atrial pressure. Note the right-sided dilatation and raised RV-RA pressure drop on the tricuspid regurgitation continuous wave Doppler, 55 mmHg

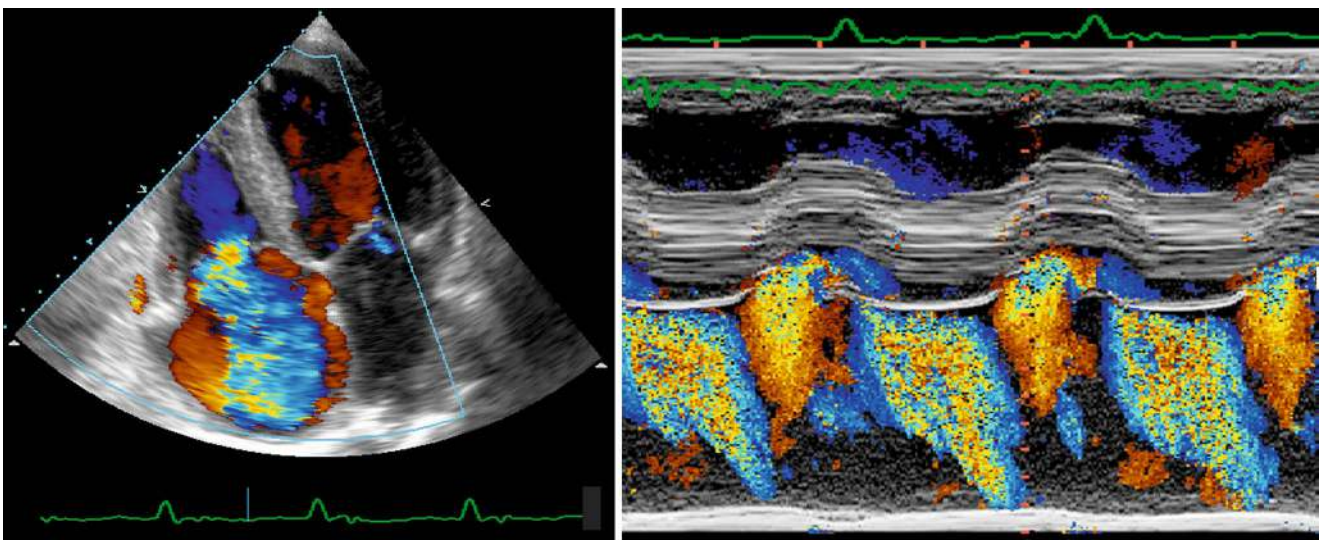


Fig. 9.9 Apical views from a patient with DCM and dilated right heart. Note the severity of tricuspid regurgitation on color Doppler (*left*) and color M-mode Doppler (*right*)

diastolic atrioventricular pressure gradient and intraventricular flow acceleration, the mitral leaflet opening is disturbed and the valve behaves as if functionally stenosed, thus adding to the disturbed cavity function in diastole (Fig. 9.10). This degree of ventricular disease may be associated with apical stagnation of blood and potential thrombus formation, suggesting the need for prophylactic anticoagulation [39].

Extracardiac Fluid Compression: Late stages of DCM with biventricular failure, pulmonary hypertension, and systemic congestion may be complicated by pericardial and/or pleural effusion. Large fluid collection increases the intrathoracic pressure and frequently exacerbates the patient's breathlessness. The consequence of the increased intrathoracic pressure on right heart physiology is assessed by studying the vena caval, tricuspid and pulmonary flows during different phases of the respiratory cycle. Right-sided filling and ejection which increase significantly during inspiration (>20% that during expiration) suggest increased extracardiac pressures (Figs. 9.11 and 9.12).

Pulsus Alternans: With severe deterioration of ventricular function and absence of extracardiac fluid collection, pulsus alternans may develop. This can easily be confirmed on

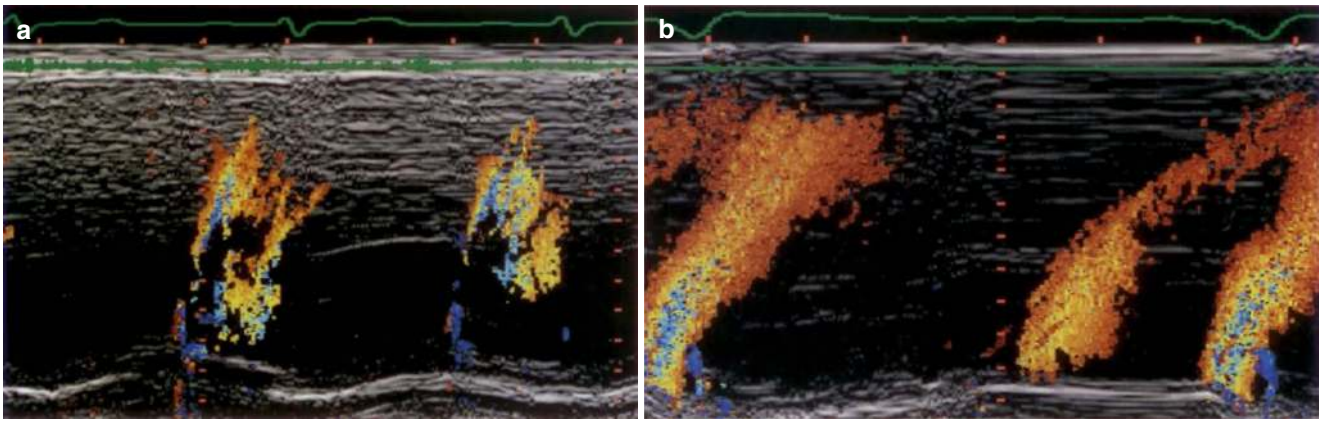


Fig. 9.10 Color M-mode of LV filling slowing fast flow acceleration (**a**) compared to normal acceleration (**b**)

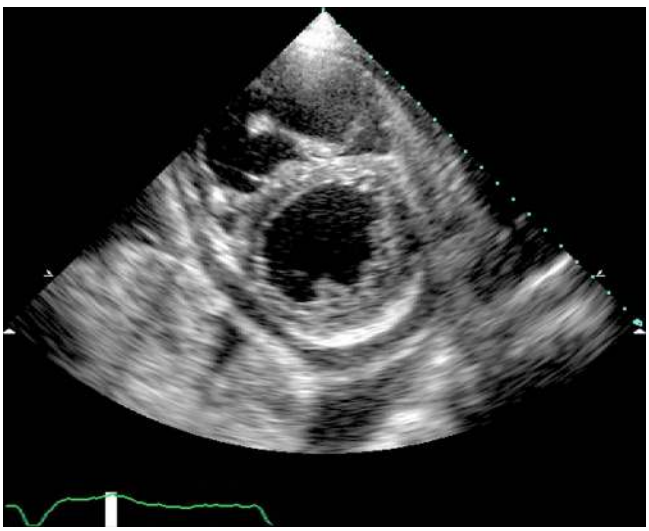


Fig. 9.11 Parasternal long axis view from a patient with DCM showing pericardial and left pleural effusion

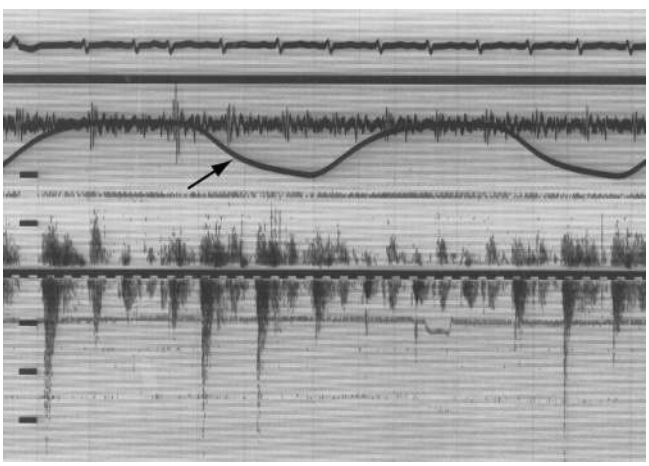


Fig. 9.12 Inferior vena caval flow from a patient with DCM and severe breathlessness showing predominant inspiratory flow (arrow) consistent with significantly raised intrathoracic pressure

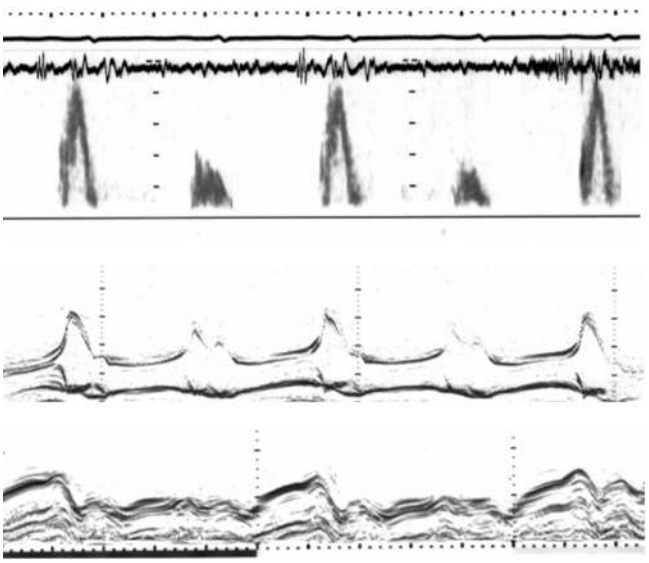


Fig. 9.13 Transmitral forward flow velocities, mitral valve echogram and ventricular long axis movement from a patient with pulsus alternating demonstrating alternating normal and compromised left ventricular filling along with failure of long axis movement in the compromised cycles

pulsed Doppler velocities of left ventricular filling and ejection as well as wall motion pattern (Figs. 9.13 and 9.14). The exact mechanism of pulsus alternans is not clearly understood.

Activation-Induced LV Dysfunction: Chronic severe left ventricular disease is almost always associated with delayed depolarization, i.e., broad QRS complex with or without classical bundle branch block pattern [40]. Progressive prolongation of ventricular depolarization has been shown to be associated with poor clinical outcome. This electrical disturbance is closely related to the delayed and prolonged ven-

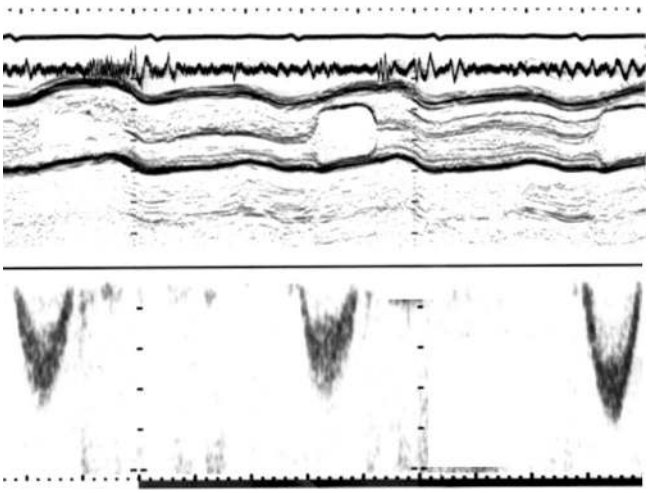


Fig. 9.14 Aortic flow velocities and valve echogram from the same patient demonstrating alternating complete cessation of aortic flow and valve opening

tricular shortening and lengthening and hence dyssynchrony. The latter contributes to raised diastolic segmental wall tension resulting in pre-systolic mitral regurgitation (Fig. 9.15). Such long mitral regurgitation can limit ventricular filling time particularly at fast heart rate and consequently reduce the stroke volume [41]. Although most of these ventricles fill with a single component "summation filling pattern" the long mitral regurgitation adds to the raised left atrial pressure and pulmonary pressures as well as compromises atrial emptying function (Fig. 9.16).

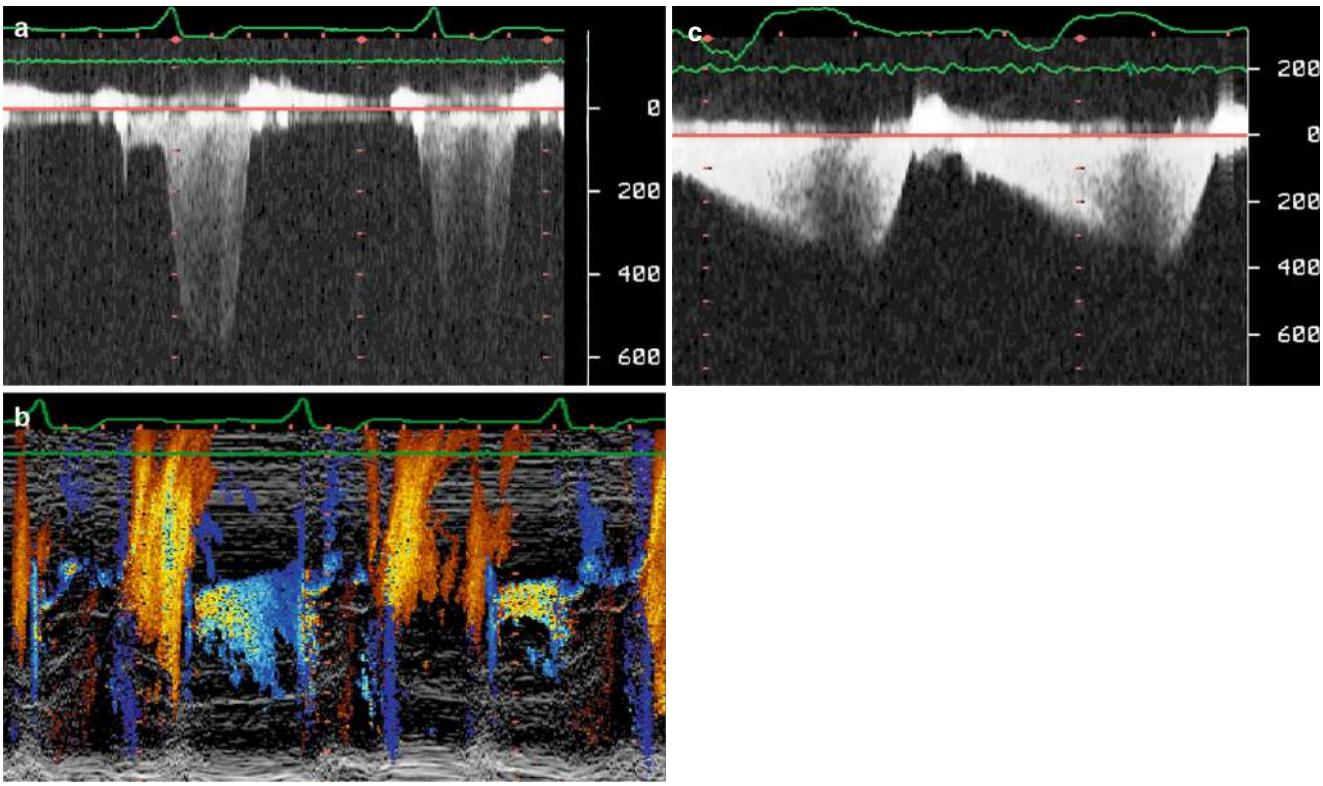


Fig. 9.15 Continuous wave Doppler recording demonstrating long mitral regurgitation in a patient with severe DCM. Note the pre-systolic component on continuous wave recording (**a**) and its corresponding velocities on color flow Doppler (**b**) An extreme example (**c**) showing total filling time of 100 ms because of very long mitral regurgitation

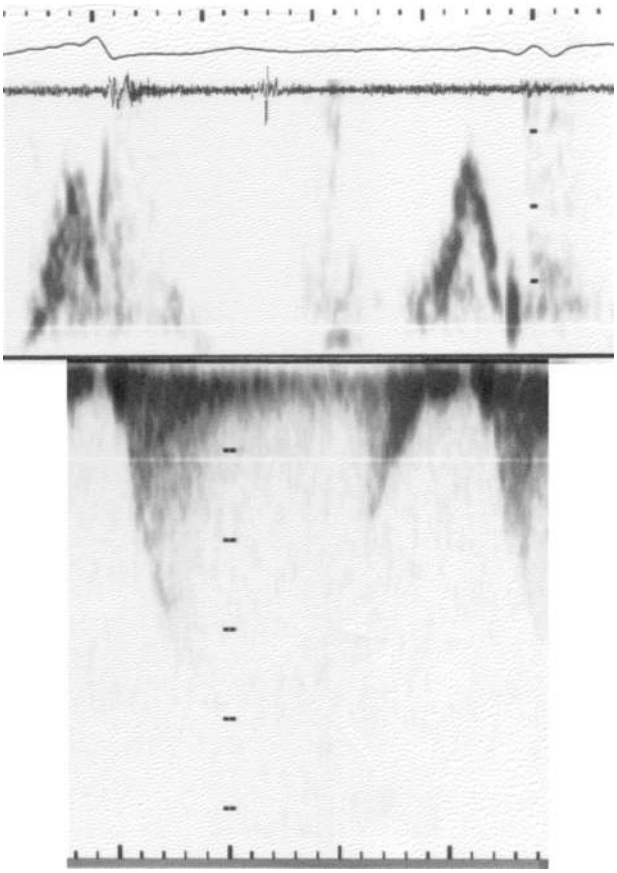


Fig. 9.16 CW Doppler from a patient with late DCM and long early diastolic mitral regurgitation that is limiting ventricular filling time

Management and Follow-Up

Patients with moderate or severe degree of left ventricular impairment should be followed up regularly by Doppler echocardiography for the assessment of left ventricular function, pressure and complications, as well as response to management. Although there are no current guidelines to suggest how frequently patients should be assessed, markers of increased filling pressure, pulmonary hypertension and mitral regurgitation, in addition to worsening symptoms, can provide accurate indication for deterioration of ventricular function or beneficial response to therapy.

Medical: Treatment is largely supportive and includes the management of heart failure, arrhythmias, and conduction system problems. The aim of this policy is to keep the filling pressures low and to protect against further deterioration of ventricular function. Angiotensin-converting enzyme (ACE) inhibitors or angiotensin receptor blockers (ARBs) if patients are intolerant to ACE, in particular have shown a significant effect on mortality reduction and improvement of clinical outcome in patients with DCM [42]. Doppler echocardiography assesses patients response to ACE inhibitors particularly those with raised left atrial pressure (restrictive filling pattern). Successful offloading of the atrium and the ventricle with ACE inhibition or ARBs reverses the restrictive filling pattern to the dominant late diastolic filling pattern and unmasks left ventricular dyssynchrony. This is usually associated with reduction of mitral regurgitation, a fall in left atrial size and significant improvement of symptoms (Fig. 9.17). As the left ventricular early diastolic pressure gradient drops and its filling becomes non-restrictive, the delay in the right ventricular filling regresses, overall right ventricular filling time increases and the degree of pulmonary hypertension reduces (Fig. 9.18). Beta blockers have also been shown to improve outcome in patients with dilated cardiomyopathy and reduce mortality. In patients with poor left ventricular function and tachycardia, small doses of beta blockers e.g. bisoprolol or carvedilol, slow the heart rate and increase left ventricular filling time and consequently stroke volume [43]. However not all patients with DCM can tolerate beta blockers, particularly those requiring faster heart rate to secure minimum physiological filling volume. Patients with late-stage ventricular disease and very short isovolumic relaxation time in particular, seem to prefer a faster heart rate in order to sustain left ventricular filling and cardiac output and therefore tolerate beta blockers poorly (Video 9.5).

Pacing: Patients presenting with a broad QRS complex (>150 ms) and long mitral regurgitation with a presystolic component that limits total LV filling time respond to DDD pacing with optimized atrioventricular delay. Short A-V delay results in immediate increase in filling time and stroke volume and improvement of overall cardiac performance (Fig. 9.19) [41]. Currently most of these patients will receive complete biventricular pacing system, and during optimization the left ventricular lead may be switched off. Long-term outcome of this intervention in individual patients is usually satisfactory.

Patients with significant early diastolic dyssynchrony, particularly of the left ventricular free wall, which prolongs early diastolic tension development and compromised early filling are usually ideal for biventricular pacing, cardiac resynchronization therapy (CRT). The procedure aims at optimizing the time of left ventricular free wall stimulation that results in regression of dyssynchronous wall motion, and an increase in the overall ventricular filling time [44]. The extent of left ventricular segmental dyssynchrony can

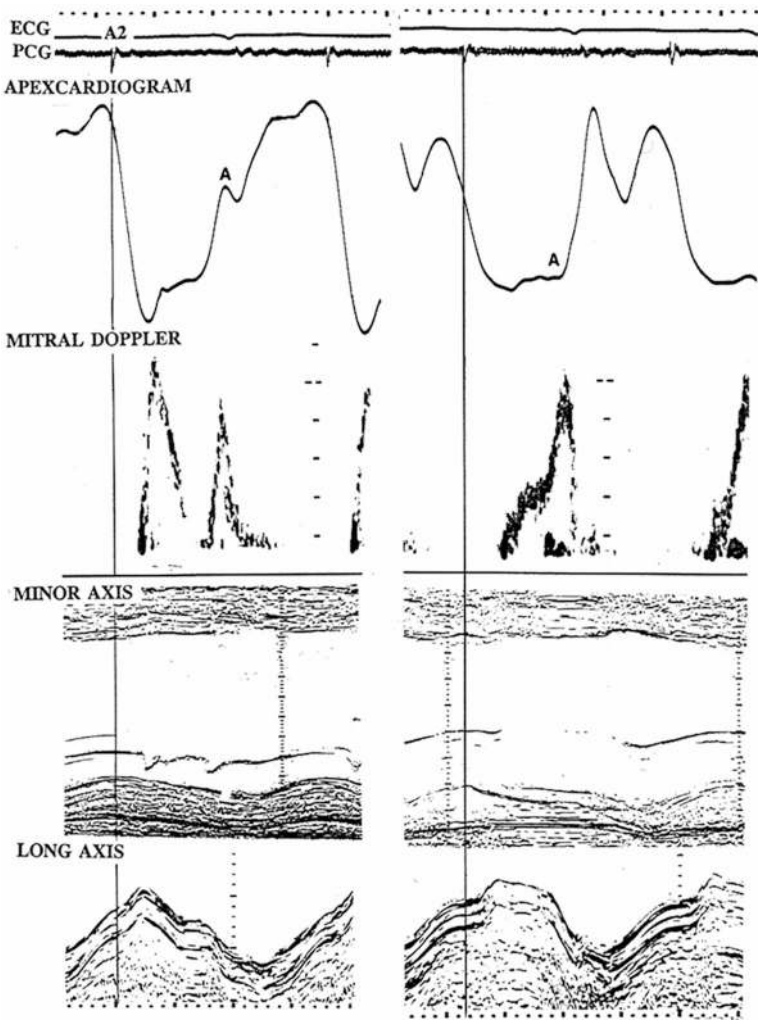


Fig. 9.17 Left ventricular filling and apexcardiogram from a patient with DCM and raised left atrial pressure (*left*) and its response to ACE inhibition (*right*). Note the significant fall in end diastolic pressure with treatment and reversal of LV filling pattern

be assessed using different echocardiographic techniques, M-mode and tissue Doppler. The extent of electromechanical delay of various segments; peak inward motion or peak systolic velocity, respectively, can be measured and compared with normal values (Fig. 9.20) [45]. Three-dimension echocardiogram has also shown a good potential for detecting dyssynchronous segments and their response to CRT [46]. Cardiac resynchronization therapy results in significant symptomatic improvement, reduction in mitral regurgitation and improved survival [47]. Since the natural history of DCM is deterioration, particularly in adults, regular follow-up of such patients provides an opportunity for potential optimization of the segmental stimulation delay and overall cardiac performance [48]. Despite the current strong evidence for the beneficial effect of CRT in DCM with poor systolic function, approximately 30% of patients receiving this treatment do not respond [49]. Modest evidence suggest that those with restrictive filling are less likely to gain symptomatic benefit from CRT since their main cardiac disturbance is raised filling pressures [50]. Ideally, patients recommended for CRT should be assessed during exercise/stress in order to determine the exact nature of cardiac disturbances which coincide with their symptoms, which should guide toward optimum management. Those developing worsening dyssynchrony should benefit from CRT, others who increase further their filling pressure and remain with restrictive filling, may need life-saving ICD (Video 9.6).

Assist Devices: Failure to control patient's symptoms by the above methods suggests the need for ventricular assist device. The rationale behind the use of the assist device is a bridge to either recovery of ventricular function or transplantation. In a minority of patients, ventricular function recovers within weeks or months of the device insertion. The pump sucks from the ventricle and ejects directly into the aorta, thus reducing wall stress and allowing the myocardium to recover. The currently available assist devices

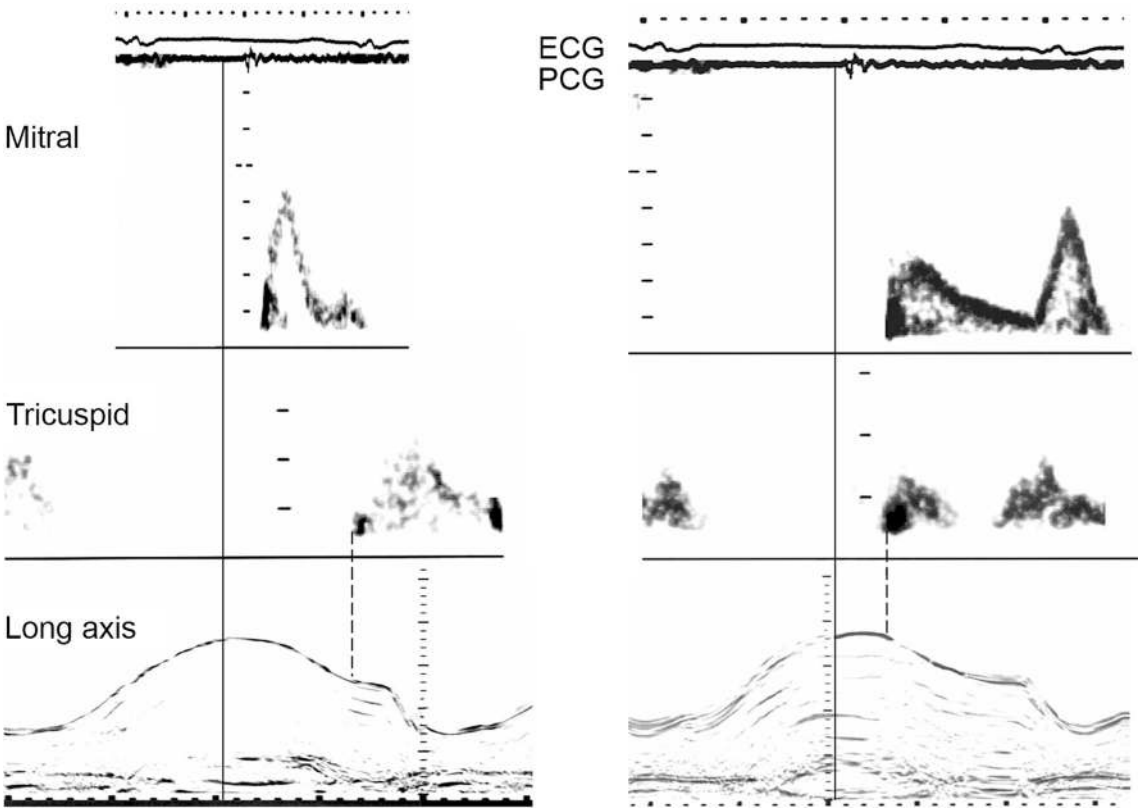


Fig. 9.18 Left and right ventricular filling from a patient with restrictive filling before (*left*) and with ACE inhibition (*right*). Note the normalization of the RV filling with off loading of the left atrium

are either phasic or continuous. The phasic Heart Mate functions independently of cardiac cycle and carries the risk of significant interference with valve function and clot formation [51]. The continuous pump is not without limitation, since at fast speed the suction force may cause mid cavity obliteration, potential free wall collapse, and high intracavity pressure difference between ventricular regions (Figs. 9.21 and 9.22) [52].

Transplantation: Cardiac transplantation is now a well-established treatment, but because of the severe shortage of adequate donor organs this form of treatment is only available for a small number of patients. In general terms the most favorable recipients are young, highly motivated people with disease confined to their heart and with excellent renal, hepatic and pulmonary function. The operation is an orthotopic heart transplant whereby the dilated heart is removed and a new donor heart inserted with anastomoses at the left atrium, pulmonary artery, aorta, and caval orifices. Over the last 20 years the use of caval orifice anastomosis has become more usual as this is found to result in a lower incidence of tricuspid regurgitation and improved right ventricular function. The main problems related to the management of these patients postoperatively remain infection and the control of rejection. Modern immunosuppressive therapy with Cyclosporin, Mycophenolate mofetil, and a short course of steroids has resulted in significant improvement in results. The 1 year survival after heart transplantation is of the order of 80% and the 5 year survival is 70%. These patients require careful life-long surveillance, largely because of the complications arising from immunosuppression. These complications comprise hypertension, which is extremely frequent and usually can be controlled by calcium antagonist, renal impairment, slowly progressive left ventricular fibrosis, B cell hyperplasia, and tumors. Nevertheless the quality of life from a good heart transplant is excellent and over 80% of these patients return to an active life for at least 10 years. This is a considerable achievement given that the majority had a prognosis of less than 6 months at the time that they are placed on the transplant waiting list.

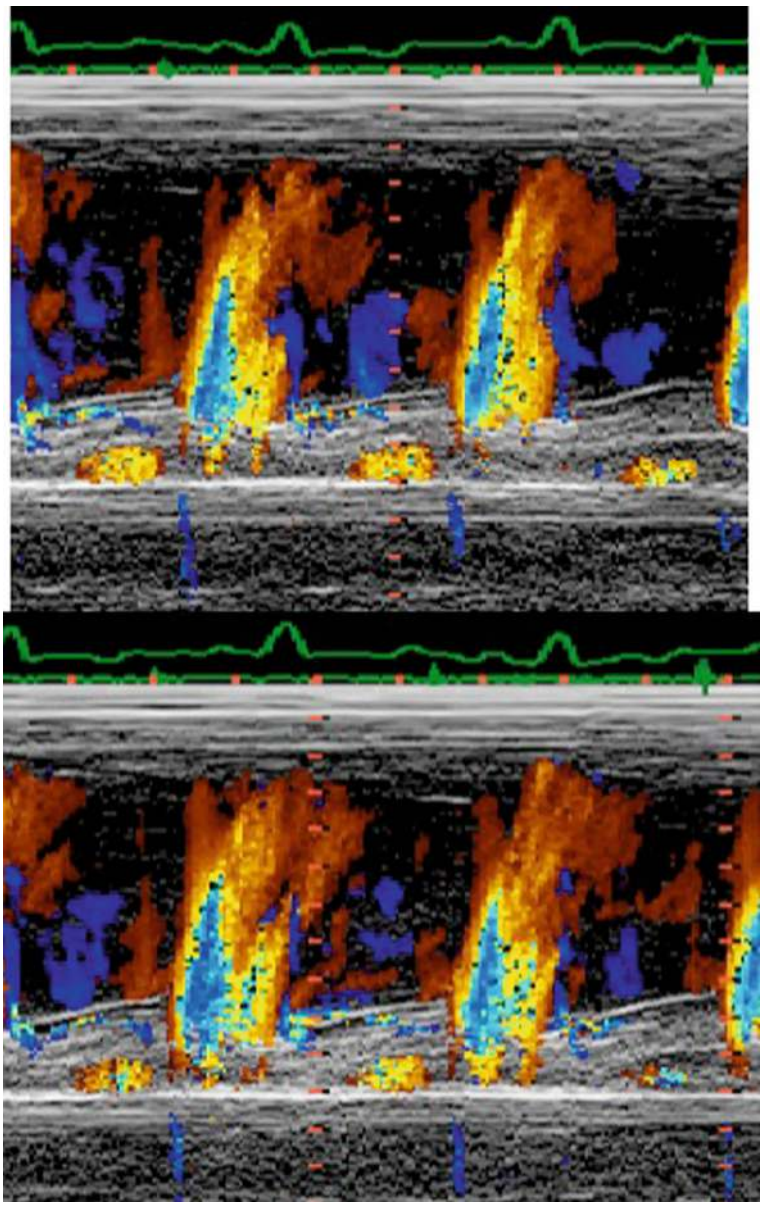


Fig. 9.19 Transmitral forward flow velocities and CW Doppler from a DCM patient with long mitral regurgitation before (top) and after (bottom) DDD pacing. Note the significant prolongation of LV filling with pacing

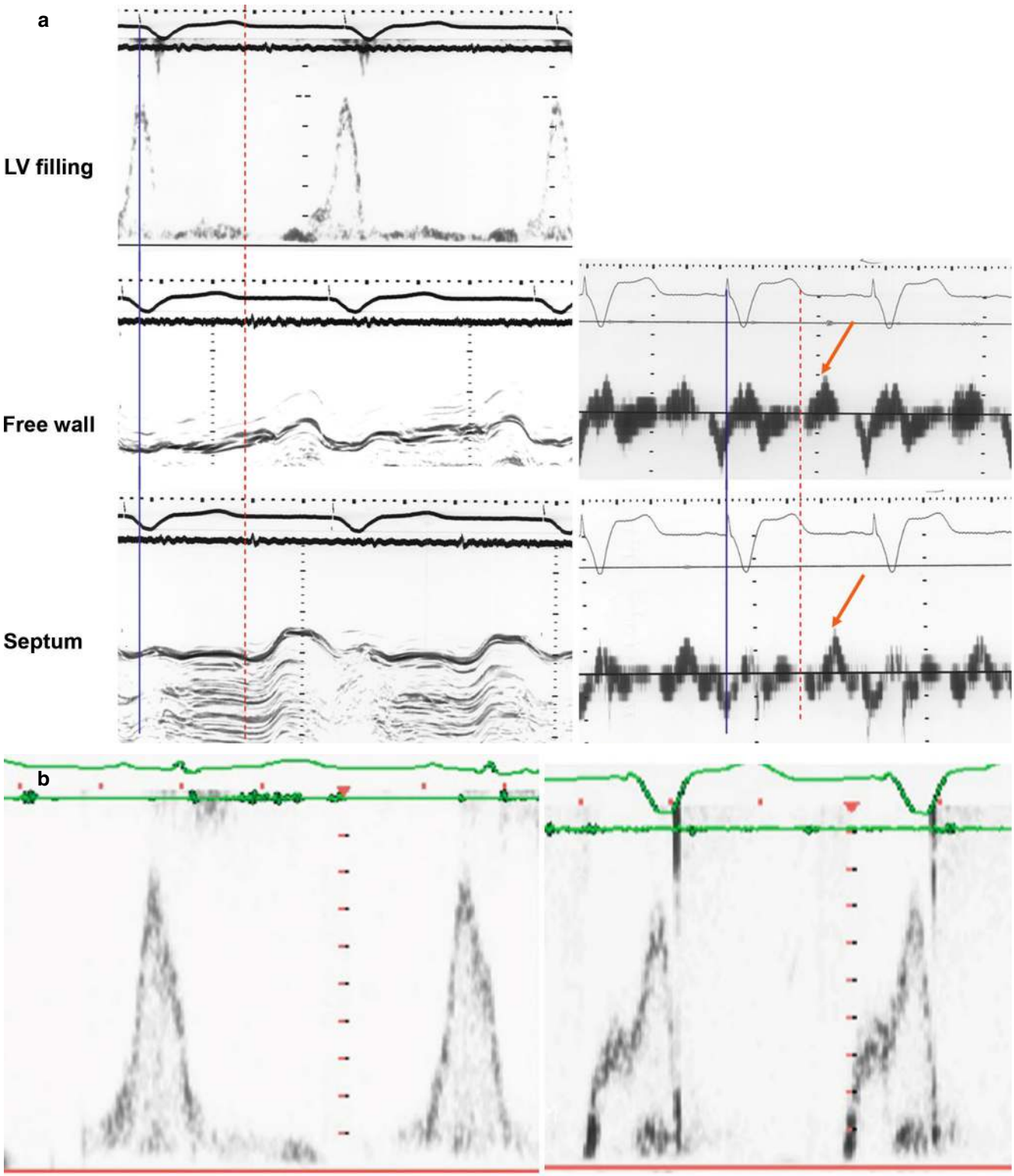


Fig. 9.20 Patient with DCM and early diastolic asynchrony (on M-mode and tissue Doppler velocities) and limited filling to late diastole (**a**) filling time of the patient before and with CRT (**b**). Note the significant increase in filling time with CRT

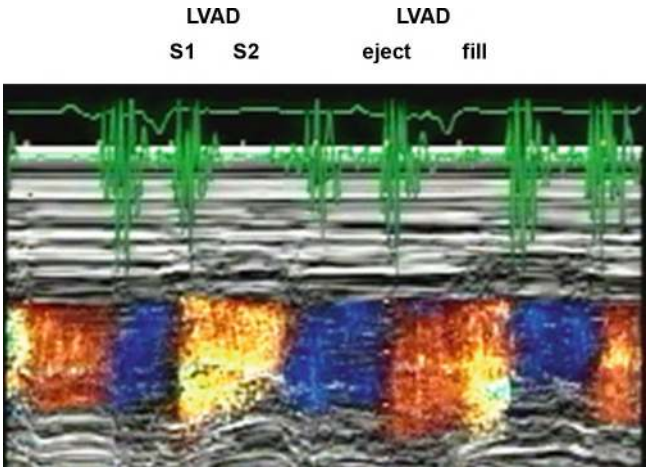


Fig. 9.21 Color M-mode of left ventricular filling from a patient with DCM and phasic assist device. Note the independent pump filling and ejection with respect to the cardiac cycle

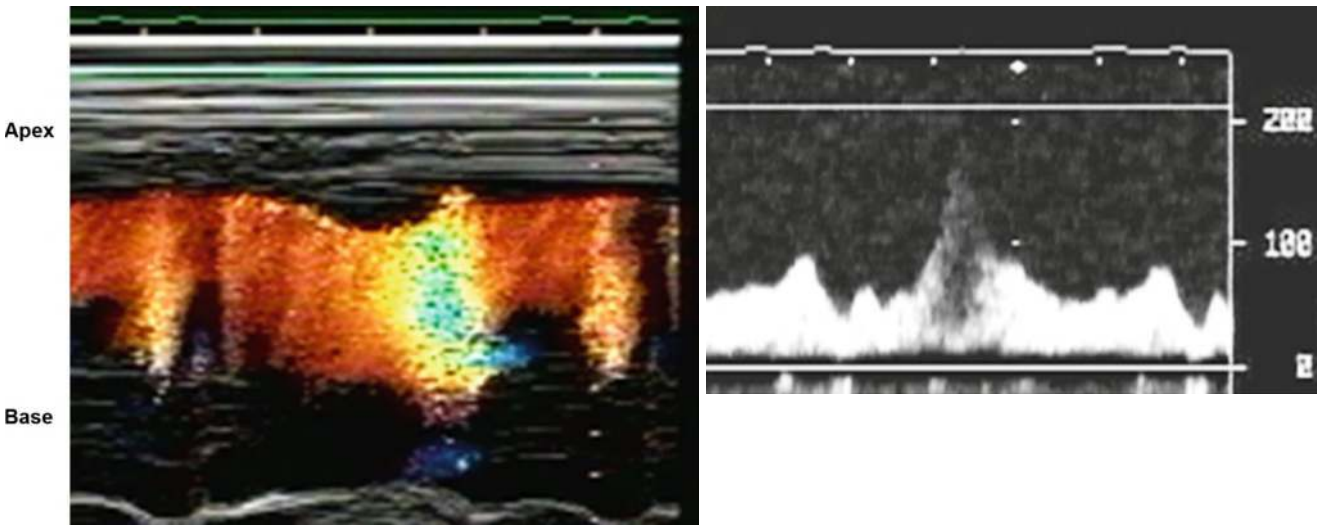


Fig. 9.22 Color M-mode from a patient with DCM and continuous assist device. Note the high mid cavity velocities with fast speed (*left*) and mid cavity obliteration (*right*)

Prognosis

The prognosis of DCM differs significantly between patients. While alcoholic cardiomyopathy tends to recover with abstinence from alcohol, other forms continue to deteriorate over time. With medical therapy, patients may respond to ACE inhibitors or ARBs showing a reduction in left atrial pressure and improvement in overall cardiac function as well as symptoms. Patients who retain high left atrial pressure are considered unstable and are at risk of developing pulmonary hypertension, subendocardial ischemia and arrhythmia. Long-standing high pulmonary wedge pressure is reflected on right ventricular function, which deteriorates irreversibly with subsequent poor outcome. Right ventricular long axis amplitude <14 mm predicts poorer outcome compared to an amplitude >14 mm [53]. Additional right ventricular disease with a restrictive filling pattern makes the outcome even poorer. While DDD pacing with A-V optimized delay has offered great assistance to overall ventricular performance in patients with DCM, no trials are available to support its beneficial use on a broader scale. Furthermore, despite the vast available evidence [53–55] for the beneficial effect of CRT in advanced disease, 30% of patients receiving such treatment remain symptomatic and with no measurable benefit. Stringent Doppler echocardiographic criteria for patient's selection for CRT remain to be ascertained. Determining the exact nature of cardiac function disturbances at the time of symptom development for optimum patient's selection seems a scientific way forward.

Furthermore, the left atrium is crucial to cardiac structure and function and should not be seen in isolation. LA volume closely relates to left ventricle volume, predicting LV size and response to CRT. Left atrial volume index (LAVI) and function are essential for predicting CRT response and reflects LA remodeling due to electrical resynchronization. This relationship helps explain why atrial fibrillation patients often do not respond to CRT, thus highlighting the importance of assessing LA structure and function in cardiac evaluations to improve treatment effectiveness [29, 44].

Signs of Disease Progression and Functional Deterioration

1. Development of restrictive left ventricular filling with very short isovolumic relaxation time, which is resistant to off loading by medication. Patients with this degree of disease poorly tolerate beta blockers and pacing seems unable to offer satisfactory benefit.
2. Right ventricular deterioration of function particularly with raised right atrial pressures. Such patients develop systemic congestion with its known complications and difficult management.
3. Severe mitral regurgitation or tricuspid regurgitation. Although medical treatment and CRT have been shown to reduce functional valve regurgitation, patients may remain with well-established ventricular remodeling, dilated valve annulus and resistant regurgitation, which carries bad prognosis.
4. Progressive broadening of QRS associated with worsening of symptoms, ventricular function and clinical outcome. CRT should be recommended for such patients, with careful optimized electrical stimulation.

Other Forms of Cardiomyopathy

Chagas Cardiomyopathy

Chagas disease is caused by *Trypanosoma cruzi* and commonly seen in South America. Early stages of the disease can only be detected in sero-positive subjects.

Late-stage ventricular dysfunction may be indistinguishable from idiopathic dilated cardiomyopathy. Although patients may be completely asymptomatic some may present with conduction disturbances (right or left bundle branch block). Echocardiographically variable degrees of localized myocardial involvement may also be present, for example, aneurysmal apex, hypokinetic basal septum or incoordinate relaxation pattern. Late disease manifests as congestive heart failure with the two ventricles grossly dilated, raised filling pressures and atrioventricular valve regurgitation (Fig. 9.23) [56].

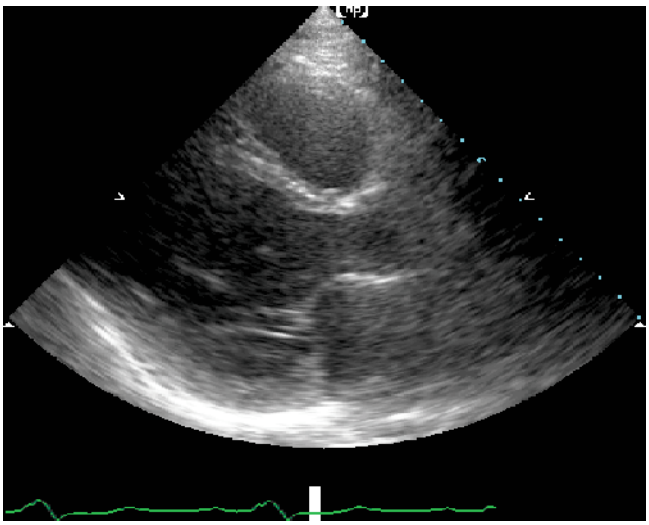


Fig. 9.23 LV parasternal images from a patient with late Chagas disease showing dilated cavity and poor systolic function

Arrhythmogenic Right Ventricular Cardiomyopathy (ARVC)

Arrhythmogenic right ventricular cardiomyopathy (ARVC) is a rare condition that presents with either serious arrhythmia or sudden death. The right ventricle is selectively dilated, particularly at the apex that looks aneurysmal, with a significant increase in myocardial echo intensity on conventional transthoracic echocardiogram (Fig. 9.24). The right ventricular inlet and exit are also dilated. Right ventricular myocardium is replaced by fibrolipomatous material as shown in the pathology specimens (Fig. 9.25) [57]. Patients with ARVC might present with completely normal right heart structure and function. Cardiac magnetic response might succeed in confirming various presentations of myocardial fibrosis, but might be completely normal. A growing evidence exists suggesting the presence of the arrhythmogenic myocardium focus in the left ventricle rather than the right, as previously conceived [58].

Pharmacological Cardiomyopathy

Cardiotoxic pharmacological agents used for treating malignancy may have a damaging effect on the myocardium. Doxorubicin and cyclophosphamide in therapeutic doses may cause severe myocardial dysfunction and deterioration of ventricular function, although end diastolic volume may remain within normal limits (Fig. 9.26). Doxorubicin toxicity is particularly dose-related, but tends to recover after reducing the drug dosage or its rate. Cyclophosphamide given as an immunosuppressive agent may cause rapid onset of interstitial myocardial hemor-

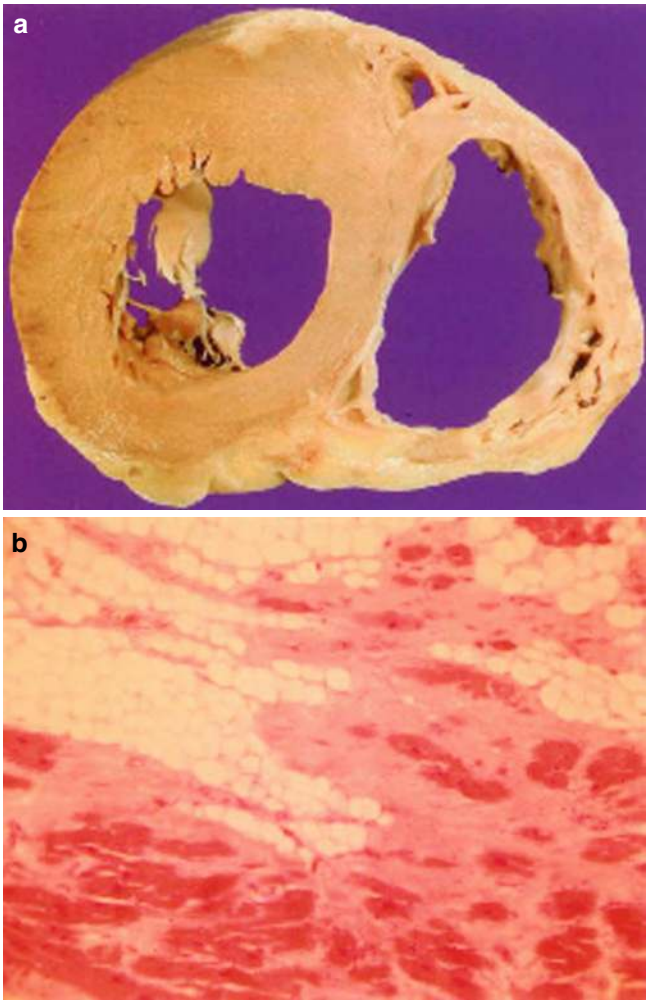


Fig. 9.24 (**a**) Transverse section of the heart showing transmural fatty replacement which extends to the anterior wall of the left ventricle with fibrous scarring. (**b**) Histological section showing distorted myocytes surrounded by pale fibrous tissue and fatty infiltration

rhage and suppression of ventricular systolic function. Chloroquine has also been documented to have significant cardiotoxic effect [59]. It is generally accepted that the myocardial toxicity could be either acute or delayed. Studies defining the two are under way.

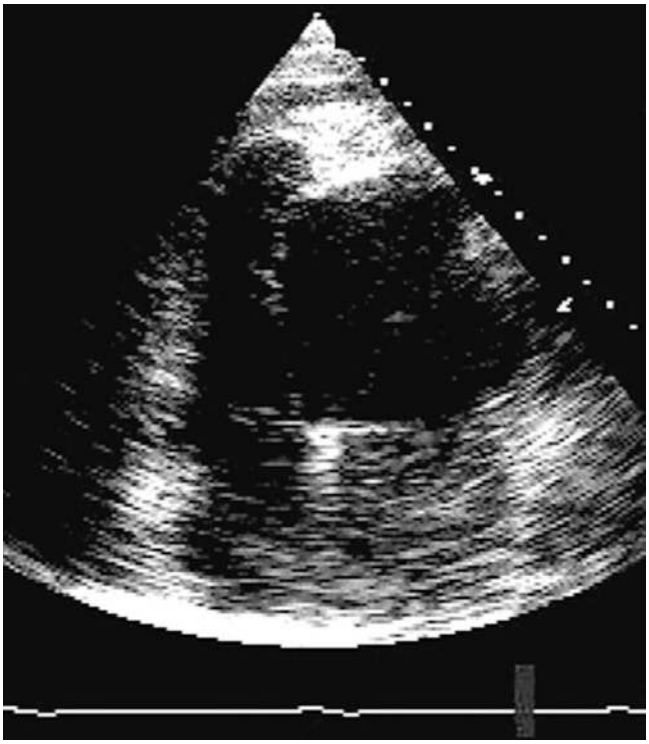


Fig. 9.25 Apical 4 chamber view from a patient with RV dysplasia showing aneurysmal RV apex

Neurological Cardiomyopathy

Ventricular involvement in neurological disorders is related to individual conditions. Friedreich's ataxia is associated with ventricular hypertrophy and Nemaline myopathy is associated with biventricular dilatation that is indistinguishable from dilated cardiomyopathy. Duchenne muscle dystrophy and Becker's disease both present with segmental ventricular dysfunction due to localized fibrosis. Finally, dystrophia myotonia is associated with conduction disturbances and localized segmental ventricular dysfunction [60]. It has recently been shown that electromechanical disturbances in myotonic dystrophy may be severe enough to have significantly bad prognosis (Figs. 9.27 and 9.28) [61, 62].

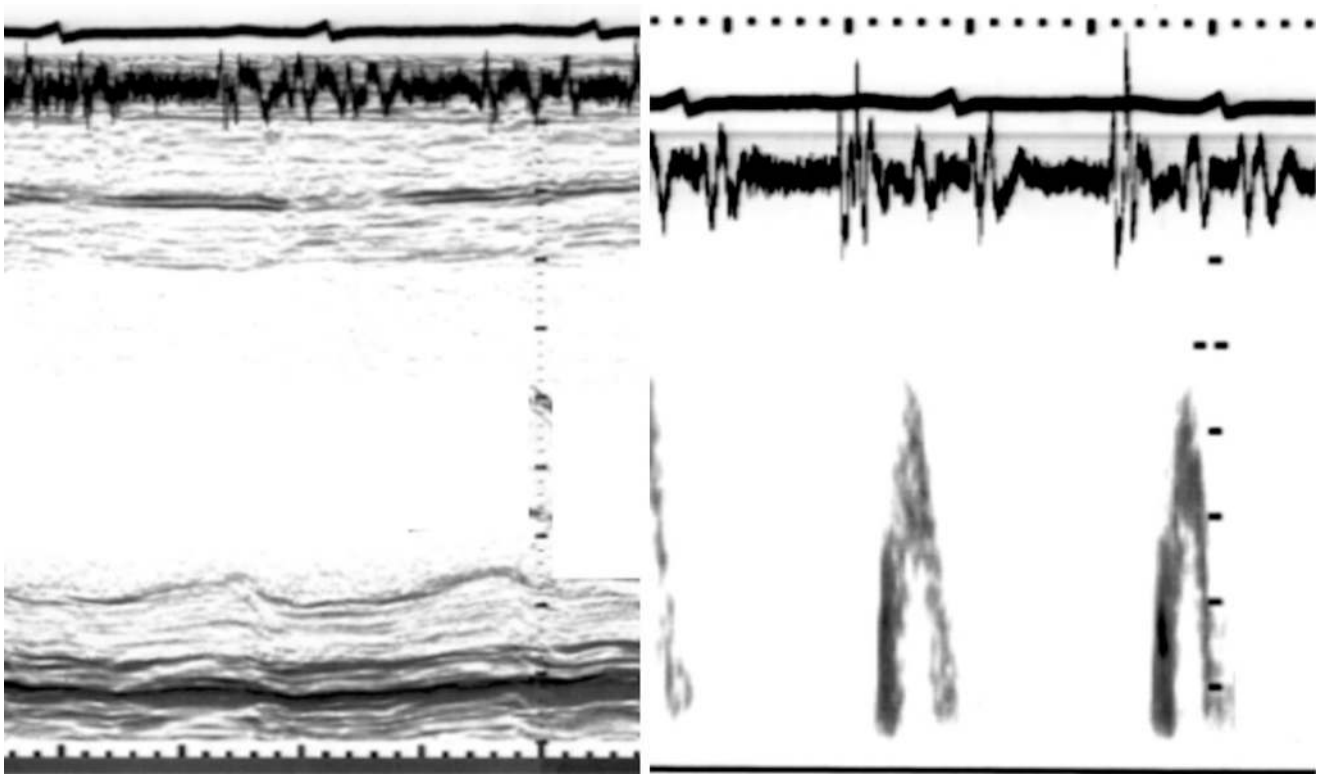


Fig. 9.26 LV minor axis recording from a patient presenting with breathlessness after doxorubicin (left). Note the poor systolic function and the limited filling time (right)

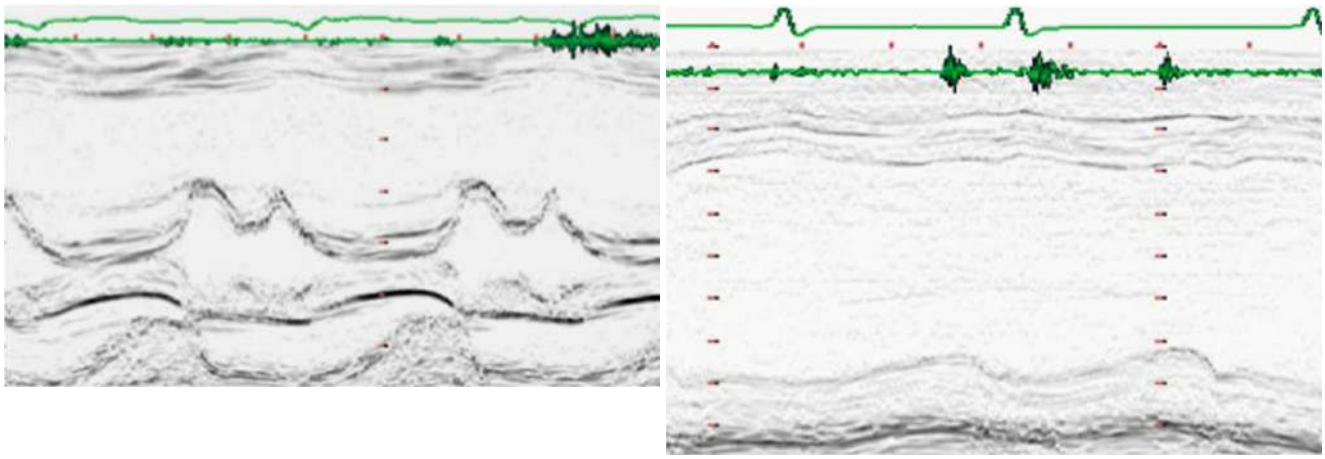


Fig. 9.27 M-mode recording from a patient with Duchenne muscle dystrophy showing enlarged LV cavity (right) with poor systatic function and zero isovolumic relaxation time (left) consistent with left atrial pressure of 30 mmHg

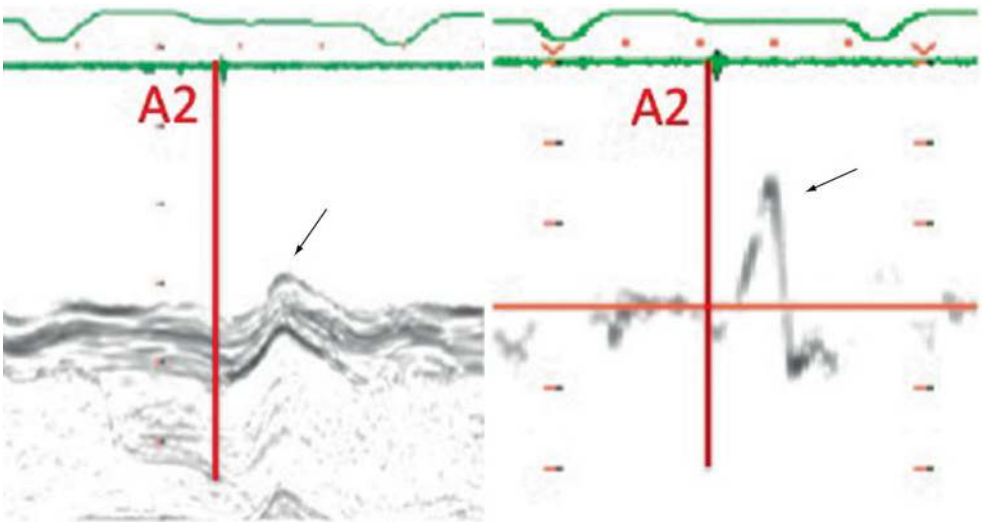


Fig. 9.28 An extreme example from a patient with DCM and septal dyssynchrony. Note the complete absence of systolic shortening on the M-mode recording (*left*) and TDI (*right*) followed by accentuated post-ejection shortening (*arrow*)

References

1. Richardson P, McKenna W, Bristow M, Maisch B, Mautner B, O'Connell J, et al. Report of the 1995 World Health Organization/ international society and Federation of Cardiology Task Force on the definition and classification of cardiomyopathies. Circulation. 1996;93:841–2.
2. Bozkurt B, Colvin M, Cook J, Cooper LT, Deswal A, Fonarow GC, et al. American Heart Association Committee on Heart Failure and Transplantation of the Council on Clinical Cardiology; Council on Cardiovascular Disease in the Young; Council on Cardiovascular and Stroke Nursing; Council on Epidemiology and Prevention; and Council on Quality of Care and Outcomes Research. Current Diagnostic and Treatment Strategies for Specific Dilated Cardiomyopathies: A Scientific Statement From the American Heart Association.Circulation. 2016;134: e579–e646.
3. Pinto YM, Elliott PM, Arbustini E, Adler Y, Anastasakis A, Böhm M, et al. Proposal for a revised definition of dilated cardiomyopathy, hypokinetic non-dilated cardiomyopathy, and its implications for clinical practice: a position statement of the ESC working group on myocardial and pericardial diseases. Eur Heart J. 2016;37:1850–8.
4. Towbin JA, Hejtmancik JF, Brink P, Gelb B, Zhu XM, Chamberlain JS, et al. X-linked dilated cardiomyopathy. Molecular genetic evidence of linkage to the Duchenne muscular dystrophy (dystrophin) gene at the Xp21 locus. Circulation. 1993;87(6):1854–65.
5. Hadjimiltiades S, Panidis IP, Segal BL, Iskandrian AS. Recovery of left ventricular function in peripartum cardiomyopathy. Am Heart J. 1986;112(5):1097–9.
6. Sutton MS, Cole P, Plappert M, Saltzman D, Goldhaber S. Effects of subsequent pregnancy on left ventricular function in peripartum cardiomyopathy. Am Heart J. 1991;121(6 Pt 1):1776–8.
7. Cambridge G, MacArthur CG, Waterson AP, Goodwin JF, Oakley CM. Antibodies to Coxsackie B viruses in congestive cardiomyopathy. Br Heart J. 1979;41(6):692–6.
8. Obeyesekere I, Hermon Y. Arbovirus heart disease: myocarditis and cardiomyopathy following dengue and chikungunya fever—a follow-up study. Am Heart J. 1973;85(2):186–94.
9. Corallo S, Mutinelli MR, Moroni M, Lazzarin A, Celano V, Repossini A, et al. Echocardiography detects myocardial damage in AIDS: prospective study in 102 patients. Eur Heart J. 1988;9(8):887–92.
10. Elliott P, Andersson B, Arbustini E, Bilinska Z, Cecchi F, Charron P, et al. Classification of the cardiomyopathies: a position statement from the European Society of Cardiology Working Group on myocardial and pericardial diseases. Eur Heart J. 2008;29:270–6.
11. Abelmann WH, Lorell BH. The challenge of cardiomyopathy. J Am Coll Cardiol. 1989;13(6):1219–39.
12. Arvidsson S, Henein MY, Wikström G, Suhr OB, Lindqvist P. Right ventricular involvement in transthyretin amyloidosis. Amyloid. 2018;25:160–6.
13. Henein MY, Lindqvist P. Diastolic function assessment by echocardiography: a practical manual for clinical use and future applications. Echocardiography. 2020;37:1908–18.
14. Bytyçi I, Dini FL, Bajraktari A, Pugliese NR, D'Agostino A, Bajraktari G, et al. Speckle tracking-derived left atrial stiffness predicts clinical outcome in heart failure patients with reduced to mid-range ejection fraction. J Clin Med. 2020;9:1244.
15. Nagueh SF, Smiseth OA, Appleton CP, Byrd BF 3rd, Dokainish H, Edvardsen T, et al. Recommendations for the evaluation of left ventricular diastolic function by echocardiography: an update from the American Society of Echocardiography and the European Association of Cardiovascular Imaging. Eur Heart J Cardiovasc Imaging. 2016;17:1321–60.
16. DeMaria AN, Bommer W, Lee G, Mason DT. Value and limitations of two dimensional echocardiography in assessment of cardiomyopathy. Am J Cardiol. 1980;46:1224–31.
17. Medina R, Panidis IP, Morganroth J, Kotler MN, Mintz GS. The value of echocardiographic regional wall motion abnormalities in detecting coronary artery disease in patients with or without a dilated left ventricle. Am Heart J. 1985;109:799–803.
18. Wallis DE, O'Connell JB, Henkin RE, Costanzo-Nordin MR, Scanlon PJ. Segmental wall motion abnormalities in dilated cardiomyopathy: a common finding and good prognostic sign. J Am Coll Cardiol. 1984;4:674–9.
19. Yazawa Y, Hayashi S, Hosokawa O, Watanabe K, Takano S, Ohno M, et al. Regional wall motion of the left ventricle in congestive cardiomyopathy: in comparison with progressive muscular dystrophy of Duchenne type (author's transl). J Cardiogr. 1981;11:1233–9.
20. Duncan AM, Francis DP, Gibson DG, Henein MY. Differentiation of ischemic from nonischemic cardiomyopathy during dobutamine stress by left ventricular long-axis function: additional effect of left bundle-branch block. Circulation. 2003;108:1214–20.

21. Laskey WK, Sutton MS, Zeevi G, Hirshfeld JW Jr, Reichek N. Left ventricular mechanics in dilated cardiomyopathy. Am J Cardiol. 1984;54:620–5.
22. Duncan AM, Lim E, Gibson DG, Henein MY. Effect of dobutamine stress on left ventricular filling in ischemic dilatedcardiomyopathy: pathophysiology and prognostic implications. J Am Coll Cardiol. 2005;46:488–96.
23. Appleton CP, Hatle LK, Popp RL. Demonstration of restrictive ventricular physiology by Doppler echocardiography. J Am Coll Cardiol. 1988;11(4):757–68.
24. Henein MY, Gibson DG. Abnormal subendocardial function in restrictive left ventricular disease. Br Heart J. 1994;72(3):237–42.
25. Henein MY, O'Sullivan CA, Coats AJ, Gibson DG. Angiotensin-converting enzyme (ACE) inhibitors revert abnormal right ventricular filling in patients with restrictive left ventricular disease. J Am Coll Cardiol. 1998;32(5):1187–93.
26. Henein MY, Amadi A, O'Sullivan C, Coats A, Gibson DG. ACE inhibitors unmask incoordinate diastolic wall motion in restrictive left ventricular disease. Heart. 1996;76(4):326–31.
27. Mancuso FJ, Moisés VA, Almeida DR, Poyares D, Storti LJ, Oliveira WA, et al. Left atrial volume determinants in patients with non-ischemic DilatedCardiomyopathy. Arq Bras Cardiol. 2015;105:65–70.
28. Bytyci I, Bajraktari G, Fabiani I, Lindqvist P, Poniku A, Pugliese NR, et al. Left atrial compliance index predicts exercise capacity in patients with heart failure and preserved ejection fraction irrespective of right ventricular dysfunction. Echocardiography. 2019;36:1045–53.
29. Bytyçi I, Bajraktari G, Henein MY. Left atrial volume index predicts response to cardiac resynchronisation therapy: a systematic review and meta-analysis. Arch Med Sci. 2020;18(4):930–8.
30. Dickerman SA, Rubler S. Mitral and tricuspid valve regurgitation in dilated cardiomyopathy. Am J Cardiol. 1989;63(9):629–31.
31. Ypenburg C, Lancellotti P, Tops LF, Boersma E, Bleeker GB, Holman ER, et al. Mechanism of improvement in mitral regurgitation after cardiac resynchronization therapy. Eur Heart J. 2008;29(6):757–65. Epub Feb 27, 2008
32. Donal E, De Place C, Kervio G, Bauer F, Gervais R, Leclercq C, et al. Mitral regurgitation in dilated cardiomyopathy: value of both regional left ventricular contractility and dyssynchrony. Eur J Echocardiogr. 2009;10(1):133–8.
33. Bytyçi I, Bajraktari G, Lindqvist P, Henein MY. Compromised left atrial function and increased size predict raised cavity pressure: a systematic review and meta-analysis. Clin Physiol Funct Imaging. 2019;39:297–307.
34. Bajraktari G, Bytyçi I, Henein MY. Left atrial structure and function predictors of recurrent fibrillation after catheter ablation: a systematic review and meta-analysis. Clin Physiol Funct Imaging. 2020;40:1–13.
35. Nishimura RA, Abel MD, Hatle LK, Tajik AJ. Relation of pulmonary vein to mitral flow velocities by transesophageal Doppler echocardiography. Effect of different loading conditions Circulation. 1990;81(5):1488–97.
36. Ritter S, Tani LY, Shaddy RE, Day RW, Orsmond GS, Pagotto LT, et al. Can Doppler systemic venous flow indices predict central venous pressure in children? Echocardiography. 2000;17(2):127–32.
37. Yock PG, Popp RL. Noninvasive estimation of right ventricular systolic pressure by Doppler ultrasound in patients with tricuspid regurgitation. Circulation. 1984;70(4):657–62.
38. Chung R, Henein MY. Apex techniques, old and new, hold the key to estimated left ventricular end-diastolic and right ventricular systolic pressure. Int J Cardiovasc Imaging. 2006;22:643–6.
39. Gottdiener JS, Gay JA, VanVoorhees L, DiBianco R, Fletcher RD. Frequency and embolic potential of left ventricular thrombus in dilated cardiomyopathy: assessment by 2-dimensional echocardiography. Am J Cardiol. 1983;52(10):1281–5.
40. Shamim W, Yousufuddin M, Cicoria M, Gibson DG, Coats AJ, Henein MY. Incremental changes in QRS duration in serial ECGs over time identify high risk elderly patients with heart failure. Heart. 2002;88(1):47–51.
41. Brecker SJ, Xiao HB, Sparrow J, Gibson DG. Effects of dual-chamber pacing with short atrioventricular delay in dilated cardiomyopathy. Lancet. 1992;340(8831):1308–12.
42. The CONSENSUS Trial Study Group. Effects of enalapril on mortality in severe congestive heart failure. Results of the cooperative north Scandinavian Enalapril survival study (CONSENSUS). N Engl J Med. 1987;316(23):1429–35.
43. Hjalmarson A, Goldstein S, Fagerberg B, Wedel H, Waagstein F, Kjekshus J, et al. Effects of controlled-release metoprolol on total mortality, hospitalizations, and Well-being in patients with heart failure: the metoprolol CR/XL randomized intervention trial in congestive heart failure (MERIT-HF). MERIT-HF Study Group JAMA. 2000;283(10):1295–302.
44. Bytyçi I, Bajraktari G, Lindqvist P, Henein MY. Improved left atrial function in CRT responders: a systematic review and meta-analysis. J Clin Med. 2020;9:298.
45. Duncan AM, Lim E, Clague J, Gibson DG, Henein MY. Comparison of segmental and global markers of dyssynchrony in predicting clinical response to cardiac resynchronization. Eur Heart J. 2006;27(20):2426–32. Epub Aug 1, 2006
46. Kapetanakis S, Bhan A, Murgatroyd F, Kearney MT, Gall N, Zhang Q, et al. Real-time 3D echo in patient selection for cardiac resynchronization therapy. JACC Cardiovasc Imaging. 2011;4(1):16–26.
47. Cleland J, Freemantle N, Ghio S, Fruhwald F, Shankar A, Marijanowski M, et al. Predicting the long-term effects of cardiac resynchronization therapy on mortality from baseline variables and the early response a report from the CARE-HF (cardiac resynchronization in heart failure) trial. J Am Coll Cardiol. 2008;52(6):438–45.
48. van Geldorp IE, Delhaas T, Hermans B, Vernooy K, Broers B, Klimusina J, et al. Comparison of a non-invasive arterial pulse contour technique and echo Doppler aorta velocity-time integral on stroke volume changes in optimization of cardiac resynchronization therapy. Europace. 2011;13(1):87–95. Epub Sep 29, 2010
49. Bajraktari G, Henein MY. The clinical dilemma of quantifying mechanical left ventricular dyssynchrony for cardiac resynchronization therapy: segmental or global? Echocardiography. 2015;32:150–5.
50. Salukhe TV, Francis DP, Clague JR, Sutton R, Poole-Wilson P, Henein MY. Chronic heart failure patients with restrictive LV filling pattern have significantly less benefit from cardiac resynchronization therapy than patients with late LV filling pattern. Int J Cardiol. 2005;100(1):5–12.
51. Dalby MC, Banner NR, Tansley P, Grieve LA, Partridge J, Yacoub MH. Left ventricular function during support with an asynchronous pulsatile left ventricular assist device. J Heart Lung Transplant. 2003;22(3):292–300.
52. Henein M, Birks EJ, Tansley PD, Bowles CT, Yacoub MH. Images in cardiovascular medicine. Temporal and spatial changes in left ventricular pattern of flow during continuous assist device "HeartMate II". Circulation. 2002;105(19):2324–5.
53. Ghio S, Recusani F, Klersy C, Sebastiani R, Laudisa ML, Campana C, et al. Prognostic usefulness of the tricuspid annular plane systolic excursion in patients with congestive heart failure secondary to idiopathic or ischemic dilated cardiomyopathy. Am J Cardiol. 2000;85(7):837–42.
54. Linde C, Leclercq C, Rex S, Garrigue S, Lavergne T, Cazeau S, et al. Long-term benefits of biventricular pacing in congestive heart failure: results from the MUltisite STimulation in cardiomyopathy (MUSTIC) study. J Am Coll Cardiol. 2002;40(1):111–8.

55. Abraham WT, Fisher WG, Smith AL, Delurgio DB, Leon AR, Loh E, et al. Cardiac resynchronization in chronic heart failure. N Engl J Med. 2002;346(24):1845–53.
56. Patel AR, Lima C, Parro A, Arsenault M, Vannan MA, Pandian NG. Echocardiographic analysis of regional and global left ventricular shape in Chagas' cardiomyopathy. Am J Cardiol. 1998;82(2):197–202.
57. Kisslo J. Two-dimensional echocardiography in arrhythmogenic right ventricular dysplasia. Eur Heart J. 1989;10(Suppl D):22–6.
58. Asimaki A, Tandri H, Huang H, Halushka MK, Gautam S, Basso C, et al. A new diagnostic test for arrhythmogenic right ventricular cardiomyopathy. N Engl J Med. 2009;360(11):1075–84.
59. Nousiainen T, Jantunen E, Vanninen E, Hartikainen J. Early decline in left ventricular ejection fraction predicts doxorubicin cardiotoxicity in lymphoma patients. Br J Cancer. 2002;86(11):1697–700.
60. de Kermadec JM, Becane HM, Chenard A, Tertrain F, Weiss Y. Prevalence of left ventricular systolic dysfunction in Duchenne muscular dystrophy: an echocardiographic study. Am Heart J. 1994;127(3):618–23.
61. Lindqvist P, Mörner S, Olofsson BO, Backman C, Lundblad D, Forsberg H, et al. Ventricular dysfunction in type 1 myotonic dystrophy: electrical, mechanical, or both? Int J Cardiol. 2010;143(3):378–84. Epub Apr 22, 2009
62. Mörner S, Lindqvist P, Mellberg C, Olofsson BO, Backman C, Henein M, et al. Profound cardiac conduction delay predicts mortality in myotonic dystrophy type 1. Intern Med. 2010;268(1):59–65. Epub Jan 11, 2010

Hypertrophic Cardiomyopathy

10

Michael Y. Henein, Per Lindqvist, Mary Sheppard, and John R. Pepper

Hypertrophic cardiomyopathy (HCM) is a primary cardiac muscle disorder with unique pathophysiology, heterogeneous expression, and diverse clinical presentations, with an annual overall mortality rate for untreated patients of approximately 1.3%. It is probably the most common genetically transmitted heart disease. HCM is often familial, of autosomal dominant transmission, and has a high degree of variable clinical penetrance. The latter is age related with typical features developing during adolescence. Approximately 50–70% of patients present mutations in one of the genes that encode different components of the cardiac sarcomere. These components are represented by β cardiac myosin heavy chain (chromosome 14), cardiac troponin T (chromosome 1), α tropomyosin (chromosome 15), cardiac myosin-binding protein C (chromosome 11), the essential and regulatory myosin light chains (chromosome 3 and 12, respectively), and cardiac actin (chromosome 15) [1–8, 59]. Mutations in three other sarcomeric protein genes (titin, Troponin C and α-cardiac myosin heavy chain) have been reported [1, 9–11]. Some adult patients, like many children, might have nonsarcomeric disease such as Anderson-Fabry disease, [12], Noonan syndrome, mitochondrial disease [13], and a phenotype that includes HCM.

Despite dramatic improvements in understanding HCM, challenges and controversies regarding its diagnosis, etiology, natural history, and management still exist. Terminology is likewise difficult, but hypertrophic cardiomyopathy is generally preferred, avoiding the term idiopathic subaortic stenosis or hypertrophic obstructive cardiomyopathy (HOCM) which implies left ventricular outflow tract obstruction. It also excludes secondary causes of left ventricular hypertrophy [14, 15].

Clinical Picture

Patients with HCM may be asymptomatic and discovered incidentally during family screening for sudden death or medical check-up that reveals left ventricular hypertrophy and T wave changes on resting ECG. Others may rarely present with exertional shortness of breath, or chest pain, with a characteristic day-to-day variation in the activity needed to cause symptoms [16–18]. Twenty percent of HCM patients complain of syncope or presyncope, which is commonly related to exertion but may also occur at rest [19]. The underlying mechanisms for these symptoms include left ventricular dysfunction, outflow tract obstruction, arrhythmias, and abnormal peripheral vascular responses during exercise. Alcohol is another provoking cause for left ventricular outflow tract (LVOT) obstruction and may cause syncope [20]. Postmortem diagnosis of HCM may be the first presentation in patients with sudden cardiac death.

Pathology

The distribution of myocardial hypertrophy in HCM may be generalized (symmetrical) [21, 22] or localized (asymmetrical) [23, 24]. The localized hypertrophy tends to affect predominantly the antero-septal wall of the left ventricle, but it may involve other regions i.e., posterior wall, ventricular apex, the right ventricle, or rarely, isolated thickened muscle trabeculae in the ventricular cavity [25]. The echocardiography criteria for HCM include increased maximal wall thickness greater than 15 mm in any myocardial segment or a septal to posterior wall thickness ratio exceeding 1.3 in

Supplementary Information The online version contains supplementary material available at https://doi.org/10.1007/978-3-031-95894-6_10.

M. Y. Henein (✉)
Imperial College London, London, UK

Siena University, Siena, Italy
e-mail: m.henein@imperial.ac.uk

P. Lindqvist
Umea University, Umea, Sweden

M. Sheppard · J. R. Pepper
Royal Brompton Hospital, London, UK

© The Author(s), under exclusive license to Springer Nature Switzerland AG 2025

M. Y. Henein (ed.), *Clinical Echocardiography*, https://doi.org/10.1007/978-3-031-95894-6_10

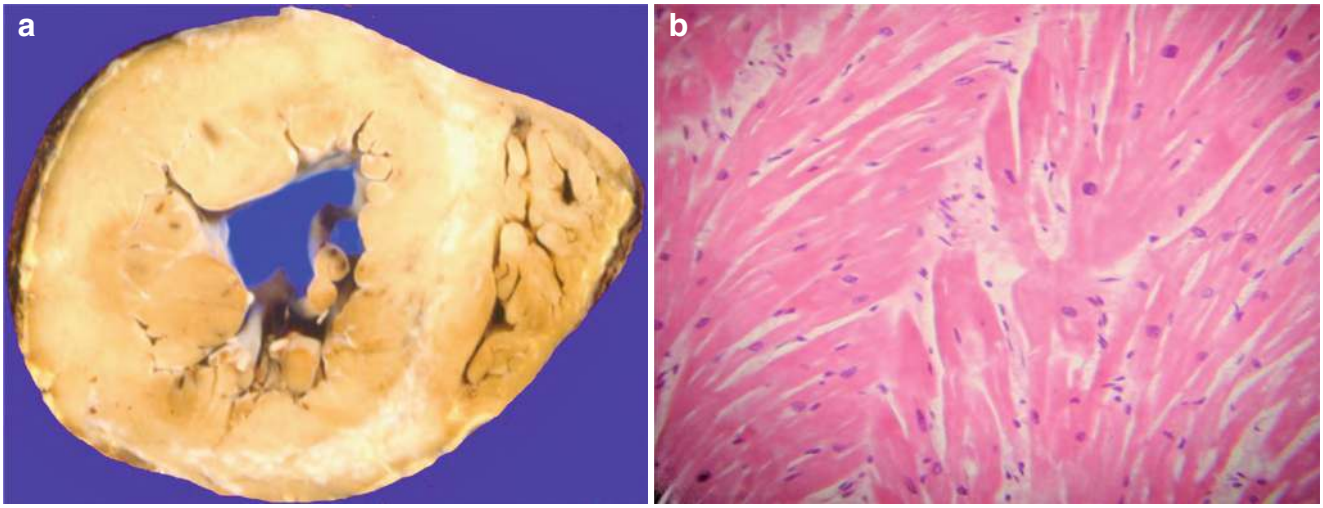


Fig. 10.1 (**a**) Transverse section of the left and right ventricles of a HCM patient showing concentric hypertrophy of the left ventricle with scaring involving the subendocardium interventricular septum and posterior wall. (**b**) Histological section showing disarray and hypertrophied myocytes at abnormal angles to each other

normotensive patients. In children, a wall thickness more thatn two standard devation above the mean, adjusted for age, gender and height suggests HCM. For wall thickness measuements in the 'gray zone' (13–15 mm) further investiagation are needed to confirm the diagnosis. The degree of segmental hypertrophy varies and may be extensive with a septal thickness up to 40 mm (Figs. 10.1, 10.2, and 10.3; Videos 10.1 and 10.2).

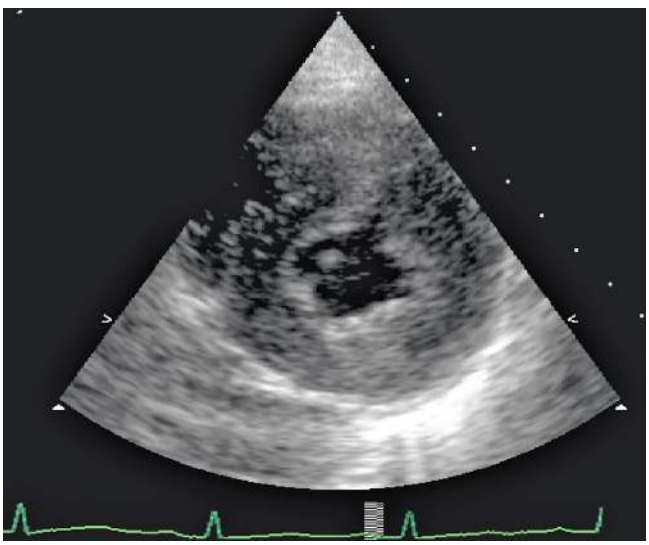


Fig. 10.2 Left ventricular minor axis view in diastole showing concentric myocardial hypertrophy

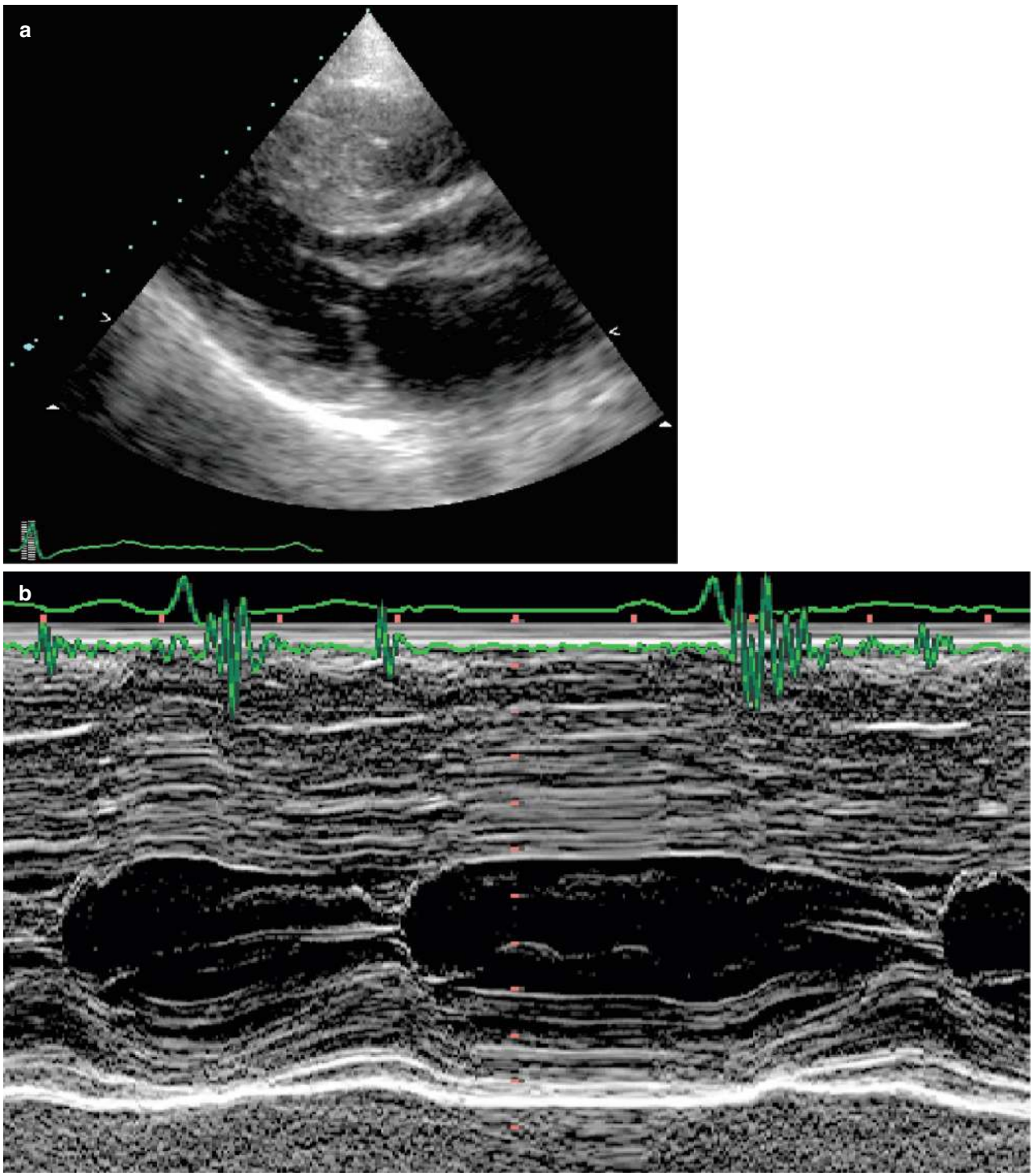


Fig. 10.3 Parasternal long axis two-dimensional view from a patient with localized anterior wall HCM (**a**) and corresponding M-mode recording (**b**)

Pathophysiology

In addition to the hypertrophic phenotypic presentation of HCM, it is generally believed that part of the left ventricular hypertrophy is subject to dynamic changes as part of the HCM disease process, through the consistent narrowing of the outflow tract by approximation of anterior mitral valve leaflet to the proximal interventricular septum in systole, possibly as a result of a pressure gradient with suction of the mitral leaflets towards septum, "Venturi effect" [26]. This systolic anterior movement (SAM) of the mitral valve is a characteristic echocardiographic feature of the LV outflow tract narrowing or obstruction, and results in significant high velocities during systole (equivalent to a pressure drop) with the increase in heart rate. In a number of patients with this condition the main site of myocardial bulk is the midcavity, which results in midcavity late systolic obliteration rather than outflow tract obstruction (Figs. 10.4, 10.5, and 10.6) [27–29]. Apical form of hypertrophic cardiomyopathy is commonly seen in Japan with characteristic ECG presentation of giant negative T waves [30].

SAM of the mitral valve is always associated with some degree of LVOT obstruction (pressure drop—high velocities) at rest. In symptomatic patients with morphological ventricular features of HCM but no signs of outflow tract obstruction, a form of stress test (Valsalva or exercise) often helps in demonstrating signs of dynamic outflow tract obstruction and high pressure drop that may coincide with development of symptoms (Fig. 10.7). Such outflow tract obstruction results in some degree of concomitant mitral regurgitation, raised left atrial pressure, pulmonary venous hypertension and hence breathlessness with or without chest pain. Also, exercise/stress-induced outflow tract obstruction results in characteristic drop of systolic blood pressure, and hence the basis for syncope and presyncope (Video 10.3).

Raised outflow tract velocities in HCM must be distinguished from intracavitary gradients which have no significant or little hemodynamic effect and are not usually associated with symptoms [31]. What confirms the direct relationship between systolic anterior movement of the mitral valve (SAM) and outflow tract velocities is the disappearance of SAM when the outflow tract gradient is abolished either by myotomy—myectomy, alcohol septal ablation, or mitral valve plication (Fig. 10.8).

SAM of the valve may result from papillary muscle coaption with the septum rather than the mitral leaflets themselves, in patients with hypertrophied papillary muscle that inserts directly into the mitral valve leaflets [32]. In addition, progonged mitral leaflets in HCM might also be part of the mechanism of outflow tract obstruction, with or without extensive increase in septal thickness (Fig. 10.9) [1]. In these cases, mitral valve plication, repair or replacement may be the most appropriate management in order to separate the papillary muscle from the mitral valve movement or mitral leaflets from septum [33] [1].

The level of left ventricular cavity narrowing or obstruction can be determined by color flow Doppler, since it demonstrates nonlinear (mosaic) flow on two-dimensional images at the site of narrowing. The degree of outflow tract obstruction or midcavity obliteration is determined by continuous wave Doppler recordings in the form of a pressure drop. The shape of the continuous wave velocity trace is also helpful in differentiating between outflow tract obstruction

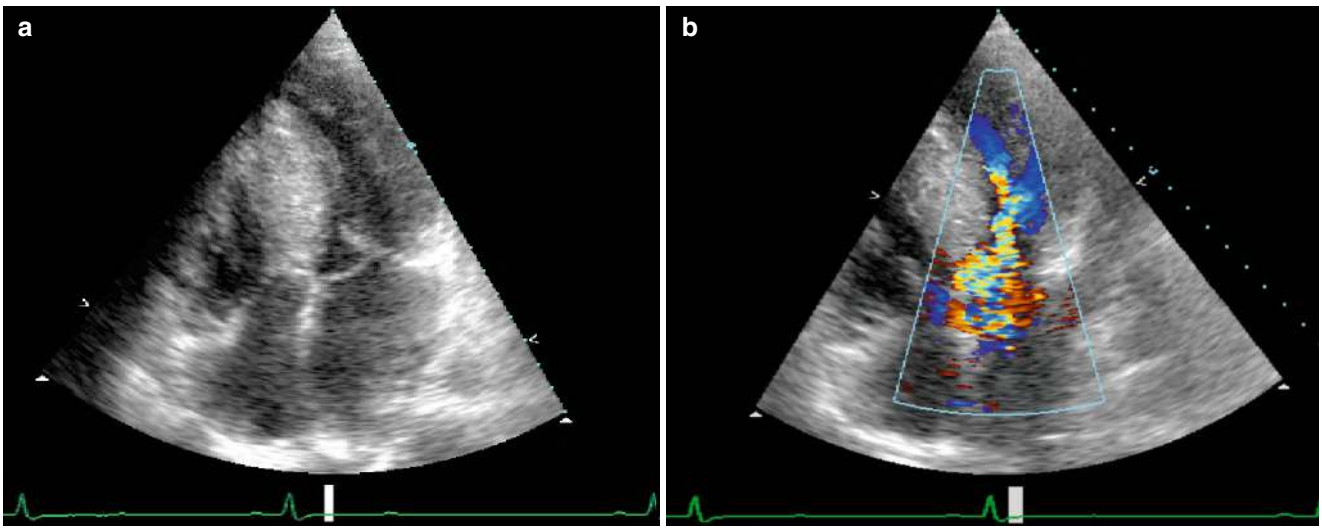


Fig. 10.4 Apical 4-chamber view from a patient with HOCM. Note the SAM of the mitral valve (**a**) and the resulting high outflow tract velocities by color Doppler (**b**)

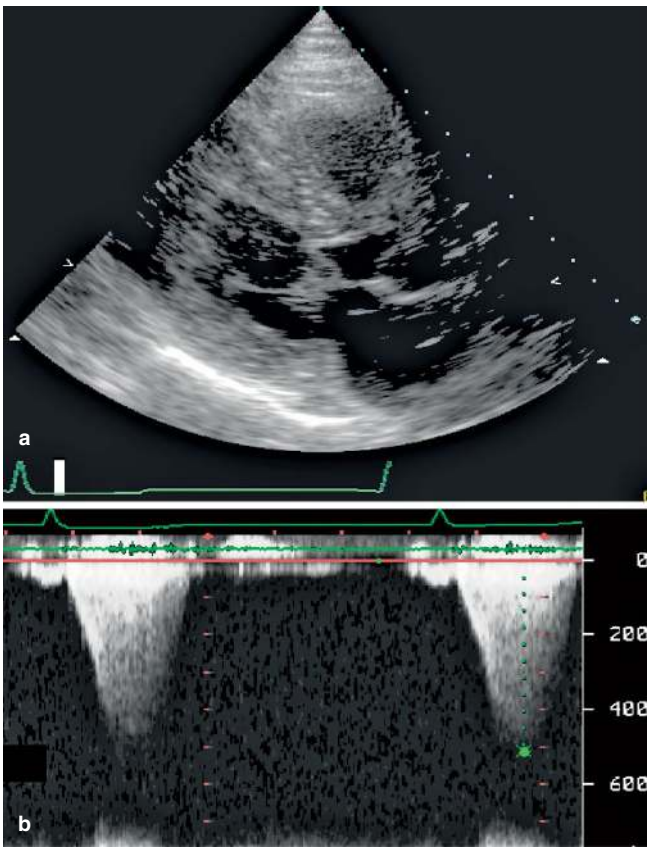


Fig. 10.5 Parasternal long axis view of the LV from a patient with HCM. Note the SAM of the mitral valve, narrowing the outflow tract in systole. 2D image (**a**) and CW Doppler gradient (**b**)

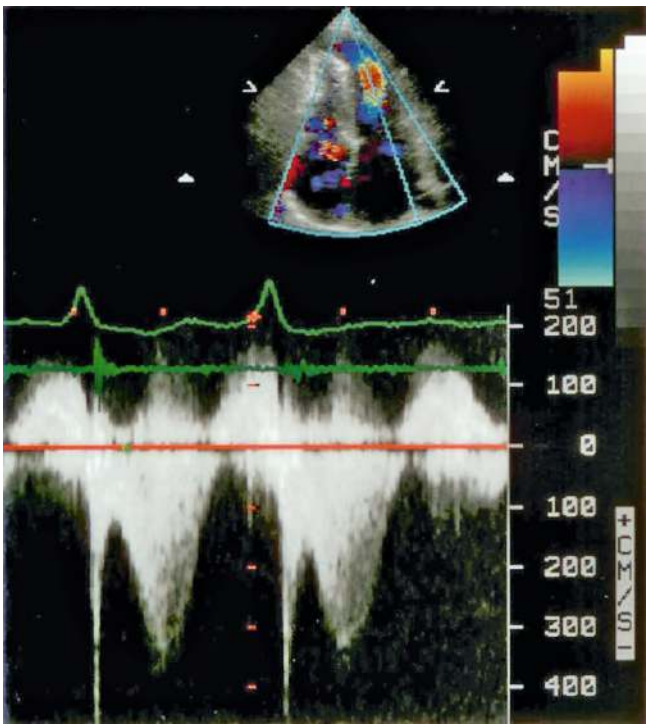


Fig. 10.6 Apical 4-chamber view from a patient with HCM and mid-cavity narrowing (*top*) demonstrating late systostic pressure drop

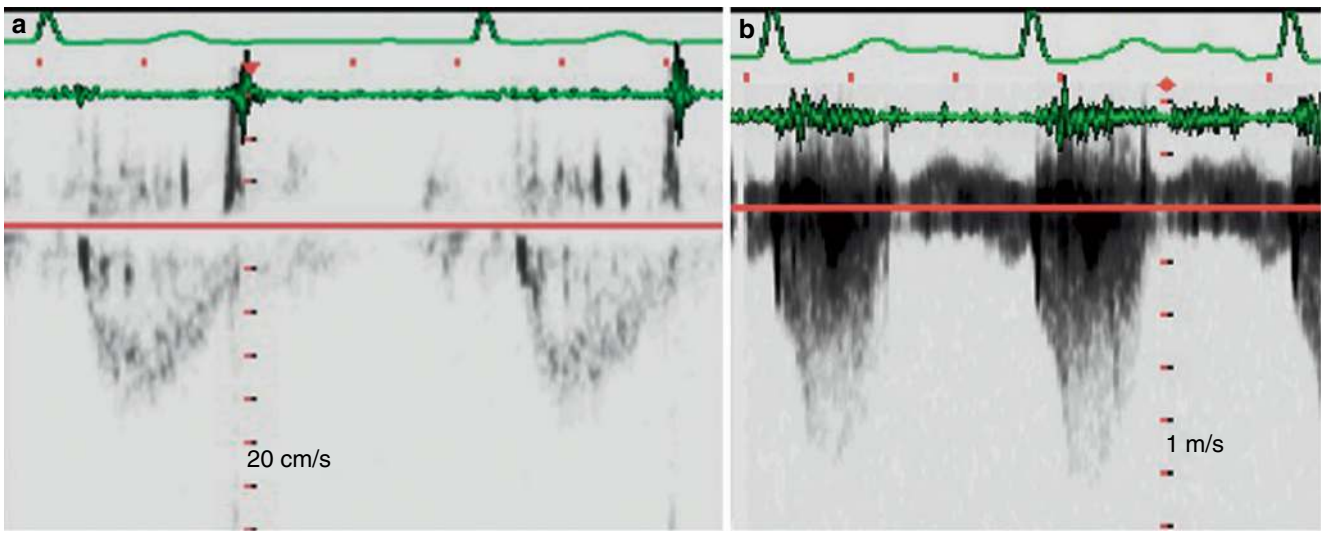


Fig. 10.7 Left ventricular outflow tract velocity (CW Doppler) from a patient with HCM, at rest (**a**) and peak stress (**b**). Note the significant increase in LV outflow tract pressure drop to 100 mm Hg with stress

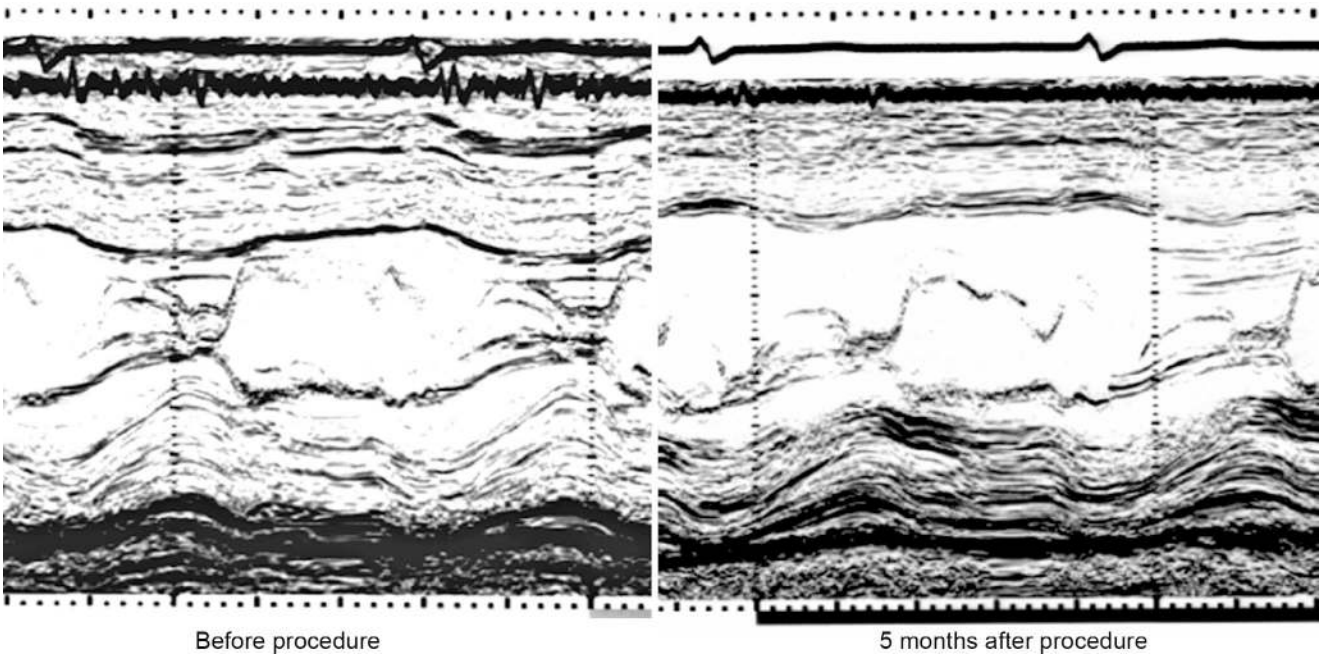


Fig. 10.8 Mitral valve echogram from a patient with HCM showing SAM (*left*) which disappeared after alcohol septal ablation (*right*)

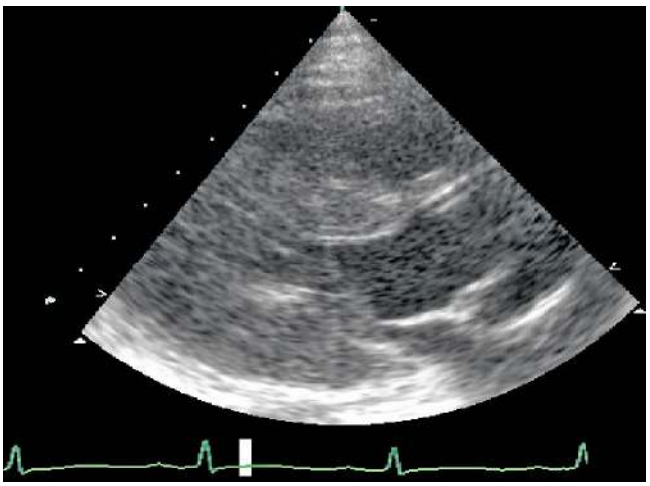


Fig. 10.9 Parasternal long axis view from a patient with HCM involving the papillary muscles. Note the anterior displacement of the papillary muscles and their movement that narrows the outflow tract

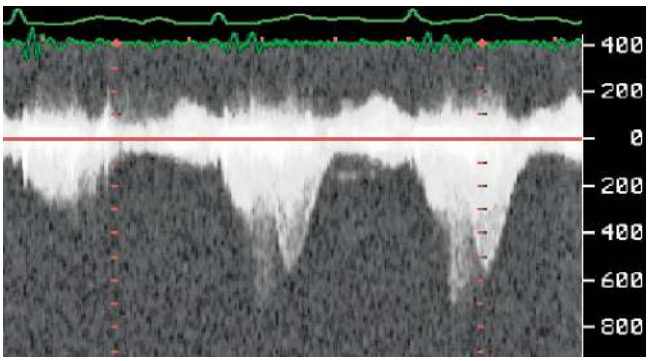


Fig. 10.10 Continuous wave Doppler of the LV outflow tract from a patient with HCM and outflow tract narrowing. Note the raised velocities that peak in midsystole in addition to another late systolic high-velocity component due to midcavity obliteration

(which peaks in mid-systole) and mid-cavity obliteration (whose velocity peaks in late systole; Fig. 10.10).

With symmetrical hypertrophy, the left ventricular cavity is crescent-like in shape rather than ellipsoid on the apical views. This shape change may itself contribute to the systolic anterior mitral valve movement and narrowing of the left ventricular outflow tract. Complete apical obliteration may occur when asymmetrical septal hypertrophy is solely apical (Fig. 10.11) [34, 35].

In HCM, the septum is commonly hypokinetic, and contributes little to the overall systolic function of the left ventricle. In order to maintain the stroke volume, the ventricular free wall becomes hyperactive. Septal hypokinesia [36, 37] should not be confused with that due to coronary artery disease, particularly its lengthening velocity, in early diastole. This can be confirmed by stress echo as it demonstrates normal increase in septal amplitude of movement but less than normal increase of its lengthening velocity. These findings suggest compromised septal distensibility rather than ischemic dysfunction. The coronary arteries themselves in HCM are commonly large and not obstructed,

although coronary velocities may be less than normal in some patients.

SAM and outflow tract obstruction accompany midsystolic aortic valve closure which probably reflects the disturbed outflow jet during systole, resulting from the obstruction. This is a frequently seen echocardiographic feature of subaortic (outflow tract) obstruction; if not present at rest, it appears with stress as SAM obstructs the outflow tract in late systole (Fig. 10.12).

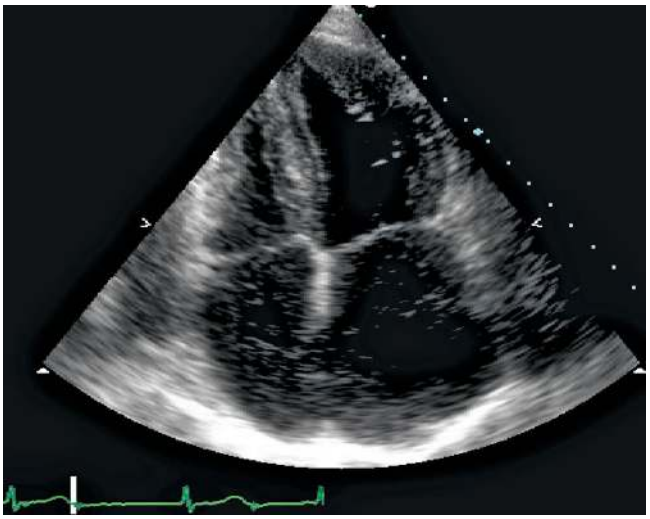


Fig. 10.11 Apical 4-chamber view from a patient with HCM demonstrating obliterated apex

Stress Echocardiography in HCM

Assessing HCM patients with stress echocardiography is important in order to establish treatment stratergy and prognosis [59] Exercise stress is preferable and recommended as pharmacological stress may give false positive response with LV outflow tract obstruction HCM [3]. While pharmacological stress does not reflect real exercise, when assessing related symptoms, exercise echo over estimates exercise severity. Patients unable to exercise could be assessed by conventional dobutamine stress echocqardiography.

Raised left ventricular outflow tract velocities at rest or with stress must be distinguished from mitral regurgitation, which is a common association, using color flow and continuous wave Doppler (Fig. 10.13) [38]. While color flow Doppler may demonstrate jet direction at rest, continuous wave Doppler is more confirmatory, particularly during stress and fast heart rate. The main difference between the two is that the outflow tract velocity signal stops at end ejection, but persists beyond A2 in mitral regurgitation.

Continuoius wave Doppler might disply concomitant mitral regurgitation flow velocity which superimposed on LVOT obstruction flow velocity. In that case, the sum of the peak mitral regurgitation pressure drop and the estimated left atrial pressure is equal to the estimated systolic left ventricular pressure. The net pressure difference between estimated LV systolic pressure and systolic blood pressure can estimate peak systolic LVOT pressure drop.

In HCM, diastolic left ventricular function is commonly disturbed, especially during exercise. A number of observa-

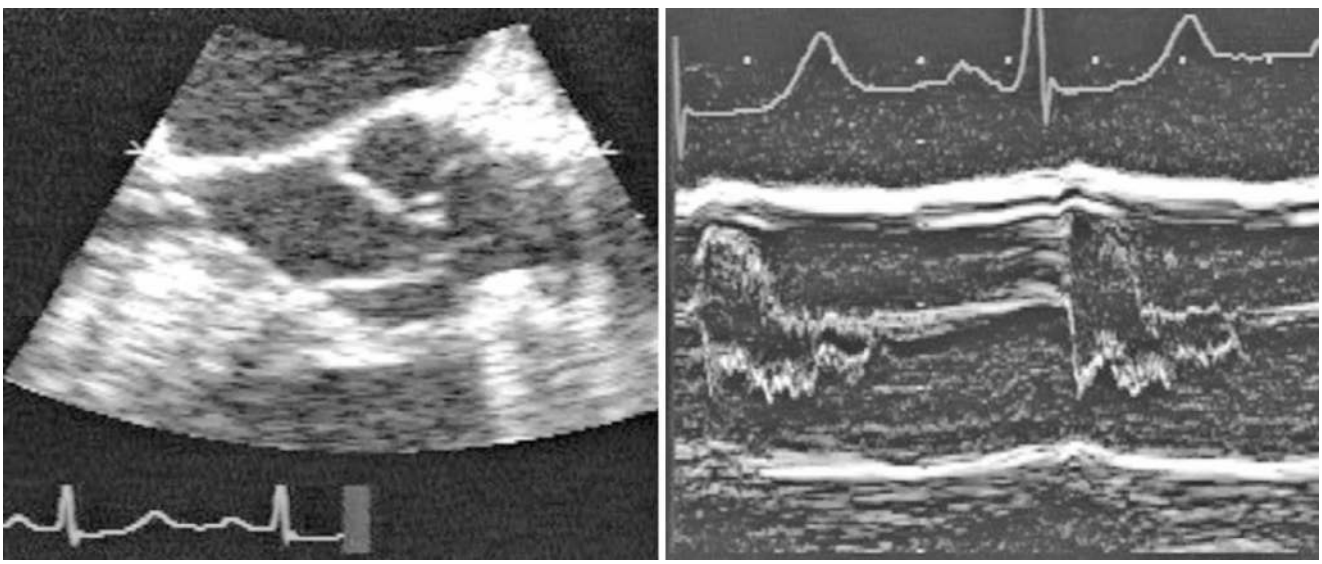


Fig. 10.12 Transesophageal echo of the aortic valve from a patient with HCM demonstrating midsystolic valve closure on 2D (*left*) and M-mode (*right*)

tions consistent with left ventricular hypertrophy but not specifically for HCM are noticed during diastole. Isovolumic relaxation time is prolonged and early diastolic left ventricular filling velocity is reduced with prolonged deceleration time, at rest. These findings are consistent with slow myocardial thinning rate and increased dispersion of early diastolic lengthening velocities and normal left ventricular filling pressure [39, 40]. Patients may also show some degree of incoordination or dyssynchrony, which does not have to be necessarily severe enough to compromise ventricular filling time (Fig. 10.14).

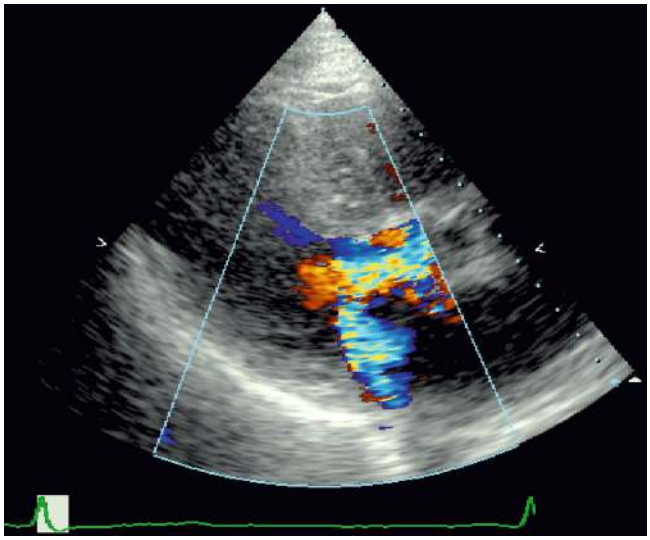


Fig. 10.13 Color flow Doppler recordings from a patient with HCM at peak dobutamine stress showing SAM, high outflow tract velocities and functional mitral regurgitation

Patients with apical hypertrophy and mid-cavity obliteration may show intracavitary flow during the isovolumic periods suggesting either differences in pressure within the ventricle or significant shape change of the cavity [41]. Late stages of HCM may demonstrate signs of stiff myocardium, raised left ventricular end-diastolic pressure and left atrial pressure. This is another cause of breathlessness and atrial arrhythmias in HCM patients. Detailed assessment of such patients confirms dilated left atrium, mitral regurgitation, and signs of pulmonary venous or even secondary (post-capillary) arterial hypertension. Management of these patients is often a challenge, since the favored vasodilators for raised left atrial pressure would exaggerate outflow tract obstruction and hence the vicious circle (Figs. 10.15 and 10.16).

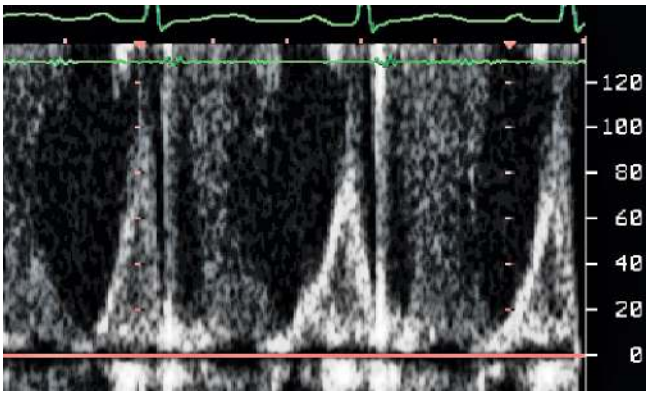


Fig. 10.14 Left ventricular filling from a patient with HCM and slow relaxation demonstrating dominant late diastolic filling

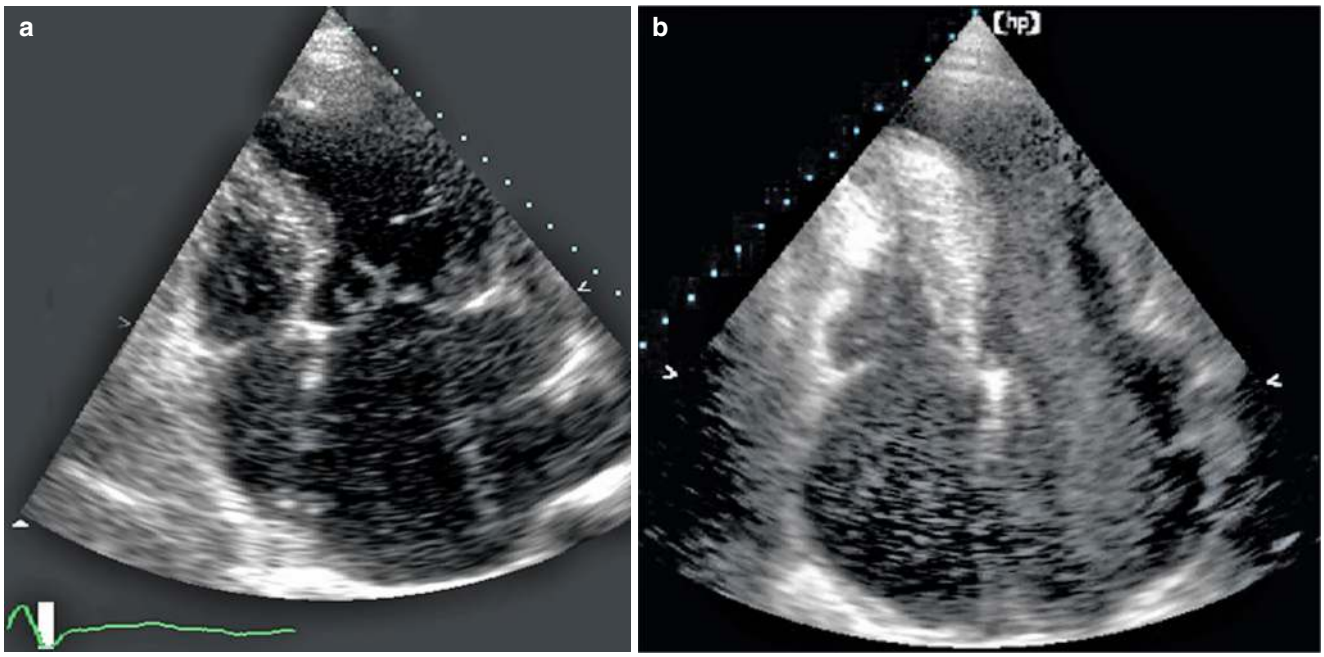


Fig. 10.15 (**a**) Apical views from a patient with HCM and stiff LV. Note the SAM of the mitral leaflets and the dilated left atrium. (**b**) Apical views from a patient with HCM showing aneurysmal apex and spontaneous echo contrast

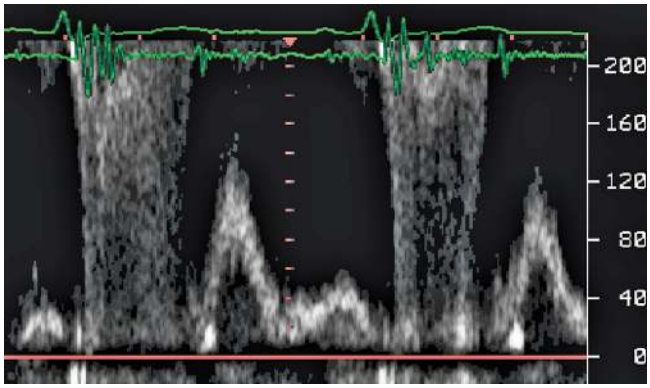


Fig. 10.16 Left ventricular filling from a patient with HCM demonstrating restrictive filling pattern and a third sound III on the phonocardiogram

Natural History

HCM may remain silent for years until it is incidentally discovered. There is no set course for the disease process. Symptoms may remain well controlled by medications for years but once the myocardium becomes stiff and intraventricular pressure rises patients complain of breathlessness or arrhythmia (often atrial fibrillation). Patients presenting with HCM later in life (sixth decade and beyond) are usually hypertensive with some degree of ventricular hypertrophy that predominantly affects the proximal septum [42]. These patients' main complaint is often exertional breathlessness rather than chest pain, arrhythmia, or syncope. Symptoms can easily be provoked and cardiac function assessed using exercise or stress echocardiography. Basal septal hypertrophy, if significant, causes LVOT obstruction during stress with the development of SAM and a drop in systolic blood pressure at the time of symptoms in a similar fashion to middle age HCM [43]. Such basal septal hypertrophy has a benign outcome in contrast to HCM and in the majority of patients symptoms can be controlled by beta blockers [44] or verapamil. Regardless of the echocardiographic picture, the clinical course in HCM is unpredictable. In a number of patients, the classical picture of HCM may change over the years to that of dilated cardiomyopathy leaving residual asymmetrical segmental hypertrophy. This progression is difficult to predict (Fig. 10.17) [45].

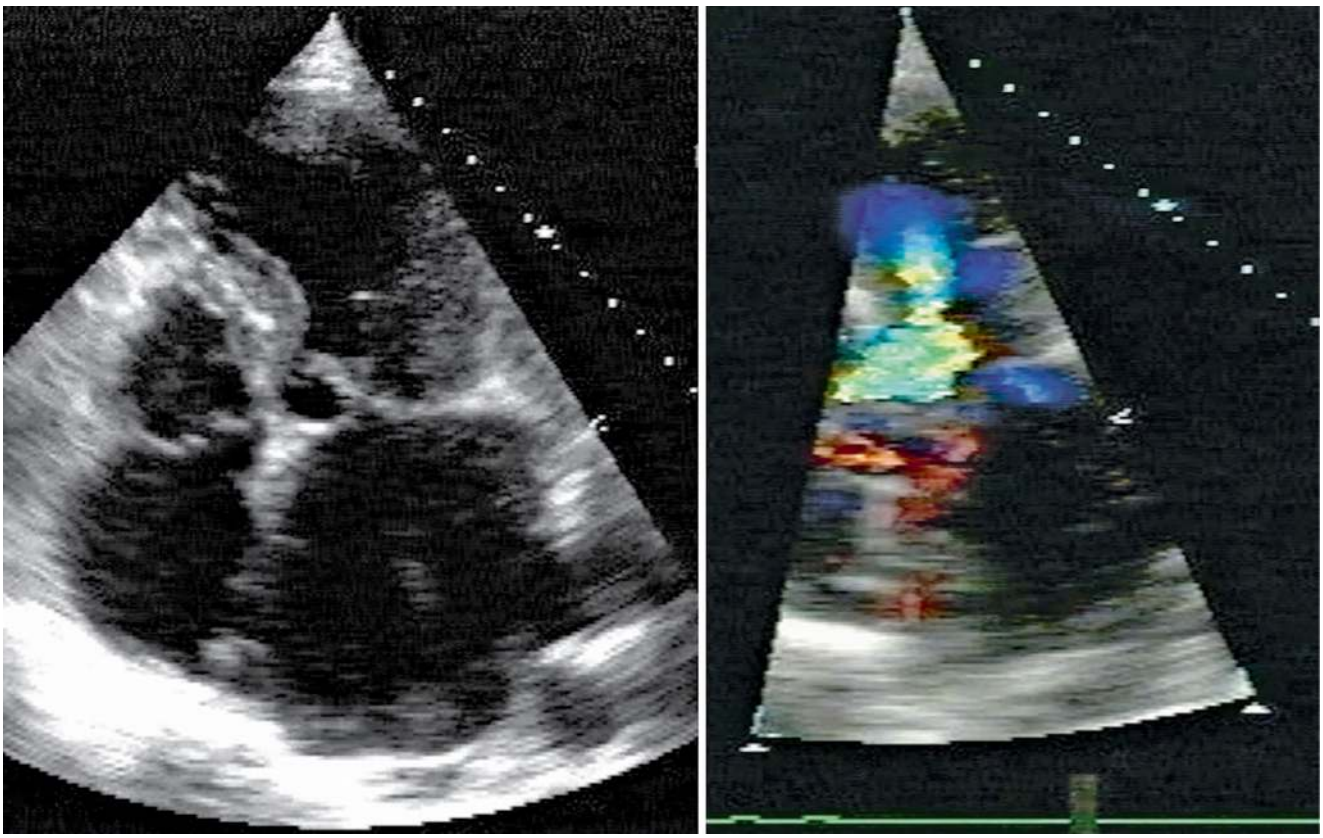


Fig. 10.17 Apical view from an elderly with basal septal hypertrophy, SAM, and color aliasing in the outflow tract (*left*). LV out flow tract velocities by continuous wave Doppler at rest and peak stress (*right*)

Mitral Valve Dysfunction in HCM

Mitral regurgitation is commonly seen in HCM. It is often mild in severity, but may become significant in advanced left ventricular dysfunction. A number of mechanisms may contribute to the alteration of normal function of the mitral valve and development of mitral regurgitation in HCM.

1. Hypertrophy of the posterior papillary muscle may displace the mitral valve anteriorly resulting in apposition of the anterior mitral valve leaflet to the septum [46].
2. Anterior mitral valve leaflet area and length are both greater than normal in HCM despite the normal diameter of the mitral valve annulus circumference. This makes the two leaflets coapt half way through their length, leaving the distal part redundant in the left ventricular cavity. With the increase in left ventricular cavity pressure during early systole the freely mobile mitral leaflet tips are pushed against the proximal part of the venticular septum, hence the reduction in the LVOT diameter resulting in raised pressure drop (Fig. 10.18) [47, 48].
3. The abnormal behavior of the mitral valve leaflets in systole (SAM) results in significant deformation of its orifice area, and consequently mitral regurgitation, of varying severity.
4. In late stages of the disease, the raised left ventricular diastolic pressure and left atrial pressure increase left ventricular and left atrial cavity size as well as the mitral annular diameters. This results in various degrees of mitral regurgitation, which may be severe (Fig. 10.19).

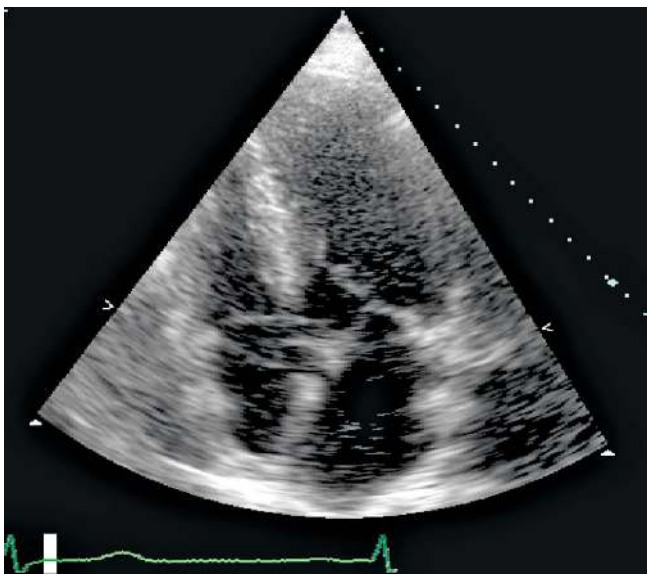


Fig. 10.18 Apical view of the mitral valve leaflets showing midlength coaption in midsystole and anterior movement of the leaflet tips (SAM)

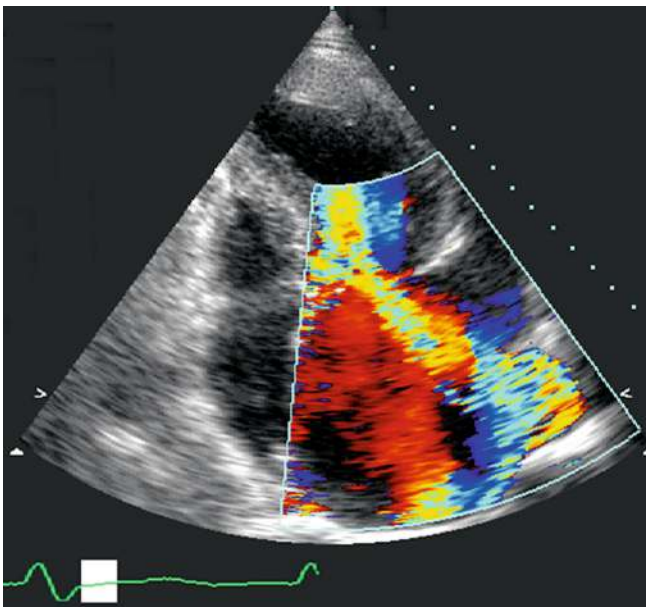


Fig. 10.19 Apical 4-chamber view from a patient with HCM and severe mitral regurgitation

Exercise Intolerance in Hypertrophic Cardiomyopathy

A number of factors may contribute to exercise intolerance known in patients with hypertrophic cardiomyopathy:

(a) An increase in LVOT velocities (gradient) with exercise results in acute drop in systolic blood pressure at the time of symptom development.
(b) High LVOT pressure drop aggravates mitral regurgitation, thus adding to the increase in atrial pressure, and pulmonary venous congestion.
(c) Exercise-induced increased LVOT pressure drop prolongs systole and shortens diastole, thus limiting ventricular filling time and stroke volume. This disturbed physiology is associated with raised left atrial pressure.
(d) The raised left atrial pressure itself may contribute to exercise intolerance by increasing pulmonary venous pressure and causing exacerbating subendocardial ischemia (Fig. 10.20).
(e) Arrhythmia may be the main exercise limiting factor in HCM. This tends to manifest at fast heart rates and during exercise/stress. Patients in atrial fibrillation might also present with shortness of breath, particularly when it is fast, due to low stroke volume.
(f) Right ventricular function is an important contributing factor to exercise tolerance. When involved in the disease process, its function is usually disturbed and hence its overall performance may influence exercise capacity (Fig. 10.21).

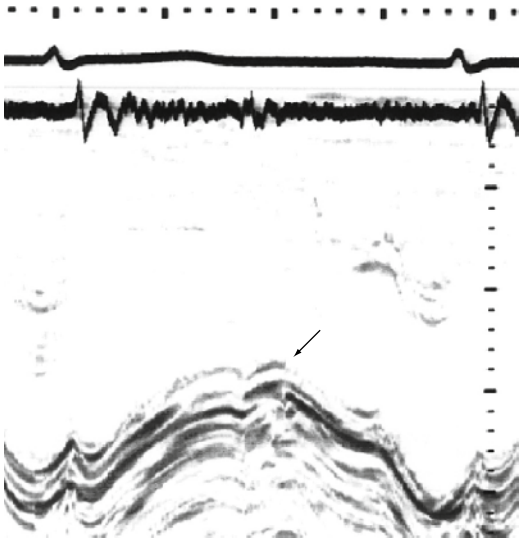


Fig. 10.20 Left ventricular free wall long axis recording demonstrating gross incoordination (postejection shortening) consistent with subendocardial ischemia (*arrow*)

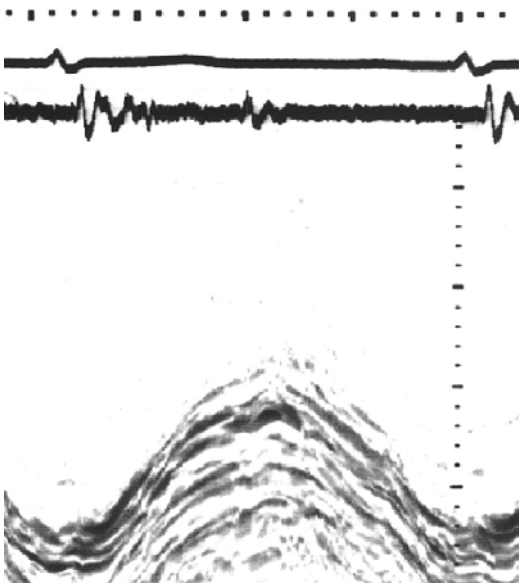


Fig. 10.21 Right ventricular long axis recording from a patient with HCM and right ventricular involvement demonstrating reduced amplitude of movement (that corresponds to ejection fraction)

Differencial Diagnosis of HCM

Conditions that can lead to thick cardiac muscle may confuse the diagnosis with HCM including cardiac amyloidosis, hypertensive heart disease, LV non-compaction, and athlete's heart and other infiltrative heart diseases.

In cardiac amyloidosis, left ventricular myocardial thickness is typically moderate and generally not asymmetric. Atrial septal thickness and valvular thickening are also present. While diastolic dysfunction occurs in the early stages of the disease systolic dysfunction typically develops in the later

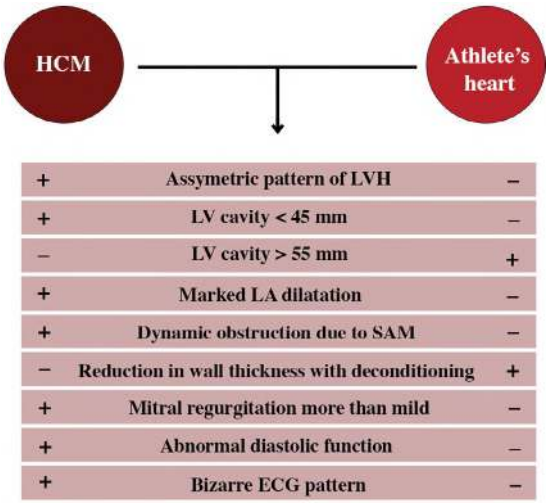


Fig. 10.22 Maron's criteria to distinguish HCM from athlete's heart

stages [49, 50]. In hypertensive heart disease, left ventricular hypertrophy is usually concentric with a sigmoid interventricular septum, and maximal wall thickness rarely exceeds 15 mm. Intensive strenuous exercise, particularly endurance sports, can lead to cardiac remodeling, increased both wall thickness and chamber size. If asymmetric LV hypertrophy is present, along with small cavity size (usually <45 mm), left atrial dilatation, dynamic obstruction, bizarre ECG findings, and abnormal left ventricular filling pressures, HCM should be suspected. Figure 10.22 illustrates the Maron criteria for distinguishing athlete's heart from HCM [51].

Management of Hypertrophic Cardiomyopathy

Medical

No current treatment is expected to prevent or stop disease progression in HCM. The main objective of medical treatment is symptom control. β blockers and/or calcium antagonists (i.e. Verapamil) have been used to control frequent arrhythmia and increases in heart rate that may be associated with syncopal attacks. Also, they have the benefit of prolonging diastole and total left ventricular filling time, which is crucial for securing optimum stroke volume; a sustained release verapamil in doses up to 480 mg/day may be useful in controlling heart rate and symptoms [52, 53]. Disopyramide with its negative inotropic effect has been used as an alternative to verapamil, mainly in patients demonstrating outflow tract obstruction at rest. Digitalis or amiodarone can be used to control the ventricular rate in patients with symptomatic atrial fibrillation along with prophylactic anticoagulation to prevent thromboembolism. Reversion to sinus rhythm either medically or electrically and its maintenance is always desirable, of course in patients with normal left atrial

size. However, patients with poor ventricular compliance and raised left atrial pressure who have dilated atria may prefer atrial fibrillation than sinus rhythm since the stroke volume generated by atrial contraction is pumped retrogradely into the pulmonary veins, resulting in worsening pulmonary congestion. When there are symptoms of congestion due to a high left atrial pressure, careful use of a diuretic or even an ACE-inhibitor may be considered. Careful use of vasodilators in HCM needs to be emphasized. While they tend to successfully reduce the preload and improve symptoms of congestion, they may also reduce the afterload and accentuate the pressure drop across the narrowed LVOT, resulting in syncopal complications. Patients presenting with signs and symptoms of cardiac decompensation are managed with conventional heart failure treatment. Recently, Mavacamten, a myosin inhibitor, has been introduced for treating HCM and early results showed improved quality of life through reduction of left ventricular outflow tract obstruction [54].

Pacing

DDD pacing has been used in patients in whom medical treatment proved not successful, in an attempt to divert septal contraction from being left-sided to become right ventricular. The rationale behind the procedure is potential widening of the left ventricular outflow tract and lowering the pressure drop, hence improvement of symptoms. Results of DDD pacing are unpredictable and early changes in ventricular behavior have not been thoroughly documented. Pacing the right ventricular apex has produced significant reduction in left ventricular outflow tract gradient compared to upper septal pacing. However, in some patients, symptoms do not change or may even become worse with DDD pacing. Long-term symptomatic improvement in the form of quality of life has not been accompanied by objective assessment of exercise tolerance [59]. Evidence exists that cardiac resynchronization therapy and biventricular pacing may benefit patients with late-stage HCM, which results in symptomatic improvement associated with reverse remodeling [55, 56].

Surgical

The standard surgical procedure for HCM is septal myectomy (the Morrow procedure) in which a small portion of the proximal septal myocardium is resected to widen the outflow tract and reduce the pressure drop across it [46]. Major complications of this operation are known: thrombo-embolism, ventricular septal defect, complete heart block, and severe aortic insufficiency. In the majority of patients, complete left bundle branch block develops which is always considered a criterion for success. Less commonly, a permanent pacemaker implantation may be required for complete heart block. Alternatively, patients with papillary muscles inserting into the mitral valve leaflets are considered as having variant degree of mitral valve disease. In these patients, attempts have been directed toward abolishing the LVOT obstruction by either plicating the mitral leaflets or replacing the entire valve with a prosthesis. Rarely, patients with disproportionately long mitral leaflets as the main cause of LVOT obstruction might need chordal repositioning [57]. Overall surgical management of HCM may completely resolve the LVOT obstruction but patients may later complain of symptoms compatible with restrictive ventricular physiology or limiting arrhythmia. It must be mentioned that even surgical myectomy does not alter the natural history of the myocardial disease, where some patients might continue to develop regional myocardial thinning picture, particularly at the apex which may carry arrhythmogenic features (Fig. 10.23).

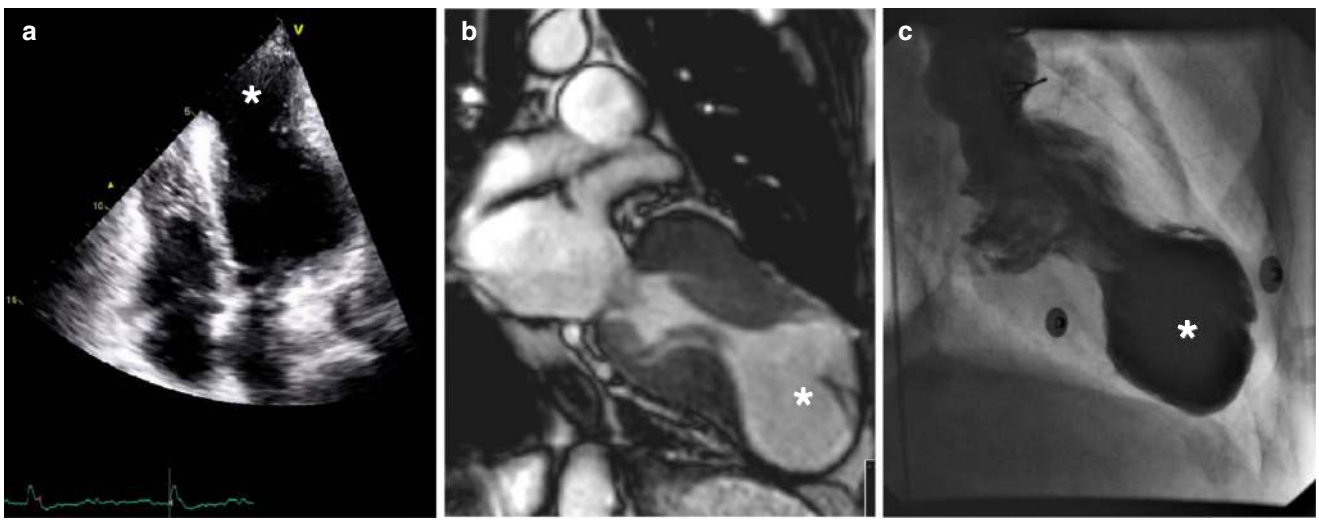


Fig. 10.23 Echo (**a**), CMR (**b**), and contrast ventriculogram (**c**) from a patient who received basal septal myectomy for obstructive HCM and 20 years later developed life-threatening arrhyth-mogenic apical aneurysm

Nonsurgical Septal Reduction

This transcatheter procedure aims at creating a small localized upper septal infarct by injection of absolute alcohol at the site of narrowing of the left ventricular outflow tract in an attempt to widen it. A balloon is inflated in the upper septal coronary branch, usually the proximal segment of the first septal branch of the left anterior descending artery. If the outflow tract pressure drops, 1–3 ml of absolute alcohol is injected down the canulated artery, distal to the inflated balloon. Outflow tract pressure drop is again assessed at rest and at peak stress with either dobutamine or isoprenaline. If the results are not satisfactory, as assessed by outflow tract gradient, the same steps are repeated again while canulating the second perforator of the left anterior descending artery and creating a larger area of septal akinesia (Fig. 10.24) [58, 59].

Echo contrast material, aids in identifying the bulk of muscle supplied by each septal branch and hence determining the target artery [60, 61]. A diluted myocardial echo contrast is injected distal to the inflated balloon in the cannulated septal perforator and the location and size of the opacified myocardium is assessed (Fig. 10.25).

Procedural success results in a significant rise in myocardial enzyme levels and a reduction in outflow tract velocities, along with the development of conduction disturbances (right bundle branch block or absent septal q wave) and septal incoordination (Fig. 10.26) [62].

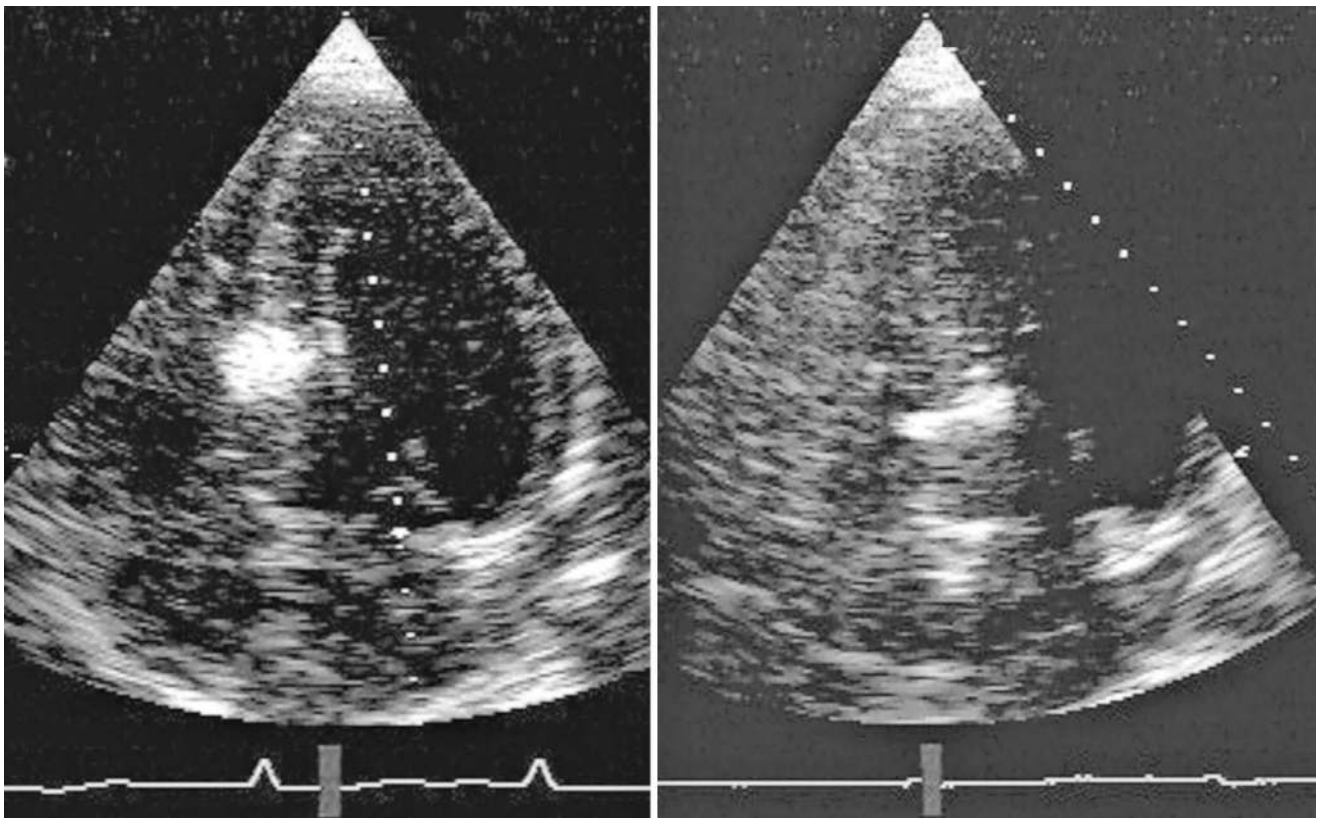


Fig. 10.24 Echo contrast injected in the second (*left*) then first (*right*) septal branches of the left anterior descending artery. Note the localization of the opacified septal myocardiun in each

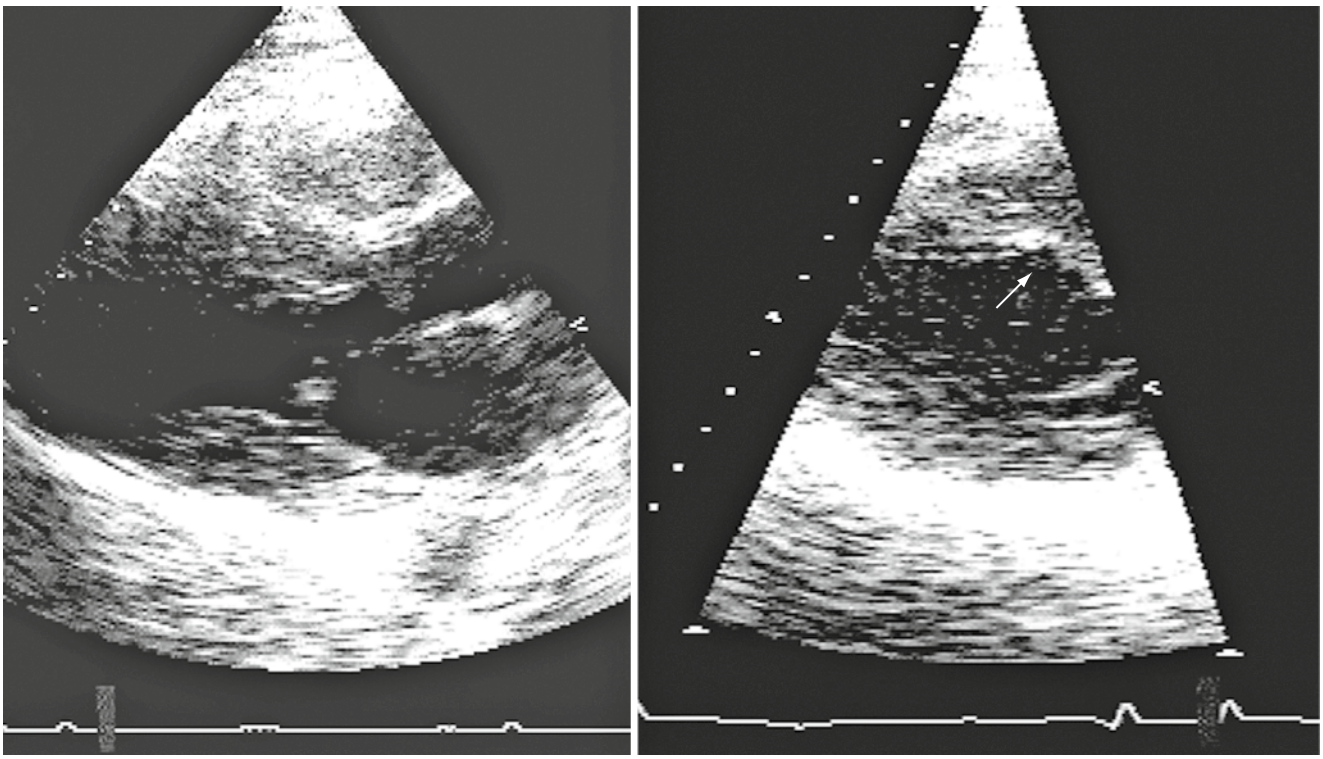


Fig. 10.25 LV long axis view of a patient with obstructive HCM before (*left*) and after (*right*) transcatheter nonsurgical septal reduction. Note the widening of the LVOT (*arrow*) at the site of the localized septal infarction

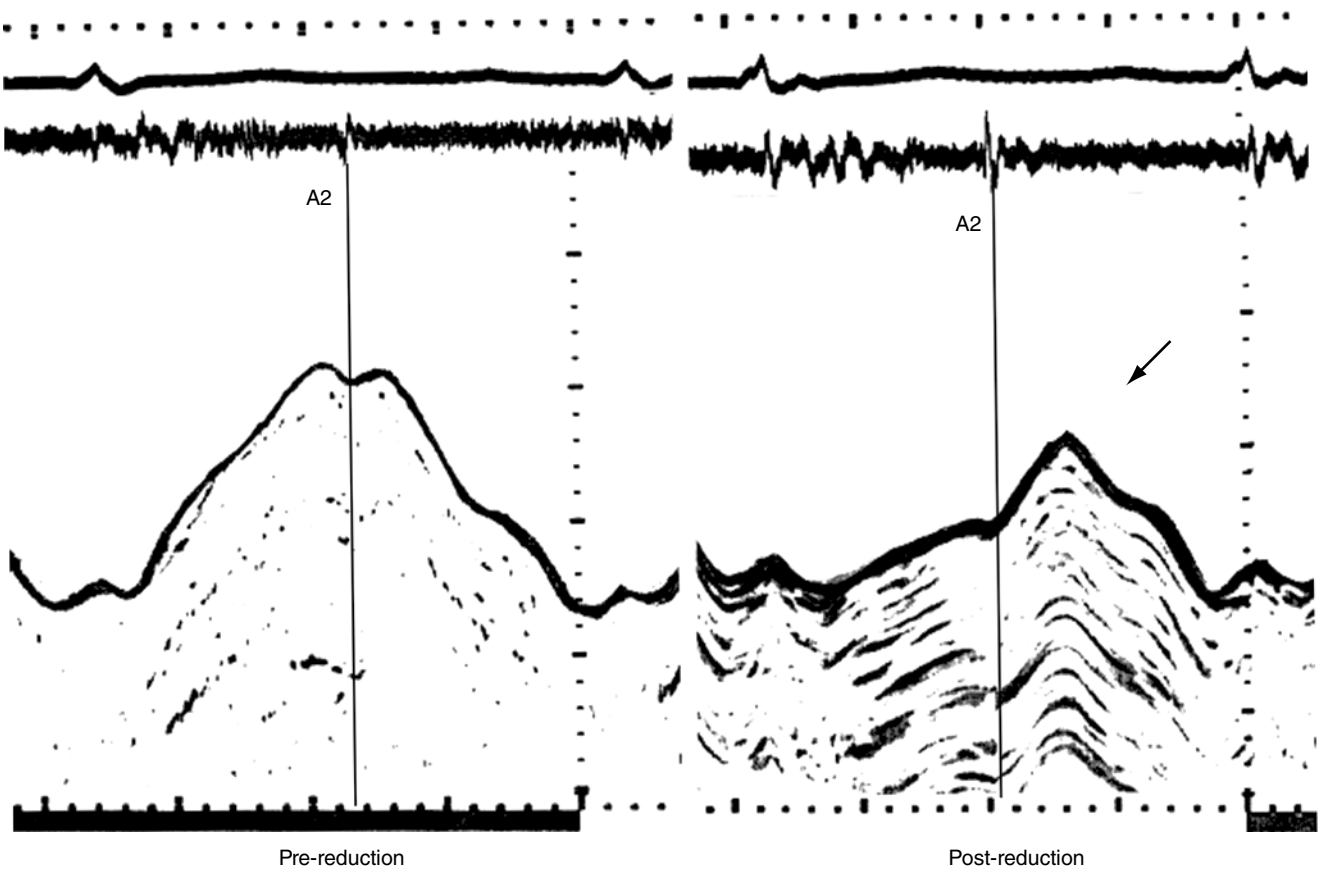


Fig. 10.26 LV septal long axis before (*left*) and after (*right*) nonsurgical septal reduction technique in a HCM patient. Note the marked incoordinate septal behavior in diastole (*arrow*)

Prognosis

In the majority of patients who symptomatically improve after the procedure, mid- and long-term follow-up demonstrate low outflow tract velocities, with a modest increase in ventricular cavity size and improved quality of life and exercise capacity. Few may require permanent pacemakers for complete heart block [63, 64]. A Recenbt meta-analysis comparing the clinical benefit of surgical myectomy and alcohol septal anblation has shown a better long term clinical outcome when using septal myectomy in the young and alcohol septal ablation in the old [65].

Family Screening

First-degree family relatives should undergo 12 lead ECG and two-dimensional echocardiographic examinations during puberty and adolescence. It is advisable that adult relatives with normal echocardiographic studies beyond age 18 have subsequent clinical assessment every 5 years, particularly if symptoms develop or there is an adverse family history. Genetic screening has been proposed but has its known problems. Family evaluation should include genetic counseling regarding the risk of developing HCM and its complications [64]. Family screening might reveal cardiac myopathic pathologies other than HCM, dilated cardiomyopathy or left atrial myopathy, although these are rare.

References

1. Seidman JG, Seidman C. The genetic basis for cardiomyopathy: from mutation identification to mechanistic paradigms. Cell. 2001;104:557–67.
2. Richard P, Charron P, Carrier L, et al. Hypertrophic cardiomyopathy: distribution of disease genes, spectrum of mutations and implications for a molecular diagnosis strategy. Circulation. 2003;107:2227–32.
3. Jarcho JA, McKenna W, Pare JA, Solomon SD, Holcombe RF, Dickie S, et al. Mapping a gene for familial hypertrophic cardiomyopathy to chromosome 14q1. N Engl J Med. 1989;321(20):1372–8.
4. Solomon SD, Geisterfer-Lowrance AA, Vosberg HP, Hiller G, Jarcho JA, Morton CC, et al. A locus for familial hypertrophic cardiomyopathy is closely linked to the cardiac myosin heavy chain genes, CRI-L436, and CRI-L329 on chromosome 14 at q11-q12. Am J Hum Genet. 1990;47(3):389–94.
5. Solomon SD, Jarcho JA, McKenna W, Geisterfer-Lowrance A, Germain R, Salerni R, et al. Familial hypertrophic cardiomyopathy is a genetically heterogeneous disease. J Clin Invest. 1990;86(3):993–9.
6. Geisterfer-Lowrance AA, Kass S, Tanigawa G, Vosberg HP, McKenna W, Seidman CE, et al. A molecular basis for familial hypertrophic cardiomyopathy: a beta cardiac myosin heavy chain gene missense mutation. Cell. 1990;62(5):999–1006.
7. Epstein ND, Fananapazir L, Lin HJ, Mulvihill J, White R, Lalouel JM, et al. Evidence of genetic heterogeneity in five kindreds with familial hypertrophic cardiomyopathy. Circulation. 1992;85(2):635–47.
8. Solomon SD, Wolff S, Watkins H, Ridker PM, Come P, McKenna WJ, et al. Left ventricular hypertrophy and morphology in familial hypertrophic cardiomyopathy associated with mutations of the beta-myosin heavy chain gene. J Am Coll Cardiol. 1993;22(2):498–505.
9. Maron BJ, WJ MK, Danielson GK, Task Force on Clinical Expert Consensus Documents, American College of Cardiologi, Committee for Practice Guidelines, European Society of Cardiology, et al. American College of Cardiology/European Society of Cardiology clinical expert consensus document on hypertrophic cardiomyopathy. A report of the American College of Cardiology Foundation Task Force on Clinical Expert Consensus Documents and the European Society of Cardiology Committee for Practice Guidelines. J Am Coll Cardiol. 2003;42(9):1687–713.
10. Elliott P, McKenna WJ. Hypertrophic cardiomyopathy. Lancet. 2004;363:1881–91.
11. Sanbe A, Nelson D, Gulick J, et al. In vivo analysis of an essential myosin light chain mutation linked to familial hypertrophic cardiomyopathy. Circ Res. 2000;87:296–302.
12. Sachdev B, Takenaka T, Teraguchi H, et al. Prevalence of Anderson-Fabry disease in male patients with late onset hypertrophic cardiomyopathy. Circulation. 2002;105(12):1407–11.
13. DiMauro S, Schon EA. Mitochondrial respiratory-chain diseases. N Engl J Med. 2003;348(26):2656–68.
14. Goodwin JF. ?IHSS. ?HOCM. ?ASH. a plea for unity. Am Heart J. 1975;89(3):269–77.
15. Maron BJ, Epstein SE. Hypertrophic cardiomyopathy: a discussion of nomenclature. Am J Cardiol. 1979;43(6):1242–4.
16. Matsumura Y, Elliott PM, Virdee MS, et al. Left ventricular diastolic function assessed using Doppler tissue imaging in patients with hypertrophic cardiomyopathy: relation to symptoms and exercise capacity. Heart. 2002;87(3):247–51.
17. Maron BJ, Tholakanahalli VN, Zenovich AG, et al. Usefulness of B-type natriuretic peptide assay in the assessment of symptomatic state in hypertrophic cardiomyopathy. Circulation. 2004;109(8):984–9.
18. Ikeda H, Maki S, Yoshida N, et al. Predictors of death from congestive heart failure in hypertrophic cardiomyopathy. Am J Cardiol. 1999;83(8):1280–3, A9.
19. Prasad K, Williams L, Campbell R, Elliott PM, McKenna WJ, Frenneaux M. Episodic syncope in hypertrophic cardiomyopathy: evidence for inappropriate vasodilation. Heart. 2008;94(10):1312–7.
20. Paz R, Jortner R, Tunick PA, et al. The effect of the ingestion of ethanol on obstruction of the left ventricular outflow tract in hypertrophic cardiomyopathy. N Engl J Med. 1996;335:938–41.
21. Maron BJ, Gottdiener JS, Bonow RO, Epstein SE. Hypertrophic cardiomyopathy with unusual locations of left ventricular hypertrophy undetectable by M-mode echocardiography. Identification by wide-angle two-dimensional echocardiography. Circulation. 1981;63(2):409–18.
22. Shapiro LM, McKenna WJ. Distribution of left ventricular hypertrophy in hypertrophic cardiomyopathy: a two-dimensional echocardiographic study. J Am Coll Cardiol. 1983;2(3):437–44.
23. Henry WL, Clark CE, Epstein SE. Asymmetric septal hypertrophy. Echocardiographic identification of the pathognomonic anatomic abnormality of IHSS. Circulation. 1973;47(2):225–33.
24. Henry WL, Clark CE, Epstein SE. Asymmetric septal hypertrophy (ASH): the unifying link in the IHSS disease spectrum. Observations regarding its pathogenesis, pathophysiology, and course. Circulation. 1973;47(4):827–32.
25. Wigle ED, Sasson Z, Henderson MA, Ruddy TD, Fulop J, Rakowski H, et al. Hypertrophic cardiomyopathy. The importance of the site and the extent of hypertrophy. A review. Prog Cardiovasc Dis. 1985;28(1):1–83.

26. Wigle ED, Adelman AG, Silver MD. Pathophysiological consideration in muscular subaortic stenosis. In: Wolstenholme GEW, editor. Hypertrophic obstructive cardiomyopathy, Ciba Foundation Study Group 47. London: Churchill; 1971.
27. Shah PM, Gramiak R, Kramer DH. Ultrasound localization of left ventricular outflow obstruction in hypertrophic obstructive cardiomyopathy. Circulation. 1969;40(1):3–11.
28. Maron BJ, Gottdiener JS, Arce J, Rosing DR, Wesley YE, Epstein SE. Dynamic subaortic obstruction in hypertrophic cardiomyopathy: analysis by pulsed Doppler echocardiography. J Am Coll Cardiol. 1985;6(1):1–18.
29. Wigle ED, Henderson M, Rakowski H, Wilansky S. Muscular (hypertrophic) subaortic stenosis (hypertrophic obstructive cardiomyopathy): the evidence for true obstruction to left ventricular outflow. Postgrad Med J. 1986;62(728):531–6.
30. Yamaguchi H, Ishimura T, Nishiyama S, Nagasaki F, Nakanishi S, Takatsu F, et al. Hypertrophic nonobstructive cardiomyopathy with giant negative T waves (apical hypertrophy): ventriculographic and echocardiographic features in 30 patients. Am J Cardiol. 1979;44(3):401–12.
31. Pellikka PA, Oh JK, Bailey KR, Nichols BA, Monahan KH, Tajik AJ. Dynamic intraventricular obstruction during dobutamine stress echocardiography. A new observation. Circulation. 1992;86(5):1429–32.
32. Maron BJ, Gottdiener JS, Epstein SE. Patterns and significance of distribution of left ventricular hypertrophy in hypertrophic cardiomyopathy. A wide angle, two dimensional echocardiographic study of 125 patients. Am J Cardiol. 1981;48(3):418–28.
33. McIntosh CL, Maron BJ, Cannon RO III, Klues HG. Initial results of combined anterior mitral leaflet plication and ventricular septal myotomy-myectomy for relief of left ventricular outflow tract obstruction in patients with hypertrophic cardiomyopathy. Circulation. 1992;86(5 Suppl):II60–7.
34. Rodger JC. Motion of mitral apparatus in hypertrophic cardiomyopathy with obstruction. Br Heart J. 1976;38(7):732–7.
35. Spirito P, Maron BJ, Bonow RO, Epstein SE. Severe functional limitation in patients with hypertrophic cardiomyopathy and only mild localized left ventricular hypertrophy. J Am Coll Cardiol. 1986;8(3):537–44.
36. Rossen RM, Goodman DJ, Ingham RE, Popp RL. Ventricular systolic septal thickening and excursion in idiopathic hypertrophic subaortic stenosis. N Engl J Med. 1974;291(25):1317–9.
37. Tajik AJ, Giuliani ER. Echocardiographic observations in idiopathic hypertrophic subaortic stenosis. Mayo Clin Proc. 1974;49(2):89–97.
38. Kinoshita N, Nimura Y, Okamoto M, Miyatake K, Nagata S, Sakakibara H. Mitral regurgitation in hypertrophic cardiomyopathy. Non-invasive study by two dimensional Doppler echocardiography. Br Heart J. 1983;49(6):574–83.
39. Spirito P, Maron BJ. Relation between extent of left ventricular hypertrophy and diastolic filling abnormalities in hypertrophic cardiomyopathy. J Am Coll Cardiol. 1990;15(4):808–13.
40. Nihoyannopoulos P, Karatasakis G, Frenneaux M, McKenna WJ, Oakley CM. Diastolic function in hypertrophic cardiomyopathy: relation to exercise capacity. J Am Coll Cardiol. 1992;19(3):536–40.
41. Nakamura T, Matsubara K, Furukawa K, Azuma A, Sugihara H, Katsume H, et al. Diastolic paradoxic jet flow in patients with hypertrophic cardiomyopathy: evidence of concealed apical asynergy with cavity obliteration. J Am Coll Cardiol. 1992;19(3):516–24.
42. Sutton MG, Tajik AJ, Smith HC, Ritman EL. Angina in idiopathic hypertrophic subaortic stenosis. A clinical correlate of regional left ventricular dysfunction: a videometric and echocardiographic study. Circulation. 1980;61(3):561–8.
43. Henein MY, O'Sullivan C, Sutton GC, Gibson DG, Coats AJ. Stress-induced left ventricular outflow tract obstruction: a potential cause of dyspnea in the elderly. J Am Coll Cardiol. 1997;30(5):1301–7.
44. Al Nasser F, Duncan A, Sharma R, O'Sullivan C, Coats AJ, Anker SD, et al. Beta-blocker therapy for dynamic left-ventricular outflow tract obstruction. Int J Cardiol. 2002;86(2–3):199–205.
45. Spirito P, Maron BJ, Bonow RO, Epstein SE. Occurrence and significance of progressive left ventricular wall thinning and relative cavity dilatation in hypertrophic cardiomyopathy. Am J Cardiol. 1987;60(1):123–9.
46. Grigg LE, Wigle ED, Williams WG, Daniel LB, Rakowski H. Transesophageal Doppler echocardiography in obstructive hypertrophic cardiomyopathy: clarification of pathophysiology and importance in intraoperative decision making. J Am Coll Cardiol. 1992;20(1):42–52.
47. Petrone RK, Klues HG, Panza JA, Peterson EE, Maron BJ. Coexistence of mitral valve prolapse in a consecutive group of 528 patients with hypertrophic cardiomyopathy assessed with echocardiography. J Am Coll Cardiol. 1992;20(1):55–61.
48. Zhu WX, Oh JK, Kopecky SL, Schaff HV, Tajik AJ. Mitral regurgitation due to ruptured chordae tendineae in patients with hypertrophic obstructive cardiomyopathy. J Am Coll Cardiol. 1992;20:242–7.
49. Liu H, Bai P, Xu HY, Li ZL, Xia CC, Zhou XY, et al. Distinguishing cardiac amyloidosis and hypertrophic cardiomyopathy by thickness and myocardial deformation of the right ventricle. Cardiol Res Pract. 2022;2022:4364279.
50. Liu D, Niemann M, Hu K, et al. Echocardiographic evaluation of systolic and diastolic function in patients with cardiac amyloidosis. Am J Cardiol. 2011;108(4):591–8.
51. Maron BJ, Pelliccia A. The heart of trained athletes: cardiac remodeling and the risks of sports, including sudden death. Circulation. 2006;114:1633–44.
52. Kaltenbach M, Hopf R, Kober G, Bussmann WD, Keller M, Petersen Y. Treatment of hypertrophic obstructive cardiomyopathy with verapamil. Br Heart J. 1979;42(1):35–42.
53. Rosing DR, Kent KM, Maron BJ, et al. Verapamil therapy: a new approach to the pharmacologic treatment of hypertrophic cardiomyopathy. II. Effects on exercise capacity and symptomatic status. Circulation. 1979;60(6):1208–13.
54. Lancellotti P, de Marneffe N, Scheen A. Mavacamten (Camzyos (R)) : first myosin modulator for obstructive hypertrophic cardiomyopathy treatment. Rev Med Liege. 2024;79(2):120–8.
55. Fananapazir L, Cannon RO III, Tripodi D, Panza JA. Impact of dual-chamber permanent pacing in patients with obstructive hypertrophic cardiomyopathy with symptoms refractory to verapamil and beta-adrenergic blocker therapy. Circulation. 1992;85(6):2149–61.
56. Rogers DP, Marazia S, Chow AW, Lambiase PD, et al. Effect of biventricular pacing on symptoms and cardiac remodelling in patients with end stage hypertrophic cardiomyopathy. Eur J Heart Fail. 2008;10(5):507–13.
57. Ashrafian H, Mason MJ, Mitchell AG. Regression of dilated-hypokinetic hypertrophic cardiomyopathy by biventricular cardiac pacing. Europace. 2007;9(1):50–4.
58. Henein M, Arvidsson S, Pilebro B, Backman C, Morner S, Lindqvist P. Long mitral valve leaflets determine left ventricular outflow tract obstruction during exercise in hypertrophic cardiomyopathy. Int J Cardiol. 2016;212:47–53.
59. Sigwart U. Non-surgical myocardial reduction for hypertrophic obstructive cardiomyopathy. Lancet. 1995;346(8969):211–4.
60. Knight C, Kurbaan AS, Seggewiss H, Henein M, Gunning M, Harrington D, et al. Nonsurgical septal reduction for hypertrophic obstructive cardiomyopathy: outcome in the first series of patients. Circulation. 1997;95(8):2075–81.
61. Faber L, Seggewiss H, Gleichmann U. Percutaneous transluminal septal myocardial ablation in hypertrophic obstructive cardiomyopathy: results with respect to intraprocedural myocardial contrast echocardiography. Circulation. 1998;98(22):2415–21.
62. Henein MY, O'Sullivan CA, Ramzy IS, Sigwart U, Gibson DG. Electromechanical left ventricular behavior after nonsurgical

septal reduction in patients with hypertrophic obstructive cardiomyopathy. J Am Coll Cardiol. 1999;34(4):1117–22.
63. Faber L, Meissner A, Ziemssen P, Seggewiss H. Percutaneous transluminal septal myocardial ablation for hypertrophic obstructive cardiomyopathy: long term follow up of the first series of 25 patients. Heart. 2000;83(3):326–31.
64. Ommen SR, Mital S, Burke MA, Day SM, Deswal A, Elliott P, et al. 2020 AHA/ACC Guideline for the Diagnosis and Treatment of Patients With Hypertrophic Cardiomyopathy: a report of the American College of Cardiology/American Heart Association Joint Committee on Clinical Practice Guidelines. J Am Coll Cardiol. 2020;76(25):e159–240.
65. Bytyçi I, Nistri S, Mörner S, Henein MY. Alcohol septal ablation versus septal myectomy treatment of obstructive hypertrophic cardiomyopathy: a systematic review and meta-analysis. J Clin Med. 2020;9(10):3062. https://doi.org/10.3390/jcm9103062.

Restrictive Cardiomyopathy

11

Michael Y. Henein, Per Lindqvist, and Mary Sheppard

Restrictive cardiomyopathy is a condition characterized by normal or subnormal left ventricular cavity size and preserved systolic function but with increased myocardial stiffness [1]. This makes the ventricle incompliant and fill predominantly in early diastole. When atrial systolic function is maintained, the ventricle may accommodate a small volume of blood during atrial systole but at the expense of further raising the end diastolic pressure (Fig. 11.1). These physiological disturbances are associated with raised left atrial pressure, atrial dilatation, and potential arrhythmias [2].

Restrictive cardiomyopathy is uncommon and usually no specific cause for it is identified.

The most common forms of restrictive cardiomyopathies are idiopathic [1], endomyocardial fibrosis (EMF) [3, 4] associated with Loffler's syndrome, and infiltrative myocardial disease [5]. In the Western World, amyloid heart disease [6] remains the most common cause of restrictive cardiomyopathy. Among other diseases of the myocardium that may present with a similar picture are cardiac sarcoidosis [7] and hemochromatosis [8].

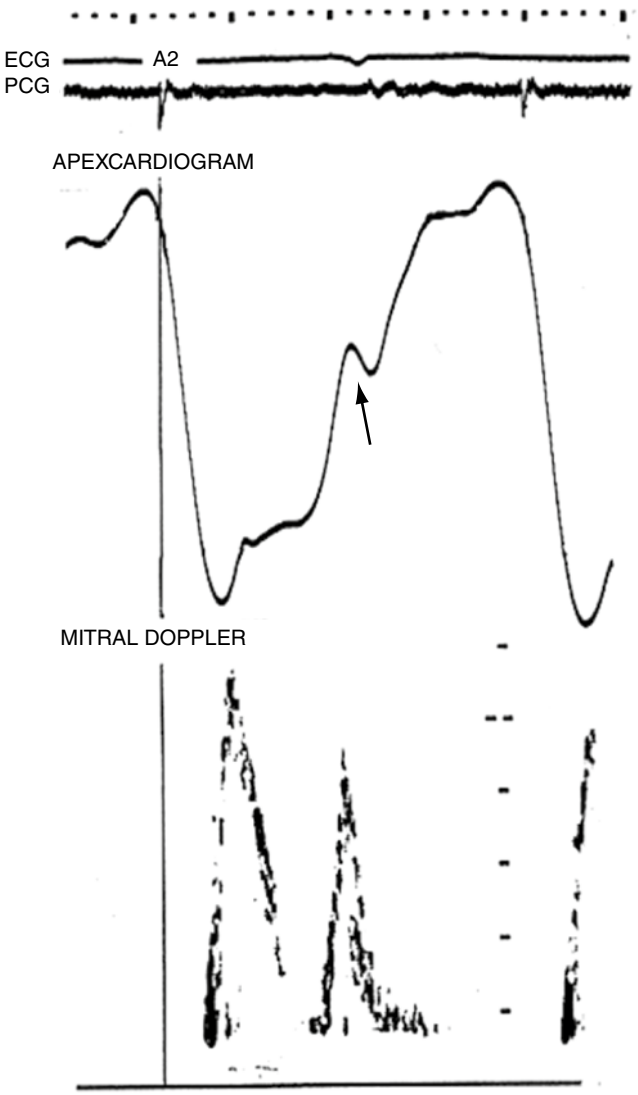


Fig. 11.1 An apexcardiogram and transmitral Doppler velocities from a patient with restrictive cardiomyopathy showing raised end diastolic pressure (arrow) with small filling volume

Supplementary Information The online version contains supplementary material available at https://doi.org/10.1007/978-3-031-95894-6_11.

M. Y. Henein (✉)
Imperial College London, London, UK

Siena University, Siena, Italy
e-mail: m.henein@imperial.ac.uk

P. Lindqvist
Umea University, Umea, Sweden

M. Sheppard
Royal Brompton Hospital, London, UK

© The Author(s), under exclusive license to Springer Nature Switzerland AG 2025

M. Y. Henein (ed.), *Clinical Echocardiography*, https://doi.org/10.1007/978-3-031-95894-6_11

Idiopathic Restrictive Cardiomyopathy

This is a benign condition, characterized by a normal left ventricular cavity size and a dilated left atrium in the absence of significant mitral valve pathology (Fig. 11.2). It is a slowly progressing disease when compared with other infiltrative restrictive cardiomyopathies [2]. Long-standing systemic hypertension with its drastic effect on the myocardial function is a common substrate for this condition. Despite the commonly maintained overall left ventricular systolic function, diastolic function is severely disturbed and could easily be assessed by studying the filling pattern and velocities. The characteristic features of restrictive left ventricular filling are short isovolumic relaxation time (IVRT), dominant early diastolic filling (E wave) with short deceleration time and small or absent late diastolic filling component (a wave). Pulmonary venous flow demonstrates late diastolic flow reversal "during atrial systole" of a longer duration than the corresponding transmitral flow (Fig. 11.3). These patients also presents with raised E/e' (e' is myocardial early diastolic Doppler velocity; Fig. 11.4). Patients diagnosed with idiopathic restrictive cardiomyopathy tend to respond to diuretics and vasodilators [9] which may successfully offload left atrium pressure. The expected satisfactory symptomatic response is usually supported by prolongation of isovolumic relaxation time, reversal of ventricular filling pattern from high E/A >1.0 to low E/A <1.0, and finally a fall in left atrial size and a fall in E/e'. With long-standing severe ventricular diastolic disease less expectation is anticipated.

Progressive rise of left atrial and pulmonary pressures and increase in cavity size result in significant impairment of myocardial function [10] and hence cavity instability and increased risk for atrial arrhythmia. So long as the left atrial pressure remains raised, medical or even DC cardioversion or ablation might not be successful. Aggressive use of renin angiotensin enzyme blocking agents [11] have proved beneficial in optimizing treatment results. Resistant cases with atrial fibrillation are not expected to have successful DC cardioversion or ablation because of the large atrium (diameter >5.0 cm) and raised pressures.

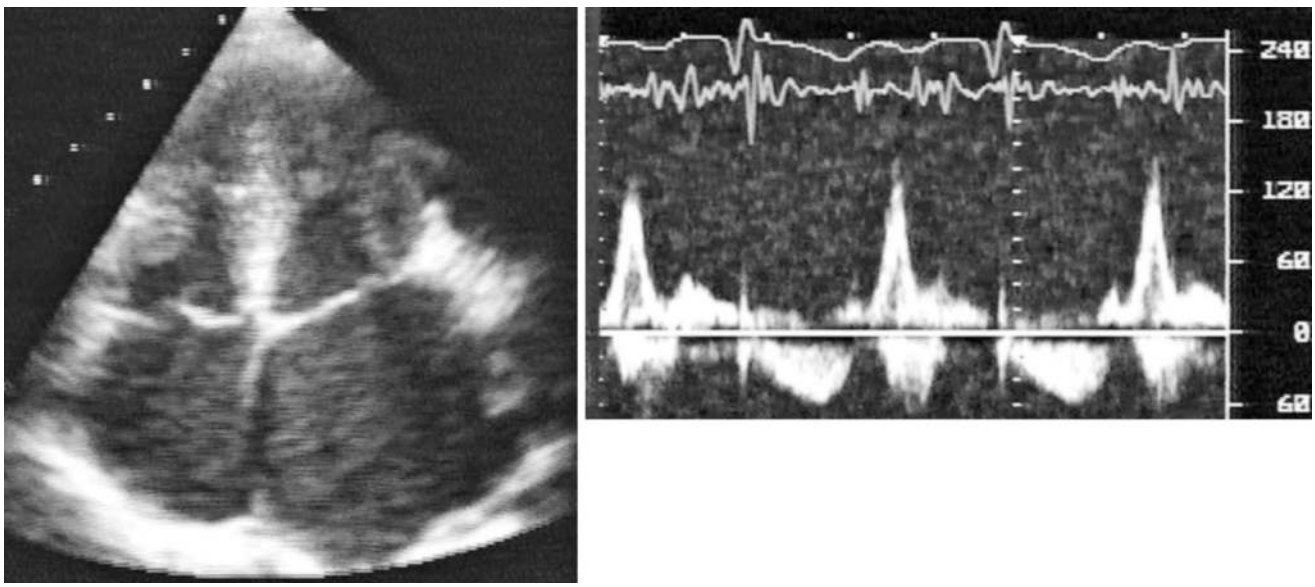


Fig. 11.2 Four chamber view from a patient with idiopathic restrictive cardiomyopathy showing normal LV cavity size, dilated left atrium (*left*) and restrictive filling pattern (*right*)

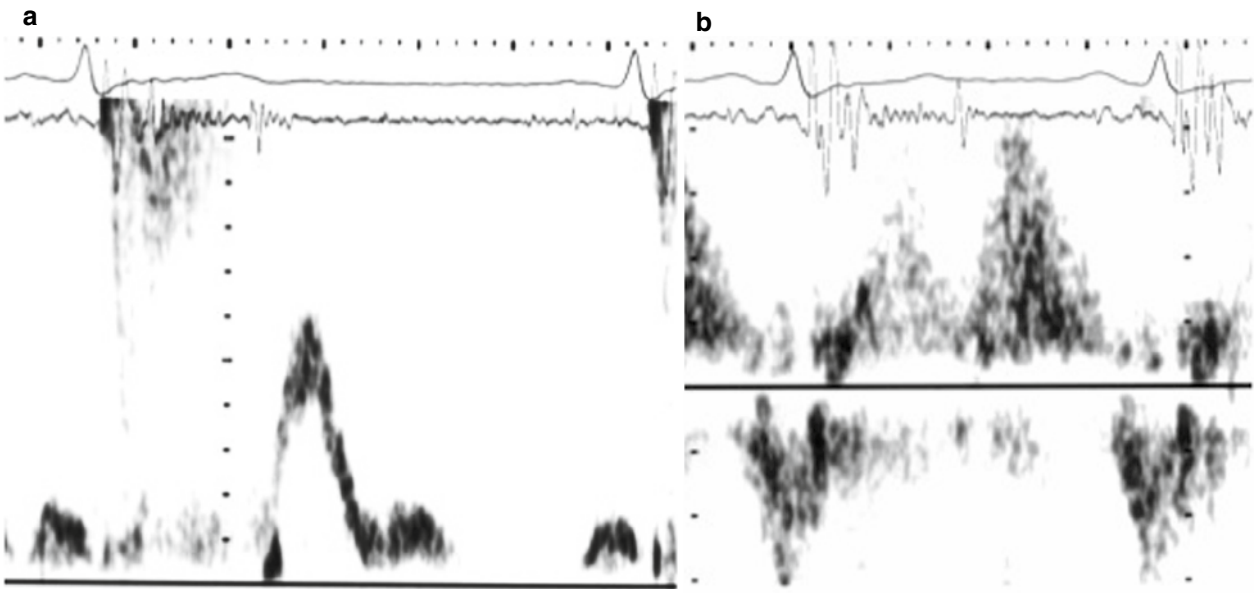


Fig. 11.3 Transmitral forward flow velocities from a patient with restrictive cardiomyopathy (**a**) along with pulmonary venous flow (**b**). Note the classical restrictive filling pattern with late diastolic flow reversal in the pulmonary veins which is significantly longer than the respective transmitral A wave

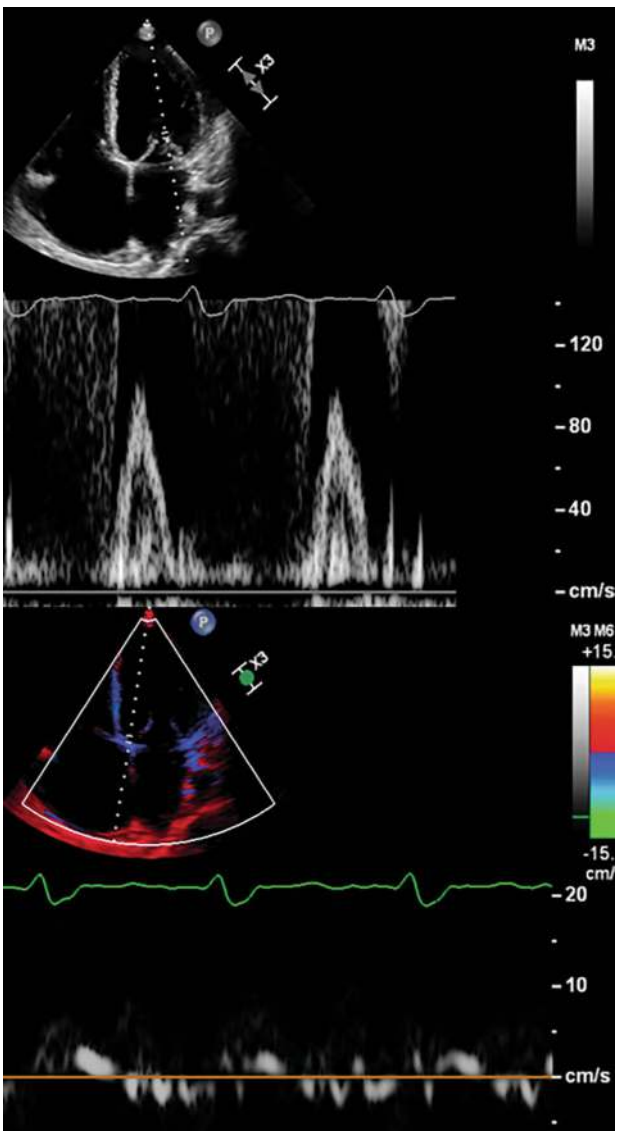


Fig. 11.4 Transmitral forward flow velocity and myocardial Doppler velocities showing raised E/e' consistent with raised left atrial prewssure

Endomyocardial Fibrosis (EMF)

This form of restrictive cardiomyopathy is prevalent in West Africa, South India, Thailand and South America among the indigenous population. Endomyocardial fibrosis is characterized by extensive fibrosis of the subendocardial layer of the myocardium involving the apices of the left and right ventricles and extending to the inflow tract. Fibrosis may be patchy or diffuse in distribution [3, 12]. Endomyocardial fibrosis results in increased chamber stiffness and hence restrictive filling. The left ventricle is normal in size but the walls are thickened with increased subendocardial myocardial echo intensity (Fig. 11.5) [13–15]. Ventricular function may initially be preserved but subsequently impaired. The endocardial fibrosis forms the substrate for thrombus formation that may obliterate the entire ventricular apex particularly the right ventricle. The atria are usually dilated, not necessarily due to the resulting mitral or tricuspid regurgitation but as a consequence of the increased atrial pressure secondary to incompliant ventricles. Severe cases may be complicated by pulmonary hypertension and significant tricuspid regurgitation. The disease may also involve the mitral and tricuspid valve leaflets themselves, thus adding to the severity of valve regurgitation. Endomyocardial fibrosis may be very similar in presentation to Löffler's syndrome [15–17].

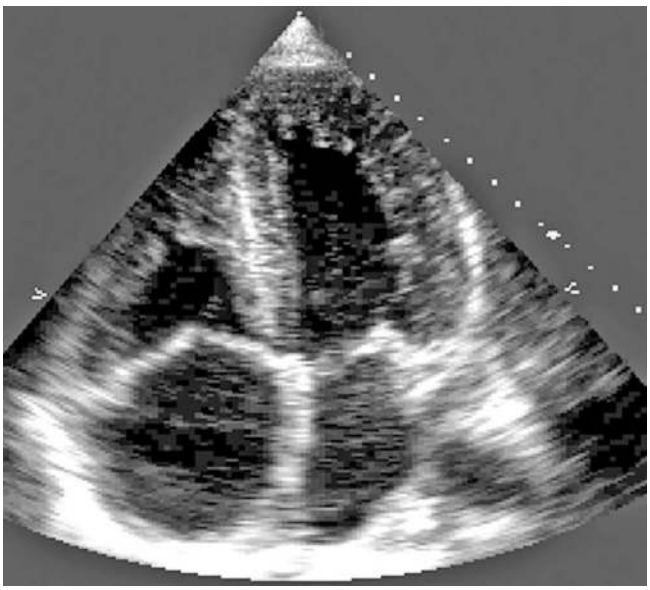


Fig. 11.5 Apical four chamber view from a patient with endomyocardial fibrosis. Note the large atria, the increased subendocardial echo intensity in the presence of normal ventricular size and mitral and tricuspid regurgitation on color Doppler

Löffler's Syndrome

Löffler's syndrome presents with echocardiographic and physiological signs similar to EMF but in addition there is hypereosinophilia [15–17]. While management of endomyocardial fibrosis is directed toward subendocardial decortication with or without valve replacement, controlling the eosinophilia is the first stage in treating Löffler's syndrome.

Infiltrative Myocardial Disease

The myocardium may be infiltrated by iron in hemochromatosis [8, 18], glycogen in Pompe's [19] and Cori's disease, or glycolipids in Fabry's disease [20]. AL (light chain) amyloid heart disease is another cause of restrictive cardiomyopathy. ATTR cardiomyopathy (ATTR-CM) is probably the most common cause for cardiac amyloidosis and can be either hereditary (ATTRv) or acquired (ATTRwt). As the ageing population increases ATTRwt is expected to be more common and probably the most common type of Amyloid Cardiac Disease [21, 22].

Myocardial infiltrates are most commonly extra cellular and the metabolism results also in fibrosis. Eventually, progressive myocardial fibrosis adds to the myocardial stiffness and increase in ventricular diastolic pressures. Amyloid deposition may be patchy or diffuse and the ventricular walls in amyloid heart disease are usually thick with poor thickening fraction wich can be seen using M-mode, myocardial Doppler velocities or strain (Figs. 11.6 and 11.8), as well as increased myocardial echo intensity (increased brightness) [6, 23]. Amyloid deposition may involve the four cardiac chambers, even the atrioventricular valves (Fig. 11.6). The amyloid disease may also involve the atrial septum and may be associated with varying degrees of pericardial effusion, commonly late in the disease (Fig. 11.7).

ATTR Cardiac Amyloidosis

Diagnosing cardiac ATTR amyloid disease needs careful assessment. The greater the ventricular wall thickness the more suspicious it is for diagnosing ATTR. Septal thickness >1.4 cm together with a concentric increase in wall thickness (increased relative wall thickness) have been found to be associated with amyloid disease (23, 24). Apical sparing ratio defined as myocardial longitudinal strain gradient between apical strain and basal and mid cavity strain is also profoundly seen in ATTR, when the value ≥1 [24].

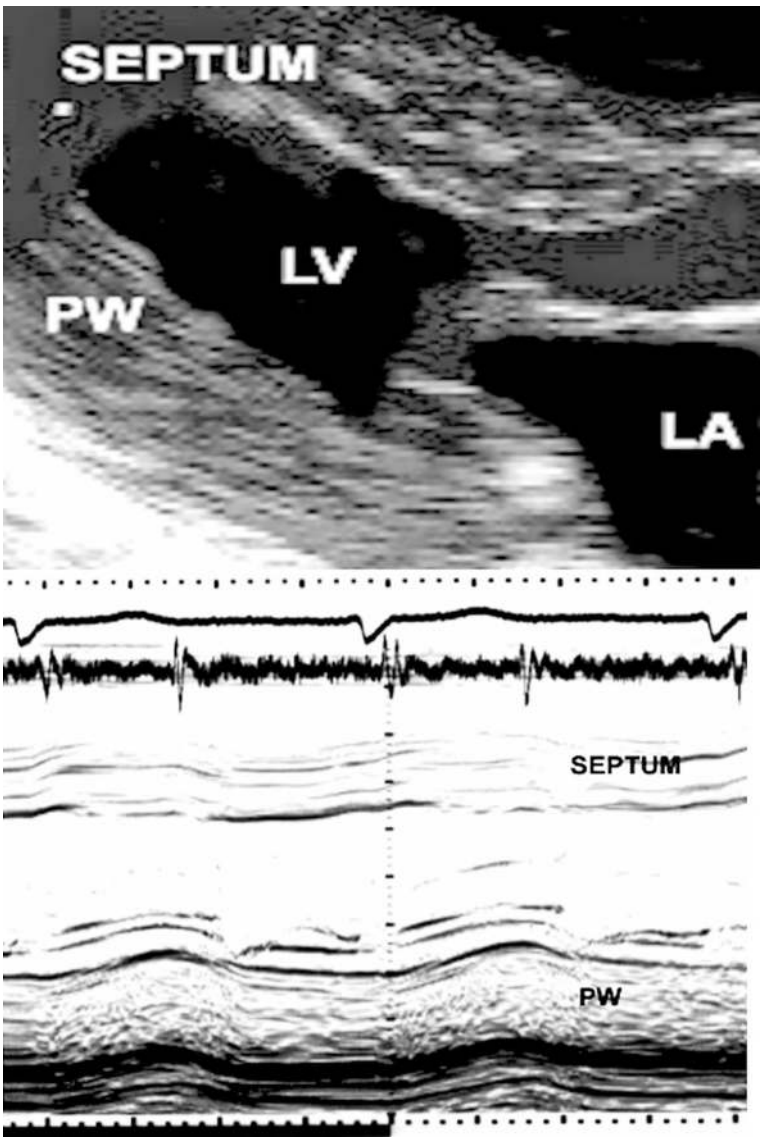


Fig. 11.6 Parasternal long axis view (*top*) and M-mode recording (*bottom*) from a patient with amyloid deposition. Note the normal LV cavity size, thick walls and poor thickening fraction

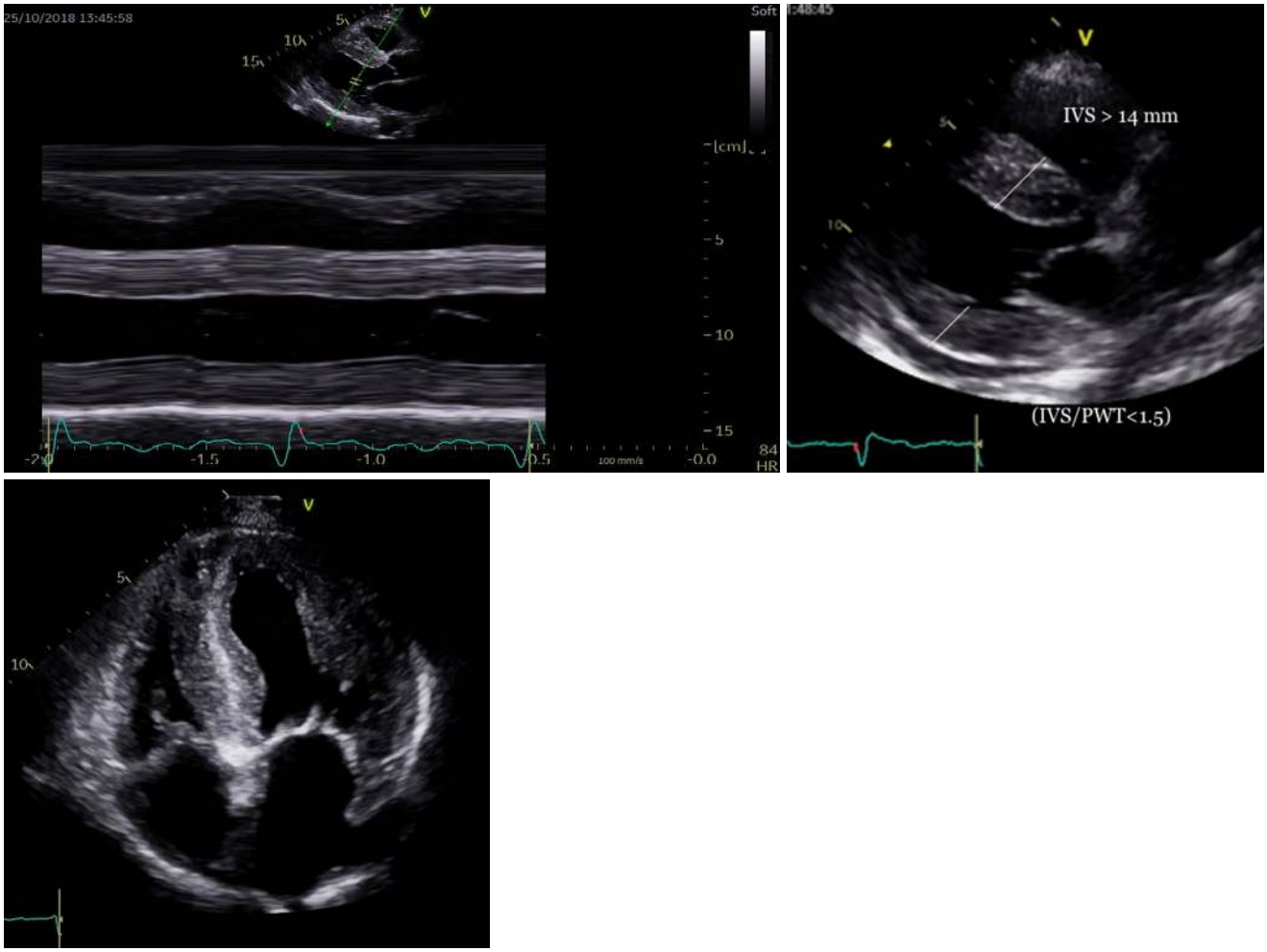


Fig. 11.7 Top: parasternal long axis view from a patient with ATTR (right) and corresponding M-mode recording (left). Note the myocardial thickness and the poor thickening fraction on M-mode. Bottom: Apical four chamber view from a patient with advanced ATTR amyloid disease involving all four chambers and atrioventricular valves

$$\text{Apical sparing ration} = \frac{\text{Apical strain mean}}{\text{Basal strain Mean} + \text{Mid cavity strain} / 2}$$

In amyloid heart disease, the extent of segmental myocardial dysfunction is usually out of proportion to the degree of wall thickness, showing markedly depressed segmental thickening and thinning rates [25]. By the time of clinical presentation and symptoms, the echocardiographic picture of amyloid heart disease is usually severe due to myocardial thickness, reduced wall motion and abnormal ventricular filling, of the restrictive pattern (Figs. 11.9 and 11.10) [26]. Mitral and tricuspid regurgitation are also commonly seen which may be severe, particularly when the valve leaflets themselves are involved in the disease process (Video 11.1).

In amyloid heart disease, the changes in ventricular filling pattern evolve as the disease progresses and ventricular function deteriorates. While in early disease the E/A ratio may be less than 1.0 and IVRT prolonged, in later stages filling becomes restrictive and IVRT shortens, consistent with raised left atrial pressures. Similar abnormalities can be seen on the right side of the heart [25, 26]. This evolving worsening of cardiac function in cardiac amyloidosis may differ when comparing AL and ATTR, with AL having rapid deteoriantation in cardiac dysfunction and less of increase in wall thickness.

Ventricular filling pattern has been shown to predict clinical outcome in amyloid heart disease. E wave deceleration time <150 ms has been shown to predict a life expectancy of 50% at 1 year compared to more than 90% survival at 1 year with deceleration time >150 ms [26].

Amyloid left ventricular disease should be differentiated from hypertrophic cardiac disease as the treatment of the two conditions is quite different [27, 28]. While the cavity volume is equally maintained or reduced in the two conditions, the overall systolic ventricular function, segmental thickening fraction and thinning rate are preserved only in hypertrophic

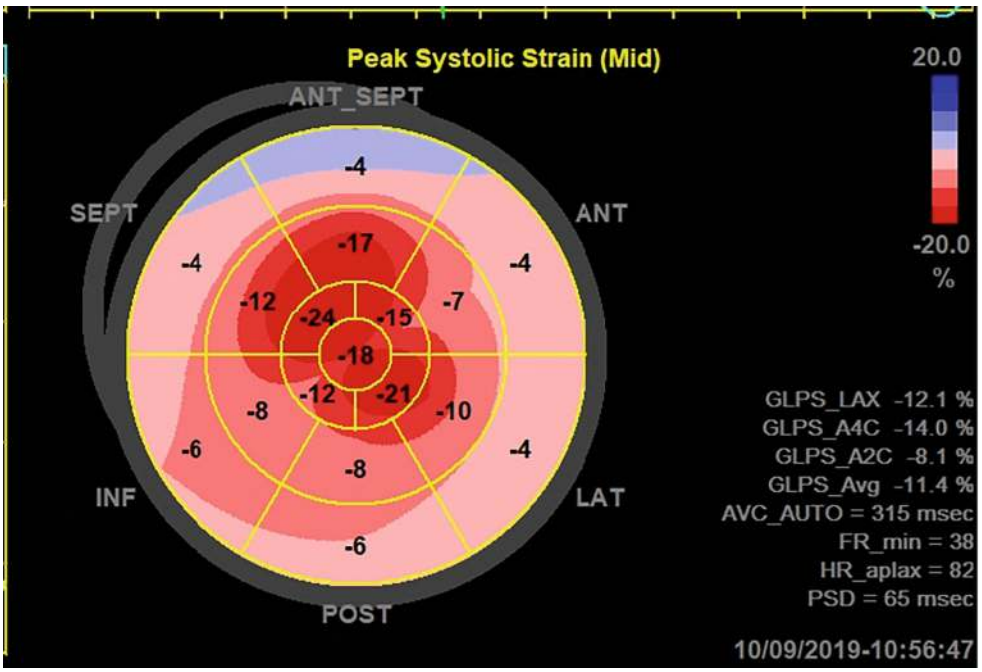


Fig. 11.8 Reduced peak atrial strain due to ventricular wall thickening from patchy myocardial infiltration

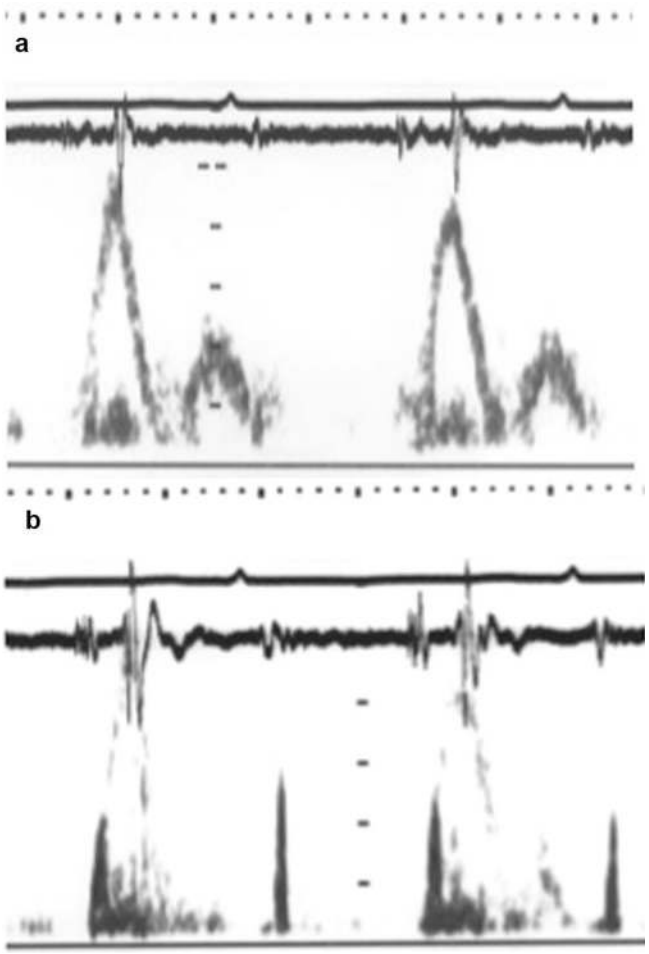


Fig. 11.9 Left ventricular filling (restrictive) from a patient with amyloid heart disease (**a**) RV filling from the same patient (**b**) Note the characteristic restrictive pattern of filling on both sides of the heart and a third heart sound on the phonocardiogram coinciding with peak 'E' wave

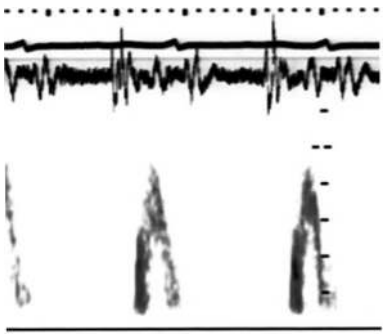


Fig. 11.10 Left ventricular filling from a patient with late-stage amyloid disease showing restrictive pattern with very short deceleration time 100 ms and a summation filling pattern

cardiomyopathy (Fig. 11.11). The QRS amplitude on conventional 12 lead ECG may also help in diffferentating cardiac amyloidosis from hypertrophic heart disease (27), demonstrating low to normal amplitude despite increased wall thickness in amyloid disease. Of note, low R wave voltage tends to be more common in AL amyloidosis compared with ATTR.

Aquired Amyloidosis or the Wild Type (ATTRwt)

ATTRwt has been recently shown as the most common type of cardiac amyloidosis, and is likely to increase in prevalence with the ageing population. Cardiac manifestation of ATTRwt is very similar to cardiac phenotype of ATTRv (fibril type) type A. It is important to note that the prevalence of ATTRwt in heart failure with preserved left

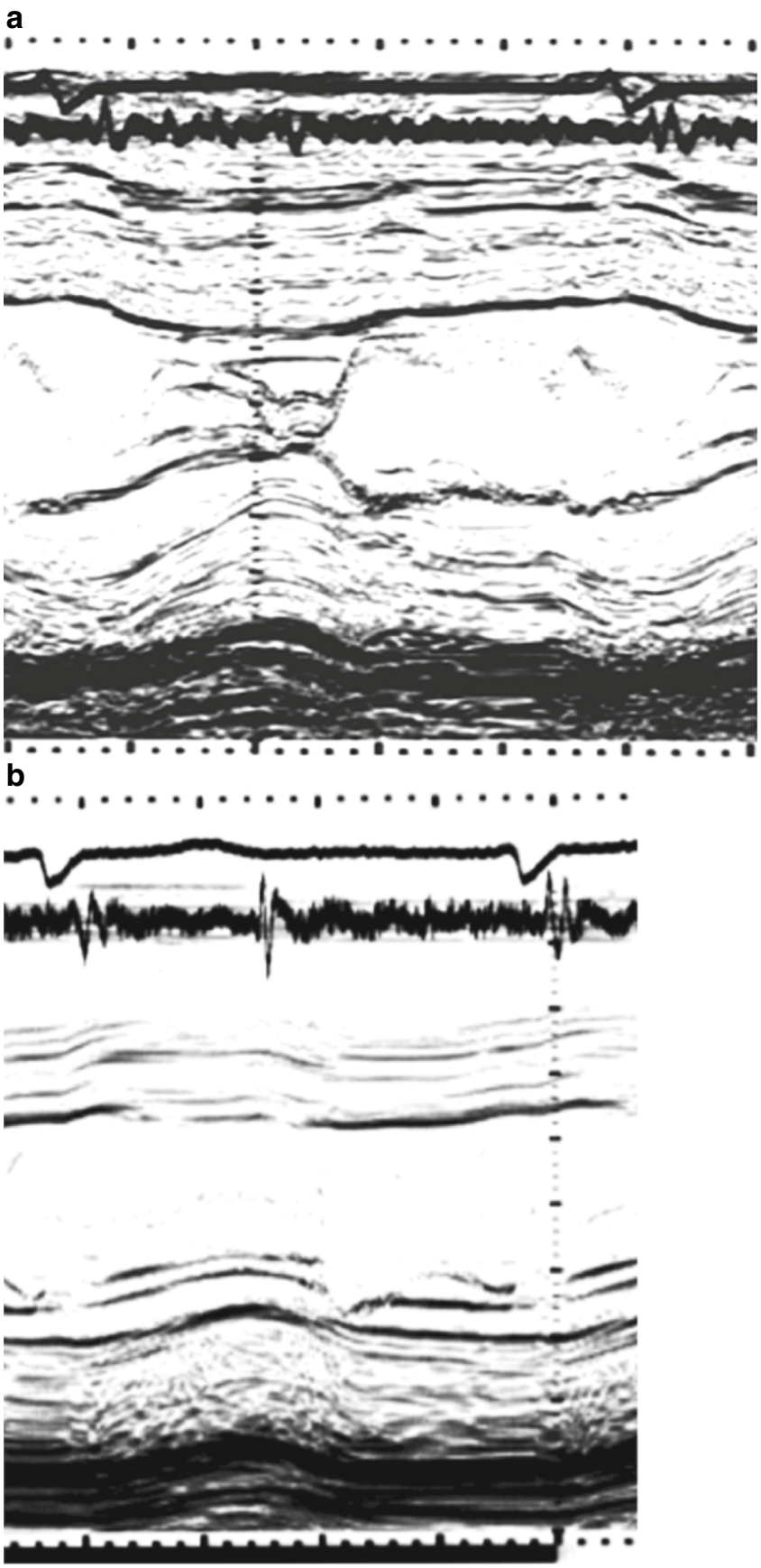


Fig. 11.11 M-mode of LV minor axis from two patients; hypertrophic cardiomyopathy (**a**) and amyloid heart disease (**b**). Note the similar extent of wall thickness but poor thickening fraction in the amyloid patient compared with the hypertrophic cardiomyopathy. (**c**, **d** and **e**) Histological sections showing amyloid (*pink*) and blood vessels replacing the myocardium. (*apple green*) florescence staining

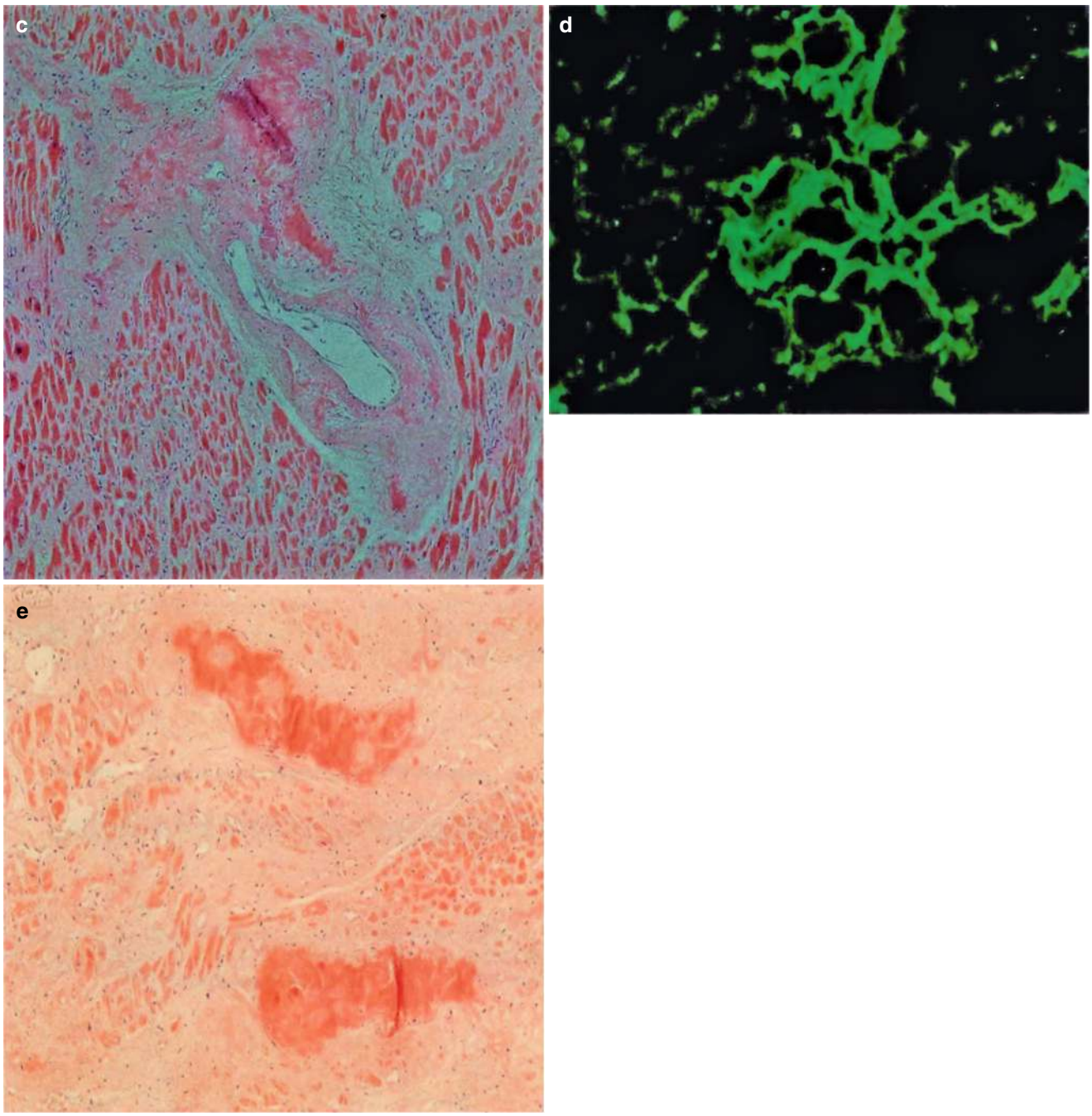


Fig. 11.11 (continued)

ventricular ejection fraction (HFpEF) has been found to be in the order of 5-13%. ATTRwt may also be detected in patients with HFmrEF and HFrEF. In patients with symptomatic heart failure septal thickness > 14 mm has been reported in 20%, particularly in those with LVEF < 50%. [29–31]

Hereditary amyloidosis (ATTRv)

Hereditary amyloidosis is often found in endemic areas in Portugal, Japan, and Sweden. Although less common than ATTRwt, hereditary amyloidosis can affect human heart and at late stages give rise to a picture similar to the AL amyloid heart disease, described before. ATTRv is a disorder which is caused by mutated transthyretin (TTR). Among over 100 documented amyloid TTR mutations, the most common mutation is the exchange of valine for methionine at position 30 (ATTR Val30Met). The typical symptom of hereditary amyloidosis is peripheral sensory-motor polyneuropathy, often accompanied by autonomic neuropathy which causes a defective autoregulation of blood pressure and heart rate. Associated cardiac complications, e.g., arrhythmia, has been described in ATTRv patients who develop increased left ventricular (LV) wall thickness, diastolic dysfunction and enlarged atria. ATTRv patients develop autonomic system dysfunction during the disease process which is progressive in nature, and may affect heart rate variability (HRV) and cause cardiac symptoms. In ATTRv there are two different fibril types, the full length type (type B) and the fragmented type (type A). Type A is more common in patients having cardiomyopathy and type B is more common in those with polyneuropathy. Studies have recently shown that the pattern of ventricular diastolic abnormalities in ATTRv patients correlate closely with the degree of disturbances of heart rate variability [32–40].

AL amyloidosis

AL amyloidosis is a clonal plasma cell expansion producing amyloid immunoglobulin light chain. This forms insoluble fibrils which deposits in organs, commonly in the heart. This leads to heart failure and also arrhythmias. The echocardiographic and CMR findings in AL amyloidosis are generally quite similar to those in ATTR-CM, especially ATTRwt (39).

Cardiac Sarcoidosis

Cardiac involvement occurs in a minority of sarcoid cases. Cardiac involvement is manifest as patchy myocardial infiltration by granulomatous sarcoid deposits followed by fibrosis (Fig. 11.12) [41]. When sarcoidosis affects the posterior wall of the left ventricle, the proximal segment is usually involved which has a similar echocardiographic picture to posterior wall myocardial infarction. It may also involve the lateral papillary muscle giving rise to some degree of mitral regurgitation. Sarcoid heart disease may affect the proximal septal segment where it may affect the electric conduction tissue resulting in conduction disease and heart block (Fig. 11.13). This explains the etiology of syncope in these patients. The left ventricular cavity may be slightly dilated at the basal region due to the fibrosed segments. Ventricular filling is commonly late diastolic.

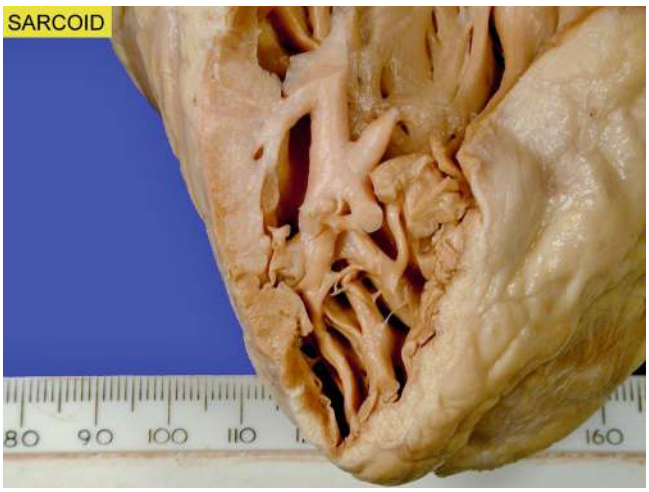


Fig. 11.12 Pathological section from a ventricle of a patient with sarcoid heart showing myocardial fibrosis

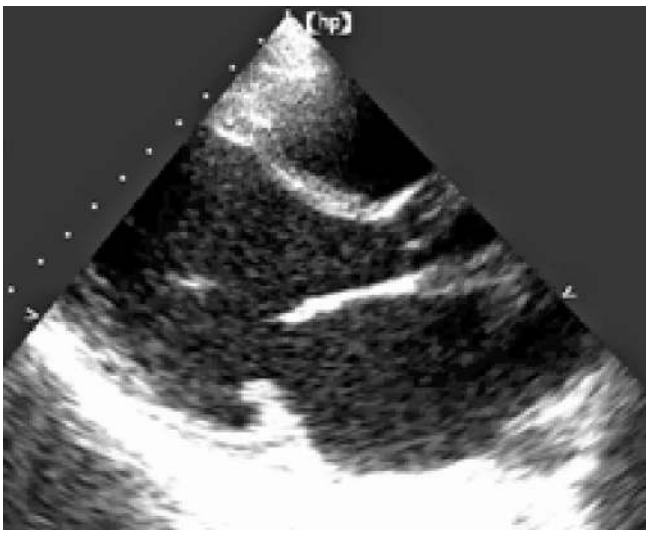


Fig. 11.13 Parasternal long axis view from a patient with sarcoid heart disease showing scarred proximal septum with increased echo intensity

Hemochromatosis

The ventricular myocardium may be infiltrated by iron in patients with hemochromatosis. It tends to invade the outer layer of the myocardium more than the subendocardium. Iron is deposited in the myocytes as well as interstitial cells, resulting in myocardial fibrosis (Fig. 11.14). Although the ventricular cavity may be dilated, the clinical outcome is better than the other infiltrative diseases since it responds well to iron chelation therapy [42].

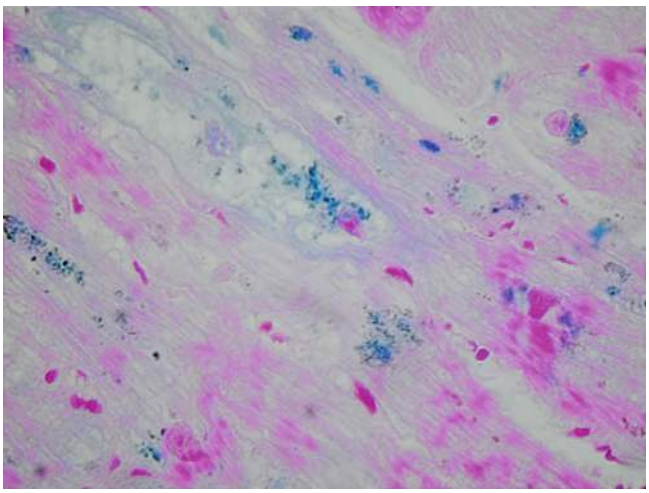


Fig. 11.14 Histological section showing hemosiderosis, *blue purple dots* of iron deposition in the myocardium

Diabetic Hypertensive Cardiomyopathy

Long-standing diabetes and hypertension may affect left ventricular function in such a way that resembles restrictive cardiomyopathy, in particular, the picture associated with amyloid (Fig. 11.15). The cavity size is maintained, walls are thickened, and sequential thickening fraction is significantly reduced. The majority of these patients become limited by breathlessness due to raised left atrial pressures in the absence of mitral valve disease. The long-term outcome of this condition, however, is more benign than that of amyloid cardiomyopathy.

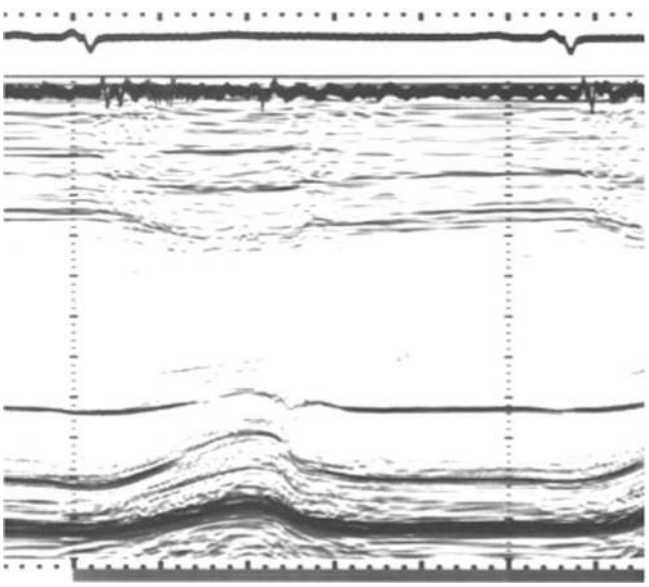


Fig. 11.15 2D and M-mode images from a patient with long-standing hypertension and diabetes. Note the reduced systolic function, and thickening fraction

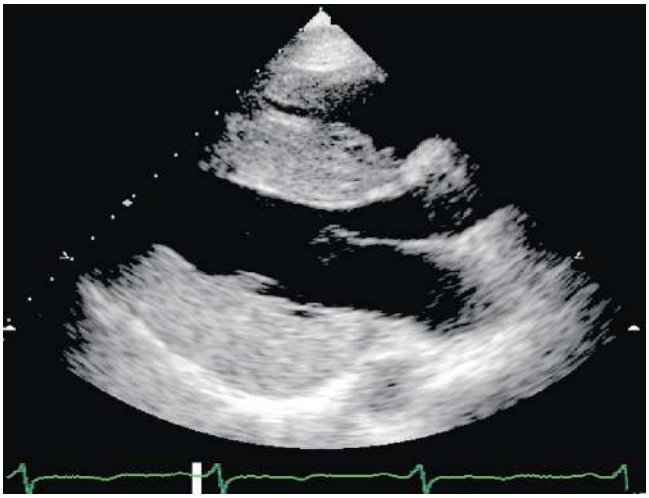


Fig. 11.16 Parasternal long axis view from a patient with glycogen storage disease showing thick walls with increased myocardial echo intensity



Fig. 11.17 Apical four chamber view from a patient with isolated right ventricular restrictive disease demonstrating large right atrium and normal size right ventricle

Myocardial storage disorders and restrictive cardiomyopathies are characterized by abnormal myocardial infiltration or fibrosis, leading to diastolic dysfunction and impaired ventricular filling. Storage disorders cause myocardial thickening with increased echogenicity due to intracellular accumulation of metabolic substrates (Figs. 11.16, 11.17 and 11.18).

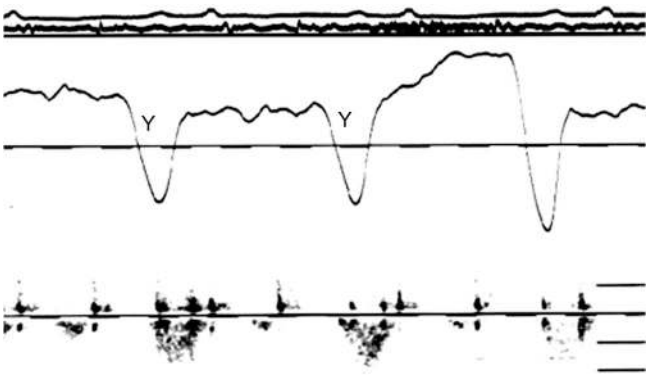


Fig. 11.18 Superior vena caval flow from a patient with restrictive right ventricular disease demonstrating deep "Y" descent consistent with early diastolic drop of RA pressure on the JVP recording

References

1. Siegel RJ, Shah PK, Fishbein MC. Idiopathic restrictive cardiomyopathy. Circulation. 1984;70(2):165–9.
2. Benotti JR, Grossman W, Cohn PF. Clinical profile of restrictive cardiomyopathy. Circulation. 1980;61:1206–12.
3. Roberts WC, Liegler DG, Carbone PP. Endomyocardial disease and eosinophilia. A clinical and pathologic spectrum. Am J Med. 1969;46:28–42.
4. Candell-Riera J, Permanyer-Miralda G, Soler-Soler J. Echocardiographic findings in endomyocardial fibrosis. Chest. 1982;82:88–90.
5. Child JS, Levisman JA, Abbasi AS, MacAlpin RN. Echocardiographic manifestations of infiltrative cardiomyopathy. A report of seven cases due to amyloid. Chest. 1976;70:726–31.
6. Cueto-Garcia L, Tajik AJ, Kyle RA, Edwards WD, Greipp PR, Callahan JA, et al. Serial echocardiographic observations in patients with primary systemic amyloidosis: an introduction to the concept of early (asymptomatic) amyloid infiltration of the heart. Mayo Clin Proc. 1984;59:589–97.
7. Silverman KJ, Hutchins GM, Bulkley BH. Cardiac sarcoid: a clinicopathologic study of 84 unselected patients with systemic sarcoidosis. Circulation. 1978;58:1204–11.
8. Short EM, Winkle RA, Billingham ME. Myocardial involvement in idiopathic hemochromatosis. Morphologic and clinical improvement following venesection. Am J Med. 1981;70(6):1275–9.
9. Henein MY, Gibson DG. Abnormal subendocardial function in restrictive left ventricular disease. Br Heart J. 1994;72(3):237–42.
10. Henein M, Lindqvist P, Mörner S, Henein MY. Effect of raised left atrial pressure on its regional and segmental chamber function: the role of speckle tracking. Scand Cardiovasc J. 2009;43:8.
11. Schneider MP, Hua TA, Böhm M, Wachtell K, Kjeldsen SE, Schmieder RE. Prevention of atrial fibrillation by renin-angiotensin system inhibition. J Am Coll Cardiol. 2010;55:2299–307.
12. Hess OM, Turina M, Senning A, Goebel NH, Scholer Y, Krayenbuehl HP. Pre- and postoperative findings in patients with endomyocardial fibrosis. Br Heart J. 1978;40:406–15.
13. George BO, Gaba FE, Talabi AI. M-mode echocardiographic features of endomyocardial fibrosis. Br Heart J. 1982;48:222–8.

14. Vijayaraghavan G, Davies J, Sadanandan S, Spry CJ, Gibson DG, Goodwin JF. Echocardiographic features of tropical endomyocardial disease in South India. Br Heart J. 1983;50:450–9.
15. Acquatella H, Schiller NB, Puigbo JJ, Gomez-Mancebo JR, Suarez C, Acquatella G. Value of two-dimensional echocardiography in endomyocardial disease with and without eosinophilia. A clinical and pathologic study. Circulation. 1983;67:1219–26.
16. Davies J, Gibson DG, Foale R, Heer K, Spry CJ, Oakley CM, et al. Echocardiographic features of eosinophilic endomyocardial disease. Br Heart J. 1982;48:434–40.
17. Gottdiener JS, Maron BJ, Schooley RT, Harley JB, Roberts WC, Fauci AS. Two-dimensional echocardiographic assessment of the idiopathic hypereosinophilic syndrome. Anatomic basis of mitral regurgitation and peripheral embolization. Circulation. 1983;67:572–8.
18. Olson LJ, Baldus WP, Tajik AJ. Echocardiographic features of idiopathic hemochromatosis. Am J Cardiol. 1987;60:885–9.
19. Hwang B, Meng CC, Lin CY, Hsu HC. Clinical analysis of five infants with glycogen storage disease of the heart–Pompe's disease. Jpn Heart J. 1986;27:25–34.
20. Bass JL, Shrivastava S, Grabowski GA, Desnick RJ, Moller JH. The M-mode echocardiogram in Fabry's disease. Am Heart J. 1980;100:807–12.
21. Brito D, Albrecht FC, de Arenaza DP, Bart N, Better N, Carvajal-Juarez I, et al. World heart federation consensus on transthyretin amyloidosis cardiomyopathy (ATTR-CM). Glob Heart. 2023;18:59.
22. Cueto-Garcia L, Reeder GS, Kyle RA, Wood DL, Seward JB, Naessens J, et al. Echocardiographic findings in systemic amyloidosis: spectrum of cardiac involvement and relation to survival. J Am Coll Cardiol. 1985;6:737–43.
23. Siqueira-Filho AG, Cunha CL, Tajik AJ, Seward JB, Schattenberg TT, Giuliani ER. M-mode and two-dimensional echocardiographic features in cardiac amyloidosis. Circulation. 1981;63:188–96.
24. Cotella J, Randazzo M, Maurer MS, Helmke S, Scherrer-Crosbie M, Soltani M, et al. Limitations of apical sparing pattern in cardiac amyloidosis: a multicenter echocardiographic study. Eur Heart J Cardiovasc Imaging. 2024;
25. Arnberg E, Eldhagen P, Lofbacka V, Venkateshvaran A, Pilebro B, Lindqvist P. RWT/SaVR-A simple and highly accurate measure screening for transthyretin cardiac amyloidosis. J Clin Med. 2022;11:4120.
26. Klein AL, Hatle LK, Burstow DJ, Seward JB, Kyle RA, Bailey KR, et al. Doppler characterization of left ventricular diastolic function in cardiac amyloidosis. J Am Coll Cardiol. 1989;13:1017–26.
27. Chandrasekaran K, Aylward PE, Fleagle SR, Burns TL, Seward JB, et al. Feasibility of identifying amyloid and hypertrophic cardiomyopathy with the use of computerized quantitative texture analysis of clinical echocardiographic data. J Am Coll Cardiol. 1989;13:832–40.
28. Lofbacka V, Suhr OB, Pilebro B, Wixner J, Sundstrom T, Lindmark K, et al. Combining ECG and echocardiography to identify transthyretin cardiac amyloidosis in heart failure. Clin Physiol Funct Imaging. 2021;41:408–16.
29. Gertz MA, Benson MD, Dyck PJ, Grogan M, Coelho T, Cruz M, et al. Diagnosis, prognosis, and therapy of transthyretin amyloidosis. J Am Coll Cardiol. 2015;66:2451–66.
30. Gillmore JD, Maurer MS, Falk RH, Merlini G, Damy T, Dispenzieri A, et al. Nonbiopsy diagnosis of cardiac transthyretin amyloidosis. Circulation. 2016;133:2404–12.
31. Lindmark K, Pilebro B, Sundstrom T, Lindqvist P. Prevalence of wild type transtyrethin cardiac amyloidosis in a heart failure clinic. ESC Heart Fail. 2021;8:745–9.
32. Cipriani A, De Michieli L, Porcari A, Licchelli L, Sinigiani G, Tini G, Zampieri M, Sessarego E, Argiro A, Fumagalli C, De Gaspari M, Licordari R, Russo D, Di Bella G, Perfetto F, Autore C, Musumeci B, Canepa M, Merlo M, Sinagra G, Gregori D, Iliceto S, Perazzolo Marra M, Cappelli F, Rapezzi C. Low QRS voltages in cardiac amyloidosis: clinical correlates and prognostic value. JACC CardioOncol. 2022;4:458–70.
33. Saraia M, Costa P, Birken S, Goodman S. Presence of an abnormal transthyretin (prealbumin) in Portuguese patients with familial amyloidotic polyneuropathy. Trans Assoc Am Physicians. 1983;96:261–70.
34. Connors LH, Lim A, Prokaeva T, Roskens VA, Costello CE. Tabulation of human transthyretin (TTR) variants. Amyloid. 2003;10:160–84.
35. Ando Y, Suhr OB. Autonomic dysfunction in familial amyloidotic polyneuropathy (FAP). Amyloid. 1998;5:288–300.
36. Backman C, Olofsson BO. Echocardiographic features in familial amyloidosis with polyneuropathy. Acta Med Scand. 1983;214:273–8.
37. Olofsson BO, Backman C, Boman K. Familial amyloidotic polyneuropathy in northern Sweden. A cross-sectional and longitudinal study of cardiac function with echocardiography. Arctic Med Res. 1988;47(Suppl 1):423–5.
38. Wiklund U, Hörnsten R, Karlsson M, Suhr OB, Jensen SM. Abnormal heart rate variability and subtle atrial arrhythmia in patients with familial amyloidotic polyneuropathy. Ann Noninvasive Eletrocardiol. 2008;13:249–56.
39. Zhao Y, Hörnsten R, Lindqvist P, Wiklund U, Suhr OB, Henein MY. Left ventricular dyssynchrony is associated with reduced heart rate variability in familial amyloidotic polyneuropathy. Int J Cardiol. 2012;155:273–8.
40. Quarta CC, Solomon SD, Uraizee I, Kruger J, Longhi S, Ferlito M, Gagliardi C, Milandri A, Rapezzi C, Falk RH. Left ventricular structure and function in transthyretin-related versus light-chain cardiac amyloidosis. Circulation. 2014;129:1840–9.
41. Lewin RF, Mor R, Spitzer S, Arditti A, Hellman C, Agmon J. Echocardiographic evaluation of patients with systemic sarcoidosis. Am Heart J. 1985;110:116–22.
42. Candell-Riera J, Lu L, Seres L, Gonzalez JB, Batlle J, Permanyer-Miralda G, et al. Cardiac hemochromatosis: beneficial effects of iron removal therapy. An echocardiographic study. Am J Cardiol. 1983;52:824–9.

Pulmonary Hypertension

12

Michael Y. Henein, Per Lindqvist, and Mary Sheppard

Pulmonary hypertension describes raised pulmonary circulatory pressure, venous or arterial. Venous pulmonary hypertension due to left ventricular disease is much more common in daily practice than primary pulmonary arterial hypertension (Fig. 12.1). The diagnosis of pulmonary hypertension is made when mean pulmonary artery systolic pressure exceeds 20 mmHg, at rest [1] The underlying pathology of pulmonary hypertension can be classified as either pre-capillary, involving the pulmonary circulation or post-capillary, when the pathology involves the left heart components and eventually result in pressure build up in the left atrium which propagates to the pulomonary venous circulation followed by the arterial circulation.

Post-capillary pulmonary hypertension is caused by any of the following pathologies [1]

(a) Mitral valve disease, stenosis or regurgitation [2, 3].
(b) Aortic valve disease, stenosis or regurgitation, particularly in the presence of left ventricular disease [4].
(c) Severe left ventricular disease due to an incompliant cavity, irrespective of its size or systolic function. Ventricular disease can be either idiopathic or secondary to coronary artery disease, systemic hypertension, valvular disease, or infiltrative myocardial disease [5, 6].
(d) Incompliant left atrium. Long-standing raised left atrial pressure results in increased wall stress, atrial dilatation, and loss of contractile function. At this stage of disease, the atrium behaves as a conduit for blood to pass through, from the left ventricle to the pulmonary veins, even with mild mitral regurgitation [7, 8].

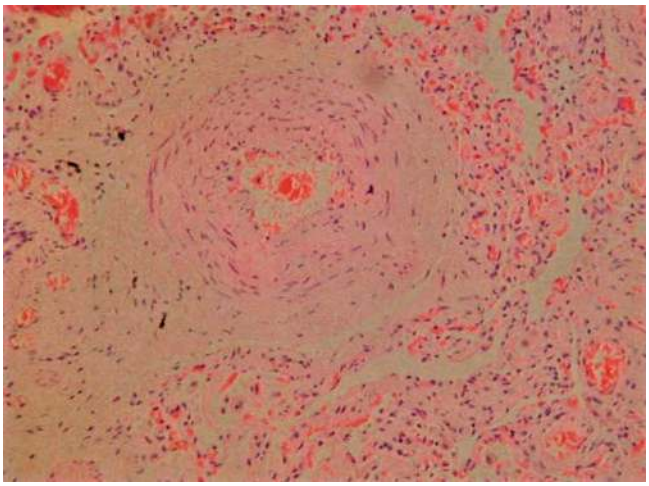


Fig. 12.1 Histological section from a patient with primary pulmonary hypertension showing medial hypertrophy of the muscular layer of the pulmonary artery, small arterial occlusion, and plexiform lesions

Pathophysiology in Post-capillary Pulmonary Hypertension

The end result of left heart valve disease is a rise in left atrial pressure, clinically referred to as "raised left ventricular filling pressure." The increase in left atrial pressure, either due to volume or pressure overload, will eventually affect passive and active atrial function. The raised atrial pressure will propagate retrogradely to the pulmonary venous system, with any further pressure increase, e.g. mitral regurgitation, resulting in pulmonary hypertension [9, 10]. Atrial contraction in late diastole against a stenosed mitral valve or raised left ventricular end diastolic pressure will accentuate the reversed flow into the pulmonary veins. With severe ventricular disease, the long-axis function of the ventricle loses its systolic component and the ventricle becomes more spherical in shape (Fig. 12.2). Atrial longitudinal function also becomes very limited and consequently, the systolic component of the pulmonary venous flow is compromised [11, 12].

M. Y. Henein (✉)
Imperial College London, London, UK

Siena University, Siena, Italy
e-mail: m.henein@imperial.ac.uk

P. Lindqvist
Umea University, Umeå, Sweden

M. Sheppard
Royal Brompton Hospital, London, UK

© The Author(s), under exclusive license to Springer Nature Switzerland AG 2025

M. Y. Henein (ed.), *Clinical Echocardiography*, https://doi.org/10.1007/978-3-031-95894-6_12

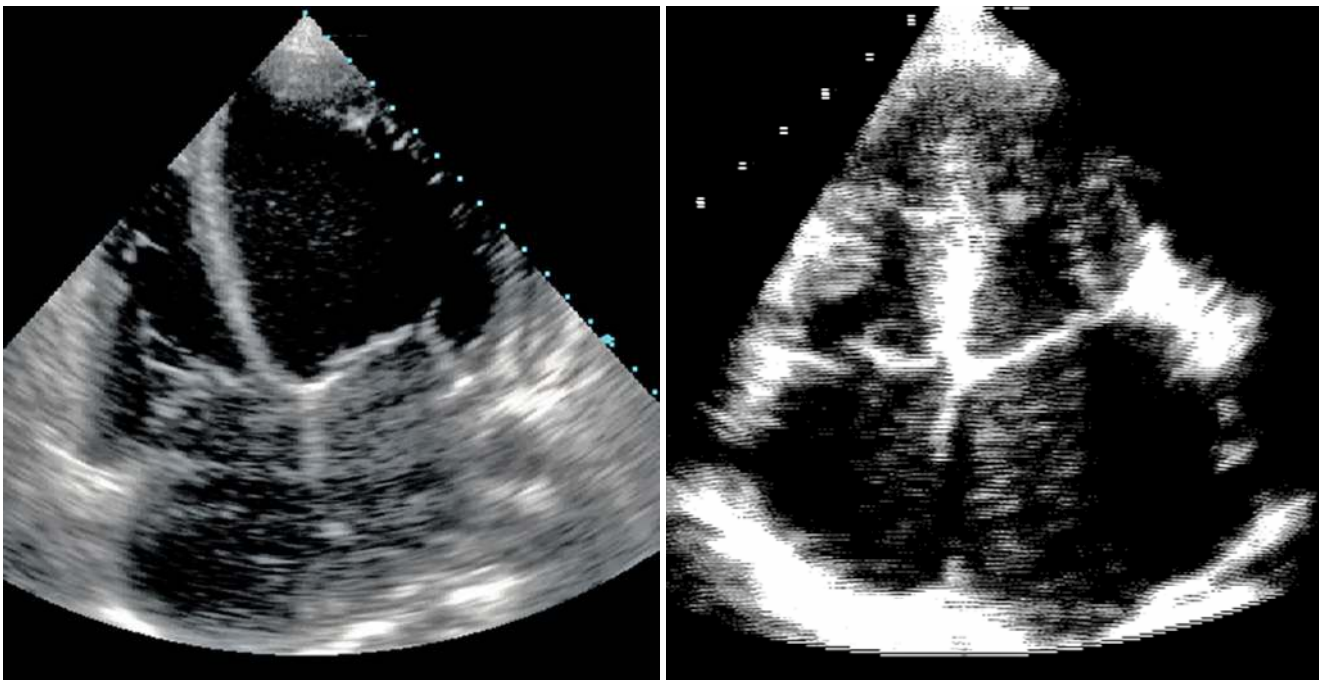


Fig. 12.2 Apical four-chamber view from a patient with severe left ventricular disease and dilated left atrium (*left*) and another with restrictive cardiomyopathy, normal size but significantly stiff left ventricle causing left atrial dilatation and secondary pulmonary hypertension (*right*). Note the left atrial dilatation in the two cases, irrespective of left ventricular size

Patients with significant mitral regurgitation, whether functional or organic, demonstrate systolic flow reversal in the pulmonary veins caused by the mitral regurgitation jet and increased pressure in the left atrium during systole (Fig. 12.3) [13].

Pre-capillary Pulmonary Hypertension This type of pulmonary arterial hypertension can broadly be classified etiologically into [1] [14]:

1. Ideopathic, heritable, drug and toxin-induced, associated with connective tissue diseases, HIV infection, portal hypertension, congenital heart diseases, schistosomiasis, chronic hemolytic anemia, persistent pulmonary hypertension of the new born, or pulmonary veno-occlusive disease and/or pulmonary capillary hemangiomatosis.
2. Pulmonary hypertension due to lung disease and/or hypoxia (Fig. 12.4).
   (a) Chronic obstructive pulmonary disease
   (b) Interstitial lung disease
   (c) Lung diseases with a mixed restrictive and obstructive pattern
   (d) Sleep disorder breathing
   (e) Alveolar hypoventilation disorders
   (f) Chronic exposure to high-altitude related hypoxia
   (g) Developmental abnormalities
3. Chronic thromboembolic pulmonary hypertension (CTEPH).
4. Pulmonary hypertension with unclear multifactorial mechanisms (Fig. 12.5).
   (a) Hematologic disorders: myeloproliferative disorders, splenectomy
   (b) Systemic disorders: sarcoidosis, pulmonary Langerhans cell histiocytosis
   (c) Metabolic disorders: glycogen storage disease, thyroid disorders
   (d) Others: tumoral obstruction, fibrosing mediastinitis, chronic renal failure on dialysis.

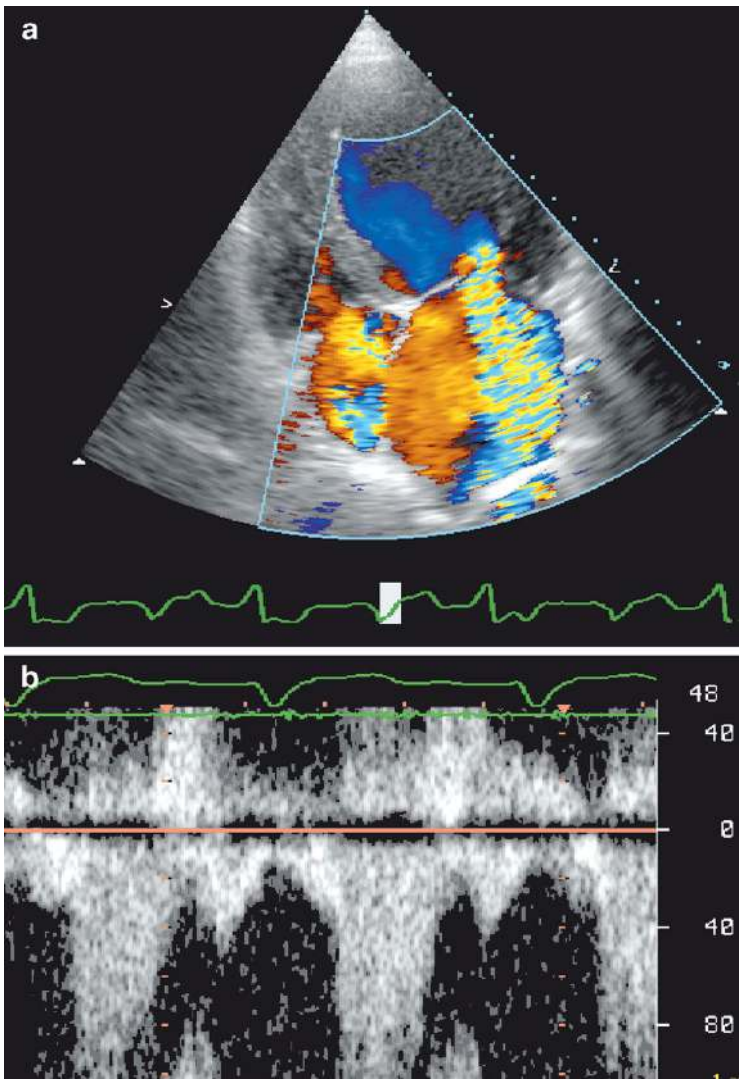


Fig. 12.3 (**a**) Apical-four chamber view from a patient with severe mitral regurgitation. Note the mitral regurgitation jet on color flow Doppler that flushes most of the left atrium until the pulmonary veins (*left*) and (**b**) the equivalent pulsed wave Doppler flow of the pulmonary veins demonstrating systolic flow reversal due to mitral regurgitation and late diastolic flow reversal consistent with raised left ventricular end-diastolic pressure

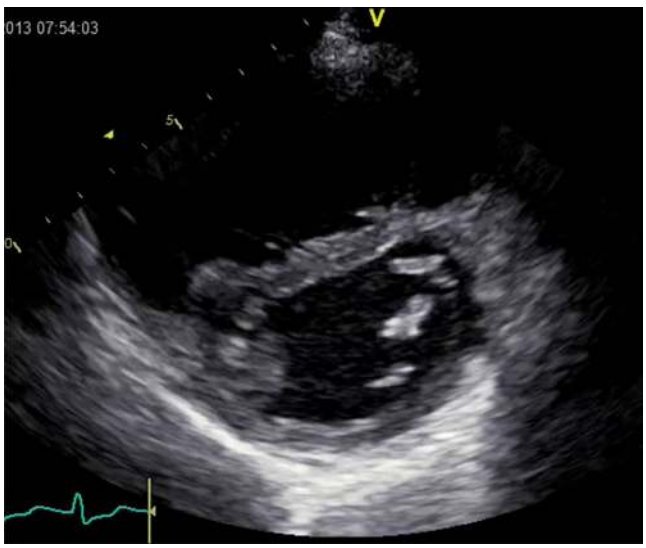


Fig. 12.4 Left ventricular short axis view from a patient with pre-capillary PH involving the lung. Notice the small size underfilled left ventricle and the disproportionate enlargement of the right ventricle



Fig. 12.5 Parasternal short-axis view showing right ventricular hypertrophy in pulmonary hypertension due to elevated right ventricular pressure

Doppler Echocardiography in Assessing Pulmonary Hypertension

1. *Peak tricuspid regurgitation pressure drop*: The most reliable marker of pulmonary hypertension in clinical practice is the peak retrograde pressure drop across the tricuspid valve, which reflects peak systolic pulmonary artery pressure (sPAP). The higher the pressure drop, the more severe the pulmonary hypertension (Fig. 12.5). Peak retrograde trans-tricuspid pressure drop added to right atrial pressure (5–10 mmHg) provides a good non-invasive estimate of peak systolic pulmonary artery pressure, although it tends to underestimate its absolute value depending on the clarity of the continuous wave Doppler signal [15]. Recent evidence suggests that adding arbitrary value to reflect right atrial pressure reduces the accuracy of retrograde transtricuspid pressure drop in estimating peak sPAP [16].
2. *Delayed onset of right ventricular filling*: In patients with pulmonary hypertension, the high retrograde pressure drop across the tricuspid valve (on the continuous wave Doppler velocity recording) usually has a long and slow pressure decline rate in early and mid diastole. This causes a significant delay in the onset of right ventricular filling with respect to end-ejection (pulmonary component of the second heart sound – P2). The normal delay in the onset of right ventricular filling is 80 ms with respect to end-ejection [17]. In patients in whom tricuspid regurgitation cannot be detected by continuous wave Doppler, a delayed onset of right ventricular filling with respect to P2 or prolonged time difference between end systole and early diastole measured by tissue Doppler, (right ventricular isovolumic relaxation time), can be taken as a surrogate marker for raised pulmonary artery pressure (Fig. 12.6) [18]. Delayed onset of right ventricular filling due to asynchronous septal or free wall relaxation, as seen in coronary artery disease, should not be taken as a sign of pulmonary hypertension.
3. *Short pulmonary acceleration time*: The increase in pulmonary vascular resistance is reflected in the pattern of the pulmonary valve flow. In a normal subject, right ventricular ejection occupies all of systole until the second heart sound (P2). In contrast, in pulmonary hypertension,

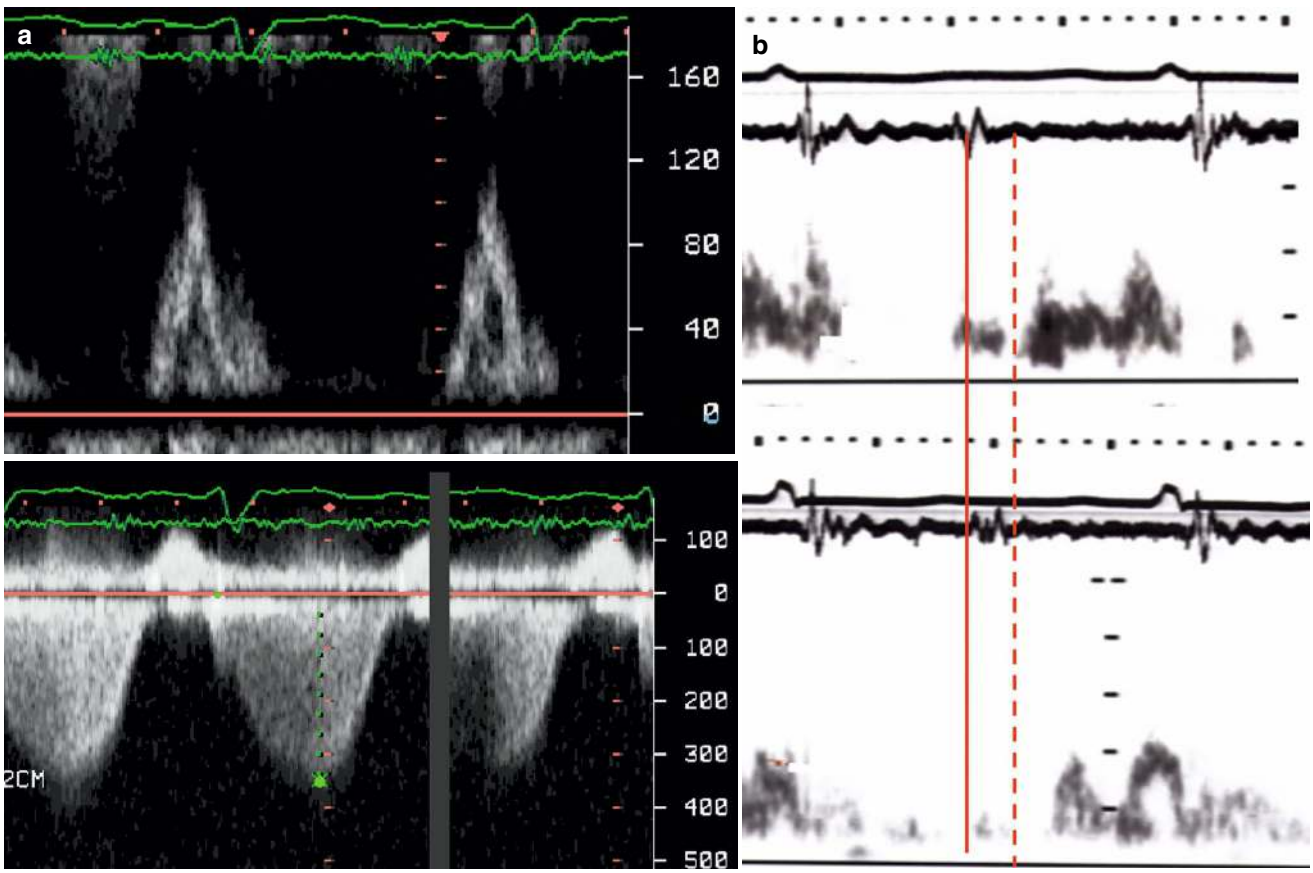


Fig. 12.6 (**a**) Pulsed wave Doppler of right ventricular filling showing delayed onset of filling (*top*) which was also short, due to long tricuspid regurgitation (*bottom*). (**b**) Delayed RV filling from a patient with pulmonary hypertension (*top*), who developed worsened delay of the onset of filling, over time (*bottom*)

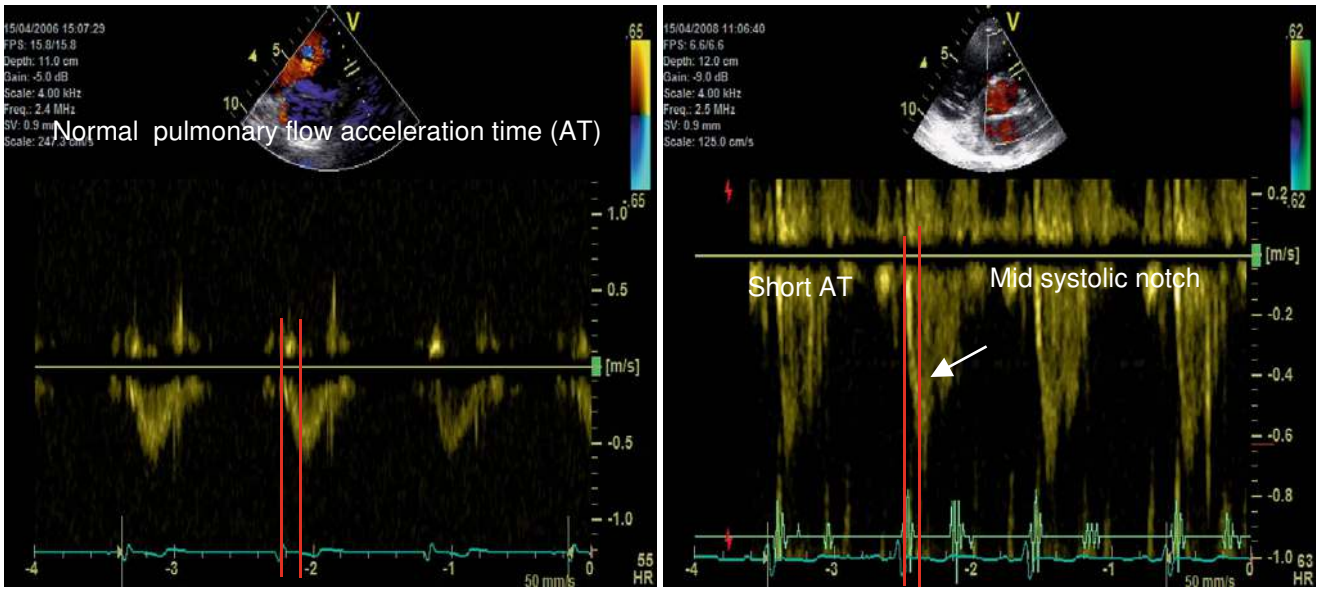


Fig. 12.7 Pulmonary forward flow from two patients: normal (*left*) and pulmonary hypertension (*right*). Note the short acceleration time in the patient

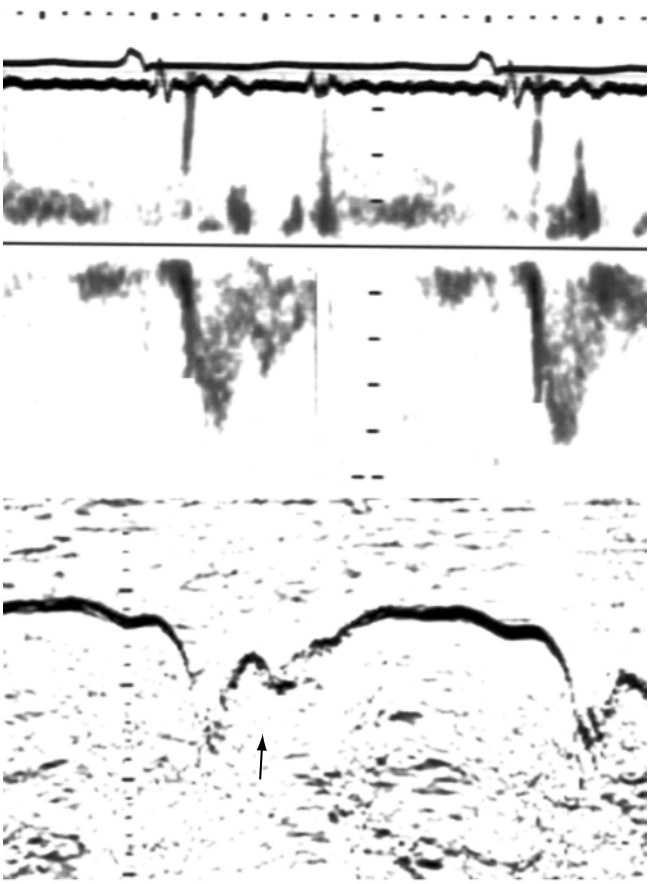


Fig. 12.8 Pulmonary flow and pulmonary valve M-mode from a patient with pulmonary hypertension showing mid-systolic valve closure (arrow) and cessation of flow

pulmonary flow is made of two components: a dominant early systolic component with a very short acceleration time, followed by a smaller late systolic component (Fig. 12.7). In general, the shorter the acceleration time of the early component, the higher the pulmonary vascular resistance and hence the pulmonary artery pressure [19].

The mid-systolic notch on the pulmonary flow in pulmonary hypertension corresponds to the mid-systolic closure of the pulmonary valve itself. This is caused by the sudden cessation of pulmonary flow in mid-systole because of the raised pulmonary vascular resistance [20]. This has been found to predict peak systolic pulmonary artery pressure of 60 mmHg (Fig. 12.8) [19].

4. *Pulmonary artery to right ventricular pressure drop*: The majority of patients with pulmonary hypertension present with some degree of functional pulmonary regurgitation on color Doppler imaging. The peak early diastolic continuous wave Doppler pressure drop of the pulmonary regurgitation provides a good estimate of mean pulmonary artery pressure in such patients (Fig. 12.9).

With slowly progressing pulmonary hypertension, all the above markers may be present. Rapidly developing pulmonary hypertension, for example, thromboembolic disease, may demonstrate raised retrograde pressure drop across the tricuspid valve in the presence of completely normal right heart size and function thus being coupled to the increased afterload. If the cause of this condition is not successfully treated, the increase in pulmonary pressures will impact RV systolic function.

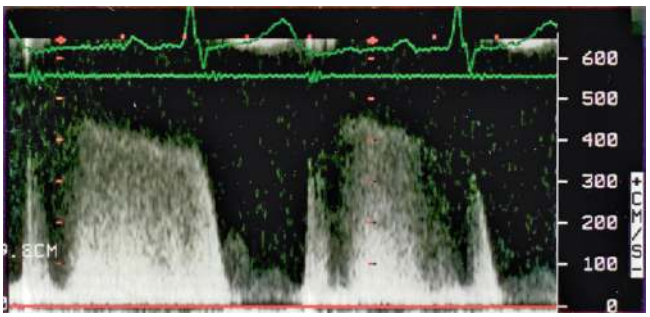


Fig. 12.9 Continuous wave pulmonary regurgitation Doppler velocities from a patient with pulmonary hypertension showing a peak early diastolic value of 65 mmHg

Pulmonary Hypertension and Vascular Resistance

Measurements of pulmonary hypertension, commonly used in clinical practice, reflect, in essence, the raised pulmonary vascular resistance (PVR). Conventional measurements of PVR are obtained by right heart catheterization. Multiple attempts have been made over the years to device Doppler-based equations for estimating pulmonary vascular resistance [21–24], but all proved to have limitations. Recently, we have proposed an equation based on the invasive measurements of PVR in a cohort of patients with both pre- and post-capillary pulmonary hypertension [25, 26].

$$\text{PVRecho} = \frac{mPAP - PWP}{CO}$$

mPAP: mean pulmonary artery pressure
PWP: pulmonary wedge pressure
CO: Cardiac output

This method has shown a specificity of 100% and a negative predictive value of 100% in identifying patients with raised PVR and a Woods unit of >3.

The table below displays the comparative accuracy measurements of the non-invasive methods proposed for the prediction of raised pulmonary vascular resistance.

	Cut-off analysis				Bland–Altman analysis	Feasibility
Echocardiographic variables	Sensitivity	Specificity	PPV	NPV	Mean difference ± SD	(%)
PVR_{echo} (WU > 3) [25]	100	63	86	100	−0.66 ± 2.1	90
PA Act/PASP, ms/mmHg (<2)	94	71	89	83	4.9 ± 4.8	83
PVR (Selimovic et al. [22], (WU > 3)	100	14	66	100	−1.8 ± 2.9	76
TRVpeak/VTIrvot (Abbas et al. [21]), (>0.175)	88	86	94	75	6.1 ± 4.0	83
PASP/HR × VTIrvot (Haddad et al. [27]), (<0.04)	94	100	100	88	6.4 ± 4.1	80
RV Strain (STE), mid, % (<−20)	88	63	82	71	21.0 ± 7.6	77

Abbreviation: *PVR* pulmonary vascular resistance, *mPAP* mean pulomonary artery preassure, *PWP* Pulmonary wedge pressure, *CO* Cardiac output, *PA* pulmonary artery, *AT* acceleration time, *PASP* pulmonary artery systolic pressure, *TRV* tricuspid regurgitation velocity, *VTI* velocity time integral, *RVOT* right ventricular outflow tract, *RV* right ventricle, *STE* speckle tracking echocardiography

Pulmonary Hypertension and Right Ventricular Function

1. *Right ventricular disease*: Severe long-standing pulmonary hypertension eventually affects right ventricular function, which, with time, becomes significantly impaired and then uncoupled from afterload. Right ventricular function can objectively be monitored by studying free wall long axis amplitude of movement (normally value >20 mm) and velocities by tissue Doppler technique (normally >10 mmHg). Assessment of right ventricular function in this way has a strong predictive value for exercise tolerance [28] and clinical outcome in different cardiac conditions (Fig. 12.10) [29]. Inability of the right ventricle to generate enough pressure to support right ventricular ejection contributes to the deterioration of the patient's clinical condition, since it compromises the stroke volume going to the left heart. Furthermore, the retrograde pressure drop across the tricuspid valve, which is usually taken as a measure of systolic pulmonary artery pressure, falls because of the right ventricular failure and the increased right atrial pressure (Fig. 12.11). Therefore, the retrograde transtricuspid pressure drop should not be taken in isolation as a sole measure of pulmonary artery pressure, in patients with severe right ventricular dysfunction. With severe right ventricular disease and raised right atrial pressure, patients may develop restrictive right ventricular physiology which itself adds to the deterioration of the condition and the poor outcome. Therefore, mPAP should be related to either stroke volume (mPAP/CO) [30] or RV function (TAPSE/mPAP) [31]
2. *Significant tricuspid regurgitation*: Severe right ventricular failure is a late stage in pulmonary hypertension. It is often associated with tricuspid annular dilatation and significant tricuspid regurgitation (Fig. 12.12). This may

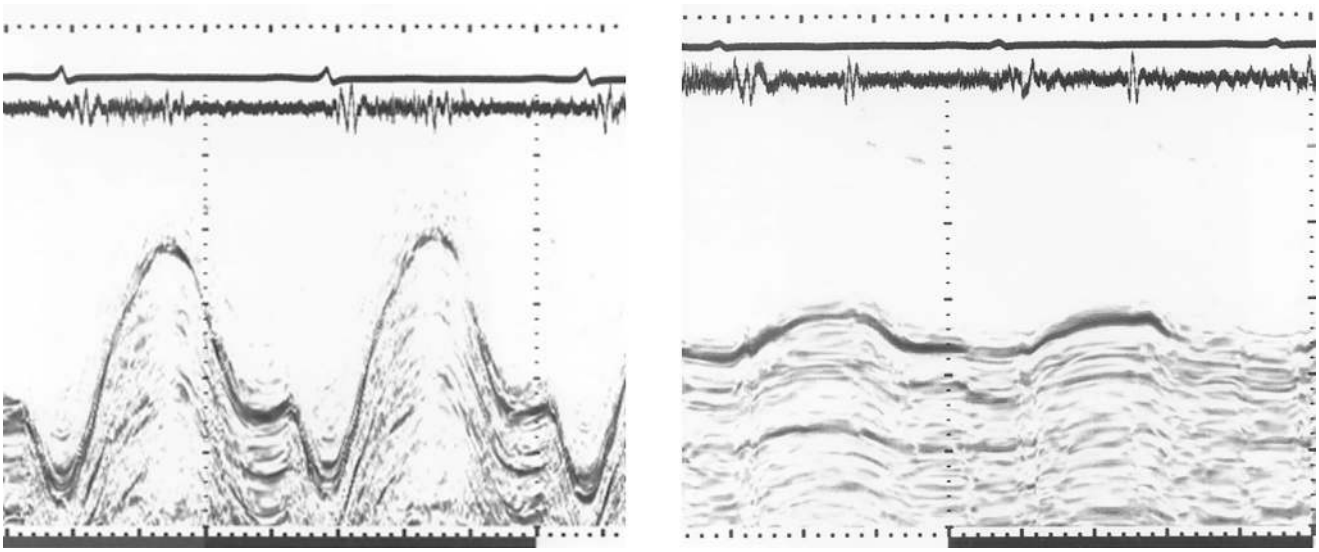


Fig. 12.10 Right ventricular long axis function from a patient with pulmonary hypertension before (*left*) and after (*right*) development of right ventricular disease. Note the significant drop in right ventricular free wall amplitude of movement over time

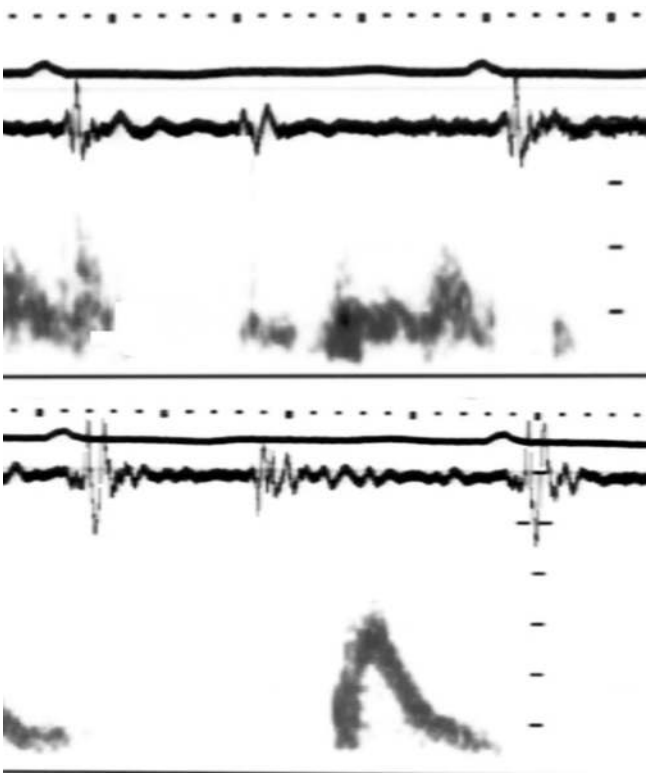


Fig. 12.11 Right ventricular filling velocities from a patient with pulmonary hypertension while the right ventricular function was maintained (*top*) showing delayed filling and after it deteriorated (*bottom*) showing restrictive filling pattern consistent with raised right atrial pressure

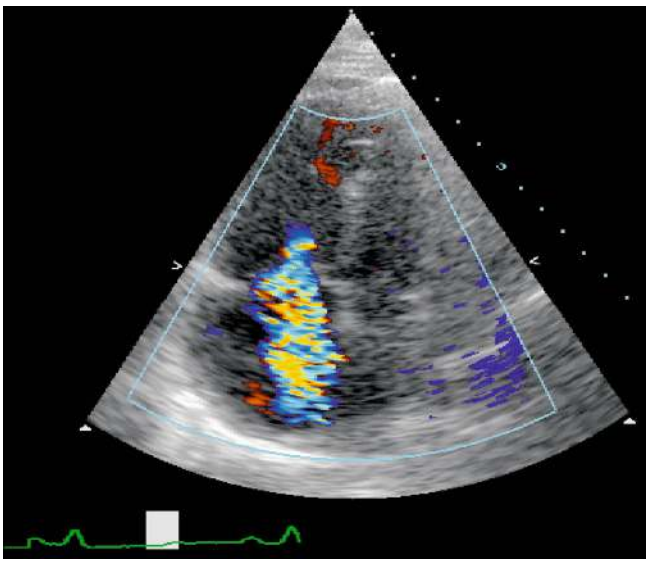


Fig. 12.12 A four-chamber view from a patient with severe pulmonary hypertension who developed right ventricular failure, dilatation of the tricuspid valve annulus, and severe tricuspid regurgitation on color Doppler. Note the extent of regurgitation, to the rear of the right atrium, on the color Doppler

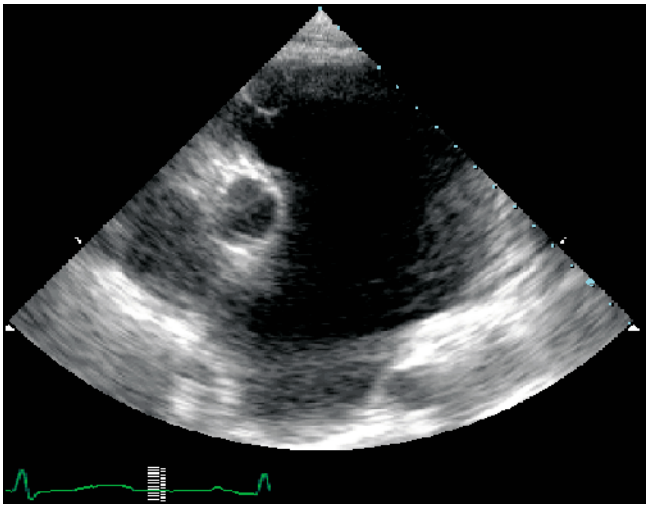


Fig. 12.13 Parasternal short axis view from a patient with pulmonary hypertension and aneurysmal pulmonary artery that involves the branch. Note that the diameter of the main pulmonary artery is 8 cm

cause right-sided heart failure and systemic congestion with elevation of central venous pressures. Tricuspid regurgitation severity can be assessed by color and continuous wave Doppler as discussed in Chap. 3.

3. *Pulmonary artery aneurysm*: The pulmonary artery may dilate in patients with significant pulmonary hypertension. In most cases, pulmonary artery dilatation is proportional to that of the right ventricle. However, an aneurysm may rarely develop, which adds to the risk of potential rupture (Fig. 12.13).

The Effect of Pulmonary Hypertension on the Left Heart

In pre-capillary PH, the right heart is frequently dilated and the left heart is normal in size. Raised right-sided ventricular pressure results in reversed septal movement, with the septum functioning as part of the right ventricle rather than the left ventricle. This can clearly be demonstrated on two-dimensional and M-mode recordings of the left ventricular minor axis from the parasternal long axis view (Fig. 12.14).

With progressive increase in right-sided pressures, the left ventricle becomes increasingly squashed and the septum flat, the so-called D-shaped ventricle during systole. This is a characteristic echocardiographic feature of pulmonary hypertension (Fig. 12.15).

The reversed septal movement in systole is characteristically followed by a septal bounce toward the left ventricular cavity in early diastole. This is caused by the relative increase in right ventricular early diastolic pressure being greater than that of the left ventricle. The inward movement of the septum in early diastole reduces left ventricular minor axis and compromises early left ventricular filling, which consequently becomes predominantly late diastolic (Fig. 12.16).

With severe pulmonary hypertension, the left ventricular shape becomes deformed, "banana shape." Consequently, the filling of the left ventricle becomes reduced and exclusively in late diastole (Fig. 12.17).

Patients with pulmonary hypertension due to long-standing systemic hypertension frequently develop left ventricular hypertrophy. The combination of the deformed septal function and the left ventricular hypertrophy in these

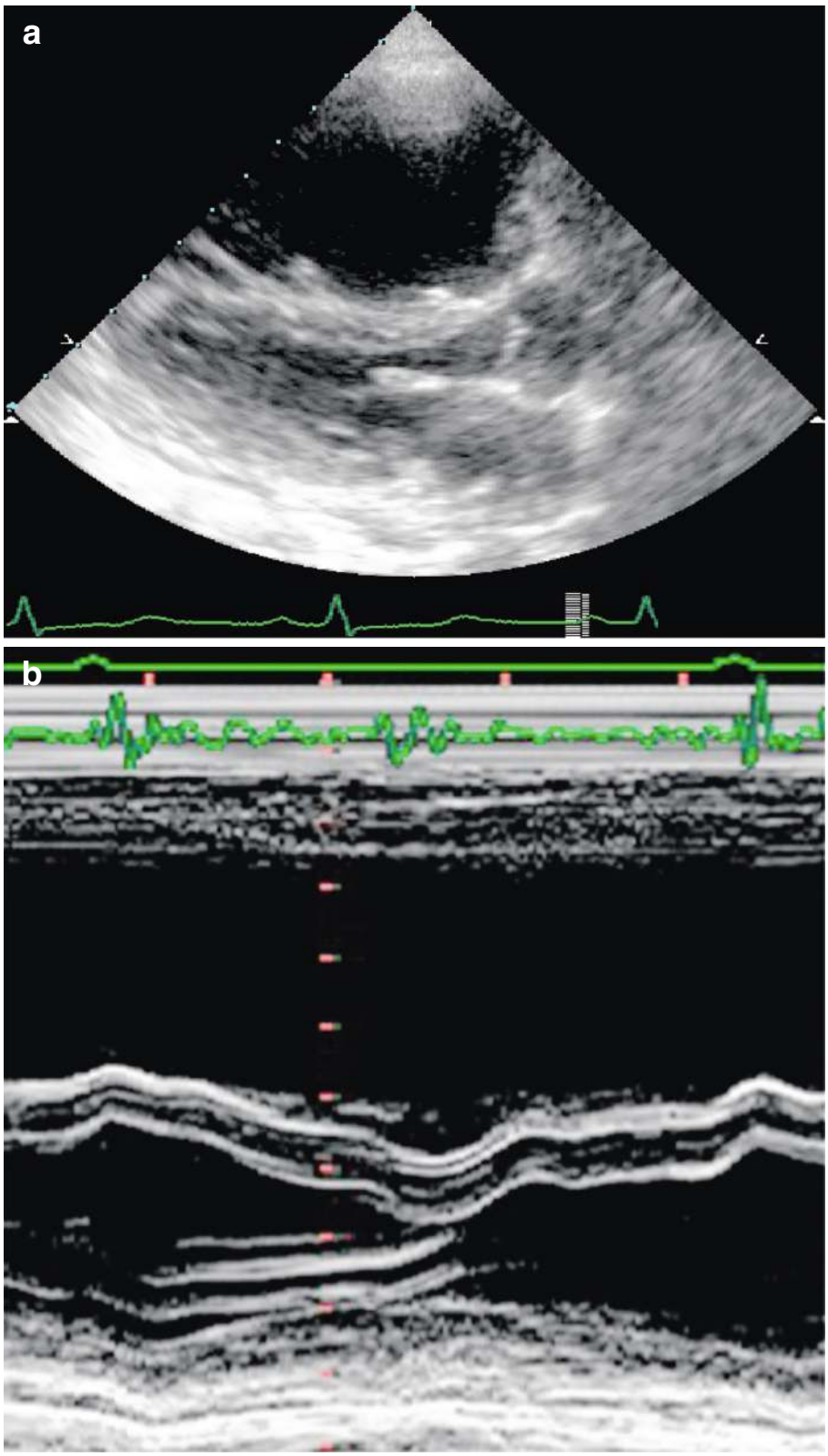


Fig. 12.14 Two-dimensional images (**a**) and M-mode recordings (**b**) of left and right ventricular cavities from a patient with advanced pulmonary hypertension demonstrating a large right ventricle and abnormal septal movement



Fig. 12.15 Parasternal short axis view of the left ventricle from a patient with pulmonary hypertension showing D-shaped cavity and dilated right ventricle

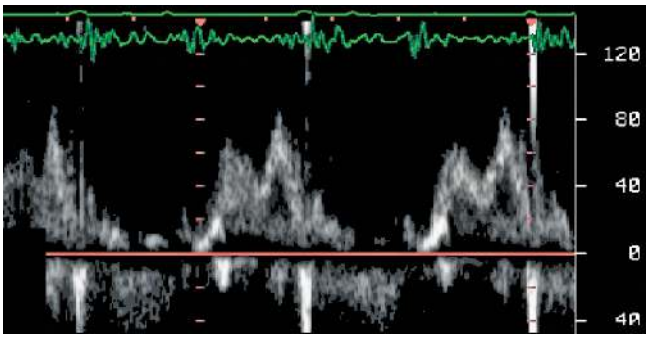


Fig. 12.16 Left ventricular filling velocities from a patient with pulmonary hypertension showing a dominant "A" wave. Notice the suppressed early diastolic filling

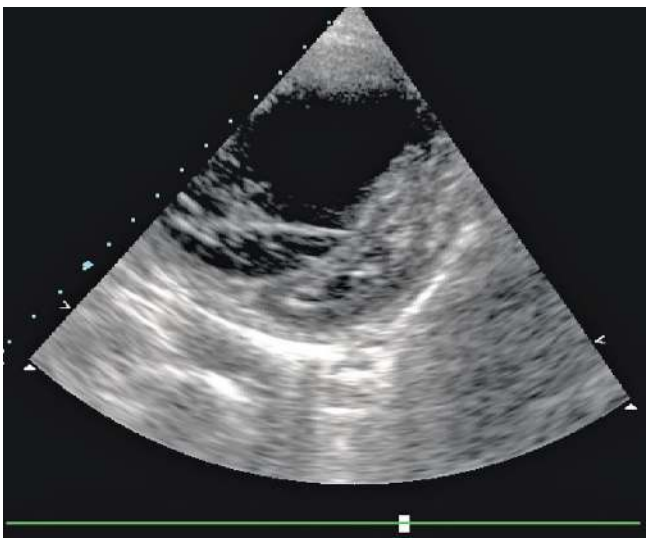


Fig. 12.17 Parasternal short axis view from a patient with advanced pulmonary hypertension showing a banana-shaped left ventricular cavity and a large right ventricular cavity

patients may cause left ventricular outflow tract obstruction, systolic anterior movement of the mitral valve, and high pressure drop (gradient) across the outflow tract, particularly with a fast heart rate. This is usually associated with a drop in systolic blood pressure and pre-syncopal attacks [32].

Management

Treatment of pulmonary hypertension is based on etiology. Pulmonary venous hypertension due to left-sided organic valvular heart disease is eminently treatable by correcting the underlying anatomical abnormality. Raised left atrial pressure due to severe left ventricular disease may respond to ACE inhibitors or ARBs, and consequently, secondary pulmonary hypertension may regress (Fig. 12.18) [33]. Patients with an incompliant left atrium may be symptomatically controlled by diuretics, although a mild degree of mitral regurgitation may still increase left atrial pressure and cause significantly limiting symptoms.

Long-standing pulmonary hypertension secondary to left heart pathology might not completely reverse even after valve surgery or the fall in left atrial pressure, due to irreversible pulmonary circulation damage. Pulmonary hypertension due to chronic obstructive airway disease or interstitial lung disease usually benefits from long-term oxygen treatment, which tends to slow down the worsening of pulmonary hypertension [34]. CTEPH patients may benefit from surgical thrombectomy, provided decision making is made through careful interdisciplinary discussions and the procedure is performed in a specialized centre with significant work experience. A successful procedure may result in a sudden drop in pulmonary artery pressure immediately after removal of the proximal thrombus. Very peripheral emboli do not usually benefit from embolectomy [35]. Pulmonary hypertension due to congenital heart disease needs special treatment in highly specialized centers with vast experience. Patients with Eisenmenger's disease have been shown to respond to bosentan treatment [36]. It is generally recommended that pulmonary hypertension patients should be managed at or under direct guidance from specialist centers, particularly with respect to the newly developed medications, e.g. endothelin receptor antagonists, PDES and Prostacycline as well as potential need for transplantation [14].

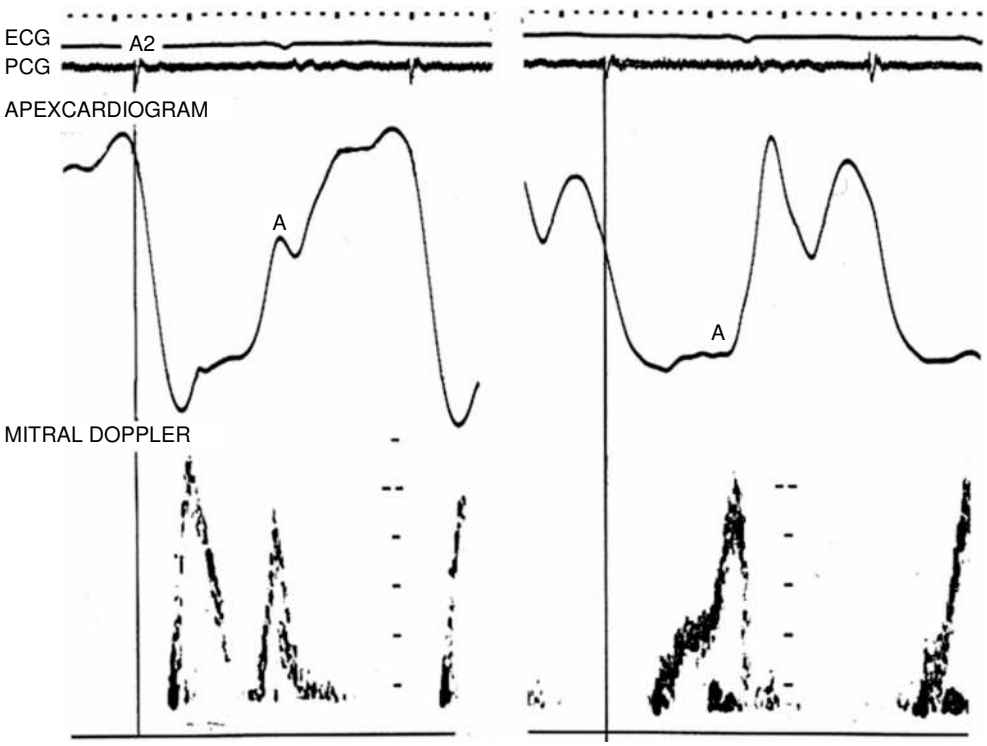


Fig. 12.18 Left ventricular filling pattern from a patient with restrictive physiology and raised left atrial pressure (*left*) and the same patient 3 weeks after commencing ACE inhibitors (*right*). Note the significant change in left ventricular physiology from the restrictive to the late diastolic filling pattern, which resulted in a significant drop in retrograde tricuspid valve pressure and improvement of symptoms

References

1. Humbert M, Kovacs G, Hoeper MM, Badagliacca R, Berger RMF, Brida M, Carlsen J, Coats AJS, Escribano-Subias P, Ferrari P, Ferreira DS, Ghofrani HA, Giannakoulas G, Kiely DG, Mayer E, Meszaros G, Nagavci B, Olsson KM, Pepke-Zaba J, Quint JK, Radegran G, Simonneau G, Sitbon O, Tonia T, Toshner M, Vachiery JL, Vonk Noordegraaf A, Delcroix M, Rosenkranz S, Group EESD. 2022 ESC/ERS Guidelines for the diagnosis and treatment of pulmonary hypertension. Eur Respir J. 2022;61(1):2200879.
2. Sajja LR, Mannam GC. Role of closed mitral commissurotomy in mitral stenosis with severe pulmonary hypertension. J Heart Valve Dis. 2001;10(3):288–93.
3. Ratwatte S, Strange G, Stewart S, Playford D, Celermajer D. Prevalence of pulmonary hypertension in mitral regurgitation and its influence on outcomes. Eur Heart J. 2023;10:e002268.
4. Snopek G, Pogorzelska H, Zielinski T, Rajecka A, Korewicki J, Biederman A, Kotlinski Z. Valve replacement for aortic stenosis with severe congestive heart failure and pulmonary hypertension. J Heart Valve Dis. 1996;5(3):268–72.
5. Lanzarini L, Fontana A, Lucca E, Campana C, Klersy C. Noninvasive estimation of both systolic and diastolic pulmonary artery pressure from Doppler analysis of tricuspid regurgitant velocity spectrum in patients with chronic heart failure. Am Heart J. 2002;144(6):1087–94.
6. Spinelli L, Petretta M, Vicario MLE, Schiavone D, De Santis V, Bonaduce D, Condorelli M. Losartan treatment and left ventricular filling during volume loading in patients with dilated cardiomyopathy. Am Heart J. 2002;143(3):433–40.
7. Ko YG, Ha JW, Chung N, Shim WH, Kang SM, Rim SJ, Jang Y, Cho SY, Kim SS. Effects of left atrial compliance on left atrial pressure in pure mitral stenosis. Catheter Cardiovasc Interv. 2001;52(3):328–33.
8. Schwammenthal E, Vered Z, Agranat O, Kaplinsky E, Rabinowitz B, Feinberg MS. Impact of atrioventricular compliance on pulmonary artery pressure in mitral stenosis – an exercise echocardiographic study. Circulation. 2000;102(19):2378–84.
9. Nishimura RA, Abel MD, Hatle LK, Tajik AJ. Relation of pulmonary vein to mitral flow velocities by transesophageal doppler echocardiography – effect of different loading conditions. Circulation. 1990;81(5):1488–97.
10. Rossvoll O, Hatle LK. Pulmonary venous flow velocities recorded by transthoracic doppler ultrasound – relation to left-ventricular diastolic pressures. J Am Coll Cardiol. 1993;21(7):1687–96.
11. Eren M, Bolca O, Dagdeviren B, Norgaz T, Tezel T. The determinants of systolic pulmonary venous flow reversal by transthoracic pulsed Doppler in mitral regurgitation: its value in determining the severity of regurgitation. Acta Cardiol. 2001;56(2):83–9.
12. Barbier P, Solomon S, Schiller NB, Glantz SA. Determinants of forward pulmonary vein flow – An open pericardium pig model. J Am Coll Cardiol. 2000;35(7):1947–59.
13. Yang H, Jones M, Shiota T, Qin JX, Kim YJ, Popovic ZB, Pu M, Greenberg NL, Cardon LA, Eto Y, Sitges M, Zetts AD, Thomas JD. Pulmonary venous flow determinants of left atrial pressure under different loading conditions in a chronic animal model with mitral regurgitation. J Am Soc Echocardiogr. 2002;15(10):1181–8.
14. 2022 ESC/ERS. Guidelines for the diagnosis and treatment of pulmonary hypertension: developed by the task force for the diagnosis and treatment of pulmonary hypertension of the European Society of Cardiology (ESC) and the European Respiratory Society (ERS). Endorsed by the International Society for Heart and Lung Transplantation (ISHLT) and the European Reference Network on rare respiratory diseases (ERN-LUNG). Eur Heart J. 2023;44(15):1312.
15. Yock PG, Popp RL. Noninvasive estimation of right ventricular systolic pressure by doppler ultrasound in patients with tricuspid regurgitation. Circulation. 1984;70(4):657–62.

16. Lindqvist P, Henein MY, Wikström G. Right ventricular myocardial velocities and timing estimate pulmonary artery systolic pressure. Int J Cardiol. 2009;137(2):130–6.
17. Yu CM, Sanderson JE, Chan S, Yeung L, Hung YT, Woo KS. Right ventricular diastolic dysfunction in heart failure. Circulation. 1996;93(8):1509–14.
18. Lindqvist P, Waldenstrom A, Wikstrom G, Kazzam E. Right ventricular myocardial isovolumic relaxation time and pulmonary pressure. Clin Physiol Funct Imaging. 2006;26(1):1–8.
19. Lindqvist P, Söderberg S, Gonzalez MC, Tossavainen E, Henein MY. Echocardiography based estimation of pulmonary vascular resistance in patients with pulmonary hypertension: a simultaneous Doppler echocardiography and cardiac catheterization study. Eur J Echocardiogr. 2011;12(12):961–6.
20. Lew W, Karliner JS. Assessment of pulmonary valve echogram in normal subjects and in patients with pulmonary arterial-hypertension. Br Heart J. 1979;42(2):147–61.
21. Abbas AE, Fortuin FD, Schiller NB, Appleton CP, Moreno CA, Lester SJ. A simple method for noninvasive estimation of pulmonary vascular resistance. J Am Coll Cardiol. 2003;41(6):1021–7.
22. Selimovic N, Rundqvist B, Bergh CH, Andersson B, Petersson S, Johansson L, Bech-Hanssen O. Assessment of pulmonary vascular resistance by Doppler echocardiography in patients with pulmonary arterial hypertension. J Heart Lung Transplant. 2007;26(9):927–34.
23. Dabestani A, Mahan G, Gardin JM, Takenaka K, Burn C, Allfie A, Henry WL. Evaluation of pulmonary-artery pressure and resistance by pulsed doppler echocardiography. Am J Cardiol. 1987;59(6):662–8.
24. Haddad F, Zamanian R, Beraud AS, Schnittger I, Feinstein J, Peterson T, Yang P, Doyle R, Rosenthal D. A novel non-invasive method of estimating pulmonary vascular resistance in patients with pulmonary arterial hypertension. J Am Soc Echocardiogr. 2009;22(5):523–9.
25. Lindqvist P, Soderberg S, Gonzalez MC, Tossavainen E, Henein MY. Echocardiography based estimation of pulmonary vascular resistance in patients with pulmonary hypertension: a simultaneous Doppler echocardiography and cardiac catheterization study. Eur J Echocardiogr. 2011;12(12):961–6.
26. Venkateshvaran A, Tossavainen E, Borneteg C, Oktay Tureli H, Vanoli D, Lund LH, Flachskampf F, Lindqvist P. A novel echocardiographic estimate of pulmonary vascular resistance employing the hydraulic analogy to Ohm's law. Int J Cardiol Heart Vasc. 2022;42:101121.
27. Haddad F, Zamanian R, Beraud AS, Peterson T, Schnittger T, Yang P, Rosenthal D. A novel method for non-invasive estimation of pulmonary vascular resistance in patients with pulmonary arterial hypertension. J Heart Lung Transplant. 2009;28(2):S157–S.
28. Webb-Peploe KM, Henein MY, Coats AJS, Gibson DG. Echo derived variables predicting exercise tolerance in patients with dilated and poorly functioning left ventricle. Heart. 1998;80(6):565–9.
29. Faris R, Coats AJS, Henein MY. Echocardiography-derived variables predict outcome in patients with nonischemic dilated cardiomyopathy with or without a restrictive filling pattern. Am Heart J. 2002;144(2):343–50.
30. Verwerft J, Verbrugge FH, Claessen G, Herbots L, Dendale P, Gevaert AB. Exercise systolic reserve and exercise pulmonary hypertension improve diagnosis of heart failure with preserved ejection fraction. Front Cardiovasc Med. 2022;9:814601.
31. Chen X, Zhang P, Lou J, Zhao R, Zhang S, Xie M, Lv Q. Application of an echocardiographic index to characterize right ventricular-pulmonary arterial coupling in heart failure. ESC Heart Fail. 2024;11(3):1290–304.
32. Henein MY, Gibbs JSR. Breathlessness in pulmonary hypertension: Heart and lung? Int J Cardiol. 2005;98(3):499–529.
33. Henein MY, O'Sullivan CA, Gibson DG. ACE-inhibitors revert abnormal right ventricular filling indices in patients with restrictive left ventricular disease. Circulation. 1998;98(17):24.
34. Weitzenblum E, Sautegeau A, Ehrhart M, Mammosser M, Pelletier A. Long-term oxygen-therapy can reverse the progression of pulmonary-hypertension in patients with chronic obstructive pulmonary-disease. Am Rev Respir Dis. 1985;131(4):493–8.
35. Galiè N, Humbert M, Vachiery JL, Gibbs S, Lang I, Torbicki A, Simonneau G, Peacock A, Noordegraaf AV, Beghetti M, Ghofrani A, Sanchez MAG, Hansmann G, Klepetko W, Lancellotti P, Matucci M, McDonagh T, Pierard LA, Trindade PT, Zompatori M, Hoeper M. 2015 ESC/ERS Guidelines for the diagnosis and treatment of pulmonary hypertension. The Joint Task Force for the Diagnosis and Treatment of Pulmonary Hypertension of the European Society of Cardiology (ESC) and the European Respiratory Society (ERS). Eur Respir J. 2015;46(6):1855–6.
36. Gatzoulis MA, Beghetti M, Galie N, Granton J, Berger R, Lauer A, Chiossi E, Landzberg MJ, Grp B-S. Bosentan shows persistent benefit in functional class and exercise capacity amongst Eisenmenger patients in the BREATHE-5 open label extension study. Eur Heart J. 2006;27:8–9.

Echocardiography in Advanced Heart Failure

13

Francesca M. Righini, Luca Martini, Matteo Lisi, Matteo Cameli, and Michael Y. Henein

Advanced heart failure (AdHF) represents an end-stage disease in which patients present with severe impairment of functional capacity despite optimum guideline-directed medical therapy (GDMT) and frequent episodes of congestive or low-output decompensated phases, causing repetitive hospitalizations and requiring aggressive therapeutic options, like mechanical circulatory support (MCS) or heart transplantation (HTx) [1].

Early recognition of the transition to AdHF is crucial to the timely selection of tailored therapeutic options and improving survival and prognosis. Despite a recent transition to a multimodality imaging approach in the cardiovascular field, echocardiography, particularly recent technological developments, has become the gold standard and first-line approach for the evaluation of patients with heart failure (HF). It provides fundamental cardiac function assessment and defines the prognostic and therapeutic landscapes in AdHF. It is the mainstay for diagnostic assessment of AdHF, being non-invasive and patient-friendly, and provides bedside fast evaluation of cardiac structure and function.

Echocardiographic examination has several targets in the HF population, including the assessment of myocardial structure and function, valvular disease, and cardiac physiology. While recent ultrasound techniques can provide additional information on myocardium deformation function, their ability to characterize tissue is inferior to that of cardiac MR [2]. Ultrasound evaluation should not occur in isolation, and a multiparametric approach is highly advised for complete evaluation of patients with AdHF [3].

HF is a progressive condition, characterized by reduced forward flow, cardiac output (CO), and/or elevated left ventricle filling pressure (LVFP) secondary to impaired myocardium function [4]. Although assessment of cardiac physiology is important for prognostic stratification and management of patients with HF, the need for an invasive method is limited because of the small but definite risk of infections, bleeding, pneumothorax, patient discomfort, and the cost of the procedure [5, 6]. In contrast, Doppler echocardiography allows accurate evaluation of most clinically relevant cardiac physiology indices, including CO and LVFP [7, 8]. The two principal mechanisms responsible for HF symptoms, impairment of left ventricular (LV) contractile function and LV filling, are not mutually exclusive and frequently coexist. However, despite the complexity of the underlying pathophysiology, the main clinical classification of chronic HF is based on LV ejection fraction (LVEF), a measure of systolic performance [9].

LV Function Assessment

The main advantage of LVEF is its simple and widespread use, which allows easy communication between various teams. However, LVEF has important limitations that compromise its ability to satisfactorily characterize individuals with HF. Visual estimation of EF is widely used, however, this approach may be misleading when the rhythm is irregular, when the LV is very large or very small, and in cases of extreme heart rates.

The main reasons for the inaccuracy of LVEF measured by echocardiography are test-retest variability [10], preload and afterload dependency, occasional sub-optimal image quality, intraventricular conduction disturbances (especially left bundle branch block when regional systole and diastole are not simultaneous) and heart rhythm irregularities, and geometric assumptions of LV shape, by 2-dimentional method, when estimating LV volumes [11]. The use of 3-dimensional echocardiography [12] in the assessment of LVEF mitigates the latter limitation. It has the advantage of reducing the test–retest variability [13]; however, this modality has its own drawbacks, such as low spatial and temporal resolution. Irrespective of the technique used for

F. M. Righini (✉) · L. Martini · M. Cameli
University of Siena, Siena, Italy

M. Lisi
Ospedale S. Maria delle Croci, Ravenna, Italy

M. Y. Henein
Imperial College London, London, UK

Siena Univesity, Siena, Italy

© The Author(s), under exclusive license to Springer Nature Switzerland AG 2025

M. Y. Henein (ed.), *Clinical Echocardiography*, https://doi.org/10.1007/978-3-031-95894-6_13

assessing LVEF, it remains limited in prognostic value when the measure is close to the reference range [14].

LV volume measurements using 2D echocardiography are susceptible to off-axis imaging, hence frequently underestimate the true volumes. The use of ultrasound contrast in such patients with enhanced contrast resolution of the true endocardial border could help improve the accuracy of the volumetric cavity assessment. The use of 3D echocardiography similarly reduces volume and function underestimation, analogous to the effect of contrast, but with the benefit of reliability [15].

In addition to the assessment of LV size, cavity shape is an important determinant of the severity of HF. The degree of LV remodelling has an important prognostic value in patients with HF and reduced EF. The transition from a bullet-shaped to a more spherical cavity is a simple subjective marker that may be quantified as a sphericity index. When using 2D imaging, LV shape may be influenced by regional involvement, thus making 3D measurements preferable [16].

Clinically, LVEF has some limitations. First, there is no clear relationship between LVEF and symptoms (NYHA functional class), and second, it is unable to predict clinical outcome in patients with end-stage HF [17]. However, the determination of LVEF has a central role in the management of HF, identifying patients who are likely to respond to HF therapy as well as those who will benefit from device therapy, either implanted defibrillators or cardiac resynchronization [18].

The limited value of LVEF in describing LV contractile function, irrespective of the method used is related to the intricacy of LV systolic function mechanics. LV ejection is governed by longitudinal and circumferential shortening, radial thickening, and rotational motion. This multidimensional pattern is achieved by the complex LV architecture, including circumferential fibers in the midmyocardium and longitudinal fibers in the subendocardium and subepicardium, forming a right-handed and left-handed helix, respectively. The rotation of the LV base and apex in opposite directions, attributable to differences in the helical geometry of the subendocardial and subepicardial layers, causes twisting of the LV, which is an important contributor to LV volume reduction during systole and untwisting and suction during diastole [9].

The subendocardial fibers responsible for LV longitudinal contraction are the most vulnerable to wall stress changes [19]. Accordingly, the selective involvement of the inner layer of the LV wall in the early phase of the disease results in LV longitudinal dysfunction. In these circumstances, when the contractile function of the subepicardial and midmyocardial fibers is preserved, it is quite common to result in increased circumferential and twist function to compensate for the compromised long-axis function and to maintain LVEF within the normal range [20]. The early reduction in LV longitudinal systolic function parallels or, in some cases, even precedes the development of diastolic abnormalities. This pattern of LV function changes is seen in the preclinical stage of HFpEF. As HF progresses, the loss of the latter compensatory mechanism may result in deterioration of overall LV performance and the HF symptoms [21]. In contrast to the above scenario, the concurrent involvement of all myocardial layers, for example, during an acute myocardial infarction or myocarditis, leads to a reduction in all components of LV contractile function and a fall in LVEF, usually with concomitant cavity dilatation [20]. These features are consistent with the morphological and functional profile of HFrEF.

Myocardial deformation imaging has emerged as an option that can provide some insight into the physiology and pathophysiology of cardiac function. The currently recommended technique for the evaluation of myocardial deformation is speckle-tracking echocardiography (STE). Despite some apparent limitations, such as relatively low temporal resolution, STE is more feasible and more likely to be implemented in daily clinical practice than the previously used modality based on tissue Doppler imaging. The measurements of myocardial deformation indices derived from STE can be carried out both in the ventricles and atria [22]. For the LV, the highest feasibility is for LV longitudinal strain. The assessment of myocardial deformation allows detection of dysfunction that would otherwise be missed. The most common deformation parameters include strain, strain rate, twist, as well as twisting and untwisting rate. Both the amplitude and timing of myocardial deformation indices can be quantified, globally and segmentally, so the technique can give additional insight into electromechanical coupling.

Applying the above parameters has shown that normal LVEF may not be synonymous with normal LV systolic function. This paradox, best seen in HFpEF, can be explained by the dependence of LVEF on a variety of geometric factors. In the presence of increased LV wall thickness and/or decreased end-diastolic volume, LVEF may remain normal despite reductions in both LV longitudinal and circumferential extent of shortening [23]. With the greater contribution of circumferential shortening than longitudinal shortening, LVEF is less prone to a decline in the context of impaired longitudinal function. These findings strongly support the use of LV deformation indices in addition to LVEF for the assessment of LV systolic function.

LVEF does not adequately assess clinical risk when it is relatively preserved [24, 25], and is of limited value for determining eligibility for device therapies in primary prevention of sudden cardiac death [26, 27]. Global longitudinal strain (GLS) has been shown to provide additional prognostic information independent of LVEF. In a meta-analysis including a wide spectrum of cardiovascular diseases, GLS was on

average 1.5-fold better prognosticator of major adverse cardiac events than LVEF, with the superiority of GLS being most discernible in the normal or near-normal ranges of LVEF [28]. Accordingly, GLS adds incremental prognostic value both in HFpEF and HFrEF, but its role as a prognosticator is more critical in the former population [29, 30]. The associations of global LV deformation with increased cardiovascular risk were also demonstrated in post-infarct patients developing HF, both for GLS and global circumferential strain [31, 32]. These measurements provide an incremental value to the diagnosis of diseases characterized by the regional heterogeneity of LV function, such as amyloidosis (relative apical sparing) or Fabry disease (functional impairment mainly in the mid or basal posterolateral segments) [33]. Myocardial deformation parameters are primarily dedicated to the assessment of cardiac contraction; however, some indices, such as strain rate during isovolumic relaxation, strain rate during early filling, and LV untwisting rate, can be used to describe diastolic function. Since deformation parameters are affected by loading conditions, probably more for strain than strain rate, they may not adequately reflect myocardial contractile function. This interplay between myocardial deformation and changing cardiac load can lead to misleading clinical conclusions, particularly in disease states characterized by high LV afterload and in serial assessments, when visit-to-visit fluctuations in blood pressure may affect the magnitude of LV deformation.

To avoid this limitation, the estimation of myocardial work correcting longitudinal deformation for systolic blood pressure on the basis of non-invasive load-strain loops has been proposed. This approach provides additional information on LV function by calculating constructive and wasted work, as well as myocardial efficiency, but further validation is warranted (Fig. 13.1) [34].

In its natural history, preclinical HF may deteriorate and progress to HFpEF or even to HFrEF. A meta-analysis of several studies of asymptomatic patients showed that diastolic dysfunction is associated with a 70% increased risk of overt HF [35]. From a pathophysiologic standpoint, the transition to symptomatic HF is related to the progression of physiological disturbances in LV filling and contractile function, which can be identified and monitored by echocardiography.

Elevated LV filling pressure (LVFP) represents the hemodynamic consequence of LV significant diastolic dysfunction. Doppler echocardiography is a well-established, reliable, reproducible, and practical non-invasive investigation for diagnosis and follow-up of patients with diastolic dysfunction. Grading diastolic dysfunction reflects different stages of myocardial disease. With disease progression, left atrial (LA) pressure rises, increasing the driving pressure across the mitral valve and consequently the increase in the E velocity on the LV filling pattern, and a restrictive pattern appears in the late stage of myocardial disease [36].

LV relaxation and LVFP can be assessed by Doppler echocardiography using a combination of parameters, including the ratio of early diastolic to late diastolic mitral inflow velocities (E/A), E wave deceleration time, mitral annular early diastolic tissue velocity (e′), ratio of mitral E/e′, pulmonary venous velocities, retrograde tricuspid regurgitation velocity and its pressure drop. It is worth noting that although e′ was suggested to be a load-independent measure of LV relaxation, it is also affected by blood pressure, systolic function, and LV minimal pressure. In general, patients with preserved systolic function, blunting of mitral annular e′ is usually indicative of the presence of abnormal relaxation and diastolic dysfunction (Fig. 13.2). Pulmonary venous velocities have also been suggested as a load-independent measure of LVFP. An increased pulmonary venous atrial contraction (PV−A) velocity and duration, and reversed S/D ratio (<1.0) are indicative of elevated LVFP [37].

It must be remembered, however, that diastolic dysfunction represents an altered interaction between elastic stiff-

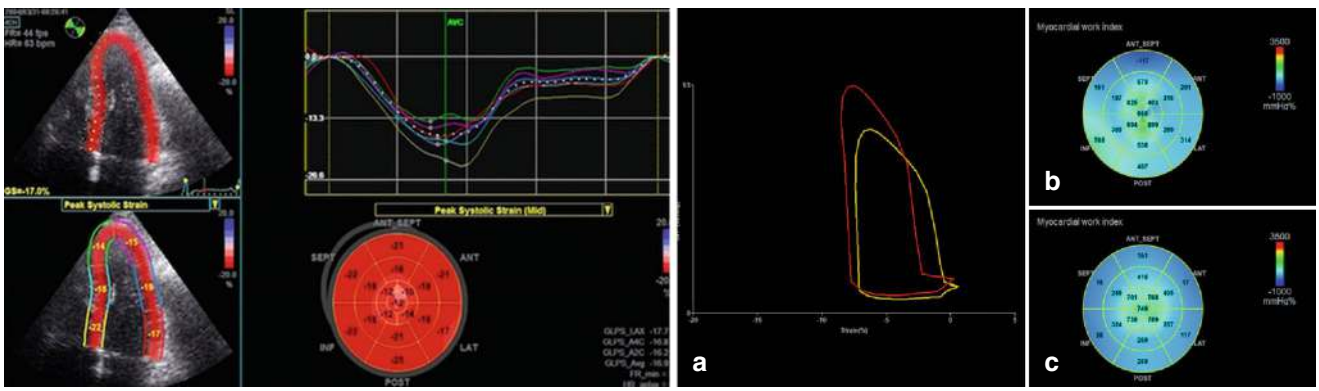


Fig. 13.1 On the left, the left ventricle global longitudinal strain (LV GLS) curve and each segment's longitudinal strain are represented by a bull's eye. On the right, the pressure-volume loop curve and myocardial work indices bull's eye, taken and adjusted under permission from 10.1002/ehf2.14339

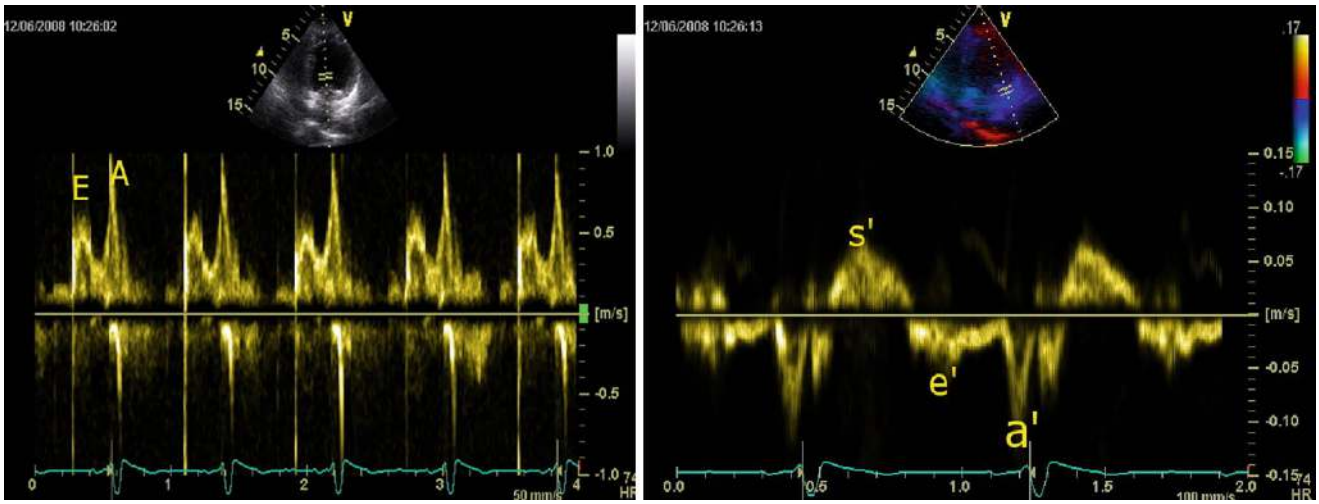


Fig. 13.2 The diastolic assessment via pulse Doppler on the mitral valve (on the left) and via tissue Doppler imaging (TDI) on the right

ness and myocardial relaxation. Conventional indices such as E/A, DT, and e′ are the result, rather than the cause, of this interplay and cannot independently quantify relaxation or stiffness [38]. Thus, for the purpose of LV diastolic function assessment, no single variable has proven to be sufficiently accurate, and therefore, algorithm-based decision trees composed of several parameters are recommended. The most recent American Society of Echocardiography guidelines [37] for the use of Doppler echocardiography in the assessment of LV diastolic function have identified the following 4 variables as the most useful for this purpose: mitral E/A ratio, average E/e′, LA volume index (LAVi), and peak retrograde tricuspid regurgitation velocity. By combining these variables, LV diastolic function and LVFP can be estimated in most patients with structural myocardial disease with or without reduced LVEF.

Echocardiographic indices of LVFP correlate with invasive estimation by catheterization. Transmitral E/A ratio, average E/e′ ratio, and LAVi have been shown to be independently associated with invasive LV diastolic pressure (LVEDP) [39, 40]. The Euro-Filling study has shown a correlation between echocardiographic indices of LVFP and invasively estimated pressures in patients based on LVEF. Lateral E/e′ was significantly related to LVEDP in patients with preserved LVEF, while the E/A ratio best correlated with LVEDP in patients with reduced LVEF.

The restrictive LV filling pattern has been consistently shown as an independent predictor of adverse clinical outcomes [41, 42] and, in a meta-analysis involving 3540 patients, it proved a powerful predictor of mortality, independent of LVEF, age, and etiology [43]. Similarly, elevated E/e′ has been shown to be an independent prognosticator in HF, both in HFrEF and HFpEF [44–47]. However, the diagnostic accuracy of the most commonly used echocardiographic marker, E/e', has been questioned, given its susceptibility to loading conditions [48] and its variable and frequently modest correlations with invasive measurements [49]. A recent meta-analysis reported a pooled r coefficient of only 0.56 [50].

Pulmonary Pressures The Guidelines' algorithm [37] was validated and proved to have 87% overall accuracy in detecting high pulmonary capillary wedge pressure—PCWP (evaluated invasively), which made it applicable in 419 (93.1%) patients and was inconclusive in 31 (6.9%) patients. This approach also has good accuracy in patients with left bundle branch block, paced rhythm, atrial fibrillation, or moderately severe to severe mitral regurgitation [51].

The validation of this approach against cardiac catheterization was carried out in two multicenter studies, which confirmed its feasibility but demonstrated some differences in its diagnostic accuracy (sensitivity and specificity of 87% and 88% in the first study and 75% and 74% in the second study, respectively) [39, 51]. The reason for this discrepancy might be the different clinical profiles of the studied cohorts and, more importantly, the different metrics of LVFP used as reference (PCWP vs LVEDP). The better correlation of the 2016 algorithm with PCWP than with LVEDP is consistent with the previous findings on the associations of individual Doppler indices used in this approach with invasive hemodynamic data [52]. However, this algorithm presents a "grey zone" of indeterminate diastolic function. Hence, it is estimated that in 10% of patients, evaluation of LVFP according to these Guidelines is inconclusive due to missing echocardiographic parameters, most often TR velocity [53].

Assessment of pulmonary artery systolic pressure is an important aspect in patients with HF. It is conventionally calculated from tricuspid regurgitation velocity, using the equation $PSPA = 4V^2$, and estimation of right atrial pressure from

the inferior vena cava diameter in response to a sniff [54]. Estimation of peak systolic pulmonary arterial pressure is important in clinical practice [55, 56]. A correct measurement of TR peak velocity is not so feasible in clinical practice, and two recent studies have shown that TR was available only in 40–60% of patients [57],. thus could be a problem, especially in patients with suspected HFpEF. The main limitations of this approach are that it depends on a tricuspid regurgitation signal and carries a risk of underestimating pulmonary artery systolic pressure in the presence of severe tricuspid regurgitation, which can contravene the assumption of low right atrial pressure.

The 2016 EACVI/ASE Guidelines suggest the use of supplementary parameters such as pulmonary venous velocities, isovolumetric relaxation time, or other methods such as STE. Particularly, recently left atrial (LA) strain, by STE, has been proved a reliable index of LVFP which could fill the gap in the previous algorithm [58, 59]. A recent multicenter study of 322 patients referred for diagnostic right- or left-side heart catheterization and with a mean LVEF of 55% demonstrated that both global peak atrial longitudinal strain (PALS) and pump strain (peak atrial contraction strain (PACS) were associated with LVFP, with an optimal cut-off of 18% and 8%, respectively to differentiate between normal and elevated LVFP (PCWP > 12 mmHg) [53]. Similar results were also confirmed [60] in 210 patients with LVEF > 50% (comparing echocardiography and right heart catheterization), showing that PALS was accurate in identifying patients with elevated LVFP (PCWP > 15 mmHg) with an AUC = 0.76. Moreover, substituting TR peak velocity for PALS (< 18%) in the 2016 ASE/EACVI algorithm resulted in 91% feasibility, 81% accuracy, and stronger agreement with invasive measurements. These results confirm that HFpEF is a challenging diagnosis, requiring an integrated approach (combination of multiple echocardiographic parameters, standard diagnostic tests, and physical examination), and they also show that LA strain is superior to TR velocity as a marker of LVFP [61]. Interestingly, the latest EACVI algorithm for the use of a multimodality imaging approach in evaluating HFpEF suggested it too in HFrEF in sinus rhythm [62], thus allowing echocardiographic estimation of LVFP in patients with HF, regardless of LVEF value.

It has recently been demonstrated that in patients with advanced HF, undergoing heart transplantation, the global PALS was inversely correlated with PCWP (**R** = − 0.83; $p < 0.0001$) and with LV fibrosis severity (**R** = − 0.78; p < 0.0001) but not with LVEF (R = 0.15; $p = 0.2$). Also, global PALS proved the strongest [AUC 0.955 (95% CI 0.87–0.99)] predictor of raised (> 18 mmHg) PCWP, evaluated invasively [63]. These results highlight the fact that LA myocardial dysfunction is strongly correlated with PCWP, thus confirming its added value in the non-invasive assessment of LVFP in HF patients, irrespective of LVEF [64].

Estimation of cardiac output (COP) is an important hemodynamic measurement to consider in AdHF. It is based on the volumetric approach based on traces diastolic and systolic volumes or uses Doppler to calculate stroke volume from blood flow, LV outflow tract diameter, and heart rate. Unfortunately, accurate tracing of end-diastolic and end-systolic borders could be problematic [65]. Measurement of the velocity time integral (VTI) at the LV outflow tract (LVOT) is a simple and useful method of estimating the forward stroke volume and CO [66–68]. LVOT VTI is useful for estimating not only CO but also prognosis in HF, irrespective of EF [69, 70]. Changes in LV inflow pattern and LVOT VTI are useful for assessing treatment response. However, the measurement of stroke volume depends on accurate estimation of LV outflow tract diameter, errors of which are squared, so likely to devalue the accuracy of the measurement.

The Left Atrium in HF

Left atrial (LA) enlargement is considered a marker of long-term rise of LVFP, analogous to the role of HbA1c as a measure of average glucose level in diabetes mellitus. During diastole, LA is directly exposed to higher LV pressures as the mitral valve is open. Along with the reduction of LV compliance and the rise of diastolic pressures, LA pressure gradually increases to maintain an adequate LV filling. This results in LA dilatation, which carries a worse prognosis [71]. In fact, LA volume is a valuable prognostic marker [72] and is predictive of events, including atrial fibrillation (AF), HF hospitalizations, stroke, and overall cardiovascular mortality [73–78]. LA volume is measured using a biplane approach in the apical views; 3D measurements have also been validated [79]. Furthermore, LA function has recently been shown to add incremental predictive information about the development of AF and in patients with AdHF.

The chronic rise of LVFP causes a continuous pressure overload on the LA, causing a range of adaptive and maladaptive cavity remodelling with alterations in the composition of extracellular matrix and interposition of fibrotic tissue. Fibrosis has dramatic effects on LA mechanics involving both reservoir and booster pump functions, the loss of which contributes further to the rise in LA pressures, the development of AF and HF symptoms [80]. Eventually, severe LA remodelling with structural, functional and electrical changes occurs with their metabolic and neurohormonal consequences, leading to a reduction of LA compliance and increased cavity stiffness [81].

Despite its high accuracy when applied to LV study, CMR assessment of LA fibrosis is still challenging mainly because of limitations in image resolution, thin atrial walls (1–2mm), and highly variable atrial shape [82, 83]. On the contrary, the growing use of a widely available STE has demonstrated

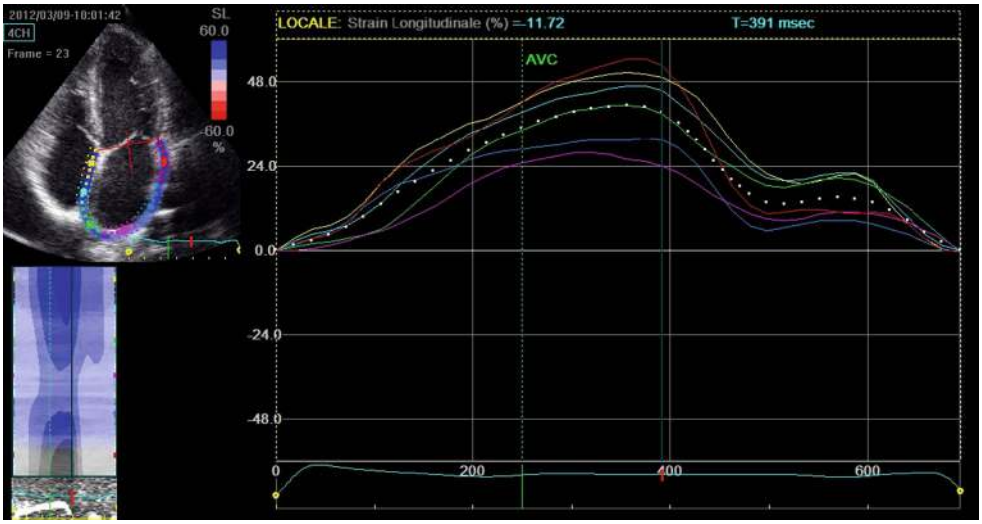


Fig. 13.3 Left atrium (LA) strain curve: the first peak represents the peak atrial longitudinal strain (PALS), while the second one represents the peak atrial contraction strain (PACS)

optimal results when applied to studying LA function, in terms of feasibility and reproducibility [84, 85].

Conventional assessment of LA function involves Doppler measurements of its conduit, reservoir, and contractile function. Assessment of LA strain is more feasible and has the ability to measure both LA contraction and LA compliance [86]. LA strain by STE has proved superior over conventional echocardiographic parameters for the diagnostic and prognostic evaluation of HF irrespective of ejection fraction [87–89], and in predicting the onset of AF [90] , which directly correlates with LA fibrosis [91]. LA enlargement, the decrease in LA pump function, the increase of LVFP, and the LV dysfunction (lower global longitudinal strain and reduced EF) have a strong impact on LA reservoir function [53]. In patients with AdHF, peak atrial longitudinal strain (PALS), an index of LA reservoir function, proved a surrogate of LVFP, while tissue Doppler imaging parameters lost their accuracy in patients with severe LV remodelling (Fig. 13.3) [92].

PALS has shown good accuracy in predicting invasively quantified atrial fibrosis in patients with mitral regurgitation [93, 94]. Moreover, the LA strain emerged as a key parameter for the estimation of LA fibrosis. A recent study [95] demonstrated an association between reduced LA function and the severity of LA wall fibrosis in patients with AdHF. In particular, PALS, severely reduced in patients with end-stage HF, was the best predictor of the extent of LA fibrosis, quantified by histopathologic studies, the gold standard measure of LA myocardial fibrosis. Furthermore, both PALS and LA fibrosis correlated with HF symptoms severity, pulmonary wedge pressure and CPET-derived exercise capacity in these patients. Therefore, severe reduction in LA function in patients with AdHF could forerun a severe degree of biventricular failure, in which the use of alternative therapeutic strategies should be considered. The increase of LA wall stress and pressure gradually leads to pulmonary hypertension and finally right ventricular (RV) overload and dysfunction with considerably worse prognosis and quality of life [96–98].

Mitral Regurgitation in HF

In patients with AdHF, the distinction between a failing LV due to severe organic mitral regurgitation and severe functional MR may have important implications, and the cornerstone distinction is the evaluation of the mitral valve. The presence and severity of MR are important parameters that should be assessed quantitatively [99]. Functional MR is characterized by tethering of the leaflets and a jet that is usually central or posteriorly directed in the absence of anterior leaflet prolapse. Ischemic MR may also be associated with a commissural jet, related to loss of support from one or the other papillary muscle [100]. Even when MR is not severe, the spectral Doppler jet provides information about LV function; the rate of increase of velocity is analogous to the measurement of LV dP/dt, a marker of LV contractile function that is particularly useful in MR, when LV function may be overestimated by EF.

The Right Ventricle in HF

Another key player in patients with HF is the right ventricle (RV). There is accumulating evidence that shows RV dysfunction as an important marker of morbidity and mortality in several clinical conditions [101] and also as an important prognostic marker, independent of pulmonary hypertension [102]. The independent and additive value of RV dysfunction and high systolic pulmonary artery pressure (sPAP) as a reflection of PH [103] has been well described. Subsequently, the presence of PH, measured by tricuspid regurgitant veloc-

ity ≥ 2.5 m/s (particularly in the presence of RV dysfunction), as a potent predictor of poor prognosis in HF patients [104] has become established. The RV responds to increases in preload or afterload and to primary myocardial pathology by cavity enlargement because of its thin walls compared to the LV [105, 106]. This results in significant disturbance of myocardial fiber architecture and interstitial tissue remodelling, localized inflammatory processes, and eventually collagen formation and fibrosis [107]. In fact, end-stage myocardial adaptation process mostly consists of collagen formation and fibrosis, which, when mild, disturbs RV function, but when severe, may have significant systemic implications.

Several echocardiographic parameters are used for quantifying RV systolic function, including tricuspid annular plane systolic excursion (M-mode), fractional area change (2D), tricuspid annular systolic velocity (tissue Doppler imaging), and RV free wall strain (STE) [108]. Although RVEF estimation by 3D echocardiography has been validated against cardiac MRI [109], it is technically challenging and not yet ready for routine use. It should be noted that the RV has unique structural and functional characteristics and differs from the LV because it essentially consists of only two walls, the septum and the free wall. RV function is accomplished through the interaction between the dominantly transverse fibers of the free wall and the oblique fibers of the septum. The traditional understanding is that the RV has longitudinal and radial motions, lengthening and shortening, as well as thickening of the RV myocardium [110]. Such anatomical design makes RV's echocardiographic function assessment challenging, in contrast to LV [111].

Traditionally, RV dysfunction has been evaluated qualitatively, but the development of RV strain and annular systolic myocardial velocity of the RV (RVs') has provided a significant improvement over existing quantitative measures such as tricuspid annular displacement (TAPSE), fractional area change, and myocardial performance index [112]. Over the last decade, the advent of 2D STE has enriched the use of echocardiography in assessing RV myocardial deformation, which has many unique advantages over and above earlier methods for evaluation of cardiac function and mechanics, particularly in early detection of subclinical myocardial dysfunction, when global ventricular function indices are normal.

Right ventricular longitudinal strain (RVLS) representing systolic shortening of the oblique fibers of the septum has been proposed as an accurate and sensitive measure of RV function that could integrate with other conventional parameters such as TAPSE, systolic RV free-wall velocity by tissue Doppler (s') and fractional area change (FAC %) [113]. RV ejection fraction is controlled by longitudinal shortening and pressing of the RV free wall against the septum. RV remodelling initially involves reduced longitudinal performance with a compensatory increase in transverse function caused by shortening of the circumferential fibers of the superficial layer. Thus, RV longitudinal strain could serve as a sensitive tool for detecting RV dysfunction [114]. In patients with end-stage HF, RV free-wall longitudinal strain has been shown to correlate with the extent of myocardial fibrosis (MF) detected by histological analysis, particularly in those with severe RV fibrosis (defined as fibrosis > 50%) (Fig. 13.4) [115].

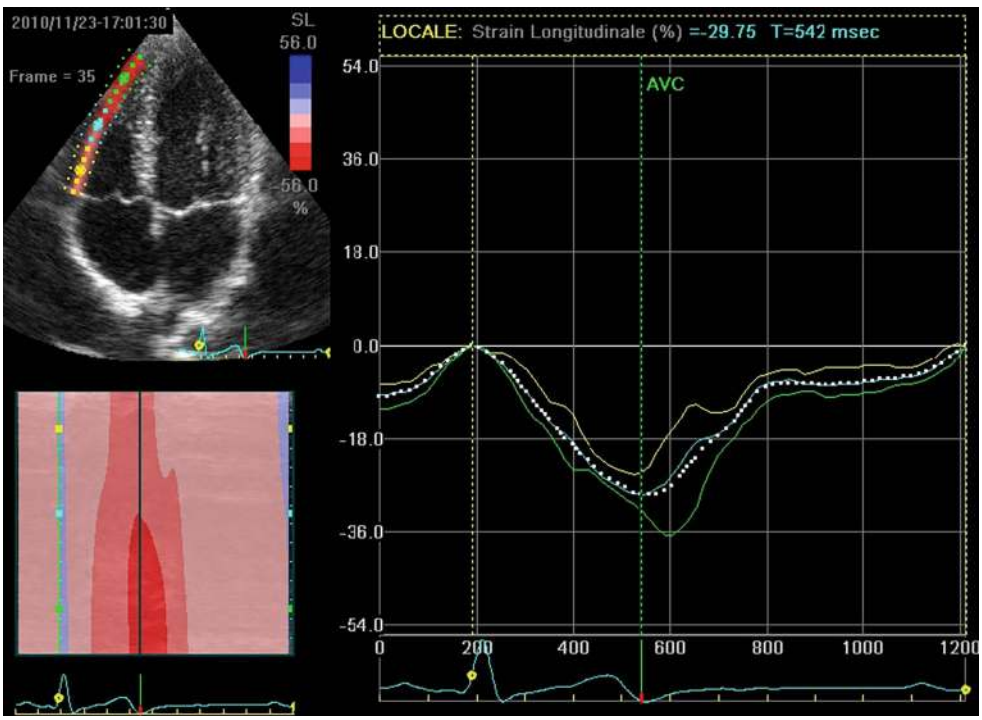


Fig. 13.4 Right ventricle free-wall longitudinal strain (RV FWLS) curve

Cardiac Resynchronization Therapy (CRT) in HF

Cardiac resynchronization therapy (CRT) has become an established means in the management of patients with heart failure (HF) with severely reduced LV EF (<35%) and a QRS > 130 msec, who remain symptomatic despite optimum medical therapy [116]. However, 30%–40% of patients receiving CRT do not experience significant LV reverse remodelling and clinical improvement [117]. In the last 20 years, efforts have been made to identify imaging-derived parameters able to identify electromechanical substrates associated with favourable CRT response. The assessment of various aspects of LV mechanics, including contractile synchrony, coordination and propagation, and myocardial work using conventional and novel ultrasound technologies provided useful information for CRT patients' selection, in particular among non-LBBB patients, who generally respond less to CRT. A multiparametric approach, based on the combination of ECG criteria and echocardiographic indices of LV dyssynchrony/discoordination, has been proved desirable for improving the prediction of CRT response.

Over time, many echocardiographic indices were developed to evaluate LV mechanical dyssynchrony, as shown by the significant delay of contraction in different LV segments. The prospective, multicenter PROSPECT trial, including 53 centers and 498 patients with standard indications for CRT, failed to propose useful markers (TDI parameters of mechanical dyssynchrony) in predicting CRT response [118], probably because of serious operators' training issues. Subsequently, STE-based quantification of LV dyssynchrony using the mechanical dispersion index (standard deviation of the averaged time-to-peak longitudinal strain, TPS-SD) ≥ 60 ms and a time difference in peak septal wall to posterior wall radial strain ≥130 ms proved accurate in identifying CRT responders [119], [120].

In order to rectify the above, dyssynchrony has to be accurately defined. Dysynchrony involves interventricular and intraventricular components. The former can be echocardiographically assessed using the pulse wave spectral Doppler of both left (LVOT) and right-ventricular outflow tract (RVOT) by determining right and left pre-ejection intervals with differences > 40 ms indicative of interventricular dyssynchrony [121]. Intraventricular dyssynchrony is detected by the "rolling rock" movement, with LV rotational movement from the interventricular septum to the free wall [122]. A delay between the onset of QRS and septal and lateral mitral annulus s' > 40 ms is indicative of cavity dyssynchrony [123]. Also, differences between septal and lateral a' > 30 ms and septal and lateral e' > 80 ms are linked with low response [124]. STE has also been used to evaluate patients' dyssynchrony and their responsiveness to CRT. Non-responders tend to have frequent continuous, severe shortening (peak strain ≥ +5%) during systole [125]. In contrast, responders have higher global longitudinal strain (GLS) and tend to increase LV, LA, and RV strain parameters (both in 2D- and 3D-STE techniques) with CRT [126].

The randomized controlled EchoCRT trial has shown that CRT does not reduce mortality or hospitalization for HF; in contrast, it may increase mortality in patients without electrical dyssynchrony (QRS < 130 ms) and with LV mechanical dyssynchrony, evaluated by both traditional and STE [127]. In light of those results and in the lack of adequate trials supporting the benefit of using echocardiographic dyssynchrony indices in predicting long-term response to CRT indications for CRT remain based on ECG measures (QRS morphology and duration) [128]. A potential use of mechanical LV dyssynchrony indices has been tested in a population of non-LBBB patients, who generally tend to respond less to CRT. STE parameters of dyssynchrony showed more favourable long-term survival in patients with dyssynchrony compared to those without [129].

Regression of dyssynchrony is defined as the coexistence of some LV segments in contraction and others in relaxation, which has been found to predict response to CRT [130, 131]. In particular, the "classical" pattern of LV dyssynchrony in LBBB is highly predictive of good response to CRT and is superior to time-to-peak methods [132]. This pattern can be evaluated by two-dimensional (2D)-STE, and consists of an early contraction of the septal wall and a simultaneous passive stretching of the opposite (lateral) wall, which begins to contract later, showing its peak contraction after aortic valve closure (post-systolic). Similarly, according to the STE-based LBBB staging proposed by Calle et al. [133], LBBB-4, characterized by early septal peak strain followed by uninterrupted stretching during systole, was associated with "super-response" in CRT-eligible patients. The systolic stretch index, a radial strain index of discoordination defined as the sum of postero-lateral systolic pre-stretch and septal systolic rebound stretch, also identified patients who benefited more favourably from CRT [134].

Recently, septal flash and apical rocking have been proposed as indices of mechanical dyssynchrony/discoordination to be incorporated in the current guidelines criteria for CRT candidate selection [135]. Septal flash is the rapid contraction, followed by a rapid relaxation, of the interventricular septum during the pre-ejection phase (isovolumetric systole). Apical rocking is the lateral motion of the apex, which can be observed in apical 4-chamber or long-axis view, due to the delayed contraction of the lateral wall, which occurs after the septal flash. The presence of septal flash and/or apical rocking assessed visually and their STE-based quantitative evaluation proved able to identify CRT responders [136–139]. STE-derived systolic rebound stretch of the interventricular septum (SRSsept), defined as the sum of

stretches that follow the premature septal shortening during systole, was found to be strongly associated with CRT-induced LV end-systolic volume reduction [140]. Moreover, in the subgroup of non-LBBB patients, high SRSsept held additional predictive information over the visual assessment of apical rocking alone.

Spatial propagation of LV contraction may also play a predictive role in patients' CRT response. In particular, the "U-shaped" propagation pattern (interruption of propagation along the LV wall, whose activation occurs with delay, counter-directional with respect to the "typical" pattern) assessed with three-dimensional (3D)-STE was detected in patients with favorable CRT response when compared to the "typical" pattern [141]. Similar information can be obtained by using 2D-STE [142].

Acute Heart Failure

Acute HF (AHF) is a "rapid onset or worsening of symptoms and/or signs of HF requiring urgent evaluation and management, initiation or intensification of treatment, including i.v. medications or procedures". The European Society of Cardiology (ESC) divides acute heart failure (AHF) into four different forms: acute decompensated heart failure (ADHF), isolated right ventricle failure (IRVF), acute pulmonary oedema (APO), and cardiogenic shock (CS) [143]. Clinical presentations of AHF are mainly based on the presence of signs of congestion and/or peripheral hypoperfusion, which require different treatments. Acute decompensated heart failure (ADHF) is the most common form of AHF, accounting for 50-70% of presentations, usually occurring in patients with a history of HF and previous cardiac dysfunction across the spectrum of LVEF and may include RV dysfunction. Compared with the acute pulmonary oedema phenotype, it has a more gradual onset with progressive fluid retention, causing systemic congestion. Congestion may be associated with hypoperfusion. Acute pulmonary oedema is related to lung congestion and may reflect advanced HF. When associated with low COP, acute pulmonary oedema would need inotropes, vasopressors, and/or Michanical Cardiac Support (MCS) in order to restore organ perfusion. RV failure is associated with raised RV and atrial pressure and systemic congestion. RV failure may also impair LV filling and ultimately reduce systemic COP, through ventricular interdependence. Cardiogenic shock is caused by primary cardiac dysfunction resulting in an inadequate COP, comprising a life-threatening state of tissue hypoperfusion, which can result in multiorgan failure and death.

The above shows that each AHF phenotype should be clearly distinguished for optimum clinical treatment. Forrester classification using pulmonary wedge pressure and cardiac index is useful for evaluating hemodynamics and determining treatment options for AHF [144, 145]. However, this is an invasive investigation including Swan-Ganz catheterization, therefore is used less frequently. In contrast, echocardiography plays a key role in the identification of AHF phenotypes and determination of treatment initiation, escalation and success.

For all AHF patients, both LV and RV dimensions, volumes, and function should be assessed in detail. Ventricular dilatation and dysfunction are common findings, especially in severe forms of AHF [146]. Echocardiography assists in quantifying the severity of LV dysfunction, elevation of LVFP, presence of valvular dysfunction, RV dysfunction and raised PASP, all of which impact treatment choice and clinical recovery. All conventional Doppler echocardiographic parameters should be used as well as deformation measurements of LV, RV and LA [147].. LV volume assessment (LV end-diastolic and end-systolic volumes) and LVEF by 2D imaging determines the categorization of patients' HF ejection fraction phenotype, which guides initiation of evidence-based treatment (including pharmacological and device-based therapies). The modified biplane Simpson's method is recommended to establish LVEF, which has the advantage of requiring only two apical views to be calculated. In patients with technically challenging TTE, intravenous echocardiographic contrast can be used to improve diagnostic accuracy or failing this, a visual estimate of LVEF can also be applied, which in experienced hands has a good correlation with the Simpsons biplane method (R = 0.898) [108]. However, in clinical practice, it is recognised that interpretation of 2D images is limited by significant intra- and inter-observer variability [65].

As mentioned above, 3D evaluation of LV volumes, and EF and STE-based deformation parameters have proved significantly accurate in providing invaluable evaluation of LV structure and function parameters [28, 148, 149]. GLS accounts for regional abnormalities that are not accounted for in the 2D calculation of LVEF by Simpson's biplane method. This is particularly important in HF caused by coronary artery disease, where overall LV systolic function may be normal and heart failure with preserved ejection fraction (HFpEF) [150]. Several studies have suggested that, irrespective of normal LVEF, GLS (by 2D or 3D) is more sensitive than LVEF in detecting minor changes in LV systolic function, which is particularly useful in AHF [151]. The underlying cardiac abnormality responsible for AHF, e.g. acute coronary artery disease, is often identifiable by characteristic patterns of RWMAs.

Moreover, LV outflow tract (OT) VTI measured in apical 5-chambers view is an important parameter that has better prognostic value than ejection fraction (EF) in patients with

EF<25%. Measurement of the velocity time integral (VTI) at the LVOT is a simple and useful method of estimating the forward stroke volume and CO, as well as clinical prognosis irrespective of LVEF [152–156]. Changes in LV inflow pattern and LVOT VTI are useful for assessing treatment response and is one of the parameters used to evaluate the weaning from mechanical circulatory support (MCS) [157] (Table 13.1).

Echocardiography is also used to study the need for MCS, especially in the case of the Impella pump and its optimum positioning. Its inlet must be at 3.5 cm from the aortic valve, free from ventricular structures, with an angle between the pump and the horizontal plane of the mitral valve >126.5° in order to reduce the risk of suction events and subsequently haemolysis. Also, the aortic valve opening is essential to be assessed in order to avoid thrombus formation [158].

More than 90% of hospitalizations due to HF result from elevations of LVFP and fluid overload [159]. It is important to recognise that the severity of impairment of LVEF does not correlate with the severity of LVFP [160]. While many patients with an LVEF <50% have elevated LVFP, up to 40% have normal filling pressures [51]. Elevated LVFP is a key contributor to symptoms in HFpEF, which accounts for ~50% of HF and 30–50% of presentations with AHF [161]. Although absolute LVFP cannot be measured using TTE, the derived indices, discussed above, have been shown to accurately reflect LV filling pressure.

It should be reiterated that estimation of LVFP and diastolic dysfunction is not as simple as evaluation of LVEF with multiple rather than single Doppler indices, often in combination with 2D-derived LA volume index (LAVi), required to accurately quantify these measures. To facilitate the clinical evaluation of diastolic function, the 2016 American Society of Echocardiography (ASE) and European Association of Cardiovascular Imaging (EACVI) simplified their guidelines to focus on four key variables (mitral E/A ratio, TRV, average E/e′ ratio, and LAVI) incorporated into two diagnostic algorithms. In 450 patients referred for cardiac catheterisation, the 2016 algorithm detected elevated pulmonary capillary wedge pressure (PCWP) in 91% of patients with EF <50% and 84% in patients with EF ≥50%, and when added to clinical criteria for HF, improved the accuracy of diagnosis by 10% [37].

Table 13.1 Echocardiographic parameters for MCS' weaning

Variable	Value
LVEF	> 25% or increase >5% in 48 h
LVOT VTI	> 10–12 cm
TDI s'_{LAT}	> 6 cm/s

LVEF left ventricle ejection fraction, *LVOT VTI* left ventricle outflow tract velocity-time integral, *TDI* tissue Doppler imaging

Congestive HF

Congestion is a major cause of HF worsening regardless of the LVEF [162]. The myocardial dysfunction worsens with each HF decompensation, leading to HF progression [163, 164]. Symptoms and signs of pulmonary and systemic congestion are the most common cause for hospitalization of acute decompensated HF, as a consequence of increased cardiac filling pressures.

Hemodynamic congestion, defined by volume overload and increased filling pressures, may precede the onset of clinical congestion by days or weeks. The risk of re-hospitalization progressively increases when invasively measured pulmonary diastolic pressure is above 18 mmHg [165].

Clinical congestion is characterized by progressive dyspnoea, weight gain, and signs of systemic venous congestion. In HF registries, one in five patients hospitalized have residual clinical or hemodynamic congestion at discharge [166]. The persistence of clinical congestion is linked to unfavourable prognosis, especially in the setting of kidney dysfunction [167, 168]. Recent studies underline the importance of the diagnosis and treatment of hemodynamic congestion before HF symptoms worsen, reducing hospitalization and improving prognosis [169]. All these data underline the importance of non-invasive detection of congestion in patients with HF, in order to reduce re-hospitalizations, to improve prognosis, and to decrease mortality by optimizing HF treatment. Several imaging markers have been proposed for the assessment of congestion. The ultrasonographic evaluation of the heart, veins and lung provides useful information about congestion and has been validated as a prognostic markers, both in acute and chronic settings [170].

LV Filling Pressures

Echocardiography has the unique ability to non-invasively estimate LV filling pressures using a comprehensive, stepwise approach, together with associated structural cardiac abnormalities in patients with unexplained dyspnoea or with clinical manifestations of HF, irrespective of EF.

Recently, two large multicenter studies with simultaneous evaluation of LVFP by echocardiography and invasive measurements (LV end-diastolic pressure, pulmonary capillary wedge pressure or LV pre-A pressure) have confirmed the high feasibility and good accuracy of the 2016 recommendations for echocardiographic assessment of LVFP. The algorithm for estimation of LVFP proved to be useful both in patients with unexplained exertional dyspnoea, and in HF patients, regardless of LVEF [51].

As mentioned above, both the E/A ratio and the E/e' ratio are fundamental to evaluate LVFP, being frequently elevated in congestive HF. Furthermore, even PALS has been noted as a variable able to predict LV diastolic function, being also included in the ASE/EACVI Guidelines in 2016 [62].

The increase in systolic pulmonary artery pressure (sPAP) is another criterion for the estimation of LVFP, if other non-cardiac causes of pulmonary hypertension or pulmonary arterial hypertension are excluded. sPAP is calculated as the sum of systolic tricuspid pressure gradient using peak TR velocity and the estimated right atrial pressure, based on the inferior vena cava (IVC) measurement. A peak TR jet velocity >2.8 m/s is strongly indicative of elevated filling pressures. However, TR jet cannot be accurately recorded in about half of the patients, mainly with preserved EF [57]. The short pulmonary artery acceleration time (AccT), less than 100 ms, is an alternative parameter indicative of sPAP elevation. Mean PAP (mPAP) can be estimated using the equation: $mPAP = 79 - 0.45 \times AccT$ [171].

RV Filling Pressure

Inferior Vena Cava

Inferior Vena Cava (IVC) diameter (IVCD) with its respiratory changes is a widely used parameter for estimating right-sided filling pressures and the assessment of changes in intravascular volume [172]. IVC is measured in the long axis from the subcostal view with the patient either in supine or in semi-recumbent position. The IVC diameter and the collapsibility index (CI) with respiration [CI = IVCD max − IVCD min/IVCD max) × 100] provide information about right atrial pressure, and pulmonary capillary wedge pressure [173, 174]. But this relationship is weak in mechanically ventilated patients [175].

In normal right atrial pressure, the IVC dimension should be less than 21 mm and the collapsibility index ≥50%. In HF patients with high right atrial pressure, the IVCD is larger, and the CI is decreased (<50%). As in almost half of HF patients, the IVC distension due to increased right atrial pressure is associated with other markers of hemodynamic congestion, despite the absence of symptoms and signs of clinical congestion, the IVC is an important subclinical marker of systemic congestion [176].

Intrarenal Venous Flow

The assessment of hemodynamic changes due to the effect of systemic congestion in HF on the intrarenal venous flow (IRVF) patterns may provide important information about the renal congestion severity, the consequences on renal function and the reversibility of abnormal IRVF patterns after de-congestion. The IRVF can be assessed by pulsed wave Doppler flow of the interlobar arteries and veins, with concomitant recording of the arterial (above the baseline) and the venous (below the baseline) Doppler signals. The normal IRVF is continuous during the cardiac cycle. As the right atrial pressure increases, progressive changes happen in the venous flow, from discontinuous, "pulsatile" flow to biphasic and even monophasic flow (the velocity progressively diminishes during systole, and the flow occurs only during diastole in patients with very high right atrial pressure) [177].

The qualitative analysis of IVRF patterns can be completed by quantitative analysis, using the venous impedance index (VII) and renal venous stasis index (RVSI). VII is calculated using the formula [(maximum velocity-minimum velocity)/maximum velocity], and RVSI is defined as the ratio between the duration of absent venous flow divided by the duration of the cardiac cycle.

The changes in IRVF patterns reflect the elevated right-side pressures transmitted backward, leading to increased interstitial and tubular hydrostatic pressure within the encapsulated kidney and lowering the glomerular filtration rate. The parenchymal vessels are compressed, and the venous flow becomes pulsatile, being dependent on the cardiac cycle, due to increased compliance of the congestive renal parenchyma. There are similar changes in hepatic venous flow [178, 179].

In a recent study in patients with stable chronic HF, the IVRF pattern became discontinuous after volume loading, even without a change in IVC size, suggesting that changes in IVRF pattern could be an earlier index of systemic congestion [180]. More recent data bring important evidence supporting the use of the IRVF pattern as a congestion marker. With decongestion therapy, normalization of the discontinuous IRVF patterns occurs in approximately half of the patients hospitalized with decompensated HF, mostly (87%) showing impaired IRVF patterns at admission. No changes in the IRVF patterns were noted in patients with renal dysfunction at baseline [181]. Serial evaluation of IRVF patterns in stable ambulatory HF patients demonstrated that discontinuous patterns during the follow-up, rather than those at baseline, were associated with poor outcomes (cardiovascular death and HF hospitalization). Moreover, the persistent discontinuous pattern was associated with renal impairment progression [182].

VExUS Score

The VExUS score is a semi-quantitative score system used to assess systemic congestion. It is based on Inferior Vena Caval (IVC) diameter and PW Doppler of portal vein, hepatic veins, and intra-renal veins. A VExUS score of 0 is consistent with IVC diameter < 21 mm. A score of 1 is consistent with dilatated IVC with a normal or mildly altered PW Doppler. In VExUS 2 there is a severe alteration of venous diastole (S-wave reversal at hepatic vein PW

Doppler, >50% of pulsatility at portal PW Doppler, and discontinuous monophasic flow with only diastolic phase at intra-renal vein PW Doppler). With a score 3, there are at least two veins where the PW Doppler is severely abnormal (Fig. 13.5) [183].

Pulmonary Congestion

The overt complete clinical picture of pulmonary congestion is a late manifestation of interstitial and alveolar oedema. However, in most patients with eminent acute HF, there is a subclinical transition in which a gradual accumulation of extravascular water occurs. Identifying subclinical pulmonary congestion offers a diagnostic advantage as well as a therapeutic window of opportunity, in which timely decongestive therapy can reduce the progression to overt symptomatic HF [184]. Moreover, complete pulmonary decongestion at hospital discharge is associated with an improved prognosis [185].

In the past 10 years, lung ultrasound (LUS) has emerged as a non-invasive imaging biomarker of pulmonary congestion with diagnostic, monitoring, therapeutic and prognostic value in the management of HF patients [186–190].

Lung Ultrasound (LUS)

LUS is a quantitative, simple and rapid method of assessing lung congestion. The main diagnostic findings suggestive of interstitial syndrome (caused by increased extravascular transudate or exudate) are the B lines [191]. These are vertical hyperechoic laser-like artefacts that arise from the pleural line and extend to the bottom of the screen without fading, moving in sync with lung sliding, and erasing A lines [185].

LUS score is a semi-quantitative scoring system developed to assess lung aeration and to guide therapy. It is based on dividing the thorax into six parts (anterior region from parasternal to anterior axillary line, lateral region from anterior to posterior axillary line and posterior region from posterior axillary to paravertebral line), and assigning, to each region, a grade between zero and three, based on the number of B-lines and pleural consolidation. Zero is defined as a physiological LUS, one as the presence of ≥3 well-spaced B-lines, two as the presence of crowded and coalescent B-lines with or without consolidations limited to the subpleural space and three as extended consolidations. The sum of each region's values grants the LUS score; the higher the score, the higher the pulmonary congestion [192]. Evaluation of the presence and number of B lines on LUS as a marker of interstitial syndrome has shown good correlation with

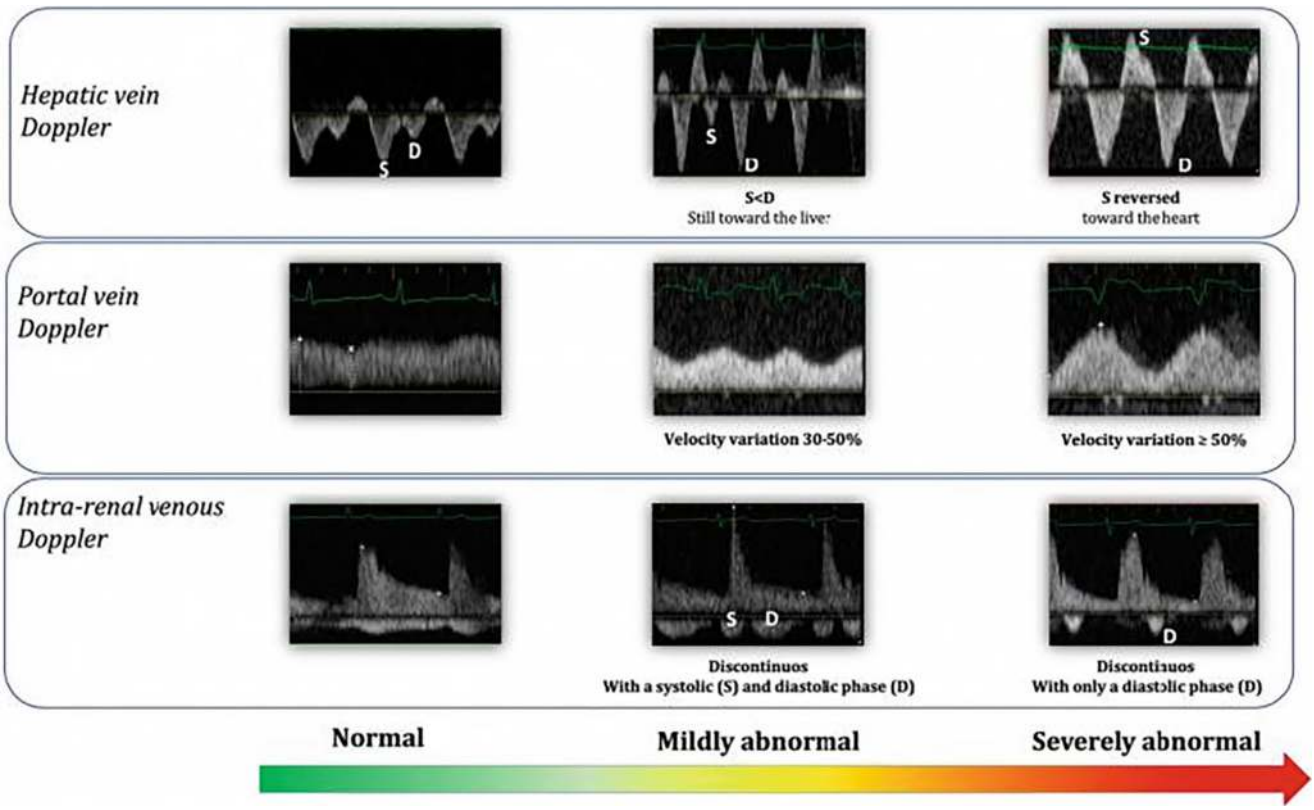


Fig. 13.5 VExUS score parameters and abnormalities. Taken and adjusted under permission from 10.3390/jcm11247538

clinical, radiological, invasive, and post-mortem markers of lung congestion and has shown prognostic and therapeutic value [193].

The B lines assessed with LUS are dynamic and their number and location can change rapidly after decongestive therapy, making them an attractive biomarker that could help in the management of pulmonary congestion [194]. Acute changes in B lines were demonstrated in patients with HF after diuretic therapy, in patients treated for hypertensive emergencies, as well as in patients undergoing hemodialysis. Moreover, a rapid increase in B lines was demonstrated with exercise in both HFpEF and HFrEF patients during stress echocardiography [195]. The number of stress-induced B lines as a marker of pulmonary congestion correlated well with brain-type natriuretic peptide (BNP) value, echographic parameters of systolic and diastolic function, and their presence was associated with a greater functional impairment [196]· [197, 198].

Therefore, B-line assessment is a promising marker of pulmonary congestion and decongestion. In a single-center small trial, LUS helped in tailoring diuretic therapy of patients with acute HF and was able to accelerate the discharge time [199]. Three recent randomized trials assessed the usefulness of LUS-guided decongestive therapy in HF in acute and chronic settings [200–202].

Pulmonary congestion as reflected by B lines assessed with LUS has an important prognostic role in ambulatory or admitted HF patients [203]. The EVEREST trial showed that clinical congestion in HF patients during hospitalization and at discharge is associated with worse prognosis. However, even patients judged to be congestion-free at discharge also have a poor prognosis [204]. It concluded that subclinical congestion conveys a poor outcome and needs to be identified early. This has been shown and proved to be reproducible [193]. LUS-detected pulmonary congestion has been shown to independently predict short-term mortality and HF hospitalization [205]. The prognostic value of LUS is preserved in ambulatory, chronic, HF patients. A higher number of B-lines on LUS identified patients at risk for urgent HF visits, HF hospitalizations, or death from any cause over 6 months, independent of age, sex, NYHA class, and clinical congestion score (Fig. 13.6) [206].

Pleural effusion can be found only in developed pulmonary oedema. The high right heart pressures increase the thoracic duct pressure, which reduces the lymphatic drainage from the pleura.

Also, the presence of pleural effusion is associated with a higher re-hospitalization rate and worse quality of life [184].

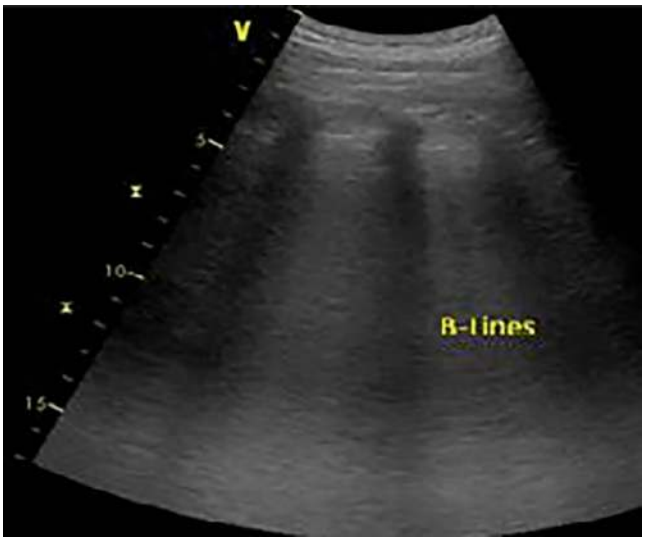


Fig. 13.6 B lines in lung ultrasonography. Taken and adjusted under permission from 10.3390/jcm11247538

Left Ventricular Assist Devices

Left ventricular assist devices (LVADs) are gaining increasing importance as a therapeutic strategy in AdHF, not only as bridge to recovery or to transplant, but also as destination therapy. A precise pre-operative, peri-operative and post-operative evaluation of these patients is crucial for the selection of LVADs candidates and management of LVADs recipients [207]. Echocardiography is an indispensable tool in the evaluation, placement, management and follow-up of patients with LVAD. While transoesophageal echocardiography is the ideal tool in guiding the implantation procedure, transthoracic echocardiography is essential during the initial evaluation, patient selection and in the post-operative follow-up.

In the pre-operative assessment, it is important to detect situations and disturbances that could predict the development of post-operative complications, so they could be treated before LVAD implantation or to turn down the recommendation for LVAD insertion. During implantation, echocardiography provides information on whether the device is correctly placed and on the response of RV to the activation of LVAD. During follow-up, it is possible to define the correct function of the device as and possible malfunctioning devices. For all these reasons, the echocardiographic evaluation of these patients is of crucial importance in order to avoid or promptly treat complications [208].

Indications for LVAD insertion include: end-stage HF due to ischaemic or non-ischaemic dilated cardiomyopathy with severe LV systolic dysfunction, LVEF <25% and the presence of an appropriate space for an LVAD inflow cannula.

Basic and advanced echocardiographic parameters help identify suitable candidates for LVAD implantation. LV geometry and function should always be assessed to determine device suitability. Markedly raised or reduced LVEF, restrictive filling pattern, and low LV end-diastolic diameter (LVEDD) are associated with higher mortality rates post-LVAD implantation [209–212]. Poor outcome of patients with high EF could be explained by the 'suck-down' mechanism when a significant shift of the interventricular septum, towards LV cavity, occurs, when the pump is turned on, which impacts RV function and consequently the pumped stroke volume [213].

A high ratio between the LA antero-posterior diameter and LVEDD [214] is another predictor of poor outcome. Assessing these geometric parameters should be better evaluated by 3-dimensional echocardiography [215]. 2D and 3D LV strain imaging have been shown to have good prognostic implications, as they correlate with hospitalization and mortality of HF [216–218].

It is also crucial to evaluate RV before LVAD implantation [219], being described as the "Achilles heel" of contemporary LVAD devices, since it is a major predictor of RV failure after the procedure, which is associated with a prolonged hospitalization and a higher morbidity and mortality [220]. For tailored risk assessment, appropriate quantification of the RV function is therefore of paramount importance.

The echocardiographic assessment of the RV remains challenging due to technical difficulties in RV imaging, in addition to its complex geometry and function [221]. Also, tricuspid regurgitation severity has to be optimally assessed. Standard echocardiographic parameters of RV longitudinal function, such as tricuspid annular plane systolic excursion (TAPSE) and tricuspid annular systolic velocity by tissue doppler (S′), failed to predict RV failure post LVAD implant [8, 222]. On the other hand, RV free-wall longitudinal strain (RVLS) derived by STE has been shown to correlate with RV stroke work index (RVSWI) after LVAD implantation [223–225]. Conflicting data exists regarding the predictive role of RV fractional area change (RVFAC) in these patients [226], even though recent studies have shown that RVFAC < 35% and RV global strain < − 12.5% are the best predictors of RV failure at 72 h post LVAD implantation [222, 227]. 3D-RV ejection fraction [228], RV index of myocardial performance (RIMP) [229], and RV sphericity index [115], which is the expression of the loss of RV physiological shape, can also modestly predict RV failure. The use of different cut-off values between studies has significantly weakened the prediction power of different echocardiographic parameters.

Heart Valve Disease in VAD patients must be assessed in detail before LVAD implantation. Aortic regurgitation (AR) has to be critically assessed, since a high proportion of LVAD patients develop AR within a year surgery [230], because of the valve leaflets being subjected to a high pressure that might cause a worsening of the regurgitation [231]. More than mild AR at the time of LVAD implantation puts the patient at risk of a 'blind-loop' phenomenon in which the blood entering the LVAD from the LV is pumped into the ascending aorta which then flows back into the LV through the incompetent aortic valve with a consequent reduction of the forward systemic with subsequent inadequate organ oxygen delivery and hypoperfusion. This 'blind-loop' competes with the effective forward systemic flow, being directly proportional to the degree of AR.

Therefore, in the presence of more than moderate aortic regurgitation, a surgical repair joint with LVAD implant should be considered [232], as recommended by recent guidelines (Fig. 13.7) [233].

In patients with aortic stenosis, surgical repair is not recommended. In those with mechanical aortic valve prosthesis, LVAD implantation is relatively contraindicated as it is considered highly thrombogenic.

Mitral regurgitation (MR) is a common finding in patients with AdHF, due to LV remodelling which leads to mitral annulus dilatation and consequently impaired leaflet coaptation. MR usually improves with LVAD implantation due to the increase in cardiac output, LV decompression, reduced LV size, and reduction of LV filling pressures. Therefore, any degree of MR is acceptable before LVAD implantation. The presence or development of severe MR after LVAD implantation could suggest inadequate LV decompression, possibly caused by malposition of the inflow cannula encroaching upon the mitral subvalvular apparatus. This scenario should be readily detected before leaving the operating theatre to allow for surgical correction. While MR repair is generally not recommended before LVAD implantation, in contrast, tricuspid regurgitation (TR) should be considered for surgical repair if it is more than moderate [234]. The presence of significant TR (at least moderate) is considered an ominous finding before LVAD implantation, as it may reflect RV dysfunction and therefore may warrant surgical repair before LVAD implantation.

Pulmonary hypertension is a common consequence of adHF. In these patients, data are conflicting with respect to their response and clinical outcome after LVAD implantation [211, 235]. Stress echocardiography using dobutamine should provide good information about the RV response, the positive inotropic response, which, if positive, should be taken as a predictor of good clinical outcome post LVAD [236].

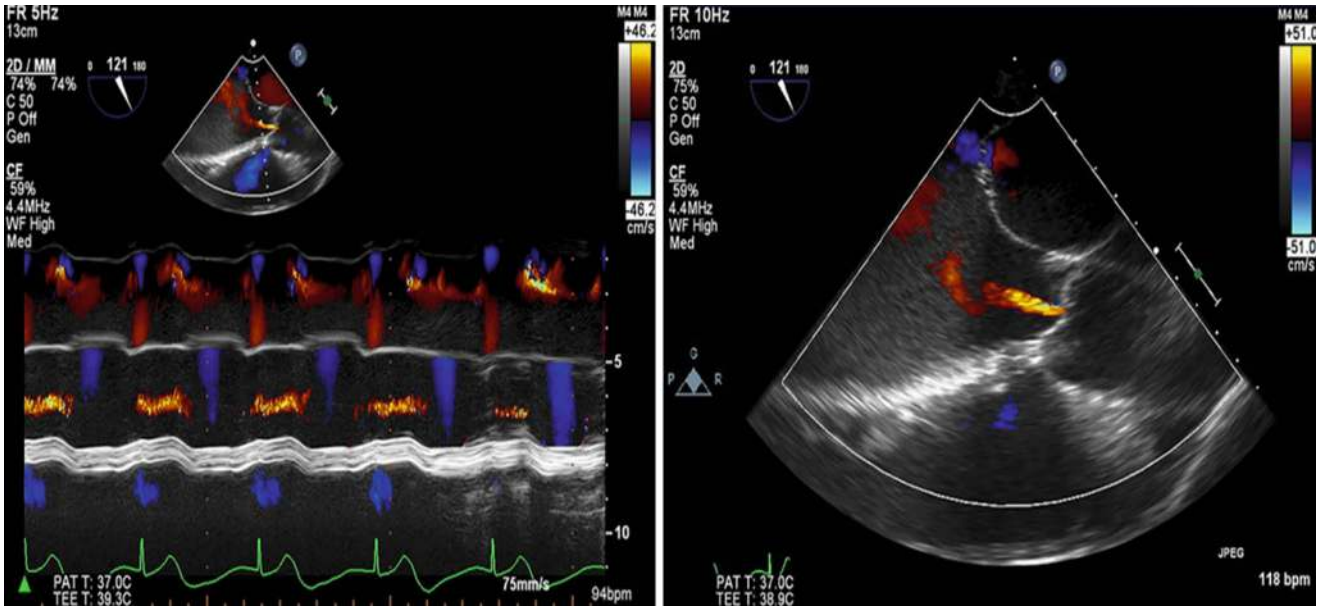


Fig. 13.7 Aortic regurgitation evaluation in LVAD patients: on the left a Colour plus M-mode modality to evidence the regurgitation duration; on the right a Colour on B-mode to evaluate the vena contracta, velocities, and the regurgitation's dimension. Taken and adjusted under permission from 10.1007/s10741-021-10073-1

Follow-up of LVAD Patients is of significant importance. Despite being limited by acoustic shadowing, TTE is the most suitable tool for long-term follow-up and should also represent the first-line evaluation in the setting of hemodynamic instability [237]. LV dimensions and volumes, at end-systole and end-diastole, should remain stable. They usually decrease with LV unloading, however, exaggerated reduction of LV or RV dimensions and volumes could indicate hypovolemia. LV ejection fraction is not an ideal parameter for assessing LV systolic function until the LVAD device is temporarily interrupted [238]. For the evaluation of diastolic dysfunction, the E/A ratio, E/e′ ratio, and deceleration time can accurately predict invasively estimated left atrial filling pressure [239].

RV evaluation should include conventional semi-quantitative methods (the analysis of the longitudinal and the radial RV function) and quantitative parameters (RVFAC, TAPSE, S′, and the Tei index) [240]. Following LVAD implantation, the RV contractile pattern changes from longitudinal to radial motion, thus making TAPSE less reliable than RVFAC as a marker of RV dysfunction. Fast pump speed might lead to impaired RV function, dilatation, and worsening TR due to increased venous return [209]. A marker of RV dilatation is an eccentricity index >1.0, which is the ratio between RV diameter and LV diameter [241].

Another important issue with LVAD is a high aorta-to-LV gradient, which keeps the aortic valve closed for a number of cycles. Opening of the valve reduces the risk of thrombus formation and valve degeneration over time; therefore, adjusting LVAD speed to allow intermittent aortic valve opening is considered a class IIb recommendation [242]. Spontaneous opening of the aortic valve is particularly important when the outflow graft is located in the descending aorta, as the aortic valve is not washed by blood [243]. A sustained aortic valve closure may suggest excessive LV unloading, while a too-frequent opening may indicate a suboptimal LVAD speed, pump dysfunction, or improvement of native LV function [216].

Moreover, as mentioned earlier, the identification of a de novo AR and its quantification is essential to avoid "futile cycles"; knowing that standard echocardiographic criteria can underestimate the AR severity given its usual eccentricity and systo-diastolic jet. For this reason and according to evidence, the systolic-to-diastolic peak velocity ratio can be determined using PWD in the outflow cannula and its increase enables the detection of AR sooner than conventional echocardiographic parameters [244].

References

1. Crespo-Leiro MG, Metra M, Lund LH, et al. Advanced heart failure: a position statement of the heart failure association of the european society of cardiology. Eur J Heart Fail. 2018;20(11):1505–35.
2. Arbustini E, Narula N, Dec GW, et al. TheMOGE(S) classification for a phenotypegenotype nomenclature of cardiomyopathy: endorsed by the World Heart Federation. J Am Coll Cardiol. 2013;62:2046–72.
3. Melillo E, Masarone D, Oh JK, Verrengia M, Valente F, Vastarella R, Ammendola E, Pacileo R, Pacileo G. Echocardiography in advanced heart failure for diagnosis, management, and prognosis. Heart Fail Clin. 2021;17(4):547–60.

4. Braunwald E, Ross J Jr, Sonnenblick EH. Mechanisms of contraction of the normal and failing heart. N Engl J Med. 1967;277(15):794–800.
5. Nagueh SF, Bhatt R, Vivo RP, Krim SR, Sarvari SI, Russell K, Edvardsen T, Smiseth OA, Estep JD. Echocardiographic evaluation of hemodynamics in patients with decompensated systolic heart failure. Circ Cardiovasc Imaging. 2011;4:220–7.
6. Ristow B, Na B, Ali S, Whooley MA, Schiller NB. Left ventricular outflow tract and pulmonary artery stroke distances independently predict heart failure hospitalization and mortality: the heart and soul study. J Am Soc Echocardiogr. 2011;24:565–72.
7. Ommen SR, Nishimura RA, Appleton CP, Miller FA, Oh JK, Redfield MM, Tajik AJ. Clinical utility of Doppler echocardiography and tissue Doppler imaging in the estimation of left ventricular filling pressures: a comparative simultaneous Doppler catheterization study. Circulation. 2000;102:1788–94.
8. Cameli M, Lisi M, Righini FM, et al. Right ventricular longitudinal strain correlates well with right ventricular stroke work index in patients with advanced heart failure referred for heart transplantation. J Card Fail. 2012;18:208–15.
9. Kosmala W, Marwick TH, Przewłocka-Kosmala M. Echocardiography in patients with heart failure: recent advances and future perspectives. Kardiol Pol. 2021;79(1):5–17.
10. Thavendiranathan P, Poulin F, Lim KD, et al. Use of myocardial strain imaging by echocardiography for the early detection of cardiotoxicity in patients during and after cancer chemotherapy: a systematic review. J Am Coll Cardiol. 2014;63:2751–68.
11. Nesbitt GC, Mankad S, Oh JK. Strain imaging in echocardiography: methods and clinical applications. Int J Cardiovasc Imaging. 2009;25(suppl. 1):9–22.
12. Dorosz JL, Lezotte DC, Weitzenkamp DA, Allen LA, Salcedo EE. Performance of3-dimensional echocardiography in measuring left ventricular volumes and ejectionfraction: a systematic review and meta-analysis. J Am Coll Cardiol. 2012;59:1799–808.
13. Thavendiranathan P, Grant AD, Negishi T, et al. Reproducibility of echocardiographic techniques for sequential assessment of left ventricular ejection fraction and volumes: application to patients undergoing cancer chemotherapy. J Am Coll Cardiol. 2013;61:77–84.
14. Marwick TH. Methods used for the assessment of LV systolic function: commoncurrency or tower of Babel? Heart. 2013;99:1078–86.
15. Jenkins C, Moir WS, Chan J, Marwick TH. Left ventricular volume measurement with echocardiography: a comparison of left ventricular opacification, 3D echocardiography or both with magnetic resonance imaging. Eur Heart J. 2009;30:98–106.
16. Mannaerts HF, van der Heide JA, Kamp O, et al. Early identification of left ventricular remodelling after myocardial infarction, assessed by transthoracic 3D echocardiography. Eur Heart J. 2004;25:680–7.
17. Mele D, Andrade A, Bettencourt P, et al. From left ventricular ejection fraction to cardiac hemodynamics: role of echocardiography in evaluating patients with heart failure. Heart Fail Rev. 2020;25:217–30.
18. Heidenreich PA, Bozkurt B, Aguilar D, et al. 2022 AHA/ACC/HFSA guideline for the management of heart failure: a report of the American College of Cardiology/American Heart Association Joint Committee on Clinical Practice Guidelines. Circulation. 2022;145(18):e895–e1032.
19. Januzzi JL, Chandrashekhar Y. Strain echocardiography: the new gold standard for imaging ventricular function? J Am Coll Cardiol. 2017;70:955–7.
20. Omar AM, Bansal M, Sengupta PP. Advances in echocardiographic imaging in heart failure with reduced and preserved ejection fraction. Circ Res. 2016;119:357–74.
21. Cikes M, Solomon SD. Beyond ejection fraction: an integrative approach for assessment of cardiac structure and function in heart failure. Eur Heart J. 2016;37:1642–50.
22. Cameli M, Caputo ML, Mondillo S, et al. Feasibility and reference values of left atrial longitudinal strain imaging by two-dimensional speckle tracking. Cardiovasc Ultrasound. 2009;7:6.
23. Stokke TM, Hasselberg NE, Smedsrud MK, et al. Geometry as a confounder when assessing ventricular systolic function: comparison between ejection fraction and strain. J Am Coll Cardiol. 2017;70:942–54.
24. Solomon SD, Anavekar N, Skali H, et al. Influence of ejection fraction on cardiovascular outcomes in a broad spectrum of heart failure patients. Circulation. 2005;112:3738–44.
25. Curtis JP, Sokol SI, Wang Y, et al. The association of left ventricular ejection fraction, mortality, and cause of death in stable outpatients with heart failure. J Am Coll Cardiol. 2003;42:736–42.
26. Dagres N, Hindricks G. Risk stratification after myocardial infarction: is left ventricular ejection fraction enough to prevent sudden cardiac death? Eur Heart J. 2013;34:1964–71.
27. Narayanan K, Reinier K, Uy-Evanado A, et al. Frequency and determinants of implantable cardioverter defibrillator deployment among primary prevention candidates with subsequent sudden cardiac arrest in the community. Circulation. 2013;128:1733–8.
28. Kalam K, Otahal P, Marwick TH. Prognostic implications of global LV dysfunction: a systematic review and meta-analysis of global longitudinal strain and ejection fraction. Heart. 2014;100:1673–80.
29. Sengeløv M, Jørgensen PG, Jensen JS, et al. Global longitudinal strain is a superior predictor of all-cause mortality in heart failure with reduced ejection fraction. JACC Cardiovasc Imaging. 2015;8:1351–9.
30. Shah AM, Claggett B, Sweitzer NK, et al. Prognostic importance of impaired systolic function in heart failure with preserved ejection fraction and the impact of spironolactone. Circulation. 2015;132:402–14.
31. Hung CL, Verma A, Uno H, et al. Longitudinal and circumferential strain rate, left ventricular remodeling, and prognosis after myocardial infarction. J Am Coll Cardiol. 2010;56:1812–22.
32. Munk K, Andersen NH, Terkelsen CJ, et al. Global left ventricular longitudinal systolic strain for early risk assessment in patients with acute myocardial infarction treated with primary percutaneous intervention. J Am Soc Echocardiogr. 2012;25:644–51.
33. Perry R, Selvanayagam JB. Echocardiography in infiltrative cardiomyopathy. Heart Lung Circ. 2019;28:1365–75.
34. Harbo MB, Nordén ES, Narula J, et al. Quantifying left ventricular function in heart failure: what makes a clinically valuable parameter? Prog Cardiovasc Dis. 2020;63:552–60.
35. Echouffo-Tcheugui JB, Erqou S, Butler J, et al. Assessing the risk of progression from asymptomatic left ventricular dysfunction to overt heart failure: a systematic overview and meta-analysis. JACC Heart Fail. 2016;4:237–48.
36. Nishimura RA, Tajik AJ. Evaluation of diastolic filling of left ventricle in health and disease: Doppler echocardiography is the clinician's Rosetta Stone. J Am Coll Cardiol. 1997;30(1):8–18.
37. Nagueh SF, Smiseth OA, Appleton CP, Byrd BF 3rd, Dokainish H, Edvardsen T, et al. Recommendations for the evaluation of left ventricular diastolic function by echocardiography: an update from the American Society of Echocardiography and the European Association of Cardiovascular Imaging. Eur Heart J Cardiovasc Imaging. 2016;17:1321–60.
38. Chung CS, Shmuylovich L, Kovács SJ. What global diastolic function is, what it is not, and how to measure it. Am J Physiol Heart Circ Physiol. 2015;309:H1392–406.
39. Lancellotti P, Galderisi M, Edvardsen T, et al. Echo-Doppler estimation of left ventricular filling pressure: results of the multicen-

tre EACVI euro-filling study. Eur Heart J Cardiovasc Imaging. 2017;18:961–8.
40. Nagueh SF, Middleton KJ, Kopelen HA, Zoghbi WA, Quiñones MA. Doppler tissue imaging: a noninvasive technique for evaluation of left ventricular relaxation and estimation of filling pressures. J Am Coll Cardiol. 1997;30(6):1527–33.
41. Dokainish H, Rajaram M, Prabhakaran D, et al. Echocardiographic Substudy of the OASIS-6 Trial Investigators. Incremental value of left ventricular systolic and diastolic function to determine outcome in patients with acute ST-segment elevation myocardial infarction: the echocardiographic substudy of the OASIS-6 trial. Echocardiography. 2014;31:569–78.
42. Somaratne JB, Whalley GA, Gamble GD, Doughty RN. Restrictive filling pattern is a powerful predictor of heart failure events post-acute myocardial infarction and in established heart failure: a literature-based meta-analysis. J Card Fail. 2007;13:346–52.
43. Doughty RN, Klein AL, Poppe KK, et al. Independence of restrictive filling pattern and LV ejection fraction with mortality in heart failure: an individual patient meta-analysis. Meta-analysis Research Group in Echocardiography (MeRGE) Heart Failure Collaborators; Meta-Analysis. Eur J Heart Fail. 2008;10(8):786–92.
44. Iwahashi N, Kimura K, Kosuge M, et al. E/e' two weeks after onset is a powerful predictor of cardiac death and heart failure in patients with a first-time ST elevation acute myocardial infarction. J Am Soc Echocardiogr. 2012;25:1290–8.
45. Okura H, Kubo T, Asawa K, et al. Elevated E/E' predicts prognosis in congestive heart failure patients with preserved systolic function. Circ J. 2009;73:86–91.
46. Møller JE, Søndergaard E, Poulsen SH, et al. Color M-mode and pulsed wave tissue Doppler echocardiography: powerful predictors of cardiac events after first myocardial infarction. J Am Soc Echocardiogr. 2001;14:757–63.
47. Hillis GS, Møller JE, Pellikka PA, et al. Noninvasive estimation of left ventricular filling pressure by E/e' is a powerful predictor of survival after acute myocardial infarction. J Am Coll Cardiol. 2004;43:360–7.
48. Park JH, Marwick TH. Use and limitations of E/e' to assess ventricular filling pressure by echocardiography. J Cardiovasc Ultrasound. 2011;19:169–73.
49. Obokata M, Reddy YNV, Borlaug BA. The role of echocardiography in heart failure with preserved ejection fraction: what do we want from imaging? Heart Fail Clin. 2019;15:241–56.
50. Nauta JF, Hummel YM, van der Meer P, et al. Correlation with invasive left ventricular filling pressures and prognostic relevance of the echocardiographic diastolic parameters used in the 2016 ESC heart failure guidelines and in the 2016 ASE /EACVI recommendations: a systematic review in patients with heart failure with preserved ejection fraction. Eur J Heart Fail. 2018;20:1303–11.
51. Andersen OS, Smiseth OA, Dokainish H, et al. Estimating left ventricular filling pressure by echocardiography. J Am Coll Cardiol. 2017;69:1937–48.
52. Nishimura RA, Appleton CP, Redfield MM, et al. Noninvasive doppler echocardiographic evaluation of left ventricular filling pressures in patients with cardiomyopathies: a simultaneous Doppler echocardiographic and cardiac catheterization study. J Am Coll Cardiol. 1996;28:1226–33.
53. Inoue K, Khan FH, Remme EW, et al. Determinants of left atrial reservoir and pump strain and use of atrial strain for evaluation of left ventricular filling pressure. Eur Heart J Cardiovasc Imaging. 2021;23(1):61–70.
54. Kirkpatrick JN, Vannan MA, Narula J, Lang RM. Echocardiography in heart failure: applications, utility, and new horizons. J Am Coll Cardiol. 2007;50:381–96.
55. Ramasubbu K, Deswal A, Chan W, Aguilar D, Bozkurt B. Echocardiographic changes during treatment of acute decompensated heart failure: insights from the ESCAPE trial. J Cardiac Fail. 2012;18:792–8.
56. Izumo M. Value of echocardiography in the treatment of patients with acute heart failure. Front. Cardiovasc Med. 2021;8:740439.
57. Balaney B, Medvedofsky D, Mediratta A, et al. Invasive validation of the echocardiographic assessment of left ventricular filling pressures using the 2016 diastolic guidelines: head-to-head comparison with the 2009 guidelines. J Am Soc Echocardiogr. 2018;31(1):79–88.
58. Nagueh SF, Appleton CP, Gillebert TC, et al. Recommendations for the evaluation of left ventricular diastolic function by echocardiography. J Am Soc Echocardiogr. 2009;22:107–33.
59. Oh JK, Miranda WR, Bird JG, et al. The 2016 diastolic function guideline: is it already time to revisit or revise them? JACC Cardiovasc Imaging. 2020;13:327–35.
60. Venkateshvaran A, Tureli HO, Faxen UL, et al. Left atrial reservoir strain improves diagnostic accuracy of the 2016 ASE/EACVI diastolic algorithm in patients with preserved left ventricular ejection fraction: insights from the KARUM haemodynamic database. Eur Heart J Cardiovasc Imaging. 2022;23(9):1157–68.
61. Boe S, OA. Left atrial strain imaging: ready for clinical implementation in heart failure with preserved ejection fraction. Eur Heart J Cardiovasc. Imaging. 2022;23(9):1169–70.
62. Smiseth OA, Morris DA, Cardim N, et al. Multimodality imaging in patients with heart failure and preserved ejection fraction: an expert consensus document of the European Association of Cardiovascular Imaging. Eur Heart J Cardiovasc Imaging. 2022;23(2):e34–61.
63. Mandoli GE, Cameli M, Pastore MC, et al. Left ventricular fibrosis as a main determinant of filling pressures and left atrial function in advanced heart failure. Eur Heart J Cardiovasc Imaging. 2024;25(4):446–53.
64. Cameli M, Sparla S, Losito M, et al. Correlation of left atrial strain and Doppler measurements with invasive measurement of left ventricular end-diastolic pressure in patients stratified for different values of ejection fraction. Echocardiography. 2016;33:398–405.
65. Marwick TH. The Role of Echocardiography in Heart Failure. J Nucl Med. 2015;56:31S–8S.
66. Iwano H, Shibayama K, Kitai T, Kusunose K, Onishi T, Tanaka H, et al. Study protocol for prospect trial to elucidate the utility of echocardiography based cardiac output in acute heart failure (PREDICT). J Echocardiogr. 2020;18:235–9.
67. Mitchell C, Rahko PS, Blauwet LA, Canaday B, Finstuen JA, Foster MC, et al. Guidelines for performing a comprehensive transthoracic echocardiographic examination in adults: recommendations from the American Society of Echocardiography. J Am Soc Echocardiogr. 2019;32:1–64.
68. Ristow B, Na B, Ali S, Whooley MA, Schiller NB. Left ventricular outflow tract and pulmonary artery stroke distances independently predict heart failure hospitalization and mortality: the Heart and Soul Study. J Am Soc Echocardiogr. 2011;24:565–72.
69. Omote K, Nagai T, Iwano H, Tsujinaga S, Kamiya K, Aikawa T, et al. Left ventricular outflow tract velocity time integral in hospitalized heart failure with preserved ejection fraction. ESC Heart Fail. 2020;7:167–75.
70. Tan C, Rubenson D, Srivastava A, Mohan R, Smith MR, Billick K, et al. Left ventricular outflow tract velocity time integral outperforms ejection fraction and Doppler-derived cardiac output for predicting outcomes in a select advanced heart failure cohort. Cardiovasc Ultrasound. 2017;15:18.
71. Cameli M, Pastore MC, Mandoli GE, Nistor D, Lisi E, Tok ÖÖ, et al. Prognosis and risk stratification of patients with advanced heart failure (from PROBE). Am J Cardiol. 2019;124:55–62.
72. Tsang TS, Barnes ME, Bailey KR, et al. Left atrial volume: important risk marker of incident atrial fibrillation in 1655 older men and women. Mayo Clin Proc. 2001;76:467–47.

73. Zile MR, Gottdiener JS, Hetzel SJ, et al. I-PRESERVE Investigators. Prevalence and significance of alterations in cardiac structure and function in patients with heart failure and a preserved ejection fraction. Circulation. 2011;124:2491–501.
74. Shah AM, Shah SJ, Anand IS, TOPCAT Investigators, et al. Cardiac structure and function in heart failure with preserved ejection fraction: baseline findings from the echocardiographic study of the treatment of preserved cardiac function heart failure with an aldosterone antagonist trial. Circ Heart Fail. 2014;7:104–15.
75. Tsang TS, Abhayaratna WP, Barnes ME, et al. Prediction of cardiovascular outcomes with left atrial size: is volume superior to area or diameter? J Am Coll Cardiol. 2006;47:1018–23.
76. Benjamin EJ, D'Agostino RB, Belanger AJ, Wolf PA, Levy D. Left atrial size and the risk of stroke and death. The Framingham Heart Study. Circulation. 1995;92:835–41.
77. Moller JE, Hillis GS, Oh JK, et al. Left atrial volume: a powerful predictor of survival after acute myocardial infarction. Circulation. 2003;107:2207–12.
78. Meris A, Amigoni M, Uno H, et al. Left atrial remodelling in patients with myocardial infarction complicated by heart failure, left ventricular dysfunction, or both: the VALIANT Echo study. Eur Heart J. 2009;30:56–65.
79. Mor-Avi V, Jenkins C, Kuhl HP, et al. Real-time 3D echocardiographic quantification of left atrial volume: multicenter study for validation with magnetic resonance imaging. JACC Cardiovasc Imaging. 2012;5:769–77.
80. Casaclang-Verzosa G, Gersh BJ, Tsang TS. Structural and functional remodeling of the left atrium: clinical and therapeutic implications for atrial fibrillation. J Am Coll Cardiol. 2008;51:1–11.
81. Melenovsky V, Hwang SJ, Redfield MM, Zakeri R, Lin G, Borlaug BA. Left atrial remodeling and function in advanced heart failure with preserved or reduced ejection fraction. Circ Heart Fail. 2015;8:295–303.
82. Donal E, Lip GY, Galderisi M, Goette A, Shah D, Marwan M, et al. EACVI/EHRA Expert Consensus Document on the role of multi-modality imaging for the evaluation of patients with atrial fibrillation. Eur Heart J Cardiovasc Imaging. 2016;17:355–83.
83. Pontecorboli G, Figueras I, Ventura RM, Carlosena A, Benito E, Prat-Gonzales S, Padeletti L, et al. Use of delayed-enhancement magnetic resonance imaging for fibrosis detection in the atria: a review. Europace. 2017;19:180–9.
84. Badano LP, Kolias TJ, Muraru D, Abraham TP, Aurigemma G, Edvardsen T, Industry representatives, et al. Standardization of left atrial, right ventricular, and right atrial deformation imaging using two-dimensional speckle tracking echocardiography: a consensus document of the EACVI/ASE/Industry Task Force to standardize deformation imaging. Eur Heart J Cardiovasc Imaging. 2018;19:591–600. [Erratum in: Eur Heart J Cardiovasc Imaging 2018;19:830–833.]
85. Cameli M, Miglioranza MH, Magne J, Mandoli GE, Benfari G, Ancona R, et al. Multicentric atrial strain comparison between two different modalities: MASCOT HIT Study. Diagnostics (Basel). 2020;10:946.
86. To AC, Flamm SD, Marwick TH, Klein AL. Clinical utility of multimodality LA imaging: assessment of size, function, and structure. JACC Cardiovasc Imaging. 2011;4:788–98.
87. Reddy YNV, Obokata M, Egbe A, Yang JH, Pislaru S, Lin G, et al. Left atrial strain and compliance in the diagnostic evaluation of heart failure with preserved ejection fraction. Eur J Heart Fail. 2019;21:891–900.
88. Malagoli A, Rossi L, Bursi F, Zanni A, Sticozzi C, Piepoli MF, et al. Left atrial function predicts cardiovascular events in patients with chronic heart failure with reduced ejection fraction. J Am Soc Echocardiogr. 2019;32:248–56.
89. Al Saikhan L, Hughes AD, Chung WS, Alsharqi M, Nihoyannopoulos P. Left atrial function in heart failure with mid-range ejection fraction differs from that of heart failure with preserved ejection fraction: a 2D speckle-tracking echocardiographic study. Eur Heart J Cardiovasc Imaging. 2019;20:279–90.
90. Park JJ, Park JH, Hwang IC, Park JB, Cho GY, Marwick TH. Left atrial strain as a predictor of new-onset atrial fibrillation in patients with heart failure. JACC Cardiovasc Imaging. 2020;13:2071–81.
91. Cameli M, Mandoli GE, Loiacono F, Sparla S, Iardino E, Mondillo S. Left atrial strain: a useful index in atrial fibrillation. Int J Cardiol. 2016;220:208–13.
92. Pastore MC, Mandoli GE, Aboumarie HS, Santoro C, Bandera F, D'Andrea A, Working Group of Echocardiography of the Italian Society of Cardiology, et al. Basic and advanced echocardiography in advanced heart failure: an overview. Heart Fail Rev. 2020;25:937–48.
93. Her AY, Choi EY, Shim CY, Song BW, Lee S, Ha JW, et al. Prediction of left atrial fibrosis with speckle tracking echocardiography in mitral valve disease: a comparative study with histopathology. Korean Circ J. 2012;42:311–8.
94. Mandoli GE, Pastore MC, Benfari G, Bisleri G, Maccherini M, Lisi G, et al. Left atrial strain as a pre-operative prognostic marker for patients with severe mitral regurgitation. Int J Cardiol. 2021;324:139–45.
95. Lisi M, Mandoli GE, Cameli M, Pastore MC, Righini FM, et al. Left atrial strain by speckle tracking predicts atrial fibrosis in patients undergoing heart transplantation. Eur Heart J Cardiovasc Imaging. 2021;23:1–7.
96. Zile MR, Baicu CF, Ikonomidis JS, Stroud RE, Nietert PJ, Bradshaw AD, et al. Myocardial stiffness in patients with heart failure and a preserved ejection fraction: contributions of collagen and titin. Circulation. 2015;131:1247–59.
97. Cameli M, Sciaccaluga C, Loiacono F, Simova I, Miglioranza MH, Nistor D, et al. The analysis of left atrial function predicts the severity of functional impairment in chronic heart failure: the FLASH multicenter study. Int J Cardiol. 2019;286:87–91.
98. Mandoli GE, Cameli M, Novo G, Agricola E, Righini FM, Santoro C, Working Group of Echocardiography of the Italian Society of Cardiology, et al. Right ventricular function after cardiac surgery: the diagnostic and prognostic role of echocardiography. Heart Fail Rev. 2019;24:625–35.
99. Zoghbi WA, Enriquez-Sarano M, Foster E, et al. Recommendations for evaluation of the severity of native valvular regurgitation with two-dimensional and Doppler echocardiography. J Am Soc Echocardiogr. 2003;16:777–802.
100. Dal-Bianco JP, Beaudoin J, Handschumacher MD, Levine RA. Basic mechanisms of mitral regurgitation. Can J Cardiol. 2014;30:971–81.
101. Lisi M, Cameli M, Mandoli GE, Pastore MC, Fm R, et al. Detection of myocardial fibrosis by speckle-tracking echocardiography: from prediction to clinical applications. Heart Fail Rev. 2022;27(5):1857–67.
102. Puwanant S, Priester TC, Mookadam F, Bruce CJ, Redfield MM, Chandrasekaran K. Right ventricular function in patients with preserved and reduced ejection fraction heart failure. Eur J Echocardiogr. 2009;10:733–7.
103. Ghio S, Gavazzi A, Campana C, Inserra C, et al. Independent and additive prognostic value of right ventricular systolic function and pulmonary artery pressure in patients with chronic heart failure. J AmColl Cardiol. 2001;37(1):183–8.
104. Shah RV, Semigran MJ. Pulmonary hypertension secondary to left ventricular systolic dysfunction: contemporary diagnosis and management. Curr Heart Fail Rep. 2008;5(4):226–32.
105. Fang F, Henein MY, Yu CM, et al. Right ventricular long axis response to different chronic loading conditions: its relevance to clinical symptoms. Int J Cardiol. 2013;167:378–82.

106. Mauritz GJ, Kind T, Marcus JT, et al. Progressive changes in right ventricular geometric shortening and long-term survival in pulmonary arterial hypertension. Chest. 2012;141:935–43.
107. Munkhammar P, Carlsson M, Arheden H, Pesonen E. Restrictive right ventricular physiologyafter tetralogy of fallot repair is associated with fibrosis of the right ventricular outflow tract visualized on cardiac magnetic resonance imaging. Eur Heart J Cardiovasc Imaging. 2013;14:978–85.
108. Lang RM, Badano LP, Mor-Avi V, et al. Recommendations for cardiac chamber quantification by echocardiography in adults: an update from the American Society of Echocardiography and the European Association of Cardiovascular Imaging. J Am Soc Echocardiogr. 2015;28:1–39.e14.
109. Sugeng L, Mor-Avi V, Weinert L, et al. Multimodality comparison of quantitative volumetric analysis of the right ventricle. JACC Cardiovasc Imaging. 2010;3:10–8.
110. Buckberg GD, Hoffman JI, Coghlan HC, Nanda NC. Ventricular structure-function relations in health and disease:part I. The normal heart. Eur J Cardiothorac Surg. 2015;47:587–601.
111. Venkatachalam S, Wu G, Ahmad M. Echocardiographic assessment of the right ventricle in the current era: application in clinical practice. Echocardiography. 2017;34(12):1930–47.
112. Rudski LG, LaiWW AJ, et al. Guidelines for the echocardiographic assessment of the right heart in adults: a report from the American Society of Echocardiography endorsed by the European Association of Echocardiography, a registered branch of the European Society of Cardiology, and the Canadian Society of Echocardiography. J Am Soc Echocardiogr. 2010;23:685–713.
113. Badano LP, Muraru D. Subclinical right ventricular dysfunction by strain analysis. Refining the targets of echocardiographic imaging in systemic sclerosis. Circ Cardiovasc Imaging. 2016;9:e005009.
114. Tadica M, Pieske-Kraighera E, Cuspidib C, et al. Right ventricular strain in heart failure: clinical perspective. Arch Cardiovasc Dis. 2017;110:562–71.
115. Lisi M, Cameli M, Righini FM, et al. RV longitudinal deformation correlates with myocardial fibrosis in patients with end-stage heart failure. JACC Cardiovasc Imaging. 2015;8(5):514–22.
116. Glikson M, Nielsen JC, Kronborg MB, Michowitz Y, Auricchio A, Barbash IM, et al. 2021 ESC guidelines on cardiac pacing and cardiac resynchronization therapy. Eur Heart J. 2021;42(35):3427–520.
117. Chung ES, Leon AR, Tavazzi L, Sun JP, Nihoyannopoulos P, Merlino J, et al. Results of the predictors of response to CRT (PROSPECT) trial. Circulation. 2008;117(20):2608–16.
118. Chung ES, Leon AR, Tavazzi L, Sun JP, et al. Results of the predictors of response to CRT (PROSPECT) trial. Circulation. 2008;117(20):2608–16.
119. Mele D, Pasanisi G, Capasso F, De Simone A, et al. Left intraventricular myocardial deformation dyssynchrony identifies responders to cardiac resynchronization therapy in patients with heart failure. Eur. Heart J. 2006;27(9):1070–8.
120. Suffoletto MS, Dohi K, Cannesson M, Saba S, Gorcsan J 3rd. Novel speckle- tracking radial strain from routine black-and-white echocardiographic images to quantify dyssynchrony and predict response to cardiac resynchronization therapy. Circulation. 2006;113(7):960–8.
121. Serri K, Lafitte S, Amyot R, Sauvé C, Roudaut R. Echocardiographic evaluation of cardiac dyssynchrony. Can J Cardiol. 2007;23(4):303–10.
122. Cleland JG, Daubert JC, Erdmann E, Freemantle N, Cardiac Resynchronization-Heart Failure (CARE-HF) Study Investigators, et al. The effect of cardiac resynchronization on morbidity and mortality in heart failure. N Engl J Med. 2005;352(15):1539–49.
123. Bader H, Garrigue S, Lafitte S, Reuter S, et al. Intra-left ventricular electromechanical asynchrony. A new independent predictor of severe cardiac events in heart failure patients. J Am Coll Cardiol. 2004;43(2):248–56.
124. Antoniou N, Kalaitzoglou M, Tsigkriki L, Baroutidou A, et al. Speckle tracking echocardiography in patients with non-ischemic dilated cardiomyopathy who undergo cardiac resynchronization therapy: a narrative review. Diagnostics (Basel). 2024;14(11):1178.
125. Carasso S, Rakowski H, Witte KK, Smith P, et al. Left ventricular strain patterns in dilated cardiomyopathy predict response to cardiac resynchronization therapy: timing is not everything. J Am Soc Echocardiogr. 2009;22(3):242–50.
126. Pescariu SA, Şoşdean R, Tudoran C, Ionac A, et al. Echocardiographic parameters as predictors for the efficiency of resynchronization therapy in patients with dilated cardiomyopathy and HFrEF. Diagnostics (Basel). 2021;12(1):35.
127. Ruschitzka F, Abraham WT, Singh JP, Bax JJ, EchoCRT Study Group, et al. Cardiac resynchronization therapy in heart failure with a narrow QRS complex. N Engl J Med. 2013;369(15):1395–405.
128. Mullens W, Auricchio A, Martens P, Witte K, et al. Optimized implementation of cardiac resynchronization therapy: a call for action for referral and optimization of care. Europace. 2021;23(8):1324–42.
129. Hara H, Oyenuga OA, Tanaka H, Adelstein EC, Onishi T, McNamara DM, et al. The relationship of QRS morphology and mechanical dyssynchrony to long-term outcome following cardiac resynchronization therapy. Eur Heart J. 2012;33(21):2680–91.
130. Kirn B, Jansen A, Bracke F, van Gelder B, et al. Mechanical discoordination rather than dyssynchrony predicts reverse remodeling upon cardiac resynchronization. Am J Physiol Heart Circ Physiol. 2008;295(2):H640–6.
131. Wang CL, Wu CT, Yeh YH, et al. Recoordination rather than resynchronization predicts reverse remodeling after cardiac resynchronization therapy. J Am Soc Echocardiogr. 2010;23(6):611–20.
132. Risum N, Jons C, Olsen NT, et al. Simple regional strain pattern analysis to predict response to cardiac resynchronization therapy: rationale, initial results, and advantages. Am Heart J. 2012;163(4):697–704.
133. Calle S, Duchenne J, Beela AS, Stankovic I, et al. Timmermans, Clinical and experimental evidence for a strain-based classification of left bundle branch block- induced cardiac remodeling. Circ Cardiovasc Imaging. 2022;15(11):e014296.
134. Lumens J, Tayal B, Walmsley J, et al. Differentiating electromechanical from non-electrical substrates of mechanical discoordination to identify responders to cardiac resynchronization therapy. Circ Cardiovasc Imaging. 2015;8(9):e003744.
135. Beela AS, Ünlü S, Duchenne J, et al. Assessment of mechanical dyssynchrony can improve the prognostic value of guideline-based patient selection for cardiac resynchronization therapy. Eur Heart J Cardiovasc Imaging. 2019;20(1):66–74.
136. Duckett SG, Camara O, Ginks MR, et al. Relationship between endocardial activation sequences defined by high-density mapping to early septal contraction (septal flash) in patients with left bundle branch block undergoing cardiac resynchronization therapy. Europace. 2012;14(1):99–106.
137. Stankovic I, Prinz C, Ciarka A, et al. Relationship of visually assessed apical rocking and septal flash to response and long-term survival following cardiac resynchronization therapy (PREDICT-CRT). Eur Heart J Cardiovasc Imaging. 2016;17(3):262–9.
138. Szulik M, Tillekaerts M, Vangeel V, et al. Assessment of apical rocking: a new, integrative approach for selection of candidates for cardiac resynchronization therapy. Eur J Echocardiogr. 2010;11(10):863–9.
139. Mada RO, Lysyansky P, Duchenne J, et al. New automatic tools to identify responders to cardiac resynchronization therapy. J Am Soc Echocardiogr. 2016;29(10):966–72.

140. Salden OAE, Zweerink A, Wouters P, Allaart CP, et al. The value of septal rebound stretch analysis for the prediction of volumetric response to cardiac resynchronization therapy. Eur Heart J Cardiovasc Imaging. 2021;22(1):37–45.
141. Seo Y, Ishizu T, Kawamura R, et al. Three-dimensional propagation imaging of left ventricular activation by speckle-tracking echocardiography to predict responses to cardiac resynchronization therapy. J Am Soc Echocardiogr. 2015;28(5):606–14.
142. Mele D, Luisi GA, Malagù M, Laterza A. Echocardiographic evaluation of cardiac dyssynchrony: does it still matter? Echocardiography. 2018;35(5):707–15.
143. McDonagh TA, Metra M, Adamo M, et al. 2021 ESC Guidelines for the diagnosis and treatment of acute and chronic heart failure: developed by the Task Force for the diagnosis and treatment of acute and chronic heart failure of the European Society of Cardiology (ESC). With the special contribution of the Heart Failure Association (HFA) of the ESC. Eur J Heart Fail. 2022;24(1):4–131.
144. Forrester JS, Diamond GA, Swan HJ. Correlative classification of clinical and hemodynamic function after acute myocardial infarction. Am J Cardiol. 1977;39:137–45.
145. Forrester JS, Waters DD. Hospital treatment of congestive heart failure. Management according to hemodynamic profile. Am J Med. 1978;65:173–80.
146. Otto CM. Textbook of clinical echocardiography. 7th ed. Elsevier–Health Sciences Division; 2023. ISBN 9780323882088
147. Fitzsimons S, Doughty RN. Role of transthoracic echocardiogram in acute heart failure. Rev Cardiovasc Med. 2021;22(3):741–54.
148. Matthews S, Levy PD, Favot M, et al. Threedimensional echocardiography in acute heart failure: can and should we do it in the emergency department? Echocardiography. 2018;35:692–4.
149. Čelutkienė J, Plymen CM, Flachskampf FA, et al. Innovative imaging methods in heart failure: a shifting paradigm in cardiac assessment. Position statement on behalf of the Heart Failure Association of the European Society of Cardiology. Eur J Heart Fail. 2018;20:1615–33.
150. Wang N, Hung C, Shin S, et al. Regional cardiac dysfunction and outcome in patients with left ventricular dysfunction, heart failure, or both after myocardial infarction. Eur Heart J. 2016;37:466–72.
151. Park JJ, Park JB, Park JH, Cho GY. Global longitudinal strain to predict mortality in patients with acute heart failure. J Am Coll Cardiol. 2018;71:1947–57.
152. Iwano H, Shibayama K, Kitai T, et al. Study protocol for prospect trial to elucidate the utility of echocardiographybased cardiac output in acute heart failure (PREDICT). J Echocardiogr. 2020;18:235–9.
153. Mitchell C, Rahko PS, Blauwet LA, et al. Guidelines for performing a comprehensive transthoracic echocardiographic examination in adults: recommendations from the American Society of Echocardiography. J Am Soc Echocardiogr. 2019;32:1–64.
154. Ristow B, Na B, Ali S, et al. Left ventricular outflow tract and pulmonary artery stroke distances independently predict heart failure hospitalization and mortality: the Heart and Soul Study. J Am Soc Echocardiogr. 2011;24:565–72.
155. Omote K, Nagai T, Iwano H, et al. Left ventricular outflow tract velocity time integral in hospitalized heart failure with preserved ejection fraction. ESC Heart Fail. 2020;7:167–75.
156. Tan C, Rubenson D, Srivastava A, et al. Left ventricular outflow tract velocity time integral outperforms ejection fraction and Doppler-derived cardiac output for predicting outcomes ina select advanced heart failure cohort. Cardiovasc Ultrasound. 2017;15:18.
157. Møller JE, Sionis A, Aissaoui N, et al. Step by step daily management of short-term mechanical circulatory support for cardiogenic shock in adults in the intensive cardiac care unit: a clinical consensus statement of the Association for Acute CardioVascular Care of the European Society of Cardiology SC, the European Society of Intensive Care Medicine, the European branch of the Extracorporeal Life Support Organization, and the European Association for Cardio-Thoracic Surgery. Eur Heart J Acute Cardiovasc Care. 2023;12(7):475–85.
158. Vranckx P. Handbook on mechanical circulatory support, Association for Acute CardioVascular Care (ACVC), 2022 edition.
159. Dini FL, Bajraktari G, Zara C, et al. Optimizing management of heart failure by using echo and natriuretic peptides in the outpatient unit. Adv Exp Med Biol. 2018;1067:145–59.
160. Tomoaia R, Beyer RS, Simu G, et al. Understanding the role of echocardiography in remodeling after acute myocardial infarction and development of heart failure with preserved ejection fraction. Med Ultrason. 2019;21:69–76.
161. Papadimitriou L, Georgiopoulou VV, Kort S, et al. Echocardiography in acute heart failure: current perspectives. J Card Fail. 2016;22:82–94.
162. Van Aelst LN, Arrigo M, Plácido R, et al. Acutely decompensated heart failure with preserved and reduced ejection fraction present with comparable haemodynamicm congestion. Eur Jr Heart Fail. 2018;20:738–47.
163. Chioncel O, Mebazaa A, Harjola V, et al. Clinical phenotypes and outcome of patients hospitalized for acute heart failure: the ESC heart failure long-term registry. Eur J Heart Fail. 2017;19:1242–54.
164. Metra M, Tomasoni D, Adamo M, et al. Worsening of chronic heart failure: definition, epidemiology, management and prevention. A clinical consensus statement by the Heart Failure Association of the European Society of Cardiology. Eur J Heart Fail. 2023;25(6):776–91.
165. Stevenson LW, Zile M, Bennett TD, et al. Chronic ambulatory intracardiac pressures and future heart failure events. Circ Heart Fail. 2010;3:580–7.
166. Girerd N, Seronde MF, Coiro S, et al. Integrative assessment of congestion in heart failure throughout the patient journey. JACC Heart Fail. 2018;6:273–85.
167. Metra M, Davison B, Bettari L, et al. Is worsening renal function an ominous prognostic sign in patients with acute heart failure? The role of congestion and its interaction with renal function. Circ Heart Fail. 2012;5:54–62.
168. Rubio-Gracia J, Demissei BG, ter Maaten JM, et al. Prevalence, predictors and clinical out-come of residual congestion in acute decompensated heart failure. Int J Cardiol. 2018;258:185–91.
169. Ilies AM, Hodorogea AS, Balahura AM, Bădilă E. Non-invasive assessment of congestion by cardiovascular and pulmonary ultrasound and biomarkers in heart failure. Diagnostics. 2022;12:962.
170. Beaubien-Souligny W, Rola P, Haycock K, et al. Quantifying systemic congestion with point-of-care ultrasound: development of the venous excess ultrasound grading system. Ultrasound J. 2020;12:16.
171. Dabestani A, Mahan G, Gardin JM, et al. Evaluation of pulmonary artery pressure and resistance by pulsed Doppler echocardiography. Am J Cardiol. 1987;59:662–8.
172. Milan A, Magnino C, Veglio F. Echocardiographic indexes for the non-invasive evaluation of pulmonary hemodynamics. Am Soc Echocardiogr. 2010;23:225–39.
173. Brennan JM, Blair JE, Goonewardena S, et al. A comparison by medicine residents of physical examination versus hand-carried ultrasound for estimation of right atrial pressure. Am J Cardiol. 2007;99:1614–6.
174. Blair JE, Brennan JM, Goonewardena SN, et al. Usefulness of hand-carried ultrasound to predict elevated left ventricular filling pressure. Am J Cardiol. 2009;103:246–7.
175. Dokainish H, Nguyen JS, Bobek J, et al. Assessment of the American Society of Echocardiography European Association of Echocardiography guidelines for diastolic function in patients with depressed ejection fraction: an echocardiographic and invasive haemodynamic study. Eur J Echocardiogr. 2011;12:857–64.

176. Miglioranza MH, Gargani L, Sant'Anna RT, et al. Lung ultrasound for the evaluation of pulmonary congestion in outpatients: a comparison with clinical assessment, natriuretic peptides, and echocardiography. JACC Cardiovasc Imaging. 2013;6:1141–51.
177. Öhman J, Harjola VP, Karjalainen P, Lassus J. Focused echocardiography and lung ultrasound protocol for guiding treatment in acute heart failure. ESC Heart Fail. 2018;5:120–8.
178. Burnett JC, Knox FG. Renal interstitial pressure and sodium excretion during renal vein constriction. Am J Physiol Renal Physiol. 1980;238:F279–82.
179. Tang WH, Kitai T. Intrarenal venous flow: a window into the congestive kidney failure phenotype of heart failure? JACC Heart Fail. 2016;4:683–6.
180. Nijst P, Martens P, Dupont M, et al. Intrarenal flow alterations during transition from euvolemia to intravascular volume expansion in heart failure patients. JACC Heart Fail. 2017;5:672–81.
181. Ter Maaten JM, Dauw J, Martens P, et al. The effect of decongestion on intrarenal venous flow patterns in patients with acute heart failure. J Card Fail. 2021;27:29–34.
182. Yamamoto M, Seo Y, Iida N, et al. Prognostic impact of changes in intrarenal venous flow pattern in patients with heart failure. J Card Fail. 2021;27:20–8.
183. Torres-Arrese M, Mata-Martínez A, Luordo-Tedesco D, et al. Usefulness of systemic venous ultrasound protocols in the prognosis of heart failure patients: results from a prospective multicentric study. J Clin Med. 2023;12(4):1281.
184. Picano E, Scali MC, Ciampi Q, Lichtenstein D. Lung ultrasound for the cardiologist. JACC Cardiovasc Imaging. 2018;11:1692–705.
185. Gargani L, Pang PS, Frassi F, et al. Persistent pulmonary congestion before discharge predicts rehospitalization in heart failure: a lung ultrasound study. Cardiovasc Ultrasound. 2015;13:40.
186. Price S, Platz E, Cullen L, Acute Heart Failure Study Group of the European Society of Cardiology Acute Cardiovascular Care Association, et al. Expert consensus document: Echocardiography and lung ultrasonography for the assessment and management of acute heart failure. Nat Rev Cardiol. 2017;14:427–40.
187. Picano E, Pellikka PA. Ultrasound of extravascular lung water: a new standard for pulmonary congestion. Eur. Heart J. 2016;37:2097–104.
188. Gargani L. Lung ultrasound: a new tool for the cardiologist. Cardiovasc Ultrasound. 2011;9:6.
189. Neskovic AN, Skinner H, Price S, et al. Focus cardiac ultrasound core curriculum and core syllabus of the European Association of Cardiovascular Imaging. Eur Heart J Cardiovasc Imaging. 2018;19:475–81.
190. Neskovic AN, Hagendorff A, Lancellotti P, et al. Emergency echocardiography: the European Association of Cardiovascular Imaging recommendations. Eur Heart J Cardiovasc Imaging. 2013;14:1–11.
191. Marini TJ, Rubens DJ, Zhao YT, et al. Lung ultrasound: the essentials. Radiol Cardiothorac Imaging. 2021;3:e200564.
192. München Barth F, Beck-da-Silva L, Ghisleni EC, et al. Lung ultrasound in congestion assessment of patients with advanced heart failure referred for heart transplant: correlations with right heart catheterization findings. Am Heart J Plus. 2023;26:100250.
193. Picano E, Scali MC. The lung water cascade in heart failure. Echocardiography. 2017;34:1503–7.
194. Pirrotta F, Mazza B, Gennari L, Palazzuoli A. Pulmonary congestion assessment in heart failure: traditional and new tools. Diagnostics. 2021;11:1306.
195. Maw AM, Hassanin A, Ho PM, et al. Diagnostic accuracy of point-of-care lung ultrasonography and chest radiography in adults with symptoms suggestive of acute decompensated heart failure: a systematic review and meta-analysis. JAMA Netw Open. 2019;2:e190703.
196. Scali MC, Cortigiani L, Simionuc A, et al. Exercise-induced B-lines identify worse functional and prognostic stage in heart failure patients with depressed left ventricular ejection fraction. Eur J Heart Fail. 2017;19:1468–78.
197. Scali MC, Zagatina A, Ciampi Q, et al. Lung ultrasound and pulmonary congestion during stress echocardiography. JACC Cardiovasc Imaging. 2020;13:2085–95.
198. Agricola E, Picano E, Oppizzi M, et al. Assessment of stress-induced pulmonary interstitial edema by chest ultrasound during exercise echocardiography and its correlation with left ventricular function. J Am Soc Echocardiogr. 2006;19:457–63.
199. Mozzini C, Perna MDD, Pesce G, et al. Lung ultrasound in internal medicine efficiently drives the management of patients with heart failure and speeds up the discharge time. Intern Emerg Med. 2018;13:27–33.
200. Araiza-Garaygordobil D, Gopar-Nieto R, Martinez-Amezcua P, et al. A randomized controlled trial of lung ultrasound-guided therapy in heart failure (CLUSTER-HF study). Am Heart J. 2020;227:31–9.
201. Pang PS, Russell FM, Ehrman R, et al. Lung ultrasound–guided emergency department management of acute heart failure (BLUSHED-AHF): a randomized controlled pilot trial. JACC Heart Fail. 2021;9:638.
202. Rivas-Lasarte M, Alvarez-Garcia J, Fernández-Martínez J, et al. Lung ultrasound-guided treatment in ambulatory patients with heart failure: a randomized controlled clinical trial (LUS-HF study). Eur J Heart Fail. 2019;21:1605–13.
203. Gargani L, Pugliese NR, Frassi F, et al. Prognostic value of lung ultrasound in patients hospitalized for heart disease irrespective of symptoms and ejection fraction. ESC Heart Fail. 2021;8:2660–9.
204. Ambrosy AP, Pang PS, Khan S, et al. Clinical course and predictive value of congestion during hospitalization in patients admitted for worsening signs and symptoms of heart failure with reduced ejection fraction: findings from the EVEREST trial. Eur Heart J. 2013;34:835–43.
205. Coiro S, Porot G, Rossignol P, et al. Prognostic value of pulmonary congestion assessed by lung ultrasound imaging during heart failure hospitalisation: a two-centre cohort study. Sci Rep. 2016;6:39426.
206. Platz E, Lewis EF, Uno H, et al. Detection and prognostic value of pulmonary congestion by lung ultrasound in ambulatory heart failure patients. Eur Heart J. 2016;37:1244–51.
207. Cameli M, Soliman Aboumarie H, Pastore MC, et al. Multimodality imaging for the evaluation and management of patients with long-term (durable) left ventricular assist devices. A Clinical Consensus Statement of the European Association of Cardiovascular Imaging (EACVI) of the ESC. Eur heart J Cardiovasc Imaging. 2024;25(10):e217–40.
208. Sciaccaluga C, Soliman-Aboumarie H, Sisti N, et al. Echocardiography for left ventricular assist device implantation and evaluation: an indispensable tool. Heart Fail Rev. 2022;27(3):891–902.
209. Todaro MC, Khandheria BK, Paterick TE, et al. The practical role of echocardiography in selection, implantation, and management of patients requiring LVAD therapy. Curr Cardiol Rep. 2014;16:468.
210. Kühl HP, Schreckenberg M, Rulands D, et al. High-resolution transthoracic real-time three-dimensional echocardiography: quantitation of cardiac volumes and function using semi-automatic border detection and comparison with cardiac magnetic resonance imaging. J Am Coll Cardiol. 2004;43:2083–90.
211. Dorosz JL, Lezotte DC, Weitzenkamp DA, et al. Performance of 3-dimensional echocardiography in measuring left ventricular volumes and ejection fraction: a systematic review and meta-analysis. J Am Coll Cardiol. 2012;59:1799–808.

212. Kato TS, Farr M, Schulze PC, et al. Usefulness of two- dimensional echocardiographic parameters of the left side of the heart to predict right ventricular failure after left ventricular assist device implantation. Am J Cardiol. 2012;109:246–51.
213. Topilsky Y, Oh JK, Shah DK, et al. Echocardiographic predictors of adverse outcomes after continuous left ventricular assist device implantation. JACC Cardiovasc Imaging. 2011;4:211–22.
214. Moon MR, De Anda A, Castro LJ, et al. Effects of mechanical left ventricular support on right ventricular diastolic function. J Heart Lung Transplant. 1997;16:398–407.
215. Neyer J, Arsanjani R, Moriguchi J, et al. Echocardiographic parameters associated with right ventricular failure after left ventricular assist device: a review. J Heart Lung Transplant. 2016;35(3):283–93.
216. Longobardo L, Kramer C, Carerj S, et al. Role of echocardiography in the evaluation of left ventricular assist devices: the importance of emerging technologies. Curr Cardiol Rep. 2016;18(7):62.
217. Cameli M, Mondillo S, Righini FM, et al. Left ventricular deformation and myocardial fibrosis in patients with advanced heart failure requiring transplantation. J Card Fail. 2016;22(11):901–7.
218. Cameli M, Mondillo S, Solari M, Righini FM, et al. Echocardiographic assessment of left ventricular systolic function: from ejection fraction to torsion. Heart Fail Rev. 2016;21(1):77–9.
219. Soliman OII, Akin S, Muslem R, et al. Derivation and validation of a novel right-sided heart failure model after implantation of continuous flow left ventricular assist devices: the EUROMACS (European Registry for Patients with Mechanical Circulatory Support) right -sided heart failure risk score. Circulation. 2018;137:891–906.
220. Matthews JC, Koelling TM, Pagani FD, Aaronson KD. The right ventricular failure risk score a pre-operative tool for assessing the risk of right ventricular failure in left ventricular assist device candidates. J Am Coll Cardiol. 2008;51:2163–72.
221. Jones N, Burns AT, Prior DL. Echocardiographic Assessment of the Right Ventricle–State of the Art. Heart. Lung Circ. 2019;28:1339–50.
222. Kato TS, Jiang J, Schulze PC, Jorde U, Uriel N, et al. Serial echocardiography using tissue Doppler and speckle tracking imaging to monitor right ventricular failure before and after left ventricular assist device surgery. JACC Heart Fail. 2013;1:216–22.
223. Cameli M, Bernazzali S, Lisi M, et al. Right ventricular longitudinal strain and right ventricular stroke work index in patients with severe heart failure: left ventricular assist device suitability for transplant candidates. Transplant Proc. 2012;44:2013–5.
224. Tamborini G, Pepi M, Galli CA, et al. Feasibility and accuracy of a routine echocardiographic assessment of right ventricular function. Int J Cardiol. 2007;115:86–9.
225. Cameli M, Lisi M, Righini FM, et al. Speckle tracking echocardiography as a new technique to evaluate right ventricular function in patients with left ventricular assist device therapy. J Heart Lung Transplant. 2013;32:424–30.
226. Kato TS, Farr M, Schulze PC, et al. Usefulness of two-dimensional echocardiographic param- eters of the left side of the heart to predict right ventricular fail- ure after left ventricular assist device implantation. Am J Cardiol. 2012;109:246–25.
227. Raina A, Seetha Rammohan HR, Gertz ZM, et al. Postoperative right ventricular failure after left ventricular assist device placement is predicted by preoperative echocardiographic structural, hemodynamic, and functional parameters. J Card Fail. 2013;19:16–24.
228. Cameli M, Loiacono F, Sparla S, Solari M, et al. Systematic left ventricular assist device implant eligibility with non-invasive assessment: the SIENA protocol. J Cardiovasc Ultrasound. 2017;25(2):39–46.
229. Field ME, Solomon SD, Lewis EF, et al. Right ventricular dysfunction and adverse outcome in patients with advanced heart failure. J Card Fail. 2006;12:616–20.
230. Aggarwal A, Raghuvir R, Eryazici P, et al. The development of aortic insufficiency in continuous-flow left ventricular assist device-supported patients. Ann Thorac Surg. 2013;95:493–8.
231. Tuzun E, Pennings K, van Tuijl S, et al. Assessment of aortic valve pressure overload and leaflet functions in an ex vivo beating heart loaded with a continuous flow cardiac assist device. Eur J Cardiothorac Surg. 2014;45:377–83.
232. Feldman D, Pamboukian SV, Teuteberg JJ, et al. The 2013 International Society for Heart and Lung Transplantation Guidelines for mechanical circulatory support: executive summary. J Heart Lung Transplant. 2013;32:157–87.
233. Cohen DG, Thomas JD, Freed BH, Rich JD, Sauer AJ. Echocardiography and continuous-flow left ventricular assist devices. Evidence and Limitations. JACC Hear Fail. 2015;3:554–64.
234. Feldman D, Pamboukian SV, Teuteberg JJ, et al. The 2013 international society for heart and lung transplantation guidelines for mechanical circulatory support: executive summary. J Heart Lung Transplant. 2013;32:157–87.
235. Rana BS, Thomas MR, Calvert PA, et al. Echocardiographic evaluation of patent foramen ovale prior to device closure. JACC Cardiovasc Imaging. 2010;3:749–60.
236. Neyer J, Arsanjani R, Moriguchi J, Siegel R, Kobashigawa J. Echocardiographic parameters associated with right ventricular failure after left ventricular assist device: a review. J Heart Lung Transplant. 2016;35(3):283–93.
237. Estep JD, Stainback RF, Little SH, et al. The role of echocardiography and other imaging modalities in patients with left ventricular assist devices. JACC Cardiovasc Imaging. 2010;3:1049–64.
238. Ishino K, Murakami T, Takata K, et al. Assessment of myocardial function during mechanical left ventricular support using serial echocardiography: a case report. Acta Med Okayama. 1994;48(165):8.
239. Frea S, Centofanti P, Pidello S, et al. Noninvasive assessment of hemodynamic status in heartware left ventricular assist device patients. JACC Cardiovasc Imaging. 2019;12:1121–31.
240. Sciaccaluga C, D'Ascenzi F, Mandoli GE, et al. Traditional and novel imaging of right ventricular function in patients with heart failure and reduced ejection fraction. Curr Heart Fail Rep. 2020;17(2):28–33.
241. Ramani G, Chen W, Patel S, Judy J, Ton VK. Noninvasive assessment of right ventricular function in patients with pulmonary arterial hypertension and left ventricular assist device. Curr Cardiol Rep. 2019;21:82.
242. Imamura T, Chung B, Nguyen A, Sayer G, Uriel N. Clinical implications of hemodynamic assessment during left ventricular assist device therapy. J Cardiol. 2018;71:352–8.
243. Kirkpatrick JN, Wiegers SE, Lang RM. Left ventricular assist devices and other devices for end-stage heart failure: utility of echocardiography. Curr Cardiol Rep. 2010;12:257–64.
244. Bouchez S, Van Belleghem Y, De Somer F, et al. Haemodynamic management of patients with left ventricular assist devices using echocardiography: the essentials. Eur Heart J Cardiovasc Imaging. 2019;20(4):373–82.

Cardio-oncology

14

Ibadete Bytyçi and Michael Y. Henein

Introduction

Advances in cancer treatments have significantly improved patient survival, but they have also led to an increase in treatment-related complications, particularly cardiotoxicity [1]. Cardiotoxicity can occur as a direct result of cancer therapies affecting heart structure and function, or it may arise from an accelerated progression of already existing cardiovascular disease (CVD), particularly in patients with CV risk factors [2].

Prevention, diagnosis, and managing cancer therapy-related cardiovascular toxicity (CTR-CVT) is crucial, as it affects the types of anticancer treatments available to patients and their long-term health outcomes, including chemotherapy, radiotherapy, targeted agents, and immunotherapies [2, 3]. The spectrum of CTR-CVT is broad, including heart failure (HF), cardiomyopathy, myocarditis, arrhythmia, valvular and pericardial diseases, but HF and cardiomyopathy are more related to cardiac injury [3, 4].

Chemotherapy

Anthracyclines are highly effective for treating cancer but can lead to cardiac side effects that affect patient's prognosis. For example, doxorubicin is associated with a 5% incidence of congestive heart failure (HF) at a cumulative dose of 400 mg/m^2, increasing to 48% at 700 mg/m^2. For patients over 65 years of age treated with standard anthracycline doses, the incidence of HF can reach up to 10%. [5]. Responses vary among individuals, with some experiencing cardiotoxicity even after a single dose.

The primary mechanism of anthracycline-induced cardiotoxicity is oxidative stress, which damages myocardial cells [6, 7]. This toxicity can be acute (such as arrhythmias or transient dysfunction), early (within the first year), or late (around 7 years after treatment) [8]. Acute effects are generally reversible but may signal more serious issues.

Recent studies show a 9% incidence of cardiotoxicity, predominantly within the first year of treatment and it is often asymptomatic [9]. Early detection of cardiotoxicity and treatment of patients with well-established HF medications can lead to better recovery, while late detection makes treatment less effective. Risk factors include cumulative dose, infusion regimen, pre-existing heart conditions, hypertension, concurrent therapies, and age. Pediatric patients, whose developing hearts are particularly vulnerable, are generally at higher risk of anthracycline cardiotoxicity compared to adults. In patients with one or more risk factors, the cumulative dose-to-cardiotoxicity curve shifts leftward, necessitating careful monitoring or consideration of alternative chemotherapeutic options. Patients with multiple risk factors may need closer monitoring or alternative treatments [1, 10].

Several conventional chemotherapies, such as cyclophosphamide, cisplatin, ifosfamide, and taxanes (paclitaxel and docetaxel), can also induce myocardial dysfunction and HF. Signs and symptoms of HF typically appear within days of drug administration, particularly with risk factors including high dose, old age, combination with other cancer drugs, and mediastinal irradiation [11]. Cisplatin and ifosfamide can infrequently cause HF due to myocardial ischemia and volume overload from high intravenous fluid requirements. This volume overload can trigger HF in patients with pre-existing myocardial impairment [12].

Docetaxel, used in breast cancer treatment, especially with or after anthracyclines, cyclophosphamide, or trastuzumab, may increase the incidence of HF. However, the exact contribution of each drug in multidrug regimens is

I. Bytyçi
Medical Faculty, University of Prishtina, Prishtina, Kosovo

Clinic of Cardiology, University Clinical Centre of Kosovo, Prishtina, Kosovo

M. Y. Henein (✉)
Imperial College, London, UK

Siena University, Siena, Italy
e-mail: m.henein@imperial.ac.uk

© The Author(s), under exclusive license to Springer Nature Switzerland AG 2025

M. Y. Henein (ed.), *Clinical Echocardiography*, https://doi.org/10.1007/978-3-031-95894-6_14

difficult to ascertain. Some reports suggest taxanes might be safer for patients with pre-existing left ventricular (LV) dysfunction, but the overall cardiotoxic risks are unclear [13].

Immunotherapies and Targeted Therapies

Immunotherapies and targeted therapies have significantly improved cancer treatment clinical outcomes. Initially, cardiotoxicity was high when trastuzumab was given with anthracyclines, but using trastuzumab after anthracyclines or in anthracycline-free regimens reduced HF rates [1]. Cardiac dysfunction rates ranged from 7 to 34%, and HF (NYHA class III or IV) rates ranged from 0 to 4%. Concomitant use with anthracyclines increases trastuzumab cardiotoxicity. Studies have shown 6.2% and 20.1% cumulative cardiac dysfunction or HF rates at 1 and 5 years, respectively, with combined anthracycline and trastuzumab treatment [14, 15].

Trastuzumab cardiotoxicity usually occurs during treatment and is not cumulative-dose related, though longer treatment durations can double LV dysfunction rates. It is typically reversible with treatment interruption and/or HF therapies [16]. The mechanism involves structural and functional changes in contractile proteins and mitochondria but rarely leads to cell death, thus allowing for potential reversibility. Risk factors include prior anthracycline exposure, short interval between anthracycline and anti-HER2 treatment, pre-existing hypertension, low LVEF, and old age [17, 18].

The cardiotoxicity risk of other anti-HER2 therapies (lapatinib, pertuzumab, and T-DM1) is similar to trastuzumab. A large trial comparing adjuvant trastuzumab alone vs. trastuzumab and lapatinib has reported cardiotoxicity incidence of 2 to 5%, with 2 to 3% experiencing HF. Cardiotoxicity risks for T-DM1 and pertuzumab appear similar, though large adjuvant trial data are pending [1, 19].

Inhibition of the Vascular Endothelial Growth Factor Signalling Pathway

Inhibiting the Vascular Endothelial Growth Factor (VEGF) signalling pathway benefits patients with various solid cancers, but VEGF inhibitors can cause cardiac side effects, especially when combined with or following conventional chemotherapies. In a large breast cancer trial, the anti-VEGF antibody bevacizumab induced LV dysfunction in 2% and HF (NYHA III or IV) in 1% of patients [20].

TKIs such as sunitinib, pazopanib, and axitinib have been reported to cause cardiotoxicity, inducing cardiac dysfunction in 3–15% and symptomatic HF in 1–10% of patients. Other anti-VEGF inhibitors like sorafenib and vandetanib show similar effects, though large prospective data are lacking [21]. A meta-analysis of 21 randomized phase II and III trials involving 10,647 patients revealed a 2.69-fold increased risk of all grades of congestive HF with VEGF receptor TKIs (e.g., sunitinib, sorafenib, pazopanib, axitinib, vandetanib, cabozantinib, ponatinib, regorafenib) compared to controls. However, the risk of severe HF was not significantly increased [22]

VEGF inhibitors also cause significant arterial hypertension, potentially impacting cardiac function. Many anti-VEGF drugs inhibit multiple pathways, complicating the identification of the cardiotoxicity mechanism. The prognosis for patients with cardiotoxicity from these drugs is challenging to determine, given their use in metastatic disease with limited life expectancy. Nonetheless, controlling hypertension and using intensive HF medications can potentially reverse cardiac dysfunction [1, 22].

BCR-ABL Kinase and Proteasome Inhibitors

Small-molecule inhibitors like imatinib have greatly improved outcomes for chronic leukemias and gastrointestinal stromal tumors. Initial concerns about imatinib-induced cardiotoxicity were not confirmed by larger studies. However, newer BCR-ABL inhibitors such as nilotinib and ponatinib are associated with cardiovascular events [23, 24]. Used in multiple myeloma treatment, proteasome inhibitors like bortezomib and carfilzomib have been shown to cause cardiac dysfunction. Bortezomib is associated with low HF incidence (up to 4%), but this can be exacerbated by steroids. Carfilzomib, a more potent inhibitor, has shown higher HF risk (up to 25%) in preliminary data [1, 25].

Radiotherapy

Evaluating radiation-induced cardiotoxicity is challenging due to long delays between exposure and onset of symptoms, use of concomitant cardiotoxic chemotherapy, improvements in radiation techniques, changes in treated populations, and underreporting results. The mortality rate ranges from 9.3 to 28 per 10,000 person-years. Among survivors, the risk of HF increases by 4.9-fold [26].

Patients treated with both left breast radiotherapy and cardiotoxic chemotherapy have the highest cardiotoxicity risk, suggesting a synergistic effect. Radiotherapy-induced cardiotoxicity commonly involves interstitial myocardial fibrosis. In a study of 1,820 adult survivors of childhood cancer exposed to anthracyclines, chest-directed radiotherapy, or both, 22% exposed to radiotherapy alone showed diastolic dysfunction, and 27.4% had reduced exercise capacity. LV systolic dysfunction often occurs when radiotherapy is com-

bined with anthracyclines. HF may also be worsened by radiation-induced valvular heart disease and coronary artery disease [27, 28].

Echocardiography Findings

Transthoracic echocardiography (TTE) is more frequently used than other cardiac imaging techniques and is vital for detecting subclinical cardiovascular disease (CVD), assessing pre-existing cardiac conditions before cancer treatment, and tracking changes during and after therapy. TEE has several inherent advantages: it is low-cost, widely available, free of ionizing radiation, and is generally patient-friendly. It is preferred for baseline risk assessment due to its ability to provide detailed quantitative and qualitative measurements of the structure and function of the LV, right ventricle (RV), left atrium (LA), and right atrium (RA), as well as pericardial disease [29–32]. Echocardiographic measurements in cardio-oncology are listed in Table 14.1.

Table 14.1 Echocardiographic measurements in cardio oncology

Echocardiography	Recommended measurements
Left heart chambers	
LV systolic function	3D LVEF/2D biplane Simpson's method
	(If the view is inadequate, using contrast is recommended)
	GLS by STE
	(In the absence of GLS by STE, TDI of mitral annulus is recommended)
LV diastolic function	LV filling pressure
	E/e' ratio
	Grading diastolic dysfunction
LV subclinical function	GLS by STE
	If GLS is not available, medial and lateral s' and MAPSE
Left atrium	LA dimension and function
	LAVI, LA area
Myocardial ischemia	WMSI
	Stress echocardiography
Right heart chambers	
Right ventricle	RV dimensions
	RV s'
	RV FAC
	TAPSE
	Pulmonary hypertension
Right atrium	RA dimension and function
Pericardial disease	Pericardial effusion
	Echocardiographic and Doppler signs of cardiac tamponade
Valvular heart disease	Cardiac valves should be carefully evaluated in patients before and after treatment
Cardiac masses	Tumor, metastasis

Abbreviations: *LA* left atrium, *DTI* Doppler Tissue Imaging, *EF* Ejection fraction, *LV* left ventricle, *RA* Right atrium, *RV* Right ventricle, *RVFAC* Right ventricular fractional area change; *s'* peak systolic velocity, *PW* Pulsed wave, *LAVI* Left atrium volume indexed, *MAPSE* Mitral annual plane systolic excursion, *TAPSE* Tricuspid annual plane systolic excursion, *WMSI* Wall motion score index

Left Heart Chambers

Left ventricular dysfunction can be divided into three main categories: (1) LV systolic dysfunction, identified by traditional indicators such as clinical symptoms of HF and a decreased LV ejection fraction (EF); (2) LV diastolic dysfunction; and (3) subclinical LV dysfunction [33, 34].

LV Systolic Dysfunction According to current guidelines, cancer therapy-related cardiac dysfunction is assessed based on a reduction in LVEF and/or relative changes in global longitudinal strain (GLS). Cardiotoxicity is defined as a 10% decrease in LVEF or a 5% drop accompanied by symptoms of HF [3, 35]. 3D echocardiography is the preferred method for assessing LVEF. If 3D echocardiography is not available, LVEF should be measured using 2D echocardiography with the biplane Simpson method. For patients with inadequate TTE images, adding ultrasound-enhancing contrast agents can help better visualize LV function and volumes when two or more LV segments are not clearly seen. While 3D echocardiography is more accurate than CMR for measuring LV volume and function, it is only feasible in about 60% of patients who have received anthracycline chemotherapy for breast cancer due to poor imaging conditions [36, 37]. Likewise, a baseline reduced LVEF or borderline LVEF (50 to 54%) is also a marker for stratifying the risk of developing cardiotoxicity from cancer therapies, especially those involving anthracyclines or trastuzumab. Additionally, an increased baseline indexed LV end-diastolic volume can predict major CV events, such as symptomatic HF or cardiac death, during anthracycline chemotherapy in patients with preserved LVEF [38, 39].

Furthermore, a decreased LVEF often represents a late manifestation of cardiotoxicity. Assessing myocardial deformation may help in detecting early changes in systolic dysfunction [29, 34]. Strain imaging, including GLS, has well-established normal values and variability. A reduction in peak GLS of over 15% can early predict cardiotoxicity (Fig. 14.1). This threshold is based on meta-analysis findings and helps maximize specificity, reduce overdiagnosis, and guide cardioprotective treatment. Evaluating GLS is especially important for patients with low-normal LVEF to detect asymptomatic myocardial damage. Consistency in GLS analysis using the same ven-

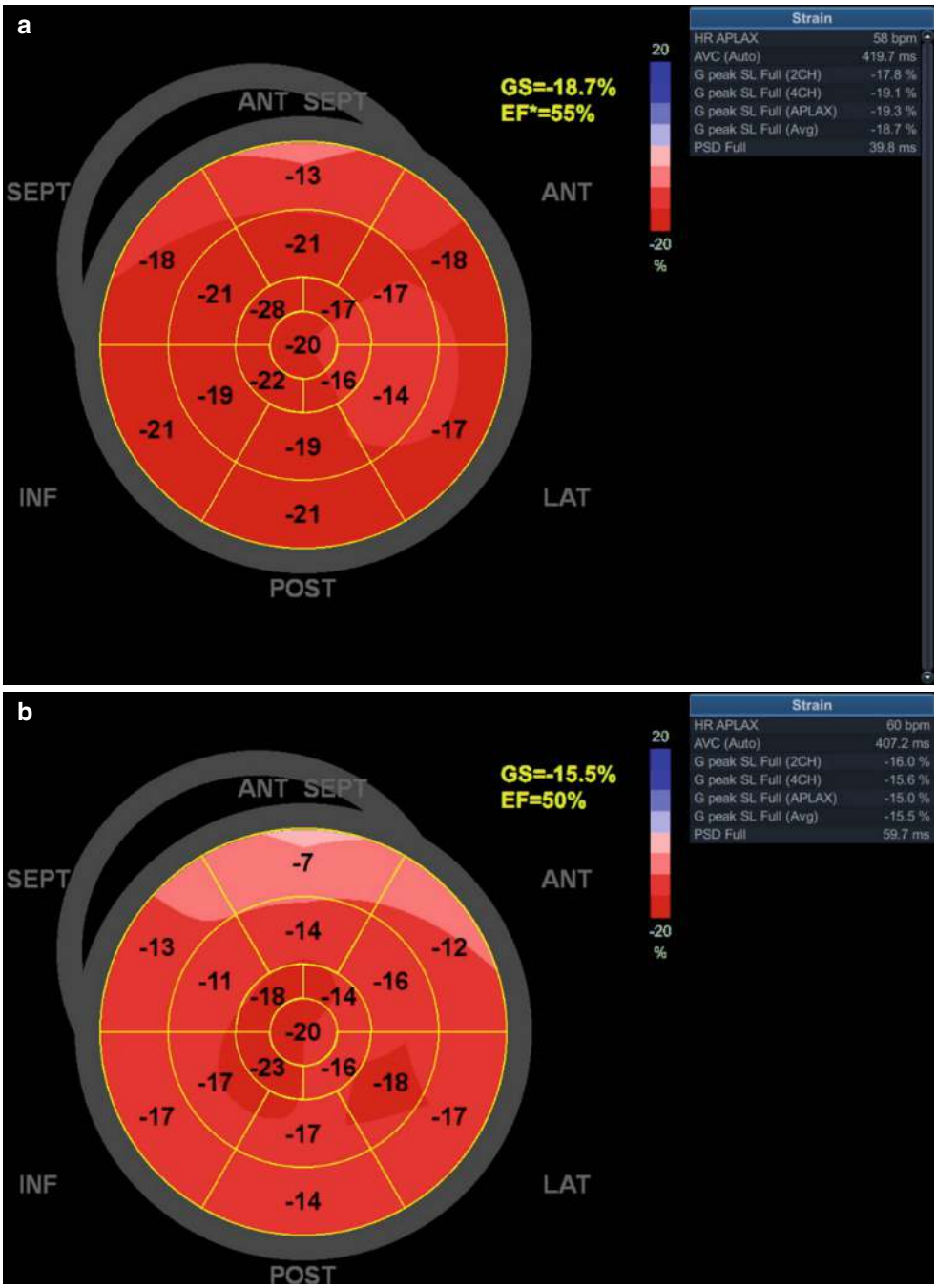


Fig. 14.1 (**a**) Baseline peak global longitudinal strain and (**b**) its reduction during follow-up, indicating early cardiotoxicity

dor is recommended during cancer treatment for accurate longitudinal comparisons [3, 40, 41].

LV Diastolic Dysfunction Monitoring diastolic dysfunction during cancer therapy is highly recommended. It is hypothesized that, similar to the ischemic cascade where blood flow mismatches and perfusion defects lead to diastolic dysfunction before systolic dysfunction occurs, diastolic dysfunction induced by cancer treatments might develop earlier than systolic dysfunction [42, 43]. Although the American Society of Echocardiography (ASE) guidelines advise the measurement of diastolic parameters during echocardiography, the ability of these parameters to predict chemotherapy-induced cardiotoxicity has not been consistently demonstrated and remains an area of ongoing research [44]. Clinical experience suggests that changes in diastolic function often precede detectable alterations in systolic function. Therefore, clinicians strongly advocate vigilant monitoring of diastolic function throughout cancer therapy. This includes evaluating parameters such as tissue relaxation, filling pressures (E/e'), and tissue Doppler indices. If any diastolic abnormalities are identified, it is important to pursue additional clinical evalu-

ations and imaging studies to ensure comprehensive monitoring and timely intervention [3, 44, 45].

LV Subclinical Dysfunction Recent efforts have focused on detecting early signs of myocardial disease and preventing LV dysfunction through a combination of biomarkers and advanced imaging techniques. In cardio-oncology, advanced methods like deformation imaging and myocardial mechanics assessments are used alongside traditional echocardiographic metrics such as LVEF and filling pressures to identify subclinical conditions [34, 40]. Despite their frequent use, the clinical impact of these advanced measures is not yet fully established. Particularly, GLS with speckle tracking and evaluations of LV function using mitral annular displacement by M-mode echocardiography or peak systolic velocity (s′) via pulsed-wave tissue Doppler are recommended for detecting chemotherapy-related cardiotoxicity. Guidelines advise measuring these myocardial mechanics at baseline and throughout treatment. A relative GLS reduction greater than 15% is likely indicative of abnormal changes when using the same ultrasound equipment [41, 46].

Left Atrium Increased LA dimension and volume, particularly LA maximal volume indexed (LAVI maximal) as an accurate marker of LV filling pressure. Reduced myocardial contraction of the LV can lead to increased end-diastolic volume, decreased ventricular compliance, and raised end-diastolic pressure, which results in high LV filling pressure. This increased volume load on the LV can cause LA remodeling [47, 48]. Additionally, the range of cardiotoxic effects now includes myocarditis caused by immune checkpoint inhibitors and cardiac dysfunction due to cytokine release syndrome from chimeric antigen receptor (CAR) T-cell therapy. There is also an anticipated rise in arrhythmias related to inflammation, such as atrial fibrillation [49, 50]. Recently, studies have highlighted the important role of LA strain as a valuable marker for detecting 'subclinical' or early diastolic dysfunction and subsequent LA dysfunction. It can also identify myocardial dysfunction in the LA of cancer patients undergoing chemotherapy, helping to predict CTR-CV before significant changes in left LVEF or clinical symptoms develop [51–53]

Right Heart Chambers

Right Ventricle The RV is often studied less than the LV in cardiovascular research, including in cardio-oncology. The unique geometry and position of the RV complicate its assessment. Traditional echocardiographic indices such as RV ejection fraction (RVEF), RV fractional area change (FAC), and tricuspid annular plane systolic excursion (TAPSE) often fail to detect subtle changes in RV systolic function in cancer patients [54, 55]. Evaluating RV diastolic function during or after chemotherapy has produced conflicting results, complicating the assessment of RV health in these patients. However, RV longitudinal strain (RV LS) has shown promise in reliably detecting myocardial injury, providing consistent results. It can identify RV cardiotoxicity almost simultaneously with LV cardiotoxicity, suggesting that cancer treatments have a uniform impact on the myocardium. Both RV GLS and RV free-wall longitudinal strain (RV FWLS) decrease during and/or after cancer treatment. Studies have shown that using 3D-speckle tracking imaging, a value of RV GLS less than −18.2% can indicate RV impairment with high sensitivity and specificity in patients with breast cancer. [56–59].

Studies, though limited, consistently show a decline in RVEF following anthracycline therapy in adult survivors of childhood cancer and breast cancer patients treated with anthracycline and trastuzumab [60, 61]. High-dose radiotherapy (>30 Gy), particularly when combined with chemotherapy, can lead to fibrosis and thinning of the RV myocardium over time. Additional mechanisms that may contribute to RV remodeling after radiotherapy include microvascular and macrovascular ischemia, accelerated atherosclerosis, and oxidative stress [62, 63].

Echocardiography is essential for monitoring RV dimensions and function in cardio-oncology. Continued research is needed to clarify the prognostic implications and improve the reliability of echocardiographic assessments in this field.

Right Atrium The assessment of the RA dimension and function in cardio-oncology is equally important. Changes in RA size and function can reflect underlying cardiac pathology and contribute to the overall assessment of right heart health in cancer patients. Echocardiographic evaluation of RA size and function, including RA area and strain measurements, can provide valuable insights into the impact of cancer treatments on the right heart [3, 54, 64]. Despite the challenges posed by the unique structures of the RV and RA, advanced techniques like RV longitudinal strain, 3D-speckle tracking imaging, and RA strain measurements offer promising tools for detecting cardiotoxicity [64].

Evaluation of Myocardial Ischemia

While cardiotoxicity from cancer therapy typically focuses on LV impairment, treatments can also cause/contribute to other cardiac syndromes, including coronary events, pericardial disease, valvular heart disease, pulmonary hypertension, and RV dysfunction. Treatments such as fluoropyrimidines,

platinum compounds, VEGF inhibitors, certain bcr-abl tyrosine kinase inhibitors, and radiotherapy have been implicated in myocardial ischemia and coronary events, including myocardial infarction. The mechanisms vary by drug and include accelerated atherosclerosis, coronary spasm, vascular endothelial damage, and arterial thrombotic events [65–67].

Resting echocardiographic diagnostic examinations, in coronary artery disease (CAD), are primarily limited to detecting regional wall motion abnormalities. In asymptomatic patients, moderate-to-severe dyssynergy has been observed in up to 17% of Hodgkin's lymphoma survivors treated with mediastinal radiotherapy (≥35 Gy). However, a hypokinetic LV segment may not necessarily indicate CAD but could reflect underlying myocardial disease [68, 69].

Stress-induced wall motion abnormalities are reliable markers of inducible ischemia in patients undergoing cancer therapies associated with myocardial ischemia and who are at intermediate or high risk of CAD. Thus, stress echocardiography is recommended as the primary cardiac imaging technique in these patients. Depending on the patient's exercise capacity, either physical exercise or pharmacological agents (such as dobutamine or dipyridamole) can be used for stress testing to diagnose inducible ischemia. Myocardial contrast agents can also be employed to improve border detection and identification of LV dyssynergy in patients with suboptimal echocardiographic windows. One of the main advantages of stress echocardiography is the absence of radiation exposure, a benefit it shares with stress CMR, which also offers high diagnostic accuracy for inducible ischemia but is more expensive and less widely available [65].

Nuclear stress testing (SPECT and PET) is a viable alternative, particularly when stress echocardiography is challenging, such as in breast cancer patients with implants or those who have had a mastectomy. Cardiac computed tomography (CCT) should be primarily used to identify coronary atherosclerosis in cancer patients who have undergone mediastinal radiotherapy, even many years after treatment completion. CT coronary angiography provides a non-invasive anatomical assessment of coronary artery disease, and with its excellent negative predictive value, it reliably excludes significant coronary disease and assists in risk stratification before surgery or the administration of high-risk drugs [70].

Pericardial Disease

Pericardial disease is a significant concern in cardio-oncology, arising from both chemotherapy and radiotherapy treatments. Pericarditis can arise acutely during radiotherapy, potentially leading to pericardial constriction that typically manifests several years later, often over a decade post-treatment. This condition has a cumulative incidence of up to 5% in patients who have received mediastinal radiotherapy. A deep 'x' descent and predominant systolic flow into the right atrium in patients with raised venous pressure that is not responding to diuretic is a supportive diagnostic criteria of pericardial constriction, which reverts back to normal early diastolic events after pericardiectomy (Chap. 15).

Echocardiography plays a crucial role in the early diagnosis and management of these conditions, while CT imaging is valuable for detecting late-stage complications such as pericardial calcification. Traditional 2D echocardiography is effective in identifying pericardial effusions, although multiple views may be needed if the effusion is loculated. Understanding these risks and utilizing appropriate diagnostic tools are essential for managing the cardiovascular health of cancer patients [71–73].

Valvular Heart Disease

Patients who have undergone radiation therapy, especially to the mediastinum, face an increased risk of long-term CV issues, including radiation-induced heart valve disease, pericardial disease, and CAD. Transthoracic echocardiography is the primary diagnostic tool for identifying valvular damage in these individuals. Distinctive echocardiographic features help differentiate radiation-induced valvular disease from rheumatic heart disease, with commissural fusion indicating radiation effects, while involvement of mitral leaflet tips suggests rheumatic disease.

Guidelines from the EACVI and ASE recommend annual physical examinations to detect symptoms or signs of radiation-induced heart disease. If symptoms are identified, further evaluation is needed. For asymptomatic patients, a transthoracic echocardiogram is advised 5 years post-exposure for high-risk individuals—those who received anterior or left-side chest radiation and have additional risk factors like smoking, diabetes, hypertension, hyperlipidemia, or obesity—and 10 years post-exposure for all other patients [3, 65, 66].

While valve disease is a rare consequence of chemotherapy, it is a well-documented late effect of high-dose mediastinal radiotherapy, particularly with older techniques like mantle field radiotherapy. There is typically a 10–20 year delay between radiation exposure and the development of clinically significant valve disease, with prevalence rates varying from 5 to 32% in Hodgkin's lymphoma survivors. Surgical outcomes for these patients often lag behind those undergoing valve replacement for other conditions, underscoring the importance of early detection and the growing role of percutaneous valve interventions [66, 74]. Echocardiography remains the gold standard for evaluating valvular heart disease, offering both qualitative and quanti-

tative insights into stenotic and regurgitant valves. Additional imaging techniques, such as CT and CMR, complement echocardiography. CT is useful for detailed assessment of stenotic valves and identifying suspected endocarditis, particularly when used with PET-CT. CMR provides accurate flow measurements across valves and is particularly valuable when echocardiographic results are inconclusive [67, 70, 72].

Cardiac Masses

Echocardiography is the first-line imaging modality for detecting cardiac masses due to its effectiveness in visualizing small and rapidly moving structures, such as valve vegetations. It provides real-time imaging and can reveal key characteristics of masses, including size, location, and mobility. It is particularly useful for initial diagnosis and assessment of mass-related hemodynamic impacts.

For more comprehensive evaluation, including assessing tissue invasion and differentiating between mass types, advanced imaging techniques may be required. CT offers detailed spatial resolution to define the mass anatomy and relationship with surrounding tissues. CMR adds value with its superior tissue characterization capabilities, utilizing techniques such as T1- and T2-weighted imaging, gadolinium enhancement, and perfusion imaging to evaluate mass nature and resectability. PET/CT imaging can assist in differentiating benign from malignant tumors and detecting metastases, although it requires precise patient preparation to ensure accurate results [70, 75, 76].

Prevention and Monitoring of Cardiovascular Complications During Cancer Therapy

Cancer therapies have significantly enhanced survival rates across various malignancies, yet this often comes with substantial risks to CV health. To safeguard long-term CV well-being, vigilant prevention and monitoring strategies are essential. Among these strategies, echocardiography plays a pivotal role in both preventing and monitoring CV complications through early detection of myocardial dysfunction. Cancer treatments, including chemotherapy agents like anthracyclines, targeted therapies such as tyrosine kinase inhibitors (TKIs), and radiation therapy, are known to cause CV complications. These can range from HF and cardiomyopathy to arrhythmias and pericardial disease. The effective management of these risks requires a proactive approach in both prevention, i.e early detection, and monitoring [77, 78].

Risk Assessment and Stratification The initial step in preventing CV complications involves thorough risk assessment and clinical stratification. Prior to initiating cancer therapy, a detailed evaluation is critical, particularly for patients with pre-existing CV conditions or those prescribed potentially cardiotoxic treatments. Echocardiography is instrumental in this phase, in providing baseline information on cardiac structure and function. This baseline assessment allows establishing tailored treatment plans that consider individual CV risk factors such as pre-existing heart conditions and the anticipated cardiotoxicity of the planned therapy [78–80].

Dose Adjustment and Therapy Modification For patients identified as high-risk based on echocardiographic findings and other clinical factors, adjusting the dose and modifying the cancer therapy can be crucial to avoid deterioration of cardiac function. For example, in the context of anthracycline therapy, regular echocardiographic assessments can assist decision making on dose reductions or the incorporation of cardioprotective agents like dexrazoxane. By monitoring cardiac function throughout treatment, healthcare providers can make informed adjustments to minimize the risk of cardiotoxicity [81–83].

Cardioprotective Medications While cardioprotective medications such as beta-blockers, ACE inhibitors, and ARBs are important in preventing cardiotoxicity, their use is often guided by echocardiographic findings. For instance, if echocardiography reveals early signs of left ventricular dysfunction, initiating or adjusting cardioprotective therapy can help mitigating further damage and preserve cardiac function [3, 84–86].

Cardiovascular Investigations

Echocardiography: Echocardiography is central to monitoring CV health during cancer therapy. Transthoracic echocardiography provides detailed, real-time insights into cardiac function, including the assessment of left and right ventricular performance. Key echocardiographic parameters, such as LVEF and GLS are critical for detecting early signs of cardiotoxicity. Regular echocardiographic evaluations are typically performed before starting therapy and periodically throughout treatment. This ongoing monitoring allows early detection of changes in cardiac function, which is crucial for initiating timely interventions and preventing severe cardiotoxic effects. By providing detailed insights into cardiac function and facilitating early detection of cardiotoxicity, echocardiography enables timely interventions and the need for adjustment of cancer treatment plans. This proactive approach, combined with advanced imaging techniques, biomarkers, and multidisciplinary care, ensures optimal management of CV risks and enhances

long-term outcomes and quality of life for cancer survivors [3, 31–33, 46].

Other Imaging Techniques: Though echocardiography is the primary tool for routine monitoring, advanced imaging techniques such as CMR and CT can complement echocardiographic findings. CMR offers high-resolution imaging of myocardial tissues, useful for assessing myocardial fibrosis and edema that might not be visible on echocardiography. CT, particularly with contrast, helps evaluating coronary artery disease and pericardial conditions. These techniques can provide additional diagnostic information when echocardiographic images are inconclusive or when a more detailed anatomical assessment is required [66, 72, 76].

Biomarkers: Cardiac biomarkers, including troponins and natriuretic peptides, serve as supplementary tools in monitoring cardiotoxicity. Elevated levels of these biomarkers, when measured alongside echocardiographic assessments, can detect myocardial injury, thus prompting further investigation. This integrated approach enhances accuracy of CV monitoring and guides necessary treatment adjustments [73, 87, 88].

Stress Testing: Stress testing, including stress echocardiography, evaluates CV function under stress conditions and identifies inducible ischemia. This approach is particularly valuable for patients at intermediate to high risk of coronary artery disease due to their cancer therapy. Stress echocardiography provides additional information on myocardial function and helps identifying patients who may benefit from further cardioprotective measures or modifications to their cancer therapy [65, 69, 70].

Patient Education and Lifestyle Modifications Educating patients about CV risks associated with cancer therapy and encouraging lifestyle modifications are crucial for prevention. Patients should be informed about the importance of adhering to prescribed medications, maintaining a heart-healthy diet, engaging in regular physical activity, and managing CV risk factors such as hypertension and diabetes [89–91].

References

1. Zamorano JL, Lancellotti P, Rodriguez Muñoz D, Aboyans V, Asteggiano R, Galderisi M, et al. 2016 ESC position paper on cancer treatments and cardiovascular toxicity developed under the auspices of the ESC Committee for Practice Guidelines. Eur Heart J. 2016;37:2768–801.
2. Lancellotti P, Suter TM, López-Fernández T, Galderisi M, Lyon AR, Van Der Meer P, et al. Cardio-oncology services: rationale, organization, and implementation. Eur Heart J. 2019;40:1756–63.
3. Lyon AR, López-Fernández T, Couch LS, Asteggiano R, Aznar MC, Bergler-Klein J, et al. 2022 ESC guidelines on cardio-oncology developed in collaboration with the European Hematology Association (EHA), the European Society for Therapeutic Radiology and Oncology (ESTRO) and the International Cardio-Oncology Society (IC-OS). Eur Heart J. 2022;43:4229–361.
4. European Society of Cardiology. ESC CardioMed. 3rd ed. Oxford: Oxford University Press; 2018.
5. Swain SM, Whaley FS, Ewer MS. Congestive heart failure in patients treated with doxorubicin: a retrospective analysis of three trials. Cancer. 2003;97:2869–79.
6. Doroshow JH. Anthracycline antibiotic-stimulated superoxide, hydrogen peroxide, and hydroxyl radical production by NADH dehydrogenase. Cancer Res. 1983;43:4543–51.
7. Lim CC, Zuppinger C, Guo X, Kuster GM, Helmes M, Eppenberger HM, Suter TM, Liao R, Sawyer DB. Anthracyclines induce calpain-dependent titin proteolysis and necrosis in cardiomyocytes. J Biol Chem. 2004;279:8290–9.
8. Steinherz LJ, Steinherz PG, Tan CT, Heller G, Murphy ML. Cardiac toxicity 4 to 20 years after completing anthracycline therapy. JAMA. 1991;266:1672–7.
9. Cardinale D, Colombo A, Bacchiani G, Tedeschi I, Meroni CA, Veglia F, Civelli M, Lamantia G, Colombo N, Curigliano G, Fiorentini C, Cipolla CM. Early detection of anthracycline cardiotoxicity and improvement with heart failure therapy. Circulation. 2015;131:1981–8.
10. Chow EJ, Chen Y, Kremer LC, Breslow NE, Hudson MM, Armstrong GT, Border WL, Feijen EA, Green DM, Meacham LR, Meeske KA, Mulrooney DA, Ness KK, Oeffinger KC, Sklar CA, Stovall M, van der Pal HJ, Weathers RE, Robison LL, Yasui Y. Individual prediction of heart failure among childhood cancer survivors. J Clin Oncol. 2015;33:394–402.
11. Gottdiener JS, Appelbaum FR, Ferrans VJ, Deisseroth A, Ziegler J. Cardiotoxicity associated with high-dose cyclophosphamide therapy. Arch Intern Med. 1981;141:758–63.
12. Mackey JR, Martin M, Pienkowski T, Rolski J, Guastalla JP, Sami A, et al. Adjuvant docetaxel, doxorubicin, and cyclophosphamide in node-positive breast cancer: 10-year follow-up of the phase 3 randomised BCIRG 001 trial. Lancet Oncol. 2013;14:72–80.
13. Gollerkeri A, Harrold L, Rose M, Jain D, Burtness BA. Use of paclitaxel in patients with pre-existing cardiomyopathy: a review of our experience. Int J Cancer. 2001;93:139–41.
14. Slamon DJ, Leyland-Jones B, Shak S, Fuchs H, Paton V, Bajamonde A, Fleming T, Eiermann W, Wolter J, Pegram M, Baselga J, Norton L. Use of chemotherapy plus a monoclonal antibody against HER2 for metastatic breast cancer that overexpresses HER2. N Engl J Med. 2001;344:783–92.
15. Goldhirsch A, Gelber RD, Piccart-Gebhart MJ, de Azambuja E, Procter M, Suter TM, Jackisch C, et al. Trial Study Team. 2 years versus 1 year of adjuvant trastuzumab for HER2-positive breast cancer (HERA): an open-label, randomised controlled trial. Lancet. 2013;382:1021–8.
16. Cote GM, Sawyer DB, Chabner BA. ERBB2 inhibition and heart failure. N Engl J Med. 2012;367:2150–3.
17. Yu AF, Yadav NU, Lung BY, Eaton AA, Thaler HT, Hudis CA, Dang CT, Steingart RM. Trastuzumab interruption and treatment-induced cardiotoxicity in early HER2-positive breast cancer. Breast Cancer Res Treat. 2015;149:489–95.
18. de Azambuja E, Bedard PL, Suter T, Piccart-Gebhart M. Cardiac toxicity with anti-HER-2 therapies: what have we learned so far? Target Oncol. 2009;4:77–88.
19. Lenihan D, Suter T, Brammer M, Neate C, Ross G, Baselga J. Pooled analysis of cardiac safety in patients with cancer treated with pertuzumab. Ann Oncol. 2012;23:791–800.
20. Ghatalia P, Morgan CJ, Je Y, Nguyen PL, Trinh QD, Choueiri TK, Sonpavde G. Congestive heart failure with vascular endothelial growth factor receptor tyrosine kinase inhibitors. Crit Rev Oncol Hematol. 2015;94:228–37.

21. Steingart RM, Bakris GL, Chen HX, Chen MH, Force T, Ivy SP, Leier CV, Liu G, Lenihan D, Lindenfeld J, Maitland ML, Remick SC, Tang WH. Management of cardiac toxicity in patients receiving vascular endothelial growth factor signaling pathway inhibitors. Am Heart J. 2012;163:156–63.
22. Qi WX, Shen Z, Tang LN, Yao Y. Congestive heart failure risk in cancer patients treated with vascular endothelial growth factor tyrosine kinase inhibitors: a systematic review and meta-analysis of 36 clinical trials. Br J Clin Pharmacol. 2014;78:748–62.
23. Valent P, Hadzijusufovic E, Schernthaner GH, Wolf D, Rea D, le Coutre P. Vascular safety issues in CML patients treated with BCR/ABL1 kinase inhibitors. Blood. 2015;125:901–6.
24. Groarke JD, Cheng S, Moslehi J. Cancer-drug discovery and cardiovascular surveillance. N Engl J Med. 2013;369:1779–81.
25. Stewart AK, Rajkumar SV, Dimopoulos MA, Masszi T, Spicka I, Oriol A, et al. ASPIRE Investigators. Carfilzomib, lenalidomide, and dexamethasone for relapsed multiple myeloma. N Engl J Med. 2015;372:142–52.
26. Jaworski C, Mariani JA, Wheeler G, Kaye DM. Cardiac complications of thoracic irradiation. J Am Coll Cardiol. 2013;61:2319–28.
27. Hooning MJ, Botma A, Aleman BM, Baaijens MH, Bartelink H, Klijn JG, Taylor CW, van Leeuwen FE. Long-term risk of cardiovascular disease in 10-year survivors of breast cancer. J Natl Cancer Inst. 2007;99:365–75.
28. Armstrong GT, Joshi VM, Ness KK, Marwick TH, Zhang N, Srivastava D, et al. Comprehensive echocardiographic detection of treatment-related cardiac dysfunction in adult survivors of childhood cancer: results from the St. Jude Lifetime Cohort Study. J Am Coll Cardiol. 2015;65:2511–22.
29. Santoro C, Arpino G, Esposito R, Lembo M, Paciolla I, Cardalesi C, et al. 2D and 3D strain for detection of subclinical anthracycline cardiotoxicity in breast cancer pa- tients: A balance with feasibility. Eur Heart J Cardiovasc Imaging. 2017;18:930–6.
30. Zhang KW, Finkelman BS, Gulati G, Narayan HK, Upshaw J, Narayan V, et al. Abnormalities in 3-dimensional left ventricular mechanics with anthracycline chemotherapy are associated with systolic and diastolic dysfunction. JACC Cardiovasc Imaging. 2018;11:1059–68.
31. Lang RM, Badano LP, Mor-Avi V, Afilalo J, Armstrong A, Ernande L, et al. Recommendations for cardiac chamber quantification by echocardiography in adults: an update from the American Society of Echocardiography and the European Association of Cardiovascular Imaging. Eur Heart J Cardiovasc Imaging. 2015;16:233–70.
32. Thavendiranathan P, Grant AD, Negishi T, Plana JC, Popović ZB, Marwick TH. Reproducibility of echocardiographic techniques for sequential assessment of left ventricular ejection fraction and volumes: application to patients undergoing cancer chemotherapy. J Am Coll Cardiol. 2013;61:77–84.
33. Armenian SH, Lacchetti C, Barac A, Carver J, Constine LS, Denduluri N, et al. Prevention and monitoring of cardiac dysfunction in survivors of adult cancers: American Society of Clinical Oncology Clinical Practice Guideline. J Clin Oncol. 2017;35(8):893–911.
34. Clasen SC, Wald JW. Left ventricular dysfunction and chemotherapeutic agents. Curr Cardiol Rep. 2018;20:20.
35. Avelar E, Strickland CR, Rosito G. Role of imaging in cardio-oncology. Curr Treat Options Cardiovasc Med. 2017;19:46.
36. Curigliano G, Cardinale D, Suter T, Plataniotis G, de Azambuja E, Sandri MT, et al. Cardiovascular toxicity induced by chemotherapy, targeted agents and radiotherapy: ESMO Clinical Practice Guidelines. Ann Oncol. 2012;23(Suppl 7):vii155–66.
37. Porter TR, Mulvagh SL, Abdelmoneim SS, Becher H, Belcik JT, Bierig M, et al. Clinical applications of ultrasonic enhancing agents in echocardiography: 2018 American Society of Echocardiography Guidelines Update. J Am Soc Echocardiogr. 2018;31:241–74.
38. Romond EH, Jeong JH, Rastogi P, Swain SM, Geyer CE, Ewer MS, et al. Seven-year follow-up assessment of cardiac function in NSABP B-31, a randomized trial com- paring doxorubicin and cyclophosphamide followed by paclitaxel (ACP) with ACP plus trastuzumab as adjuvant therapy for patients with node-positive, human epi- dermal growth factor receptor 2-positive breast cancer. J Clin Oncol. 2012;30:3792–9.
39. Mousavi N, Tan TC, Ali M, Halpern EF, Wang L, Scherrer-Crosbie M. Echocardiographic parameters of left ventricular size and function as predictors of symptomatic heart failure in patients with a left ventricular ejection fraction of 50–59% treated with anthracyclines. Eur Heart J Cardiovasc Imaging. 2015;16:977–84.
40. Yingchoncharoen T, Agarwal S, Popovic ZB, et al. Nor- mal ranges of left ventricular strain: a meta-analysis. J Am Soc Echocardiogr. 2013;26:185–91.
41. Oikonomou EK, Kokkinidis DG, Kampaktsis PN, Amir EA, Marwick TH, Gupta D, et al. Assessment of prognostic value of left ventricular global longitudinal strain for early prediction of chemotherapy-induced cardiotoxicity: a systematic review and meta-analysis. JAMA Cardiol. 2019;4:1007–18.
42. Dorup I, Levitt G, Sullivan I, et al. Prospective longitu- dinal assessment of late anthracycline cardiotoxicity after childhood cancer: the role of diastolic function. Heart. 2004;90(10):1214–6.
43. Stoddard MF, Seeger J, Liddell NE, et al. Prolongation of isovolumetric relaxation time as assessed by Dopp- ler echocardiography predicts doxorubicin-induced systolic dysfunction in humans. J Am Coll Cardiol. 1992;20(1):62–9.
44. Plana JC, Galderisi M, Barac A, Ewer MS, Ky B, Scherrer-Crosbie M, et al. Expert consensus for multimodality imaging evaluation of adult patients during and after cancer therapy: a report from the American Society of Echocardiography and the European Association of Cardiovascular Imaging. Eur Heart J Cardiovasc Imaging. 2014;15(10):1063–93.
45. Galderisi M, Cosyns B, Edvardsen T, Cardim N, Delgado V, Di Salvo G, et al. Standardization of adult transthoracic echocardiography reporting in agreement with recent chamber quantification, diastolic function, and heart valve disease re- commendations: an expert consensus document of the European Association of Cardiovascular Imaging. Eur Heart J Cardiovasc Imaging. 2017;18:1301–10.
46. Thavendiranathan P, Poulin F, Lim KD, Plana JC, Woo A, Marwick TH. Use of myocardial strain imaging by echocardiography for the early detection of cardiotoxicity in patients during and after cancer chemotherapy: a systematic review. J Am Coll Cardiol. 2014;63(25 Pt A):2751–68.
47. Yaylali YT, Saricopur A, Yurtdas M, Senol H, Gokoz-Dogu G. Atrial function in patients with breast cancer after treatment with Anthracyclines. Arq Bras Cardiol. 2016;107:411–9.
48. Chen N, Liu A, Sun S, Wei H, Sun Q, Shang Z, et al. Evaluation of left atrial function and mechanical dispersion in breast cancer patients after chemotherapy. Clin Cardiol. 2022;45:540–8.
49. Herrmann J. Adverse cardiac effects of cancer therapies: cardiotoxicity and arrhythmia. Nat Rev Cardiol. 2020;17:474–502.
50. Farmakis D, Filippatos G. Cancer begets atrial fibrillation … and vice versa? Eur Heart J. 2024;45:2214–6.
51. Park H, Kim KH, Kim HY, Cho JY, Yoon HJ, Hong YJ, Park HW, Kim JH, Ahn Y, Jeong MH, et al. Left atrial longitudinal strain as a predictor of Cancer therapeutics-related cardiac dysfunction in patients with breast Cancer. Cardiovasc. Ultrasound. 2020;18:28.
52. Bytyçi I, Bajraktari G. Left atrial changes in early stages of heart failure with preserved ejection fraction. Echocardiography. 2016;33:1479–87.
53. Goyal A, Abbasi HQ, Yakkali S, Khan AM, Tariq MD, Sohail AH, Khan R. Left atrial strain as a predictor of early anthracycline-induced chemotherapy-related cardiac dysfunction: a pilot systematic review and meta-analysis. J Clin Med. 2024;13:3904.

54. Keramida K, Farmakis D. Right ventricular involvement in cancer therapy-related cardiotoxicity: the emerging role of strain echocardiography. Heart Fail Rev. 2021;26:1189–93.
55. Rossetto L, Di Lisi D, Madaudo C, Sinagra FP, Di Palermo A, Triolo OF, et al. Right ventricle involvement in patients with breast cancer treated with chemotherapy. Cardiooncology. 2024;10:24.
56. Zhang L, Zhang R, Shuai P, Chen J, Yin L, et al. A global case meta-analysis of three-dimensional speckle tracking for evaluating the cardiotoxicity of anthracycline chemotherapy in breast cancer. Front Cardiovasc Med. 2022; 9:942620.
57. Keramida K, Farmakis D, Bingcang J, Sulemane S, Sutherland S, Bingcang RA, et al. Longitudinal changes of right ventricular deformation mechanics during trastuzumab therapy in breast cancer patients. Eur J Heart Fail. 2019;21:529–35.
58. Boczar KE, Aseyev O, Sulpher J, Johnson C, Burwash IG, Turek M, et al. Right heart function deteriorates in breast cancer patients undergoing anthracycline-based chemotherapy. Echo Res Pract. 1016;3(3):79–84.
59. Wang Y, Zhang P, Liu K, Zhang J, Ma X, Li L, et al. Evaluation of changes in right ventricular myocardial mechanical properties in breast cancer patients receiving pirarubicin using three-dimensional speckle tracking imaging. Nan fang yi ke da xue xue bao = J South Med Univ. 2018;38(9):1032–8.
60. Christiansen JR, Massey R, Dalen H, Kanellopoulos A, Hamre H, Ruud E, et al. Right ventricular function in long-term adult survivors of childhood lymphoma and acute lymphoblastic leukaemia. Eur Heart J Cardiovasc Imaging. 2016;17(7):735–41.
61. Lange SA, Ebner B, Wess A, Kogel M, Gajda M, Hitschold T, et al. Echocardiography signs of early cardiac impairment in pa- tients with breast cancer and trastuzumab therapy. Clin Res Cardiol. 2012;101(6):415–26.
62. Tuohinen SS, Skytta T, Virtanen V, Luukkaala T, Kellokumpu-Lehtinen PL, Raatikainen P. Early effects of adjuvant breast cancer radiotherapy on right ventricular systolic and diastolic function. Anticancer Res. 2015;35(4):2141–7.
63. Murbraech K, Holte E, Broch K, Smeland KB, Holte H, Rosner A, et al. Impaired right ventricular function in long-term lymphoma survivors. J Am Soc Echocardiogr. 2016;29(6):528–36.
64. Tadic M, Cuspidi C, Hering D, Venneri L, Grozdic-Milojevic I. Radiotherapy-induced right ventricular remodelling: the missing piece of the puzzle. Arch Cardiovasc Dis. 2017;110(2):116–23.
65. Plana JC, Galderisi M, Barac A, Ewer MS, Ky B, Scherrer-Crosbie M, et al. Expert consensus for multimodality imaging evaluation of adult patientsduring and after cancer therapy: a report from the American Society of Echocardiography and the European Association of Cardiovascular Imaging. J Am Soc Echocardiogr. 2014;27:911–39.
66. Lancellotti P, Nkomo VT, Badano LP, Bergler-Klein J, Bogaert J, Davin L, et al. European society of cardiology working groups on nuclear cardiology and cardiac computed tomography and cardiovascular magnetic resonance; american society of nuclear cardiology; society for cardiovascular magnetic resonance; society of cardiovascular computed tomography. expert consensus for multi-modality imaging evaluation of cardiovascular complications of radiotherapy in adults: a report from the european association of cardiovascular imaging and the American society of echocardiography. Eur Heart J Cardiovasc Imaging. 2013;14:721–40.
67. Addison D, Neilan TG, Barac A, Scherrer-Crosbie M, Okwuosa TM, Plana JC, et al. American heart association council on cardiovascular radiology and intervention; cardio-oncology committee of the council on clinical cardiology and council on genomic and precision medicine; and council on cardiovascular and stroke nursing. cardiovascular imaging in contemporary cardio-oncology: a scientific statement from the American heart association. Circulation. 2023;148:1271–86.
68. Lange SA, Reinecke H. Coronary artery disease and cancer: treatment and prognosis regarding gender differences. Cancers (Basel). 2022;14:434.
69. Hamada H, Ohkubo T, Maeda M, Ogawa S. Evaluation of cardiac reserved function by high-dose dobutamine-stress echocardiography in asymptomatic anthracycline-treated survivors of childhood. Cancer. 2006;48:313–20.
70. Cottin Y, L'huillier I, Casasnovas O, Geoffroy C, Caillot D, Zeller M, et al. Dobutamine stress echocardiography identifies anthracycline cardiotoxicity. Eur J Echocardiogr. 2000;1:180–3.
71. Danad I, Szymonifka J, Twisk JWR, Norgaard BL, Zarins CK, Knaapen P, et al. Diagnostic performance of cardiac imaging methods to diagnose ischaemia-causing coronary artery disease when directly compared with fractional flow reserve as a reference standard: a meta-analysis. Eur Heart J. 2017;38:991–8.
72. Gambril JA, Chum A, Goyal A, Ruz P, Mikrut K, Simonetti O, et al. Cardiovascular imaging in cardio-oncology: the role of echocardiography and cardiac MRI in modern cardio-oncology. Heart Fail Clin. 2022;18:455–78.
73. Campia U, Moslehi JJ, Amiri-Kordestani L, et al. Cardio-oncology: vascular and metabolic perspectives: a scientific statement from the American Heart Association. Circulation. 2019;139:e579–602.
74. Bhakta N, Liu Q, Yeo F, Baassiri M, Ehrhardt MJ, Srivastava DK, Metzger ML, et al. Cumulative burden of cardiovascular morbidity in paediatric, adolescent, and young adult survivors of Hodgkin's lymphoma: an analysis from the St Jude Lifetime Cohort Study. Lancet Oncol. 2016;17:1325–34.
75. Fussen S, De Boeck BWL, Zellweger MJ, Bremerich J, Goetschalckx K, Zuber M, et al. Cardiovascular magnetic resonance imaging for diagnosis and clinical management of suspected cardiac masses and tumours. Eur Heart J. 2011;32:1551–60.
76. Rahbar K, Seifarth H, Schäfers M, Stegger L, Hoffmeier A, Spieker T, et al. Differentiation of malignant and benign cardiac tumors using 18F-FDG PET/CT. J Nucl Med. 2012;53:856–63.
77. Visseren FLJ, Mach F, Smulders YM, Carballo D, Koskinas KC, Bäck M, et al. 2021 ESC Guidelines on cardiovascular disease prevention in clinical practice. Eur Heart J. 2021;42:3227–337.
78. Ferdinandy P, Baczkó I, Bencsik P, Giricz Z, Görbe A, Pacher P, et al. Definition of hidden drug cardiotoxicity: paradigm change in cardiac safety testing and its clinical implications. Eur Heart J. 2019;40:1771–7.
79. Lyon AR, Dent S, Stanway S, Earl H, Brezden-Masley C, Cohen-Solal A, et al. Baseline cardiovascular risk assessment in cancer patients scheduled to receive cardiotoxic cancer therapies: a position statement and new risk assessment tools from the Cardio-Oncology Study Group of the Heart Failure Association of the European Society. Eur J Heart Fail. 2020;22:1945–60.
80. Oliveira GH, Al-Kindi SG, Guha A, Dey AK, Rhea IB, DeLima MJ. Cardiovascular risk assessment and management of patients undergoing hematopoietic cell transplant- ation. Bone Marrow Transplant. 2021;56:544–55.
81. Van Nimwegen FA, Schaapveld M, Cutter DJ, Janus CPM, Krol ADG, Hauptmann M, et al. Radiation dose-response relationship for risk of coronary heart disease in survivors of Hodgkin lymphoma. J Clin Oncol. 2016;34:235–43.
82. Jacob S, Camilleri J, Derreumaux S, Walker V, Lairez O, Lapeyre M, et al. Is mean heart dose a relevant surrogate parameter of left ventricle and coronary arteries exposure during breast cancer radiotherapy: a dosimetric evaluation based on individually-

determined radiation dose (BACCARAT study). Radiat Oncol. 2019;14:29.
83. Persson GF, Scherman Rydhög J, Josipovic M, Maraldo MV, Nygård L, Costa J, et al. Deep inspiration breath-hold volumetric modulated arc radiotherapy decreases dose to mediastinal structures in locally advanced lung cancer. Acta Oncol (Madr). 2016;55:1053–6.
84. Kalam K, Marwick TH. Role of cardioprotective therapy for prevention of cardiotoxicity with chemotherapy: a systematic review and meta-analysis. Eur J Cancer. 2013;49:2900–9.
85. Li X, Li Y, Zhang T, Xiong X, Liu N, Pang B, et al. Role of cardioprotective agents on chemotherapy-induced heart failure: a systematic review and network meta-analysis of randomized controlled trials. Pharmacol Res. 2020;151:104577.
86. Fang K, Zhang Y, Liu W, He C. Effects of angiotensin-converting enzyme inhibitor/ angiotensin receptor blocker use on cancer therapy-related cardiac dysfunction: a meta-analysis of randomized controlled trials. Heart Fail Rev. 2021;26:101–9.
87. Demissei BG, Hubbard RA, Zhang L, Smith AM, Sheline K, McDonald C, et al. Changes in cardiovascular biomarkers with breast cancer therapy and associations with cardiac dysfunction. J Am Heart Assoc. 2020;9:e014708.
88. Pavo N, Raderer M, Hülsmann M, Neuhold S, Adlbrecht C, Strunk G, et al. Cardiovascular biomarkers in patients with cancer and their association with all- cause mortality. Heart. 2015;101:1874–80.
89. Sharifi-Rad J, Rodrigues CF, Sharopov F, Docea AO, Karaca AC, Sharifi-Rad M, et al. Diet, lifestyle and cardiovascular diseases: linking pathophysiology to cardioprotec- tive effects of natural bioactive compounds. Int J Environ Res Public Health. 2020;17:2326.
90. Michos ED, Marshall CH. Healthy lifestyle benefits both cancer and cardiovascular disease: more bang for the buck. JACC Cardio Oncol. 2021;3:675–7.
91. Cao Z, Xu C, Yang H, Li S, Wang Y. The role of healthy lifestyle in cancer incidence and temporal transitions to cardiometabolic disease. JACC CardioOncol. 2021;3:663–74.

The Left Atrium

15

Alessandro Campora, Matteo Lisi, Matteo Cameli, and Michael Y. Henein

Left Atrial Anatomical, Geometrical and Structural Features

The left atrium (LA) is the cardiac chamber most posteriorly situated in the chest. It is anteriorly connected to the aortic root, from which it is separated by the transverse pericardial sinus. Posteriorly, the LA is related to the tracheal bifurcation, the oesophagus, the descending aorta and the vertebral column. The LA has 4 main anatomical components: the vestibule, the appendage, the portion of the pulmonary veins outlet and the septal portion. Because of the LA proximity to the esophagus, transoesophageal echocardiography (TOE) has become the echocardiographic investigation of choice for the assessment of LA anatomy.

Left Atrial Physiology

LA plays a pivotal role in maintaining optimum cardiac performance and LV filling. LA impacts LV filling volume through its reservoir, conduit and booster pump functions, with a close interdependence with the LV function. During the cardiac cycle, LA performs three different functions: during LV systole and isovolumic relaxation, it acts as a reservoir, receiving blood from the pulmonary veins and storing energy in the form of restoring forces. During early LV diastole and diastasis, it acts as a conduit, transferring blood into the LV via a small pressure difference during early diastole and passively from the pulmonary veins into the LV during diastasis. During LV late diastole, LA acts as an active pump, augmenting LV stroke volume by approximately 20-30% in normal subjects and substantially more in the presence of LV dysfunction (Fig. 15.1).

Left Atrial-Left Ventricular Interdependence

LA phasic functions demonstrate the close interdependence between atrial and ventricular performances. LA reservoir function is modulated by LV contraction, through the descent of the atrioventricular ring and LV base during systole, and by the diastolic properties of the LA (i.e. relaxation and chamber stiffness). The LA conduit function is impacted by the relaxation of the LV, the early diastolic chamber pressures, and LA cavity compliance, while the LA booster pump function is affected by LV compliance and end-

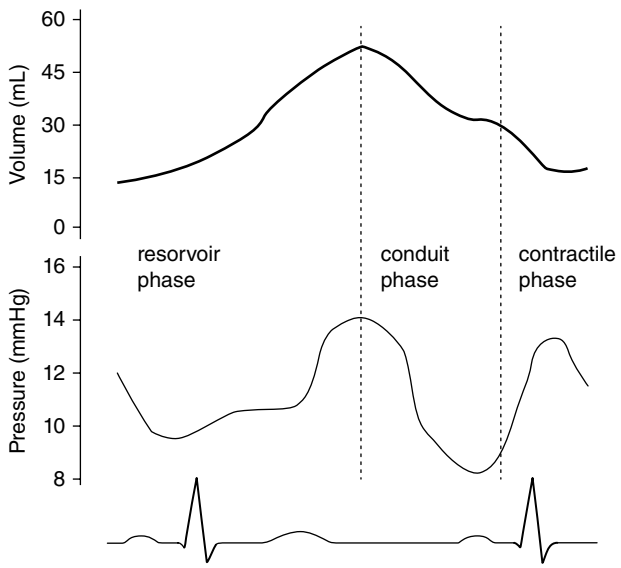


Fig. 15.1 *Left atrial function*: during the *reservoir phase* there is an increase in atrial volume accompanied by continuous rise in pressure; in the *conduit phase* there is a decrease in atrial volume accompanied by a pressure fall; during the *contractile phase* there is a volume decrease coupled with a new increase in atrial pressure

A. Campora (✉) · M. Cameli
University of Siena, Siena, Italy

M. Lisi
Ospedale S. Maria delle Croci, Ravenna, Italy

M. Y. Henein
Imperial College London, London, UK

Siena University, Siena, Italy

© The Author(s), under exclusive license to Springer Nature Switzerland AG 2025
M. Y. Henein (ed.), *Clinical Echocardiography*, https://doi.org/10.1007/978-3-031-95894-6_15

diastolic pressure, as well as LA intrinsic contractile function.

LA remodelling, including changes in shape, dimension, structure, and function, occurs in response to pressure overload, caused by LV dysfunction, mitral valve stenosis, stiff LA syndrome, as well as volume overload, caused by valvular regurgitation, left-to-right shunts and high output states. In the absence of primary atrial pathology or mitral valve disease, LA remodelling mainly reflects LV dysfunction, being proposed as a barometer of diastolic burden. LA reservoir and contractile function can be exaggerate in order to maintain adequate LV filling in the presence of abnormal LV relaxation and compromised LA conduit function. With the worsening of LV diastolic function and the increase in LV filling pressures, LA reservoir and contractile function decrease and the cavity functions predominantly as a conduit [1].

Left Atrial Volume–Pressure Relations

As LA diameter increases, its output increases, in order to maintain adequate stroke volume until the optimal Frank-Starling relationship is exceeded [2]. Beyond this point and with severe LA dilatation, contractile cavity function decreases. Such physiological changes propose the importance of regular assessment of LV dimensions and volumes as a marker for myocardial dysfunction, that reflects worsening pathology; valve disease (particularly mitral) or LV myocardial disease. Although the most accurate means for assessing LA pressure/volume relations is by recording their curves [3], the clinical use of such a method is limited as it requires invasive measurements.

Left Atrial Neuroendocrine Function

LA mechanical stretch stimulates the release of atrial natriuretic peptide (ANP), which promotes direct vasodilation, reduces renin and endothelin secretion, and fibroblast collagen synthesis. This physiological behaviour aims at preventing LA remodelling. With the development of severe LA fibrosis, there is a depletion of ANP stores, hence the limited compensatory effect of the ANP secretion. On the other hand, the overproduction of ANP can accumulate as amyloid, leading to isolated atrial amyloidosis and consequently atrial fibrillation (AF) [4].

Echocardiographic Examination of the Left Atrium

Left Atrial Dimensions

Assessment of LA dimensions is of clinical importance since cavity enlargement is now established as a strong predictor of major adverse cardiovascular outcomes in the general population and several pathological conditions [5]. The traditional method for estimating LA size is a measurement of its anterior-posterior diameter, which has been extensively used in clinical and academic studies. However, considering that the LA is a 3D structure and that its enlargement occurs preferentially in the superior-inferior or medial-lateral axes as the LA is constrained by the aortic root anteriorly, and the tracheal bifurcation posteriorly, changes in the anterior-posterior LA diameter often underestimate changes in other LA dimensions. This makes the linear anterior-posterior measurement inaccurate for quantification of LA size. Measuring LA area, as a reflection of cavity size suffers from the same limitation.

In contrast, evaluation of LA volume assures accurate assessment of the asymmetric cavity remodelling, providing superior prognostic information when compared with LA area or diameter [6]. Maximum LA volume (obtained just before mitral valve opening) is routinely recommended in standard echocardiographic examination. In bi-dimensional (2D) echocardiography, the modified section should be obtained in order to maximize LA volume. Biplane area–length or Simpson's methods are available on most echocardiographs. However, those methods make assumptions that may be inaccurate and, hence, may underestimate LA volumes when compared with cardiac computed tomography (CT) or cardiac magnetic resonance (CMR). Moreover, LA's maximum volume is only a snapshot of LA remodelling. The extension of the assessment to LA phasic volumes might add significant prognostic information. Evaluation of LA phasic volumes includes maximum volume, minimal volume (measured at mitral valve closure), and the volume just before atrial contraction (measured at the onset of P wave on the electrocardiogram). The main limitation of LA volume measurements is being time-consuming and dependent on the operator's accuracy based on the geometric assumptions of biplane volume calculations, acoustic window, and timing of atrial events. As body size is a major determinant of LA size, LA volumes must be reported indexed to body surface area [7].

Three-dimensional (3D) echocardiography overcomes these 2D echocardiography limitations by avoiding geometric assumptions. It guarantees an accurate assessment of LA volume, with a lower variability compared to 2D echocardiography. Modern 3D echocardiographic software are able to automatically obtain phasic LA volumes (minimum, maximum, and before atrial contraction) and calculate active LA ejection fraction (EF). The feasibility of 3D echocardiography for the assessment of LA volumes has been proved and the technique has been validated against CMR [8, 9]. Nevertheless, 3D echocardiography also has some limitations: arrhythmias such as AF prevent multi-beat full-volume acquisitions and inadequate apical acoustic window. Reference values derived from large populations remain currently lacking.

For 2D echocardiography, the normal value for indexed LA volume established by current guidelines is 22+/−6 ml/m^2 [7]. The increase in LA volume by more than one standard deviation (SD) i.e. >28 ml/m^2, based on sensitivity and specificity for prediction of cardiac adverse events, is considered as mild enlargement. The increase in LA volume by more than two SD (>34 ml/m^2) is considered the cut-off that provides more specific discrimination of abnormal versus normal LA volume for diastolic function assessment [10]. Despite the extensive evidence on the prognostic value of LA dilatation, clear cut-offs with an impact on patient management have been merely arbitrarily set.

Left Atrial Function

With technical advances new methods have developed that allow quantitative assessment of LA function. In addition to classical parameters based on pulsed wave Doppler, volumetric analysis and tissue Doppler imaging (TDI), novel post-processing imaging methodologies based on speckle tracking echocardiography (STE) have provided a more comprehensive understanding of LA mechanics.

Spectral Doppler-Derived Parameters

Analysis of pulmonary venous flow can estimate atrial filling and emptying status, as well as diastolic transmitral flow, which provides a broad estimation of LA functions. Transmitral peak A-wave velocity reflects LA booster pump function, while the measurement of systolic, diastolic, and atrial reversal waves at the level of pulmonary venous flow reflects all three LA functions (reservoir, conduit and booster pump, respectively). These flow analyses provide an easy method to recognize atrial stunning and its mechanical recovery after sinus rhythm restoration, post cardioversion. The atrial fraction, represented as the ratio between velocity time integral (VTI) of the A wave and VTI of diastolic transmitral flow, may also be used as an estimate of LA contractile function:

$$\text{Atrial fraction} : \text{VTI}_{\text{a wave}} / \text{VTI}_{\text{mitral inflow}}.$$

Atrial ejection force is another parameter that describes atrial systolic function. It can estimate the force imposed by the LA to accelerate blood flow to the LV:

$$\text{Atrial ejection force} : 0.5 \times 1.06 \times \text{mitral annulus area} \times \left(\text{peak A velocity}\right)^2.$$

These Doppler indices are limited by their dependence on heart rate and loading conditions.

On TOE, LA appendage contraction can be assessed by pulsed Doppler flow interrogation. A reduction in the LA appendage velocities below < 20 cm/s has been shown to be predictive of the risk of thrombus formation and, therefore may be used to guide anticoagulation therapy. On the other hand, the presence of good LA appendage function post cardioversion (high emptying velocities > 40 cm/s) indicates a low embolic risk and has also been associated with a low risk of AF recurrences [11].

Left Atrial Phasic Volume-Derived Parameters

The most common methods used for LA function assessment are based on the measurement of LA phasic volumes and the calculation of the following indices [12]:

$$\text{LA EF} = \left(\text{Vol}_{\text{max}} - \text{Vol}_{\text{min}}\right) / \text{Vol}_{\text{max}} \times 100$$

$$\text{LA expansion index} = \left(\text{Vol}_{\text{max}} - \text{Vol}_{\text{min}}\right) / \text{Vol}_{\text{min}} \times 100$$

$$\text{LA passive emptying fraction} = \left(\text{Vol}_{\text{max}} - \text{Vol}_{\text{p}}\right) / \text{Vol}_{\text{max}} \times 100$$

$$\text{LA active emptying fraction} = \left(\text{Vol}_{\text{p}} - \text{Vol}_{\text{min}}\right) / \text{Vol}_{\text{p}} \times 100$$

$\text{Vol}_{p=}$ volume just before the atrial contraction, measured at the onset of *P* wave on the electrocardiogram (ECG).

3D echocardiography provides accurate and reproducible volume measurements automatically. It has emerged as the best and preferred method to obtain LA phasic volumes and

functional parameters. Like spectral Doppler-derived parameters, the main limitation of LA phasic volumes-derived parameters is their load dependency.

Left Atrial Assessment by Tissue Doppler imaging (TDI)

The TDI method can characterize intrinsic myocardial velocities and provide relatively load-independent measurements of LA function. Care should be taken to setting adjustments (minimum gain, reduced sector size and depth, frame rate >100 frames/s, parallel alignment of the sampling window with the region of interest) in order to obtain an accurate measurement of LA myocardial velocities. Assessment of peak velocity of the mitral annulus in late diastole (a') has shown a good correlation with LA EF and LA ejection force, and thus can be used as a marker of atrial contraction [13]. The offline color TDI waveforms analysis allows multiple atrial regions to simultaneous assessment. One of the main limitations of this method is that the velocities may be influenced by translation and tethering, therefore might fail to distinguish between intrinsic atrial movement and the displacement induced by ventricular motion through the mitral annulus movement. This potential limitation has been overcome with the advent of atrial strain and strain rate, which have shown good site specificity, being able to describe the intrinsic movement of LA longitudinal shortening and lengthening which is discordant with ventricular longitudinal motion. LA strain can be quantified in two different ways, depending on whether measuring the onset of the atrial cycle is taken as that of the P wave on the ECG or that of the QRS complex [14]. Using the P wave as a reference point does not apply to patients in AF. This has led to differences in nomenclature and cut-offs, and to difficulties in practical application of these parameters. Regardless of the reference point used, the LA strain rate curve is triphasic, with strain rates in ventricular systole, early diastole, and late diastole corresponding to reservoir, conduit, and contractile function [15], respectively. TDI is also capable of determining atrial electromechanical delay, calculated as the time interval from the onset of the P wave on the ECG to the peak or onset of the a' wave on the atrial myocardial velocities curves [16]. Total atrial conduction time can be estimated as the time from the beginning of the P wave to the peak of the a' wave velocity measured at the level of the lateral LA wall. This method provides information on the atrial wall's electrical vulnerability or stability, which can be associated with the risk of AF. The main limitations of TDI-derived strain are the angle dependency, the time needed for wall-by-wall sampling, and the setting of cut-offs, which limit the routine use of this method in clinical practice.

Left Atrial Assessment by Speckle Tracking Echocardiography (STE)

STE is a non-Doppler-based technique derived from standard 2D data acquisition, which can provide objective quantification of myocardial deformation. Over the last few years, STE has demonstrated significant feasibility and measurement reproducibility [17–20]. The method has shown several advantages in contrast to conventional Doppler-derived indexes, being not angle-dependent and having lower reverberation effects, side lobes and drop-out artifacts.

STE was originally developed to study LV deformation, but it has been extensively used also to evaluate atrial chamber function in recent years [21]. Atrial longitudinal strain, in particular, has been proven an excellent parameter of LA function in many conditions, even in AF. 2D STE uses standard B-mode images for speckle tracking analysis: the speckle pattern (acoustic back-scatter generated by the reflected ultrasound beam) is followed frame-by-frame, identifying the best matching area by a statistical approach. The displacement of the analyzed pattern is considered to follow myocardial movement and every change between speckles is evaluated as a myocardial deformation [22].

LA apical 4- and 2-chamber views images are obtained using conventional 2D grey scale echocardiographic images, during a brief breath hold and with a stable ECG recording. Typically, three consecutive heart cycles are recorded and averaged but patients with AF require an averaged measurement of at least five consecutive beats. The recommended STE frame rate is set between 60 and 80 frames per second [17]. Recordings are then processed using a specific acoustic-tracking software, that allows off-line semi-automated analysis of speckle-based strain (Fig. 15.2).

LA endocardium surface is manually traced in both 2- and 4-chamber views by a point-and-click method. The epicardial surface tracing is automatically generated by the system in order to obtain a region of interest (ROI). The ROI can be manually adjusted in width and shape then the software divides it into 6 segments and the resulting tracking quality for each segment is automatically scored as either acceptable or non-acceptable, with the possibility of further additional corrections. Segments in which no adequate image quality can be obtained, are rejected by the software and automatically excluded from the analysis. If the patient has adequate image quality, a total of 12 segments are then analyzed [17], and for each of these segments, the software provides the longitudinal strain curves as well as a mean curve of all segments that reflects the overall LA deformation measurement (Fig. 15.2) [23].

During the LA reservoir phase, the cavity stretches so the strain curve increases, reaching a positive peak at the end of atrial filling, before the mitral valve opening. After mitral opening, LA empties quickly and its volume decreases, so

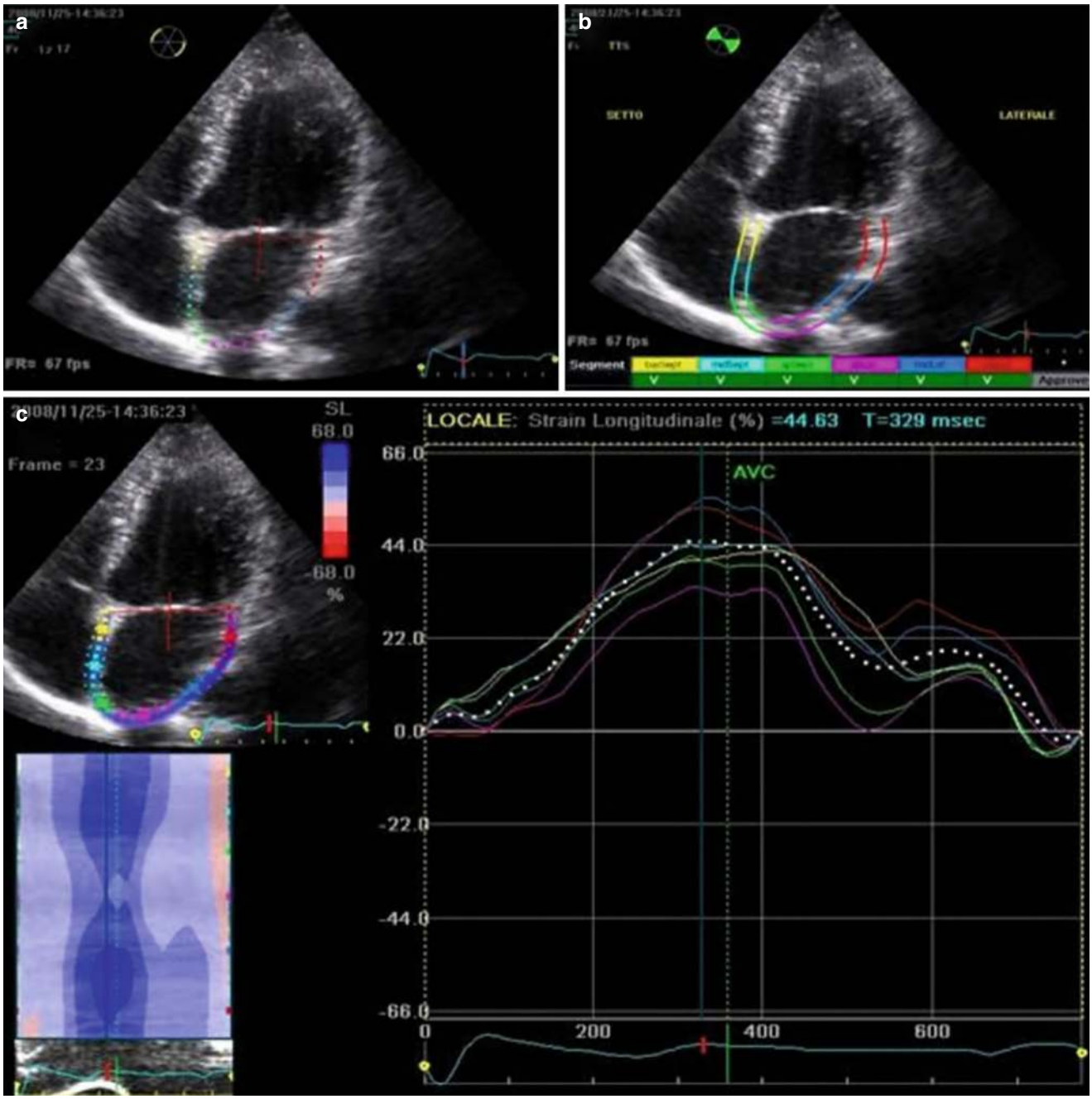


Fig. 15.2 Measurement of left atrial longitudinal strain by speckle tracking. (**a**) The border of the atrial endocardium is traced with a point-and-click method; (**b**) the software elaborates an automatic region of interest, divided into 6 subregions. Segmental tracking quality is analyzed; (**c**) once approved by the user, the software generates segmental longitudinal strain curves. The average strain is represented by the dashed curve. Adapted from M. Cameli, M. Caputo, S. Mondillo, et al., Feasibility and reference values of left atrial longitudinal strain imaging by two-dimensional speckle tracking, Cardiovasc. Ultrasound 7 (Feb 8 2009) 6, https://doi.org/10.1186/1476-7120-7-6. [17]

the strain initially decreases, until it reaches a plateau corresponding to the diastasis phase. In patients with sinus rhythm, the plateau is followed by a second positive wave, in the same direction as the first, which corresponds to the period preceding atrial contraction and finally by a negative wave during atrial contraction [17].

Peak atrial longitudinal strain (PALS) measured at the end of the reservoir phase, is the most important strain parameter in AF, since this phase depends essentially on atrial compliance. Peak atrial contraction strain (PACS) can be measured only in patients in sinus rhythm, just before the start of active atrial contractile phase (Fig. 15.3.).

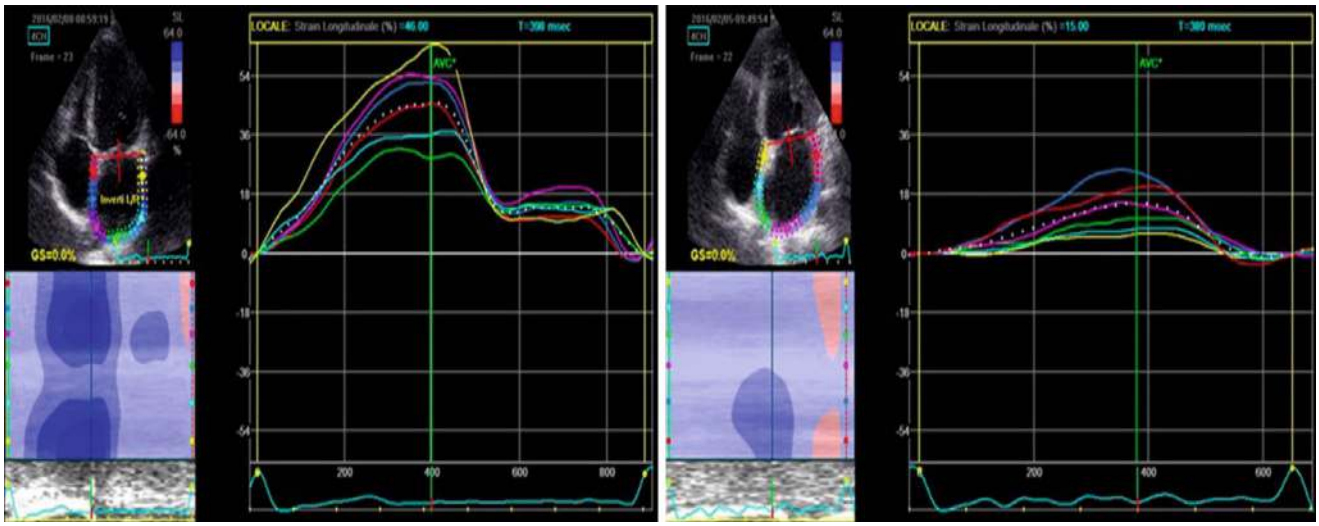


Fig. 15.3. Atrial strain in sinus rhythm vs atrial strain in atrial fibrillation: in this figure we can see the differences between atrial strain in a healthy subject (left) and a patient with atrial fibrillation (right). In the atrial fibrillation subject, besides a reduced PALS, we can note the disappearance of PACS, the second deflection of the curve, relative to the atrial systole. Adapted from Cameli M, Mandoli GE, Loiacono F, Sparla S, Iardino E, Mondillo S. Left atrial strain: a useful index in atrial fibrillation. Int J Cardiol. 2016;220: 208–213. [23]

Atrial strain and strain rate have been shown to inversely relate to the extent of LA fibrosis, detected by CMR [24] or histolopathology [25], making deformation measurements taken as a surrogate for identifying the degree of atrial wall fibrosis. The failure of 2D STE to address the complexities of cardiac geometry and motion is an important limitation of the method. Recently developed 3D STE by eliminating the effect of through-plane motion has enabled the evaluation of LA area strain by combining longitudinal and circumferential strain information [26]. A recent study demonstrated that 3D STE-derived LA volume measurement had a good correlation with CT measurements. Regional strain analysis indicated that region-specific LA reservoir strain changes might be affected by the restriction of the surrounding structures. Furthermore, the lateral segmental LA reservoir strain can reveal early LA functional changes before LA remodeling occurs. Given the accuracy of 3D STE, segmented LA strain, together with other conventional parameters, seems to have a good applicability in daily practice [27].

In recent years studies have demonstrated the usefulness of LA mechanics assessment obtaining excellent correlations with clinical end-points, risk stratification, and prognosis [28]. This has contributed to the increase in the popularity of using STE assessment of LA function. However, the current guidelines assessment of LA mechanics by STE remains recommended only for limited conditions including regional LA assessment in patients with LV diastolic dysfunction, after AF to predict the maintenance of sinus rhythm, or to identify patients at risk for LA failure or arrhythmias [9]. Nevertheless, the continuous evidence that has emerged, the spectrum of potential applications in clinical practice and the resulting growing interest in the method, set important prerequisites towards its progressive greater involvement in the guidelines.

Left Atrial Stiffness

Physiologically, LA stiffness is defined as the pressure change required to increase by unit amount of the volume of a passive container. LA stiffness is invasively measured as mean pulmonary wedge pressure divided by LA systolic strain. Non-invasive estimation of LA stiffness can be made with relatively good agreement with the invasively assessed LA stiffness [29], using the intra-cavity filling pressure (E/e' ratio) in conjunction with the percentage of maximum LA myocardial deformation [30]. This parameter has been shown to relate to LV diastolic dysfunction, LA dilatation, and collagen synthesis [30], and has been used to identify patients with diastolic heart failure (HF) [29]. Furthermore, LA stiffness has been shown to be able to predict the maintenance of sinus rhythm after cardioversion for AF [31] and to predict AF recurrence after pulmonary vein isolation [30]. The evaluation of atrial stiffness in athletes has clarified the adaptation of the atria to training (physiologic remodelling) demonstrating that, despite a greater LA size, exercise-induced physiological remodelling is accompanied by lower LA stiffness in contrast to patients with cardiomyopathies, in whom atrial stiffness is high (pathologic remodelling) [32]. Thus, this echocardiographic parameter can potentially represent a new tool that can further clarify the LA function properties.

Clinical Indications for Left Atrium Assessment

Echocardiographic assessment of LA has been for many years limited to dimensional assessment only, with clinical correlates mainly in AF patients aiming at assessing the likelihood of post-cardioversion recurrence of AF or the indication for electrophysiological procedures. Functional studies have always been relegated to research activities. With technological advances and the greater availability of STE software there has been a greater shift of focus to LA function component analysis, rather than only the dimensional component. This resulted in the emergence of important new scientific evidence of clinical relevance. This has also shed light on the importance of studying the thin-walled chamber function, which is affected early in patients with LV disease.

In this section we will review current and potential clinical applications of echocardiographic assessment of LA, focusing on available new evidence.

Atrial Fibrillation, Stroke/Dementia and Atrial Myopathy

AF is the most frequently sustained cardiac arrhythmia, with a prevalence of 0.4% to 1% in the general population and 9% in the elderly, carrying high morbidity and mortality [33]. Importantly, the presence of AF is associated with a 5-fold increased risk of stroke, which represents the first manifestation of AF in 2% to 5% of patients [34]. Its genesis has been attributed to LA appendage thrombi formation as a result of blood stasis, with subsequent dislodgement and cerebral embolization. AF has also been shown to correlate with various forms of dementia, independent of the history of stroke. An increase in LA size is one of the major determinants of AF onset [35, 36] and LA volume index (LAVi) has proved to be superior to LA diameter (I), being a more reliable marker of LA remodelling. Among the prospective studies, Paciaroni et al. reported that severe LA dilatation (defined by LA diameter ≥ 5.0 cm/m^2 or LAVi ≥ 40 ml/m^2) predicted recurrence of thromboembolic events on multivariate analysis (OR 2.05, 95% CI 1.08–2.87, $p = 0.027$) in a population of 854 AF patients admitted for acute ischaemic stroke [37]. In 150 AF patients undergoing the Maze surgical procedure, LAVi predicted thromboembolic events in the whole population (HR = 3.23, 95% CI 1.10–9.48, $p = 0.03$) but not in patients on anticoagulation [38]. In the study of Asinger et al., LA diameter (RR = 1.6, 95% CI 1.0–2.5, $p = 0.04$) proved an independent predictor of thromboembolic events in AF patients [39]. Conversely, in two other studies, LA diameter [40] and LAVi [41] showed univariate relations with thromboembolic events, which were lost in subsequent multivariable analyses.

It has become recognised that LA function more than LA size itself could have a greater impact on LA thrombosis development [38, 42]. For years, atrial blood stasis due to AF was acknowledged as the mechanism of AF-related thromboembolism [43]; however, recent evidence has proposed atrial myopathy (AM) as an alternative mechanism. AM, defined as "any complex structural, architectural, contractile, or electrophysiological changes affecting the atria with the potential to produce clinically relevant manifestations" appears with LA dysfunction and dilation [44]. Emerging evidence suggests that thromboembolism can occur in AM even without AF [45]. However, AM and AF are strictly correlated with a cause-consequence relationship. In fact, LA fibrosis, characterizing AM, affects LA compliance and function and often leads to AF [46]. Furthermore, AF and the subsequent hemodynamic overload may provoke atrial remodeling, stiffness, and fibrosis, leading to AM [47]. Although cardiac magnetic resonance is the gold standard investigation to assess the extent of fibrosis, STE has emerged as a noninvasive, quicker, and more available alternative technique.

The study of LA deformation also offers important information on the early modification of LA structure and function and predicts the occurrence and persistence of AF [23]. Patients with paroxysmal AF proved to have increased LA stiffness [48]. Also, the LA strain provides additional information on acute embolisms over CHA_2DS_2-VASc score in patients with paroxysmal/permanent AF [49]. Sade et al [50] have shown that a reduction in LA strain could stratify AF risk in patients with cryptogenic stroke. Moreover, in the low-risk general population, a reduction in LA reservoir strain proved an independent predictor of the long-term risk of AF and ischemic stroke [51]. These studies suggest that LA strain may be used to assess LA fibrosis and stiffness characterizing AM, which may drive the risk of stroke, independent of AF. Considering its feasibility and increasing availability, LA strain may thus improve risk stratification for stroke and dementia in clinical practice. This may lead to alternative indications for anticoagulation treatment for primary prevention of stroke, not only extending the indication to patients without AF who are at high risk of stroke but also the potential commencement of anticoagulants in patients with AF in "grey-zone" risk categories for stroke according to current indices.

Heart Failure (HF)

For a long time, LV systolic dysfunction has been considered as the main determinant of symptoms in HF [52]. However, the loss of the LA reservoir and active functions can be responsible for the progression towards a symptomatic systolic HF, with subsequent development of pulmonary congestion and neuro-hormonal instability, the common features of advanced HF [53]. In diastole, LA is directly exposed to higher LV pressures while the mitral valve is open. Along with the reduction of LV compliance and the rise of diastolic pressures, LA pressure gradually increases in order to maintain adequate LV filling. This results in LA dilatation which carries a worse prognosis and quality of life [54–57]. The pressure overload imposed on LA causes a range of adaptive and maladaptive remodelling with structural, functional, electrical, metabolic, and neurohormonal consequences. Fibrosis has dramatic effects on LA mechanics involving both reservoir and booster pump functions, the loss of which further contributes to the rise in LA pressures, AF and worsening HF symptoms [58].

LA strain by STE has proved superior compared to conventional echocardiographic parameters in patients with HF symptoms, for both diagnosis and prognosis, irrespective of LV EF [59–61]. STE has also been shown to better predict the onset of AF [62], which is directly correlated to the presence of LA fibrosis [23]. Furthermore, in patients with advanced HF, PALS and LA reservoir function, showed an important role as a surrogate of LV filling pressures [63] over and above TDI parameters [64]. Identification of advanced LA remodelling, correlated with worsening symptoms and increased pulmonary pressures. Therefore, in patients with advanced HF, a severe reduction in LA function could forerun a more severe stage of biventricular failure, in which the high risk of post-implant RV acute failure could contraindicate the use of alternative therapeutic strategies such as LV assist devices (LVAD). In fact, poor RV function represents a contraindication to LVAD implant which can be the only available option in many patients with end-stage HF considering the shortage of donors for heart transplantation [65].

Recently [66], M. Lisi et al have shown global PALS was the strongest predictor of invasively assessed LA fibrosis in patients with end-stage HF, carrying the best diagnostic accuracy for detecting severe LA fibrosis (>50%), over and above other parameters of LA performance and diastolic function. They also confirmed the association of a reduced global PALS with HF symptoms (New York Heart Association, NYHA class) and exercise capacity, evaluated by Cardiopulmonary exercise testing (CPET)-derived oxygen consumption (VO2 max), which were also associated with the extent of myocardial fibrosis. Due to its direct correlation with AF burden, LA fibrosis quantification in HF patients could represent a future target to optimize management. Indeed, the onset of AF lead to a worse prognosis and to the need of a different approach with cardiac resynchronization therapy.

Mitral Regurgitation

Severe chronic mitral regurgitation (MR) determines progressive and insidious LV and LA volume overload, and symptoms could be masked for a long time [67]. In these patients, the evaluation of LV structure and function parameters such as LV EF may be misleading [68]. Chronic LA volume overload causes progressive LA dilatation and LA intrinsic myocardial dysfunction and fibrosis [69] which causes increased LA cavity stiffness and produces supraventricular arrhythmias such as AF. AF itself then deteriorates atrial and ventricular function, with progressive worsening of MR and further myocardial dysfunction [70]. If managed only medically, severe symptomatic MR would lead to high morbidity and mortality. Current guidelines recommend mitral valve repair (MVR) if operable and not at high risk. In asymptomatic patients, surgery is still controversial and current guidelines suggest intervention in the presence of LV systolic dysfunction, as shown by LV EF $\leq$ 60% and/or LV end-systolic diameter $\geq$ 40 mm [71].

Severe MR determines progressive systolic and diastolic dysfunction by increasing ventricular wall stress [72] and mass, causing ultra-structural fiber rearrangement, and myocardial fibrosis also in patients with preserved LV EF [73]. Due to the thinner LA walls, cavity dilatation and reduction in myocardial strain occur much earlier and in a greater extent than that of the LV [74–76], similar to what occurs in other conditions such as diabetes and hypertension [77]. Increased LA volume and reduced PALS before MVR have been independently associated with postoperative AF in patients with severe MR [78]. Furthermore, death and the need for mitral valve surgery due to HF were found to be predicted by PALS in a cohort of 104 patients with asymptomatic severe primary MR [79].

Surgical correction of MR removes the volume overload, unmasking pre-operative LV myocardial dysfunction. This is revealed by the reduction in post-operative EF [80], LV global longitudinal and circumferential myocardial strain and strain rate [70]. Similar post-operative myocardial abnormalities have been observed in the LA. After correction of MR, LA volume and LA strain are reduced with residual intrinsic myocardial dysfunction and increased volume, [70] suggesting that pre-operative LA function does not necessarily reflect the magnitude of intrinsic chamber dysfunction, [81] but preferably a progressive process of tissue remodeling and fibrosis [82]. These myocardial abnormalities, together with the chronic volume overload, may trigger the well-known high incidence of postoperative AF

[83], especially when exposed to the acute stress of surgical intervention, creating a pro-arrhythmic environment that is manifested clinically as post-operative AF [84]. This has been especially seen in patients undergoing combined coronary artery bypass surgery and MVR [70, 85, 86]. The meta-analysis performed by Kawcznski M et al. [87] confirmed those observations, as increased pre-operative LA volume and reduced LA global PALS emerged as strong predictors of postoperative AF. Moreover, in patients with paroxysmal AF, mean pre-operative LA volume predicted the development of postoperative AF, after aortic or mitral valve surgery [84].

The other parameter that emerged as a predictor of post-operative AF was LV diastolic dysfunction, due to the raised LV filling pressure and consequently LA pressure and volume overload. That provokes stretching of the pulmonary veins and increased cavity arrhythmogenic activity [84, 88]. In MR, conventional echocardiographic measurements of LV filling pressure (such as E/e′) could not be taken as a net expression of increased LA chamber pressure, because absolute "E" wave velocity depends on the severity of volume overload and "e′" wave reflects how healthy the subendocardium is before the surgical intervention [71]. Therefore, LA volumes are often increased to compensate for the rise in LA pressure, and could be associated with a normal or only slightly raised LA pressure [88, 89]. These features support the emerging role of LV and LA strain in predicting post-operative outcomes. Therefore, LA intrinsic function (global PALS) is considered an early tool for evaluating subclinical signs of HF, also showing a potential role in predicting post-operative AF and HF symptoms [69].

Sugimoto et al. [90] demonstrated that in patients with MR, undergoing exercise stress echocardiography, global PALS and PACS reserve have a primary role in the abnormal response to exercise, influencing the right heart hemodynamic status, cardiac output increase, and ventilation efficiency. They also carry a predictive value of all-cause mortality and hospitalization for HF.

The information gathered with these recent studies has demonstrated the significant association between global PALS and event-free survival (HF and mortality), over and above conventional prognostic indices. Global PALS is also capable of predicting functional capacity (assessed by NYHA class and Borg CR10 score) and the extent of LA fibrosis [91].

In summary, global PALS has emerged as an important predictor, over and above current mitral surgery indications [71], of postoperative survival in patients with chronic severe MR [92, 93]. However, the most recent ESC guidelines on valvular disease do not mention LA strain measurement in these patients [71] but only point out the importance of LA dilatation and the occurrence of AF. Further research is warranted on this topic.

Mitral Stenosis

In patients with mitral stenosis (MS), LA strain and strain rate during LV systole are impaired even before symptoms occur. Reduced PALS could predict a worse prognosis over a 3-year follow-up in patients with moderate MS, irrespective of LA volume, age, and mitral valve area [78]. In addition, PALS proved the most powerful predictor of new-onset AF at 4-year follow-up in asymptomatic patients with isolated rheumatic MS [94]. These findings indicate that impaired LA reservoir function determined by PALS can predict the development of AF and cardiovascular events independent of mitral valve area in asymptomatic patients with MS, hence LA STE should be considered during the evaluation for MS procedures to determine the best timing for intervention.

Aortic Stenosis

Decreased LA strain assessed by 2D STE has been shown in patients with aortic stenosis (AS) [78], but in those with aortic regurgitation, it has not been characterized by 2D-STE yet.

The aortic valve obstruction causes pressure overload on the LV, with the consequent development of concentric myocardial hypertrophy as an adaptive mechanism to reduce wall stress. These changes lead to early diastolic dysfunction, due to the reduction of LV compliance, while initially systolic performance is only mildly compromised. Later on, myocardial contractile function and deformation become impaired with a consequent fall in cardiac output. The interdependence between the atrium and the ventricle is reflected in the LA which, similar to what happens in MR, undergoes adverse remodeling, with its size increasing due to chronic pressure overload, which eventually leads to an increase in pulmonary venous and arterial pressure [95], with resulting HF symptoms development and, often, AF [81].

As mentioned in MR and MS, reduction in PALS in AS has been associated with an increase in all-cause mortality, worsening HF, and a need for cardiac-related hospitalization [96], and PALS was also been shown to correlate with prognosis in patients with severe AS [96, 97], with the development of post-operative AF, increased myocardial stiffness, and altered relaxation [98], regardless of pre-existing LA dilatation [99]. In addition, LA strain proved the major determinant of pulmonary hypertension in patients with severe AS and preserved LV EF [100] and a marker of LA remodeling after transcatheter aortic valve replacement [101], supporting serial monitoring of LA function to identify patients requiring early surgical treatment before the development of pulmonary hypertension and irreversible LA damage.

The latest ESC/EACTS guidelines for the management of valvular disease, intervention for severe AS is indicated, irre-

spective of symptoms, in patients with one of the following conditions, either isolated or associated systolic dysfunction in the absence of other causes; severe AS with mean gradient ≥ 60 mmHg; rapid progression and markedly elevated BNP levels, particularly in those with estimated poor prognosis [71]. The type of intervention should be decided based on the heart team evaluation. Surgical aortic valve replacement remains the first choice in patients <75 years of age with low surgical risk, while transcatheter aortic valve replacement is preferred in those >75 years with high surgical risk [71].

Even in this setting the latest guidelines consider invasive treatment of AS based on the patient's symptoms or LV impairment evaluated by EF, but do not consider strain evaluation when deciding on the optimal timing of valve replacement. This strategy often results in late management with irreversible cardiac structural changes. Alterations in LV GLS and PALS detect myocardial dysfunction before reduction of EF and LA enlargement take place. In the near future, their routine use in clinical practice could help identify patients requiring earlier invasive treatment in order to improve post-operative outcomes and recovery.

Thus, studies indicate the development of LA dysfunction at the early phase of MR, MS, and AS and the significant impact of LA dysfunction on prognosis, including all-cause mortality and outcome after surgery. Hence, assessment of LA reservoir function by 2D STE in patients with valvular diseases is likely to provide a guide for therapy, particularly timely surgery in patients with asymptomatic severe valvular diseases.

Ischemic Heart Diseases

Although the change in LA strain caused by ischemic heart disease (IHD) has not been fully characterized, several studies have shown that assessment of LA strains can provide useful information for the management of patients with IHD. Firstly, the reduction in global PALS has been shown to predict an increased risk of new-onset AF after coronary artery bypass graft surgery [28, 78]. Secondly, PALS may be useful in the prediction of the prognosis of patients with acute myocardial infarction (AMI) [28], as LA reservoir and booster pump functions determined by 2D echocardiography or cardiac MRI have shown to independently predict all-cause mortality in patients with AMI [28]. Antoni et al. [102] showed in a cohort of 320 patients with AMI treated with percutaneous coronary intervention that global PALS and LA volume could independently predict all-cause mortality, re-infarction, and hospitalization for HF. Ersbøll et al. [103] also demonstrated that LA strain was associated with all-cause mortality and hospitalization for HF in an 843 patient's cohort with AMI. However, in this last study, LA did not emerge as an independent predictor of outcome when adjusted for age, LV longitudinal strain, and LA volume. It is unclear whether the discrepancy between the two studies results can be totally explained by the use of LV longitudinal strain and LA volume as adjustment variables in the multivariate analyses.

Hypertension and Diabetes Mellitus

Particularly in the elderly, hypertension and diabetes are very common diseases, and both are major risk factors for HF (including HFpEF). Similar to patients with paroxysmal AF, reduced LA PALS and PACS were demonstrated in hypertensive and diabetic patients with normal LA size (LA volume index < 28 mL/m^2) [28]. In asymptomatic patients with hypertension, Oki et al. [104] demonstrated that 2D STE could detect, beyond LA dysfunction, also LV - arterial coupling dysfunction. Furthermore, they showed worsening of LA–LV–arterial interaction when asymptomatic hypertensives developed HF with preserved EF. These findings suggest that 2D STE could be useful for early diagnosis of LA and LV dysfunction in patients with hypertension and/or diabetes.

2D STE can also be used for the evaluation of the effects of treatments on LA function in hypertensive patients. Degirmenci et al. [105] showed an improvement in LA reservoir, conduit, and booster pump functions after 12 months of treatment with renin-angiotensin receptor blockers (irbesartan) and beta blockers (nebivolol) in patients with mild–moderate hypertension. The improvement of LA strain was associated with better control of blood pressure and a decrease in LA volume. Interestingly, no significant difference between the irbesartan treatment group and the nebivolol treatment group was found. This indicates that improvement of the LA function primarily depends on the blood pressure control level, and not on the class of antihypertensive agents. The study of subclinical LA dysfunction's impact on the prognosis in patients with hypertension and diabetes mellitus, considering its close association with the onset of AF, is an interesting issue.

These findings indicate that 2D STE is a sensitive tool for detecting LA involvement in various non-cardiac diseases. Its usefulness for stratifying AF risk or risk of cardiovascular death in non-cardiac diseases remains to be investigated.

Interventional Procedures

3D TOE can provide images from multiple perspectives and can be used to identify anatomical landmarks, assess the size of different structures and defects, and as a guide during interventional procedures involving atrial septum, LA appendage, or pulmonary veins [106]. 3D TOE has a

better ability to discriminate between thrombus and LA appendage pectinate muscles than 2D TOE and to improve the assessment of LA appendage morphology and size [106], hence might be crucial in guiding its percutaneous closure. The 3D TOE can provide high-quality images of the interatrial septum, identifying anomalies such as patent foramen ovale, septal aneurysmal (defined as a saccular excursion of > 10 mm from the plane of the atrial septum), or septal lipomatous hypertrophy (defined as a septal thickness of >20 mm) [106]. A septal defect position and relationship with surrounding structures can be accurately visualized by 3D TOE.

Left Atrial Myopathy

Myopathy, by definition, reflects primary muscle pathology irrespective of the chamber, LV or LA. Evidence exists supporting LA dysfunction in patients with LV cardiomyopathy; hypertrophic, dilated and restrictive. The nature of LA dysfunction is similar to what is seen in other valve and LV pathologies, in the form of cavity dysfunction with or without enlargement [44]. With the significant improvement of cardiac imaging techniques, we have now started seeing some evidence for disproportionate LA enlargement and consequently dysfunction in patients with only mild mitral or aortic valve disease and mild arterial hypertension [107, 108]. Such changes might represent an early stage of LA myopathy that could be determined by other factors, that are yet to be identified. Another example is committed runners who develop LA enlargement and AF at a very young age. A third group is family members of patients with well-documented LV cardiomyopathy who are found incidentally to have LA electric and mechanical failure with absent P wave and no mechanical activity.

The diagnosis of AM could be suggested based on ECG findings, as AF or other atrial arrhythmias, serum biomarkers, and imaging evidence for LA dilation and dysfunction, often associated with myocardial fibrosis. Echocardiography, capable of providing a precise assessment of both morphological and functional parameters of the LA, has proven to be an extremely useful technique for evaluating the presence of AM. The LA, due to its thinner wall compared to the ventricular chambers, is more susceptible to early alterations in various pathological processes; therefore, early identification of morpho-functional alterations can reveal the presence of early myopathic changes, irrespective of symptoms.

Although these examples are clinically rare, clinicians should look out for them since they might benefit from specifically tailored protective management strategies, particularly for preventing the development of arrhythmia with its thromboembolic risk (Fig. 15.4).

Future Perspectives

Despite considerable data regarding the prognostic role of LA size and function assessed by multiple imaging techniques, the exploitation of these parameters in clinical practice is still limited.

Clinical relevance of LA function determined by 2D STE has emerged, and this modality is considered to be a promising technique for diagnosis, therapeutic decision-making, and assessment of prognosis [109]. However, most previous findings were derived from single-center studies with relatively small sample sizes. Hence, nonbiased large-scale multicenter studies are required to test and strengthen the clinical utility of LA function determined by 2D STE. Also, the standardization of image acquisition, software application, and data analysis could lead to significant advancement of the field. In addition, establishing specific cut-offs for 3D echocardiography-derived volumes will help implementation of this method in clinical practice. Until then, 3D echocardiography remains an invaluable tool for LA anatomy assessment, providing useful, unique information for percutaneous procedures.

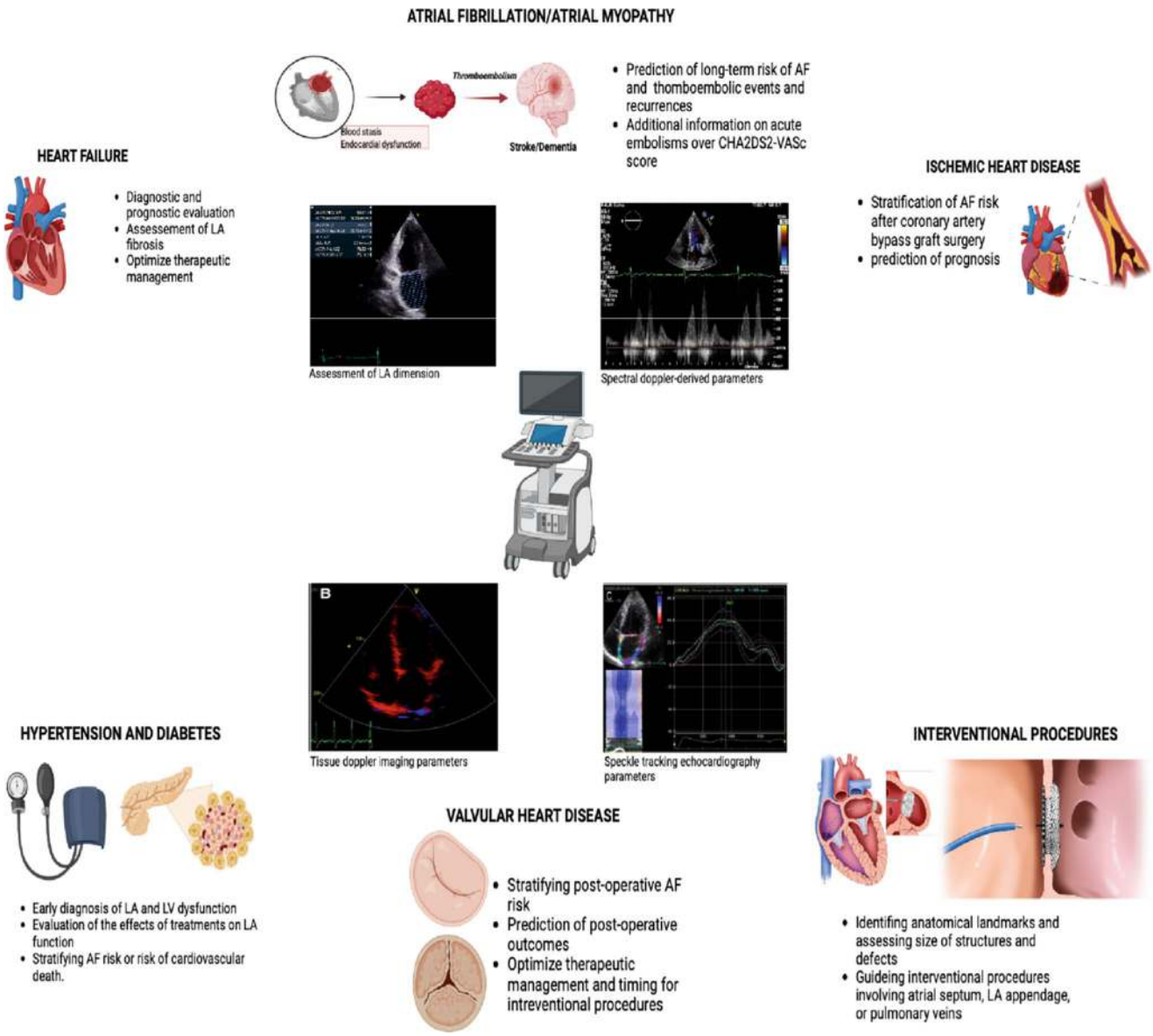


Fig. 15.4 Current and potential clinical applications of the echocardiographic study of the left atrium. *AF* atrial fibrillation, *LA* left atrium, *LV* left ventricle

References

1. Prioli A, Marino P, Lanzoni L, Zardini P. Increasing degrees of left ventricular filling impairment modulate left atrial function in humans. Am J Cardiol. 1998;82(6):756–61. https://doi.org/10.1016/s0002-9149(98)00452-4.
2. Payne RM, Stone HL, Engelken EJ. Atrial function during volume loading. J Appl Physiol. 1971;31(3):326–31. https://doi.org/10.1152/jappl.1971.31.3.326.
3. Hoit BD, Shao Y, Gabel M, Walsh RA. In vivo assessment of left atrial contractile performance in normal and pathological conditions using a time-varying elastance model. Circulation. 1994;89(4):1829–38. https://doi.org/10.1161/01.cir.89.4.1829.
4. Röcken C, Peters B, Juenemann G, et al. Atrial amyloidosis: an arrhythmogenic substrate for persistent atrial fibrillation. Circulation. 2002;106(16):2091–7. https://doi.org/10.1161/01.cir.0000034511.06350.df.
5. Tsang MY, Barnes ME, Tsang TS. Left atrial volume: clinical value revisited. Curr Cardiol Rep. 2012;14(3):374–80. https://doi.org/10.1007/s11886-012-0268-8.
6. Tsang TS, Abhayaratna WP, Barnes ME, et al. Prediction of cardiovascular outcomes with left atrial size: is volume superior to area or diameter? J Am Coll Cardiol. 2006;47(5):1018–23. https://doi.org/10.1016/j.jacc.2005.08.077.
7. Evangelista A, Flachskampf F, Lancellotti P, et al. European Association of Echocardiography recommendations for standardization of performance, digital storage and reporting of echocardiographic studies. Eur J Echocardiogr. 2008;9(4):438–48. https://doi.org/10.1093/ejechocard/jen174.
8. Rodevan O, Bjornerheim R, Ljosland M, Maehle J, Smith HJ, Ihlen H. Left atrial volumes assessed by three- and two-

dimensional echocardiography compared to MRI estimates. Int J Card Imaging. 1999;15(5):397–410. https://doi.org/10.1023/a:1006276513186.
9. Mor-Avi V, Yodwut C, Jenkins C, et al. Real-time 3D echocardiographic quantification of left atrial volume: multicenter study for validation with CMR. JACC Cardiovasc Imaging. 2012;5(8):769–77. https://doi.org/10.1016/j.jcmg.2012.05.011.
10. Nagueh SF, Smiseth OA, Appleton CP, et al. Recommendations for the evaluation of left ventricular diastolic function by echocardiography: an update from the American Society of Echocardiography and the European Association of Cardiovascular Imaging. J Am Soc Echocardiogr. 2016;29(4):277–314. https://doi.org/10.1016/j.echo.2016.01.011.
11. Troughton RW, Asher CR, Klein AL. The role of echocardiography in atrial fibrillation and cardioversion. Heart. 2003;89(12):1447–54. https://doi.org/10.1136/heart.89.12.1447.
12. Triposkiadis F, Tentolouris K, Androulakis A, et al. Left atrial mechanical function in the healthy elderly: new insights from a combined assessment of changes in atrial volume and transmitral flow velocity. J Am Soc Echocardiogr. 1995;8(6):801–9. https://doi.org/10.1016/s0894-7317(05)80004-5.
13. Sohn DW, Chai IH, Lee DJ, et al. Assessment of mitral annulus velocity by Doppler tissue imaging in the evaluation of left ventricular diastolic function. J Am Coll Cardiol. 1997;30(2):474–80. https://doi.org/10.1016/s0735-1097(97)88335-0.
14. Mor-Avi V, Lang RM, Badano LP, et al. Current and evolving echocardiographic techniques for the quantitative evaluation of cardiac mechanics: ASE/EAE consensus statement on methodology and indications endorsed by the Japanese Society of Echocardiography. Eur J Echocardiogr. 2011;12(3):167–205. https://doi.org/10.1093/ejechocard/jer021.
15. Sirbu C, Herbots L, D'hooge J, et al. Feasibility of strain and strain rate imaging for the assessment of regional left atrial deformation: a study in normal subjects. Eur J Echocardiogr. 2006;7(3):199–208. https://doi.org/10.1016/j.euje.2005.06.001.
16. Merckx KL, De Vos CB, Palmans A, et al. Atrial activation time determined by transthoracic Doppler tissue imaging can be used as an estimate of the total duration of atrial electrical activation. J Am Soc Echocardiogr. 2005;18(9):940–4. https://doi.org/10.1016/j.echo.2005.03.022.
17. Cameli M, Caputo M, Mondillo S, et al. Feasibility and reference values of left atrial longitudinal strain imaging by two-dimensional speckle tracking. Cardiovasc Ultrasound. 2009;7:6. Published 2009 Feb 8. https://doi.org/10.1186/1476-7120-7-6.
18. Vianna-Pinton R, Moreno CA, Baxter CM, Lee KS, Tsang TS, Appleton CP. Two-dimensional speckle-tracking echocardiography of the left atrium: feasibility and regional contraction and relaxation differences in normal subjects. J Am Soc Echocardiogr. 2009;22(3):299–305. https://doi.org/10.1016/j.echo.2008.12.017.
19. Kim DG, Lee KJ, Lee S, et al. Feasibility of two-dimensional global longitudinal strain and strain rate imaging for the assessment of left atrial function: a study in subjects with a low probability of cardiovascular disease and normal exercise capacity. Echocardiography. 2009;26(10):1179–87. https://doi.org/10.1111/j.1540-8175.2009.00955.x.
20. Saraiva RM, Demirkol S, Buakhamsri A, et al. Left atrial strain measured by two-dimensional speckle tracking represents a new tool to evaluate left atrial function. J Am Soc Echocardiogr. 2010;23(2):172–80. https://doi.org/10.1016/j.echo.2009.11.003.
21. Cameli M, Lisi M, Righini FM, Mondillo S. Novel echocardiographic techniques to assess left atrial size, anatomy and function. Cardiovasc Ultrasound. 2012;10:4. Published 2012 Feb 1. https://doi.org/10.1186/1476-7120-10-4.
22. Mondillo S, Galderisi M, Mele D, et al. Speckle-tracking echocardiography: a new technique for assessing myocardial function. J Ultrasound Med. 2011;30(1):71–83. https://doi.org/10.7863/jum.2011.30.1.71.
23. Cameli M, Mandoli GE, Loiacono F, Sparla S, Iardino E, Mondillo S. Left atrial strain: A useful index in atrial fibrillation. Int J Cardiol. 2016;220:208–13. https://doi.org/10.1016/j.ijcard.2016.06.197.
24. Kuppahally SS, Akoum N, Burgon NS, et al. Left atrial strain and strain rate in patients with paroxysmal and persistent atrial fibrillation: relationship to left atrial structural remodeling detected by delayed-enhancement MRI. Circ Cardiovasc Imaging. 2010;3(3):231–9. https://doi.org/10.1161/CIRCIMAGING.109.865683.
25. Her AY, Choi EY, Shim CY, et al. Prediction of left atrial fibrosis with speckle tracking echocardiography in mitral valve disease: a comparative study with histopathology. Korean Circ J. 2012;42(5):311–8. https://doi.org/10.4070/kcj.2012.42.5.311.
26. Mochizuki A, Yuda S, Oi Y, et al. Assessment of left atrial deformation and synchrony by three-dimensional speckle-tracking echocardiography: comparative studies in healthy subjects and patients with atrial fibrillation. J Am Soc Echocardiogr. 2013;26(2):165–74. https://doi.org/10.1016/j.echo.2012.10.003.
27. Kuraoka A, Ishizu T, Sato M, et al. Left atrial regional strain assessed by novel dedicated three-dimensional speckle tracking echocardiography. J Cardiol. 2021;78(6):517–23. https://doi.org/10.1016/j.jjcc.2021.07.002.
28. Vieira MJ, Teixeira R, Gonçalves L, Gersh BJ. Left atrial mechanics: echocardiographic assessment and clinical implications. J Am Soc Echocardiogr. 2014;27(5):463–78. https://doi.org/10.1016/j.echo.2014.01.021.
29. Kurt M, Wang J, Torre-Amione G, Nagueh SF. Left atrial function in diastolic heart failure. Circ Cardiovasc Imaging. 2009;2(1):10–5. https://doi.org/10.1161/CIRCIMAGING.108.813071.
30. Machino-Ohtsuka T, Seo Y, Tada H, et al. Left atrial stiffness relates to left ventricular diastolic dysfunction and recurrence after pulmonary vein isolation for atrial fibrillation. J Cardiovasc Electrophysiol. 2011;22(9):999–1006. https://doi.org/10.1111/j.1540-8167.2011.02049.x.
31. Shaikh AY, Maan A, Khan UA, et al. Speckle echocardiographic left atrial strain and stiffness index as predictors of maintenance of sinus rhythm after cardioversion for atrial fibrillation: a prospective study. Cardiovasc Ultrasound. 2012;10:48. Published 2012 Dec 3. https://doi.org/10.1186/1476-7120-10-48.
32. D'Ascenzi F, Pelliccia A, Natali BM, et al. Morphological and functional adaptation of left and right atria induced by training in highly trained female athletes. Circ Cardiovasc Imaging. 2014;7(2):222–9. https://doi.org/10.1161/CIRCIMAGING.113.001345.
33. January CT, Wann LS, Calkins H, et al. 2019 AHA/ACC/HRS Focused Update of the 2014 AHA/ACC/HRS Guideline for the Management of Patients With Atrial Fibrillation: A Report of the American College of Cardiology/American Heart Association Task Force on Clinical Practice Guidelines and the Heart Rhythm Society [published correction appears in J Am Coll Cardiol. 2019 Jul 30;74(4):599]. J Am Coll Cardiol. 2019;74(1):104–32. https://doi.org/10.1016/j.jacc.2019.01.011.
34. Lubitz SA, Yin X, McManus DD, et al. Stroke as the initial manifestation of atrial fibrillation: the Framingham heart study. Stroke. 2017;48(2):490–2. https://doi.org/10.1161/STROKEAHA.116.015071.
35. Bang CN, Dalsgaard M, Greve AM, et al. Left atrial size and function as predictors of new-onset of atrial fibrillation in patients with asymptomatic aortic stenosis: the simvastatin and ezetimibe in aortic stenosis study. Int J Cardiol. 2013;168(3):2322–7. https://doi.org/10.1016/j.ijcard.2013.01.060.
36. Gardner JD, Skelton WP 4th, Khouzam RN. Is it time to incorporate the left atrial size to the current stroke risk scoring systems

for atrial fibrillation?*. Curr Probl Cardiol. 2016;41(9-10):251–9. https://doi.org/10.1016/j.cpcardiol.2016.10.004.
37. Paciaroni M, Agnelli G, Falocci N, et al. Prognostic value of trans-thoracic echocardiography in patients with acute stroke and atrial fibrillation: findings from the RAF study. J Neurol. 2016;263(2):231–7. https://doi.org/10.1007/s00415-015-7957-3.
38. Buber J, Luria D, Sternik L, et al. Left atrial contractile function following a successful modified Maze procedure at surgery and the risk for subsequent thromboembolic stroke. J Am Coll Cardiol. 2011;58(15):1614–21. https://doi.org/10.1016/j.jacc.2011.05.051.
39. Predictors of thromboembolism in atrial fibrillation: II. Echocardiographic features of patients at risk. The stroke prevention in Atrial Fibrillation Investigators. Ann Intern Med. 1992;116(1):6–12. https://doi.org/10.7326/0003-4819-116-1-6.
40. Kim TH, Shim CY, Park JH, et al. Left ventricular diastolic dysfunction is associated with atrial remodeling and risk or presence of stroke in patients with paroxysmal atrial fibrillation. J Cardiol. 2016;68(2):104–9. https://doi.org/10.1016/j.jjcc.2015.10.008.
41. Lee SH, Choi S, Chung WJ, et al. Tissue Doppler index, E/E', and ischemic stroke in patients with atrial fibrillation and preserved left ventricular ejection fraction. J Neurol Sci. 2008;271(1-2):148–52. https://doi.org/10.1016/j.jns.2008.04.006.
42. Lancellotti P, Galderisi M. Prediction of ischaemic stroke in non-valvular atrial fibrillation if advanced echocardiography plays the game. Eur Heart J. 2018;39(16):1426–8. https://doi.org/10.1093/eurheartj/ehy025.
43. Watson T, Shantsila E, Lip GY. Mechanisms of thrombogenesis in atrial fibrillation: Virchow's triad revisited. Lancet. 2009;373(9658):155–66. https://doi.org/10.1016/S0140-6736(09)60040-4.
44. Goette A, Kalman JM, Aguinaga L, et al. EHRA/HRS/APHRS/SOLAECE expert consensus on atrial cardiomyopathies: definition, characterization, and clinical implication. Heart Rhythm. 2017;14(1):e3–e40. https://doi.org/10.1016/j.hrthm.2016.05.028.
45. Brambatti M, Connolly SJ, Gold MR, et al. Temporal relationship between subclinical atrial fibrillation and embolic events. Circulation. 2014;129(21):2094–9. https://doi.org/10.1161/CIRCULATIONAHA.113.007825.
46. Triposkiadis F, Pieske B, Butler J, et al. Global left atrial failure in heart failure. Eur J Heart Fail. 2016;18(11):1307–20. https://doi.org/10.1002/ejhf.645.
47. Miller JD, Aronis KN, Chrispin J, et al. Obesity, Exercise, Obstructive Sleep Apnea, and Modifiable Atherosclerotic Cardiovascular Disease Risk Factors in Atrial Fibrillation. J Am Coll Cardiol. 2015;66(25):2899–906. https://doi.org/10.1016/j.jacc.2015.10.047.
48. Yoon YE, Kim HJ, Kim SA, et al. Left atrial mechanical function and stiffness in patients with paroxysmal atrial fibrillation. J Cardiovasc Ultrasound. 2012;20(3):140–5. https://doi.org/10.4250/jcu.2012.20.3.140.
49. Obokata M, Negishi K, Kurosawa K, et al. Left atrial strain provides incremental value for embolism risk stratification over CHA_2DS_2-VASc score and indicates prognostic impact in patients with atrial fibrillation. J Am Soc Echocardiogr. 2014;27(7):709–716.e4. https://doi.org/10.1016/j.echo.2014.03.010.
50. Sade LE, Keskin S, Can U, et al. Left atrial mechanics for secondary prevention from embolic stroke of undetermined source. Eur Heart J Cardiovasc Imaging. 2022;23(3):381–91. https://doi.org/10.1093/ehjci/jeaa311.
51. Alhakak AS, Biering-Sørensen SR, Møgelvang R, et al. Usefulness of left atrial strain for predicting incident atrial fibrillation and ischaemic stroke in the general population. Eur Heart J Cardiovasc Imaging. 2022;23(3):363–71. https://doi.org/10.1093/ehjci/jeaa287.
52. Braunwald E. Heart failure. JACC Heart Fail. 2013;1(1):1–20. https://doi.org/10.1016/j.jchf.2012.10.002.
53. Karayannis G, Kitsios G, Kotidis H, Triposkiadis F. Left atrial remodelling contributes to the progression of asymptomatic left ventricular systolic dysfunction to chronic symptomatic heart failure. Heart Fail Rev. 2008;13(1):91–8. https://doi.org/10.1007/s10741-007-9021-6.
54. Zile MR, Baicu CF, Ikonomidis JS, et al. Myocardial stiffness in patients with heart failure and a preserved ejection fraction: contributions of collagen and titin. Circulation. 2015;131(14):1247–59. https://doi.org/10.1161/CIRCULATIONAHA.114.013215.
55. Cameli M, Sciaccaluga C, Loiacono F, et al. The analysis of left atrial function predicts the severity of functional impairment in chronic heart failure: The FLASH multicenter study. Int J Cardiol. 2019;286:87–91. https://doi.org/10.1016/j.ijcard.2019.03.063.
56. Mandoli GE, Cameli M, Novo G, et al. Right ventricular function after cardiac surgery: the diagnostic and prognostic role of echocardiography. Heart Fail Rev. 2019;24(5):625–35. https://doi.org/10.1007/s10741-019-09785-2.
57. Cameli M, Pastore MC, Mandoli GE, et al. Prognosis and Risk Stratification of Patients With Advanced Heart Failure (from PROBE). Am J Cardiol. 2019;124(1):55–62. https://doi.org/10.1016/j.amjcard.2019.03.041.
58. Casaclang-Verzosa G, Gersh BJ, Tsang TS. Structural and functional remodeling of the left atrium: clinical and therapeutic implications for atrial fibrillation. J Am Coll Cardiol. 2008;51(1):1–11. https://doi.org/10.1016/j.jacc.2007.09.026.
59. Reddy YNV, Obokata M, Egbe A, et al. Left atrial strain and compliance in the diagnostic evaluation of heart failure with preserved ejection fraction. Eur J Heart Fail. 2019;21(7):891–900. https://doi.org/10.1002/ejhf.1464.
60. Malagoli A, Rossi L, Bursi F, et al. Left atrial function predicts cardiovascular events in patients with chronic heart failure with reduced ejection fraction. J Am Soc Echocardiogr. 2019;32(2):248–56. https://doi.org/10.1016/j.echo.2018.08.012.
61. Al Saikhan L, Hughes AD, Chung WS, Alsharqi M, Nihoyannopoulos P. Left atrial function in heart failure with mid-range ejection fraction differs from that of heart failure with preserved ejection fraction: a 2D speckle-tracking echocardiographic study. Eur Heart J Cardiovasc Imaging. 2019;20(3):279–90. https://doi.org/10.1093/ehjci/jey171.
62. Park JJ, Park JH, Hwang IC, Park JB, Cho GY, Marwick TH. Left atrial strain as a predictor of new-onset atrial fibrillation in patients with heart failure. JACC Cardiovasc Imaging. 2020;13(10):2071–81. https://doi.org/10.1016/j.jcmg.2020.04.031.
63. Inoue K, Khan FH, Remme EW, et al. Determinants of left atrial reservoir and pump strain and use of atrial strain for evaluation of left ventricular filling pressure. Eur Heart J Cardiovasc Imaging. 2021;23(1):61–70. https://doi.org/10.1093/ehjci/jeaa415.
64. Pastore MC, Mandoli GE, Aboumarie HS, et al. Basic and advanced echocardiography in advanced heart failure: an overview. Heart Fail Rev. 2020;25(6):937–48. https://doi.org/10.1007/s10741-019-09865-3.
65. Cameli M, Pastore MC, Campora A, Lisi M, Mandoli GE. Donor shortage in heart transplantation: How can we overcome this challenge? Front Cardiovasc Med. 2022;9:1001002. Published 2022 Oct 17. https://doi.org/10.3389/fcvm.2022.1001002.
66. Lisi M, Mandoli GE, Cameli M, et al. Left atrial strain by speckle tracking predicts atrial fibrosis in patients undergoing heart transplantation. Eur Heart J Cardiovasc Imaging. 2022;23(6):829–35. https://doi.org/10.1093/ehjci/jeab106.
67. Delahaye JP, Gare JP, Viguier E, Delahaye F, De Gevigney G, Milon H. Natural history of severe mitral regurgitation. Eur Heart J. 1991;12(Suppl B):5–9. https://doi.org/10.1093/eurheartj/12.suppl_b.5.
68. Lee R, Marwick TH. Assessment of subclinical left ventricular dysfunction in asymptomatic mitral regurgitation. Eur J

Echocardiogr. 2007;8(3):175–84. https://doi.org/10.1016/j.euje.2006.11.002.
69. Cameli M, Lisi M, Righini FM, et al. Usefulness of atrial deformation analysis to predict left atrial fibrosis and endocardial thickness in patients undergoing mitral valve operations for severe mitral regurgitation secondary to mitral valve prolapse. Am J Cardiol. 2013;111(4):595–601. https://doi.org/10.1016/j.amjcard.2012.10.049.
70. Lisi M, Cameli M, Di Tommaso C, et al. Mitral regurgitation severity correlates with symptoms and extent of left atrial dysfunction: Effect of mitral valve repair. J Clin Ultrasound. 2018;46(1):32–40. https://doi.org/10.1002/jcu.22521.
71. Vahanian A, Beyersdorf F, Praz F, et al. 2021 ESC/EACTS Guidelines for the management of valvular heart disease. Eur Heart J. 2022;43(7):561–632. https://doi.org/10.1093/eurheartj/ehab395.
72. Zile MR, Gaasch WH, Levine HJ. Left ventricular stress-dimension-shortening relations before and after correction of chronic aortic and mitral regurgitation. Am J Cardiol. 1985;56(1):99–105. https://doi.org/10.1016/0002-9149(85)90574-0.
73. Starling MR, Kirsh MM, Montgomery DG, Gross MD. Impaired left ventricular contractile function in patients with long-term mitral regurgitation and normal ejection fraction. J Am Coll Cardiol. 1993;22(1):239–50. https://doi.org/10.1016/0735-1097(93)90840-w.
74. Lisi M, Cameli M, Mandoli GE, et al. Detection of myocardial fibrosis by speckle-tracking echocardiography: from prediction to clinical applications. Heart Fail Rev. 2022;27(5):1857–67. https://doi.org/10.1007/s10741-022-10214-0.
75. Thiedemann KU, Ferrans VJ. Left atrial ultrastructure in mitral valvular disease. Am J Pathol. 1977;89(3):575–604.
76. Ferrans VJ, Massumi RA, Shugoll GI, Ali N, Roberts WC. Ultrastructural studies of myocardial biopsies in 45 patients with obstructive or congestive cardiomyopathy. Recent Adv Stud Cardiac Struct Metab. 1973;2:231–72.
77. Mondillo S, Cameli M, Caputo ML, et al. Early detection of left atrial strain abnormalities by speckle-tracking in hypertensive and diabetic patients with normal left atrial size. J Am Soc Echocardiogr. 2011;24(8):898–908. https://doi.org/10.1016/j.echo.2011.04.014.
78. Hoit BD. Left atrial size and function: role in prognosis. J Am Coll Cardiol. 2014;63(6):493–505. https://doi.org/10.1016/j.jacc.2013.10.055.
79. Yang LT, Liu YW, Shih JY, et al. Predictive value of left atrial deformation on prognosis in severe primary mitral regurgitation. J Am Soc Echocardiogr. 2015;28(11):1309–1317.e4. https://doi.org/10.1016/j.echo.2015.07.004.
80. Witkowski TG, Thomas JD, Delgado V, et al. Changes in left ventricular function after mitral valve repair for severe organic mitral regurgitation. Ann Thorac Surg. 2012;93(3):754–60. https://doi.org/10.1016/j.athoracsur.2011.11.034.
81. Henein MY, Holmgren A, Lindqvist P. Left atrial function in volume versus pressure overloaded left atrium. Int J Cardiovasc Imaging. 2015;31(5):959–65. https://doi.org/10.1007/s10554-015-0638-6.
82. Ahmed MI, Gladden JD, Litovsky SH, et al. Increased oxidative stress and cardiomyocyte myofibrillar degeneration in patients with chronic isolated mitral regurgitation and ejection fraction >60%. J Am Coll Cardiol. 2010;55(7):671–9. https://doi.org/10.1016/j.jacc.2009.08.074.
83. Goette A, Juenemann G, Peters B, et al. Determinants and consequences of atrial fibrosis in patients undergoing open heart surgery. Cardiovasc Res. 2002;54(2):390–6. https://doi.org/10.1016/s0008-6363(02)00251-1.
84. Melduni RM, Suri RM, Seward JB, et al. Diastolic dysfunction in patients undergoing cardiac surgery: a pathophysiological mechanism underlying the initiation of new-onset post-operative atrial fibrillation. J Am Coll Cardiol. 2011;58(9):953–61. https://doi.org/10.1016/j.jacc.2011.05.021.
85. Maesen B, Nijs J, Maessen J, Allessie M, Schotten U. Post-operative atrial fibrillation: a maze of mechanisms. Europace. 2012;14(2):159–74. https://doi.org/10.1093/europace/eur208.
86. Dobrev D, Aguilar M, Heijman J, Guichard JB, Nattel S. Postoperative atrial fibrillation: mechanisms, manifestations and management. Nat Rev Cardiol. 2019;16(7):417–36. https://doi.org/10.1038/s41569-019-0166-5.
87. Kawczynski MJ, Gilbers M, Van De Walle S, et al. Role of pre-operative transthoracic echocardiography in predicting post-operative atrial fibrillation after cardiac surgery: a systematic review of the literature and meta-analysis. Europace. 2021;23(11):1731–43. https://doi.org/10.1093/europace/euab095.
88. Chang SL, Chen YC, Chen YJ, et al. Mechanoelectrical feedback regulates the arrhythmogenic activity of pulmonary veins. Heart. 2007;93(1):82–8. https://doi.org/10.1136/hrt.2006.089359.
89. Diwan A, McCulloch M, Lawrie GM, Reardon MJ, Nagueh SF. Doppler estimation of left ventricular filling pressures in patients with mitral valve disease [published correction appears in Circulation. 2005 Jul 26;112(4):e76. Diwan, Abhvinav [corrected to Diwan, Abhinav]]. Circulation. 2005;111(24):3281–9. https://doi.org/10.1161/CIRCULATIONAHA.104.508812.
90. Sugimoto T, Bandera F, Generati G, et al. Left atrial dynamics during exercise in mitral regurgitation of primary and secondary origin: pathophysiological insights by exercise echocardiography combined with gas exchange analysis. JACC Cardiovasc Imaging. 2020;13(1 Pt 1):25–40. https://doi.org/10.1016/j.jcmg.2018.12.031.
91. Mandoli GE, Pastore MC, Benfari G, et al. Left atrial strain as a pre-operative prognostic marker for patients with severe mitral regurgitation. Int J Cardiol. 2021;324:139–45. https://doi.org/10.1016/j.ijcard.2020.09.009.
92. Debonnaire P, Leong DP, Witkowski TG, et al. Left atrial function by two-dimensional speckle-tracking echocardiography in patients with severe organic mitral regurgitation: association with guidelines-based surgical indication and postoperative (long-term) survival. J Am Soc Echocardiogr. 2013;26(9):1053–62. https://doi.org/10.1016/j.echo.2013.05.019.
93. Bonow RO. Left atrial function in mitral regurgitation: guilt by association. JACC Cardiovasc Imaging. 2014;7(3):233–5. https://doi.org/10.1016/j.jcmg.2014.01.009.
94. Ancona R, Comenale Pinto S, Caso P, et al. Two-dimensional atrial systolic strain imaging predicts atrial fibrillation at 4-year follow-up in asymptomatic rheumatic mitral stenosis. J Am Soc Echocardiogr. 2013;26(3):270–7. https://doi.org/10.1016/j.echo.2012.11.016.
95. Strauer BE. Ventricular function and coronary hemodynamics in hypertensive heart disease. Am J Cardiol. 1979;44(5):999–1006. https://doi.org/10.1016/0002-9149(79)90235-2.
96. Galli E, Fournet M, Chabanne C, et al. Prognostic value of left atrial reservoir function in patients with severe aortic stenosis: a 2D speckle-tracking echocardiographic study. Eur Heart J Cardiovasc Imaging. 2016;17(5):533–41. https://doi.org/10.1093/ehjci/jev230.
97. Meimoun P, Djebali M, Botoro T, et al. Left atrial strain and distensibility in relation to left ventricular dysfunction and prognosis in aortic stenosis. Echocardiography. 2019;36(3):469–77. https://doi.org/10.1111/echo.14258.
98. Cameli M, Lisi M, Reccia R, et al. Pre-operative left atrial strain predicts post-operative atrial fibrillation in patients undergoing

aortic valve replacement for aortic stenosis. Int J Cardiovasc Imaging. 2014;30(2):279–86. https://doi.org/10.1007/s10554-013-0323-6.

99. Pernigo M, Benfari G, Geremia G, et al. Atrial function as an independent predictor of postoperative atrial fibrillation in patients undergoing aortic valve surgery for severe aortic stenosis. J Am Soc Echocardiogr. 2017;30(10):956–965.e1. https://doi.org/10.1016/j.echo.2017.07.001.
100. Calin A, Mateescu AD, Rosca M, et al. Left atrial dysfunction as a determinant of pulmonary hypertension in patients with severe aortic stenosis and preserved left ventricular ejection fraction. Int J Cardiovasc Imaging. 2017;33(12):1939–47. https://doi.org/10.1007/s10554-017-1211-2.
101. D'Ascenzi F, Cameli M, Iadanza A, et al. Improvement of left ventricular longitudinal systolic function after transcatheter aortic valve implantation: a speckle-tracking prospective study. Int J Cardiovasc Imaging. 2013;29(5):1007–15. https://doi.org/10.1007/s10554-012-0175-5.
102. Antoni ML, ten Brinke EA, Atary JZ, et al. Left atrial strain is related to adverse events in patients after acute myocardial infarction treated with primary percutaneous coronary intervention. Heart. 2011;97(16):1332–7. https://doi.org/10.1136/hrt.2011.227678.
103. Ersbøll M, Andersen MJ, Valeur N, et al. The prognostic value of left atrial peak reservoir strain in acute myocardial infarction is dependent on left ventricular longitudinal function and left atrial size. Circ Cardiovasc Imaging. 2013;6(1):26–33. https://doi.org/10.1161/CIRCIMAGING.112.978296.
104. Oki T, Miyoshi H, Oishi Y, Mizuguchi Y, Ara N, Iuchi A. The impact of hypertension as a road to heart failure with preserved ejection fraction: diagnostic value of two-dimensional speckle tracking echocardiography for the early impairment of left atrial-left ventricular-arterial coupling. Curr Hypertens Rev. 2014;10(4):177–88. https://doi.org/10.2174/1573402111666150206123245.
105. Degirmenci H, Duman H, Demirelli S, et al. Assessment of effect of irbesartan and nebivolol on the left atrium volume and deformation in the patients with mild-moderate hypertension. Eur Rev Med Pharmacol Sci. 2014;18(6):781–9.
106. Farina JM, Barry T, Arsanjani R, Ayoub C, Naqvi TZ. Three-dimensional transesophageal echocardiography in percutaneous catheter-based cardiac interventions. J Clin Med. 2023;12(17):5664. Published 2023 Aug 31. https://doi.org/10.3390/jcm12175664.
107. O'Connor K, Magne J, Rosca M, et al. Left atrial function and remodelling in aortic stenosis. Eur J Echocardiogr. 2011;12(4):299–305. https://doi.org/10.1093/ejechocard/jer006.
108. Wang Z, Tan H, Zhong M, Jiang G, et al. Strain rate imaging for noninvasive functional quantification of the left atrium in hypertensive patients with paroxysmal atrial fibrillation. Cardiology. 2008;109(1):15–24. https://doi.org/10.1159/000105322.
109. Cameli M, Lisi M, Focardi M, et al. Left atrial deformation analysis by speckle tracking echocardiography for prediction of cardiovascular outcomes. Am J Cardiol. 2012;110(2):264–9. https://doi.org/10.1016/j.amjcard.2012.03.022.

Cardiac Tumors

16

Michael Y. Henein, Mary Sheppard, and Michael Rigby

Benign Tumors

Cardiac tumors are rarely suspected clinically but usually appear as unexpected findings when patients are investigated for syncope, breathlessness, thromboembolism, or constitutional manifestations such as congestive heart failure or pulmonary hypertension [1]. Transthoracic echocardiography provides a great opportunity to identify clinically silent tumors [2], although an extension to extracardiac structures should be further investigated by transesophageal echocardiography [3], computed tomography (CT) scanning, or cardiac magnetic resonance (CMR). Benign tumors form approximately 80% of all cardiac tumors, 70% of which are myxomas [4].

Myxomas

Myxomas affect adults in the third to sixth decade of life with 3:1 female predominance [5, 6]. They may remain completely silent until either accidentally discovered or become large enough to interfere with cardiac function and give symptoms [7]. Myxomas may occur anywhere in the heart but in over 80% of patients, the left atrium is involved, followed by a right atrium, while the ventricles can be involved only in 5% of cases [8]. They rarely occur concurrently in more than one chamber [9]. Left atrial myxomas originate from the inter-atrial septum. They may increase in size and eventually occupy nearly the whole of the atrial cavity

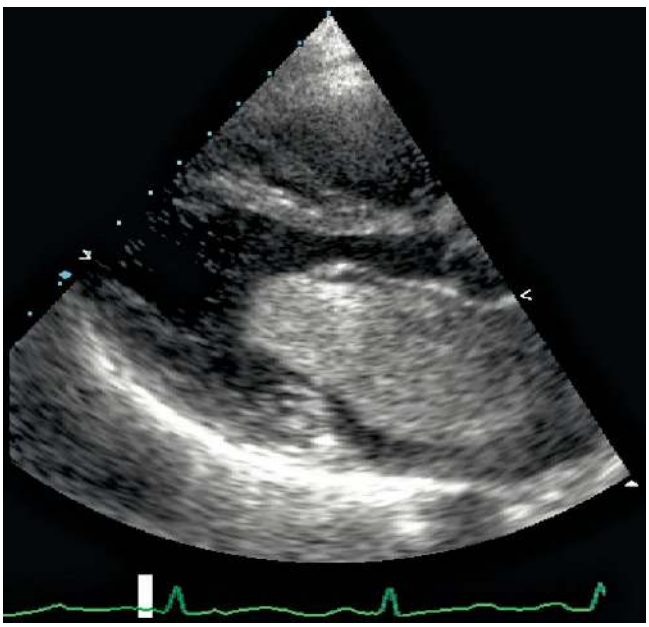


Fig. 16.1 Parasternal long-axis view from a patient with left atrial myxoma. Note the size of the tumor and its relationship to anterior mitral valve leaflet

(Fig. 16.1). Being redundant, they may obstruct the left ventricular inlet, and prolapse into the left ventricle in diastole, a so-called tumor plop (Fig. 16.2). Large tumors may thus cause functional mitral stenosis, and consequently secondary pulmonary hypertension and tricuspid regurgitation (Figs. 16.3 and 16.4) [10].

Right atrial myxoma is much less common [11]. It may obstruct the right ventricular inlet, damage the tricuspid valve leaflets and cause obstruction of the right ventricular inflow tract [12]. Papillary fragments on the tumor surface may break off and cause systemic thromboemboli (Fig. 16.5) [13, 14].

The most important differential diagnosis of atrial myxoma is atrial thrombus. In contrast to atrial myxoma, a thrombus is commonly attached to the atrial wall by a large base and at any segment (Fig. 16.6). The atrial thrombus is

Supplementary Information The online version contains supplementary material available at https://doi.org/10.1007/978-3-031-95894-6_16.

M. Y. Henein (✉)
Imperial College, London, UK

Siena University, Siena, Italy
e-mail: m.henein@imperial.ac.uk

M. Sheppard · M. Rigby
Royal Brompton Hospital, London, UK

© The Author(s), under exclusive license to Springer Nature Switzerland AG 2025
M. Y. Henein (ed.), *Clinical Echocardiography*, https://doi.org/10.1007/978-3-031-95894-6_16

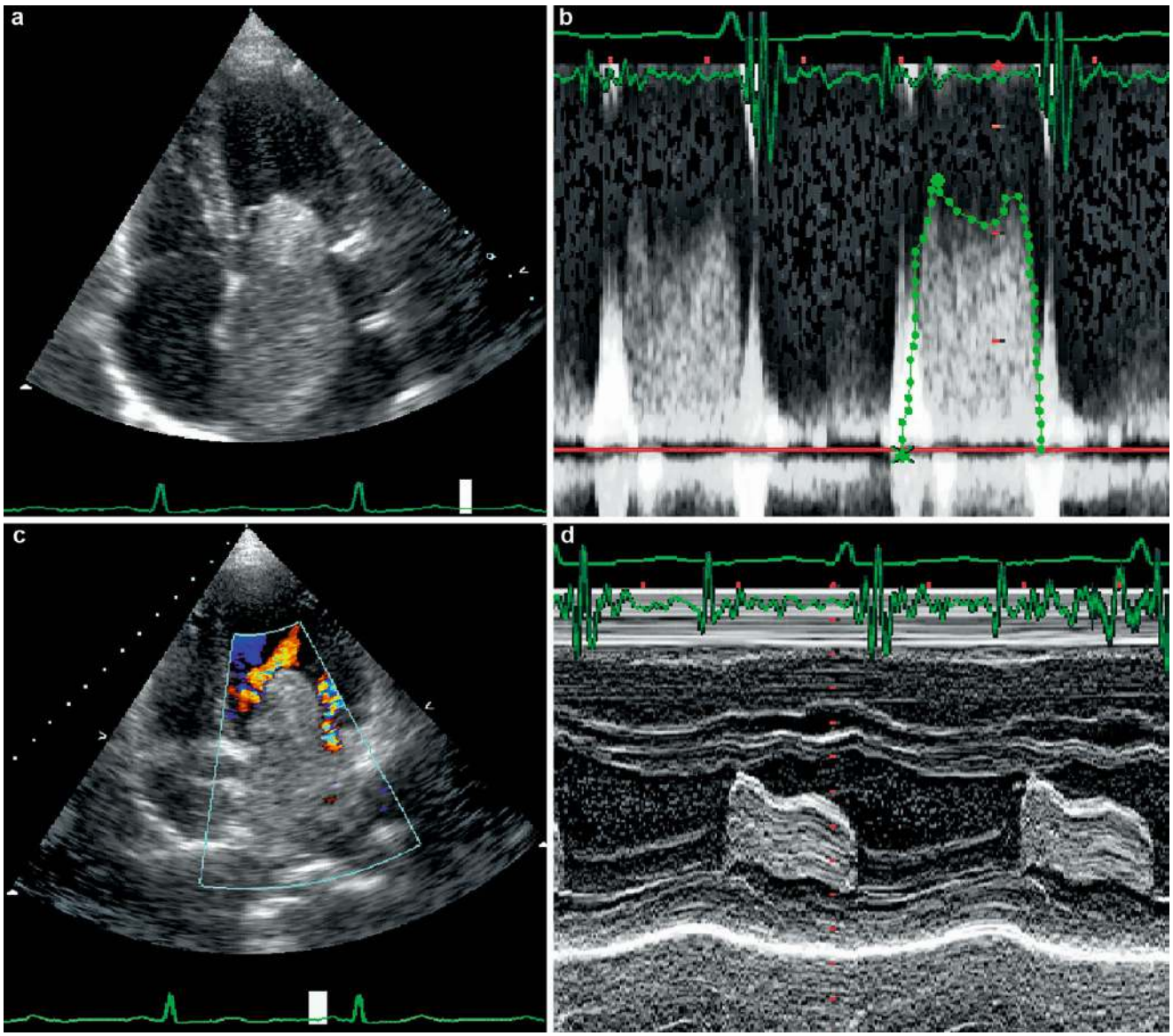


Fig. 16.2 Apical four-chamber images from the same (**a**) patient demonstrating left atrial myxoma (**b**) prolapsing into the LV cavity. Note the aliasing of the color flow Doppler, raised inflow velocities consistent with narrowed ventricular inflow tract (**c**) and the classical mitral valve M-mode of prolapsing myxoma (**d**)

not pedunculated and is immobile [15]. Thrombus usually does not have a rounded contour as does the myxoma but could take any shape and form, commonly obliterating corners. Atrial thrombus is also commonly associated with other pathologies e.g. mitral valve disease, dilated atrium, atrial fibrillation and raised atrial pressures secondary to left ventricular disease.

Surgical excision is the only management for large tumors and results in normalization of atrial size and function (Fig. 16.7). Atrial myxoma may recur after excision either in the same area or in adjacent segments if its origin in the left atrium is not completely removed.

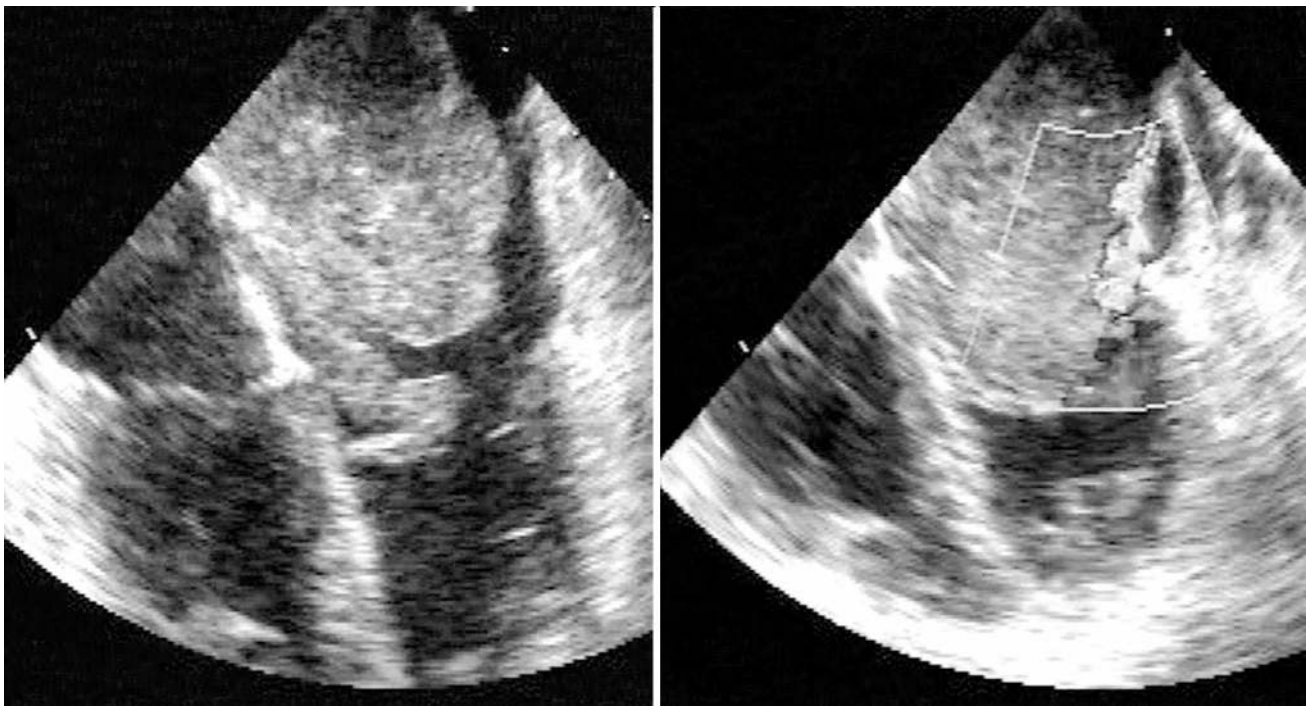


Fig. 16.3 TOE from a patient with left atrial myxoma demonstrating the prolapsing tumor in diastole (left) that narrows ventricular inlet causing raised filling velocities (right)

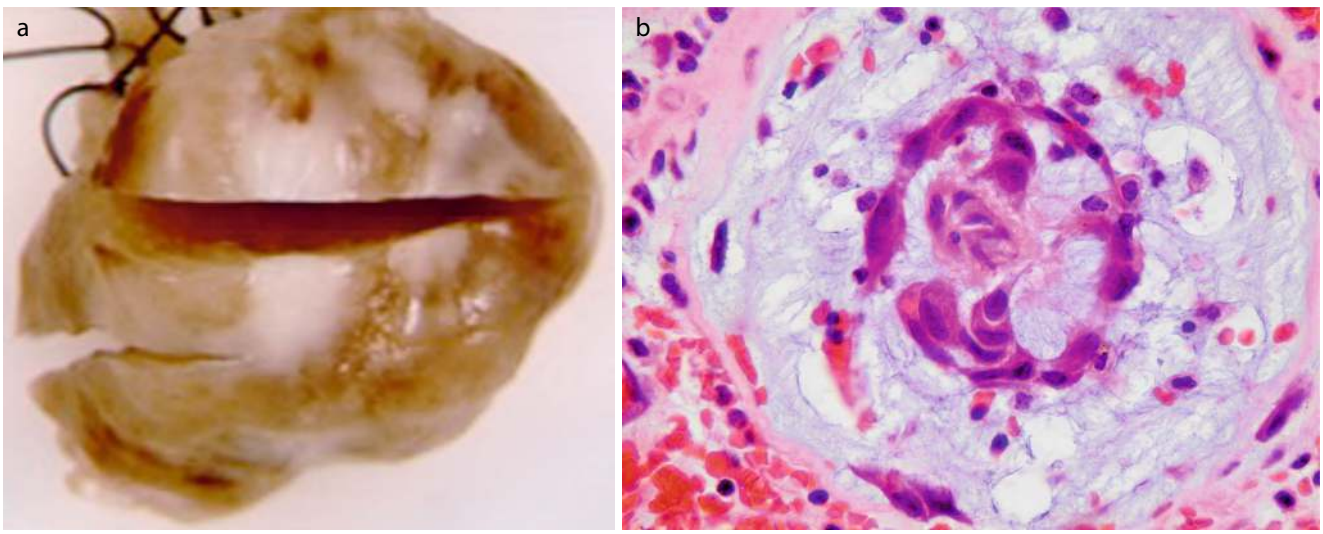


Fig. 16.4 (**a**) Pathological specimen of left atrial myxoma showing myxoid tissue (**b**) histological section

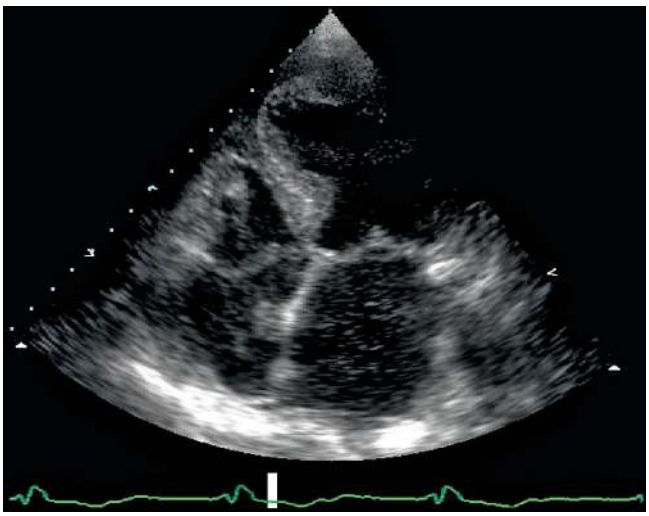


Fig. 16.5 Apical four-chamber view from a patient with small right atrial myxoma

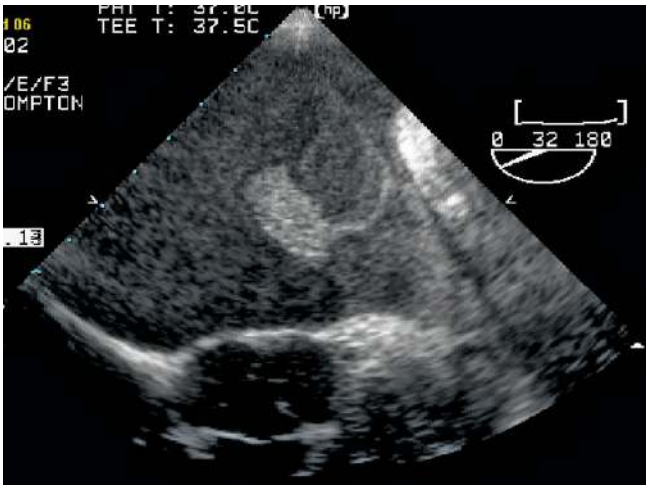


Fig. 16.6 TOE demonstrating large left atrium, spontaneous contrast and a free wall thrombus

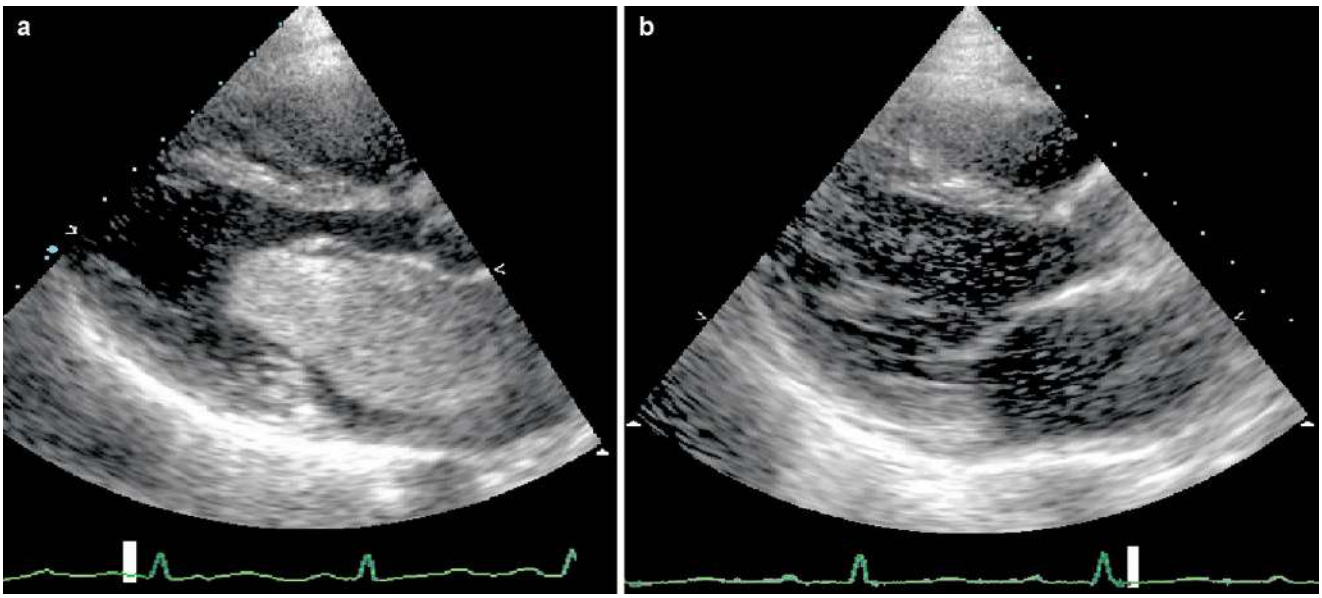


Fig. 16.7 Parasternal long-axis view from a patient with left atrial myxoma (left). Note the normalization of the left atrial size after excision of the tumor (right)

Fibroelastoma

This benign mass appears as a small frond-like tumor, and is usually solitary but rarely multiple [16, 17]. Although it can be found anywhere in the heart, it is commonly attached to the valves or ventricular outflow tract (Figs. 16.8 and 16.9). A fibroelastoma is not usually associated with any symptoms but is accidentally found either during routine scanning or surgery for other pathology.

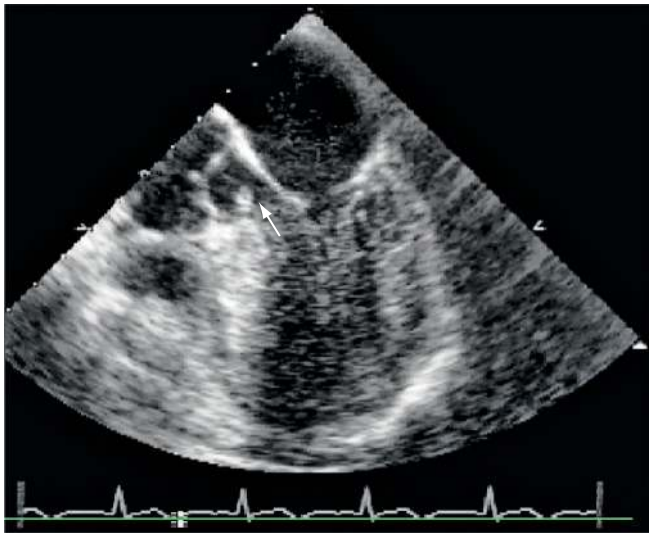


Fig. 16.8 Apical four-chamber view demonstrating a small fibroelastoma attached to LV outflow tract (arrow)

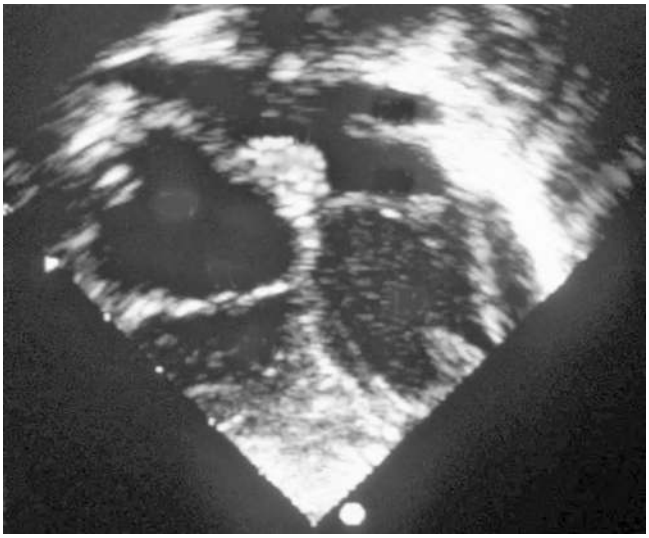


Fig. 16.10 Subcostal views from a patient with atrial septal lipoma

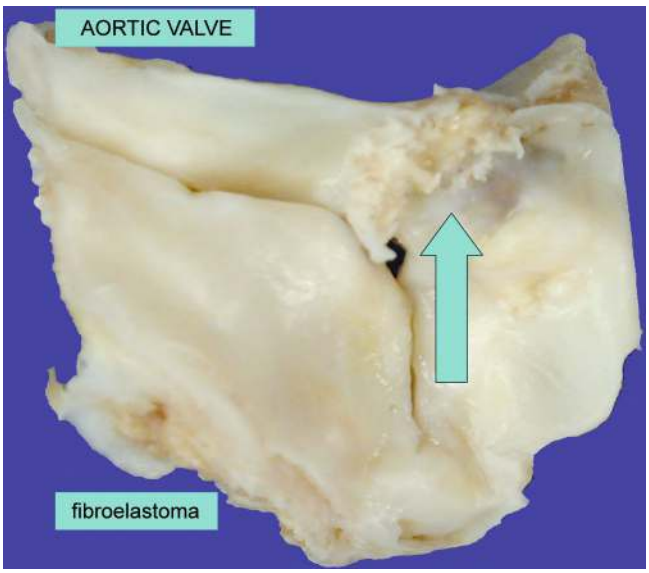


Fig. 16.9 Pathological section showing a small fibroelastoma attached to the mitral valve (arrow)

Lipomas

Lipomas are rare benign tumors that are found attached to the endocardium or epicardium. Demonstrating that they are encapsulated and sessile may help in differentiating them from fat deposition inside and outside the heart [18, 19]. Lipomas are rarely associated with symptoms or clinical manifestations. Although lipomas attached to the interatrial septum may be difficult to differentiate from benign septal hypertrophy their localization and encapsulation may support the diagnosis of lipoma (Fig. 16.10).

Rhabdomyoma [20]: This congenital tumor may grow large enough to obstruct valves and cause sudden death. Characteristically it is associated with tuberosclerosis and multiple tumors are usually found. After birth, the tumors tend to regress in size (Fig. 16.11).

Fibroma: Cardiac fibroma is usually solitary, occurring either at the ventricular free wall or at the septum when involving the septal myocardium (Fig. 16.12). Large fibromas are often inoperable. They are benign and can regress with increasing age in childhood.

Teratoma: Often detected antenatally, these are evident in infancy (Fig. 16.13).

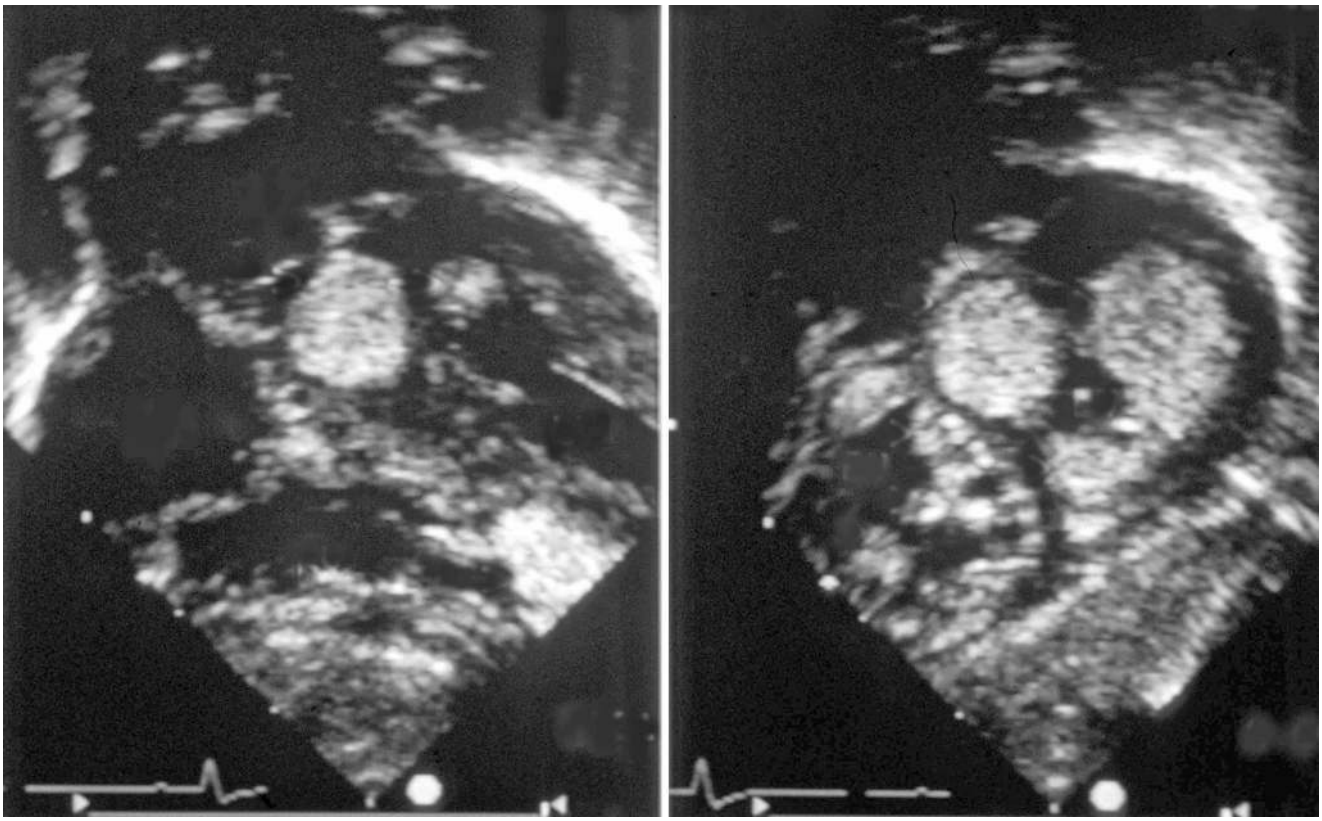


Fig. 16.11 Subcostal views from a patient with multiple rabdomiomata

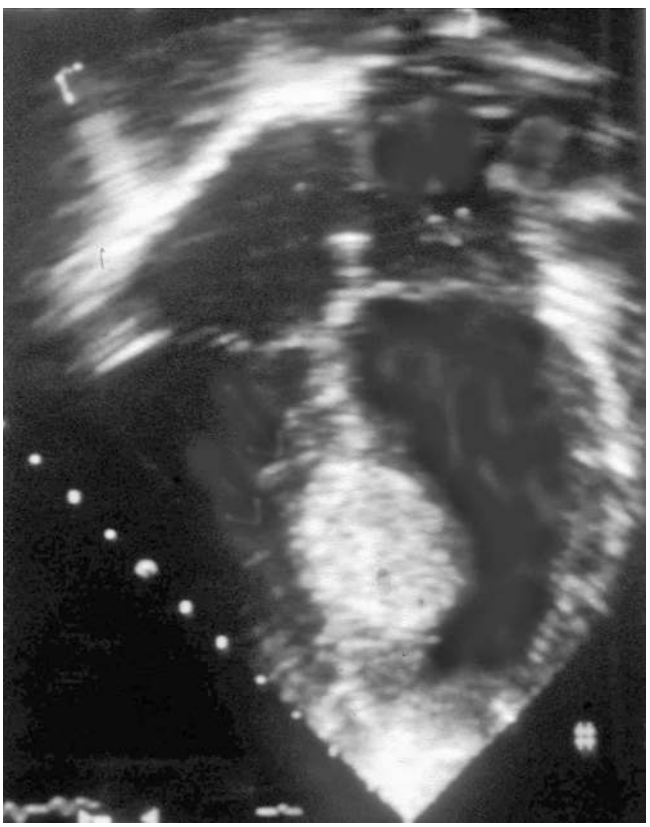


Fig. 16.12 Subcostal view from a patient with ventricular septal fibroma. Notice the tumor size and its distant relationship to the LV inlet



Fig. 16.13 Subcostal views from a patient with teratoma invading the distal septum and right ventricular apex

Malignant Tumors

Primary Malignant Tumors

While benign tumors favor the left atrium, malignant ones tend to occur more commonly in the right heart [21]. Over 80% of primary malignant tumors are sarcomas, the most common one being angiosarcoma [22]. In over 70% of cases, it occurs in the right atrium, invading the myocardium, epicardium and pericardium, and frequently metastasizes to the lungs (Figs. 16.14 and 16.15). Other sarcomas may also occur but are extremely rare. Osteosarcoma may occur in the left atrium as well.

Mesothelioma: The second most common primary malignant tumor which grows from the visceral or parietal layer of the pericardium [23]. It rarely invades the myocardium. It is rarely intracardiac and may mimic a myxoma.

Secondary Malignant Tumors

Secondary malignant tumors are commonly found in autopsies. However, their incidence in the heart is much less than in other organs, possibly due to frequent obliteration of the malignant cells by myocardial contraction, sliding of its layers and poor lymphatic cardiac flow. Secondary tumors may complicate carcinoma of the lung and breast and are less frequently seen with melanoma [24], leukemia and lymphoma [25]. When blood-borne secondaries invade the heart, the right heart is most commonly affected, particularly with malignant melanoma and renal cell carcinoma. Direct invasion of the heart via lung or breast carcinoma is usually associated with large pericardial effusions. Lymphatic spread as in breast carcinoma and lymphoma may invade the pericardium without any obvious intracardiac secondary growth. Melanoma and leukemia commonly involve the heart without pericardial effusion (Figs. 16.16, 16.17, 16.18, 16.19, 16.20, 16.21 and 16.22; Videos 16.1, 16.2, and 16.3).



Fig. 16.15 Apical four-chamber view showing right atrial angiosarcoma invading the atrial wall and disturbing atrial blood flow

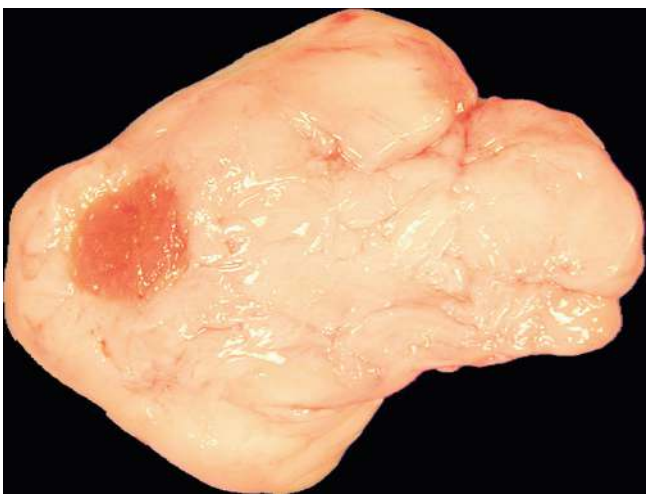


Fig. 16.14 Pathological section demonstrating malignant secondaries invading the right atrium



Fig. 16.16 Parasternal long axis showing melanoma invading right ventricular free wall

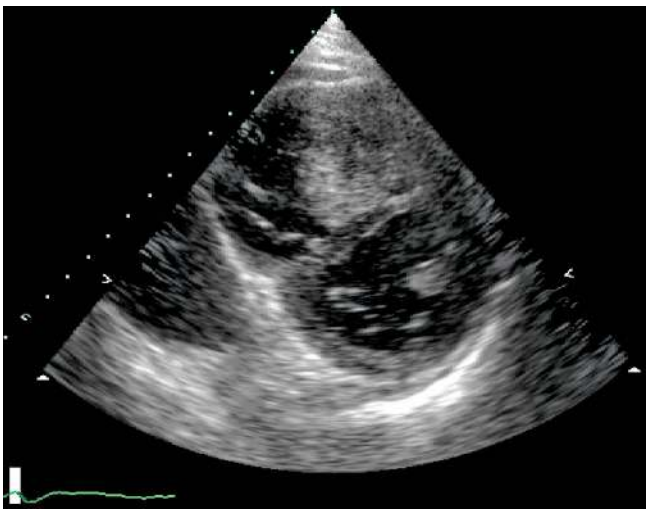


Fig. 16.17 Short axis view showing malignant melanoma invading right venticular free wall

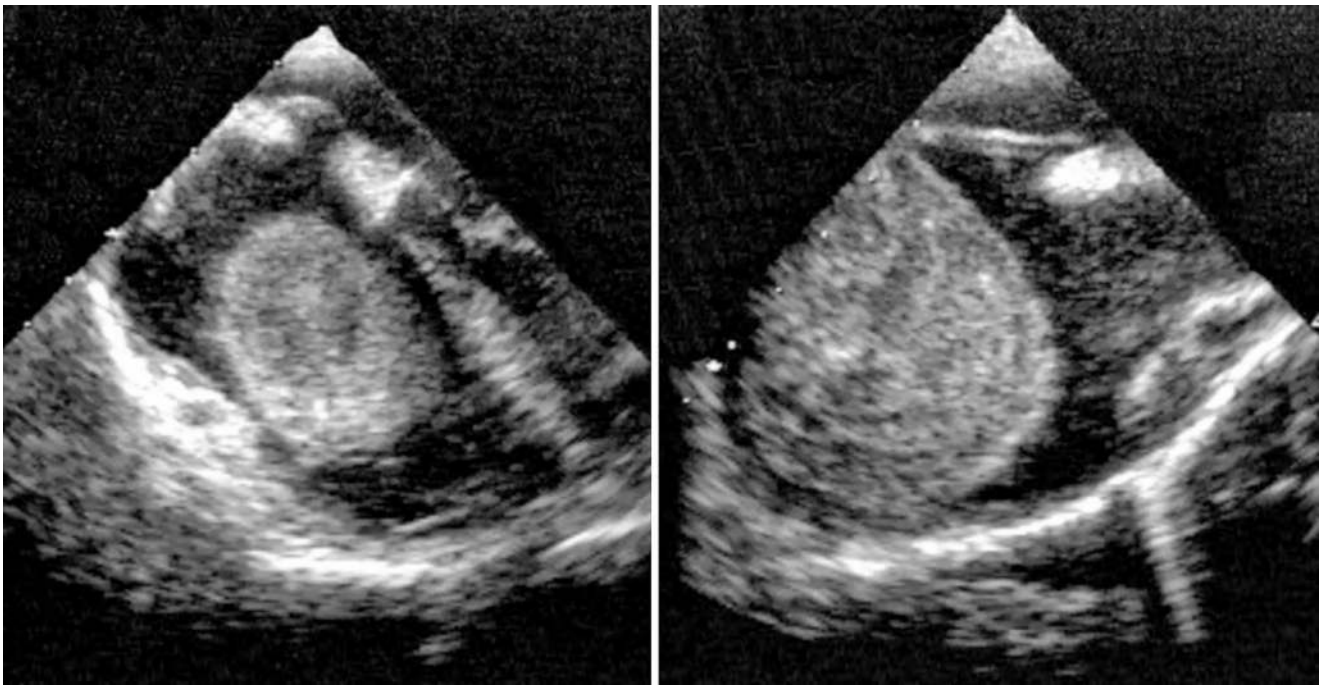


Fig. 16.18 TOE from a patient with renal cell carcinoma with secondaries invading the IVC and the right atrium

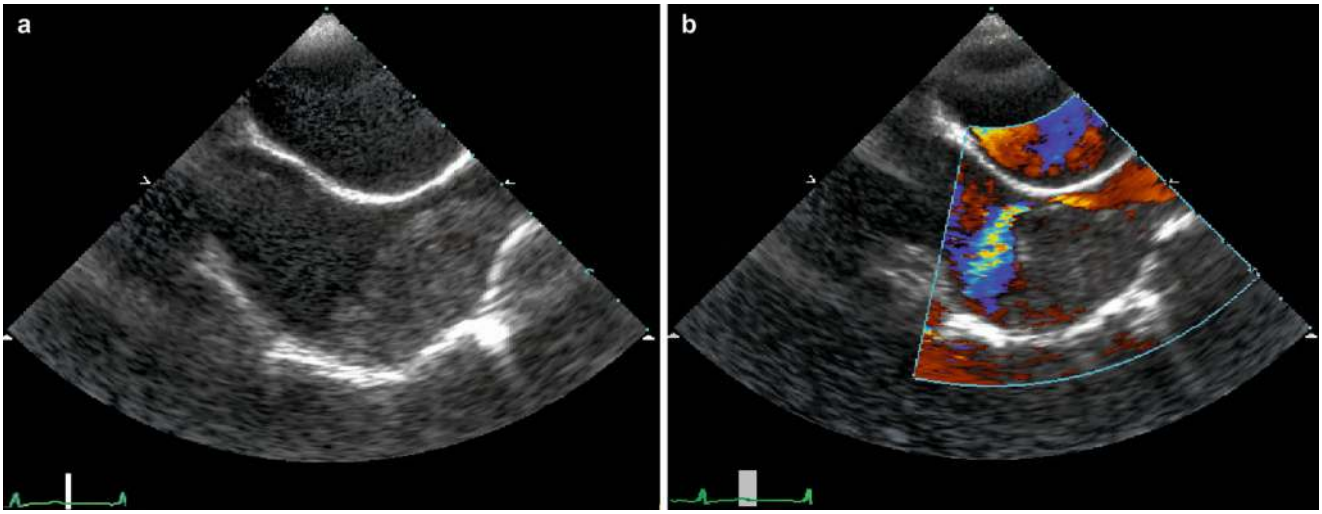


Fig. 16.19 TOE showing osteosarcoma invading the right atrial free wall (**a**) and causing narrowing of its inflow (**b**)



Fig. 16.20 Apical view showing malignant melanoma invading right ventricular septal region near the apex



Fig. 16.21 Apical view showing renal cell carcinoma invading right ventricular free wall

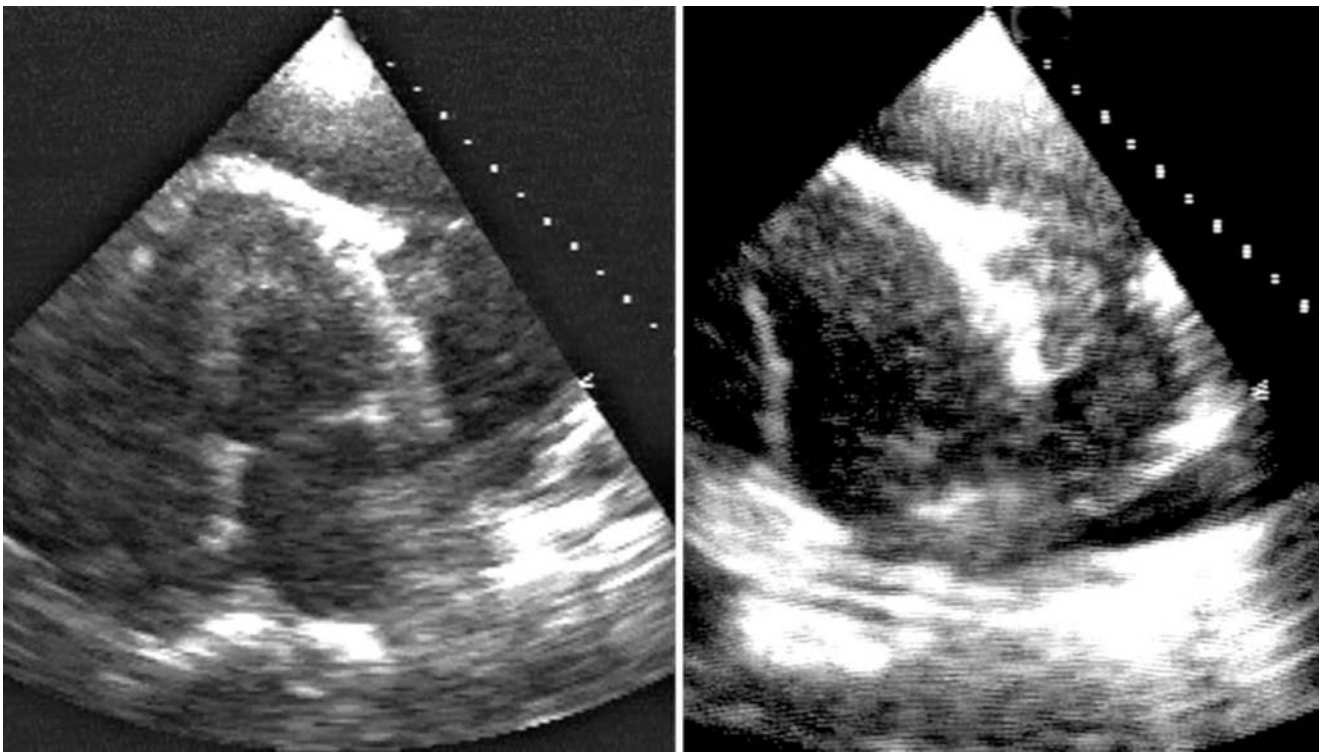


Fig. 16.22 Apical views demonstrating left pleural carcinoma invading and eroding the pericardium and the epicardium of the LV free wall

References

1. Bloor CM, O'Rourke RA. Cardiac tumors: clinical presentation and pathologic correlations. Curr Probl Cardiol. 1984;9(6):7–48.
2. Fyke FE III, Seqard JB, Edwards WD, Miller FA Jr, Reeder GS, Schattenberg TT, et al. Primary cardiac tumors: experience with 30 consecutive patients since the introduction of two-dimensional echocardiography. J Am Coll Cardiol. 1985;5(6):1465–73.
3. Reeder GS, Khandheria BK, Seward JB, Tajik AJ. Transesophageal echocardiography and cardiac masses. Mayo Clin Proc. 1991;66(11):1101–9.
4. Goodwin JF. The spectrum of cardiac tumors. Am J Cardiol. 1968;21(3):307–14.
5. Prichard RW. Tumors of the heart: review of the subject and report of one hundred and fifty cases. Arch Pathol. 1951;51:98–128.
6. Nasser WK, Davis RH, Dillon JC, Tavel ME, Helmen CH, Feigenbaum H, et al. Atrial myxoma. I. Clinical and pathologic features in nine cases. Am Heart J. 1972;83(5):694–704.
7. McAllister HA, Fenoglio JJ. Tumors of the cardiovascular system. Atlas of tumor pathology. Washington: Armed Forces Institute of Pathology; 1978.
8. Salcedo EE, Adams KV, Lever HM, Gill CC, Lombardo H. Echocardiographic findings in 25 patients with left atrial myxoma. J Am Coll Cardiol. 1983;1(4):1162–6.
9. Vargas-Barron J, Romero-Cardenas A, Villegas M, Keirns C, Gomez-Jaume A, Delong R, et al. Transthoracic and transesophageal echocardiographic diagnosis of myxomas in the four cardiac cavities. Am Heart J. 1991;121(3 Pt 1):931–3.
10. Gorcsan J III, Blanc MS, Reddy PS, Marrone GC. Hemodynamic diagnosis of mitral valve obstruction by left atrial myxoma with transesophageal continuous wave Doppler. Am Heart J. 1992;124(4):1109–12.
11. Dashkoff N, Boersma RB, Nanda NC, Gramiak R, Andersen MN, Subramanian S. Bilateral atrial myxomas. Echocardiographic considerations. Am J Med. 1978;65(2):361–6.
12. Turlapati RV, Jacobs LE, Kotler MN. Right atrial myxoma causing total destruction of the tricuspid valve leaflets. Am Heart J. 1990;120(5):1227–31.
13. Bryhn M, Gustafson A, Stubbe I. Two-dimensional echocardiography in the diagnosis of hemorrhages in a left atrial myxoma. Acta Med Scand. 1982;212(6):433–5.
14. Rahilly GT Jr, Nanda NC. Two-dimensional echographic identification of tumor hemorrhages in atrial myxomas. Am Heart J. 1981;101(2):237–9.
15. Reeder GS, Tajik AJ, Seward JB. Left ventricular mural thrombus: two-dimensional echocardiographic diagnosis. Mayo Clin Proc. 1981;56(2):82–6.

16. Lee KS, Topol EJ, Stewart WJ. Atypical presentation of papillary fibroelastoma mimicking multiple vegetations in suspected subacute bacterial endocarditis. Am Heart J. 1993;125(5 Pt 1):1443–5.
17. Richard J, Castello R, Dressler FA, Willman VL, Nashed A, Lewis B, et al. Diagnosis of papillary fibroelastoma of the mitral valve complicated by non-Q-wave infarction with apical thrombus: transesophageal and transthoracic echocardiographic study. Am Heart J. 1993;126(3 Pt 1):710–2.
18. Shirani J, Roberts WC. Clinical, electrocardiographic and morphologic features of massive fatty deposits ("lipomatous hypertrophy") in the atrial septum. J Am Coll Cardiol. 1993;22(1):226–38.
19. Kamiya H, Ohno M, Iwata H, Ohsugi S, Sawada K, Koike A, et al. Cardiac lipoma in the interventricular septum: evaluation by computed tomography and magnetic resonance imaging. Am Heart J. 1990;119(5):1215–7.
20. Smythe JF, Dyck JD, Smallhorn JF, Freedom RM. Natural history of cardiac rhabdomyoma in infancy and childhood. Am J Cardiol. 1990;66(17):1247–9.
21. Burke AP, Cowan D, Virmani R. Primary sarcomas of the heart. Cancer. 1992;69(2):387–95.
22. Glancy DL, Morales JB Jr, Roberts WC. Angiosarcoma of the heart. Am J Cardiol. 1968;21(3):413–9.
23. Skhvatsabaja LV. Secondary malignant lesions of the heart and pericardium in neoplastic disease. Oncology. 1986;43(2):103–6.
24. Glancy DL, Roberts WC. The heart in malignant melanoma. A study of 70 autopsy cases. Am J Cardiol. 1968;21(4):555–71.
25. Roberts WC, Glancy DL, DeVita VT Jr. Heart in malignant lymphoma (Hodgkin's disease, lymphosarcoma, reticulum cell sarcoma and mycosis fungoides). A study of 196 autopsy cases. Am J Cardiol. 1968;22(1):85–107.

Pericardial Disease

17

Michael Y. Henein and Mary Sheppard

Anatomy

The pericardium consists of two layers, a visceral layer lined by mesothelial cells and a parietal or fibrous layer lined also by mesothelial cells but with attached fat and fibrous tissue (Fig. 17.1). The mesothelial layer secretes a small amount of pericardial fluid, usually 50 ml of clear fluid which allows both surfaces to slide together during the cardiac cycle. The fibrous layer is usually 1 mm in thickness while the visceral layer is a transparent membrane on the surface of the heart [1].

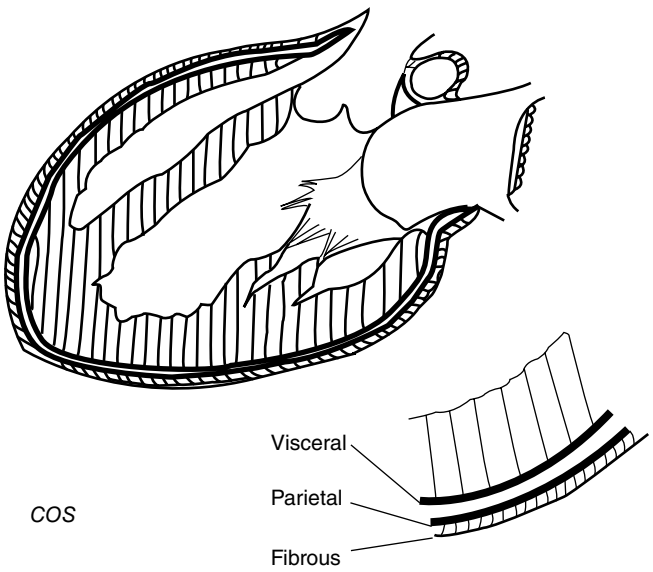


Fig. 17.1 A diagram demonstrating pericardial layers

Physiology

Intrapericardial pressure normally ranges between −2 and 2 mmHg, thus it is less than that of the right heart. It falls with the intrapleural pressure during inspiration resulting in a fall in right-sided cardiac pressure. This causes a modest increase in right heart-filling velocities with inspiration. These effects are often exaggerated in patients with clinically significant pericardial disease.

Pericardial Effusion

Diagnosis of pericardial effusion is only made when the volume of the fluid in the pericardial space is more than the physiological amount of 50 ml. Hundred milliliters of fluid collection in the pericardial space can be visualized by two-dimensional echocardiography [2]. Pericardial effusion can

M. Y. Henein (✉)
Imperial College London, London, UK

Siena University, Siena, Italy
e-mail: m.henein@imperial.ac.uk

M. Sheppard
Royal Brompton Hospital, London, UK

© The Author(s), under exclusive license to Springer Nature Switzerland AG 2025
M. Y. Henein (ed.), *Clinical Echocardiography*, https://doi.org/10.1007/978-3-031-95894-6_17

be secondary to cardiac or noncardiac etiology [3]. The acute rapid collection is usually caused by traumatic injury, iatrogenic ventricular puncture, or aortic dissection with fluid collection inside the pericardium. Chronic effusion is more common than acute effusion. The common causes of chronic fluid accumulation in the pericardial sac are viral infection, uremia, collagen vascular disease, myocardial infarction, myxedema, and malignancy. Also, conditions associated with salt and water retention such as congestive cardiac failure, renal failure, and hepatic cirrhosis may be complicated by pericardial effusion. Most of the pericardial effusion seen in clinical practice however is idiopathic in origin.

A small rapidly accumulated effusion may result in raised intrapericardial pressure and development of symptoms whereas with a slowly accumulating effusion patients may remain asymptomatic even with large volumes [4]. Symptoms in pericardial effusion are not specific and may be in the form of reduced exercise tolerance or dull aching chest pain. Patients may develop symptoms of mediastinal syndrome (cough caused by bronchial compression, dyspnea due to lung compression, or hoarseness of voice caused by recurrent laryngeal nerve compression). Distant heart sounds and widespread dullness to percussion may be the only physical signs until tamponade develops.

Investigations: Chest X-ray does not always confirm the presence of pericardial effusion if it is less than 250 ml. CMR and CT scanning are ideal for assessing pericardial thickness. Echocardiography is the investigation of choice for confirming the presence of pericardial effusion and for assessing its volume [5]. An echo-free space in the pericardium both in M-mode and 2D should be distinguished from anterior pericardial fat [6]. More than 1 cm of pericardial densites that are moving with the pericardium and the epicardium suggest the presence of pericardial fat. A localized effusion should always be looked for from different views; even a small amount adjacent to the left atrium or right atrium can be visualized on two-dimensional echocardiographic images. With a large pericardial collection, the entire heart may swing in the effusion causing electrical alternans. The latter is defined as alternating small R wave amplitudes with normal ones (Figs. 17.2, 17.3, and 17.4) [7].

Pericardial effusion should be differentiated from pleural effusion by identifying the location of the pericardial effusion with respect to the descending aorta and fibrous pericardium (from the parasternal long axis view; Fig. 17.5) [8].

Quantitation of pericardial effusion: semiquantitative estimation with either M-mode or 2D techniques is usually adequate for clinical management. A 1 cm global collection around the heart suggests an approximate amount of 200 mL. With localized effusion a comparative assessment of the effusion size with that of the left ventricle gives a rough estimation of the collection volume. The hemodynamic effects of pericardial effusion depend on the pressure–volume relation of the pericardium, the speed of fluid collection, and the volume of the effusion. In patients with ventricular disease, ventricular compliance may also add to the hemodynamic effects of pericardial effusion [9].

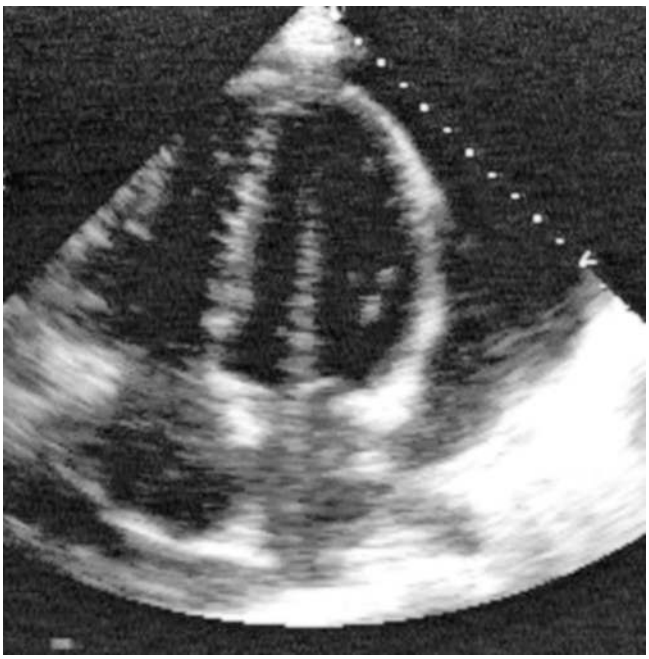


Fig. 17.2 Apical four-chamber view from a patient with a large pericardial effusion. Note the large space between the pericardium and the epicardium

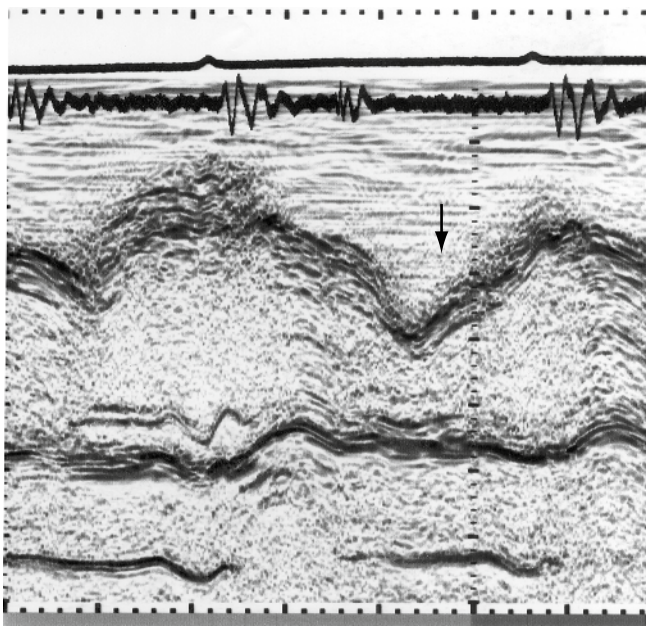


Fig. 17.3 M-mode of the aortic valve and root demonstrating diastolic right ventricular collapse (arrow)

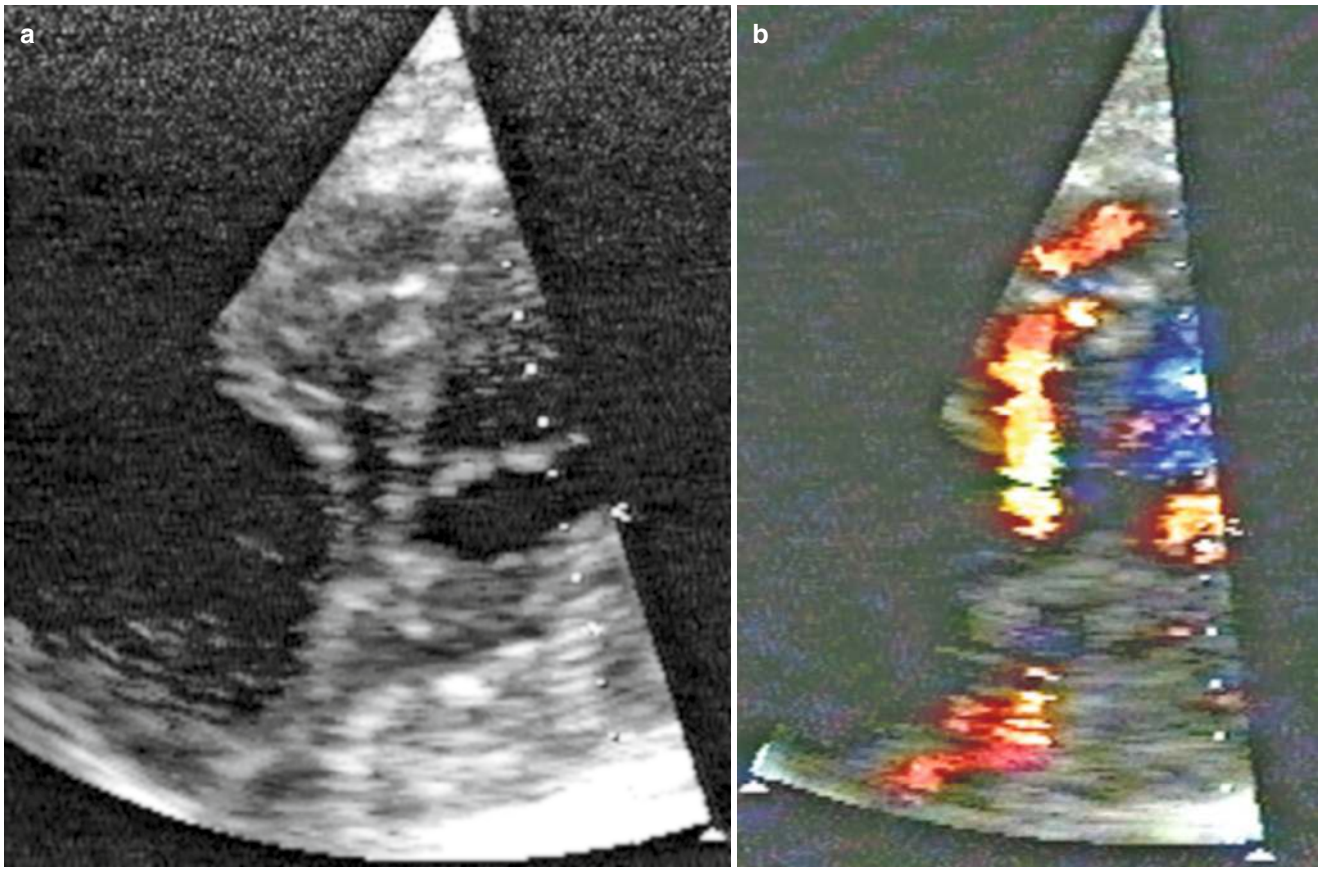


Fig. 17.4 (**a**) Apical four-chamber view from a patient with a localized pericardial effusion behind the right atrium. Note the collapsed right atrial cavity that causes iatrogenic narrowing of the right ventricular inflow tract proximal to the tricuspid valve leaflets and hence the functional raised filling velocities similar to tricuspid stenosis (**b**)

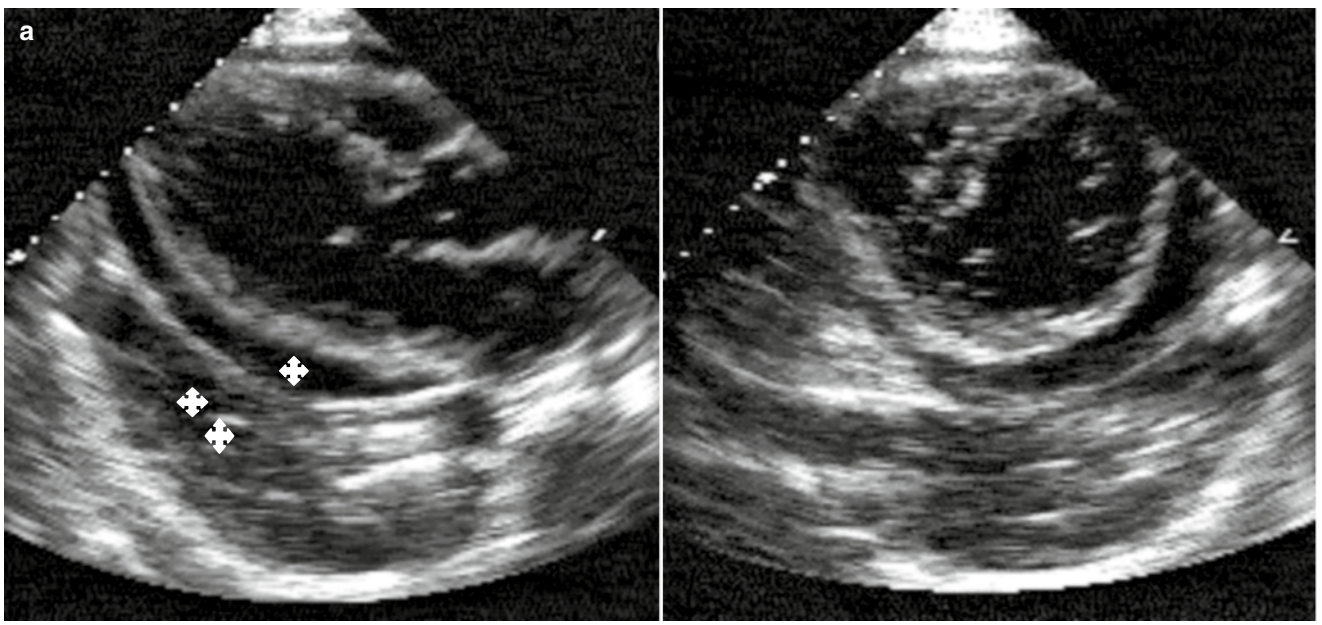


Fig. 17.5 Parasternal long axis (**a**) and short axis (**b**) views from a patient with pericardial (*) and pleural effusions (**). Note the relationship of the latter with respect to the descending aorta and the pericardial effusion

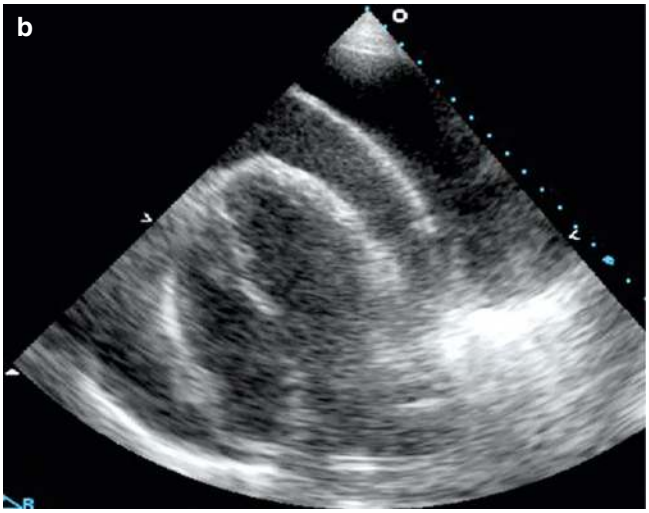


Fig. 17.5 (continued)

Pericardial Tamponade

Pericardial tamponade is a condition of cardiac hemodynamic instability presenting as chamber compression caused by increased intrapericardial pressure greater than the filling pressure of the right and left ventricles. The most common cause of tamponade is malignant effusion or acute fluid collection after cardiac surgery. Right ventricular collapse is a sensitive (92%) and highly specific (100%) diagnostic sign for tamponade. It reflects transient negative transmural early diastolic pressure as pericardial pressure exceeds right ventricular pressure. Right ventricular collapse is better seen from the short axis view across the right ventricular outflow tract and should be confirmed to be diastolic in timing. Right atrial collapse is less sensitive (82%) but equally specific (100%) for pericardial tamponade [10]. Also, a right atrial inversion index greater than 34% strongly suggests tamponade. In the absence of hemodynamically significant pericardial effusion, right ventricular diastolic collapse may be caused by bilateral large pleural effusion [11]. In contrast, the onset of right ventricular collapse may be delayed by myocardial hypertrophy, pulmonary hypertension, or free wall adhesions, commonly associated with malignant effusions [11].

Pathophysiology The pericardium is normally able to stretch to accommodate more than 2000 ml of slowly accumulated fluid without a significant increase in pressure. Rapid accumulation of as little as 200 ml increases pericardial pressure. The inability of the pericardium to distend causes its pressure to rise above right atrial pressure followed by right ventricular pressure and eventually results in right ventricular collapse. Normally intrapericardial and intrapleural pressures fall equally during inspiration. With tamponade intrapericardial pressure does not fall as much, resulting in less pressure gradient between intrathoracic pressure and pulmonary veins and left atrium and ventricle [12]. This results in reduced left-sided filling velocities and stroke volume during inspiration [13]. On the right side of the heart, the increase in right ventricular dimensions during inspiration enhances right-sided filling and ejection during inspiration. A progressive increase in pericardial pressure and right ventricular pressure may affect the left heart adding to its compromised filling during inspiration and significantly drops the stroke volume (Fig. 17.6). The combined effect of the two mechanisms may eventually compromise cardiac output [14]. Intrapericardial pressure greater than 10 mmHg results in right ventricular collapse and raised diastolic pressures of both ventricles as well as increased capillary wedge pressure. This leads to an inspiratory fall of aortic pressure and hence pulsus paradoxus and hypotension. Pericardial effusion to that extent is not the sole cause of arterial paradox, since its mechanisms are complex [15]. Loculated high-pressure posterior pericardial effusion may have a similar effect on left ventricular physiology in the absence of large-volume effusion. Patients with such disturbed hemodynamics often present with raised JVP, tachycardia, and tachypnea. In the absence of pericardial effusion, right ventricular diastolic collapse may be caused by a large pleural effusion that results in a similar disturbed physiology to that of pericardial effusion (Fig. 17.7).

Left ventricular and left atrial collapse are much less commonly seen with tamponade. However, left ventricular invagination caused by localized collection around the free wall has been reported after open heart surgery (Fig. 17.8) [16]. Significant localized posterior effusion is usually caused by anterior adhesions between the right ventricle, the right atrium, and pericardium [17].

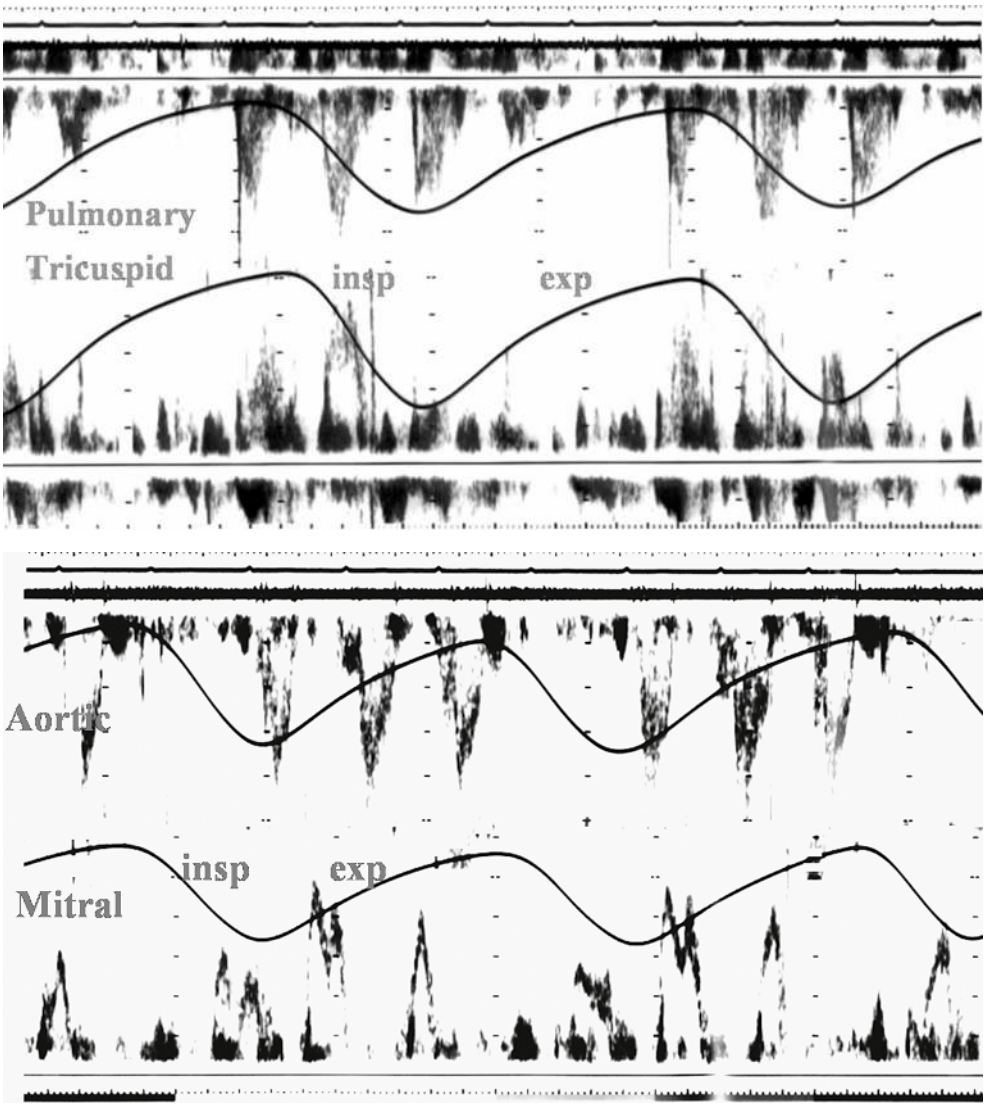


Fig. 17.6 Transtricuspid and pulmonary pulsed wave Doppler velocities from a patient with large pericardial effusion and tamponade (*upper*) and transmitral and aortic Doppler velocities from the same patient (*lower*) demonstrating reciprocal significant alteration of right and left-sided filling and ejection velocities with respiration, being predominantly inspiratory on the right and expiratory on the left side of the heart

Intrapericardial clot formation after cardiac surgery or as a complication of an interventional procedure, for example, transseptal puncture, may result in signs of tamponade due to the rapid increase in intrapericardial pressure even in the absence of a significantly large fluid volume, because of fluid absorption (Fig. 17.9). Diagnosis of this condition is important since it does not usually respond to percutaneous needle aspiration. Transoesophageal echo postoperatively is of great value in making the differential diagnosis [18].

Management of pericardial tamponade: Pericardiocentesis is traditionally performed under fluoroscopy but currently available ultrasound imaging can provide enough guidance to achieve maximum drainage [19]. However, ultrasound cannot provide guidance for needle aspiration since the needle tip is poorly visualized on ultrasound images. Substernal window drainage is usually recommended in patients with resistant, recurrent, or fast-accumulating effusion. Although surgical in nature the procedure allows for therapeutic symptomatic pressure relief, fluid drainage, and pericardial biopsy for cytology. It is generally successful with a large effusion and much less successful with small collections. A subcostal window is also the ideal means for dealing with localized effusion that is not accessible by needle drainage.

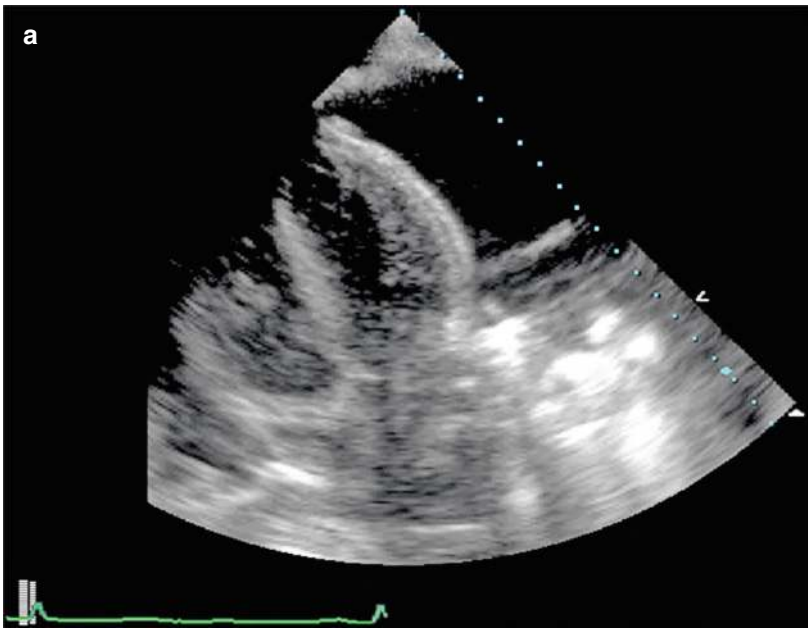


Fig. 17.7 Large left pleural effusion (**a**) from a patient with the phasic right heart filling (**b**) and IVC flow (**c**) showing tamponade-like picture with predominant flow during inspiration

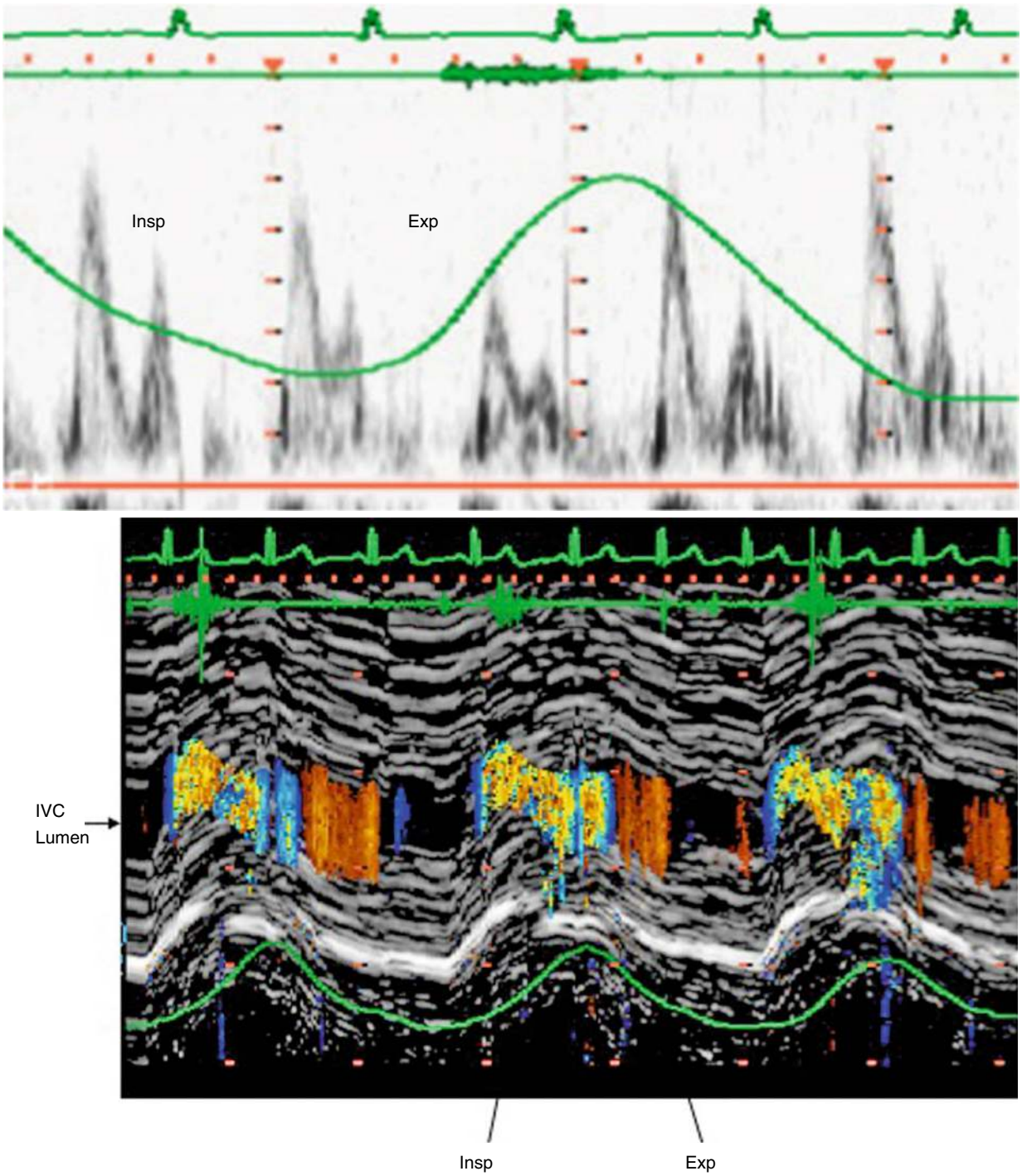


Fig. 17.7 (continued)

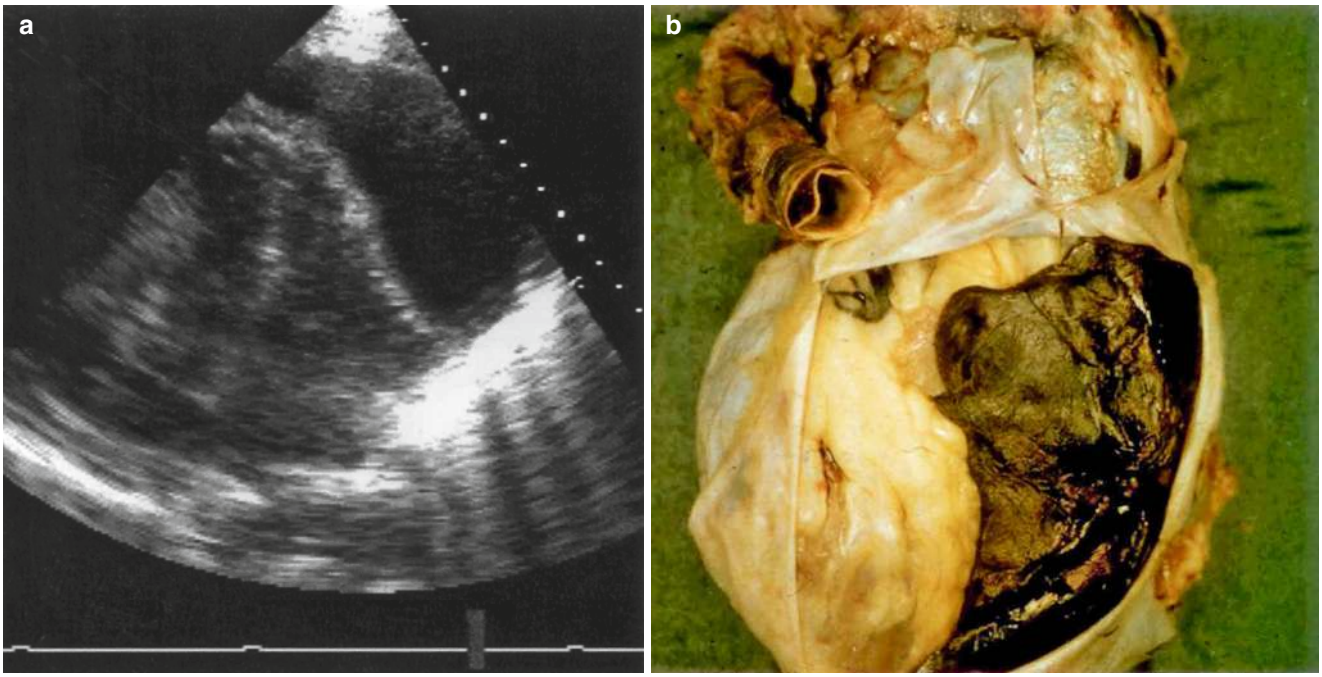


Fig. 17.8 (**a**) Apical four-chamber view from a patient with localized pericardial effusion around the left ventricular free wall. Note the effect of the raised localized pericardial pressure compressing the ventricular free wall. (**b**) Pathological section from a patient with hemopericardium

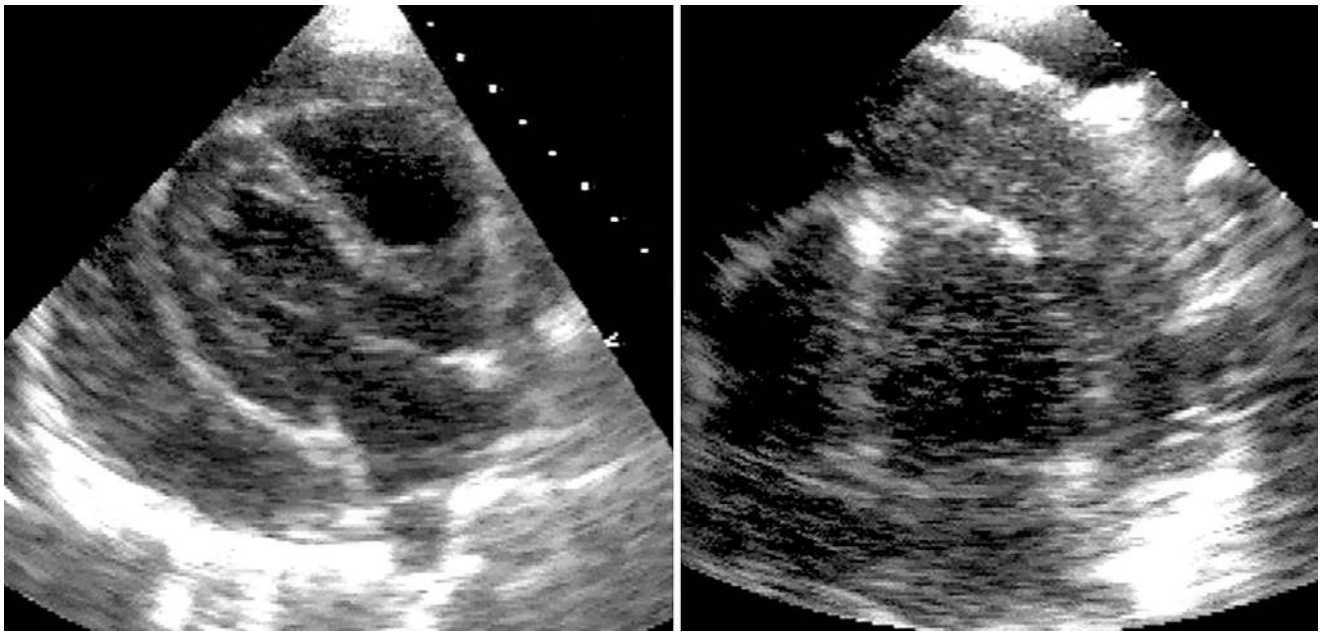


Fig. 17.9 Left parasternal long axis view (*left*) and apical view (*right*) from a patient with postoperative clotting in the pericardial space

Constrictive Pericarditis

Pericardial constriction is a pathological condition characterized by pericardial thickening and fibrosis that results in the adhesion of its two layers and calcium deposition [20]. Constrictive pericarditis is usually seen by the pathologist as a thickened adherent sheet on the cardiac surface, which cannot be separated from the underlying myocardium. Both fibrous and visceral layers fuse together (Fig. 17.10).

Etiology The most common cause of constrictive pericarditis is viral infection which can be missed for a long time until



Fig. 17.10 Specimen of the posterior pericardial segment demonstrating thickened pericardium with complete fusion of its layers (constriction) in a postcardiac surgery subject

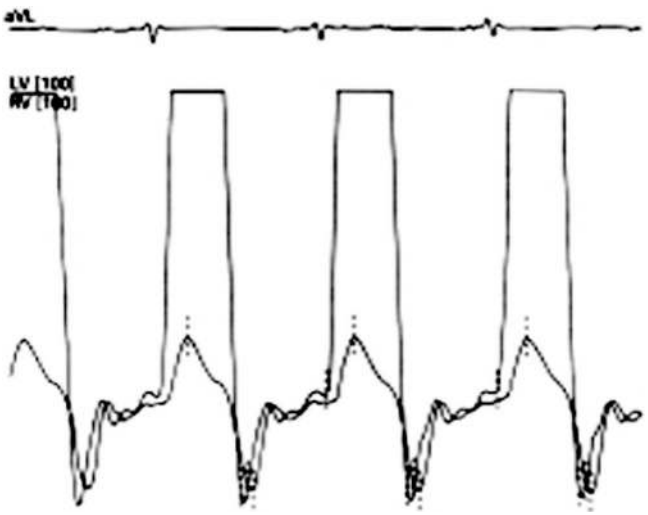


Fig. 17.11 Combined right and left ventricular pressures from a patient with constrictive pericarditis. Note the equalization of the two ventricular pressures in late diastole

presentation. Viral etiology is frequently invoked when no cause is found [21]. Tuberculosis is currently an uncommon cause particularly in the West. Other causes may be radiation, connective tissue disease, chronic renal failure, neoplastic disease, and previous cardiac surgery.

Pathophysiology The stiff pericardium loses its stretching ability to accommodate normal changes in intracardiac pressures. This is demonstrated by the equalization of end-diastolic pressures in the right and left ventricles "dip and plateau pattern," a cardinal sign for diagnosing pericardial constriction (Fig. 17.11). Since this pathology is uniform it manifests itself in the form of raised venous pressure, usually seen in the jugular veins and with systemic fluid retention. This picture also complicates acute or chronic inflammatory processes that involve the pericardium. A thickened pericardium on any imaging technique is not an exclusive diagnostic criterion for constrictive physiology. Furthermore, in rare cases of rapidly increasing ventricular volumes as in dilated cardiomyopathy, the pericardium may be completely normal but demonstrates an external constricting effect, thus adding to the deterioration of the clinical condition.

A fibrosed and unstretchable pericardium being adherent to the epicardial layer of the myocardium can limit its normal movement during the cardiac cycle, particularly in systole, along the ventricular transverse axis. It cannot however affect shortening and lengthening of the longitudinal myocardial fibers that are located in the subendocardium. This longitudinal myocardial function can easily be studied from the movement of the mitral and tricuspid valve annuli in systole and diastole, respectively. The downward displacement of the tricuspid ring and valve in systole results in increased right atrial surface area and volume and a fall in right atrial pressure. This allows a column of blood to fill the atrium and hence the characteristic systolic drop of venous pressure, "the X descent" [1]. A similar presentation can be seen in the left heart physiology. The chronic increase in venous pressure results in systemic congestion and dilatation of hepatic veins, which demonstrate a similar pattern to that of the jugular veins (Fig. 17.12).

The above-disturbed physiology results in fluid retention due to low cardiac output and venous return: raised JVP, congested liver, and lower limb edema. Calcification of the pericardial border may be seen in the chest X-ray but is not always a diagnostic criterion. Pericardial thickening may be better demonstrated by CMR or CT scanning.

Echocardiographic findings: A deep X descent on JVP recording from a patient with very high venous pressure along with the predominant systolic flow in the superior or inferior vena cavae is a very reliable finding for pericardial constriction. The thickened pericardium is a poorly sensitive marker since it can easily be confused with small pericardium effusion with adhesions, fibrous strands, or pericardial fat. In constrictive pericarditis, there is less intracardiac than extracardiac respiratory variation particularly on the right side when compared to that seen with pericardial tamponade [22]. Nonspecific signs include: (a) rapid early diastolic posterior motion of the aortic root, with little additional movement in mid and late diastole caused by pressure equalization between the atrium and the ventricle in late diastole, limiting filling and ring movement [23], (b) premature opening of the pulmonary valve occurring before the P wave of the ECG suggesting significant increase in right ventricular pressures

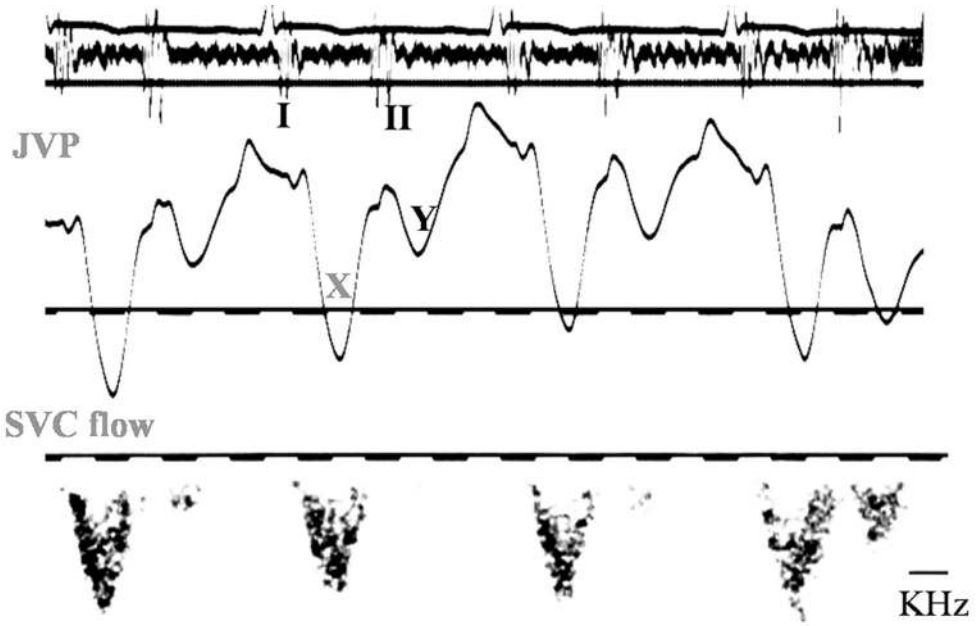


Fig. 17.12 JVP from a patient with pericardial constriction. Note the dominant systolic "X" descent (*top*) coinciding with a systolic right atrial filling component from the superior vena cava (*bottom*)

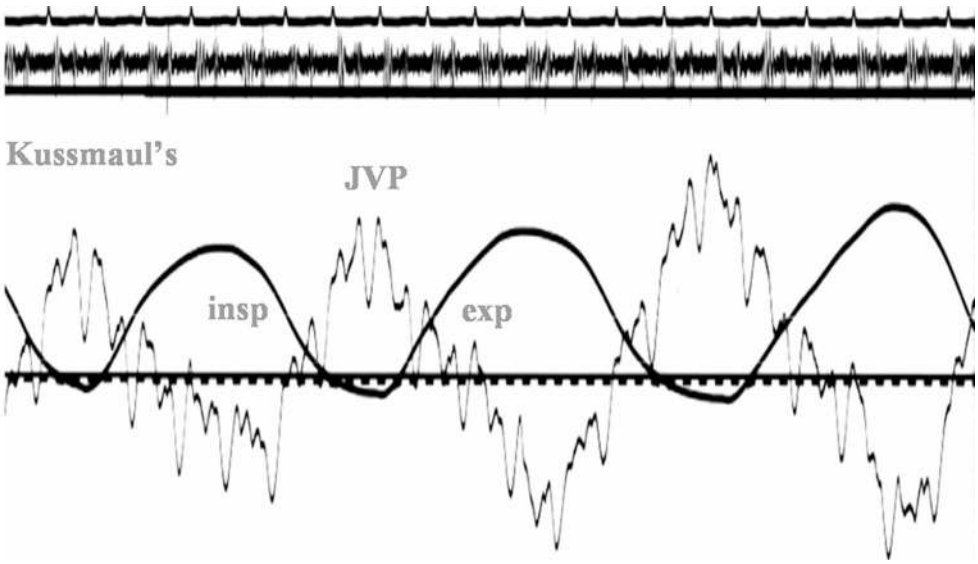


Fig. 17.13 Jugular venous pulse with superimposed respiration recording demonstrating increased venous pressure during inspiration (Kussmaul's sign)

in mid-diastole, and occasionally raised right atrial pressure during inspiration (Kussmaul's sign; Fig. 17.13).

These findings can similarly be seen in other conditions such as left bundle branch block, right ventricular disease, etc. Although a dilated inferior vena cava is commonly seen it is not solely a diagnostic sign for pericardial constriction. Spontaneous contrast in the inferior vena cava, resulting from the limited venous return may be an additional finding in favor of constrictive pericarditis [24].

In summary, therefore, the most sensitive Doppler sign for pericardial constriction in patients with persistent raised venous pressure is the predominant systolic atrial filling along with the "X" descent on the jugular venous pulse.

Management of pericardial constriction: Diuretics are usually given as an attempt to control the raised venous pressures and fluid retention. Pericardiectomy is usually recommended in patients resistant to pharmacological therapy. After surgical removal of the pericardium, the venous pressure drops and the "X" descent disappears on the JVP (Fig. 17.14). This is not always instantaneous and may take up to a few days or even weeks to settle.

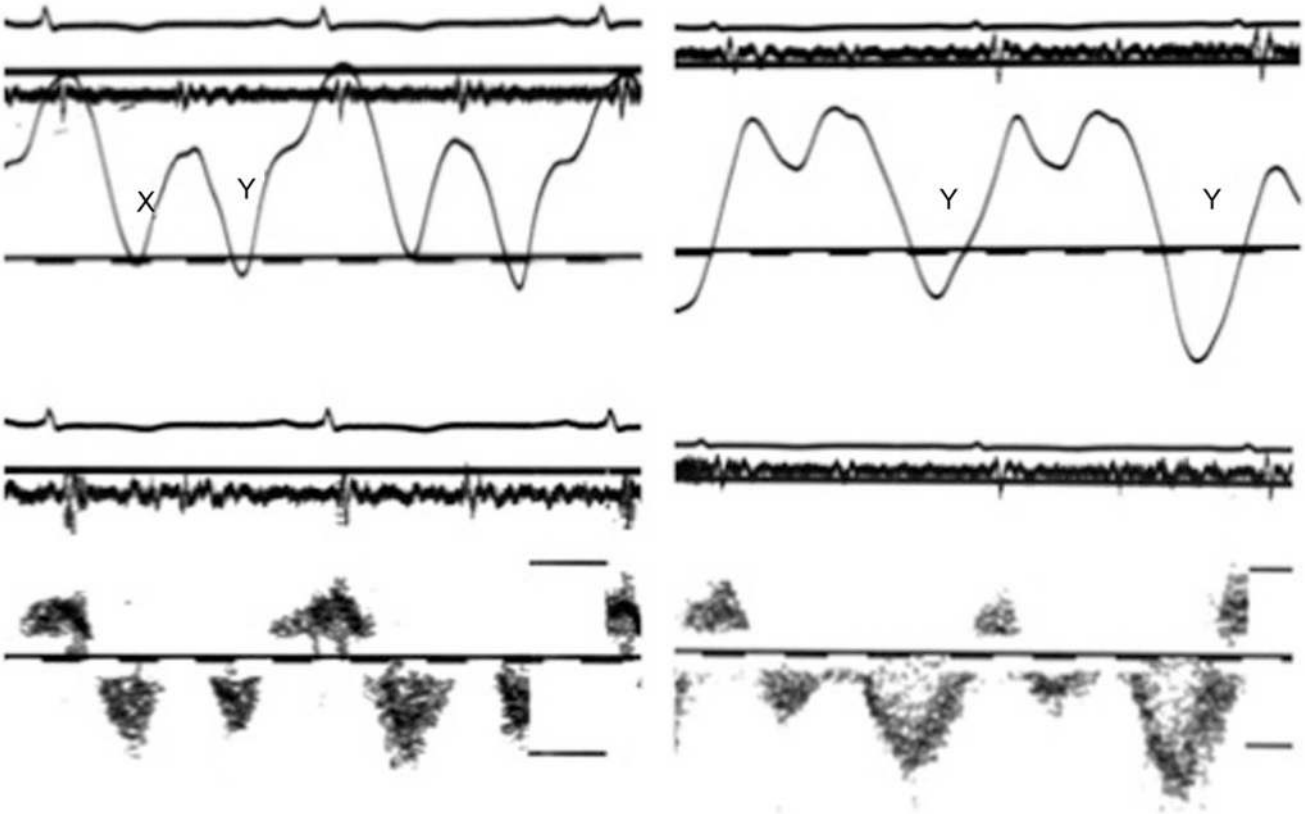


Fig. 17.14 JVP from a patient with constrictive pericarditis before (*left*) and after (*right*) pericardiectomy. Note the diagnostic deep "X" descent and systolic right atrial filling before surgery which disappeared a few days after surgery

Differentiation Between Constrictive Pericarditis and Restrictive Cardiomyopathy [25]

The clinical similarity between these two conditions makes the differential diagnosis difficult i.e. raised venous pressure and fluid retention resistant to medical therapy. While constrictive pericarditis is an extracardiac constraint, restrictive cardiomyopathy is an intrinsic myocardial disease of the ventricle. Restrictive cardiomyopathy is either idiopathic or infiltrative in origin (e.g. amyloid disease). The ventricular muscle may preserve its contractile function but lose its compliance, thereby becoming stiff and incompliant. This is specifically manifested in late diastole as the ventricle becomes unable to fill without a significant rise in the end-diastolic pressure. Therefore, ventricular filling becomes restricted to early diastole with high acceleration and deceleration frequently associated with right-sided third heart sound. A concurrent fall in systemic venous pressure in early diastole, "deep Y descent" is an additional diagnostic sign. Since restrictive cardiomyopathy is a chronic condition it results in a gradual increase in right atrial pressure and size

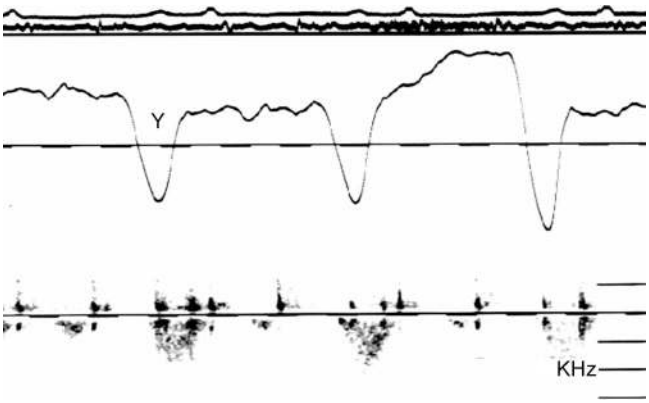


Fig. 17.15 JVP from a patient with restrictive cardiomyopathy. Note the predominant early diastolic "Y" descent and right atrial filling (superior vena caval flow)

which in advanced stages may become the cause of arrhythmia, particularly atrial flutter (Figs. 17.15, 17.16, and 17.17).

Respiratory variation of ventricular filling and ejection velocities may be modestly present in constriction but is absent in restrictive right ventricular disease [26]. As pericardiectomy is largely a radical surgical management for con-

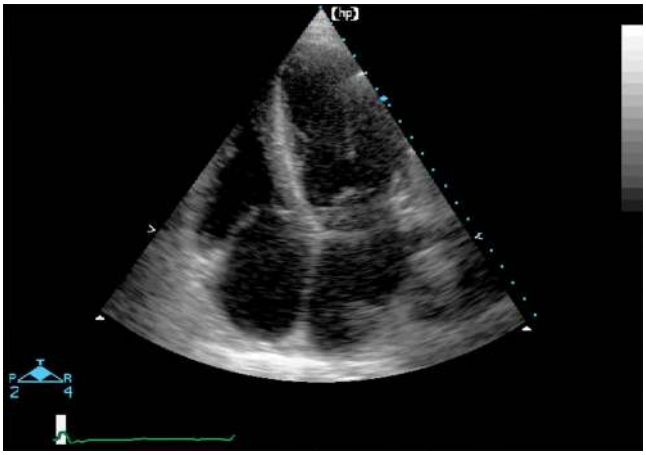


Fig. 17.16 Apical four-chamber view from a patient with restrictive cardiomyopathy showing normal right ventricular size and dilated right atrium in the absence of tricuspid valve stenosis

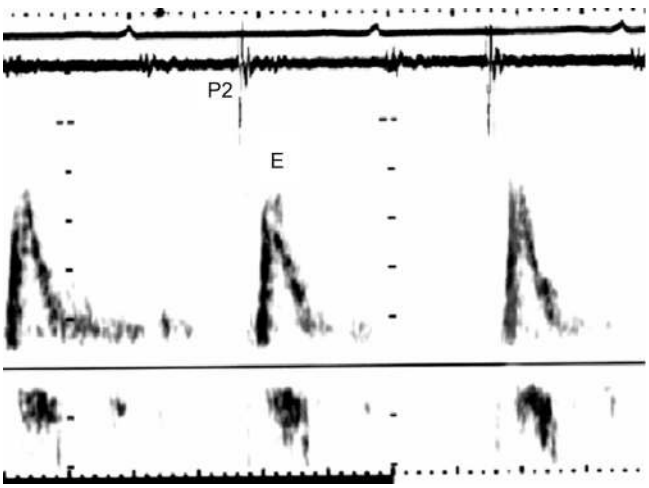


Fig. 17.17 Transtricuspid flow from a patient with restrictive cardiomyopathy showing signs of raised right atrial pressure; fast acceleration, and short deceleration time

striction, empirical medical treatment remains the only available management to control patient symptoms in restrictive cardiomyopathy. Isolated right ventricular restrictive disease is rare, however may be seen in patients with pulmonary stenosis even after surgical treatment [27]. Right ventricular restriction is commonly seen in association with restrictive left ventricular disease particularly amyloid infiltration and occasionally after recurrent open heart surgery or coronary artery disease (Fig. 17.18). When right ventricular restriction and constriction physiology are present, even pericardiectomy does not provide radical cessation of the venous retention because it only alleviates the extracardiac



Fig. 17.18 Apical four-chamber view from a patient with amyloid heart disease. Note the massive infiltration of the ventricles and atria judged by the increased myocardial echo intensity

effect of constriction, being unable to alter the restrictive behavior of the right ventricle.

Pericardial Complications Post- Open Heart Surgery

Apart from the commonly seen pericardial effusion other complications, although rare, may occur:

1. *Pericardial clot*: Clot collection in the pericardial space with or without pericardial effusion is often associated with delayed postoperative clinical recovery. Irrespective of the amount present, it may have an important physiological effect on the overall cardiac function. With time, the clot results in increased intrapericardial pressure and hence disturbed hemodynamics. Surgical removal of the clot is the ideal management of this condition through reopening and emptying the pericardial space. Early detection and management ensure complete recovery [18].
2. "*Tight*" *pericardium*: In the absence of postoperative pericardial effusion or detectable clotting, intrapericardial pressure may be raised to the extent that it affects right-sided physiology, making it phasic with respect to

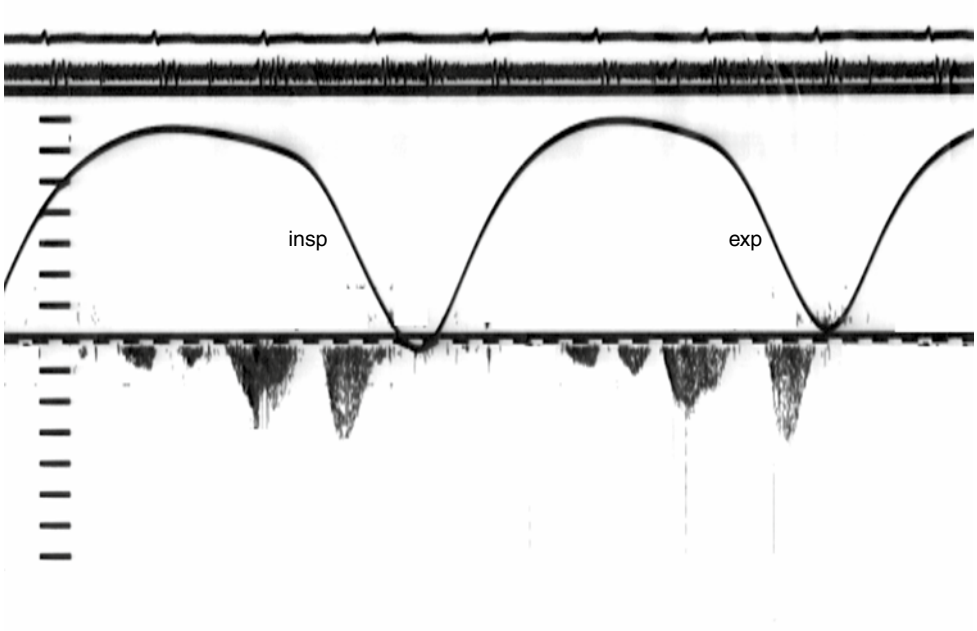


Fig. 17.19 JVP and SVC flow from a patient with postop tight pericardium. Note predominantly right-sided filling during inspiration

respiration, a tamponade-like picture. This condition is uncommon but may be seen after open heart surgery with signs of raised venous pressure. JVP is raised and right-sided physiology, filling and ejection, is predominantly inspiratory (Fig. 17.19). On two-dimensional images, there is no evidence for right atrial or right ventricular collapse. The exact underlying etiology is not clear, although a potential element of pericardial tightness that is self-limited, may be involved. Although these signs may resolve with time, delayed sternal closure has proved beneficial in some of the patients presenting with this phenomenon. The condition tends to settle within days if not few weeks after surgery, with complete normalization of venous pressure. This self-limited course supports the idea of it being iatrogenic pericardial inflammation that resolves itself with time.

3. *Restrictive pericarditis*: This is a rare clinical presentation that usually occurs following open heart surgery [25]. It presents with resistant fluid retention and raised venous pressure. Two-dimensional echocardiographic images may not show any specific abnormality although CMR may demonstrate a thickened pericardium. The underlying pathology seems to be chronic combined pericardial and epicardial inflammation that consequently results in massive fibrosis and adhesions between the two layers. Patients with restrictive pericarditis are usually resistant to medical therapy demonstrating signs of restrictive physiology on both sides of the heart with a dominant early diastolic filling component and short deceleration time. Atrial pressures are usually raised as shown by the extraordinarily short isovolumic relaxation period (Fig. 17.20). Ventricular filling is predominantly early diastolic due to the raised end-diastolic cavity pressure. The jugular venous pulse demonstrates a deep "Y" descent. Although left ventricular minor axis dimensions and systolic function may be preserved, ventricular long axis amplitude is consistently depressed in keeping with myocardial dysfunction.

Management: Resistant cases to medical therapy may respond to surgical decortication of the pericardium. This does not always secure complete recovery since the epicardial layer of the myocardium is usually involved in the pathology with fibrosis extending into the underlying myocardium (Fig. 17.21).

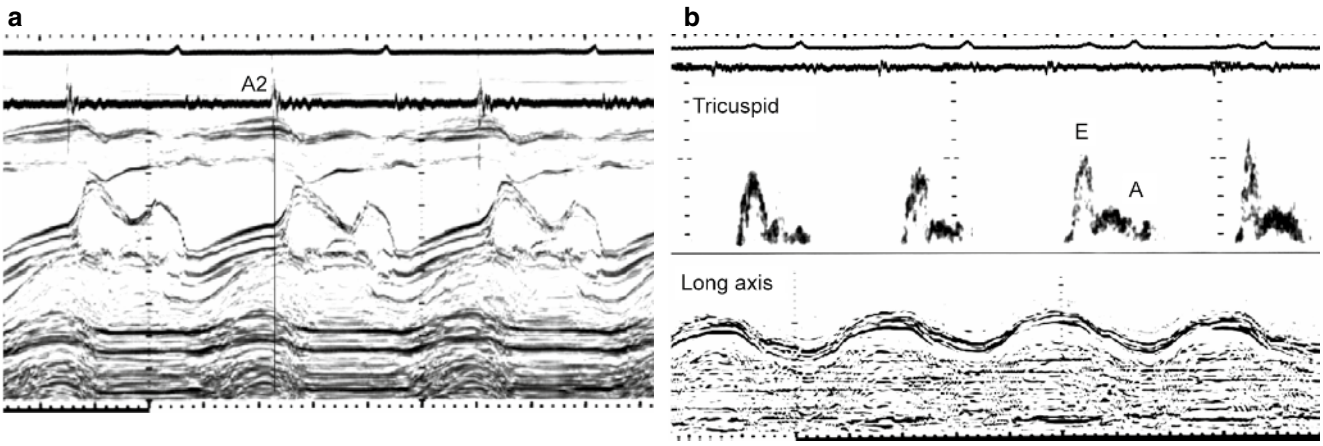


Fig. 17.20 (**a**) Mitral echogram from a patient with restrictive pericarditis. Note the short isovolumic relaxation time consistent with raised left atrial pressure. (**b**) Right ventricular long axis recording from the same patient showed markedly depressed amplitude and systolic function along with restrictive filling

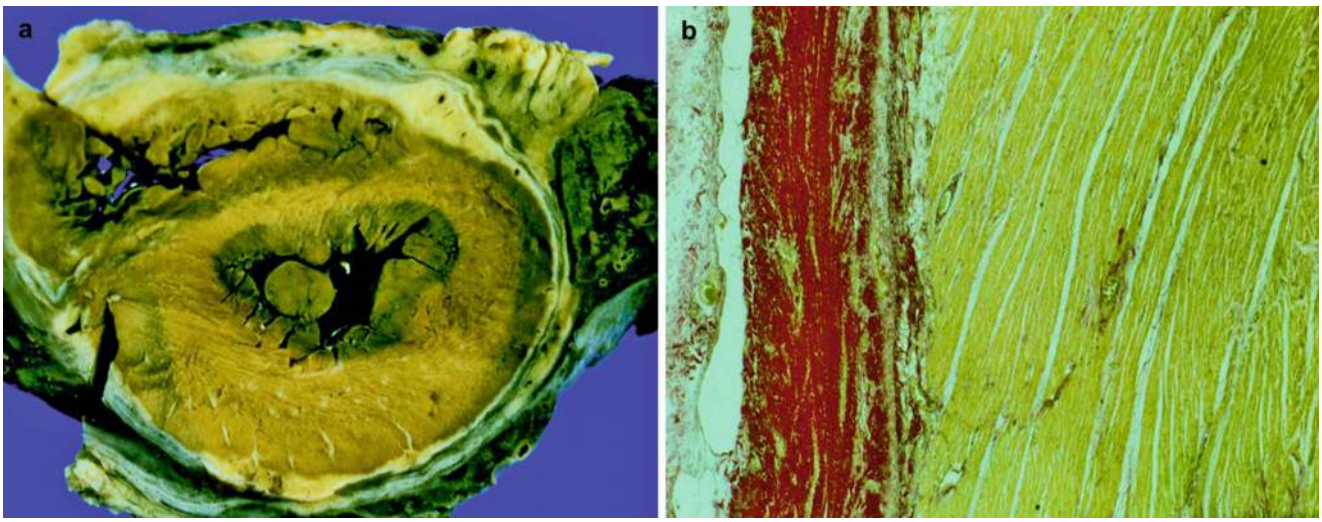


Fig. 17.21 (**a**) Section of the heart and pericardium from a case of restrictive pericarditis showing pericardial fibrosis invading the epicardium. (**b**) respective histology

Pericardial Tumors

The most common tumors of the pericardium are secondaries from elsewhere. The most frequent are carcinoma of the breast and lung, malignant melanoma, lymphoma, and leukemia [28]. They invade the pericardium either directly or via lymphatics or hematogenous dissemination. Primary tumors are rare but usually include malignant mesothelioma and sarcomas. While carcinomas metastasize in the pericardium in the form of localized masses, lymphomas and leukemia present in the form of uniform pericardial infiltration and thickening which may cause tumor incarceration of the heart and hence the clinical syndrome of "constrictive physiology." A mild degree of pericardial thickening may easily be missed on two-dimensional images. Cardiac magnetic resonance or CT scanning may offer a more conclusive diagnostic picture for pericardial thickening. Recurrent pericardial effusion of unknown etiology should suggest malignancy until otherwise proven. In addition, pericardial effusion in the presence of intracardiac mass suggests malignancy (Figs. 17.22, 17.23, and 17.24).

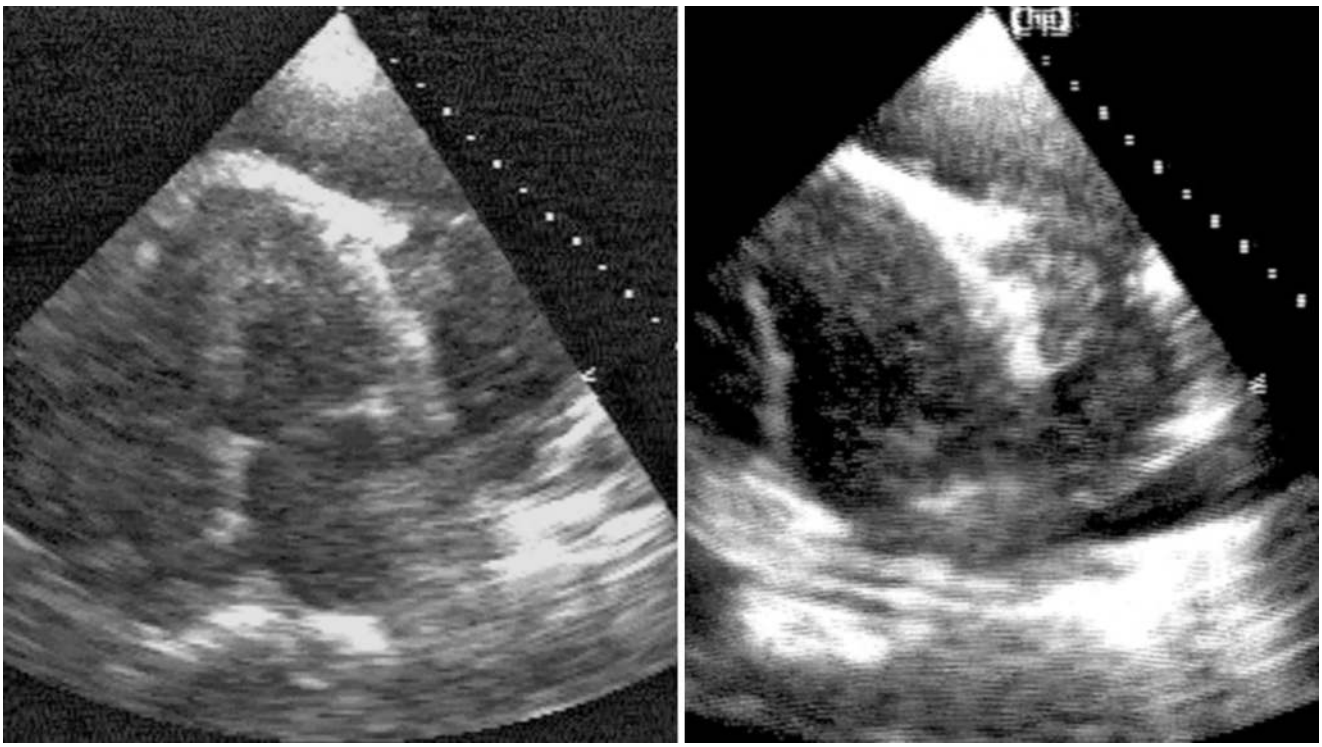


Fig. 17.22 Apical four-chamber view from a patient with pleural carcinoma invading the pericardium (left) and the apical free wall (right) of the left ventricle

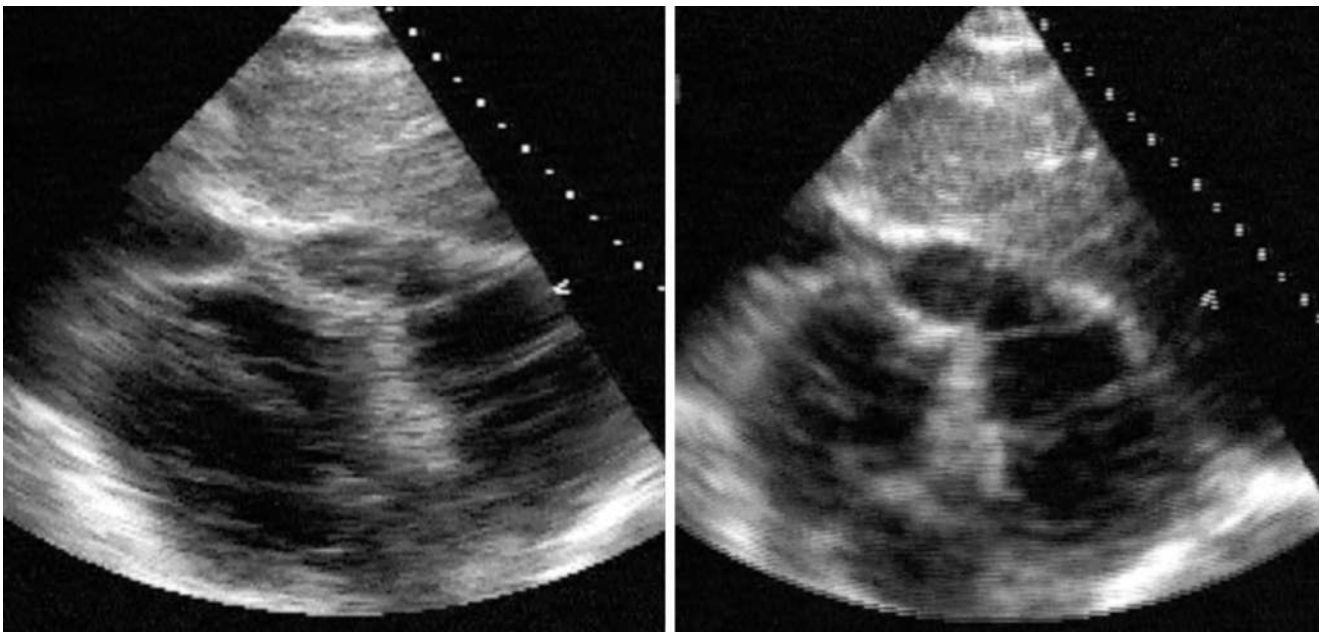


Fig. 17.23 Subcostal view from a patient with small cell carcinoma that invaded the pericardium causing effusion and adhesions to the right ventricular free wall

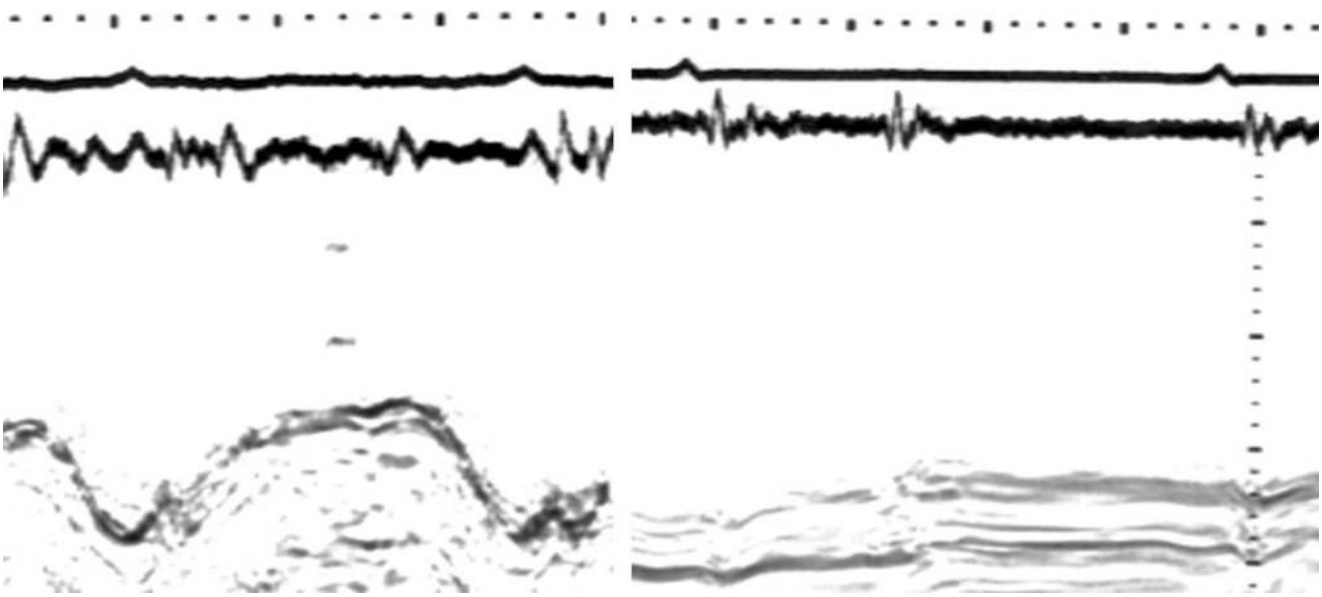


Fig. 17.24 Right ventricular free wall long axis before (*left*) and after (*right*) pericardial invasion showing significantly reduced free wall amplitude caused by adhesion

References

1. Lorell BH, Braunwald E. Pericardial disease. In: Braunwald E, editor. Heart disease. Philadelphia: WB Saunders; 1992. p. 1465–516.
2. Hagan AD. Evaluation of pericardial diseases by M-mode and two-dimensional echocardiography. In: Mason DT, editor. Advances in heart disease. New York: Grune & Stratton; 1980. p. 699–702.
3. Guberman BA, Fowler NO, Engel PJ, Gueron M, Allen JM. Cardiac tamponade in medical patients. Circulation. 1981;64(3):633–40.
4. Chandraratna PA. Echocardiography and Doppler ultrasound in the evaluation of pericardial disease. Circulation. 1991;84(3 Suppl):I303–10.
5. Horowitz MS, Schultz CS, Stinson EB, Harrison DC, Popp RL. Sensitivity and specificity of echocardiographic diagnosis of pericardial effusion. Circulation. 1974;50(2):239–47.
6. Isner JM, Carter BL, Roberts WC, Bankoff MS. Subepicardial adipose tissue producing echocardiographic appearance of pericardial effusion. Documentation by computed tomography and necropsy. Am J Cardiol. 1983;51(3):565–9.
7. Nanda NC, Gramiak R, Gross CM. Echocardiography of cardiac valves in pericardial effusion. Circulation. 1976;54(3):500–4.
8. Come PC, Riley MF, Fortuin NJ. Echocardiographic mimicry of pericardial effusion. Am J Cardiol. 1981;47(2):365–70.
9. D'Cruz IA, Hoffman PK. A new cross sectional echocardiographic method for estimating the volume of large pericardial effusions. Br Heart J. 1991;66(6):448–51.
10. Singh S, Wann LS, Schuchard GH, Klopfenstein HS, Leimgruber PP, Keelan MH Jr, et al. Right ventricular and right atrial collapse in patients with cardiac tamponade—a combined echocardiographic and hemodynamic study. Circulation. 1984;70(6):966–71.
11. Gillam LD, Guyer DE, Gibson TC, King ME, Marshall JE, Weyman AE. Hydrodynamic compression of the right atrium: a new echocardiographic sign of cardiac tamponade. Circulation. 1983;68(2):294–301.
12. Katz LN, Gauchat HW. Observations on pulsus paradoxus (with special reference to pericardial effusions): II. Experimental. Arch Intern Med. 1924;33:371–93.
13. Appleton CP, Hatle LK, Popp RL. Cardiac tamponade and pericardial effusion: respiratory variation in transvalvular flow velocities studied by Doppler echocardiography. J Am Coll Cardiol. 1988;11(5):1020–30.
14. Shabetai R, Fowler NO, Fenton JC, Masangkay M. Pulsus paradoxus. J Clin Invest. 1965;44(11):1882–98.
15. Reddy PS, Curtiss EI, O'Toole JD, Shaver JA. Cardiac tamponade: hemodynamic observations in man. Circulation. 1978;58(2):265–72.
16. Chuttani K, Pandian NG, Mohanty PK, Rosenfield K, Schwartz SL, Udelson JE, et al. Left ventricular diastolic collapse. An echocardiographic sign of regional cardiac tamponade. Circulation. 1991;83(6):1999–2006.
17. Kronzon I, Cohen ML, Winer HE. Diastolic atrial compression: a sensitive echocardiographic sign of cardiac tamponade. J Am Coll Cardiol. 1983;2(4):770–5.
18. Kochar GS, Jacobs LE, Kotler MN. Right atrial compression in postoperative cardiac patients: detection by transesophageal echocardiography. J Am Coll Cardiol. 1990;16(2):511–6.
19. Callahan JA, Seward JB, Nishimura RA, Miller FA Jr, Reeder GS, Shub C, et al. Two-dimensional echocardiographically guided pericardiocentesis: experience in 117 consecutive patients. Am J Cardiol. 1985;55(4):476–9.
20. Nishimura RA, Kazmier FJ, Smith HC, Danielson GK. Right ventricular outflow obstruction caused by constrictive pericardial disease. Am J Cardiol. 1985;55(11):1447–8.
21. Cameron J, Oesterle SN, Baldwin JC, Hancock EW. The etiologic spectrum of constrictive pericarditis. Am Heart J. 1987;113(2 Pt 1):354–60.
22. Shabetai R, Fowler NO, Guntheroth WG. The hemodynamics of cardiac tamponade and constrictive pericarditis. Am J Cardiol. 1970;26(5):480–9.

23. Voelkel AG, Pietro DA, Folland ED, Fisher ML, Parisi AF. Echocardiographic features of constrictive pericarditis. Circulation. 1978;58(5):871–5.
24. Himelman RB, Lee E, Schiller NB. Septal bounce, vena cava plethora, and pericardial adhesion: informative two-dimensional echocardiographic signs in the diagnosis of pericardial constriction. J Am Soc Echocardiogr. 1988;1(5):333–40.
25. Henein MY, Rakhit RD, Sheppard MN, Gibson DG. Restrictive pericarditis. Heart. 1999;82(3):389–92.
26. Hatle LK, Appleton CP, Popp RL. Differentiation of constrictive pericarditis and restrictive cardiomyopathy by Doppler echocardiography. Circulation. 1989;79(2):357–70.
27. Lam YY, Kaya MG, Goktekin O, Gatzoulis MA, Li W, Henein MY. Restrictive right ventricular physiology: its presence and symptomatic contribution in patients with pulmonary valvular stenosis. J Am Coll Cardiol. 2007;50(15):1491–7. Epub Sep 24, 2007; 9(2):357–70.
28. Kutalek SP, Panidis IP, Kotler MN, Mintz GS, Carver J, Ross JJ. Metastatic tumors of the heart detected by two-dimensional echocardiography. Am Heart J. 1985;109(2):343–9.

Simple Adult Congenital Heart Lesions

18

Wei Li and Michael Y. Henein

Introduction

Congenital heart disease (CHD) is one of the most common inborn defects, occurring in about 0.9% of newborn infants. As a result of various advances in medical treatment, percutaneous intervention and cardiac surgery, most patients born with CHD can now survive into adulthood. Patients often have residual or developed acquired hemodynamic lesions, hence the need for lifelong follow-up. Echocardiography is the most commonly used diagnostic tool for such service [1, 2].

Atrial Septal Defect (ASD)

ASD is an anatomical defect in the interatrial septum that results in shunting at the atrial level. It is one of the most common defects seen in adult congenital heart disease (ACHD) clinics [1–3].

Classification

According to the location of the defect, ASD can be classified into the following types.

1. Secundum ASD

   The majority (80%) of ASDs are of secundum type. The defect is localized in the region of the fossa ovalis and is best viewed from the modified parasternal four-chamber view and sub-costal view (Fig. 18.1).



Fig. 18.1 Apical four-chamber view showing a secundum ASD

2. Primum ASD

   This defect is less common (15%) and forms part of the spectrum of atrioventricular septal defect. The defect is located near the atrioventricular junction (Fig. 18.2). The defect is best viewed from an apical four-chamber view. Atrioventricular valves are typically malformed (Fig. 18.3). The abnormal left AV valve is best seen in the parasternal short-axis view.

W. Li (✉)
Department of Cardiology, Royal Brompton Hospital, London, UK
e-mail: w.li@rbht.nhs.uk

M. Y. Henein
Imperial College London, London, UK

Siena University, Siena, Italy

© The Author(s), under exclusive license to Springer Nature Switzerland AG 2025

M. Y. Henein (ed.), *Clinical Echocardiography*, https://doi.org/10.1007/978-3-031-95894-6_18

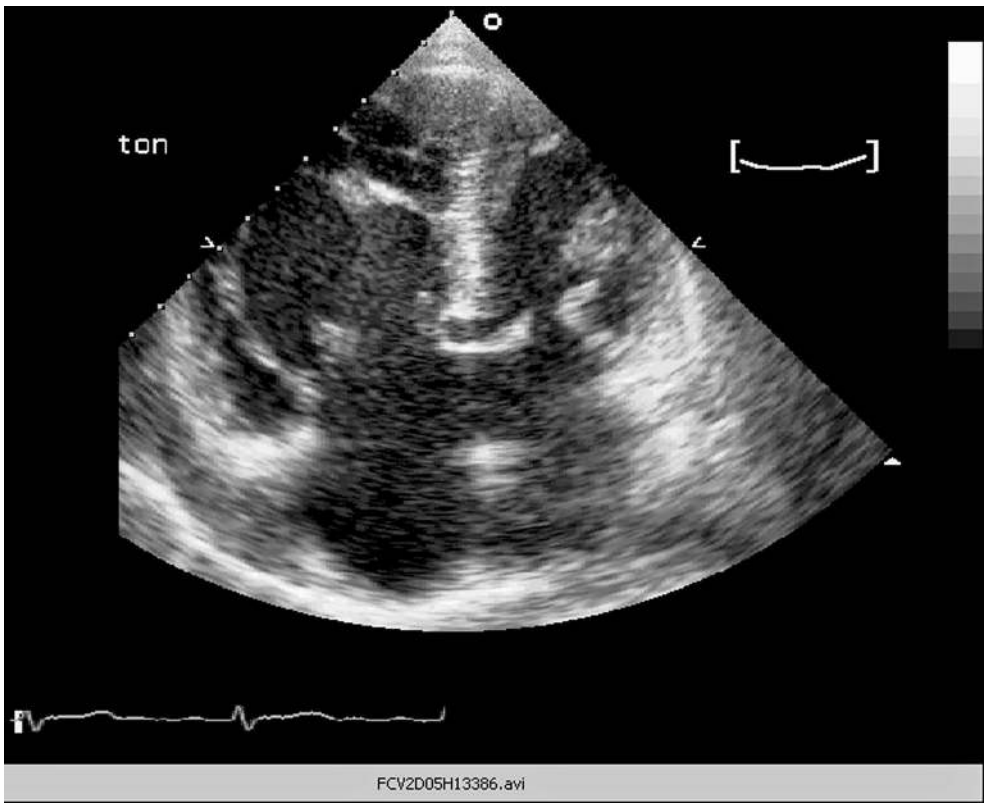


Fig. 18.2 Apical four-chamber view showing a primum ASD

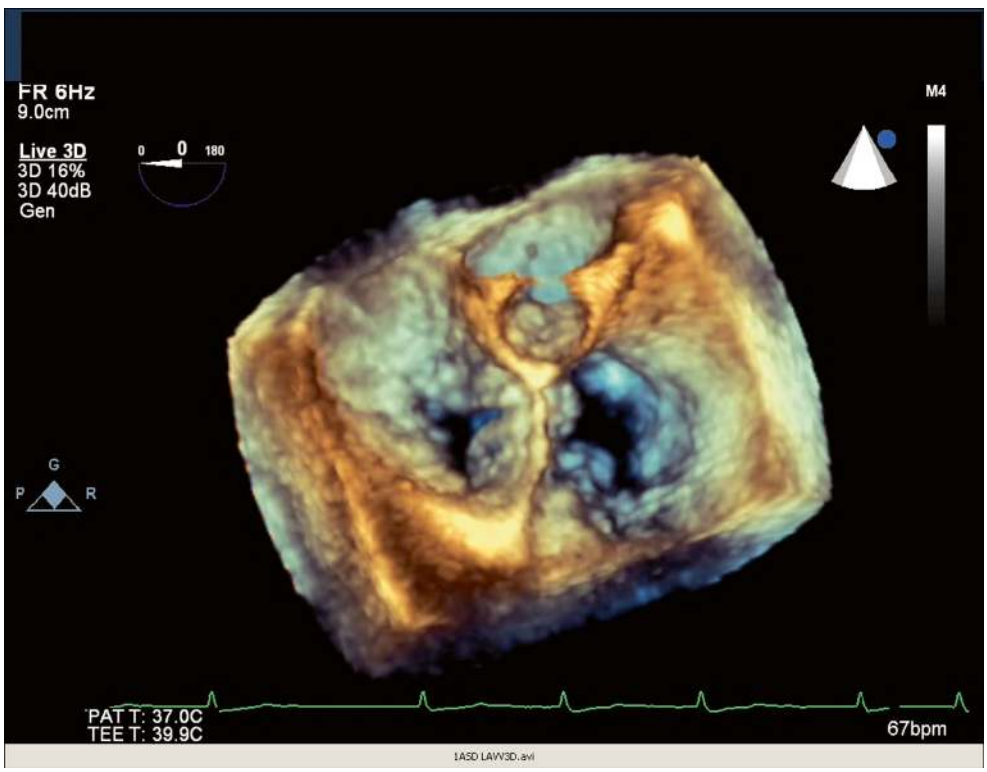


Fig. 18.3 3D TOE demonstrating tri-leaflet left AV valve and quadra cuspid right AV valve in primum ASD

3. Superior sinus venosus defect (5%)

   This defect is located outside the limbus of the fossa ovalis near the superior vena caval entry. The caval vein has a bilateral connection, overriding the septum. Partial anomalous venous return of the right upper pulmonary vein is a common association. Superior sinus venosus defect can be visualized from the modified parasternal short-axis view or sub-costal view in echogenic adult patients. Transesophageal echocardiography at the mid-esophagus with a 90-degree view (caval view) is the diagnostic tool (Figs. 18.4 and 18.5).
4. Inferior sinus venosus defect (2%)

   This type of defect is also located outside the limbus of the fossa ovalis but near the inferior vena caval entry. The caval vein overrides the septum. The inferior sinus venosus defect is best visualized from the sub-costal view in echogenic adults. Otherwise, transesophageal echocardiography with a caval view can identify the defect.

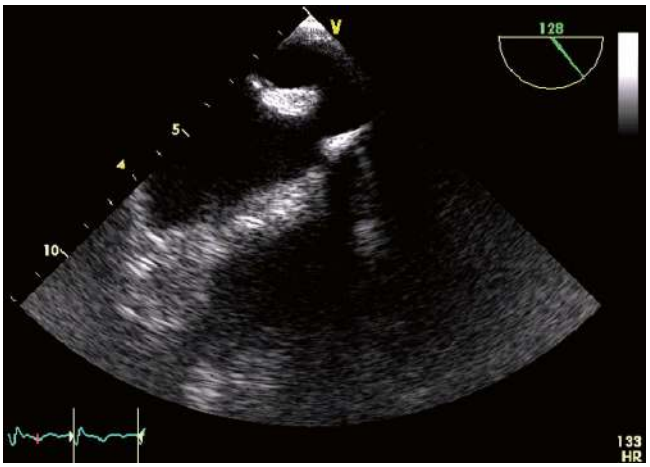


Fig. 18.4 TOE showing SVC type ASD

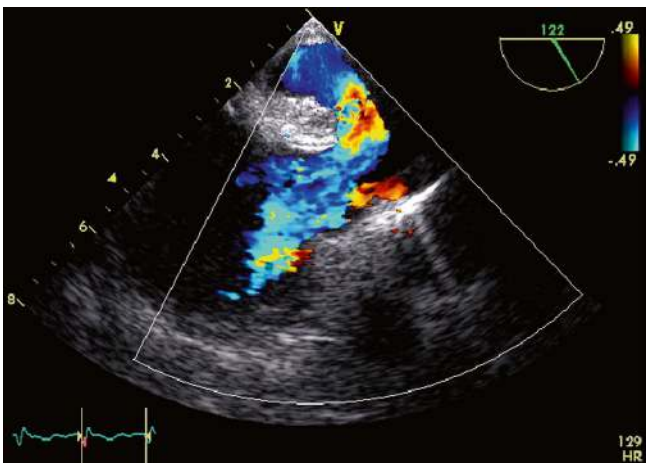


Fig. 18.5 TOE SVC type ASD, color Doppler demonstrate shunt through the defect

5. Coronary sinus defect (unroofed coronary sinus).

   This defect is very rare (<1%) and is located in the wall that separates the coronary sinus from the left atrium. It may be partially or completely missing. The best view to visualize the defect is the apical four-chamber view with slight posterior angulation.

Echocardiography

Echocardiography is the investigation of choice for diagnosing ASD. It not only provides a diagnosis demonstrated as defect size and location but also quantification of the shunt size. Right heart dilatation and volume overloading are the key findings and best characterize the hemodynamic relevance of the defect (preferable to the shunt ratio). Left to right shunt can be quantified by using the continuity equation (RVOT TVI × RVOT area/LVOT VTI × LVOT area), where RVOT is the right ventricular outflow tract, LVOT is left ventricular outflow tract and VTI is the velocity time integral. The shunt volume depends on RV/LV compliance, defect size and LA/RA pressure. A simple ASD causes left-to-right shunt because of the higher compliance of the RV compared with the LV and and consequently RV and pulmonary circulation volume overload. Reduction of LV compliance or any condition that causes raised LA pressure, e.g. ischemic heart disease, cardiomyopathy, aortic and mitral valve disease or hypertension increases left to right shunt. Reduced RV compliance (pulmonary stenosis, pulmonary artery hypertension, RV disease) or tricuspid valve disease may decrease the left to right shunt and eventually result in shunt reversal. Pulmonary artery pressure should always be assessed by using tricuspid regurgitation and pulmonary Doppler [2, 3].

Associated Anomalies

Associated lesions with ASD include anomalous pulmonary venous connection, persistent left SVC, pulmonary valve stenosis and mitral valve prolapse should also be assessed. In patients with primum ASD, atrioventricular valve morphology and function should be assessed in detail. The left AV valve is usually three leaflets and the degree of valve regurgitation or stenosis should be quantified. Hypoplastic or absent papillary muscle with parachute-type valve anomaly is often seen associated with this lesion.

Indication for Closure

In patients with evidence of RV volume overload and no PAH or LV disease, ASD closure is recommended. The size and position of the defect determine the method of closure. Currently, secundum defects with stretched diameter < 38 mm and a sufficient rim of 5 mm except towards the aorta are feasible for device closure. With the recent development in interventional technology, SVC-type defects with favourable pulmonary venous anatomy can also be closed

percutaneously. Other types of defects will need surgical repair at present.

In patients after interventional closure or surgical repair, the following should be assessed:

- Presence of residual shunt and its clinical significance.
- Position of the device and its relationship to other cardiac structures.
- Right and left ventricular size and function.
- Presence of pulmonary hypertension.
- Atrioventricular valve function.
- Left ventricular outflow tract obstruction (seen in patients after primum ASD closure).

Persistence of right heart dilatation is usually the sign of residual left to right shunt. Impaired ventricular function (especially of the left ventricle) is common in patients with coronary artery disease or arrhythmias [4].

Ventricular Septal Defect

Ventricular septal defect (VSD) represents discontinuity of the ventricular septum that results in left to right shunt across the inter-ventricular septum [1, 3, 5].

Classification

1. Peri-membranous VSD. The defect is located in the membranous septum with possible extension into the inlet, trabecular or outlet septum or part of its border is formed by fibrous continuity between the leaflets of the atrioventricular valve and semilunar valve (Fig. 18.6).
2. Muscular VSD. This defect has a muscular border and can be described as a muscular inlet, outlet or apical trabecular, frequently multiple.
3. Doubly committed subarterial VSD. This type of defect is characterized by fibrous continuity between the adjacent leaflets of the aortic and pulmonary valves. Superiorly, these defects are roofed by arterial valves while postero-inferiorly the margin may be muscular or perimembranous.

VSD seen in adult patients can be

(a) Small VSD with no hemodynamic consequences but carries the risk of potential superimposed infection (endocarditis).
(b) Large VSD, the majority of which develop pulmonary hypertension (Eisenmenger syndrome).
(c) Residual defects after repair.

Echocardiography

Ventricular septal defects should be imaged from several planes in order to provide a precise diagnosis. The type and location of VSD should be determined from multiple views. For the perimembranous VSD, parasternal short-axis and apical four-chamber views show the proximity of the defect to the tricuspid valve, while parasternal and apical long-axis views demonstrate the relation of the defect with the aortic valve. Perimembranous VSDs extending to the inlet portion are best shown in the apical four chamber or sub-costal para-coronal view. For apical trabecular muscular VSD, parasternal long-axis view, apical four-chamber view and parasternal short-axis view scanning towards the apex can demonstrate the defect and left to right shunt on color flow Doppler. For doubly committed and juxta-arterial defects, the parasternal

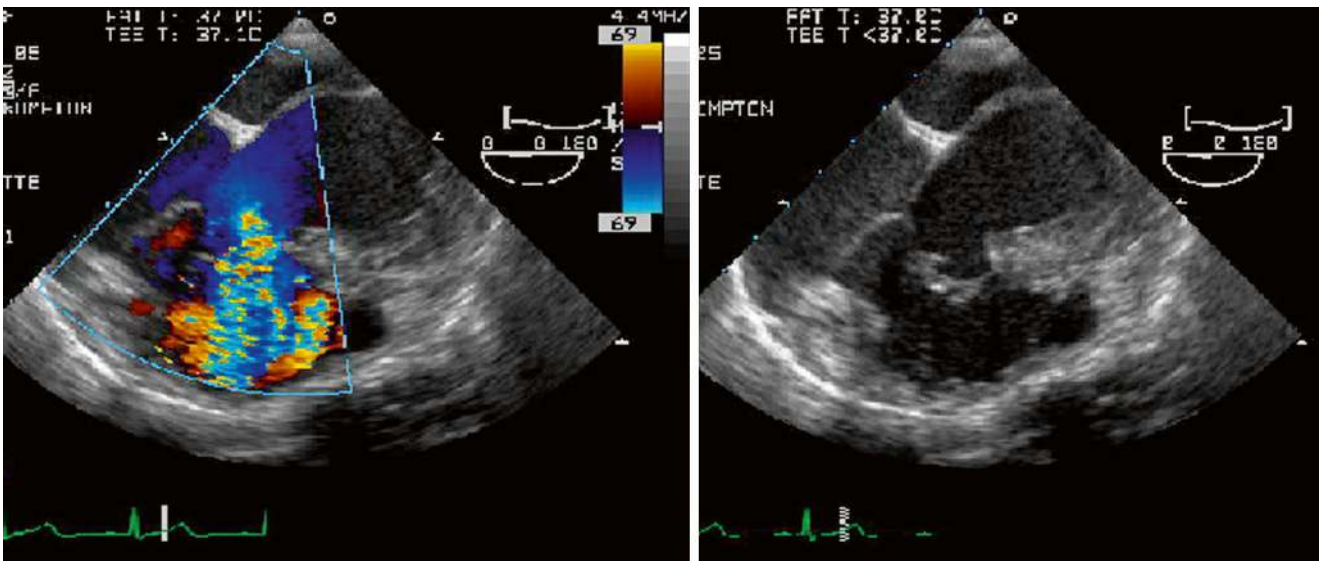


Fig. 18.6 TOE showing perimembranous VSD with aneurysmal formation

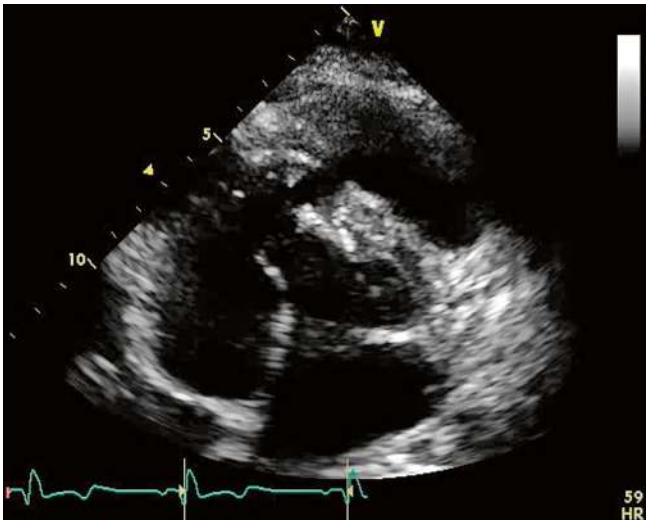


Fig. 18.7 Short-axis view from a patient with peri-membranous subtricuspid VSD showing muscle band distal to the defect forming double chamber of right ventricle (DCRV)

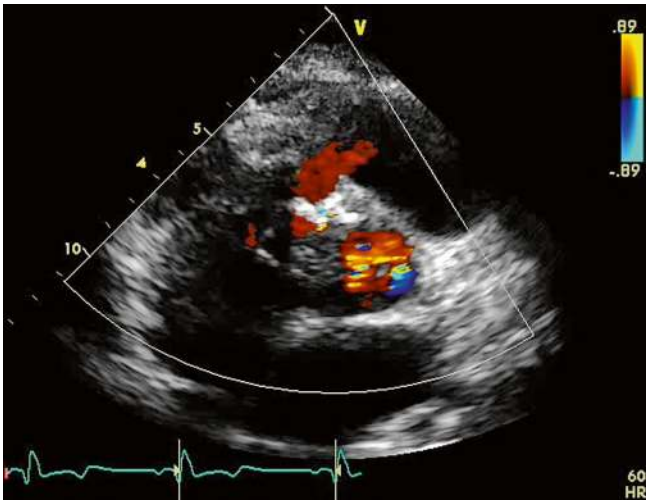


Fig. 18.8 Same patient as above. Color Doppler showing turbulent flow through the DCRV

long axis with antero-superior angulation, short axis view or sub-costal parasagittal planes can display the continuity of both arterial valves and also the presence, if any, of herniation of the right-facing aortic sinus. Residual VSD post-surgical repair or device closure is often around the patch or device [3, 5].

Defect Size and Hemodynamic Significance

VSDs can be described as small (less than 5 mm), moderate (5–10 mm) or large (more than 10 mm) in adult patients. Large VSD results in left heart dilatation. A restrictive VSD has a significant peak instantaneous gradient (>75 mmHg) and is not associated with left heart dilatation or pulmonary hypertension. A non-restrictive VSD will have a low peak instantaneous gradient (<25 mmHg) and heave significant left heart dilatation with pulmonary hypertension. Right ventricular pressure can be estimated with continuous Doppler interrogation of the gradient across the VSD (right ventricular systolic pressure = systolic blood pressure − 4 × (VSD peak velocity^2)). Significant pulmonary vascular disease may result in bidirectional or predominantly right-to-left shunting across the VSD (Eisenmenger's syndrome). Left to right shunt across a small VSD can become continuous when there is raised LV diastolic pressure. As a result, shunt volume increases and the left heart dilates.

Associated Anomalies

Important associated lesions with VSDs include prolapse of the right or non-coronary aortic cusp with progressive aortic regurgitation and development of double-chamber right ventricle from hypertrophy of right ventricular muscle band (Figs. 18.7 and 18.8).

Indications for VSD Closure

A VSD associated with LV volume overload should be considered for closure, transcatheter or surgical. Patients with VSD and aortic leaflet prolapse causing significant aortic regurgitation should also be considered for surgical closure [5].

Atrioventricular Septal Defects

Atrioventricular septal defect (AVSD) occurs at the atrioventricular junction (top of the ventricular septum and bottom end of the inter-atrial septum) and is characterized by the presence of a common AV valve guarded by five leaflets. In the partial form, the anterior and posterior bridging leaflets are fused centrally, creating separate left and right-sided orifice. When the VSD is big, pulmonary hypertension develops early in life. Patients with small lesions may remain asymptomatic for a long time. Complete atrioventricular septal defects are often seen in patients with Down's syndrome [2, 3].

In the adult population, the following groups of patients could be seen:

(a) Primum ASD or AVSD with small ventricular component with no or mild–moderate pulmonary hypertension.
(b) Large AVSD with established Eisenmenger physiology, is often associated with Down syndrome.
(c) Repaired AVSD (including primum ASD). The majority of patients after surgical repair have good hemodynamic results and remain asymptomatic. Some patients may have residual shunt, left or right atrioventricular valve

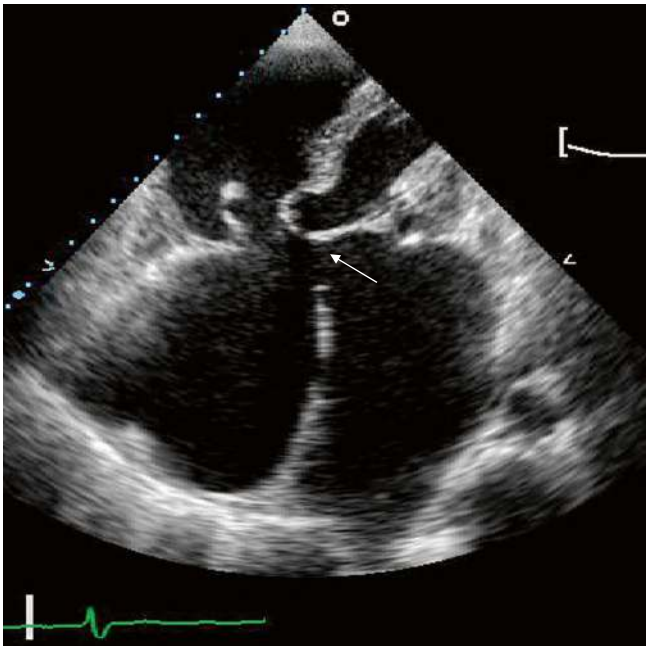


Fig. 18.9 Apical four-chamber view showing AVSD with small ventricular component

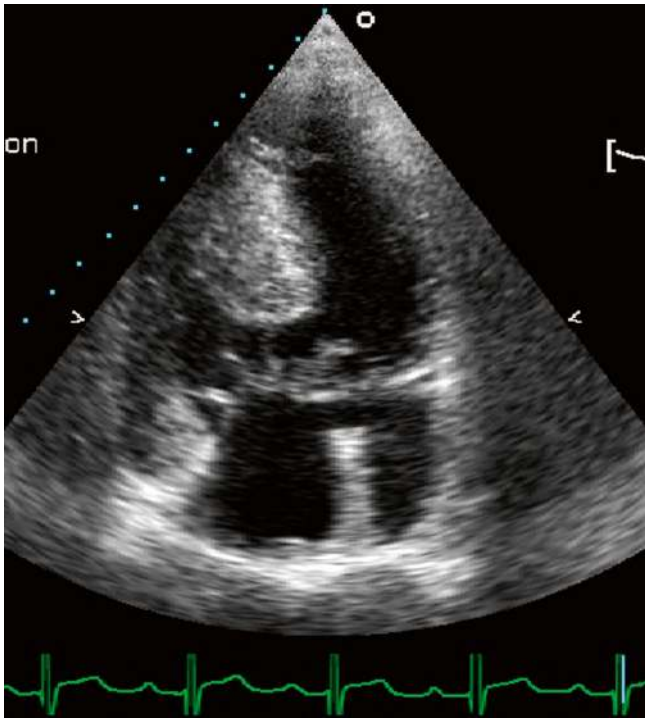


Fig. 18.10 Apical four-chamber view showing complete AVSD with common AV valve

regurgitation or left ventricular outflow tract obstruction. In rare cases, pulmonary hypertension progresses despite the repair of the shunt lesion. Atrioventricular valve stenosis is rarely seen after repair.

Echocardiography

The commonly used view for diagnosis AVSD is the parasternal long-axis view which demonstrates the elongated left ventricular outflow tract (the characteristic goose-neck deformity) and the abnormal left AV valve with septal attachment. The apical four-chamber view is the preferred diagnostic image that displays the loss of the offset arrangement of left and right AV valve leaflets (Figs. 18.9 and 18.10). Anterior angulation of the transducer displays the anterosuperior bridging leaflet. Parasternal short-axis view demonstrates five leaflet arrangement of the common AV valve. In adults with atrioventricular septal defect, either the left or the right atrioventricular valve may be incompetent and results in significant clinical consequences. Significant left ventricular outflow tract obstruction may develop later after surgical repair.

Associated Lesions

Associated lesions include secundum ASD, tetralogy of Fallot and other forms of complex congenital heart disease.

Patent Ductus Arteriosus

Patent ductus arteriosus is a blood vessel connecting the proximal left pulmonary artery to the descending aorta just distal to the left subclavian artery. During fetal life, the ductus arteriosus is a vital structure that bypasses the pulmonary circulation. A persistent shunt that remains patent well after birth is usually managed either surgically or interventionally by device (mostly coils) implantation early in life. Most adult cases with PDA are small or silent without clinical hemodynamic significance. Moderate size ductus with significant left to right shunt causes left heart enlargement and some degree of pulmonary hypertension are rarely seen in adults. Large ductus in adults usually result in Eisenmenger physiology with eventually right to left shunt which can be difficult to diagnose using echocardiography [3, 4, 6].

Echocardiography

Parasternal sagittal ductus cut (in an infraclavicular location in the second left intercostal space) demonstrates the ductus between the anteriorly located main pulmonary artery and posterior descending aorta. With normal pulmonary vascular

resistance, the flow is left to right and continuous. Flow velocity is usually high in restrictive PDA. With increasing pulmonary vascular resistance, the flow becomes bidirectional with right-to-left in systole and left-to-right shunting in diastole. With progressive pulmonary vascular disease, the shunt can be exclusively right to left. Ductus can also be visualized from the parasternal short-axis view (Figs. 18.11 and 18.12). In this view, the ductus is imaged as a connection between the bifurcation of the pulmonary artery and the descending aorta. It is possible for the left pulmonary artery to be mistaken for the ductus. Color Doppler is of great help in demonstrating left to right shunt in patients with small Ductus. Left atrial and ventricular dilatation is the indirect sign of significant left to right shunt. Continuous wave flow velocity across the ductus reflects the pulmonary pressure. Tricuspid regurgitation velocity may more accurately reflect the pressure difference between the right ventricle and right atrium and the pulmonary artery pressure [3].

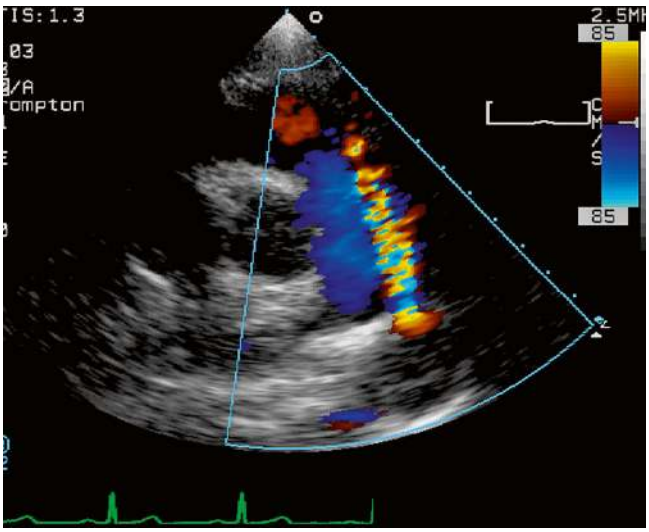


Fig. 18.11 Parasternal short-axis view showing small duct on color Doppler

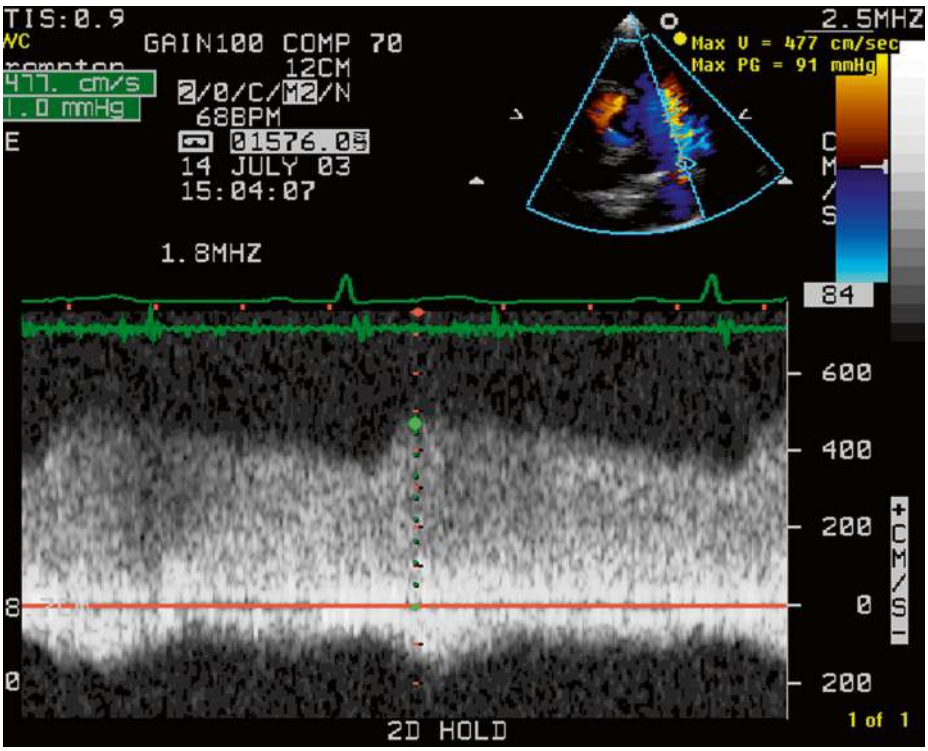


Fig. 18.12 Continuous wave Doppler recording of duct flow

Coarctation of Aorta

Aortic coarctation is defined as a narrowing or obstruction of the aortic arch. The region of the aortic arch frequently affected is between the origin of the left subclavian artery and the insertion of the arterial duct, the region known as the isthmus. Two major variants of morphological coarctation; tubular hypoplasia and discrete coarctation, are recognized and the two may co-exist.

Aortic coarctation can be imaged best from the high parasternal or suprasternal parasagittal plane. Discrete coarctation is characterized by a shelf of echo-dense tissue obstructing the aortic lumen from its posterior aspect. This shelf is usually located just distal to the origin of the left subclavian artery (Figs. 18.13 and 18.14). In some patients, coarctation is associated with hypoplasia of the proximal aortic arch, as well as with the presence of additional stenosis in the region of the transverse aorta and proximal descending aorta, or with a patent ductus arteriosus. Doppler is very helpful in assessing the severity of the coarctation. Direct interrogation of the site by continuous wave Doppler is char-

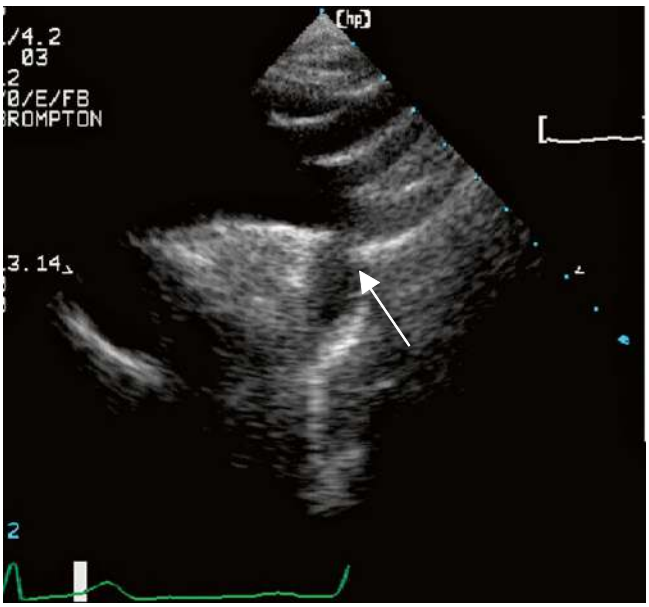


Fig. 18.13 Suprasternal view of the aortic arch and proximal descending aorta demonstrating discrete narrowing (arrow)

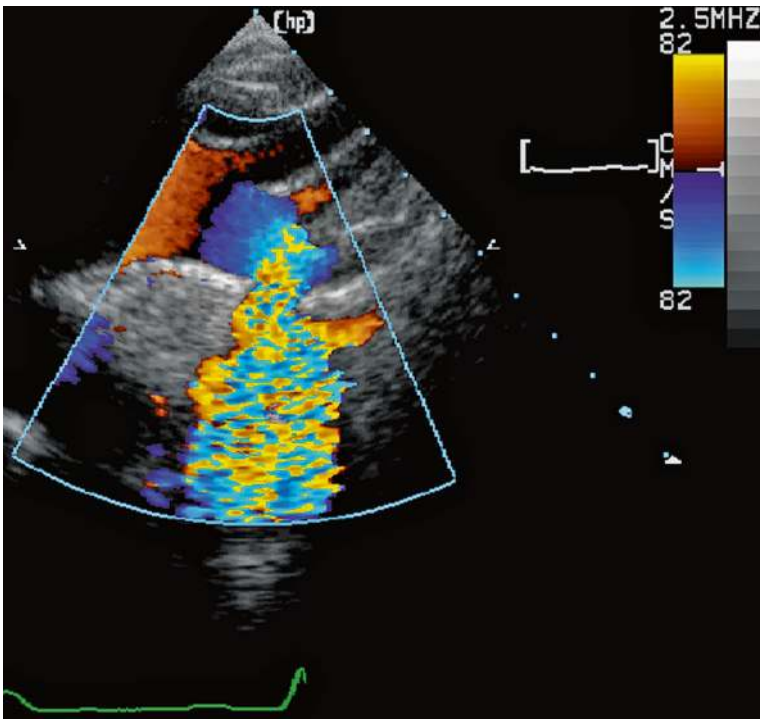


Fig. 18.14 Color Doppler across coarctation area showing turbulent flow

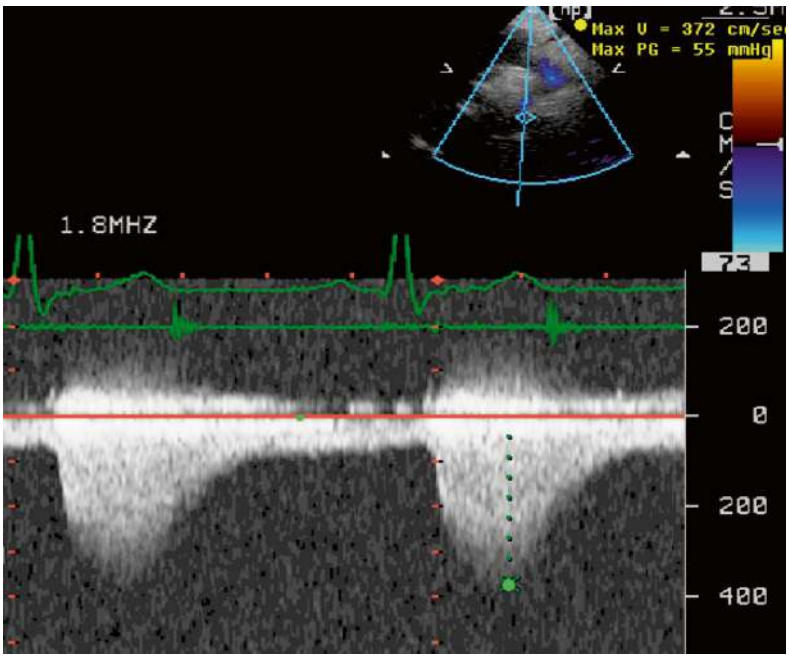


Fig. 18.15 Continuous wave Doppler flow across the descending aorta from a patient with coarctation of the aorta demonstrating high systolic velocity and continuous flow during the whole diastolic period

acteristic. The high systolic velocity, which may continue throughout the cardiac cycle (diastolic tail) is characteristic of severe coarctation (Fig. 18.15). Pulsed wave Doppler velocities of the descending aorta from the sub-costal sagittal plane demonstrate reduced systolic flow, a characteristically low peak velocity and prolonged acceleration and deceleration times. Studies have shown a close relationship between systolic and diastolic velocities across the coarctation. In cases with pinpoint severe coarctation, the systolic velocity may be low and the flow becomes continuous. The severity of stenosis can be underestimated by using the peak systolic velocity alone.

Secondary effects: left ventricular hypertrophy and left ventricular dysfunction.

Associated lesions: bicuspid aortic valve, mitral valve disease (parachute mitral valve, a complex known as Shone syndrome) and left ventricular outflow trace obstruction.

Management: while traditional treatment of aortic coarctation used to be surgical repair percutaneous aortic coarctation stenting has become an attractive alternative with promising results [4, 7].

Ebstein Anomaly

Ebstein anomaly is the most common form of congenital tricuspid valve disease. It is defined as a displaced origin of some part of the hinge point of the valve leaflets within the right ventricular cavity instead of the atrioventricular junction. It is almost always accompanied by dysplasia of the tricuspid valve leaflets. Leftward and inferior displacement of the proximal attachment is the more common form of Ebstein anomaly that may involve the septal and posteroinferior (mural) leaflets, whereas the anterosuperior leaflet is usually normally attached, but enlarged ('sail-like) [8].

The displacement of the septal leaflet of the tricuspid valve (more than 0.8 cm/m^2) is best displayed in the apical four-chamber views (Fig. 18.16). The mobility of the tricuspid valve leaflets is also reduced in Ebstein anomaly. Displacement of the posteroinferior leaflet can be demonstrated in the sub-costal coronal and sagittal views. Parasternal long-axis views with medial angulation to image the right ventricle may also display the tethering of the posteroinferior leaflet to its underlying myocardium. The proximal segment of the anterosuperior leaflet is commonly attached to the atrioventricular groove. Typically, the tricuspid valve orifice is rotated superiorly toward the right ventricular outflow tract. As a result of the tricuspid valve leaflet displacement the atrialized portion of the right ventricle becomes large, adding to the dilatation of the right atrium caused by tricuspid regurgitation [9].

Ebstein anomaly is often associated with significant tricuspid valve regurgitation. This can easily be confirmed by color Doppler as it demonstrates a large regurgitation jet originating down in the right ventricular cavity near the

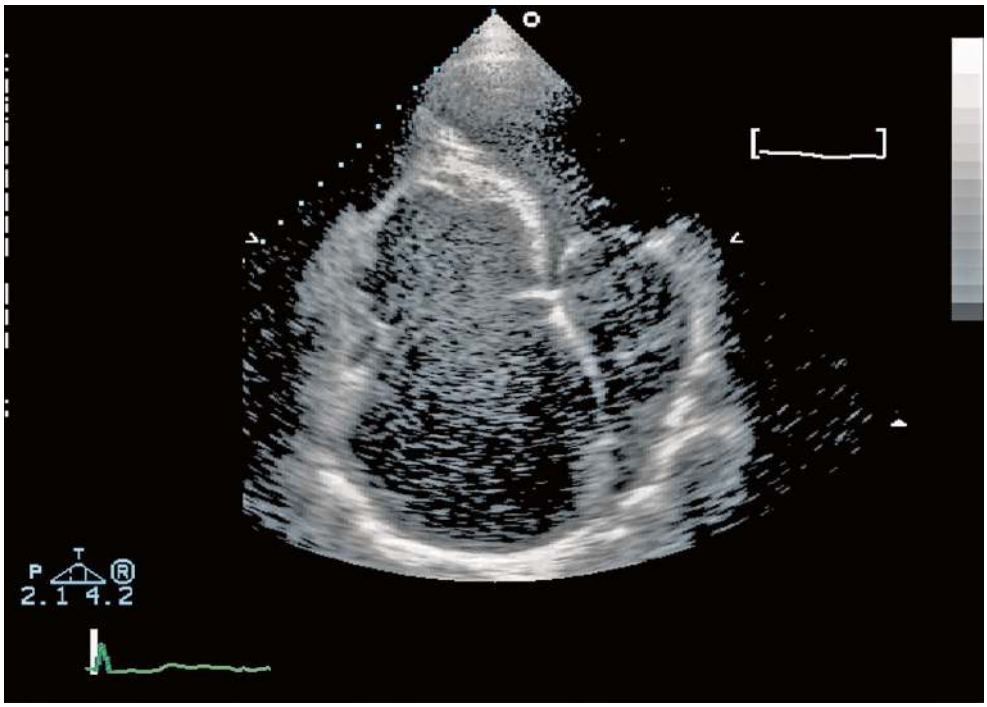


Fig. 18.16 Apical four-chamber view demonstrating apical displacement of the septal leaflet, as a result, the coapting point of the tricuspid valve is displaced deep into RV cavity

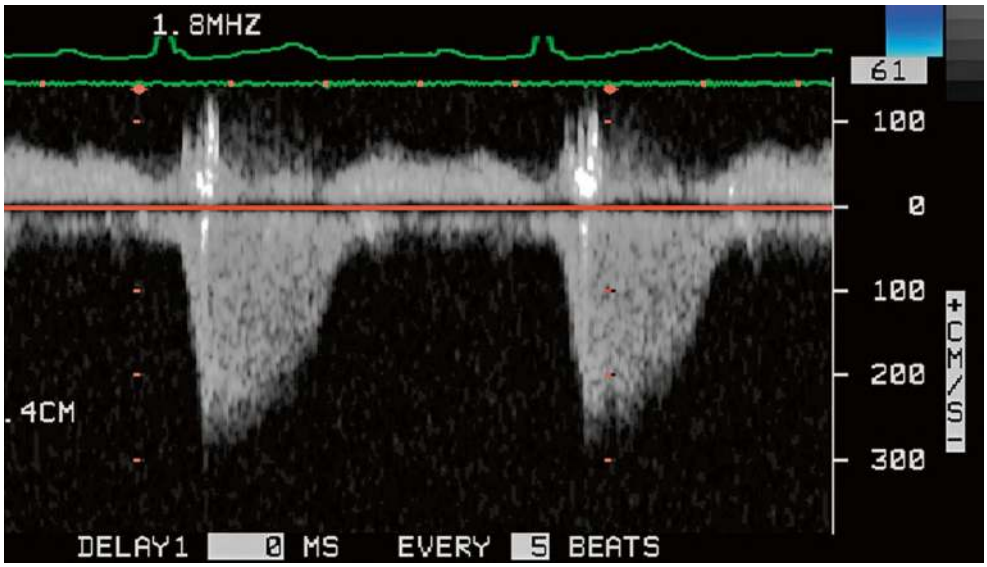


Fig. 18.17 Continuous wave Doppler recording of severe tricuspid regurgitation

apex and fills the dilated right atrium. Color flow aliasing should not be taken as a diagnostic feature because with severe regurgitation velocities might be too low to aliase. Continuous wave Doppler can be used to assess the severity of the tricuspid regurgitation. Signs of severity are low retrograde velocity and pressure drop across the tricuspid valve (due to raised right atrial pressure) that underestimates systolic right ventricular pressure, equalization of right ventricular and right atrial pressure drop at end-ejection and laminar flow of the tricuspid regurgitation flow pattern (Fig. 18.17). Pulsed wave Doppler recording of superior and inferior vena caval flow demonstrates systolic flow reversal and dominant early diastolic filling of the right atrium.

The most frequent additional anomaly seen in Ebstein malformation is atrial septal defect. If right atrial pressure is raised, right-to-left shunting may be seen. Agitated saline contrast may be used to demonstrate this. Ebstein anomaly has a wide spectrum of anatomic and clinical presentation and there is no close correlation between severities of anatomic abnormality and clinical symptom. Usually, clinical symptoms determine the treatment [8, 9].

Tetralogy of Fallot

Definition

Tetralogy of Fallot is the most common form of cyanotic congenital heart anomalies, accounting for approximately 10% of all congenital heart diseases. The hallmark of the condition is an antero-cephalad location of the outlet septum resulting in right ventricular outflow tract (RVOT) obstruction. As a result of this malalignment, a ventricular septal defect exists in the subaortic region. Rightward deviation of the aortic orifice, with overriding of the valvar leaflets is relative to the crest of the ventricular septum. Right ventricular hypertrophy is an adaptive phenomenon to the systemic afterload shared by both left and right ventricles. RVOT obstruction may be infundibular, valvar or a combination of both. In some cases, there is branch pulmonary artery stenosis. Most patients presenting in adulthood would have undergone some extent of palliation or primary repair [1, 4, 10].

Echocardiographic Assessment of Un-Operated Tetralogy of Fallot Includes

Ventricular Septal Defect

The VSD in tetralogy is usually perimembranous outlet (92%), few doubly committed (5%), very rare inlet VSD or AVSD (2%). The parasternal long-axis and short-axis images demonstrate the size and location of the VSD.

Level of RVOT Obstruction and its Severity

There is a degree of right ventricular infundibular stenosis in almost all cases of tetralogy of Fallot. The pulmonary valve itself is abnormal in most cases of tetralogy of Fallot. Acquired atresia of the infundibulum or the valve may also occur. Pulmonary artery stenosis may occur at branch points from the bifurcation onwards. Hypoplasia of the pulmonary arteries has been reported as frequently as in 50%. Lack of origin of one pulmonary artery (typically the left) from the pulmonary trunk is not infrequently seen. In adult patients, the parasternal long-axis view with lateral angulation is valuable for imaging the right ventricular outflow, the pulmonary valve area, the main pulmonary artery and the bifurcation.

Aortic Overriding

The classical parasternal long-axis view is the best to image the aortic override of the ventricular septum (Fig. 18.18). The degree of aortic override can vary from 5% to 95% of the valve being connected to the right ventricle. Tetralogy of Fallot therefore, may coexist with double outlet right ventricle, when more than half (50%) of the aorta is connected to the right ventricle. It is important to examine the coronary arteries and their relationship to the right ventricular outflow tract (using a short-axis view); this may be difficult to achieve in adult patients.

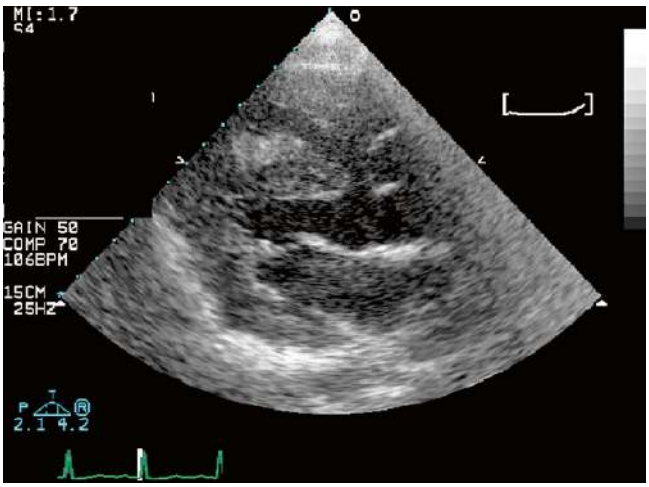


Fig. 18.18 Parasternal long-axis view showing aortic overriding and sub-aortic VSD in a patient with tetralogy of Fallot

Associated Lesions

Patency of the oval fossa, atrial septal defect (ASD), a second muscular VSD or an atrioventricular septal defect. A right aortic arch is common and sometimes associated with anomalous origin of the subclavian artery. Coronary arterial abnormalities, such as a left anterior descending artery originating from the right coronary artery, crossing the right ventricular outflow tract, may occur in about 3% and may be of surgical importance [9–11].

Patients with Palliative Procedures

There are occasional patients who may reach adulthood with a palliative procedure only. The types of different palliative procedures that augment pulmonary blood flow in tetralogy of Fallot are:

- *Blalock-Taussig shunt* (*classical*): subclavian artery-to-pulmonary artery anastomosis (end-to-side).
- *Blalock-Taussig shunt* (*modified*): interposition graft between subclavian artery and uni or bilateral pulmonary artery.
- *Waterston shunt*: ascending aorta-to-main or right pulmonary artery (side-by-side).
- *Potts shunt*: descending aorta-to-left pulmonary artery (side-by-side).
- *Central interposition tube graft.*
- *Infundibular resection* (*Brock procedure*) or closed pulmonary valvotomy.
- Relief of right ventricular outflow tract obstruction without VSD closure or with fenestrated VSD closure.

Shunts can usually be detected from supra-sternal view. Color and continuous wave Doppler are usually very helpful for assessing the patency, tortuosity and/or stenosis of the shunt. Magnetic Resonance Imaging (MRI) is capable of providing clearer images of the shunt.

Pulmonary pressures can be estimated as:

$$\text{Pulmonary artery systolic pressure} = \text{peak systolic systemic arterial pressure} - 4V^2\,(\text{peak velocity across the shunt}).$$

It is important to exclude peripheral pulmonary artery stenosis when using this method. Left ventricular dilatation and dysfunction may also develop secondary to volume overload. Patients with previous Brock procedures, residual right ventricular outflow tract obstruction and significant pulmonary regurgitation can still be present.

In view of the potential right-sided complications in patients with unoperated or previously palliated tetralogy of Fallot, late repair should be considered in those suitable for surgery which in turn should improve functional status and quality of life [4, 10].

Patient with Reparative Surgery

Reparative surgery for tetralogy of Fallot involves closing the VSD and relieving the right ventricular outflow tract obstruction. Echocardiographic assessment should include:

- Degree of pulmonary regurgitation.
- Right ventricular dimension and function.
- Residual right ventricular outflow tract obstruction.
- Residual VSD.
- Aortic dilatation and regurgitation.
- Left ventricular function.

Pulmonary regurgitation and right ventricular outflow tract obstruction are the most common residual hemodynamic lesions that contribute to the morbidity and mortality of these patients. Replacement of the pulmonary valve can prevent irreversible damage to the right ventricle and arrhythmic complications.

Pulmonary regurgitation can be quantified by using two criteria: jet diameter on a color flow map and Pulmonary Regurgitation index (PR index).

- Jet diameter is measured at the pulmonary valve leaflets level during early diastole. Jet diameter > 0.98 cm indicates significant regurgitation.
- Pulmonary Regurgitation index (PR index) is the ratio between pulmonary regurgitation time and total diastolic time. An index of <0.77 suggests severe pulmonary regurgitation.

From the pulmonary artery spectral Doppler, total diastolic time is measured as the time interval between the end of the previous ejection to the beginning of the succeeding one. Pulmonary regurgitation time is measured from the onset of regurgitation to the end when the regurgitation signal reaches the baseline (pressure equalization between the pulmonary artery and right ventricle). The ratio of pulmonary regurgitation time to total diastolic time is taken as the pulmonary regurgitation index. The lower the value, the more severe the regurgitation is (Fig. 18.19).

Right ventricular dilatation and reversed septal motion are indirect signs of significant pulmonary regurgitation.

Residual Right Ventricular Outflow Obstruction

- This is classified into mild (peak gradient <40 mmHg), moderate (40–70 mmHg) and severe (>70 mmHg).
- Residual right ventricular afterload is also undesirable, because of the increased risk of ventricular dysfunction and arrhythmia. Residual or progressive pulmonary stenosis after repair may happen at different levels.
- Severity of right ventricular outflow tract obstruction may be underestimated in the presence of right ventricular dysfunction and reduced stroke volume.

Residual Shunt

Residual VSDs are commonly around the VSD patch area. It is important to measure the VSD size and shunt velocity. From the shunt velocity, right ventricular pressure can be evaluated. Significant left to right shunt usually results in left atrial and left ventricular volume overload and dilatation. Furthermore, shunts at atrial and arterial levels may be present in some patients. When there is a significant left-to-right shunt at the atrial level, right atrial and right ventricular dilatation usually co-exist.

Assessment of the Right Ventricle

Assessment of the right ventricle includes assessment of its morphology (size and wall thickness) and function (systolic and diastolic); the former includes right ventricular inflow

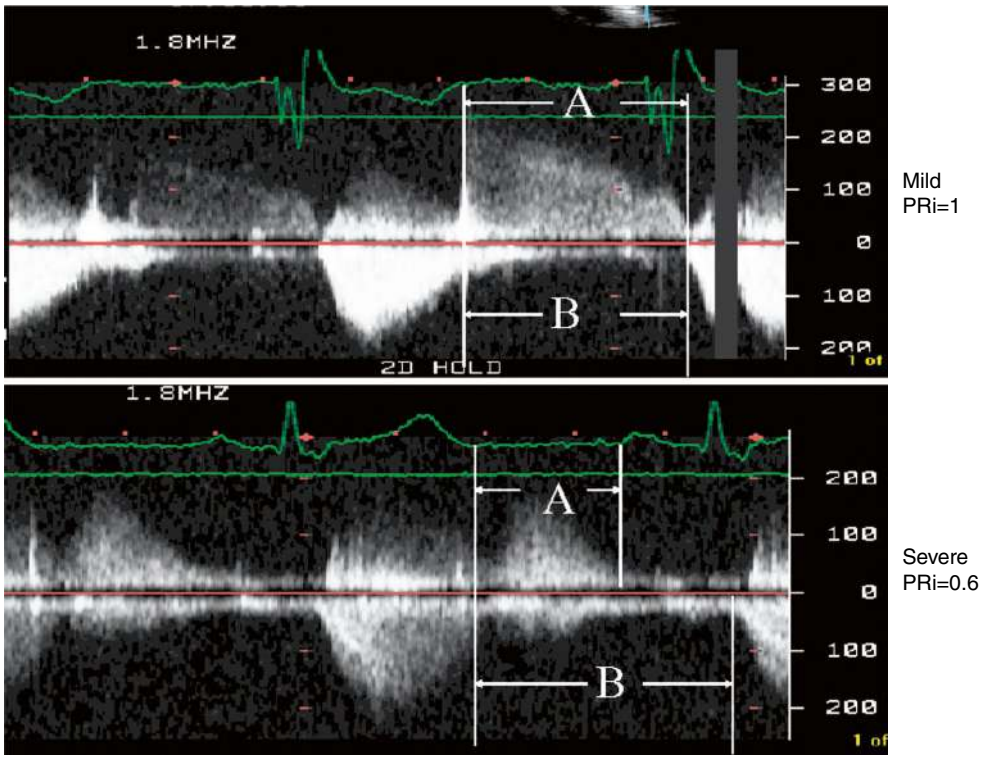


Fig. 18.19 Pulsed wave Doppler from two patients with pulmonary regurgitation, mild (*top*) and severe (*bottom*). Note the shortening regurgitation signal in the patient with severe lesion and hence low PRi (*A*/*B*)

and outflow tracts. The outflow tract is the region where the frequent presence of akinesis and aneurysmal formation contributes to ventricular dysfunction and predisposes to sustained ventricular tachycardia. Right ventricular size can be measured from the parasternal long-axis view which represents the right ventricular outflow dimension and from the apical four-chamber view by measuring the right ventricular inlet diameter or ventricular area. RV outflow diameter > 2.7 cm is compatible with increased end-diastolic volumes by MRI. The literature suggests that a right ventricular inlet diameter > 4 cm is consistent with cavity dilatation. Right ventricular aneurysmal dilatation and akinetic patch area are best visualized from the parasternal short-axis view and can be more clearly demonstrated by MRI.

Right Ventricular Function

Right ventricular function has been known to be an echo challenge in part due to the complex geometry of the right ventricle. The following parameters can be used:

- Right ventricular free wall long-axis excursion and myocardial tissue Doppler velocity.
- Right ventricular fraction area change.
- Right ventricular myocardial performance index.
- RV dp/dt can also be measured from a tricuspid regurgitation trace.
- Strain and strain rate indicates.
- Right ventricular restrictive physiology as demonstrated by antegrade diastolic flow detected by pulsed wave Doppler in the main pulmonary artery coinciding with atrial systole ('a' wave), presenting throughout the respiratory cycle. Retrograde flow during atrial systole can also be detected on superior and inferior vena cava flow.
- Right ventricular end-diastolic and end-systolic volume and ejection fraction derived from MRI are very accurate in assessing RV systolic function. Regional wall motion (right ventricular outflow tract akinesia) and aneurysmal dilatation can be demonstrated by both echo and MRI.

Aortic Root Dimension and Aortic Regurgitation

Progressive dilatation of the aorta has been shown late after the repair of the tetralogy of Fallot.

The number of patients seen with increasing aortic dimensions after tetralogy of Fallot repair has been increasingly noticed, who needed aortic root repair and aortic valve replacement. Therefore, the aortic dimension and presence of aortic regurgitation should be closely monitored.

Left Ventricular Diameter and Function

Left ventricular dysfunction may relate to previous longstanding cyanosis prior to repair, and inadequate myocardial

protection during repair and/or development of coronary artery disease as patients get older. Conventional methods for assessing LV function (such as ejection fraction and fractional shortening) as well as myocardial velocities and deformation parameters can be applied in these patients [4, 11].

References

1. Baumgartner H, Bonhoeffer P, De Groot NMS, et al. ESC Guidelines for the management of grown-up congenital heart disease (new version 2010). Eur Heart J. 2010;31:2915–57.
2. Gatzoulis MA, Webb G, Daubeney PF, editors. Diagnosis and management of adult congenital heart disease. Philadelphia: Elsevier/Saunders; 2011.
3. Li W, Henein M, Gatzoulis MA. Echocardiography in adult congenital heart disease. New York: Springer; 2007.
4. Riahi M, Velasco Forte MN, Byrne N, Hermuzi A, Jones M, et al. Early experience of transcatheter correction of superior sinus venosus atrial septal defect with partial anomalous pulmonary venous drainage. EuroIntervention. 2018;14:868–76.
5. Minette MS, Sahn DJ. Ventricular septal defects. Circulation. 2006;114(20):2190–7.
6. Schneider DJ, Moore JW. Patent ductus arteriosus. Circulation. 2006;114:1873–82.
7. Tan JL, Babu-Narayanan SV, Henein MY, et al. Doppler echocardiographic profile and indexes in the evaluation of aortic coarctation in patients before and after stenting. J Am Coll Cardiol. 2005;46:1045–53.
8. Brown ML, Dearani JA, Danielson GK, et al. Effect of operation for Ebstein anomaly on left ventricular function. Am J Cardiol. 2008;102:1724–7.
9. Shiina A, Seward JB, Edwards WD, et al. Two-dimensional echocardiographic spectrum of Ebstein's anomaly: detailed anatomic assessment. J Am Coll Cardiol. 1984;3:356–70.
10. Li W, Davlouros PA, Kilner PJ, et al. Doppler-echocardiographic assessment of pulmonary regurgitation in adults with repaired tetralogy of Fallot: comparison with cardiovascular magnetic resonance imaging. Am Heart J. 2004;147:165–72.
11. Haddad F, Hunt SA, Rosenthal DN, Murphy DJ. Right ventricular function in cardiovascular disease: I. Anatomy, physiology, aging, and functional assessment of the right ventricle. Circulation. 2008;117(11):1436–48.

Percutaneous Device Closure of Atrial Septal Defect (ASD) and Patent Foramen Ovale (PFO)

19

Evelyn M. Lee, Kwang How Mok, Ting Ting Low, and Leonard M. Shapiro

Introduction

There is now good evidence for consideration of PFO closure for secondary prevention of stroke in younger patients with cryptogenic stroke [1–4], especially if patients have high-risk clinical and anatomical features [5] [6]. Percutaneous device closure is the method of choice for ASD and PFO closure in the majority of cases, but sometimes surgical closure may be necessary [7, 8]. Echocardiography has been invaluable in pre-, intra- and post-procedural assessment [9, 10], in determining suitability for device closure, guiding closure [11], detecting complications and understanding reasons for failure.

Two-dimensional (2D) echo provides excellent resolution for detailed analysis, while three-dimensional (3D) echo is particularly helpful in understanding complex shapes and spatial relationships [12]. Transoesophageal echocardiography (TOE) and intracardiac echocardiography (ICE) are both useful for intraprocedural guidance for device closure.

A wide range of devices have been designed and used over the years, but the majority are no longer in widespread use. Common devices in current use include the Amplatzer device and the Gore Cardioform Septal Occluder [13].

This chapter explains the uses of, and lessons learnt, from echocardiography. Standard abbreviations used in the text and figures are listed in Table 19.1.

Table 19.1 Abbreviations

ASD	Atrial septal defect
PFO	Patent foramen ovale
2D	2-dimensional
3D	3-dimensional
TTE	Transthoracic echocardiography
TOE	Transoesophageal echocardiography
ICE	Intracardiac echocardiography
LA	Left atrium
RA	Right atrium
IAS	Interatrial septum
SP	Septum primum
SS	Septum secundum
FO	Fossa Ovalis
DASP	Deviated atrial septum primum
Ao	Aorta
SVC	Superior vena cava
IVC	Inferior vena cava
SB	Sizing balloon
GW	Guide wire
DW	Delivery wire

The Percutaneous Closure Procedure

Most closure devices have consisted of a left atrial disk and right atrial disk linked by a waist that straddles the defect, and that holds the 2 disks flush against the interatrial septum like a clamp to stabilize the device position. A guidewire is passed from the femoral vein to the right atrium, across the defect and into the left atrium, often with the tip parked in the left upper pulmonary vein. A long sizing balloon is placed within the defect and inflated until indentations appear to form a "waist" (Fig. 19.1).

Balloon sizing is advisable in most cases, especially if the septum primum is floppy, aneurysmal or folds readily, as the stretched size can be considerably larger than the measured size (Fig. 19.2).

Larger devices are more difficult to deploy and have greater potential for non-endothelialization, thrombus formation and atrial wall erosion. Occasionally, an ASD with firm, well-aligned rims, involving a non-aneurysmal septum,

Supplementary Information The online version contains supplementary material available at https://doi.org/10.1007/978-3-031-95894-6_19.

E. M. Lee (✉) · K. How Mok
Department of Cardiology, Tan Tock Seng Hospital, Singapore, Singapore

T. T. Low
Department of Cardiology, Tan Tock Seng Hospital, Singapore, Singapore

Department of Cardiology, National University Hospital, Singapore, Singapore

L. M. Shapiro
Department of Cardiology, Papworth Hospital, Cambridge, UK

© The Author(s), under exclusive license to Springer Nature Switzerland AG 2025

M. Y. Henein (ed.), *Clinical Echocardiography*, https://doi.org/10.1007/978-3-031-95894-6_19

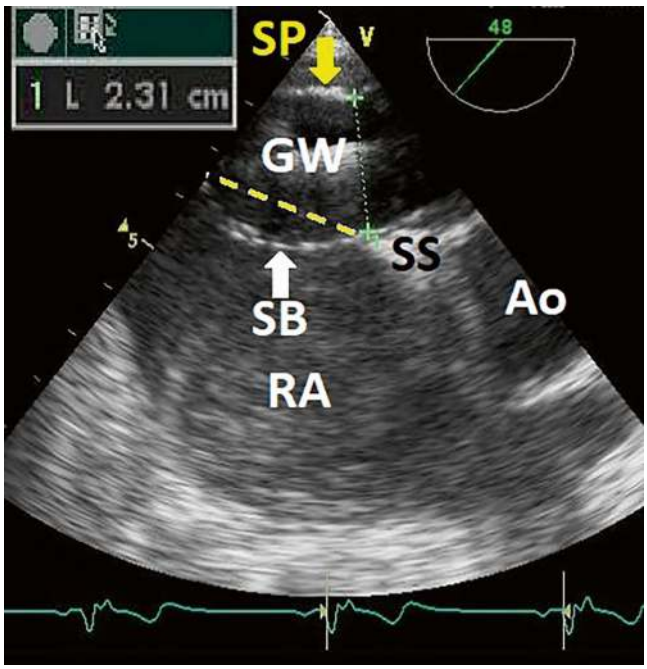


Fig. 19.1 Sizing balloon (SB, white arrow) in situ across the ASD. Indentations from the septum secundum (SS) and from the septum primum (SP, yellow arrow) cause a waist (dotted white line) to form in the balloon. The balloon often displaces septum primum into the left atrium, especially if septum is aneurysmal, such that the waist is not, as might be intuitively expected, in the plane of the fossa ovalis (dashed yellow line). The septum primum is thin and may be difficult to see lying flush against the balloon surface, as in this patient. This balloon waist represents the stretched diameter of the defect, and device waist size needed for closure

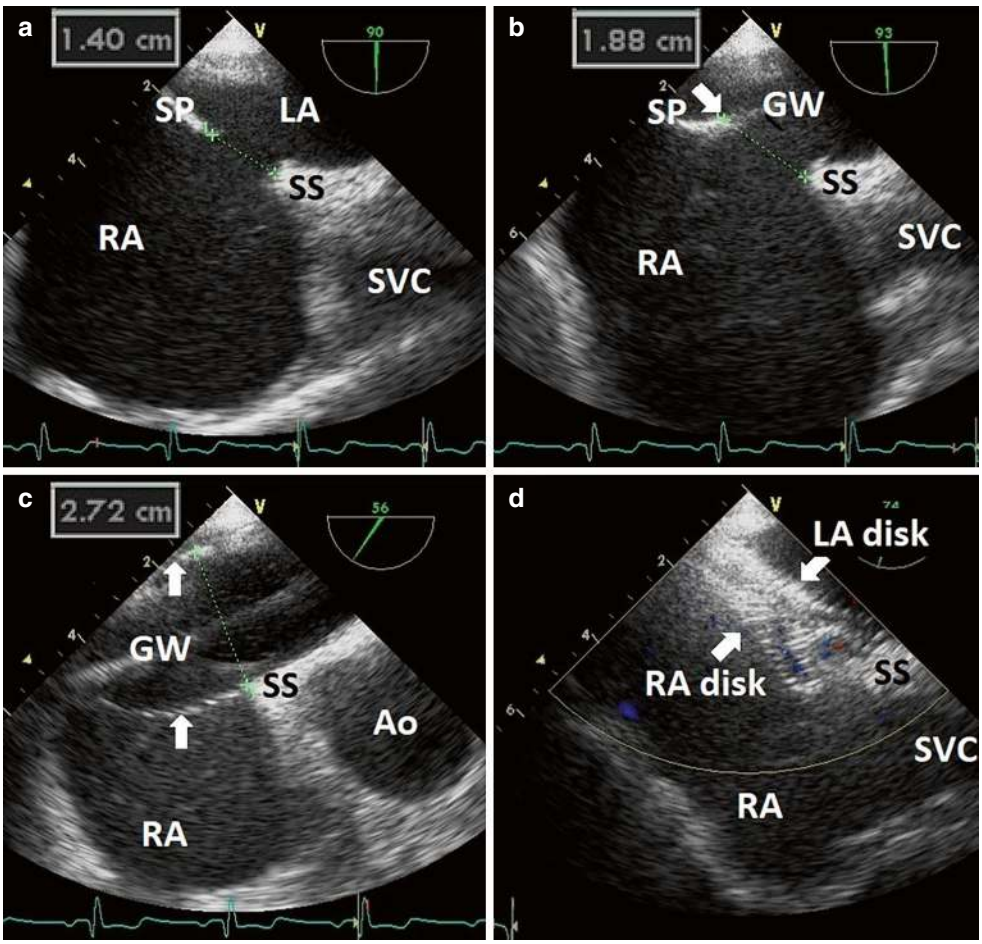


Fig. 19.2 (**a**) This ASD measures only 1.4 cm on TOE. (**b**) Although the septum primum (SP) looks straight in this view, it was redundant and aneurysmal in other views. It bent and displaced readily with just the stiffness of a standard guide wire (GW), increasing ASD diameter by 34% to 1.9 cm. (**c**) Sizing balloon stretched diameter was even bigger at 2.7 cm. Arrows point to the surfaces of the inflated sizing balloon. (**d**) The defect was closed satisfactorily with a 2.8 cm-waisted Amplatzer ASD occluder

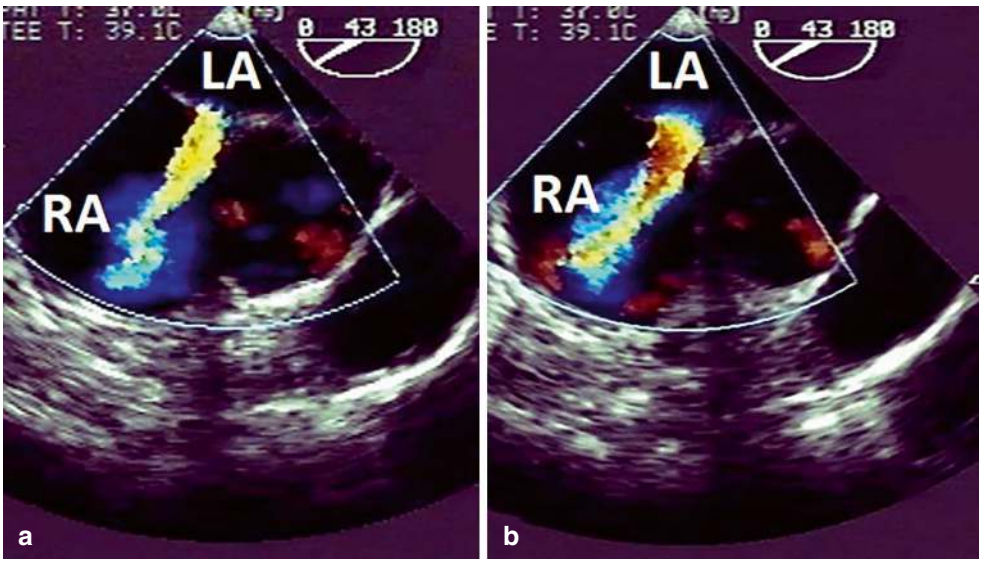


Fig. 19.3 (**a**) Secundum ASD with left to right shunt, before balloon sizing. (**b**) Same ASD, now larger after balloon sizing

may be sized by TOE alone. Measurements are adjusted for potential changes in ASD size with atrial filling and elasticity by adding a minimum of 20% to the average TOE-measured diameter, and 25–30% if the septum primum is flimsy and slightly redundant. The average 2D-TOE diameter is the mean of 1 or 2 sets of maximum diameters measured on 2D on 2 views at 90° to each other (e.g. 0° and 90°, 45° and 135°). 3D TOE is often used to corroborate 2D findings, but care must be taken with 3D measurements to avoid mistakes from echo dropout, high gains and oblique views. TOE sizing avoids enlargement of defects by balloon stretch (Fig. 19.3), and helps to minimize device size, but carries a risk of under-sizing if case selection is poor.

A delivery sheath is passed into the left atrium, the guidewire removed and the closure device passed up the delivery catheter into the left atrium. The left atrial disk is deployed in the left atrium, pulled back and apposed to the interatrial septum. The right atrial disk is then deployed and the device released from the delivery system if the intraprocedural assessment is satisfactory (Fig. 19.4).

Devices that have been deployed but not released from the delivery system can be re-sheathed and retrieved. Some may be re-deployed, allowing multiple attempts at closure with the same device.

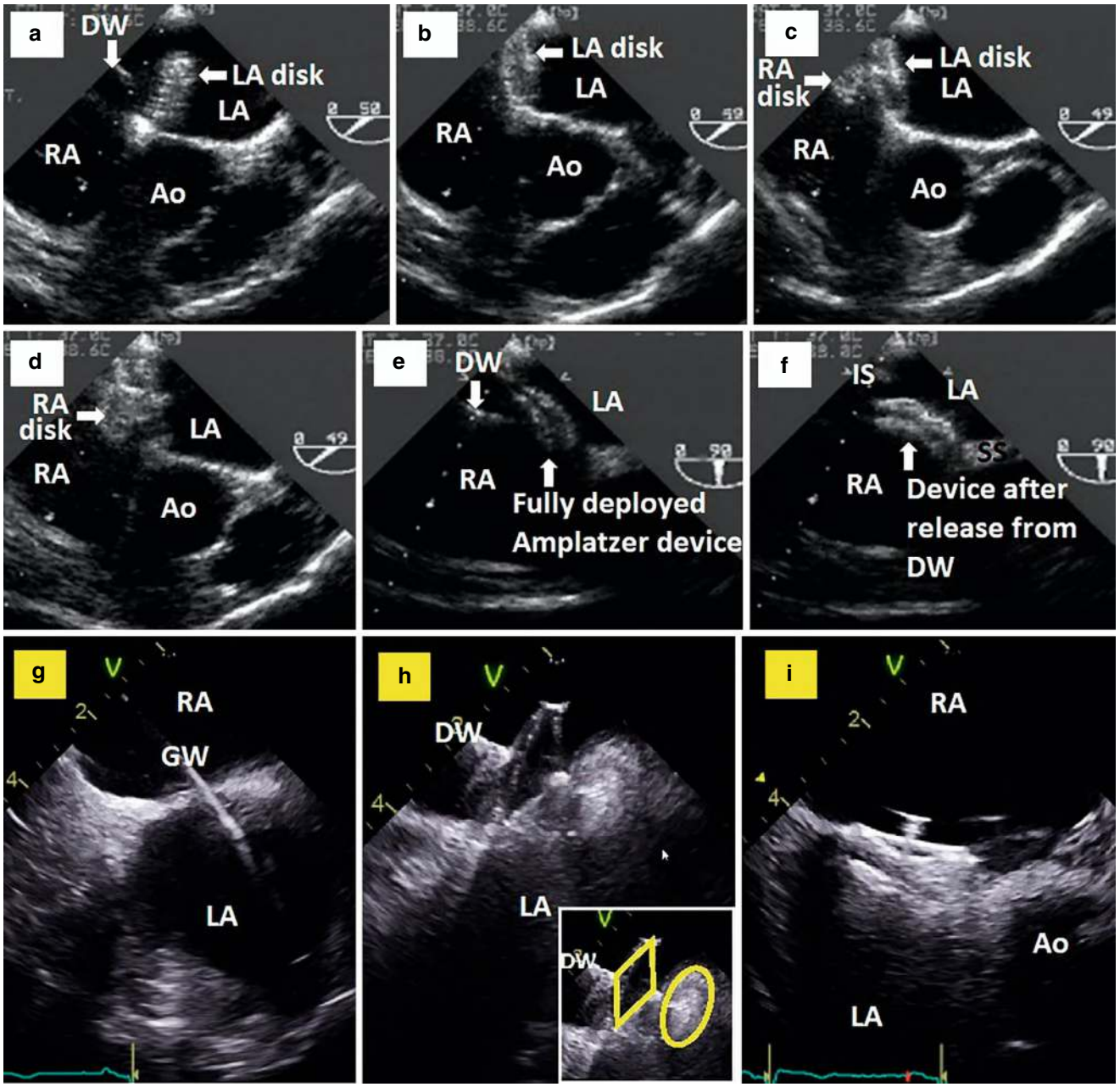


Fig. 19.4 (**a**–**f**) Amplatzer ASD occluder closure of a secundum ASD with aneurysmal interatrial septum under TOE guidance. (**a**) Left atrial (LA) disk deployed in left atrium. (**b**) LA disk pulled back onto interatrial septum. (**c**) Right atrial disk partially deployed in right atrium. (**d**) RA disk fully deployed and pulled upon. The device is pushed and pulled to check for stability and imaged from all angles to ensure circumferential septal capture between disks. (**e**) The unreleased device is often poorly aligned with the septal plane as the rigidity of the delivery wire causes device angulation and septal distortion. (**f**) Upon release, the device "jumps" into its final position. The aneurysmal interatrial septum sags into the right atrium bringing the device with it, so this device does not sit within the plane of the fossa ovalis, but it was stable and the ASD successfully closed. (**g**–**i**) Amplatzer PFO closure using ICE. (**g**). Guidewire through the PFO. (**h**) Device deployed but not yet released, pulled on to check for stability. The stretched RA disk is marked by the diamond in the insert. The oblique cut through the LA disk is marked by the oval. (**i**) Well-seated device after release

Device Design

There have been a wide range of devices used, with a wide range of designs (Fig. 19.5), but many are no longer in use [13]. Disks range from bulky, three-dimensional (3D) frames of nitinol wire meshwork filled with felt sheets (Amplatzer—Abbott Cardiovascular and second and third-generation similar devices like Occlutech—Occlutech Holding AG and Cera—Lifetech Scientific Corporation), to flat sheets of material mounted on a supportive wire frame of radial struts (e.g. Cardiastar and Intrasept—Cardia, Cardioseal, Starflex and Biostar—NMT Medical Inc.), radial loops (Premere, right atrial disk—St. Jude Medical Inc.), interlaced loops or spirals round central support (e.g. Solysafe—Swiss implant AG,. Helex and the newer iteration CARDIOFORM—WL Gore and Associates, Ultrasept—Cardia), to the minimalistic left atrial disk of the Premere, which consists only of an uncovered, propeller-shaped wire frame. Covering materials on the wire frames include various synthetics (e.g. Intrasept, Helex, Starflex, Premere right atrial disk) and biodegradables such as collagen (e.g. Biostar).

Disks vary in radial and circumferential strength. Stronger 3D devices (e.g. Amplatzer) may be better at handling the tensions required to pull awkward PFO tunnels into suitable shapes for closure. Independent radial struts or loops may conform better to 3D contours than circular constructs but may need sufficient redundancy in disk material to permit flush coverage of a non-planar 3D surface underneath with a surface area greater than that of the disk. Otherwise, flat planar disks may be distorted by the 3D atrial surface and provide an incomplete seal.

Simple fixed-short-waist radial spoke planar devices such as Biostar and Starflex are no longer in general use. Simple radial spokes had less radial strength and could fold easily into PFO long tunnels, especially with funnel-like left atrial openings. (Fig. 19.6, Video 19.1). Spoke tips were small and could prolapse more readily through small spaces, e.g. narrow fossa ovalis or fenestrations. (Fig. 19.7, Video 19.2).

Disk bulk, rigidity and materials may be important. Thin disks may allow for perforation for trans-septal catheter-based interventions in the future. Soft and highly malleable disks have a lower risk of erosion. Although biodegradable

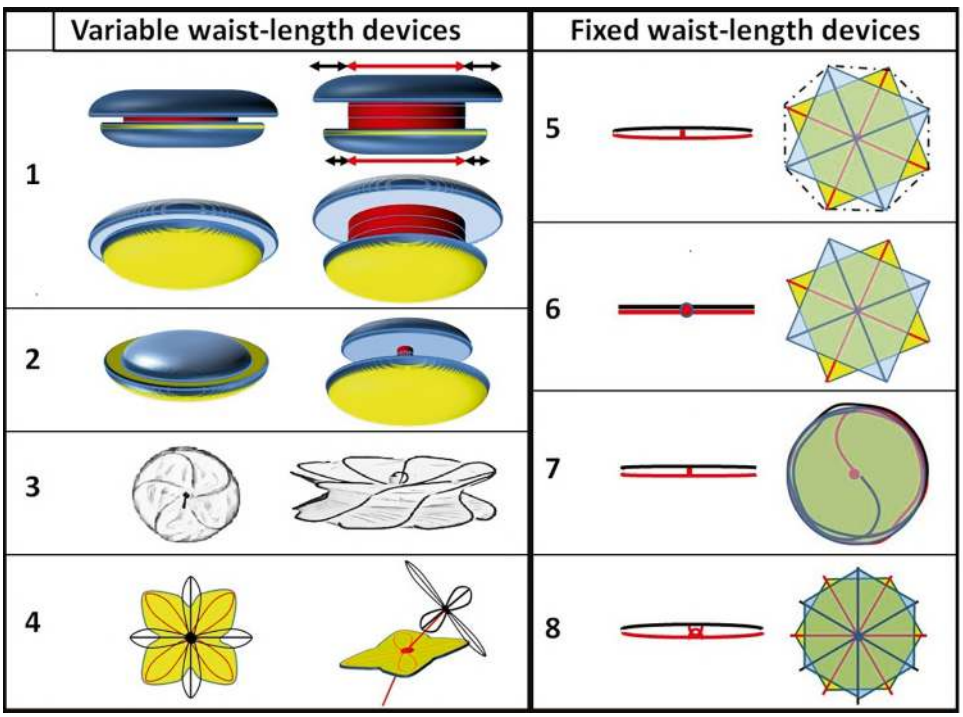


Fig. 19.5 Device designs. (1 and 2) Nitinol mesh porous devices with 3D disks, adaptable 3D waists and felt inserts that thrombose to render the device non-porous, e.g. Amplatzer ASD device. (2) Amplatzer PFO devices differ from ASD devices by having a right atrial disk larger than the left. (3) Cardioform wire loops and spirals that flatten into planar disks and adaptable 3D waist. (4) Premere device with bare wire "propeller" as left atrial disk, planar material-covered wire "propeller" as right atrial disk, and variable length thread for the waist. (5) Planar disk device (Biostar) with elastic springs linking left and right atrial disks. These springs traverse the ASD and abut its edges to enable self-centering. (6, 7, and 8) Non-self-centering planar disk devices with sheet material covered radial struts or wire loops with short fixed waist lengths and no waist angulations (6 and 7) or variable angulation, e.g. Intrasept with 2 interlinked metal loops as its waist (8)

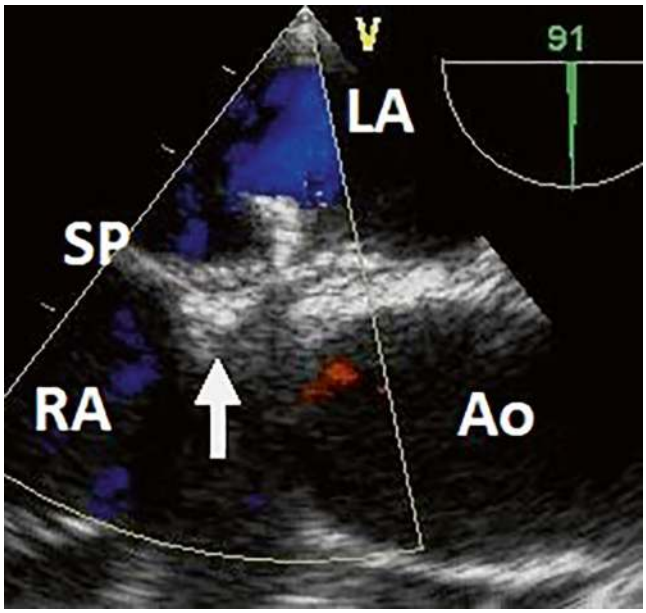


Fig. 19.6 Cardioseal PFO closure device (arrow) folded into the PFO tunnel

devices have the theoretical benefit of leaving little or no foreign material in the heart, extensively biodegradable devices have not been successful [14] [15]. The ideal degradation time for biodegradable disks is unknown, with risks of perforation, residual shunting, device fragmentation, device displacement and increased thrombogenicity from premature degradation.

Amplatzer and Occlutech ASD devices have 3D bulk in both disks and waists, with self-centering cylindrical waists that will ultimately thrombose off to occlude the ASD. Newer ASD devices have combined low-profile planar disks with 3D self-centering wire frame sheet material-covered waists, e.g. Gore Cardioform and Cardia Ultrasept ASD occluders. These 3D waists have some adaptability in both shape and length to better fit different septal morphologies. The current Gore Cardioform Septal Occluder 2 sets of 5 spiraling wires on either side of the central waist, covered in PTFE to form a complex PTFE lantern. These flatten out to form planar left and right atrial disks composed of 5 overlapping petals with redundancy of material between petals, allowing independent positioning and greater 3D conformability. Some self-

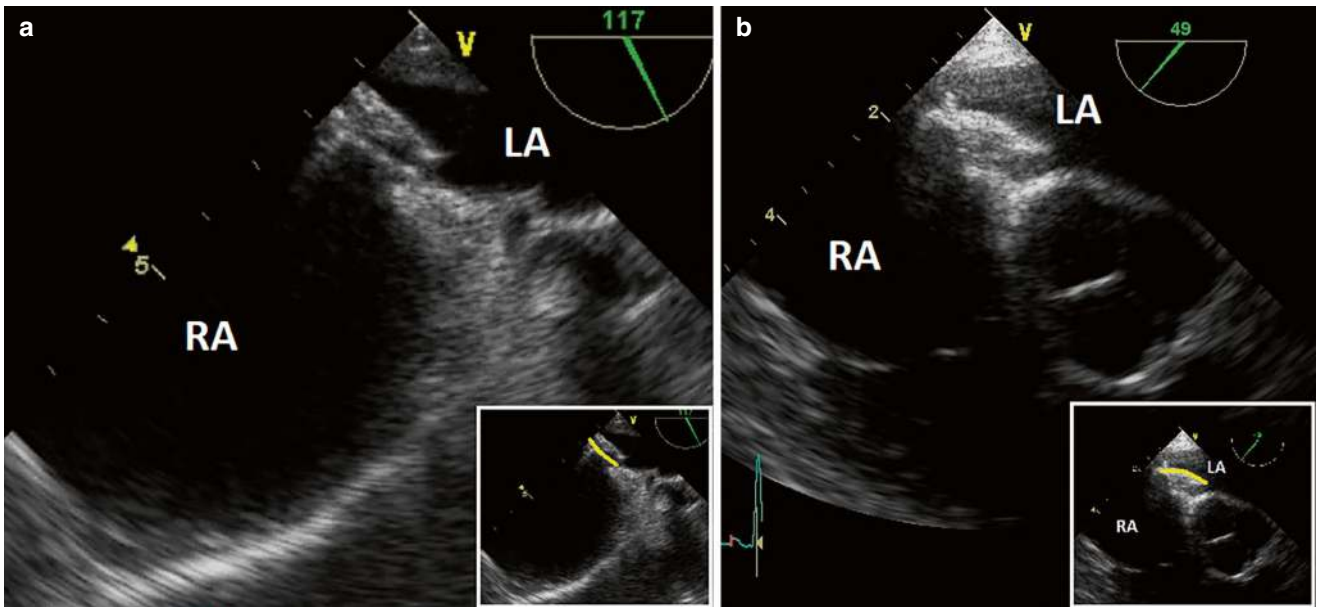


Fig. 19.7 Two patients with residual shunts due to spoke malposition following PFO closure with radial spokes planar devices. (**a**) Late displacement of one spoke of the RA disk (yellow line on insert) into the PFO tunnel stented the PFO open, causing recurrent shunting. (**b**) One of the left atrial disk spokes of this Intrasept was caught within a fenestration causing a mal-positioned, poorly apposed left atrial disk (yellow line on insert)

centering devices are no longer in use. The Solysafe had sparse wire spirals between disks. Starflex and Biostar had micro springs linking right and left atrial disk struts.

Without self-centering, larger device disks are required for ASD closure (disk radius > ASD diameter) to ensure that the disk covers the entire ASD and does not prolapse through the defect, should the waist become positioned asymmetrically at the edge of the ASD. Most non-self-centering devices had a thin waist of wire, interlocking structures, or thread. Some had fixed waist length and inflexible waist angulation. Premere used a non-biodegradable thread on which the right atrial disk could be locked at a suitable point, allowing a variable and highly adaptable waist length and angulation to match widely varying PFO anatomy.

Non-disk-based techniques may add to the versatility and success of percutaneous closure e.g. FlatStent from Coherex (no longer manufactured), NobleStitch™ EL from HeartStitch [16–18].

Multiple device-related factors influence the completeness of defect closure, device endothelialization, device thrombogenicity, device embolization and risk of erosion through the atrial wall. Many devices are no longer in use. Common devices in current use include Amplatzer, Occlutech, Gore Cardioform and Cardia Ultrasept devices. Device selection is driven by individual anatomy, clinical indication and operator experience. The bulk of available evidence for PFO closure was derived from clinical trials using AMPLATZER™ PFO Occluder [2–4] and GORE® HELEX® Septal Occluder (not available anymore) or the GORE® CARDIOFORM [1], with the latter being associated with a higher rate of AF and incomplete closure. A European position paper was published in 2019 recommending a shared decision approach for the potential use of devices outside of AMPLTAZER and CARDIOFORM for PFO closure [19]. For ASD closure, there are no specific guideline recommendations on device selection.

Echocardiography has provided insights into the performance of these varied devices and how best to match device design to individual anatomy.

Assessment of Suitability for ASD Closure

TOE is routinely used to assess suitability for percutaneous closure.

TOE Criteria for Closure

1. *Suitable defect size for the available device*s. Closure of ASDs is generally limited to sizes of approximately 3 cm or less, due to the available device sizes and poor rims often associated with very large ASDs.
2. *Sufficient rim around the defect to seat a stable device*. Poor aortic rims are technically acceptable as devices can splay across the aorta, but good rims are required for support elsewhere (Fig. 19.8, Videos 19.3, 19.4 and 19.5). There is a small risk of rare but potentially fatal erosion into the aorta or pericardial space. The risk is greater with an oversized 3D device in a constrained space, and rims <5 mm wide. Risk may be lower with softer and less bulky devices such as the Gore Septal Occluder. No cases of erosion have been reported so far with the latter [20].
3. *Suitably flat apposition surfaces on which to sit the atrial disks*. Protruding structures and atrial wall curvature may cause device distortion and malposition (Figs. 19.8 and 19.9, Video 19.6). If disk apposition is poor, endothelialization may be suboptimal, with a small risk of thrombus formation. To achieve complete closure without residual shunting, there must be a complete seal by optimal apposition of at least one disk, or complete plugging of the defect by the device waist.
4. *Adequate separation from adjacent structures.* It is important to check the proximity of important adjacent structures—superior and inferior vena cava, coronary sinus (Fig. 19.10), right pulmonary veins, mitral (Fig. 19.11) and tricuspid valves, and atrial free wall—to avoid encroachment upon these structures. Only secundum ASDs are suitable for percutaneous device closure. Device closure of sinus venosus defects risks venous obstruction, while primum ASD closure will affect the atrioventricular valves.
5. *Absence of other abnormalities requiring surgical correction*, such as second ASD unsuitable for closure, deviant anatomy that would complicate device closure, anomalous pulmonary venous drainage or valvular heart disease.
6. *Absence of intracardiac thrombus*, which may embolise if accidentally disturbed. Guidewires often enter the left atrial appendage.
7. *Adequate closure for the clinical indication* [7, 8]. Closure is sometimes predictably incomplete. Fenestrations distant from the device or inadequately trapped between supporting rims may still shunt. More than 1 device may be required for multiple defects. Small residual shunts are acceptable where the aim is shunt reduction for right heart volume overload from left-to-right shunting, or hypoxaemia [21] from right-to-left shunting in severe sleep apnoea [22] or platypnoea orthodeoxia [23]. They may be unacceptable in suspected paradoxical embolism in cryptogenic stroke or arterial "bends" in divers [24]. Although risk of recurrent paradoxical embolism seems related to shunt size [5, 25] and partial closure may perhaps still be beneficial, patients should nevertheless be aware of procedural limitations.

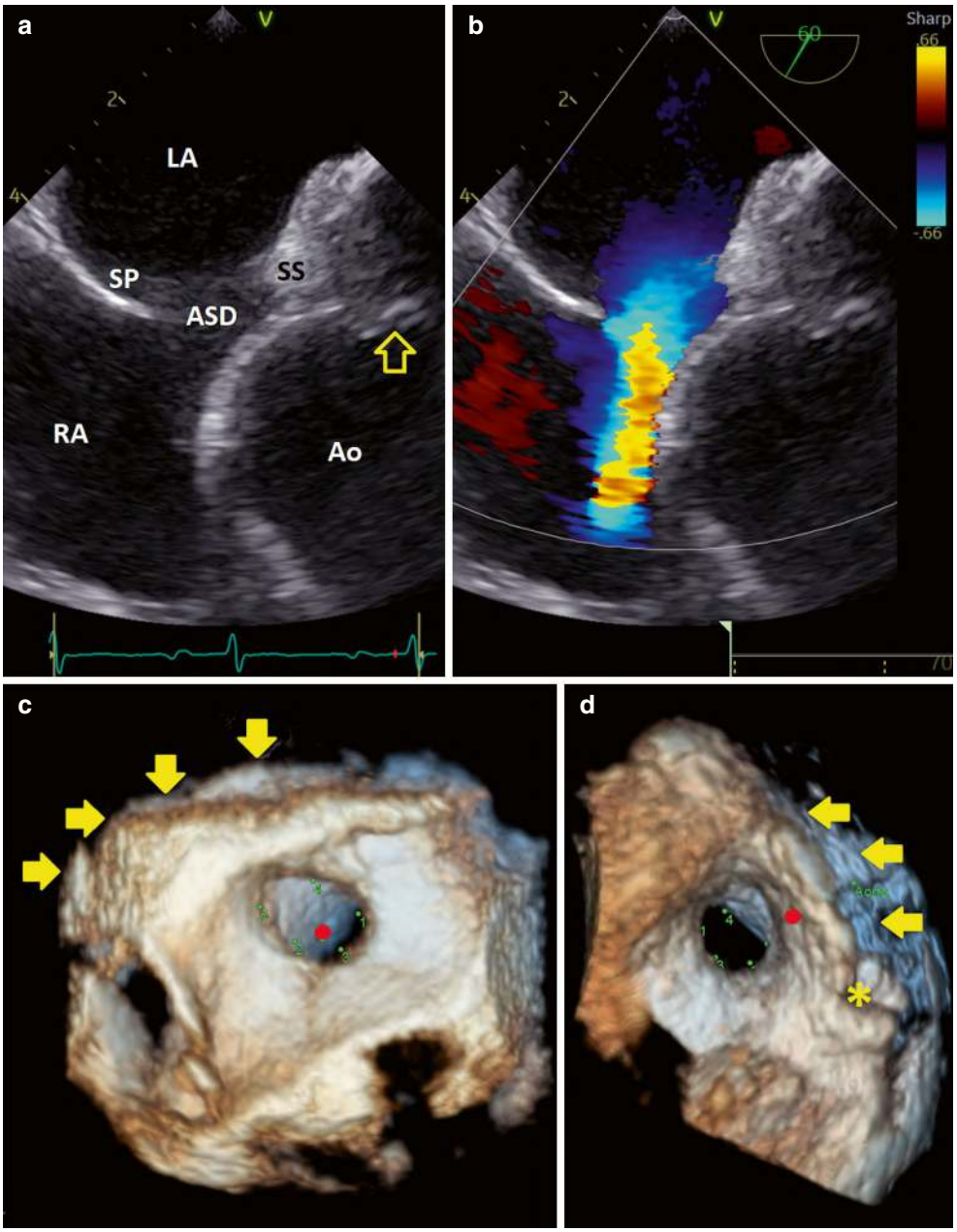


Fig. 19.8 TOE. ASD deemed unsuitable for device closure. (**a**) The aortic rim is minimal, and the bulging unfolded aorta distorts the right atrial wall. There is no space for device disks to splay across the aorta. Yellow arrow points to the aortic valve. (**b**) The ASD shunts left to right on colour doppler. (**c**, **d**) 3D TOE views. Yellow arrows point to the position of the aorta behind the LA wall in C, and the aorta itself in (**d**). The bulge in the right atrial wall caused by the unfolded aorta is marked by the red dot. Green dots mark the rims of the ASD. (**c**) View from LA, showing the lack of rim, steep curvature of the LA wall from the ASD rim, and lack of space to seat the LA disk in the aortic quadrant of the ASD. (**d**) View from RA showing the distorted superior RA lumen-like a funnel leading down to the ASD. Only the inferior third of the rim is flat enough to be gripped by the ASD device, and there is a high risk of RA disk displacement

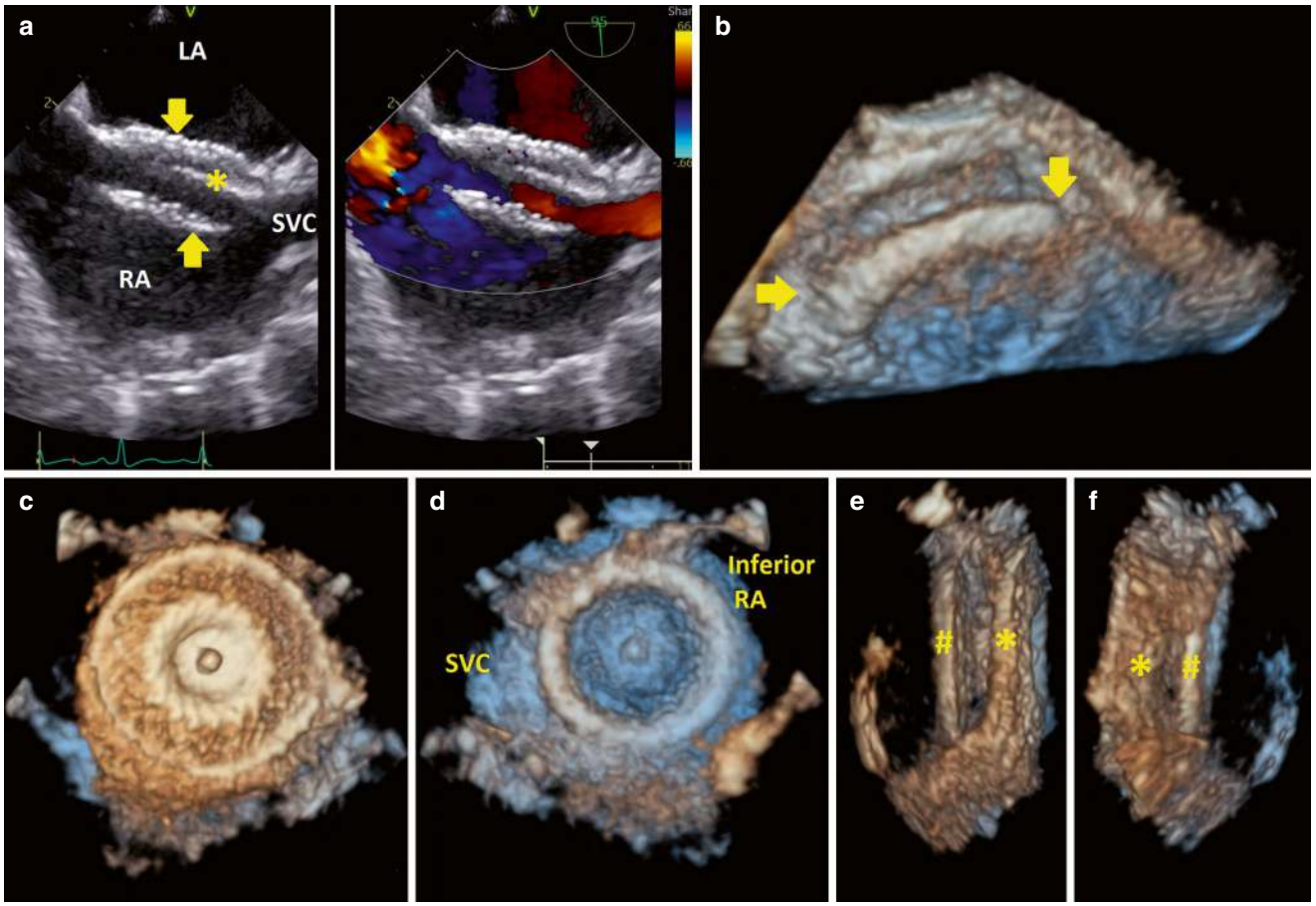


Fig. 19.9 TOE of Amplatzer device ASD closure. (**a**) The left atrial disk (Down arrow) was well apposed, but the right atrial disk did not sit flush against the interatrial septum (Up arrow). Blood from SVC and IVC flowed freely around and between right atrial disk and interatrial septum (*). (**b**) 3D TOE view of the right atrial disk viewed from the inferior right atrium. The disk edges are held up by the curvature of the right atrial walls anteriorly and posteriorly (arrows), preventing it from sitting flush with the septum. (**c**) The left atrial disk is well formed and well seated. (**d**) The right atrial disk is deformed into a shallow bowl. E. Inferior view from inferior RA, and F. superior view from the SVC, show the RA disk (#) held well away from the interatrial septum (*) inferiorly and posterosuperiorly. There was a small area of suboptimal LA disk apposition superiorly due to LA wall curvature, with flow between the disk and interatrial septum. However, there was no residual shunt as the well-sized device waist completely occluded the ASD

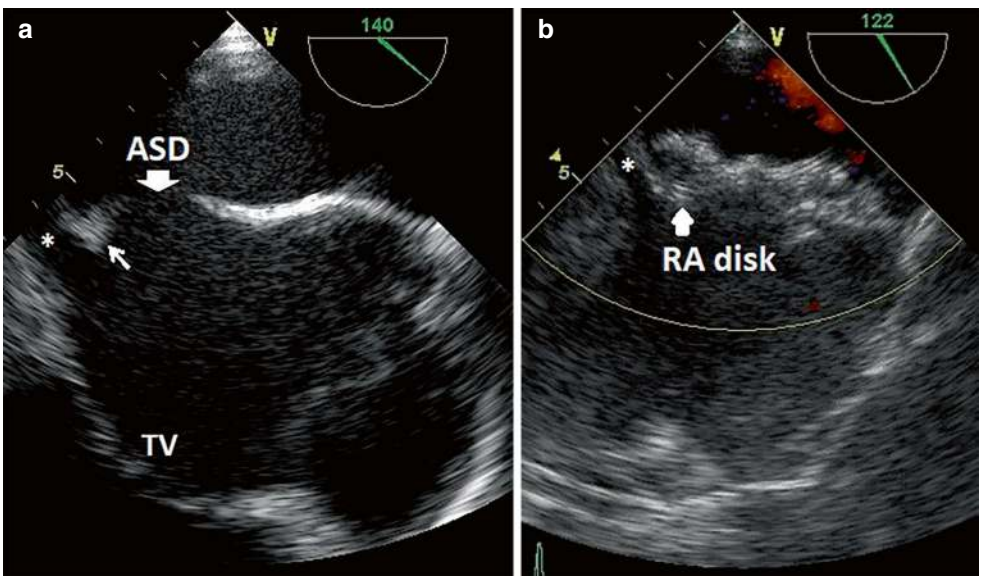


Fig. 19.10 TOE of an inferior ASD. (**a**) The interatrial septum ends (small arrow) next to the ostium of the coronary sinus (*). (**b**) The inferior rim of the device is close to the coronary sinus ostium but there is just enough inferior rim to avoid obstructing the ostium

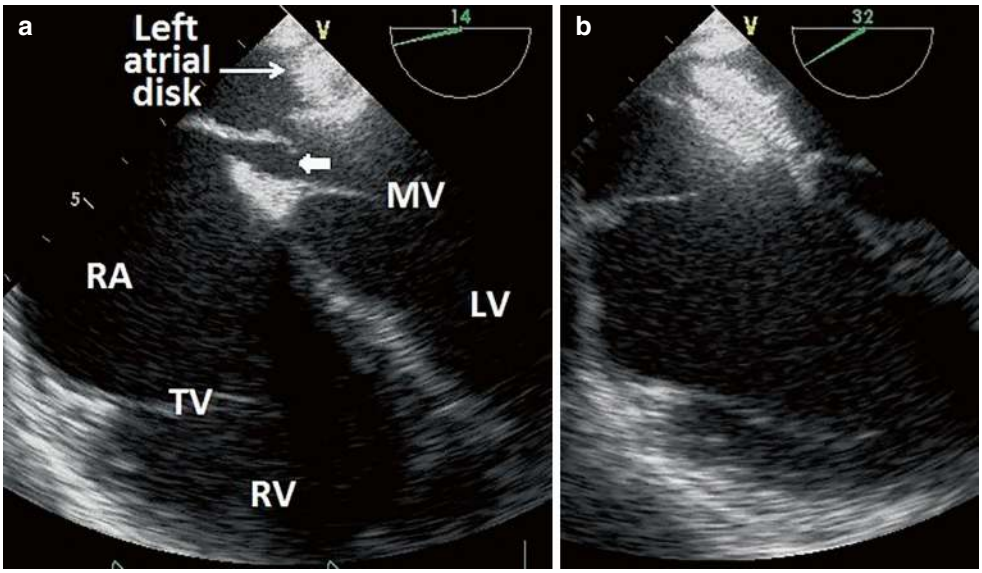


Fig. 19.11 (**a**) This hybrid PFO-ASD defect (white thick arrow) extended anteriorly and inferiorly to an unusual extent. (**b**) The defect was closed with a small Amplatzer ASD device which centered in the ASD higher up in the septum and just avoided impingement on the mitral valve

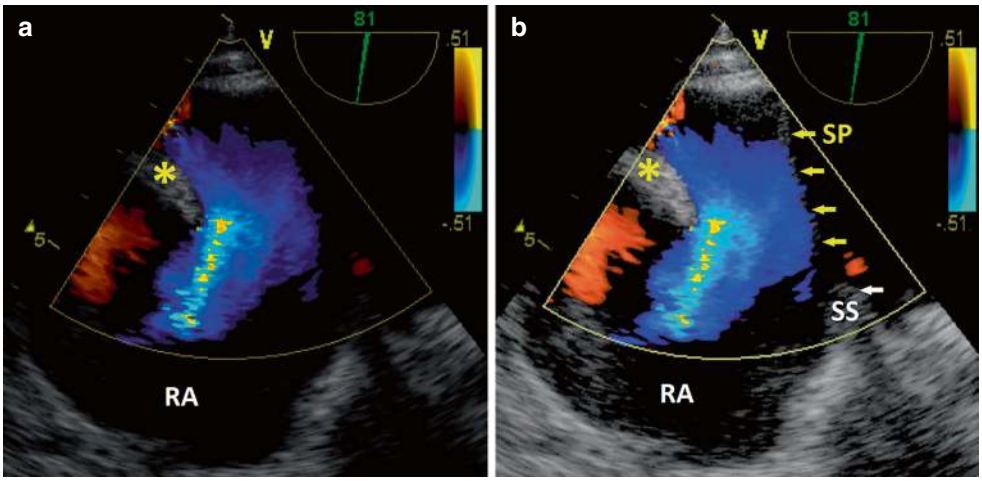


Fig. 19.12 Low oesophageal TOE view. (**a**). With suboptimal gains, colour doppler suggests a large ASD with left to right shunt. (**b**) The same image with higher gain settings. The interatrial septum is now visible. The apparent ASD-like flow is actually IVC flow redirected through the gap between the prominent Eustachian valve ridge (*) and the interatrial septum (arrows)

Common TOE Pitfalls

The most common or significant mistakes on TOE assessment that we encountered in patients referred from general hospitals to tertiary centres for ASD or PFO closure were:

1. *Missed concomitant pathology:* Excessive concentration on the obvious ASD at TOE by inexperienced operators resulted in other missed pathology, e.g. concomitant inferiorly positioned second secundum ASD, concomitant sinus venosus defect, partial anomalous pulmonary venous drainage.

Some patients have very poor low oesophageal TOE windows, causing an inferior "blind spot". Nevertheless, visualization of the inferior septum is often still possible by probe retroflexion, or use of a 90-degree angle, from a higher and better oesophageal window. If parts of the septum and pulmonary veins cannot be imaged adequately, consider alternative imaging modalities e.g. MRI.

High caval inflows create prominent and mildly turbulent colour doppler flows in the right atrium that might obscure smaller ASD flows, resulting in missed fenestrations. Use of colour doppler in the 90 degree views may be helpful in separating the different flows by optimizing their directional disparity—caval flows move parallel to the septum, while ASD flows are perpendicular to the septum and cut across caval flow.

2. *ASD misdiagnosis:* In a few cases, the normal gap between a prominent Eustachian valve and the partially visible atrial septum was mistaken for an inferior secundum ASD, and the IVC inflow was mistaken for shunt flow. With low oesophageal TOE windows, the atrial septum is often thin, perpendicular to the probe, and prone to echo dropout (Figs. 19.12 and 19.31).

Intraprocedural Guidance

Use of Intraprocedural Echo Guidance

Intraprocedural echocardiographic guidance is invaluable for:

1. *Positioning the guidewire*, particularly when defects are difficult to cross.
2. *Identifying which of multiple defects is crossed*.
3. *Sizing of defects*. Appearances can be deceptive. PFO size and shape and tendency for aneurysmal atrial septa to fold are often better appreciated when traversed by the guidewire than at pre-assessment (Fig. 19.2).
4. *Guiding delivery sheath position and device deployment*. Poor delivery angle can lead to device malposition. Large left atrial disks may get stuck mid-atrium due to small anteroposterior diameters. Entrapment of septal tissue within the delivery catheter when re-sheathing a device results in a stuck catheter that cannot be withdrawn. This is easily recognized on TOE by the failure of the sheath tip to come off the septum and septal "tugging" with manipulation.
5. *Assessing residual shunts*. Trivial residual shunts are common immediately post-procedure, but most close by 6 months. Mild shunting through the porous Amplatzer devices immediately post-implantation resolves as devices thrombose. Shunts through visibly open channels of flow often persist and should be avoided (Fig. 19.13, Video 19.7).
6. *Assessing device stability*. Stability may be tested with pushing and pulling and combinations of the 2 to "wiggle" the device (Video 19.8).
7. *Detecting complications.* Intraprocedural echo is indispensable for the detection of encroachment upon adjacent structures, device deformity, malposition, or displacement, haemopericardium and assessment of transient inferior ST elevation. Despite rigorous prior de-airing, device deployment invariably releases microbubbles, which may enter the up-pointing right coronary ostium of the supine patient. Fortunately, this usually has little or no impact on left ventricular function. Inferior hypokinesia, if any, is brief. Thrombus rarely forms on the device within the sheath, despite heparinization, but can cause serious embolic complications such as embolic stroke. Thrombus found at deployment should be withdrawn into the right atrium before device re-sheathing and removal to avoid systemic embolization, or left safely sandwiched between right atrial disk and interatrial septum (Fig. 19.14, Videos 19.9 and 19.10).

Choice of Echo Modality for Intraprocedural Guidance

Both TOE and ICE are useful for intraprocedural guidance [26]. TOE is frequently used for intra-procedural echo, but requires heavy sedation for patient tolerance, or preferably, general anaesthesia for airway protection in the supine

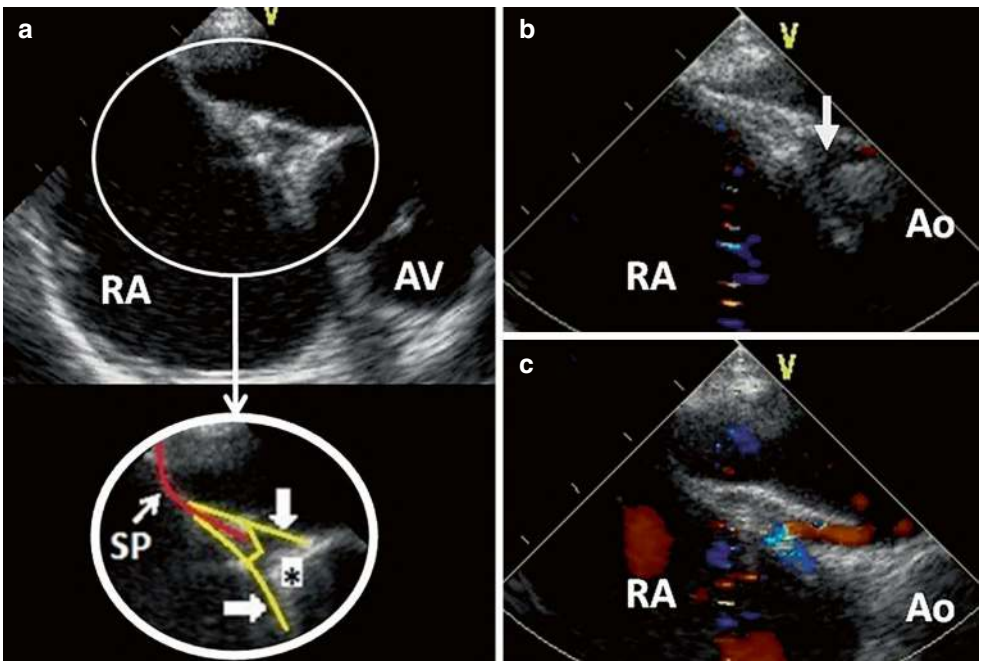


Fig. 19.13 (**a**) This Intrasept PFO closure device with articulated waist (marked in yellow in insert) splayed across the aorta but retracted the septum primum (marked in red in insert) to create an iatrogenic flap retraction ASD (arrow in **b**) with residual shunting seen on colour doppler in **c**. The shunt was present and unchanged 17 months later

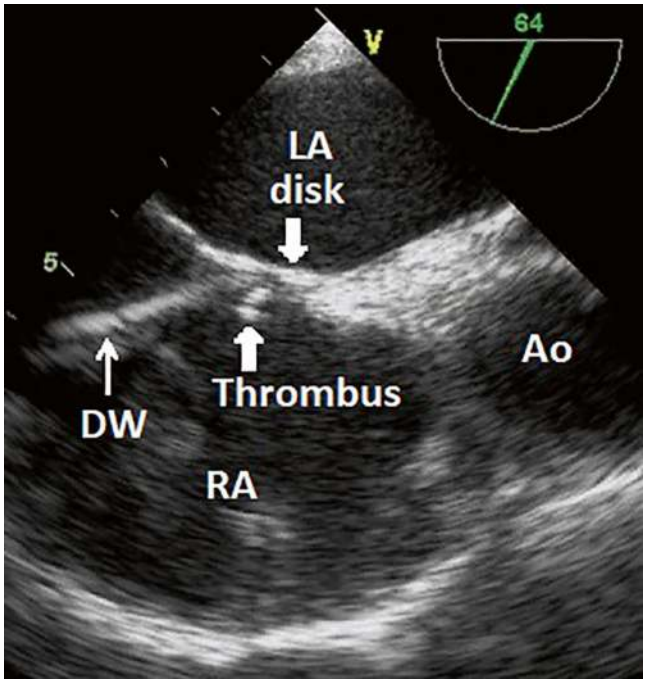


Fig. 19.14 PFO closure. Mobile thrombus was present on the LA disk of this Premere device when it was deployed in the left atrium. The thrombus remained attached as the disk was drawn down onto the interatrial septum. As the thrombus was small, unlikely to cause significant pulmonary embolism, and could easily embolize at re-sheathing of the device, the RA disk was deployed and the PFO closure was completed. The thrombus was left sandwiched tightly by the right atrial disk against the septum, with no clinical sequelae

patient. ICE is also used. Although costly and less versatile than TOE, it does not require sedation or general anaesthesia. Depending on anaesthesia and recovery facilities, this may also improve turnaround time for closure procedures. However, it may be less suitable for cases with complex anatomy due to the limitations in available ICE imaging planes, and it requires additional venous puncture with the associated risk of vascular complications.

Functional Atrial Septal Anatomy: Secundum ASD, PFO, Hybrid Defect, Aneurysmal Septum and Interatrial Septal Aneurysm

The Double-Layered Septum and Flap Valve (PFO)

The interatrial septum is a complex bi-layered structure containing a flap valve which can be defective in different ways (Figs. 19.15, 19.16, and 19.17) [12, 27]. Its anatomical relations are shown in Fig. 19.16. The septum can roughly be divided into four quadrants—aortic or antero-superior, SVC or postero-superior, IVC or postero-inferior, and valvular or anteroinferior. The left atrial surface is formed by the septum primum, a thin, continuous sheet spanning the whole interatrial space except superiorly where it breaks down in embryonic development to create the ostium secundum. It ranges from being taut, flat and immobile, to redundant, aneurysmal

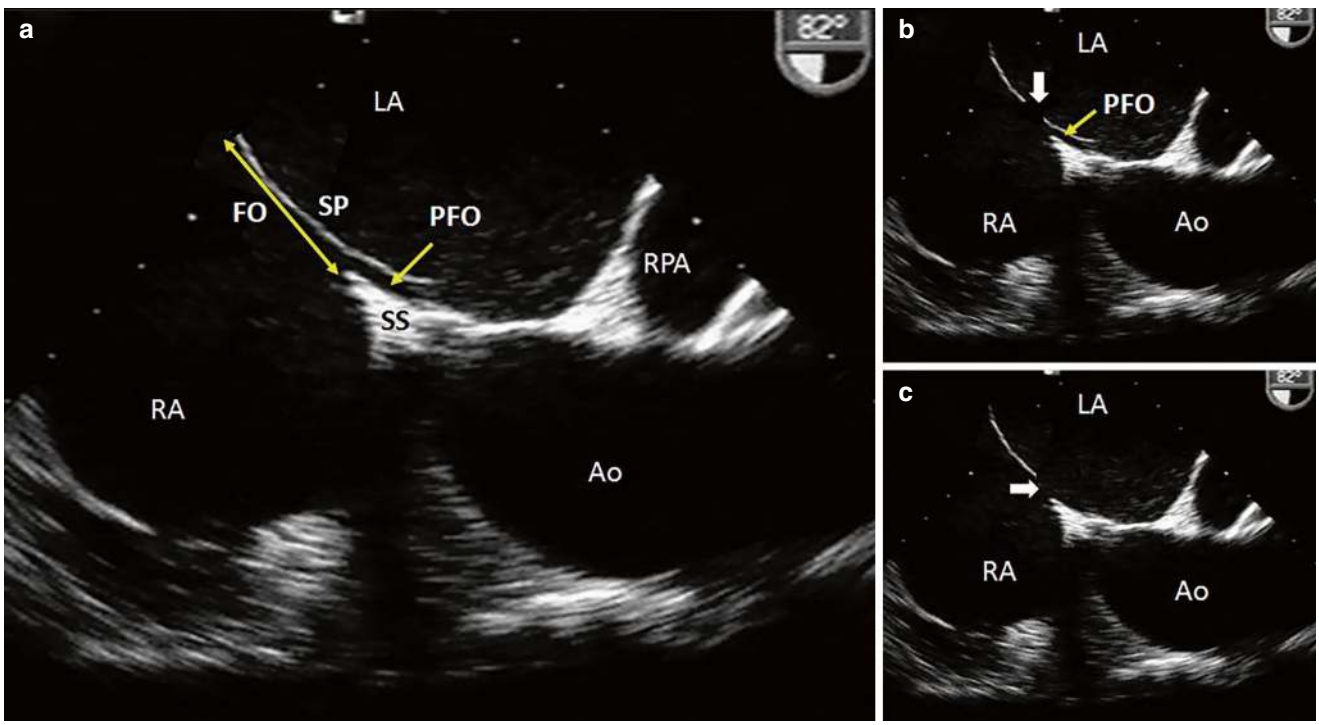


Fig. 19.15 Anatomy of the atrial septum on TOE. (**a**) PFO. (**b**) Secundum ASD, fenestration type. (**c**) Secundum ASD, flap valve type

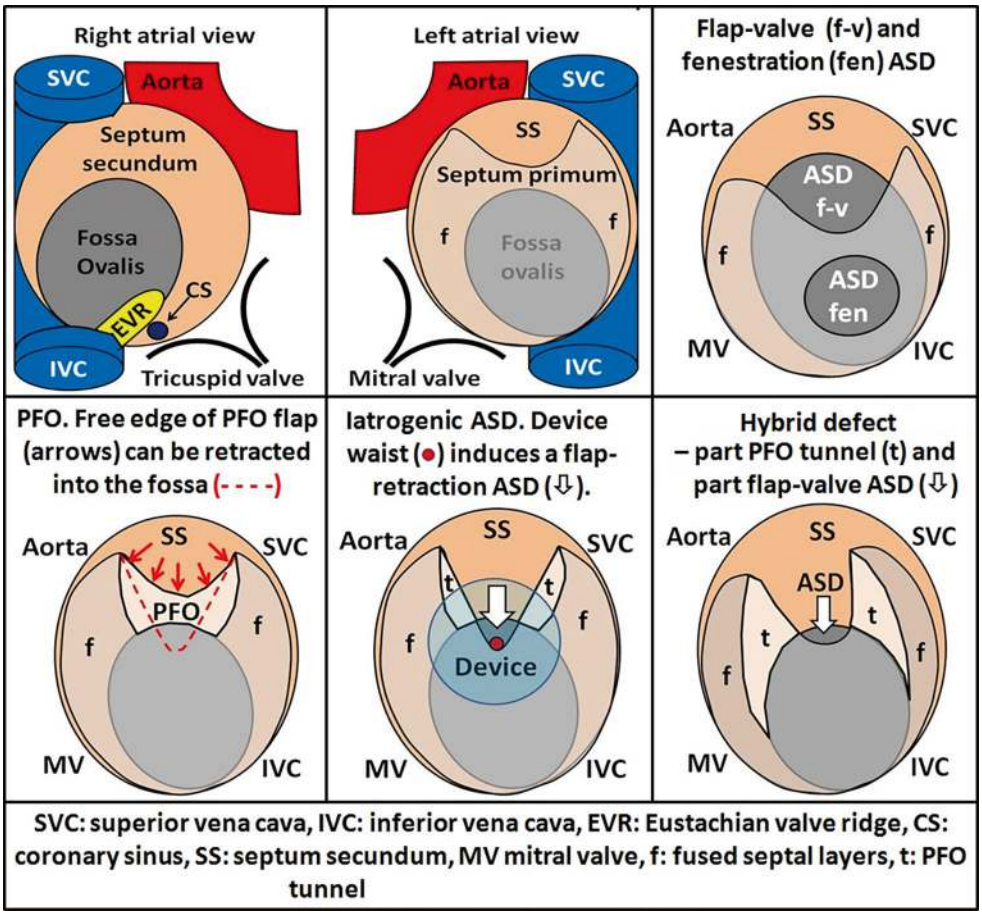


Fig. 19.16 Anatomy of the atrial septum, en face views. Top row from left to right—RA view of interatrial septum, LA view of interatrial septum, LA view of flap-valve and fenestration types of ASD. Bottom row. LA views of interatrial septum. Left: The unfused septum primum, marked "PFO", forms the mobile roof of the PFO tunnel. It is often sufficiently redundant and elastic such that the free edge (red arrows) can be retracted to the level of the fossa ovalis (dotted red line) to create a flap valve ASD. Middle: An iatrogenic flap-valve ASD is formed at PFO device closure (middle diagram) when the flap is pulled back by the waist (red circle) of the closure device (transparent blue circle). Right: This configuration may also occur naturally (right diagram), resulting in a PFO-ASD hybrid defect that has a combination of features of both PFO and flap valve ASD

and very mobile, and may contain true septal aneurysms. The secundum septum is a thicker C-shaped outer rim of tissue around the interatrial space, formed by the in-folding of left and right atrial walls where they meet. Secundum septum is usually minimal inferiorly. Its inner rim forms the rim of the fossa ovalis.

The two layers overlap circumferentially and fuse to form a single septum, except antero-superiorly where they fail to fuse till after birth. The unfused septum primum acts as a mobile flap, opening into the left atrium and shutting against the septum secundum to form a flap valve, the PFO. The right atrial entrance to the flap valve is at the edge of the fossa ovalis, and left atrial exit above, with a tunnel between them that can vary in width and range from virtually non-existent to 2 cm long. Flap valves remain probe-patent in a quarter of the adult population [28], making PFO essentially a normal variant. The flap may be congenitally displaced into the left atrium (deviated atrial septum primum, DASP), causing complete or partial failure of flap valve closure (Fig. 19.18, Videos 19.11 and 19.12).

Secundum ASD: Fenestrations and Flap-Valve ASD

A secundum ASD is a hole in the fossa ovalis. There are two basic types—fenestration and flap-valve ASDs (Figs. 19.15, 19.16, and 19.17).

A fenestration ASD is a hole entirely within the primum septum. Its boundaries are continuous within a single layer and not subject to changing shape and size due to the separation of layers, unlike the flap-valve ASD. TOE-sizing reflects maximum ASD size in uncomplicated fenestrations that do not involve aneurysmal parts of the septum, and balloon-sizing is less critical. Stretching by balloon sizing may enlarge the hole, resulting in the need for larger devices.

The flap-valve ASD is formed when primum septum fails to overlap the secundum septum. The septum primum may simply be deficient in tissue, or aneurysmal with excess tissue allowing the superior rim of the primum septum to sag into the fossa. The rims of a flap valve ASD are therefore formed by two different layers with varying degrees of over-

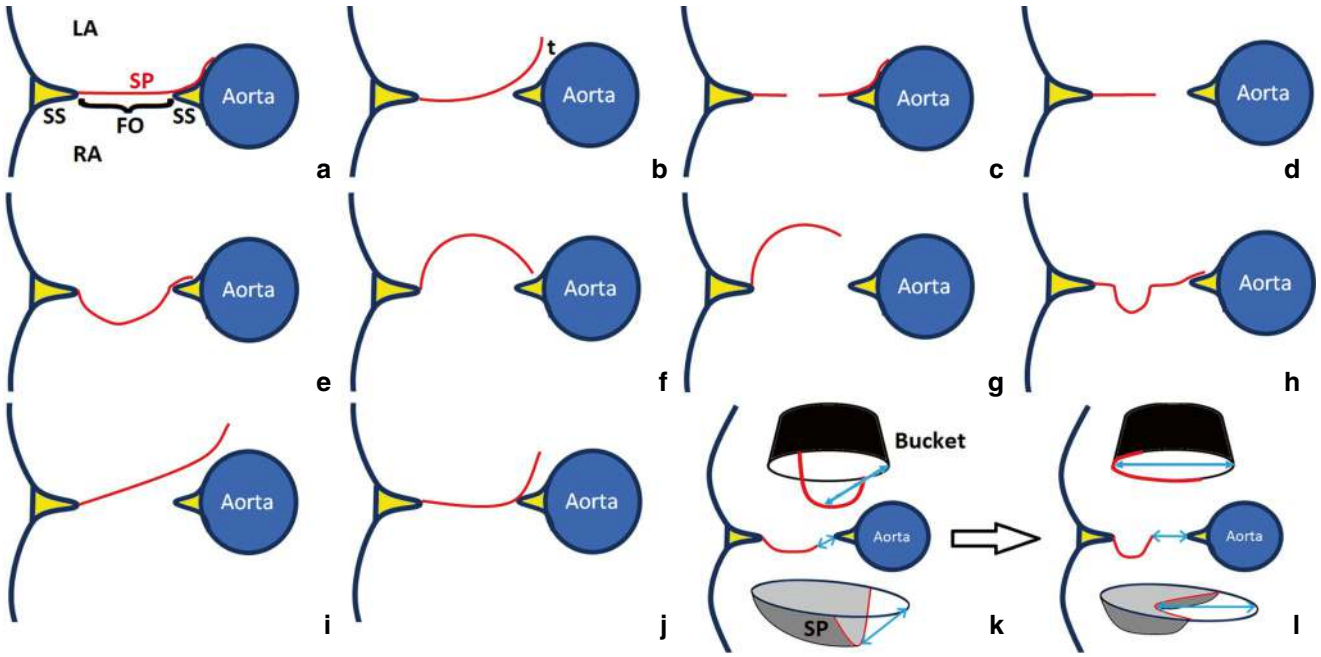


Fig. 19.17 (**a**) PFO in the closed position. (**b**) PFO in the open position with a visible tunnel (t) between LA and RA. (**c**) Secundum ASD, fenestration type. (**d**) Secundum ASD, flap valve type. (**e**) Aneurysmal interatrial septum, PFO in closed position. (**f**) Aneurysmal interatrial septum, PFO in the open position. If the PFO flap is tethered by its attachments inside the left atrium, the PFO flap may retract inadequately even though most of the septum primum displaces widely, resulting in a significant minimum PFO tunnel length that causes problems with fixed length short waist devices. (**g**) Untethered PFO flaps may retract and displace considerably. (**h**) Interatrial septal aneurysm. (**i**) Long tunnel PFO with taut flap valve completely displaced into the left atrium (deviated atrial septum primum, DASP). The complete DASP shunts continuously throughout the cardiac cycle like an ASD. (**j**) Partial DASP with redundant septum sagging onto the fossa edge to close that end of the tunnel. It behaves more like a PFO. Since primum and secundum septum layers do not oppose well, devices will also not sit well. (**k**, **l**) "Bucket handle effect". Defects involving aneurysmal septum are deceptive in size and must be balloon-sized. The hole seems small in **k** but redundant septum folds back (**l**) when swung into the plane of the fossa ovalis by an ASD closure device, markedly increasing the defect diameter (blue double arrow). This is analogous to the distance from the handle to the bucket edge, depending on the position of the handle

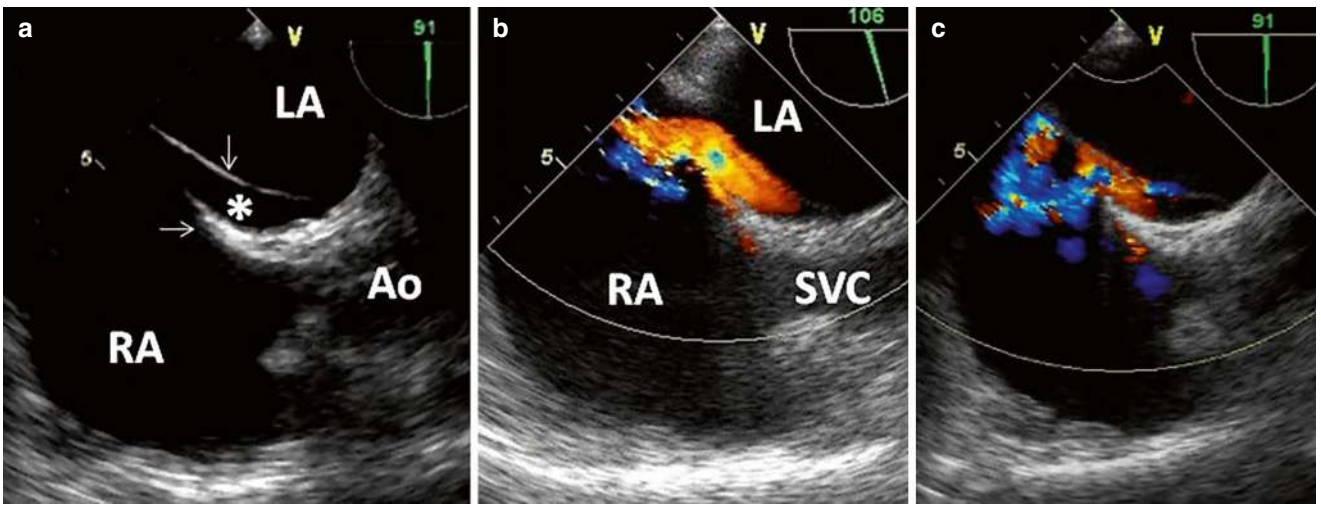


Fig. 19.18 Complete deviated atrial septum primum (DASP). (**a**) Septum primum (down arrow) and secundum (right arrow) are never apposed throughout the cardiac cycle, creating a permanently open tunnel (*). (**b**) The PFO shunts continuously like an ASD. (**c**) The defect is associated with a multifenestrated true septal aneurysm

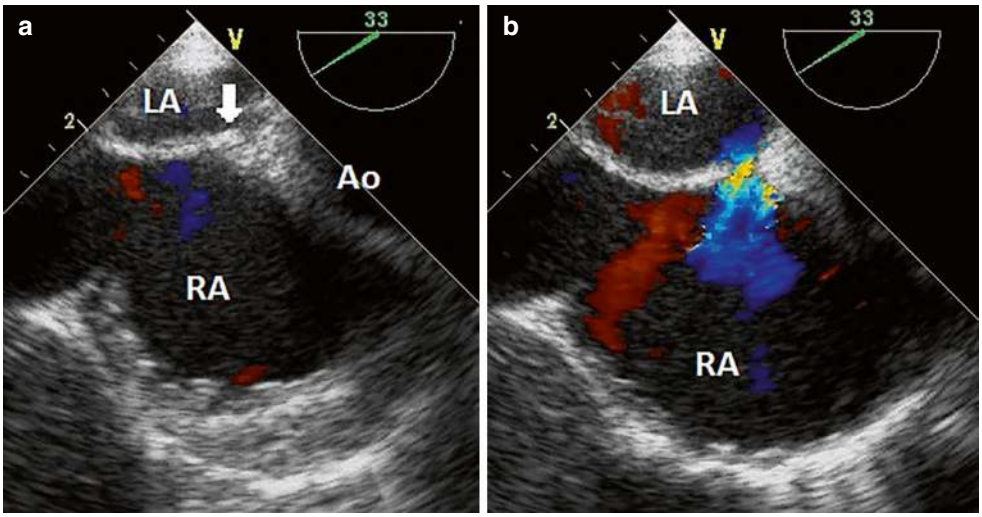


Fig. 19.19 Defects with minimal tunnel length may morph from PFO to ASD and back with each cardiac cycle as the atria change in shape and size, as shown in these images from the same cardiac cycle in the same patient. The defect has the configuration of a PFO in **a** but becomes an ASD in **b** when the septum is stretched

lap and adhesion. These 2 layers may move somewhat independently of each other, changing the size and plane of the defect with atrial pressure changes during the cardiac cycle, or iatrogenic manipulation. Size changes can be considerable and unpredictable from baseline imaging, especially with an aneurysmal and floppy septum, and balloon-sizing is essential in these cases to reduce the risk of device undersizing.

Aneurysmal Interatrial Septum and Interatrial Septal Aneurysm

The aneurysmal interatrial septum (Fig. 19.17) is conventionally defined as one in which the entire septum primum of the fossa ovalis is redundant and aneurysmal, with at least 10 mm maximum displacement from the septal plane (plane of the septum secundum). The 10 mm cut-off is arbitrary and the problems caused by aneurysmal anatomy are not absolutely proportional to the degree of displacement. Displacement separates the 2 layers that form the boundaries of a flap valve ASD, and aneurysmal septa often fold back when reshaped by a closure device, causing 3D alterations in ASD shape and size that are difficult to predict accurately. Balloon sizing is essential. Folding retracts the free edge of the septum primum, creating iatrogenic flap-valve ASDs from PFOs, and increasing native flap-valve ASD size (Fig. 19.17).

An atrial septal aneurysm is a localised saccular outpouching of a section of septum primum, (Figs. 19.17 and 19.18c, Video 19.13) and can co-exist with an aneurysmal septum. Similar unpredictable sizing problems arise if fenestration-type ASDs straddle normal septum and septal aneurysms.

3D TOE may improve sizing by imaging alone in the future, but difficulties in sizing accuracy due to echo dropout, overgained images, and the unpredictability of 3D size and position changes in flap valve ASD with mobile aneurysmal septum primums, are currently prohibitive.

The Continuum Between PFO and Flap-Valve ASD, and the Iatrogenic Flap Valve ASD

PFO and flap-valve ASD are not dichotomous but a dynamic continuum. When the PFO flap is retracted back into the fossa so that it no longer overlaps, a flap valve ASD is formed. Iatrogenic flap-retraction ASDs are formed routinely at PFO closure when the device waist retracts the flap, shortening the tunnel to suit the short device waist (Fig. 19.16). Spontaneous flap retraction may occur intermittently, with cyclical and circulatory volume changes in atrial size, alternating the defect between PFO and ASD anatomy (Fig. 19.19, Video 19.14).

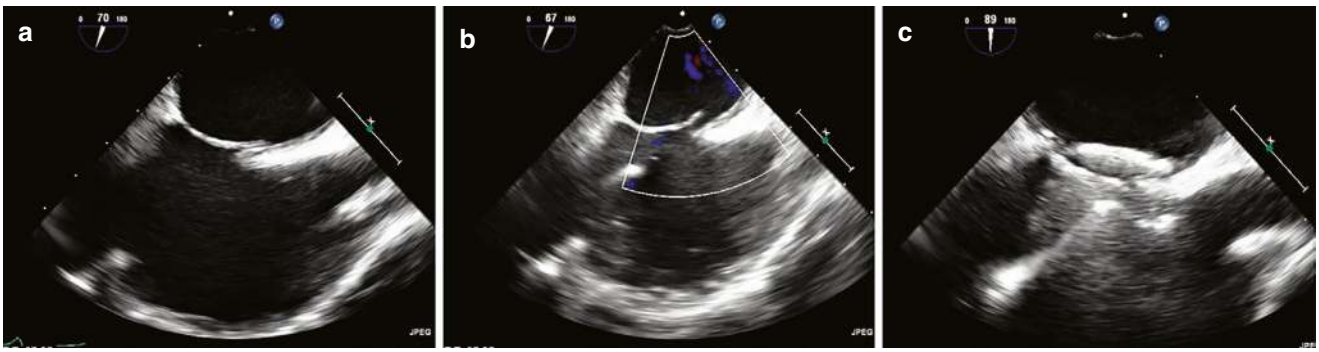


Fig. 19.20 30-year-old male with transient ischaemic attack. (**a**) TOE showing a double-layered structure of the inter-atrial septum but with no convincing opening or color flow. His bubble study was negative. (**b**) PFO was easily crossed when probed with a 0.035″ wire on a multi-purpose catheter. (**c**) Closure of PFO with a 25 mm Amplatz PFO occluder

Detection of Patency: Left Atrial Pocket or PFO?

It is not uncommon for only the right atrial orifice of a PFO to fuse shut, leaving the remaining tunnel as a blind left atrial pocket. This pocket retains its bi-layered appearance on echo and can only be differentiated from a PFO by demonstrating a lack of patency on visual assessment of tunnel opening, colour doppler, bubble contrast study, or manual probing at surgery or catheterization. Tunnels may be held shut by the higher pressure on the left atrial aspect, and open only with good Valsalva manoeuvres and, sometimes, sharp sniffs, which are best achieved at transthoracic echo or transcranial doppler bubble studies. In most centres, these are the screening tests of choice for a PFO [29].

TOE is also highly sensitive for the detection of PFO because of its excellent, higher resolution, but good Valsalva manoeuvres are more difficult to achieve [30]. Where a double-layered pocket is seen without evidence of patency, patency cannot be excluded unless spontaneous right-to-left septal displacement, often called "septal bounce", occurs to provoke flap opening during bubble studies (Videos 19.15 and 19.16 show the same PFO with and without "septal bounce"). Not all areas with a double-layered appearance may be patent. The lack of PFO opening on 2D despite a septal bounce on 2D alone may be misleading because the imaging plane does not traverse the patent section, hence the need for simultaneous bubble study. "Septal bounce" can be momentary and infrequent, caught only with prolonged, careful observation. Intravenous fluids to improve volume status and increase septal "bounce" may improve TOE sensitivity [31].

Reliance on bubble counting to assess PFO size should be tempered by anatomical appearances, including the extent of a distinct bilayered structure with a potential space in between, the extent of septal bounce and adequacy of Valsalva manoevres. A PFO with potential to open widely may shunt minimally or not at all on bubble study, simply because a high LA to RA pressure difference maintains functional closure of the PFO. Where there is a high suspicion for paradoxical embolism, a double-layered interatrial septal anatomy and lack of good septal bounce during bubble studies, it may be appropriate to probe the patency and size of PFO with a guidewire even if TOE and bubble studies fail to demonstrate patency (Fig. 19.20, Videos 19.17 and 19.18).

Positive bubble studies merely indicate there is a shunt but may not show where the shunt is, unless bubbles are actually seen traversing the septum. Although PFOs are said to shunt early and pulmonary level shunts are seen several beats later, delayed shunting can still be due to a PFO if the flap valve fails to open on earlier beats.

Complex Functional Anatomy and Its Impact on Device Closure

The atrial septum varies greatly in mobility, redundancy, attachments, aneurysms, number and position of defects, and size of fossa ovalis. Surfaces around defects may not be smooth and flat. PFO and ASD may merge to form a complex hybrid defect. PFO tunnel size and shape are very variable. Tunnel length and width may vary within the same tunnel. Tunnels may not even be straight. Left and right atrial openings may be asymmetric or multiple. Multiple views are required with 2D TOE to define defect anatomy. 3D TOE greatly improves understanding of complex 3D contours and relationships, but resolution is less good, and visualization of thin septum is limited by echo drop-out**.** 2D TOE is still required for fine detail.

Multiple factors interact to affect the success of percutaneous closure:

1. *ASD and PFO anatomical size and shunt size.*
2. *Septum primum characteristics: Aneurysmal septum and septal displacement. Tunnel length and PFO flap retractability.*

3. *Support: Supporting rims, tunnel width and fossa width.*
4. *3D conformation of the apposition surfaces*
5. *Multiple defects.*
6. *Hybrid defects.*
7. *Proximity to major cardiac structures.*
8. *Complete and partial DASP tunnels, ramps and funnels.*

ASD and PFO Anatomical Size and Shunt Size

ASDs may exceed the maximum available size of closure device. Unstretched TOE size is usually less than balloon-stretched size by at least 20%, more if the septum is flimsy and redundant. Patients with ASDs of diameter 3 cm or more should be made aware that they have a high risk of procedural failure should they opt for percutaneous device closure.

Even if a large-size of the device is available, deployment of a large left atrial disk may be difficult. Large devices may be caught on the left atrial free wall in fasted supine patients with narrow left atrial diameters, preventing the left atrial disk from turning to align with the septum. Suboptimal, fixed 90-degree device angulation on the stiff delivery wire together with poor aortic septal rim predisposes to LA disk prolapse through the ASD into the right atrium (Fig. 19.21a, b). This can be improved by the use of an extra guidewire parked in

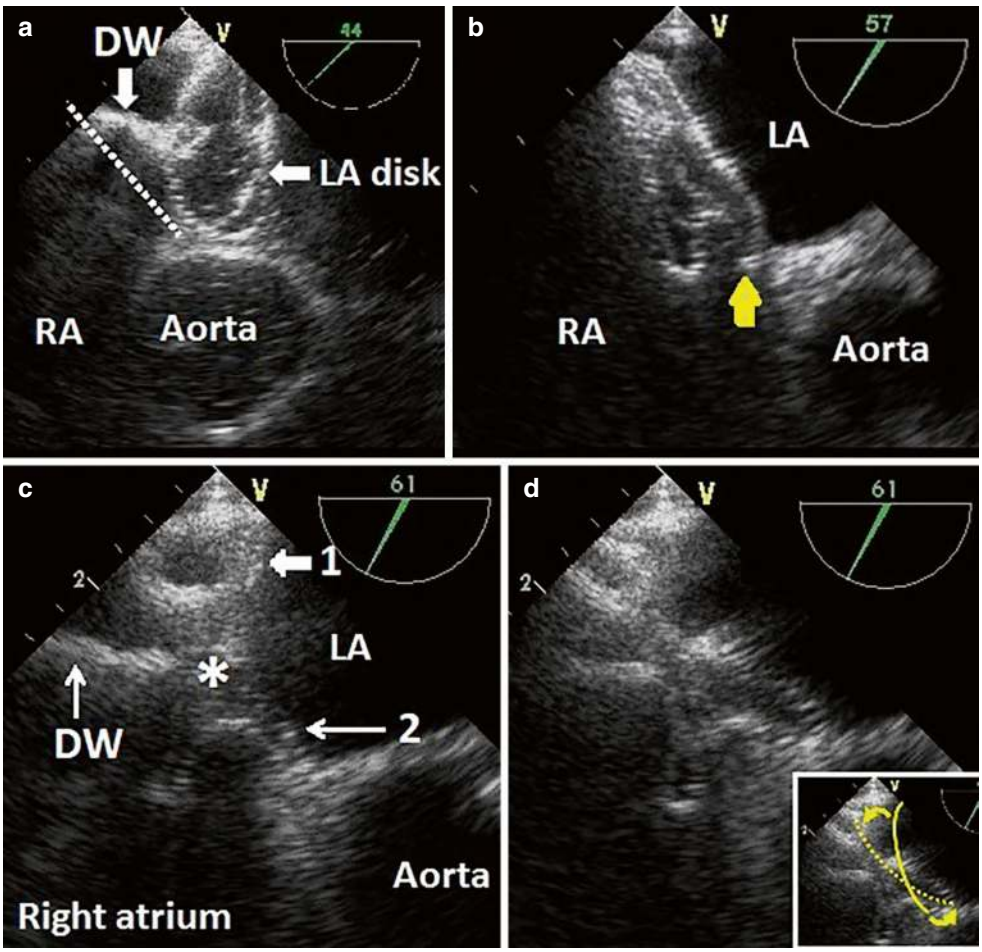


Fig. 19.21 Two patients with LA disk larger than intraprocedural LA anteroposterior diameter. (**a**, **b**) Patient 1—"kiting" malposition. (**a**) The bulbous LA disk was deformed from pulling while its edges were stuck at a point of narrower LA diameter. Harder pulls brought the LA disk past the narrow point and down onto the septum, but the 90 degree inflexible angulation between device and delivery wire, like a kite on a string, prevented the LA disk from aligning with the plane of the fossa ovalis (white dotted line). (**b**) The lack of aortic rim allowed "kiting" malposition with recurrent LA disk prolapse (yellow arrow) through the ASD into right atrium. The problem was resolved by simultaneous partial deployment of the right atrial disk while positioning the LA disk. The flexible device waist then acted as the hinge, allowing the LA disk to rotate into the correct plane. (**c**, **d**) Patient 2–counter-intuitive pushing. Pulling failed to move the LA disk past the obstruction in the second patient. (**c**) The device waist (*) simply stretched with pulling while the LA disk remained hung up (1) on the anterior LA wall. However, the aortic rim prevented "kiting" malposition (2). Further pulling either resulted in kiting malposition, or more often, the entire device slipping back into the right atrium. (**d**) Keeping the LA and RA disks correctly deployed in their respective atria as in C, the whole device was pushed and eased forward into the splayed position over the aortic rim, rotating the LA disk from the stuck position (full yellow line in the insert) into septal apposition (dotted yellow line) while simultaneously pulling the opposite side of the LA disk off the free wall

the left upper pulmonary vein (Figs. 19.22 and 19.23) and minimal partial right atrial disk deployment to release the more flexible waist. This flexibility allows the left atrial disk to tilt into a more favourable alignment with the septum. Pulling will usually free the left atrial disk, but occasionally fails when a mismatch in disk and LA diameter is too great. When it is possible to catch the aortic rim between the left atrial disk and a partially deployed right atrial disk, pushing may paradoxically be more effective. (Fig. 19.21c, d).

Tiny PFO's and ASD's may be incidental rather than causal to stroke and may not require closure. Tiny fenestrations may be hard to wire but may be left when closing a larger ASD for shunt, since they contribute little to shunt size.

ASD diameter is often larger at TOE than TTE. A TOE average diameter of about 0.9 to 1.0 cm is the usual threshold size giving rise to the 1.5:1 shunt for which prophylactic closure is recommended. However, pressure differences between atria and atrial stretch may alter shunt size significantly. Even a small hole may shunt left-to-right significantly with raised left atrial pressures in the presence of mitral stenosis.

Septum Primum Characteristics: Aneurysmal Septum and Septal Displacement. Tunnel Length and PFO Flap Retractability

Figure 19.24 shows some of the problems that arise from aneurysmal septa and mismatched tunnel and device waist length.

The entire septum primum may be aneurysmal and redundant, prolapsing through the fossa ovalis into the right atrium and displacing into the left atrium when RA pressure exceeds LA pressure, such that the septum "bounces". Unless the septum primum is well adherent to the septum secundum, it may displace and retract considerably to open a PFO widely, resulting in the association between aneurysmal interatrial septum, large PFO and increased risk of stroke by paradoxical embolism. This displacement may convert a PFO into a large, iatrogenic flap retraction ASD, requiring closure with an ASD occluder rather than PFO occluder (Fig. 19.25, Videos 19.19, 19.20, and 19.21). In the same way, the sep-

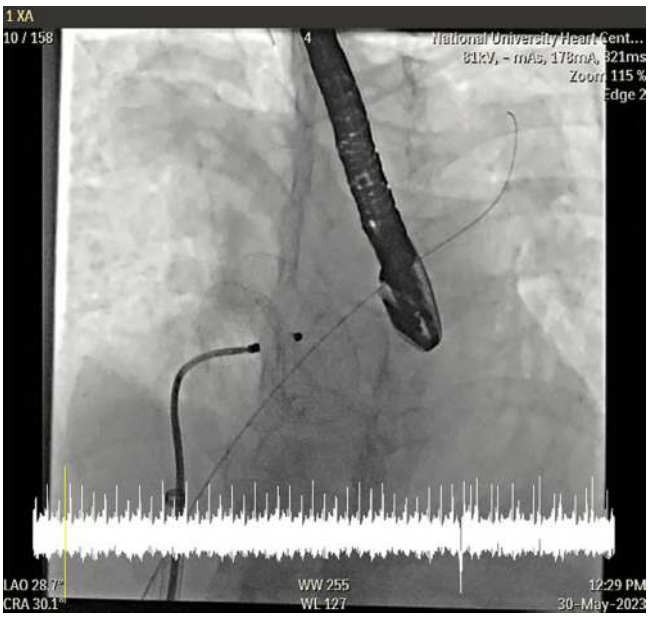


Fig. 19.23 Fluoroscopic image of a 32 mm Amplatzer septal occluder deployed in a 29 mm secundum ASD, deployment supported by a 0.035″ stiff angled Terumo guidewire M parked in the left upper pulmonary vein to prevent "kiting" malposition

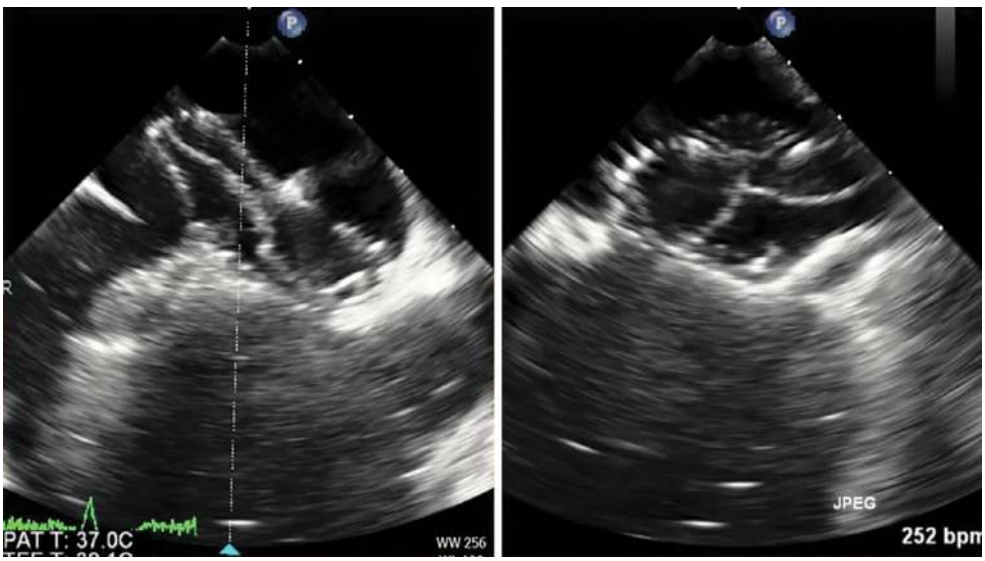


Fig. 19.22 Biplane of a 32 mm Amplatzer septal occluder deployed in 29 mm secundum ASD. Left image showing a bi-caval view of the LA disk, tilted with inferior rim well within the LA, but superior rim abutting the septum secundum and at risk of prolapse into the RA ("kiting" malposition) when pulled back to achieve close septal apposition and correctly sited release of the RA disk. Not well appreciated is a guidewire supporting the device, better appreciated on fluoroscopy (Fig. 19.23)

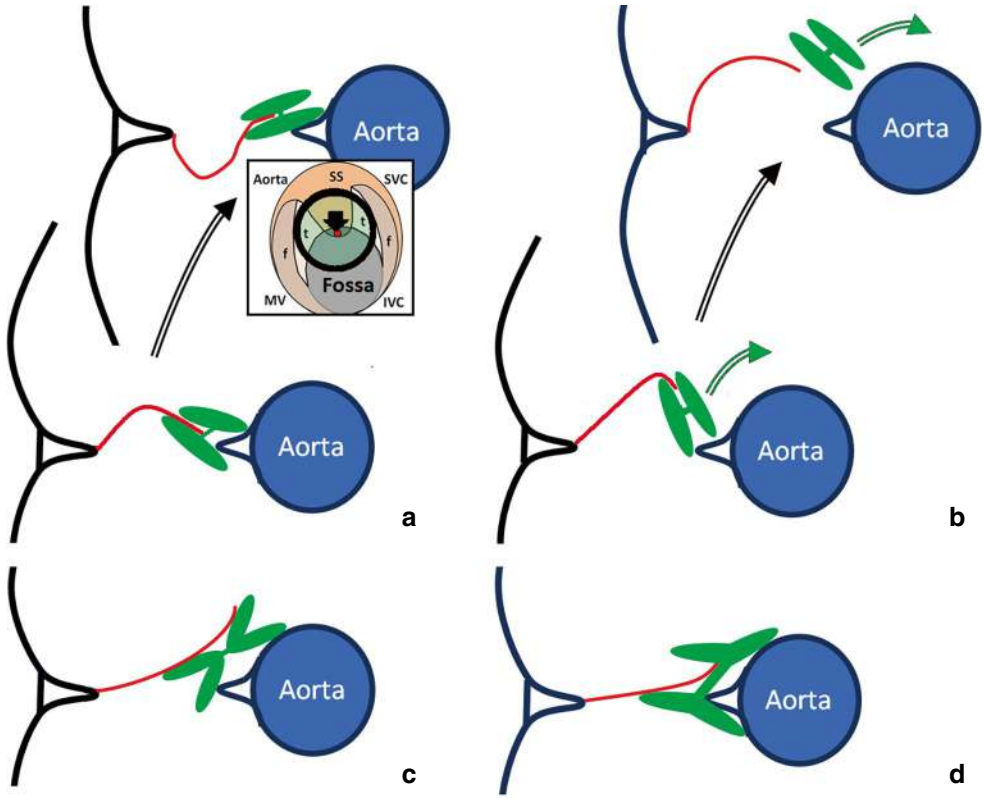


Fig. 19.24 Aneurysmal interatrial septum and device displacement, (**a**) PFO-ASD hybrid defect. The mobile septum allows the device to tilt out of position and the RA disk to displace into the partially unroofed PFO tunnel. Since the device is wider than the left atrial orifice of the tunnel, the device displaces no further but stents the defect open. The insert uses the same schematic as Fig 19.16. (**b**) A small flap valve ASD. The septum's large capacity for displacement allows for transformation into a large defect. Displacement results in device tilting and instability, and ultimate device embolization. C and D. Inadequate PFO flap retraction. (**c**) Device waist-tunnel length mismatch may cause disks to fold and displace into the tunnel. (**d**) Even with adaptable device waist lengths, the distortion may prevent good LA disk apposition, especially if there is a degree of DASP. The RA disk may be tilted towards the left atrium, lifting the septum primum and stenting the PFO open. An ASD device may be more appropriate for such PFO, plugging the tunnel with the device waist instead of relying on a good seal from disk apposition

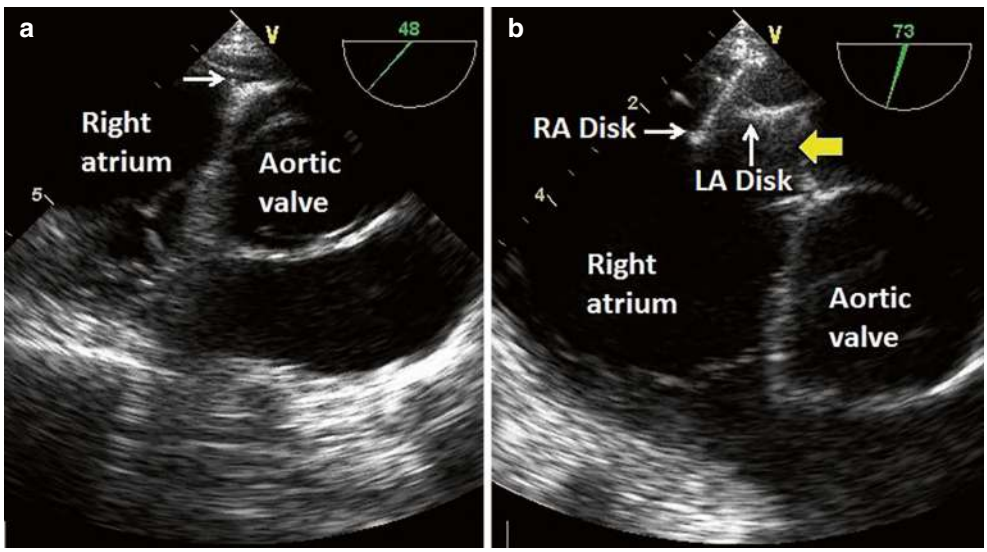


Fig. 19.25 (**a**) This PFO appears to be a normal short tunnel PFO. (**b**) However, the septum primum folded readily with traction, converting the PFO into a large flap retraction ASD (yellow arrow), into which the LA disk of the Premere PFO closure device prolapsed. The PFO was successfully closed with a balloon-sized 26 mm Amplatzer ASD device

tum primum rim of an ASD can retract and displace to markedly enlarge the ASD, and it is essential to balloon-size the defect to avoid undersizing.

Excessive mobility of the septum with significant displacement into either atrium, commonly seen with aneurysmal septa, may be associated with excessive mobility of the closure device, and its partial or complete displacement (Figs. 19.24 and 19.26).

Long PFO tunnel length > 1 cm is often quoted as a relative contra-indication to trans-tunnel PFO device closure. However, absolute tunnel length is less important than minimum retracted tunnel length. Disk deformation and displacement may result from mismatched minimum tunnel length and device waist length.

Tunnel lengths vary greatly between PFOs. They may also differ considerably in different parts of the same PFO, and 3-D TOE is helpful in locating the minimum length for measurement (Figs. 19.27 and 19.28).

PFO flaps vary widely in their extent of adherence to the secundum septum and in how tautly strung they are between their attachments on either side of the tunnel. Redundant flaps of long tunnels may retract easily all the way back to the edge of the fossa ovalis. Taut flaps may retract minimally even though they are <1 cm long, causing problems from mismatched tunnel length and device waist-length. Devices with short, fixed waist lengths less than tunnel length generate tensions that cause disk deformation and displacement into the tunnel (Figs. 19.6 and 19.24).

Variable waist-length planar devices such as the Premere are no longer in use, but devices with 3D waists are adaptable and can stretch moderately to match longer tunnel lengths. Some interventionalists deal with long tunnels by puncturing the septum in the adjacent fossa ovalis and placing a PFO closure device through the puncture instead. However, trans-septal puncture requires a stable septum, and is difficult with freely mobile septum primum.

PFO closure devices are liable to centre themselves at the point of minimum tunnel length, where tension on the device is least. With asymmetric tunnels, the closure device will center itself eccentrically on the short side, such that only half of the device diameter covers the PFO flap. Bigger devices may be needed to ensure the flap is pinned down adequately (Fig. 19.29).

Excessive PFO flap retraction may result in an iatrogenic ASD larger than the device waist, associated with residual shunting, unless disk apposition on at least one side of the septum is perfect, or an ASD device with a wide waist is used to plug the hole. Otherwise, the defect will effectively be stented open by the device (Fig. 19.13).

Severe retraction, usually in association with a redundant, aneurysmal septum, converts PFOs into large, iatrogenic flap-retraction ASDs. Such PFOs need to be treated as flap-valve ASDs with balloon-sizing to avoid undersizing and displacement of devices (Fig. 19.25, Videos 19.19, 19.20, and 19.21).

Support: Supporting Rims, Tunnel Width and Fossa Width

Supporting rims must be adequate to avoid device displacement and malposition. The minimum acceptable rim is usu-

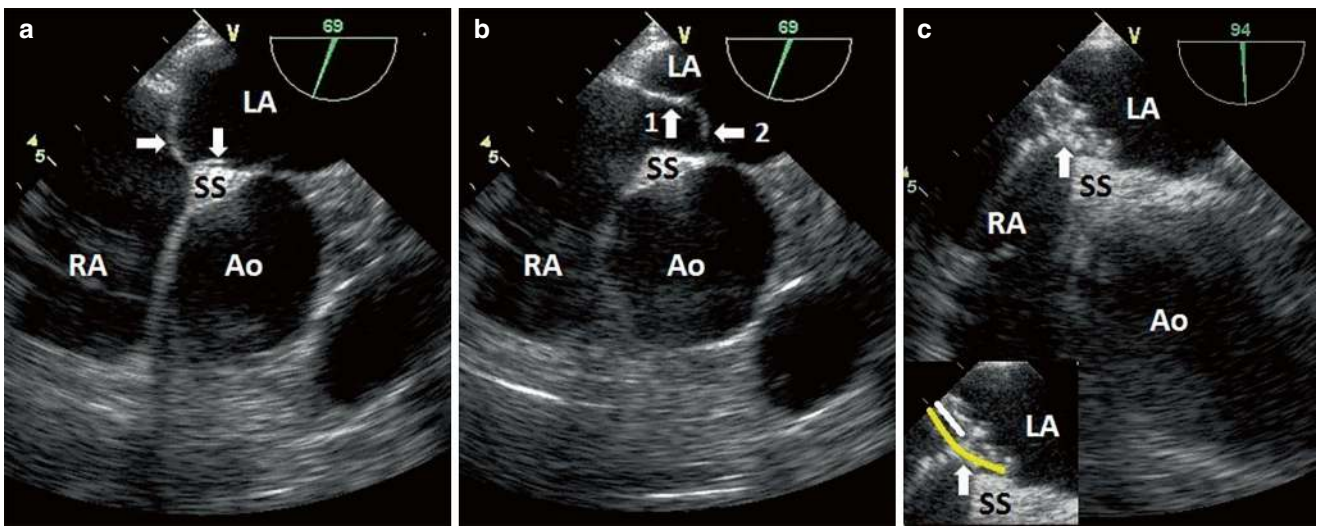


Fig. 19.26 (**a**) PFO with aneurysmal septum (arrows). (**b**) The septum primum flap displaces widely (1) but remains tethered inside the left atrium (2). However, it did retract satisfactorily with the guidewire, and the PFO was closed successfully with a Biostar (radial spoke planar disk device with short fixed-length waist). (**c**) Six months later, the RA disk had displaced into the PFO tunnel (arrow), stenting the tunnel open. The insert shows the RA disk marked in yellow and the septum primum in white. The PFO was finally closed with a 30 mm Amplatzer cribriform (large disk, small adaptable waist) device

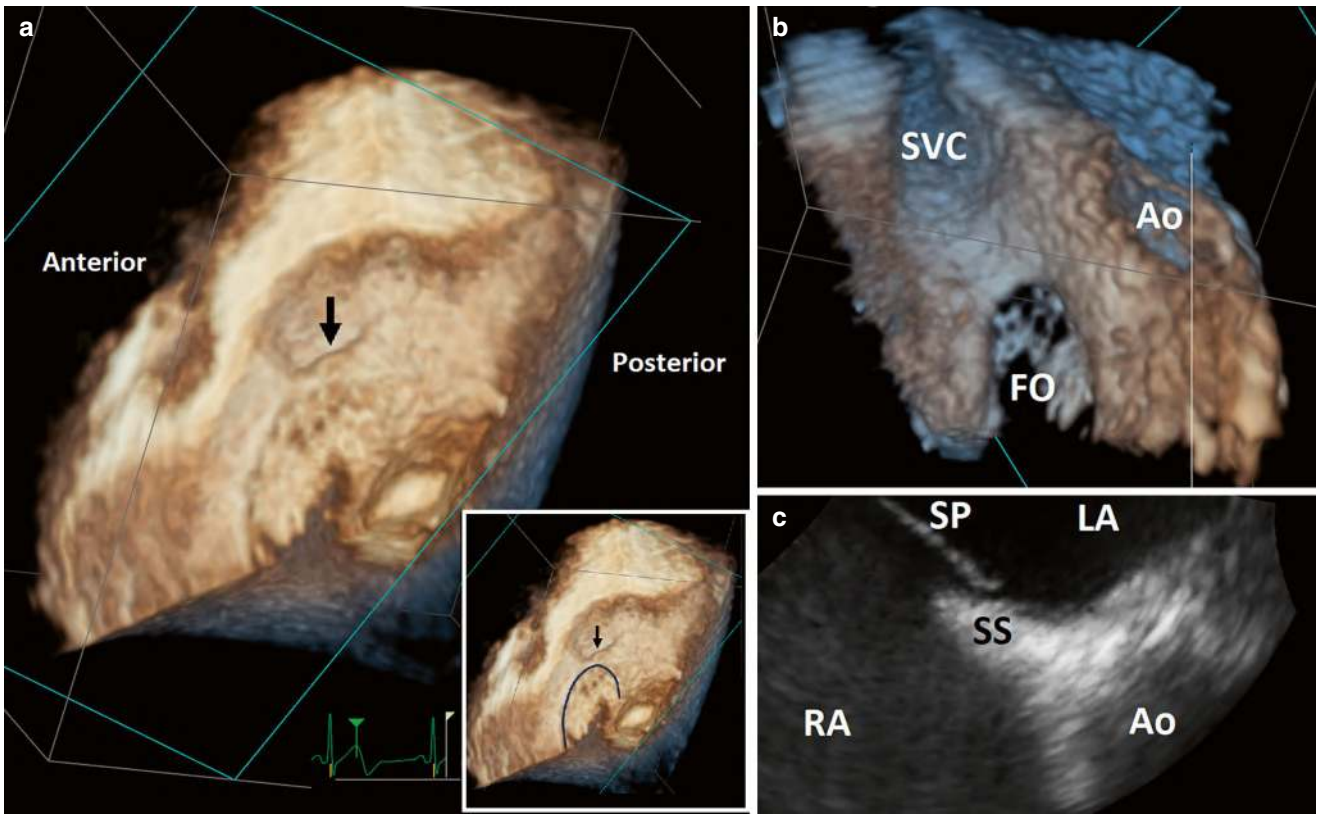


Fig. 19.27 Short tunnel PFO. (**a**) 3D TOE, view from LA, showing the LA opening of the PFO tunnel (arrow). The black line in the insert outlines the fossa ovalis. (**b**) 3D TOE, view from RA, showing edges of the fossa ovalis. The septum primum was intact. The ASD-like defects in the fossa ovalis are due to echo dropout. (**c**) 2D TOE. PFO flap in the open position

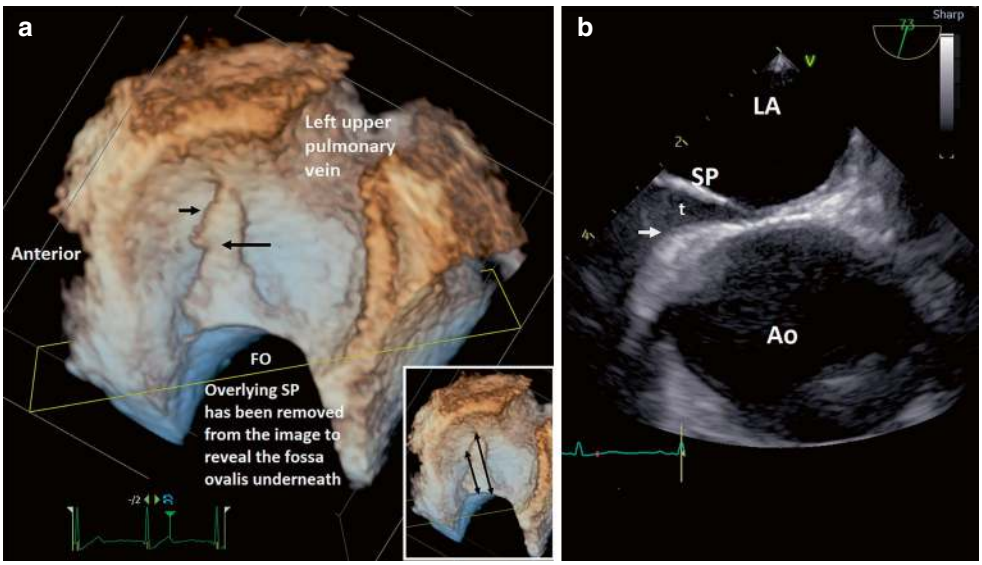


Fig. 19.28 Long tunnel PFO. (**a**) 3D TOE, view from LA, showing the long PFO tunnel (long arrow) with its slanted opening high up in the left atrium (short arrow). The septum primum has been removed from the fossa ovalis by image post-processing to show the edges of the secundum septum. Double-headed arrows in the insert show the minimum and maximum echocardiographic tunnel lengths. (**b**) 2D TOE showing an oblique cut through the open PFO tunnel (t) and the adjacent septum primum adhering well to the atrial wall. The septum secundum is deficient at the aortic rim of the fossa (arrow) and the rim practically non-existent

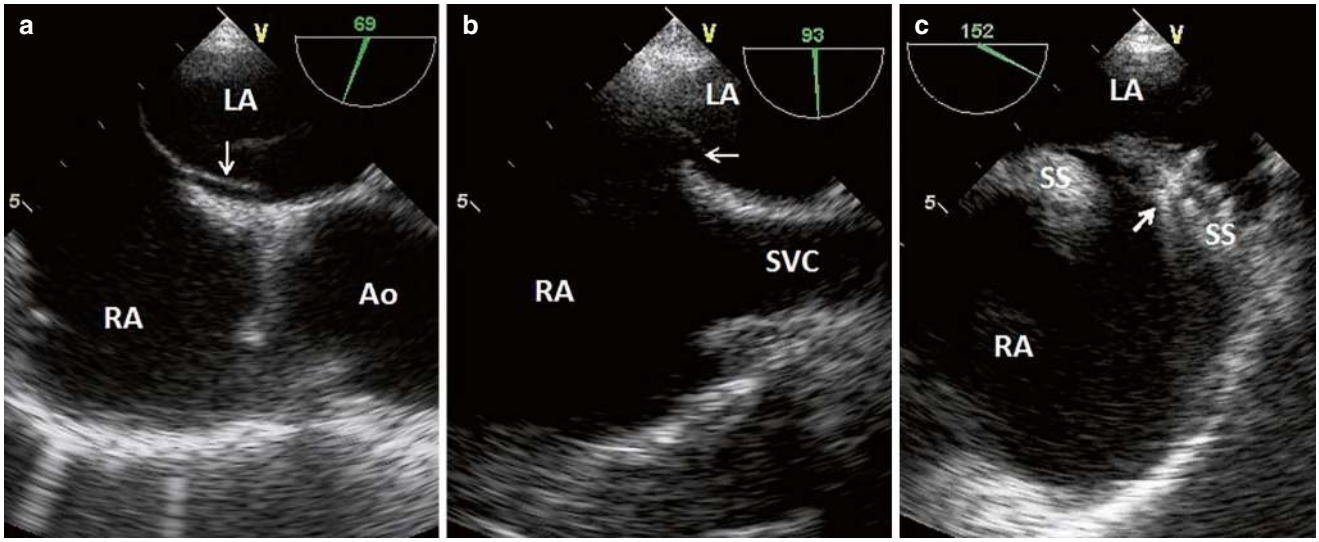


Fig. 19.29 Highly asymmetric PFO tunnel. (**a**) This tunnel (arrow) measured 1.4 cm long anteriorly. (**b**) There was almost no tunnel posteriorly (arrow). (**c**) The PFO device centred eccentrically and posteriorly (arrow) where the tunnel was shortest. A large device was chosen since only its anterior half would cover the PFO

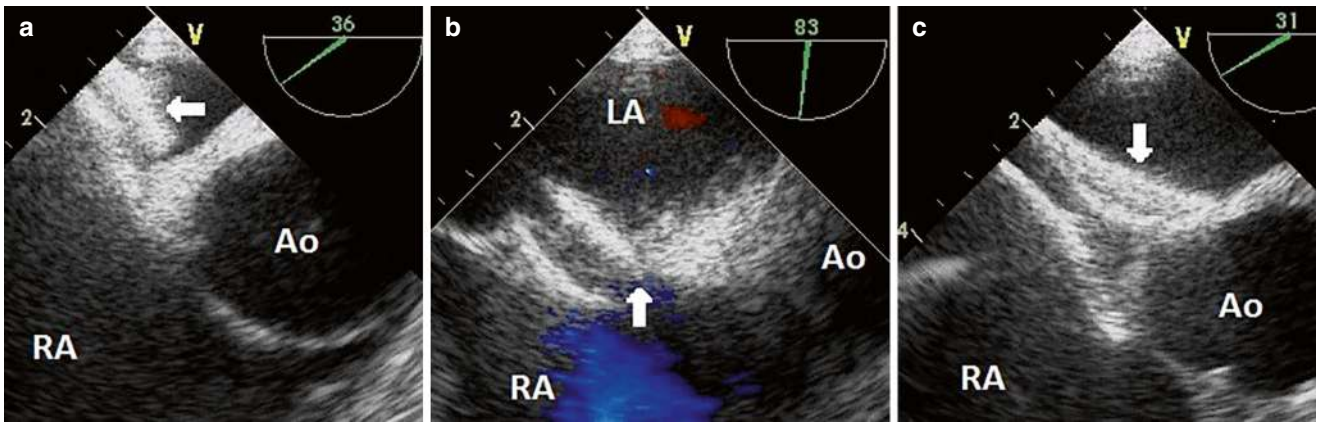


Fig. 19.30 Amplatzer PFO closure. (**a**) The device appears well-positioned but without much splay across the aorta. (**b**) A gentle wiggle of the device caused it to displace into the right atrium. (**c**) The Cribriform device splayed well across the aorta and was stable

ally 5 mm. Large devices may have wider disk-septum overlap zones, e.g. 8 mm with large Amplatzer devices. Narrow rims, especially with oversized, stiffer 3D devices such as Amplatzer or Occlutech, carry a small (0.04–0.3%), but potentially catastrophic risk of erosion into pericardial space or aorta [32]. Softer devices like the Gore Septal Occluder may carry a lower risk of erosion. There have been no reported cases of erosion with this device so far [33].

Deficient aortic quadrant rim is common, and the rounded aortic contour allows disks to slide around the aorta easily and displace, especially with a mobile interatrial septa and small devices that prolapse through the fossa easily. It may be compensated for by splaying the device across the aorta. Large disk-to-waist ratio devices such as the 30 mm Amplatzer cribriform device can also grip the immobile septum secundum on both sides of the fossa instead of just septum primum, thus stabilizing both septum primum and closure device in the plane of the fossa ovalis (Fig. 19.30).

A wide fossa is permissive and may allow partial or whole disk displacement through the fossa, especially in conjunction with a highly mobile interatrial septum (Fig. 19.25). Displacement may be partial, with a wide PFO tunnel being permissive, allowing RA disk displacement into the tunnel (Figs. 19.24 and 19.26).

Three-Dimensional Conformation of Apposition Surfaces

The thinly separated, parallel disks of closure devices are designed to sit flush against a thin flat septum. However, surfaces that device disks rest on are often not flat, except with

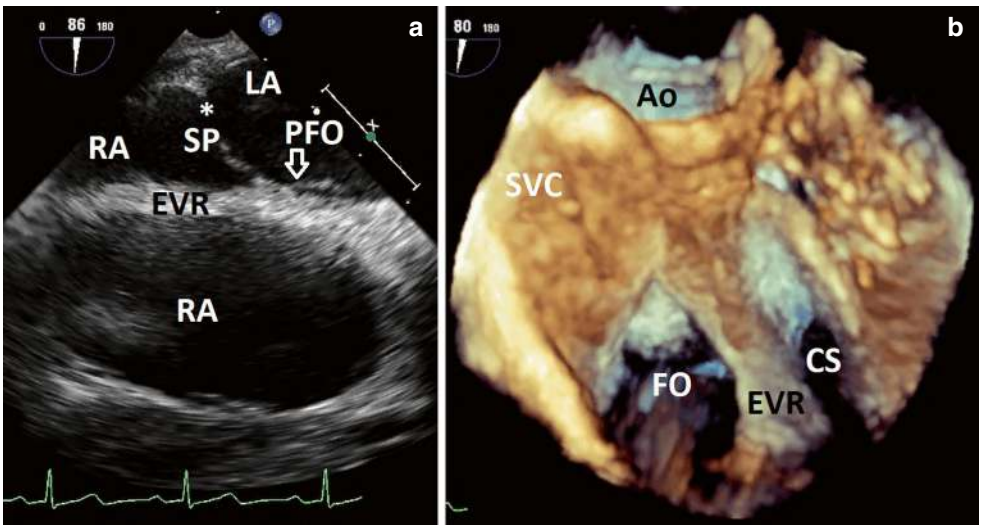


Fig. 19.31 2D-TOE of PFO and 3D-TOE RA view of the same patient. The prominent Eustachian valve ridge (EVR) runs across the floor of the right atrium and rises up the anterior edge of the fossa behind the coronary sinus (CS). Together with thick secundum septum, this forms a deep archway at the top of the fossa ovalis where the entrance to the PFO tunnel is situated. Good all round RA disk apposition is unlikely. Echo dropout artefact gives a false impression of an inferior ASD (*)

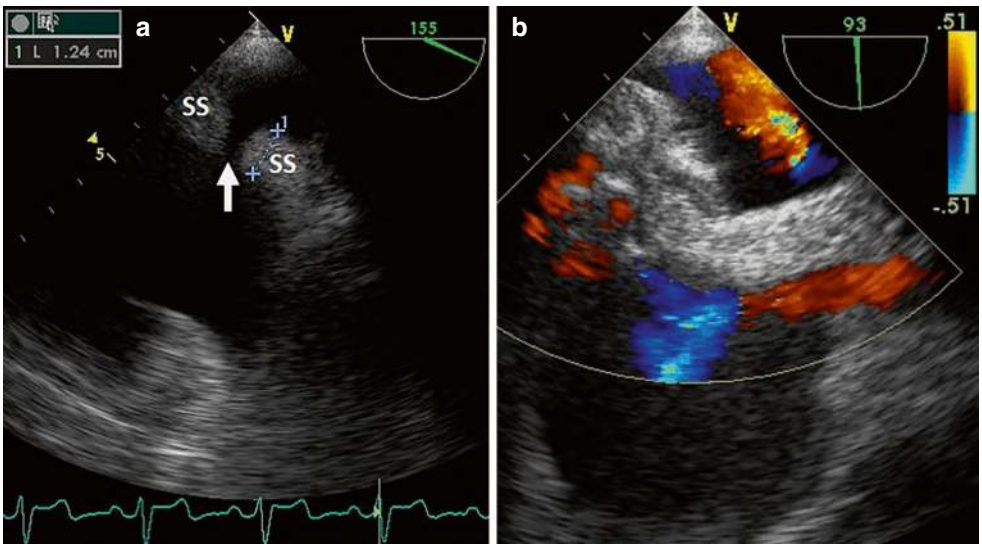


Fig. 19.32 (**a**) This thick lipomatous secundum septum did not taper down to the fossa ovalis in most areas, resulting in a long narrow slot-shaped ASD (arrow). (**b**) This ASD was closed with a balloon-sized 1.8 cm Amplatzer ASD occluder. Its variable waist shape and length allowed a good fit without device distortion and with no residual shunting

smaller mid-fossa fenestrations. This is especially true with flap valve ASDs and PFOs which are not positioned centrally in the septum. The curve of adjacent atrial free wall, the bulge of the aorta across which disks are splayed, the variable thickness of the secundum septum, and the Eustachian valve ridge may create complex 3D conformations of the left and right atrial apposition surfaces (Fig. 19.31). Septum secundum can be extensive, resulting in a small fossa and an ASD that is more like a long slot in thick tissue than a hole in a thin planar sheet (Fig. 19.32, Video 19.22). There may not be enough flat septum between fossa and atrial free walls curving away from the septum to accommodate a large device, resulting in device distortion (Fig. 19.8).

If disks do not lie flush against the septum to produce a complete seal, there may be substantial residual shunting. The malleability of 3D wide-waisted devices allows better conformation to odd-shaped holes, and their wide waists will occlude defects even if disk apposition is incomplete.

Multiple Defects

Care should be taken to inspect the entire septum for multiple defects, especially if the identified index defect seems incongruously small for the degree of right heart dilatation. A second secundum ASD may be sizeable but unsuitable for percutaneous device closure, e.g. due to poor supporting rims. There is no particular association between secundum ASD and other shunts, but they may occasionally co-exist. Concomitant sinus venosus defects and anomalous pulmonary veins would require surgical closure instead.

Multiple ASDs and PFOs may co-exist. A PFO tunnel may have single or multiple entrances or exits (Fig. 19.33a). Some ASDs are separated by thin tissue strands that can be stretched or broken by balloon inflation, converting the multiple ASDs into a single defect, closable by a single device. Tiny fenestrations that do not contribute significantly to shunt size may be left untouched if thought to be of little

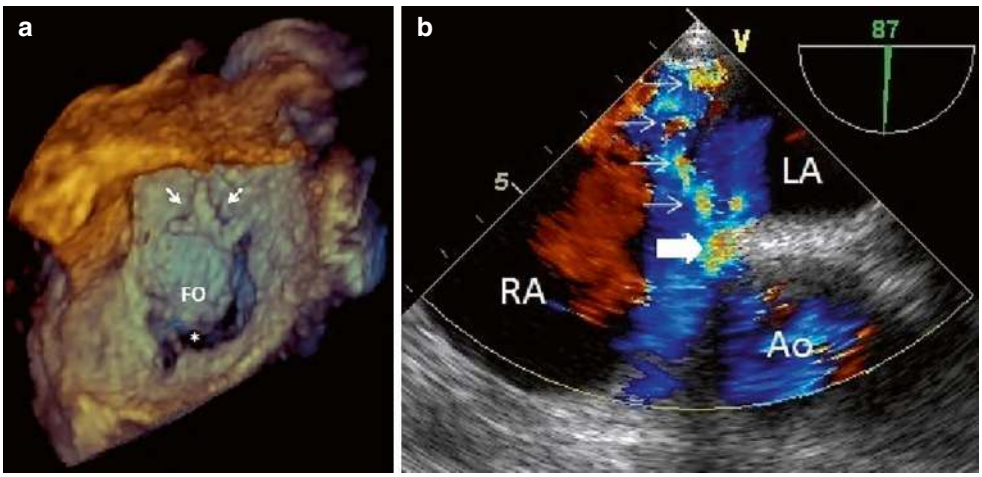


Fig. 19.33 (**a**) LA view on 3D TOE showing 2 LA tunnel exits (arrows) separated by a strand of septum primum tissue. There were no ASDs. Apparent defects (*) are due to echo dropout. (**b**) Pepper pot septum with multiple small fenestration ASD's (thin arrows) and a flap valve ASD (thick arrow)

clinical significance. Small fenestrations in a pepper pot septum (Fig. 19.33b) may be closed with a small waist—large disk device centred in a fenestration in the middle of the scattered fenestrations, sandwiching surrounding defects between the disks to reduce shunting. When an aneurysmal septum is straightened between device disks, redundant tissue will crumple with concertina folds, collapsing small defects to reduce their shunting further. Multiple defects may require multiple closure devices.

Hybrid Defects

The ASD-PFO Hybrid

Flap valve secundum ASDs may merge seamlessly into an adjacent PFO, resulting in a PFO-ASD hybrid where the ASD merges seamlessly with the partially unroofed PFO tunnel (Fig. 19.16). Their hybrid nature complicates closure and it is essential to understand how each component behaves.

Balloon sizing may open up a large gap by flap displacement rather than retraction, leading to the use of an oversized ASD device that sits badly and worsens the tilt into the left atrium (Fig. 19.34). Use of a small waist—large disk device such as the Amplatzer Cribriform device may improve disk alignment and apposition with the septum, while the large disks grip the immobile septum secundum over large arcs of the disk circumference to stabilize the device (Figs. 19.34, 19.35, and 19.36).

Proximity to Major Cardiac Structures

Septum secundum defects may occur in any part of the septum. Although PFOs are usually located in the anterosuperior (aortic) quadrant, failure of primum to secundum septum adherence can occur in other locations. It is important to note any proximity to major structures (vena cavae, pulmonary veins, atrioventricular valves, coronary sinus) and check that there is no significant impact on these structures from device closure (Fig. 19.37, Videos 19.23 and 19.24)

Complete and Partial DASP Tunnels, Ramps and Funnels

Complete and partial DASP PFO configurations occur when the septum primum is displaced away from the secundum septum throughout the cardiac cycle. This fixed separation may affect the entire length of the tunnel (Figs. 19.17 and 19.18), or only part of it, most commonly in "ramp" and "funnel" configurations [34, 35].We have not attempted to close long tunnel DASP-type PFOs. Current devices are not designed for such anatomy. DASP complicates closure and is a risk factor for procedural failure.

With partial DASP, the layers appose at the fossa edge, then separate in the left atrium, with the flap rising off the septum secundum as it extends superiorly. If the flap is deficient centrally and the tunnel partially unroofed, a shorter central tunnel results, flanked by long ramps on either side

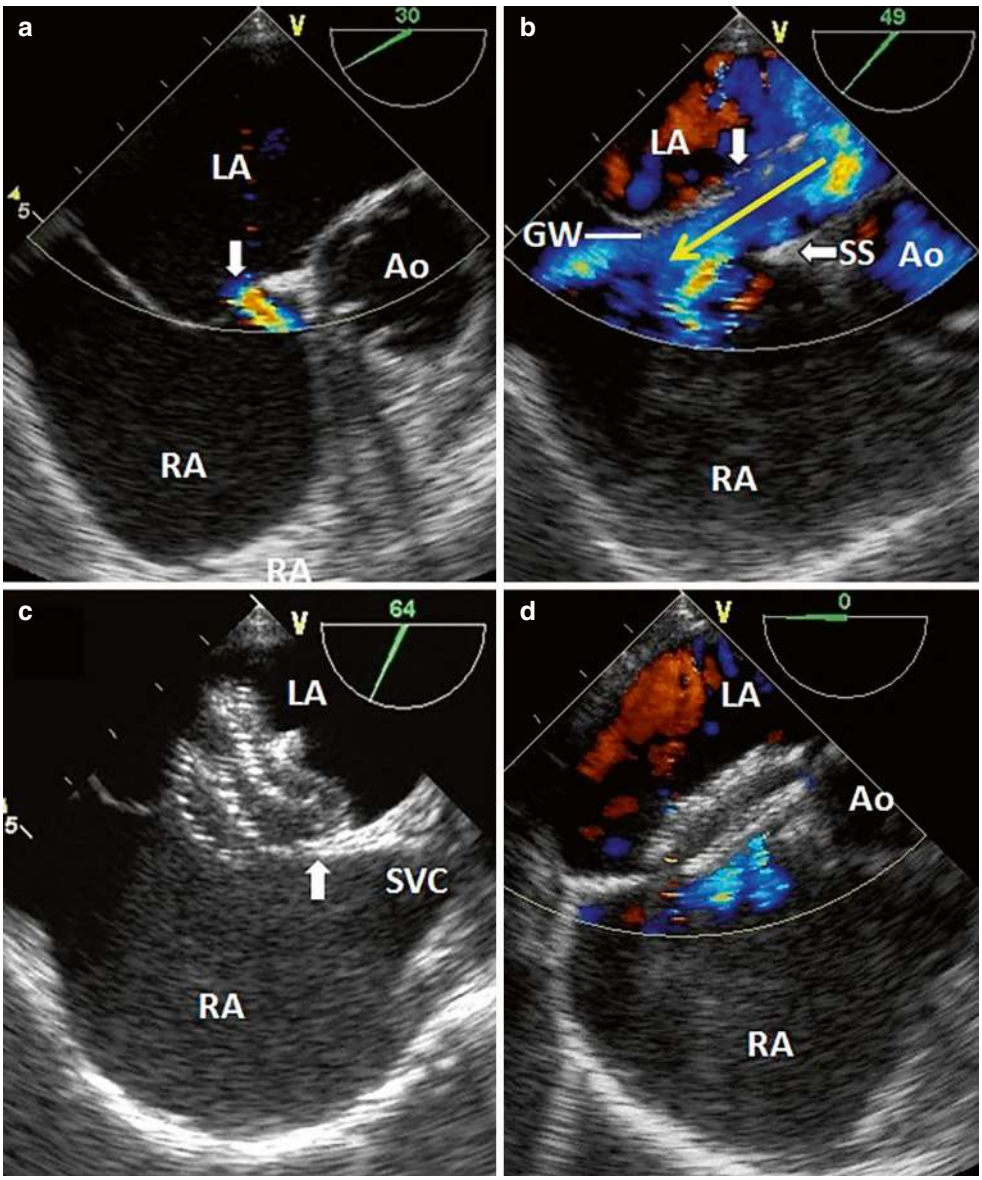


Fig. 19.34 Amplatzer closure of PFO-ASD hybrid defect. (**a**) Small ASD (white arrow). (**b**) The ASD merges with an unfused flap valve (white arrow). This opens up into a long, large PFO tunnel with large left to right shunt (yellow arrow) with the guidewire (GW). Balloon stretched size of the defect was 19 mm. (**c**) The oversized 20 mm ASD device is tilted into the left atrium by the oversized waist (arrow) and its grip on the septum secundum is very precarious. (**d**) Moments later, the RA disk has slipped over the edge and through the fossa, halfway into the PFO tunnel. Half of it is malpositioned inside the PFO tunnel, stenting the defect open with persistent shunting. The ASD device was removed and the defect successfully closed with a 30 mm Amplatzer cribriform device

(Fig. 19.38). With taut ramps, septal layers do not oppose even when clamped with a closure device. The 2 disks are held apart and the tunnel between them remains open. Flap retraction by the device waist may hold the PFO open. For these reasons, Helex (planar disks, short wire waist) device closure failed and worsened the shunt (Fig. 19.39) in the case in Fig. 19.38.

The PFO flap may be strung tautly between its superior attachments in the left atrium, pulling the tunnel floor into a curved recess, creating a tunnel-like an open funnel (Fig. 19.40). Left atrial disks like the radial spoke devices that are no longer in use had little radial strength and would fold readily into open funnels.

Taut flaps retract poorly to shorten the tunnel, even when considerable manual force is applied. The left atrial disk may cap the funnel at an angle to the atrial wall. The LA disk pushes against the wall, with a possibly increased risk of atrial wall erosion. Elsewhere, it protrudes into left

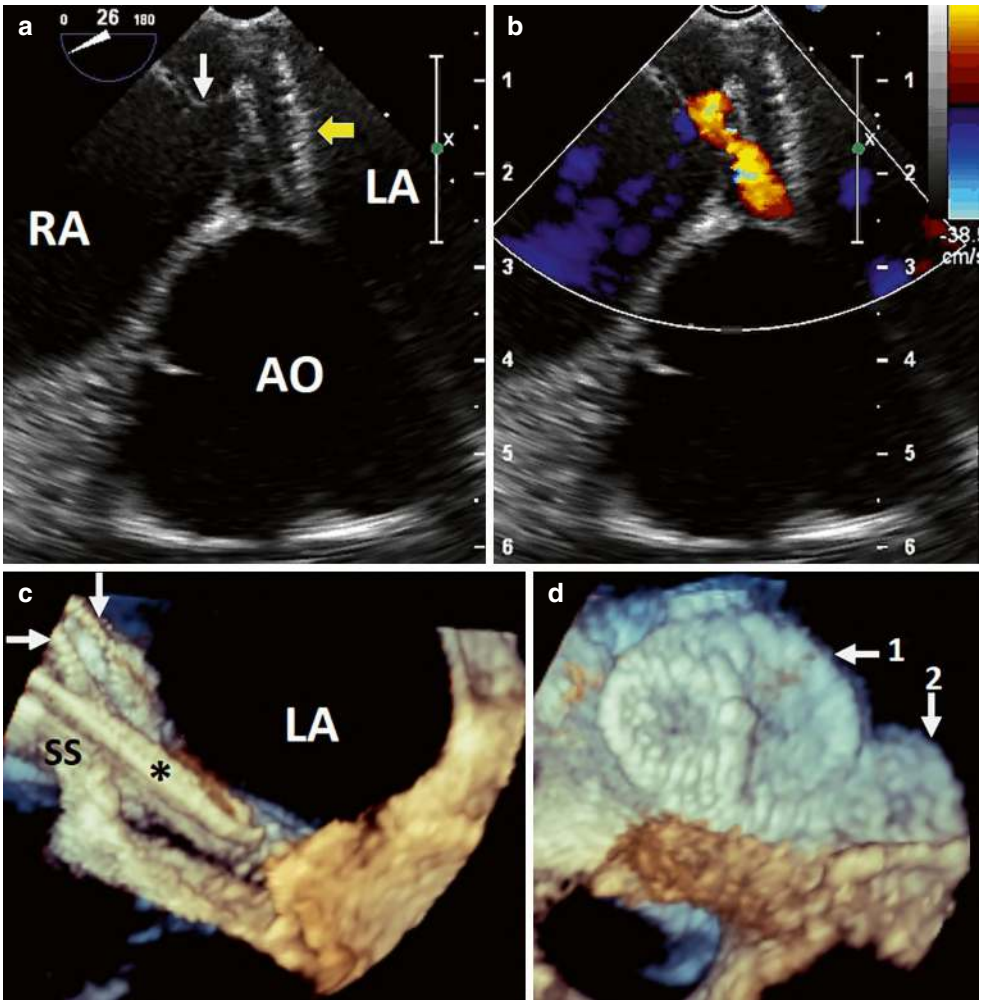


Fig. 19.35 (**a**) This PFO-ASD hybrid defect comprised of a small flap valve ASD merged with an unusually anterior, unroofed PFO and redundant atrial septum primum (white arrow). This was successfully closed with a small Amplatzer ASD occluder (yellow arrow) but she had late, and fortunately, only partial displacement of RA disk into the tunnel, stenting the PFO open. (**b**) Recurrent and now continuous left to right shunt. (**c**) A second procedure was performed. The delivery sheath (*) is seen entering the LA from the fossa, pushing the old device aside. The old LA disk (down arrow) is in the LA. The old RA disk (right arrow) has prolapsed into the PFO tunnel. (**d**) A large cribriform device (1) was deployed. This clamped down on the smaller first device (2) to close the residual shunt, and onto the superior half of the secundum septum, simultaneously stabilizing both devices

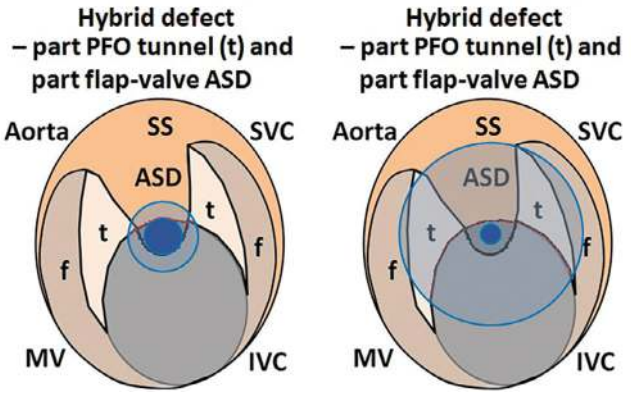


Fig. 19.36 Hybrid defect with device. This diagram uses the same schematic as in Fig. 19.16. Left: The small Amplatzer ASD device waist (darker blue) fills the ASD, but its disks (light blue) are small, the rims are narrow, grip only a short arc (red dotted line) of the immobile septum secundum, and are much narrower than the fossa. If the septum primum displaces into the left atrium, the right atrial disk can easily prolapse through the fossa to become displaced. Right: The cribriform PFO device has only a small waist that does not fully fill the ASD, but its disks are large and the rims are long. They grip a large arc of the immobile septum secundum with a large amount of overlap, thus stabilizing the device in the plane of the fossa. In addition, being wider than the fossa, the right atrial disk will not displace easily through the fossa. If disk apposition is good, a good seal of the ASD may be achieved despite the small non-occlusive waist.

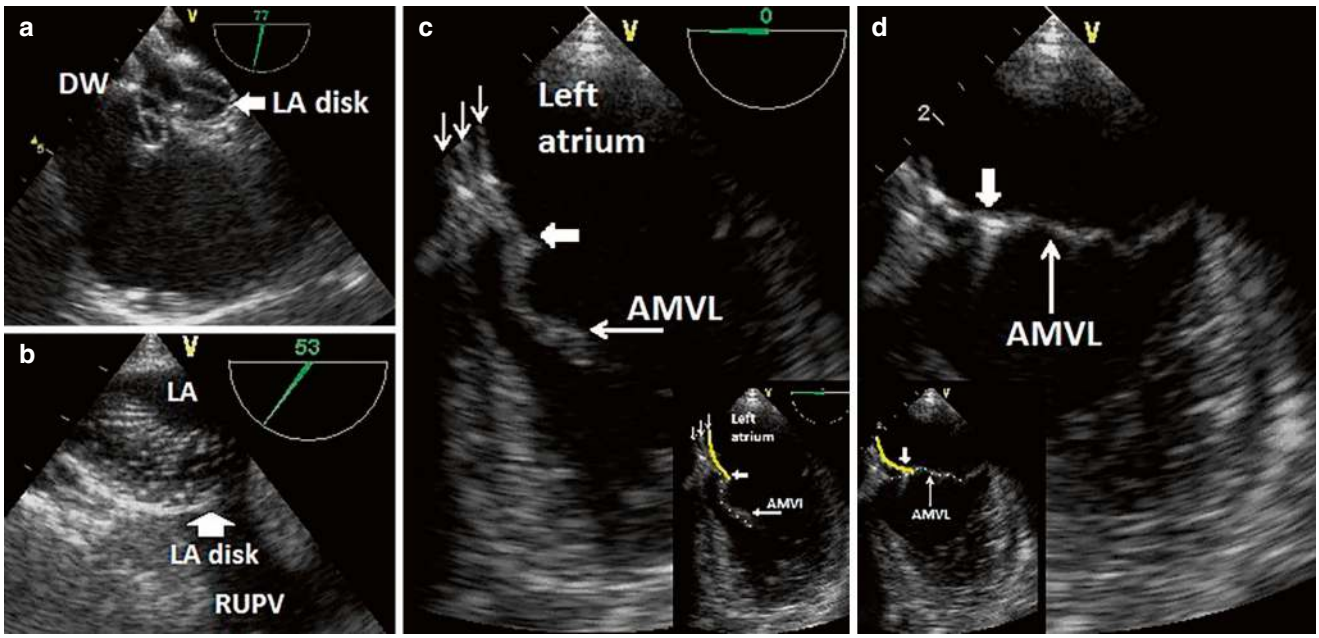


Fig. 19.37 (**a**, **b**) Right upper pulmonary vein (RUPV) obstruction. (**a**) The LA disk fails to shape well, causing the bulbous outline of the disk with felt layer inside. (**b**) The misshapen LA disk obstructs the ostium of the right upper pulmonary vein (RUPV). (**c**, **d**, Videos 19.23 and 19.24) The intrasept planar PFO device is positioned in an abnormally inferior PFO-like defect. From left to right, the 3 small thin arrows in C point to the RA disk, interatrial septum and LA disk respectively. The LA disk (yellow line in the insert) impinges on the anterior mitral valve leaflet (white dotted line), straightening in diastole (**c**) and bending in systole (**d**) with leaflet movement. The unreleased device was recaptured and removed due to risk of leaflet erosion and device strut fracture. The defect was later closed successfully with a smaller Helex device.

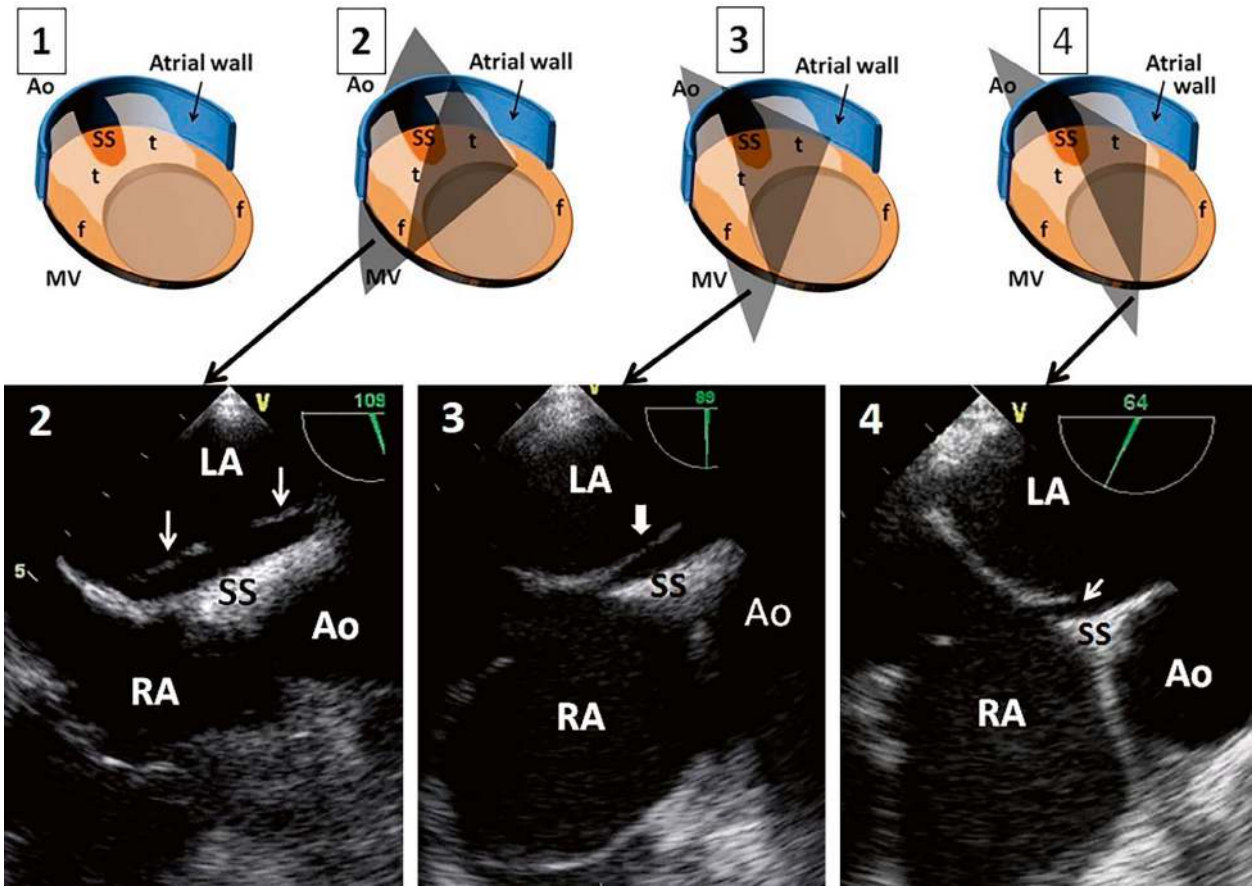


Fig. 19.38 Double-ramp, partial DASP PFO. 1. Diagrammatic representation using the same schematic as Fig. 19.16. Diagrams 2, 3 and 4 show cut-planes through the defect and their corresponding 2D TOE images, with arrows in TOE images pointing to the double-ramp in cross-section, the long ramp-like side of the PFO, and short central tunnel respectively

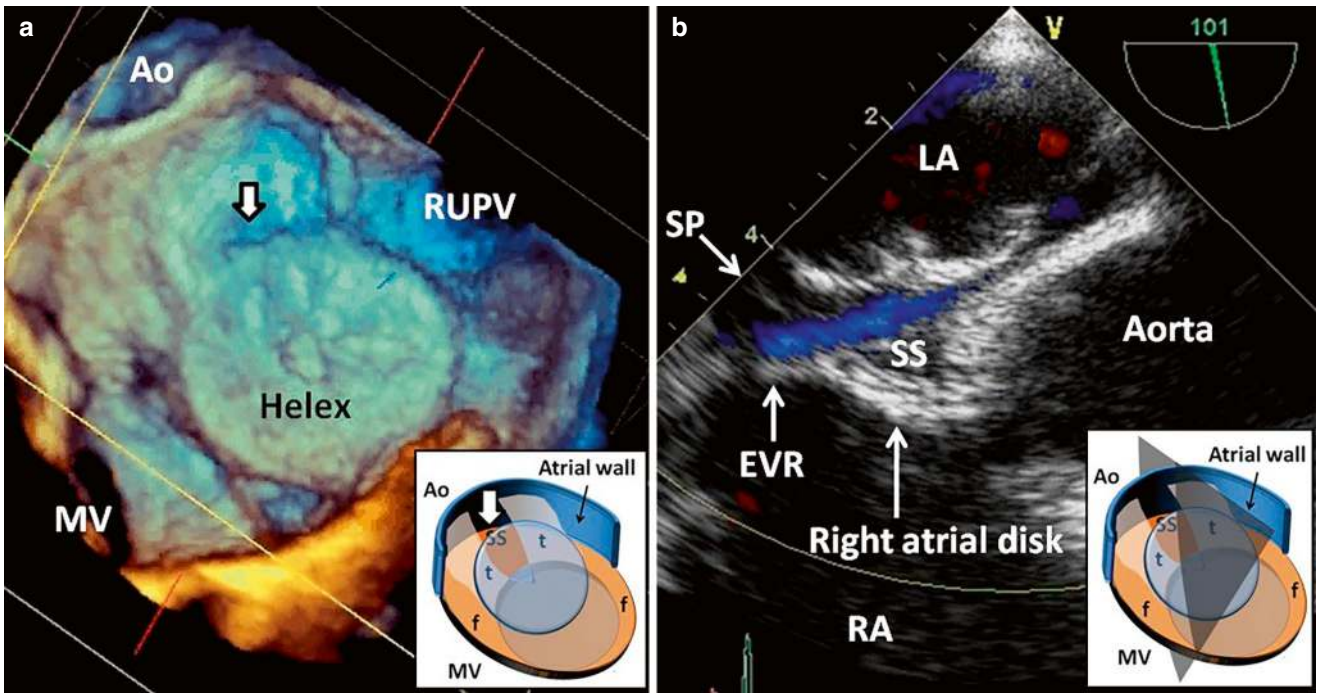


Fig. 19.39 Failed closure of the large double-ramp, partial DASP PFO in Fig. 19.38. Diagrams use the same schematics as Fig. 19.16. (**a**) Three-dimensional modeling (insert) warned that a 30 mm Helex device (blue disk) might fail to seal the left atrial tunnel exit, fail to clamp tunnel layers together, and possibly stent the fossa tunnel entrance open by creating a flap retraction ASD. All three problems occurred and shunting was continuous and worse post-procedure. One year later, the continuous shunt was still present. 3D TOE (left atrial view) shows the open tunnel exit (arrow). (**b**) 2D TOE showed residual continuous shunting. Helex implantation had converted the centrally unroofed tunnel into an open funnel. This was successfully closed by the unorthodox deployment of an Amplatzer ASD device over the Helex with a 3D waist to occlude the tunnel

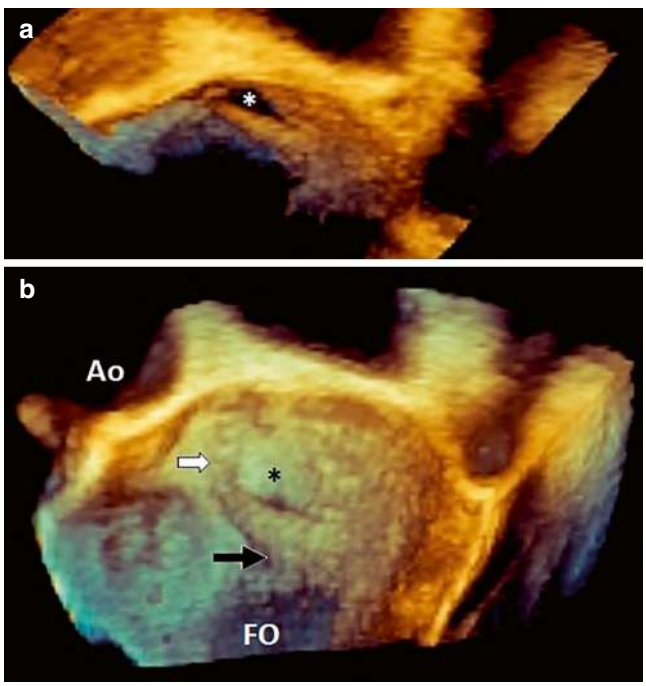


Fig. 19.40 3D TOE images from the LA showing the funnel configuration of this partial DASP PFO tunnel (*). (**a**) View from above the tunnel exit at its minimum size. (**b**) Oblique view of the maximally open tunnel with a wide rim (white arrow) funneling down to a much narrower tunnel below (black arrow)

atrium, with associated risks of incomplete endothelialization and thrombus formation. Tension from poor flap retraction may tilt the right atrial disk towards the tunnel, causing flap displacement, thus stenting the tunnel open. Disks may not achieve adequate seals, and closure is more reliable with tunnel occlusion. We have successfully closed smaller, open-funnel, DASP PFOs with Amplatzer ASD devices, choosing them for their radial strength, occlusive waist of adaptable length, and small rims (Fig. 19.41, Videos 19.25, 19.26 and 19.27).

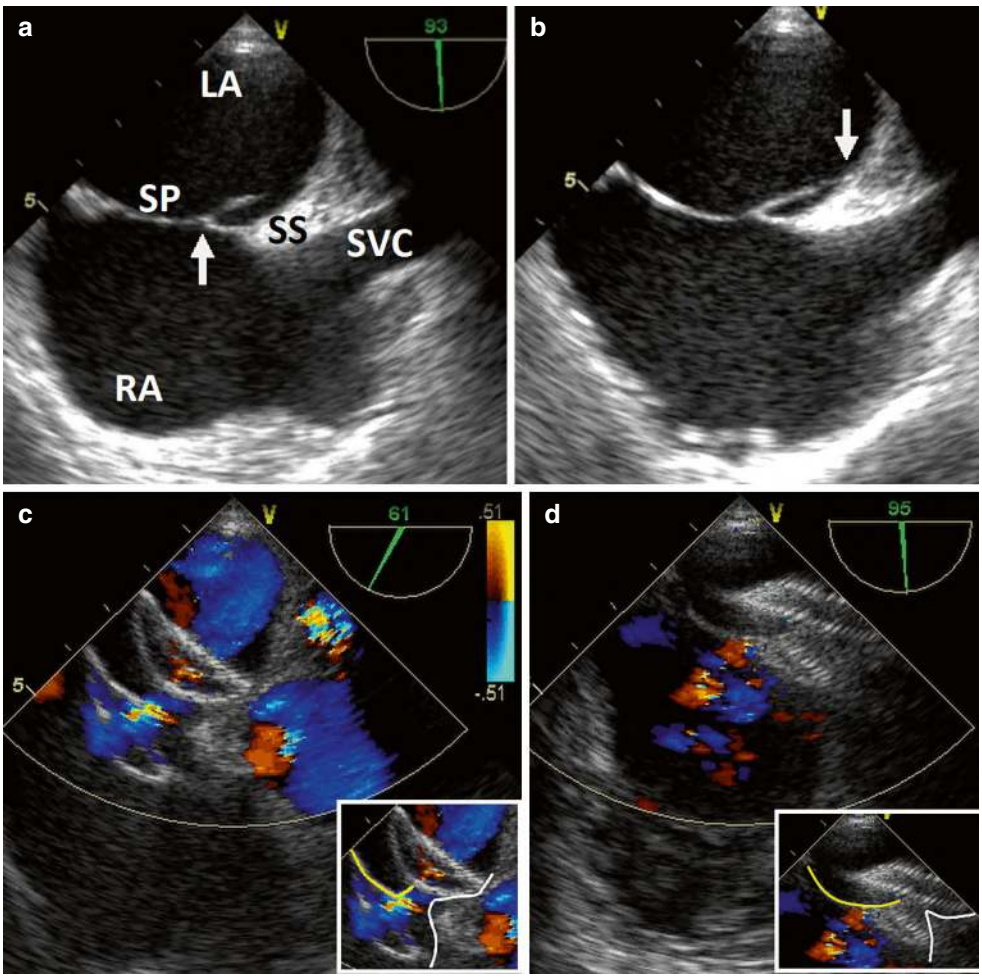


Fig. 19.41 (**a**) The septum primum is aneurysmal and sags down just enough onto the fossa edge (arrow) to close the PFO (Video 19.25). (**b**) The rest of the PFO flap does not appose and is tethered inside the left atrium (arrow). (**c**) Closure with an Amplatzer PFO occluder (Video 19.26) failed. The LA disk was hung up in the left atrium as the flap would not retract. The poorly apposed LA disk protruded into the left atrium. The waist stented the tunnel open. We were not confident that the RA disk could provide a good seal. (**d**) The PFO occluder was removed and replaced with a balloon-sized 15 mm-waisted Amplatzer device (Video 19.27). The LA disk was similarly malpositioned but the waist filled the defect with the usual immediate post-procedure shunting through, but not around, the porous waist. The shunt had resolved when reassessed a year later. Septum primum is outlined in yellow, atrial wall and septum secundum in white, in the inserts

Conclusions

Echocardiography has emphasized the complexities of ASD and PFO closure, and clearly shown that one size does not fit all. Choice and size of device are determined by many different anatomical and functional characteristics acting in concert. These characteristics matter more than whether the defect is a PFO or ASD. Indeed, there is an anatomical continuum between PFO and flap-valve ASD and hybrid defects have features of both. Some PFOs require an ASD device for closure and vice versa. Ideal devices for some anatomical variants have yet to be devised and the principles discussed above should be taken into consideration for future designs. Three-dimensional modeling allows the simultaneous incorporation of the many different features that influence defect and device behaviour. The limitations of 3D model construction from 2D images have been overcome with 3D TOE, but resolution remains better with 2D TOE. Where support from anaesthesia and TOE services are limited, ICE is a helpful alternative, although less versatile in terms of available views and perhaps less suitable for complex anatomy. Both 2-D and 3D echocardiography are invaluable for pre-procedural assessment, planning and peri-procedural guidance. They help us pre-empt trouble, and continue to confirm, refute and refine our current imperfect concepts.

References

1. Søndergaard L, et al. Patent foramen Ovale closure or antiplatelet therapy for cryptogenic stroke. N Engl J Med. 2017;377(11):1033–42. https://doi.org/10.1056/NEJMoa1707404.
2. Saver JL, et al. Long-term outcomes of patent foramen Ovale closure or medical therapy after stroke. N Engl J Med. 2017;377(11):1022–32. https://doi.org/10.1056/NEJMoa1610057.
3. Mas J-L, et al. Patent foramen ovale closure or anticoagulation vs. antiplatelets after stroke. N Engl J Med. 2017;377(11):1011–21. https://doi.org/10.1056/NEJMoa1705915.
4. Lee PH, et al. Cryptogenic stroke and high-risk Patent Foramen Ovale. The DEFENSE-PFO Trial. 2018. https://doi.org/10.1016/j.jacc.2018.02.046.
5. Nakayama R, et al. Identification of high-risk patent foramen Ovale associated with cryptogenic stroke: development of a scoring system. J Am Soc Echocardiogr. 2019;32(7):811–6. https://doi.org/10.1016/J.ECHO.2019.03.021.

6. Tobis JM, et al. Proposal for updated nomenclature and classification of potential causative mechanism in patent foramen ovale-associated stroke. JAMA Neurol. 2020;77(7):878–86. https://doi.org/10.1001/JAMANEUROL.2020.0458.
7. Stout KK, et al. 2018 AHA/ACC guideline for the management of adults with congenital heart disease: a report of the American College of Cardiology/American Heart Association task force on clinical practice guidelines. Circulation. 2019;139(14):e698–800. https://doi.org/10.1161/CIR.0000000000000603.
8. Baumgartner H, et al. 2020 ESC Guidelines for the management of adult congenital heart disease. Feb. 07, 2021, Oxford University Press. https://doi.org/10.1093/eurheartj/ehaa554.
9. Sorajja P, Nishimura RA. Patent foramen ovale closure without echocardiography: are we closing the door too fast too soon? JACC Cardiovasc Interv. 2009;2(2):124–6. https://doi.org/10.1016/J.JCIN.2008.12.001.
10. Davison P, Clift PF, Steeds RP. The role of echocardiography in diagnosis, monitoring closure and post-procedural assessment of patent foramen ovale. Eur J Echocardiogr. 2010;11(10):i27. https://doi.org/10.1093/EJECHOCARD/JEQ120.
11. Martin-Reyes R, et al. Role of real-time three-dimensional transoesophageal echocardiography for guiding transcatheter patent foramen ovale closure. Eur J Echocardiogr. 2009;10(1):148–50. https://doi.org/10.1093/EJECHOCARD/JEN214.
12. Rana BS, Shapiro LM, McCarthy KP, Ho SY. Three-dimensional imaging of the atrial septum and patent foramen ovale anatomy: defining the morphological phenotypes of patent foramen ovale. Eur J Echocardiogr. 2010;11(10):i19. https://doi.org/10.1093/EJECHOCARD/JEQ122.
13. Nassif M, et al. Historical developments of atrial septal defect closure devices: what we learn from the past. Expert Rev Med Devices. 2016;13(6):555–68. https://doi.org/10.1080/17434440.2016.1182860.
14. Li Y, et al. Initial clinical experience with the biodegradable AbsnowTM device for percutaneous closure of atrial septal defect: a 3-year follow-up. J Interv Cardiol. 2021;2021:1. https://doi.org/10.1155/2021/6369493.
15. Van Den Branden BJ, Post MC, Plokker HW, Ten Berg JM, Suttorp MJ. Patent foramen ovale closure using a bioabsorbable closure device: safety and efficacy at 6-month follow-up. JACC Cardiovasc Interv. 2010;3(9):968–73. https://doi.org/10.1016/J.JCIN.2010.06.012.
16. Gaspardone A, et al. Novel percutaneous suture-mediated patent foramen ovale closure technique: early results of the NobleStitch EL Italian registry. EuroIntervention. 2018;14(3):e272–9. https://doi.org/10.4244/EIJ-D-18-00023.
17. Sievert H, et al. Transcatheter closure of patent foramen ovale with radiofrequency: acute and intermediate term results in 144 patients. Catheter Cardiovasc Interv. 2009;73(3):368–73. https://doi.org/10.1002/CCD.21809.
18. Zimmermann WJ, et al. Patent foramen ovale closure with the SeptRx device initial experience with the first 'In-Tunnel' device. JACC Cardiovasc Interv. 2010;3(9):963–7. https://doi.org/10.1016/J.JCIN.2010.04.019.
19. Pristipino C, et al. European position paper on the management of patients with patent foramen ovale. General approach and left circulation thromboembolism. EuroIntervention. 2019;14(13):1389–402. https://doi.org/10.4244/EIJ-D-18-00622.
20. Ivens E, Hamilton-Craig C, Aroney C, Clarke A, Jalali H, Burstow DJ. Early and late cardiac perforation by Amplatzer atrial septal defect and patent foramen ovale devices. J Am Soc Echocardiogr. 2009;22(9):1067–70. https://doi.org/10.1016/J.ECHO.2009.06.013.
21. Gelernter-yaniv L, Khoury A, Schwartz Y, Lorber A. Transcatheter closure of right-to-left interatrial shunts to resolve hypoxemia. Congenit Heart Dis. 2008;3(1):47–53. https://doi.org/10.1111/J.1747-0803.2007.00157.X.
22. Johansson MC, Eriksson P, Peker Y, Hedner J, Råstam L, Lindblad U. The influence of patent foramen ovale on oxygen desaturation in obstructive sleep apnoea. Eur Respir J. 2007;29(1):149–55. https://doi.org/10.1183/09031936.00035906.
23. Toffart AC, Bouvaist H, Feral V, Blin D, Pison C. Hypoxemia-orthodeoxia related to patent foramen ovale without pulmonary hypertension. Heart Lung. 2008;37(5):385–9. https://doi.org/10.1016/J.HRTLNG.2007.09.006.
24. Lairez O, et al. Risk of neurological decompression sickness in the diver with a right-to-left shunt: literature review and meta-analysis. Clin J Sport Med. 2009;19(3):231–5. https://doi.org/10.1097/JSM.0B013E31819B0FA2.
25. Torti SR, et al. Risk of decompression illness among 230 divers in relation to the presence and size of patent foramen ovale. Eur Heart J. 2004;25(12):1014–20. https://doi.org/10.1016/J.EHJ.2004.04.028.
26. Ponnuthurai FA, van Gaal WJ, Burchell A, Mitchell AR, Wilson N, Ormerod OJ. Safety and feasibility of day case patent foramen ovale (PFO) closure facilitated by intracardiac echocardiography. Int J Cardiol. 2009;131(3):438–40. https://doi.org/10.1016/J.IJCARD.2007.07.141.
27. Calvert PA, Rana BS, Kydd AC, Shapiro LM. Patent foramen ovale: anatomy, outcomes, and closure. Nat Rev Cardiol. 2011;8(3):148–60. https://doi.org/10.1038/NRCARDIO.2010.224.
28. Koutroulou I, Tsivgoulis G, Tsalikakis D, Karacostas D, Grigoriadis N, Karapanayiotides T. Epidemiology of patent foramen Ovale in general population and in stroke patients: a narrative review. Front Neurol. 2020;11:281. https://doi.org/10.3389/FNEUR.2020.00281.
29. Katsanos AH, et al. Transcranial Doppler versus transthoracic echocardiography for the detection of patent foramen ovale in patients with cryptogenic cerebral ischemia: a systematic review and diagnostic test accuracy meta-analysis. Ann Neurol. 2016;79(4):625–35. https://doi.org/10.1002/ANA.24609.
30. Mojadidi MK, Bogush N, Caceres JD, Msaouel P, Tobis JM. Diagnostic accuracy of transesophageal echocardiogram for the detection of patent foramen ovale: a meta-analysis. Echocardiography. 2014;31(6):752–8. https://doi.org/10.1111/echo.12462.
31. Afonso L, et al. Usefulness of intravenously administered fluid replenishment for detection of patent foramen ovale by transesophageal echocardiography. Am J Cardiol. 2010;106(7):1054–8. https://doi.org/10.1016/J.AMJCARD.2010.05.037.
32. McElhinney DB, Quartermain MD, Kenny D, Alboliras E, Amin Z. Relative risk factors for cardiac erosion following transcatheter closure of atrial septal defects: a case-control study. Circulation. 2016;133(18):1738–46. https://doi.org/10.1161/CIRCULATIONAHA.115.019987.
33. Qureshi AM, et al. Long-term results of the atrial septal defect occluder ASSURED trial for combined pivotal/continued access cohorts. JACC Cardiovasc Interv. 2024;17(19):2273–83. https://doi.org/10.1016/J.JCIN.2024.07.013.
34. Roberson DA, Javois AJ, Cui W, Madronero LF, Cuneo BF, Muangmingsuk S. Double atrial septum with persistent interatrial space: echocardiographic features of a rare atrial septal malformation. J Am Soc Echocardiogr. 2006;19(9):1175–81. https://doi.org/10.1016/J.ECHO.2006.04.001.
35. Cohen MS, Weinberg P, Coon PD, Gaynor JW, Rychik J. Deviation of atrial septum primum in association with normal left atrioventricular valve size. J Am Soc Echocardiogr. 2001;14(7):732–7. https://doi.org/10.1067/MJE.2001.111875.

Carotid Scanning

20

Eugenio Picano and Ana Cristina Camarozano

Carotid ultrasound has traditionally been used to evaluate the presence of obstructive atherosclerosis in the setting of symptomatic cerebrovascular disease or asymptomatic carotid bruit. More recently, carotid ultrasound has been performed in epidemiologic studies to measure carotid intima-media thickness (CIMT) and detect nonobstructive plaque to evaluate the relation of these findings to cardiovascular disease risk factors and cardiovascular disease morbidity and mortality. In addition, changes in CIMT may be used as a measure of the efficacy of a pharmacologic intervention. The present chapter will focus on carotid ultrasound as an imaging biomarker of cardiovascular risk, diagnostic assessment in asymptomatic patients with known or suspected carotid stenosis or coronary artery disease, and follow-up in treated patients. Moreover, training and certification will be addressed. Carotid ultrasound remains an important imaging modality for initial assessment but is reserved for evaluation of the carotid bulb region. Based on the 2023 recommendations of the European Society of Cardiovascular Radiology, in asymptomatic patients, computed tomography or magnetic resonance should be the second-line imaging technique that is always performed after an initial ultrasound exam has identified severe stenosis, plaque features possibly correlated to increased stroke risk or was not conclusive [1]. Carotid ultrasound detects different stages of atherosclerosis, from a pre-intrusive increase in CIMT to protrusive plaque to hemodynamically significant plaques [2]. In addition to plaque geometry, the plaque texture may supply critical information on plaque histologic structure and vulnerability (Fig. 20.1).

E. Picano (✉)
University of Belgrade, Belgrade, Serbia

A. C. Camarozano
Federal University of Paranà, Paranà, Brazil

© The Author(s), under exclusive license to Springer Nature Switzerland AG 2025
M. Y. Henein (ed.), *Clinical Echocardiography*, https://doi.org/10.1007/978-3-031-95894-6_20

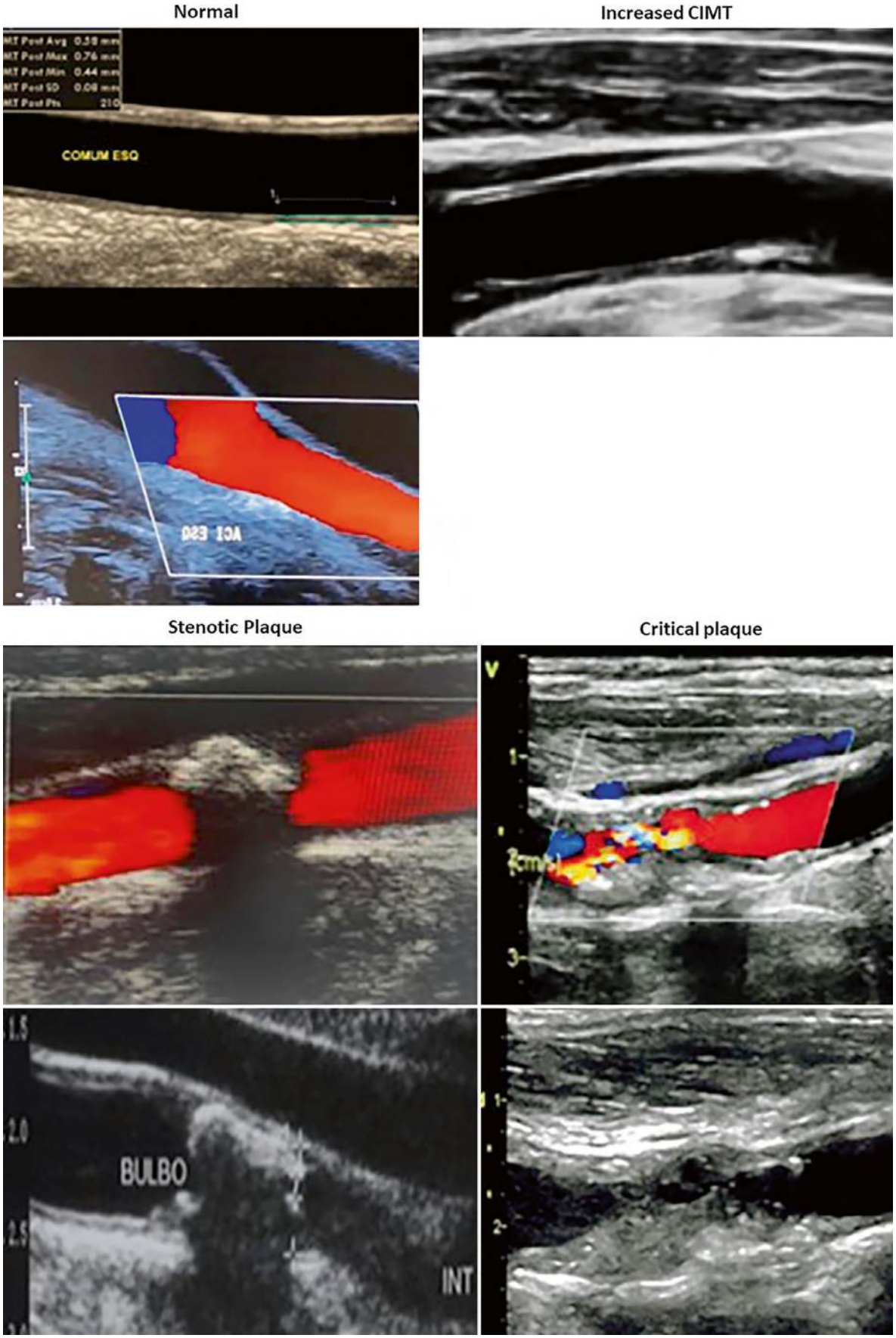


Fig. 20.1 (**a**–**c**) The figure shows 2D and Doppler patterns of a normal carotid wall (panel A); an increased CIMT (panel B); a carotid plaque (panel C); a hemodynamically critical carotid plaque (panel D)

Table 20.1 Carotid phenotypes by ultrasound

	CIMT	Plaque
Carotid wall thickness	<1.5 mm	≥ 1.5 mm
Arterial wall layer involved	Intima	Media
Pathogenesis	Aging	Atherosclerosis
Impact on risk	Modest	Marked

CIMT

Carotid arterial atherosclerosis is thought to develop beneath the intimal layer in the sub-intima. In contrast, the medial layer is subject to non-atherosclerotic medial hypertrophy commonly induced by aging and hypertension. Since the largest portion of CIMT (99% in healthy individuals and 80% when diseased) consists of the medial layer, CIMT has not been shown to consistently add to cardiovascular disease risk prediction. Carotid plaque, on the other hand, represents the atherosclerotic process itself and starts in the intimal layer and has thus been shown to predict cardiovascular disease events better than CIMT [3] (Table 20.1).

A CIMT ≥1.5 mm be considered a clinically significant lesion for patients less than 65 years of age [4]. Progression can be slowed by medical therapy and other risk factor modifications (e.g., control of blood pressure). However, serial scanning of CIMT is challenging in individual patients due to variability in measurement in relation to the rate of disease progression and is therefore not recommended in clinical settings.

Imaging Protocol

The carotid arteries should be interrogated using state-of-the-art ultrasound equipment with a linear-array transducer operating at a fundamental frequency of at least 7 MHz. 2D measurement corresponds to the thickness of the first 2 echogenic lines of the arterial wall of the common carotid artery, 1–2 cm upstream of the carotid bifurcation, in the far wall. The image represents the far wall of the common carotid artery showing the intima and media, defined by the distance between the endothelium and the external elastic membrane. For clinical purposes, the distance between the endothelium and the tunica adventitia is measured to obtain the CIMT. The CIMT should be parallel to the ultrasound beam and the measurement should be performed in the distal part of the common artery using a diastolic frame and excluding carotid plaque. The use of contrast agents in this setting is not recommended. B-mode imaging is preferred over M-mode imaging even though M-mode has better temporal resolution but it allows the scanning of one single point [2, 4].

Reporting

Echo scientific societies do not recommend partial reporting, but CIMT may be performed for risk stratification purposes. It should be stated clearly that the exam does not replace the conventional carotid duplex ultrasound, as clinically indicated.

Significant Carotid Artery Disease

Color-flow duplex scan is the appropriate technique to identify carotid plaques, determine the degree of stenosis, and assess plaque structure. Two main features are always analyzed: morphology (by 2D echo) and hemodynamics (by Doppler and color codification). Diameter and area may be measured during 2D echo. American Society of Echocardiography 2020 recommends that first, the carotid arterial wall be visually scanned for the presence of protuberant plaque, and if absent, then a CIMT measurement be performed to identify the presence of diffuse plaque (defined as CIMT ≥1.5 mm) (Table 20.2). If performed, CIMT should be measured as described in the American Society of Echocardiography Consensus Statement on the Use of Carotid Ultrasound to Identify Subclinical Vascular Disease and Evaluate Cardiovascular Risk.

Table 20.2 Carotid plaque types and associated risk

Grade	Plaque type	Plaque thickness	Risk
0	No plaque	CIMT <1.5 mm	Very low
1	Protuberant	CIMT <1.5 mm	Low
2	Protuberant or diffuse	CIMT 1.5–2.4 mm	Intermediate
3	Protuberant or diffuse	CIMT ≥2.5 mm	High

Modified from Johri et al., American Society of Echocardiography 2020 [4]

Table 20.3 Doppler criteria to assess stenosis severity

Degree of stenosis %	ICA/PSV cm/s	Plaque estimates %	ICA/EDV cm/s	ICA CCA PSV ratio
Normal	<125	0	<40	<2.0
<50	<125	<50	<40	<2.0
50–69	125–230	>50	40–100	2.0–4.0
>70	>230	>50	>100	>4.0
Subtotal occlusion	Variable	>50 narrow lumen	>0	Variable
Total occlusion				NA

CCA common carotid artery, *EDV* end-diastolic velocity, *ICA* internal carotid artery, NA, not applicable *PSV* peak systolic velocity

The combination of morphology, diameter, and hemodynamics allows the quantification of the degree of stenosis (see Table 20.3).

In 2003, the American Society of Radiology held a conference and standardized the ultrasound criteria to determine stenosis [4]. They recommended duplex velocity criteria (measurements of internal carotid artery peak systolic velocity and end-diastolic velocity as well as the internal carotid artery /common carotid artery peak systolic velocity ratio) and morphological characteristics (Table 20.1). The classification by Grant 2003 remains the most used and recommended criteria in clinical practice [5]. The disadvantages of Duplex Ultrasound include limited visualization of the proximal common carotid artery and distal internal carotid artery and technical difficulties related to the patient's physical condition (e.g. obesity, heart failure, postoperative status). Also, there are no widely acknowledged standardized criteria for pseudo-occlusion on ultrasound. Furthermore, contrast-enhanced ultrasound is increasingly being used to evaluate patients with known or suspected atherosclerosis; it can help identify carotid plaque ulcerations, differentiate occlusion from pseudo occlusion, identify carotid dissection, and identify intraplaque neovascularization. With improved technology, the accuracy of this imaging test has increased significantly over time [6].

Risk Stratification with Carotid Plaque

A simple approach for early detection of atherosclerotic disease is to assess, at rest, also carotid ultrasound for the detection of subclinical carotid atherosclerosis that has the same value as coronary subclinical atherosclerosis to improve risk prediction and re-classification compared with conventional risk factors [7]. There is a moderate correlation between carotid and coronary stenosis and between carotid and coronary calcification [8]. The presence of a subclinical and pre-obstructive carotid lesion is associated with a higher likelihood of subsequent events. Incremental value of carotid plaque assessment is especially useful in patients without inducible ischemia, as the incidence of hard events is reduced to 0.34% annually when stress echo is normal for wall motion in patients with the absence of carotid plaques, and increases four-fold in the presence of any carotid plaque and no regional wall motion abnormality during stress echo [9]. Atherosclerotic plaque detection by carotid ultrasound may be considered a risk modifier in the cardiovascular risk assessment of asymptomatic subjects but is not recommended by the European Society of Cardiology guidelines 2019 [10]. With the systematic application of carotid scans to patients referred to stress echo, indications can be extended [11].

Plaque Characterization

Plaque composition can be even more important than plaque severity in determining plaque vulnerability and prognosis, and carotid ultrasound can identify the composition of atherosclerotic plaques, with lipid and hemorrhagic plaques hypoechoic, fibrotic plaques hyperechoic, and calcified plaques hyperechoic with shadowing and increased ultrasound, as shown by in vitro [12–14] and in vivo studies [15–17]. In particular, lipid-rich necrotic core, plaque neovascularization with dense vasa vasorum network, intraplaque hemorrhage, and perivascular plaque inflammation are strong predictors of plaque vulnerability and subsequent events, while plaque calcification is a sign of plaque stability [18, 19]. Although computed tomography and especially magnetic resonance imaging offer more relevant information on plaque characterization, ultrasound may offer some clues relevant to plaque characterization and prognosis. When a carotid plaque shows features of vulnerability, also the contralateral carotid plaque shows similar features of vulnerability, suggesting the presence of a systemic, generalized activation of the atherosclerotic process [20]. Vulnerable, complex carotid plaques by ultrasound are more often associated with indices of systemic inflammation such as C-reactive protein and accompany the phase of instabilization of chronic coronary syndromes suggesting, again, that the plaque instability is not confined to coronary plaques [21]. Vulnerable carotid plaques also respond better to statin therapy [22], likely for their higher lipid content, and more susceptible to stabilization than fibrotic tissue. Reliable characterization of plaque tissue content and features suggestive of plaque instability (ulceration, thin fibrous cap) is not yet available using standard carotid ultrasound techniques. Plaques may be characterized as homogeneous (i.e., of uniform echogenicity) or as heterogeneous. Highly echogenic portions of heterogeneous plaques may correspond to areas of calcification, whereas echolucent areas may represent either lipid or hemorrhagic content [20, 21]. The presence of significant calcification is indicated by shadowing or a signal void beyond the highly echogenic calcium. Homogeneous, hyperechogenic, and with regular outer borders, without plaque neo-vascularization from the vascular luminal side after contrast, are less vulnerable than inhomogeneous, hypoechoic plaques with positive intra-plaque neovascularization localized to plaque shoulder with contrast-enhanced ultrasound, which shows larger lipoid-rich necrotic cores and more frequent intraplaque hemorrhage, and are an inde-

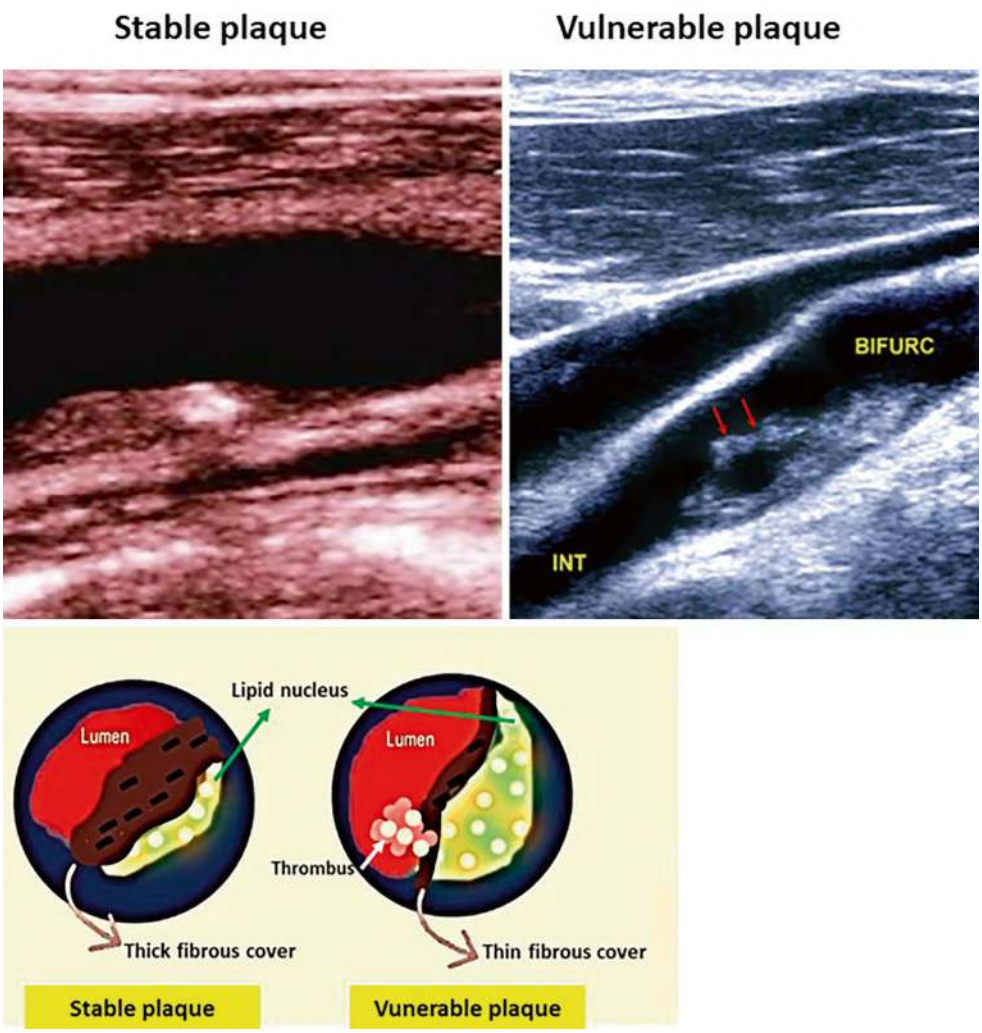


Fig. 20.2 Subjective assessment of carotid plaque echogenicity.On the left, a stable plaque; on the right, a vulnerable plaque. In the lower panel: schematic drawing of the plaques adapted from Falk E at al [26].

Table 20.4 Ultrasound criteria for carotid plaque vulnerability

	Vulnerable plaque	Stable plaque
Plaque severity	Mild to severe	Mild to severe
Homogeneity	Dishomogeneous	Homogeneous
Echodensity	Hypoechoic (lipidic core)	Hyperechoic (calcium)
Intimal profile	Irregular (ulcer)	Smooth
Contrast	Intraplaque (Vascularized)	Nonvascularized
Videodensitometry	Average low, skewed	Average high, plateau-like

pendent predictor of cardiovascular events even in patients with negative stress echocardiography (Fig. 20.2). This approach started in the early eighties and is now revived under the radiomics approach, consisting of an advanced mathematical quantitative description of the image through methods of artificial intelligence. Quantitative methods of plaque radiomics will greatly enhance the diffusion and the impact of plaque characterization by ultrasound [23–25] (Table 20.4).

References

1. Saba L, Loewe C, Weikert T, Williams MC, Galea N, Budde RPJ, Vliegenthart R, Velthuis BK, Francone M, Bremerich J, Natale L, Nikolaou K, Dacher JN, Peebles C, Caobelli F, Redheuil A, Dewey M, Kreitner KF, Salgado R. State-of-the-art CT and MR imaging and assessment of atherosclerotic carotid artery disease: standardization of scanning protocols and measurements-a consensus document by the European Society of Cardiovascular Radiology (ESCR). Eur Radiol. 2023;33(2):1063–87. https://doi.org/10.1007/s00330-022-09024-7.
2. Stein JH, Korcarz CE, Hurst RT, et al. Use of carotid ultrasound to identify subclinical vascular disease and evaluate cardiovascular disease risk: a consensus statement from the American Society of Echocardiography Carotid Intima-Media Thickness Task Force. J Am Soc Echocardiogr. 2008;21:93–111.

3. Polak JF, Alexandrov AV. Accuracy of the Society of Radiologists in Ultrasound (SRU) Carotid Doppler velocity criteria for grading North American Symptomatic Carotid Endarterectomy Trial (NASCET) stenosis: a meta-analysis. J Ultrasound Med. 2023;42(7):1423–35. https://doi.org/10.1002/jum.16150.
4. Johri AM, Nambi V, Naqvi TZ, Feinstein SB, Kim ESH, Park MM, Becher H, Sillesen H. Recommendations for the assessment of carotid arterial plaque by ultrasound for the characterization of atherosclerosis and evaluation of cardiovascular risk: from the American Society of Echocardiography. J Am Soc Echocardiogr. 2020;33(8):917–33. https://doi.org/10.1016/j.echo.2020.04.021.
5. Grant EG, Benson CB, Moneta GL, Alexandrov AV, Baker JD, Bluth EI, Carroll BA, Eliasziw M, Gocke J, Hertzberg BS, Katarick S, Needleman L, Pellerito J, Polak JF, Rholl KS, Wooster DL, Zierler E, Society of Radiologists in Ultrasound. Carotid artery stenosis: gray-scale and Doppler ultrasound diagnosis--Society of Radiologists in Ultrasound consensus conference. Ultrasound Q. 2003;19(4):190–8. https://doi.org/10.1097/00013644-200312000-00005.
6. Cassola N, Baptista-Silva JC, Nakano LC, Flumignan CD, Sesso R, Vasconcelos V, Carvas Junior N, Flumignan RL. Duplex ultrasound for diagnosing symptomatic carotid stenosis in the extracranial segments. Cochrane Database Syst Rev. 2022;7(7):CD013172. https://doi.org/10.1002/14651858.CD013172.pub2.
7. Baber U, Mehran R, Sartori S, Schoos MM, Sillesen H, Muntendam P, et al. Prevalence, impact, and predictive value of detecting subclinical coronary and carotid atherosclerosis in asymptomatic adults: the BioImage study. J Am Coll Cardiol. 2015;65:1065–74.
8. Bytyçi I, Shenouda R, Wester P, Henein MY. Carotid atherosclerosis in predicting coronary artery disease: a systematic review and meta-analysis. Arterioscler Thromb Vasc Biol. 2021;41(4):e224–37. https://doi.org/10.1161/ATVBAHA.120.315747.
9. Ahmadvazir S, Pradhan J, Khattar RS, Senior R. Long-term prognostic value of simultaneous assessment of atherosclerosis and ischemia in patients with suspected angina: implications for routine use of carotid ultrasound during stress echocardiography. J Am Soc Echocardiogr. 2020;33:559–69.
10. Knuuti J, Wijns W, Saraste A, Capodanno D, Barbato E, Funck-Brentano C, Prescott E, Storey RF, Deaton C, Cuisset T, Agewall S, Dickstein K, Edvardsen T, Escaned J, Gersh BJ, Svitil P, Gilard M, Hasdai D, Hatala R, Mahfoud F, et al. 2019 ESC Guidelines for the diagnosis and management of chronic coronary syndromes. Eur Heart J. 2020;41(3):407–77. https://doi.org/10.1093/eurheartj/ehz425.
11. Picano E, Pierard L, Peteiro J, Djordjevic-Dikic A, Sade LE, Cortigiani L, Van De Heyning CM, Celutkiene J, Gaibazzi N, Ciampi Q, Senior R, Neskovic AN, Henein M. The clinical use of stress echocardiography in chronic coronary syndromes and beyond coronary artery disease: a clinical consensus statement from the European Association of Cardiovascular Imaging of the ESC. Eur Heart J Cardiovasc Imaging. 2024;25(2):e65–90. https://doi.org/10.1093/ehjci/jead250.
12. Picano E, Landini L, Distante A, Benassi A, Sarnelli R, L'Abbate A. Fibrosis, lipids, and calcium in human atherosclerotic plaque. In vitro differentiation from normal aortic walls by ultrasonic attenuation. Circ Res. 1985;56(4):556–62. https://doi.org/10.1161/01.res.56.4.556.
13. Picano E, Landini L, Lattanzi F, Mazzarisi A, Sarnelli R, Distante A, et al. The use of frequency histograms of ultrasonic backscatter amplitudes for detection of atherosclerosis in vitro. Circulation. 1986;74:1093–8.
14. Picano E, Landini L, Lattanzi F, Salvadori M, Benassi A, L'Abbate A. Time domain echo pattern evaluations from normal and atherosclerotic arterial walls: a study in vitro. Circulation. 1988;77(3):654–9. https://doi.org/10.1161/01.cir.77.3.654.
15. Urbani MP, Picano E, Parenti G, Mazzarisi A, Fiori L, Paterni M, Pelosi G, Landini L. In vivo radiofrequency-based ultrasonic tissue characterization of the atherosclerotic plaque. Stroke. 1993;24(10):1507–12. https://doi.org/10.1161/01.str.24.10.1507.
16. Mazzone AM, Urbani MP, Picano E, Paterni M, Borgatti E, De Fabritiis A, Landini L. In vivo ultrasonic parametric imaging of carotid atherosclerotic plaque by videodensitometric technique. Angiology. 1995;46(8):663–72. https://doi.org/10.1177/000331979504600804.
17. Nicolaides A, Panayiotou AG. Screening for atherosclerotic cardiovascular risk using ultrasound. J Am Coll Cardiol. 2016;67(11):1275–77. https://doi.org/10.1016/j.jacc.2016.01.016. Latha S, Muthu P, Dhanalakshmi S, Kumar R, Lai KW, Wu X. Emerging feature extrac tion techniques for machine learning-based classification of carotid artery ultrasound images. Comput Intell Neurosci. 2022;2022:1847981
18. Huang R, DeMarco JK, Ota H, Macedo TA, Abdelmoneim SS, Huston J III, et al. Prognostic value of intraplaque neovascularization detected by carotid contrast-enhanced ultrasound in patients undergoing stress echocardiography. J Am Soc Echocardiogr. 2021;34:614–24.
19. Petersen C, Peçanha PB, Venneri L, Pasanisi E, Pratali L, Picano E. The impact of carotid plaque presence and morphology on mortality outcome in cardiological patients. Cardiovasc Ultrasound. 2006;4:16. https://doi.org/10.1186/1476-7120-4-16.
20. Ibrahimi P, Jashari F, Johansson E, Gronlund C, Bajraktari G, Wester P, Henein MY. Vulnerable plaques in the contralateral carotid arteries in symptomatic patients: a detailed ultrasound analysis. Atherosclerosis. 2014;235(2):526–31. https://doi.org/10.1016/j.atherosclerosis.2014.05.934.
21. Lombardo A, Biasucci LM, Lanza GA, Coli S, Silvestri P, Cianflone D, Liuzzo G, Burzotta F, Crea F, Maseri A. Inflammation as a possible link between coronary and carotid plaque instability. Circulation. 2004;109(25):3158–63. https://doi.org/10.1161/01.CIR.0000130786.28008.56.
22. Ibrahimi P, Jashari F, Bajraktari G, Wester P, Henein MY. Ultrasound assessment of carotid plaque echogenicity response to statin therapy: a systematic review and meta-analysis. Int J Mol Sci. 2015;16(5):10734–47. https://doi.org/10.3390/ijms160510734.
23. Skandha SS, Nicolaides A, Gupta SK, Koppula VK, Saba L, Johri AM, Kalra MS, Suri JS. A hybrid deep learning paradigm for carotid plaque tissue characterization and its validation in multicenter cohorts using a supercomputer framework. Comput Biol Med. 2022;141:105131. https://doi.org/10.1016/j.compbiomed.2021.105131.
24. Paraskevas KI, Mikhailidis DP, Ringleb PA, Brown MM, Dardik A, Poredos P, Gray WA, Nicolaides AN, Lal BK, Mansilha A, Antignani PL, de Borst GJ, Cambria RP, Loftus IM, Lavie CJ, Blinc A, Lyden SP, Matsumura JS, Jezovnik MK, Bacharach JM, et al. An international, multispecialty, expert-based Delphi Consensus document on controversial issues in the management of patients with asymptomatic and symptomatic carotid stenosis. J Vasc Surg. 2024;79(2):420–435.e1. https://doi.org/10.1016/j.jvs.2023.09.031.
25. Alexandratou M, Papachristodoulou A, Li X, Partovi S, Davidhi A, Rafailidis V, Prassopoulos P, Kamperidis V, Koutroulou I, Tsivgoulis G, Grigoriadis N, Krogias C, Karapanayiotides T. Advances in noninvasive carotid wall imaging with ultrasound: a narrative review. J Clin Med. 2022;11(20):6196. https://doi.org/10.3390/jcm11206196.
26. Falk E, Shah PK, Fuster V. Coronary plaque disruption. Circulation. 1995;92:657–71.

Diseases of the Aorta

21

Michael Y. Henein, Mary Sheppard, Harry Smith, John R. Pepper, and Mario Petro

Congenitally Small Aortic Root

Please refer to chapter aortic valve disease, Chap. 2.

Acute Aortic Syndrome (AAS)

Acute aortic syndrome (AAS), as defined, encompasses life-threatening aortic conditions characterized by acute onset and shared pathophysiological features. It includes aortic dissection, intramural hemoatoma, and penetrating atherosclerotic ulcer. Acute aortic dissection is a surgical emergency that requires accurate diagnosis and prompt management. A number of classifications exist, the simplest of which classifies aortic dissection according to the location of the entry point into: type "A," which involves all forms that include the ascending aorta, and type "B," which does not involve the ascending aorta. While type "A" is always an emergency diagnosis and management, type "B" can be managed medically or conservatively. Mortality from type "A" dissection may be up to 60% within the first 24 hours, 80% over the first 2 weeks, and 90% within 3 months of acute attack. Dissection of the proximal ascending aorta can often be seen on transthoracic echocardiographic imaging, and even those involving the distal ascending aorta may occasionally be detected. However, transthoracic echo cannot always exclude "A" dissection. Instead, transesophageal echo is the investigation of choice when there is a suspicion [1–3].

The diagnostic marker of dissection is the luminal flap that can take different shapes and forms during the cardiac cycle according to its size.

(a) Freely mobile flap with detached edges that prolapse back into the left ventricle in diastole. This tends to hold the leaflets apart and the valve open during diastole resulting in severe aortic regurgitation (Fig. 21.1).
(b) Mobile flap that is distal to the aortic valve leaflets. Blood fills the false lumen at the entry point which may thrombose if left untreated. This results in dilatation of the distal part of the aortic root and ascending aorta and consequently significant aortic regurgitation. Identifying the true and false aortic lumens depends on the position of the dissection flap in the aortic lumen and its relationship to the image planes and flow patterns (Fig. 21.2). In acute presentation, the aortic lumen with normal blood flow velocities is the true lumen in comparison to the other lumen with significantly lower velocities. Late diagnosed cases may show no flow in the false lumen but rather organized blood clots.
(c) Co-incidental chronic dissection which has settled spontaneously and is thrombosed (organized) in the distal ascending aorta. Such cases may be followed up clinically without the need for intervention (Fig. 21.3).

An apparent dissection flap may be mimicked on transthoracic echo by other conditions such as calcified aortic valve, pacing leads, aortic wall calcification, or pericardial effusion. However, an independently moving flap-like layer in a dilated ascending aorta is suggestive of dissection until proven otherwise (Fig. 21.4; Video 1).

Transesophageal echo provides clear images of the aortic root and ascending aorta in the majority of patients with suspected aortic dissection. The entry site is usually identified, the flap is clearly seen, and the extent of dissection, to the arch or even to the descending aorta, can be followed. Associated coronary artery or carotid artery dissection can

Supplementary Information The online version contains supplementary material available at https://doi.org/10.1007/978-3-031-95894-6_21.

M. Y. Henein (✉)
Imperial College London, London, UK

Siena University, Siena, Italy
e-mail: m.henein@imperial.ac.uk

M. Sheppard · H. Smith · J. R. Pepper · M. Petro
Royal Brompton Hospital, London, UK

© The Author(s), under exclusive license to Springer Nature Switzerland AG 2025

M. Y. Henein (ed.), *Clinical Echocardiography*, https://doi.org/10.1007/978-3-031-95894-6_21

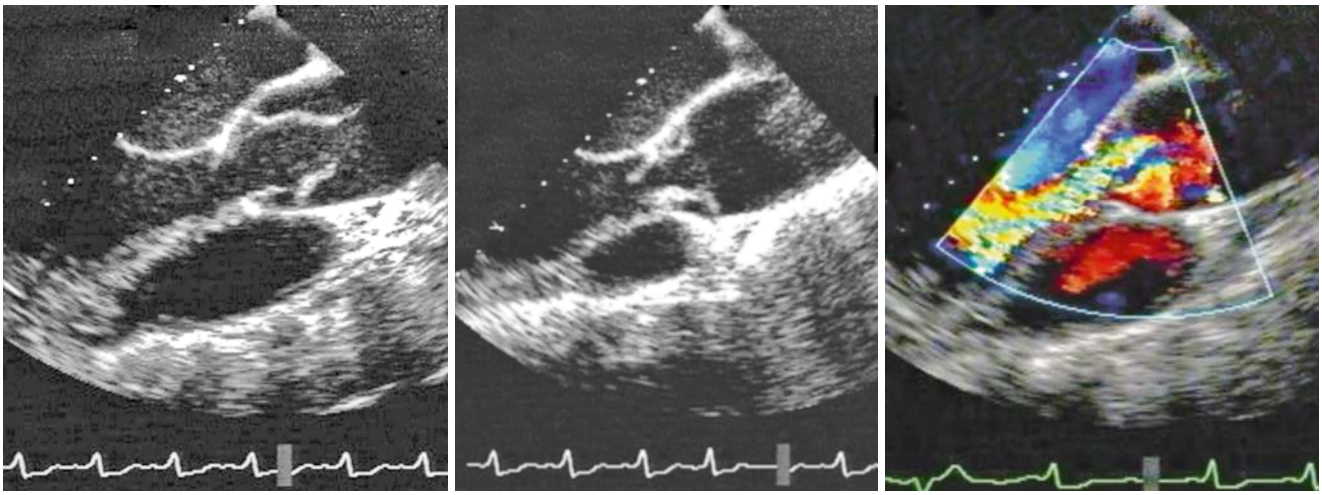


Fig. 21.1 Transesophageal echo from a patient with aortic dissection. Note the freely mobile flap in the ascending aorta in systole (*left*) which prolapses into the left ventricle in diastole (*middle*) resulting in severe aortic regurgitation on color flow Doppler (*right*)

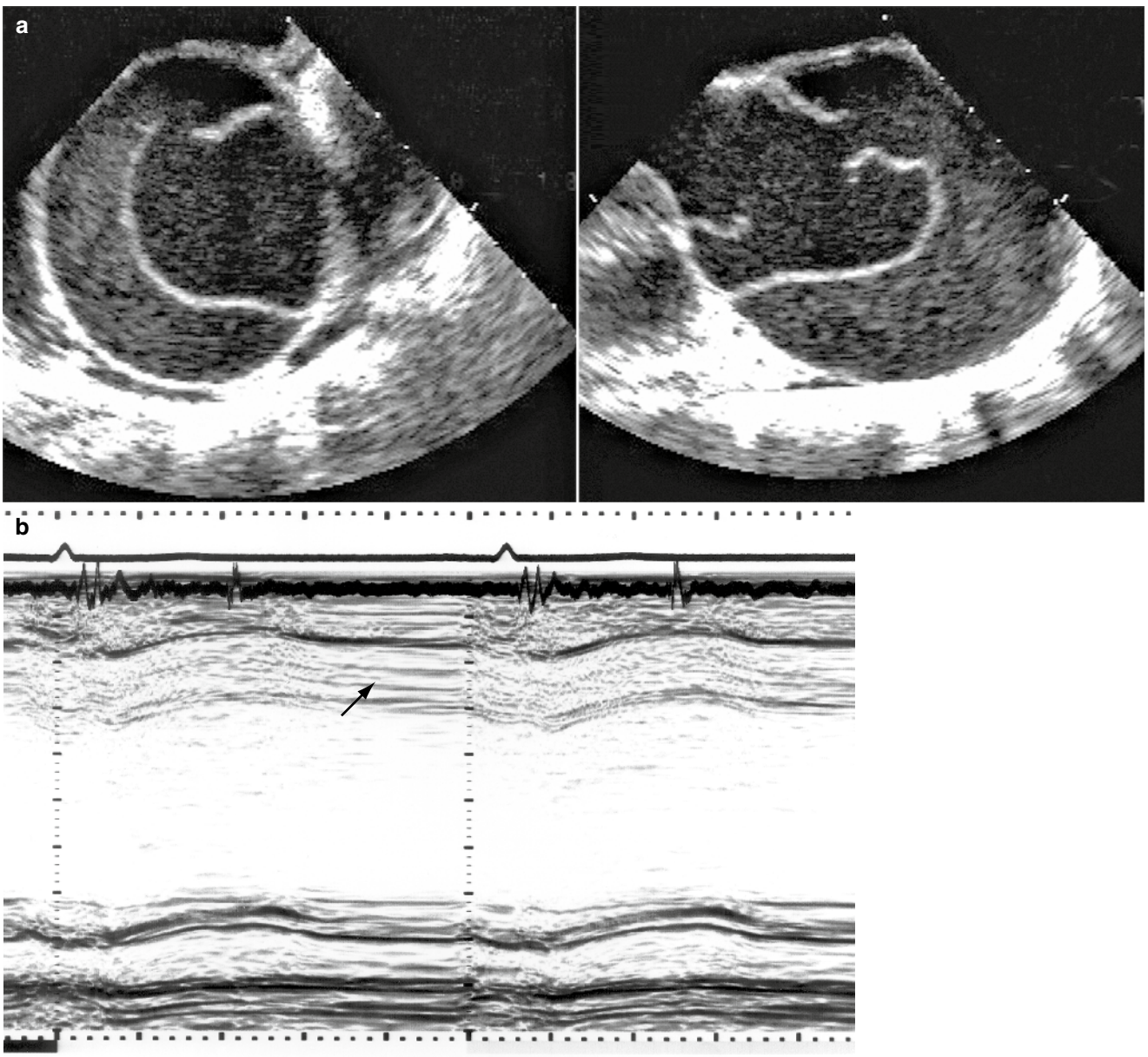


Fig. 21.2 (**a**) TOE of the aorta showing dilated ascending aorta with a dissection flap in the middle separating the true from the false lumen. (**b**) M-mode of the proximal ascending aorta showing the true aortic lumen and a clotted dissection (*arrow*)

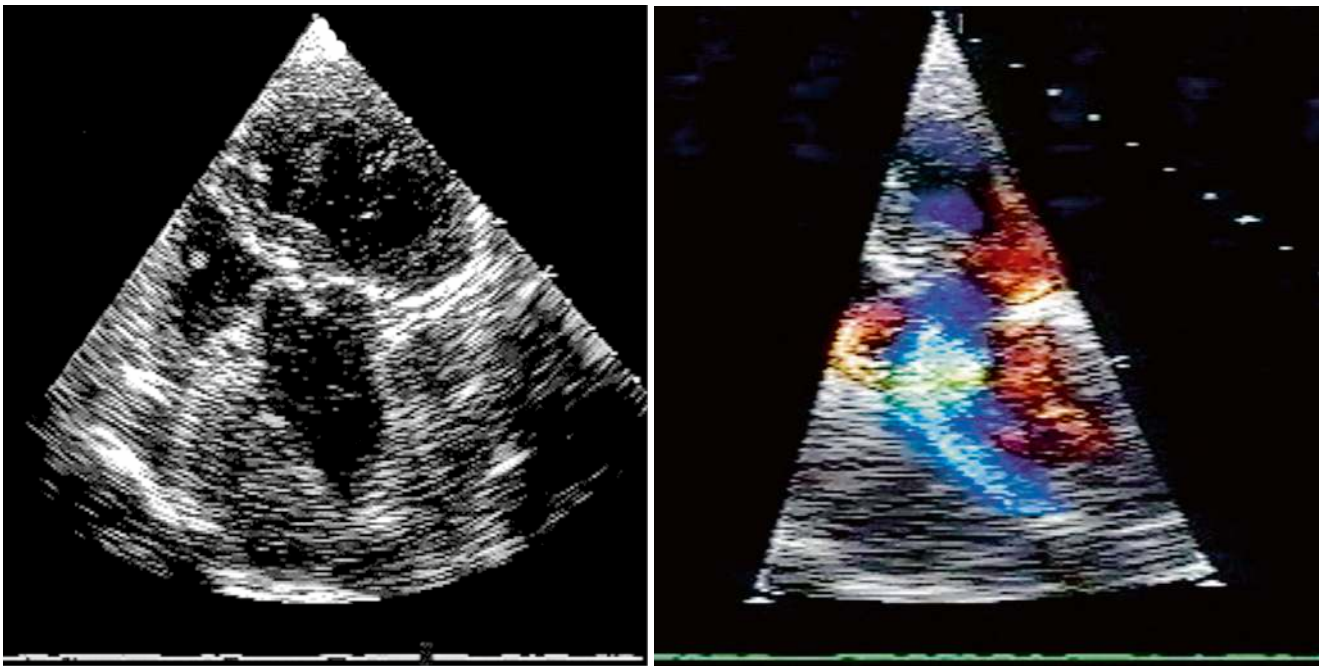


Fig. 21.3 Apical four-chamber view from an elderly patient with dissection in the distal ascending aorta. Note the organized thrombus in the false lumen (*left*) and the blood flow in the true lumen parallel to the flap edge (*right*)

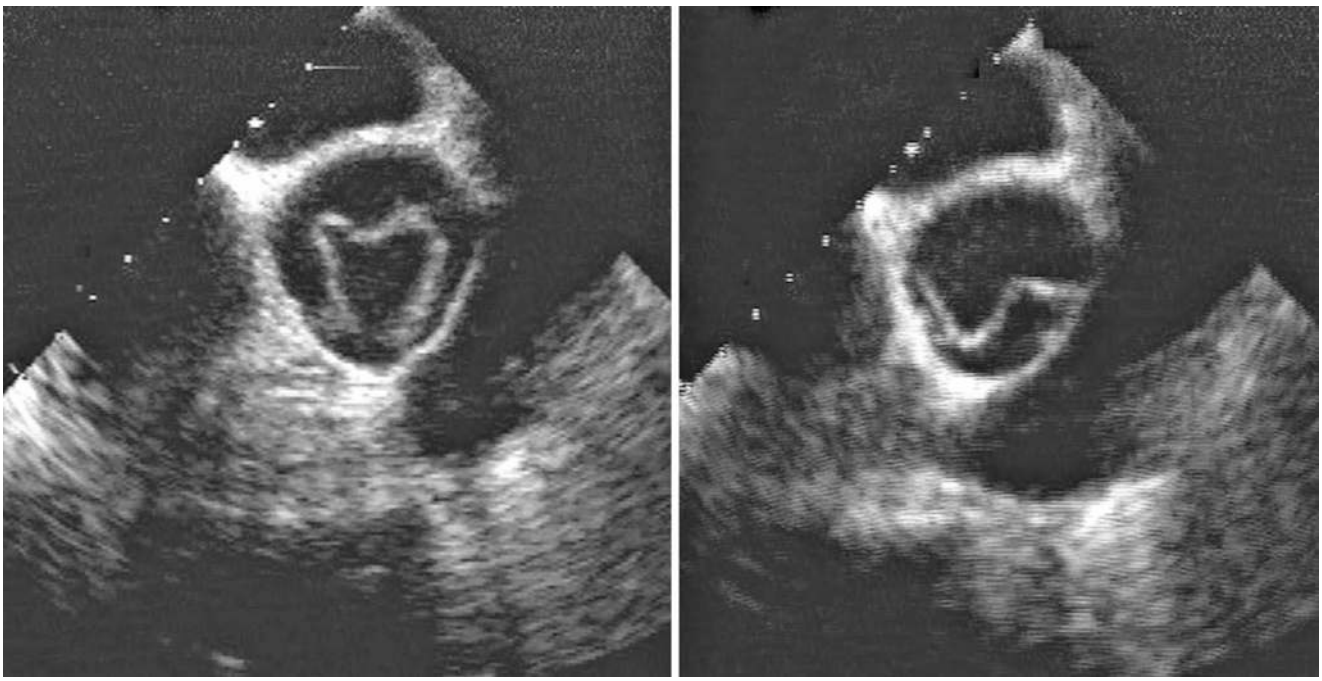


Fig. 21.4 Short axis of the ascending aorta from a patient with dissection showing freely mobile flap, changing its shape during the cardiac cycle

be confirmed, although it occurs in a very small percentage of patients (Fig. 21.5) [4–6].

Color flow Doppler with transthoracic and transesophageal echo imaging helps in identifying the entry site and in assessing the severity of aortic regurgitation. Transesophageal echo has similar sensitivity to cardiovascular magnetic resonance (CMR) and computed tomography (CT) scanning for diagnosing aortic dissection but lower specificity, particularly for the ascending aorta. This has been attributed to the extent of aortic calcification, plaque formation, debris, and echo reverberations. It has the advantage, though, of being performed at bedside and on ventilated patients in the intensive care unit [7, 8].



Fig. 21.5 Transverse section in the ascending aorta demonstrating a dissection flap dividing the aorta into two lumens

Management

The classification of dissection of the aorta is closely related to the optimal initial treatment; thus, Type A dissection involving either the ascending aorta or the ascending arch and descending aorta is an indication for urgent surgical repair. A Type B dissection, which classically originates in the proximal third of the descending aorta immediately distal to the origin of the left subclavian artery, is initially treated by medical therapy with surgical repair reserved for selected patients, 8–12 weeks later. . The objective of surgery for acute Type A aortic dissection is fourfold: to protect the aortic valve, prevent cardiac tamponade, protect the coronary ostia, and stabilize the aorta. These operations are performed using cardiopulmonary bypass, and frequently the distal aortic anastomosis is made during a period of circulatory arrest involving core cooling of the patient to between 15 °C and 18 °C for a period of approximately 20–25 min. Deep hypothermic circulatory arrest is necessary if the cross clamp needs to be opened to visualize the entry tear in the aorta, the subsequent anastomosis will be considered an open distal anastomosis rather than a closed distal anastomosis. In these instances, careful consideration is to be given to the patient and whether they are able to tolerate periods of deep hypothermic circulatory arrest. For example, octogenarian patients may benefit from a "defensive strategy" (closed anastomosis with isolated repair of the ascending aorta) when it comes to dissection repair in respect of their reduced physiological reserve [9].

The principle of the operation is to remove the area of the aorta where the entry site or tear exists and to reconstitute the layers of the aorta, both proximal and distal to this point. The complexity of surgery can vary depending on the degree of dissection, accompanying malperfusion syndrome, or any retrograde extension involving the aortic root or valve. In the vast majority of patients, it is possible to resuspend the commissures of the aortic valve, thus saving the aortic valve, the leaflets of which are usually quite normal. An interposition graft of collagen-impregnated Dacron is then placed between the two reconstructed areas of the aorta. Frequently, it is necessary to extend the distal anastomosis into the proximal part of the aortic arch. The risk of this surgery is of the order of 8–10% mortality with a 1–2% incidence of stroke. By comparison, acute operations on the descending aorta, which are not routinely done, carry a similar mortality risk and a small risk of paraplegia [10]. It is vital that these patients remain under surveillance, preferably by a surgeon interested in surgery of the aorta, and that they undergo CMR scans annually or CT scans if this is inappropriate, since they continue to suffer from aortic disease (aortopathy). In the majority of these cases, the distal part of the aorta heals and the false lumen thromboses, but in a small minority, this does not occur, and further dilatation of the descending aorta may take place, requiring intervention at a later date.

Complex aortic and aortic arch pathology can be addressed using a frozen elephant trunk (F.E.T) procedure which can create a secure landing zone for future endovascular intervention. For example, when the disease involves the proximal descending aorta or future treatment involves the descending aorta the F.E.T is a good option [11]. Historically the elephant trunk repair originally referred to a technique developed in the 1980s whereby a segment of the aortic graft hung freely in the descending aorta like an "elephant's trunk" [12]. The frozen modification incorporates a stent graft into the trunk, allowing immediate repair of the descending thoracic aorta. This is particularly useful in dissections where a distal extension is necessary to obliterate the false lumen.

Aortic dissection is the commonest cause of death in young Marfan patients, even those with no clear evidence for root dilatation. In these patients, the strongest predictor of dissection is the rate of change of the aortic root dimensions over time, using critical echocardiographic assessment. Prevention of this life-threatening problem is by aortic root replacement with a Dacron composite and artificial valve, or valve suspension procedure. Although the prophylactic results of this procedure are satisfactory, it remains a major heart surgery with potential serious complications and an eventual need for redo surgery at some stage. Recently, the development of a bespoke external aortic root support (EARS) using imaging and computer-aided design to fit the individual patient's ascending aorta has been achieved with very satisfactory protective results for vulnerable patients [14, 15].

More recently, newer classifications of acute aortic dissection have been proposed, including the introduction of the non-A, non-B acute aortic dissection, and the type, entry, and malperfusion (TEM) staging. Non-A non-B can be defined as an entry intimal tear, located beyond the left subclavian, with a retrograde extension of the dissection into the aortic arch. An alternative definition includes an entry tear located between the innominate and the left subclavian artery, with or without distal extension of the dissection. The F.E.T with interventional repair is a suitable option for this demograph where TEVAR is not suitable. TEM staging is an extension of the Stanford classification, incorporating non-A, non-B dissections, adding further clarity to the extent of the disease process [13].

Intramural Hematoma

Intramural hematoma appears as a thickening of the aortic wall, typically >5 mm, and is a more localized process compared to classic aortic dissection. Differentiating intramural hematoma from a thrombosed false lumen in aortic dissection can be challenging, particularly on transthoracic echo. A key diagnostic feature is the displacement of intimal calcification, caused by blood accumulation within the aortic media, which helps in the differential diagnosis. However, for a definitive diagnosis, additional investigations are needed, such as CT angiography or MRI, which offer superior visualization of the aorta, enabling clear distinction between intramural hematoma, dissection, and other aortic pathologies.

Penetrating Atherosclerotic Ulcer

Penetrating atherosclerotic ulcer occurs when an atherosclerotic plaque develops an ulcer that breaks through the internal elastic lamina and invades the aortic media. This process usually leads to the formation of a localized intramural hematoma. It typically presents with rough, uneven edges, along with multiple irregularities in the intimal layer, and may also be associated with localized hematoma formation.

Aortic Atherosclerotic Debris

These are small localized atherosclerotic plaques in the aortic wall that protrude into the aortic lumen and can be identified by transesophageal echo. Different grades of debris may be recognized, varying from thickened intima, atherosclerotic plaques, and mobile atheromata greater than 5 mm in diameter. An atherosclerotic aortic wall can be the source of strokes in a number of conditions [16, 17]:

(a) Patients undergo aortic clamping as part of cardiopulmonary bypass.
(b) High-risk patients with carotid or peripheral vascular disease.
(c) Patients with recurrent embolization.

Aortic Aneurysm

A dilated ascending aorta can be readily diagnosed by transthoracic echocardiography and the diameter measured from M-mode recordings. Aneurysms involving the arch or the descending thoracic aorta are better studied by transesophageal echo, CMR, or CT scanning (Figs. 21.6 and 21.7). A true aneurysm may be differentiated from a dissecting aneurysm [18, 19]. A common cause of aortic aneurysm is Marfan syndrome but the lesion may occur in the absence of external stigmata of the disease [20], commonly referred to as Marfanoid disease. According to Laplace's law, wall tension increases directly with diameter, so that a dilated aorta is inherently unstable, particularly if medial necrosis is present (Fig. 21.8). Such patients should therefore be regularly monitored for changes in aortic diameter. Patients with an aortic root exceeding 5 cm are likely to be taking prophylactic beta blocker therapy to prevent progressive aortic dilatation [20]. Aortic replacement with resuspension or replacement of the aortic valve is a commonly applied surgical management for aortic aneurysm, when the aortic diameter exceeds 5.5–6 cm [21]. Such patients are at high risk of dissection, and ideally, the operation should be performed before this occurs. Whether or not prophylactic aortic root replacement should be considered in patients with normal aortic diameter but a strong family history of dissection, particularly at a young age, remains controversial.

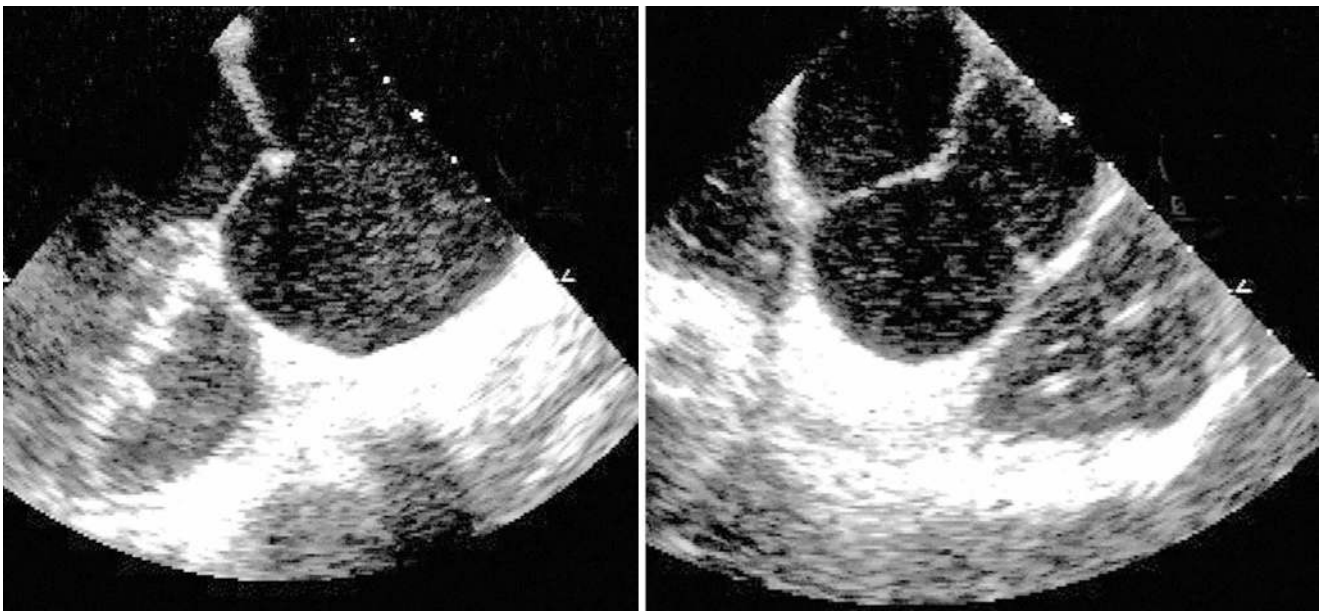


Fig. 21.6 TOE from a patient with aortic root aneurysm (localized)

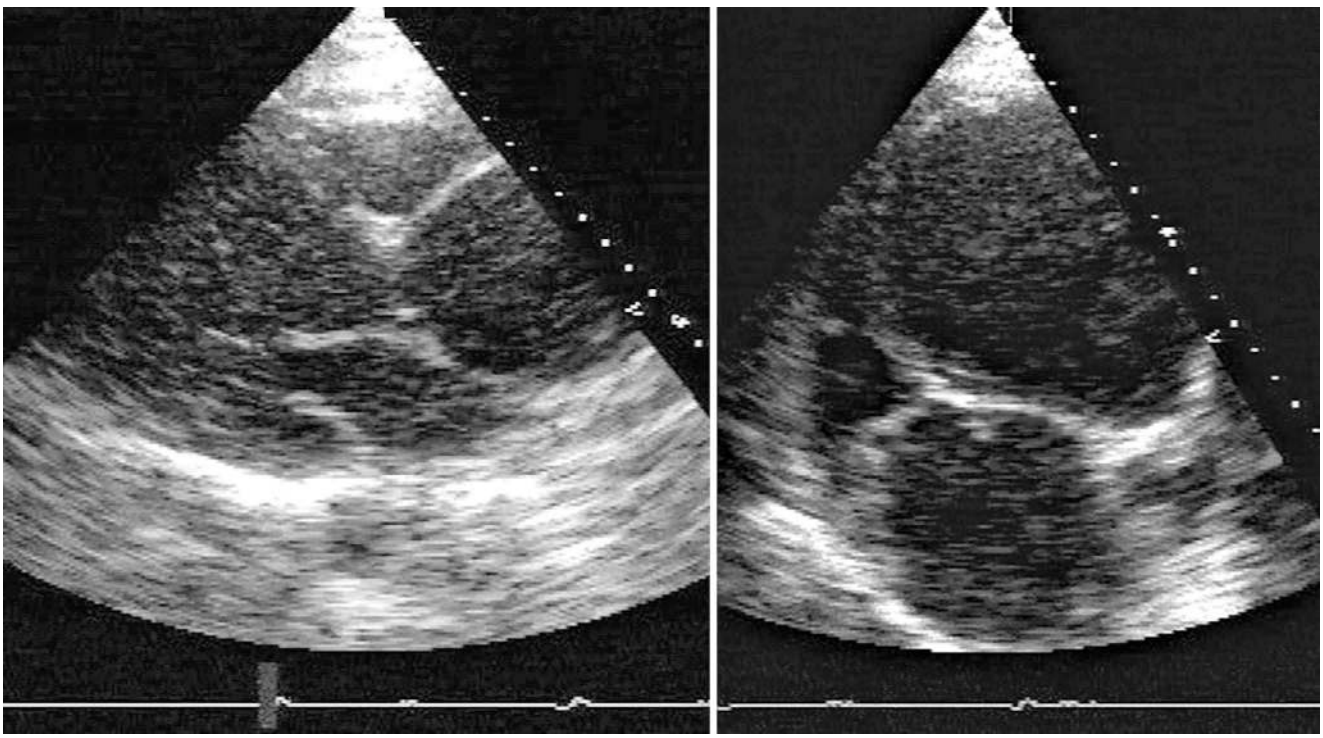


Fig. 21.7 Parasternal view from a patient with aneurysmal ascending aorta (*left*) and equivalent image from apical five-chamber views (*right*) demonstrating aneurysm diameter of 8 cm

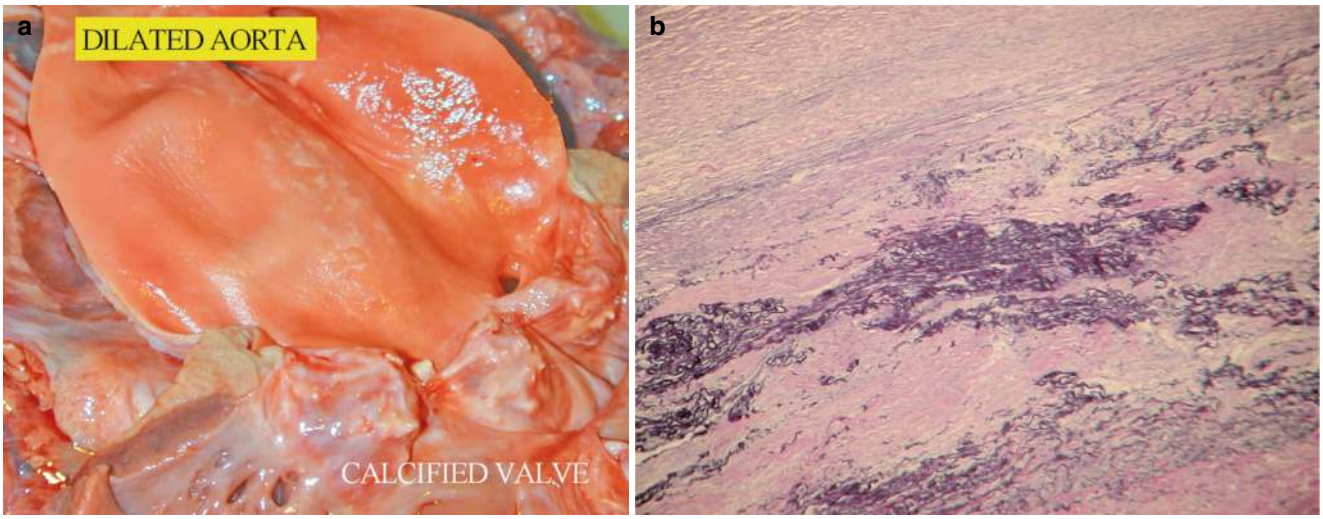


Fig. 21.8 (**a**) Section demonstrating dilated and aneurysmal ascending aorta. (**b**) Histological section from the aorta showing cystic medial necrosis characteristic of aortic aneurysm

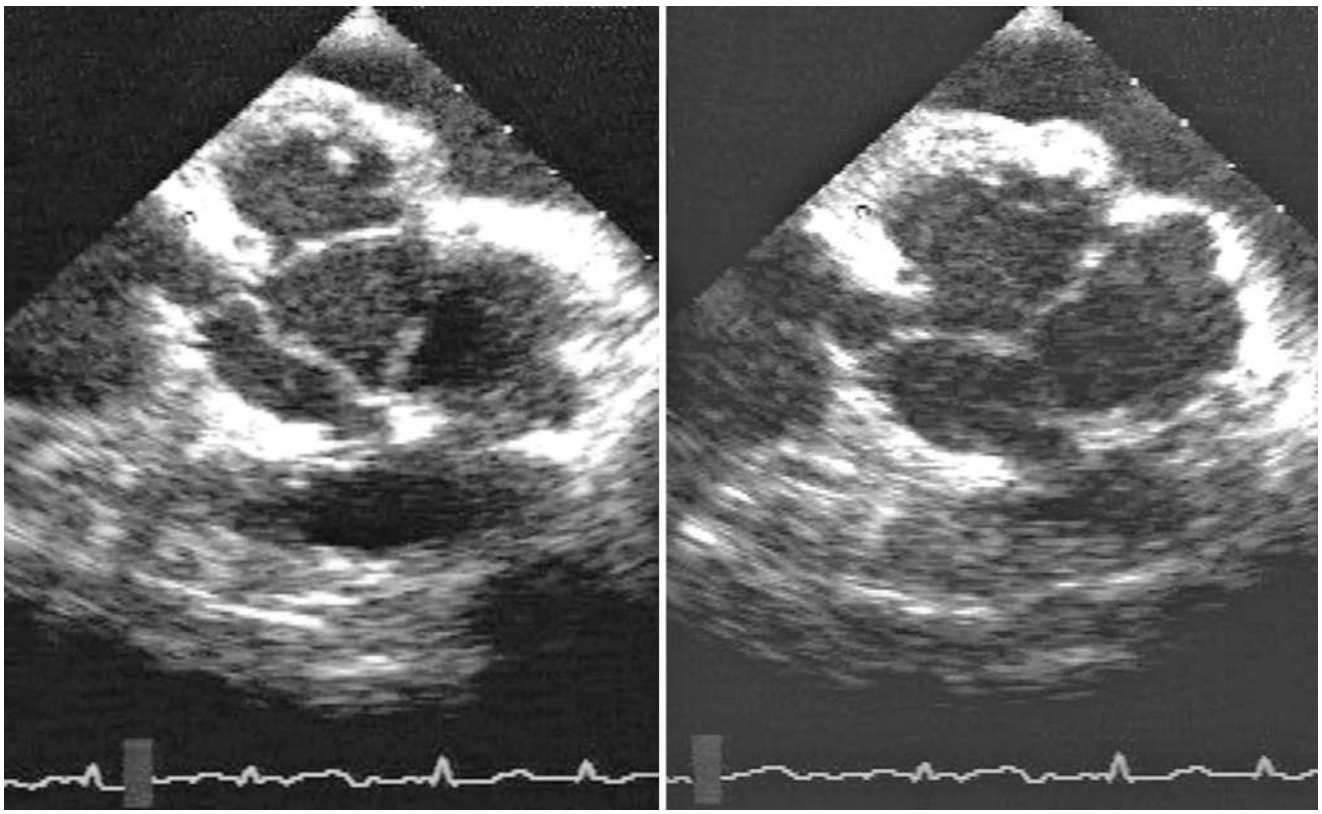


Fig. 21.9 Parasternal short axis views from a patient with aneurysmal aortic sinuses. Note the large sinus diameter and the retained clot behind the corresponding leaflet

Aortic Sinus Aneurysm

Aneurysm of the aortic sinuses has been reported in Marfan syndrome. The congenital form of aneurysmal sinuses is rare but has been reported with the sinus diameter exceeding 2.5 cm. Intact dilated sinuses carry the risk of blood clots inside them, and hence the need for prophylactic anticoagulants. Coronary sinus rupture into the right heart establishes a fistulous connection between the aorta and the right atrium or right ventricle. Color flow Doppler helps to establish the exact relationship between the aortic sinuses and right heart chambers (Figs. 21.9, 21.10, and 21.11) [21–23].

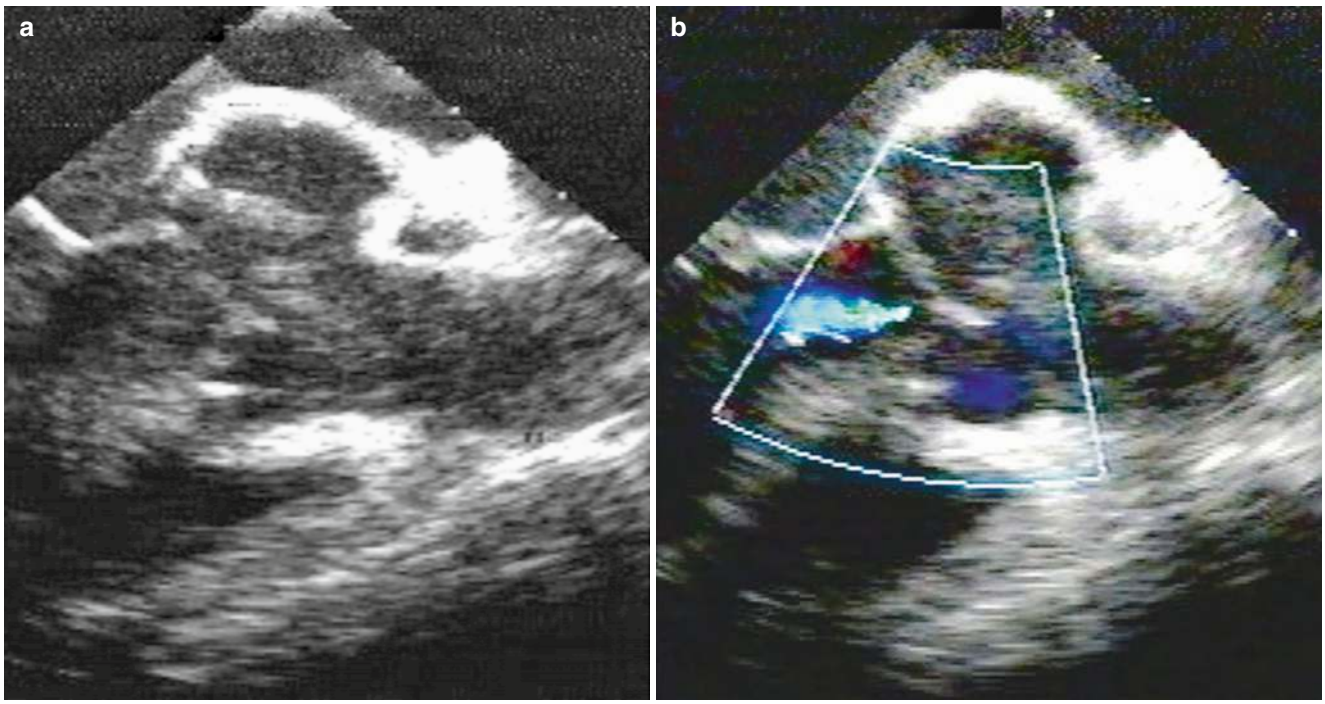


Fig. 21.10 Parasternal long axis view from the same patient showing additional mild aortic regurgitation



Fig. 21.11 TOE images of the aortic root from a patient with infective endocarditis showing ruptured sinus of Valsalva aneurysm into the right atrium demonstrating continuous flow

Aortic Root Abscess

This is a form of infective endocarditis that can involve the paravalvular tissue of the aortic root. It is commonly associated with prolongation of the PR interval and conduction disturbances. Transthoracic echo often confirms the presence of paravalvular space lesions. A well-defined abscess enlarges during systole due to the blood flowing in and out of it (Figs. 21.12 and 21.13). Aortic root abscess may consist of one or more small compartments, either in isolation or connected together. Transesophageal echocardiography, particularly the short axis view, is ideal for demonstrating an aortic root abscess, and color flow Doppler may confirm space continuity between the compartments and the aortic root. If the latter is found, it is usually demonstrated as a fistula between the cavity and the aortic root with the hemodynamics of aortic regurgitation. Aortic root abscess is a strong indication for early surgery. Small cavities may be sterilized, repaired, or grafted with pericardial tissue during surgery, followed by aortic valve replacement. Large and widely spread cavities may require the entire aortic root replacement [24, 25].

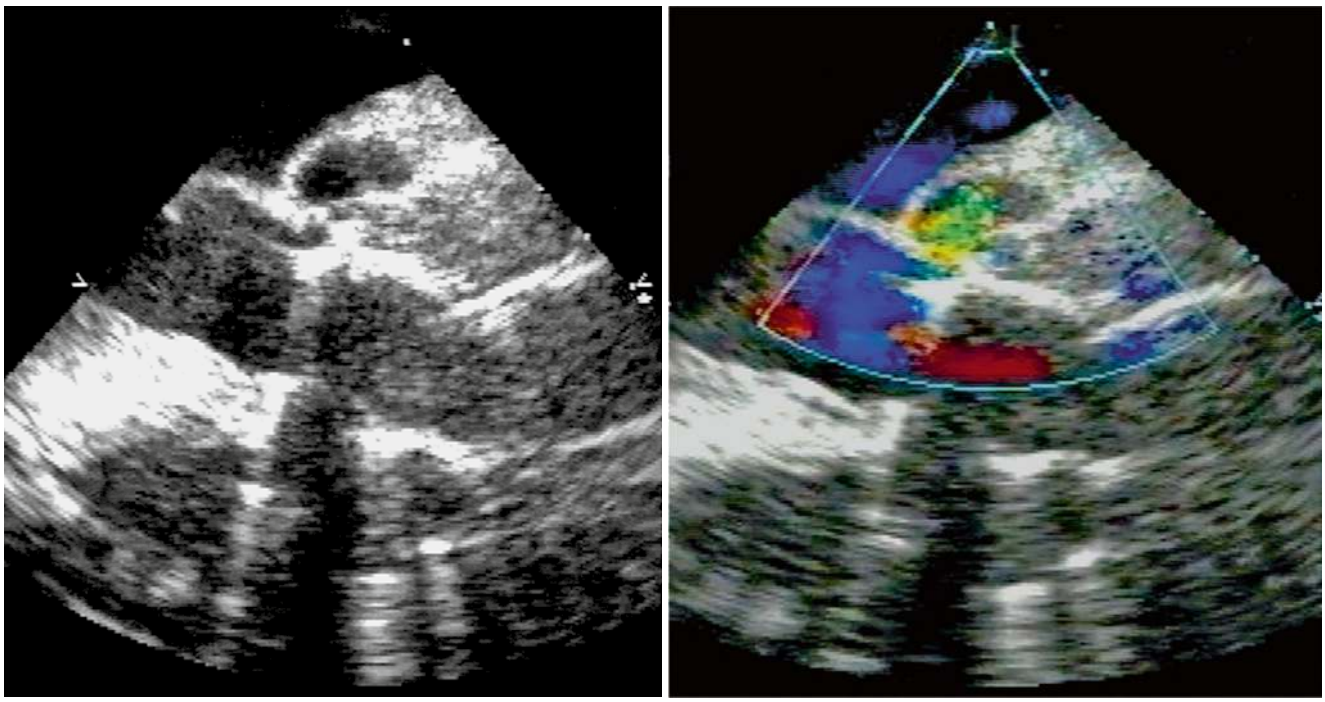


Fig. 21.12 Parasternal long axis view from a patient with localized abscess cavity

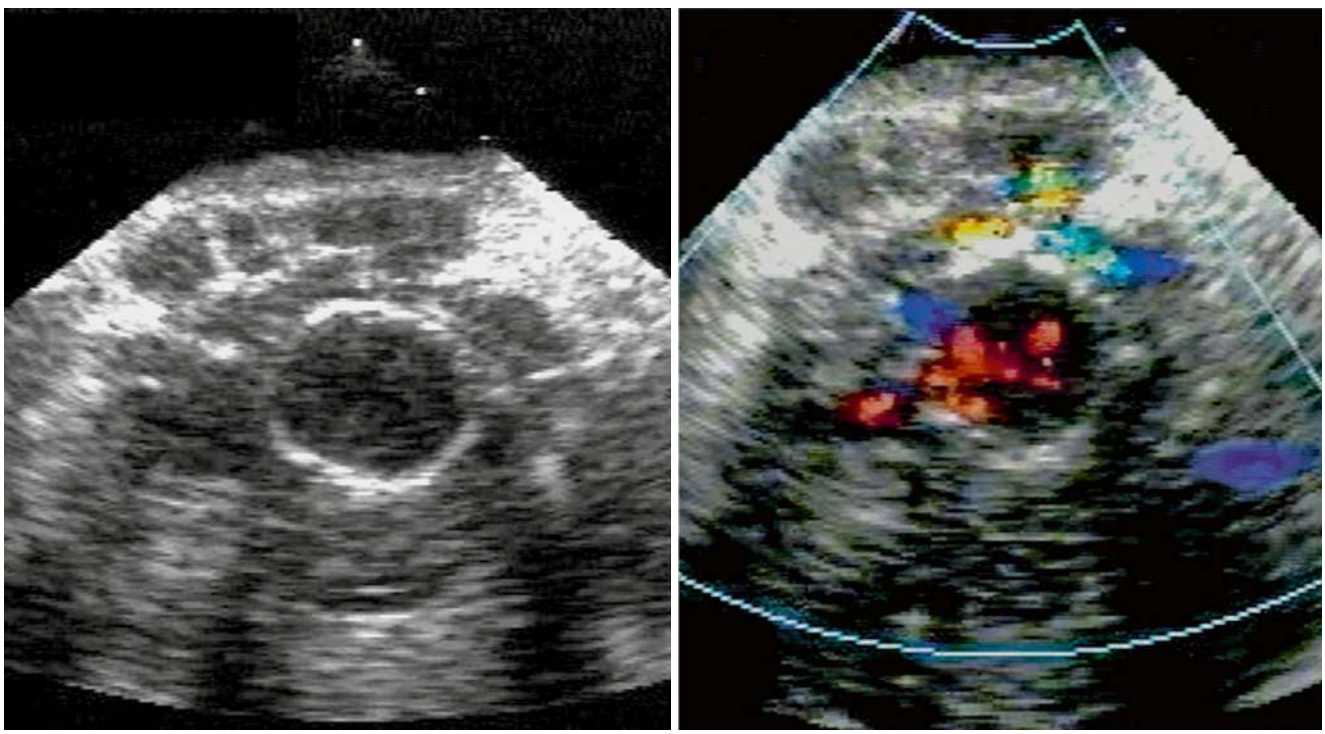


Fig. 21.13 Short axis of the aortic root showing paravalvular abscess cavities with color flow inside them

Intraoperative Echocardiography

Intraoperative transesophageal echocardiography provides an invaluable tool for assessing early results of aortic surgery. In patients with aortic dissection, the inlet site of the dissection as well as its extent site can be confirmed. The flap morphology and lumens can all be clearly visualized, and hence the right surgical strategy can be made. Early results of dissection repair (with homograft or Dacron) can be evaluated, and the aortic valve function (suspended native valve

or substitute) can be assessed. The same benefits apply to surgical procedures for aortic aneurysms. Additional information on left ventricular size and function is provided, and any pericardial collection that may delay early postoperative recovery can also be quantified.

Coarctation of the Aorta

Coarctation of the aorta is a localized aortic stricture that commonly affects the descending aorta distal to the origin of the left subclavian artery, with significant aortic narrowing. Coarctation of the aorta results in collateral development between the proximal and distal aortic segments to the coarctation in order to secure the peripheral circulation. Coarctation of the aorta may present as a single congenital anomaly or may be associated with bicuspid aortic valve, atrial septal defect, ventricular septal defect, or patent ductus arteriosus. Most patients with coarctation survive until adulthood. Coarctation is best visualized from the suprasternal notch with leftward angulation of the imaging probe (Fig. 21.14). Post-stenotic dilatation is commonly seen as well as prestenotic dilatation of the descending thoracic aorta. Color flow Doppler helps in localizing the segment involved, but continuous wave Doppler is the diagnostic technique to confirm the presence and severity of aortic coarctation. With a mild degree of aortic lumen narrowing, the velocity across the coarctation is low and its deceleration limb stops at end ejection. With significant stenosis, the systolic velocities are increased and the pressure decline continues through diastole, so-called diastolic tail. This is a diagnostic Doppler criterion for significant coarctation (Fig. 21.15) [26, 27].

From continuous wave Doppler recordings, peak pressure drop across the coarctation site can be calculated from the peak blood flow velocity using the modified Bernoulli equation. This may overestimate the pressure drop across the coarctation. Therefore, applying the eq. $4 \times (V_2^2 - V_1^2)$ as a measure of the pressure drop, where V_2 is the distal velocity and V_1 the proximal velocity, provides a closer value to that from catheterization [28]. Patients who demonstrate a modest systolic pressure drop but raised diastolic pressure drop across the coarctation site, greater than 16 mmHg, should be considered as having significant coarctation. Combined significant aortic stenosis, commonly due to a morphologically bicuspid valve, and coarctation may exist, and decision-making for managing such patients may be difficult, since severe aortic stenosis can underestimate the degree of coarctation narrowing and vice versa. The situation may be even more complex when there is additional significant left ventricular disease and low cardiac output state. Stress echo may have an important role in confirming the severity of aortic stenosis and coarctation based on changes in the effective valve orifice area and lumen diameter, respectively, with stress.



Fig. 21.14 Suprasternal images of the aortic arch and proximal descending aorta from a patient with coarctation (*left*). Note the color aliasing at the site of aortic narrowing (*right*)

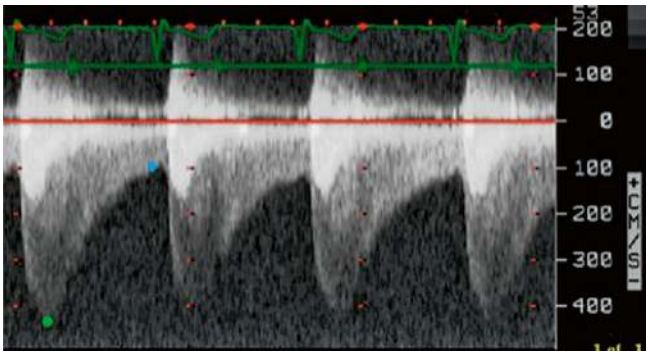


Fig. 21.15 Continuous wave Doppler recording from a patient with severe coarctation of the aorta showing velocity of 4.5 m/s equivalent to a pressure drop of 90 mmHg and a diastolic tail

Management

Significant coarctation can be treated by balloon aortoplasty (particularly in the young) or surgical resection with end-to-end anastomosis in adults who are not suitable for the non-surgical procedure. Transesophageal echo monitoring during balloon aortoplasty and surgery provides excellent imaging of the site of stricture and anastomosis. In patients with coexisting aortic stenosis and coarctation, current surgical policy recommends managing the coarctation first, preferably by percutaneous balloon intervention, followed by aortic valve replacement.

Surgery for coarctation in children is an operation that is usually carried out before the child attends school. An end-to-end anastomosis is the primary aim following resection of the coarctation segment. Interrupted sutures are used over the anterior third of the anastomosis to allow for subsequent growth. In situations where the aorta is hypoplastic particularly in the neonate more complex methods of repair are required and one of the commonest approaches is the use of the subclavian flap. By this operation, the left subclavian artery is sacrificed, and the proximal part of this artery is used as a flap to augment the area adjacent to the coarctation. Flow to the arm in the majority of instances is maintained by the collateral circulation from the suprascapular arteries.

In adult patients, coarctation of the aorta is a more complex operation as there is commonly calcification at the site of the duct, and if collaterals are not well developed, it is vital to ensure that the lower half of the body is well perfused during the clamping period. It is in this group of patients that there is an incidence of paraplegia of approximately 3–5%, which can be reduced by techniques to ensure adequate perfusion to the lower half of the body and, in some instances, a drainage of the cerebrospinal fluid via a lumbar catheter. The overall mortality for a coarctation in childhood is of the order of 1–2% and in adult life it is around 2–3%. Postoperatively, patients need to be followed up in specialized clinics for life, as there are significant complications that can arise from the coarctation, particularly if Dacron grafts are employed for the intervening segment when a direct end-to-end anastomosis cannot be achieved. Approximately two-thirds of such patients still require lifelong medical treatment for hypertension. It should be mentioned that even after complete repair of the aortic coarctation and removal of afterload, patients may present with significant impairment of left ventricular function. Recent studies have shown that the intrinsic elastic properties of the aorta in such patients are significantly abnormal, suggesting that the disease is not simply a localized stricture but rather a form of aortopathy [29–31].

Aortitis

Takayasu Disease

Takayasu disease is a form of aortitis that affects people in the second to fifth decade of life. It is characterized by intimal proliferation and fibrosis along with fibrous scarring of the arterial media. Takayasu disease affects mainly the aorta and its major branches, more markedly at the arterial origin. Clinically, the disease is manifested by weak or absent pulses along the arterial course. Takayasu aortitis rarely affects the aortic root, but when it does occur, it results in aortic regurgitation and post-stenotic dilatation. An echocardiogram may be inconclusive, but in some cases, significant diffusely thickened aortic wall may be demonstrated by two-dimensional (2D) echo imaging. This picture should be differentiated from an aortic root abscess, where the site of infection is always localized to one segment of the root. Once the diagnosis is made, conservative management is usually recommended, but pacemaker insertion may be required if the condition is complicated by heart block [32] (Fig. 21.16).

Aortitis of Rheumatic Disease

As in rheumatoid arthritis and ankylosing spondylitis, arteritis is the result of complex immune disturbances. When the aorta is involved, the inflammatory process results in pan aortitis affecting the three arterial layers. The only echocardiographic finding may be mild aortic regurgitation, which rarely progresses. This is probably because of the early disease recognition, the arthritis, and the commencement of therapy that limits further progression. However, extensive involvement with severe aortic regurgitation may occur [33].

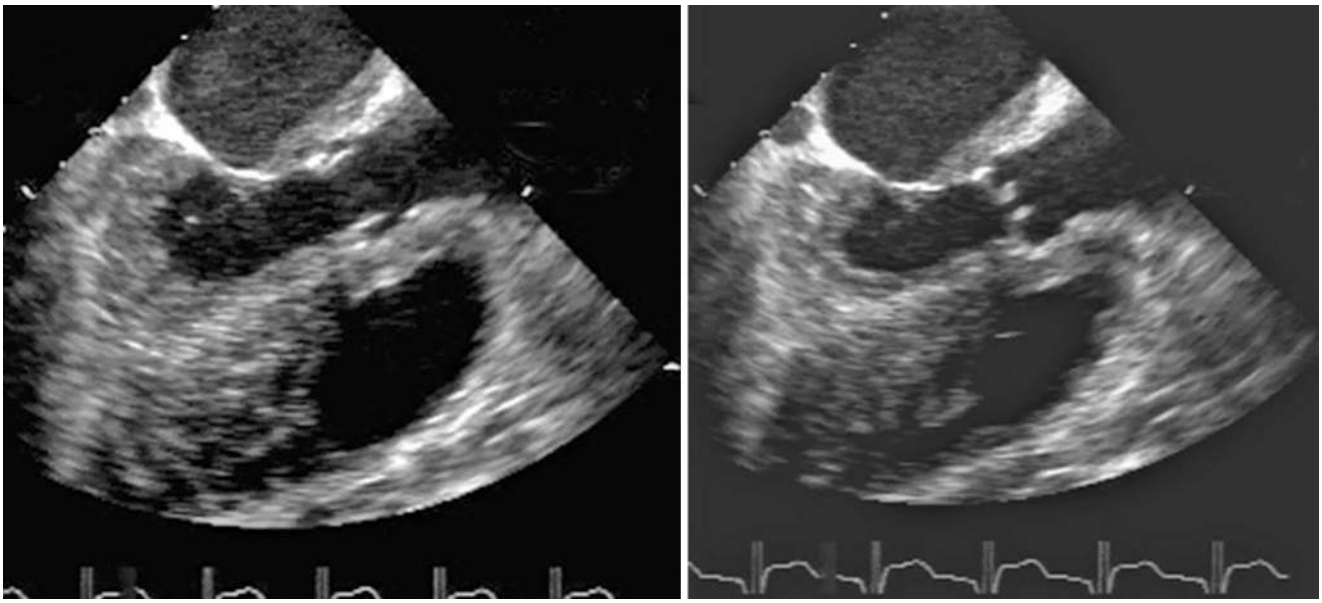


Fig. 21.16 Parasternal long axis view from a patient with Takayasu disease showing significantly thickened aortic root wall (10 mm)

Syphilitic Aortitis

This is a rare condition that results in scarring of the media and adventitia. It is manifested late after the onset of infection (10–30 years). The ascending aorta is the commonly affected site that becomes dilated. In severe disease, a large aneurysm is formed which may result in mediastinal syndrome by causing pressure on the adjacent structures: bronchi, esophagus, and recurrent laryngeal nerve. Surgery is the only means for managing complications of syphilitic aortic aneurysm [34, 35].

References

1. Erbel R, Engberding R, Daniel W, Roelandt J, Visser C, Rennollet H. Echocardiography in diagnosis of aortic dissection. Lancet. 1989;1(8636):457–61.
2. Harris PD, Bowman FO Jr, Malm JR. The management of acute dissections of the thoracic aorta. Am Heart J. 1969;78(3):419–22.
3. Nienaber CA, von Kodolitsch Y, Nicolas V, Siglow V, Piepho A, Brockhoff C, et al. The diagnosis of thoracic aortic dissection by noninvasive imaging procedures. N Engl J Med. 1993;328(1):1–9.
4. Ayala K, Chandrasekaran K, Otto J. Are the Doppler characteristics of the entry site of an intimal flap useful in the evaluation and follow up of aortic dissection? J Am Coll Cardiol. 1992;19:279A.
5. Khandheria BK, Tajik AJ, Taylor CL, Safford RE, Miller FA Jr, Stanson AW, et al. Aortic dissection: review of value and limitations of two-dimensional echocardiography in a six-year experience. J Am Soc Echocardiogr. 1989;2(1):17–24.
6. Kotler MN. Is transesophageal echocardiography the new standard for diagnosing dissecting aortic aneurysms? J Am Coll Cardiol. 1989;14(5):1263–5.
7. Chia BL, Yan PC, Ee BK, Choo MH, Tay MB, Lee CN. Two-dimensional echocardiography and Doppler color flow abnormalities in aortic root dissection. Am Heart J. 1988;116(1 Pt 1):192–4.
8. Iliceto S, Nanda NC, Rizzon P, Hsuing MC, Goyal RG, Amico A, et al. Color Doppler evaluation of aortic dissection. Circulation. 1987;75(4):748–55.
9. Ghazy T, Eraqi M, Mahlmann A, Hegelmann H, Matschke K, Kappert U, et al. Quality of life after surgery for Stanford type A aortic dissection: influences of different operative strategies. Heart Surg Forum. 2017;20(3):E102–6.
10. Glower DD, Speier RH, White WD, Smith LR, Rankin JS, Wolfe WG. Management and long-term outcome of aortic dissection. Ann Surg. 1991;214(1):31–41.
11. Mazzolai L, Teixido-Tura G, Lanzi S, Boc V, Bossone E, Brodmann M, et al. 2024 ESC Guidelines for the management of peripheral arterial and aortic diseases. Eur Heart J. 2024;45(36):3538–700.
12. Beckmann E, Shrestha ML. The 7 pillars of the frozen elephant trunk. Innovations: technology and techniques in cardiothoracic and vascular. Surgery. 2022;17(4):255–8.
13. Sievers HH, Rylski B, Beyersdorf F, Czerny M, Kari FA, Kreibich M, et al. Aortic dissection reconsidered: type, entry site, malperfusion classification adding clarity and enabling outcome prediction. Interact Cardiovasc Thorac Surg. 2020;30(3):451–7.
14. Pepper J, John Chan KM, Gavino J, Golesworthy T, Mohiaddin R, Treasure T. External aortic root support for Marfan syndrome: early clinical results in the first 20 recipients with a bespoke implant. J R Soc Med. 2010;103(9):370–5.
15. Pepper J, Golesworthy T, Utley M, Chan J, Ganeshalingam S, Lamperth M, et al. Manufacturing and placing a bespoke support for the Marfan aortic root: description of the method and technical results and status at one year for the first ten patients. Interact Cardiovasc Thorac Surg. 2010;10(3):360–5. Epub Dec 11, 2009.
16. Karalis DG, Chandrasekaran K, Victor MF, Ross JJ Jr, Mintz GS. Recognition and embolic potential of intraaortic atherosclerotic debris. J Am Coll Cardiol. 1991;17(1):73–8.
17. Tobler HG, Edwards JE. Frequency and location of atherosclerotic plaques in the ascending aorta. J Thorac Cardiovasc Surg. 1988;96(2):304–6.
18. Fox R, Ren JF, Panidis IP, Kotler MN, Mintz GS, Ross J. Anuloaortic ectasia: a clinical and echocardiographic study. Am J Cardiol. 1984;54(1):177–81.

19. Pyeritz RE. Propranolol retards aortic root dilatation in the Marfan syndrome, abstracted. Circulation. 1983;68(Suppl III):365.
20. el Habbal MH. Cardiovascular manifestations of Marfan's syndrome in the young. Am Heart J. 1992;123(3):752–7.
21. Rothbaum DA, Dillon JC, Chang S, Feigenbaum H. Echocardiographic manifestation of right sinus of Valsalva aneurysm. Circulation. 1974;49(4):768–71.
22. Haaz WS, Kotler MN, Mintz GS, Parry W, Spitzer S. Ruptured sinus of Valsalva aneurysm: diagnosis by echocardiography. Chest. 1980;78(5):781–4.
23. Nishimura K, Hibi N, Kato T, Fukui Y, Arakawa T. Real-time observation of ruptured right sinus of Valsalva aneurysm by high speed ultrasono-cardiotomography. Report of a case. Circulation. 1976;53(4):732–5.
24. Ellis SG, Goldstein J, Popp RL. Detection of endocarditis-associated perivalvular abscesses by two-dimensional echocardiography. J Am Coll Cardiol. 1985;5(3):647–53.
25. Shively BK, Gurule FT, Roldan CA, Leggett JH, Schiller NB. Diagnostic value of transesophageal compared with transthoracic echocardiography in infective endocarditis. J Am Coll Cardiol. 1991;18(2):391–7.
26. Carvalho JS, Redington AN, Shinebourne EA, Rigby ML, Gibson D. Continuous wave Doppler echocardiography and coarctation of the aorta: gradients and flow patterns in the assessment of severity. Br Heart J. 1990;64(2):133–7.
27. Houston AB, Simpson IA, Pollock JC, Jamieson MP, Doig WB, Coleman EN. Doppler ultrasound in the assessment of severity of coarctation of the aorta and interruption of the aortic arch. Br Heart J. 1987;57(1):38–43.
28. Marx GR, Allen HD. Accuracy and pitfalls of Doppler evaluation of the pressure gradient in aortic coarctation. J Am Coll Cardiol. 1986;7(6):1379–85.
29. Lam YY, Mullen MJ, Kaya MG, Gatzoulis MA, Li W, Henein MY. Left ventricular and ascending aortic function after stenting of native coarctation of aorta. Am J Cardiol. 2010;105(9):1343–7.
30. Lam YY, Mullen MJ, Kaya MG, Gatzoulis MA, Li W, Henein MY. Left ventricular long axis dysfunction in adults with "corrected" aortic coarctation is related to an older age at intervention and increased aortic stiffness. Heart. 2009;95(9):733–9.
31. Lam YY, Kaya MG, Li W, Mahadevan VS, Khan AA, Henein MY, et al. Effect of endovascular stenting of aortic coarctation on biventricular function in adults. Heart. 2007;93(11):1441–7. Epub Jun 17, 2007.
32. Choe YH, Kim DK, Koh EM, Do YS, Lee WR. Takayasu arteritis: diagnosis with MR imaging and MR angiography in acute and chronic active stages. J Magn Reson Imaging. 1999;10(5):751–7.
33. Townend JN, Emery P, Davies MK, Littler WA. Acute aortitis and aortic incompetence due to systemic rheumatological disorders. Int J Cardiol. 1991;33(2):253–8.
34. Frank MW, Mehlman DJ, Tsai F, Lomasney JW, Joob AW. Syphilitic aortitis. Circulation. 1999;100(14):1582–3.
35. Pugh PJ, Grech ED. Images in clinical medicine. Syphilitic aortitis. N Engl J Med. 2002;346(9):676.

Cardiac Function and Renal Disease

22

Bernd Stegmayr and Michael Y. Henein

The Cardio-Renal Syndrome (Table 22.1)was introduced by Ronco et al. almost 20 years ago [1]. Acute cardiac events, such as myocardial infarction, may cause subsequent acute kidney impairment that may later be established as chronic kidney disease (CKD). The other scenario is the relationship between cardiac dysfunction and the subsequent development of kidney failure. Many, particularly elderly patients, suffer from the unspecified diagnosis of CKD, which also progresses with age. Most of these patients suffer from arteriosclerosis involving the renal vessels and hence secondary hypertension.

Once kidney impairment progresses and the residual function is reduced to below 15% the normal function, patients start accumulating more uremic toxins within all body cells. Some of these toxins, such as urea, will cause an osmotic effect hence retaining water in the cells (Fig. 22.1a–f). The subsequent impairment of other organ functions causes progressive fatigue. Fluid retention may appear in the tissues, including the pericardial space. Low concentration of intravascular albumin, such as in malnutrition, vasculitis, or extensive proteinuria, increases the risk of edema and organ function impairment. The best current clinical practice dictates the serious need to establish a well-structured collaboration between cardiologists and nephrologists for optimum management of such patients, in order to determine the timely commencement of renal dialysis or graft transplantation. Once the decision is made to start dialysis, hemodialysis, in most countries, is the first and main choice, while peritoneal dialysis is a rare alternative. The following sections will focus on factors that need the clinical attention of both nephrologists and cardiologists in order to provide the best possible patient care.

Table 22.1 The cardio-renal syndrome is a based on five principal interactions

Acute cardio-renal syndrome (type 1)
Acute worsening of heart function leading to kidney injury and/or dysfunction
Mainly due to patients hospitalized for acute de-compensated heart failure that subsequent induce acute kidney injury (AKI)
Chronic cardio-renal syndrome (type 2)
Chronic abnormalities in heart function lead to kidney injury or dysfunction. The syndrome is common in patients hospitalized with congestive heart failure
Acute reno-cardiac syndrome (type 3)
Acute worsening of kidney function that leads to heart injury and/or dysfunction
The pathophysiological mechanisms go beyond volume overload such as in severe septic shock initiated with AKI and subsequently involving the heart either by uremic toxins and/or fluid retention due to restricted urinary output
Chronic reno-cardiac syndrome (type 4)
Chronic kidney disease (CKD) leading to heart injury, disease, and/or dysfunction
There is an exponential relation between the severity of renal dysfunction and the risk for all-cause mortality with excess cardiovascular deaths
Secondary cardio-renal syndromes (type 5)
Systemic conditions leading to simultaneous injury and/or dysfunction of heart and kidney. This subtype refers to situations where both organs are simultaneously affected by systemic illnesses, either acute or chronic such as sepsis, systemic lupus erythematosus, diabetes mellitus, or other chronic inflammatory conditions

B. Stegmayr (✉)
Umea University, Umea, Sweden
e-mail: bernd.stegmayr@umu.se

M. Y. Henein
Imperial College London, London, UK

Siena University, Siena, Italy

© The Author(s), under exclusive license to Springer Nature Switzerland AG 2025

M. Y. Henein (ed.), *Clinical Echocardiography*, https://doi.org/10.1007/978-3-031-95894-6_22

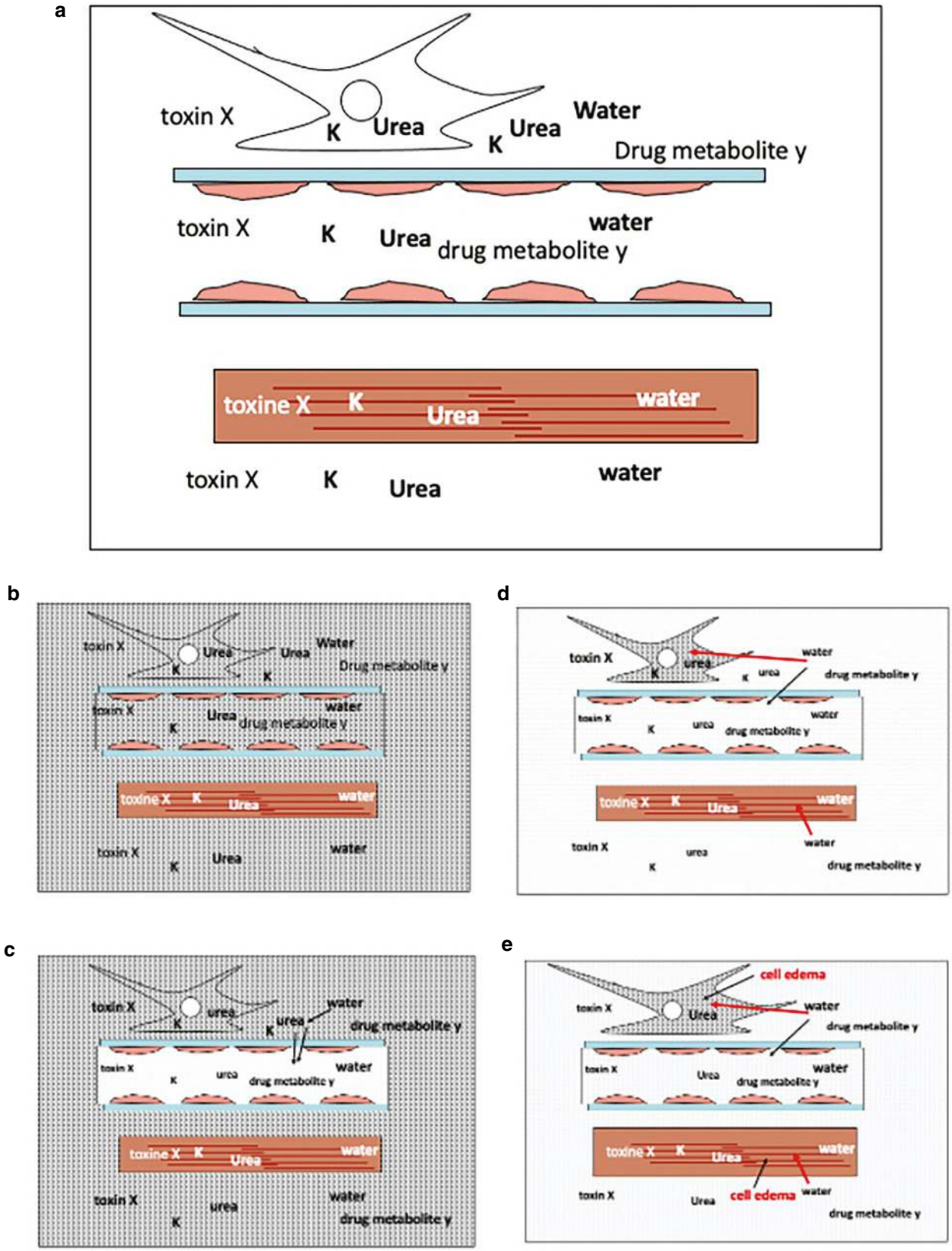


Fig. 22.1 Legend: Distribution of uremic toxins and water (**a**) healthy condition, normal concentration of substances in general; (**b**) Dialysis necessary condition with uremic toxins in all compartments; (**c**) Initiated dialysis reduces the concentration of water-soluble substances and excess water in the vessels; (**d**) Diffusion of substances and convection of water from the extracellular compartment into the vessels lowers the local concentrations; Osmotic effects of uremic solutes may influence cells to absorb water by osmotic effects; (**e**) Enlargement/edema of cells while diffusion of substances lags behind from the intracellular to the extracellular compartment. Meanwhile, a prolonged dialysis enables a shift toward equilibration of compartments

Access in Dialysis

Patients with kidney disease requiring dialysis usually receive hemodialysis or hemodiafiltration intermittently (HD) or continuously, in the intensive care unit, which requires a large venous access for the extracorporeal circuit in order to incorporate the dialyzer before returning to a vein (CVVHD). A common vascular access is a dual lumen central dialysis catheter (CDC), which is inserted subcutaneously through the external or internal jugular vein with the tip just placed in the right atrium. The catheter may be of the "acute version" or "permanent version." The acute catheter has no cuff in order to allow its easy movement in and out through the skin entry, at the expense of increased risk of migration of bacteria and contamination of the blood. Such infection may be a cause for endocarditis. The permanent catheter, on the other hand, has a cuff that is fixed a few centimeters inside the skin entry with a subsequent subcutaneous channel, and after a distance, it enters the jugular vein. This design restricts skin-borne tunnel-related infections, as is the case with the "acute catheter." However, still the opening and closing of the catheter, such as in each dialysis, carries the risk of bacterial contamination of the blood line. Catheters also carry the risk of blood clotting, which may cause subsequent embolic episodes to the lungs. If the patient has an open foramen ovale, embolic contamination may cross over directly to the left heart, causing potential systemic thromboembolism.

Echocardiography plays a pivotal role in the comprehensive assessment of dialysis patients. Transthoracic imaging ascertains the presence of the catheter tip in the right atrium, its exact distance from the tricuspid valve to safeguard any potential interference with valve function. It confirms/refutes the presence of a patent foramen ovale and provides a detailed assessment of the anatomy and function of the interatrial septum. This is achieved by a simple contrast (bubble) study with the Valsalva maneuver in order to exclude contrast bubble shunt reversal from the right to the left atrium. Finally, echocardiography is the most feasible noninvasive imaging investigation that confirms the presence of endocarditis in the form of vegetations or abscess formation in highly suspicious cases.

Patients with progressive CKD may enter the dialysis program through a planned protocol. However, 30% of the patients show up on an acute basis, unaware of their CKD. They may suffer from fatigue or various other symptoms of breathlessness and/or palpitations, as well as other signs of congestive heart failure. The latter group usually receives a central dialysis catheter to initiate hemodialysis, while the "planned" group receives an arteriovenous fistula (AVF). If lower arm vessels only hold a low blood flow, an arteriovenous graft (AVG) may be necessary or an upper arm and brachial artery AVF or AVG. Overall, the arteriovenous (AV) accesses are preferred over the catheter since morbidity related to the AV access is less common [2].

Cardiac consideration for AVF is a risk for increased recirculation and cardiac strain. This shunted recirculation may progress into congestive heart failure, especially in patients with upper arm AVF or AVG [3], and hence the need for optimum cardiac assessment by Doppler echocardiography to establish baseline chamber structure and function.

Cardiac Response to Dialysis

Establishing an AV access for dialysis will result in a shunt from the arterial to the venous circulation of at least 600 ml/min, which is a preferred flow for a patent fistula [2]. This volume and flow rate are bound to cause an increased cardiac strain [4]. In some patients, the AVF flow could increase up to 1000 ml/min and even higher, depending on body surface area and any other existing cardiac condition [2]. Many patients on hemodialysis may suffer from hypertension besides evolving arteriosclerosis related to various conventional risk factors, including hereditary, dietary, and metabolic. Myocardial stunning may also develop, unexpectedly, in patients on hemodialysis [5]. The progressive loss of residual renal function and urinary output causes fluid retention between the dialyses. The retained fluid is usually successfully removed by the dialysis device during the 3–5 hours of dialysis three times/week. The intermittent change in fluid retention influences the intermittent removal of toxic substances. Those toxins interfere with cellular function when retained, at their highest concentrations before dialysis, in all compartments, including intracellularly. During dialysis, a passage of water-soluble molecules occurs between compartments, most rapidly removed from the blood line and least from the intracellular compartment. This results in a shift of osmotic effects and subsequently interferes with organ function. Rapid removal of the osmotic effect can cause complications in the course of dialysis that may even end up in convulsions and death (called disequilibrium) [6]. On the other hand, too fast fluid removal from the body (ultrafiltration) may induce hypotension in vulnerable cardiac patients, particularly those with blood pressure below 100 mmHg, at the start of dialysis. In patients with congestive heart failure that worsens by fluid overload, during the dialysis and ultrafiltration procedure, the blood pressure will rise by withdrawal of fluid up to a point when it again starts to decrease. This reflects the Frank-Starling mechanism of the heart and can be used to optimize patient's dry weight.

Body Weight in Dialysis Patients

Under normal renal and cardiac conditions without fluid retention, a person will have the "Ideal" weight (described as "Dry weight"). With severe kidney failure and limited urine output, fluid is retained following ingestion and hence increases body weight above the ideal expected for body surface area, a condition described as "Wet weight" or Predialysis weight. Fluid retention is related to body weight and can be calculated as an Inter Dialytic Weight Gain (IDWG), given as the increase in percentage of body weight (Fig. 22.2) [7–9]. Since it may be difficult to estimate the Ideal body weight in dialysis patients, various methods are used to estimate fluid retention, including jugular vein dilatation in supine position, peripheral edema, chest x-ray, ultrasound evaluation based dilatation of lung vessels and bioimpedance, ultrasound assessment of cardiac enlargement, and myocardial strain before and after dialysis [10–12]. Echocardiography plays an important role in such patients in assessing the presence of pericardial effusion and pleural effusion, also in excluding a cardiac dysfunction that could contribute to fluid retention, such as pericardial constriction, tamponade, irrespective of its volume, and restrictive myocardial disease.

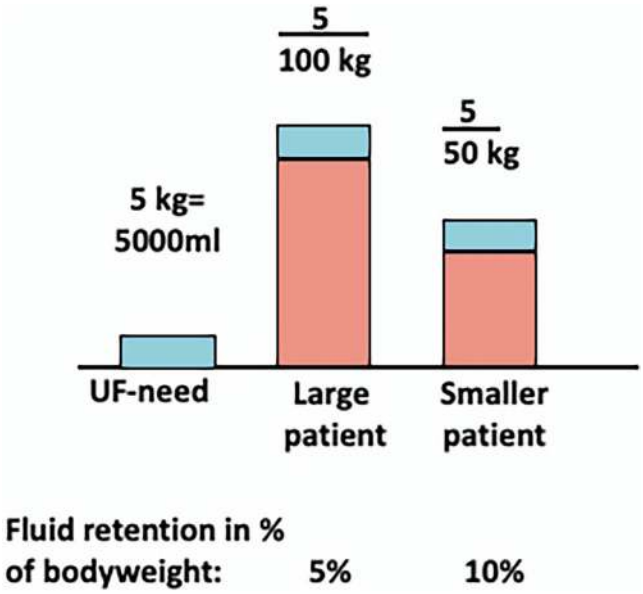


Fig. 22.2 Patients with dialysis-dependent kidney failure often have reduced or ceased urine output. This results in retention of fluid in the body due to ingestion of fluid or food. The weight of the patient will increase from the ideal weight (Dry weight) until the fluid is removed from the patient with the dialysis technique (ultrafiltration). The intradialytic weight gain (IDWG) that appears between two dialysis sessions is then expressed in kg and related to the ideal weight of the patient given in percentage. Five percent IDWG represents approximately a condition of pulmonary stasis and 10% pulmonary edema unless a right heart failure is dominant. Here, the importance of weight gain in relation to the ideal body weight is shown

Cardiac Biomarkers in Dialysis Patients

Since the half-life of cardiac markers such as troponin and NT-pro-BNP is prolonged in dialysis patients, the reference level is usually set higher [13, 14] than in normal conditions. Many HD patients already have high levels of Troponin and NT-pro-BNP before dialysis [13, 14] thus indicating cardiac strain. A relationship between the NT-pro-BNP and the extent of IDWG has been found [14]. Even using optimal dialysis protocol, high NT pro-BNP and Troponin values may be detected, again indicating cardiac strain. Besides a myocardial infarction or endocarditis, consideration should be given to clarify whether the rise in cardiac biomarkers is an acute or a chronic condition. The latter situation may be due to myocardial stunning and an acute or chronic unnoticed overhydration, e.g., related to malnutrition or catabolic situations [9] (Fig. 22.3a, b).

Patients with already raised cardiac biomarkers before dialysis are known to have worse prognosis [15]. The values correlate with the IDWG with a breakpoint of >2.5% at start for NT pro-BNP and even lower for Troponin [14]. After initiating hemodialysis, pro-BNP and Troponin T frequently rise further within 180 min of dialysis (Fig. 22.4) [14]. This is often seen in patients with worse fluid retention (Fig. 22.5a, b) [14], but also in those who had undergone fast ultrafiltration during dialysis (fluid removal) (Fig. 22.6) [16]. The significant rise in cardiac biomarkers in these patients could be related to reduced global and segmental myocardial blood flow with or without additional coronary artery disease. Episodes of hypotension may also contribute. Another potential mechanism for the compromised coronary blood supply to the myocardium is air embolism caused by bubbles developing in the extracorporeal circuit during hemodialysis (Fig. 22.7) [17–19].

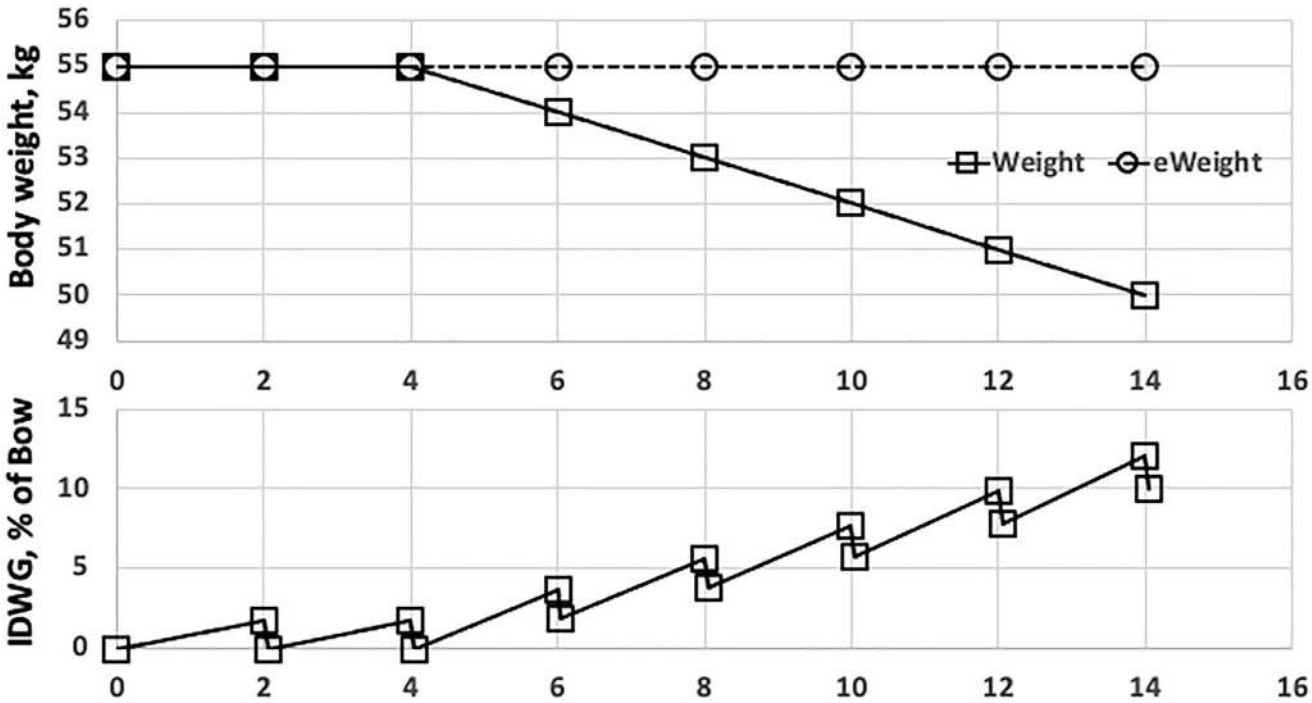


Fig. 22.3 Ideal body weight over time in relation to the interdialytic weight gain (IDWG) in %. (**a**) The upper part shows the hatched line with open circles with an estimation of the ideal weight (eWeight) over time (here on the x-axis given as days, weeks, or months). The filled line with open squares shows the reduction of the ideal weight (e.g., by malnutrition) that may be missed unless repeated adjustments of the eWeight are done. (**b**) The lower part shows an IDWG of 1.8% during the first two episodes. When the patient loses weight, the assessed IDWG is wrong, and a retention of fluid appears. The ideal weight needs to be corrected to make the right assumption of the IDWG. Here, a real IDWG of 12% appears at period 14. The clinical evaluation needs to take this into account upon unexpected congestive heart failure

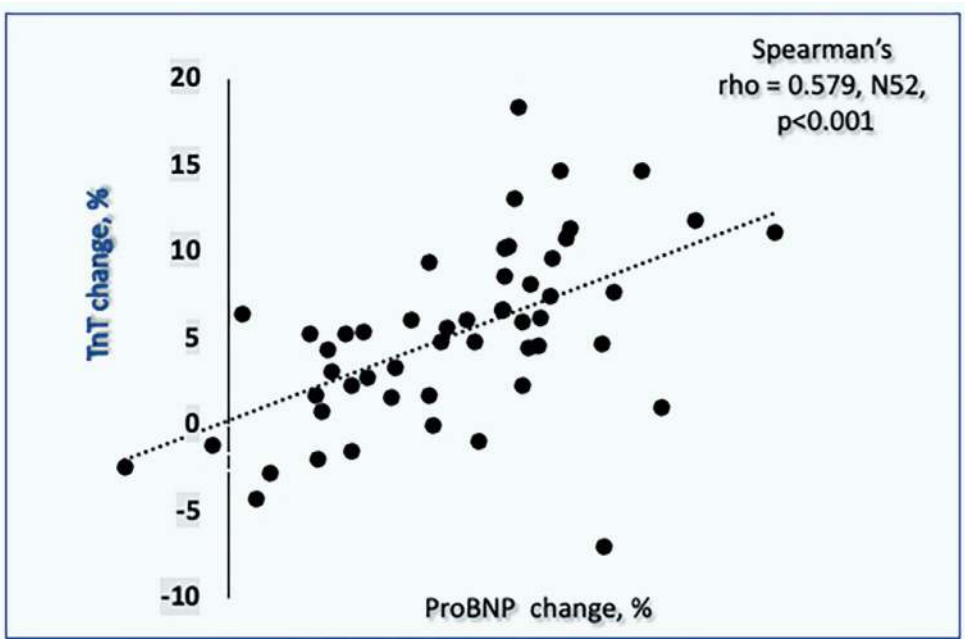


Fig. 22.4 Relation between ProBNP and troponin T (TnT) in their change (in %) from start to 180 min of hemodialysis from Goto et al. [14]

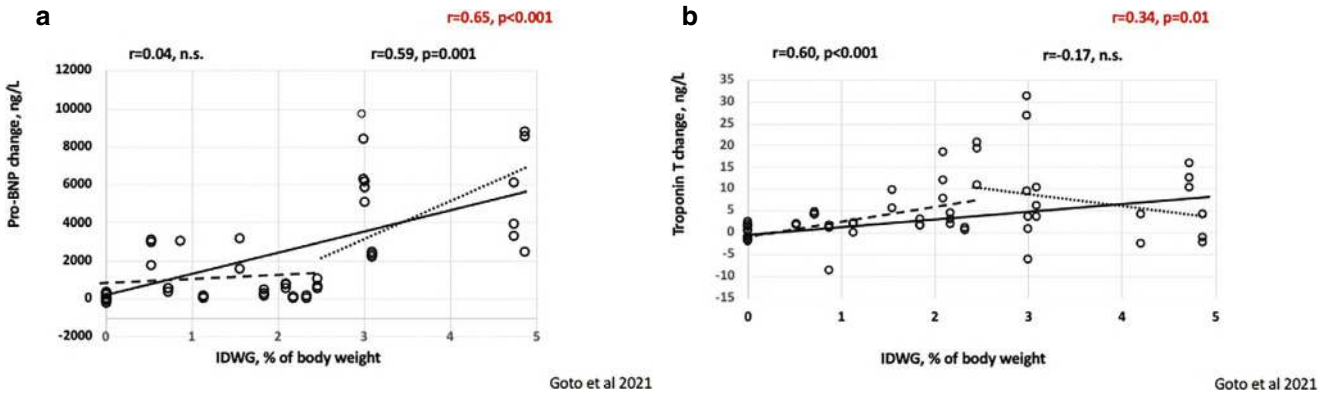


Fig. 22.5 The change in cardiac markers from start to 180 min of dialysis in relation to IDWG. (**a**) The overall correlation of proBNP is significant to IDWG but more evidently a break appears at 2.5%. (**b**) Troponin T is related to the IDWG throughout the analysis

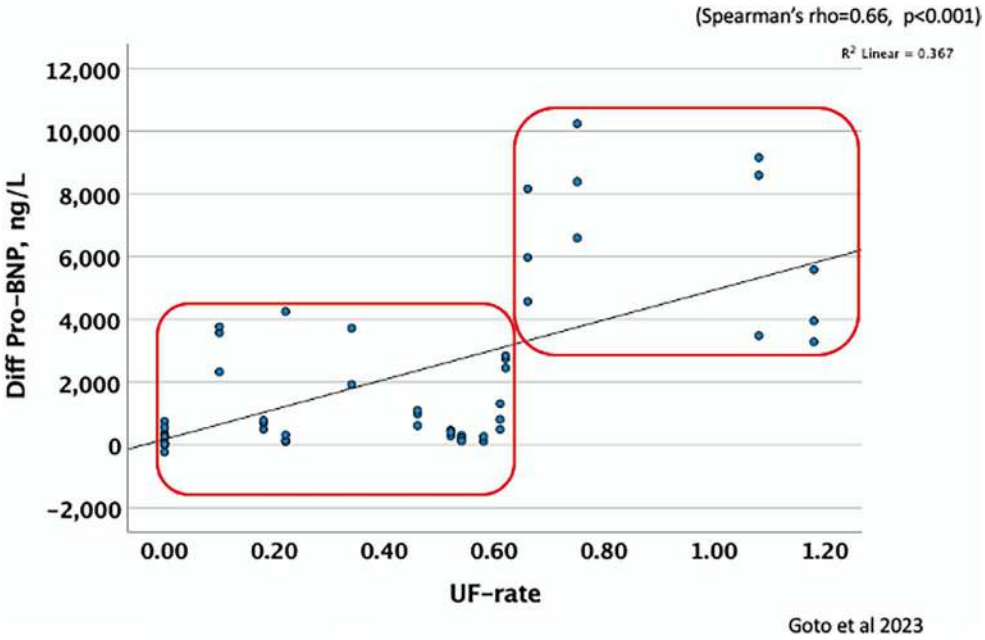


Fig. 22.6 The change in proBNP from start to 180 min of dialysis shows a breakpoint at the ultrafiltration rate of 0.60 (calculated as the speed of removal of fluid in IDWG%/hour of dialysis)

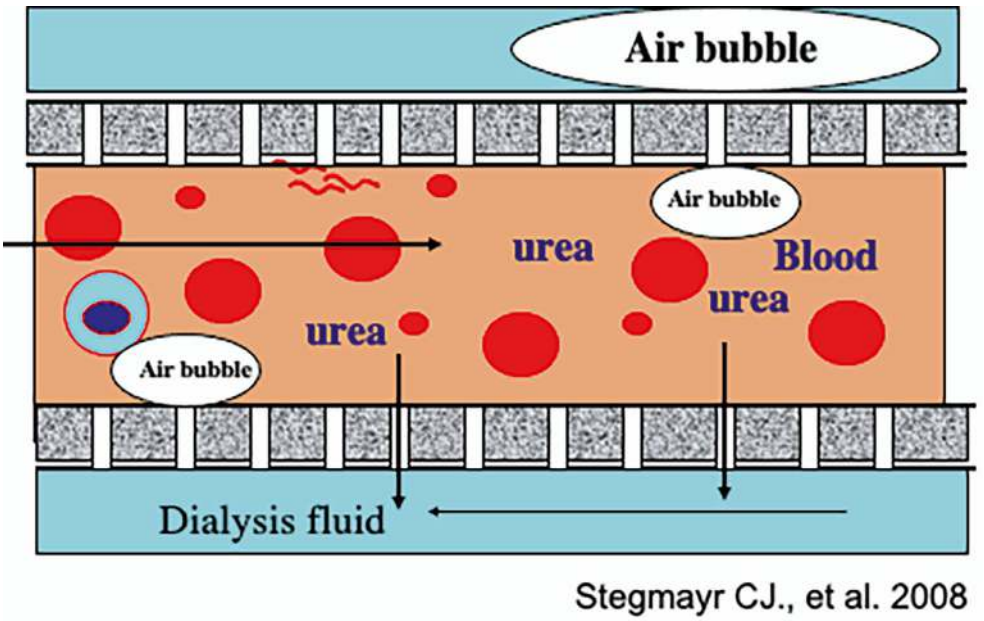


Fig. 22.7 A longitudinal view of a dialyzer semipermeable capillaries with perfusing dialysis fluid at the outside enabling diffusion of uremic solutes from the blood to the dialysate. Air bubbles present in blood are only partly removed by venous chambers while the residing bubbles pass into the venous line of the patient. (Modified after Stegmayr C et al. [23])

Cardiac Arrhythmia and Hemodialysis

Rare cases of sudden cardiac death during and early after HD have been reported, which suggested cardiac arrhythmia as the potential cause. Bradycardia and QT dispersion have been reported as the most common type of arrhythmia, rather than tachycardia. It has also been suggested to be related to long dialysis cycle length. However, the current evidence supporting such suggestion is only modest, and larger cohort studies need to confirm it [14, 20, 21].

Clinical Considerations for Hemodialysis Patients with Cardiac Problems

- To consider various reasons for cardio-renal syndrome and direct cardiac injuries.
- To accurately evaluate cardiac function from a recent echocardiographic examination.
- To re-evaluate the vascular access in case of significant recirculation and, if so, consider surgical adjustments for optimum access; change to a CDC or peritoneal dialysis [21, 22] while ceasing the recirculation of the AVF.
- -To estimate adequate dialysis procedure (extent of uremic solutes, including potassium levels and acidosis).
- -To estimate the predicted dry weight of the patient.
- -To check IDWG (such as >2.5%), and limit fluid intake or prescribe more frequent dialysis sessions.
- -To ascertain the presence of any catabolic condition or malnutrition that could have contributed to the reduction of the optimal (dry weight) that needs adjusting dialysis protocols. Addition or change to peritoneal dialysis will help eliminate waste products and fluid, and in parallel add calories by glucose transfer from the peritoneal fluid into the body, at no cost of fluid retention if the right osmotic fluid is chosen.

The above measures should help improving cardiac function and optimizing predialysis levels of Troponin and pro-BNP. Unsuspected increase in these markers would suggest a significant myocardial infarction, probably caused by numerous air emboli. The use of dialyzers with a high sieving coefficient will eliminate cardiac markers from the dialysate and cause falsely low values when drawn after the dialysis session [13].

References

1. Ronco C, McCullough P, Anker SD, et al. Cardio-renal syndromes: report from the consensus conference of the acute dialysis quality initiative. Eur Heart J. 2010;31:703–11.
2. Stegmayr B, Willems C, Groth T, et al. Arteriovenous access in hemodialysis: a multidisciplinary perspective for future solutions. Int J Artif Organs. 2021;44:3–16.
3. Warja M, Laveborn E, Ott M, Jonsson AP, Stegmayr B. NT-pro-BNP as marker for cardiac strain that may be caused by high-output arteriovenous shunting in a haemodialysis patient. A case report. BMC Nephrol. 2020;21:544.
4. Hadimeri U, Smedby Ö, Fransson S-G, Stegmayr B, Hadimeri H. Fistula diameter correlates with echocardiographic characteristics in stable hemodialysis patients. Nephrology @ Point of Care. 2015;1:e44–e8.
5. Burton JO, Jefferies HJ, Selby NM, McIntyre CW. Hemodialysis-induced repetitive myocardial injury results in global and segmental reduction in systolic cardiac function. Clin J Am Soc Nephrol. 2009;4:1925–31.
6. Bhandari B, Komanduri S. Dialysis disequilibrium syndrome. In: StatPearls. Treasure Island: ineligible companies. Disclosure: Saketram Komanduri declares no relevant financial relationships with ineligible companies; 2024.
7. Stegmayr BG, Brannstrom M, Bucht S, et al. Minimized weight gain between hemodialysis contributes to a reduced risk of death. Int J Artif Organs. 2006;29:675–80.
8. Holmberg B, Stegmayr BG. Cardiovascular conditions in hemodialysis patients may be worsened by extensive interdialytic weight gain. Hemodial Int. 2009;13:27–31.
9. Matsuda K, Fissell R, Ash S, Stegmayr B. Long-term survival for hemodialysis patients differ in Japan versus Europe and the USA. What might the reasons be? Artif Organs. 2018;42:1112–8.
10. Elgenidy A, Amin MA, Awad AK, et al. The use of lung ultrasound in evaluation of extravascular lung water in hemodialysis patients: systematic review and meta-analysis. Hemodial Int. 2024;28:148–61.
11. Georgianos PI, Agarwal R. Resistant hypertension in dialysis: epidemiology, diagnosis, and management. J Am Soc Nephrol. 2024;35:505–14.
12. Mambelli E, Grandi F, Santoro A. Comparison of blood volume biofeedback hemodialysis and conventional hemodialysis on cardiovascular stability and blood pressure control in hemodialysis patients: a systematic review and meta-analysis of randomized controlled trials. J Nephrol. 2024;37:897.
13. Laveborn E, Lindmark K, Skagerlind M, Stegmayr B. NT-proBNP and troponin T levels differ after haemodialysis with a low versus high flux membrane. Int J Artif Organs. 2015;38:69–75.
14. Goto J, Forsberg U, Jonsson P, et al. Interdialytic weight gain of less than 2.5% seems to limit cardiac damage during hemodialysis. Int J Artif Organs. 2021;44:539–50.
15. Satyan S, Light RP, Agarwal R. Relationships of N-terminal pro-B-natriuretic peptide and cardiac troponin T to left ventricular mass and function and mortality in asymptomatic hemodialysis patients. Am J Kidney Dis. 2007;50:1009–19.

16. Goto J, Ott M, Stegmayr B. Myocardial markers are highly altered by higher rates of fluid removal during hemodialysis. Hemodial Int. 2024;28:17–23.
17. Stegmayr B. Air contamination during hemodialysis should be minimized. Hemodial Int. 2017;21:168–72.
18. Forsberg U, Jonsson P, Stegmayr B. Air contamination during medical treatment results in deposits of microemboli in the lungs: an autopsy study. Int J Artif Organs. 2019;42:477–81.
19. Forsberg U, Jonsson P, Stegmayr B. Microemboli induced by air bubbles may be deposited in organs as a consequence of contamination during medical care. Clin Kidney J. 2023;16:159–66.
20. Edwards JC, Mosman A, Hauptman PJ, et al. Arrhythmia in chronic hemodialysis as a function of predialysis electrolytes and interdialytic interval. Hemodial Int. 2023;27:45–54.
21. Francois K, Ronco C, Bargman JM. Peritoneal dialysis for chronic congestive heart failure. Blood Purif. 2015;40:45–52.
22. Stegmayr BG, Banga R, Lundberg L, Wikdahl AM, Plum-Wirell M. PD treatment for severe congestive heart failure. Perit Dial Int. 1996;16:S231–5.
23. Stegmayr C, Jonsson P, Forsberg U, Stegmayr B. Hemodialysis dialyzers contribute to contamination of air microemboli that bypass the alarm system in the air trap. Int J Artif Organs. 2008;31:317–22.

Index

A
Advanced heart failure (AdHF), 227–241
American Heart Association (AHA), 130
Amyloid heart disease, 201, 204, 206–208, 210, 300
Angina, CAD
  inherent limitations, 130
  stable, 130, 131
  stress long axis, 131, 133, 134
Aorta diseases
  aortic
    aneurysm, 361, 363
    arch and proximal descending aorta, 366
    root abscess, 364, 365
    sinus aneurysm, 363, 364
  aortic arch and proximal descending aorta, 367
  aortitis (*see* Aortitis)
  apical four-chamber view, elderly patient, 359
  ascending aorta, patient, 359
  coarctation, 366
  congenitally small aortic root (*see* Aortic valve)
  continuous wave Doppler recording, patient, 367
  dissection, 357
  intraoperative echocardiography, 365
  management, 360, 361, 367
  parasternal view, patient, 362–365
  paravalvular abscess cavities, 365
  TOE, 358, 362, 364
  transesophageal echo, patient, 358
  transverse section, ascending aorta, 360
Aortic aneurysm, 50, 361, 363, 366
Aortic coarctation
  continuous wave Doppler flow, 315
  continuous wave Doppler recording, duct flow, 313
  defined, 314
  management, 315
  pulsed wave Doppler velocities, 315
  secondary effects and lesions, 315
  suprasternal view, discrete narrowing, 314
Aortic dissection, 61, 290, 357, 358, 360, 361, 365
Aortic regurgitation
  etiology, 49, 50, 53
  intraoperative echo assistance, 62
  management
    symptomatic and asymptomatic patients, 58
    transthoracic echocardiography, 58
  pathophysiology, 53, 55
  physiological disturbances, 54, 56
  severity assessment, 56, 57, 60
  signs modification, conditions, 56
  surgery, 60, 61
Aortic root, 14, 37, 39, 42, 47–53, 57, 58, 60, 61, 103, 117, 118, 261, 262, 297, 319, 357, 360, 364, 365, 367
Aortic stenosis
  causes
    acquired aortic, 40–42
    congenital aortic tubular, 37
    congenital cusp malformation, 36, 38
    sub-aortic, 37, 40
    supra-aortic, 40
  congenital, 36
  management
    valve replacement surgery, 44
    valvuloplasty, 45
  pathophysiology, 42
  patients, asymptomatic, 49
  severity assessment
    color flow Doppler, 43
    continuity equation, 43
    CW Doppler, 42
    leaflet separation extent, 42
  symptoms and physiological disturbances, 43
  TAVI procedure, 48
  valve surgery
    echocardiography role, 47, 48
    homografts, 46
    mechanical/bioprosthetic, 46
    pulmonary autograft/Ross procedure, 46
Aortic valve, 1, 4, 10, 14, 20, 21, 83, 84, 91, 96, 98, 100, 101, 103, 108, 117, 189, 234, 236, 240, 241, 269, 290, 310, 315, 328, 357, 360, 361, 366
  anatomy, 35
  aneurysm, aortic root, 50
  aortic regurgitation secondary, leaflet prolapse, 50
  aortic root tubular narrowing and proximal ascending aorta, 39
  apexcardiogram, 55
  ascending aorta and LV outflow tract, 52
  bicuspid, 36
  calcific AV disease, 42
  calcified aortic valve and dilated ventricle, poor systolic function, 43
  color flow Doppler, 45
  color flow jet, aortic regurgitation, 57
  combined rheumatic mitral and disease, 41
  cusp formation presentations, 37
  CW Doppler, 40, 43, 44, 47, 60
  disease, 9, 40, 41, 47, 49, 103, 106, 215, 271
  double barreled aorta, 53
  eccentric closure point, 38
  infected xenograft, 54
  infective endocarditis, 50
  jugular venous pulse, 46
  left ventricle and ascending aorta, 36
  LV minor axis M-mode, 47
  LV M-mode recording, 56, 61

© The Editor(s) (if applicable) and The Author(s), under exclusive license to Springer Nature Switzerland AG 2025

M. Y. Henein (ed.), *Clinical Echocardiography*, https://doi.org/10.1007/978-3-031-95894-6

Aortic valve (*cont.*)
mitral valve echogram, 55
mitral valve M-mode recording, 57
M-mode echogram, 38
normal tricuspid and parasternal short axis, 35
pathological specimen, 51
proximal dissection, 53
pulmonary homograft peak velocity, 47
pulsed wave Doppler recording, 60
replacement, 14, 101, 103, 108, 269, 270, 319, 367
regurgitation, 49, 50, 54, 56, 58, 61
rheumatic aortic valve, 41
senile degenerative calcification, 41
septal LV long axis recording, 45
stenosis, 36, 37, 40–44, 46–49
stenotic rheumatic, 41
sub-aortic stenosis, 40
supra-aortic stenosis, 40
TOE, 51, 55, 57
transesophageal echo, 49
transmitral Doppler flow velocities, 45
2-cm long vegetation, 51
Aortitis
rheumatic, 367
syphilitic, 368
Takayasu, 367, 368
Arrhythmogenic right ventricular cardiomyopathy (ARVC), 176
ASD, *see* Atrial septal defect
Atrial pressure, 9, 22, 43, 45, 70, 71, 78–80, 92, 122, 166, 192, 204, 215, 218, 220, 230, 231, 237, 261, 278, 292, 297–301, 316, 335
Atrial septal defect (ASD), 19, 39, 68, 70, 72, 321–349, 366
apical four-chamber view, primum, 308
assessment, interventional closure/surgical repair, 310
classification, 307
description, 307
patent foramen ovale, 321–349
right heart dilatation and volume overload, 309
RV and LV, 309
3D TOE, primum, 308
TOE, SVC type, color Doppler, 309
Atrial septal devices, 324, 326, 337
Atrioventricular septal defect (AVSD)
adult population, 311
apical four-chamber view
AV valve, 312
small ventricular component, 312
description, 311
Atrioventricular valve, 19, 28, 67, 72, 176, 204, 307, 309–312, 327, 344
AVSD, *see* Atrioventricular septal defect

B

Bicuspid aortic valve
associated lesions, 315
description, 36
M-mode echogram, 38
parasternal long and short axis, 38
section, 37
Bioprosthetic valve, 28, 46, 95, 98, 103

C

Cancer therapy-related cardiovascular toxicity (CTR-CVT), 249
Cardiac resynchronization therapy, 125, 164, 170, 194, 268
Cardiac sarcoidosis, 201, 210
Cardiac tumors
atrial septal lipoma, 281
benign, 277
fibroelastoma, 280, 281
free wall thrombus, 280
left atrial myxoma, 277, 279
lipomas, 281, 282
LV cavity, 278
malignant
melanoma invading, 284–286
primary, 283
secondary, 283–286
multiple rabdomiomata, 282
myxoid tissue, 279
myxomas, 277, 279, 280
normalization, 278, 280
pleural carcinoma and pericardium, 286
renal cell carcinoma invading, 284, 285
right atrial angiosarcoma, 283
TOE, osteosarcomal invading, 285
Cardio-renal syndrome, 378
Carotid intima-media thickness (CIMT), 351, 353, 354
Carotid plaque, 353, 354
Carotid scanning
artery disease, 353, 354
description, 351, 352
imaging protocol and reporting, 353
plaque characterization, 354, 355
Catheter-based mitral valve clip repair (CBMCR), 29
Chagas Cardiomyopathy, 176
Constrictive pericarditis
echocardiographic findings, 297
etiology and pathophysiology, 296, 297
JVP, patient, 298, 299
management, 298
and restrictive cardiomyopathy
clinical similarity, 299
description, 299, 300
respiratory variation, 299
right and left ventricular pressures, 297
Coronary artery anomalies (CAAs), 115, 117
Coronary artery disease (CAD)
acquired, 117
anatomy
anterior myocardial infarction, 120
IVUS imaging, 119
pathological specimen, 122
recordings, 135
right and left coronary sinuses, 118
right ventricular free wall longitudinal motion, 123
scarred and kinetic segment, LV long axis, 121
angina, 130, 131, 134, 135
anomalous left coronary artery origin, 116
anterior infarction, apical aneurysm, 124
aortic root
origin, 117
TOE, 118
aortic valve leaflets and root, 117
apical ventricular septal defect, 124
balloon inflation, proximal LAD, 142
biventricular ischemic myopathy, 140
cavity full opacification and endocardium clear delineation, 131
changes, QRS duration, 133
congenital, 115
CW Doppler and color flow M-mode recordings, 126

echocardiographic imaging, 118–120
exertional angina, 132
free wall infarction and posterior mitral valve leaflet prolapse, 125
intraoperative TOE, 143–145
ischemic cardiomyopathy, 135, 136
left ventricular M-mode recording, 143
limiting dyspnea and ischemic cardiomyopathy, 141
LV free wall long axis recording, 142
LV septal long axis recording, 142
management
bypass surgery, 143, 146
medical follow-up, 140
PCI, 140
mitralclip in situ creation, 125
mitral regurgitation disappearance, 145
multiple vein grafts and LIMA, LAD, 146
myocardial infarction, 120, 122
myocardial tissue Doppler recordings, 138
parasternal long axis view, left ventricle, 121
QRS broadening and septal onset delay, 134
resistant dyspnea and ischemic cardiomyopathy, 141
right ventricular filling velocities, 123
right ventricular infarction
ischemic left ventricular disease, 127
left ventricular thrombus, 126
mitral regurgitation, 123
papillary muscle rupture, 123
pericardial effusion, 126
ventricular aneurysms, 122
ventricular septal defect, 123
septal long axis
function, 135
recording, 133
stress-induced apical and inferior wall perfusion abnormalities, 127
stress isovolumic time and peak cardiac output, 139
TOE, posterolateral ruptured papillary muscle, 125
transesophageal echocardiogram, 143
transmitral and pulmonary venous Doppler flow velocities, 129
unstable angina, 135
Coronary atherosclerosis, 254
Coronary flow reserve, 130

D

Dental procedures, 105, 106
Diagnosis, 2, 17, 19, 21, 36, 40, 80, 98, 103, 106, 107, 110, 115, 117, 120, 122, 126, 155, 183, 184, 193
Dilated cardiomyopathy (DCM), 15, 26, 76, 136, 138, 191, 197, 240, 297
activation-induced LV dysfunction, 168
apical 4 chamber view
mitral regurgitation, 165
spherical-shaped LV cavity, 165
apical views, large left ventricular cavity, 167
ARVC, 176
assist devices, 171, 175
Chagas cardiomyopathy, 176
continuous wave Doppler recording, 169
description, 161
and diastolic asynchrony, 174
etiology, 161, 162
extracardiac fluid compression, 167
follow-up, 170, 172
inferior vena caval flow, patient, 168
left and right ventricular filling, patient, 172
left ventricular thrombus, 166
LV filling pattern, patient, 164
mitral regurgitation, 164
neurological, 177
pacing, 170, 174
parasternal long axis view, pericardial and left pleural effusion, 168
pharmacological, 176
prognosis, 175
pulmonary hypertension, 166
pulsus alternans, 167
raised left atrial pressure, 165
signs, disease progression and functional deterioration, 176
transmitral flow, restrictive left ventricular filling, 166
transmitral forward flow velocities and CW Doppler, 166
transplantation, 172
treatment, 170
tricuspid regurgitation, 166
ventricular filling, 164
ventricular function, 170
Dobutamine stress, 132, 143, 155, 189, 190

E

Ebstein anomaly
apical four-chamber view, septal leaflet, 315, 316
description, 315
displacement, posterio-inferior leaflet, 315
tricuspid valve regurgitation, 315
Echocardiography, 6, 7, 9, 11, 13–16, 25, 26, 28, 29, 31, 36, 44, 47, 48, 58, 61, 68, 71, 90, 92, 95, 98, 106–109, 111, 115, 117, 118, 120, 123, 125–127, 129, 130, 135, 143, 151, 153–155, 157, 158, 162–164, 170, 183, 189, 191, 227–241, 251–255, 262, 263, 270, 271, 290, 310, 321, 327, 349, 353, 373, 374
Echocardiography, congenital heart lesions
aortic coarctation, 314, 315
ASD (*see* Atrial septal defect (ASD))
Ebstein anomaly, 315, 316
PDA (*see* Patent ductus arteriosus (PDA))
tetralogy, fallot, 317–320
VSD (*see* Ventricular septal defect (VSD))
Embolic events, 110, 111
Endomyocardial fibrosis (EMF)
description, 204
mitral/tricuspid regurgitation, 204
External aortic root support (EARS), 360

H

HCM, *see* Hypertrophic cardiomyopathy
Heart disease, 9, 10, 84, 106, 115, 117, 156, 157, 161, 183, 193, 207, 210, 216, 224, 251, 253, 254, 309, 312
Heart rate variability (HRV), 210
Hypertrophic cardiomyopathy (HCM), 39, 85, 106, 118, 156, 183, 186, 192
apical 4-chamber view, HOCM, 186
apical view
basal septal hypertrophy, 191
mitral valve leaflets, 192
clinical picture, 183
color flow Doppler recordings, patient, 190
continuous wave Doppler, LV outflow tract, 188
echo contrast injection, 195
exercise intolerance, 192
left ventricular minor axis, concentric myocardial hypertrophy, 184
left ventricular outflow tract velocity, 187

Hypertrophic cardiomyopathy (HCM) (*cont.*)
LV long axis view, patient, 196
LV septal long axis, nonsurgical septal reduction technique, 196
management
family screening, 197
medical, 193
nonsurgical septal reduction, 195, 196
pacing, 194
prognosis, 197
surgical, 194
mitral valve dysfunction, 192
mitral valve echogram, patient, 188
natural history, 191
parasternal long axis two-dimensional view, 185
parasternal long axis view, LV, 187
pathology, 183
pathophysiology, 186, 188, 189
right ventricular long axis recording, patient, 193
transesophageal echo, aortic valve, 189
transverse section, left and right ventricle, 184

I
Idiopathic restrictive cardiomyopathy, 202, 203
Infective endocarditis (IE), 20, 36, 50, 51, 56, 60, 61, 103, 364
abscess
surgery/necropsy, 108
TEE, 108
dehiscence, prosthetic valve
surgery/necropsy, 109
2D TTE, 109
echocardiography role, 106, 107
fistula
surgery/necropsy, 109
TEE, 109
modified duke criteria, 106
perforation, 109
preventive measures
cardiac conditions, risk, 106
prophylactic antibiotics, 105
transient bacteremia, 105
pseudoaneurysm
surgery/necropsy, 109
2D TTE, 108
surgery, left-sided native valve
indications and timing, 110, 111
2D TTE e 3D TTE, 112
types, 110
valve aneurysm, 109
vegetation
aortic valve, 108
mitral valve, 108
surgery/necropsy, 108
2D TTE, 108
Interstitial lung disease, 216, 224
Intravascular ultrasound (IVUS)
accurate information, plaque characterization, 119
imaging, 119
scanning, 120
Ischemic cardiomyopathy, 16, 126, 129, 134–137, 139–141, 143, 145
CAD
functional mitral regurgitation, 136
hibernating myocardium, 135
ventricular long axis function, 136, 137

K
Kawasaki disease, 117, 156
Kidney disease, 373

L
Left atrial (LA) pressure, 4, 7, 9, 11, 16, 21, 22, 25, 26, 43, 120, 127, 136, 140, 141, 143, 164–167, 169–171, 175, 178, 186, 189, 190, 192, 194, 201, 202, 206, 211, 215, 224, 229, 302, 338
Left atrium (LA), 1–4, 8, 11, 13, 16, 17, 21, 22, 24, 129, 143, 162, 164, 172, 176, 190, 202, 215–217, 224, 231, 232, 251, 253, 261–264, 266–271, 277, 278, 280, 283, 290, 292, 309, 321, 323, 324, 332–334, 337, 338, 340, 341, 344–348, 373
Left heart chambers, 251
Left ventricular and function, 319
Left ventricular outflow tract, 14, 37, 48, 50, 98, 183, 188, 189, 194, 195, 224, 310, 312
Löffler's syndrome, 204

M
Malignant tumors
primary, 283
secondary, 283
Management, 9, 14, 26, 29, 87, 93, 103, 106, 110, 119, 120, 122, 123, 125, 140, 158, 170–172, 176, 183, 186, 190, 193, 194
Marfan's syndrome, 18, 50, 61, 361
Mechanical cardiac support (MCS), 236
Mechanical valve, 46, 81, 95, 97, 98
Mesothelial cells, 289
Mitral annular calcification
description, 14
management, 14
Mitral clip procedure, 29
Mitral regurgitation (MR), 42, 43, 55, 56, 95–99, 101, 103, 115, 120, 123, 125–127, 129, 136, 140, 141, 143, 145, 156, 157, 162, 164–166, 169–171, 173, 176, 186, 189, 190, 192, 210, 215–217, 224, 230, 232, 240, 268, 269
congenital, 19
endomyocardial fibrosis, 24
infective endocarditis, 20
ischemic
acute myocardial infarction, 16
normal left ventricle, 16
papillary muscle rupture, 16
ventricular dysfunction, 16
management, 26
myxomatous degeneration, 17
pathophysiology
left atrial pressure, 21
stroke volume, 21
preoperative and perioperative patient assessment, 28
ruptured chordae tendineae, 24
severity assessment
color flow area, 21
continuity equation, 22
continuous wave Doppler, 22
large LV stroke volume, 21
left atrial emptying volume, 22
PISA, 21
systolic flow reversal, pulmonary veins, 22
three-dimensional color Doppler, 22
vena contracta, 21
stress echocardiography, 25
surgery, 28
valve replacement complications
disintegrating mitral xenograft, 29
endocarditis, 29
fibrin strands/thrombi, 29
para-prosthetic, 29
stuck mitral prosthesis, 29
Mitral stenosis (MS), 40, 55, 56, 71, 269, 277, 338
complications
aortic valve disease, 9

leaflet fibrosis and deformation, 7
left atrial dilatation, 7
left ventricular dysfunction, 8
pulmonary hypertension, 9
right heart disease, 9
tricuspid regurgitation, 9
tricuspid valve stenosis, 9
congenital, 2
disturbed physiology, 7
interventional treatment
surgery, 11–13
valvuloplasty, 11
non-interventional treatment
follow-up, 11
medical therapy, 11
patient selection, surgery, 13, 14
rheumatic, 3, 4
severity assessment
continuity equation, 6
flow convergence method, 5
planimetry technique, 5
pressure ½ time, 6
transmitral pressure drop, 5
vena contracta, 5
Mitral valve, 35, 36, 41, 42, 49, 53, 55, 57, 70, 72, 75, 81, 97, 98, 100–103, 108, 111, 112, 125, 145, 164, 168, 186–188, 192, 194, 215, 224, 230, 262, 264, 268, 269, 277, 278, 281, 309, 347
anatomy, 1, 2
annular calcification, 14
clip procedure, 29
color Doppler regurgitation, 24
color flow Doppler, 2
CW Doppler, 30, 42
dense pale fibrous tissue, 26
disease, 6, 11, 12, 17, 21, 40, 81, 194, 211, 215, 278, 309, 315
extensive nodular calcification, mitral annulus, 14
flail anterior leaflet, Marfan's syndrome, 18
flow velocities and rheumatic disease, 12
functional regurgitation, patient, 9
long axis recording, 13
LV filling velocities, CW Doppler, 6
LV parasternal view, dilated cavity, 8
minor axis, left ventricle, 2
mitral xenograft and large vegetation, patient, 30
M-mode echogram, patient, 5
M-mode, LV minor axis, 2
parasternal long axis, 4, 10, 12
parasternal short axis, rheumatic, 5
pathological specimen from, disintegrated MV xenograft, 29
pathology section, rheumatic MVD, 3
patient
endomyocardial fibrosis, 26
rheumatic heart disease, 10
physiology, 2
posterior MV leaflet and late systolic prolapse, 1
regurgitation, 15–17, 19, 21, 22, 26, 28–30
rheumatic, 3
Starr–Edwards ball cage metallic valve, 29
Starr–Edwards prosthesis, small fibrin strands, 30
Starr–Edward valve, 30
stenosis, 2–5, 7–14
subcostal views, patients, 3
thickened leaflet, ballooning, 15
TOE, 8, 18, 24
transmitral Doppler flow velocities, 2, 7
transmitral flow convergence velocities, 6
2D parasternal long axis, rheumatic leaflets, 4
vena contracta, 5
Mitral valve replacement, 9, 12, 13, 26–28
Myocardial infarction, echo-Doppler technique, 120, 122

N

Neurological Cardiomyopathy, 177, 179
Noonan's syndrome, 91

O

Open heart surgery, 292, 300–302
Outflow tract (OT), 25, 37, 39, 40, 43, 45, 49, 50, 52, 56, 86, 88, 90, 91, 95, 98, 127, 156, 183, 186–191, 193–195, 197, 224, 231, 235, 281, 319

P

Papillary muscle, 1–3, 13, 15, 16, 21, 24–26, 67, 81, 122, 123, 125, 164, 186, 192, 194, 210, 232, 309
Patent ductus arteriosus (PDA)
description, 312
echocardiography, 312
hemodynamic significance, 312
Patent foramen ovale (PFO), 92, 143, 271, 321–349
complex functional anatomy, device closure, 336–341
description, 321
detection, patency
momentary "bounce", septum, 336
tunnels, 336
device design
description, 325
materials, wire frames, 325
nonself-centering devices, 325
variations, 325
intraprocedural guidance
aneurysmal atrial septa, 335
antero-posterior diameters, 337
atrial septal anatomy, 332
description, 331, 332
intraprocedural assessment, 323
sizing defects, 335
percutaneous closure procedure
intraprocedural assessment, 323, 324
TOE sizing, 322, 323
stable device, 327
suitability, closure
coronary sinus, 327
secundum-type ASDs, 327
stable device, 327
TOE and ICE, 321
PDA, *see* Patent ductus arteriosus
Percutaneous coronary intervention (PCI), 321
Pericardial disease
anatomy, 289
apical four-chamber view
amyloid heart disease, 300
pleural carcinoma, 303
complications, post open heart surgery
clot and "Tight" pericardium, 301, 302
management, 301
restrictive pericarditis, 302
constrictive pericarditis and restrictive cardiomyopathy (*see* Constrictive pericarditis)
effusion (*see* Pericardial effusion)
heart and pericardium, 302

Pericardial disease (*cont.*)
jugular venous pulse, 298
JVP and SVC flow, 301
JVP, patient, 298, 299
large left pleural effusion, patient, 296
left parasternal long axis and apical views, pericardial space, 296
mitral echogram, 302
M-mode, aortic valve, 289
physiology, 289
specimen, posterior pericardial segment, 297
tamponade, 292, 294, 296
transtricuspid flow, patient, 300
tumors, 302
Pericardial effusion, 42, 48, 69, 71, 120, 126, 143, 204, 254, 283, 302, 357, 374
apical four-chamber view, patient, 290, 291
cause, chronic fluid accumulation, 290
complications, 300
diagnosis, 289
investigations, 290
parasternal long and short axis views, patient, 291
quantitation, 290
subcostal view, small cell carcinoma, 303
symptoms, 290
transtricuspid and pulmonary pulsed Doppler velocities, 293
Pericardial tamponade
intrapericardial clot formation, 294
pathophysiology, 292
pericardiocentesis, 294
right ventricular collapse, 292
Pericardial tumors
cardiac magnetic resonance/CT scanning, 302
primary, 302
Pharmacological cardiomyopathy, 175
Plaque characterization, carotid scanning, 354, 355
Plaque vulnerability, 354, 355
Prosthetic valve, 61, 81, 95–98, 103, 105–107, 109, 111
Proximal isovelocity surface area (PISA), 7, 8
Pulmonary artery pressure, 166, 218–220, 224, 309, 313
Pulmonary hypertension, 4, 7–9, 11, 12, 29, 48, 55, 56, 72, 78, 90, 98, 127, 143, 156, 157, 162, 166, 167, 170, 175, 204, 215, 224, 237, 240, 253, 310
apical-four chamber view, mitral regurgitation, 217
Doppler echocardiography, 218–220
flow and valve M-mode, patient, 219
four-chamber view, systemic sclerosis, 221
histological section, patient, 215
management, 224
parasternal short axis view, 224
pathophysiology, 215–217
recordings, diastolic RV filing, 218
and right ventricular function, 220–222
tricuspid pulsed wave flow, patient, 218
2D images and M-mode recordings, 223
and vascular resistance, 220
Pulmonary regurgitation, 219, 220, 318, 319
arrhythmia, 89
assessment, right ventricular function, 89
isolated congenital, 88
restrictive right ventricular disease complications, 92
right ventricular dilatation, 88
right ventricular dysfunction, 89
Pulmonary stenosis, 72, 300, 309
severity, 84
subvalvar, 85
supravalvar, 87
treatment, 87
valvular, 84
Pulmonary valve, 47, 79, 101, 218, 219, 297, 309, 310, 317
anatomy, 83
aortic valve and right ventricular outflow tract, 91
CW Doppler, 85, 88, 90–92
dilated right ventricular cavity, 91
electron beam angiography, 88
mild and severe, post valvotomy, 89
regurgitation, 88, 89, 92, 93
restrictive RV disease and cyanosis, 92
right ventricular filling pattern, 91
right ventricular M-mode recording, 92
and right ventricular outflow tract, leaflets, 83
stenosis
severity, 84
subvalvar, 85
supravalvar, 87
treatment, 87
valvular, 84
stiff and fibrosed leaflets, 85
stiff right ventricle and arrhythmia, 93
subvalvar/infundibular stenosis, 86
superior vena caval flow, 91
supravalvar stenosis, 87
thread-like artery, 88
transpulmonary CW Doppler, 91
transthoracic and transesophageal, 84
tricuspid regurgitation, 92
2D images, subvalvar stenosis, 86
Pulmonary valve replacement, 93
Pulmonary vascular resistance (PVR), 4, 9, 218–220, 313

R

Regurgitation
aortic valve
etiology, 49, 50, 54
intraoperative echo assistance, 62
management, 58, 60, 61
pathophysiology, 53, 55
physiological disturbances, 54, 55
severity assessment, 56, 57
signs modification, conditions, 56
surgery, 61
mitral valve
causes, 15–17, 19
endomyocardial fibrosis, 25
infective endocarditis, 20
management, 26
pathophysiology, 21
preoperative and perioperative patient assessment, 28
ruptured chordae tendineae, 24
severity assessment, 21, 22
stress echocardiography, 25
surgery, 28
valve replacement complications, 29, 30
tricuspid
assessment, 79–81
etiology, 72, 75, 78
pathophysiology, 78
surgical procedures, 81
treatment, 81
Reiter's syndrome, 50
Restrictive cardiomyopathy, 72
apex cardiogram and transmitral Doppler velocities, 201

apical four chamber view, 204
cardiac sarcoidosis, 210
description, 204
diabetic hypertensive, 211, 212
EMF, 204
hemochromatosis, 211
histological section, hemosiderosis, 211
idiopathic, 202, 203
infiltrative myocardial disease, 204–206
left ventricular filling, 207
Löffler's syndrome, 204
M-mode, LV minor axis, 208
parasternal long axis view and M-mode recording, 205
pathological section, ventricle, 210
superior vena cava, restrictive right ventricular disease, 212
2D and M-mode images, 211
transmitral forward flow velocities, 203
Rheumatic fever, 2, 3, 7, 11, 61, 105
Right heart chambers, 251, 253, 363
Right ventricular function, 220, 222, 319
Right ventricular outflow tract (RVOT), 83, 88, 91, 234, 292, 309, 315, 317, 318

S

Speckle tracking echocardiography (STE), 90, 228, 263–266
Stratification, 15, 120, 155, 156, 227, 254, 255, 266, 267, 353, 354
Stress echocardiography, 25, 44, 125, 189, 191, 239, 240, 254, 256, 269
appropriateness
description, 151
indications, 156
comparison
cardiac magnetic resonance, 158
effective dose ranges, medical procedures, 158
ESC guidelines, 158
competence, 157
contraindications
dobutamine and dipyridamole, 156
exercise, 156
coronary flow reserve, 154
description, 151
diagnosis
necrotic and viability response, 153
normal and ischemic response, 153
diagnostic value, 155, 157
examples, 152, 153
feasibility and safety
adenosine, 155
dipyridamole, 155
dobutamine, 155
exercise, 155
external pacing, 155
myocardial viability, 152
dobutamine, 156
pathophysiology, 152
prognostic value, 155
pathophysiology, 151, 152
prognostic value, 155–156
test protocols, 152–155
valvular heart disease, 156, 157
advantages, 156
description, 156, 157
non-cardiac surgery, 157
Suspected coronary artery disease, 351

T

Test protocols, stress echocardiography
adenosine, 155
diagnostic and submaximal non-diagnostic endpoints, 152
dipyridamole, 155
dobutamine, 155
echocardiographic imaging, 157
ergonovine, 155
pacing, 155
sensitivity and specificity, dipyridamole *vs*. dobutamine, 155
Tetralogy of fallot
aortic overriding, 317
aortic root dimension and regurgitation, 319
assessment, right ventricle, 318, 319
associated lesions, 317
continuous wave Doppler recording, tricuspid regurgitation, 316
definition, 317
left ventricular diameter and function, 319
obstruction and severity, RVOT, 317
patients
palliative procedures, 317, 318
reparative surgery, 318
residual right ventricular outflow obstruction, 318
residual shunt, 318
right ventricular function, 319
VSD, 317
Transcatheter aortic valve implantation (TAVI), 48, 49
Transesophageal echocardiogram (TEE)
extensive fibrosis, 69
left ventricular outflow, 98
para-prosthetic abscess, 108
Transthoracic and transesophageal echocardiography (TTE)
paravalvular regurgitation, 109
role, 109
Transthyretin, 41, 210
Tricuspid annulus, 76, 78, 81, 166
Tricuspid regurgitation (TR), 4, 7, 9, 10, 101, 122, 162, 166, 167, 172, 176, 204, 206, 218, 220, 222, 229–231, 240, 277, 309, 313, 315, 316
assessment, 79–81
etiology, 72, 73, 75
pathophysiology, 78
surgical procedures, 81
treatment, 81
Tricuspid stenosis
assessment, 71
etiology, 68, 70
pathophysiology, 70
treatment, 71
Tricuspid valve, 7, 9, 10, 13, 14, 25, 83, 99, 101, 103, 106, 118, 131, 218–220, 225, 277, 291, 297, 300, 309, 310, 315, 316, 327, 373
anatomy, 67
apical 4 chamber view
carcinoid, 69
Ebstein anomaly, 72
pericardial effusion, 70
pulmonary hypertension, 73
rheumatic mitral valve disease, 74
and color Doppler, 73
continuous wave Doppler recordings, 80
endomyocardial fibrosis, 75
ischemic cardiomyopathy, 78
Jugular venous pulse, 79
M-mode recording, LV minor axis, 81
narrowed inflow and high velocities, 70

Tricuspid valve (*cont.*)
parasternal view, 71, 77
pathological section, 75
pulsed wave Doppler velocities, 80
regurgitation, 72, 78, 79, 81
replacement, 81
rheumatic tricuspid valve leaflets, 68
right heart, 67
stenosis, 68, 71, 72
3D views, histological section, 75
TOE
Ebstein anomaly, 73
renal cell carcinoma, 71
transesophageal echocardiogram, fibrosis, 69
transtricuspid flow velocities, atrial septal defection, 70
TV leaflets, 75, 77
TTR, *see* Transthyretin

V
Valve replacement, 13, 14, 16, 20, 25, 26, 28, 29, 37, 41, 43–49, 58, 60, 68, 71, 72, 81, 87, 93, 95, 98, 204, 254, 270
Valve substitutes
and aortic root, 103
artificial, mechanical and bioprostheses, 95
color flow Doppler, 96, 97
CW Doppler, 97, 100
dehiscence area, mitral valve prosthesis, 103
endocarditis, 102
homografts, 101
large vegetation attachment, 102
M-mode recording, left ventricular minor axis, 98
normal transvalvular flow pattern and continuous wave velocities, 102
pathological section and M-mode recording, 99
TOE, 96, 103
transesophageal echocardiogram, 98
transthoracic and transesophageal echo, 97
valve replacement, 97, 101–103
Ventricular outflow tract, 14, 37, 48, 50, 280
Ventricular septal defect (VSD), 50, 87, 123, 194, 317
associated anomalies, 311
associated lesions, 312
AVSD, 311, 312
classification, 310
description, 310
indications, closure, 311
parasternal short-axis view, 310
short-axis view, peri-membranous subtricuspid, 311
size defect and hemodynamic significance, 311
Visceral layers, 289, 296

W
Wall motion abnormality, 151, 154, 354
Williams syndrome, 87